WOODS HOLE
OCEANOGRAPHIC INSTITUTION

COLLECTED REPRINTS

1961

LIBRARY
SEP 2[illegible] 1962
FISH & WILDLIFE SERVICE

JULY, 1962

LIBRARY
BUREAU OF COMMERCIAL FISHERIES
U. S. FISH AND WILDLIFE SERVICE
P. O. BOX 3830
HONOLULU 12, HAWAII

WOODS HOLE
OCEANOGRAPHIC INSTITUTION

COLLECTED REPRINTS

1961

JULY, 1962

This volume contains contributions from the WOODS HOLE OCEANOGRAPHIC INSTITUTION which were published in 1961; also the Annual Report of the Director for the year 1961.

TABLE OF CONTENTS

Contribution No.

ARONS, A. B., A. P. INGERSOLL, and T. GREEN III.
Experimentally Observed Instability of a Laminar Ekman Flow in a Rotating Basin 1135

BACKUS, RICHARD H.
Stranded Killer Whale in the Bahamas 1085

BACKUS, RICHARD H., CHARLES S. YENTSCH and ASA WING
Bioluminescence in the Surface Waters of the Sea 1191

BENSON, BRUCE B. and PETER D. M. PARKER
Nitrogen/Argon and Nitrogen Isotope Ratios in Aerobic Sea Water 1153

BENSON, BRUCE B. and PETER D. M. PARKER
Relations among the Solubilities of Nitrogen, Argon and Oxygen in Distilled Water and Sea Water 1154

BLUMER, MAX
Benzpyrenes in Soil 1193

BLUMER, MAX and GILBERT S. OMENN
Fossil Chlorins in a Triassic Sediment 1063

BLUMER, MAX and GILBERT S. OMENN
Fossil Porphyrins: Uncomplexed Chlorins in a Triassic Sediment 1155

BODMAN, R. H., L. V. SLABAUGH and V. T. BOWEN
A Multipurpose Large Volume Sea-Water Sampler 1208

BOLIN, BERT and HENRY STOMMEL
On the Abyssal Circulation of the World Ocean. IV. Origin and Rate of Circulation of Deep Ocean Water as Determined with the Aid of Tracers 1170

BROCKHURST, R. R., J. G. BRUCE, JR. and A. B. ARONS
Refraction of Underwater Shock Waves by a Strong Velocity Gradient 1147

CIFELLI, RICHARD
227. *Globigerina incompta*, a New Species of Pelagic Foraminifera from the North Atlantic 1165

CONOVER R. J.
Addendum. The Turnover of Phosphorus by *Calanus finmarchicus* 1050

CURL, HERBERT, JR. and GUY C. McLEOD
The Physiological Ecology of a Marine Diatom, *Skeletonema costatum* (Grev.) . . 1198

CURL, HERBERT, JR. and JUDITH SANDBERG
The Measurement of Dehydrogenase Activity in Marine Organisms 1209

DAVID, CHARLES N. and ROBERT J. CONOVER
Preliminary Investigation on the Physiology and Ecology of Luminescence in the Copepod, *Metridia lucens* 1183

DUGDALE, R. C., DAVID W. MENZEL and JOHN H. RYTHER
Nitrogen Fixation in the Sargasso Sea 1159

Contribution No.

EDWARDS, ROBERT L.
The Fishes of Richmond Gulf, Ungava, Canada 1109

FARMER, H. G. and D. D. KETCHUM
Chap. 5. An Instrumentation System for Wave Measurements, Recording and Analysis 1131

GRICE, GEORGE D.
Calanoid Copepods from Equatorial Waters of the Pacific Ocean 1072

GRICE, GEORGE D.
Candacia ketchumi, a New Calanoid Copepod from the North-Western Part of the Sargasso Sea 1127

HAYS, EARL E.
Comparison of Directly Measured Sound Velocities with Values Calculated from Hydrographic Data 1066

HOSKINS, HARTLEY and S. T. KNOTT
Geophysical Investigation of Cape Cod Bay, Massachusetts, Using the Continuous Seismic Profiler 1137

KRAUS, ERIC B.
Physical Aspects of Deduced and Actual Climatic Change 1186

KRAUS, ERIC B. and CLAËS ROOTH
Temperature and Steady State Vertical Heat Flux in the Ocean Surface Layers 1199

LEVINE, JOSEPH
A Spherical Vortex Model of the Buoyant Thermal in Cumulus and Dry Convection 1139

LEWIN, JOYCE C.
The Dissolution of Silica from Diatom Walls 1110

MALKUS, JOANNE S., CLAUDE RONNE and MARGARET CHAFFEE
Cloud Patterns in Hurricane Daisy, 1958 1145

MALKUS, W. V. R. and G. VERONIS
Surface Electroconvection 1138

MARSHALL, S. M. and A. P. ORR
On the Biology of *Calanus finmarchicus*. XII. The Phosphorus Cycle: Excretion, Egg Production, Autolysis 1050

McLACHLAN, JACK
The Effect of Salinity on Growth and Chlorophyll Content in Representative Classes of Unicellular Marine Algae 1150

MENZEL, D. W. and J. H. RYTHER
Annual Variations in Primary Production of the Sargasso Sea off Bermuda 1119

MENZEL, D. W. and J. H. RYTHER
Zooplankton in the Sargasso Sea off Bermuda and its Relation to Organic Production 1121

	Contribution No.
MENZEL, D. W. and J. H. RYTHER Nutrients Limiting the Production of Phytoplankton in the Sargasso Sea, with Special Reference to Iron	1123
NICHOLLS, G. D. and V. T. BOWEN Natural Glass from Beneath Red Clay on the Floor of the Atlantic	1215
PRATT, R. M. Erratic Boulders from Great Meteor Seamount	1122
RAYMONT, J. E. G. and ROBERT J. CONOVER Further Investigations on the Carbohydrate Content of Marine Zooplankton	1114
REDFIELD, ALFRED C. The Tidal System of Lake Maracaibo, Venezuela	1045
REITZEL, JOHN Some Heat-Flow Measurements in the North Atlantic	1194
RICHARDS, FRANCIS A. and BRUCE B. BENSON Nitrogen/Argon and Nitrogen Isotope Ratios in Two Anaerobic Environments, the Cariaco Trench in the Caribbean Sea and Dramsfjord, Norway	1057
RIEHL, HERBERT and JOANNE MALKUS Some Aspects of Hurricane Daisy, 1958	1156
RYTHER, JOHN H. and DANA D. KRAMER Relative Iron Requirement of Some Coastal and Offshore Plankton Algae	1177
RYTHER, JOHN H. and DAVID W. MENZEL Primary Production in the Southwest Sargasso Sea, January–February, 1960	1120
RYTHER, JOHN H., DAVID W. MENZEL and R. F. VACCARO Diurnal Variations in Some Chemical and Biological Properties of the Sargasso Sea	1118
SAUNDERS, PETER M. An Observational Study of Cumulus	1152
SCHELTEMA, RUDOLF S. Metamorphosis of the Veliger Larvae of *Nassarius obsoletus* (Gastropoda) in Response to Bottom Sediment	1132
SHAW, EVELYN The Development of Schooling in Fishes. II.	1176
SHAW, EVELYN Minimal Light Intensity and the Dispersal of Schooling Fish	1211
SIEVER, RAYMOND, ROBERT M. GARRELS, JOHN KANWISHER and ROBERT A. BERNER Interstitial Waters of Recent Marine Muds off Cape Cod	1168
SOULE, FLOYD M., PETER A. MORRILL and ALFRED P. FRANCESCHETTI Physical Oceanography of the Grand Banks Region and the Labrador Sea in 1960	1160

Contribution No.

STERN, MELVIN E.
The Stability of Thermoclinic Jets 1166

SUGIHARA, T. T. and VAUGHAN T. BOWEN
Radioactive Rare Earths from Fallout for a Study of Particle Movement in the Sea 1136

SWALLOW, J. C. and L. V. WORTHINGTON
An Observation of a Deep Countercurrent in the Western North Atlantic 1129

TEAL, JOHN M. and JOHN KANWISHER
Gas Exchange in a Georgia Salt March 1218

TRASK, PARKER D.
Sedimentation in a Modern Geosyncline off the Arid Coast of Peru and Northern Chile 1144

VOORHIS, ARTHUR D.
Evidence of an Eastward Equatorial Undercurrent in the Atlantic from Measurements of Current Shear 1189

WEBSTER, FERRIS
A Description of Gulf Stream Meanders off Onslow Bay 1173

WEBSTER, FERRIS
The Effect of Meanders on the Kinetic Energy Balance of the Gulf Stream 1174

WELANDER, PIERRE
Theory of Very Long Waves in a Zonal Atmospheric Flow 1157

WIESER, WOLFGANG and JOHN KANWISHER
Ecological and Physiological Studies on Marine Nematodes from a Small Salt Marsh near Woods Hole, Massachusetts 1167

WOODCOCK, A. H. and A. T. SPENCER
Lava-Sea-Air Contact Areas as Sources of Sea-Salt Particles in the Atmosphere 1171

ZEIGLER, JOHN M. and SHERWOOD D. TUTTLE
Beach Changes Based on Daily Measurements of Four Cape Cod Beaches 1158

THE WOODS HOLE OCEANOGRAPHIC INSTITUTION

Report for the Year 1961

LIST OF CONTRIBUTIONS

The following contribution is not included in this volume:

BUMPUS, D. F.
Drift Bottle Records for the Gulf of Maine, Georges Bank, and the Bay of Fundy, 1956–58 1146

Contribution No. 1045

Made in United States of America
Reprinted from Limnology and Oceanography
Vol. 6, No. 1, January, 1961
pp. 1–12

THE TIDAL SYSTEM OF LAKE MARACAIBO, VENEZUELA[1]

Alfred C. Redfield
Woods Hole, Massachusetts

ABSTRACT

The tides of the Lake Maracaibo system are attributable to a standing wave produced by tidal waves entering from the Gulf of Venezuela and their reflection from the head of the lake. A node for the semidiurnal constituents occurs in the northern part of the lake. An antinode for the semidiurnal constituents occurs in Tablazo Bay, and this antinode may be presumed to coincide with the node of the diurnal constituents.

When the dimensions of the basin and friction are taken into account by the step-by-step integration of finite difference equations for continuity and gravitational acceleration, estimates of tidal elevations and currents agree approximately with those observed.

The presence of significant rotary tidal currents in Lake Maracaibo or effects of the rotation of the earth on the tide is excluded.

The influence of the antinode in Tablazo Bay on sedimentation and on the exclusion of salt water from the lake are discussed.

In a study of the hydrography of Lake Maracaibo it became evident that the tide is an important factor in depositing marine sediments in its approaches and in controlling the salt content of its water. The tide of the lake is too small to be of practical importance, but along the channel leading from Maracaibo to the Gulf of Venezuela the tidal conditions are of great interest to navigation and have been under continuous observation, formerly by the Maracaibo Bar Survey and presently by the Instituto Nacional de Canalizaciones. The phenomena are apparently complex but yield to analysis by principles commonly applied to the tides in narrow embayments when the topography of the tidal basin is taken into account, it being shown that the effects of the rotation of the earth are negligibly small even in the broad basin of the lake. The situation is an example of the degree to which a standing tidal wave may become distorted by extreme variations in the dimensions of the channel without losing its fundamental characteristics.

The topography of the lake and its approaches is shown in Figure 1.

The tide in the Caribbean is mainly diurnal and at Aruba has a mean range at spring tides of 21 cm. In the Gulf of Venezuela the semidiurnal constituents of the Caribbean tide are greatly augmented by resonance with the result that at Zaparita Island at its southwestern extremity, where the tide has access to the lake, the tide is semidiurnal and has a mean range of 90 cm (Redfield 1958).

---

[1] Contribution No. 1045 from the Woods Hole Oceanographic Institution. This study was made in the course of investigations conducted for the Creole Petroleum Corporation which has granted permission for its publication. Grateful acknowledgment is made to the Creole Petroleum Corporation, the Compãnia Shell de Venezuela and Servicios Hidrograficos for making tidal data available, to Mr. L. A. Earlston Doe and other employees of Creole for assistance in the course of the work, to Dr. Bostwick H. Ketchum and Mr. Dean F. Bumpus who participated in the field, and to Mr. A. R. Miller for the harmonic analyses of tide records from La Salina.

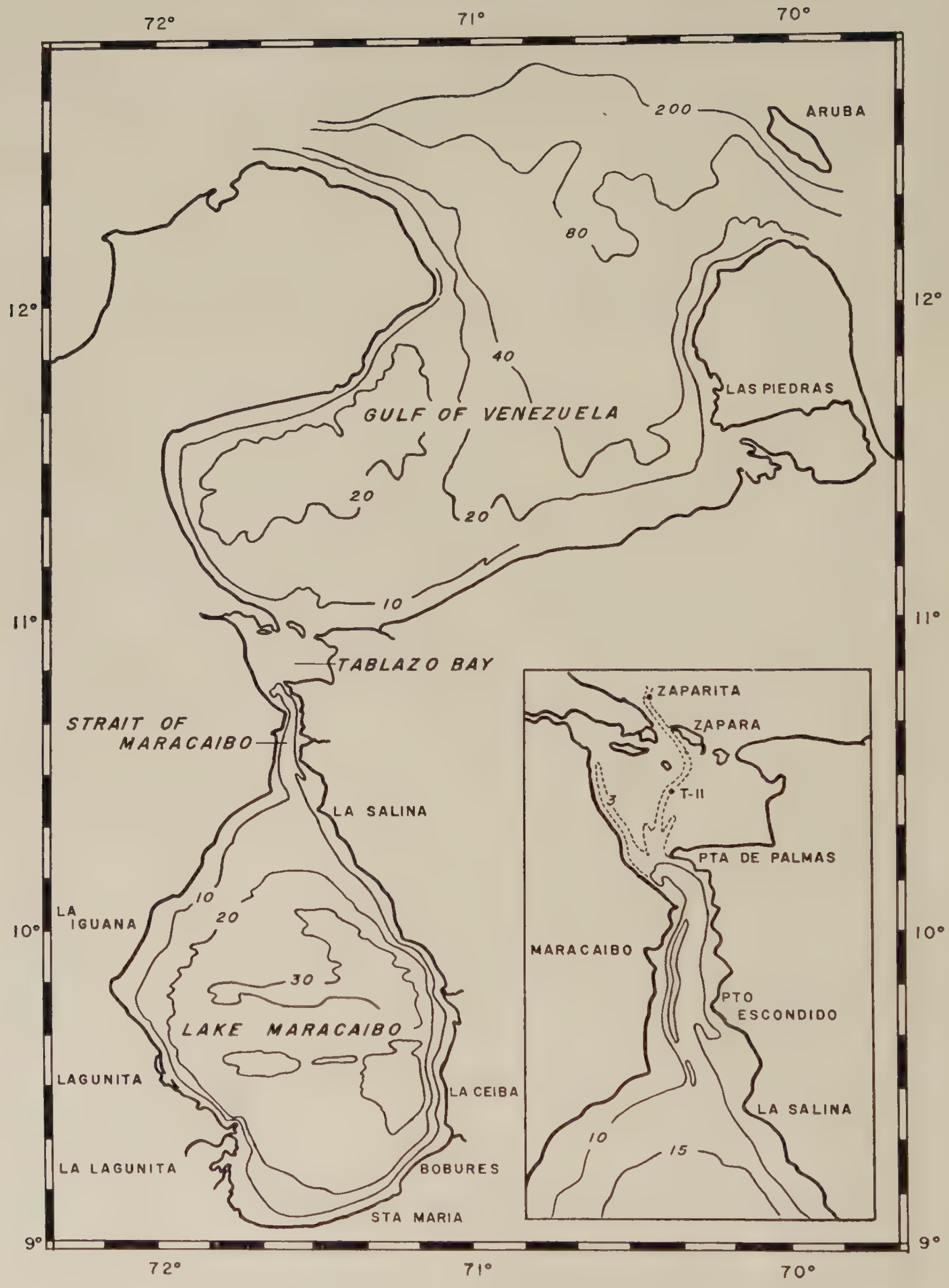
72°
71°
70°
12°
11°
10°
9°
200
ARUBA
80
40
GULF OF VENEZUELA
LAS PIEDRAS
20
20
10
TABLAZO BAY
STRAIT OF MARACAIBO
LA SALINA
LA IGUANA
10
20
30
LAKE MARACAIBO
LAGUNITA
LA CEIBA
LA LAGUNITA
BOBURES
STA MARIA
ZAPARITA
ZAPARA
T-11
3
PTA DE PALMAS
MARACAIBO
PTO ESCONDIDO
LA SALINA
10
15

FIG. 1. Topography and place names of Lake Maracaibo and approaches.

Immediate access to the lake is by narrow and shallow channels across a barrier bar, and between barrier islands, and thence across Tablazo Bay to the Strait of Maracaibo. Tablazo Bay is shallow, the depths being reduced to some 2 m on the average by the deposition of sediments of marine origin (U. S. Waterways Experiment Station 1938). A dredged channel of 7-m depth across Tablazo Bay has been deep-

TABLE 1. *Harmonic constants*

	Constituent	Aruba 12°31′N 70°03′W	Zaparita 11°01′N 71°39′W	Zapara 10°58′N 71°34′W	Tablazo Bay 10°53′N 71°37′W	La Salina 10°23′N 71°28′W
Amplitude (H) cm						
	K_1	9.2	12.2	6.1	4.3	1.5
	O_1	6.1	9.2	3.1	2.4	0.4
	M_2	4.0	42.7	30.5	23.2	0.73
	S_2	2.1	3.1	3.1	3.1	—
Epoch (G)						
	K_1	241	251	247	247	021
	O_1	228	242	246	250	029
	M_2	161	269	284	296	287
	S_2	084	184	216	220	—

ened to 12 m since the present study was made. In contrast, the Strait of Maracaibo is a narrow trough 10 to 20 m deep extending some 20 km to widen into the lake. Lake Maracaibo is a broad shallow basin, unbroken by irregular physical features, which is some 85 km in length with a mean depth of 24 m and maximum depth of 35 m.

The tide retains its semidiurnal character across Tablazo Bay and along the Strait of Maracaibo. Along this stretch, after some delay in the entrance passages, high water is very nearly synchronous but the range of tide diminishes progressively lakeward. The relations of current to tidal elevation in the entrance passages is similar to that usually found in the inlets through barrier islands, the current flowing lakeward while the tide is rising (U. S. Waterways Experiment Station 1938). In the strait, in contrast, the current flows seaward at that time.

At the northern end of the lake the range of tide is greatly reduced. Spring tides appear to be diurnal, while semidiurnal components are evident during neap tides. At the southern end the semidiurnal character of the tide is restored and the range is increased to about 6 cm. High water occurs about 6 hr after high water in the Gulf of Venezuela.

Tides in embayments can usually be attributed to standing waves resulting from the interference of primary progressive waves entering from the outer sea and reflected waves engendered when the preceding primary wave is reflected from the head of the basin (Defant 1919). The varied tidal relations observed in the Maracaibo system may be explained quantitatively on this basis if the dimensions of the basin are taken into account. It can be shown that for the semidiurnal constituents a node exists in the northern part of the lake and that an antinode is present in Tablazo Bay. For the diurnal constituents a node is presumably present at the latter position.

DATA

The available harmonic analyses are given in Table 1. The constants for Aruba, Zaparita, Zapara and Tablazo Bay are from the Admiralty Tide Tables. The analysis for La Salina was made by Mr. A. R. Miller from records of Creole Petroleum Corporation for three periods of 15, 23 and 29 days.

Table 2 lists the available information on the amplitude and epoch of the semidiurnal tide. Data for positions between Las Piedras and Maracaibo represent long term averages supplied by Servicios Hidrograficos, formerly the Maracaibo Bay Survey. For Aruba and La Salina the characteristics listed are those of the M_2 constituent as found by harmonic analysis. The data for Bobures, near the head of the lake, was supplied by Creole Petroleum Corporation. Tidal observations in the lake are difficult because of the small range of tide, rapid changes in lake level and the frequent occurrence of seiches which obscure the tidal record. The Bobures data are based on an average of 6 successive days of record selected for a period when seiches were absent. Additional information supplied by the Compãnia Shell de Venezuela

TABLE 2. *Data on semidiurnal tide*

Position	Latitude (N.)	Amplitude (cm)	High Water* (hr)	Slack Water* Turns South (hr)
Aruba	12°31′	4	−3.5	
Las Piedras	11°42′	12.5	−0.5	
Zaparita	11°01′	46.0	0	−3.6
Zapara I	10°58′	32.4	+0.8	−3.2
Tablazo Bay				
Buoy T-5	10°56′			−2.8
Buoy T-11	10°54′	25.0	+1.1	−1.1
Buoy T-17	10°52′			+0.6
Buoy T-23	10°50′			+1.4
Punta de Palmas	10°47′	24.6		+1.8
Capitan Chico	10°43′			+0.5
Maracaibo	10°38′	10.7	+1.2	
Puerto Escondido	10°30′			+0.8
La Salina	10°23′	0.7	+1.4	−0.5
Bobures	9°15′	3.0	+6.0	−1.0

* Time relative to high water at Zaparita.

indicates that at five other positions on the southern margin of the lake, extending from La Iguana (10°02′N, 71°60′W) to La Ceiba (9°28′N, 71°14′W), the range and time of high water were similar to that observed at Bobures.

The current data listed in Table 2 were obtained by field observations, using current poles and drags (Pritchard and Burt 1951), extending usually over not more than one day. Because of the variations in amplitude which occur in the course of the lunar cycle, and the considerable and variable outflow of fresh water from the lake, these data give only rough approximations of the mean tidal motion.

THE SEMIDIURNAL TIDE

Two independent methods of analysis have been employed. The first depends on the characteristic phase relations of elevation and current in a standing oscillation. The second employs step-by-step integration of finite difference equations for continuity and acceleration under the force of gravity.

Location of node and antinode by phase relations

If the tide in an embayment is considered to be a standing wave resulting from the combined effects of a primary wave entering from the outer sea and a secondary wave resulting from the reflection of the preceding entering wave at the barrier formed by the head of the embayment, these waves will be in phase to a different degree at different positions along the channel. Nodes will exist where the two waves have opposite phases at distances of ¼, ¾, etc., wave lengths from the barrier. Antinodes will exist, where the two waves have the same phase at ½, 1, etc., wave lengths from the barrier. Equations expressing the relation of the times of high water, slack water, elevation, current along the channel, and the effect of friction on these relations are available (Redfield 1958). For present purposes it will serve to summarize the conditions found at the barrier and at the first node and antinode. If friction is neglected:

1) At the barrier high water and slack water are synchronous, the amplitude of elevation is maximal and that of current is zero.

2) At the node the amplitude of elevation is zero, that of current is maximal and the time of high water changes abruptly by ½ period, with the result that the elevation is rising beyond the node while it is falling between the node and the barrier.

3) At the antinode the amplitude of elevation is again maximal and that of the current is zero. The time of slack water changes abruptly by ½ period with the result that high water and slack water become synchronous beyond the antinode and occur ½ period before high water at the barrier.

If friction is taken into account the changes in phase at the node and antinode are less abrupt. The amplitude of elevation at the node and of current at the antinode are not reduced to zero but remain minimal, and while the change in phase is less abrupt, these points are still marked by a maximal rate of change of the time of high and slack water. These relations are shown in Figure 5.

Current measurements made off Captain Chico showed that in the Strait of Maracaibo the tidal current flowed seaward during the period when the tide was rising. This is the relation expected between a node and

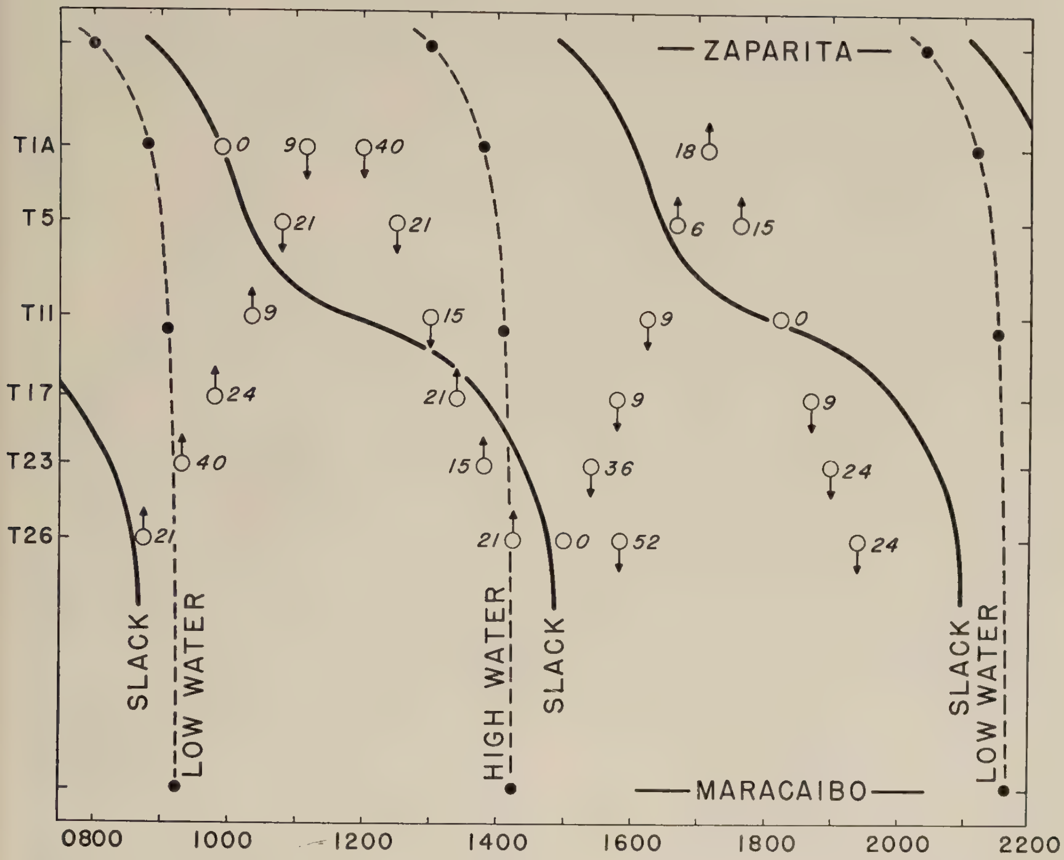

FIG. 2. Relation of time of high water and slack water in Tablazo Bay. March 15, 1954 Time meridian 67°30′W. Current velocities in cm/sec.

antinode (see Fig. 5). Since the current flows landward while the tide is rising in the passage leading from the Gulf of Venezuela it was suspected that an antinode existed in Tablazo Bay. The position of this antinode was determined by the following expedient.

Four traverses of the channel between Punta de Palmas (Buoy T-26) and Zapara Island (Buoy T-1A) were made in alternate directions. At 6 positions marked by navigation buoys the direction and velocity of current were measured in passing. The measurements are plotted in Figure 2 against the time of observation. The continuous curves show the time of slack water with very little uncertainty. The dashed lines indicate the predicted time of high water. The figure shows that the direction of flow is opposite at all times at Zaparita and Punta de Palmas, and that the time of slack water changes rapidly through ½ period in the neighborhood of Buoy T-11 at about 10°54′N. Since these are the relations expected in the neighborhood of an antinode it is concluded that the antinode of the semidiurnal tidal components exists near this point.

The position of the node of the semidiurnal tide cannot be located precisely from the available data on the times of high and slack water. They indicate that the node must lie in the lake at a point south of La Salina, since high water is delayed at La Salina only 0.3 hr relative to its time at the antinode. La Salina must lie close to the node, however, since the amplitude of the semidiurnal tide is greatly reduced there.

Analysis by Consideration of Continuity and Acceleration

If the dimensions of an embayment are accurately known the distribution along its axis of the amplitude of elevation, flux and current velocity for an oscillation of given period may be estimated. The procedure, first developed by Sterneck (1915) has been used by him, by Defant (1919) and by Grace (1936) in examining the tides in various landlocked seas, and is described by Proudman (1953). It consists in determining from a chart the dimensions of a series of segments separated by vertical sections across the axis of the basin. Begining at high or low water at the landward segment, the amplitude of elevation in each segment and of the flux and mean current across each section is obtained by the alternate use of two finite difference equations and successive integration.

For frictionless flow the approximate finite difference equations are:

$$\delta\,(AU) = \left(\frac{2\pi}{T}\cdot b\cdot\delta x\right) Z \qquad (1)$$

$$\delta Z = -\left(\frac{2\pi}{gT}\cdot\delta x\right) U \qquad (2)$$

where A = area of each vertical section
U = amplitude of mean current across section
b = breadth at section
δx = distance between sections
Z = amplitude of elevation of each section
g = acceleration due to gravity
T = period of tidal component

If friction is considered, equation (1) is replaced by

$$\delta\,(AU_1) = \left(\frac{2\pi}{T}\cdot b\cdot\delta x\right) Z_1 \qquad \text{and}$$

$$\delta\,(AU_2) = \left(\frac{2\pi}{T}\cdot b\cdot\delta x\right) Z_2 \qquad (3)$$

and equation (2) by

$$\delta Z_1 = \left(-\frac{1}{gT}\,U_1 + \frac{1}{g\tau}\,U_2\right) 2\pi\delta x \qquad \text{and}$$

$$\delta Z_2 = \left(-\frac{1}{gT}\,U_2 - \frac{1}{g\tau}\,U_1\right) 2\pi\delta x \qquad (4)$$

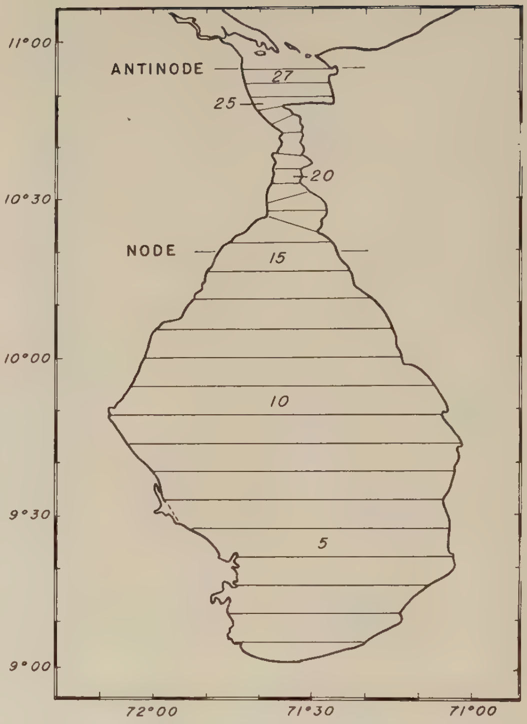

FIG. 3. Scheme of segmentation employed in calculation of tidal characteristics by stepwise integration.

At each section the amplitude of the mean current $= \sqrt{U_1^2 + U_2^2}$ and the amplitude of elevation $= \sqrt{Z_1^2 + Z_2^2}$. The characteristic damping time constant, τ, is given by $\frac{2\pi}{\tau} = \frac{\delta k}{3\pi h} C$ where k is the coefficient of friction, h is the mean depth, and $C = \sqrt{U_1^2 + U_2^2}$.

The distribution of amplitude of elevation, of flux and of mean current along the axis of the Maracaibo system was estimated by dividing the area into 27 segments, as shown in Figure 3. The spacing of the sections, δx, was 10 km in the lake and about 5 km along the strait and across Tablazo Bay. The dimensions of the sections and of the surface areas between sections were obtained from a large-scale chart, contoured at 1-m depth intervals, provided by the Creole Petroleum Corporation.

The results of application of equations (1) and (2) for frictionless flow are shown in Figure 4 by solid lines. They indicate the

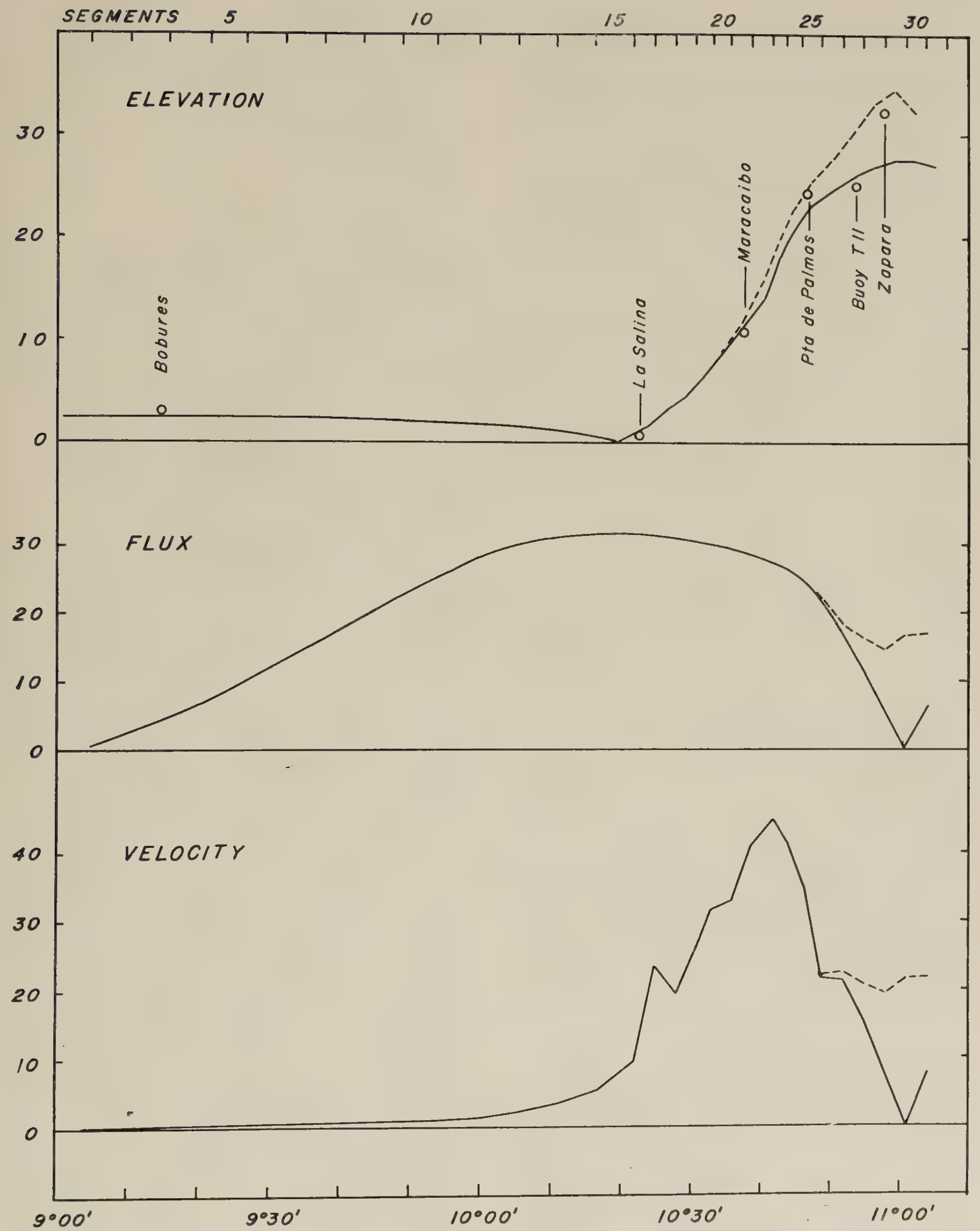

FIG. 4. Amplitude of elevation, flux and mean velocity of current estimated by stepwise integration. Solid lines show estimates for frictionless flow; dashed lines assuming coeffficient of friction, $k = 0.0025$. Scale of ordinate: elevation, cm; flux, 10^4 cm^3/sec; mean velocity, cm/sec. Abscissa—latitude N. and position of segments.

TABLE 3. *Comparison of observed and calculated amplitude of semidiurnal tide (cm)*

Position	Observed	Calculated ($k=0$)	Difference	Calculated ($k=0.0025$)	Difference
Zapara I	32.4	29.0	−3.4	33.0	+0.6
Buoy T-11	25.0	26.4	+1.4	30.5	+5.5
Punta de Palmas	24.6	22.0	−2.7	24.0	−0.6
Maracaibo	10.7	12.5	+1.8	12.0	+1.3
La Salina	0.7	0.75	+0.05	1.0	+0.3
Bobures	3.0	2.5	−0.5	2.5	−0.5

TABLE 4. *Comparison of observed and calculated amplitude of current (cm/sec)*

	Observed	Calculated
Punta de Palmas	30	32
Capitan Chico	30	42
Pt. Esundido	16	25
La Salina	12	12

location of a node in the lake at 10°20′N where the elevation passes through zero, and where the flux is maximal. If the calculation is extended to include several hypothetical segments, similar in dimensions to segment 27, current velocity and flux are found to pass through zero in segment 29 indicating that an antinode would exist in that region if Tablazo Bay were somewhat longer. The available data for the amplitude of elevation may be fitted best by the estimates if the amplitude at the head of the lake is taken as 2.5 cm. See Table 3. If the value of 3 cm observed at Bobures is used the amplitudes at Maracaibo and in Tablazo Bay become too large.

The calculation was repeated employing equations (3) and (4) which take bottom friction into account. The value of the coefficient of friction, k, was taken as 0.0025 following the estimations of Taylor (1918) and Grace (1936) for tidal movement in the Irish Sea and Bristol Channel. The results are shown in Figure 3 by dashed lines.

In the lake, where the estimated mean velocity of the tidal current is less than 10 cm/sec, the friction terms are insignificant and flow may be regarded as frictionless. In the strait of Maracaibo and Tablazo Bay, where the estimated velocities of the tidal current are higher, the friction terms increase the estimates of the amplitudes, flux and current. The estimated amplitudes agree with the available observations shown in Table 3 about as well as they do in the frictionless case. The position of the node is unchanged. Current velocity and flux do not fall to zero in the apparent position of the antinode, but pass through minima between the hypothetical segments 28 and 29. Such a condition is to be expected at the antinode in the presence of friction because the reflected tidal wave is attenuated and complete interference with the incoming wave does not occur, with the result that some residual current is present. It also corresponds to the observation that tidal currents are present at all positions across Tablazo Bay as shown in Figure 2.

Data are not available for a precise comparison of the currents, but a few short-term current measurements shown in Table 4 agree roughly with the estimations. The observed currents may be expected to differ from the estimated mean currents because of differences in the amplitude of the tide during the lunar month and because of variations in the current with depth and with position across the channel.

The stepwise integration indicates clearly the position of the node, and the insignificance of friction in the lake. It estimates approximately the relative amplitudes of the elevations and currents along the channel. It does not yield completely satisfactory estimates since the solutions with or without friction do not develop the antinode within Tablazo Bay. Nevertheless, when it is considered that the stepwise integration is carried out over a half wave length of the tide, in a channel which varies 15 fold in both depth and breadth the effectiveness of the method in estimating the general characteristics of the tide in an irregular basin is impressive.

Discussion of the semidiurnal system

The relations of the times of high water and slack water, and the approximate results of the stepwise integration justify the conclusion that the tide of the Maracaibo Sys-

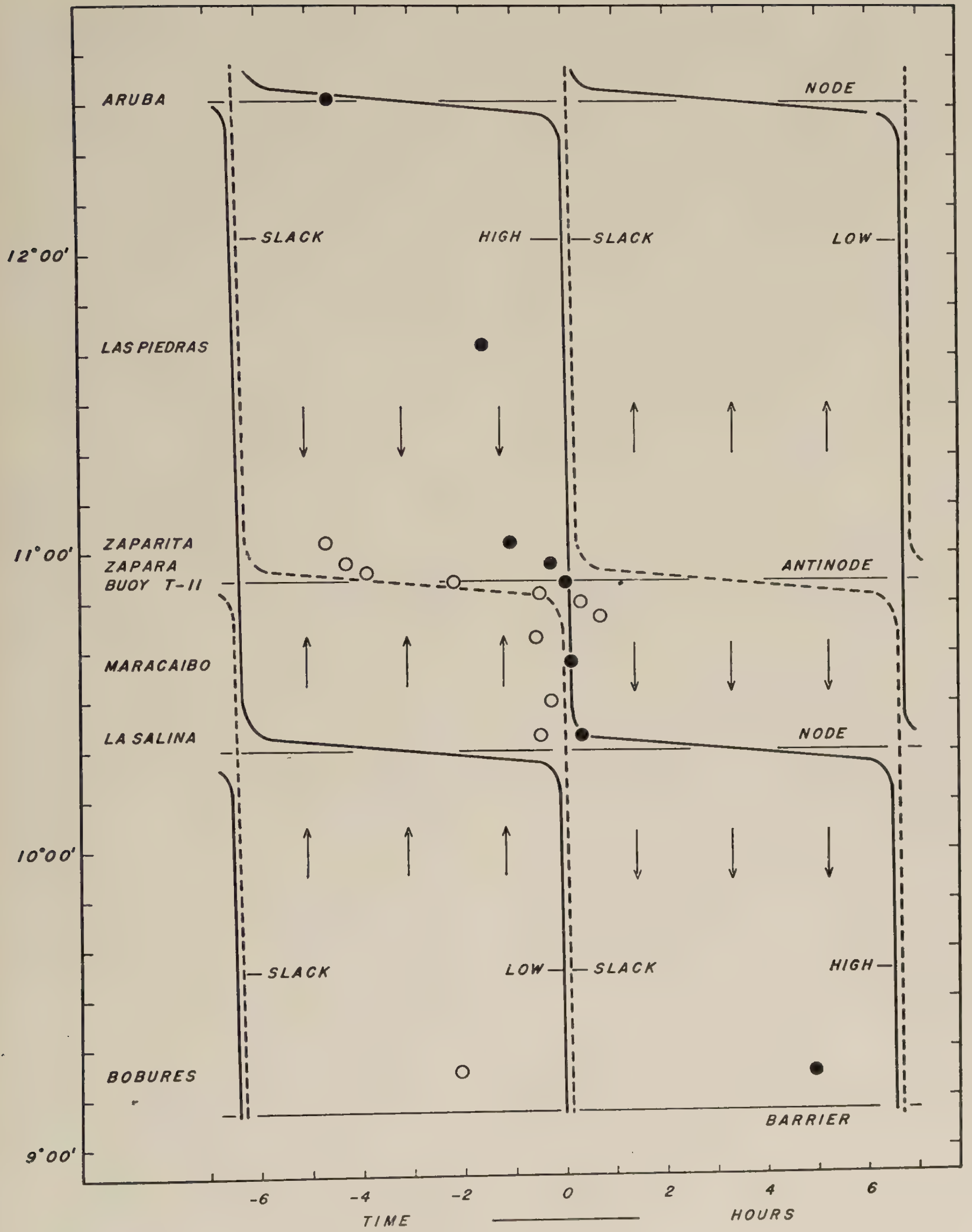

FIG. 5. Diagram of theoretical relations of times of high and low water (solid lines), slack water (dashed lines) and current direction (arrows) for a standing wave reflected from a barrier. Solid circles show data for time of high water, and open circles for time of slack water as listed in Table 2. Ordinate, time in hours relative to high water at Buoy T-11; abscissa, latitude N.

tem behaves as a standing wave resulting from reflection at the head of the lake.

Figure 5 attempts to present the available data on tide and current in relation to this conclusion. The heavy lines in this figure represent in a diagrammatic way the relations between the time of high water and slack water to be expected on this hypothesis in a channel of uniform section ¾ wave length in extent, and having a node at 10°20′N, an antinode at 10°54′N, and a second node at about 12°30′N, near Aruba. The arrows indicate the synchronous direction of current and the points show the times of high and slack water recorded in Table 2. The observed data corresponds in a general way to the theoretical curves. However, there are departures which require comment.

The scatter of the points indicating the time of slack water is attributable to the inadequacy of current data obtained from a single day's observation where the diurnal inequality of the tides is pronounced. Similarly the time of high water at Bobures is based on short term observations made under difficult conditions and cannot be very dependable. On the other hand, the times of high water at the other positions is based on long term averages and should be quite reliable. They show that there is a delay of more than one hour between high water in the Gulf of Venezuela (at Las Piedras and Zaparita) and high water in Tablazo Bay and the Strait of Maracaibo. Such a delay is not to be expected if the tides are due to the simple cooscillation postulated.

Tablazo Bay is separated from the Gulf of Venezuela by narrow passages in which swift currents develop in response to differences in level. The delay in the time of high water in Tablazo Bay is adequately explained by the restriction of these passages. Because of the break in continuity of unrestricted flow in the channels leading to Tablazo Bay it is probably mistaken to consider the Gulf of Venezuela and Lake Maracaibo as forming a simple system of oscillation.

It is perhaps more correct to consider the motion of the lake to be a uninodal seiche which, because of the dimensions of the lake basin and its approaches, oscillates with the period of the semidiurnal tide. The tide in the Gulf of Venezuela, which appears to be a simple cooscillation dominated by the semidiurnal constituents of the motion in the Caribbean Sea, provides the energy to maintain the lake's oscillation. The flow in the restricted connecting passages is similar to that commonly observed in inlets to embayments behind barrier islands, where the rise and fall of the tide is delayed. Similarly the oscillation of the lake is delayed relative to that in the Gulf, by which it is engendered.

THE DIURNAL TIDE

Data on the diurnal tide are limited to the 5 positions, listed in Table 1, for which harmonic analyses are available. These data should conform to certain expectations determined by the position of the nodes and antinodes of the semidiurnal system.

Since the diurnal and semidiurnal waves travel at the same rate and the former waves are twice the length of the latter, the first node of the diurnal system should occur in Tablazo Bay, near the position of the antinode of the semidiurnal system. The antinode of the diurnal system should coincide with the second antinode of the semidiurnal system, but since no such second antinode develops within the limits of the coastal waters no antinode for the diurnal tide is to be expected.

Considering the epochs of the diurnal constituents, the value of G should be about the same seaward of the expected node in Tablazo Bay, which may be seen to be the case. Landward of the node the value of G should increase 180°. Actually the value changes about 135° between Tablazo Bay and La Salina.

Consideration of the amplitudes of the constituents is complicated by the influence of the dimensions of the basin. It may be noticed that between Aruba and Zaparita the amplitudes of the diurnal constituents are not greatly augmented as is that of the M_2 constituent, for which the dimensions of the Gulf produce a high degree of resonance. Between Zaparita and Tablazo Bay both species of constituent diminish about in proportion, presumably as the result of changes in the dimensions of the channel. At La Salina the amplitude of M_2 is reduced much more than that of the diurnal constituents because this position is close to the node of the semidiurnal system.

It may be concluded that the diurnal constituents conform reasonably, if not exactly, to the characteristics of the system deduced for the semidiurnal tide.

DISCUSSION

The tide in the Maracaibo system has been treated as linear motion parallel to the axis of the basin. The existence of a significant rotatory system is excluded by the following consideration.

It may be inferred from the existence of the node for the semidiurnal tide near the northern extremity of the lake that the natural period of lengthwise oscillation of the lake proper is about 6 hr. Since the width of the lake is about ⅔ of the length a transverse oscillation would have a period of perhaps 4 hr. A rotatory system requires the components of motion at right angles to be comparable in period. Consequently such a system could not exist for a tide of 12-hr period.

In the Northern Hemisphere the rotation of the earth frequently causes the range of tide in an embayment to be greater on the right of the inflowing current—the Kelvin effect. Such effects in Lake Maracaibo appear to be insignificant because of the low current velocities and the low latitude. Taking the mean velocity of the tidal current at the widest part of the lake to be 0.5 cm per sec and applying the geostrophic equation, it appears that if equilibrium between the Coriolis force and gravity were reached the transverse slope of the lake surface would be about 10^{-8} and the difference in elevation on opposite sides would be less than 2 mm. A similar computation for the Strait of Maracaibo at Capitan Chico, where tidal currents of 30 cm/sec occur, indicates a slope of less than 10^{-6} and a difference of elevation of less than 5 mm.[2]

The presence of the antinode in Tablazo Bay appears to have an important bearing on the problem of maintaining the channel, and, in fact, on the development of the physiography of the area. The topography suggests that in comparatively recent times Lake Maracaibo stood above sea level. The form of the strait resembles a river valley eroded under arid conditions, and a deeper trough along its western side indicates the course of the river which once drained the lake. The postglacial rise in sea level appears to have drowned this valley and to have given access of tidal water to the lake. Subsequently marine deposits filled the bight in which Tablazo Bay lies and built the barrier islands and bars which separate it from the Gulf of Venezuela (Redfield 1958).

With the admission of the tide into the lake the antinode would have developed. Since an antinode is a region where flux and current are greatly reduced, sedimentation would be encouraged there. When sea level was lower and the water shallower the antinode may have been located south of its present position. It is possible that a sill at the southern end of the strait, which separates the deeper waters of the strait from those of the lake basin and where the remnants of the old river course appear to have been buried, may have been deposited when the antinode occupied this position. However that may have been, at the present time the antinode is in a position to account for the deposition of the marine sediments which fill Tablazo Bay. In 1954 the ship channel across Tablazo Bay had shoaled in just the region where the antinode was located, and dredges were at work there removing the recent sedimentation.

The antinode appears to be important also in restraining the entrance of salt water into the lake. The low chloride content of lake water, which has varied between 400 and 1,200 ppm during the past 14 years, is due to the large discharge of lake water required to balance the precipitation over the lake basin. During rainy periods this discharge is sufficient to displace the water of Tablazo Bay almost completely—a possibility arising from its very shallowness and which, in turn, may be attributed to sedimentation at the antinode. During dry periods this flow diminishes and salt moves inward across Tablazo Bay and into the lake by tidal mixing. The reduction of tidal flux in the region of the antinode limits this process and thus reduces at such times the rate at which salt penetrates to the lake waters.

---

[2] Within Lake Maracaibo currents, presumably wind-driven, circulate in an anticlockwise sense with velocities of the order of 25 cm/sec (Redfield 1958). The tidal currents under discussion are superimposed upon this motion and the discussion refers only to the tidal component of motion.

REFERENCES

DEFANT, A. 1919. Untersuchungen über die Gezeitenerscheinungen in Mittel- und Randmeeren, in Buchten und Kanälen. Denkschr. Akad. Wiss. Wien, **86**: 57–174.

GRACE, S. F. 1936. Friction in the tidal currents of the Bristol Channel. Geophys. Supp. MNR Astron. Soc., **3**: 388–395.

HYDROGRAPHIC DEPARTMENT, ADMIRALTY. 1956. The Admiralty Tide and Tidal Stream Tables. Vol. 11, Atlantic and Indian Oceans for the year 1957. London. 436 pp.

PRITCHARD, D. W., AND W. V. BURT. 1951. An inexpensive and rapid technique for obtaining current profiles in estuarine waters. J. Mar. Res., **10**: 180–189.

PROUDMAN, J. 1953. Dynamical Oceanography. London, Methuen, 409 pp.

REDFIELD, A. C. 1950. The analysis of the tidal phenomena in narrow embayment. Papers in Phys. Oceanogr. and Meteorol., **2**(4), 36 pp.

———. 1958. Preludes to the entrapment of organic matter in the sediments of Lake Maracaibo. Habitat of Oil, Am. Assoc. Petrol. Geol. pp. 968–981.

STERNECK, R. 1915. Hydrodynamische Theorie der halbtägigen Gezeiten des Mittelmeeres. Sitz. K. Akad. Wiss. Wien., math-naturwis. Kl. Abt 2a, **124**: 905–979.

TAYLOR, G. I. 1918. Tidal friction in the Irish Sea. Phil. Trans. Royal Soc. A, **220**: 1–33.

U.S. WATERWAYS EXPERIMENT STATION. CORPS OF ENGINEERS, U.S. ARMY. 1938. Model study of channel improvements at Outer Bar, Lake Maracaibo, Venezuela. Technical Memo. 106-1, 3 Vols.

Contribution No. 1050

. mar. biol. Ass. U.K. (1961) 41, 463–488
Printed in Great Britain

ON THE BIOLOGY OF *CALANUS FINMARCHICUS*

XII. THE PHOSPHORUS CYCLE: EXCRETION, EGG PRODUCTION, AUTOLYSIS*

By S. M. Marshall, D.Sc., and A. P. Orr, D.Sc.
The Marine Station, Millport

With an Addendum

The turnover of phosphorus by *Calanus finmarchicus*

By R. J. Conover
Woods Hole Oceanographic Institution

(Text-figs. 1–5)

The return of plant nutrients to sea water by the zooplankton has been nvestigated by Cooper (1935), Gardiner (1937), and Harris (1959). The first wo showed experimentally that living zooplankton organisms rapidly increased the concentration of phosphorus in the sea water, and Harris showed hat excretion was important in supplying nitrogen to the phytoplankton of Long Island Sound. The breakdown of dead organisms was studied by Hoffmann (1956) and Krause (1959). Marshall & Orr (1955) made some measurements of the excretion of P by *Calanus finmarchicus* and showed that t was most rapid during the first week after a period of feeding. The very igh losses after 2–3 weeks of starvation led them to suppose that the ^{32}P they were measuring had not been in equilibrium through the animals.

In view of the importance of phosphate regeneration as a factor in the roductivity of the sea, it was decided to follow in more detail, using the opepod *Calanus*, the role of the zooplankton in the turnover of P.

METHODS

Early experiments on the excretion of soluble P, after feeding with labelled ood cultures (Marshall & Orr, 1955), were unsatisfactory because the P xcreted disappeared from solution, presumably being taken up by bacteria n the walls of the container. The loss of P from the body was therefore measured instead.

---

* Contribution no. 1050 from the Woods Hole Oceanographic Institution.

Addition of antibiotics to the water, however, prevents the loss by bacterial action, and from 1958 the excretion was measured only in the water in which the *Calanus* were kept. Streptomycin and chloromycetin were the antibiotics used (Oppenheimer, 1955), but it was later found that the chloromycetin had a depressing effect on feeding. In the 1959–60 experiments penicillin and streptomycin were used, neither of which had a deleterious effect in a concentration of 50 mg/l.

The P in the body was measured only at the beginning and end of an experiment. Initial measurement was made by putting the *Calanus* in a Perspex cell of the same diameter as a planchette (2 cm) and having, excavated in the centre, a cylindrical cavity 5·5 mm in diameter and 1·5 mm deep. The *Calanus* is put in the cavity in a drop of water and the excess sucked off until the water is just level with the top of the cell. For comparable readings the *Calanus* must be measured always in the same position. The highest readings are got if the dorsal side is uppermost because of the dorsal position of the ovary, the most highly radioactive tissue. The reading when the ventral side is up is the lowest and that when the copepod is on its side is intermediate. The last position was chosen because it is the easiest to get a *Calanus* to adopt. The cavity was not large enough to let them move freely, but an occasional one may have turned over during the course of the reading. Since the cell is appreciably higher than the planchettes normally used and since water is present, the relation between wet and dry readings had to be found by reading a considerable number of *Calanus*, first alive in the cell and then torn and dried on a planchette. The factor varied considerably from about 1 to 1·25, and the average used was 1·185. To avoid damaging the *Calanus* used for an experiment, only one 40 sec initial reading was taken.

Another improvement in accuracy was made by using a liquid counter of 10 ml. capacity for the water samples instead of a series of dried 0·2 ml. samples. Conversion factors for the liquid counters were made against readings on planchettes and the mean of a large number of counts taken. Considering the variability of these two conversion factors and the short duration of the initial reading of the *Calanus* it is satisfactory that the initial direct reading and the final calculated reading (made by adding the radioactivity gained by the water to the reading of the *Calanus* body at the close of the experiment) usually agreed fairly well (see, for example, Table 2). The calculated initial value is used in the tables and figures.

Calanus of the stage desired were picked out of a tow-netting and put in a culture of radioactive phytoplankton, usually either *Skeletonema costatum* or *Syracosphaera elongata*. Either *Calanus finmarchicus* or *C. helgolandicus* were used according to their abundance. If necessary they were changed to fresh culture at intervals and when they had been fed for a given time they were washed individually and their radioactivity measured in the Perspex cell. They were then put singly in calibrated bottles of about 35 ml. capacity filled with membrane-filtered water containing antibiotics. The bottles were put in dark cloth bags and kept in a tank at 10° C.

Earlier experiments had shown that, although a *Calanus* can take up ^{32}P from solution, the amount is negligible when compared with that taken up in the food.

In some experiments half of the copepods were starved and half fed by the addition of non-radioactive culture to the membrane-filtered water. Survival was good, but on several occasions the starved *Calanus* survived better than the fed (see Table 1). To measure excretion each *Calanus* was transferred to a fresh bottle and duplicate samples from the original bottle read in a liquid counter. Measurements were usually made after 6 and 24 h. and thereafter at longer intervals.

At the end of an experiment the *Calanus* bodies were either torn up and dried on a planchette or else a final reading of the living animal was made in a Perspex cell. Occasionally the body was torn and dried on a coverslip laid on a planchette and was subsequently used for total P analysis.

Most excretion experiments were done on females because they feed best, and in the winter because they are not then laying eggs. Several, however, were done on laying females and, before sampling, the water in each bottle was examined for eggs. When these were present they were washed and dried and their radioactivity measured. A few drops of a 1 % solution of ethylene-diamine-tetracetic acid was added per 100 ml. of medium in these experiments to ensure the healthy development of the eggs (Cleland, 1953).

On some occasions analyses of total phosphorus were made by Harvey's method (1948). From 1 to 6 *Calanus* were used in each determination.

EXCRETION

The results of the excretion experiments are shown in Tables 1–4 and Figs. 1–3. Table 2 and Fig. 2 give one experiment set out in full to show the extent of the individual variation and the comparison of the initial and final readings of the bodies. On the whole it can be said that the shorter the period of feeding on radioactive culture, the more rapid is the initial excretion of phosphorus. This can be said only of the average curves; in each series there may be individuals which excrete more quickly or more slowly than the rest. The results of the longer term feeding were not so plain. Of the two series fed for 7 days, one excreted during the first few days at a slower rate than the other which was only slightly slower than the 1-day feeding series. Of two series fed for 2 weeks or longer one was more like the slower and one like the faster of the 7-day feeding series. In a final experiment where the *Calanus* were fed first on radioactive food for a week, then on non-radioactive food for a week, the resulting curve was the same as the slow 7-day series. It seems probable that in the experiments showing a very gradual fall, the ^{32}P had reached equilibrium throughout the body. In the curves showing a rapid

TABLE 1. EXCRETION OF *CALANUS* AFTER FEEDING FOR DIFFERENT TIMES

f, *C. finmarchicus*; h, *C. helgolandicus*

Date ...	9–22.xii.59		15–28.xii.59		4–16.xi.59		24.xi.–8.xii.59		17.xi.–1.xii.59		1–15.xii.59		10–26.v.58		28.xii.59–12.i.60		1–7.vi.60	20–27.iv.60
^{32}P feeding ...	3 h		3 h		1 day		1 day		7 days		7 days		14 days		18 days		7 days then non-r.a. 7 days	2 days
No. and stage	7♀h	6♀h	7♀h	7♀h	7♀h	6♀h	7♀h	7♀h	7♀h	7♀h	7♀h	7♀h	5♀f	5♀f	7♀h	7♀h	15♀f	14V
Treatment	Fed	Starved	Fed	Starved	Fed	Starved	Fed	Starved	Fed	Starved	Fed	Starved	Fed	Starved	Fed	Starved	Starved	Starved
Time	Av. % loss	Av. % loss	Av. % loss	Av. % loss	Av. % loss	Av. % loss	Av. % loss	Av. % loss	Av. % loss	Av. % loss	Av. % loss	Av. % loss	Av. % loss	Av. % loss	Av. % loss	Av. % loss	Av. % loss	Av. % loss
6 h	18·6	9·9	15·7	9·7	21·0	9·6	15·5	7·1	6·6	7·1	5·6	3·8	6·3†	5·4†	5·9	5·5	1·8	—
1 day	36·4	18·5	30·1	18·8	34·9	23·6	35·4	21·1	13·3	18·2	11·5	8·4	—	—	12·7	13·4	7·5	15·2
2 days	—	—	—	—	—	—	—	—	—	—	—	—	13·1	11·7	—	—	13·1	24·8
3 days	52·4	41·4	44·1	39·3	49·9	42·1	49·4	42·5	22·8	32·2	23·9	17·5	$16{\cdot}1_4$	$17{\cdot}6_4$	23·1	27·6	—	30·1
4 days	—	—	—	—	—	—	—	—	—	—	—	—	—	—	—	—	21·4	—
5 days	$57{\cdot}4_6$	49·9	—	—	58·4	49·9	—	—	—	—	—	—	$23{\cdot}6_4$	$24{\cdot}3_4$	—	—	—	37·4
6 days	—	—	55·1	52·8	—	—	59·5	55·4	38·9	46·7	29·7	28·7	—	—	$37{\cdot}8_6$	42·5	27·6	—
7 days	—	—	—	—	—	—	—	—	—	—	—	—	—	—	—	—	—	43·8
8 days	$63{\cdot}7_6$	55·8	—	—	62·9	59·0	—	—	—	—	—	—	—	—	—	—	—	—
9 days	—	—	All dead	62·1	—	—	66·8 All dead	63·2	52·5	57·0	—	—	—	—	$47{\cdot}9_4$	53·8	—	—
10 days	—	—	—	—	—	—	—	—	—	—	$43{\cdot}4_1$	$43{\cdot}5_6$	—	—	—	—	—	—
11 days	—	—	—	—	—	—	—	—	—	—	—	—	$39{\cdot}0_4$	$42{\cdot}5_4$	—	—	—	—
12 days	—	—	—	—	67·6	68·1	—	—	—	—	—	—	—	—	$56{\cdot}6_4$	$64{\cdot}0_8$	—	—
13 days	$73{\cdot}3_2$	66·9	—	70·3	—	—	—	—	—	—	—	—	—	—	—	—	—	—
14 days	—	—	—	—	—	—	—	$73{\cdot}1_5$	$68{\cdot}1_6$	$68{\cdot}8_3$	$54{\cdot}3_1$	$55{\cdot}1_6$	—	—	—	—	—	—
15 days	—	—	—	—	—	—	—	—	—	—	—	—	—	—	$61{\cdot}7_4$ all dead	$72{\cdot}1_5$	—	—
16 days	—	—	—	—	—	—	—	—	—	—	—	—	$51{\cdot}1_4$	$54{\cdot}7_4$	—	—	—	—

Suffix indicates number of *Calanus*. † 12 hours

TABLE 2. EXCRETION OF FEMALE *CALANUS* FED 3 HOURS WITH ^{32}P LABELLED FOOD

All counts, No./ml./min.

Fed ...	1		2		3		4		5		6		7		Average % loss	
Days	Count	% loss	Count	% loss	Count	% loss	Count	% loss	Count	% loss	Count	% loss	Count	% loss		Sum
0 (wet)	45,990		20,880		26,340		39,040		37,260		39,860		26,070			
0 (calc.)	45,334		20,511		25,231		36,250		35,500		38,955		23,133			
¼ (6 h)	11,510	25·4	4,399	21·4	4,096	16·2	5,637	15·5	6,191	17·4	6,023	15·5	4,306	18·6	18·6	
1 (18 h)	8,389	18·5	4,521	22·0	3,945	15·6	4,180	11·5	6,965	19·6	6,128	15·7	4,963	21·4	17·8	36·4
3	5,957	13·1	4,707	23·0	2,900	11·5	6,483	17·9	5,833	16·4	5,236	13·4	3,828	16.5	16·0	52·4
5	3,232	7·1	327	1·6	2,039	8·1	Killed	—	1,744	4·9	1,349	3·5	1,119	4·8	5·0	57·4
8	2,505	5·5	1,350	6·6	1,367	5·4	—	—	2,228	6·3	3,338	8·6	1,235	5·3	6·3	63·7
13	6,686	14·7	3,563	17·4	2,645	10·5	—	—	3,038	8·6	5,641	14·5	6,064	26·2	9·6	73·3
		Dead		Dead								Dead		Dead		
Body at end	7,055		1,644		8,239		19,950		9,501		11,240		1,618			

Starved ...	1		2		3		4		5		6		Average % loss	
Days	Count	% loss	Count	% loss	Count	% loss	Count	% loss	Count	% loss	Count	% loss		Sum
0 (wet)	32,010		65,120		33,670		49,870		31,660		32,000			
0 (calc.)	35,764		71,035		36,073		48,107		32,211		32,134			
¼ (6 h)	7,820	21·9	4,757	6·7	3,329	9·2	4,064	8·4	2,067	6·4	2,096	6·5	9·9	
1 (18 h)	2,905	8·1	3,918	5·5	2,696	7·5	2,188	4·6	3,292	10·2	5,036	15·7	8·6	18·5
3	5,801	16·2	16,070	22·6	10,120	28·0	11,980	24·9	6,094	21·4	7,838	24·4	22·9	41·4
5	1,927	5·4	8,506	12·0	4,851	13·4	5,365	11·1	1,945	6·0	956	3·0	8·5	49·9
8	1,257	3·5	4,943	7·0	3,178	8·8	3,434	7·1	2,043	6·3	767	2·4	5·9	55·8
13	2,524	7·1	9,541	13·4	4,635	12·9	6,756	14·0	4,150	12·9	1,981	6·2	11·1	66·9
Body at end	13,530		23,300		7,264		14,320		11,810		13,460			

TABLE 3. EFFECT OF TEMPERATURE ON EXCRETION

Fed one day and starved during experiment

Date ...	7–21. i. 60			27. i–8. ii. 60		
Calanus ...	7 ♀ f	7 ♀ f	7 ♀ f	7 ♀ f	7 ♀ f	5 ♀ f
Temp. (° C)	5°	10°	15°	5°	10°	15°
	Mean loss %	Mean loss %	Mean loss %	Mean loss %	Mean loss %	Mean loss %
6 h	1·7	2·2	3·9	6·7	4·1	6·7
1 day	6·2	7·9	10·4	15·8	13·1	15·9
3 days	18·1	20·1	27·1	27·1	30·6	35·0
6 days	—	—	—	40·6	46·4	51·1
7 days	34·0	37·3	48·6	—	—	—
9 days	—	—	—	51·5	55·9	60·4
11 days	44·5	46·9	61·9*	—	—	—
12 days	—	—	—	59·1	63·6	67·3†
14 days	50·6	52·9	69·2*	—	—	—

* Average of 6. † Average of 4. f = *finmarchicus*

TABLE 4. EXCRETION OF LAYING FEMALE *CALANUS*

Mean loss %

Date ...	4–9. v. 58				4–9. v. 58			
^{32}P feeding ...	1 day				1 day			
Calanus ...	5 *C. finmarchicus* (starved)				5 *C. finmarchicus* (fed)			
	Excretion				Excretion			
	Eggs	Total	Egg layers	Non layers	Eggs	Total	Egg layers	Non layers
8 h	0	7·2	—	7·2	—	18·3	—	18·3
1 day	$6{\cdot}1_2$	13·6	23·9	6·7	$5{\cdot}5_1$	8·6	11·9	8·6
2 days	$1{\cdot}0_1$	13·9(3)	11·1	15·3	0	18·5(4)	—	18·5
3 days	—	—	—	—	—	—	—	—
4 days	—	—	—	—	—	—	—	—
5 days	$3{\cdot}1_1$	10·3(3)	10·0	10·4	0	9·2(4)	—	9·2

Date ...	5–11. iv. 60				6–12. vii. 60			
^{32}P feeding ...	1 day				5 days, then non-^{32}P 4 days			
Calanus ...	14 *C. finmarchicus* (starved)				7 *C. finmarchicus* (fed)			
	Excretion				Excretion			
	Eggs	Total	Egg layers	Non layers	Eggs	Total	Egg layers	Non layers
8 h	—	—	—	—	—	—	—	—
1 day	$6{\cdot}1_6$	12·3	18·1	7·9	$0{\cdot}4_1$	6·8	3·9	7·4
2 days	$12{\cdot}1_1$	14·6	15·9	10·1	$0{\cdot}2_2$	4·5	3·2	5·0
3 days	$2{\cdot}2_6$	10·4	13·5	8·2	$2{\cdot}1_3$	5·5(6)	2·9	8·1
4 days	0	4·9	—	4·9	$2{\cdot}0_3$	2·2(5)	2·2	2·2
5 days	$1{\cdot}3_1$	2·6(2)	2·4	2·7	$0{\cdot}7_2$	1·6(5)	0·9	2·2
6 days	0	3·5(2)	—	3·5	$1{\cdot}5_3$	3·0(5)	2·3	3·9
7 days	0	2·7(2)	—	2·7	—	—	—	—

Suffix indicates number of *Calanus* laying; number in brackets indicates number averaged.

initial fall, on the other hand, a large proportion of the ^{32}P must be in a labile form. This is confirmed by the results of the total P analyses (see p. 477).

There is, during the first day or two, a difference in excretion of ^{32}P between fed and starved *Calanus*. Those being fed (on non-radioactive food) excrete more than those being starved (see Fig. 2 and Tables 1 and 2). The more food taken in therefore the more is metabolized and this agrees with the fact that the percentage of food digested is high, even in *Calanus* that are kept in a rich culture and are producing faecal pellets rapidly.

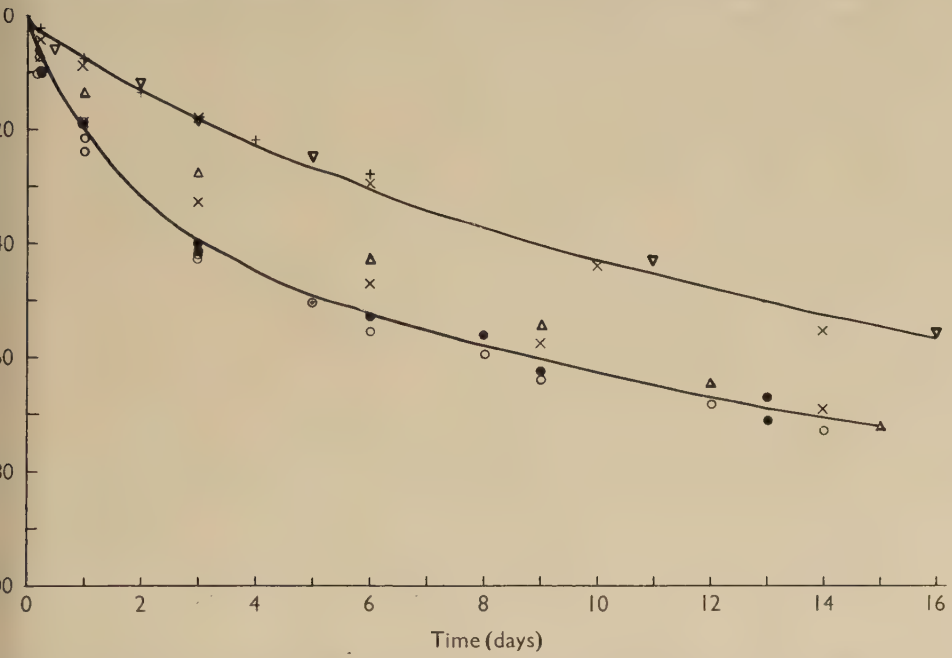

Fig. 1. Effect of short-term (lower curve) and long-term (upper curve) feeding on excretion in starved female *Calanus*. ●, 3 h; ○, 1 day; ×, 7 days; ▽, 14 days; △, 18 days; + 7 days radioactive, then 7 days non-radioactive.

Two experiments were made on the effect of temperature on excretion in starved *Calanus* (Table 3 and Fig. 3). The temperatures compared were 5°, 10°, and 15° C. Although there was the usual variation and the curves for individuals in the three series usually overlapped, the averages show a slightly greater excretion as the temperature rises. One peculiarity of these particular experiments was that in all the *Calanus*, excretion, although following the usual curve, was much lower than normal. Most of the excretion experiments were done in late autumn and winter on *C. helgolandicus*, a few females of which are to be found throughout that time. The temperature experiments were done, however, with *C. finmarchicus* females newly moulted from over-wintering Stage V. They must have been immature and low in total P (see

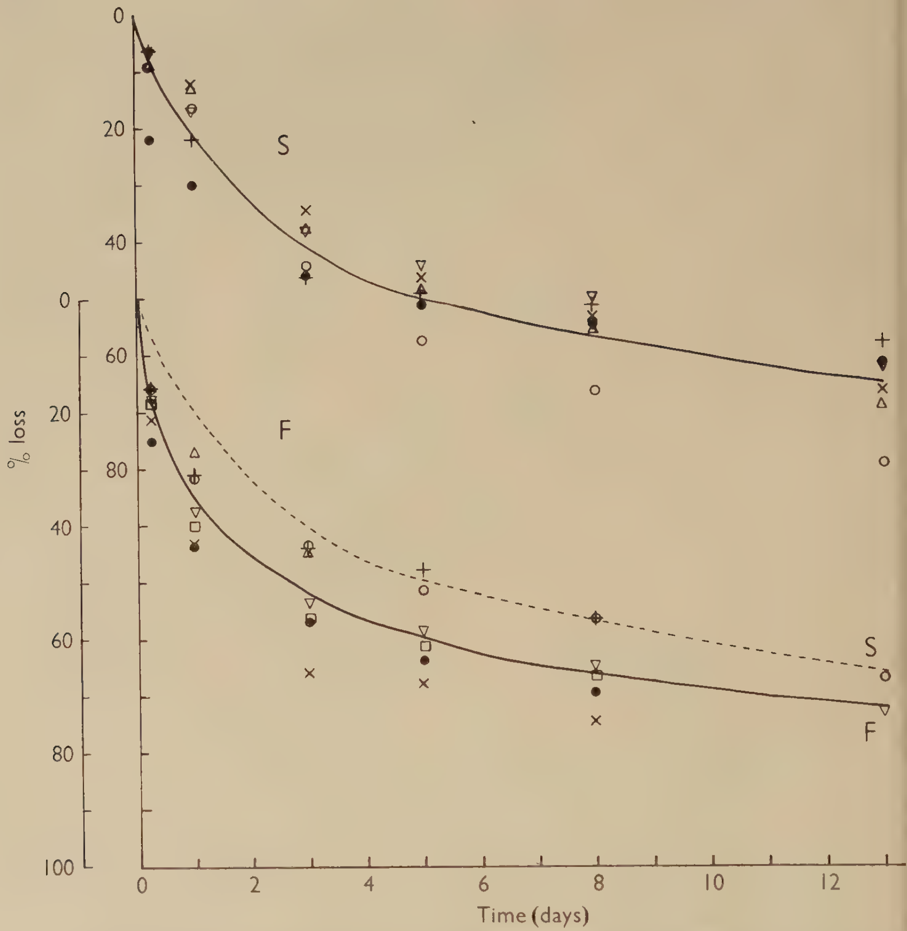

Fig. 2. Excretion in fed and starved *Calanus* after 3 h feeding with labelled culture to show variation between individuals. The curve for starved is repeated (dotted line) for comparison with that for fed. Each symbol represents one *Calanus* in both fed and starved.

p. 478). The *C. finmarchicus* females were not tested again until April when they were ripe and may have belonged to the next generation. The excretion figures had then risen and were much the same as the *C. helgolandicus* in autumn.

Stage V were used only once, in April, and their average excretion was slightly lower than that of females fed for the same length of time.

EGG PRODUCTION

It has previously been found (Marshall & Orr, 1955), by rough dissection of *Calanus* females fed on cultures labelled with ^{32}P, that a large proportion of this is concentrated in the ovary and reproductive system. Some experiments were therefore made to find out how large a proportion of the ^{32}P entering the *Calanus* body could be recovered in the eggs laid.

Preliminary experiments showed that *Calanus* females fed on radioactive and non-radioactive food laid much the same number of eggs, i.e. the ^{32}P in the concentrations used did not in itself affect the ovary.

When ripe female *Calanus* are brought into the laboratory almost all of them lay eggs on the first night. If fed they go on laying at irregular intervals for some weeks or months. For most experiments ripe females were picked

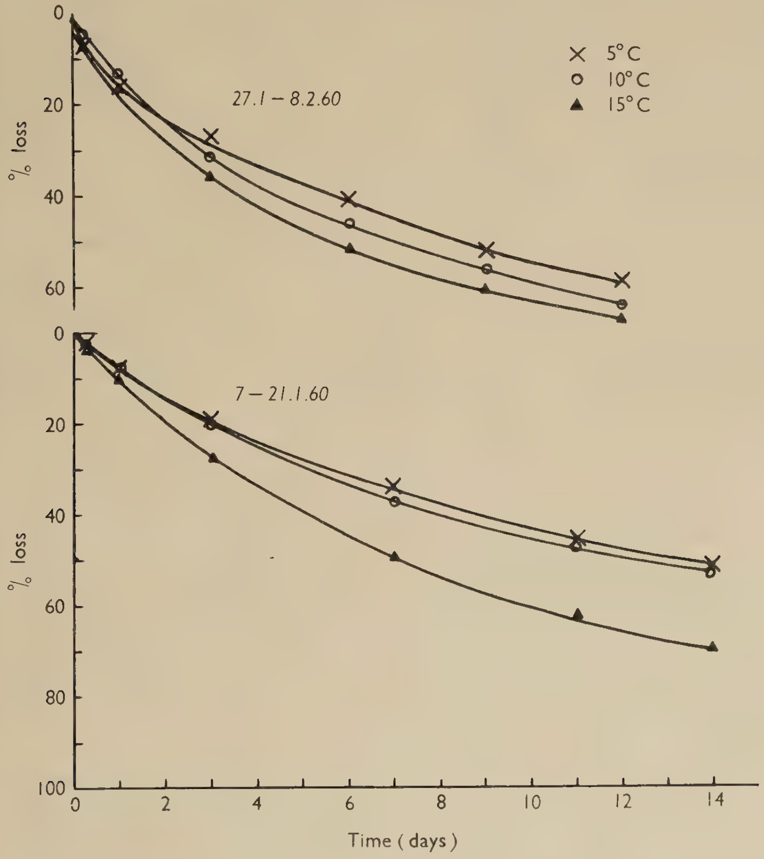

Fig. 3. Effect of temperature on excretion in starved female *Calanus*.

out from a tow-netting and put overnight into a culture of radioactive phytoplankton. Next morning they were washed and the activity measured in a Perspex cell. The eggs laid were also washed and read dry. These two figures added give the initial body value, although it will be slightly too low owing to he overnight excretion.

The results varied according to the time of year at which the experiments were carried out. In an experiment made in August 1959, the 24 females used survived badly, but those which lived more than 5 or 6 days produced eggs which contained 15–34% of the initial ^{32}P. These *Calanus* may have been laying for some time in the sea, and later experiments were carried out in early spring either before, or just about, the time at which *Calanus* eggs normally appear here in the plankton in numbers. All the females were given less than 24 h of radioactive feeding and were then fed on non-radioactive culture for a varying time (Table 5).

TABLE 5. EGG LAYING EXPERIMENTS IN FEBRUARY

Date	No.	Time (days)	Total no. eggs laid	% ^{32}P in eggs	% ^{32}P in body at end	% ^{32}P excreted (excluding eggs)
C. helgolandicus						
3–29. ii. 60	1	22	111	33·8	6·7	89·9
3–29. ii. 60	2	22	142	26·3	5·2	92·9
4–24. ii. 60	3	21	59	27·8	12·1	83·3
4–24. ii. 60	4	21	58	24·8	10·2	86·4
4–24. ii. 60	5	21	72	25·1	13·1	82·5
4–24. ii. 60	6	21	48	17·0	10·1	87·8
5–24. ii. 60	7	20	49	21·1	13·0	83·5
6–24. ii. 60	8	19	55	14·2	18·1	78·9
7–24. ii. 60	9	18	152	31·1	10·1	85·3
C. finmarchicus						
9–27. ii. 60	10	19	93	10·4	11·2	87·5
10–27. ii. 60	11	18	192	48·7	7·0	86·4
10–27. ii. 60	12	18	169	52·0	15·2	68·3
10–27. ii. 60	13	18	153	44·3	12·5	77·5
10–27. ii. 60	14	18	83	21·2	18·3	76·8
10–27. ii. 60	15	18	82	24·7	12·1	83·9
10–27. ii. 60	16	18	139	28·2	13·2	81·6
10–27. ii. 60	17	18	173	37·0	13·6	78·4
11–27. ii. 60	18	17	139	44·6	20·1	63·7
11–27. ii. 60	19	17	92	40·4	11·4	80·9
11–27. ii. 60	20	17	96	37·0	15·6	75·2

At this time the sea was poor in phytoplankton and the eggs in the females were developing slowly. In many the number of eggs per lay rose rather than fell towards the end of the period, but in spite of this the radioactivity per lay decreased steadily. The maximum percentage of ^{32}P produced in any one lay was 25–30%, and this was invariably in the first. The results from two of these individuals are shown in Figs. 4, nos. 11 and 16, and a summary of the results is given in Table 5. Because of the rapid loss of ^{32}P later experiments were stopped after about a week.

In the two final series (Table 6) the *Calanus* were caught about 6 a.m., which is shortly after the time (midnight to 4 a.m.) at which the majority of females lay in spring, and were fed on radioactive culture till evening. They ere then removed, washed, measured for ^{32}P and given non-radioactive od. In the experiment on 7 March only two *Calanus* out of 24 had laid eggs y evening, so that, apart from these, the readings of the live bodies gave the ue figures for the initial values. Of the 25 *Calanus* females set up in the same ay on 14 March, 10 had laid eggs by evening. These two experiments were rried on for only 6 and 5 days. The results are given in Table 6, and Fig. 4, os. 21, 23, 24, but only for these *Calanus* which laid more than once and rvived till the end of the experiment.

It is surprising how large a proportion (up to 38 %) of the ^{32}P ingested can me out again within 24 h as eggs. The largest number of eggs is usually id on the first night and the highest percentage return of ^{32}P accordingly pears then also. There is usually a steady decrease thereafter but occasion- ly, with a larger number of eggs laid, the downward trend is temporarily versed. At the end of the experiments the *Calanus* were killed and the ^{32}P maining in the body measured. When this, plus the value of the eggs laid, is ibtracted from the original reading, the difference may be taken as the hosphorus lost by excretion.

In the two experiments where the *Calanus* were caught early and fed during e day the total percentage returned as eggs in the 6 days following the dioactive meal averaged 47·3 %; the maximum was 72·4 %. These high gures indicate an insistent demand for phosphorus on the part of the ovary id explain why *Calanus* females lay freely only when well fed.

It seemed possible that the ^{32}P might be adsorbed on the surface of the egg id not really incorporated in its substance. To test this, some ripe *Calanus* males were fed on labelled phytoplankton and their eggs collected and ashed. Half were then measured for ^{32}P; half were allowed to hatch and the P in the resulting nauplii measured. There was no significant difference etween the radioactivity of eggs and nauplii from the same lay, which dicates that the ^{32}P was not merely on the surface.

In Fig. 4 the loss of ^{32}P as eggs is plotted cumulatively, but the loss in cretion is calculated only by difference and the curve for this drawn to semble the usual excretion curves. Fig. 4, nos. 11, 16, show the results of e experiments in February. In the March experiments (Fig. 4, nos. 21, 23, , 25) the ripe females obviously have a large number of eggs ready, or almost ady to lay, and these were produced during the next 5 or 6 days. It seems ear from these two series of experiments that when much of the P is used in g production, the excretion is reduced. Even when we subtract from the itial reading the P in the eggs, the excretion, as a percentage of the mainder (Tables 5 and 6, last column), is still low for those which lay well.

Three series of experiments were made on laying females in which excre- on of ^{32}P was measured as well as that produced in eggs (Table 4). In the st two of these, the females were given labelled food for one day only and rved for the rest of the experiment. The average loss by excretion followed

TABLE 6. EGG LAYING EXPERIMENTS IN MARCH

Date	No.	Number of, and percentage of ^{32}P in, eggs laid on day														Total no. eggs laid	% ^{32}P in eggs	% ^{32}P in body at end	% ^{32}P excreted (excluding eggs)
		Day of capture		1		2		3		4		5		6					
7–13.iii.60	21	58	17·0	—	—	15	5·2	46	10·1	5	0·9	6	0·8	15	1·9	145	36·0	19·1	70·2
	22	—	—	71	35·0	43	14·8	33	7·2	24	3·8	10	1·4	—	—	181	62·1	22·1	41·7
	23	—	—	56	37·8	38	16·9	30	8·2	28	5·4	14	2·2	13	1·8	179	72·4	20·0	27·5
	24	—	—	65	33·7	—	—	37	9·2	—	—	27	3·9	—	—	129	46·7	34·1	36·0
	25	—	—	—	—	128	37·0	47	12·8	—	—	36	5·0	41	5·3	252	60·0	28·6	28·5
14–19.iii.60	26	—	—	24	13·3	64	16·2	10	1·8	17	2·1	—	—	—	—	115	33·4	21·4	67·9
	27	47	36·9	—	—	29	12·1	20	3·9	12	1·7	4	0·4	—	—	112	55·1	25·3	43·6
	28	32	22·6	—	—	32	8·7	14	2·8	26	4·4	32	3·3	—	—	136	41·8	25·6	56·0
	29	—	—	35	22·3	62	18·4	30	6·3	—	—	—	—	—	—	127	47·0	23·4	55·9
	30	—	—	49	28·9	32	12·3	21	4·1	—	—	—	—	—	—	102	45·3	34·4	37·1
	31	—	—	27	22·8	26	9·7	8	1·9	16	3·1	—	—	—	—	77	37·5	38·8	37·9
	32	45	18·6	—	—	65	21·5	31	5·1	—	—	—	—	—	—	141	45·2	19·0	65·3
	33	—	—	17	0·3	—	—	—	—	22	4·6	—	—	—	—	39	4·9	33·5	64·8
	34	—	—	—	—	20	11·6	53	22·3	—	—	9	1·2	—	—	82	35·1	26·8	58·7

osely the curve appropriate for one day's feeding, but when the excretion by g-layers and non-egg-layers on any one day was compared, the former were und to have excreted considerably more than the latter. In the third series e females were fed 5 days on radioactive and then 4 days on non-radioactive od before measurements started, so that the ^{32}P would be in equilibrium

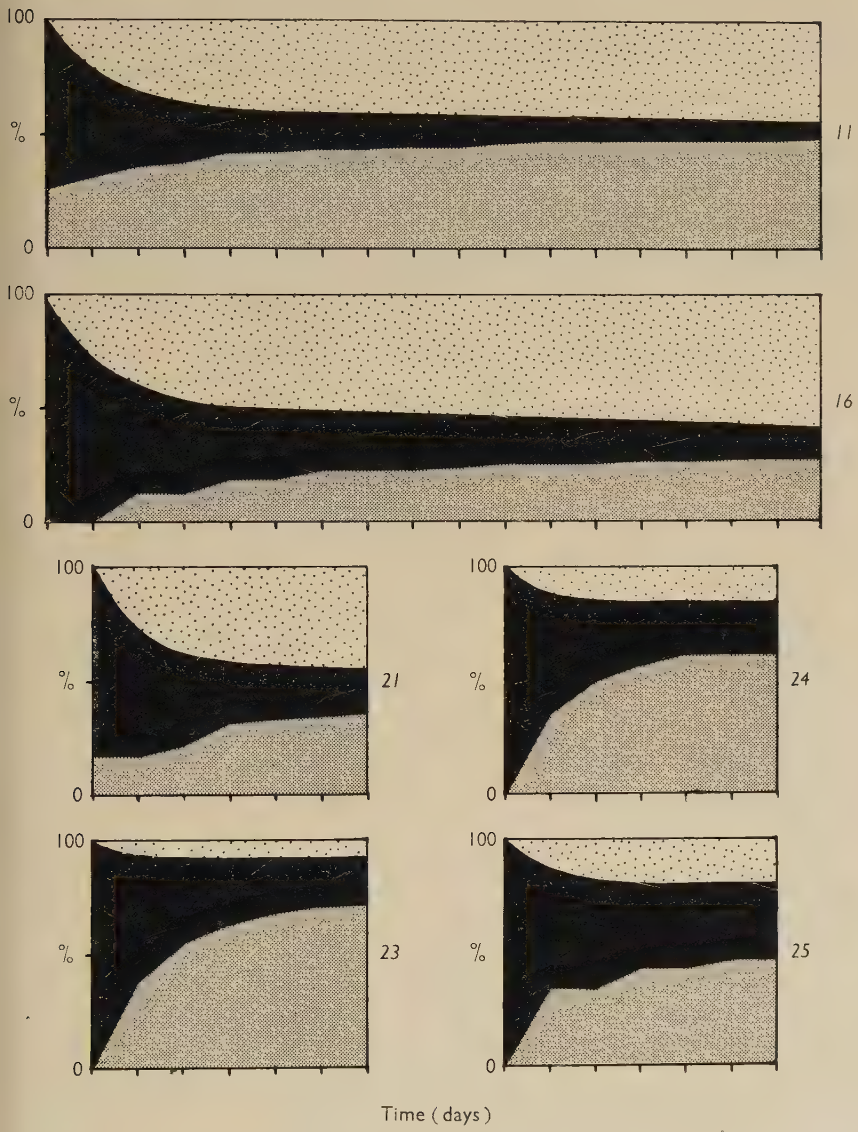

g. 4. Fate of one meal in laying female *Calanus finmarchicus*. Black, ^{32}P in body; dark stippling, in eggs; light stippling, in excretion.

throughout the body. Non-radioactive feeding was continued throughout th experiment, and some of the females laid regularly although the number c eggs was small. Excretion of ^{32}P was low, and there was no marked differenc between egg-layers and non-egg-layers.

A possible explanation of this difference is that in the starved females the for excretion must come from the pool of labelled P in the body, whereas i the fed it will come mainly from the food newly taken in which was nc labelled and would therefore not be measured.

TOTAL PHOSPHORUS IN *CALANUS*

It was unexpected that the losses in excretion as measured by ^{32}P should b so high and some total P analyses were made for comparison.

Those at Woods Hole were done through the kindness of Dr Bostwick Ketchum. In these several *Calanus* from the same batch as the experimenta animals were used to give initial P values, but there was so much variatio between individuals that this cannot be a very reliable figure. In the late analyses at Millport a considerable number of controls (up to 20 in groups c 3–5) gave a more reliable initial result. The mean of these was compared wit the mean of groups of 1–5 at the end of the experiment. The results are show in Table 7.

TABLE 7. PHOSPHORUS ANALYSES

	Initial		Final		% change total P	% chang ^{32}P
Experiment	No. *Calanus**	µg P/*C.*	No. *Calanus**	µg P/*C.*		
March 1960						
Fed 6 days	15 ♀ (3)	1·39	10 ♀ (2)	1·60	+15	—
Fed 7 days			2 ♀ (1)	1·95	+40	—
Starved 6 days			10 ♀ (2)	0·93	−33	—
Starved 7 days			3 ♀ (1)	0·84	−40	—
April 1960						
Fed 3 days	16 ♀ (4)	1·95	8 ♀ (2)	1·43	−27	—
Starved 2 days			6 ♀ (2)	0·87	−55	—
Fed 7 days			10 ♀ (2)	1·80	−8	—
Starved 6 days			6 ♀ (2)	1·01	−49	—
Starved 4 days			11 ♀ (4)	1·14	−42	−62
April 1960						
Starved 2 days	12 ♀ (3)	1·80	9 ♀ (3)	1·43	−21	−40
Starved 4 days			11 ♀ (3)	1·32	−27	−44
June 1960						
Starved 6 days	16 ♀ (4)	1·33	13 ♀ (3)	0·97	−31	−29
April 1960						
Starved 7 days	10 V (2)	1·18	7 V (2)	0·84	−30	−45
May 1960						
Fed 1 day	20 V (4)	1·80	20 V (4)	1·68	−7	—
Fed 2 days			20 V (4)	1·36	−25	—
May 1960						
Autolysed 3 days	Estimated	1·62	9 ♀ (2)	0·015	−91	−94

* Number of determinations in brackets

There is evidently a considerable variation in the P content of individual *Calanus*. The values vary from 1·12 to 2·39 μg/*Calanus* female. They are artly dependent on the state of maturity and may also be dependent on eeding either before or after capture. Even after feeding in the laboratory, owever, the total P was increased only in two experiments, and it was more sual for there to be a slight fall. At Woods Hole the chloromycetin used was ater found to inhibit feeding in *Calanus* to a marked extent, and the loss in ed *Calanus* there was greater than at Millport where penicillin was used nstead. After starving, the loss in total P was always considerable.

At Woods Hole the total P was measured in individual *Calanus* at the end f the experiment and was compared with the average initial value. In spite f the great individual variation, the average percentage change given by both he radioactive and the total P methods agreed well for starved *Calanus* in ong- as well as in short-term feeding experiments. Even in one *Calanus* vhich had lost as much as 70 % the agreement was close. For fed *Calanus* the verage values by the two methods naturally differed more.

At Millport most of the total P analyses were done after short-term feeding xperiments, and in these the loss calculated from radioactive measurements vas much above that from total P. In the one long-term feeding experiment 1. vi. 60) the results from the two methods were closer.

Stage V was used in two experiments. The initial values were only slightly elow those for females and were 1·18–1·80 μg P/*Calanus*. As with females, eeding in the laboratory did not prevent the loss of total P and in a short-term eeding experiment excretion as measured by ^{32}P was much above that as neasured by total P.

It appears that it is only when the radioactive feeding period is long enough or the ^{32}P to be in equilibrium throughout the body that the two methods ive comparable results.

Since such a high proportion of the P goes to the ovary it seemed that it hould be possible to measure the total P in *Calanus* eggs. In April eggs were ollected from 50–60 females of both *C. finmarchicus* and *C. helgolandicus*. The numbers were 2227 and 2452 respectively. In duplicate estimations the irst contained 0·68 and 0·71 and the second 0·96 and 1·08 μg P/100 eggs. In May these analyses were repeated after the females had been fed overnight to ind out if this would raise the P content of the eggs. The numbers were 878 nd 815, the P content 0·65 and 0·65 μg P/100 eggs for *C. finmarchicus* and ·08 and 1·12 for *C. helgolandicus*. It thus appears that short-term feeding loes not increase the P content of the individual egg laid. Since at the peak of he egg-laying period as many as 60 to 100 eggs may be produced in a single ay, a *Calanus* can part with up to a third of its total P in one lay. This conirms the egg-laying experiments with ^{32}P.

One would also expect unripe females to be less rich in P than ripe, and his was tested in June 1960. Most females in the tow-nettings were ripe, but a few in an early stage of reproductive development were obtainable. The analyses showed that the unripe contained 1·27 and the ripe 2·01 μg P/*Calanus*.

Stage V may contain as much P as do females, depending presumably on their state of nutrition. The early copepodite stages rarely have more than a small quantity of fat, but Stage V varies from having only a small amount to having an enormous bolster which fills most of the body. In the rough dissections already mentioned of *Calanus* fed with labelled P, we found that much was in the fat (up to 40 %). Since after moulting into females the fat rapidly disappears with the growth of the eggs, it was assumed that the fat was used to build up the eggs. Total P was estimated in Stage V of different fatness and found to vary from 0·71 μg/*Calanus* in lean up to 1·84 in fat. In samples taken in mid-July most of the fat Stage V were larger than the lean (length of cephalosome 2·32 and 2·02 mm) and perhaps belonged to a different generation. In a comparison of 5 lean and 5 fat of the same length, however, the P content was 0·79 and 1·24 μg P/*Calanus*.

LIBERATION OF PHOSPHORUS FROM DEAD *CALANUS*

Phosphorus is returned to the sea by the break-down of dead zooplankton. To find out the rate at which this happens, some experiments were made by measuring the loss of ^{32}P from dead *Calanus*. After feeding overnight with cultures labelled with ^{32}P, the radioactivity of the body was measured in a Perspex cell and the animals killed and put singly in bottles of membrane-filtered sea water. To some of these the usual antibiotics were added, to some antibiotics plus toluol, to others only chloroform, and finally there were some controls with no addition. The bottles were kept rotating slowly on a vertical wheel to keep the bodies moving and so simulate sinking in the sea. They were kept at a temperature of about 18° C.

In some experiments (Table 8) the *Calanus* were killed by gentle heat. A surprising feature was the high rate of loss of ^{32}P even after only 24 h. After 3 days it was over 90 % and analyses of total P confirmed this. Even in 2 h, the loss, though variable, might be as high as 75 %. The results were much the same in the controls and in those to which chloroform had been added.

Since the heating might have reduced enzyme or bacterial activity some *Calanus* were killed by freezing, but the results confirmed those in which the *Calanus* had been killed by heat.

The breakdown of P compounds may be caused by autolysis or by bacterial action since the presence of antibiotics, toluol or chloroform does not entirely rule out the latter. From the point of view of re-cycling of P in the sea, it is perhaps immaterial which is responsible but since all the *Calanus*, including the controls, released P at much the same rate, autolysis seems the most likely explanation.

TABLE 8. AUTOLYSIS OF DEAD *CALANUS* AT 18° C

(Loss %)

Date ...	11–14. v. 60		17–19. v. 60		4–6. vii. 60						24–26. v. 60			
Method of killing ...	Heat		Heat		Heat		Heat		Heat		Cold		Cold	
Addition ...	P and S		P and S		P and S		CHCl$_3$		None		P and S		P and S and toluol	
No. *Calanus* ...	9♀		9♀		3V 1♀		4V 1♀		4V		8♀		8♀	
Loss %	Range	Mean	Range	Mean	Range	Mean	Range	Mean	Range	Mean	Range	Mean	Range	Mean
2 h	—	—	4·6–74·6	31·8	*43·0–70·3	60·1	*64·4–73·4	70·2	*45·1–66·3	57·1	—	—	68·9–82·6	75·8
8 h	—	—	21·9–83·5	55·4	—	—	—	—	—	—	†73·0–86·4	80·4	75·4–88·1	82·0
1 day	70·1–90·4	81·0	53·7–92·8	74·4	76·9–83·1	80·4	78·3–83·9	81·5	68·2–96·3	79·1	88·0–94·0	92·2	88·3–95·2	91·8
2 days	88·3–95·2	90·8	67·6–94·9	81·4	82·2–89·3	85·6	85·3–89·8	87·3	74·0–97·0	84·1	93·0–97·0	95·6	93·1–98·0	95·5
3 days	92·0–96·1	93·7	—	—	—	—	—	—	—	—	—	—	—	—

P = penicillin; S = streptomycin; * 5 h; † 5–7 h.

DISCUSSION

One of the most important points to consider in any experiment using ^{32}P is the relation between the radioactive and the total P. The total P analyses done in conjunction with the excretion experiments show that not all the P compounds in the *Calanus* body are labelled immediately. It needs a period of feeding of at least a week before labelled P is in equilibrium throughout the body. Some compounds are more labile and in them P is metabolized more rapidly than in others. From the rate of loss of metabolized P by excretion in *Calanus* which have been fed long enough for the ^{32}P to be in equilibrium (Table 1, p. 466) we can estimate that the biological half-life is about 14 days. From this we can calculate the turnover time, i.e. the time required to liberate the amount of P present in a *Calanus*. This is given (Zilversmit, Entenman & Fishler, 1943) as half-life × 1·44, i.e. about 20 days.

The large reduction in P which can be tolerated during starvation was unexpected, especially as it did not seem to affect the activity of the animals. It was usual, however, to find a high mortality when the ^{32}P loss rose to about 70 %.

The high rate of excretion during the first 24 h after a short-term feeding experiment with labelled culture has a bearing on the use of such cultures in the measurement of filtering rates. In the early excretion experiments (Marshall & Orr, 1955) the *Calanus* were fed for a week, excretion on the first day was 10 % or less, and it was concluded that the effect in feeding experiments would be negligible. *Calanus* in a feeding experiment lasting usually about 18–24 h is, however, more properly compared with those in excretion experiments after one day's feeding and the 'volume filtered', at least that part of it which is calculated on food assimilated, may have thus been underestimated by an amount varying from 10 % up to 50 %.

The figures we gave for volumes filtered varied from less than 1 ml. up to 84 ml./24 h. A corrected maximum figure of 120 ml./day is above the average found by Gauld (1951) when calculating filtration by cell counts (70 ml.) but is still much below that postulated by some recent workers (Cushing, 1959; Steele, 1959) to account for changes in the phytoplankton populations in the sea.

A surprising feature of the results of total P analyses is the relatively big difference in the P content of individual *Calanus*. Apart from this the value probably varies seasonally. There is usually more P in females than in Stage V, more in ripe than in unripe females, and more in fat than in lean Stage V. The normal value for the P content of one female may be taken as 0·05–0·06 μg atom P (1·55–1·86 μg P) which corresponds to the mean value for 100 ml. sea water at E 1 in the English Channel in winter (Armstrong & Butler, 1960).

Our earlier observations showed that in females much of the ingested P was rapidly transferred to the ovary and one of the most striking facts about the P metabolism is the large quantity which goes into egg production. Barnes & Barnes (1956) also noted this in the freshwater copepod *Cyclops strenuus*. In this species females without egg-sacs contained two-thirds of the P of females with them, i.e. as in *Calanus* the P in the eggs was about one-half the P in the rest of the body. In *Cyclops* there was 0·35 μg P/100 eggs, in *Calanus finmarchicus* 0·68 μg in eggs of about the same size.

The observations on the fate of the ^{32}P of one short feeding period (p. 473) show that in the course of 5–6 days up to 70% may appear as eggs. The percentage of P excreted in these actively laying females is lower than usual (Fig. 4) and this seems to indicate that egg-laying females use their food more efficiently.

Richman (1958) has made a detailed study of the energy budget of *Daphnia pulex*, and has found that in the pre-adult stage 55–58% of the energy assimilated was used for growth. Once reproduction had begun only 3–4% was used for growth and 52–70% went into the eggs and young. His experiments dealt with animals over the greater part of their life span, whereas ours deal with a relatively short feeding time, but they confirm one another in indicating that the metabolism of these Crustacea is efficiently geared for reproduction.

These studies on excretion and autolysis emphasize the importance of the role of zooplankton in the regeneration of P in the sea. Some of the P is inorganic and some organic (Cooper, 1935; Hoffmann, 1956). The organically bound P may be available for plant growth either directly (Harvey, 1945; Chu, 1946) or after further breakdown.

Harris (1959) has already shown that excretion by the zooplankton is important in the re-cycling of nitrogen in Long Island Sound. In spring and summer there, zooplankton excretion accounts for half the nitrogen required by the phytoplankton.

Calanus in a rich food culture can produce faecal pellets at the rate of one every 5 or 6 min. These are, however, low in P (Harvey, Cooper, Lebour & Russell, 1935) and these authors thought that this was because P from undigested cells was liberated directly into the water as phospho-proteins and phospholipids. Our digestion experiments and the present results, however, suggest that assimilation of P is high; the rate of loss from faecal pellets is low.

The seasonal and diurnal migrations of the zooplankton and the length of their stay in the surface waters rich in phytoplankton will be significant in deciding whether the regenerated P will be immediately available for plant production or only after its introduction there by vertical mixing.

Hoffmann (1956) measured the rate of breakdown of P in both phyto- and zooplankton after death and his figures for the autolysis of mixed copepod plankton are in fairly close agreement with ours for female *Calanus*. According to him 20–25% of inorganic P and 30–40% of organic P is liberated very shortly after death and between 80 and 90 % in 24 h. We found that breakdown was almost complete in 2 days. It is probably autolytic, and we agree with Hoffmann that bacterial action (Harris, 1959) or enzymes in the water (Kreps, 1934; Steiner, 1938) are of relatively small importance.

Gardiner (1933) measured the rate of sinking of anaesthetized *Calanus* and found it to be dependent on size. For females it was about 15 m/h so that a dead *Calanus* might liberate as much as 75 % of its P in sinking through the top 50 m. It is probable that, after the formation of a thermocline, the growth of the phytoplankton depends more on the excretion of the zooplankton than on nutrients supplied from below or from bacterial decomposition.

We should like to thank the Director and staff of the Woods Hole Oceanographic Institution for their generous support, especially Dr G. L. Clarke for his advice and unfailing help and Dr B. H. Ketchum for the early P analyses. We are also indebted to Dr R. J. Conover and Dr J. Steele for fruitful discussion of the results.

SUMMARY

It is shown that equilibrium of ^{32}P throughout the body of *Calanus* is reached only after a feeding period of about a week. The time required to liberate by excretion the amount of P present in a *Calanus* is about 20 days. Fed *Calanus* excrete at a higher rate than starved. The implications of excretion in feeding experiments using ^{32}P is discussed.

There are large differences in the total P content of individual *Calanus*. Figures are given for ripe and unripe females, fat and lean Stage V, and eggs. A high percentage, up to 55 % of the total P, may be lost by excretion during starvation.

A high proportion of the P in the food assimilated (up to 70 %) may appear within a week as eggs laid.

Liberation of P from dead *Calanus* is very rapid and is almost complete in three days.

The relation of excretion and autolysis to the P cycle in the sea is discussed.

REFERENCES

Armstrong, F. A. J. & Butler, E. I., 1960. Chemical changes in sea water off Plymouth during 1958. *J. mar. biol. Ass. U.K.*, Vol. 39, pp. 299–302.

Barnes, H. & Barnes, M., 1956. Contenuto di fosforo totale in alcuni stadi di due comuni animali d'acqua dolce e suo rapporto con quello delle loro uova. *Mem. Ist. ital. Idrobiol. di Marchi*, Vol. 9, pp. 113–24.

Chu, S. P., 1946. The utilization of organic phosphorus by phytoplankton. *J. mar. biol. Ass. U.K.*, Vol. 26, pp. 285–95.

Cleland, K. W., 1953. Heavy metals, fertilization and cleavage in the eggs of *Psammechinus miliaris*. *Exp. Cell Res.*, Vol. 4, 246–8.

Cooper, L. H. N., 1935. Rate of liberation of phosphate in sea water by the breakdown of plankton. *J. mar. biol. Ass. U.K.*, Vol. 20, pp. 197–200.

Cushing, D. H., 1959. On the nature of production in the sea. *Fish. Invest., Lond.*, Ser. 2, Vol. 22, No. 6, 40 pp.

Gardiner, A. C., 1933. Vertical distribution in *Calanus finmarchicus*. *J. mar. biol. Ass. U.K.*, Vol. 18, pp. 575–610.

—— 1937. Phosphate production by planktonic animals. *J. Cons. int. Explor. Mer*, Vol. 12, pp. 144–46.

Gauld, D. T., 1951. The grazing rate of planktonic copepods. *J. mar. biol. Ass.U.K.*, Vol. 29, pp. 695–706.

Harris, E., 1959. The nitrogen cycle in Long Island Sound. *Bull. Bingham oceanogr. Coll.*, Vol. 17, pp. 31–65.

Harvey, H. W., 1945. *Recent Advances in the Chemistry and Biology of Sea Water.* Cambridge University Press.

—— 1948. The estimation of phosphate and of total phosphorus in sea water. *J. mar. biol. Ass. U.K.*, Vol. 27, pp. 337–59.

Harvey, H. W., Cooper, L. H. N., Lebour, M. V. & Russell, F. S., 1935. Plankton production and its control. *J. mar. biol. Ass. U.K.*, Vol. 20, pp. 407–42.

Hoffman, C., 1956. Untersuchungen über die Remineralisation des Phosphors im Plankton. *Kieler Meeresforsch.*, Bd. 12, pp. 25–36.

Krause, H. R., 1959. Biochemische Untersuchungen über den postmortalen Abbau von totem Plankton unter aeroben und anaeroben Bedingungen. *Arch. Hydrobiol.*, Suppl., Bd. 24, Bd. 3, pp. 297–337.

Kreps, E., 1934. Organic catalysts or enzymes in sea water. *James Johnstone Memorial Volume*, pp. 193–202. Liverpool.

Marshall, S. M. & Orr, A. P., 1955. On the biology of *Calanus finmarchicus*. VIII. Food uptake, assimilation and excretion in adult and Stage V *Calanus*. *J. mar. biol. Ass. U.K.*, Vol. 34, pp. 495–529.

Oppenheimer, C. H., 1955. The effect of marine bacteria on the development and hatching of pelagic fish eggs and the control of such bacteria by antibiotics. *Copeia*, 1955, pp. 43–9.

Richman, S., 1958. The transformation of energy by *Daphnia pulex*. *Ecol. Monogr.*, Vol. 28, pp. 273–91.

Robertson, J. S., 1957. Theory and use of tracers in determining transfer rates in biological systems. *Physiol. Rev.*, Vol. 37, pp. 133–54.

Steele, J. H., 1959. The quantitative ecology of marine phytoplankton. *Biol. Rev.*, Vol. 54, pp. 129–59.

Steiner, M., 1938. Zur Kenntnis des Phosphatkreislaufes in Seen. *Naturwissenschaften*, Heft 44, pp. 723–4.

Zilversmit, D. B., Entenman, C. & Fischler, M. C., 1943. On the calculation of 'turnover time' and 'turnover rate' from experiments involving the use of labelling agents. *J. gen. Physiol.*, Vol. 26, pp. 325–31.

ADDENDUM

THE TURNOVER OF PHOSPHORUS BY *CALANUS FINMARCHICUS*

By R. J. CONOVER

Woods Hole Oceanographic Institution

It has been shown above that the rate of loss of ^{32}P from *Calanus* is in part dependent on the length of time of feeding on the radioactive culture prior to the start of the excretion measurements. It was also observed that the ^{32}P was excreted from *Calanus* more rapidly in fed than in starved animals after short-term feeding with labelled cultures (see Fig. 2 and Tables 1 and 2, pp. 466, 467 and 470). Finally, it was shown that the rate of loss of ^{32}P in starved *Calanus* was frequently more rapid than the loss in total phosphorus (see Table 7, p. 476). Thus the radioactive phosphorus must be presumed to pass through several different physiological or chemical 'pools' each with a different turnover time before equilibrium is approached.

In the series of experiments described, the culture medium was changed each time the ^{32}P loss from the animals was measured and, therefore, the design conforms more closely to an open than a closed system, i.e. to one in which there is a continuous flow into and out of the system with no reversible reactions in contrast to one in which there is maximum recycling. Changes in total phosphorus with feeding are sometimes positive and sometimes negative (Table 7); in the absence of any pronounced trend toward an increase or decrease in total phosphorus in the experiments, a steady state will be presumed.

In the simplest type of open system, assuming excretion from a single phosphorus pool under steady-state conditions and with no recycling, the amount of isotope in the pool would decrease according to the expression

$$X = ae^{-kt}, \tag{1}$$

where X is the amount of radioactivity at any time t, a is the initial concentration of ^{32}P and k is the turnover rate. Under these experimental conditions a semilog plot of the amount of ^{32}P in the animal against time should give a straight line with slope k. In Fig. 5, the data for fed animals from Table 2 (Expt. 9–22.xii.59), taken as percentage ^{32}P remaining in the copepod body, have been plotted on semilog paper against time. After 2–3 days the loss would seem to be linear, but over the first 24 h at least it is much more rapid than would be anticipated if only a single rate function applied. These animals were fed only 3 h on labelled phytoplankton before the excretion measurements were begun. With a longer initial labelling period, the percentage loss of ^{32}P from the bodies of the experimental animals during the first few hours after excretion measurements were started was not so great (see Fig. 1 and Table 1). It must, therefore, be presumed that there is at least one additional pool of small size, but with a high turnover rate, that is intermediate between the external phosphorus supply and the larger, stable pool of body phosphorus. Because this pool is proportionately so small compared with the stable pool, its turnover rate can be studied with precision only if the initial labelling period is kept short.

Since the data strongly suggest that more than a single rate process is involved in the uptake and loss of phosphorus by *Calanus*, it was decided to perform the analysis with a two-compartment rate function, assuming a steady state and no recycling, such that

$$X = a_1 e^{-k_1/t} + a_2 e^{-k_2 t}, \tag{2}$$

where a_1 and k_1 represent the initial concentration and daily turnover rate for the labile pool and a_2 and k_2 are the concentration and turnover rate for the stable pool. In Fig. 5, a smooth curve has been fitted by eye to the data for animals labelled 3 h and an asymptote to the straight part of the curve extended to the ordinate. The slope of this line k_2 is the turnover rate for the slow reaction and its y intercept is equivalent to the radioactivity in a_2 at the end of the labelling period, i.e. $t = 0$. When the ordinates of this line are subtracted from the portion of the curve which does not correspond with it, a second curve describing the fast reaction is obtained with slope k_1 and y intercept a_1.

The slopes (k_i) of the curves may be determined from the expression

$$k_i = 0{\cdot}693/T_i, \tag{3}$$

where T_i is the half time of the reaction determined from the graph by inspection. For the fast reaction the half life T_1 is 0·375 days ($k_1 = 1{\cdot}848$) and for the slow reaction $T_2 = 13$ days ($k_2 = 0{\cdot}053$). The y intercepts $a_1 = 0{\cdot}44$ and $a_2 = 0{\cdot}56$ indicate that the amount of ^{32}P in the two pools after 3 h feeding was nearly equal.

A similar analysis procedure was carried out for the other experiments ısing the data for fed animals contained in Table 2. These results are summarized in Table 9. As in the case of the experiment shown in Fig. 5, when he labelling period was kept short the ^{32}P in the labile pool constituted an ippreciable percentage of the total and it was possible to evaluate the rate onstants (k's) for both the slow and fast reactions. However, in experiments vith more than one day's labelling, over 90 % of the tracer appeared in the table pool and only the slow reaction could be studied. Variability in the stimate for k_1 (31·8 %) was somewhat greater than that for k_2 (24·5 %) which nay in part be due to the small number of measurements made during the ritical first few hours after the excretion measurement was begun; however, articularly in Expts. 15–28.xii.59 and 4–16.xi.59 (Table 1), the graphic analysis suggested that a third metabolic pool might exist intermediate between a_1 and a_2.

The values for a_1 and a_2 in Table 9 give some idea of the partitioning of the isotopic phosphorus between the two pools with different periods of feeding on labelled phytoplankton culture. However, in order to determine the relative dimensions of the two pools, it is necessary to estimate how much ^{32}P each could acquire at infinite time. At initial time the ^{32}P will all be in the algae and will have a certain concentration in relation to the total phosphorus which determines the upper limit of radioactivity which can be acquired by each of the pools. The uptake of ^{32}P then, in each pool, behaves according to the expression

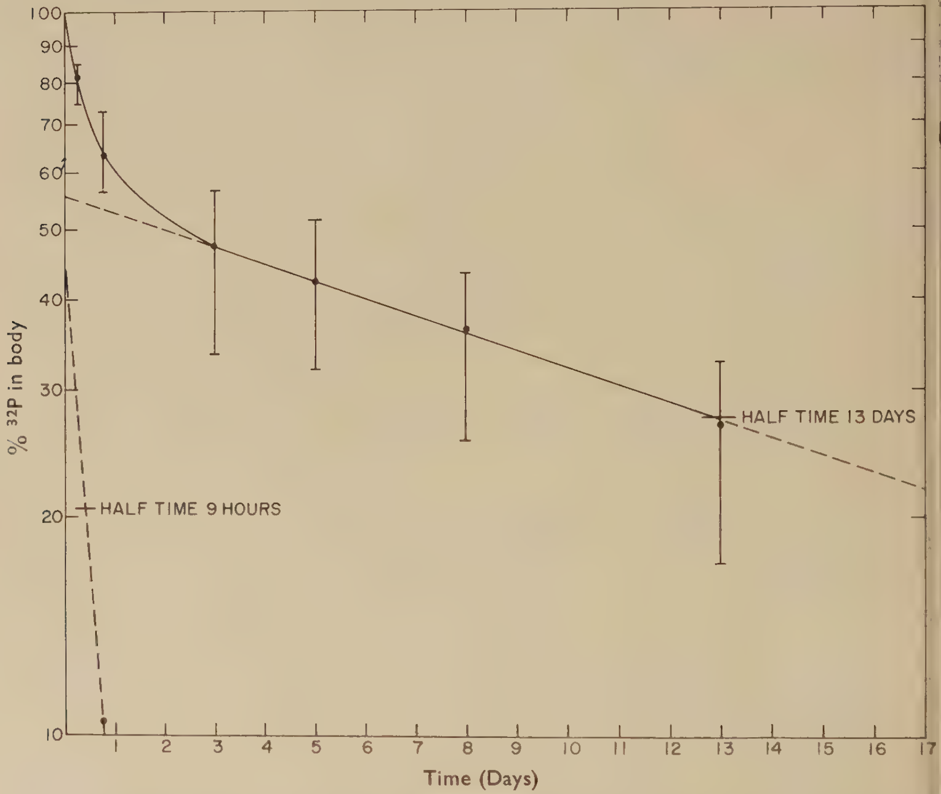

Fig. 5. Semi-logarithmic plot of the percentage of the initial burden of ^{32}P in the body of *Calanus finmarchicus* against time (data taken from Table 2, experiment of 9–22. xii. 59). The smooth curve has been fitted by eye to the mean percentage ^{32}P in the animals. Vertical lines indicate the range of individual variation. The dashed lines represent graphic extrapolations carried out using the procedure outlined in the text.

$$X_i = a_{i\infty} (1 - e^{-k_i t}), \tag{4}$$

where $a_{i\infty}$ represents the radioactive concentration at infinite time in the

ith pool and k_i is the rate constant governing uptake by this pool (for derivation of this and other formulae used, see Robertson, 1957). If the system is in a steady state with no recycling, it can be shown that the rate constants governing the uptake must equal those governing the loss from each pool. The total ^{32}P burden after 3 h or after one day's feeding on labelled phytoplankton is known for the four experiments shown in Table 10. It is also known how this radioactivity is distributed between the two pools a_1 and a_2 (see Table 9). Therefore, if the radioactivity in counts/minute in a_1 or a_2 is set equal to X_i and if the corresponding values for k and for t from Table 9 are inserted, equation (4) may be solved for $a_{i\infty}$. Since the proportion of radioactive phosphorus to total phosphorus should be the same for each pool at infinite time, the relative dimensions of the two pools can now be computed as percentage of total body phosphorus. Thus in Table 10 it is shown that somewhere between 94 % and 99 % of the total phosphorus content of *Calanus* is in relatively stable form.

TABLE 9. VALUES FOR TURNOVER RATE (k_i) AND PROPORTION OF RADIOACTIVITY IN THE PHOSPHORUS POOLS (a_i) IN *CALANUS FINMARCHICUS*

Date of experiment	Length of labelling period (feeding with labelled phytoplankton)	Fast reaction		Slow reaction	
		Turnover rate k_1	Proportion in a_1	Turnover rate k_2	Proportion in a_2
9–22. xii. 59	3 h	1.848	0·44	0·053	0·56
15–28. xii. 59	3 h	2·081	0·375	0·037	0·625
4–16. xi. 59	1 day	0·924	0·50	0·036	0·50
24. xi.–18. xii. 59	1 day	2·081	0·38	0·069	0·62
17. xi.–1. xii. 59	7 days	—	—	0·072	0·915
1–15. xii. 59	7 days	—	—	0·048	0·965
10–26. v. 58	14 days	—	—	0·048	0·92
28. xii.–12. 59. i. 60	18 days	—	—	0·060	0·915
		Mean = 1·734		Mean = 0·053	
		σ = 0·551		σ = 0·013	
		C.V. = 31·8 %		C.V. = 24·5 %	

TABLE 10. POOL SIZE AT INFINITE TIME AND TOTAL PHOSPHORUS EXCRETION FOR *CALANUS FINMARCHICUS* LABELLED FOR PERIODS OF ONE DAY OR LESS

Date of experiment	Length of labelling period	Mean initial radioactivity (ct/min)	Size of pool a_1 (% total P)	Size of pool a_2 (% total P)	Total daily turnover of E_T (%/day)
9–22.xii.59	3 h	32,116	2·3	97·7	9·4
15–28.xii.59	3 h	17,926	1·3	98·7	6·4
4–16.xi.59	1 day	21,358	6·1	93·9	9·0
24.xi.–8.xii.59	1 day	58,556	4·5	95·5	16·0

It would also be of considerable importance for the understanding of nutrient cycles in the sea to determine the phosphorus turnover rate for the whole animal. Since the amount of phosphorus excreted by the animal will depend on the fraction lost per unit time from each pool and the relative amount of phosphorus in each pool, it is necessary to use the differential form of expression 2 to obtain an estimate of turnover for *Calanus*. Thus, the excretion rate

$$-\frac{d(a_1+a_2)}{dt} = E_T = k_1 a_1 + k_2 a_2. \qquad (5)$$

Values for phosphorus excretion for the four experiments where the labelling period was short are shown in the last column of Table 10. The mean turnover rate would seem to be about 10 %/day. As many members of the zooplankton community are smaller than *Calanus* and may be expected to be more active metabolically, the possibility that excretion by plankton animals contributes significantly to aquatic nutrient budgets should not be overlooked.

Contribution No. 1057

Deep-Sea Research, 1961, Vol. 7, pp. 254 to 264. Pergamon Press Ltd., London. Printed in Great Britain

Nitrogen/argon and nitrogen isotope ratios in two anaerobic environments, the Cariaco Trench in the Caribbean Sea and Dramsfjord, Norway*

FRANCIS A. RICHARDS** and BRUCE B. BENSON

(*Received* 10 *July* 1959)

Abstract—Mass spectrometric measurements of nitrogen/argon and nitrogen isotope ratios have been used to examine the fate of nitrogen arising from the decomposition of organic matter in two anaerobic marine environments, the Cariaco Trench in the Caribbean Sea and the Dramsfjord in Norway.

Values of N_2/A in these waters are larger than would be expected from dissolved atmospheric gases. By assuming that the A concentration is biologically unaffected, the excess quantities of N_2 can be calculated. These are in good agreement with the amounts of nitrogen which would be expected to arise from the decomposition of organic matter. The latter values are computed from the observed concentrations of nitrogen compounds and either the observed concentrations of inorganic phosphate or the amounts of oxygen (either free or bound in the sulphate ion) consumed from the water.

It is shown that nitrogen isotope ratios are markedly different in the nitrogen of biogenic origin from those in nitrogen dissolved from the atmosphere.

It is shown that it is probable that free nitrogen can be formed from organic matter only through the denitrification of nitrate, formed as an intermediate.

INTRODUCTION

THE statistically constant ratio of phosphorus to nitrogen in sea-water and in marine organisms, N : P = 15 or 16 : 1, by atoms, has been established by REDFIELD (1934, 1942), COOPER (1938), FLEMING (1940) and others. FLEMING also reported the average ratios of carbon to these elements in marine plankton to be C : N : P = 106 : 16 : 1, and REDFIELD (1934) has shown that in sea-water the ratio of the change of carbonate-carbon to nitrogen is C : N = 7 : 1. Upon the ultimate decomposition of organic matter having the above composition, inorganic forms of phosphorus, nitrogen and carbon are released to the water in these same ratios. In aerobic waters this latter process is accompanied by the consumption of free oxygen from the water in, statistically, the ratios AOU : C : N : P = 270 : 106 : 15 : 1 (RICHARDS and VACCARO, 1956), where AOU is the apparent oxygen utilization.

In the oxygen-free waters of the Cariaco Trench, however, RICHARDS and VACCARO found the ratio of oxygen consumption to phosphorus release to be only 235 : 1. This ratio takes into account the oxygen from the sulphate ions which, in the absence of free oxygen, are reduced to sulphides (H_2S, HS^-, $S^=$). Furthermore, under anaerobic conditions, the nitrogen, assumed to be released initially in the amino ($-NH_2$) form, does not appear in the form of nitrate (NO_3^-). In the Cariaco Trench, RICHARDS and VACCARO found that nitrate and nitrite either were absent or were present in traces quantitatively unimportant to the discussion to follow. The quantities of ammonia-nitrogen in the anaerobic depths, although larger than found in the open ocean, were too small to account for all the nitrogen which should have been present, as estimated from the above ratios and either the phosphate concentrations or the quantities of oxygen consumed. They suggested that the balance of nitrogen might be present as free, molecular N_2 in solution, amounting to approximately 0·35 ml/l or about 3·5 per cent of the quantity of atmospheric nitrogen in the water.

---

*Contribution No. 1057 from Woods Hole Oceanographic Institution.

**Present address : Department of Oceanography, University of Washington, Seattle 5, Washington.

In order to elucidate further the fate of nitrogen in anaerobic environments, we have carried out studies on the Cariaco Trench, off the north coast of Venezuela, and on the Dramsfjord, an arm of the Oslofjord in Norway.

THEORETICAL CONSIDERATIONS

The amount of free nitrogen expected from biological sources can be computed from the ratios quoted above and either the phosphate concentration or the sum of the dissolved oxygen consumption (AOU) plus four times the sulphide concentration:

$$N_2^{B\,(P)} = 15\,(PO_4^{\equiv}) - (NH_3 + NO_2^- + NO_3^-) \tag{1}$$

$$N_2^{B\,(0)\,\text{aerobic}} = 0{\cdot}056\,(\text{AOU}) - (NH_3 + NO_2^- + NO_3^-) \tag{2}$$

$$N_2^{B\,(0)\,\text{anaerobic}} = 0{\cdot}064\,(\text{AOU} + 4S^=) - (NH_3 + NO_2^- + NO_3^-) \tag{3}$$

The AOU values are expressed in microgramme atoms per litre and can be estimated from the observed concentrations of oxygen and the equilibrium solubilities of oxygen in sea-water at the observed temperatures and salinities, using the nomogram of RICHARDS and CORWIN (1956), constructed from the solubility results of TRUESDALE *et al.* (1955). The symbols $PO_4^{\equiv}$, $S^=$, NH_3, NO_2^- and NO_3^- are the concentrations of phosphate-phosphorus, sulphide-sulphur, and ammonia-, nitrite-, and nitrate-nitrogen, respectively, in microgramme atoms per litre.

For reasons discussed in the preceding paper (BENSON and PARKER, 1961a), the uncertainties involved in estimating the concentrations of dissolved atmospheric nitrogen are larger than the small amounts of the hypothesized free biogenic nitrogen. Consequently, absolute gasometric determinations of the concentrations of total dissolved nitrogen would yield no information. On the other hand, the method employed by BENSON and PARKER, using dissolved argon as a reference, is particularly appropriate for this problem. The presence of biogenic nitrogen would alter the nitrogen/argon ratios in the dissolved gases, making the ratios larger than if only atmospheric nitrogen were present.

BENSON and PARKER have shown (on the basis of certain assumptions, which, from their results in aerobic waters, seem to be valid) that the measured nitrogen/argon ratios can be used to compute ΔN_2, the amount of nitrogen in excess of that expected from the atmosphere, from the equation

$$\Delta N_2 = \left(\frac{N_2}{A} - \frac{N_2'}{A'}\right) A \tag{4}$$

N_2/A is the measured volumetric nitrogen/argon ratio in the dissolved gas from a sample. N_2'/A' is the ratio of the solubilities of nitrogen and argon in water equilibrated with air at the potential temperature and salinity of the sample. BENSON and PARKER (1961a) have reported preliminary determinations of N_2'/A' vs. temperature and salinity. The absolute concentration of argon dissolved in the sample is denoted by A.

If free biogenic nitrogen is produced, it might be expected to have an isotope ratio, $R_B = {}^{29}N_2{}^B/{}^{28}N_2{}^B$, different from that of the dissolved atmospheric nitrogen (see, for example, HOERING, 1955). Although the proportion of biogenic nitrogen to atmospheric nitrogen in the dissolved gas would be small, its presence might alter the total dissolved nitrogen isotope ratio, R, sufficiently to be detectable with very precise measurements. Furthermore, if biological processes do alter the isotope ratio it is possible to calculate an approximate value for R_B, as follows :

Let R_A and R_S be the isotope ratios in atmospheric nitrogen and in atmospheric nitrogen dissolved in ‘ normal ’ aerobic sea-water. Let δ_S, δ and δ_B be the per mille differences between R_S, R and R_B, respectively, and R_A, *i.e.*,

$$\delta_S \equiv \left(\frac{R_S}{R_A} - 1\right) 10^3, \qquad \delta \equiv \left(\frac{R}{R_A} - 1\right) 10^3, \qquad \delta_B \equiv \left(\frac{R_B}{R_A} - 1\right) 10^3. \tag{5}$$

By definition,

$$R \equiv \frac{{}^{29}N_2{}^S + {}^{29}N_2{}^B}{{}^{28}N_2{}^S + {}^{28}N_2{}^B},$$

or

$${}^{28}N_2{}^S\, R + {}^{28}N_2{}^B\, R = {}^{29}N_2{}^S + \frac{{}^{29}N_2{}^B}{{}^{28}N_2{}^B}\, {}^{28}N_2{}^B.$$

Dividing by ${}^{28}N_2{}^S$, substituting R_S and R_B for their equivalents, and rearranging gives

$$R_B = R + \frac{{}^{28}N_2{}^S}{{}^{28}N_2{}^B}(R - R_S).$$

Upon substituting for R_B, R and R_S from (5) and simplifying :

$$\delta_B = \delta + \frac{{}^{28}N_2{}^S}{{}^{28}N_2{}^B}(\delta - \delta_S).$$

Moreover, to a very good approximation

$$\frac{{}^{28}N_2{}^S}{{}^{28}N_2{}^B} \simeq \frac{N_2{}^S}{\Delta N_2} = \frac{N_2 - \Delta N_2}{\Delta N_2} = \frac{N_2/A - \Delta N_2/A}{\Delta N_2/A} = \frac{N_2'/A'}{N_2/A - N_2'/A'},$$

where equation 4 has been used.

Therefore,
$$\delta_B = \delta + (\delta - \delta_S)\frac{N_2'/A'}{N_2/A - N'_2/A'}. \tag{6}$$

The result is expressed in terms of the δ's rather than the R's since it is δ which is measured with the mass spectrometer.

PROCEDURES, DATA AND RESULTS

Samples were collected in the Dramsfjord on 14 August 1957, and from the Cariaco Trench on 8 and 9 November 1957, for measurements of the dissolved gases. Simultaneous observations of salinity, temperature, dissolved oxygen or sulphide, nitrate, nitrite, ammonia and phosphate were made.

Inorganic phosphates were determined by the method described by WATTENBERG (1937), WOOSTER and RAKESTRAW (1951) and ROBINSON and THOMPSON (1948a). Nitrates were determined by the method of MULLIN and RILEY (1955), ammonia by either the method of RILEY and SINHASENI (1957) or by a modification of ATKINS' (1957) adaptation of the method of KRUSE and MELLON (1953). ROBINSON and THOMPSON (1948b) have described the method used for determining nitrites, and oxygen was determined by the Winkler method. Sulphide analyses were made by a modification of the standard colourimetric method of the American Public Health Association (1946) due to Dr. S. A. el Wardani (private communication).

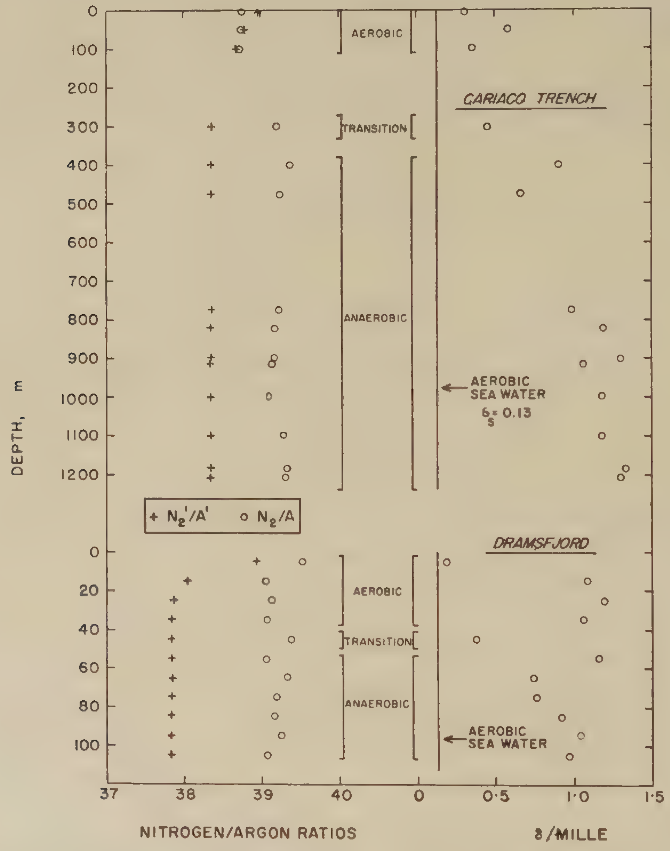

Fig. 1. Vertical distribution of the nitrogen/argon ratios expected from atmospheric gases (N_2'/A') and those observed (N_2/A), and of the values of δ in the Cariaco Trench and Dramsfjord.

BENSON and PARKER (1961a) have described the techniques for obtaining and processing samples of sea-water for dissolved gas analyses, and the mass spectrometric methods used for the N_2/A and $^{29}N_2/^{28}N_2$ ratio measurements. The water samples were stored for several months before the gases were extracted, but we have no reason to believe this had any effect on the dissolved nitrogen or argon in the anaerobic samples. As will be discussed below, it is improbable that biogenic nitrogen can be formed except through the intermediate formation of nitrate, so that any organic matter present in the samples would not be expected to yield N_2 upon its decomposition during storage.

After extraction from the water, the gas was prepared for analysis by immersing the gas sample tubes in liquid air for several minutes and then introducing the gas phase into a vacuum system. There it was cyclically Toepler-pumped through a Vycor furnace filled with pure copper turnings at 700 °C, and a liquid air trap, until all the oxygen was removed. This procedure eliminated any oxides of nitrogen which might have been present, before the gas was introduced into the furnace manifold. The observed excesses of nitrogen, therefore, did not arise from the reduction of oxides of nitrogen.

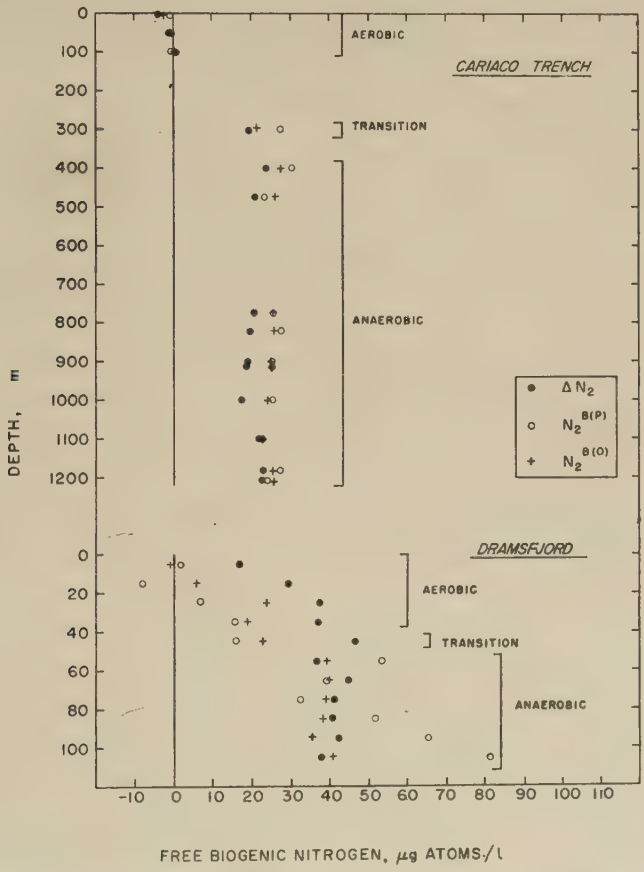

Fig. 2. Vertical distribution of ΔN_2, $N_2^{B(P)}$ and $N_2^{B(0)}$ in the Cariaco Trench and Dramsfjord.

Since the absolute concentration of dissolved argon was not measured, the approximation that A = A′ was used in calculating the values of ΔN_2. The uncertainty of *ca.* ± 5 per cent involved in this approximation (Rakestraw and Emmel, 1938a), corresponded to an uncertainty in ΔN_2 of only about ± 0·01 ml/l for the Cariaco Trench samples and ± 0·02 ml/l for the Dramsfjord samples. The values of A′ given by Benson and Parker (1961b), calculated from their N_2'/A' values and the N_2' values of Rakestraw and Emmel (1938b) were used.

Table 1. *Variables in the Cariaco Trench and Dramsfjord*

Depth (m)	*T* °C	*S*‰	$NO_3^- - N$	$NO_2^- - N$	$NH_3 - N$	$PO_4^{\equiv} - P$	AOU	$S^{=} - S$	N_2/A (*by volume*)	δ‰		Δ N_2 ml/l	Δ N_2 μga/l	N_2B(P)	N_2B(0)	δ_B ‰
Cariaco Trench																
Aerobic Zone :																
5	28·56	35·90	0·10	± 0	3·0	0·15	9	—	38·76	0·31	—	− 0·045	− 4·0	− 0·8	− 2·6	—
50	25·21	36·53	0·07	0·03	1·8	0·10	22	—	38·74	0·50,	0·65	− 0·011	− 1·0	− 0·4	− 0·7	—
100	23·27	36·70	2·17	0·07	2·1	0·27	88	—	38·73	0·21,	0·51	+ 0·009	0·8	− 0·3	+ 0·6	—
Transition Zone :																
300	16·99	36·22	2·39	0·02	2·8	2·19	471	0·04	39·21	0·46	—	0·219	19·6	27·6	21·2	—
Anaerobic Zone :																
400	16·84	36·20	0·21	0·03	3·6	2·27	471	4·1	39·38	0·91	—	0·267	23·8	30·2	27·3	30·2
476	16·84	36·21	1·37	0·05	5·0	2·00	471	10·4	39·25	0·67	—	0·234	20·9	23·6	26·4	23·9
775	16·88	36·18	0·14	—	9·9	2·38	471	21·6	39·24	0·99	—	0·231	20·6	25·7	25·6	38·5
823	16·76	36·17	± 0	—	10·1	2·50	471	21·9	39·18	1·19	—	0·218	19·5	27·4	25·7	50·2
(900)	16·87	36·18	± 0	± 0	10·5	2·41	471	17·7	39·17	1·30	—	0·213	19·0	25·6	24·6	56·7
915	16·81	36·20	± 0	—	10·6	2·42	471	20·4	39·14	1·06	—	0·208	18·6	25·1	25·7	46·2
(1000)	16·82	36·17	± 0	0·07	11·0	2·38	471	24·0	39·09	1·18	—	0·195	17·4	25·2	24·3	55·6
1101	16·89	36·18	± 0	—	11·3	2·26	471	14·5	39·29	1·18	—	0·245	21·9	22·6	22·6	44·5
1184	16.93	36·17	0·12	0·01	8·5	2·38	471	14·8	39·33	1·22,	1·44	0·255	22·8	27·1	25·3	48·8
1208	16·87	36·17	± 0	0·02	8·4	2·15	471	15·3	39·31	1·30	—	0·252	22·5	23·8	25·6	48·0
Dramsfjord																
Aerobic Zone :																
5	17·65	± 0	6·4	0·48	0·2	0·60	114	—	39·52	0·19	—	0·188	16·8	1·9	− 0·7	—
15	8·62	24·88	13·0	± 0	± 0	0·33	337	—	39·05	1·08	—	0·332	29·6	− 8·0	5·9	—
25	6·48	29·81	7·2	± 0	0·6	0·97	570	—	39·12	1·20	—	0·420	37·5	6·8	24·1	—
35	5·98	30·23	9·2	± 0	0·2	1·68	511	—	39·07	1·06	—	0·416	37·2	15·8	19·2	—
Transition Zone :																
45	6·02	30·90	8·3	0·19	0·8	1·68	575	—	39·38	0·38	—	0·522	46·6	15·9	22·9	—
Anaerobic Zone :																
55	6·06	30·90	0·4	± 0	4·4	3·90	619	18·0	39·06	1·13,	1·20	0·412	36·7	53·7	39·4	33·1
65	6·00	30·90	± 0	± 0	3·8	2·87	620	16·0	39·32	0·74	—	0·502	44·9	39·2	40·0	16·3
75	5·89	30·90	± 0	± 0	1·2	2·24	621	2·0	39·19	0·79,	0·74	0·462	41·3	32·4	39·1	18·3
85	5·86	30·90	± 0	± 0	1·8	3·57	622	1·0	39·17	0·92	—	0·456	40·7	51·8	38·3	23·2
95	5·84	30·99 (?)	± 0	± 0	5·3	4·73	623	4·0	39·23	1·04	—	0·476	42·5	65·6	35·6	25·6
105	5·83	30·90	± 0	± 0	8·8	6·03	623	38·0	39·08	0·97	—	0·425	38·0	81·6	40·8	26·4

N.B.—Bracketed depths are estimated.

Concentrations, except as indicated, given in microgramme atoms per litre.

In aerobic sea-water, BENSON and PARKER have found a very small, but perhaps significant, difference between R_S and R_A, corresponding to $\delta_S = 0{\cdot}13‰$. This value was used in calculating the values of δ_B in anaerobic waters, but even if the δ_S they found was an artifact arising from a very small systematic error in the isotope ratio measurements, the effect on the calculated values for δ_B would be negligible. (The isotope ratios reported in this paper were measured under identical conditions and concurrently with those reported by BENSON and PARKER, so that if the $\delta_S = 0{\cdot}13‰$ value is too high, our δ values are also high by the same amount. Consequently, the factor $(\delta - \delta_S)$ in the dominant second term in equation 6 would remain unchanged).

The observations of depth, temperature, salinity, chemical variables, nitrogen/argon ratios, and δ values are shown in the first eleven columns of Table 1. As in the Cariaco Trench, the quantities of nitrate and nitrite were negligible in the anaerobic parts of the Dramsfjord. Nitrogen/argon ratios and δ values are plotted against depth in Fig. 1. Values of ΔN_2, $N_2^{B(P)}$, $N_2^{B(0)}$ and δ_B, calculated from the basic data, are entered in the final columns of Table 1. Fig. 2 is a graphical comparison of the values of ΔN_2, $N_2^{B(P)}$ and $N_2^{B(0)}$.

ERRORS

The sources of error in the determination of ΔN_2 have been discussed by BENSON and PARKER (1961a, 1961b). On the basis of their results, we would estimate random errors of approximately ± 5 and ± 7 μga/l (or ± 0·06 and ± 0·08 ml/l) for the Cariaco Trench and Dramsfjord, respectively. From the uncertainties in the chemical determinations, we estimate random errors in $N_2^{B(P)}$ and $N_2^{B(0)}$ of ± 2·5 and ± 1·4 μga/l, respectively, in the anaerobic parts of the Cariaco Trench, and for the corresponding Dramsfjord quantities, ± 5·6 and ± 4·8 μga/l. It is evident from the data that, in the anaerobic zones, the variations of ΔN_2, $N_2^{B(P)}$ and $N_2^{B(0)}$ must be considered to be the result of random errors in measurement. The one exception, $N_2^{B(P)}$ in the Dramsfjord, will be discussed below.

Table 2. Summary of the mean values, and standard deviations from the mean, for ΔN_2, $N_2^{B(P)}$, $N_2^{B(0)}$ *and* δ_B *in the anaerobic zones of the Cariaco Trench and the Dramsfjord*

	μga/l						‰	
	ΔN_2	*Std. Dev.*	$N_2^{B(P)}$	*Std. Dev.*	$N_2^{B(0)}$	*Std. Dev.*	δ^B	*Std. Dev.*
Cariaco Trench	20·7	1·8	25·6	2·2	25·3	1·3	44	11
Dramsfjord	40·7	3·0	54·0	18·0	38·9	1·8	24	6

Table 2 is a summary of the mean values, and the standard deviations from the means, of ΔN_2, $N_2^{B(P)}$, $N_2^{B(0)}$ and δ_B, in the anaerobic regions of the Cariaco Trench and the Dramsfjord. The standard deviations in ΔN_2 are much smaller than the estimated random errors. This may have resulted from better sampling techniques than those employed in the work of BENSON and PARKER, from the more homogeneous origin of the anaerobic waters, or both.

Any possible systematic error in N_2'/A', associated with the calibration of the mass spectrometer (BENSON and PARKER, 1961b), would cause no error in the calculated values for ΔN_2, since the same calibration was used in the present measurements. On the other hand, it is estimated that their choice of a linear least squares solution for N_2'/A' vs. temperature might lead to a systematic error in ΔN_2 of up to 4 μga/l in the Cariaco Trench and 6 μga/l in the Dramsfjord, depending upon the temperature. This, together with systematic errors in the AOU values, and in the value for the N : P ratio chosen, could explain the fact that the mean ΔN_2 in the anaerobic Cariaco Trench is slightly smaller than the mean $N_2^{B(P)}$ or $N_2^{B(0)}$, even though the mean values of ΔN_2 and $N_2^{B(0)}$ are essentially equal in the Dramsfjord.

The dominant second term in equation 6 contains the ratio of two small differences, so that even very small errors will affect δ_B considerably. For example, if the mean ΔN_2 for the anaerobic Cariaco samples were increased by 4 μga/l (to be nearly equal to the mean $N_2^{B(0)}$), the mean δ_B would decrease to approximately 37‰.

DISCUSSION

The hypothesis that free molecular nitrogen of biogenic origin is released in anaerobic zones seems to be confirmed by the observations. In the Cariaco Trench, the calculated values of ΔN_2 and N_2^B are in good agreement throughout the water column. The negative values in the aerobic zone, and the differences between the mean values of ΔN_2 and of N_2^B in the anaerobic zone are probably not significant.

In the anaerobic zone of the Dramsfjord, the values of ΔN_2 and $N_2^{B(0)}$ agree very well, but as noted above, the mean value of $N_2^{B(P)}$ is high, with large, statistically significant fluctuations in the individual values. Other observations made in the fjord throughout the preceding year show that the nitrogen to phosphorus ratio there is highly variable and reaches extreme values. It is apparent that neither the nitrogen to phosphorus ratio used (N : P = 15), nor any constant ratio of nitrogen to phosphorus, is applicable in this environment. The fjord receives domestic sewage from the city of Drammen and wastes from wood pulp manufacture (BRAARUD *et al.* 1958). Under these circumstances, it may be merely fortuitous that the biogenic nitrogen computed from the consumption of oxygen is in agreement with the values of ΔN_2. It is more likely, however, that the C : N ratios in the decomposing organic matter are near the ‘ normal ’ 7 : 1 ratio found in plankton organisms, while the phosphate contribution varies independently.

The excesses of free nitrogen, ΔN_2, found in the aerobic zone in the Dramsfjord could be the result of the mixing of aerobic and anaerobic waters. Fig. 3 shows the distribution of oxygen and sulphides at this location (Station bm of BRAARUD *et al.*, 1958) from November, 1956, until the time of the observations. In the last two months of 1956, a sulphide zone was centred at about 40 m, and extended upward to about 30 m (as determined by FØYN's 1955 oxygen recording device). During the year 1957, the layer was mixed with aerated water, a process which would destroy the sulphides (and perhaps ammonia) by oxidation, but would leave the previously formed free biogenic nitrogen unaffected, except by dilution. Neither Equation (2) nor (3) would be applicable in such a mixture of anaerobic and aerobic waters, but would yield values smaller than the actual ΔN_2, especially if the sulphides are oxidized only to free sulphur instead of all the way to sulphates. The observed values of ΔN_2 and $N_2^{B(0)}$ in the aerobic zone indicate such an effect, although the differences are larger than would be predicted. (Despite the fact that the Dramsfjord samples were ' poisoned ' with mercuric chloride, it is possible that some free nitrogen was formed in the samples from the aerobic zone between the time of collection and analysis. However, the aerobic Cariaco Trench samples were stored without poisoning, and the values of ΔN_2 and $N_2^{B(0)}$ agree quite well). A similar mixing of aerated and anaerobic waters apparently accounts for the biogenic nitrogen found at 300 m in the Cariaco Trench.

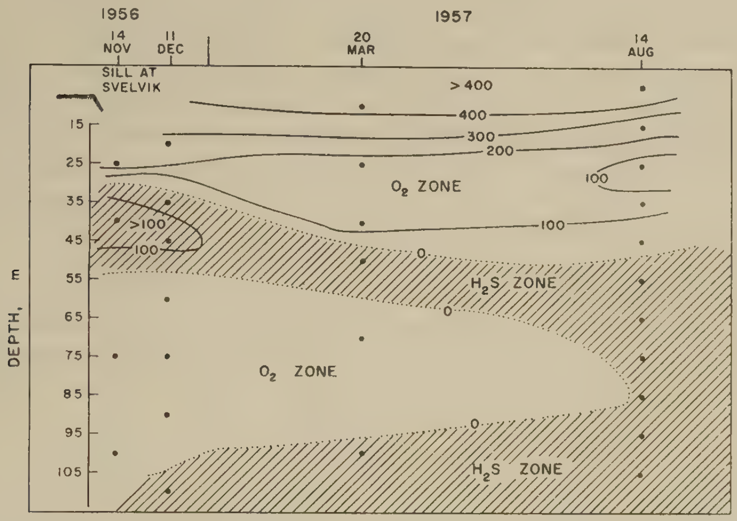

FIG. 3. Vertical distribution of sulphides and dissolved oxygen at station bm in the Dramsfjord, 14 November 1956–14 August 1957. Concentrations are in microgramme atoms per litre.

The hypothesis that biogenic nitrogen is released as dissolved gas is further substantiated by the fact that the nitrogen isotope ratio in the anaerobic zones is different from that in ' normal ' aerobic sea-water. Although the accuracy of the calculated values for δ_B is low, it is believed that the difference in the mean values of 44‰ and 24‰ for the Cariaco Trench and the Dramsfjord is significant, a result which might be expected from the difference in the sources of organic material. Both values for δ_B are large compared with other values given in the literature. HOERING (1955), for instance, found a range of − 13 to + 13‰. Among the animal and plant proteins he analyzed, the largest value was 8·1‰ for seaweed from Tokyo Bay.

THE MECHANISM OF NITROGEN FORMATION

The anaerobic production of free N_2 from organic matter, in which it can be assumed that the nitrogen is present in the reduced (amino, $-NH_2$) form, is an overall oxidation, but the most probable pathway is *via* the reduction, or denitrification, of nitrate-nitrogen, since this is the only known metabolic pathway (FRY, 1955). However, direct anaerobic conversion of $-NH_2$ to N_2, with sulphate ion as the oxidant, might occur concurrently with, or subsequently to, the nitrate reduction. The data from the Cariaco Trench make it possible to examine this question, and to conclude that the direct oxidation does not take place.

Assume that the Cariaco Trench was at one time filled with water containing oxygen and nitrate in the approximate concentrations now found at sill depth (150 m) in the nearby open Caribbean, *i.e.*, about 7 μga/l of nitrate-nitrogen and 3 ml/l, or about 270 μga/l of dissolved oxygen. The disappearance of this quantity of oxygen would be accompanied by the oxidation of additional organic matter, giving rise to an additional 15 μga/l of nitrate-nitrogen (AOU : N = 270 : 15). Therefore, at the time the water became anaerobic the total nitrate-nitrogen available was 22 μga/l. The reduction of this nitrate to the observed zero would release 22 μga/l of free nitrogen, which is essentially equal to the observed mean value of ΔN_2 of 20·7 μga/l. It is evident that direct oxidation of amino-nitrogen to free nitrogen by sulphate does not *accompany* the reduction of nitrate, because otherwise ΔN_2 would be significantly larger. It is also unlikely that the sampling was carried out at the moment when the nitrate was all just reduced, and before direct oxidation could occur. Therefore, it follows within experimental errors, that direct oxidation does not take place. Were significantly higher concentrations of ΔN_2 present, it would be necessary to examine further the possibility of the direct oxidation.

The requirement for the intermediate formation of nitrate ion accounts for the essentially uniform distribution of biogenic nitrogen in the anaerobic part of the trench (just as the salinity is essentially uniform), although neither ammonia nor sulphides are uniformly distributed. The relatively high concentrations of ammonia now present have presumably accumulated from hydrolysis reactions (involving no oxidation of nitrogen), following the disappearance of the oxygen and nitrogen. Simultaneously, the oxidation of the organic residues, stripped of their amino groups, proceeds, with sulphate ions as the oxidant, giving rise to the accumulation of carbonates, phosphates and sulphides. Thus, there is no necessary relationship between the distribution of biogenic nitrogen and sulphides or ammonia, although there should be a direct relationship between the distribution of sulphides and ammonia.

Note added in proof.

The word " anaerobic " used in this paper and by RICHARDS and VACCARO (1956) is a misnomer since the word properly is applicable only to living bodies. The word ' anaeric (ally) ' was proposed by WILEN (WILEN, F., 1929. Use of the word " anaeric " proposed. *Ind.-Eng. Chem.*, News Ed. **1**, No. 17, p. 8) for the adjectival and adverbial motion of mere freedom from, or performance in the absence of, free oxygen. In describing this notion, the word ' anoxic ' appears more accurate, because the other gases found in air may be present. The words anoxic and anoxia, having a precedent in medical terminology, imply solely the absence of oxygen and their use is recommended.

Acknowledgements—Both authors wish to thank the John Simon Guggenheim Foundation for fellowship awards which made possible the work of one (R) in Norway, and part of the work of the other (B) at Woods Hole. The co-operation of the Director and personnel of Universitetet Biologiske Laboratorium of the University of Oslo made the work on the Dramsfjord not only possible but a real pleasure. Special thanks are due to Dr. ERNST FØYN, L. A. E. DOE, NATHANIEL CORWIN, RALPH VACCARO, PETER D. M. PARKER and Dr. EVA M. KUHN, who gave invaluable help in the various analyses, to the Captain and Company of R.V. *Atlantis*, and to Captain H. HØIUM of M/C *Gunnar Knudsen*. Part of the work was supported by the Office of Naval Research, Contract Nonr-2196 (00) NR 083-004 with the Woods Hole Oceanographic Institution and part by the National Science Foundation under Grant G-4650 to Amherst College.

Woods Hole Oceanographic Institution,
Woods Hole, Mass., U.S.A. and
Amherst College,
Amherst, Mass., U.S.A.

REFERENCES

AMERICAN PUBLIC HEALTH ASSOCIATION (1946) *Standard methods for the examination of water and sewage.* 9th Ed. Amer. Publ. Health Assn., N.Y.

ATKINS W. R. G. (1957) The direct estimation of ammonia in sea water, with notes on nitrate, copper, zinc and sugars. *J. du. Cons.* **22**, 271-277.

BENSON B. B. and PARKER P. D. M. (1961a) Nitrogen/argon and nitrogen isotope ratios in aerobic sea water. *Deep-Sea Res.*

BENSON B. B. and PARKER P. D. M. (1961b) Relations among the solubilities of nitrogen, argon and oxygen in distilled water and sea water.

BRAARUD T., FØYN B. and HASLE G. R. (1958) The marine and fresh-water phytoplankton of the Dramsfjord and the adjacent part of the Oslofjord March-December 1951. *Hvalrådets Skr.*, No. 43, 102 pp.

COOPER L. H. N. (1938) Redefinition of the anomaly of the nitrate-phosphate ratio. *J. Mar. Biol. Assoc. U.K.* **23**, 179.

FLEMING R. H. (1940) The composition of plankton and units for reporting populations and production. *Proc. Sixth Pac. Sci. Congr. Calif.* 1939 **3**, 535-540.

FØYN E. (1955) Continuous oxygen recording in sea water. *Rept. Norweg. Fish. Mar. Inves.* **11**, No. 3, 88 pp.

FRY B. A. (1955) *The nitrogen metabolism of micro-organisms.* Methuen and Co. Ltd., London ix + 166 pp.

HOERING T. C. (1955) Variations of nitrogen-fifteen abundance in naturally occurring substances. *Science* **122**, 1233-1234.

KRUSE J. and MELLON M. G. (1953) Colorimetric determinations of ammonia and cyanate. *Anal. Chem.* **25**, 1188-1192.

MULLIN J. B. and RILEY J. P. (1955) The spectrophotometric determination of nitrate in natural waters, with particular reference to sea water. *Analyt. Chim. Acta.* **12**, (5), 464-480.

RAKESTRAW N. W. and EMMEL V. M. (1938a) The relation of dissolved oxygen to nitrogen in some Atlantic waters. *J. Mar. Res.* **1**, 207-216.

RAKESTRAW N. W. and EMMEL V. M. (1938b) The solubility of nitrogen and argon in sea water. *J. Phys. Chem.* **42**, 1211-1215.

REDFIELD A. C. (1934) *On the proportions of organic derivatives in sea water and their relation to the composition of plankton.* In *James Johnstone Memorial Vol.* Univ. Press of Liverpool, pp. 176-192.

REDFIELD A. C. (1942) The process determining the concentrations of oxygen, phosphate and other organic derivatives within the depths of the Atlantic Ocean. *Pap. Phys. Oceanogr. Meteorol.* **9**, No. 2, 22 pp.

RICHARDS F. A. and CORWIN N. (1956) Some oceanographic applications of recent determinations of the solubility of oxygen in sea water. *Limnol. and Oceanogr.* **1**, No. 4, 263-267.

RICHARDS F. A. and VACCARO R. F. (1956) The Cariaco Trench, an anaerobic basin in the Caribbean Sea. *Deep-Sea Res.* **3**, No. 3, 214-228.

RILEY J. P. and SINHASENI P. (1957) The determination of ammonia and total ionic inorganic nitrogen in sea water. *J. Mar. Biol. Assoc. U.K.* **36**, 161-168.

ROBINSON R. J. and THOMPSON T. G. (1948a) The determination of phosphates in sea water. *J. Mar. Res.* **7**, No. 1, 33-41.

ROBINSON R. J. and THOMPSON T. G. (1948b) The determination of nitrites in sea water. *J. Mar. Res.* **7**, No. 1, 42-48.

TRUESDALE G. A., DOWNING A. L. and LOWDEN G. F. (1955) The solubility of oxygen in pure water and sea water. *J. Appl. Chem.* **5**, 53-62.

WATTENBERG H. (1937) Critical review of the methods used for determining nutrient salts and related constituents in sea water. I Methoden zur Bestimmung von Phosphat, Silikat, Nitrit, Nitrat, und Ammoniak im Seewasser. *Rapp. Proc. Verb. Cons. Perm. Int. Explor. Mer.* **103**, 1-26.

WOOSTER W. S. and RAKESTRAW N. W. (1951) The estimation of dissolved phosphate in sea water. *J. Mar. Res.* **10**, No. 1, 91-100.

Printed in Great Britain by The Salisbury Press Ltd., Publicity House, Wilton Road, Salisbury Wilts. (27335)

Contribution No. 1063

(*Reprinted from Nature, Vol.* 191, *No.* 4784, *pp.* 161–162,
July 8, 1961)

Fossil Chlorins in a Triassic Sediment*

SPECTROSCOPIC evidence for the presence of green chlorophyll-derivatives in ancient sediments and crude oils has been reported by Treibs[1] and by Blumer[2]. We have now succeeded in isolating and characterizing the green pigments responsible for the absorption band at about 640 mμ in the extracts of the porphyrin-rich Triassic oil-shale from Serpiano (Switzerland) (Fig. 1*A*). The pigments are isolated by first removing from the extracts the asphaltenes by iso-octane precipitation and extracting the ether solution of the pigment-concentrate with 6 *N* hydrochloric acid. Subsequent partitioning between ether and hydrochloric acid of increasing concentration removes the stronger bases deoxophyllerythroetioporphyrin (DPEP) and meso-etioporphyrin (MEP). The final purification of the green pigment is then accomplished by repetitive chromatography over partially deactivated alumina (Brockman III). The spectrum of the pure pigment (Fig. 1*B*) is characteristic of the chlorin (dihydroporphin) configuration, and the partial resolution of the band at 490 mμ in addition to the presence of a small band at 612 mμ is indicative of a meso-chlorin, a chlorophyll-derivative in which the vinyl-group in the 2-position has been hydrogenated to an ethyl-group[3]. The high chromatographic mobility of this pigment on alumina and on paper ($R_F = 0 \cdot 75$ on Whatman No. 3 paper, carbon tetrachloride–iso-octane developer, 7 : 3, see ref. 4) eliminates the possibility of the presence of acid-, ester- and other polar groups like —COH, —CO, —OH.

The pigment, which is thus characterized as a meso-etiochlorin, can be converted to the corresponding porphin by dehydrogenation with excess chloranil in boiling xylene. The reaction product (Fig. 1*C*) exhibits a typical porphyrin spectrum, intermediate between those of DPEP and MEP and identical with that of the DPEP/MEP-mixture present as uncomplexed pigments in the same sediment. This dehydrogenation product can be resolved by chromatography over alumina into fractions with the etio-spectrum of MEP and phyllo-spectrum of DPEP. Paper chromatography of these fractions confirms the spectroscopic evidence, the R_F-values agreeing within $\pm 0 \cdot 01$ unit with those for pure DPEP and MEP.

For additional structural confirmation, the unknown dihydroderivative of DPEP was synthesized

---

* Contribution Number 1063 of the Woods Hole Oceanographic Institution.

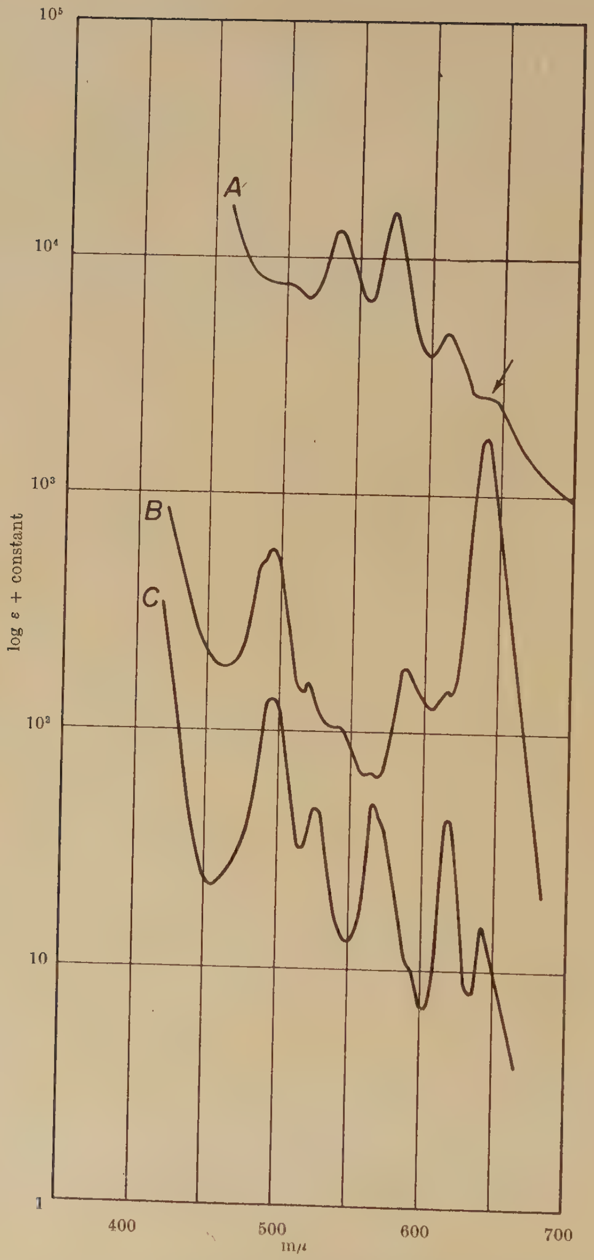

Fig. 1. Spectra. *A*, Benzene–methanol extract of Serpiano oil-shale; *B*, natural dihydro-DPEP containing some dihydro-MEP; *C*, porphyrin mixture obtained by dehydrogenation; the small peak at 641 mμ is a trace of residual chlorin

by hydrogenating with Raney-nickel a DPEP concentrate isolated from the oil shale. The spectrum of the hydrogenation product is identical to that of the fossil chlorin. A small difference in the R_F-values (0·68 for the synthetic compound, compared with 0·75 for the natural chlorin) is explained by the presence of a larger fraction of the more rapidly moving dihydro-MEP in the natural pigment.

Thus, the fossil chlorin is characterized as a mixture of dihydro-DPEP (deoxo-meso-etio-pyro-pheophorbide *a*) with some dihydro-MEP (etiochlorin III). The etiochlorin must have been formed by intensive reduction from hæmin, protoporphyrin, mesoporphyrin and meso-etioporphyrin being intermediates. The chlorin structure of dihydro-DPEP is also more likely to be of secondary than of primary origin. The vinyl-group of the chlorophyll-pigments disappears early in geological history, probably by isomerization of the vinyl-chlorins to meso-porphyrins. Any meso-chlorins that might be formed at this stage would be re-oxidized to meso-porphyrins because of their extremely low redox-potential. Only much later, after complete reduction of all carbonyl-groups, can the porphyrin-system be partially reduced with formation of the fossil chlorins.

A more detailed report of this work is being prepared for publication elsewhere. This investigation has been supported by a research contract with the United States Office of Naval Research (Contract *NONR*-2196 (00)) and the grant of a summer fellowship to one of us (G. O.).

MAX BLUMER
GILBERT OMENN

Woods Hole Oceanographic Institution,
Woods Hole,
Mass.

---

[1] Treibs, A., *Ann.*, **517**, 172 (1935); *Angew. Chem.*, **49**, 682 (1936).
[2] Blumer, M., *Helv.*, **33**, 1627 (1950).
[3] Stern, A., and Pruckner, F., *Z. phys. Chem.*, A, **180**, 321 (1937).
[4] Blumer, M., *Anal. Chem.*, **28**, 1640 (1956).

Printed in Great Britain by Fisher, Knight & Co., Ltd., St. Albans

Contribution No. 1066

Reprinted from THE JOURNAL OF THE ACOUSTICAL SOCIETY OF AMERICA, Vol. 33, No. 1, 85–88, January, 1961
Copyright, 1961 by the Acoustical Society of America.
Printed in U. S. A.

Comparison of Directly Measured Sound Velocities with Values Calculated from Hydrographic Data*

EARL E. HAYS
Woods Hole Oceanographic Institution, Woods Hole, Massachusetts
(Received June 16, 1960)

Hydrographic data (temperature, salinity, depth) and directly measured sound velocities were obtained from a section made at 6°E across the Mediterranean Sea in June and July, 1959. Sound velocities were calculated from the hydrographic data and compared with the measured values. Two methods were used to calculate the sound velocity from the hydrographic data. One method used Del Grosso's zero depth values with the depth correction from Matthew's tables. (This has been the usual method of calculation at the Woods Hole Oceanographic Institution until now.) The other method used the empirical equation of Wilson derived from laboratory measurements made at the Naval Ordnance Laboratory. The significant difference observed in the comparisons appears below 200 m. Here the corrections using Matthew's tables result in too large values for the velocities at depth, the magnitude of the difference being about 2.5 m/sec at 2500 m depth. The calculated values from Wilson's equation agree with the experimental values more closely (about 0.5 m/sec difference at 2200 m depth).

INTRODUCTION

WO important advances have recently taken place
that affect the study of the sound velocity distri-
n in the oceans. One has been the development of
nd velocimeter by Greenspan and Tschiegg[1] at the
onal Bureau of Standards capable of measuring
d velocities to within 0.3 m/sec, at any depth in
oceans (unit is tested at 16 000 psi). The other
nce has been the careful measure in the laboratory
und velocity in sea water as a function of tempera-
pressure, and salinity, and the fitting of an
rical equation to the data by Wilson[2] at the Naval
ance Laboratory.

is unlikely that the density of sound velocimeter
rings in the ocean will approach that of hydro-
hic stations for some time so that velocity infor-
on will continue to depend upon existing hydro-
hic data. For this reason we have made a com-
on of sound velocities as measured *in situ* with
calculated from hydrographic data taken as
ly as possible at the same locations and times.

e measurements were made at seven locations
ning the width of the Mediterranean Sea at 6°E in
and July, 1959. The work was done from the
ds Hole Oceanographic Institution's (WHOI) Re-
h Vessel USNS *Chain*, Captain W. Olivey,
nanding.

PROCEDURE

each location the ship would maneuver in such a
ner as to maintain the wire in a vertical position.
hydrographic station was made, followed immedi-
by the sound velocimeter lowering. The total time
station averaged about three hours.

A hydrographic station is made by collecting water samples from various depths. By using two thermometers on each bottle (one protected from the pressure) it is possible to measure the pressure (depth) of each bottle and the ambient temperature at the time the sample is collected.[3] Aboard ship the salinity of each sample is determined[4] as well as other properties of interest (O_2, PO_4, etc.). The amount of wire paid out with the bottles is also measured but the depth-wire out relation is modified by the wire attitude. In addition for this series of hydrographic stations the depths of the deep samples (>1350 m) were measured by a sonic method.[5]

The depth of the sound velocimeter was measured by the sonic method only. The recordings of the depths are based on a sound velocity of 4800 ft/sec and the true depths are derived from these using the measured sound velocity values.

The sound velocimeter[6] is of the "sing-around" type, and its use in deep water has been described. In these measurements the procedure was to lower the instrument steadily at a rate near 1.5 m/sec while averaging the velocity-of-sound measurement over every other second. The raising procedure consisted of making several 10-sec counting-period measurements with the velocimeter held steady near the depth of each deep water sample taken.

DATA

A typical plot of sound velocity versus depth for one lowering is given in Fig. 1. The continuous curves are plotted from the 1-sec averages from the descent and the circle's are from the 10-sec averages of the ascent.

Contribution No. 1066 from the Woods Hole Oceanographic
tution. This work was supported by the Office of Naval
arch and the Bureau of Ships.

I. Greenspan and C. Tschiegg, Rev. Sci. Instr. **28**, 897 (1957).

V. Wilson, U. S. Naval Ordnance Laboratory, Reports 6746,
(1959); J. Acoust. Soc. Am. **31**, 1067 (1959); **32**, 641 (1960).

[3] H. Sverdrup, M. Johnson, and R. Fleming, *The Oceans* (Prentice-Hall, Inc., Engelwood Cliffs, New Jersey, 1942), pp. 347–350.

[4] A. Bradshaw and C. Schleicher, Woods Hole Oceanog. Inst. Ref. No. 56-20 (unpublished).

[5] H. Edgerton and J. Cousteau, Rev. Sci. Instr. **30**, 1125 (1959).

[6] C. E. Tschiegg and E. Hays, J. Acoust, Soc. Am. **31**, 1038 (1959).

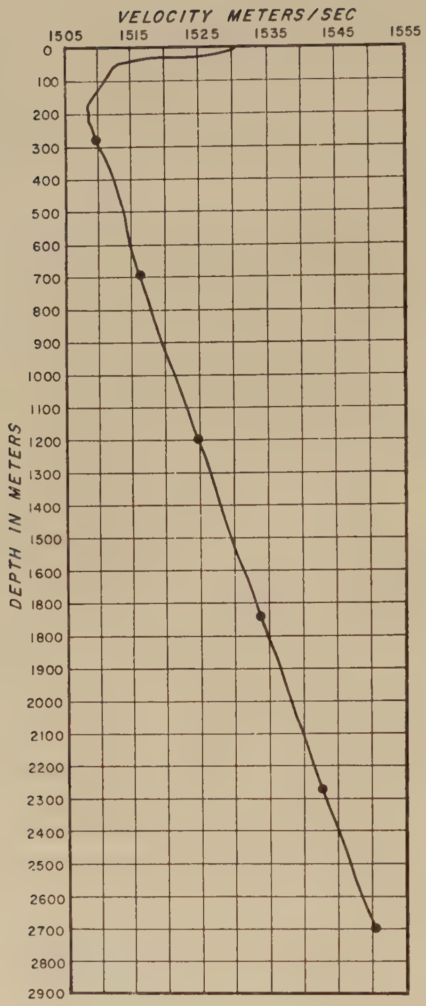

FIG. 1. Sound velocity profile.

Figure 2 is a plot of the difference between the sound velocity values calculated by the Del Grosso-Matthews method and the directly measured values.

Figure 3 is a plot of the differences between the sound velocity values calculated using Wilson's equation and the directly measured values. Wilson's equation is based on measurements in the salinity range $33^0/_{00}$–$37^0/_{00}$ and we are taking some liberty in extrapolating for $38.4^0/_{00}$ water. The numbers on the curves refer to the oceanographic stations at which the data were collected.

ERRORS

Lateral motion of the ship guarantees that the measurements taken by the sound velocimeter and the collection of water samples did not occur at exactly the same location. The trends of the differences indicate that this is not a serious situation except in the shallower measurements (1, 50, and 100 m). The sizable differences occurring in these measurements can be attributed to variations in water structure in the
horizontal direction or possibly to depth measuren
errors, as the thermal gradients are largest in t
regions.

The error in the depth measurement when the s
method is used for both hydrographic and velocim
depths is dominated by any change in total depth of
water during the run. The depth is given by total w
depth minus height above bottom. The water depth
checked periodically and we assign a maximum e
here of 3 m. The error in the actual measurement of
travel times associated with these depths is a facto
three smaller. An error of 3 m in depth represent
error in sound velocity of 0.05 m/sec.

These measurements started out to compare a velo
profile obtained with ordinary hydrographic techn
with that obtained from the velocimeter using s
depth determinations. Figure 2 is plotted on this ba
that is, the depth determination for the hydrogra
values were from the hydrographic data. Included is
run in which the water depth changed apprecia

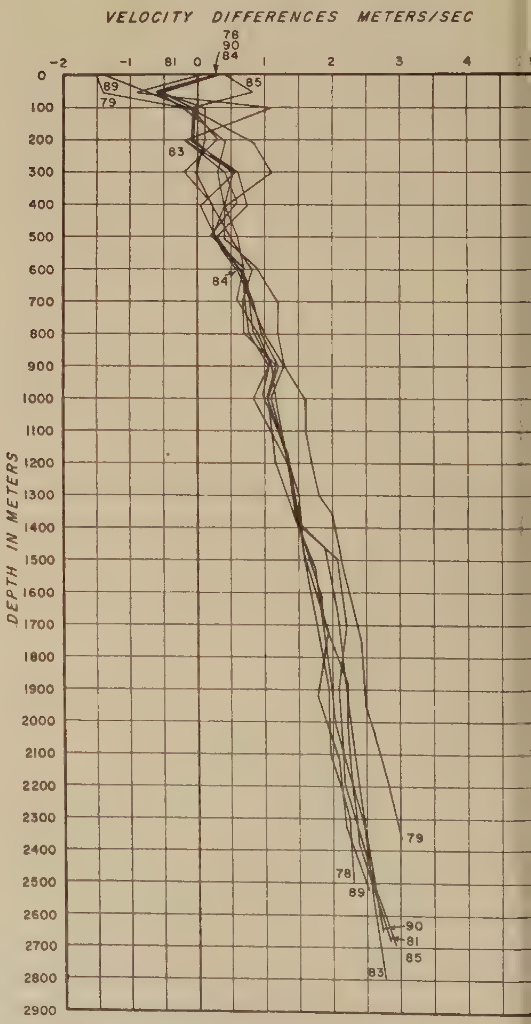

FIG. 2. Sound velocity differences, Del Grosso-Matthew
minus directly measured values.

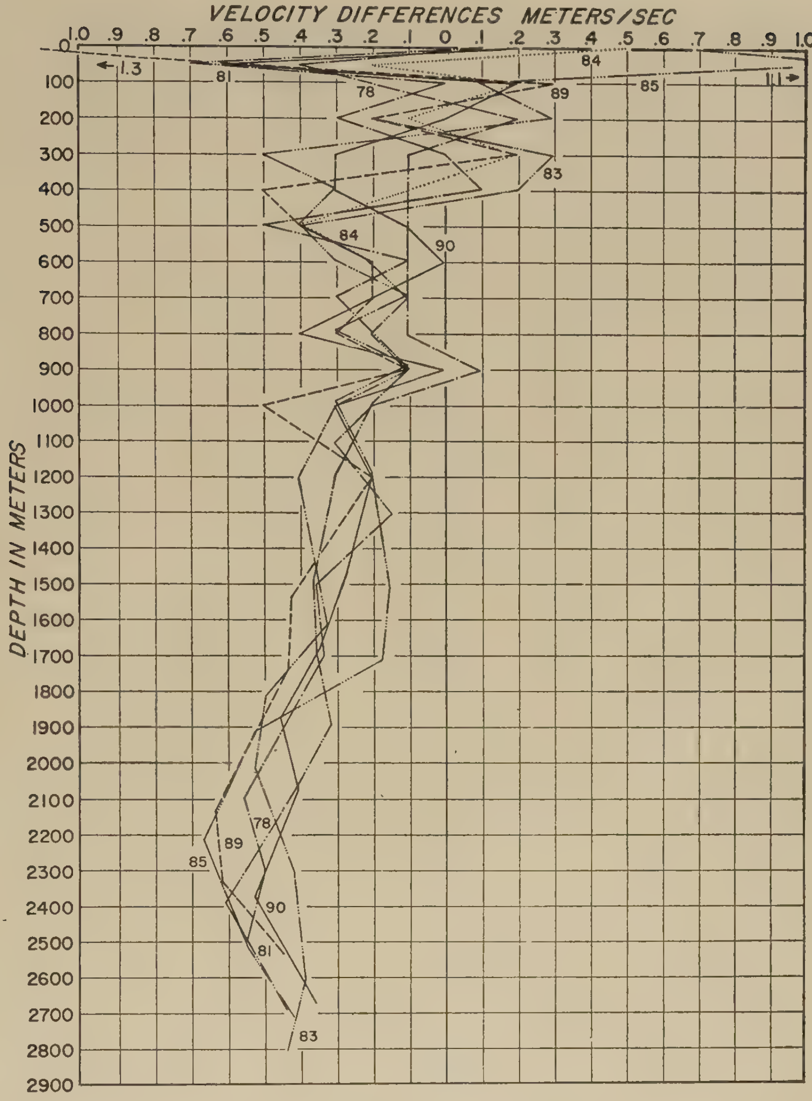

IG. 3. Sound velocity differ-
es. Wilson's equation minus
ectly measured values.

Dow of Woods Hole has just developed an upside echo sounder that measures depth rather than t above the bottom, thus eliminating this problem e future.) We had just completed the above when ere informed of Wilson's work and realized that our could be used to compare field measurements with atory measurements. Therefore, in Fig. 3 all depths er than 1350 m are based on sonic measurements r than hydrographic data. For depths less than hydrographic data was used in the calculated ities. The rms deviation between the sonic depths hydrographically calculated depths for all those ter than 1350 m was 7.8 m which was another tity we were interested in checking.

mperatures of the water samples are measured to C and we assign a maximum error of 0.03°C, h means a change in the sound velocity about m/sec.

e salinity values are read to 0.01 parts per thousand and an error of 0.03 parts per thousand is assigned. The resulting variation in sound velocity is about 0.03 m/sec.

To use Wilson's equation, depths must be converted to pressures. This conversion was made using tables Wilson constructed from data given in Dorsey.[7] This again required extrapolation and a gravitational correction.

In view of the two extrapolations used, the total sum of error in measurement for the calculated values, that is depth, temperature, and salinity, totaling 0.18 m/sec seems small.

The sound velocimeter was calibrated before the cruise and was within ±0.15 m/sec of the values for distilled water given by Greenspan and Tschiegg.[8] At the end of the cruise the instrument was calibrated at several temperatures and was 0.25 m/sec lower than Greenspan's and Tschieggs' values. A subsequent check recently after considerable more use at sea has shown an increase in this trend. Thus during this particular cruise the instrument has a variation of ±0.15 m/sec with a possible mean drift of 0.00 to −0.25 m/sec in relation to our reference.

---

[7] N. Dorsey, Am. Chem. Soc. Monograph No. 81 (Reinhold Publishing Corporation, New York, 1940), pp. 249–250.

[8] M. Greenspan and C. E. Tschiegg, J. Research Natl. Bur. Standards 59, 249 (1957).

There are two corrections that can be made to the sound velocimeter data. One compensates for the change in path length with temperature, and this correction was made, using the temperature data from the hydrographic stations. The correction ranges from 0.33 to 0.55 m/sec, and the error introduced by temperature uncertainties is small. A pressure correction for the change in path length was not made, as this is only −0.025 m/sec at the 2500 meter depth.

Figure 3 seems to be consistent with the foregoing errors as far as the spread in the data goes, that is, if we take the rms of the random errors involved, most of the spread is within this value except near the surface, with some embarrassment at the 300 and 400 m depths. The sudden jog at 900 m is most easily explained by a faulty thermometer. Reconciling the data to Wilson's equation is not as satisfactory.

The instrument at depth was reporting a sound velocity greater than that predicted by Wilson, for example at 2200 m the difference is about 0.5 m/sec. At this temperature, approximately 13°C, Greenspan's and Tschiegg's distilled water values at atmosphere pressure are lower than those of Wilson and Del Grosso b proximately 0.2–0.3 m/sec. This coupled with the drift of the instrument, using 0.25 m/sec can mea the instrument is giving a value 1.00 m/sec highe Wilson's value. We do not believe these difference be resolved at the present time.

CONCLUSIONS

As Wilson's equation and the velocimeter agree closely at depth than do the Del Grosso-Matthew velocimeter comparison, we believe the Matt depth correction to be in error. In using the veloci as the standard, the error in m/sec is approximatel thousandth of the depth in meters. The differ between the velocimeter and Wilson's equation only be resolved by future work under carefully trolled conditions.[9]

ACKNOWLEDGMENTS

In conclusion the author wishes to acknowledg efforts of many others; David McGill of WHOI was in charge of the hydrographic stations and ana Mrs. Betty Curl and R. Brockhurst of WHOI sup the calculated values of *S*/*V*, C. Tschiegg of NB W. Wilson of USNOL supplied prepublication data Dennis Moore of WHOI helped on the veloci lowerings and computations.

---

[9] K. V. Mackenzie, J. Acoust. Soc. Am. 32, 100 (1960).

Contribution No. 1072

UNITED STATES DEPARTMENT OF THE INTERIOR, Stewart L. Udall, *Secretary*
FISH AND WILDLIFE SERVICE, Clarence F. Pautzke, *Commissioner*
BUREAU OF COMMERCIAL FISHERIES, Donald L. McKernan, *Director*

CALANOID COPEPODS FROM EQUATORIAL WATERS OF THE PACIFIC OCEAN

By GEORGE D. GRICE

March 3, 1849

FISHERY BULLETIN 186
From Fishery Bulletin of the Fish and Wildlife Service
VOLUME 61

Issue date - Jan. 25, 1962

[Contribution No. 1072, Woods Hole Oceanographic Institution]
Published by the U.S. Fish and Wildlife Service • 1961
Printed at the U.S. Government Printing Office, Washington

For sale by the Superintendent of Documents, U.S. Government Printing Office,
Washington 25, D.C.—Price 45 cents

Library of Congress catalog card for the series, Fishery Bulletin of the Fish and Wildlife Service:

U. S. *Fish and Wildlife Service.*
Fishery bulletin. v. 1–
Washington, U. S. Govt. Print. Off., 1881–19

v. in illus., maps (part fold.) 23–28 cm.

Some vols. issued in the congressional series as Senate or House documents.
Bulletins composing v. 47– also numbered 1–
Title varies: v. 1–49, Bulletin.
Vols. 1–49 issued by Bureau of Fisheries (called Fish Commission, v. 1–23)

1. Fisheries—U.S. 2. Fish-culture—U.S. I. Title.

SH11.A25 639.206173 9—35239*

Library of Congress [59r55b1]

CONTENTS

Page
Materials ---- 172
Methods ---- 172
General remarks ---- 174
Taxonomy ---- 175

Family:

- Calanidae ---- 175
- Eucalanidae ---- 180
- Paracalanidae ---- 183
- Pseudocalanidae ---- 189
- Aetideidae ---- 190
- Euchaetidae ---- 199
- Phaennidae ---- 203
- Scolecithricidae ---- 206
- Temoridae ---- 213
- Metridiidae ---- 215
- Centropagidae ---- 218
- Lucicutiidae ---- 220
- Heterorhabdidae ---- 222
- Augaptilidae ---- 223
- Arietellidae ---- 226
- Candaciidae ---- 228
- Pontellidae ---- 239
- Acartiidae ---- 240

Literature cited ---- 241

ABSTRACT

A systematic study was made of the calanoid copepods found in 14 zooplankton samples, four of which were obtained from within the recently discovered equatorial undercurrent (Cromwell current), collected between 5° N. and 5° S. and 130° E. and 120° W.

One hundred and ten species belonging to 18 families were recorded. Descriptive notes, measurements and figures were given for most species with citations to previous occurrences in the Pacific Ocean.

Except for *Scolecithricella tenuiserrata* (Giesbrecht), the copepod species in samples collected from within the equatorial undercurrent were not very different from those in samples obtained adjacent to the current. The numerical abundance and species diversity in equatorial waters were briefly compared with that reported for the northwestern Pacific Ocean. *Acrocalanus andersoni* Bowman, *Chirundina indica* Sewell and *Haloptilus fertilis* (Giesbrecht) were reported for the first time from the Pacific Ocean.

Three species, *Xanthocalanus dilatus*, *Amallophora smithae* and *Scolecithricella tropica*, are described as new, and hitherto unknown males of *Gaetanus miles* Giesbrecht and *G. minor* Farran are briefly illustrated from juvenile specimens. It was proposed that *Euchirella brevis* Sars is a synonym for *E. amoena* Giesbrecht; *Euchaeta consimilis* Farran for *E. concinna* Dana; *Scoecithrix longicornis* Scott, and *Scolecithricella spinipedata* Mori for *Scolecithricella ctenopus* (Giesbrecht); and *Centropages pacificus* Chiba for *C. elongatus* Giesbrecht.

CALANOID COPEPODS FROM EQUATORIAL WATERS OF THE PACIFIC OCEAN

By GEORGE D. GRICE, *Woods Hole Oceanographic Institution* [1]

The present paper concerns the calanoid copepods found in plankton samples collected along the equator, an area which has been relatively unexplored taxonomically.

Systematic studies on calanoid copepods have made these microcrustaceans one of the better known groups of the holoplankton of the Pacific Ocean. Extensive taxonomic reports are available for the north Pacific (Brodsky, 1950), the northeast Pacific (Davis, 1949), the western Pacific (Vervoort, 1946; Tanaka, 1953), and the Pacific sector of the Antarctic (Vervoort, 1957). In addition there are numerous smaller but nevertheless valuable papers concerning the calanoid copepods of more restricted areas. Although there remain large, unexplored areas, these recent papers and certain of the older ones (e.g., Scott, 1909) provide a framework for a zoogeographic study of Pacific calanoids and, moreover, show where additional investigations are needed.

Most of the laboratory work of this study was done in Honolulu, Hawaii, in 1958 and 1959 under a fellowship from the John Simon Guggenheim Memorial Foundation. I wish to express my appreciation to the Foundation for the opportunity to make this study. The U.S. Fish and Wildlife Biological Laboratory furnished space for the work, the use of their library facilities and a part of their extensive plankton collections. It is a pleasure to acknowledge the cooperation of Thomas S. Aus-

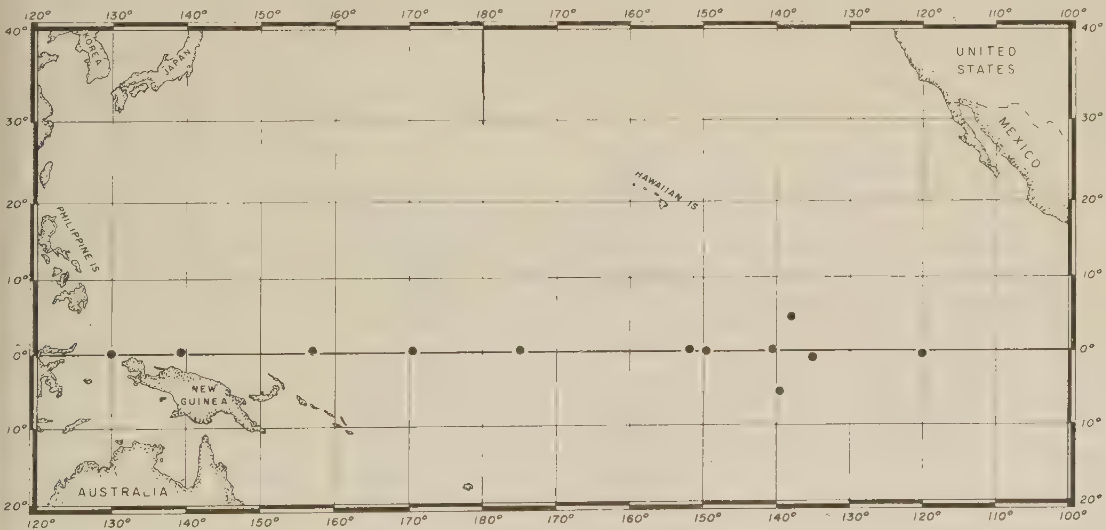

FIGURE 1. Positions where plankton samples were obtained.

---

[1] Woods Hole, Mass.

Fishery Bulletin 186. Approved for publication July 21, 1960.

tin and E. C. Jones. I wish also to thank Dr. Paul Illg for his advice during the course of the work, Dr. Thomas E. Bowman for reviewing the manuscript, and my wife, Joan, for assistance in completing the drawings.

MATERIALS

The present report is based on the examination of 14 plankton samples collected between 5° N. and 5° S. latitude and between 130° E. and 120° W. longitude in the Pacific Ocean (fig. 1). The pertinent data associated with each plankton collection are presented in table 1. Hydrographic data associated with these collections are given by King, Austin, and Doty (1957) for the research vessel *Hugh M. Smith*, cruise 31, and by Austin (1957) for cruise 35. Processed reports containing hydrographic data have been issued for *Orsom* cruise 56–4 (Legand, 1957), for *Stranger* and *Horizon* cruises (Scripps Institution of Oceanography, 1957), and for *Satsuma* and *Kagoshima* cruises (Japanese Hydrographic Office, 1956).

Four of the 14 samples (*Smith* cruise 31, stations 94, 144, 178, and cruise 47, station 31) were obtained from the recently discovered equatorial undercurrent (Knauss and King, 1958) by means of closing net gear. In addition, one oblique tow (*Smith* cruise 35, station 63) apparently passed within the undercurrent at least during part of the tow.

The three samples obtained on cruise 47 were oriented with respect to the undercurrent. One sample (cruise 47, station 31) was collected within the current, and the other two were obtained from below it (cruise 47, station 29) and from above it (cruise 47, station 30).

Six collections (*Smith* cruise 35, station 63, *Stranger* 34, *Orsom* 10, *Horizon* 32, *Satsuma* 32, and *Kagoshima* 613) were selected from a large number of plankton samples obtained by vessels participating in a large scale quasi-synoptic study (Operation Equapac) in Pacific equatorial waters. The samples used in the present studies are those obtained nearest to the Equator by each of the vessels.

METHODS

Owing to the large volume of most of the samples, except *Kagoshima* 613, it was not practical to examine the entire contents of each. In order to estimate the percentage representation and the numerical abundance of the common species, small quantities of the original samples were examined. These sub-samples, the sizes of which are given in table 2, were obtained by means of a plankton splitter (McEwen, Johnson, and Folsom, 1954). On

TABLE 1.—*Plankton station data*

Research vessel	Agency	Cruise No.	Station No.	Position	Date	Time [1]	Size of net	Mesh (mm.)	Depth [2] (m.)	Water filtered (m.^{3})
Hugh M. Smith	U.S. Fish and Wildlife Service.	31	94–2	00°11′S 119°58′W	*1955* Nov. 7	0916–0946 ZT	1 m.	0.65	146–72 CN	590.2
Do	do	31	132–2	04°40′N 138°14′W	Nov. 17	0921–0950 ZT	1 m.	65	119–63 CN	690.8
Do	do	31	144–2	00°16′N 140°12′W	Nov. 20	1000–1036 ZT	1 m.	65	122–61 CN	38.0
Do	do	31	153-3	05°31′S 139°54′W	Nov. 22	1008–1039 ZT	1 m.	65	126–63 CN	966.4
Do	do	31	178–2	00°21′N 151°40′W	Dec. 6	0917–0947 ZT	1 m.	.65	146–68 CN	283.8
Do	do	47	30	00°00′ 149°36′W	*1958* Oct. 27	1118–1151 ZT	1 m.	.65	surface	1342.0
Do	do	47	31	00°00′ 149°33′W	do	1153–1246 ZT	1 m.	.65	100 CN	380.0
Do	do	47	29	00°00′ 149°38′W	do	0953–1112 ZT	1 m.	.65	500 CN	922.0
Do	do	35	63–1	01°10′S 134°57′W	*1956* Aug. 19	2116–2152 ZT	1 m.	.66	169 Q	
Stranger	Scripps Institution of Oceanography.		34	00°01′N 174°59′W	Sept. 15	0352 GMT	1 m.	56	0–140 Q	
Orsom	Institut Français d'Océanie.	56–4	10	00°35′N 170°11′E	Oct. 4	2338–2457 LT	50 cm.	.366	150 Q( )	616.0
Horizon	Scripps Institution of Oceanography		32	00°03′S 157°00′E	Aug. 25	0428 GMT	1 m.	.56	0–280 Q	
Satsuma	Japan Hydrographic Office.		32	00°29′N 139°49′E	Aug. 18	2100–2210 ZT	45 cm.	.33	0–150 Q	20.71
Kagoshima-Maru	Kagoshima University, Japan.		613	00°38′N 130°20′E	Aug. 1	0725–0955 ZT	22.5 cm.	.11	0–50 V	

[1] ZT, zone time; LT, local time; GMT, Greenwich mean time.
[2] CN, closing net; Q, oblique open net; V, vertical open net.

TABLE 2.—*List of species and number of specimens in each sub-sample*

["X" indicates the species was found during the examination of other fractions of original sample]

Species	*Hugh M. Smith*									*Stranger*	*Orsom*	*Horizon*	*Satsuma*	*Kagoshima*
	94	132	144	153	178	30	31	29	63	34	10	32	32	613
1. Calanus tenuicornis	2	1		3	2							1		
2. Nannocalanus minor	1	44	2	21	41		2	X	2	6	6	12		
3. Canthocalanus pauper									1	1		2		
4. Neocalanus gracilis	X	8		6			17			X	X		X	
5. N. robustior				1	X				1	X				
6. Undinula vulgaris													X	
7. U. darwini	1	1	4	72	57	20	11	X	39	6	2	11	6	
8. Eucalanus attenuatus		1		15	4	1	15		15	X		11		
9. E. mucronatus												2		
10. E. subtenuis	1	85	86	2	173		39		45					
11. E. pileatus													1	
12. E. subcrassus									3	X	4			
13. Rhincalanus cornutus	X		1	1			3	48	9	1	2	1	5	
14. R. nasutus	1													
15. Paracalanus aculeatus			X	3	3		1		11	3	4	1		
16. P. parvus	X													
17. P. dubia														1
18. Acrocalanus longicornis				2			1		1	X				
19. A. andersoni										1	X			1
20. A. monachus										X	X	3		
21. Calocalanus pavo				1					1	1	1	X		
22. C. plumulosus													X	
23. Clausocalanus arcuicornis	3	75	4	9	27	15	11		3	12	18	9	5	
24. C. furcatus		30		14	3		1		6	6		4	1	
25. Euaetideus giesbrechti	1		1					X	X					
26. E. acutus	5	2	3	X	11	X	4		X	X				
27. E. bradyi	13		3						X					
28. Chiridius poppei	2								X					
29. Gaetanus miles								2	X					
30. G. minor								6	3			X		
31. Euchirella bella				X			X		X	X				
32. E. venusta									X					
33. E. pulchra									X					
34. E. amoena		X	X	X	X				X					
35. E. curticauda											X			
36. E. maxima								X						
37. Pseudochirella sp.								X						
38. Chirundina streetsi												X		
39. C. indica									X					
40. Undeuchaeta plumosa									X			X	1	
41. U. intermedia									1			X		
42. Euchaeta marina		1	X	33	8	34	12		7	5	X	2		
43. E. wolfendeni		1							1	5		4	2	
44. E. media									1					
45. E. tenuis								1	1			X		
46. E. concinna													4	
47. E. longicornis	2	4												
48. E. spinosa								X						
49. Phaenna spinifera	3	X					X		1		X	X		
50. Xanthocalanus dilatus n. sp.			X											
51. Amallophora smithae n. sp.			X											
52. Scolecithrix danae		2	4	18	5	X	26	X	17	3	1	7	6	
53. S. bradyi	14	4	X		1		1							
54. Scolecithricella ctenopus	1				1					1	X			
55. S. abyssalis	8		X					1	1					
56. S. vittata	4													
57. S. tenuiserrata			6		9		2		1	2				
58. S. marginata			X		X									
59. S. tropica n. sp.	4	4			2									
60. S. sp.			X											
61. Scaphocalanus echinatus									X					
62. S. longifurca	1							X	1					
63. Scottocalanus securifrons												X		
64. S. farrani								X						
65. S. sedatus								X			X			
66. Temoropia mayumbaensis	X										X			
67. Metridia venusta			7											
68. Pleuromamma xiphias									X		X		1	
69. P. abdominalis	2							13	7		X	1	5	
70. P. indica													1	
71. P. quadrungulata								5	X					
72. P. gracilis	1							12	X			1	X	
73. P. borealis									X		X		1	
74. Centropages gracilis		1		X	X	7				X			X	
75. C. elongatus				X								X	X	
76. C. calaninus						X						1		
77. Lucicutia flavicornis	15	3	X		11		3	X		1			1	
78. L. ovalis		X		1	4				X	2	1	1		
79. Heterorhabdus spinifrons			2					3	1				X	
80. H. papilliger	5	6	10		27		9	1	1	X	X			
81. Haloptilus longicornis	19	12	43	X	26		50		1	X	1	X	13	
82. H. acutifrons	X													
83. H. fertilis												X		
84. H. ornatus									X					
85. H. spiniceps	X									X	X	X	X	
86. H. austini	1													
87. Augaptilus longicaudatus	X													
88. Euaugaptilus hecticus							2			X			X	

TABLE 2.—*List of species and number of specimens in each sub-sample*—Continued

["X" indicates the species was found during the examination of other fractions of original sample]

Species	*Hugh M. Smith*									*Stranger*	*Orsom*	*Horizon*	*Satsuma*	*Kagoshima*
	94	132	144	153	178	30	31	29	63	34	10	32	32	613
89. Arietellus setosus									X					
90. A. giesbrechti								X						
91. A. plumifer	1								X					
92. A. aculeatus									X					
93. Candacia longimana												X	X	
94. C. guggenheimi								X						
95. C. tenuimana								X						
96. C. aethiopica						X						X	X	
97. C. pachydactyla		X		X	X	X			1	X	X	X		
98. C. curta								X			X	X		
99. C. bipinnata			X		X									
100. C. varicans							1		X					
101. C. catula					X				1	X	X	X		
102. C. bispinosa				3	X					X	X		1	
103. C. simplex	X	5	X	X	1									
104. C. truncata		X		1		X			X	1	X	8	15	
105. Pontella securifer						X	X							
106. P. tenuiremis												X		
107. Labidocera detruncata						X						X		
108. Pontellina plumata		X			X	7	X		X	1	X	1		
109. Acartia danae	1	1			X									
110. A. negligens				2	2	70	5		X	X	27		X	
Unidentified copepodids	22	70	18	5	22	0	0	41	44	30	2	23	28	5
Number of specimens in sub-sample	134	361	194	213	440	154	216	133	228	88	67	106	97	7
Sub-sample size	1/16	1/64	1/8	1/256	1/16	1/32	1/4	1/64	1/512	1/256	1/256	1/256	1/2	all
Number of copepods per cubic meter	3.6	33.4	40.8	56.4	24.8	3.7	2.3	9.2			27.8		9.3	
Number of species	34	27	26	27	31	15	25	25	55	35	31	39	29	2

completing the analysis of the sub-sample, portions of the original sample were examined for species not found in the aliquot. The species in each sample are listed in table 2 along with the number of specimens of each found in the aliquot.

Representatives of most species from each station were segregated by sex and placed in labeled vials. This material will be deposited in the U.S. National Museum.

GENERAL REMARKS

Species composition

A total of 110 species of calanoid copepods was found in the samples (table 2). Of these, three species belonging to the genera *Xanthocalanus*, *Amallophora*, and *Scolecithricella* are described as new, and three species, *Acrocalanus andersoni*, *Chirundina indica*, and *Haloptilus fertilis*, are reported for the first time from the Pacific Ocean.

The collections examined were obtained from along the Equator from 120° W. to 130° E., a distance of approximately 5,800 miles (fig. 1). Many of the species were widely distributed and occurred in samples collected in the eastern Pacific (east of 170° W.) and those collected in the western Pacific (west of 170° W.). Disregarding the small collection made at *Kagoshima* station 613, the most frequently occurring species were *Nannocalanus minor*, *Undinula darwini*, *Clausocalanus arcuicornis*, and *Scolecithrix danae*. These four species were present in all but one or two samples.

A study of table 2 will reveal that there were at least 6 species which were frequently found (4 or more samples) in the eastern Pacific, but which were not found in the samples examined from the western Pacific. One of these, *Eucalanus subtenuis*, was the most abundant copepod in three of the eastern Pacific samples and its apparent absence from the western Pacific samples is noteworthy. It is not, however, restricted to the eastern Pacific, as it has been reported from Japan (Fukase, 1957; Tanaka, 1956a) and from the Dutch East Indies (Vervoort, 1946). The other eastern Pacific species have also been reported from these two areas.

Equatorial undercurrent samples

Four of the fourteen samples examined were obtained from within the equatorial current (*Smith* 94, 144, 178, 31). The species composition of these samples, when compared with samples collected from adjacent waters—north (*Smith* 132), south (*Smith* 153), and above (*Smith* 30) and below (*Smith* 29) the undercurrent—was not particularly distinctive. *Scolecithricella tenuiserrata,* although apparently absent from one undercurrent sample (*Smith* 94), did appear in the other three samples and also in two other samples (*Smith* 63, *Stranger* 34) that were collected from depths where the undercurrent could be located, if present, but several hundred miles west of its known limits. Knauss (1959), has indicated that the current may extend as far west as about 160° E.; in that event the above two samples could have been collected from the current. Even if *S. tenuiserrata* is typically found within the undercurrent, it cannot be considered as an "indicator" *sensu stricto* of the current. In addition to the present samples, this species has been reported from near the Great Barrier Reef (Farran, 1936) and from Japan (Tanaka, 1953).

Numerical abundance

The number of copepods calculated for those collections in which a current meter was employed, varied from 2.3 to 56.4 with a mean of 21.8 copepods per cubic meter (table 2). These data may be compared to numerical data presented by Brodsky (1952) for the northwestern Pacific Ocean. Using only those collections in which closing nets were used (*Smith* 94, 132, 144, 153, 178, and 31), a mean number of 26.8 copepods per cubic meter was calculated for depths between approximately 50 and 150 meters in the eastern Pacific Ocean. Brodsky's data included numerical abundances for seven different vertical levels. For the 50 to 100–m. level he gave a figure of 5,040 calanoids per cubic meter and for the 100 to 200–m. level, 320 per cubic meter. Nine species were present at the former level and ten at the latter level. In comparison, there were no less than 25 species in any of the aforementioned eastern Pacific closing net samples.

TAXONOMY

For each species I have given references to its occurrence in the Pacific Ocean, with the exception of those early records summarized by Giesbrecht and Schmeil (1898) and those cited by Vervoort (1946, 1957). The former reference has usually been omitted in the following sections. I have given measurements for several individuals of a species and usually at all stations where it occurred. The total-length measurements are from the tip of the forehead to the end of the furca, without regard to the telescoped portions of the abdominal segments, and are recorded in mm. unless otherwise indicated. Except for *Pseudochirella,* copepodids which could not be assigned to a species are not mentioned.

Included under Remarks are certain taxonomic or ecological notes and usually a few brief statements on the diagnostic characters of the species. It is hoped that the specific characters mentioned and the figures presented for each species will be useful to others making identifications of tropical calanoid copepods. All illustrations were made with a camera lucida.

Family CALANIDAE

Calanus tenuicornis Dana, 1849

Pacific records: Vervoort, 1946. Also, Yamada, 1933; Johnson, 1942; Mori, 1942; Davis, 1949; Brodsky, 1950; Motoda, Iizuka, and Anraku, 1950; Motoda and Anraku, 1951; Anraku, 1952; Honjo, 1952; Motoda and Anraku, 1952b; Nakai, 1952; Anraku, 1953; Tanaka, 1953; Yamazi, 1953a; 1953c; Anraku, 1954a; 1954b; Motoda and Anraku, 1954; Tsuruta and Chiba, 1954a; 1954b; Yamazi, 1954b; 1954d; Bowman, 1955; Chiba, Tsuruta, and Maéda, 1955; Motoda and Anraku, 1955; Nagaya et al., 1955; Yamazi, 1955a; Chiba, 1956; Tanaka, 1956a; Heinrich, 1957a; Honjo et al., 1957; Heinrich, 1958b; Yamazi, 1958a; 1958b; Brodsky, 1959; Lindberg, 1959; Ponomareva, 1959.

Vessel:	*Station*	*Occurrence*
Hugh M. Smith	94	1 female, 1.87 mm.; 1 male, 1.80 mm.
Do	132	present.
Do	153	1 female, 1.75 mm.; 1 male, 1.56 mm.
Do	178	present.
Horizon	32	1 female, 1.68 mm.

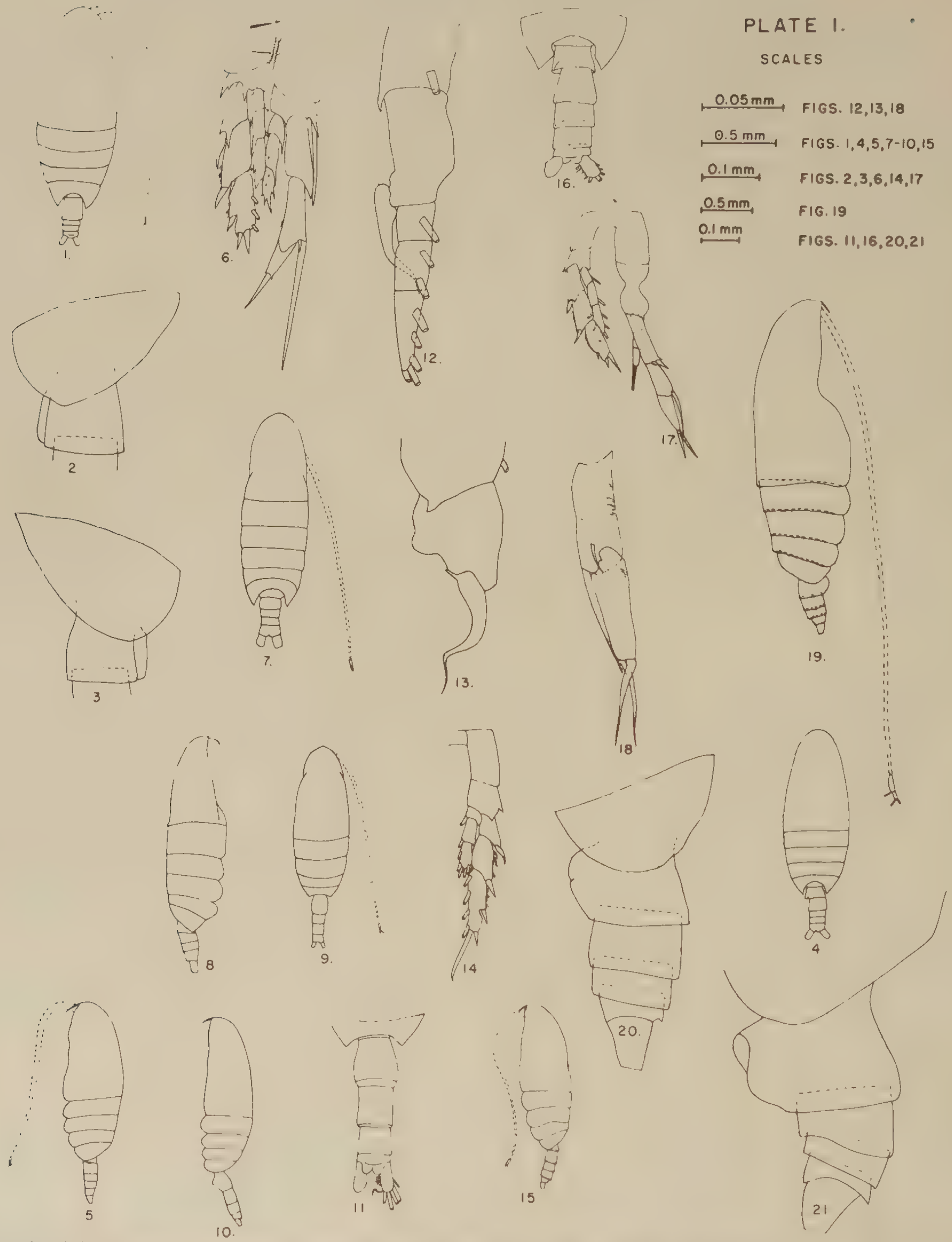
PLATE I.
SCALES
0.05 mm FIGS. 12,13,18
0.5 mm FIGS. 1,4,5,7-10,15
0.1 mm FIGS. 2,3,6,14,17
0.5 mm FIG. 19
0.1 mm FIGS. 11,16,20,21
1.
6.
12.
16.
17.
2
7.
13.
18
19.
3
8
9.
14
20.
4
5
10.
11
15
21

PLATE 1—(1) *Nannocalanus minor*, female, dorsal view; (2) posterior part of thorax and genital segment, left side; (3) posterior part of thorax and genital segment, right side; (4) male, dorsal view; (5) lateral view; (6) fifth pair of feet; (7) stage V female, dorsal view; (8) lateral view; (9) *Canthocalanus pauper*, female, dorsal view; (10) lateral view; (11) posterior part of thorax and abdomen, dorsal view; (12) endopod of first foot, lateral view; (13) first and second basipodal segments of first foot, oblique view; (14) fifth foot; (15) male, lateral view; (16) posterior part of thorax and abdomen, dorsal view; (17) fifth pair of feet; (18) distal two segments of left fifth foot; (19) *Neocalanus gracilis*, female, lateral view; (20) posterior part of thorax and abdomen, lateral view; (21) *Neocalanus robustior*, female, posterior part of thorax and abdomen, lateral view.

Remarks: Most of the present specimens have their furcal setae eroded. Bowman (1955) has previously observed this in specimens collected from the northeastern Pacific. He attributed this erosion to protozoan parasites which were present in the furcae. The majority of my specimens also contain these parasites in the furcae. Bowman (1955) has fully figured *C. lighti*, a species which differs morphologically from *tenuicornis* only in size.

Nannocalanus minor (Claus, 1863)

(Plate 1, figs. 1–8)

Pacific records: Vervoort, 1946. Also, as *Calanus minor;* Yamada, 1933a; Mori, 1937; 1942; Wilson, 1942; Anraku, 1952; Chiba, 1952c; Honjo, 1952; Nakai, 1952; Tanaka, 1953; Yamazi, 1953a; 1953b; 1953c; Anraku, 1954b; Motoda and Anraku, 1954; Tsuruta and Chiba, 1954b; Yamazi, 1954b; 1954d; Chiba, Tsuruta, and Maéda, 1955; Hida and King, 1955; Motoda and Anraku, 1955; Nagaya et al., 1955; Yamazi, 1955d; Chiba, 1956; Tanaka, 1956a; Honjo et al., 1957; Yamazi, 1958a. As *Nannocalanus minor;* Wilson, 1950; Brodsky, 1955; Rose, 1955; Heinrich, 1957b; 1958a; Brodsky, 1959.

Vessel:	*Station*	*Occurrence*
Hugh M. Smith	94	1 female, 1.73 mm.
Do	132	14 females, 1.56–1.70 mm.; 7 males, 1.39–1.43 mm.
Do	144	1 female, 1.73 mm.
Do	153	10 females, 1.58–1.67 mm.; 3 males, 1.44–1.46 mm.
Do	178	25 females, 1.51–1.65 mm.; 12 males, 1.31–1.51 mm.
Do	31	1 female, 1.75 mm.
Do	29	1 female, 1.80 mm.
Do	63	1 female, 1.80 mm.
Stranger	34	6 females, 1.53–1.70 mm.
Orsom	10	2 females, 1.58, 1.61 mm.; 4 males 1.24–1.46 mm.
Horizon	32	9 females (stage V), 1.53–1.70 mm.

Remarks: All the above female specimens belong to *N. minor* f. *major* (Sewell, 1929). Although Sewell (1947) has recently recognized two forms of the male (f. *major* and f. *minor*), I was unable to distinguish these forms among the above specimens. Presumably, they are all referable to f. *major* as Vervoort (1946) has reported smaller males (1.20–1.29) from one *Snellius* station (113) in Netherlands East Indies.

Canthocalanus pauper (Giesbrecht, 1888)

(Plate 1, figs. 9–18)

Pacific records: Vervoort, 1946. Also, as *Calanus pauper;* Mori, 1937; 1942; Honjo, 1952; Yamazi, 1953a; 1953b; Anraku, 1954b; Johnson, 1954; Tsuruta and Chiba, 1954b; Motoda and Anraku, 1955; Nagaya et al., 1955. As *Canthocalanus pauper;* Wilson, 1942; 1950; Tanaka, 1953; Brodsky, 1955; Rose, 1955; Tanaka, 1956a; Yamazi, 1958a.

Vessel:	*Station*	*Occurrence*
Hugh M. Smith	63	1 female, 1.42 mm.
Stranger	34	1 male, 1.31 mm.
Orson	32	2 females, 1.42, 1.46 mm.; 1 male, 1.36 mm.

Remarks: This small copepod is most easily recognized by the peculiarly shaped spine on the second basipodal segment of the first pair of feet (figs. 12, 13) in the female and the structure of the fifth pair of feet (figs. 17, 18) in the male.

Neocalanus gracilis (Dana, 1849)

(Plate 1, figs. 19–20)

Pacific records: Vervoort, 1946; 1957. Also, as *Calanus gracilis;* Mori, 1942; Honjo, 1952; Tsuruta and Chiba, 1954b; Motoda and Anraku, 1955; Nagaya et al., 1955; Chiba, 1956; Honjo et al., 1957. As *Neocalanus gracilis;* Tanaka, 1953; Hida and King, 1955; Tanaka, 1956a; Yamazi, 1958a.

Vessel:	*Station*	*Occurrence*
Hugh M. Smith	94	present.
Do	132	8 females (stage V), 2.34–2.48 mm.
Do	153	1 female, 3.09 mm.
Do	31	2 females, 3.33 mm.
Stranger	34	4 females, 3.01–3.06 mm.
Orsom	10	1 female, 2.96 mm.
Satsuma	32	1 female, 2.11 mm.

Remarks: Vervoort (1946) has listed the differences between this species and *Neocalanus robustior* (Giesbrecht). The adult females of *N. gracilis* are smaller (maximum 3.33) and the genital segment is less produced ventrally (fig. 20). No males were encountered in the present collections.

Neocalanus robustior (Giesbrecht, 1888)

(PLATE 1, FIG. 21)

Pacific records: Vervoort, 1946. Also, as *Calanus robustior;* Mori, 1937; Honjo, 1952; Yamazi, 1953a; Tsuruta and Chiba, 1954b; Chiba, Tsuruta, and Maéda, 1955; Nagaya et al., 1955; Chiba 1956; Honjo et al., 1957. As *Neocalanus robustior;* Wilson, 1942; 1950; Tanaka, 1953; Brodsky, 1955; Tanaka, 1956a; Yamazi, 1958a.

Vessel:	*Station*	*Occurrence*
Hugh M. Smith	153	1 female, 4.08 mm.
Do	178	1 female, 3.40 mm.
Do	63	1 female (stage V), 2.99 mm., 3 females, 3.80–3.89 mm.
Stranger	34	1 female, 3.61 mm.

Remarks: The large size (greater than 3.4 mm.) and greatly produced genital segment (fig. 21) of this species distinguishes it from *N. gracilis.* No males were found in the present samples.

Undinula vulgaris (Dana, 1849)

Pacific records: Vervoort, 1946. Also, as *Calanus vulgaris;* Yamada, 1933a; Mori, 1937; 1942; Chiba, 1952c; Honjo, 1952; Anraku, 1954b; Tsuruta and Chiba, 1954b; Motoda and Anraku, 1955; Chiba, 1956; Honjo et al., 1957. As *Undinula vulgaris;* Wilson, 1942; Johnson, 1949; Wilson, 1950; Tanaka, 1953; Johnson, 1954; Brodsky, 1955; Hida and King, 1955; Rose, 1955; Tanaka, 1956a; Yamazi, 1958a.

Vessel:	*Station*	*Occurrence*
Satsuma	32	1 male, 2.04 mm.

Remarks: Both Vervoort (1946) and Wilson (1950) speak of the great abundance of this species in the Netherlands East Indies and near the Hawaiian Islands, respectively. Scott (1909) also found it abundantly in the Malay Archipelago area as did Johnson (1949) in Bikini Lagoon and Tanaka (1956a) in the Izu region of Japan. In view of its extreme scarcity in the present collections, it is apparently more of an insular and nearshore species in contradistinction to *Undinula darwini,* a widespread species in the present collections.

Undinula darwini (Lubbock, 1860)

(PLATE 2, FIGS. 1–9)

Pacific records: Vervoort, 1946. Also, as *Calanus darwini;* Yamada, 1933a; Mori, 1937; 1942; Anraku, 1952; Honjo, 1952; Nakai, 1952; Yamazi, 1953a; 1953b; 1953c; Anraku, 1954b; Chiba and Tsuruta, 1954; Yamazi, 1954b; Motoda and Anraku, 1955; Nagaya et al., 1955; Yamazi, 1955a; 1955d; Chiba, 1956; Honjo et al., 1957; Yamazi, 1958b. As *Undinula darwini;* Wilson, 1942; 1950; Tanaka, 1953; Johnson, 1954; Brodsky, 1955; Rose, 1955; Tanaka, 1956a; Heinrich, 1957b; 1958a; Yamazi, 1958a; 1958b.

Remarks: All female specimens of this species have a group of inwardly projecting spines on the inner sides of the fifth thoracic segment (fig. 1). Also characteristic of this sex is the shape of the genital segment, which in dorsal view, is seen to narrow anteriorly (fig. 1).

The three forms of the female of this species (described by Sewell, 1929) are distinguished by the shape of the left fifth thoracic margin and spinulation of the proximal segments of the first antennae. The right fifth thoracic margin in all three forms is rounded and has

Vessel:	*Station*	*Occurrence (measurement in mm.; number of specimens in paren.)*			
		f. *typica* female	f. *symmetrica* female	f. *intermedia* female	male
Hugh M. Smith	94				(1)
Do	132		1.97 (1)		
Do	144	1.90 (1)	1.87–2.04 (7)		1.80 (3)
Do	153	1.90–2.00 (2)	1.80–1.90 (7)		present.
Do	178	present	1.84–1.90 (20)		1.60–1.67 (4)
Do	30	2.00 (2)	1.95–2.04 (4)		
Do	31	1.90–2.18 (2)	2.00 (1)		(2)
Do	29				(1)
Do	63	1.90 (1)	1.94–2.04 (5)		(8)
Stranger	34	2.04 (1)	2.04 (1)	2.07 (1)	(3)
Orsom	10			1.90 (1)	1.73 (1)
Horizon	32		2.04 (1)	1.94–2.07 (4)	
Satsuma	32	1.80 (1)		1.84–1.90 (5)	1.63 (1)

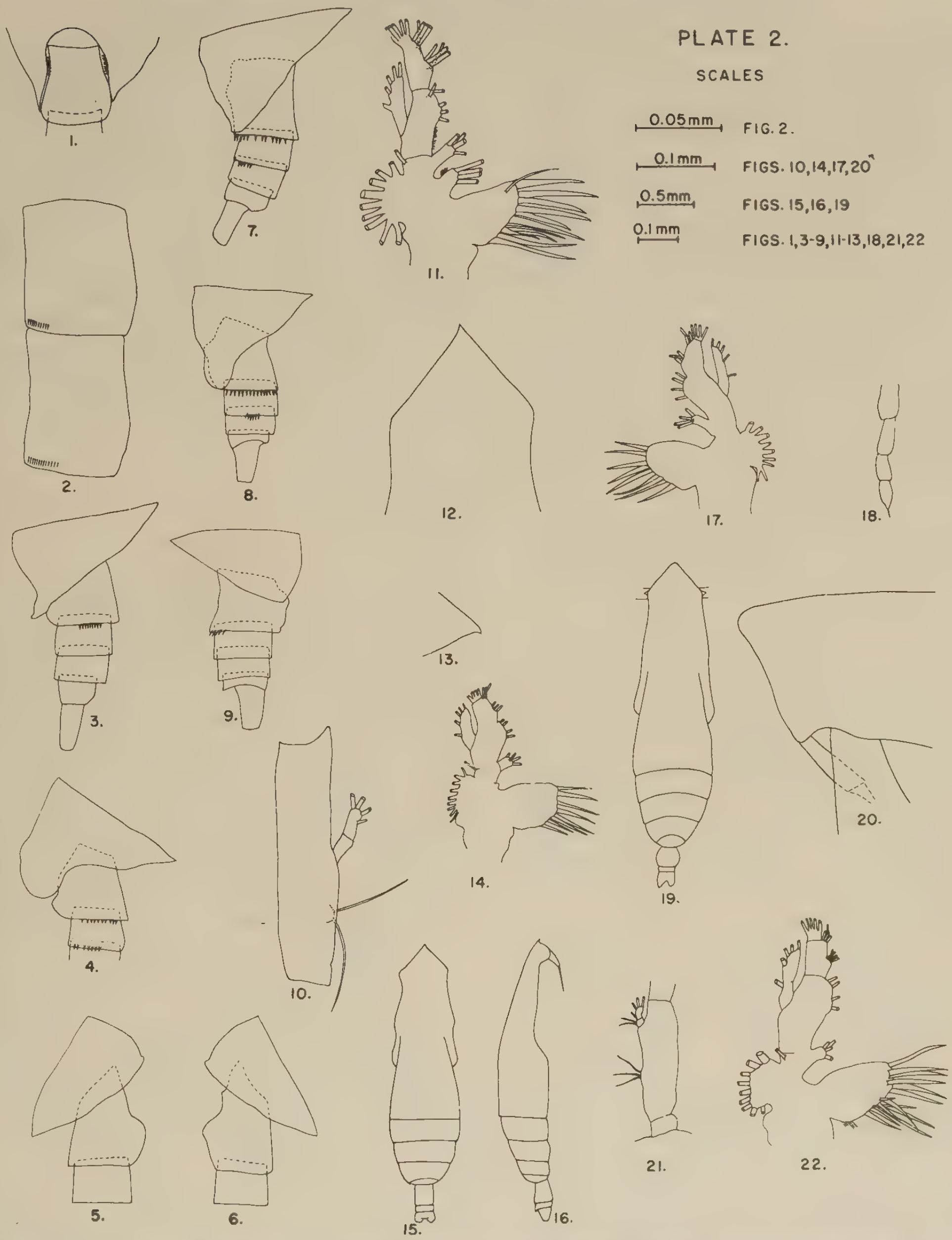
PLATE 2.
SCALES
0.05mm FIG. 2.
0.1mm FIGS. 10,14,17,20
0.5mm FIGS. 15,16,19
0.1mm FIGS. 1,3-9,11-13,18,21,22
1.
2.
3.
4.
5.
6.
7.
8.
9.
10.
11.
12.
13.
14.
15.
16.
17.
18.
19.
20.
21.
22.

PLATE 2.—(1) *Undinula darwini* f. *typica*, female, posterior part of thorax and genital segment, dorsal view; (2) segments 6 and 7 of first antenna; (3) posterior part of thorax and abdomen, left side; (4) posterior part of thorax and abdomen, left side; (5) *U. darwini* f. *symmetrica*, female, posterior part of thorax and genital segment, right side; (6) posterior part of thorax and genital segment, left side; (7) *U. darwini* f. *intermedia*, female, posterior part of thorax and abdomen, left side; (8) posterior part of thorax and abdomen, left side; (9) posterior part of thorax and abdomen, right side; (10) *Eucalanus attenuatus*, female, second basal segment and endopod of mandible; (11) first maxilla; (12) *E. mucronatus*, stage IV, female, forehead, dorsal view; (13) forehead, lateral view; (14) first maxilla; (15) stage V, male, dorsal view; (16) lateral view; (17) first maxilla; (18) fifth foot; (19) *E. subtenuis* var. *japonica*, female, dorsal view; (20) forehead, lateral view; (21) basal segments and endopod of mandible; (22) first maxilla.

a small notch. In forma *typica*, both segments 6 and 7 of the first antennae have a row of spinules along the distal margin (fig. 2). The left fifth thoracic margin is somewhat variable in shape. Typically, it is produced into a point which is directed ventrally (fig. 3). In a few individuals this margin was expanded and rounded (fig. 4). In forma *symmetrica*, a row of spinules is also present on segments 6 and 7 of the first antennae, but the two thoracic margins are symmetrical (figs. 5, 6). In forma *intermedia*, spinules are present on segments 3 through 7 of the first antennae, and the left fifth thoracic margin is usually more or less triangular in shape (fig. 7). In several specimens, this margin was rounded similar to that of forma *symmetrica* (fig. 8). Most examples of forma *intermedia* also had a small group of spines situated on the left mid-lateral margin of the second abdominal segment.

Chiba (1953a) has recently discussed and presented figures of small (40–60μ) spherical bodies which he detected within the furcae of the female of this species. He considered these objects to be eggs and analogized the "egg chamber" (furca) to the brood sac of daphnids. I too have seen these bodies in the furcae of this species. They are possibly protozoan parasites but not the reproductive eggs of the species.

Family EUCALANIDAE

Eucalanus attenuatus (Dana, 1849)

(PLATE 2, FIGS. 10, 11)

Pacific records: Vervoort, 1946. Also, Yamada, 1933a; Tanaka, 1935a; Mori, 1937; Johnson, 1942; Mori, 1942; Wilson, 1942; Brodsky, 1950; Wilson, 1950; Anraku, 1952; Honjo, 1952; Tanaka, 1953; Yamazi, 1953c; Anraku, 1954b; Johnson, 1954; Tsuruta and Chiba, 1954b; Yamazi, 1954d; Brodsky, 1955; Chiba, Tsuruta and Maéda, 1955; Hida and King, 1955; Motoda and Anraku, 1955; Nagaya et al., 1955; Rose, 1955; Yamazi, 1955a; 1955d; Chiba, 1956; Tanaka, 1956a; Honjo et al., 1957; Heinrich, 1958a; 1958b; Yamazi, 1958a; Brodsky, 1959; Lindberg, 1959; Ponomareva, 1959.

Vessel:	*Station*	*Occurrence*
Hugh M. Smith	132	1 female, 3.89 mm.
Do	153	present.
Do	178	2 females, 3.61, 3.80 mm.; 1 male, 2.96 mm.
Do	30	1 female, 3.16 mm.
Do	31	5 males, 2.92–3.06 mm.
Do	63	2 females, 3.90, 4.08 mm.
Stranger	34	1 female, 3.06 mm.
Horizon	32	7 females, 3.90–4.28 mm.; 1 female (stage V) 3.20 mm.

Remarks: Vervoort (1946) noted that there were large variations in the sizes of his specimens (females, 3.55–5.80; males 2.95–4.35) from the Netherlands East Indies, but he could find no anatomical differences between the size groups. Tanaka (1956a) likewise observed that there were large size variations (female, 4.32–6.19; male, 3.24–4.67) in the lengths of specimens obtained from the Izu region of Japan. He reported differences (shape of genital segment, presence of hair on female, relative lengths of segments of fifth pair of feet in the male) between the larger specimens of this species and suggested that a northern variety may have been present. The lengths of the present specimens were not nearly so variable as those reported by Vervoort or Tanaka.

Eucalanus mucronatus Giesbrecht, 1888

(PLATE 2, FIGS. 12–18)

Pacific records: Vervoort, 1946; 1957. Also, Yamada, 1933; Tanaka, 1935a; Honjo, 1952; Nakai, 1952; Tanaka, 1953; Yamazi, 1953a; Anraku, 1954b; Chiba, Tsuruta, and Maéda, 1955; Motoda and Anraku, 1955; Nagaya et al., 1955; Tanaka, 1956a; Honjo et al., 1957; Yamazi, 1958a; 1958b.

Vessel:	*Station*	*Occurrence*
Horizon	32	1 female (stage IV), 2.07 mm.; 1 male (stage V), 2.55 mm.

Remarks: Juveniles of this species were found in one collection. They are easily recognized by the pointed forehead, which is present in both sexes.

Eucalanus subtenuis Giesbrecht, 1888

(Plate 2, figs. 19–21; Plate 3, figs. 1–4)

Pacific records: Vervoort, 1946. Also, Mori, 1937; Tanaka, 1935a; Johnson, 1942; Mori, 1942; Wilson, 1942; 1950; Tanaka, 1953; 1956a; Fukase, 1957; Honjo et al., 1957; Heinrich, 1958b.

Vessel:	*Station*	*Occurrence*
Hugh M. Smith	94	1 female, 3.12 mm.
Do	132	13 females, 2.55–2.96 mm.
Do	144	10 females, 2.40–2.60 mm.
Do	153	present.
Do	178	15 females, 2.65–2.72 mm.; 6 males, 2.45–2.52 mm.
Do	31	15 females, 2.55–2.79 mm.
Do	63	16 females, 2.69–2.96 mm.; 1 male, 2.51 mm.

Remarks: All of the present specimens are referable to *E. subtenuis* var. *japonica* Fukase, 1957. This variety is distinguished from *subtenuis* chiefly by the number of setae on the mandibular palpus (both sexes) and the structure of the fifth feet of the male. There are 3 setae on the mandibular palpus (fig. 21; fig. 3) and the distal segment of the fifth foot is longer than the terminal spine (fig. 4). In *subtenuis* there are 2 setae on the mandibular palpus and the terminal spine of the fifth foot is longer than the distal segment.

According to Fukase, Tanaka's (1935a) *E. subtenuis* and Mori's (1937) *E. mucronatus* are both referable to *subtenuis* var. *japonica*.

This species was present in seven of the samples and in four of these (*Smith* 132, 144, 178, 63) it was the most abundant species.

Eucalanus pileatus Giesbrecht, 1888

(Plate 3, figs. 5–12)

Pacific records: Scott, 1909; Tanaka, 1935a; Wilson, 1950; Tanaka, 1953; 1956a.

Vessel:	*Station*	*Occurrence*
Satsuma	32	2 females, 1.80 and 1.94 mm.

Remarks: This species closely resembles *E. subcrassus* and the two may prove to be conspecific. Until a detailed study is made of each, it seems best to keep them separate. The females may be distinguished as follows (Pacific specimens):

1. Size. *E. pileatus*, 1.80–2.41; *E. subcrassus*, 2.23–2.82. (length data from Tanaka, 1935a; Mori, 1937; Vervoort, 1946; and present data). Farran (1936) has reported *E. subcrassus* with total lengths of 1.84–2.92 from the Great Barrier Reef. He did not record *E. pileatus*.
2. Shape of forehead. In dorsal view anterior end of forehead more produced in *E. pileatus* (fig. 7) than in *E. subcrassus* (plate 3, fig. 15).
3. Shape of genital segment. *E. pileatus*, greatest diameter at a point approximately one-half the length of the segment (fig. 10); *E. subcrassus*, greatest diameter in lower third of segment (plate 3, fig. 16).

Eucalanus subcrassus Giesbrecht, 1888

(Plate 3, figs. 13–17)

Pacific records: Vervoort, 1946. Also, Tanaka, 1935a; Mori, 1937; 1942; Wilson, 1950; Anraku, 1952; Honjo, 1952; Tanaka, 1953; Anraku, 1954b; Tsuruta and Chiba, 1954b; Brodsky, 1955; Chiba, Tsuruta, and Maéda, 1955; Motoda and Anraku, 1955; Nagaya et al., 1955; Rose, 1955; Tanaka, 1956a; Honjo et al., 1957; Yamazi, 1958a.

Vessel:	*Station*	*Occurrence*
Hugh M. Smith	63	3 females, 2.44–2.52 mm.
Stranger	34	3 females, 2.24–2.48 mm.
Orsom	10	4 females, 2.31–2.48 mm., 3 males (stage V), 2.11–2.18 mm.

Remarks: Vervoort (1946) stated that there are 4 setae on the second basal joint of the first maxilla. The present specimens, however, have 5 (fig. 17).

Rhincalanus cornutus (Dana, 1849)

(Plate 3, figs. 18–19)

Pacific records: Vervoort, 1946. Also, Yamada, 1933; Tanaka, 1935a; Mori, 1937; 1942; Wilson, 1942; 1950; Honjo, 1952; Tanaka, 1953; Anraku, 1954b; Tsuruta and Chiba, 1954b; Chiba, Tsuruta and Maéda, 1955; Hida and King, 1955; Nagaya et al., 1955; Rose, 1955;

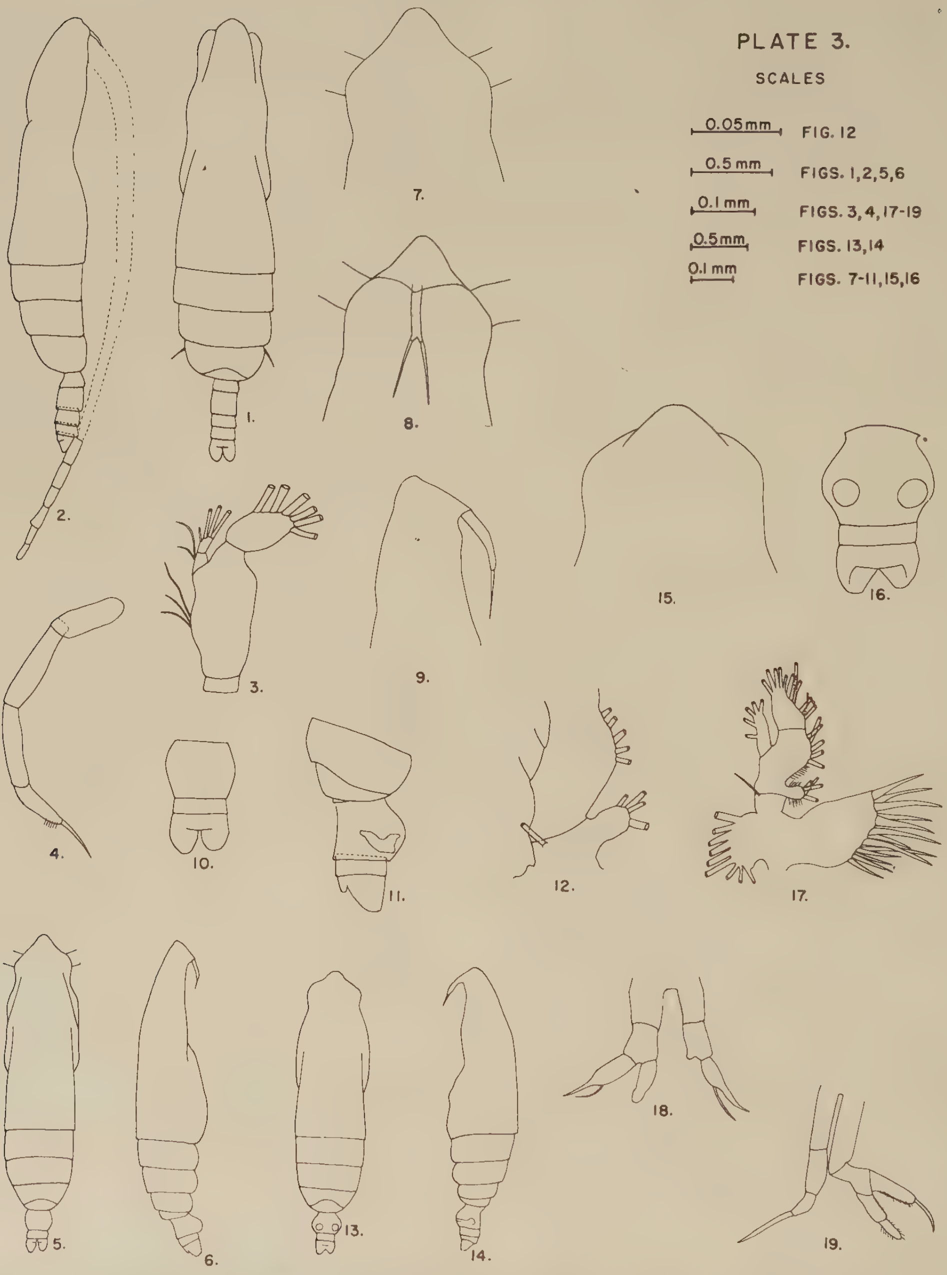
PLATE 3.
SCALES
0.05mm FIG. 12
0.5 mm FIGS. 1,2,5,6
0.1 mm FIGS. 3,4,17-19
0.5mm FIGS. 13,14
0.1 mm FIGS. 7-11,15,16
1.
2.
3.
4.
5.
6.
7.
8.
9.
10.
11.
12.
13.
14.
15.
16.
17.
18.
19.

PLATE 3.—(1) *Eucalanus subtenuis* var. *japonica*, male, dorsal; (2) lateral; (3) mandible palpus; (4) fifth foot; (5) *E. pileatus*, female, dorsal view; (6) female, lateral view; (7) forehead, dorsal view; (8) forehead, ventral view; (9) forehead, lateral view; (10) abdomen, dorsal view; (11) posterior part of thorax and abdomen, lateral view; (12) first maxilla (part); (13) *E. subcrassus*, female, dorsal view; (14) lateral view; (15) forehead, dorsal view; (16) abdomen, dorsal view; (17) first maxilla; (18) *Rhincalanus cornutus*, stage V, male, fifth pair of feet; (19) adult male, fifth pair of feet.

Chiba, 1956; Tanaka, 1956a; Honjo et al., 1957; Yamazi, 1958a.

Vessel:	Station	Occurrence
Hugh M. Smith	94	2 females, 2.79, 3.20 mm.
Do	144	1 female, 3.09 mm.
Do	153	1 male, 2.89 mm.
Do	31	2 females, 3.33; 2 males (stage V), 2.70, 2.80 mm.
Do	29	18 females, 3.20–3.33 mm.; 6 males, 2.79–2.86 mm.
Do	63	3 females, 3.09–3.24 mm.
Stranger	34	1 female, 3.09 mm.
Orsom	10	2 males, 2.69, 2.72 mm.
Horizon	32	2 females, 3.40 mm.; 1 male (stage V), 2.52 mm.
Satsuma	32	1 male, 2.95 mm.

Remarks: All of the above females belong to *R. cornutus* f. *typica* Schmaus. This species was widely distributed in the samples.

Rhincalanus nasutus Giesbrecht, 1888

Pacific records: Vervoort, 1946; 1957. Also, Yamada, 1933; Tanaka, 1935a; Johnson, 1942; Brodsky, 1950; Anraku, 1952; Honjo, 1952; Tanaka, 1953; Anraku, 1954b; 1954c; Chiba and Tsuruta, 1955; Tanaka, 1956a; Honjo et al., 1957; Heinrich, 1958a; Yamazi, 1958a.

Vessel:	Station	Occurrence
Hugh M. Smith	94	4 females, 4.08–4.37 mm.

Remarks: This species occurred in but one sample which was collected in the eastern Pacific by a closing net at a depth between 146 and 172 meters. As Vervoort (1946) mentioned, it is primarily a subsurface species.

Family PARACALANIDAE

Paracalanus aculeatus Giesbrecht, 1888

(PLATE 4, FIGS. 1–3)

Pacific records: Vervoort, 1946; 1957. Also, Yamada, 1933a; 1933b; Mori, 1942; Anraku, 1952; Chiba, 1952a; 1952b; Honjo, 1952; Nakai, 1952; Anraku, 1953; Tanaka, 1953; Yamazi, 1953c; Anraku, 1954b; Tsuruta and Chiba, 1954b; Chiba, Tsuruta, and Maéda, 1955; Motoda and Anraku, 1955; Nagaya et al., 1955; Rose, 1955; Chiba, 1956; Tanaka, 1956b; Honjo et al., 1957; Yamazi, 1958a.

Vessel:	Station	Occurrence
Hugh M. Smith	144	1 female, 1.0 mm.
Do	153	2 females, 1.09, 1.17 mm.
Do	178	2 females, 1.10 mm.
Do	31	1 female, 1.10 mm.
Do	63	9 females, 1.04–1.16 mm.
Stranger	34	4 females, 1.07–1.17 mm.
Orsom	10	3 females, 1.07–1.12 mm.
Horizon	32	2 females, 1.05, 1.10 mm.

Remarks: All the present specimens belong to *P. aculeatus* f. *major* Sewell, 1929. It was widely distributed in the present collections, but no males were observed.

Paracalanus parvus (Claus, 1863)

Pacific records: Vervoort, 1946; 1957. Also, Mori, 1942; Lowe, 1936; Chiba, 1949; Kokubo, 1950; Yamazi, 1950; 1951; Anraku, 1952; Honjo, 1952; Motoda and Anraku, 1952a; Yamazi, 1952a; 1952b; 1952c; Anraku, 1953; Tanaka, 1953; Yamazi, 1953a; 1953b; 1953c; Anraku, 1954a; 1954b; Tsuruta and Chiba, 1954b; Yamazi, 1954a; 1954b; 1954c; 1954d; 1954e; Chiba, Tsuruta, and Maéda, 1955; Motoda and Anraku, 1955; Nagaya et al., 1955; Nakai, 1955; Rose, 1955; Yamazi, 1955a; 1955b; 1955c; 1955d; Chiba, 1956; Shen and Bai, 1956; Tanaka, 1956b; Honjo et al., 1957; Légaré, 1957; Yamazi, 1957; 1958a; 1958b; Brodsky, 1959; Lindberg, 1959.

Vessel:	Station	Occurrence
Hugh M. Smith	94	2 females, 0.99 mm.

Remarks: Although this is a cosmopolitan species, it was observed in but one sample. Possibly its small size permitted most of the specimens to pass through the meshes of the nets employed or perhaps it is not too abundant in the waters sampled.

Paracalanus dubia Sewell, 1912

(PLATE 4, FIGS. 4–12)

Pacific records: Rose, 1955.

Vessel:	Station	Occurrence
Kagoshima	613	1 female, 0.49 mm.

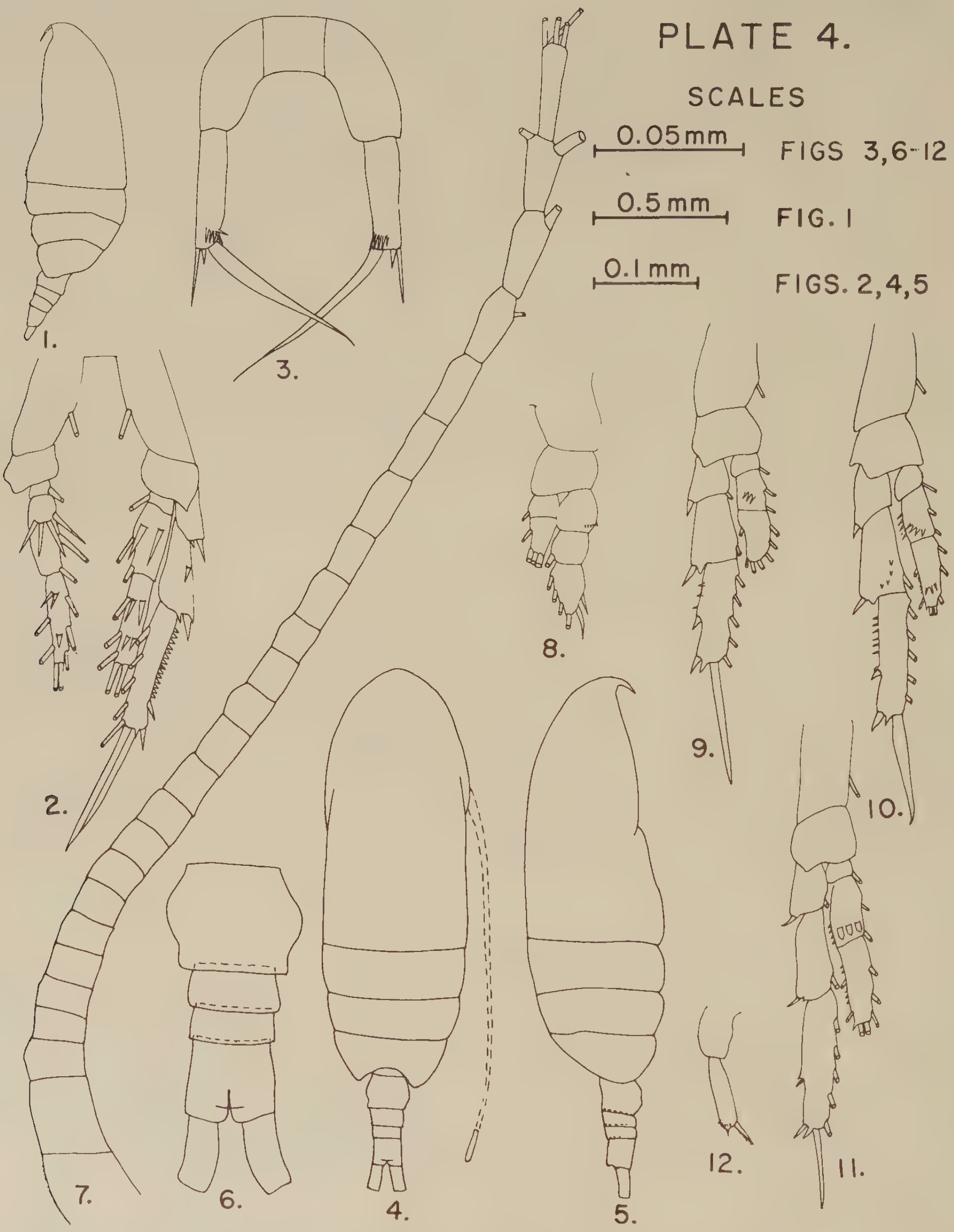
PLATE 4.
SCALES
0.05 mm FIGS 3,6-12
0.5 mm FIG. 1
0.1 mm FIGS. 2,4,5
1.
2.
3.
4.
5.
6.
7.
8.
9.
10.
11.
12.

Plate 4.—(1) *Paracalanus aculeatus*, female, lateral view; (2) fourth pair of feet (one exopod missing); (3) fifth pair of feet; (4) *P. dubia*, female, dorsal view; (5) lateral view; (6) abdomen, dorsal view; (7) first antenna; (8) first foot; (9) second foot; (10) third foot; (11) fourth foot; (12) fifth foot.

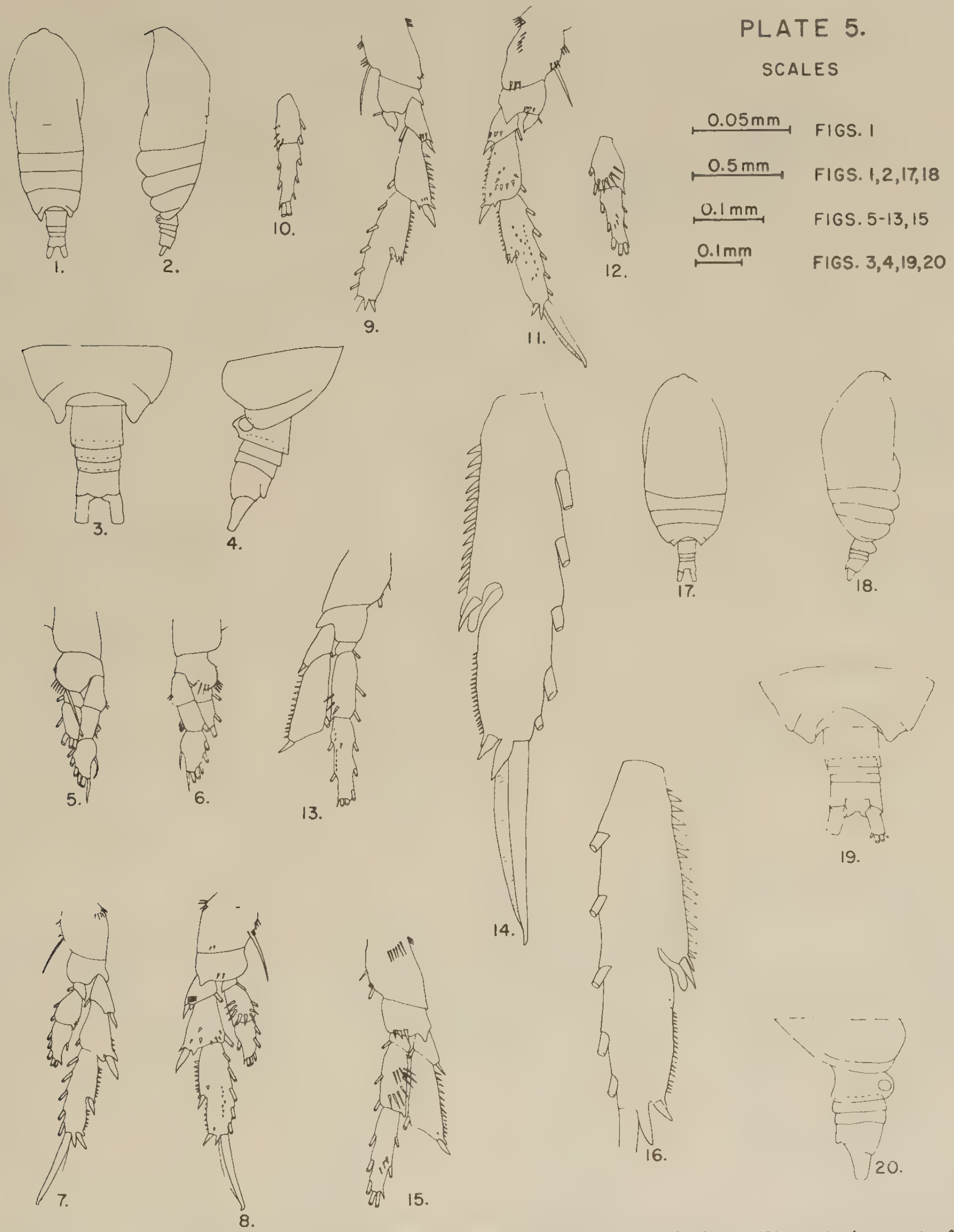
PLATE 5.
SCALES
0.05mm FIGS. 1
0.5mm FIGS. 1,2,17,18
0.1mm FIGS. 5-13,15
0.1mm FIGS. 3,4,19,20
1.
2.
3.
4.
5.
6.
7.
8.
9.
10.
11.
12.
13.
14.
15.
16.
17.
18.
19.
20.

PLATE 5.—(1) *Acrocalanus longicornis*, female, dorsal view; (2) lateral view; (3) posterior part of thorax and abdomen, dorsal view; (4) posterior part of thorax and abdomen, lateral view; (5) first foot, anterior; (6) first foot, posterior; (7) second foot, anterior; (8) second foot, posterior; (9) third foot, anterior, without distal 2 segments of endopod; (10) distal 2 segments of endopod of third foot, anterior; (11) third foot, posterior, without distal 2 segments of endopod; (12) distal 2 segments of endopod, posterior; (13) fourth foot, anterior, without third exopodal segment; (14) third exopodal segment of fourth foot, anterior; (15) fourth foot, posterior, without third exopodal segment; (16) third exopodal segment of fourth foot, posterior; (17) *A. andersoni*, female, dorsal view; (18) lateral view; (19) posterior part of thorax and abdomen, dorsal view; (20) posterior part of thorax and abdomen, lateral view.

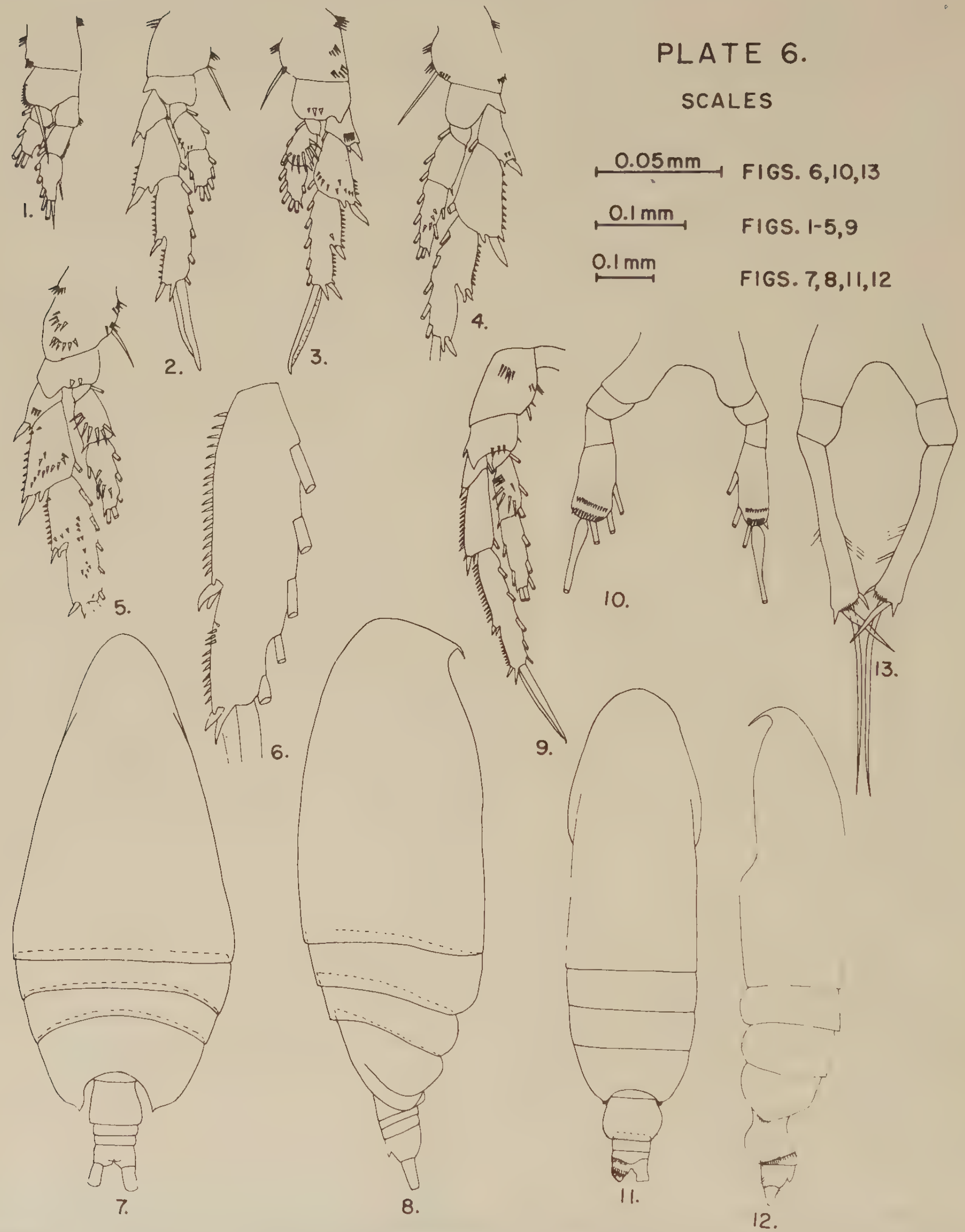
PLATE 6.
SCALES
0.05 mm FIGS. 6,10,13
0.1 mm FIGS. 1-5,9
0.1 mm FIGS. 7,8,11,12
1.
2.
3.
4.
5.
6.
7.
8.
9.
10.
11.
12.
13.

PLATE 6.—(1) *Acrocalanus andersoni*, first foot, anterior; (2) second foot, anterior; (3) second foot, posterior; (4) third foot, anterior; (5) third foot, posterior; (6) third exopodal segment of fourth foot, posterior; (7) *A. monachus*, female, dorsal view; (8) lateral view; (9) fourth foot, posterior; (10) *Calocalanus pavo*, female, fifth pair of feet; (11) *C. plumulosus*, female, dorsal view; (12) lateral view; (13) fifth pair of feet.

Remarks: The forehead of the present specimen as well as the spination of certain of the first four pairs of swimming feet differ somewhat from Sewell's description. The fifth pair of feet of Sewell's *P. serratipes* are similar to those of *P. dubia* but the former is a larger species (1.10 mm.).

The small spinules on the distal end of the terminal segment of the fifth feet can best be seen under oil immersion. The other feet, except the first pair, were also examined under oil in order to ascertain the number of setae, surface spines and lateral teeth on the various segments.

Only one specimen was obtained and this was partly destroyed in the process of dissection.

Acrocalanus longicornis Giesbrecht, 1888

(PLATE 5, FIGS. 1–16)

Pacific records: Vervoort, 1946. Also, Yamada, 1933; Mori, 1937; 1942; Wilson, 1942; 1950; Tanaka, 1953; Tsuruta and Chiba, 1954b; Chiba, Tsuruta and Maéda, 1955; Nagaya et al., 1955; Rose, 1955; Yamazi, 1955a; Tanaka, 1956b; Honjo et al., 1957; Yamazi, 1958a.

Vessel:	*Station*	*Occurrence*
Hugh M. Smith	153	2 females, 1.20, 1.22 mm.
Do	31	1 female, 1.26 mm.
Do	63	2 females, 1.19, 1.24 mm.
Stranger	34	7 females, 1.17–1.27 mm.

Remarks: The presence of a partial suture between the head and first thoracic segment (figs. 1, 2) and the spination of the swimming feet, particularly the number of teeth (more than 18) on the distal part of the third exopodal segment of the fourth pair of feet (figs. 14, 16), distinguished this species from others in the genus.

Acrocalanus andersoni Bowman, 1958

(PLATE 5, FIGS. 17–20; PLATE 6, FIGS. 1–6)

Pacific records: None.

Vessel:	*Station*	*Occurrence*
Stranger	34	1 female, 0.95 mm.
Orsom	10	3 females, 1.12–1.17 mm.
Kagoshima	613	1 female, 1.12 mm.

Remarks: This species was recently described from specimens obtained from the south Atlantic coast of the United States (Bowman, 1958). It is recognized by the lack of partial suture between the head and first thoracic segment (figs. 17, 18) and the number of lateral teeth (11) on the distal part of the third exopodal segment of the fourth pair of feet (fig. 6).

Acrocalanus monachus Giesbrecht, 1888

(PLATE 6, FIGS. 7–9)

Pacific records: Scott, 1909; Farran, 1936; Mori, 1937; 1942; Wilson, 1942; 1950; Tanaka, 1953; Tsuruta and Chiba, 1954b; Chiba, Tsuruta, and Maéda, 1955.

Vessel:	*Station*	*Occurrence*
Stranger	34	2 females, 1.02, 1.05 mm.
Orsom	10	1 female, 1.00 mm.
Horizon	32	3 females, 1.00–1.10 mm.

Remarks: The truncate appearance of this species in lateral view (fig. 8) readily distinguishes it from others in the genus.

Calocalanus pavo (Dana, 1849)

(PLATE 6, FIG. 10)

Pacific records: Vervoort, 1946. Also, Yamada, 1933a; Mori, 1937; Johnson, 1942; Mori, 1942; Wilson, 1942; 1950; Tanaka, 1953; Yamazi, 1953b; 1953c; Johnson, 1954; Tsuruta and Chiba, 1954b; Yamazi, 1954d; Brodsky, 1955; Chiba, Tsuruta, and Maéda, 1955; Nagaya et al., 1955; Rose, 1955; Yamazi, 1955d; Chiba, 1956; Tanaka, 1956b; Heinrich, 1957b; Honjo et al., 1957; Heinrich, 1958b; Yamazi, 1958a; 1958b.

Vessel:	*Station*	*Occurrence*
Hugh M. Smith	153	1 female, 0.85 mm.
Do	63	1 female, 1.00 mm.
Stranger	34	1 female, 1.19 mm.
Orsom	10	1 female, 0.97 mm.
Horizon	32	1 female, 1.00 mm.

Remarks: Bernard (1958) has recently revised the genus *Calocalanus* based on material collected in the Bay of Algiers. She proposed the family Calocalanidae, which consists of the genus *Calocalanus* s. str. and two new genera, *Leptocalanus* and *Dolichocera*. She has also

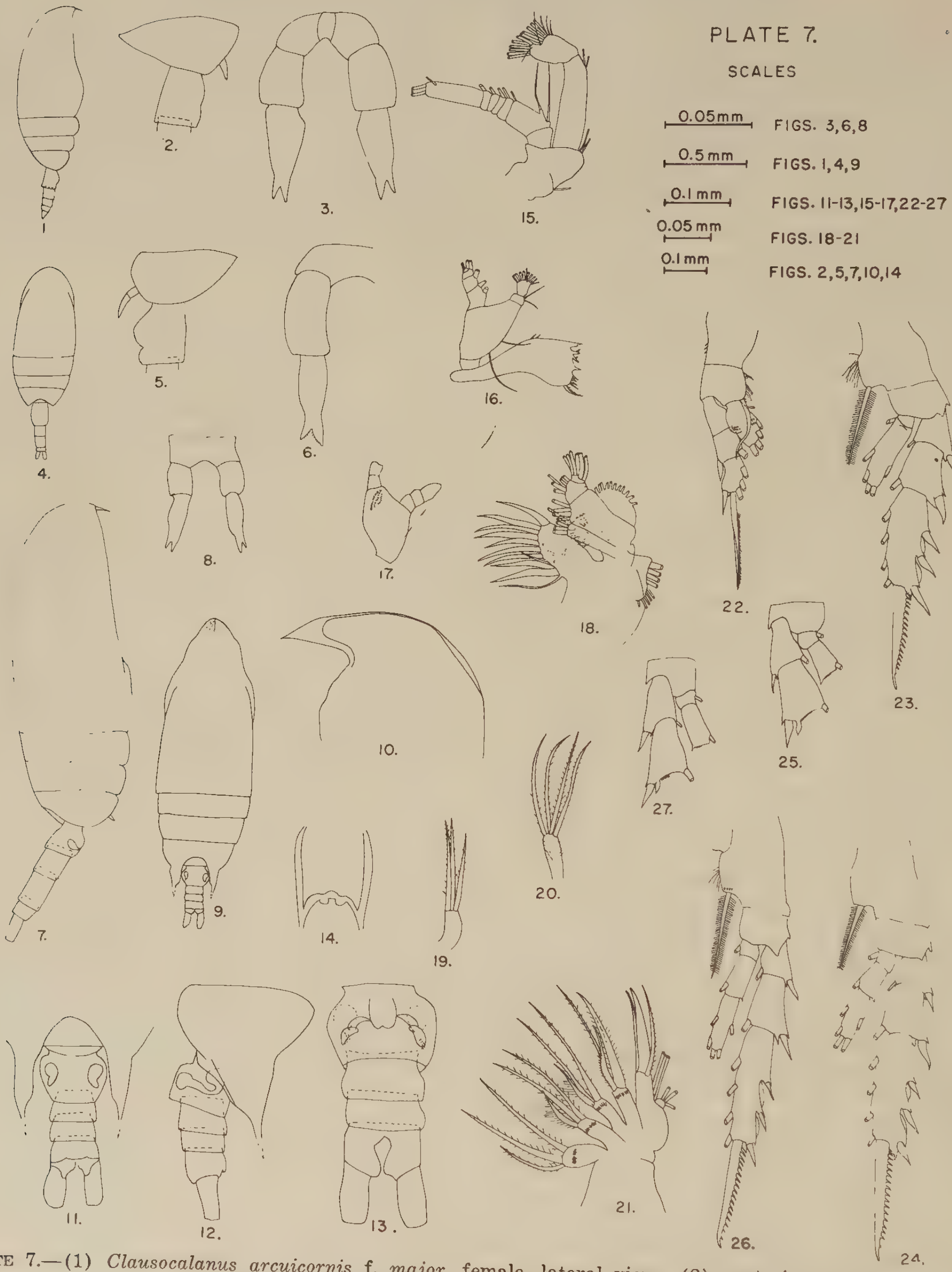
PLATE 7.
SCALES
0.05mm FIGS. 3,6,8
0.5 mm FIGS. 1,4,9
0.1 mm FIGS. 11-13,15-17,22-27
0.05 mm FIGS. 18-21
0.1 mm FIGS. 2,5,7,10,14
1
2.
3.
15.
4.
5.
6.
16.
8.
17.
18.
22.
23.
25.
27.
10.
20.
7.
9.
14.
19.
11.
12.
13.
21.
26.
24.

Plate 7.—(1) *Clausocalanus arcuicornis* f. *major*, female, lateral view; (2) posterior part of thorax and genital segment, lateral view; (3) fifth pair of feet; (4) *C. arcuicornis* f. *minor*, female, dorsal view; (5) posterior part of thorax and genital segment, lateral view; (6) fifth foot; (7) *C. furcatus*, female, lateral view; (8) fifth pair of feet; (9) *Euaetideus giesbrechti*, female, dorsal view; (10) forehead, lateral view; (11) posterior part of thorax and abdomen, dorsal view; (12) posterior part of thorax and abdomen, lateral view; (13) abdomen, ventral view; (14) rostrum; (15) second antenna; (16) mandible; (17) mandible palpus (other side); (18) first maxilla; (19) second inner lobe of first maxilla; (20) third inner lobe of first maxilla; (21) second maxilla; (22) first foot, anterior; (23) second foot, posterior; (24) third foot, posterior; (25) second basipodal segment and first and second segments of endopod and exopod of third foot, anterior; (26) fourth foot, posterior; (27) second basipodal segment and first and second segments of endopod and exopod of fourth foot, anterior.

described two new species and presented descriptions of five hitherto unknown males. *Calocalanus gracilis* Tanaka, 1956, is not included in her revision.

Calocalanus plumulosus (Claus, 1863)

(Plate 6, figs. 11–13)

Pacific records: Scott, 1909; Farran, 1929; 1936; Dakin and Colefax, 1940; Mori, 1942; Wilson, 1942; Anraku, 1953; Tanaka, 1953; Tanaka, 1956b; Heinrich, 1957b; 1958b; Yamazi, 1958a.

Vessel:	Station	Occurrence
Satsuma	32	2 females, 0.87 mm.

Remarks: According to Bernard's revision (see Remarks under preceding species), this species belongs to a new genus, *Leptocalanus*. The descriptions presented by Tanaka (1956b) and Bernard (1958) of the male are quite different and the two are not unispecific.

Family PSEUDOCALANIDAE

Clausocalanus arcuicornis (Dana, 1849)

(Plate 7, figs. 1–6)

Pacific records: Vervoort, 1946; 1957. Also, Yamada, 1933; Johnson, 1942; Mori, 1942; Brodsky, 1950; Nakai, 1952; Anraku, 1954b; Tsuruta and Chiba, 1954b; Brodsky, 1955; Chiba, Tsuruta, and Maéda, 1955; Motoda and Anraku, 1955; Nagaya et al., 1955; Rose, 1955; Chiba, 1956; Tanaka, 1956b; Heinrich, 1957b; Honjo et al., 1957; Heinrich, 1958a; Yamazi, 1958a; Brodsky, 1959; Lindberg, 1959; Ponomareva, 1959.

Vessel:	Station	Occurrence (*measurement in mm.; number of specimens in paren.*)		
		f. *minor*, female	f. *major*, female	male
Hugh M. Smith	94	1.26–1.29 (2)		
Do	132	1.07–1.24 (17)		
Do	144	present	1.34–1.46 (8)	present.
Do	153	1.15–1.25 (4)	1.37 (1)	
Do	178	1.08–1.28 (21)	1.33 (1)	
Do	30		1.43–1.56 (14)	1.21–1.26 (2)
Do	31	1.19–1.31 (4)	1.42–1.53 (5)	
Do	63	1.33 (1)	1.51 (1)	
Stranger	34	1.16–1.28 (10)		
Orsom	10	1.16–1.24 (13)	1.53 (1)	
Horizon	32	1.14–1.24 (6)	1.30-1.46 (2)	
Satsuma	32	1.08–1.12 (3)		

Remarks: I have tentatively equated the females of this species to two forms which were described by Sewell, 1929. The two forms are distinguished by size and the total and relative lengths of the segments of the fifth feet. Forma *major* is large (1.30–1.60 mm.), and the fifth pair of feet is small (fig. 2). The distal segment is about twice as long as the proximal one (fig. 3). Forma *minor* is distinguished by its small size and its longer fifth feet (fig. 5). The distal and proximal segments are about equal in length.

Tanaka (1956b) has described two types of males of this species which differ in size and in the structure of the fifth feet. Although rare in the present collections, males with fifth feet referable to Tanaka's large form were found in the sample from the *Hugh M. Smith*, station 30.

Clausocalanus furcatus (Brady, 1883)

(Plate 7, figs. 7–8)

Pacific records: Vervoort, 1946. Also, Mori, 1937; 1942; Wilson, 1942; Brodsky, 1950; Wilson, 1950; Nakai, 1952; Anraku, 1953; Tanaka, 1953; Yamazi, 1953c; Anraku, 1954b; Tsuruta and Chiba, 1954b; Motoda and Anraku, 1955; Nagaya et al., 1955; Rose, 1955; Chiba, 1956; Tanaka, 1956b; Honjo et al., 1957; Heinrich, 1958a.

Vessel:	Station	Occurrence
Hugh M. Smith	132	present.
Do	153	present.

Vessel:	*Station*	*Occurrence*
Do	178	2 females, 1.10, 1.12 mm.
Do	31	1 female, 1.14 mm.
Do	63	5 females, 1.00–1.17 mm.
Stranger	34	4 females, 1.12–1.19 mm.
Horizon	32	3 females, 1.02–1.19 mm.
Satsuma	32	1 female, 1.05 mm.

Remarks: This species is easily distinguished from the preceding by its short genital segment (fig. 7) and very small fifth feet (figs. 7, 8).

Family AETIDEIDAE

Euaetideus giesbrechti (Cleve, 1904)

(Plate 7, figs. 9–27)

Pacific records: Vervoort, 1957. Also, as *Aetideus giesbrechti;* Johnson, 1942; Mori, 1942; Honjo, 1952; Anraku, 1954b; 1954c; Chiba, Tsuruta, and Maéda, 1955; Motoda and Anraku, 1955; Nagaya et al., 1955; Chiba, 1956; Honjo et al., 1957; Tanaka, 1957a; Yamazi, 1958a. As *Euaetideus giesbrechti*; Heinrich, 1957b; 1958a; 1958b.

Vessel:	*Station*	*Occurrence*
Hugh M. Smith	94	1 female, 1.95 mm.
Do	144	1 female, 1.95 mm.
Do	29	1 female, 1.97 mm.
Do	63	2 females, 1.97 mm.

Remarks: Vervoort (1957) has recently described a new species of *Euaetideus* (*E. australis*) as well as redescribed and figured the other three species (*E. giesbrechti, E. bradyi, E. acutus*) in this genus. The latter three species were represented in the present collections and as all three of them differ in a few details from Vervoort's descriptions, I have included a brief discussion and several figures of each of them. The chief differences between my specimens of *E. giesbrechti* and those described by Vervoort are listed below. The numbers in parenthesis are those given by Vervoort.

1. Second antennae (fig. 15). Four (3) setae on distal segment of exopod. Seven (6) setae on outer lobe and 9 (8) setae on inner lobe of endopod.
2. First maxillae (figs. 18–20). Second basal segment with 4 (5) setae. Second inner lobe with 3 (2) setae. Three (4) setae on the first segment of the endopod. It should be pointed out that Vervoort stated that the first maxilla of *E. giesbrechti* is like that of *E. australis.* The second basal segment of the first maxilla of the latter species is shown to have 4 setae, which agrees, in this respect, with the number on the present specimens.

The three species found in the present collections are distinguished by the shape of the anterior margin of the head (dorsal view); the character of the rostrum; and the posterior lateral thoracic margins. In *E. giesbrechti* the forehead is evenly rounded and the rostral plate is not visible (fig. 9). There are two small knobs between the rostral spines (fig. 14), and the posterior lateral thoracic margins have a characteristic shape (fig. 12). This species is also larger (1.95–2.00) than the other two.

Euaetideus acutus (Farran, 1929)

(Plate 8, figs. 1–2)

Pacific records: Vervoort, 1957. Also, as *Aetideus acutus;* Tanaka, 1957a.

Vessel:	*Station*	*Occurrence*
Hugh M. Smith	94	5 females, 1.65–1.70 mm.
Do	132	2 females, 1.65, 1.70 mm.
Do	144	3 females, 1.70 mm.
Do	153	1 female, 1.70 mm.
Do	178	9 females, 1.55–1.65 mm.
Do	30	1 female, 1.61 mm.
Do	31	2 females, 1.55, 1.65 mm.
Do	63	1 female, 1.60 mm.
Stranger	34	1 female, 1.60 mm.

Remarks: Certain differences were noted in the second antennae and first maxillae of the present specimens and the descriptions and figures of these appendages given by Vervoort. These differences are summarized below:

1. Second antennae. Same as that described for *E. giesbrechti.* Vervoort shows 3 setae on the terminal segment of the exopod and 6 setae on the outer lobe and 8 setae on the inner lobe of the endopod.

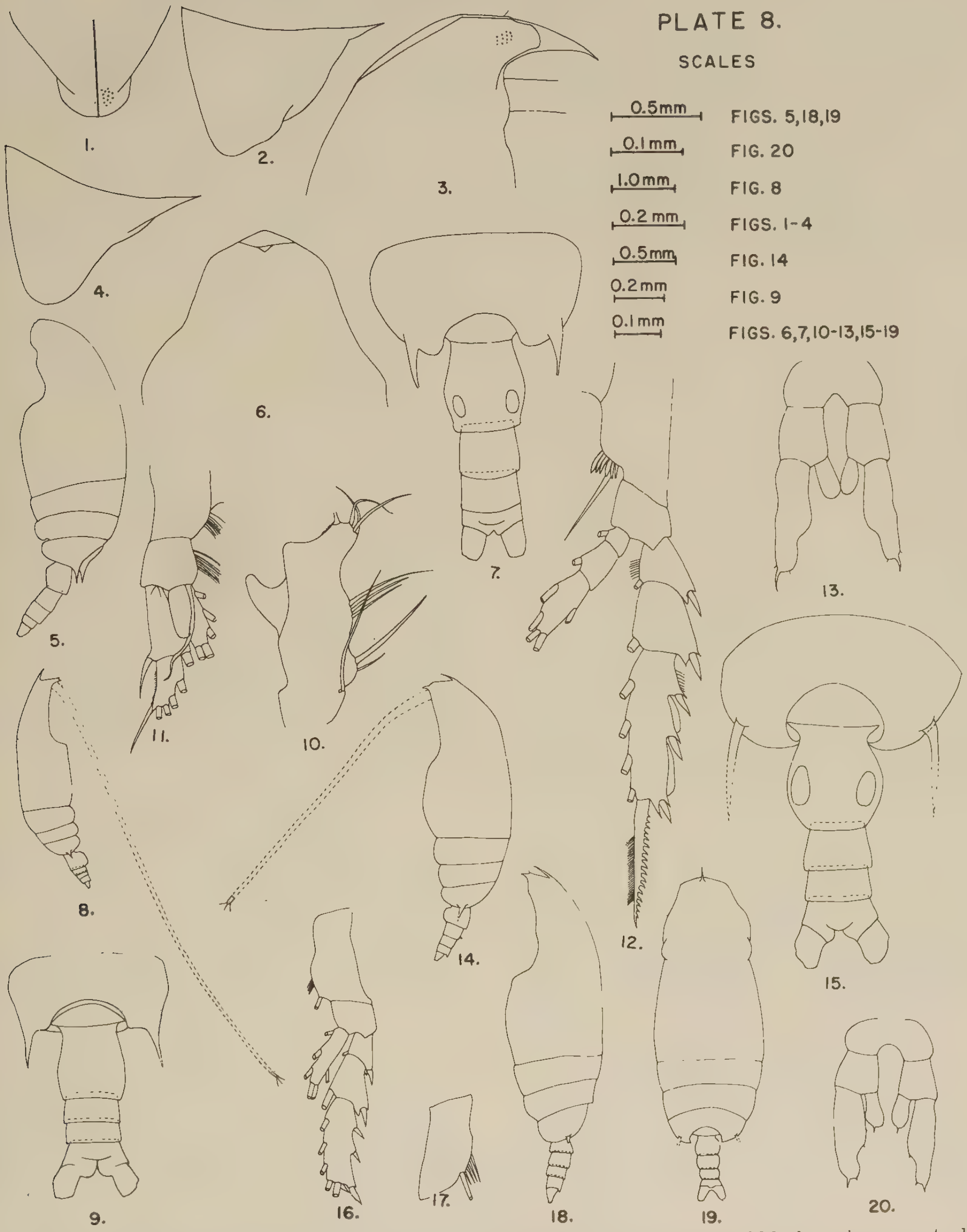
PLATE 8.
SCALES
0.5mm FIGS. 5,18,19
0.1mm FIG. 20
1.0mm FIG. 8
0.2mm FIGS. 1-4
0.5mm FIG. 14
0.2mm FIG. 9
0.1mm FIGS. 6,7,10-13,15-19
1.
2.
3.
4.
5.
6.
7.
8.
9.
10.
11.
12.
13.
14.
15.
16.
17.
18.
19.
20.

PLATE 8.—(1) *Euaetideus acutus*, female, forehead, dorsal view; (2) fourth and fifth thoracic segments, lateral view; (3) *E. bradyi*, female, forehead, lateral view; (4) fourth and fifth thoracic segments, lateral view; (5) *Chiridius poppei*, female, lateral view; (6) forehead, ventral view; (7) posterior part of thorax and abdomen, dorsal view; (8) *Gaetanus miles*, female, lateral view; (9) posterior part of thorax and abdomen, dorsal view; (10) first basipodal segment of maxilliped; (11) first foot; (12) fourth foot; (13) stage V, male, fifth pair of feet; (14) *Gaetanus minor*, female, lateral view; (15) posterior part of thorax and abdomen, dorsal view; (16) second foot; (17) first basipodal segment of fourth foot; (18) stage V, male, lateral view; (19) dorsal view; (20) fifth pair of feet.

2. First maxillae. Same as that described for *E. giesbrechti.* Vervoort shows 5 setae on the second basal segment, 2 setae on the second inner lobe and 4 setae on the first segment of the endopod.

E. acutus may be identified by the large rostral plate which is visible in dorsal view (fig. 1) and the character of the posterior lateral thoracic margins (fig. 2).

Euaetideus bradyi (A. Scott, 1909)

(PLATE 8, FIGS. 3–4)

Pacific records: Vervoort, 1957; Also, as *Aetideus bradyi;* Tanaka, 1957a.

Vessel:	*Station*	*Occurrence*
Hugh M. Smith	94	12 females, 1.60–1.65 mm.
Do	144	3 females, 1.65 mm.
Do	63	1 female, 1.70 mm.

Remarks: The second antennae differ from that figured by Vervoort in the manner described above for *E. giesbrechti.* The first maxilla of the present specimens has 4 setae on the basal segment and 3 setae on the second inner lobe. Vervoort showed 5 and 2 setae, respectively, on these parts of the maxilla. The anterior margin of the head of this species appears to be pitted similar to that of the preceding two species.

E. bradyi is distinguished from the above two species by the absence of knobs between the rostral spines and the character of the posterior lateral thoracic margins (fig. 4). In lateral view, a short hair is visible just dorsad of the base of the rostrum. I have not observed this hair in the other two species.

Chiridius poppei Giesbrecht, 1892

(PLATE 8, FIGS. 5–7)

Pacific records: Scott, 1909; Farran, 1929; Tanaka, 1937; Wilson, 1942; Brodsky, 1950; Tanaka, 1953; 1957a.

Vessel:	*Station*	*Occurrence*
Hugh M. Smith	94	2 females, 1.59, 1.83 mm.
Do	63	1 female, 1.70 mm.

Remarks: This species was found in two samples collected in the eastern Pacific. Vervoort (1957) suggested that *C. poppei* and *C. gracilis* Farran, 1905 may represent different size groups of the same species. He has also indicated how the two forms differ.

Gaetanus miles Giesbrecht, 1888

(PLATE 8, FIGS. 8–13)

Pacific records: Scott, 1909; Farran, 1936; Wilson, 1942; Brodsky, 1950; Tanaka, 1953; 1957b. As *G. secundus* Esterly, 1911; Johnson, 1942.

Vessel:	*Station*	*Occurrence*
Hugh M. Smith	29	2 females, 3.40, 3.50 mm.
Do	63	2 females, 3.52 mm.; 1 male (stage V), 2.89 mm.

Remarks: The female of this species is easily recognized by the elongate antennae which exceed the furca by the last 9 segments. Accompanying the females in the collection from *Smith* 63 was an immature male (stage V) which is apparently referable to this species. The fifth feet are shown in figure 13. The adult male is undescribed, although Esterly (1911) mentions that he has observed this sex, presumably in company with the females of his *G. secundus* (=*G. miles*).

Gaetanus minor Farran, 1905

(PLATE 8, FIGS. 14–20)

Pacific records: Vervoort, 1957. Also, Anraku, 1954b; 1954c; Tanaka, 1957b; Heinrich, 1958b.

Vessel:	*Station*	*Occurrence*
Hugh M. Smith	29	2 females, 2.18 mm.
Do	63	2 females, 2.15, 2.24 mm.; 1 male (stage V), 1.87 mm.
Horizon	32	1 female, 2.00 mm.

Remarks: The female is distinguished from *G. miles* by the short antennae and the presence of numerous small spines (fig. 17) on the first basipodal segment of the fourth feet. Rose (1933) states that the endopods of the second feet are composed of 2 segments. These endopods of the present specimens, as well as the one figured by Scott (1909), consist of only 1 segment (fig. 16). Associated with the females in the collection from *Smith* 63 was a juvenile

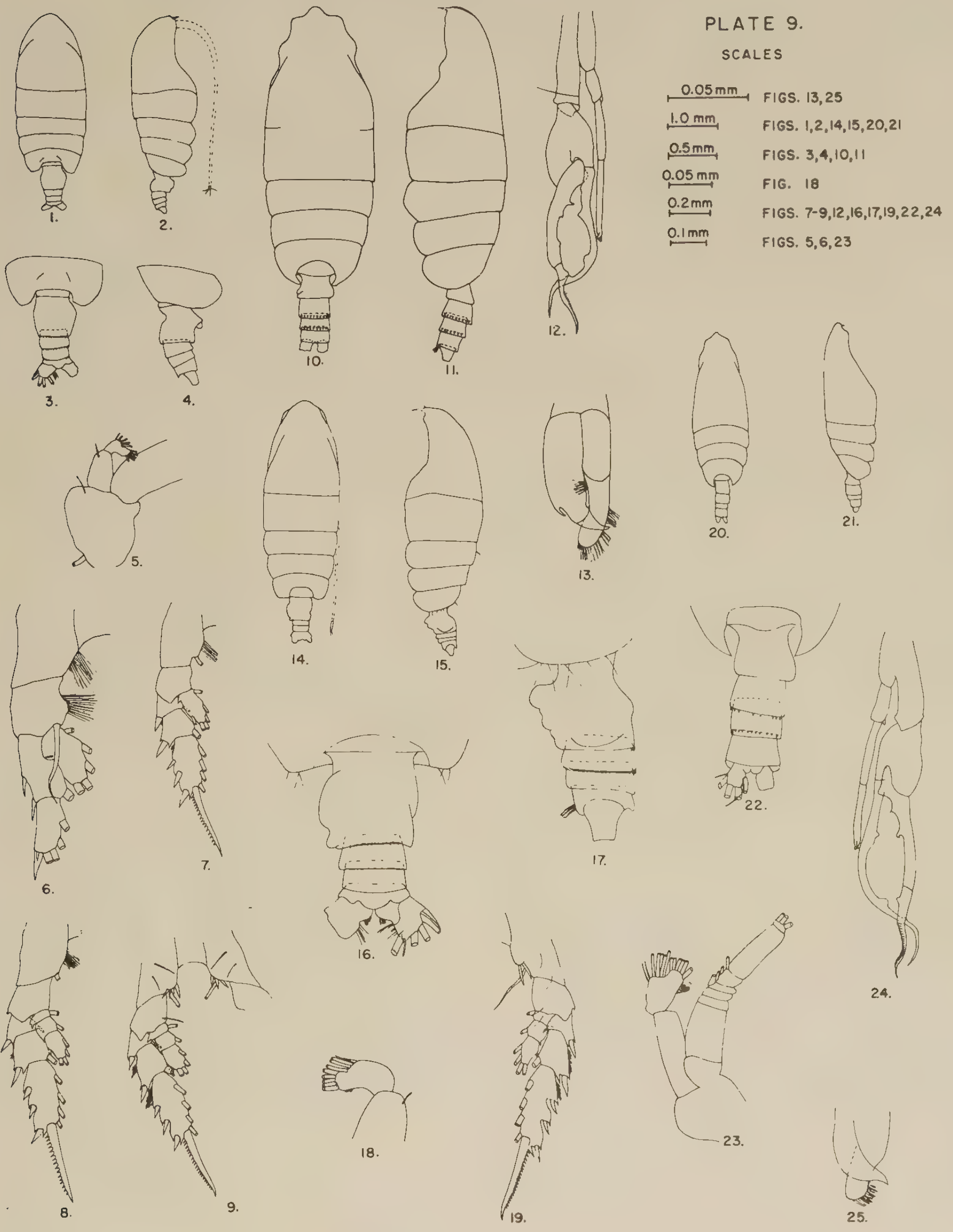
PLATE 9.
SCALES
0.05 mm FIGS. 13, 25
1.0 mm FIGS. 1, 2, 14, 15, 20, 21
0.5 mm FIGS. 3, 4, 10, 11
0.05 mm FIG. 18
0.2 mm FIGS. 7-9, 12, 16, 17, 19, 22, 24
0.1 mm FIGS. 5, 6, 23
1.
2.
3.
4.
5.
6.
7.
8.
9.
10.
11.
12.
13.
14.
15.
16.
17.
18.
19.
20.
21.
22.
23.
24.
25.

PLATE 9.—(1) *Euchirella bella*, female, dorsal view; (2) lateral view; (3) posterior part of thorax and abdomen, dorsal view; (4) posterior part of thorax and abdomen, lateral view; (5) endopod of second antenna; (6) first foot; (7) second foot; (8) third foot; (9) fourth foot; (10) male, dorsal view; (11) lateral view; (12) fifth pair of feet; (13) terminal part of left fifth foot; (14) *E. venusta*, female, dorsal view; (15) lateral view; (16) abdomen, dorsal view; (17) abdomen, lateral view; (18) endopod of second antenna; (19) fourth foot; (20) male, dorsal view; (21) lateral view; (22) abdomen, dorsal view; (23) second antenna; (24) fifth pair of feet; (25) terminal part of left fifth foot.

male (stage V), which is apparently referable to this species (figs. 18–20). The male of this species has been hitherto unknown.

Euchirella bella Giesbrecht, 1888

(Plate 9, figs. 1–13)

Pacific records: Vervoort, 1949; Wilson, 1950.

Vessel:	Station	Occurrence
Hugh M. Smith	153	2 females, 3.90, 4.18 mm.; 1 male, 3.33 mm.
Do	31	2 females, 3.80 mm.; 1 male, 3.36 mm.
Do	63	1 female, 3.80 mm.
Stranger	34	1 female, 3.80 mm.

Remarks: The species of female *Euchirella* are distinguished by the shape of the genital segment, number of setae on the endopod of the second antennae and the spination of the first basipodal segment of the fourth pair of feet. The males are identified by the structure of the fifth feet. The genital segment of *E. bella* is nearly symmetrical in dorsal view (figs. 1, 3) and is produced in ventral view (figs. 2, 4). The second segment of the endopod of the second antennae in the specimens examined has 5 setae on the outer and 5 setae on the inner lobe (fig. 5). Giesbrecht and Schmeil (1898) state that there are 6 and 5 setae on these respective lobes. The males in the present collections have 6 setae on the external lobe and 7 on the internal lobe, the 2 most internal ones being very small and slender. Vervoort (1949) indicated that there were 6 setae on each lobe. The number of spines on the first basipodal segment of the fourth feet is variable. Some specimens have 5 on each side and others have 4 on one side and 3 on the other (fig. 9). Scott (1909) and Sewell (1947) have also noted a variable number of spines on this segment.

Wilson (1950) has erroneously synonymized *E. amoena* with this species. See discussion of this under *E. amoena* below.

Euchirella venusta Giesbrecht, 1888

(Plate 9, figs. 14–25)

Pacific records: Scott, 1909; Farran, 1929; Vervoort, 1949; Wilson, 1950; Tanaka, 1953; 1957b.

Vessel:	Station	Occurrence
Hugh M. Smith	63	4 females, 4.37–4.84 mm.; 1 male, 3.80 mm.

Remarks: The female is identified by the knob-like protrusion from the left posterior margin of the genital segment (fig. 16); the presence of 4 setae on the inner lobe and 5 setae on the external lobe of the endopod of the second antennae (fig. 18); and the two long spines on the first basipodal segments of the fourth pair of feet. Sewell (1947) has recently described the male, additional figures of which are given herein (figs. 20–25). The second antennae (fig. 23) have 6 setae on the outer lobe and 7 setae on the inner lobe, 2 of which are small. Sewell reported 6 setae on each lobe. The structure of the fifth feet agrees quite well with Sewell's figure of this appendage.

Euchirella pulchra (Lubbock, 1856)

(Plate 10, figs. 1–4)

Pacific records: Esterly, 1905; Scott, 1909; Johnson, 1942; Wilson, 1942; Davis, 1949; Vervoort, 1949; Brodsky, 1950; Wilson, 1950; Tanaka, 1953; 1957b.

Vessel:	Station	Occurrence
Hugh M. Smith	63	1 female, 3.42 mm.

Remarks: The genital segment is produced into a rounded swelling to the left (fig. 2). The second segment of the endopod of the second antennae has 6 setae on each lobe (fig. 3). This is the number reported also by Tanaka (1957b), but Giesbrecht and Schmeil (1898) and Vervoort (1952) stated that the internal lobe has 5 setae. Possibly the very small, innermost seta on the internal lobe was overlooked. An additional identification character is the presence of 2 spines on the first basipodal segment of the fourth pair of feet (fig. 4).

Euchirella amoena Giesbrecht, 1888

(Plate 10, figs. 5–10)

Synonymy

Euchirella amoena Giesbrecht, 1888, Atti Acc. Lincei. Rend., Ser. 4, 4, sem. 2: 336.

Euchirella brevis, Sars, 1905. Bull. Mus. Oceanogr., Monaco, 26: 12.

Euchirella bella (partim), Wilson, 1950, U.S.N.M., Bull. 100, 14: 218.

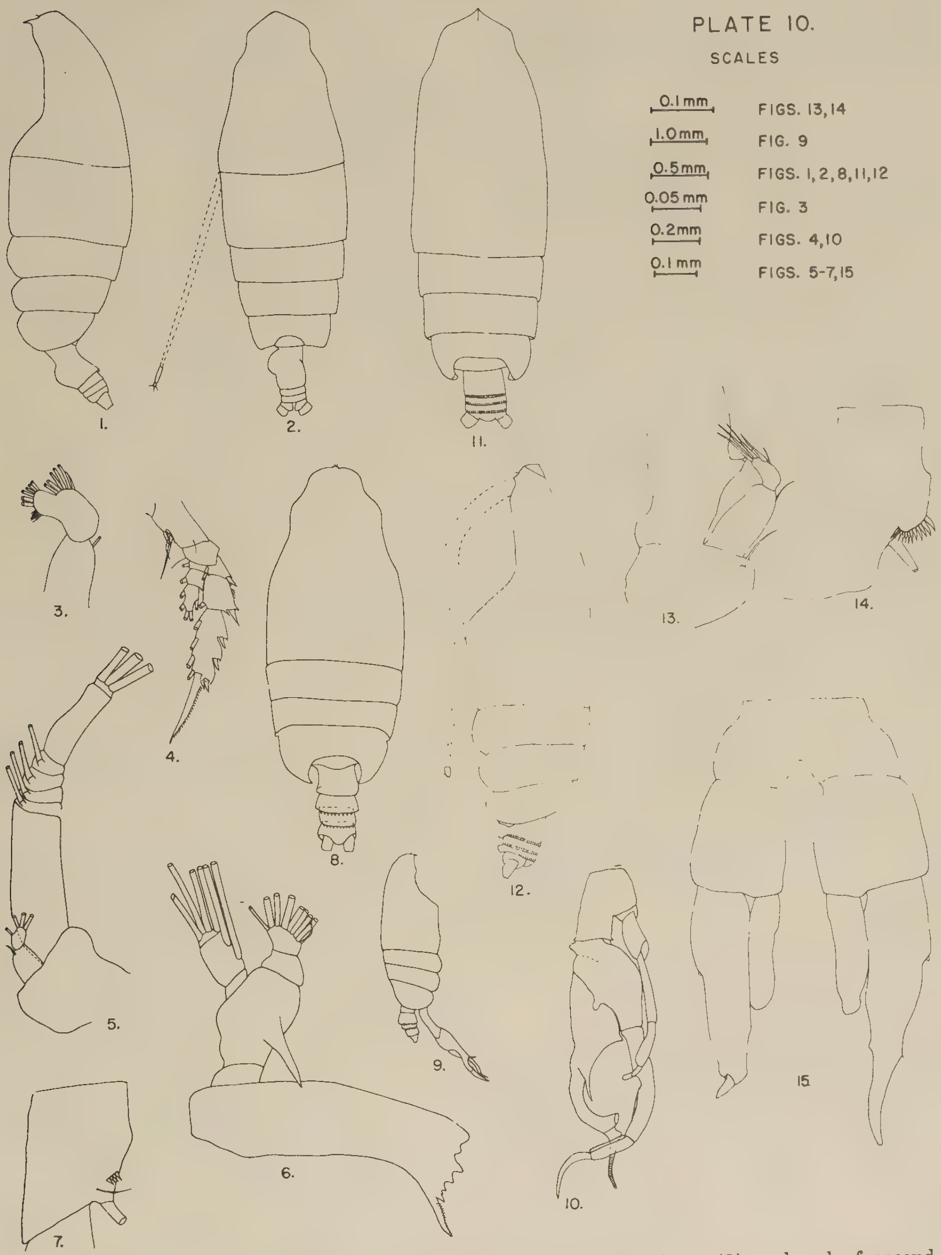
PLATE 10.
SCALES
0.1 mm FIGS. 13,14
1.0 mm FIG. 9
0.5 mm FIGS. 1,2,8,11,12
0.05 mm FIG. 3
0.2 mm FIGS. 4,10
0.1 mm FIGS. 5-7,15
1.
2.
11.
3.
4.
8.
13.
14.
12.
5.
6.
9.
10.
15
7.

PLATE 10.—(1) *Euchirella pulchra*, female, lateral view; (2) dorsal view; (3) endopod of second antenna; (4) fourth foot; (5) *E. amoena*, female, second antenna; (6) mandible: (7) first basipodal segment of fourth foot; (8) male, dorsal view; (9) lateral view; (10) fifth pair of feet; (11) *E. curticauda*, female, dorsal view; (12) lateral view; (13) endopod of second antenna; (14) first basipodal segment of fourth foot; (15) *E. maxima*, stage V, male, fifth pair of feet.

Pacific records: Esterly, 1905; Scott, 1909; Farran, 1929; Mori, 1937; Wilson, 1942; Brodsky, 1950; Wilson, 1950; Tanaka, 1953; Chiba, Tsuruta, and Maéda, 1955; Nagaya et al., 1955; Chiba, 1956; Tanaka, 1957b; Yamazi, 1958a.

Vessel:	*Station*	*Occurrence*
Hugh M. Smith	132	1 male, 3.20 mm.
Do	144	1 female, 3.70 mm.
Do	153	2 females, 3.61, 3.70 mm.; 3 males, 3.33 mm.
Do	178	1 female, 3.80 mm.
Do	63	1 male, 3.33 mm.

Remarks: Fleminger (1956) is no doubt correct in placing Sars' (1905) *brevis* (described from female) in synonymy with Giesbrecht's (1888) *amoena* (described from male). This synonymy is further substantiated by Mori's (1937) description of the female of *amoena*. Although Mori did not describe the fourth pair of feet, the total length, abdomen-cephalothorax ratio, length of the first antennae, length of the endopod of the second antennae and the number of setae on the distal segment of the endopod of the second antennae clearly establish that Mori's *E. amoena* and Sars' *E. brevis* are unispecific.

As Fleminger has stated, Wilson's synonymy of *E. amoena* under *E. bella* is an error. The male of *E. bella* was described by Sewell (1947) and Vervoort (1949); neither author was cited by Wilson. It should be noted, however, that Dr. Wilson's paper was published nine years after his death.

Euchirella curticauda Giesbrecht, 1888

(PLATE 10, FIGS. 11–14)

Pacific records: Esterly, 1906; Scott, 1909; Johnson, 1942; Mori, 1942; Wilson, 1942; Davis, 1949; Brodsky, 1950; Wilson, 1950; Anraku, 1952; Tanaka, 1953; 1957b.

Vessel:	*Station*	*Occurrence*
Orsom	10	2 females, 3.52, 3.62 mm.

Remarks: This species is recognized by the presence of a crest, absence of a rostrum (fig. 12) and the presence of a comb of spines on the first basipodal segment of the fourth pair of feet (fig. 14).

Euchirella maxima Wolfenden, 1905

(PLATE 10, FIG. 15)

Pacific records: Scott, 1909; Wilson, 1950.

Vessel:	*Station*	*Occurrence*
Hugh M. Smith	29	1 female (stage V), 5.79 mm.; 1 male (stage V), 5.70 mm.

Remarks: A male and female were obtained in the 500 m. collection made at the above station. Both sexes have a crest on the forehead. Sewell (1929) has described the stage V individuals of this species.

Pseudochirella sp.

Vessel:	*Station*	*Occurrence*
Hugh M. Smith	29	4 juveniles, 6.93–7.14 mm.

Remarks: These large juvenile copepods could not be assigned to a species. They were obtained from the 500–meter plankton tow.

Chirundina streetsi Giesbrecht, 1895

(PLATE 11, FIGS. 1–4)

Pacific records: Esterly, 1906; Scott, 1909; Farran, 1929; Johnson, 1942; Brodsky, 1950; Wilson, 1950; Tanaka, 1953; 1957b.

Vessel:	*Station*	*Occurrence*
Horizon	32	1 female, 4.94 mm.

Remarks: This species is distinguished from the following one by its large size, pronounced crest on forehead (fig. 1), and the presence of 2 spines on the first exopodal segment of the first feet (fig. 4).

Chirundina indica Sewell, 1929

(PLATE 11, FIGS. 5–20)

Pacific records: None.

Vessel:	*Station*	*Occurrence*
Hugh M. Smith	63	1 female, 4.66 mm.

Remarks: I have compared in some detail (figs. 5–20) the present species with the descriptions of *C. indica* provided by Sewell (1929, 1947). On the basis of his description the latter species is distinguished from *C.*

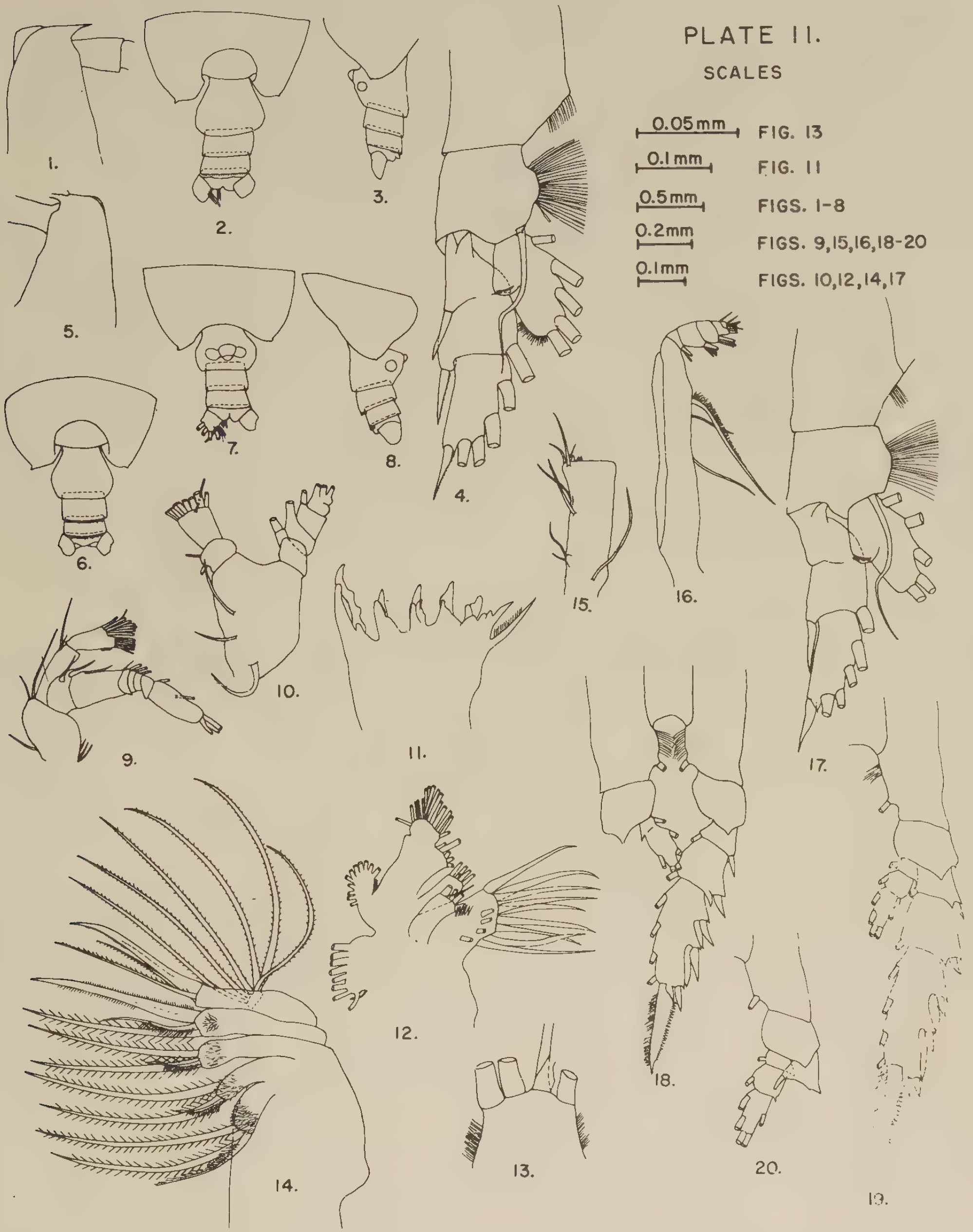
PLATE 11.
SCALES
0.05mm FIG. 13
0.1mm FIG. 11
0.5mm FIGS. 1-8
0.2mm FIGS. 9,15,16,18-20
0.1mm FIGS. 10,12,14,17
1.
2.
3.
4.
5.
6.
7.
8.
9.
10.
11.
12.
13.
14.
15.
16.
17.
18.
19.
20.

Plate 11.—(1) *Chirundina streetsi*, female, forehead, lateral view; (2) posterior part of thorax and abdomen, dorsal view; (3) abdomen, lateral view; (4) first foot; (5) *C. indica*, forehead, lateral view; (6) posterior part of thorax and abdomen, dorsal view; (7) posterior part of thorax and abdomen, ventral view; (8) posterior part of thorax and abdomen, lateral view; (9) second antenna; (10) mandible palpus; (11) gnathal lobe of mandible; (12) first maxilla; (13) terminal part of third inner lobe of first maxilla; (14) second maxilla; (15) first basipodal segment of maxilliped; (16) distal part of maxilliped; (17) first foot; (18) second pair of feet (one exopod and one endopod missing); (19) third foot; (20) fourth foot (distal part of exopod missing).

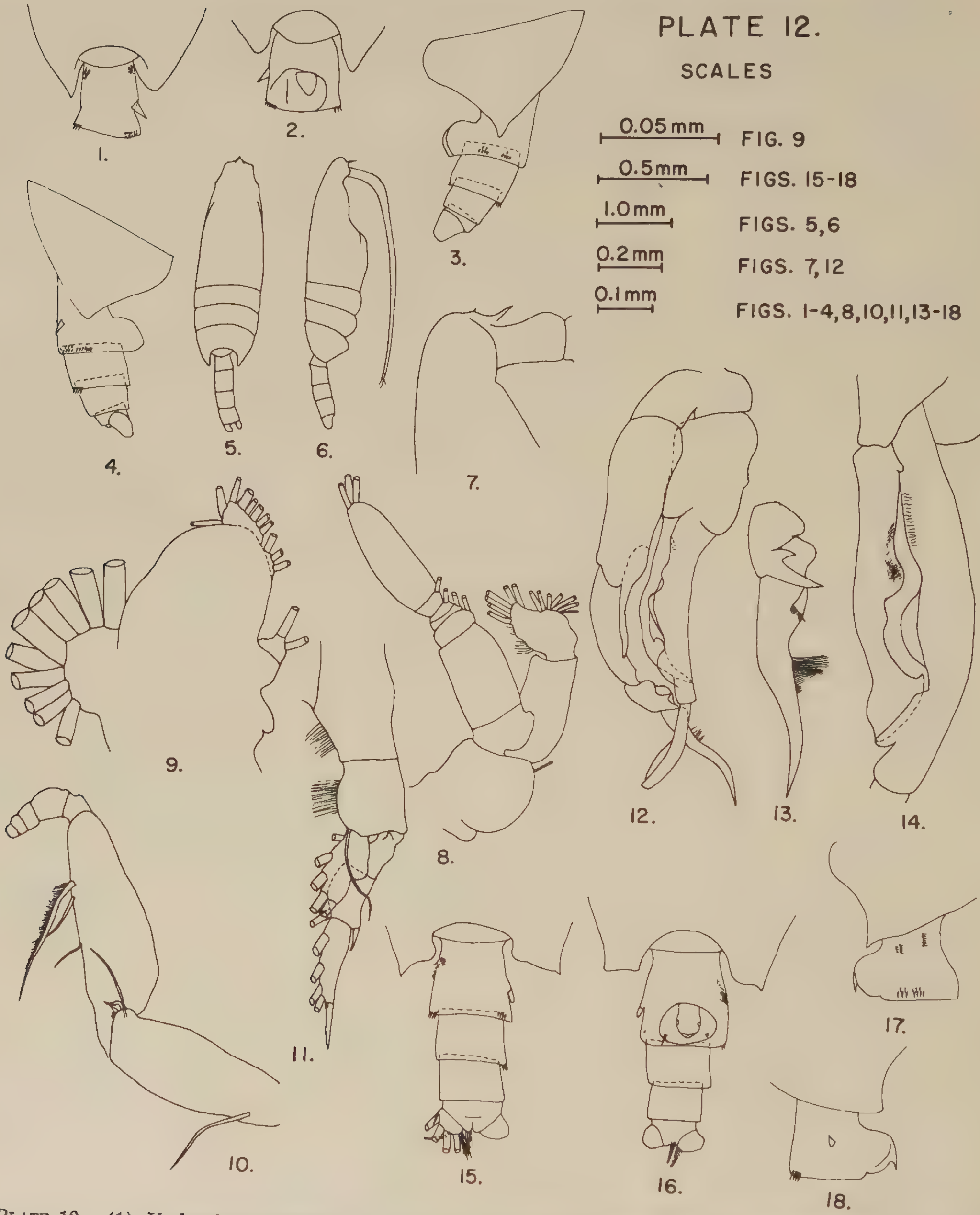
PLATE 12.
SCALES
0.05 mm FIG. 9
0.5mm FIGS. 15-18
1.0mm FIGS. 5,6
0.2mm FIGS. 7,12
0.1mm FIGS. 1-4,8,10,11,13-18
1.
2.
3.
4.
5.
6.
7.
8.
9.
10.
11.
12.
13.
14.
15.
16.
17.
18.

PLATE 12.—(1) *Undeuchaeta plumosa*, female, genital segment, dorsal view; (2) ventral view; (3) posterior part of thorax and abdomen, left side; (4) posterior part of thorax and abdomen, right side; (5) male, dorsal view; (6) lateral view; (7) forehead, lateral view; (8) second antenna; (9) first maxilla (part); (10) maxilliped (setae on distal part omitted); (11) first foot; (12) fifth pair of feet; (13) terminal part of left fifth foot; (14) right fifth foot (part); (15) *U. intermedia*, female, dorsal view; (16) abdomen, ventral view; (17) genital segment, left side; (18) genital segment, right side.

streetsi by its low crest, the smoothly rounded posterior thoracic margins and the presence of but 1 external spine on the first exopodal segment of the first feet. Except for the posterior thoracic margins, which have 1 small projection (figs. 7–9), my specimen agrees with Sewell's *indica*. In details of the mouth parts, two minor differences were noted. Sewell's specimens have 6 setae on the outer lobe of the second antenna, while the present specimen has 7 (fig. 10); the exopod of the mandible has 9 setae (Sewell probably referred to the distal segment); the present specimen has 10, one of which is extremely small (fig. 11).

The projections on the posterior thoracic margins may be a variable character as Vervoort (1957) has observed in several species of a related genus, *Undeuchaeta*. It seems best therefore to refer the present species to *C. indica*.

Undeuchaeta plumosa (Lubbock, 1856)

(PLATE 12, FIGS. 1–14)

Pacific records: Vervoort, 1957. Also, Brodsky, 1950; Heinrich, 1957b; Tanaka, 1957b.

Vessel:	*Station*	*Occurrence*
Hugh M. Smith	63	1 male, 3.52 mm.
Horizon	32	1 female, 3.47 mm.
Satsuma	32	1 female, 3.41 mm.

Remarks: The female is distinguished by the presence of a spine on the right side of the genital segment (figs. 1, 2) near the dorsal surface, and the male by the structure of the fifth feet (figs. 12–14).

Undeuchaeta intermedia A. Scott, 1909

(PLATE 12, FIGS. 15–18)

Pacific records: Vervoort, 1957. Also, Johnson, 1942; Brodsky, 1950 (as *U. bispinosa*)

Vessel:	*Station*	*Occurrence*
Hugh M. Smith	63	4 females, 3.99–4.28 mm.
Horizon	32	3 females, 3.99–4.08 mm.

Remarks: The large ventral spine-like protrusion of the genital segment in the female (figs. 17, 18) distinguishes this species from the preceding one.

Family EUCHAETIDAE

Euchaeta marina (Prestandrea, 1833)

(PLATE 13, FIG. 1)

Pacific records: Scott, 1909; Marukawa, 1921; Yamada, 1933b; Mori, 1937; Dakin and Colefax, 1940; Mori, 1942; Wilson, 1942; Brodsky, 1950; Motoda, Iizuka, and Anraku, 1950; Wilson, 1950; Anraku, 1952; Honjo, 1952; Nakai, 1952; Anraku, 1953; Chiba, 1953b; Tanaka, 1953; Anraku, 1954b; Tsuruta and Chiba, 1954b; Chiba, Tsuruta, and Maéda, 1955; Motoda and Anraku, 1955; Nagaya et al., 1955; Rose, 1955; Chiba, 1956; Heinrich, 1957b; Honjo et al., 1957; Gilmartin, 1958; Heinrich, 1958a; Tanaka, 1958; Yamazi, 1958a; Lindberg, 1959.

Vessel:	*Station*	*Occurrence*
Hugh M. Smith	132	1 male, 3.12 mm.
Do	144	1 female, 3.61 mm.
Do	153	2 females, 3.32, 3.42 mm.
Do	178	1 female, 3.06 mm.
Do	30	3 females, 2.96–3.06 mm.; 1 male, 2.99 mm.
Do	31	present.
Do	63	4 females, 3.40–3.60 mm.; 1 male, 3.37 mm.
Stranger	34	4 females, 3.13–3.26 mm.; 5 males, 3.06–3.23 mm.
Orsom	10	3 females, 3.13–3.23 mm.
Horizon	32	2 females, 3.13, 3.23 mm.

Remarks: This is probably the most widespread species in the genus. It occurred in ten of the present samples and in two (*Smith* 153 and 30), it comprised a fairly significant percentage of the total number of copepods.

Euchaeta wolfendeni A. Scott, 1909

(PLATE 13, FIGS. 2–9)

Pacific records: Farran, 1936; Mori, 1937; Wilson, 1950; Honjo, 1952; Tanaka, 1953; Tsuruta and Chiba, 1954b; Chiba, Tsuruta, and Maéda, 1955; Nagaya et

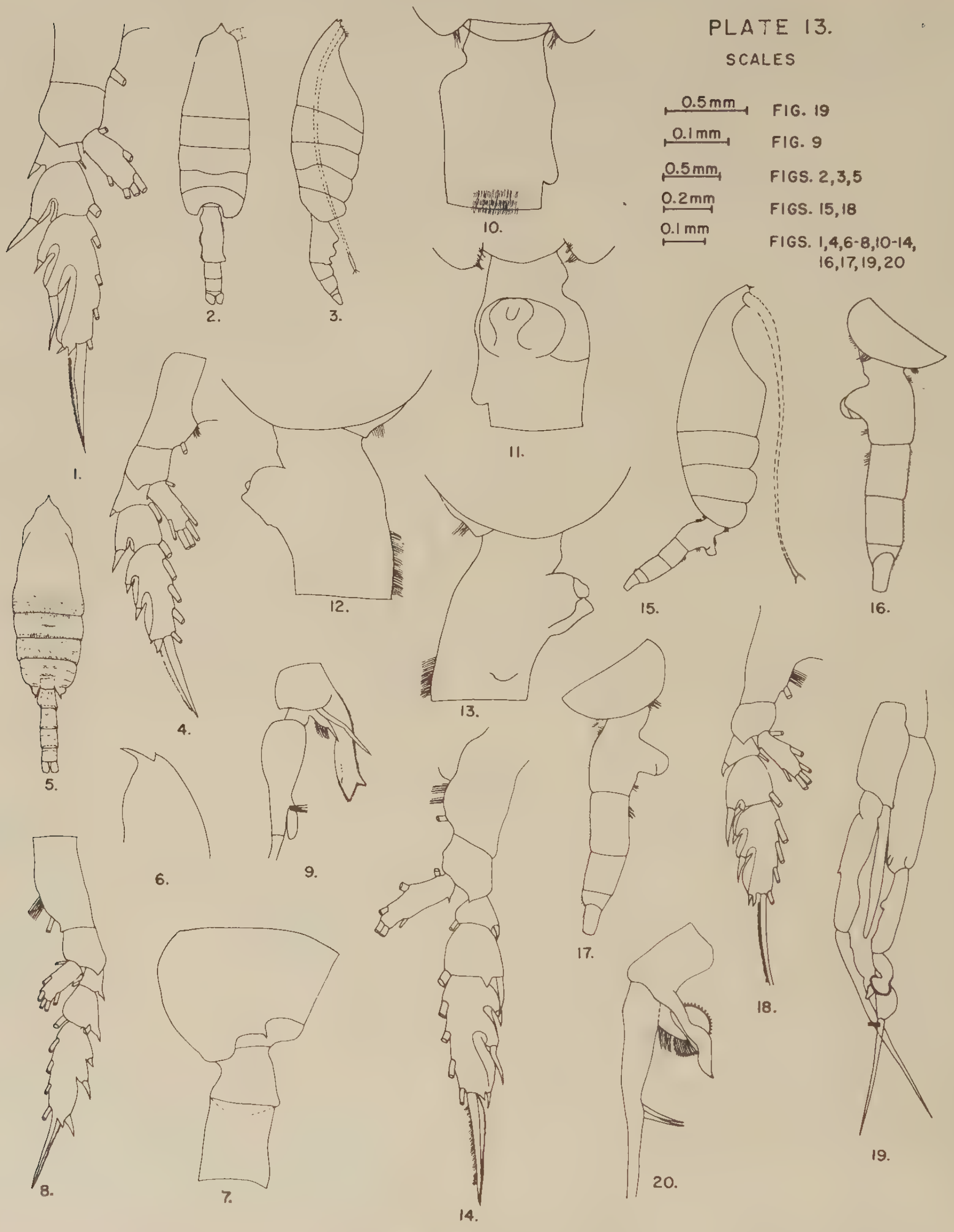
PLATE 13.
SCALES
0.5 mm FIG. 19
0.1 mm FIG. 9
0.5 mm FIGS. 2,3,5
0.2 mm FIGS. 15,18
0.1 mm FIGS. 1,4,6-8,10-14, 16,17,19,20
1.
2.
3.
4.
5.
6.
7.
8.
9.
10.
11.
12.
13.
14.
15.
16.
17.
18.
19.
20.

PLATE 13.—(1) *Euchaeta marina*, female, second foot; (2) *E. wolfendeni*, female, dorsal view; (3) lateral view; (4) second foot; (5) male, dorsal view; (6) forehead, lateral view; (7) posterior part of thorax and first two abdominal segments, lateral view; (8) second foot; (9) terminal part of left fifth foot; (10) *E. media*, female, genital segment, dorsal view; (11) genital segment, ventral view; (12) genital segment, left side; (13) genital segment, right side; (14) second foot; (15) *E. tenuis*, female, lateral view; (16) posterior part of thorax and abdomen, left side; (17) posterior part of thorax and abdomen, right side; (18) second foot; (19) male, fifth pair of feet; (20) terminal part of left fifth foot.

al., 1955; Chiba, 1956; Honjo et al., 1957; Tanaka, 1958; Yamazi, 1958a.

Vessel:	Station	Occurrence
Hugh M. Smith	132	1 female, 2.50 mm.
Do	63	1 female, 2.52 mm.
Stranger	34	3 females, 2.24–2.38 mm.; 2 males, 2.21, 2.35 mm.
Horizon	32	1 female, 2.55 mm.; 3 males, 2.31–2.44 mm.
Satsuma	32	2 females, 2.38, 2.40 mm.; 1 male, 2.31 mm.

Remarks: The female is distinguished by the long genital segment, the right posterior margin of which is produced into a rounded knob (fig. 2). The relative lengths of the outer-edge spines on the second and third exopodal segments of the second feet (fig. 4) are also diagnostic (cf. *E. marina*, plate 13, fig. 1). The male is identified by the structure of the terminal part of the left fifth foot (fig. 9).

Euchaeta media Giesbrecht, 1888

(Plate 13, figs. 10–14)

Pacific records: Vervoort, 1957. Also, Johnson, 1942; Brodsky, 1950; Tsuruta and Chiba, 1954b; Chiba, Tsuruta, and Maéda, 1955; Nagaya et al., 1955; Heinrich, 1957b; Honjo et al., 1957; Tanaka, 1958.

Vessel:	Station	Occurrence
Hugh M. Smith	63	1 female, 3.52 mm.

Remarks: The female of *E. media* is recognized by the characteristic swelling on the left side and the knob-like protrusion on the right side of the genital segment (figs. 10, 11). The middle spine on the outer edge of the third exopodal segment of the second pair of feet is elongate and the spine on the second exopodal segment reaches beyond the base of the proximal spine on the third segment (fig. 14).

Euchaeta tenuis Esterly, 1906

(Plate 13, figs. 15–20)

Pacific records: Esterly, 1906; Scott, 1909; Brodsky, 1950. As *E. solida*, Esterly, 1911.

Vessel:	Station	Occurrence
Hugh M. Smith	29	4 females, 5.60–5.98 mm.; 3 males, 5.03–5.22 mm.
Do	63	1 female, 5.13 mm.; 1 male, 4.75 mm.
Do	32	present.

Remarks: The large and asymmetrical ventral protrusions (figs. 16, 17) of the female genital segment will identify this species. The outer-edge spines of the second pair of feet (fig. 18) are also diagnostic. In the male the structure of the second segment of the left fifth foot (figs. 19, 20) is characteristic. It is dilated and coarsely serrate.

Euchaeta concinna Dana, 1849

(Plate 14, figs. 1–13)

Synonymy:

Euchaeta consimilis Farran, 1936, Great Barrier Reef Exped. 1928–29. Sci. Rept. 5(3): 90.

Pacific records: Scott, 1909; Farran, 1936; Mori, 1937; Dakin and Colefax, 1940; Wilson, 1950; Tanaka, 1953; Rose, 1955; Honjo et al., 1957; Heinrich, 1958b; Tanaka, 1958. As *E. consimilis;* Farran, 1936; Rose, 1955.

Vessel:	Station	Occurrence
Satsuma	32	3 females, 2.52–2.55 mm.; 1 male, 2.24 mm.

Remarks: Farran (1936) described *E. consimilis* from 4 female specimens collected near the Great Barrier Reef. He also found *E. concinna* in his collections, but this species was observed only inside the reef where it was one of the most characteristic of the copepods. According to Farran, *consimilis* differs, morphologically, from *concinna* in the form of the protrusion on the right side of the genital segment in the female (see Farran's fig. 6) and in size. As Farran pointed out, Sewell (1929) observed "a considerable degree of variation" in the form of the genital protrusion in *concinna* collected in the Indian Ocean. The latter author suggested that this variation may be correlated with egg laying which causes the protrusion to increase in size.

The size of specimens, as recorded in the literature is also variable.

Source:	Female	Male
Mori, 1937 (Japan)	3.0 mm.	
Tanaka, 1958 (Japan)	2.87–3.25 mm.	----------

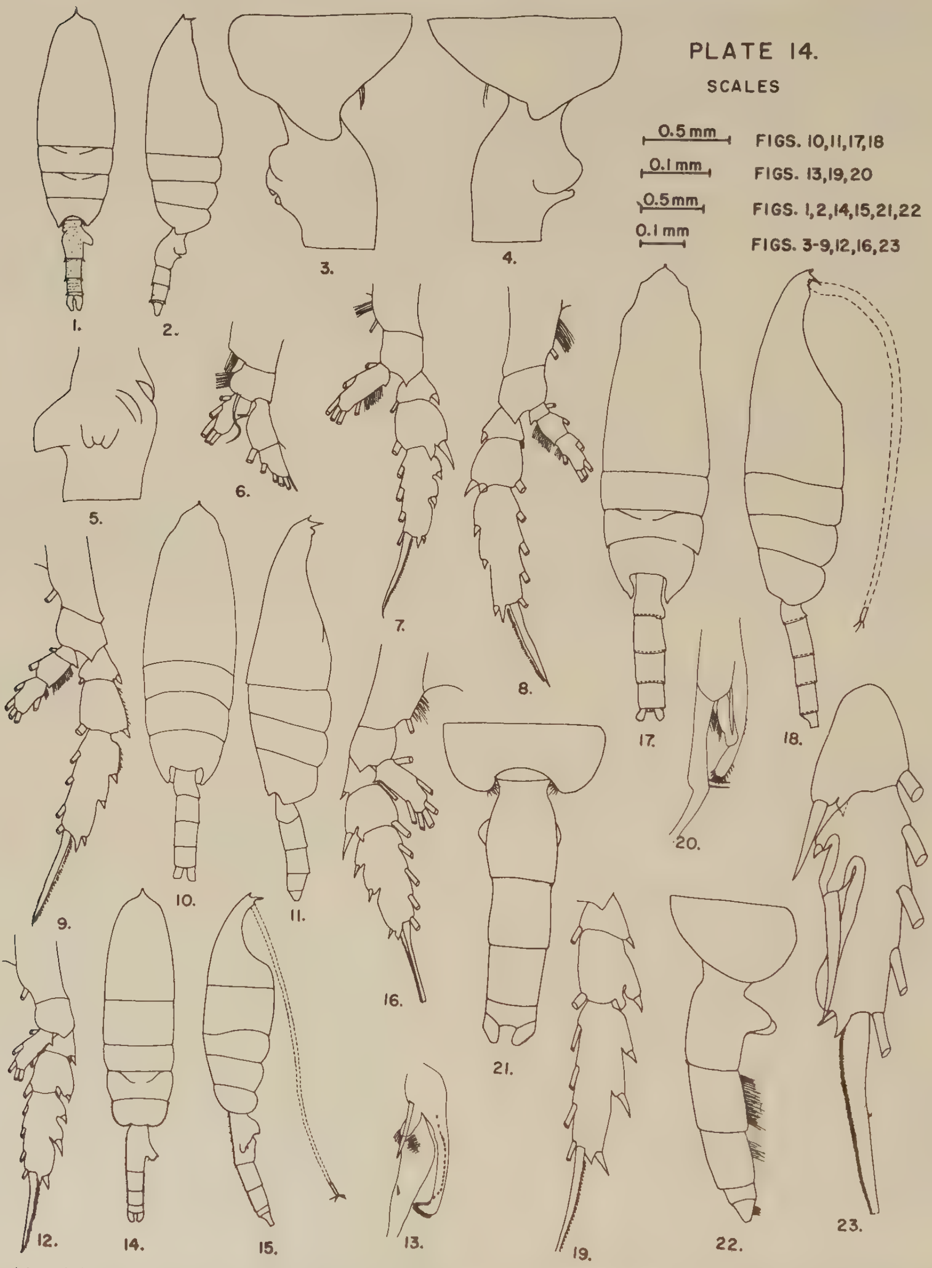
PLATE 14.
SCALES
0.5 mm FIGS. 10,11,17,18
0.1 mm FIGS. 13,19,20
0.5 mm FIGS. 1,2,14,15,21,22
0.1 mm FIGS. 3-9,12,16,23
1.
2.
3.
4.
5.
6.
7.
8.
9.
10.
11.
12.
13.
14.
15.
16.
17.
18.
19.
20.
21.
22.
23.

PLATE 14.—(1) *Euchaeta concinna*, female, dorsal view; (2) lateral view; (3) posterior part of thorax and genital segment, left side; (4) posterior part of thorax and genital segment, right side; (5) genital segment, ventral side; (6) first foot; (7) second foot; (8) third foot; (9) fourth foot; (10) male, dorsal view; (11) lateral view; (12) second foot; (13) terminal part of left fifth foot; (14) *E. longicornis*, female, dorsal view; (15) lateral view; (16) second foot; (17) male, dorsal view; (18) lateral view; (19) exopod of second foot; (20) terminal part of left fifth foot; (21) *E. spinosa*, female, posterior part of thorax and abdomen, dorsal view; (22) lateral view; (23) second and third segments of exopod of second foot.

Vessel:	Station	Occurrence
Giesbrecht and Schmeil, 1898 (tropical Pacific)	3.3 mm.	2.75 mm.
Heinrich, 1958b (tropical Pacific)	2.5 mm.	
Farran, 1936 (inside Barrier Reef)	3.25–3.40 mm.	2.54–2.76 mm.
Farran, 1936 (outside Barrier Reef)	2.36–2.67 mm.	
Dakin and Colefax, 1940 (Australia)	3.75 mm.	2.6 mm.
Sewell, 1929 (Indian Ocean)	2.5–3.5 mm.	2.4–3.0 mm.
Wolfenden, 1905 (Indian Ocean)	2.75–3.0 mm.	

In view of the wide size range in both sexes and the variable nature of the genital segment in the female, it seems best to consider *E. consimilis* as a synonym of *E. concinna.*

Euchaeta longicornis Giesbrecht, 1888

(PLATE 14, FIGS. 14–20)

Pacific records: Scott, 1909; Farran, 1929; 1936; Mori, 1937; Wilson, 1950; Honjo, 1952; Nakai, 1952; Tanaka, 1953; Anraku, 1954b; Chiba, Tsuruta, and Maéda, 1955; Nagaya et al., 1955; Honjo et al., 1957; Tanaka, 1958.

Vessel:	Station	Occurrence
Hugh M. Smith	94	3 females, 2.88 mm.
Do	132	8 females, 2.65–2.92 mm.; 1 male, 2.65 mm.

Remarks: The female genital segment has a large protrusion on the right side from which arises a smaller spine-like process.

Wilson (1950) described the male sex of this species. I have compared my single male specimen (except the body, which was destroyed in dissection) to one identified by G. O. Sars and loaned to me by the U.S. National Museum. The two are unispecific. In the Museum specimen a small spine is present on the superior-lateral margins of the fifth thoracic segment as is also found on the male of *E. wolfendeni* (see plate 13, fig. 7). I probably overlooked these spines in my specimen and therefore they are not shown in the figure given of the male (fig. 18).

Euchaeta spinosa Giesbrecht, 1892

(PLATE 14, FIGS. 21–23)

Pacific records: Esterly, 1905; Johnson, 1942; Brodsky, 1950; Wilson, 1950; Tanaka, 1953; 1958. As male of *Undeuchaeta major;* Esterly, 1905.

Vessel:	Station	Occurrence
Hugh M. Smith	29	1 female, 6.94 mm.

Remarks: The ventral projections of the genital segment (fig. 22) are visible in dorsal view. The middle spine on the outer margin of the third exopodal segment of the second feet is greatly elongate, and the spine on the second exopodal segment surpasses the tip of the first spine on the third segment (fig. 23).

Family PHAENNIDAE

Phaenna spinifera Claus, 1863

(PLATE 15, FIG. 1)

Pacific records: Scott, 1909; Farran, 1929; Mori, 1937; Wilson, 1942; 1950; Tanaka, 1953; Anraku, 1954b; 1954c; Tsuruta and Chiba, 1954b; Chiba, Tsuruta, and Maéda, 1955; Motoda and Anraku, 1955; Nagaya et al., 1955; Chiba, 1956; Honjo et al., 1957; Yamazi, 1958a. As *Onchocalanus nudipes;* Wilson, 1942.

Vessel:	Station	Occurrence
Hugh M. Smith	94	present.
Do	132	3 females, 1.87–1.90 mm.
Do	31	1 female, 1.60 mm.
Do	63	present.
Orsom	10	1 female, 1.87 mm.
Horizon	32	present.

Remarks: The globular thorax, small abdomen, and lack of fifth feet (in the female) make this species easily recognized. Vervoort (1950) placed Wilson's *Onchocalanus nudipes* in synonymy with *Phaenna spinifera.*

Xanthocalanus dilatus n. sp.

(PLATE 15, FIGS. 2–11)

Vessel:	Station	Occurrence
Hugh M. Smith	144	2 females, 1.56, 1.60 mm.

Description: The head and first thoracic segment and fourth and fifth thoracic segments are separate (figs. 2, 3). The posterior lateral margins of the first thoracic segment are dis-

PLATE 15.

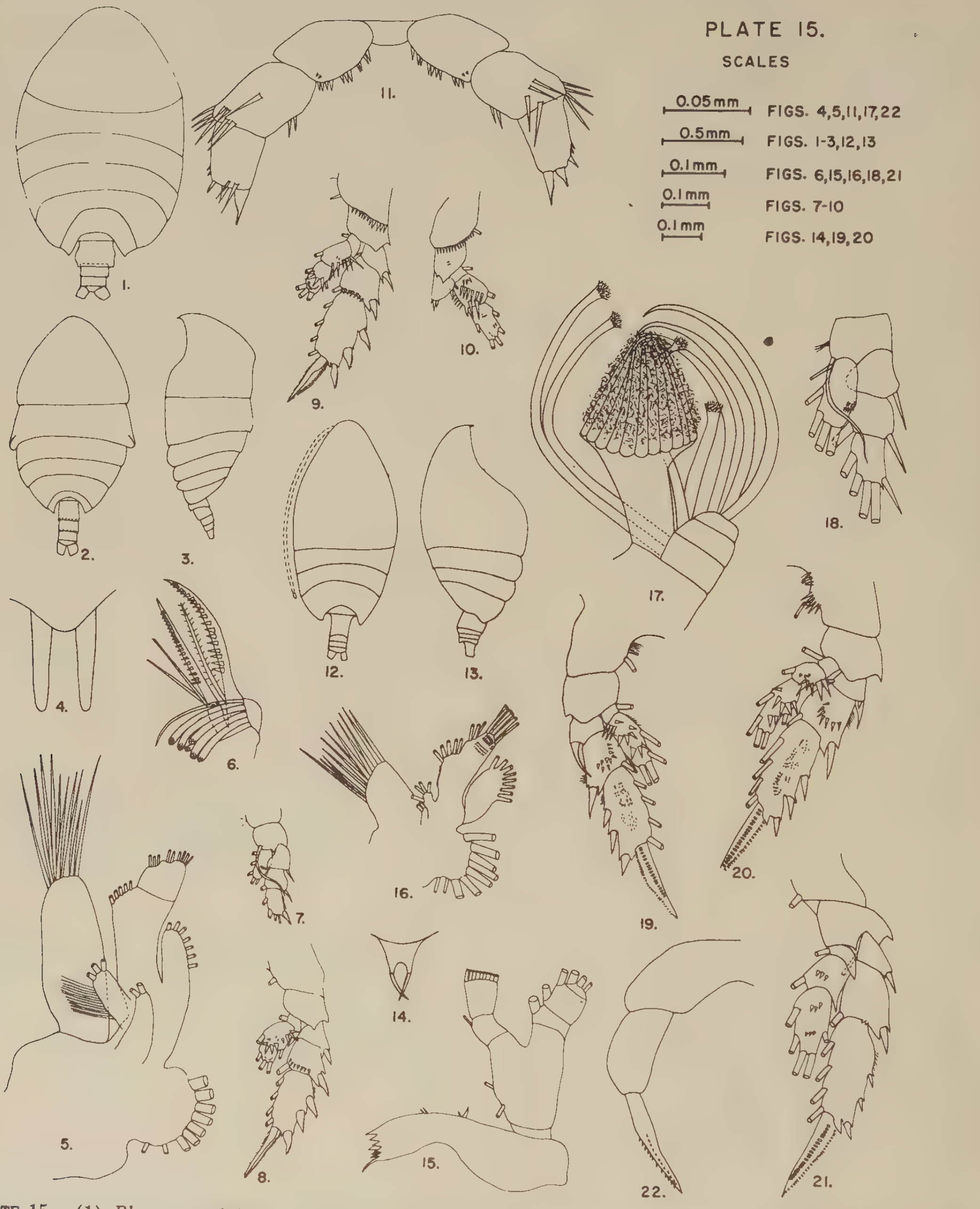
SCALES
0.05 mm FIGS. 4,5,11,17,22
0.5 mm FIGS. 1-3,12,13
0.1 mm FIGS. 6,15,16,18,21
0.1 mm FIGS. 7-10
0.1 mm FIGS. 14,19,20
1.
2.
3.
4.
5.
6.
7.
8.
9.
10.
11.
12.
13.
14.
15.
16.
17.
18.
19.
20.
21.
22.

PLATE 15.—(1) *Phaenna spinifera*, female, dorsal view; (2) *Xanthocalanus dilatus* n.sp., female, dorsal view; (3) lateral view; (4) rostrum; (5) first maxilla, (6) terminal part of second maxilla; (7) first foot; (8) second foot; (9) third foot; (10) fourth foot (distal two segments of exopod missing); (11) fifth pair of feet (figs. 2–6 and 11 of holotype, figs. 7–10 of paratype); (12) *Amallophora smithae* n. sp., female, dorsal view; (13) lateral view; (14) rostrum; (15) mandible; (16) first maxilla; (17) terminal part of second maxilla; (18) first foot; (19) second foot; (20) third foot; (21) fourth foot; (22) fifth foot (figs. 12–22 of holotype).

tended and there is a distinct dilation on the dorsal surface of the head. The rostrum is straight and club-like (fig. 4).

The first antennae of both specimens are broken off near the proximal end. Although somewhat mutilated, the second antennae appear to have 1 seta on the first segment of the endopod. The second segment of the endopod has 14 setae on the distal margin (8 on the inner lobe and 6 on the outer lobe). The exopod has a total of 6 setae but some may be missing from the various segments.

The mandible has 3 setae on the basipod, 11 setae on the endopod and 6 on the exopod.

The first maxilla (fig. 5) has the following number of setae: 9 on the external lobe, 7 on the exopod, 9 on the endopod, 5 on the second basal segment, 2 on the second internal lobe and 3 on the third internal lobe.

The terminal part of the second maxilla (fig. 6) has 6 sensory organs and 1 worm-like appendage.

The exopods of the first 4 pairs of feet are 3-segmented (figs. 7–10), although the second and third exopodal segments of the fourth pair are broken off. The endopod of the first foot consists of 1 segment, of the second foot of 2 segments and of the third and fourth feet of 3 segments. The endopodal segments of the second and third feet have numerous spines arising from their posterior surfaces. A row of spines is present at the junction of the first and second basipodal segments, on the posterior side, of the third and fourth feet. The fifth foot (fig. 11) consists of 3 segments, all of which are furnished with either marginal or surface spines.

Remarks: This species differs from other described *Xanthocalanus* in (1) the dilations of the dorsal surface of the head and lateral margins of the first thoracic segment, (2) the spines on the basipodal segments of the third and fourth feet, and (3) the details of the fifth pair of feet. The fifth pair of feet closely resemble those of *X. agilis* Giesbrecht but *agilis* lacks the characteristic dilations of the head and first thoracic segment of the present species. In addition, *X. agilis* is a larger species (2.40 mm.). The presence of spines on the basipodal segments may also be found in other species of *Xanthocalanus*. Figures of these segments are available for only a few species.

The name proposed for this species is derived from the Latin word "dilato" and refers to the characteristic protrusions on the head and first thoracic segment. The holotype (U.S.N.M. No. 104, 420) and 1 paratype (No. 104, 421) have been deposited in the U.S. National Museum.

Amallophora smithae n. sp.

(PLATE 15, FIGS. 12–22)

Vessel:	*Station*	*Occurrence*
Hugh M. Smith	144	1 female, 1.40 mm.

Description: The head and first thoracic segments and the fourth and fifth thoracic segments are fused (fig. 12). In lateral view the posterior margin of the cephalothorax has a small indentation (fig. 13).

The first antennae are short and do not reach the end of the cephalothorax. Each antenna consists of 23 segments.

The endopod of the second antenna is slightly less than three-fourths the length of the exopod. Endopodal segment 1 has 2 setae. Segment 2 has 8 setae on the inner lobe and 7 setae on the outer lobe. The exopod has 8 setae all of which are densely plumose.

The basal segment of the mandibular palpus has 2 setae (fig. 15). There are 9 setae on the distal segment of the endopod and 1 seta on the proximal segment. The exopod has a total of 6 setae.

The first maxilla (fig. 16) has the following number of setae: 11 on the first inner lobe, 2 on the second inner lobe, 4 on the third inner lobe, 5 on the second basal segment, 9 on the endopod, 8 on the exopod and 9 on the external lobe. Two groups of small spines are present on the surface of the endopod.

The terminal part of the second maxilla (fig. 17) has 1 enlarged sensory organ, 4 smaller sensory organs and 3 worm-like appendages.

The first and second basal segments of the maxilliped have 7 and 5 setae, respectively. The 5 endopodal segments have the following number of setae: 4, 4, 3, 3 (plus 1 external seta), and 4.

The first pair of feet have 3-segmented exopods and 1-segmented endopods (fig. 18). The second pair of feet have exopods composed of 3 segments and endopods of 2 segments while the succeeding 2 pairs of feet each have 3-segmented exopods and endopods (figs. 19–21). The terminal spine of the second, third, and fourth pair of feet is characterized by an outer serrate margin and an inner row of small perforations. The endopods of the second and third feet have large spines arising from their surfaces. Numerous smaller spines are present on the 2 distal exopodal segments of the second and third feet. The fourth feet have a reduced number of spines.

The fifth feet (fig. 22) are small and consist of 2 segments. There is a stout and finely toothed spine arising from the distal segment.

Remarks: This species is closely related to *A. vorax* (Esterly, 1911). It differs from Esterly's species in the segmentation of the cephalothorax, cephalothorax-abdomen ratio, and the structure of the fifth feet. The fourth and fifth thoracic segments are separate in *A. vorax* but fused in *A. smithae*. Davis (1949) also reported that these segments in his specimen of *A. vorax* were fused. The cephalothorax is 6½ times longer than the abdomen in *A. vorax* according to Esterly; in the present species it is approximately 4 times the length of the abdomen. Davis stated that the abdomen of his specimen was longer than that reported by Esterly. In *A. vorax* there are two spines on the distal segment of the fifth feet. In *A. smithae* there is one robust spine.

Vervoort (1957) has discussed the genus *Amallophora* and pointed out differences between it and the genus *Xanthocalanus*. The structures of the maxillae and fifth feet appear to exclude the present species from the genus *Xanthocalanus* although the articulated rostral filaments are unlike those found in *Amallophora*. If Brodsky (1950) is correct in assigning Esterly's species (described as *Scolecithrix vorax*) to the genus *Amallothrix* then perhaps the present species should also be placed in this genus. Until the *Xanthocalanus–Amallothrix–Amallophora* complex is revised, I am referring the present species to the genus *Amallophora*.

The species is named for the research vessel *Hugh M. Smith*. The holotype is deposited in the U.S. National Museum (No. 104, 422).

Family SCOLECITHRICIDAE

Scolecithrix danae (Lubbock, 1856)

Pacific records: Esterly, 1905; Scott, 1909; Farran, 1929; Yamada, 1933; Farran, 1936; Mori, 1937; Dakin and Colefax, 1940; Johnson, 1942; Mori, 1942; Wilson, 1942; 1950; Anraku, 1952; Honjo, 1952; Nakai, 1952; Tanaka, 1953; Anraku, 1954b; Johnson, 1954; Tsuruta and Chiba, 1954b; Chiba, Tsuruta, and Maéda, 1955; Hida and King, 1955; Motoda and Anraku, 1955; Nagaya et al., 1955; Chiba, 1956; Honjo et al., 1957; Heinrich, 1958a; Yamazi, 1958a.

Vessel:	*Station*	*Occurrence*
Hugh M. Smith	132	present.
Do	144	present.
Do	153	present.
Do	178	present.
Do	30	present.
Do	31	3 females, 2.04–2.14 mm.
Do	29	3 females, 2.01–2.04 mm.
Do	63	4 females, 2.04–2.14; 3 males, 2.07–2.21 mm.
Stranger	34	2 females, 2.00, 2.04 mm.
Orsom	10	2 females, 2.01, 2.11; 1 male, 1.97 mm.
Horizon	32	3 females, 2.04; 2 males, 2.04, 2.11 mm.
Satsuma	32	2 females, 1.90, 2.00 mm.

Remarks: The posteriorly directed ventral protrusion on the female genital segment and the structure of the fifth feet of the male serve to identify this species. Figures of both these characters are given in Rose, 1933.

Scolecithrix bradyi Giesbrecht, 1888

(PLATE 16, FIGS. 1–5)

Pacific records: Esterly, 1905; Farran, 1929; 1936. As *Scolecithricella bradyi;* Scott, 1909; Mori, 1937; 1942; Wilson, 1942; 1950; Honjo, 1952; Tanaka, 1953; Chiba, Tsuruta, and Maéda, 1955; Motoda and Anraku, 1955; Nagaya et al., 1955; Chiba, 1956; Honjo et al., 1957.

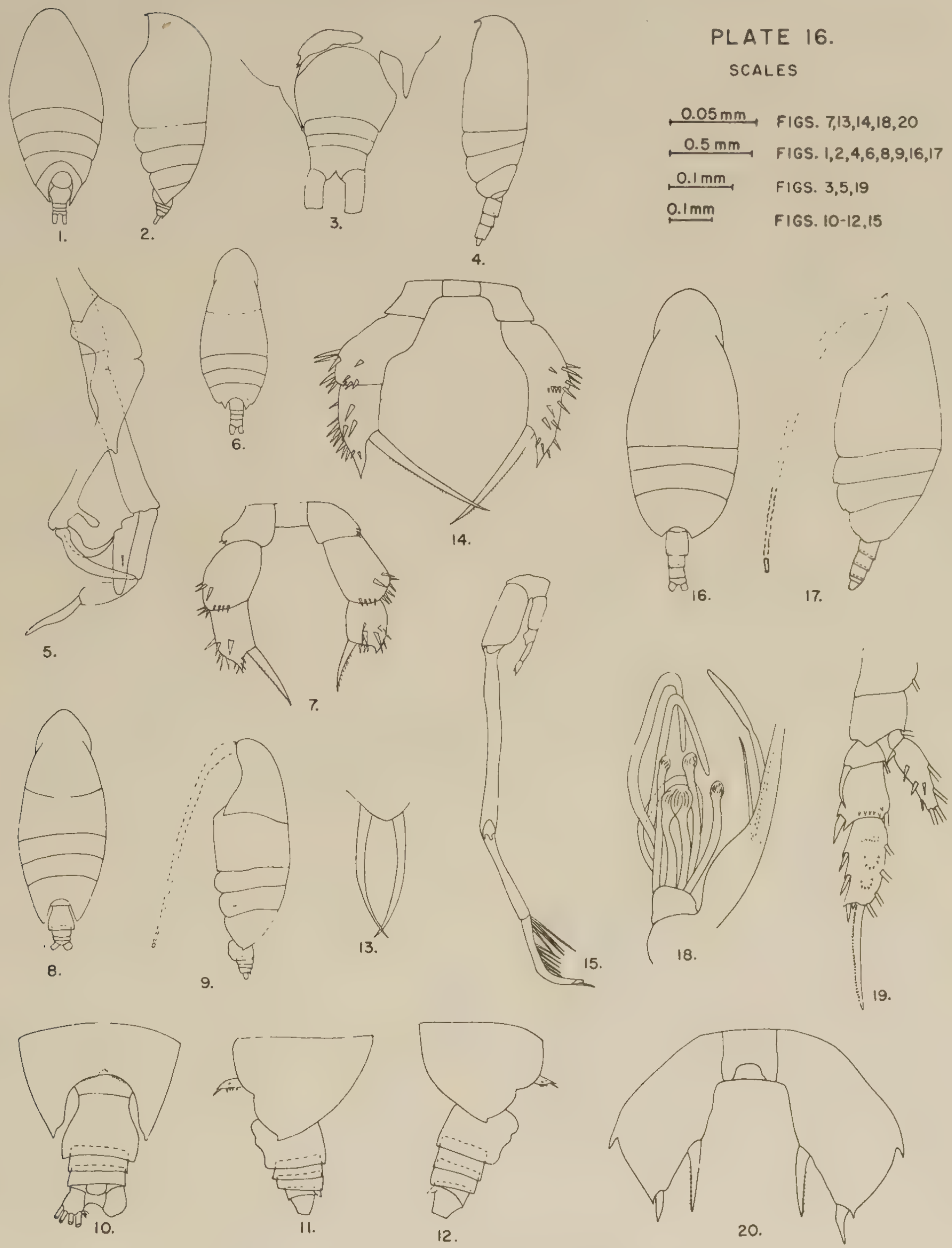
PLATE 16.
SCALES
0.05 mm FIGS. 7,13,14,18,20
0.5 mm FIGS. 1,2,4,6,8,9,16,17
0.1 mm FIGS. 3,5,19
0.1 mm FIGS. 10-12,15
1.
2.
3.
4.
5.
6.
7.
8.
9.
10.
11.
12.
13.
14.
15.
16.
17.
18.
19.
20.

PLATE 16.—(1) *Scolecithrix bradyi*, female, dorsal view; (2) lateral view; (3) posterior part of thorax and abdomen, ventral view; (4) male, lateral view; (5) fifth pair of feet; (6) *Scolecithricella ctenopus*, female, juvenile, dorsal view; (7) fifth pair of feet; (8) adult, dorsal view; (9) lateral view; (10) posterior part of thorax and abdomen, dorsal view; (11) left side; (12) right side; (13) rostrum; (14) fifth pair of feet; (15) male, fifth pair of feet; (16) *S. abyssalis*, female, dorsal view; (17) lateral view; (18) terminal part of second maxilla; (19) second foot; (20) fifth pair of feet.

Vessel:	Station	Occurrence
Hugh M. Smith	94	11 females, 1.36–1.41; 2 males, 1.51, 1.56 mm.
Do	132	4 females, 1.33–1.36 mm.
Do	144	present.
Do	178	present.
Do	31	present.

Remarks: The asymmetrical posterior thoracic margins, the right one of which extends beyond the genital segment (fig. 1), serve to identify the female of this species. The male is recognized by the structure of the fifth feet (fig. 5).

Scolecithricella ctenopus (Giesbrecht, 1888)

(PLATE 16, FIGS. 6–15)

Synonymy:

Scolecithrix ctenopus Giesbrecht, 1888, Atti Acc. Lincei Rend., ser. 4, 4 sem. 2: 338.

Scolecithricella ctenopus Sewell, 1929, Mem. Ind. Mus., 10: 212.

Scolecithrix longicornis T. Scott, 1894, Trans. Linn. Soc., Zool., 6: 50.

Scolecithricella spinipedata Mori, 1937, The pelagic Copepoda from the neighbouring waters of Japan, p. 53.

Pacific records: Scott, 1909; Farran, 1936; Tanaka, 1953.

Vessel:	Station	Occurrence
Hugh M. Smith	94	1 juvenile female, 1.28 mm.
Do	178	2 females, 1.49, 1.53; 1 male, 1.54 mm.
Stranger	34	1 female, 1.46; 1 male, 1.46 mm.
Orsom	10	1 female, 1.48 mm.

Remarks: Farran (1936) found two females which differed in size, segmentation of thorax and structure of fifth feet. He also reviewed the records and descriptions of *S. longicornis* (Scott, 1894) and considered it a synonym of *S. ctenopus*.

The present female specimens also fall into two size groups, the smaller of which is very similar to Farran's small specimen. The head and thorax in this form are separated by a fine line (in Farran's specimen they were fused) and a faint line is also seen to separate the fourth and fifth thoracic segments (fig. 6). Although the fifth feet are fairly well differentiated, the genital segment is undeveloped in this small specimen. In the larger form (figs. 8–14) the head and first thoracic segment are incompletely fused and the fourth and fifth thoracic segments are completely fused. The genital segment is well developed as are the fifth feet.

Although it is slightly larger, Mori's *S. spinipedata*, is, in my opinion, a synonym of *S. ctenopus*.

Scolecithricella abyssalis (Giesbrecht, 1888)

(PLATE 16, FIGS. 16–20)

Pacific records: Scott, 1909; Mori, 1937; Tanaka, 1937; Wilson, 1942; 1950; Anraku, 1952; Tanaka, 1953; Brodsky, 1955; Chiba, Tsuruta, and Maéda, 1955; Nagaya et al., 1955; Chiba, 1956.

Vessel:	Station	Occurrence
Hugh M. Smith	94	6 females, 1.87–1.90 mm.
Do	144	1 female, 1.74 mm.
Do	29	1 female, 2.21 mm.
Do	63	1 female, 1.87 mm.

Remarks: Some variation was noted in the structure of the fifth feet of this species. Several specimens did not have the small spine-like protrusion near the terminal spine as shown in the fifth feet figured here (fig. 20).

Scolecithricella vittata (Giesbrecht, 1892)

(PLATE 17, FIGS. 1–8)

Pacific records: Farran, 1936; Wilson, 1950; Tanaka, 1953.

Vessel:	Station	Occurrence
Hugh M. Smith	94	2 females, 1.66 mm.

Remarks: As in the preceding species, variation was noted in the fifth feet of this species. The terminal seta in one specimen was approximately twice the length of the proximal one (fig. 8) while in the other specimen it was somewhat shorter (fig. 4).

Scolecithricella tenuiserrata (Giesbrecht, 1892)

(PLATE 17, FIGS. 9–21; PLATE 18, FIG. 1)

Pacific records: Farran, 1936; Tanaka, 1953.

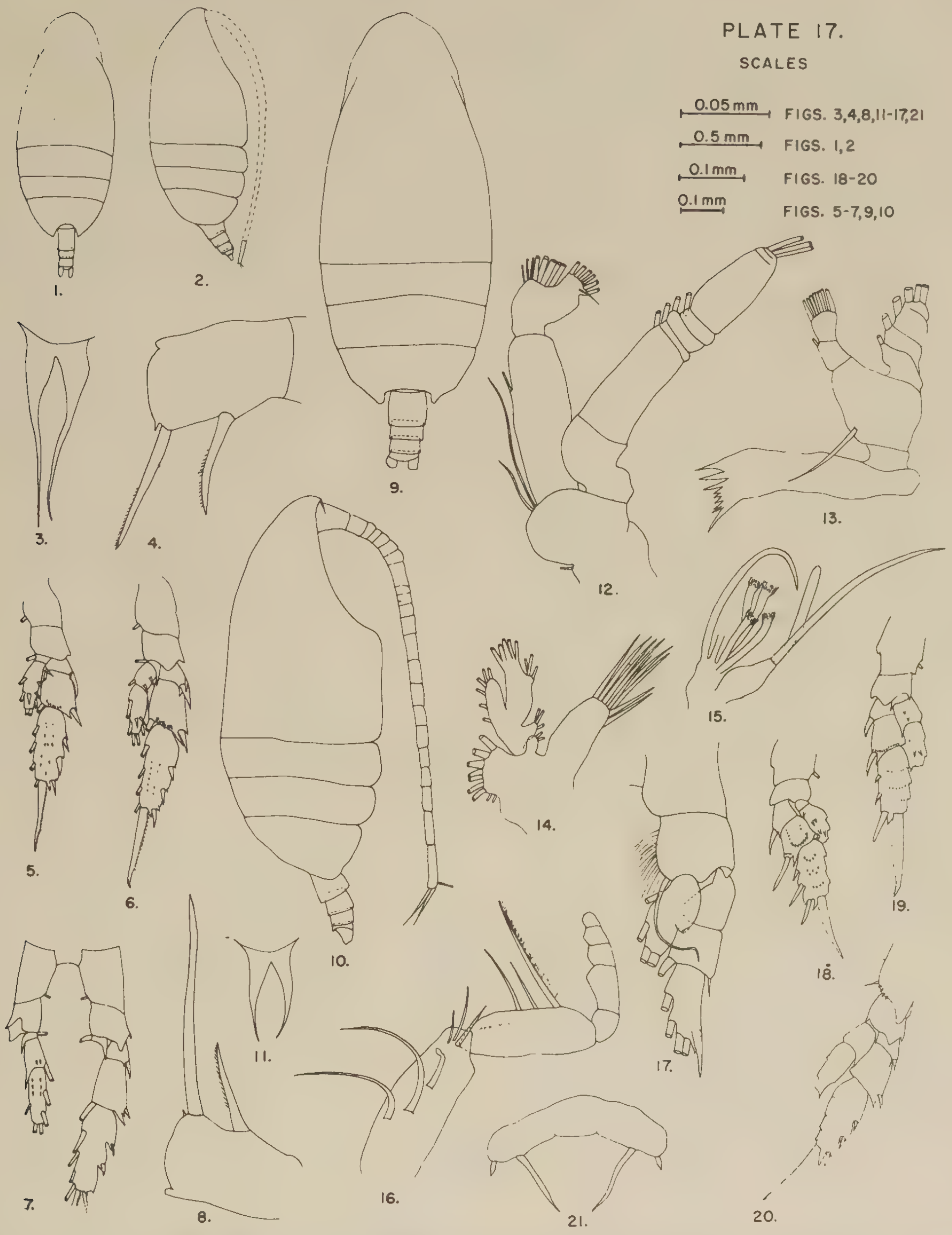
PLATE 17.
SCALES
0.05 mm FIGS. 3,4,8,11-17,21
0.5 mm FIGS. 1,2
0.1 mm FIGS. 18-20
0.1 mm FIGS. 5-7,9,10
1.
2.
3.
4.
5.
6.
7.
8.
9.
10.
11.
12.
13.
14.
15.
16.
17.
18.
19.
20.
21.

Plate 17.—(1) *Scolecithricella vittata*, female, dorsal view; (2) lateral view; (3) rostrum; (4) fifth foot; (5) second foot; (6) third foot; (7) fourth pair of feet (one exopod and one endopod missing); (8) fifth foot; (9) *S. tenuiserrata*, female, dorsal view; (10) lateral view; (11) rostrum; (12) second antenna; (13) mandible; (14) first maxilla; (15) terminal part of second maxilla; (16) maxilliped (setae on endopod not shown); (17) first foot; (18) second foot (setae not shown); (19) third foot (setae not shown); (20) fourth foot (setae not shown); (21) fifth pair of feet.

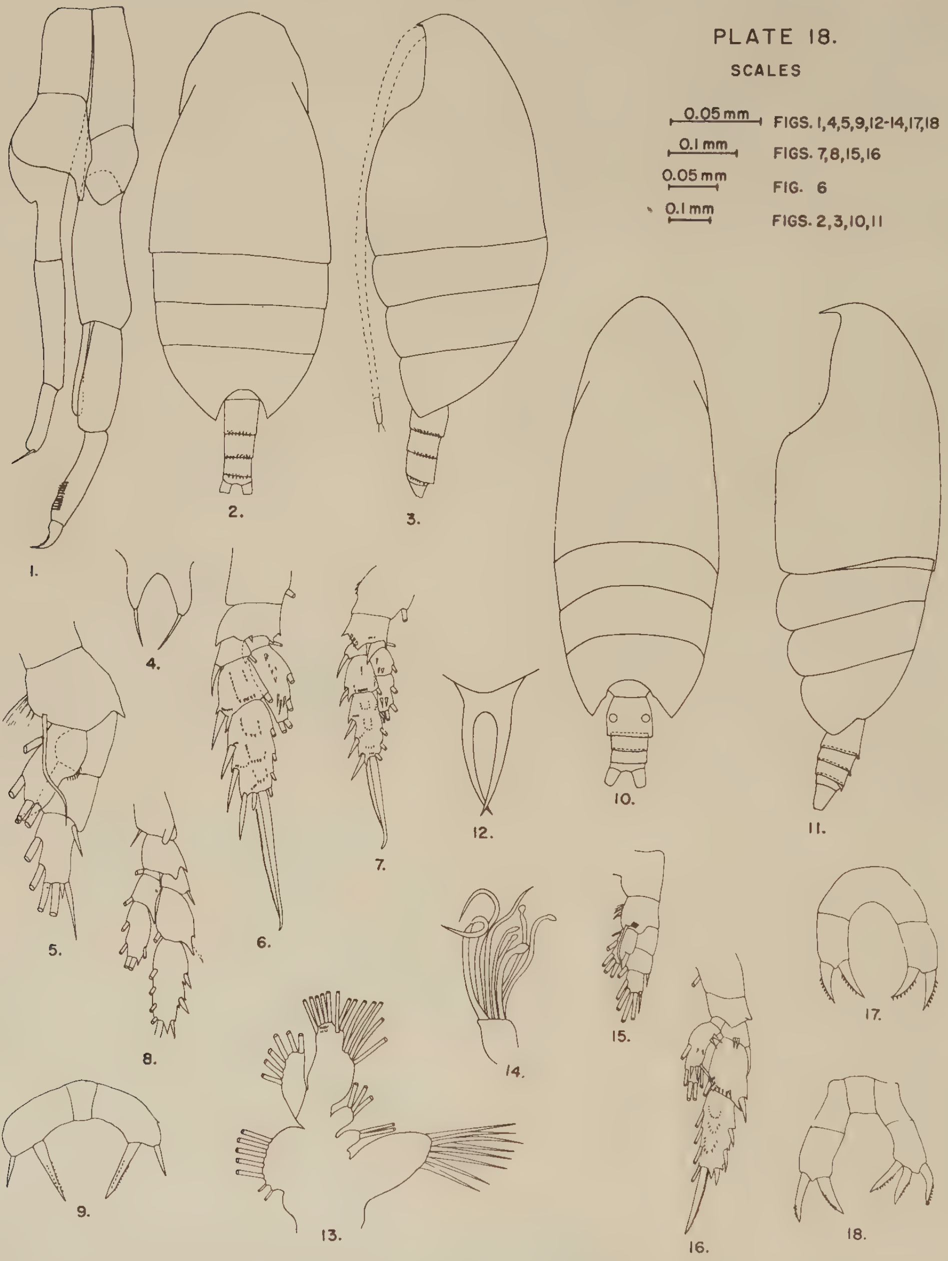
PLATE 18.
SCALES
0.05 mm FIGS. 1,4,5,9,12-14,17,18
0.1 mm FIGS. 7,8,15,16
0.05 mm FIG. 6
0.1 mm FIGS. 2,3,10,11
1.
2.
3.
4.
5.
6.
7.
8.
9.
10.
11.
12.
13.
14.
15.
16.
17.
18.

PLATE 18.—(1) *Scolecithricella tenuiserrata*, male, fifth pair of feet; (2) *S. marginata*, female, dorsal view; (3) lateral view; (4) rostrum; (5) first foot; (6) second foot; (7) third foot; (8) fourth foot; (9) fifth pair of feet; (10) *Scolecithricella tropica* n. sp., female, dorsal view; (11) lateral view; (12) rostrum; (13) first maxilla; (14) terminal part of second maxilla; (15) first foot; (16) second foot; (17) fifth pair of feet; (18) fifth pair of feet, abnormal (figs. 10–18 of paratype).

Vessel:	Station	Occurrence
Hugh M. Smith	144	1 female, 1.08 mm.; 1 male, 1.17 mm.
Do	178	4 females, 1.05–1.10 mm.; 4 males, 1.0–1.27 mm.
Do	31	present.
Stranger	34	3 females, 1.02–1.10 mm.

Remarks: Because of the difficulty encountered in identifying this species, I have included several figures of the female and a figure of the fifth feet of a specimen that I consider to be the male of this species. Giesbrecht and Schmeil (1898) stated that the second basal segment of the first maxilla of the female has 5 setae. The present specimens have 3 setae on this segment. Although these authors indicated that the male of this species is questionable, they gave the length as 1.45 mm. as compared to 1.15 mm. for the female. The present males are also larger than the females.

Scolecithricella marginata (Giesbrecht, 1888)

(PLATE 18, FIGS. 2–9)

Pacific records: Scott, 1909; Wilson, 1942.

Vessel:	Station	Occurrence
Hugh M. Smith	144	2 females, 1.05 mm.
Do	178	2 females, 1.00, 1.02 mm.

Remarks: The small size and fifth feet (fig. 9) serve to identify this species.

Scolecithricella tropica n. sp.

(PLATE 18, FIGS. 10–18)

Vessel:	Station	Occurrence
Hugh M. Smith	94	4 females, 1.22–1.30 mm.
Do	132	5 females, 1.15–1.27 mm.
Do	178	2 females, 1.13, 1.14 mm.

Description: Of the 11 specimens of this species examined, none was intact. The following description is based, therefore, on several specimens and even with these a discussion of certain appendages will not be possible.

The cephalothorax is considerably longer than the abdomen, the ratio of these two body parts is approximately 4.4: 1.0 (figs. 10, 11). The posterior thoracic border has a well-defined indentation at a point just anterior to the apex. The genital segment is longer than the combined lengths of the next 2 segments. The rostral filaments are long and apparently not articulated to the base (fig. 12).

The first maxilla (fig. 13) has the following number of setae: 2 on the second inner lobe, 3 on the third inner lobe, 5 on the second basal segment, 8 on the endopod, and 6 on the exopod.

The terminal portion of the second maxilla (fig. 14) has 5 sensory and 3 worm-like appendages.

The first pair of feet (fig. 15) has a 3-segmented exopod and 1-segmented endopod. A group of small spines is present on the second basal segment near the distal margin. The exopod of the second pair of feet consists of 3 segments and the endopod of 2 segments (fig. 16). Two spines are present on the surface of the first exopodal segment, a group of large and small spines on the second segment and three groups of spines on the third exopodal segment. Five large and 2 small spines are present on the second endopodal segment.

As in certain other species of *Scolecithricella*, the fifth feet are variable. Most of the specimens examined have 2, approximately equal, terminal spines (fig. 17) but at least 2 specimens were observed to have 3 on one side and 2 on the other (fig. 18).

This species is distinguished from other species of *Scolecithricella* by the indentation on the posterior thoracic margin and the structure of the fifth feet.

Remarks: An undissected female from Station 94 was selected as the holotype (U.S.N.M. No. 104, 416). This specimen and 6 paratypes (Nos. 104, 417–104, 419) have been deposited in the U.S. National Museum.

Scolecithricella sp.

(PLATE 19, FIGS. 1–5)

Vessel:	Station	Occurrence
Hugh M. Smith	144	2 males, 1.20, 1.22 mm.

Remarks: Two male specimens which are apparently referable to the genus *Scolecithri-*

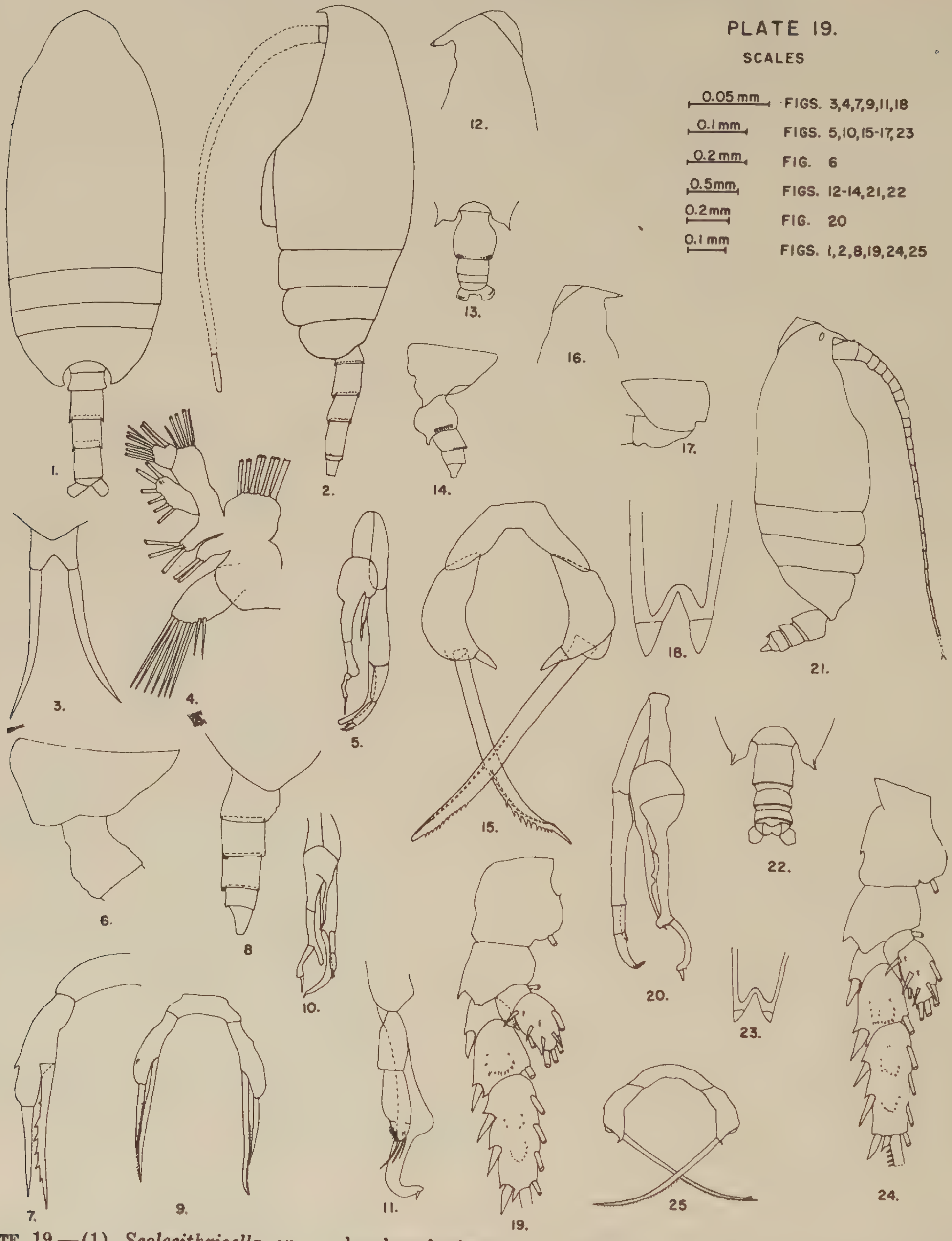
PLATE 19.
SCALES
0.05 mm FIGS. 3,4,7,9,11,18
0.1 mm FIGS. 5,10,15-17,23
0.2 mm FIG. 6
0.5 mm FIGS. 12-14,21,22
0.2 mm FIG. 20
0.1 mm FIGS. 1,2,8,19,24,25
1.
2.
3.
4.
5.
6.
7.
8
9.
10.
11.
12.
13.
14.
15.
16.
17.
18.
19.
20.
21.
22.
23.
24.
25

PLATE 19.—(1) *Scolecithricella sp.*, male, dorsal view; (2) lateral view; (3) rostrum; (4) first maxilla; (5) fifth pair of feet; (6) *Scaphocalanus echinatus*, female, posterior part of thorax and genital segment; (7) fifth foot; (8) *S. longifurca*, female, posterior part of thorax and abdomen, lateral view; (9) fifth pair of feet; (10) male, fifth pair of feet; (11) left fifth foot; (12) *Scottocalanus securifrons*, female, forehead, lateral view; (13) abdomen, dorsal view; (14) posterior part of thorax and abdomen, lateral view; (15) fifth pair of feet; (16) *S. farrani*, male, forehead, lateral view; (17) posterior part of thorax and genital segment, lateral view; (18) rostrum; (19) second foot; (20) fifth pair of feet; (21) *S. sedatus*, female, lateral view; (22) abdomen, dorsal view; (23) rostrum; (24) second foot; (25) fifth pair of feet.

cella were found in the above sample. As the males of several described females, including the preceding species, are not known, I hesitate to describe the present species as new.

Scaphocalanus echinatus (Farran, 1905)

(PLATE 19, FIGS. 6, 7)

Pacific records: Farran, 1929, 1936; Mori, 1937; Wilson, 1950; Honjo, 1952; Tanaka, 1953; Tsuruta and Chiba, 1954a; Chiba, 1956; Honjo et al., 1957.

Vessel:	*Station*	*Occurrence*
Hugh M. Smith	63	1 female, 2.00 mm.

Remarks: *S. echinatus* resembles *S. longifurca* but the inner edge setae on the fifth feet of the former species are coarsely toothed (fig. 7).

Scaphocalanus longifurca (Giesbrecht, 1888)

(PLATE 19, FIGS. 8–11)

Pacific records: Tanaka, 1953. As *Scolecithricella longifurca*, Scott, 1909. As ?*Scaphocalanus gracilicauda*, Tanaka, 1937.

Vessel:	*Station*	*Occurrence*
Hugh M. Smith	94	1 male, 1.53 mm.
Do	29	2 females, 1.87, 1.94 mm.
Do	63	1 female, 1.94 mm.

Remarks: The similarity of this species to *S. subbrevicornis* has been pointed out by Farran (1929) and Vervoort (1951). The latter author has indicated that Tanaka's *S. gracilicauda* (male) is identical to a male doubtfully referred by Rose (1942) to *S. dentata*. Vervoort (1951) suggests that these two males may be the male of *S. longifurca*. I, too, have found a male specimen which I am tentatively referring to *S. longifurca* rather than to *S. subbrevicornis*, as figured by Vervoort, because of the small size of the present specimen (1.53). Vervoort's specimens measured 2.19 mm. and Tanaka's single specimen was 1.75 mm. The former author has also suggested (1957) that Wilson's (1950) records of *S. subbrevicornis* are probably referable to *S. longifurca*.

Scottocalanus securifrons (T. Scott, 1894)

(PLATE 19, FIGS. 12–15)

Pacific records: Scott, 1909; Farran, 1929; Tanaka, 1937; Brodsky, 1950; Wilson, 1950; Tanaka, 1953; Hida and King, 1955; Heinrich, 1958b.

Vessel:	*Station*	*Occurrence*
Horizon	32	1 female, 4.08 mm.

Remarks: The ventral surface of the genital segment is produced posteriorly and partly overlaps the following segment (fig. 14). The spine on the left fifth foot is thicker than that on the right (fig. 15). These two characters will identify the female of this species. No male has been found in the present samples.

Scottocalanus farrani A. Scott, 1909

(PLATE 19, FIGS. 16–20)

Pacific records: Scott, 1909; Wilson, 1950.

Vessel:	*Station*	*Occurrence*
Hugh M. Smith	29	1 male, 3.50 mm.

Remarks: The structure of the fifth pair of feet particularly the relative lengths of the exo- and endopods and the presence of a tooth-like process on the second basal segment of the right foot will identify the male of this species. No females were found.

Scottocalanus sedatus Farran, 1936

(PLATE 19, FIGS. 21–25)

Pacific records: Farran, 1936.

Vessel:	*Station*	*Occurrence*
Hugh M. Smith	29	1 female, 3.40 mm.
Orsom	10	1 female, 3.30 mm.

Remarks: This species is distinguished by the long setae and small, outwardly directed spines on the terminal segments of the fifth pair of feet (fig. 25).

Family TEMORIDAE

Temoropia mayumbaensis T. Scott, 1894

(PLATE 20, FIGS. 1–12)

Pacific records: Scott, 1909; Farran, 1929; 1936; Wilson, 1942; Heinrich, 1957b.

Vessel:	*Station*	*Occurrence*
Hugh M. Smith	94	6 females, 0.94–0.99; 3 males, 0.88–0.92 mm.
Orsom	10	2 females, 0.98 mm.

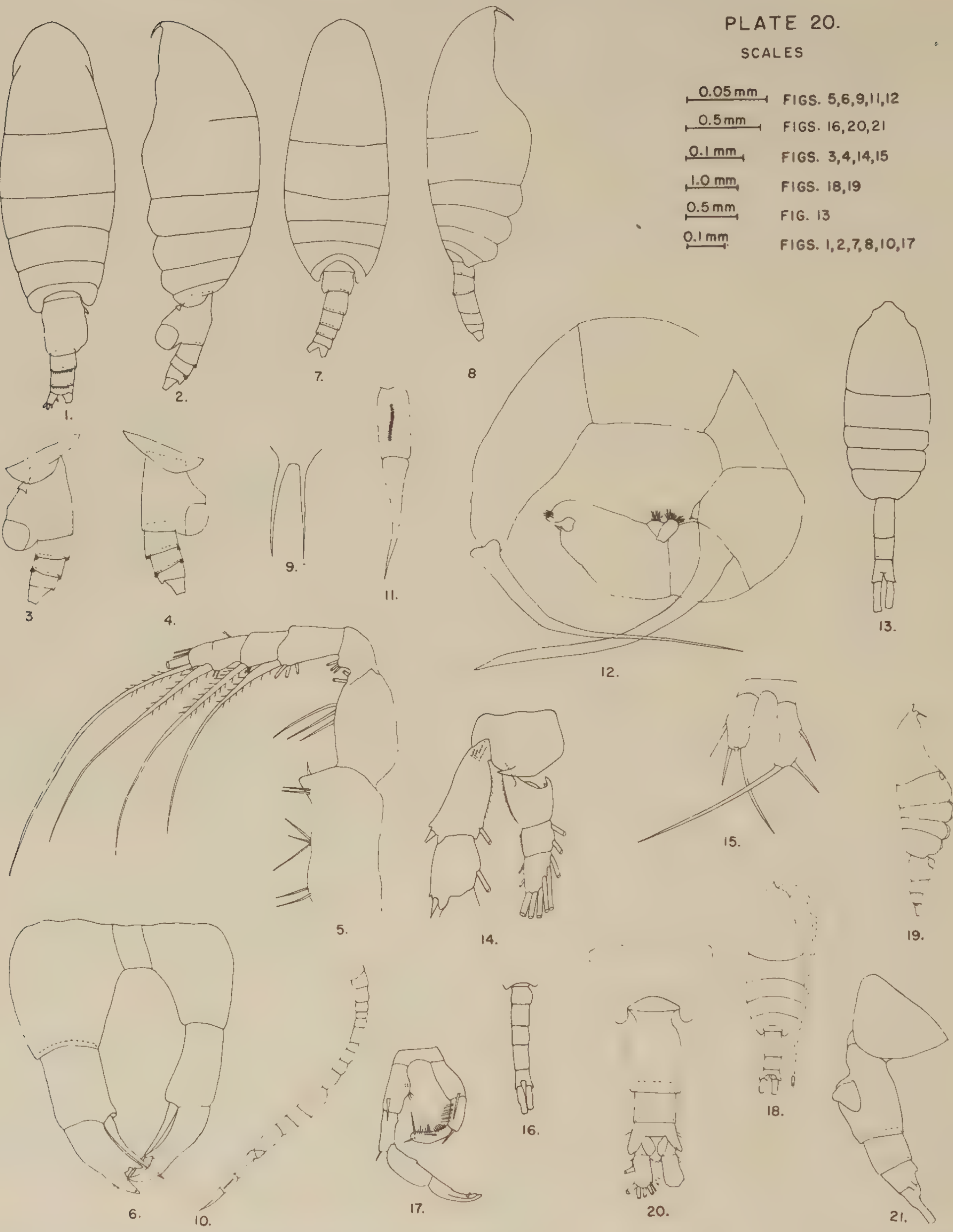
PLATE 20.
SCALES
0.05 mm FIGS. 5,6,9,11,12
0.5 mm FIGS. 16,20,21
0.1 mm FIGS. 3,4,14,15
1.0 mm FIGS. 18,19
0.5 mm FIG. 13
0.1 mm FIGS. 1,2,7,8,10,17
1.
2.
7.
8.
3
4.
9.
11.
12.
13.
5.
14.
15.
19.
6.
10.
17.
16.
20.
18.
21.

PLATE 20.—(1) *Temoropia mayumbaensis*, female, dorsal view; (2) lateral view; (3) posterior part of thorax and abdomen, left side; (4) posterior part of thorax and abdomen, right side; (5) maxilliped; (6) fifth pair of feet; (7) male, dorsal view; (8) lateral view; (9) rostrum; (10) first antenna; (11) distal two segments of first antenna; (12) fifth pair of feet; (13) *Metridia venusta*, female, dorsal view; (14) second foot (third exopodal segment omitted); (15) fifth pair of feet; (16) male, abdomen, dorsal view; (17) fifth pair of feet; (18) *Pleuromamma xiphias*, female, dorsal view; (19) lateral view; (20) posterior part of thorax and abdomen, dorsal view; (21) posterior part of thorax and abdomen, lateral view.

Remarks: The small size and large ventral protrusion on the genital segment (figs. 3, 4) will identify the female. The geniculate right antenna and the pointed terminal segment of this antenna (figs. 10, 11) will aid in recognizing the male sex.

Family METRIDIIDAE

Metridia venusta Giesbrecht, 1889

(PLATE 20, FIGS. 13–17)

Pacific records: Vervoort, 1957.

Vessel:	*Station*	*Occurrence*
Hugh M. Smith	144	1 juvenile female, 2.88 mm.; 1 male, 2.82 mm.

Remarks: This species is recognized by the asymmetrical furca. In both sexes the left furca is longer than the right one (figs. 13, 16).

Pleuromamma xiphias (Giesbrecht, 1888)

(PLATE 20, FIGS. 18–21, PLATE 21, FIGS. 1–5)

Pacific records: Vervoort, 1957. Also, Johnson, 1942; Mori, 1942; Brodsky, 1950; Anraku, 1952; Honjo, 1952; Anraku, 1954b; Tsuruta and Chiba, 1954a; 1954b; Chiba, Tsuruta, and Maéda, 1955; Hida and King, 1955; Nagaya et al., 1955; Chiba, 1956; Heinrich, 1957b; Honjo et al., 1957; Heinrich, 1958b; Yamazi, 1958a.

Vessel:	*Station*	*Occurrence*
Hugh M. Smith	63	1 male, 4.28 mm.
Orsom	10	2 females, 3.99, 4.08 mm.; 2 males, 3.99, 4.08 mm.
Satsuma	32	1 female, 4.25 mm.; 1 male, 4.18 mm.

Remarks: The large spine-like protrusion on the forehead of this species (figs. 19, 3) readily distinguishes it from other species in the genus.

Pleuromamma abdominalis (Lubbock, 1856)

(PLATE 21, FIGS. 6–15)

Pacific records: Vervoort, 1957. Also, Johnson, 1942; Mori, 1942; Brodsky, 1950; Anraku, 1952; Honjo, 1952; Anraku, 1954a; 1954b; Tsuruta and Chiba, 1954b; Chiba, Tsuruta, and Maéda, 1955; Hida and King, 1955; Nagaya et al., 1955; Chiba, 1956; Heinrich, 1957b; Honjo et al., 1957; Heinrich, 1958a; Yamazi, 1958a.

Vessel:	*Station*	*Occurrence* (*measurements in mm.; number of specimens in paren.*)			
		f. *typica*		f. *edentata*	f. *abyssalis*
		female	male	female	male
Hugh M. Smith	94	3.02 (2)			
Do	29		3.13 (1)	2.75–3.06 (11)	3.06 (1)
Do	63			2.75–2.82 (2)	
Orsom	10		2.79–3.02 (3)		
Horizon	32	3.06 (1)			
Satsuma	32	2.85–3.13 (5)	2.99–3.06 (4)		

Remarks: All three forms of this species appeared in the above cited samples. Figures and descriptions of these have been presented by Steuer (1932). The female of forma *abyssalis* is not known. The female of forma *typica* and forma *edentata* are distinguished by the teeth on the first and second antennal segments. In forma *typica* these segments each has a large tooth (fig. 6) while in forma *edentata* these segments have only small teeth (fig. 10). Although Steuer mentions that segment 16 of the first antenna is smaller than segment 17 in forma *edentata*, these length differences are difficult to observe.

The male of forma *edentata* is unknown. Forma *typica* is easily recognized by the greatly asymmetrical and hairy abdomen (fig. 7) while the male of forma *abyssalis* has a less asymmetrical and less hairy abdomen (fig. 12). The small tooth on segment 17 (fig. 13) makes this specimen referable to what Steuer termed subform *thermophila* of forma *abyssalis*.

Pleuromamma indica Wolfenden, 1905

(PLATE 22, FIGS. 1–7)

Pacific records: Tanaka, 1953.

Vessel:	*Station*	*Occurrence*
Satsuma	32	1 male, 2.04 mm.

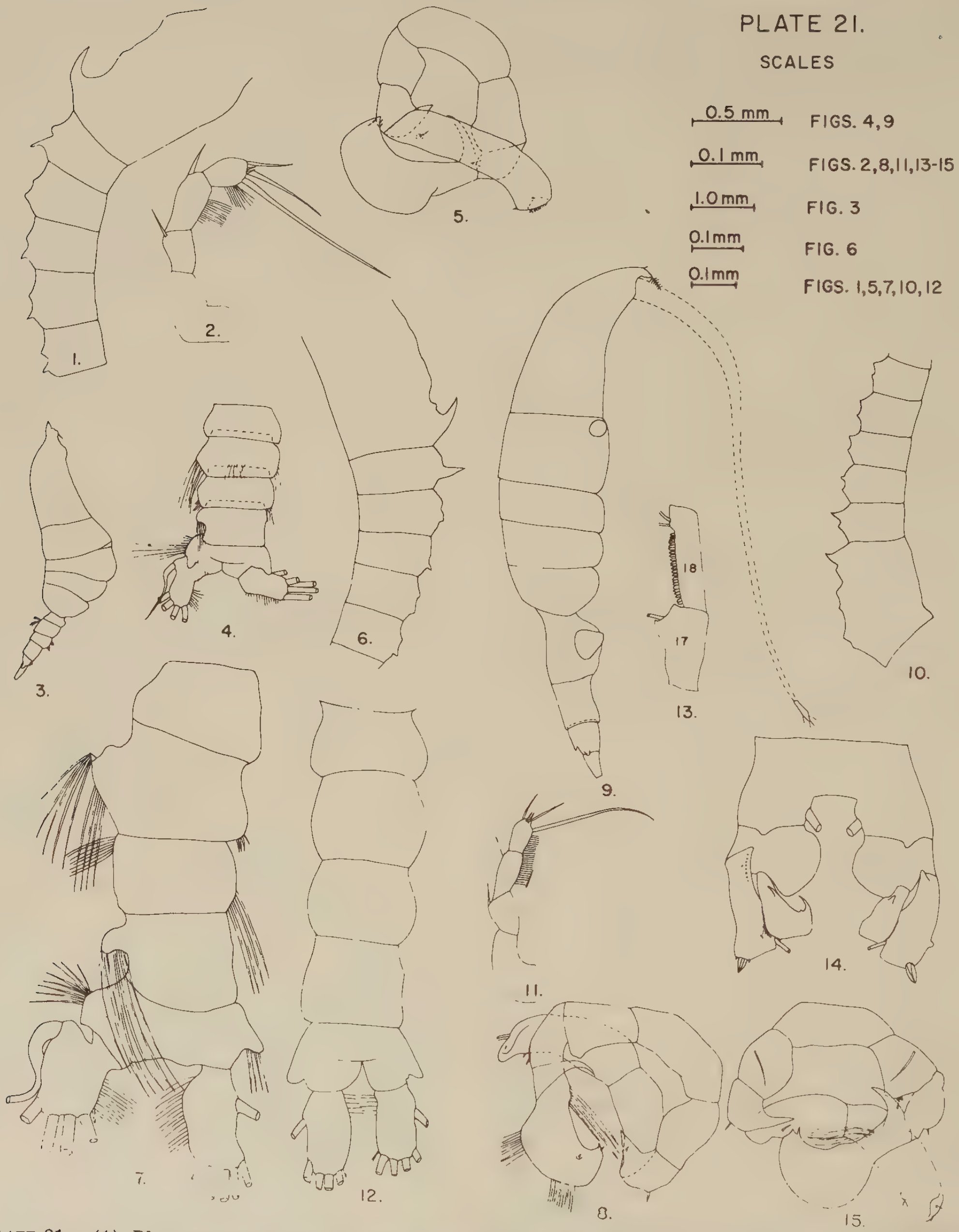
PLATE 21.
SCALES
0.5 mm FIGS. 4,9
0.1 mm FIGS. 2,8,11,13-15
1.0 mm FIG. 3
0.1mm FIG. 6
0.1mm FIGS. 1,5,7,10,12
1.
2.
3.
4.
5.
6.
7.
8.
9.
10.
11.
12.
13.
14.
15.
18
17

PLATE 21.—(1) *Pleuromamma xiphias*, female, proximal part of first antenna; (2) fifth foot; (3) male, lateral view; (4) abdomen, dorsal view; (5) fifth pair of feet; (6) *P. abdominalis* f. *typica*, female, proximal part of first antenna; (7) male, abdomen, dorsal view; (8) fifth pair of feet; (9) *P. abdominalis* f. *edentata*, female, lateral view; (10) proximal part of first antenna; (11) fifth foot; (12) *P. abdominalis* f. *abyssalis*, male, abdomen, dorsal view; (13) segments 17 and 18 of right first antenna; (14) second pair of feet (distal end of exopods and endopods not shown); (15) fifth pair of feet.

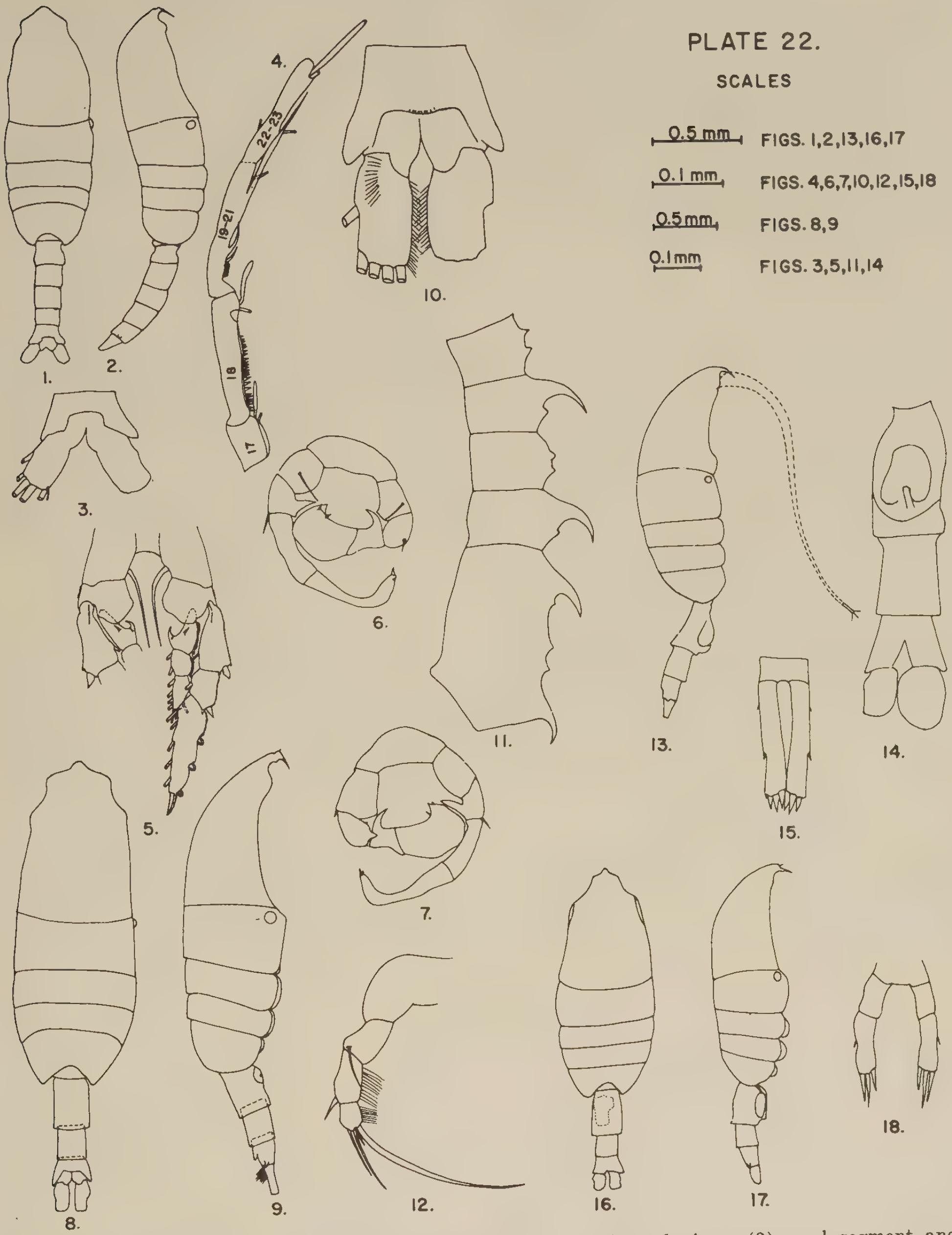
PLATE 22.
SCALES
0.5 mm FIGS. 1,2,13,16,17
0.1 mm FIGS. 4,6,7,10,12,15,18
0.5mm FIGS. 8,9
0.1mm FIGS. 3,5,11,14
1.
2.
3.
4.
22-23
19-21
18
17
5.
6.
7.
8.
9.
10.
11.
12.
13.
14.
15.
16.
17.
18.

Plate 22.—(1) *Pleuromamma indica*, male, dorsal view; (2) lateral view; (3) anal segment and furcae, dorsal view; (4) segments 17 to 23 of right first antenna; (5) second pair of feet (only part of one foot shown); (6) fifth pair of feet, anterior side; (7) posterior side; (8) *P. quadrungulata* f. *typica*, female, dorsal view; (9) lateral view; (10) anal segment and furcae, dorsal view; (11) proximal part of first antenna; (12) fifth foot; (13) *P. gracilis* f. *minima*, female, lateral view; (14) abdomen, ventral view; (15) fifth pair of feet; (16) *P. borealis*, female, dorsal view; (17) lateral view; (18) fifth pair of feet.

Remarks: Only a single male of this species was found. It is distinguished from males of *abdominalis* and other species by the symmetrical abdomen (fig. 1), divergent furcae (fig. 3) and absence of teeth on segment 17 of the right first antenna (fig. 4). The first segment of both endopods of *indica* are indented and claw-like (fig. 5) in contradistinction to *abdominalis* which has this claw-like indentation on only one endopod.

Pleuromamma quadrungulata (Dahl, 1893)

(PLATE 22, FIGS. 8–12)

Pacific records: Vervoort, 1957. Also, Brodsky, 1950.

Vessel:	*Station*	*Occurrence*
Hugh M. Smith	29	1 female, 3.77 mm.
Do	63	1 female, 3.51 mm.

Remarks: The above specimens are referable to forma *typica* Steuer, 1932. It is distinguished from forma *psychrophila* Steuer, 1931, by the presence of a large curved tooth on the fourth segment of the first antennae (fig. 11). In forma *psychrophila* this tooth is reduced in size and not curved.

Pleuromamma gracilis (Claus, 1863)

(PLATE 22, FIGS. 13–15)

Pacific records: Esterly, 1905; Scott, 1909; Farran, 1929; 1936; Mori, 1937; Tanaka, 1937; Dakin and Colefax, 1940; Johnson, 1942; Mori, 1942; Wilson, 1942; Brodsky, 1950; Wilson, 1950; Anraku, 1952; Honjo, 1952; Tanaka, 1953; Anraku, 1954b; Tsuruta and Chiba, 1954b; Chiba, Tsuruta, and Maéda, 1955; Nagaya et al., 1955; Chiba, 1956; Heinrich, 1957b; Honjo et al., 1957; Heinrich, 1958a; 1958b; Yamazi, 1958a.

Vessel:	*Station*	*Occurrence*
Hugh M. Smith	94	1 female, 1.80 mm.
Do	29	6 females, 2.01–2.07 mm.
Do	63	1 female, 1.90 mm.
Horizon	32	1 female, 1.94 mm.
Satsuma	32	1 female, 1.97 mm.

Remarks: All the specimens obtained of this species are referable to Steuer's (1932) forma *minima*. This form is distinguished from forma *piseki* (Farran, 1929) and *maxima* (Steuer, 1932) by the divergent margins of the anal segment (fig. 14) and by the fused second basal and exopodal segments of the fifth feet (fig. 15). In most of the present specimens the left furca is enlarged (fig. 14).

Pleuromamma borealis (Dahl, 1893)

(PLATE 22, FIGS. 16–18)

Pacific records: Farran, 1929; Brodsky, 1950; Wilson, 1950.

Vessel:	*Station*	*Occurrence*
Hugh M. Smith	63	1 female, 2.01 mm.
Orsom	10	1 female, 1.83 mm.
Satsuma	32	2 females, 1.90 mm.

Remarks: The long spines on the fifth feet of the female (fig. 18) distinguished this species from the preceding one.

Family CENTROPAGIDAE

Centropages gracilis (Dana, 1849)

(PLATE 23, FIGS. 1–3)

Pacific records: Scott, 1909; Yamada, 1933; Farran, 1936; Mori, 1937; Dakin and Colefax, 1940; Mori, 1942; Wilson, 1950; Tanaka, 1953; Tsuruta and Chiba, 1954b; Chiba, Tsuruta, and Maéda, 1955; Nagaya et al., 1955; Chiba, 1956; Honjo et al., 1957; Yamazi, 1958a.

Vessel:	*Station*	*Occurrence*
Hugh M. Smith	132	3 females, 1.90–1.97 mm.
Do	153	present.
Do	178	2 females, 2.00 mm.
Do	30	3 females, 1.97–2.01 mm.; 1 male, 2.04 mm.
Stranger	34	1 female, 1.90 mm.
Satsuma	32	1 male, 1.84 mm.

Remarks: The female is recognized by the spines on the sides on the second abdominal segment and the short spine-like protrusions on the inner sides of the second exopodal segments (fig. 1) of the fifth feet. The thumb of the chela of the right foot of the male has a

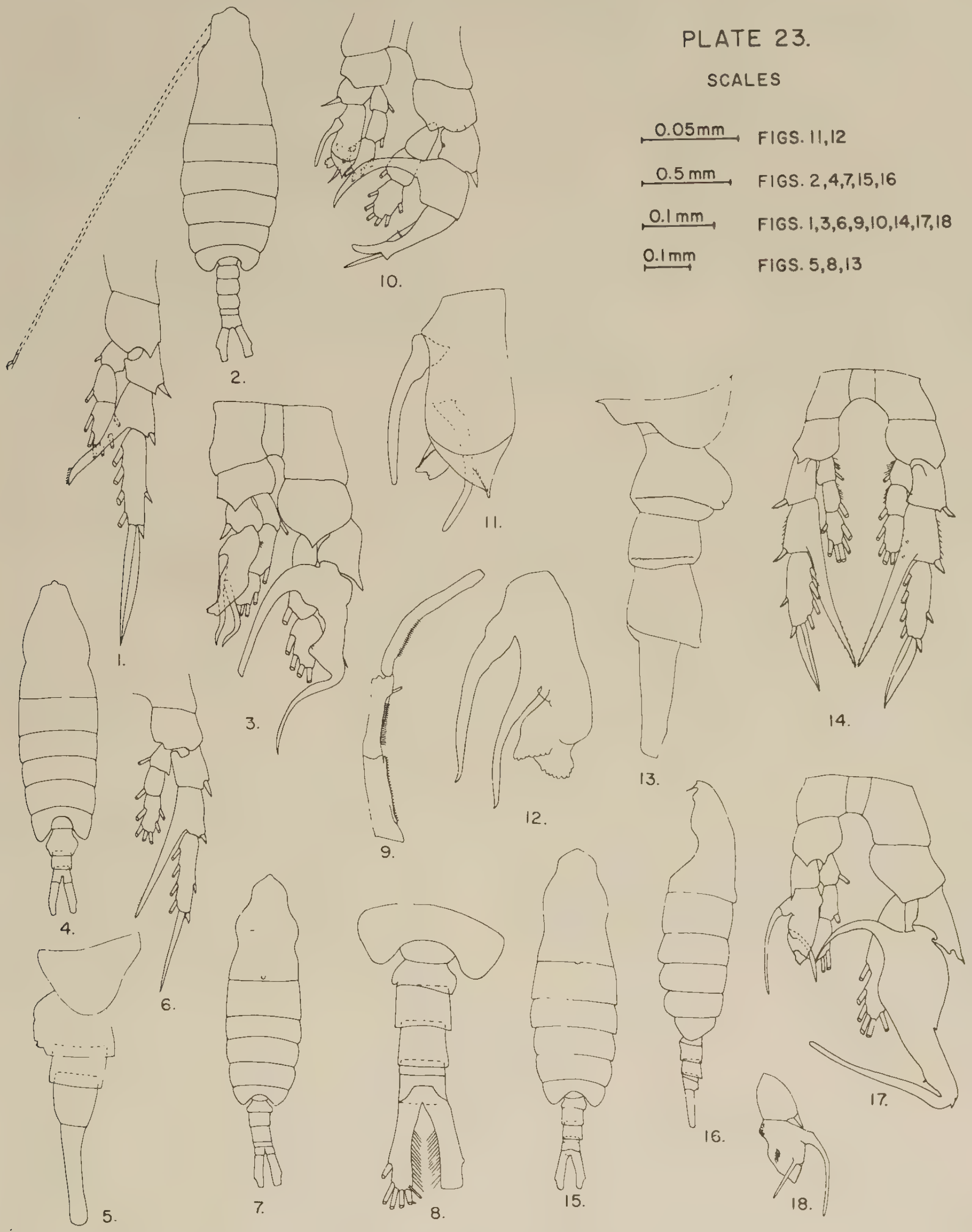
PLATE 23.
SCALES
0.05mm FIGS. 11,12
0.5 mm FIGS. 2,4,7,15,16
0.1 mm FIGS. 1,3,6,9,10,14,17,18
0.1 mm FIGS. 5,8,13
1.
2.
3.
4.
5.
6.
7.
8.
9.
10.
11.
12.
13.
14.
15.
16.
17.
18.

PLATE 23.—(1) *Centropages gracilis*, female, fifth foot; (2) male, dorsal view; (3) fifth pair of feet; (4) *C. elongatus*, female, dorsal view; (5) posterior part of thorax and abdomen, lateral view; (6) fifth foot; (7) male, dorsal view; (8) posterior part of thorax and abdomen, dorsal view; (9) segments 17 to 21 of right first antenna; (10) fifth pair of feet; (11) terminal part of exopod of left fifth foot; (12) terminal part of exopod of left fifth foot, other side; (13) *C. calaninus*, female, posterior part of thorax and abdomen, lateral view; (14) fifth pair of feet; (15) male, dorsal view; (16) lateral view; (17) fifth pair of feet; (18) exopod of left fifth foot.

pronounced triangular protrusion which is absent in other species in the genus (fig. 3).

Centropages elongatus Giesbrecht, 1896

(PLATE 23, FIGS. 4–12)

Synonymy:

Centropages pacificus Chiba, 1956, Jour. Shimonoseki College of Fisheries, 6(1): 47–48.

Pacific records: Scott, 1909; Mori, 1937; 1942; Wilson, 1942; Johnson, 1954; Tsuruta and Chiba, 1954b; Chiba, Tsuruta, and Maéda, 1955; Nagaya et al., 1955; Yamazi, 1958a.

Vessel:	*Station*	*Occurrence*
Hugh M. Smith	153	1 female, 1.87 mm.
Horizon	32	2 males, 1.74, 1.76 mm.
Satsuma	32	1 female, 1.66 mm.

Remarks: The female genital segment is only slightly asymmetrical (figs. 4, 5) and the abdomen lacks the spines which are present in the preceding species and in a related species (*C. violaceus*). The spine-like extensions of the second exopodal segments of the fifth feet exceed the distal end of the third exopodal segments (fig. 6). The male is recognized by the structure of the fifth feet, particularly the long external spine near the distal end of the thumb (fig. 10) and the form of the left exopod (figs. 11, 12).

Chiba (1956) has described a new species, *C. pacificus* (based on males), from specimens collected in the Bikini area. I believe these specimens are the males of *C. elongatus*, a species which has also been reported from Bikini by Johnson (1954).

Mori (1937) stated in his discussion of this species that the last thoracic segments of the female are pointed. He also presented a figure showing this point on one lateral margin. However, no mention was made of the pointed margins of the last thoracic segments by Giesbrecht (1896) in his original description of the species nor in the synopsis of this species presented later by Giesbrecht and Schmeil (1898). The latter authors stated that *C. elongatus* is related to *C. violaceus* which has round posterior thoracic margins. The present specimens also have rounded margins (fig. 5).

Centropages calaninus (Dana, 1849)

(PLATE 23, FIGS. 13–18)

Pacific records: Scott, 1909; Farran, 1936; Mori, 1937; Dakin and Colefax, 1940; Mori, 1942; Wilson, 1942; 1950; Tanaka, 1953; Tsuruta and Chiba, 1954b; Chiba, Tsuruta, and Maéda, 1955; Nagaya et al., 1955; Chiba, 1956; Gilmartin, 1958; Yamazi, 1958a.

Vessel:	*Station*	*Occurrence*
Hugh M. Smith	30	1 female, 2.18 mm.; 1 male, 2.06 mm.
Horizon	32	3 females, 1.97–2.04 mm.; 5 males, 1.80–2.00 mm.

Remarks: The anal segment of the female has a small knob on the ventral surface near the posterior end and the spine-like protrusions of the second exopodal segments of the fifth feet exceed the tip of the third exopodal segments (figs. 13, 14). The male is recognized by the structure of the fifth feet, especially the long and bent thumb of the chela (fig. 17).

Family LUCICUTIIDAE

Lucicutia flavicornis (Claus, 1863)

(PLATE 24, FIGS. 1–4)

Pacific records: Esterly, 1905; Scott, 1909; Farran, 1929; Mori, 1937; Dakin and Colefax, 1940; Johnson, 1942; Mori, 1942; Wilson, 1942; Davis, 1949; Brodsky, 1950; Wilson, 1950; Anraku, 1952; Honjo, 1952; Tanaka, 1953; Anraku, 1954b; Tsuruta and Chiba, 1954b; Chiba, Tsuruta, and Maéda, 1955; Motoda and Anraku, 1955; Nagaya et al., 1955; Chiba, 1956; Heinrich, 1957b; Honjo et al., 1957; Heinrich, 1958a; Yamazi, 1958a.

Vessel:	*Station*	*Occurrence*
Hugh M. Smith	94	12 females, 1.46–1.90 mm.; 7 males, 1.43–1.77 mm.
Do	132	3 males, 1.29–1.66 mm.
Do	144	4 females, 1.63–1.80 mm.; 5 males, 1.44–1.48 mm.
Do	178	3 females, 1.36–1.53 mm.; 7 males, 1.28–1.42 mm.

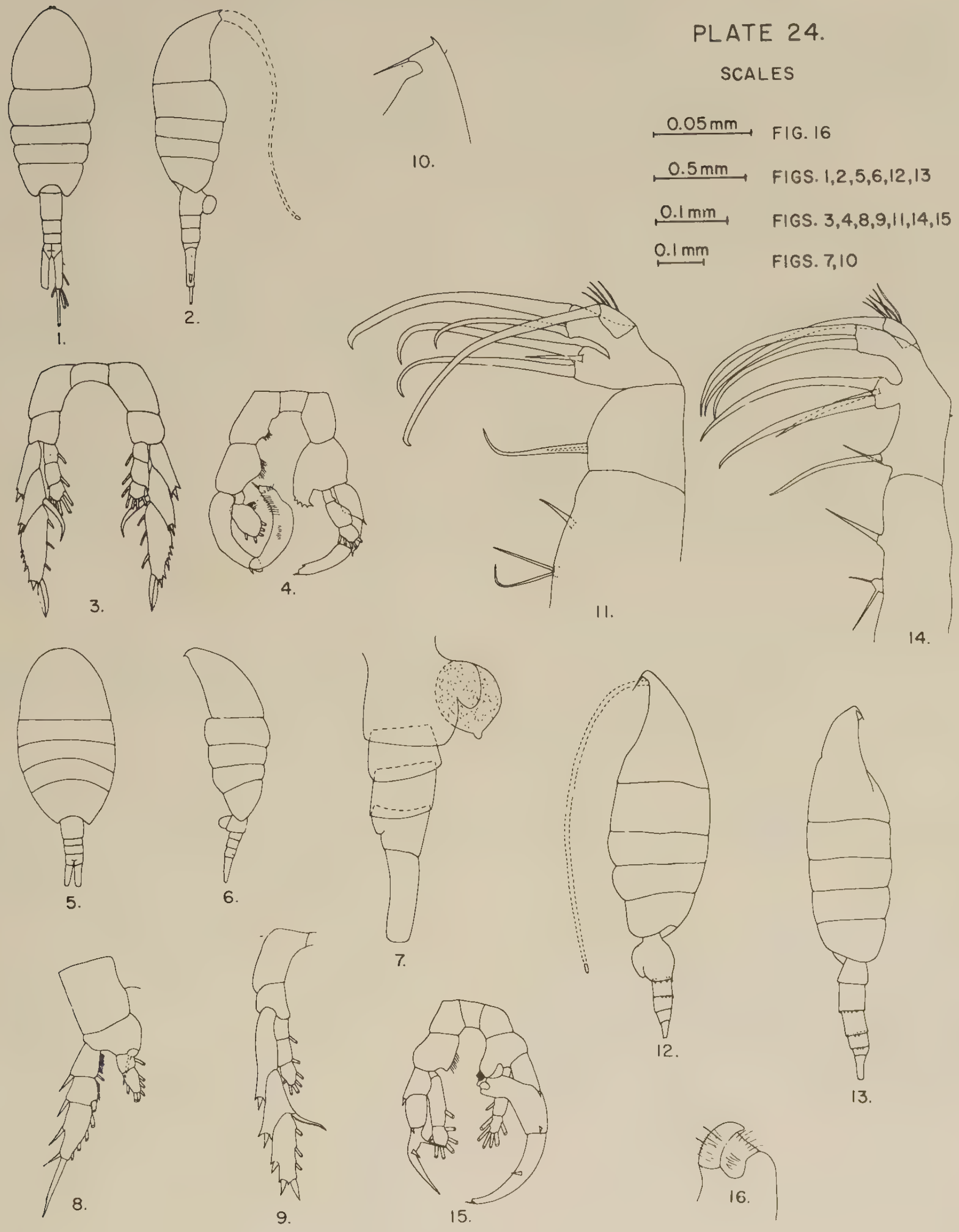
PLATE 24.
SCALES
0.05 mm FIG. 16
0.5 mm FIGS. 1,2,5,6,12,13
0.1 mm FIGS. 3,4,8,9,11,14,15
0.1 mm FIGS. 7,10
1.
2.
3.
4.
5.
6.
7.
8.
9.
10.
11.
12.
13.
14.
15.
16.

Plate 24.—(1) *Lucicutia flavicornis*, female, dorsal view; (2) lateral view; (3) fifth pair of feet; (4) male, fifth pair of feet; (5) *L. ovalis*, female, dorsal view; (6) lateral view; (7) abdomen, lateral view; (8) first foot; (9) fifth foot; (10) *Heterorhabdus spinifrons*, female, forehead, lateral view; (11) second maxilla; (12) *H. papilliger*, female, lateral view; (13) male, lateral view; (14) second maxilla; (15) fifth pair of feet; (16) distal end of protrusion of second right exopodal segment.

Vessel:	*Station*	*Occurrence*
Do	31	3 females, 1.41–1.55 mm.
Do	29	present.
Stranger	34	1 female, 1.39 mm.
Satsuma	32	1 female, 1.26 mm.

Remarks: The female is distinguished from other species of the genus by the short anal segment (figs. 1, 2) and by the form of the fifth feet (fig. 3). The male is recognized by the protrusion of the second basipodal segment of the left foot and the long terminal segment of the right exopod (fig. 4).

Other authors, including Farran, 1929, mention that considerable variation occurs in the length of this species. In at least one collection (*Smith* 94), two size groups were noted as follows: females 1.46–1.53 (6); 1.87–1.90 (6); males 1.39–1.53 (7); 1.77 (1) mm.

Lucicutia ovalis Wolfenden, 1911

(Plate 24, figs. 5–9)

Pacific records: Farran, 1929; 1936; Mori, 1937; Wilson, 1950; Tanaka, 1953; Anraku, 1954b; Tsuruta and Chiba, 1954b; Chiba, Tsuruta, and Maéda, 1955; Motoda and Anraku, 1955; Nagaya et al., 1955; Chiba, 1956; Honjo et al., 1957; Yamazi, 1958a.

Vessel:	*Station*	*Occurrence*
Hugh M. Smith	132	2 females, 1.32, 1.36 mm.
Do	153	1 female, 1.37 mm.
Do	178	3 females, 1.34–1.36 mm.
Do	63	1 female, 1.46 mm.
Stranger	34	1 female, 1.39 mm.
Orsom	10	present.
Satsuma	32	1 female, 1.44 mm.

Remarks: The female is most easily recognized by its small size, the two-segmented endopod of the first feet (fig. 8), and the structure of the fifth feet (fig. 9).

Family HETERORHABDIDAE

Heterorhabdus spinifrons (Claus, 1863)

(Plate 24, figs. 10–11)

Pacific records: Vervoort, 1957. Also, Brodsky, 1950; Tanaka, 1953.

Vessel:	*Station*	*Occurrence*
Hugh M. Smith	144	present.
Do	29	3 females, 2.69–3.57 mm.; 3 males, 3.04–3.20 mm.
Do	63	1 male, 2.41 mm.
Satsuma	32	3 females, 2.10–2.18 mm.

Remarks: In both sexes the forehead is prolonged into a point (fig. 10), a character which will identify this species. In the female, one of the distal 3 spines of the maxilliped is small and slender (fig. 11).

Heterorhabdus papilliger (Claus, 1863)

(Plate 24, figs. 12–16)

Pacific records: Esterly, 1905; Scott, 1909; Farran, 1929; 1936; Mori, 1937; Tanaka, 1937; Dakin and Colefax, 1940; Johnson, 1942; Mori, 1942; Wilson, 1942; Brodsky, 1950 Wilson, 1950; Anraku, 1952; Honjo, 1952; Tanaka, 1953; Anraku, 1954a; 1954b; 1954c; Chiba, Tsuruta, and Maéda, 1955; Motoda and Anraku, 1955; Nagaya et al., 1955; Chiba, 1956; Heinrich, 1957b; Yamazi 1958a.

Vessel:	*Station*	*Occurrence*
Hugh M. Smith	94	2 females, 2.04, 2.07 mm.; 3 males, 1.80–1.94 mm.
Do	132	2 females, 1.87, 1.90 mm.; 1 male, 1.87 mm.
Do	144	1 female, 2.14 mm.; 1 male, 2.11 mm.
Do	178	6 females, 1.80–1.87 mm.; 6 males, 1.70–1.84 mm.
Do	29	1 female, 2.00 mm.
Do	31	4 females, 1.90–1.94 mm.; 1 male, 1.97 mm.
Do	63	2 females, 1.77, 1.97 mm.
Stranger	34	1 female, 1.94 mm.
Orsom	10	1 female, 1.84 mm.

Remarks: The female forehead is rounded (fig. 12) and the 3 distal spines of the maxilliped are all about equal in length in both sexes (fig. 14).

Family AUGAPTILIDAE

Haloptilus acutifrons (Giesbrecht, 1892)

(PLATE 25, FIGS. 1–8)

Pacific records: Vervoort, 1957. Also, Johnson, 1942; Brodsky, 1950; Tanaka, 1953; Anraku, 1954b; Chiba, Tsuruta, and Maéda, 1955; Nagaya et al., 1955; Chiba, 1956; Yamazi, 1958a.

Vessel:	Station	Occurrence
Hugh M. Smith	94	1 female, 3.80 mm.

Remarks: Although closely resembling *H. oxycephalus*, *H. acutifrons* may be distinguished by (1) its small size, (2) less produced forehead (fig. 1) and (3) structure of the gnathal lobe of the mandible (fig. 3).

Haloptilus fertilis (*Giesbrecht*, 1892)

(PLATE 25, FIGS. 9–11)

Pacific records: none.

Vessel:	Station	Occurrence
Hugh M. Smith	32	1 male, 2.47 mm.

Remarks: The male is recognized by its small size and structure of the fifth feet (fig. 11).

Haloptilus longicornis (Claus, 1863)

Pacific records: Scott, 1909; Farran, 1929; 1936; Mori, 1937; Johnson, 1942; Mori, 1942; Wilson, 1942; Brodsky, 1950; Wilson, 1950; Tanaka, 1953; Yamazi, 1953c; Chiba, Tsuruta, and Maéda, 1955; Nagaya et al., 1955; Chiba, 1956; Heinrich, 1957b; Honjo et al., 1957; Heinrich, 1958b; Yamazi, 1958a.

Vessel:	Station	Occurrence
Hugh M. Smith	94	present.
Do	132	9 females, 1.80–1.90 mm.
Do	144	present.
Do	153	Do
Do	178	Do
Do	31	Do
Do	63	Do
Stranger	34	Do
Orsom	10	Do
Horizon	32	Do
Satsuma	32	5 females, 1.77–1.83 mm.

Remarks: The long first antennae which exceed the end of the furca and the knob-like button on the forehead will identify the female. No males were found.

As the occurrence records indicate, this was a widespread species in the present collections. It was also the most abundant species of *Haloptilus* and occurred in fair numbers in several samples (*Smith* 94, 144, 31).

Haloptilus ornatus (Giesbrecht, 1892)

(PLATE 25, FIGS. 12–16)

Pacific records: Scott, 1909; Mori, 1937; Johnson, 1942; Wilson, 1942; Wilson, 1950; Tanaka, 1953; Anraku, 1954b; Chiba, Tsuruta, and Maéda, 1955; Nagaya et al., 1955; Chiba, 1956.

Vessel:	Station	Occurrence
Hugh M. Smith	63	1 female, 4.56 mm.

Remarks: This is a large species and has a rounded forehead. As in other species of *Haloptilus*, the form of the gnathal lobe of the mandible is also diagnostic (fig. 13).

Haloptilus spiniceps (Giesbrecht, 1892)

(PLATE 25, FIGS. 17–20; PLATE 26, FIGS. 1–5)

Pacific records: Scott, 1909; Farran, 1929; 1936; Mori, 1937; Dakin and Colefax, 1940; Johnson, 1942; Wilson, 1942; 1950; Tanaka, 1953.

Vessel:	Station	Occurrence
Hugh M. Smith	94	1 female, 3.99 mm.
Stranger	34	1 female, 3.70 mm.
Orsom	10	present.
Horizon	32	1 female, 3.80 mm.
Satsuma	32	1 female, 3.80 mm.

Remarks: The short pointed forehead (fig. 17) which is curved downward in lateral view (fig. 18) and the structure of the gnathal lobe of the mandible (fig. 20) will identify the female of this species. No male has been found.

Haloptilus austini Grice, 1959

Pacific records: Grice, 1959.

Vessel:	Station	Occurrence
Hugh M. Smith	94	2 females, 3.16, 3.33 mm.

Remarks: I have recently described this species. It has a rounded forehead and, as in other species of *Haloptilus*, the gnathal lobe of the mandible is diagnostic.

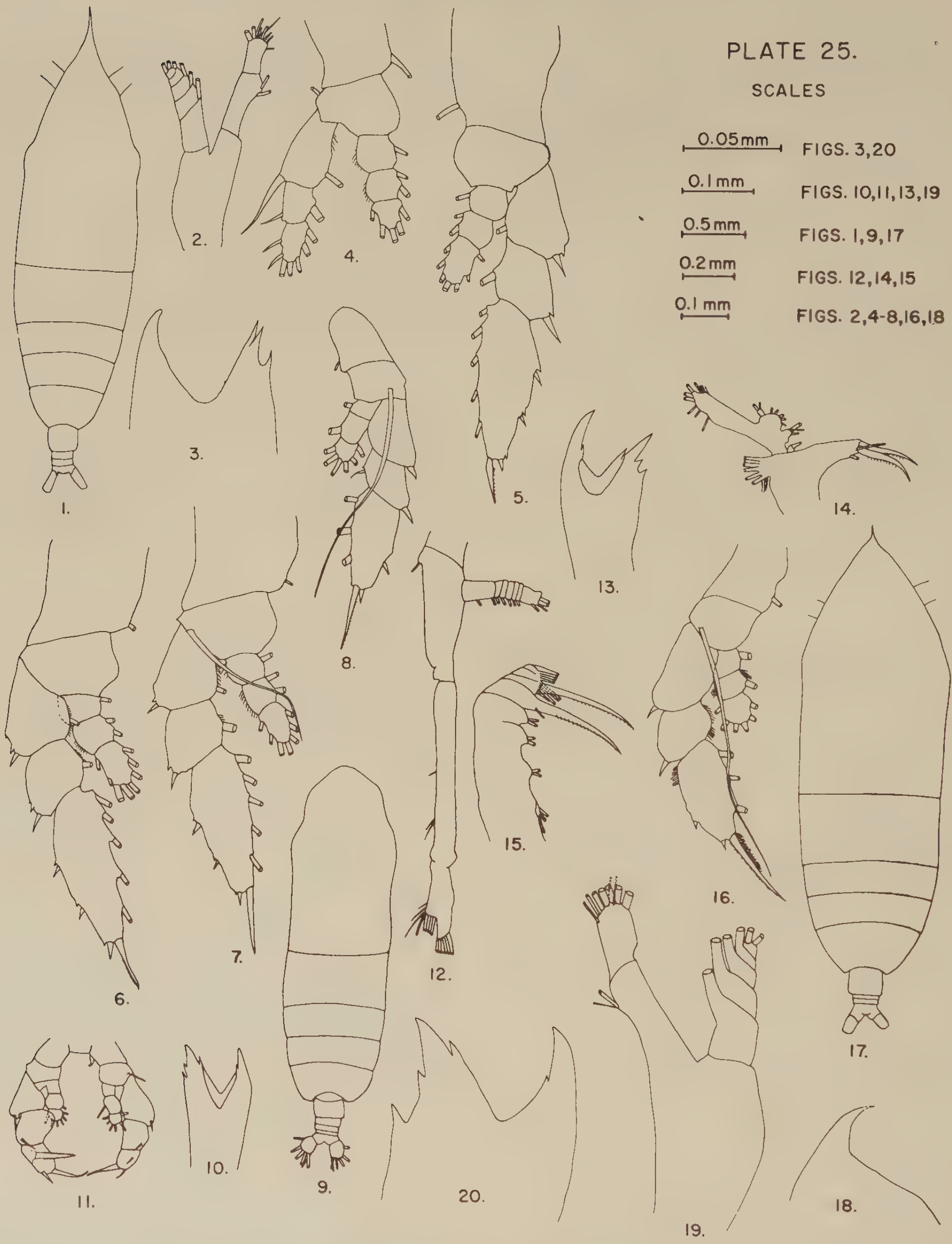
PLATE 25.
SCALES
0.05mm FIGS. 3,20
0.1 mm FIGS. 10,11,13,19
0.5mm FIGS. 1,9,17
0.2mm FIGS. 12,14,15
0.1 mm FIGS. 2,4-8,16,18
1.
2.
3.
4.
5.
6.
7.
8.
9.
10.
11.
12.
13.
14.
15.
16.
17.
18.
19.
20.

Plate 25.—(1) *Haloptilus acutifrons*, female, dorsal view; (2) mandible palpus; (3) gnathal lobe of mandible; (4) first foot; (5) second foot; (6) third foot; (7) fourth foot; (8) fifth foot; (9) *H. fertilis*, male, dorsal view; (10) gnathal lobe of mandible; (11) fifth pair of feet; (12) *H. ornatus*, female, second antenna; (13) gnathal lobe of mandible; (14) first maxilla; (15) second maxilla; (16) fifth foot; (17) *H. spiniceps*, female, dorsal view; (18) forehead, lateral view; (19) mandible palpus; (20) gnathal lobe of mandible.

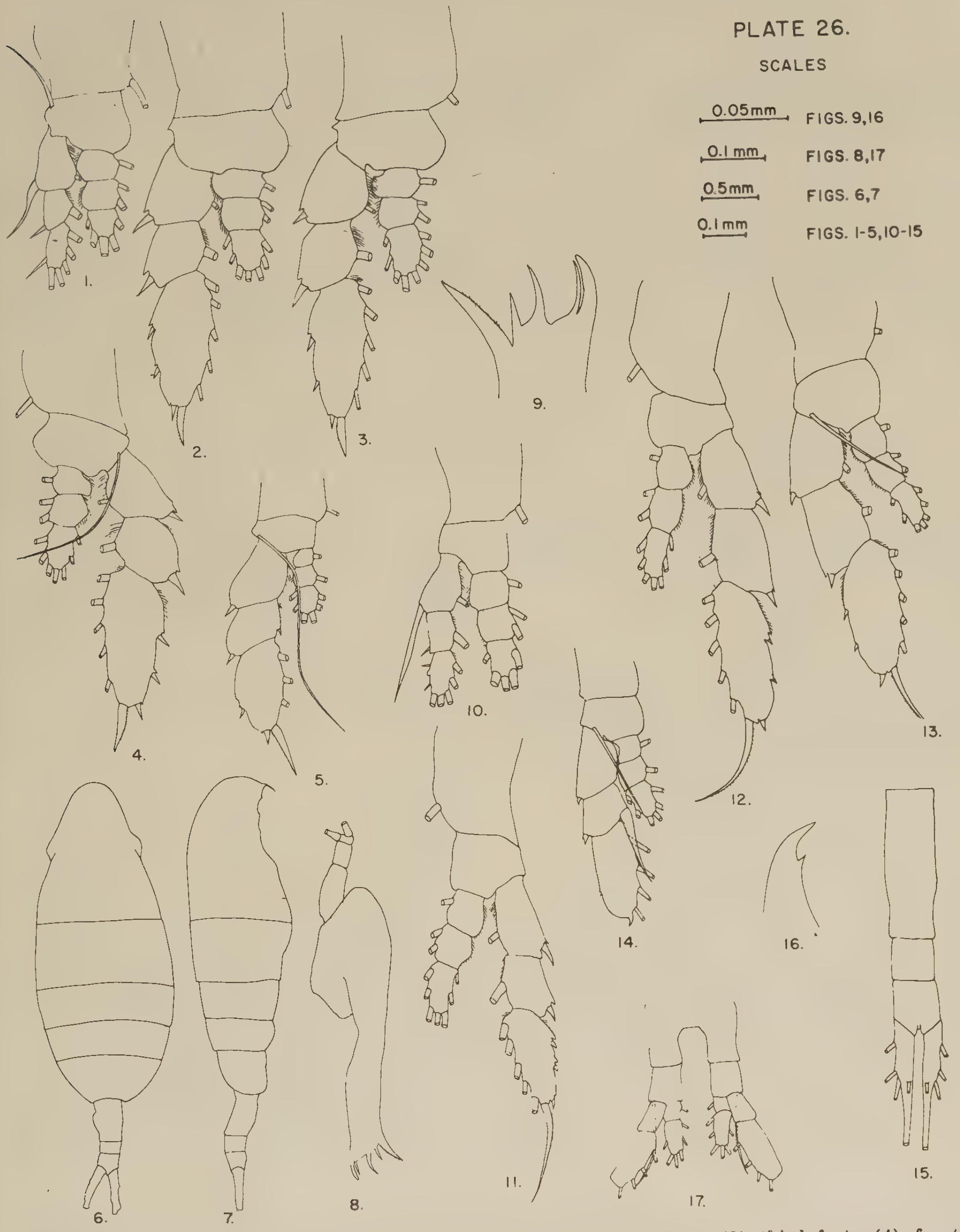
PLATE 26.
SCALES
0.05mm FIGS. 9,16
0.1 mm FIGS. 8,17
0.5mm FIGS. 6,7
0.1 mm FIGS. 1-5,10-15
1.
2.
3.
4.
5.
6.
7.
8.
9.
10.
11.
12.
13.
14.
15.
16.
17.

PLATE 26.—(1) *Haloptilus spiniceps*, female, first foot; (2) second foot; (3) third foot; (4) fourth foot; (5) fifth foot; (6) *Augaptilus longicaudatus*, female, dorsal view; (7) lateral view; (8) mandible; (9) gnathal lobe of mandible; (10) first foot; (11) second foot; (12) third foot; (13) fourth foot; (14) fifth foot; (15) *Euaugaptilus hecticus*, female, abdomen; (16) gnathal lobe of mandible; (17) fifth pair of feet.

Augaptilus longicaudatus (Claus, 1863)

(PLATE 26, FIGS. 6–14)

Pacific records: Esterly, 1905; Scott, 1909; Farran, 1929; 1936; Wilson, 1942; Brodsky, 1950; Wilson, 1950; Tanaka, 1953.

Vessel:	*Station*	*Occurrence*
Hugh M. Smith	94	1 female, 3.60 mm.

Remarks: The asymmetrical genital segment (fig. 6), mandibular dentition (fig. 8), and structure of the fifth feet (fig. 14) will identify the female. No males were observed in the present collections.

Euaugaptilus hecticus (Giesbrecht, 1889)

(PLATE 26, FIGS. 15–17)

Pacific records: Farran, 1929; Wilson, 1950; Tanaka, 1953. As *Augaptilus hecticus;* Scott, 1909.

Vessel:	*Station*	*Occurrence*
Hugh M. Smith	31	2 females, 2.70 mm.
Stranger	34	1 female, 2.28 mm.
Satsuma	32	1 female, 2.38 mm.

Remarks: The very long genital segment (fig. 15), claw-like mandibular blade (fig. 16) and the 2-segmented exopods of the fifth feet (fig. 17) serve to identify this species.

Family ARIETELLIDAE

Arietellus setosus Giesbrecht, 1892

(PLATE 27, FIGS. 1–4)

Pacific records: Esterly, 1905; Scott, 1909; Esterly, 1911; Farran, 1929; Johnson, 1942; Wilson, 1942; Brodsky, 1950; Wilson, 1950.

Vessel:	*Station*	*Occurrence*
Hugh M. Smith	63	1 male, 3.99 mm.

Remarks: The posterior thoracic margins are widely divergent (figs. 1, 3) and the forehead terminates in an acute point (fig. 2). Only the male has been found in the present samples.

Arietellus giesbrechti Sars, 1905

(PLATE 27, FIG. 5)

Pacific records: Wilson, 1950; Tanaka, 1953.

Vessel:	*Station*	*Occurrence*
Hugh M. Smith	29	1 male, 4.75 mm.

Remarks: In the male the left posterior thoracic margin is slightly longer than the right. The fifth feet, shown here (fig. 5), are also diagnostic. No females were observed.

Arietellus plumifer Sars, 1905

(PLATE 27, FIGS. 6–10)

Pacific records: Wilson, 1950.

Vessel:	*Station*	*Occurrence*
Hugh M. Smith	94	1 juvenile female.
Do	63	1 female, 5.51 mm.

Remarks: The posterior margins of the thorax are symmetrical and turned upward (figs. 6, 7, 9), and the head has a small point (figs. 7, 8). No males were found.

Arietellus aculeatus (T. Scott, 1894)

(PLATE 27, FIGS. 11–14)

Pacific records: Scott, 1909; Farran, 1929; Wilson, 1950.

Vessel:	*Station*	*Occurrence*
Hugh M. Smith	63	1 juvenile female, 4.08 mm.

Remarks: The forehead is produced into a long point (fig. 11). The posterior thoracic margins are asymmetrical and the spinous protrusion of the right side is more divergent and longer than the one on the left (figs. 11, 13).

Farran (1929) has suggested that *A. armatus* Wolfenden, 1911 is probably a synonym of *A. aculeatus.* Wilson (1950), however, recognized *armatus* as a valid species and redescribed both sexes.

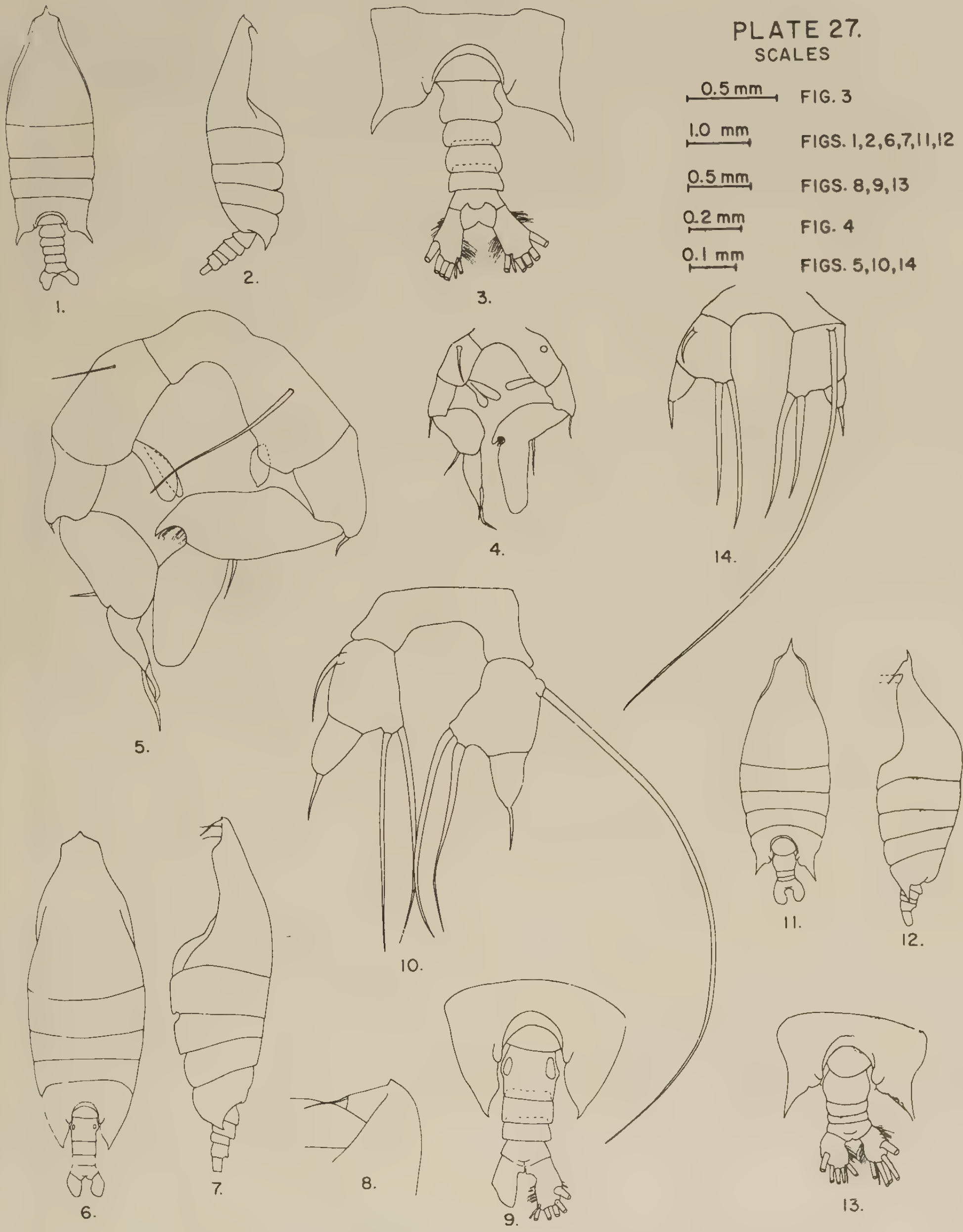
PLATE 27.
SCALES
0.5 mm FIG. 3
1.0 mm FIGS. 1,2,6,7,11,12
0.5 mm FIGS. 8,9,13
0.2 mm FIG. 4
0.1 mm FIGS. 5,10,14
1.
2.
3.
4.
5.
6.
7.
8.
9.
10.
11.
12.
13.
14.

Plate 27.—(1) *Arietellus setosus*, male, dorsal view; (2) lateral view; (3) posterior part of thorax and abdomen, dorsal view; (4) fifth pair of feet; (5) *A. giesbrechti*, male, fifth pair of feet; (6) *A. plumifer*, female, dorsal view; (7) lateral view; (8) forehead, lateral view; (9) posterior part of thorax and abdomen, dorsal view; (10) fifth pair of feet; (11) *A. aculeatus*, juvenile female, dorsal view; (12) lateral view; (13) posterior part of thorax and abdomen, dorsal view; (14) fifth pair of feet.

Family CANDACIIDAE

Candacia longimana (Claus, 1863)

(Plate 28, figs. 1–12)

Pacific records: Scott, 1909; Farran, 1929; 1936; Mori, 1937; 1942; Wilson, 1942; 1950; Honjo, 1952; Tanaka, 1953; Anraku, 1954b; Tsuruta and Chiba, 1954b; Chiba, Tsuruta, and Maéda, 1955; Nagaya et al., 1955; Chiba, 1956; Heinrich, 1957b; Honjo et al., 1957; Yamazi, 1958a.

Vessel:	Station	Occurrence
Horizon	32	2 females, 2.82, 2.92 mm.; 1 male, 2.69 mm.
Satsuma	32	1 female, 2.89 mm.

Remarks: Twelve species of *Candacia* were found in the collections. For each species, excepting *C. guggenheimi* which has recently been described (Grice and Jones, 1960), I have usually included figures of the dorsal and lateral views of both sexes. Figures are also given of the fifth feet of each species and, for most species, figures of certain of the cephalic appendages (gnathal lobe of the mandible, second maxilla and maxilliped) are given. The females of the species herein described are easily recognized by the forms of the genital segment and fifth feet. The males are recognized by the character of the spine-like protrusion of the right posterior thoracic margin, the structure of the abdomen and the form of the fifth feet.

The female of *C. longimana* has a symmetrical genital segment (fig. 1), the basal tooth of the mandible is tricuspate (fig. 3), and the fifth foot terminates in 3 sub-equal points (figs. 4, 5). The right posterior thoracic margin of the male ends in an irregular protrusion (figs. 6, 7) which in lateral view is seen to turn upward (fig. 9). The right side of the genital segment has a large finger-like protrusion. The right fifth foot is chelate (fig. 11) and the distal margin of the last segment of the left foot ends in 3 small points (fig. 12).

Candacia guggenheimi Grice and Jones, 1960

Pacific records: Grice and Jones, 1960.

Vessel:	Station	Occurrence
Hugh M. Smith	29	present.

Remarks: This species has recently been described elsewhere (Grice and Jones, 1960). The genital segment of the female has two small spines on the dorsal surface and the genital segment of the male has a bilobed protrusion extending from the right side.

Candacia tenuimana (Giesbrecht, 1889)

(Plate 28, figs. 13–18; plate 29, figs. 1–4)

Pacific records: Scott, 1909; Johnson, 1942; Wilson, 1942; 1950.

Vessel:	Station	Occurrence
Hugh M. Smith	29	1 female, 2.07 mm.; 1 male, 2.20 mm.

Remarks: The female genital segment is slightly asymmetrical, the right side being more produced than the left (fig. 13, 15). The basal tooth of the mandible has 2 unequal cusps (fig. 17). The innermost spine-like protrusion of the distal segment of the fifth foot (fig. 18) is considerably longer than the other two. The spine-like protrusion on the right posterior thoracic margin of the male has a bifid tip (fig. 1, 2) and the genital segment is produced to the right in the form of a narrow, curved, spine-like process (fig. 2). As in the preceding species, the right fifth foot is chelate (fig. 4).

Candacia aethiopica (Dana, 1849)

(Plate 29, figs. 5–16)

Pacific records: Streets, 1877; Esterly, 1905; Scott, 1909; Farran, 1929; Yamada, 1933a; Tanaka, 1935b; Farran, 1936; Mori, 1937; Dakin and Colefax, 1940; Johnson, 1942; Mori, 1942; Wilson, 1942; 1950; Tanaka, 1953; Anraku, 1954b; Tsuruta and Chiba, 1954b; Chiba, Tsuruta, and Maéda, 1955; Nagaya et al., 1955; Chiba, 1956; Honjo et al., 1957; Gilmartin, 1958.

Vessel:	Station	Occurrence
Hugh M. Smith	30	1 male, 2.24 mm.
Horizon	32	1 female, 2.21 mm.; 3 males 2.18–2.24 mm.
Satsuma	32	1 female, 1.97 mm.

Remarks: Of the two spine-like protrusions on the female genital segment, the one on the left is the larger (figs. 5, 7). The basal tooth of the mandible has 3 cusps, the middle one of which is the larger (fig. 9). The distal segment of the fifth foot has 1 external spine, 3

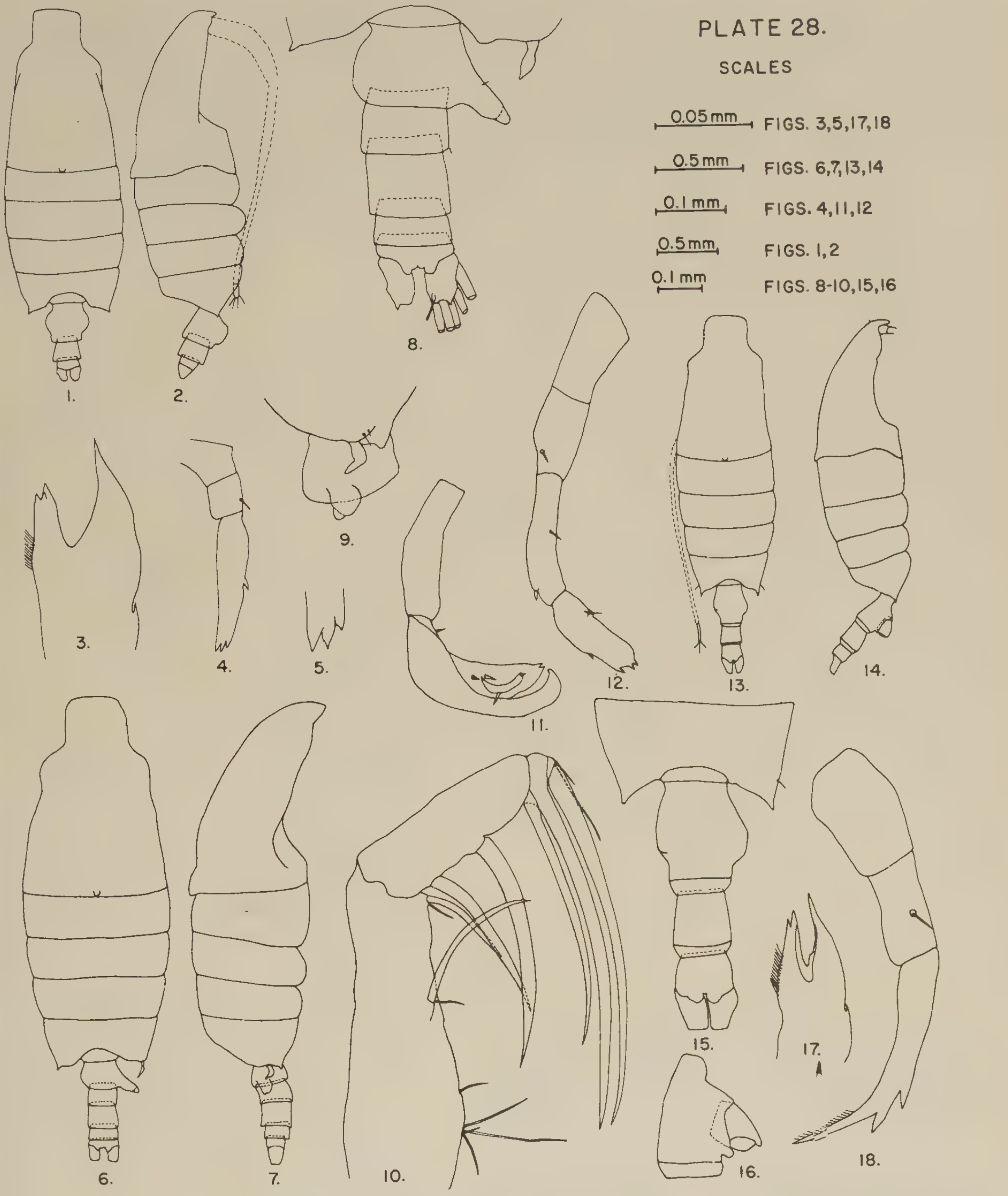
PLATE 28.
SCALES
0.05 mm FIGS. 3,5,17,18
0.5 mm FIGS. 6,7,13,14
0.1 mm FIGS. 4,11,12
0.5 mm FIGS. 1,2
0.1 mm FIGS. 8-10,15,16
1.
2.
8.
9.
3.
4.
5.
11.
12.
13.
14.
6.
7.
10.
15.
16.
17.
18.

Plate 28.—(1) *Candacia longimana*, female, dorsal view; (2) lateral view; (3) gnathal lobe of mandible; (4) fifth foot; (5) tip of fifth foot; (6) male, dorsal view; (7) lateral view; (8) abdomen, dorsal view; (9) posterior lateral corner of thorax and genital segment, right side; (10) second maxilla; (11) right fifth foot; (12) left fifth foot; (13) *C. tenuimana*, female, dorsal view; (14) lateral view; (15) posterior part of thorax and abdomen, dorsal view; (16) genital segment, lateral view; (17) gnathal lobe of mandible; (18) fifth foot.

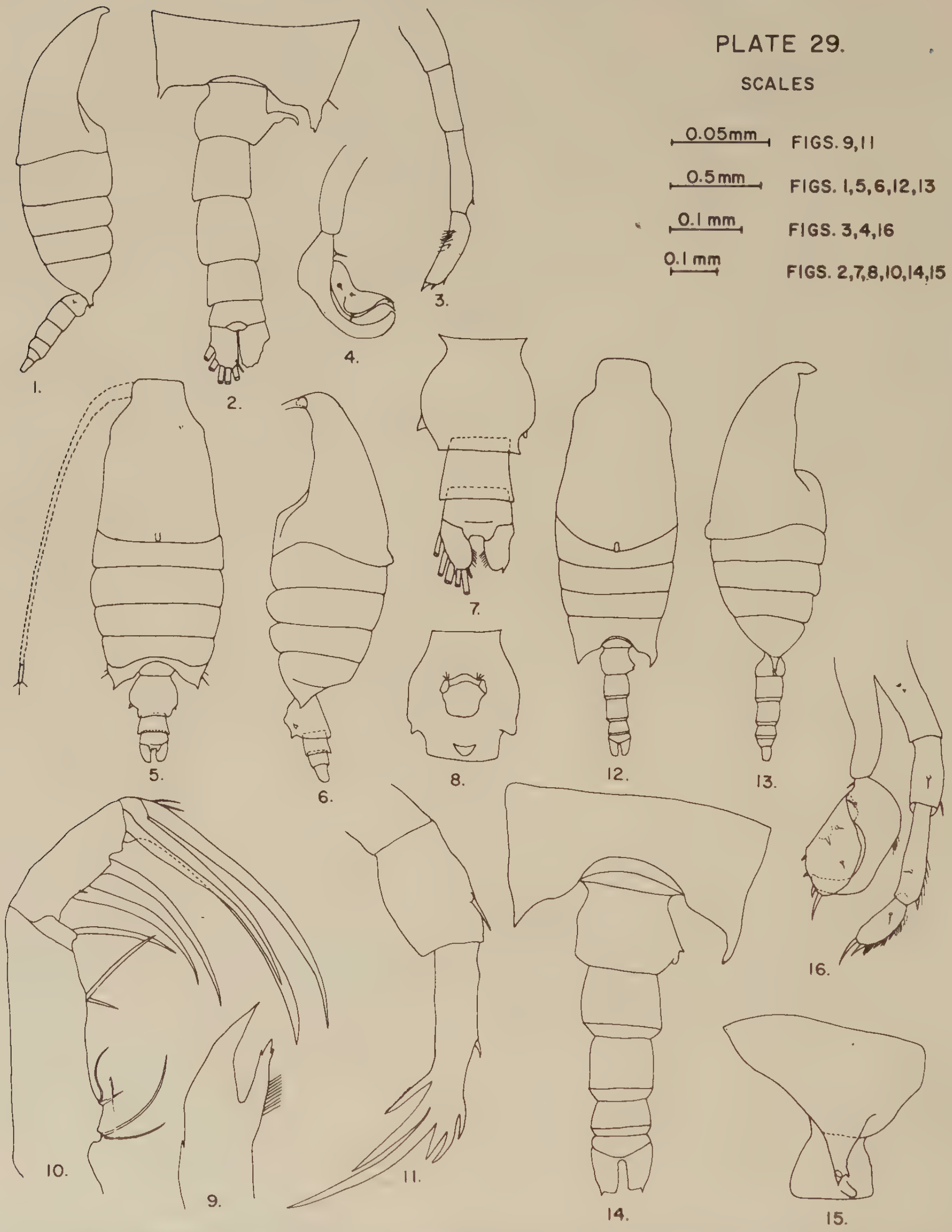
PLATE 29.
SCALES
0.05mm FIGS. 9,11
0.5mm FIGS. 1,5,6,12,13
0.1 mm FIGS. 3,4,16
0.1 mm FIGS. 2,7,8,10,14,15
1.
2.
3.
4.
5.
6.
7.
8.
9.
10.
11.
12.
13.
14.
15.
16.

PLATE 29.—(1) *Candacia tenuimana*, male, lateral view; (2) posterior part of thorax and abdomen, dorsal view; (3) left fifth foot; (4) right fifth foot; (5) *C. aethiopica*, female, dorsal view; (6) lateral view; (7) abdomen, dorsal view; (8) genital segment, ventral view; (9) gnathal lobe of mandible; (10) second maxilla; (11) fifth foot; (12) male, dorsal view; (13) lateral view; (14) posterior part of thorax and abdomen, dorsal view; (15) posterior lateral corner of thorax and genital segment, right side; (16) fifth pair of feet.

terminal points and 3 internal, apparently unarticulated, setae (fig. 11). The male has a bifid spine-like protrusion (lateral view) extending from the right posterior margin of the thorax (figs. 13, 15). There is a rounded tubercle and a spine-like point arising from the right side of the genital segment (fig. 14). The chela of the right fifth foot is broad and spinous (fig. 16).

Candacia pachydactyla (Dana, 1849)

(PLATE 30, FIGS. 1–9)

Pacific records: Scott, 1909; Tanaka, 1935; Mori, 1937; Dakin and Colefax, 1940; Wilson, 1942; 1950; Chiba, 1952c; Tanaka, 1953; Tsuruta and Chiba, 1954b; Chiba, Tsuruta, and Maéda, 1955; Hida and King, 1955; Nagaya et al., 1955; Chiba, 1956; Honjo et al., 1957; Yamazi, 1958a.

Vessel:	Station	Occurrence
Hugh M. Smith	132	2 males, 2.52 mm.
Do	153	1 female, 2.82 mm.; 1 male, 2.07 mm.
Do	178	2 males, 2.52 mm.
Do	30	4 females, 2.48–2.55 mm.; 1 male, 2.48 mm.
Do	63	1 female, 2.88 mm.; 4 males, 2.45–2.72 mm.
Stranger	34	3 females, 2.62–2.65 mm.; 2 males, 2.38, 2.52 mm.
Orsom	10	1 male, 2.48 mm.
Horizon	32	6 females, 2.55–2.62 mm.; 6 males, 2.31–2.55 mm.

Remarks: This is a robust species and is easily distinguished by the coarse spine-like protrusions of the genital segment of the female (figs. 1, 2). The basal tooth of the mandible ends in 3 very unequal cusps (fig. 3). The distal segment of the fifth feet ends in 3 points, the innermost one of which is curved (fig. 4). The right posterior margin of the thorax of the male (figs. 5, 6) is similar to that of *C. aethiopica* but the protrusion of the genital segment is quite large (fig. 7). The thumb of the chela on the right fifth foot ends in a long spine as does the distal segment of the left foot (figs. 8, 9).

Candacia curta (Dana, 1849)

(PLATE 30, FIGS. 10–14; PLATE 31, FIGS. 1–3)

Pacific records: Esterly, 1905; Scott, 1909; Farran, 1935b; Farran, 1936; Mori, 1937; Johnson, 1942; Wilson, 1942; 1950; Tanaka, 1953; Tsuruta and Chiba, 1954b; Chiba, Tsuruta, and Maéda, 1955; Nagaya et al., 1955; Chiba, 1956; Honjo et al. 1957; Yamazi, 1958a. As *C. bicornuta;* Mori, 1932.

Vessel:	Station	Occurrence
Hugh M. Smith	29	2 females, 2.48. 2.62 mm.; 2 males, 2.28, 2.34 mm.
Orsom	10	1 female, 2.44 mm.; 1 male, 2.20 mm.
Horizon	32	1 female, 2.58 mm.

Remarks: The female genital segment is slightly asymmetrical in dorsal view (fig. 10) and has a spine-like protrusion on the ventral side (fig. 11). This spine-like protrusion originates from the right side of the segment (fig. 12). The basal tooth of the mandible has 3 cusps, the lowermost one of which arises from behind the other two (fig. 13). There are 2 points on the distal end of the fifth foot and another point a short distance back of the distal end (fig. 14). The right posterior thoracic margin of the male ends in a hooked spine-like point (fig. 1) and there is a curved, pointed protrusion from the right side of the genital segment (fig. 2). The chela of the fifth foot is also diagnostic (fig. 3).

Candacia bipinnata (Giesbrecht, 1889)

(PLATE 31, FIGS. 4–7)

Synonymy:

Candacia bipinnata (Giesbrecht, 1889, Atti Acc. Lincei Rend., ser. 4, 5 sem. 1: 815).

Candacia pectinata (not of Brady, 1878) Esterly (1905, Univ. Calif. Publ. Zool., 2(4): 193); Mori (1937, The pelagic Copepoda from the neighboring waters of Japan, p. 83); Dakin and Colefax (1940, Publ. Univ. Sydney Dept. Zool. Monogr. 1, p. 105). (*C. pectinata* Brady, 1878=*C. armata* Boeck, 1873.)

Pacific records: Esterly, 1905; Scott, 1909; Tanaka, 1929; Yamada, 1933; Tanaka, 1935b; Mori, 1937; Dakin and Colefax, 1940; Johnson, 1942; Wilson, 1942; Davis, 1949; Motoda, Iizuka, and Anraku, 1950; Brodsky, 1950; Wilson, 1950; Anraku, 1952; Honjo, 1952; Anraku, 1953; Tanaka, 1953; Anraku, 1954b; Chiba, Tsuruta, and Maéda, 1955; Motoda and Anraku, 1955; Nagaya et al., 1955; Chiba, 1956; Honjo et al., 1957;

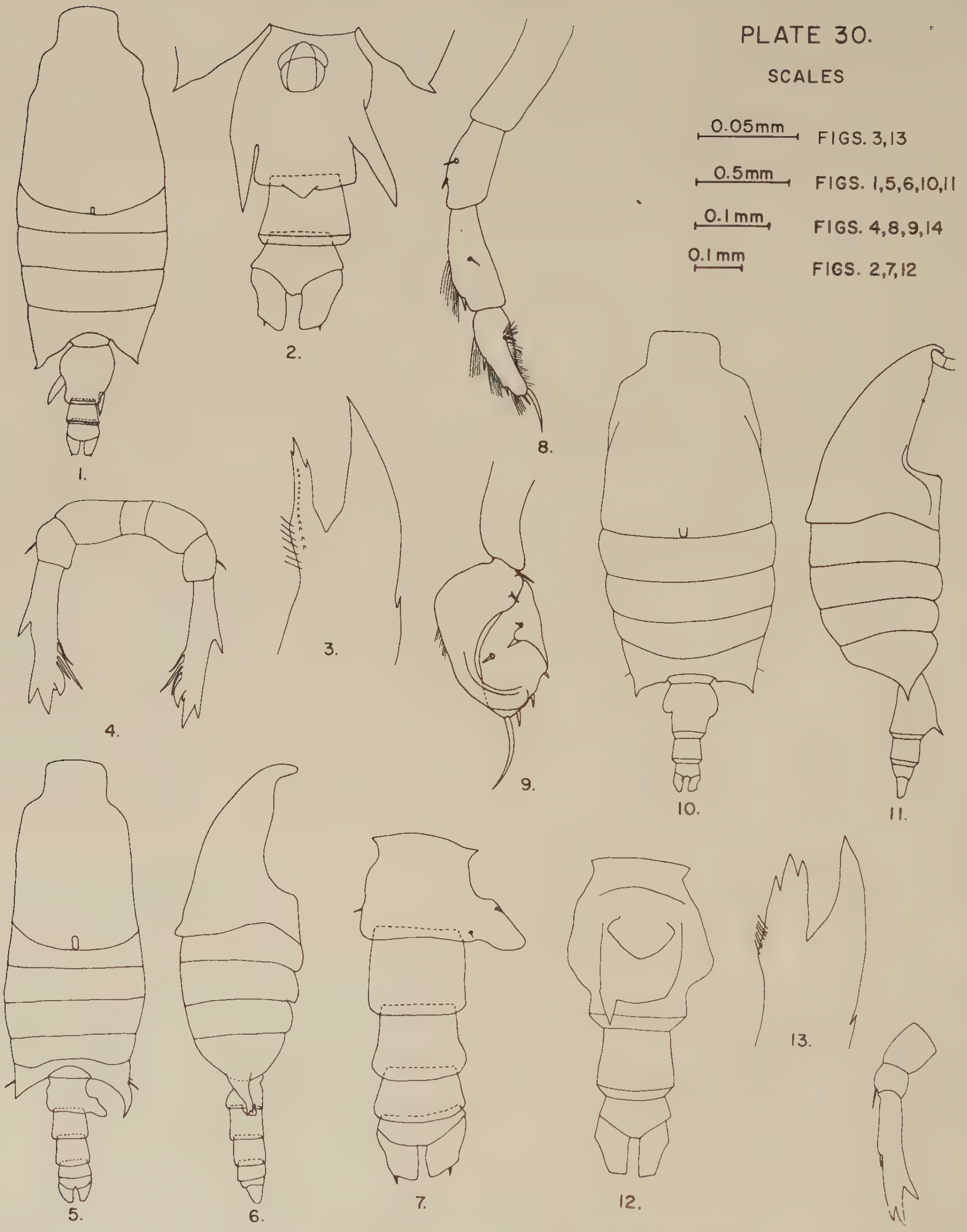
PLATE 30.
SCALES
0.05mm FIGS. 3,13
0.5mm FIGS. 1,5,6,10,11
0.1mm FIGS. 4,8,9,14
0.1mm FIGS. 2,7,12
1.
2.
3.
4.
5.
6.
7.
8.
9.
10.
11.
12.
13.

PLATE 30.—(1) *Candacia pachydactyla*, female, dorsal view; (2) abdomen, ventral view; (3) gnathal lobe of mandible; (4) fifth pair of feet; (5) male, dorsal view; (6) lateral view; (7) abdomen, dorsal view; (8) left fifth foot; (9) right fifth foot; (10) *C. curta*, female, dorsal view; (11) lateral view; (12) abdomen, ventral view; (13) gnathal lobe of mandible; (14) fifth foot.

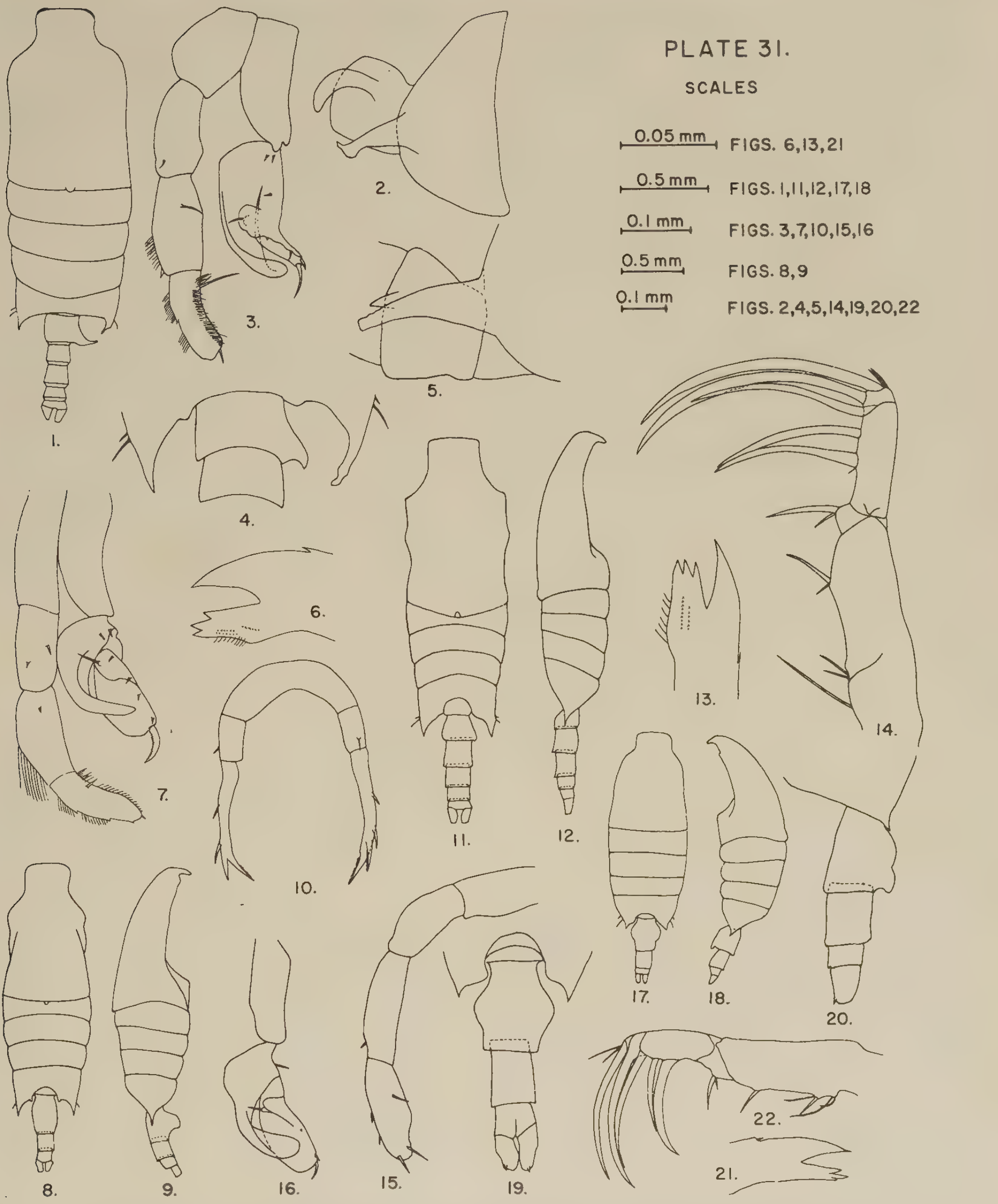
PLATE 31.
SCALES
0.05 mm FIGS. 6,13,21
0.5 mm FIGS. 1,11,12,17,18
0.1 mm FIGS. 3,7,10,15,16
0.5 mm FIGS. 8,9
0.1 mm FIGS. 2,4,5,14,19,20,22
1.
2.
3.
4.
5.
6.
7.
8.
9.
10.
11.
12.
13.
14.
15.
16.
17.
18.
19.
20.
21.
22.

PLATE 31.—(1) *Candacia curta*, male, dorsal view; (2) posterior part of thorax and genital segment, right side; (3) fifth pair of feet; (4) *C. bipinnata*, male, posterior part of thorax and abdomen, dorsal view; (5) posterior part of thorax and abdomen, right side; (6) gnathal lobe of mandible; (7) fifth pair of feet; (8) *C. varicans*, female, dorsal view; (9) lateral view; (10) fifth pair of feet; (11) male, dorsal view; (12) lateral view; (13) gnathal lobe of mandible; (14) second maxilla; (15) left foot; (16) right foot; (17) *C. catula*, female, dorsal view; (18) lateral view; (19) abdomen, dorsal view; (20) abdomen, lateral view; (21) gnathal lobe of mandible; (22) second maxilla.

Yamazi, 1958a; Brodsky, 1959; Lindberg, 1959. As *C. bipunctata* [=*C. bipinnata*?]; Yamazi, 1953a.

Vessel:	Station	Occurrence
Hugh M. Smith	178	1 male, 1.90 mm.
Do	144	1 male, 2.28 mm.

Remarks: Only two males of this species were found. The right posterior lateral protrusion of the thorax is characteristic. This protrusion exceeds the end of the genital segment and its tip, as seen in dorsal view, is irregular (fig. 4). In lateral view the distal end appears to be somewhat truncate (fig. 5). A small, posteriorly directed hook arises from the right side of the genital segment (fig. 4). The basal tooth of the gnathal lobe of the mandible is tricuspate (fig. 6). The thumb of the chela of the right fifth foot has a stout spine at its tip.

In regard to the above indicated synonymy, Sars (1903) redescribed *C. armata* (Boeck, 1873) and pointed out that *C. pectinata* (Brady, 1878) is a synonym of the former species. *C. armata* is a north Atlantic species which occurs along the east coast of the United States as far south as off Beaufort, North Carolina (Fleminger and Bowman, 1956), and along the coast of Europe probably as far south as off Spain. It has also been reported from the Mediterranean Sea (Rose, 1934) and from the Adriatic Sea (Hure, 1955).

I have examined specimens identified by Esterly (1905) and labeled *C. bipinnata* ♀, *C. pectinata* ♂, which were loaned to me by Dr. Abraham Fleminger of the Scripps Institution of Oceanography. Included in the vial were two females, *C. bipinnata*. Esterly's figure of the fifth foot of his female *C. pectinata* is probably that of a stage V female *C. bipinnata*, a species which also occurred in his collections. The figure of the genital segment of his male *C. pectinata* is clearly referable to *C. bipinnata*. Esterly stated in regard to *C. bipinnata* that he did not find the male of this species.

Mori (1937) reported only the male of *C. pectinata* from Japanese waters. His figures and description of this species indicate that it is actually *C. bipinnata*. The protrusion of the right posterior lateral margin of the thorax, the form of the hook on the right side of the genital segment, and the structure of the fifth pair of feet all agree with those of *C. bipinnata*. Mori also presented figures of male *C. bipinnata* which are not unlike those of his *C. pectinata*.

Dakin and Colefax's (1940) *C. pectinata* (both sexes) which were questionably referred to this species are also *C. bipinnata*. I have examined specimens which were obtained from the east coast of Australia and which are similar to the figures presented by these authors for *C. pectinata*. These copepods are stage V female and adult male *C. bipinnata*.

As to other reports of *C. pectinata* from the Pacific Ocean, Scott (1909) has previously stated that Brady's (1883) figures of this species "represents at least four distinct species, none of which are identical with it" (*C. pectinata*=*C. armata*). *C. pectinata* has also been reported by Honjo (1952) and Honjo et al. (1957). As the species is included in lists, without descriptions or figures, these records too are questionable and in need of confirmation.

Candacia varicans (Giesbrecht, 1892)

(PLATE 31, FIGS. 8–16)

Pacific records: Farran, 1929; Johnson, 1942; Wilson, 1942; 1950.

Vessel:	Station	Occurrence
Hugh M. Smith	31	2 males, 2.14, 2.18 mm.
Do	63	1 female, 2.55 mm.; 2 males, 2.26, 2.28 mm.

Remarks: The female has a long and symmetrical genital segment (fig. 8) which is produced on the ventral side (fig. 9). The fifth feet are slightly asymmetrical and terminate in two rather long, but unequal, points (fig. 10). The thorax and genital segment of the male are symmetrical (figs. 11, 12). The basal tooth of the mandible ends in three approximately equal cusps. The right fifth foot is chelate (fig. 16).

Candacia catula (Giesbrecht, 1889)

(PLATE 31, FIGS. 17–22; PLATE 32, FIGS. 1–6)

Pacific records: Scott, 1909; Tanaka, 1935b; Farran, 1936; Mori, 1937; Dakin and Colefax, 1940; Mori, 1942; Wilson, 1942; Anraku, 1952; Tanaka, 1953;

Tsuruta and Chiba, 1954b; Chiba, Tsuruta, and Maéda, 1955; Nagaya et al., 1955; Yamazi, 1958a.

Vessel:	Station	Occurrence
Hugh M. Smith	178	present.
Do	63	2 females, 1.56, 1.63 mm.; 2 males, 1.46, 1.53 mm.
Stranger	34	7 females, 1.60–1.67 mm.; 2 males, 1.53, 1.62 mm.
Orsom	10	1 female, 1.53 mm.; 1 male, 1.43 mm.
Horizon	32	1 female, 1.59 mm.

Remarks: This is a small species, the females of which have a symmetrical genital segment (figs. 17, 19). The ventral surface is produced into a lobe (figs. 18, 20). The basal tooth of the mandible ends in 3 cusps, the lowermost one of which is quite small (fig. 21). The fifth foot terminates in 3 unequal points (fig. 1). The male posterior thoracic margins are symmetrical (figs. 2, 4) and the chela of the right fifth foot is small. The thumb of the chela has a long spine protruding from its tip (fig. 6).

Candacia bispinosa (Claus, 1863)

(PLATE 32, FIGS. 7–14)

Pacific records: Scott, 1909; Farran, 1929; Tanaka, 1935b; Farran, 1936; Mori, 1937; Johnson, 1942; Wilson, 1942; 1950; Honjo, 1952; Tanaka, 1953; Anraku, 1954b; Tsuruta and Chiba, 1954b; Chiba, Tsuruta, and Maéda, 1955; Motoda and Anraku, 1955; Nagaya et al., 1955; Chiba, 1956; Heinrich, 1957b; Honjo et al., 1957; Heinrich, 1958a; Yamazi, 1958a.

Vessel:	Station	Occurrence
Hugh M. Smith	153	3 females, 1.66–1.80 mm.
Do	178	1 female, 1.60 mm.
Stranger	34	1 female, 1.67 mm.; 1 male, 1.73 mm.
Orsom	10	1 female, 1.56 mm.; 1 male, 1.56 mm.
Satsuma	32	1 male, 1.70 mm.

Remarks: This species and the following two species, *C. simplex* (Giesbrecht) and *C. truncata* (Dana), differ in a few details (e.g., structure of right, first antenna in male and fifth feet in both sexes) from the preceding nine species. It has been suggested by Sars (1903) that these three may have to be removed from the genus *Candacia*.

The female of *C. bispinosa* has two spine-like protrusions arising from the genital segment (fig. 7). These protrusions, particularly the one on the left side, are quite variable in shape and in size. In one specimen (*Smith* 178) the left protrusion reaches nearly to the anal segment. There is a small rounded knob arising from the ventral side of the genital segment near the posterior end (fig. 8). The pre-anal segment is asymmetrical. The left side is dilated near the anterior end, but there is some variation in the size of the protrusion. The ventral surface of this segment may or may not have a row of hairs arising from near the posterior end. The basal tooth of the mandible is undivided, but one or more spine-like processes are present on this tooth (fig. 9). The large terminal finger-like protrusion of the distal segment of the fifth foot is finely serrate on both sides (fig. 12).

Segment 20 of the right first antenna of the male is swollen distally (fig. 13). There are 3 outer edge spines on the distal segment of the right fifth foot (fig. 14). The proximal spine is shorter than the distal two spines. The penultimate segment of the left fifth foot is enlarged and the outer edge seta of the distal segment is shorter than the terminal ones.

Candacia simplex (Giesbrecht, 1889)

(PLATE 32, FIGS. 15–18; PLATE 33, FIGS. 1–5)

Pacific records: Scott, 1909; Farran, 1929; 1936; Mori, 1937; Johnson, 1942; Mori, 1942; Wilson, 1942; 1950; Tanaka, 1953; Tsuruta and Chiba, 1954b; Chiba, Tsuruta, and Maéda, 1955; Nagaya et al., 1955; Rose, 1955; Chiba, 1956.

Vessel:	Station	Occurrence
Hugh M. Smith	94	1 female, 1.93 mm.
Do	132	8 females, 1.73–1.87 mm.; 3 males 1.73–1.83 mm.
Do	144	present.
Do	153	1 female, 1.67 mm.
Do	178	2 females, 1.90 mm.; 1 male, 1.80 mm.

Remarks: The genital segment of the female is slightly asymmetrical and has a group of small hair-like structures which are visible on the right side (figs. 15, 16). The terminal finger of the distal segment of the fifth foot is

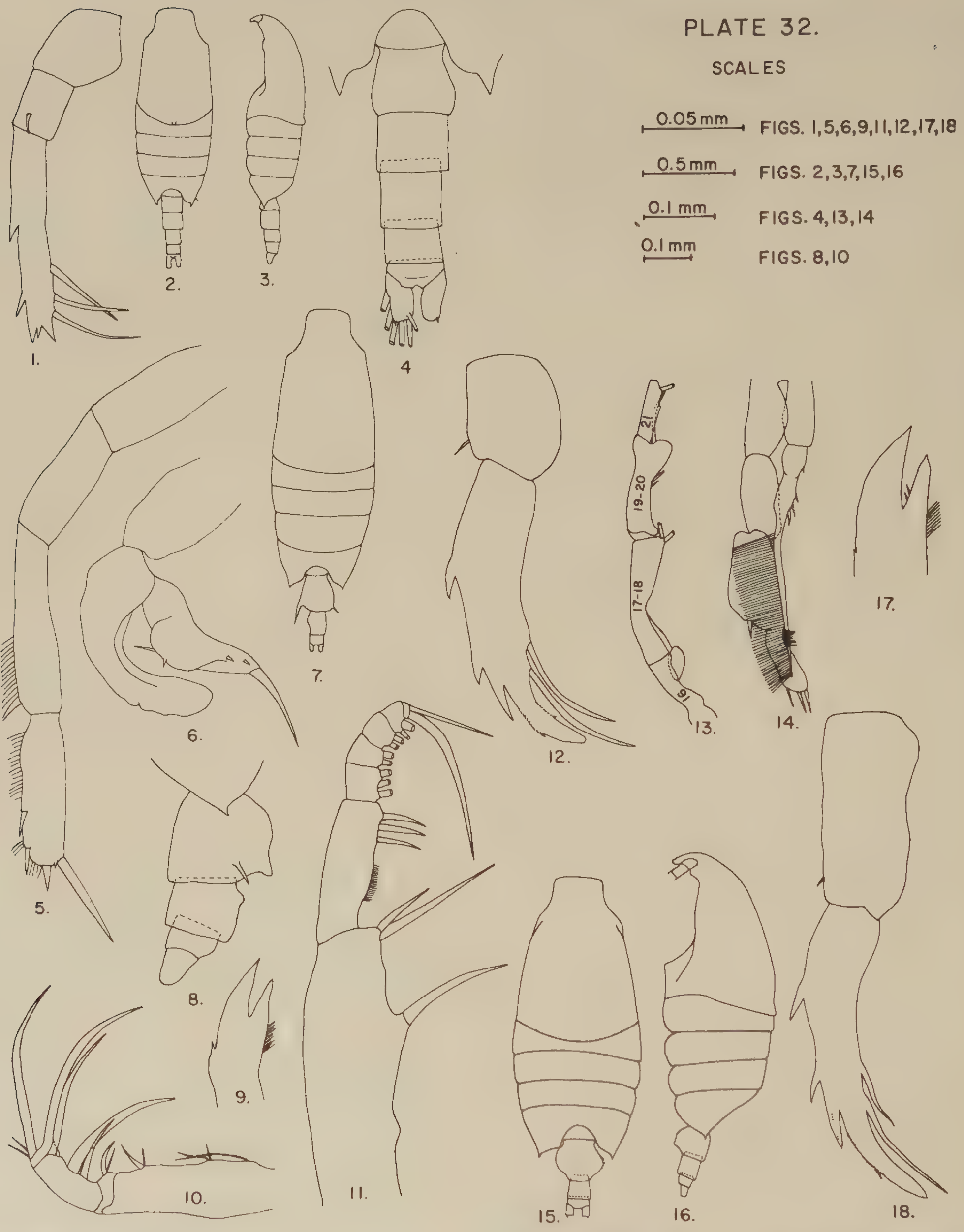
PLATE 32.
SCALES
0.05 mm FIGS. 1,5,6,9,11,12,17,18
0.5 mm FIGS. 2,3,7,15,16
0.1 mm FIGS. 4,13,14
0.1 mm FIGS. 8,10
1.
2.
3.
4
5.
6.
7.
8.
9.
10.
11.
12.
13.
14.
15.
16.
17.
18.
21
19-20
17-18
16

Plate 32.—(1) *Candacia catula,* female, fifth foot; (2) male, dorsal view; (3) lateral view; (4) abdomen, dorsal view; (5) left fifth foot; (6) right fifth foot; (7) *C. bispinosa,* female, dorsal view; (8) abdomen, right side; (9) gnathal lobe of mandible; (10) second maxilla; (11) maxilliped; (12) fifth foot; (13) male, segments 16 to 21 of right first antenna; (14) fifth pair of feet; (15) *C. simplex,* female, dorsal view; (16) lateral view; (17) gnathal lobe of mandible; (18) fifth foot.

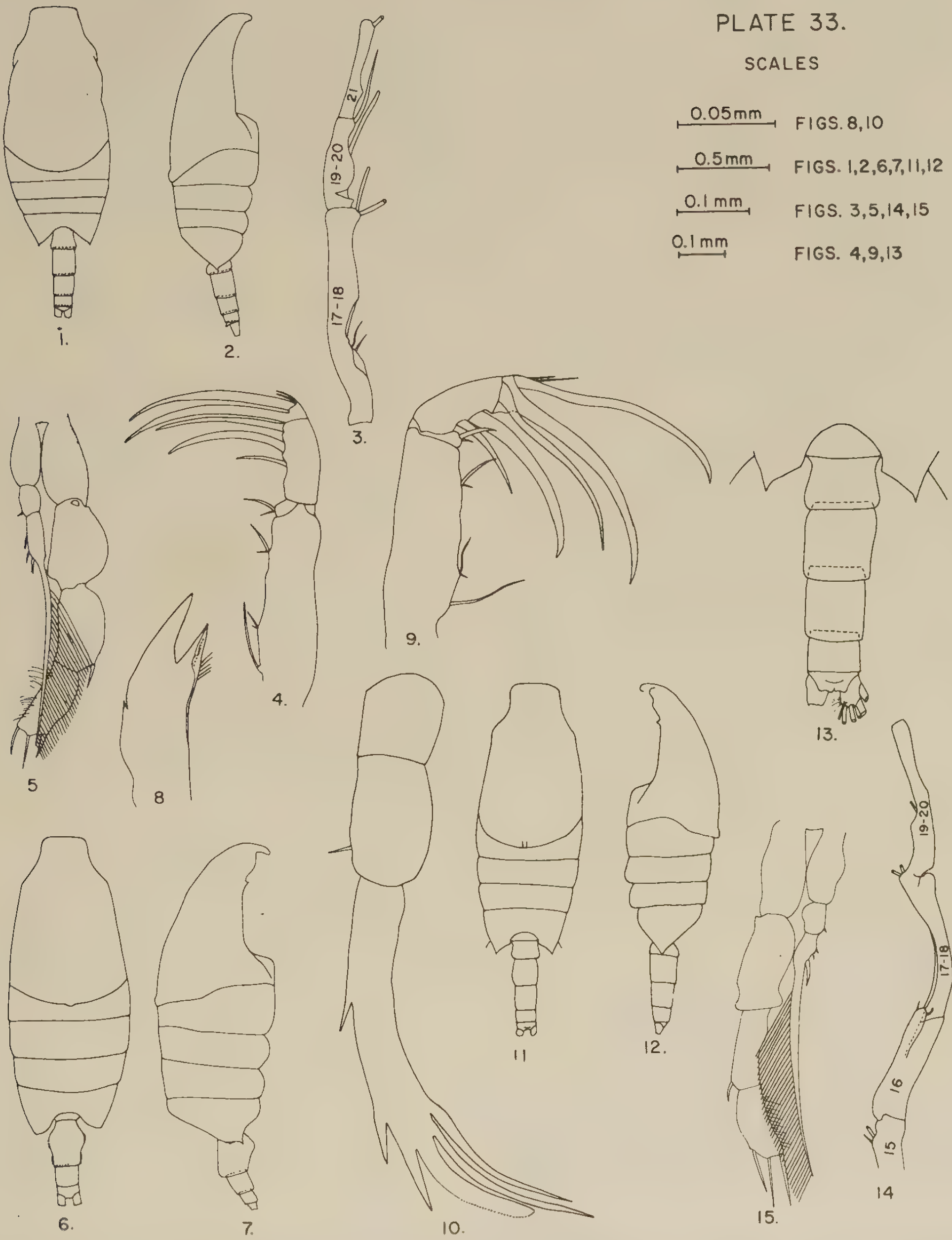
PLATE 33.
SCALES
0.05mm FIGS. 8,10
0.5mm FIGS. 1,2,6,7,11,12
0.1 mm FIGS. 3,5,14,15
0.1 mm FIGS. 4,9,13
1.
2.
3.
21
19-20
17-18
4.
5
8
9.
10.
11
12.
13.
14
19-20
17-18
16
15
15.
6.
7.

PLATE 33.—(1) *Candacia simplex*, male, dorsal view; (2) lateral view; (3) segments 17 to 21 of right first antenna; (4) second maxilla; (5) fifth pair of feet; (6) *C. truncata*, female, dorsal view; (7) lateral view; (8) gnathal lobe of mandible; (9) second maxilla; (10) fifth foot; (11) male, dorsal view; (12) lateral view; (13) abdomen, dorsal view; (14) segments 15 to 20 of right first antenna; (15) fifth pair of feet.

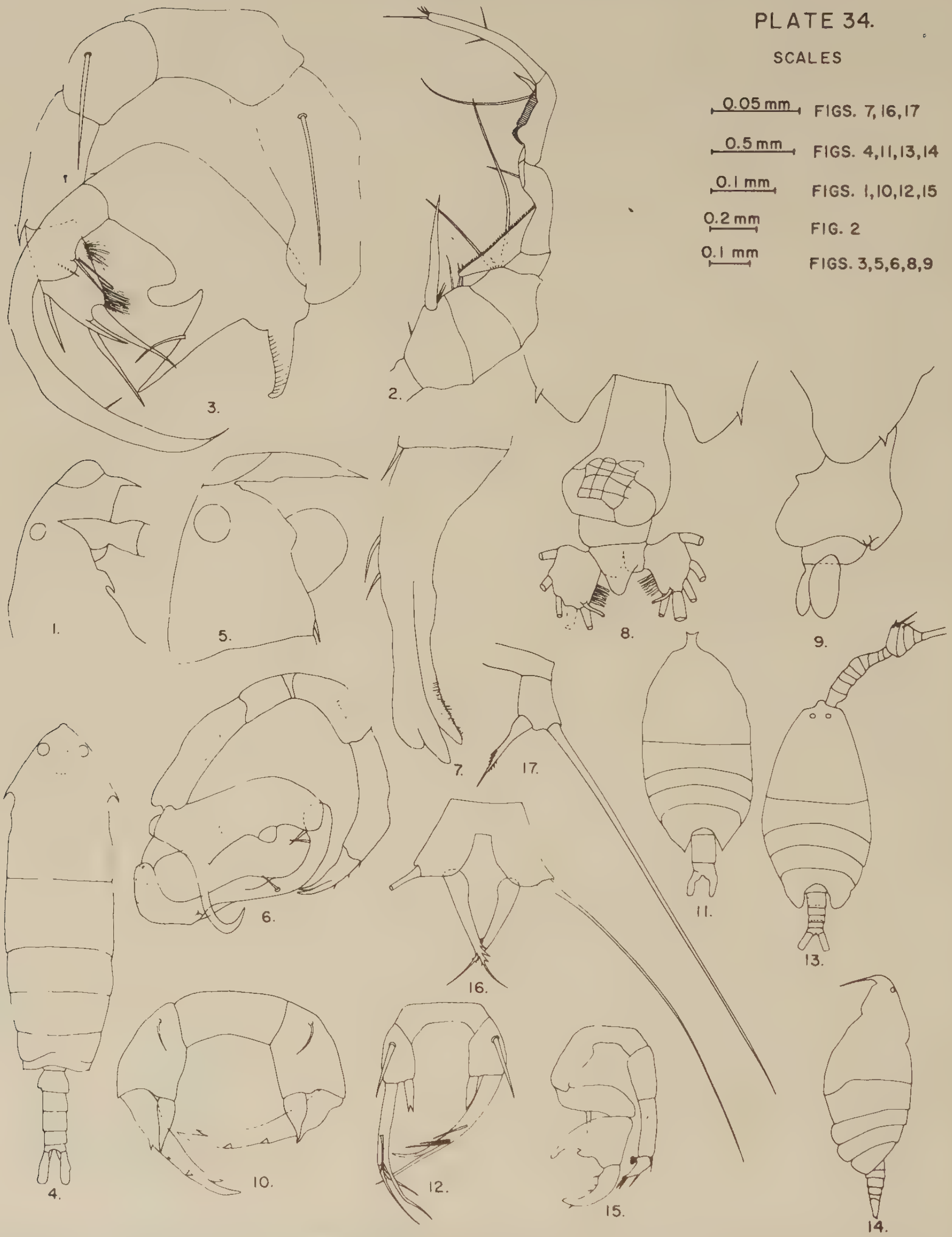
PLATE 34.
SCALES
0.05 mm FIGS. 7, 16, 17
0.5 mm FIGS. 4, 11, 13, 14
0.1 mm FIGS. 1, 10, 12, 15
0.2 mm FIG. 2
0.1 mm FIGS. 3, 5, 6, 8, 9
1.
2.
3.
4.
5.
6.
7.
8.
9.
10.
11.
12.
13.
14.
15.
16.
17.

PLATE 34.—(1) *Pontella securifer*, male, forehead, lateral view; (2) distal end of right first antenna; (3) fifth pair of feet; (4) *P. tenuiremis*, male, dorsal view; (5) forehead, lateral view; (6) fifth pair of feet; (7) left fifth foot; (8) *Labidocera detruncata*, female, abdomen, dorsal view; (9) lateral view; (10) fifth pair of feet; (11) *Pontellina plumata*, female, dorsal view; (12) fifth pair of feet; (13) male, dorsal view; (14) lateral view; (15) fifth pair of feet; (16) *Acartia danae*, female, fifth foot; (17) *A. negligens*, female, fifth pair of feet.

finely serrate on the external margin (fig. 18). Of the 2 internal setae on this segment, the distal one is approximately twice the length of the proximal one. The male thorax and abdomen are symmetrical (figs. 1, 2). The right fifth foot is similar to that of *C. bispinosa* (fig. 5). The left fifth foot terminates in 3 setae, the middle one of which is the longer. The penultimate segment is not particularly enlarged.

Candacia truncata (Dana, 1849)

(Plate 33, figs. 6–14)

Pacific records: Scott, 1909; Yamada, 1933a; Tanaka, 1935b; Farran, 1936; Mori, 1937; Dakin and Colefax, 1940; Mori, 1942; Wilson, 1942; Tanaka, 1953; Anraku, 1954b; Tsuruta and Chiba, 1954b; Chiba, Tsuruta, and Maéda, 1955; Motoda and Anraku, 1955; Nagaya et al., 1955; Chiba, 1956; Heinrich, 1957b; Honjo et al., 1957; Yamazi, 1958a; 1958b; Grice and Jones, 1960. As *C. turgida;* Wilson, 1950.

Vessel:	*Station*	*Occurrence*
Hugh M. Smith	132	3 females, 1.90–2.00 mm.; 2 males, 2.11 mm.
Do	153	3 males, 1.97–2.11 mm.
Do	30	present.
Do	63	1 female, 1.87 mm.
Stranger	34	7 females, 1.94–2.04 mm.; 3 males, 1.94–1.97 mm.
Orsom	10	3 females, 1.97–2.04 mm.; 1 male, 2.06 mm.
Horizon	32	11 females, 1.84–2.00 mm.; 5 males, 1.94–2.00 mm.
Satsuma	32	5 females, 1.87–1.90 mm.; 3 males, 1.87–2.00 mm.

Remarks: The female genital segment is symmetrical and finely pubescent on the lateral margins (fig. 16). The terminal finger of the distal segment of the fifth foot is finely serrate along its outer distal margin (fig. 10). The proximal seta on the internal margin is slightly shorter than the distal one. The male thorax and abdomen are symmetrical (figs. 11, 12). Segment 16 of the right first antenna is produced into an elongate process (fig. 14). The distal spine on the terminal segment of the right fifth foot (fig. 15) is considerably larger than the preceding two spines. The terminal seta on some specimens is articulated to this segment while in others it is not.

Family PONTELLIDAE

Pontella securifer Brady, 1883

(Plate 34, figs. 1–3)

Pacific records: Scott, 1909; Farran, 1936; Dakin and Colefax, 1940; Wilson, 1942; 1950; Tanaka, 1953.

Vessel:	*Station*	*Occurrence*
Hugh M. Smith	30	2 females, 4.40, 4.46 mm.
Do	31	1 male, 4.40 mm.

Remarks: Both sexes have a large lens situated at the base of the rostrum. Figures of the male sex are given (figs. 1–3).

Pontella tenuiremis Giesbrecht, 1889

(Plate 34, figs. 4–7)

Pacific records: Wilson, 1942; 1950.

Vessel:	*Station*	*Occurrence*
Horizon	32	1 male, 2.80 mm.

Remarks: The structure of the fifth feet (figs. 6, 7) distinguishes the male of this species from other *Pontella*.. No females were found.

Labidocera detruncata (Dana, 1849)

(Plate 34, figs. 8–10)

Pacific records: Scott, 1909; Yamada, 1933; Farran, 1936; Mori, 1937; Dakin and Colefax, 1940; Mori, 1942; 1950; Tanaka, 1953; Anraku, 1954b; Chiba, Tsuruta, and Maéda, 1955; Nagaya et al., 1955; Chiba, 1956; Yamazi, 1958a; 1958b.

Vessel:	*Station*	*Occurrence*
Hugh M. Smith	30	1 female, 2.72 mm.
Do	32	1 female, 2.68 mm.

Remarks: The lateral margins of the last thoracic segment (figs. 8, 9) are pointed and the genital segment is asymmetrical. These two characters plus the structure of the fifth feet (fig. 10) will identify the female. No male was found in the present collections.

Pontellina plumata (Dana, 1849)

(Plate 34, figs. 11–15)

Pacific records: Scott, 1909; Farran, 1929; 1936; Mori, 1937; Dakin and Colefax, 1940; Mori, 1942; Wilson, 1950; Anraku, 1952; Tanaka, 1953; Anraku, 1954b; Tsuruta and Chiba, 1954b; Chiba, Tsuruta, and Maéda, 1955; Motoda and Anraku, 1955; Nagaya et al., 1955; Chiba, 1956; Heinrich, 1958a; Yamazi, 1958a.

Vessel:	*Station*	*Occurrence*
Hugh M. Smith	132	1 female, 1.66 mm.; 2 males, 1.49, 1.59 mm.
Do	178	present.
Do	30	9 females, 1.43–1.84 mm.; 1 male, 1.56 mm.
Do	31	2 females, 1.62, 1.80 mm.
Do	63	present.
Stranger	34	2 females, 1.56, 1.63 mm.
Orsom	10	present.
Horizon	32	present.

Remarks: The female is distinguished by the symmetrically pointed posterior margins of the last thoracic segment (fig. 11) and the right furca. This furca is fused to the anal segment. The posterior lateral margins of the last thoracic segment of the male are rounded (figs. 13, 14) and the right fifth foot is chelate (fig. 15).

Family ACARTIIDAE

Acartia danae Giesbrecht, 1889

(Plate 34, fig. 16)

Pacific records: Scott, 1909; Farran, 1929; 1936; Mori, 1937; Dakin and Colefax, 1940; Johnson, 1942; Mori, 1942; Wilson, 1942; Davis, 1949; Wilson, 1950; Anraku, 1952; Tanaka, 1953; Anraku, 1954b; Motoda and Anraku, 1955; Heinrich, 1957b; Honjo et al., 1957; Heinrich, 1958a; Yamazi, 1958a; 1958b.

Vessel:	*Station*	*Occurrence*
Hugh M. Smith	94	present.
Do	132	1 female, 1.12 mm.
Do	178	present.

Remarks: The female has a large spine on the first segment of the first antennae and the posterior lateral margins of the thorax end in a large point. The external seta on the fifth foot (fig. 16) is slightly more than twice the length of the internal spine.

Acartia negligens Dana, 1849

(Plate 34, fig. 17)

Pacific records: Scott, 1909; Farran, 1929; 1936; Mori, 1937; 1942; Wilson, 1942; 1950; Anraku, 1952; Honjo, 1952; Tanaka, 1953; Anraku, 1954b; Tsuruta and Chiba, 1954b; Chiba, Tsuruta, and Maéda, 1955; Motoda and Anraku, 1955; Nagaya et al., 1955; Chiba, 1956; Heinrich, 1957b; 1958a; Yamazi, 1958a; 1958b.

Vessel:	*Station*	*Occurrence*
Hugh M. Smith	153	2 females, 1.05, 1.10 mm.
Do	178	present.
Do	30	10 females, 1.08–1.21 mm.
Do	31	5 females, 1.10–1.17 mm.
Do	63	present.
Stranger	34	2 females, 1.08, 1.12 mm.
Orsom	10	14 females, 1.10–1.16 mm.
Satsuma	32	present.

Remarks: In contradistinction to *A. danae*, the posterior lateral margins of the last thoracic segment have a series of very small points. The external seta on the fifth foot (fig. 17) is more than four times the length of the internal spine.

LITERATURE CITED

ANRAKU, M.

1952. Plankton copepods collected by R. S. *Yushino-Maru* in Pacific waters to the east of northern Japan during her cruise in November, 1948. Bulletin of the Faculty of Fisheries. Hokkaido University 3(1): 31–39. [In Japanese.]

1953. Seasonal distribution of pelagic copepods at Oshora Bay, west coast of Hokkaido. Bulletin of the Faculty of Fisheries. Hokkaido University 3(3): 187–192.

1954a. Distribution of plankton copepods off Kitami, Hokkaido, in Okhotsk Sea in summer, 1949 and 1950. Bulletin of the Faculty of Fisheries. Hokkaido University 4(4): 249–255.

1954b. Copepods collected on the whaling grounds off northern Japan and Bonin Islands. Bulletin of the Faculty of Fisheries. Hokkaido University 5(1): 1–8.

1954c. Gymnoplea Copepoda collected in Aleutian waters in 1953. Bulletin of the Faculty of Fisheries. Hokkaido University 5(2): 123–136.

AUSTIN, T. S.

1957. Summary, oceanographic and fishery data, Marquesas Islands area, August-September, 1956 (Equapac). U.S. Fish and Wildlife Service, Special Scientific Report—Fisheries No. 217, 186 p.

BARY, B. M.

1959. Species of zooplankton as a means of identifying different surface waters and demonstrating their movements and mixing. Pacific Science 13(1): 14–54.

BERNARD, M.

1958. Révision des *Calocalanus* (Copépodes Calanoida) avec description d'un genre nouveau et deux espèces nouvelles. Bulletin de la Société zoologique de France 83(2–3): 185–199.

BOECK, A.

1873. Nye slaegter og arter af saltvands-copepoder. Christiania Videnskabs-Selskabet Forhanlinger, p. 37–60.

BOWMAN, T. E.

1955. A new copepod of the genus *Calanus* from the northeastern Pacific with notes on *Calanus tenuicornis* Dana. Pacific Science 9(4): 413–422.

1958. A new species of *Acrocalanus* (Copepoda: Calanoida) from off the southeastern coast of the United States. Bulletin of Marine Science of the Gulf and Caribbean 8(2): 118–124.

BRADY, G. S.

1878. A monograph of the free and semi-parasitic Copepoda of the British Islands. Vol. 1. The Ray Society, p. 1–148.

1883. Report on the Copepoda collected by *H.M.S. Challenger* during the years 1873–76. Report on the Scientific Results of *HMS Challenger*, Zoology. Vol. 8, p. 1–142.

1899. On the marine Copepoda of New Zealand. Transactions of the Zoological Society of London 15, pt. 2:31–54.

BRODSKY, K. A.

1950. Calanoida of polar and far eastern seas of the U.S.S.R. Opredeliteli po Fauna S.S.S.R., Izdavaemi, Zoologicheskim Institutom Akademii Nauk SSSR. 35: 1–442. [In Russian.]

1952. On the vertical distribution of copepods in the northwestern Pacific Ocean. Investigations of the far eastern seas of the U.S.S.R. *III*. Deep water fauna of the northwestern Pacific Ocean, p. 88–94. [Translated by W. G. Van Campen, 1956, U.S. Fish and Wildlife Service, Special Scientific Report—Fisheries No. 192, p. 1–6.]

1955. Plankton of the northwestern part of the Kuroshio and waters of the Pacific Ocean adjacent to the Kurile Islands. Transactions of the Institute of Oceanology, Academy of Sciences, U.S.S.R. 18: 124–133. [Translated by W. G. Van Campen, 1956, U.S. Fish and Wildlife Service, Special Scientific Report—Fisheries No. 192, p. 16–24.]

1959. Zooplankton of sea waters of south Sakhalin and south Kurile Islands. Investigations of Far Eastern Seas VI, Academy of Sciences, U.S.S.R., p. 5–46. [In Russian.]

CAMPBELL, M. H.

1929. Some free swimming copepods of the Vancouver Island region. Transactions of the Royal Society of Canada 23, pt. 2, sect. 5: 303–332.

CHIBA, T.

1949. On the distribution of the plankton in the eastern China Sea and Yellow Sea. I. Plankton composition in spring. The Journal of the Shimonoseki College of Fisheries 1(1): 57–63. [In Japanese.]

1952a. On the distribution of the plankton in the eastern China Sea and Yellow Sea. II. Observation on the plankton in spring during the period 1949–50. Bulletin of the Japanese Society of Scientific Fisheries 17(7): 183–186. [In Japanese.]

1952b. On the distribution of the plankton in the eastern China Sea and Yellow Sea. III. Observations on the plankton in autumn during the years 1948–1949. Bulletin of the Japanese Society of Scientific Fisheries 17(7): 187–190. [In Japanese.]

1952c. On the plankton of Nakano-Umi in summer, 1948. The Journal of the Shimonoseki College of Fisheries 2(1): 48–53. [In Japanese.]

1953a. Some observations on the morphological characteristics especially on the reproductive organ of Copepoda, *Calanus darwini*. The Journal of the Shimonoseki College of Fisheries 3(3): 235–238. [In Japanese.]

1953b. Studies on the pelagic Copepoda from the Japan Sea. 1. On the genus *Euchaeta* Philippi, 1843. Bulletin of the Japanese Society of Scientific Fisheries 18(11): 613–617.

1956. Studies on the development and the systematics of Copepoda. The Journal of the Shimonoseki College of Fisheries 6(1): 1–90. [In Japanese.]

CHIBA, T., A. TSURUTA, and H. MAÉDA.

1955. Report on zooplankton samples hauled by larva-net during the cruise of Bikini expedition, with special reference to copepods. The Journal of the Shimonoseki College of Fisheries 5(3): 189–213.

DAKIN, W. J., and A. N. COLEFAX.

1940. The plankton of the Australian coastal waters off New South Wales. Pt. 1. Publications of the University of Sydney, Department of Zoology Monograph 1, p. 1–211.

DAVIS, C. C.

1949. Pelagic Copepoda of the northeastern Pacific Ocean. University of Washington Publications in Zoology. Vol. 14, 117 p.

ESTERLY, C. O.

1905. The pelagic Copepoda of the San Diego region. University of California Publications in Zoology 2(4): 113–233.

1906. Additions to the copepod fauna of the San Diego region. University of California Publications in Zoology 3(5): 53–92.

1911. Third report on the Copepoda of the San Diego region. University of California Publications in Zoology 6(14): 313–352.

1913. Fourth taxonomic report on the Copepoda of the San Diego region. University of California Publications in Zoology 11(10): 181–196.

1924. The free swimming Copepoda of San Francisco Bay. University of California Publications in Zoology 26(5): 81–129.

FARRAN, G. P.

1929. Crustacea. Part X. Copepoda. British Antarctic (*Terra Nova*) Expedition, 1910, Natural History Report, Zoology 8(3): 203–306.

1936. Copepoda. Great Barrier Reef Expedition 1928–29. Scientific Reports 5(3): 73–142.

FLEMINGER, A.

1956. Taxonomic and distributional studies on the epiplanktonic calanoid copepods (Crustacea) of the Gulf of Mexico. Doctoral Dissertation, Harvard University Library.

FLEMINGER, A., and T. E. BOWMAN.

1956. A new species of *Candacia* (Copepoda: Calanoida) from the western north Atlantic Ocean. Proceedings of the U.S. National Museum 106(3370): 331–337.

FUKASE, S.

1957. Note on a variety of *Eucalanus subtenuis* Giesbrecht from the Japanese waters. Journal of the Oceanographical Society of Japan 13(1): 17–21.

GIESBRECHT, W.

1888, 1889, 1891. Elenco dei copepodi pelagici raccolti dal tenente di vascello Gaetano Chierchia durante il viaggio della R. Corvetta *Vettor Pisani* negli anni 1882–1885 e dal tenente di vascello Francesco Orsini nel Mar Rosso, nel 1884. Atti della R. Accademia Nazionale dei Lincei Rendiconti, (4). Vol. 4, sem. 2 (1888): 284–287, 330–338. Vol. 5 (1889), sem. 1: 811–815; sem. 2: 24–29. Vol. 7 (1891), sem. 1: 474–481; sem. 2: 63–68, 276–282.

1892. Systematik und faunistik der pelagischen Copepoden des Golfes von Neapel. Fauna u. Flora des Golfes von Neapel u. d. angrenz Meeresabschnitte 19: 1–831.

1895. Die pelagischen Copepoden. Bulletin of the Museum of Comparative Zoology at Harvard College 25(12): 243–263.

1896. Ueber pelagische Copepoden des Rothen Meeres gesammelt vom marinestabsarzt Dr. Augustin Krämer. Zoologische Jahrbucher, Abt. Systematik. Vol. 9, p. 315–327.

GIESBRECHT, W., and O. SCHMEIL.

1898. Copepoda I. Gymnoplea. Das Tierreich, Lief. 6, 169 p.

GILMARTIN, M.

1958. Some observations on the lagoon plankton of Eniwetok Atoll. Pacific Science 12(4): 313–316.

GRICE, G. D.

1959. A new species of *Haloptilus* (Copepoda: Calanoida) from equatorial and subtropical waters of the east-central Pacific Ocean. Journal of the Washington Academy of Sciences 49(6): 193–195.

GRICE, G. D., and E. C. JONES.

1960. Two new species of *Candacia* (Copepoda: Calanoida) from the central Pacific with notes on two other species. Pacific Science 14(3): 280–291.

HEINRICH, A. K.

1957a. The distribution of *Calanus tenuicornis* Dana and *Calanus lighti* Bowman in the north Pacific. Doklady Akademii Nauk S.S.S.R. 116 (4): 691–693 [In Russian.]

1957b. The vertical distribution of the plankton to the southeast from the Bonin Islands. Doklady Akademii Nauk S.S.S.R. 117(2): 321–324. [In Russian.]

1958a. The vertical distribution of copepods in the Kuroshio Current and the way they penetrate into the zone of mixing of subtropical and subarctic waters. Doklady Akademii Nauk S.S.S.R. 118(6): 1191–1193. [In Russian.]

1958b. On the feeding of copepods in the tropical region. Doklady Akademii Nauk S.S.S.R. 119 (5): 1028–1031. [In Russian.]

HIDA, T., and J. E. KING.

1955. Vertical distribution of zooplankton in the central equatorial Pacific, July–August 1952. U.S. Fish and Wildlife Service, Special Scientific Report—Fisheries No. 144, 22 p.

HONJO, K.
1952. Distribution of Copepoda in the adjacent sea of the Izu Islands during winter and spring. Bulletin of the Tokai Regional Fisheries Research Laboratory, No. 4, p. 1–5. [In Japanese.]

HONJO, K., H. OHTA, T. KIDACHI, K. UMEDA, and S. KUDOH.
1957. Distribution of Copepoda in the "Kuroshiro" area, south of Honshu, May, 1955. Records of Oceanographic Works in Japan, Special No. March 1957, p. 120–129.

HURE, J.
1955. Distribution annuelle verticale du zooplancton sur une station de l'Adriatique meridionale. Acta Adriatica Institut za Oceanografiju i Ribarstvo–Split fnr Jugoslavija 7(7): p. 1–72.

JAPANESE HYDROGRAPHIC OFFICE.
1956. Plankton observation. Equapac Expedition. Japanese Hydrographic Office. [Unpublished processed report.]

JOHNSON, M. W.
1942. Notes on Zooplankton. Records of Observations, Scripps Institution of Oceanography. Vol. 1, No. 1, Oceanographic Observations on the E. W. Scripps Cruises of 1938, p. 27–29.
1949. Zooplankton as an index of water exchange between Bikini Lagoon and the open sea. Transactions of the American Geophysical Union 30(2): 238–244.
1954. Bikini and nearby atolls. Pt. 2. Oceanography (biologic). Plankton of northern Marshall Islands. U.S. Geological Survey, Professional Paper F, p. 301–314.

KING, J. E., T. S. AUSTIN, and M. S. DOTY.
1957. Preliminary report on expedition *Eastropic.* U.S. Fish and Wildlife Service, Special Scientific Report—Fisheries No. 201, 155 p.

KNAUSS, J. A.
1959. Direct current measurements at the equator–the Cromwell Current. International Oceanographic Congress, 31 August–12 September 1959. Preprints, American Association for the Advancement of Science, p. 515–516.

KNAUSS, J. A., and J. E. KING.
1958. Observations of the Pacific equatorial undercurrent. Nature 182 (4635): 601–602.

KOKUBO, S.
1950. The ecology of certain Copeda in Japan Sea, and Mutsu Bay. Bulletin of the Japanese Society of Scientific Fisheries 16(5): 215–220. [In Japanese.]

LEGAND, M.
1957. *Orsom III.* Résultats biologiques de l'expédition Equapac. Institut Français d'Océanie, Rapport Scientifique No. 1. [Processed report.]

LÉGARÉ, J. E. H.
1957. The qualitative and quantitative distribution of plankton in the Strait of Georgia in relation to certain oceanographic factors. Journal of the Fisheries Research Board of Canada 14(4): 551–552.

LINDBERG, G. U.
1959. A list of the fauna of sea waters of the south Sakhalin and south Kurile Islands. Investigations of Far Eastern Seas. VI. Academy of Sciences of the U.S.S.R., p. 173–256. [In Russian.]

LOWE, C. W.
1936. Observations on some Pacific diatoms as the food of copepods and fishes. Journal of the Biological Board of Canada 3(1): 12–19.

MCEWEN, G. F., M. W. JOHNSON, and T. R. FOLSOM.
1954. A statistical analysis of the performance of the Folsom plankton sample splitter, based upon test observations. Archiv für Meteorologie, Geophysik und Bioklimatologie, Ser. A., 7: 502–527.

MCMURRICH, J. P.
1916. Notes on the plankton of the B. C. coast. Transactions of the Royal Society of Canada 10, Ser. 3, sect. 5:75–89.

MARUKAWA, H.
1921. Plankton list and some new species of Copepoda from the northern waters of Japan. Bulletin Institute of Oceanography No. 384.

MORI, T.
1930. An annotated list of the pelagic Copepoda from the S. W. part of the Japan Sea with descriptions of two new species. Zoological Magazine 41(487): 199–209. [In Japanese.]
1932. New copepods from southern Japan. Zoological Magazine, 44(523): 167–177. [In Japanese.]
1937. The pelagic Copepoda from the neighbouring waters of Japan. Tokyo. 150 p.
1942. Systematic studies of the plankton organisms occurring in Iwayama Bay, Palao. IV Copepoda from the Bay and adjacent waters. Palao Tropical Biological Station Studies, 2(3): 549–580.

MOTODA, S., and M. ANRAKU.
1951. An observation on the vertical distribution of plankton at Ishikari Bay, Hokkaido. Journal of the Oceanographic Society of Japan 6(4): 194–201. [In Japanese.]
1952a. Observations on the plankton of Funka Bay, Hokkaido. I. Vertical distribution of plankton at the mouth of the bay in August 1950. Bulletin of the Hokkaido Region Fisheries Laboratory, No. 5, p. 17–20. [In Japanese.]
1952b. Plankton investigations (spring and summer, 1951). Report of the Deep Sea Fisheries of the Northern Japan Sea, No. 3, p. 71–76. [In Japanese.]
1954. Daily change of vertical distribution of plankton animals near western entrance to the Tsugaru Strait, Northern Japan. Bulletin of the

Faculty of Fisheries, Hokkkaido University 5(1): 15–19.

1955. Marine plankton copepods from the Hachijo Island, Idzu Islands, with special reference to their vertical distribution. Records of Oceanographic Works in Japan 2(1): 210–214.

Motoda, S., A. Iizuka, and M. Anraku.

1950. Plankton distribution to the northwest of Hokkaido in summer 1949. Report of the Deep Sea Fisheries of the Northern Japan Sea, No. 1, p. 78–109. [In Japanese.]

Nagaya, Y., Y. Komaki, T. Chiba, A. Tsuruta, and H. Maéda.

1955. Effects of artificial radioactivity on plankton. Publication of the Fishery Agency of Japan, p. 33–54. [In Japanese.]

Nakai, Z.

1952. On quantitative distribution of plankton reproduced in the northern Pacific. Tokai Regional Fisheries Laboratory, Special Publication No. 2, p. 1–6.

1955. The chemical composition, volume, weight, and size of the important marine plankton. Tokai Regional Fisheries Research Laboratory, Special Publication No. 5, p. 12–24.

Ponomareva, L. A.

1959. Some data on the zooplankton of the western coast of the south Sakhalin Island. Investigations of Far Eastern Seas. VI. Academy of Sciences of the U.S.S.R., p. 47–57. [In Russian.]

Rose, M.

1933. Copépodes pélagiques. Faune de France, 26: 1–374.

1934. Recherches complementaires sur les copépodes pélagiques de baie d'Alger. Bulletin de la Société d'histoire naturelle de l'Afrique du Nord 25(5): 145–148.

1942. Les Scolecithricidae (Copépodes pélagiques) de la Baie d'Alger. Annales de l'Institut Océanographique, n. s. 21, Pt. 3: 113–170.

1955. Quelques notes sur le plancton marin recueilli en 1953, par M. G. Ranson, dans la baie de Nhatrang-Canda (Viet Nam). Bull. du Muséum, 2ᵉ serie, vol. 27, No. 5.

Sars, G. O.

1903. Copepoda. Calanoida. Crustacea of Norway, Volume IV. 171 p.

1905. Listes preliminaires de Calanoides recueillis pendant les campagnes de S.A.S. le Prince Albert de Monaco avec diagnoses des genres et des espèces nouvelles. Bulletin du Musée Océanographique de Monaco, No. 26, 22 p.

Schmitt, W. L.

1939. Decapoda and other crustacea collected on the Presidential cruise of 1938. Smithsonian Miscellaneous Collections 98(6): 29 p.

Scott, A.

1909. The Copepoda of the *Siboga* expedition. Pt. 1. Free swimming, littoral and semi-parasitic Copepoda. Siboga-Expéditie Monographie 29a, p. 1–323.

Scott, T.

1894. Report on Entomostraca from the Gulf of Guinea. Transactions of the Linnean Society of London, series 2, Zoology. Vol. 6, Pt. 1, 161 p.

Scripps Institution of Oceanography.

1957. Data collected by Scripps Institution vessels on Equapac Expedition, August 1956. Scripps Institution of Oceanography Data Report, ref. 57–25. [Processed report.]

Sewell, R. B. S.

1929, 1932. The Copepoda of Indian Seas. Calanoida. Memoirs of the Indian Museum 10: 1–221 (1929), 223–407 (1932).

1947. The free swimming planktonic Copepoda. Systematic Account. *John Murray* Expedition 1933–34. Scientific Report 8(1): 1–303.

Shen, Chia-Jui, and Sye-O Bai.

1956. The Marine Copepoda from the spawning ground of *Pneumatophorus japonicus* (Houttuyn) off Chefoo, China. Acta Zoologica Sinica 8(2): 177–234. [In Chinese.]

Steuer, A.

1932. Copepoda 6: *Pleuromamma* Giesbr. 1898 der Deutschen Tiefsee-Expedition. Wissenschaftliche Ergebnisse der Deutschen Tiefsee-Expedition, 1898–1899, 24(1): 1–119.

Streets, T. H.

1877. Contribution to the natural history of the Hawaiian and Fanning Islands and lower California. Bulletin, U.S. National Museum, No. 7, p. 1–172.

Tanaka, O.

1935a. The Copepoda of Sagami Bay. Family Eucalanidae I. Suisan Gakkwai Ho (Tokyo) 6(3): 142–165. [In Japanese.]

1935b. The Copepods of Sagami Bay. Pt. II. The family Candaciidae. Suisan Gakkwai Ho (Tokyo) 6(4): 210–227. [In Japanese.]

1936. On some new species of Copepoda from Sagami Bay. Japanese Journal of Zoology 7(1): 31–36.

1937. Copepods from the deep water of Suruga Bay. Japanese Journal of Zoology 7(2): 251–271.

1953. The pelagic copepods of the Izu region. Records of Oceanographic Works in Japan 1(1): 126–137.

1956a. The pelagic copepods of the Izu Region, middle Japan. Systematic Account. I. Families Calanidae and Eucalanidae. Publications of the Seto Marine Biological Laboratory 5(2): 251–272.

1956b. The pelagic copepods of the Izu Region, middle Japan. Systematic Account. II. Families Paracalanidae and Pseudocalanidae. Publications of the Seto Marine Biological Laboratory 5(3): 367–406.

1957a. The pelagic copepods of the Izu Region, middle Japan. Systematic Account. III. Family Aetideidae (Part 1). Publications of the Seto Marine Biological Laboratory 6(1): 31–68.

1957b. The pelagic copepods of the Izu Region, middle Japan. Systematic Account. IV. Family Aetideidae (Pt. 2). Publications of the Seto Marine Biological Laboratory 6(2): 169–207.

1958. The pelagic copepods of the Izu Region, middle Japan. Systematic Account. V. Family Euchaetidae. Publications of the Seto Marine Biological Laboratory 6(3): 327–367.

TSURUTA, A., and T. CHIBA.

1954a. On the distribution of plankton at the fishing ground of salmons in the north Pacific Ocean, 1952. Journal of the Shimonoseki College of Fisheries 3(3): 239–245. [In Japanese.]

1954b. On the plankton at the fishing ground of tuna in the mid-Pacific Ocean. (1953.) Journal of the Shimonoseki College of Fisheries 3(3): 247–253. [In Japanese.]

VERVOORT, W.

1946. Biological results of the *Snellius* Expedition. XV. The bathypelagic Copepoda Calanoida of the *Snellius* Expedition. I. Families Calanidae, Eucalanidae, Paracalanidae, and Pseudocalanidae. Temminckia 8: 1–181.

1949. Some new and rare Copepoda Calanoida from east Indian Seas. Zoologische Verhandelingen, No. 5, 53 p.

1950. On the identity of *Onchocalanus nudipes* C. B. Wilson, 1942. Proceedings of the Section of Sciences, Koninklijke Nederlandse Akademie van Wetenschappen 53(1): 83–92.

1951. Plankton copepods from the Atlantic sector of the Antarctic. Verhandelingen der Koninklijke Nederlandse Akademie van Wetenschappen Afdeeling Natuurkunde, Sect. 2. Vol. 47 (no. 4): 1–156.

1952. Copepoda. Sub-order Calanoida. Family Aetideidae, Genus *Euchirella*. Fiches d'Identification du Zooplancton 47. Conseil Permanent International pour l'Exploration de la Mer.

1957. Copepods from Antarctic and sub-Antarctic plankton samples. B.A.N.Z. Antarctic Research Expedition 1929–1931. Reports, Ser. B (Zoology and Botany), 160 p.

WILSON, C. B.

1942. The copepods of the plankton collected during the last cruise of the *Carnegie*. Carnegie Institution of Washington Publication No. 536, 237 p.

1950. Copepods gathered by the U.S. Fisheries steamer *Albatross* from 1887 to 1909, chiefly in the Pacific Ocean. U.S. National Museum Bulletin 100, 14(4): 141–441.

WOLFENDEN, R. N.

1905. Notes on the collection of Copepoda. The Fauna and Geography of the Maldive and Laccadive Archipelagoes. Vol. 2. Suppl. 1: 989–1040.

YAMADA, T.

1933a. On the distribution of the temperate plankton in the western part of the Korean Strait. Bulletin of the Japanese Society of Scientific Fisheries 1(6): 281–286. [In Japanese.]

1933b. Report on the distribution of the plankton in the neighboring seas of Tyosen in June 1932. Annual Report of the Hydrographic Observatory of the Fishery Experiment Station. Government General of Tyosen, No. 7. Appendix. [In Japanese.]

YAMAZI, I.

1950. Plankton investigations in inlet waters of Japan. I. Introductory notes and the plankton of Akkeshi Bay, Hanasaki Inlet and Nemuro Harbour. Publications of the Seto Marine Biological Laboratory 1(3): 93–113.

1951. Plankton investigations in inlet waters of Japan. II. The plankton of Hakodate Harbour and Yoichi Inlet in Hokkaido. Publications of the Seto Marine Biological Laboratory 1(4): 185–194.

1952a. Plankton investigations in inlet waters of Japan. III. The plankton of Imari Bay in Kyusyu. Publications of the Seto Marine Biological Laboratory 2(2): 289–304.

1952b. Plankton investigations in inlet waters of Japan. IV. The plankton of Nagasaki Bay and Nagasaki Harbour in Kyusyu. Publications of the Seto Marine Biological Laboratory 2(2): 305–318.

1952c. Plankton investigations in inlet waters of Japan. V. The plankton of Hiroshima Bay in the Seto-Naikai (Inland Sea). Publications of the Seto Marine Biological Laboratory 2(2): 319–330.

1953a. Plankton investigations in inlet waters of Japan. VII. The plankton collected during the cruises to the new Yamato Bank in the Japan Sea. Publications of the Seto Marine Biological Laboratory 3(1): 75–108.

1953b. Plankton investigations in inlet waters of Japan. IX. The plankton of Onagawa Bay on the eastern coast of Tôhoku district. Publications of the Seto Marine Biological Laboratory 3(2): 173–187.

1953c. Plankton investigations in inlet waters of Japan. X. The plankton of Kamaisi Bay on the eastern coast of Tôhoku district. Publications of the Seto Marine Biological Laboratory 3(2): 189–204.

1954a. Plankton investigations in inlet waters of Japan. XI. The plankton of Kozima Bay in the Seto-Naikai (Inland Sea). Publications of the Seto Marine Biological Laboratory 3(3): 399–421.

1954b. Plankton investigations in inlet waters of Japan. XII. Plankton of Miyako Bay on the eastern coast of Tôhoku district. Publications of the Seto Marine Biological Laboratory 3(3): 423–441.

1954c. Plankton investigations in inlet waters of Japan. XIII. The plankton of Obama Bay on the Japan Sea coast. Publications of the Seto Marine Biological Laboratory 4(1): 103–114.

1954d. Plankton investigations in inlet waters of Japan. XIV. The plankton of Turuga Bay on the Japan Sea coast. Publications of the Seto Marine Biological Laboratory 4(1): 115–126.

1954e. Plankton investigations in inlet waters of Japan. XV. The plankton of Yosa–Naikai and Kumihama Bay, enclosed bays on the Japan Sea coast. Publications of the Seto Marine Biological Laboratory 4(1): 127–145.

1955a. Plankton investigations in inlet waters of Japan. VIII. The plankton of Miyazu Bay in relation to the water movement. Publications of the Seto Marine Biological Laboratory 4(2–3): 269–284.

1955b. Plankton investigations in inlet waters of Japan. XVI. The plankton of Tôkyô Bay in relation to the water movement. Publications of the Seto Marine Biological Laboratory 4(2–3): 285–309.

1955c. Plankton investigations in inlet waters of Japan. XVII. Seasonal succession of zooplankton in the inner area of Tanabe Bay from June to October 1954. Publications of the Seto Marine Biological Laboratory 4(2–3): 311–320.

1957. Plankton investigations in inlet waters of Japan. XX. Diurnal change of plankton animals at an innermost station in Wakayama Harbor. Publications of the Seto Marine Biological Laboratory 6(2): 209–224.

1958a. Preliminary check-list of plankton organisms found in Tanabe Bay and its environs. Publications of the Seto Marine Biological Laboratory 7(1): 111–163.

1958b. A study on the productivity of the Tanabe Bay. Pt. I, IV. On some plankton indicating the water exchange in the Tanabe Bay. Records of Oceanographic Works in Japan Special Publication No. 2, p. 25–35.

YAMAZI, I., and T. HORIBATA.

1955. Plankton investigations in inlet waters of Japan. XVIII. Seasonal succession of plankton in Taizi Bay in the years 1951–1953. Publications of the Seto Marine Biological Laboratory 4(2–3): 321–336.

☆U.S. GOVERNMENT PRINTING OFFICE: 1961—597171

Contribution No. 1085

Made in United States of America
Reprinted from Journal of Mammalogy
Vol. 42, No. 3, 21 August 1961
pp. 418–419

STRANDED KILLER WHALE IN THE BAHAMAS

Because records of the killer whale, *Orcinus orca,* off the southeastern United States are few, the stranding of one of these animals on Great Abaco Island, Bahamas, is reported. The record is of additional interest since this cetacean only rarely beaches itself. The writer is indebted to Mr. and Mrs. John W. Coolidge, Cambridge, Massachusetts, for the data pertaining to the stranding, including eight good photographs of the skull in various aspects, isolated teeth, the cervical bloc, and ribs (Plate I).

The animal stranded alive on the eastern shore of Man O'War Cay, Great Abaco Island, sometime in June 1960. There were several open wounds in the tail region and the whale was followed inshore by a number of large sharks, the appearance of the latter at this spot being considered unusual in itself. The animal is reported as having been about 20 feet long, with a large dorsal fin. The skull is described as being about 4 feet long and the teeth about 5 inches in length with about 3 inches imbedded in the gum. The teeth numbered 14 pairs in the upper jaw and the same (with some question) in the lower jaw.

It is clear from the photographs of the skull that it belongs to *Orcinus orca* and the few other data are all compatible with this identification. Although most authorities state that *Orcinus* has from 10 to 13 pairs of teeth in each jaw, according to Tomilin (Zveri SSSR i prilezhashchikh stran. IX. Kitoobraznyye. Acad. Sci. USSR, Moscow: 1–756, 1957), 14 pairs are occasionally encountered.

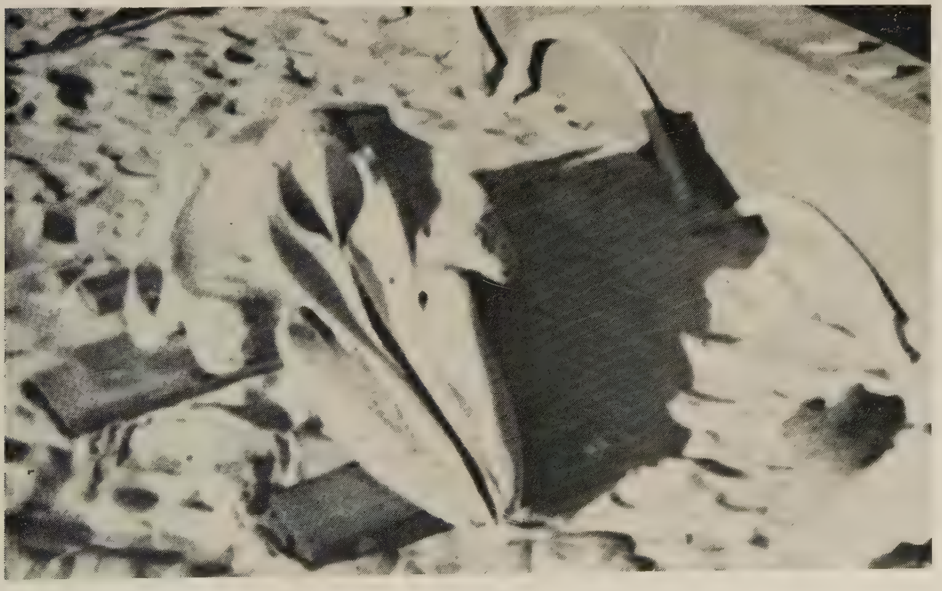

PLATE I

Skull and isolated teeth and ribs of *Orcinus orca* stranded on Great Abaco Island, Bahamas, in June 1960. (*Photo by J. W. Coolidge.*)

Moore (Am. Midl. Nat., 49: 117–158, 1953) gives Florida records for the killer whale. In addition to two strandings, he lists five sightings of this animal, all in the Gulf Stream off the Florida east coast. According to Moore's informants, this animal is not often encountered in these waters. Caldwell, Layne and Siebenaler (Quart. J. Fla. Acad. Sci., 19: 189–196, 1956) report an additional Florida stranding, and Gunter (U. S. F. W. S., Fish. Bull. 89: 543–551, 1954) reports a sighting off Port Aransas, Texas. On the occasion of the present stranding, Man O'War Cay inhabitants stated that the animal was completely unknown to them.

In addition to the one reported here, strandings on the east coast of North America are as follows (of single individuals unless otherwise noted): New Melbourne, Trinity Bay, Nfld., 27 April 1957, 19 or more individuals (Dearden, Canad. Field-Nat., 72: 166–167, 1958); Chapel Arm, Trinity Bay, Nfld., 9 June 1955 (Sergeant and Fisher, J. Fish. Res. Bd. Canada, 14: 83–115, 1957); Economy, Minas Basin, N. S., 4 Jan. 1950 (*ibid.*); Eastport, Me., March 1902, 2 individuals (True, Proc. U.S. Nat. Mus., 27: 227–230, 1904); Tenant's Harbor, Me., 14 Dec. 1957 (Mairs and Scattergood, Maine Field Nat., 15: 111–113, 1959); Harpswell, Me., 14 Nov. 1904 (Norton, Proc. Portland Soc. Nat. Hist., 4: 101, 1930); Barnegat, N. J., Jan. 1909 (True, Science, 29: 790–791, 1909); Wildwood Crest, N. J., 27 Jan. 1941 (Ulmer, Not. Nat., 83: 1–5, 1941); Summerland Key, Fla., about March 1948 (Moore, *op. cit.*); Everglades, Fla., Dec. 1921 (*ibid.*); 6 miles E of East Pass, Okaloosa Co., Fla., May 1956 (Caldwell, Layne and Siebenaler, *op. cit.*).

In these 12 strandings the whales have come ashore alive in four cases. In one case the whale was first noted dead in the surf but may have come ashore alive earlier. In the remaining seven cases this information is not available.—Richard H. Backus, *Woods Hole Oceanographic Inst., Woods Hole, Massachusetts. Received 25 January 1961.*

[Contribution No. 1085 from the Woods Hole Oceanographic Institution.]

Contribution No. 1109

THE FISHES OF RICHMOND GULF, UNGAVA, CANADA [1]

ROBERT L. EDWARDS

Biological Laboratory, Bureau of Commercial Fisheries, Woods Hole

INTRODUCTION

THIS REPORT is based on material collected uring the 1953 R/V *Lemming* Expedition to Richmond Gulf. This expedition was financed rincipally by the American Philosophical Society Penrose Fund) with additional assistance from he Geological Society of America, the Woods Hole Oceanographic Institution, and the American Academy of Arts and Sciences. The 1953 trip was primarily concerned with the general ecology f the Richmond Gulf area, both land and water.

The research was accomplished from the R/V *Lemming,* a surplus Navy whaleboat, modified nto a small oceanographic research vessel. In ddition to fish, large collections of small mammals, marine mollusks, and other invertebrates were made. Sufficient temperature, salinity, and epth data were obtained to present a clear picure of the marine environment of Richmond Gulf during the summer months. Dr. J. Lockwood Chamberlin [1] and the author collected all f the data and material discussed.

RICHMOND GULF

Richmond Gulf (fig. 1) is a large triangular ody of essentially marine water on the eastern ide of Hudson Bay. It is about 30 miles long n its western edge and approximately 20 miles wide. It is deepest along its western side with epths to at least 70 fathoms. The eastern edge s generally shoal. Navigation amongst the small slands was a hazardous business even with a hallow draft vessel, although one could reach lmost any general area with the R/V *Lemming* draft 4 feet) with proper care and navigation.

The gulf is connected with Hudson Bay by a arrow channel, the Hazard, at its southwestern orner. At its narrowest, the Hazard is about 00 yards wide and probably nowhere deeper han about 60 feet. On two transects made with he R/V *Lemming,* the depths recorded here were 0 and 48 feet. Tracings of the depths recorded by echo-sounder on these two trips through the Hazard are presented in figure 2.

HYDROGRAPHY

Numerous rivers enter Richmond Gulf, especially along its eastern edge (see fig. 1). The influx of this relatively warm fresh water in the spring and summer decreases the salinity of the surface waters and raises its temperature. Average summer temperature and salinity data are presented in table 1. Conditions in Richmond Gulf differ from those in Hudson Bay in two significant aspects. First, there is no clearly defined thermocline in neighboring Hudson Bay water. Second, temperatures drop rapidly to values less than zero below 200 feet in Richmond Gulf. While it drops similarly in Hudson Bay, it does not reach these sub-zero values so quickly.

Some typical bathythermograph traces are presented in figure 3 to illustrate the temperature depth relationships observed. It would appear that the cold, relatively saline water entering Richmond Gulf during the winter months is not rapidly flushed out during the summer months. The layer of relatively fresh water on the surface, the thermal stratification, and the depth threshold of the Hazard would all contribute to the trapping of this cold water. These conditions are reminiscent of similar conditions observed by others in arctic fiords where the entrance is shallower than the fiord proper.

Richmond Gulf is not, however, stagnant in the deeper holes. Even the deepest areas had an epi-, and an infauna that was thriving if not populous. This is not really surprising. The turbulence of water entering Richmond Gulf just beyond the Narrows of the Hazard is legendary and undoubtedly provides for at least minimal exchange of even the deepest water.

BOTTOM TYPES, CONDITIONS AND ASSOCIATED INVERTEBRATES

SHALLOW WATER, 0–25 FEET

The shallowest waters, with temperatures of 8 to 15° C. and salinities of 15 to 21 parts per

---

[1] Contribution No. 1109 from the Woods Hole Oceano-raphic Institution, Woods Hole, Massachusetts.

ROCEEDINGS OF THE AMERICAN PHILOSOPHICAL SOCIETY, VOL. 105, NO. 2, APRIL, 1961
eprint *Printed in U.S.A.*

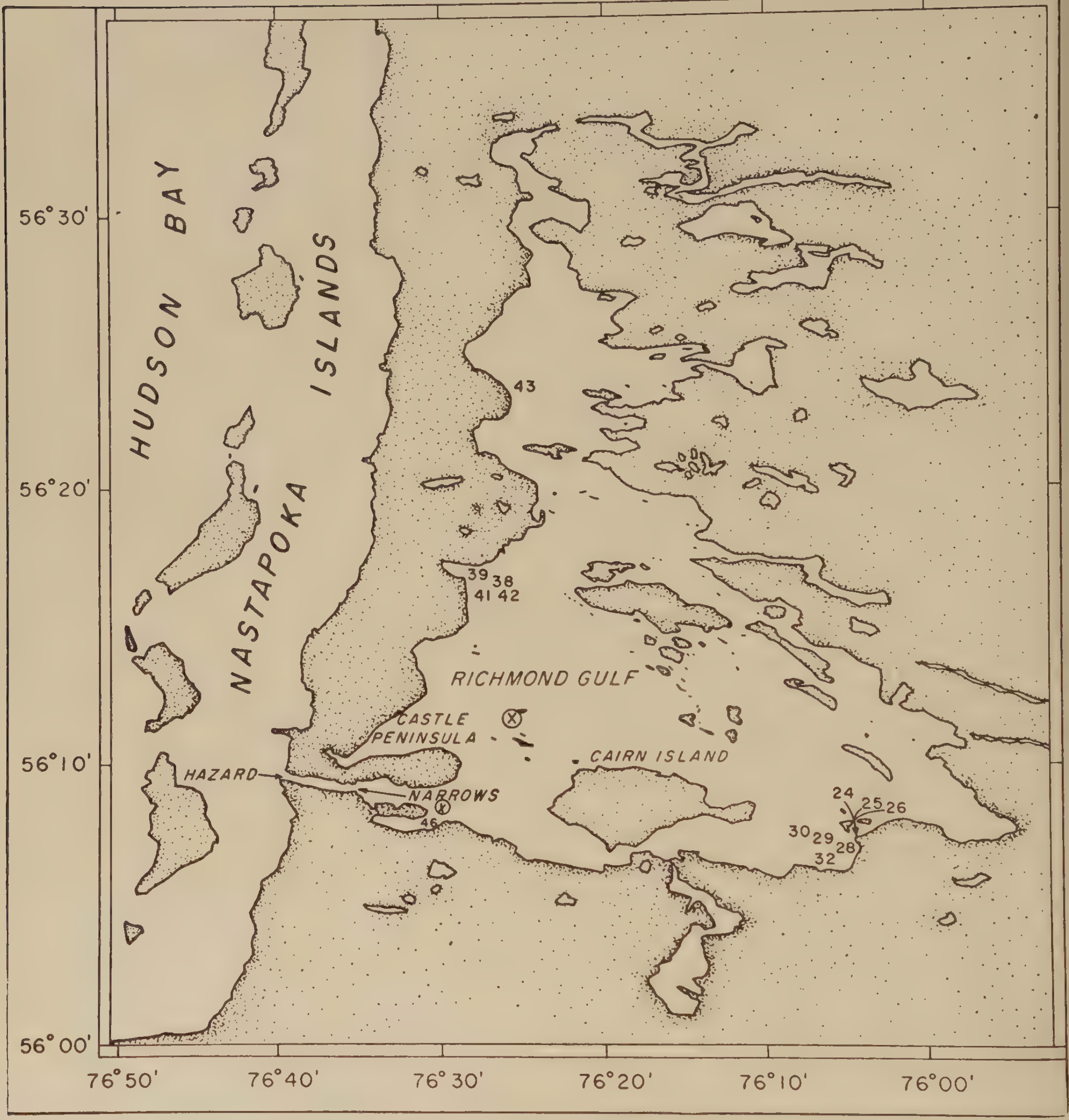
HUDSON BAY
NASTAPOKA ISLANDS
RICHMOND GULF
CASTLE PENINSULA
CAIRN ISLAND
HAZARD
NARROWS
43
39 38
41 42
46
24
25 26
30 29
28
32
56°30'
56°20'
56°10'
56°00'
76°50'
76°40'
76°30'
76°20'
76°10'
76°00'

FIG. 1. Stations mentioned in text where fish were collected in Richmond Gulf, summer of 1953. X indicates otter trawl stations at which fish were not collected.

thousand, usually support thriving communities of fucoid algae and mollusks, depending on the bottom type and the amount of molar action. The bottom may be bare rock, underwater talus, boulders, gravel, sand, clay, or mud.

Where streams and rivers enter, it is usually sand and/or gravel. Off the beaches, which are only a small part of the coast line, the sand and gravel are succeeded by clay and mud. Th greatest part of the coast line is bare rock an talus, and the bottom in these areas is usuall similar.

Sand and gravel bottoms in relatively shallo water usually had a thriving community c *Mytilus, Mya, Macoma, Buccinum, Strongylo centrus,* and fucoid algae as obvious member

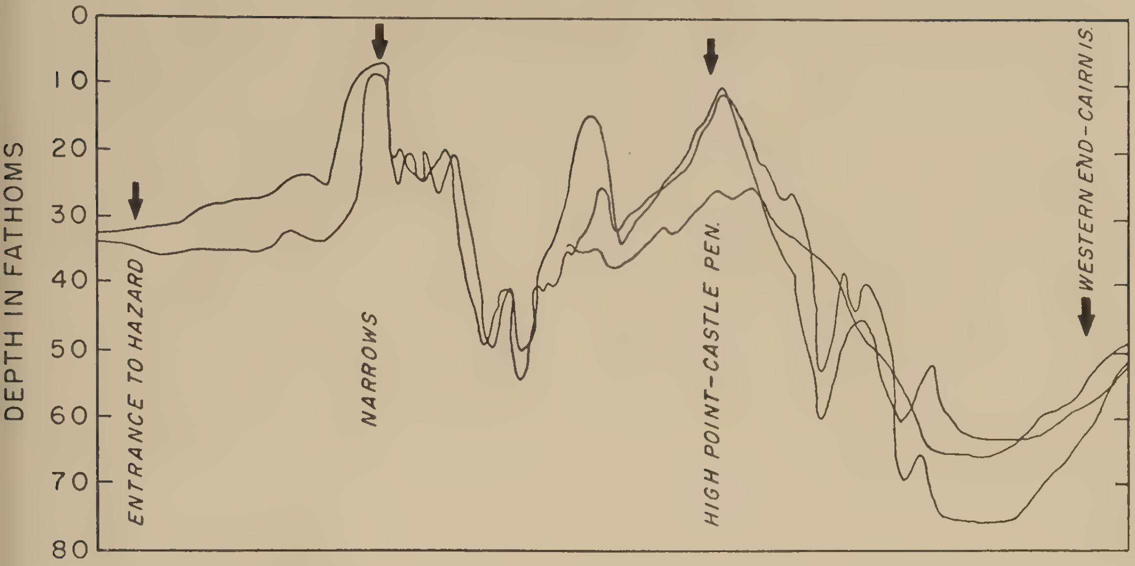

FIG. 2. Echo sounder traces from Hudson Bay entrance of Hazard to Cairn Island, Richmond Gulf. Total distance about 10 miles.

the fauna and flora. The plain rock bottoms pported little else than the sea urchin, whater the depth.

MID-DEPTHS, 25–150 FEET

The waters referred to here as the mid-depths ve temperatures above 0° C. and salinities of 22 26 parts per thousand. The bottom is usually ay or gray and/or brown muds. Rock, talus, d boulders were encountered only where the eep cliffs made up the shore line or where there ere were sharp changes in the bottom topogphy.

The middle depth muds supported extensive pulations of invertebrates. The mollusks were represented by species of *Astarte, Trichotropis, Macoma, Portlandia, Pandora, Thracia, Buccinum,* and others. Small decapod shrimp of several genera were present as well as the large isopod, *Mesidothea.* The crinoid, *Heliometra glacialis,* was occasionally collected on these bottoms. Starfish were common and included species of the genera *Solaster, Ctenodiscus, Pteraster, Leptasterias,* and *Ophiura.* Polychaete worm tubes were common. In certain areas, a very large worm, probably *Echiurus,* was an abundant member of the bottom fauna.

TABLE 1

VERAGE TEMPERATURES AND SALINITIES OF RICHMOND GULF, AUGUST AND SEPTEMBER, 1953

verages at depths in feet, salinities to the nearest tenth of $^0/_{00}$ and temperatures to nearest 0.5° C.

Depth	S $^0/_{00}$	° C.
0	17.00	10
25	21.90	8
50	23.00	5
75	23.80	3
100	24.80	2
125	25.10	1.5
150	26.00	0.5
200	26.90	0.0
300	27.00	−0.5

DEEP WATER, MORE THAN 200 FEET

This deep water characteristically had temperatures at and below 0° C. The salinities were at least as great as 27 parts per thousand. The bottom in these deep areas is usually red or red-brown mud. None of the bottom samples collected had an H_2S odor. There was not an abundant infauna, and the epifauna was certainly depauperate.

The ubiquitous *Portlandia* occurred, along with *Nucula, Thyasira,* and *Buccinum.* Worm tubes were relatively common. Except for an occasional *Ophiura,* starfish did not occur on these muds.

STATION LIST AND GEAR

A list of the stations where fish were collected is presented in table 2. Data concerning these stations pertinent to this report are included, We usually depended on the otter trawl to collect fish. Our trawl was a scaled down model of the standard "german-type" trawl used in commercial fisheries. It was about fifteen feet long with a spread of eight feet between the otter boards. The cod end mesh was one inch. The otter boards were frequently upset on the rough bottom and many tows were accordingly failures. The standard towing time was five minutes. Gillnets with one- and three-inch stretched mesh proved to be very useful in well-protected places. Much of the Richmond Gulf area, however, is too open, too rough, and too subject to strong winds to use gillnets effectively. We occasionally hand lined for fish when we were penned up in harbor. The dipnet was used at night from time to time to collect the fish and invertebrates that gathered in the light of our lanterns.

Only minimum numbers of the larger species of fish were saved to conserve space and preservative. As is usually the case, this decision was later regretted.

A small aquarium was carried on board into which we placed specimens for observation. When time permitted, color notes were made of living material.

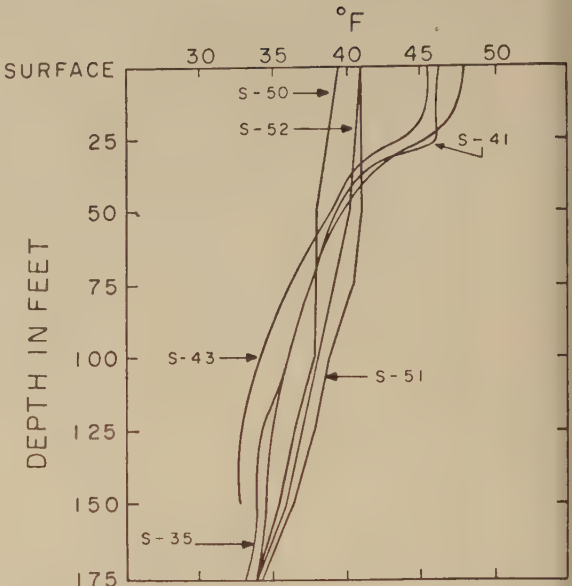

FIG. 3. Comparative bathythermograph traces from Richmond Gulf (Stations 35, 41, and 43) and Hudson Ba (Stations 50, 51, and 52).

ANNOTATED LIST OF SPECIES

The remarks contained in this list are based on the material collected and preserved and on material examined in the field. Only the preserved specimens are listed in the material examined. All of the material will be deposite in the Museum of Comparative Zoology, Cambridge, Massachusetts.

Raja radiata Donovan
Prickly Skate

Material examined: One immature male, 11 mm., and numerous egg cases from station 4

TABLE 2

STATIONS WHERE FISH WERE COLLECTED, WITH PERTINENT DATA, AUGUST AND SEPTEMBER, 1953
HL = handline, GN = gillnet, DN = dipnet, OT = otter trawl

Station No.	Depth in feet	Date	Gear	Bottom	Temp. ° C.	Location
24	0	31 Aug.	DN, GN	Sand	9	56°07.5′ N. 76°04′ W.
24b	12	7 Sept.	OT, GN	Rocky	11	56°07.5′ N. 76°04′ W.
25a	15	31 Aug.	HL	Talus	7	56°07.5′ N. 76°04′ W.
25b	50	9 Sept.	HL	Talus	7	56°07.5′ N. 76°04′ W.
—	0	9 Sept.	DN	Talus	12	56°07.5′ N. 76°04′ W.
26a	40	1 Sept.	OT	Gray-brown mud	1.9	56°07.5′ N. 76°04′ W.
26b	50	2 Sept.	OT	Gray-brown mud	1.9	56°07.5′ N. 76°04′ W.
28c	0	22 Sept.	DN	Sand	3.3	56°07′ N. 76°04′ W.
29c	50	5 Sept.	OT	Gray-brown mud	2.1	56°07′ N. 76°06′ W.
30a	60	2 Sept.	OT	Brown mud and boulders	5.0	56°07′ N. 76°05′ W.
31b	40	5 Sept.	OT	Brown mud	5.7	56°07′ N. 76°04′ W.
38	230	9 Sept.	OT	Brown mud	−0.3	56°17′ N. 76°28′ W.
39a	0	11 Sept.	DN	Sand	5.7	56°17′ N. 76°28′ W.
41c	300	17 Sept.	OT	Red-brown mud	0.0	56°17′ N. 76°27′ W.
42a	350	17 Sept.	OT	Red mud	−0.4	56°17′ N. 76°27′ W.
43a	150	19 Sept.	OT	Brown mud and clay	0.3	56°24′ N. 76°27′ W.
46	90	26 Sept.	OT	Clay	2.2	56°08′ N. 76°31′ W.

This species was well known to the local Indians nd Eskimos who have caught it while fishing for od. They describe it as reaching lengths of bout 18 inches.

Coregonus (*Leucichthys*) *artedi* (*Le Sueur*)
Cisco

Material examined: 3 specimens from station 4b.

Notes: The cisco was to be seen everywhere long the shore line. Although many specimens vere collected, most of them were sacrificed to he frying pan to relieve our otherwise monotonus diet.

Scales from 15 specimens varying in length rom 225 to 246 mm. (fork length) were examhed for annuli. All had what appeared to be vell-defined annuli, and all were in their fourth ummer if the writer properly interpreted the cales. Dymond (1932) also determined that sh of this size from Hudson Bay were of this ge. It is notable that all of the fish that we ollected were in the size range mentioned above.

Gadus m. ogac Richardson
Ogac

This cod was frequently seen. The material xamined was all as previously described by variis authors. We collected only a few specimens o verify the identification.

It was locally abundant. The Eskimos aparently understood the winter movements of his fish, and at this season fished for it through he ice. Mrs. George Papp, wife of the freerader in Richmond Gulf, knew of a few places o catch ogac. That she could catch large quanities was demonstrated to Chamberlin and myelf when, with two visitors, she caught about 00 pounds one morning in the neighborhood of ur station No. 26. The fish were generally arge, running about 18 to 24 inches in length. Chamberlin and I were notoriously unsuccessful n making any such catch ourselves.

The few cod that we did catch had been feeding argely on fish, especially *Ammodytes hexapterus.* One specimen, 23 cm. in length, was in its third ummer (two annuli plus a zone of further rowth), while another, 29 cm. long, was in its ourth summer. Needless to say, this is slow rowth for a codfish.

Boreogadus saida (Lepechin)
Polar Tomcod

Material examined: 18 specimens from stations 26a, 38, 41c, 42a and 46.

Size: Largest specimen 163 mm., smallest specimen 87 mm. Most of the specimens averaged just over 100 mm. fork length.

Notes: The polar cod was obviously a fish of the greater depths in Richmond Gulf. The greatest number of specimens (12) were obtained at our deepest station where the water temperature was significantly below zero.

All of these fish had a few scales in the pectoral fin area. An annulus could not be detected on any of the scales. These fish were smooth to the touch as none of the scales had yet developed the bony tubercles.

Color: Very sketchy color notes in my log state that this fish was a "steely greenish blue above, whitish below."

Gasterosteus aculeatus Linnaeus
Two-spined Stickleback

Material examined: Station 39, 18 specimens, 52 to 67 mm., aver. 56 mm. Tide pool, 17 specimens, 20 to 26 mm., aver. 22 mm.

Notes: The two-spined stickleback was observed anywhere on the gulf that we anchored, collecting in small numbers at the surface in the light of our lanterns. They were usually busily engaged in feeding on the gammarids that were also attracted to the light.

Every tide pool and almost every puddle in the spray zone that was examined had large numbers of young two-spined sticklebacks.

Pungitius pungitius pungitius (Linnaeus)
Ninespine Stickleback

Material examined: Station 39, 1 specimen, 45 mm.

This stickleback was observevd and collected in numbers in James Bay and Hudson Bay proper. It seems likely that it is more abundant in Richmond Gulf than our collections indicate, and that we somehow missed it.

Ammodytes hexapterus Pallas
Sand Launce

Material examined: 49 specimens from stations 24, 25, 26a, 27 and 39. There appeared to be two general size categories, the first averaging 65 mm., the second averaging 93 mm.

Remarks: Our material has been assigned to the species *hexapterus* Pallas on the basis of the vertebral numbers. Five specimens from each of three lots were examined, and all fish had 68 vertebrae except two which had 70 and 71 vertebrae. That this species was to be expected in the Hudson Bay area has been pointed out by Walters (1955).

Notes: From the standpoint at least of the casual observer, the sand launce is the most abundant fish in Richmond Gulf. It may be observed in large schools wherever the bottom is sandy. At night schools of this fish collected in the light cast by our vessel. They have been observed in number at low tide, right at the water's edge, burying themselves in the sand as the waves receded and left them stranded. That this activity was not without its hazard was evidenced by the large numbers of sand launces found dead along the strand line during these periods. Indian children were observed gathering these fish when they were to be found at the water's edge.

The sand launce was eaten by *Myoxocephalus quadricornis* and *Gadus m. ogac.* These two fish frequently had their stomachs and even their mouths filled with this species. Chamberlin examined some seal stomachs at Great Whale River in the winter of 1954 and found their stomachs packed with *Ammodytes.*

Most of our material was collected with a dip-net. Chamberlin dredged one specimen up in the summer of 1950 when he was collecting mollusks in some sandy bottom. The material collected at station 24 consisted of launces that gilled themselves in the hardware cloth liner of our bottom dredge one night when it was hanging over the side at the surface.

Aspidophoroides olriki Lütken
Arctic Sea-poacher

Material examined: Three specimens from stations 38 and 46.

Color: Generally white on sides and underneath. Brown line around snout dorsally, extending obliquely under eye to opercle. Two oblique brown bars extending up from the base of the pectorals more or less outlining a diamond-shaped light brown area on the top of the head. Dorsal milky white or transparent with brown bands (color in rays). Caudal with dark brown basal spot and terminated with a similarly colored band.

Icelus spatula Gilbert and Burke
Two-horned Sculpin

Material examined: 19 specimens from stations 38, 41c, 42a and 46.

Size: Largest female 117 mm., largest male 102 mm. Eight specimens measured from 70 to 75 mm. in length.

Notes: The two-horned sculpin was apparently relatively common in the deeper water. It was usually taken along with *Boreogadus saida, Lumpenus medius,* and *Careproctus reinhardi.*

Color: Body and fins generally transparent-whitish. Fins with spotty horizontal bands of light brown. Area including first three rays of pectoral fin white. Two large brown spots below eyes. Two darker brown "bars" on back at level of soft dorsal. Body sparingly "square" spotted with light chocolate brown. Base of caudal fin with brown patch. The color of the gills and black eyeball obviously due to general transparency of fish. Figure 201, page 360 of Andriashev (1953) is an excellent presentation of the pattern seen in the Richmond Gulf specimens.

Gymnocanthus tricuspis (Reinhardt)
Staghorn Sculpin

Material examined: 13 specimens from stations 26b, 28c, 31b.

Size: Largest female 222 mm., largest male 211 mm. Smallest specimens collected were 38 and 42 mm. in length. Six specimens measured from 81 to 145 mm.

Meristics: D XI, 15–16, A 16–18, P 17–18.

Notes: This is an exceedingly difficult species to deal with. I have referred it to *tricuspis* with misgivings about the separateness of the species *tricuspis* and *galeatus.* The history of sculpin systematics has been one of ever-increasing awareness of the morphological plasticity of this genus and of consequent synonymizing of apparently good species as more material becomes available.

Dunbar and Hildebrand (1952) have already detailed the variation in number of bony tubercles on the head of this species. Some of the specimens examined from Richmond Gulf are exactly as pictured in Andriashev (1954: fig. 208–1, page 373), while others lack figured bony tubercles entirely.

TABLE 3

SUMMARY OF MERISTIC VARIATION IN *Gymnocanthus tricuspis* IN ARCTIC AND SUBARCTIC NORTH AMERICA

	Labrador (Backus, 1957)	Hudson Bay (Vladykov, 1933 and Edwards)	Western arctic America[1]
1st dorsal spines			
Mean	11.2	11.0	10.7
Range	X–XII	X–XII	X–XI
No. of specimens	119	36	55
2nd dorsal rays			
Mean	15.7	15.7	15.2
Range	14–17	15–17	15–17
No. of specimens	118	36	55
Anal rays			
Mean	17.8	17.4	17.3
Range	15–19	17–19	16–18
No. of specimens	119	36	55
Pectoral rays			
Mean	18.7	17.8	18.8
Range	17–21	17–18	17–20
No. of specimens	119	6	55

[1] Based on data presented by Andriashev, 1954, 369, for the Laptev Sea.

Fin ray counts certainly indicate that Richmond Gulf specimens are *tricuspis*.

None of our specimens have a "tricuspid" opercular spine. This spine varies greatly, usually bearing two accessory branches directed dorsally. The proximal branch is often bifid. One specimen had only one dorsally directed branch. The spine of the two smallest specimens was gracefully curved upwards as reported previously by Dunbar and Hildebrand (1952).

The interorbital space also varied greatly in width, varying from 18 to 47 per cent of the horizontal diameter of the eye. Although my sample was small, this variation did not appear to be a matter of sex.

All of the females (four) over 190 mm. had well-developed eggs (diameter about one mm.) in the ovaries.

Color: The following color notes of a small, 31 mm., specimen from station 28c were made: Generally light brown with head back to pectorals a brighter orange brown. Dark chocolate brown bar extending from snout to eye and onto the opercle. Three similarly colored vertical bars on the body, the first under the first section of the dorsal fin, the second under the anterior edge of the second section of the dorsal, and the third just behind the dorsal. A white bar, checkered with black, extended from the base of the pectoral fin to the base of the caudal fin. Belly generally a clear white. Ventral portion of trunk transparent. Pectoral fin yellowish at base, white posteriorly. Four bright reddish-brown bands of color across the pectoral, the color principally in the fin rays. First part of dorsal banded from top to bottom with a relatively broad reddish brown band, a white band, another reddish brown band and a last white band. As in the pectoral, this color was mostly in the fin rays themselves. Second part of dorsal (soft rays) with three such bands of reddish brown, with less white color in between. Pelvic and anal white. Caudal with three vertical bands of reddish brown.

Myoxocephalus quadricornis (Linnaeus)
Four-horned Sculpin

Material examined: 7 specimens from station 24. Two specimens were also available from Fort George on the east coast of James Bay.

Size: Largest male 278 mm., largest female 263 mm.

Notes: This handsome sculpin is always present in those shallow water areas where *Mytilus* and fucoid algae abound. It was frequently taken in numbers in our shallow gillnet sets and never in otter trawl sets in depths greater than 40 feet. Richmond Gulf four-horned sculpins are, as elsewhere, restricted to shallow waters of low salinity.

TABLE 4

SUMMARY OF MERISTIC VARIATION IN *M. quadricornis* IN ARCIC AND SUBARCTIC NORTH AMERICA

	Labrador (Backus, 1957)	Hudson Bay (Vladykov, 1933 and Edwards)	Western arctic America (Walters, 1955)
1st dorsal spine			
Mean	7.9	7.9	7.9
Range	VII–IX	VI–X	VI–X
No. of specimens	9	134	116
2nd dorsal rays			
Mean	14.7	14.6	13.8
Range	14–16	13–17	11–15
No. of specimens	9	134	114
Anal rays			
Mean	14.4	14.7	13.6
Range	14–16	13–17	12–16
No. of specimens	9	134	111
Pectoral rays			
Mean	15.5	15.6	16.3
Range	15–16	15–17	15–18
No. of specimens	9	28	98

The males and females collected in September were nearly ripe. Their stomachs almost invariably contained gammarids. A few specimens were feeding on sand launces.

Color: This sculpin is most distinctly colored, especially during the breeding season. The following color notes were made from several male specimens collected early in September: General color above brown to dark greenish brown with a mottling of light cream or very light brown. Occasional specimens are very light green-brown above. Rays of all fins cream to light brown, the tissue between a dull black. Some specimens had the rays of the pelvic fin pink, in others the pelvic fin rays and the tips of the pectoral rays were yellow to yellow-orange. Bony "combs" on head dirty white. Belly and sides bright canary yellow. Ventral part of gill cover frequently bright pink. Membranous portion of jaw rosy. Ventral portion of trunk white.

Myoxocephalus scorpius (Linnaeus)
Sea Scorpion

Material examined: 4 specimens from stations 24 and 30a.

Meristics: D IX-X, 15–16, A 13–15, P 16–17.

Notes: This species was relatively common in shallow-water areas with sandy and bare-rock bottoms where we caught many with handlines in the summer of 1950. Only one specimen was taken in relatively deep water in 1953 (station 30a). One was taken in a gillnet in 7 feet of water. During the summer months at least *scorpius* may be frequently found in low salinity, shallow water.

TABLE 5

Summary of Meristic Variation in *M. scorpius* in Arctic and Subarctic North America

	Labrador (Backus, 1957)	Hudson Bay (Vladykov, 1933 and Edwards)	Western arctic America (Walters, 1955)
1st dorsal spines			
Mean	10.0	10.3	10.4
Range	IX–XI	IX–XII	IX–XI
No. of specimens	241	49	29
2nd dorsal rays			
Mean	16.9	16.5	15.1
Range	15–19	15–18	14–16
No. of specimens	241	49	27
Anal rays			
Mean	13.7	13.2	11.8
Range	12–16	12–15	11–14
No. of specimens	241	49	25
Pectoral rays			
Mean		17.3	17.4
Range		16–18	16–18
No. of specimens		21	29

Specimens collected in September were approaching ripeness; the eggs of one female exceeded one millimeter in diameter. Their stomachs contained the remains of gammarids, isopods, and fish.

Eumicrotremus spinosus (Muller)
Spiny Lumpfish

Notes: One small specimen, about 10 mm., was taken by dipnet at night on station 39a. We put it in a beaker with some gammarids to watch it for a while. The gammarids disposed of all but a few remnants in just a few minutes while we were occupied dipnetting. Fortunately, there was no doubt as to its identity.

Careproctus reinhardi (Kroyer)
Jellyfish

Material examined: 3 specimens from stations 29c and 38, measuring 40, 60 and 68 mm.

Notes: Unless one has been previously prepared, this fish presents an unbelievable and shocking first appearance. When our first specimen dropped on the deck, we thought it was a partially digested fish from the stomach of a cod. On closer examination, it proved quite lively, and we kept it in the aquarium for a day, examining it with great interest.

This tadpole-shaped fish is surrounded by a clear, gelatinous layer that is particularly thick over the trunk. Most of the dorsal and anal fins are included in this sheath forward. The pectorals and caudal are free. The various organs and major nerves and blood vessels were easily traced in our largest specimen (68 mm. long). The only color in the fish was the normal color of the internal organs, black eyeballs, red muscles, brownish liver, etc.

The local Eskimos and Indians are familiar with the species and say that it reaches lengths of up to 6 inches or more. Eskimo children play a game with it (described by two creditable witnesses). It is placed on the bare arm to which it apparently fastens with its sucker. The child then runs around with it, and the other children attempt to snatch it away.

It is reported caught in fair numbers when fishing for cod through the ice in winter.

Our material has been referred to *reinhardi* (Kroyer). Until large collections of fish of this genus from arctic and boreal areas are available, the status of many of the species in the genus will be questionable. The Richmond Gulf specimens had about 52 dorsal rays, 48 anal rays, and 30 pectoral rays. The eye is about 20 per cent of head length and slightly larger than the ventral sucker. The pectoral fin was not obviously notched. The rays of the lower lobe were separated distally and barely extended beyond the anus. The anus was situated well forward, close to the ventral sucker. The ventral sucker was squarish, not triangular, and situated well forward under the eye. There were no "prickles" on the body, such as those reported by Backus (1957) for *C. longipinnis* Burke from Labrador. The extent descriptions of *longipinnis* are sufficiently broad, however, to include our material "prickles" or no, as are those of *C. reinhardi* (Kroyer).

Lycodes reticulatus Reinhardt
Reticulated Eelpout

Material examined: 2 specimens from stations 26a and 41c, measuring 95 and 105 mm.

Notes: Each of these specimens had scales with a few circuli, no annuli.

Color: General body color a warm orange with a pink overtone. Dorsal fin dark brown barred, the bars extending down onto body and breaking up into irregular vertical lines. One fish had 7 such bars, the other 10. Andriashev's (1954) figure 156, page 285, of *L. rossi* shows a similar pattern, especially on the head. Figure 158, page 287 (*op. cit.*) of *L. reticulatus* lacks the reticulations on the head that were so obvious on our younger specimens.

Lumpenus medius Reinhardt
Stout Eelblenny

Material examined: 10 specimens from stations 26a, 29c, 30a, 32 and 38.

Size: Largest specimen 133 mm., smallest 70 mm.

Notes: This small fish was captured frequently enough in our relatively large mesh otter trawl to suggest that it may have been quite common.

It is easily distinguished from *fabricii* by the manner in which both the dorsal and anal fins are joined to the caudal. *L. fabricii* does not have its dorsal and anal fins so joined with the caudal; rather they end just short of the caudal.

Color: Body generally pink-transparent. Spotted or mottled with light brown. Irregular black spot behind eyes. Caudal and dorsal faintly banded with brown. Underneath head and belly milky white.

Lumpenus fabricii (Cuvier and Valenciennes)
Slender Eelblenny

Material examined: 4 specimens from station 38, measuring 163, 163, 170 and 192 mm.

Notes: Despite their length, these are very slender fishes. It is probable that they are much commoner than the data indicate, since they could easily escape through the meshes of the trawl.

DISCUSSION

Three species of fish are added to the Hudson Bay list in this report—*Ammodytes hexapterus, Lumpenus medius,* and *Careproctus reinhardi.* None of this material does any violence to the generally accepted opinion that Hudson Bay fishes re-entered the area from Atlantic refugia following the Wisconsin glaciation.

The presence of *A. hexapterus* in Hudson Bay was predicted by Walters. This euryhaline species could easily have made its way from the western Canadian arctic into Hudson Bay at almost any time. While the vertebral counts do indicate a western origin for this population, it must be remembered that vertebral numbers are subject to modification by the environmental temperatures and that the vertebral numbers of our material may merely be the result of temperature differences between Hudson Bay and the rest of the eastern Canadian arctic (where *Ammodytes dubius* occurs).

The meristic data available for *G. tricuspis, M. quadricornis,* and *M. scorpius* are presented in tables 3, 4, and 5. It is to be regretted that little further data are available. *M. quadricornis* and *M. scorpius* from Hudson Bay are similar meristically to fish from Labrador, and are quite different from the fish of western arctic America. In general these remarks apply as well to the *G. tricuspis* population from Hudson Bay. In this case the pectoral fin ray count appears anomalous but it is based on only six specimens.

There is a suggestion of trends in these data that someone in the future with access to good collections of *Myoxocephalus* from the arctic should look into, with respect to the interrelationships of populations, the relation of meristics to water temperatures, and with respect to the manner in which the numbers of rays vary in one fin with respect to another. It will be observed in the *Myoxocephalus* meristic data for both species that the total counts of rays tend to be greater for Labrador individuals than for Hudson Bay specimens, and that Labrador and Hudson Bay counts are generally higher than are those of western arctic American material. There is a suggestion that the pectoral rays counts vary in the opposite direction.

The fauna of Hudson Bay, as collected in Richmond Gulf and elsewhere, quite clearly appears to be derived from the Atlantic side. The present writer agrees completely with the remarks on this subject expressed by Walters (1953: 353).

The Richmond Gulf area merits further study of all groups. It is especially interesting from the hydrographic point of view. It is, at least, a convenient place to work in, having depths in excess of 70 fathoms and being relatively protected from the otherwise extremely harsh weather conditions that one experiences on Hudson Bay proper. The fauna includes many species generally considered as indicators of true arctic conditions as well as quite typical subarctic and even boreal species. It is apparent that there are often limitations of the arctic environment besides sub-zero temperatures, and these problems could be profitably pursued in Richmond Gulf.

The following species were observed and/or collected in the shallow, low salinity water of Richmond Gulf:

Gadus m. ogac
Myoxocephalus quadricornis
Myoxocephalus scorpius
Ammodytes hexapterus
Gasterosteus aculeatus
Pungitius pungitius
Mallotus villosus
Eumicrotremus spinosus
Salvelinus alpinus
Coregonus (Leucichthys) artedi

The following marine species were collected in water above 0° C. in salinities varying from 22 to 26 parts per thousand.

Raja radiata
Gadus m. ogac
Boreogadus saida
Lumpenus fabricii
Lumpenus medius
Lycodes reticulatus
Gymnocanthus tricuspis
Icelus spatula
Myoxocephalus scorpius
Aspidophoroides olriki
Careproctus reinhardi

The following species were collected in water near or below 0° C. and in salinities of 27 parts per thousand or greater.

Boreogadus saida
Icelus spatula
Careproctus reinhardi

REFERENCES

ANDRIASHEV, A. P. 1954. Fishes of the northern seas of the SSSR. Moscow and Leningrad, Acad. Sci., SSSR.

BACKUS, R. H. 1957. The fishes of Labrador. *Bull. Amer. Mus. Nat. Hist.* **113**: art. 4.

DUNBAR, M. J., and H. H. HILDEBRAND. 1952. Contribution to the study of the fishes of Ungava Bay. *Jour. Fish. Res. Board Canada* **9** (2).

DYMOND, J. R. 1933. Biological and oceanographic conditions in Hudson Bay. 8. The coregonine fishes of Hudson and James Bays. *Contrib. Canadian Biol. Fish.*, N. S. **8** (1).

VLADYKOV, V. D. 1933. Biological and oceanographic conditions in Hudson Bay. 9. Fishes from the Hudson Bay region (except the Coregonidae). *Contrib. Canadian Biol. Fish.*, N. S. **8** (2).

WALTERS, V. 1955. Fishes of western arctic America and eastern arctic Siberia. Taxonomy and zoogeography. *Bull. Amer. Mus. Nat. Hist.* **106**: art. 5.

Contribution No. 1110

Geochimica et Cosmochimica Acta, 1961, Vol. 21, pp. 182 to 198. Pergamon Press Ltd. Printed in Northern Ireland

The dissolution of silica from diatom walls*

JOYCE C. LEWIN†
Woods Hole Oceanographic Institution, Woods Hole, Massachusetts

(*Received* 18 *July*, 1960)

Abstract—Silica walls of diatoms, prepared by digesting cultured cells with nitric acid, dissolved more rapidly in media of higher pH or at higher temperatures. Most of the studies reported here were carried out in Tris buffer at pH 9·0–9·3 and at 19°C. The rate of dissolution under these conditions was slightly less than in sea water at pH 8·0, since NaCl accelerates the dissolution of silica. The silica from cleaned diatom walls dissolved in Tris buffer until, after 3–4 weeks, the solution had become saturated at 40–50 mg Si/l. (85–110 mg SiO_2/l.). The rate of solution decreased with time, probably due to the presence of silica in different states of hydration. Living cells suspended in buffer in darkness remained viable for many weeks during which time very little silicon dissolved from their walls. However, every treatment which killed the cells (heat, protein-denaturing agents, organic solvents, breakage) resulted in an increase in the rate of silica dissolution, although this rate was never as great as from acid-cleaned walls.

Experiments with EDTA indicated that a cationic inorganic factor was retarding silica dissolution from killed cells. Pretreatment of cleaned silica walls with salts of Al, Be, Fe, Ga, Gd, Sc, Ti, Y and Yb at pH values between 2·0 and 9·0, and with Mn at pH values between 4·0 and 11·0, had various effects on the subsequent rate of dissolution of the silica at pH 9·0. At certain pH values each of these elements can evidently combine superficially with amorphous silica and thereby retard its rate of dissolution. Pretreatment of cleaned silica walls with salts of La, Mo, Cr, at pH values between 2·0 and 9·0, and with Ca and Mg at pH values between 4·0 and 11·0, had no effect on their subsequent dissolution at pH 9·0. Al, Be, Fe, Ga, Gd and Y were all capable of combining with silica walls at pH 8·0, which is the pH of sea water, and thereby retarding their subsequent dissolution. A single determination showed that the walls adsorbed Al equivalent to 1 per cent of their weight. In retarding dissolution of the silica, Al was as effective on killed, but intact, cells as on acid-cleaned walls.

The silica of nine samples of untreated diatomaceous earth of fresh-water and marine origins, ranging in age from Upper Cretaceous through Pliocene, was essentially insoluble under these conditions. Digestion in strong nitric acid freed only a small fraction of the silica for dissolution. The factor which retarded the initial dissolution of silica from natural marine phytoplankton could be removed completely by pretreating the cells with a chelation mixture of EDTA and oxalate. DHEG, which is reported to complex certain cations such as Fe, but to have no effect on Ca or Mg, was equally effective.

It can be concluded that certain adsorbed inorganic cations decrease the rate of dissolution of diatomaceous silica. In living diatom cells there may be an additional mechanism for stabilizing silica walls.

INTRODUCTION

NATURAL waters, both fresh and marine, are generally far from saturated with respect to silicic acid, i.e. more could be dissolved than is normally present in solution (COOPER, 1952; BRUEVICH, 1953; and KRAUSKOPF, 1956). The equilibrium in nature would therefore be in the direction of silica dissolution.

The amorphous silica structures in diatoms, radiolarians, sponges and silicoflagellates have been deposited by vital activity, and appear to be prevented from dissolving in their aqueous habitat while intact and associated with the living organisms. Under certain conditions, the siliceous structures remaining after the death of such organisms also appear to be resistant to solution, since silica deposits of biological origin are sometimes found in vast quantity in both fresh-water and

---

* Contribution No. 1110 from Woods Hole Oceanographic Institution, Woods Hole, Massachusetts. These studies were aided by a contract between the Office of Naval Research, Department of the Navy, and the Woods Hole Oceanographic Institution, NR–104–392. Acknowledgment is made to Dr. G. DALLAS HANNA, California Academy of Sciences, and to the Great Lakes Carbon Corp. for supplying samples of fossil diatoms.

† Present address: Division of Marine Biology, Scripps Institution of Oceanography, La Jolla, California.

marine environments (see CONGER, 1942; BRAMLETTE, 1946; and RIEDEL, 1959). COOPER (1952) has postulated that the surfaces of the siliceous skeletons may be protected against solution by some sort of an organic skin, possibly only a few molecules in thickness. ILER (1955) has likewise speculated that: (a) the magnesium, iron, aluminium, or other polyvalent cations in natural waters may produce a coating of insoluble silicates and thus prevent the enclosed silica from dissolving; or alternatively (b) organic complexes on the surface of the silica may prevent dissolution.

The present paper deals with studies on dissolution of the silica frustules of diatoms, in an attempt to adduce evidence for the presence of such a protective coating and to investigate its nature. In particular, the relative effects of various inorganic cations as protective agents have been studied. In principle, the method consisted of pretreating living or killed cells, or cleaned frustules, in various ways, and then allowing them to dissolve under controlled conditions over a period of days. The rate of solution was determined by sampling at intervals, removing the cells by centrifugation, and determining colorimetrically the silica in the supernatant solution.

MATERIALS AND METHODS

In order to obtain a supply of silica walls of uniform size and known composition, cells of *Navicula pelliculosa* (Bréb.) Hilse were grown in an inorganic medium containing (g/l.): K_2HPO_4, 0·2; $MgSO_4 0{\cdot}7H_2O$, 0·2; $Ca(NO_3)_2{\cdot}4H_2O$, 1·0, dissolved in glass-distilled water. Trace elements were added as follows: 0·1 p.p.m. each B, Co, Cu, Mn, Mo; 0·3 p.p.m. Zn; 0·5 p.p.m. Fe. Silicate was added as $Na_2SiO_3{\cdot}9H_2O$ to give a soluble silicon concentration of 10 p.p.m.

Two-litre Pyrex Erlenmeyer flasks containing 1·5 l. of medium were sterilized by autoclaving and inoculated under sterile conditions. The cultures were constantly aerated by filtered air and illuminated at 3000 lux, at 20°C for 10 days. At the end of the growth period, the cells were allowed to settle and were concentrated to approximately 40 ml by decanting and removal of the supernatant medium. The cells harvested from 1·5 l. of culture provided sufficient siliceous frustules for one experimental run. The pH of the suspension was adjusted to 2·5–3·0 to dissolve precipitated phosphates, and the cells were immediately washed by repeated centrifuging and resuspending in distilled water. They were then concentrated to a suitable volume, and dispensed into small test tubes, 2 ml of cell suspension per tube, to give the same concentration of diatom silica in each tube of a given experiment. This varied between 2 and 3 mg SiO_2 from one experiment to another.

When "cleaned" frustules were required, 2 ml concentrated nitric acid were added to each tube and the mixture heated at 100°C for 15 min to decompose the organic matter. The frustules were freed from the acid by diluting with water and centrifuging, followed by three washings with distilled water.

In each experiment the cells or frustules in the small test tubes were first subjected to various pretreatments, with suitable control samples retained as required. The chemical agents used were removed by washing. The final cell or frustule preparation was suspended in 20 ml of 0·01 M Tris buffer, at pH 9·0–9·3, in polyethylene bottles (125 ml). Polyethylene centre wells containing 10% KOH were inserted into the containers to remove atmospheric CO_2 and thereby to aid in maintaining the pH of the suspension throughout the experimental period. The polyethylene bottles were then capped and stored at 20°C. When sea water was employed as the dissolving medium, centre wells were not used.

Although it would have been desirable to shake the suspensions during the time while the walls were dissolving, this was not feasible because of the large number of bottles involved and because of the presence of the centre wells containing KOH. All bottles were therefore left at rest during the dissolution period.

In order to follow the dissolution of the silica, samples were removed at intervals and the soluble silicic acid appearing in the medium was determined colorimetrically by the use of ammonium molybdate and hydroquinone (LEWIN, 1954).

Soluble salts of the various elements tested were prepared in the following ways: aluminium metal powder, iron wire, gallium metal, Sc_2O_3, Yb_2O_3, Y_2O_3 or Gd_2O_3 dissolved in hot concentrated hydrochloric acid; TiO_2 dissolved in concentrated sulphuric acid; $FeSO_4 \cdot 7H_2O$, La acetate, $(NH_4)_6Mo_7O_{24} \cdot 4H_2O$, $Cr_2K_2(SO_4)_4$, $Be(NO_3)_2 \cdot 3H_2O$, $MnCl_2 \cdot 4H_2O$, $Ca(NO_3)_2 \cdot 4H_2O$, and $MgSO_4 \cdot 7H_2O$ dissolved directly in the acetate-Tris buffer. Tris (hydroxymethyl) aminomethane buffer was obtained from the Sigma Chemical Company. EDTA or Versene (disodium salt of ethylenediaminetetra-acetic acid) and DHEG or Versene Fe–3 Specific (N:N′-di(2-hydroxyethyl) glycine) were obtained from Versenes, Incorporated, Framingham, Mass.

RESULTS

1. *Preliminary*

(a) *Effect of pH.* In preliminary experiments, acid-cleaned silica walls were suspended in Tris buffer (0·01 M) adjusted with HCl to pH 3, 6, 7, 8 and 9, and kept at 20°C. In media of higher pH, the silica frustules dissolved more rapidly (Fig. 1). Similar observations were made by JØRGENSEN (1955a, 1957). The rate at pH 9 was found to be most convenient for sampling purposes, and 0·01 M Tris buffer adjusted to pH 9·0–9·3 was employed in screw-capped polyethylene bottles for most of the experiments reported in this paper. By the use of centre wells containing KOH (see Methods) the pH was maintained at a constant level for many weeks (or it decreased in some cases to pH 8·6 if the bottles were opened several times). In those cases where sea water at pH 8 was employed for dissolution of the silica walls, no KOH-containing tube was inserted since it was found to cause the pH of the sea water to rise to pH 9.

(b) *Effect of temperature.* In preliminary experiments, silica walls were suspended in 0·01 M Tris buffer and kept at different temperatures. The rates of dissolution at 10°C, 15°C, 21°C, and 35°C are shown in Fig. 2. For the following experiments reported in this paper, the polyethylene containers were stored in a dark cupboard at about 19°C.

(c) *The rate of dissolution of silica walls in Tris buffer compared with that of sea water.* Silica walls dissolved more rapidly in sea water (pH 8·0) than in Tris buffer adjusted to the same pH (see Fig. 3). The lower rate in Tris buffer was not due to an inhibitory effect of the buffer, since walls dissolved in sea water *plus* Tris at the same rate as in sea water alone. The accelerated dissolution in sea water is attributable to NaCl (DIÉNERT and WANDENBULCKE, 1923). Silica walls in 2·5% NaCl and Tris at pH 8·2 dissolved at the same rate as in sea water (Fig. 3). Fluoride at concentrations of 1, 10 and 100 p.p.m. in Tris buffer at pH 8·0 was found to have no appreciable effect on the rate of dissolution of silica walls.

(*d*) *Removal of organic matter.* For the microscopic examination of diatom walls it is customary to "clean" the frustules, i.e. to free them of organic matter, by heating them with concentrated nitric acid. There was some question that the use of such strong acid might dehydrate or change the structure of the silica in the walls, thereby altering its subsequent dissolution. However, it was found that walls cleaned by heating at 100°C with 10% (by volume) nitric acid for 15 min dissolved in buffer at exactly the same rate as those cleaned with the concentrated acid. Lower concentrations were ineffective in destroying all organic cellular material.

1

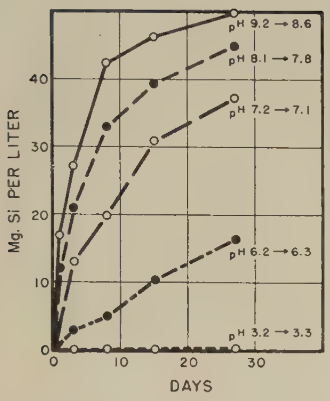

2

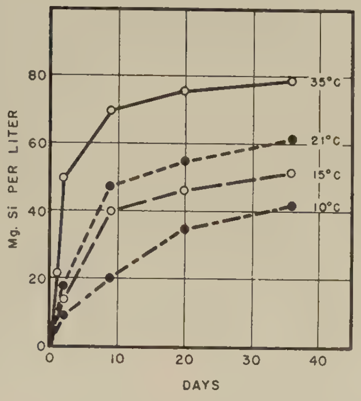

3

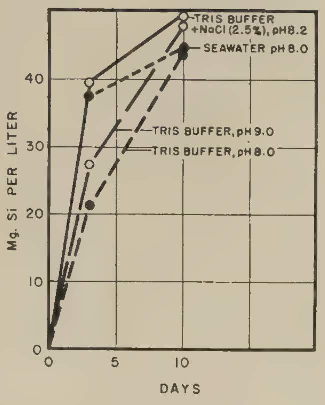

4

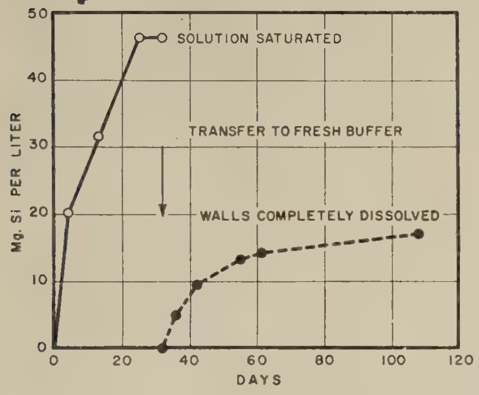

5

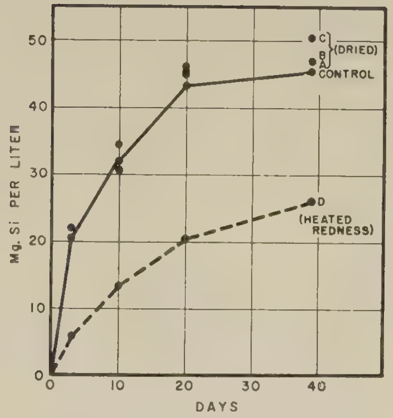

Fig. 1. Dissolution of silica from acid-cleaned valves at 19°C in 0·01 M Tris buffer, initial pH adjusted with HCl, final pH also shown.

Fig. 2. Dissolution of silica from acid-cleaned valves in 0·01 M Tris buffer, pH 9·0–9·3, at 10, 15, 21 and 35°C.

Fig. 3. Dissolution of silica from acid-cleaned valves in Tris buffer, in sea water, and in Tris buffer + NaCl, at 19°C.

Fig. 4. Dissolution of silica from acid-cleaned valves in 0·01 M Tris buffer, pH 9·0–9·3, at 19°C, showing decrease in rate with time.

Fig. 5. Dissolution of silica in 0·01 M Tris buffer, pH 9·0–9·3, at 19°C, from acid-cleaned valves: (a) dried in air, (b) dried in air and then in a vacuum desiccator over H_2SO_4 for 20 hr, (c) dried at 45°C for 23 hours, and (d) heated to redness for 3 min in a platinum crucible. Control valves not dried.

(e) *Change of solution rate with time.* The number of silica walls employed in each experiment was usually in excess of that required to saturate the medium with dissolved silicic acid. In most experiments the levelling of the dissolution curve between 40 and 50 mg Si/l. was therefore due to the attainment of the solubility equilibrium rather than to the complete dissolution of all the silica from the walls. To illustrate this, in one experiment the silica walls remaining after equilibrium had been reached were collected by centrifugation, resuspended in fresh buffer, and made up to the same volume as before. Silica from the walls then continued to pass into solution until they completely dissolved (see Fig. 4). From the shape of the curve it is apparent that the rate of solution of the silica in water decreases with time (JØRGENSEN, 1955a, 1957), presumably indicating the existence of silica in different states of hydration.

(f) *Dissolution of silica from dried silica walls.* In the experiments reported in this paper the silica walls were never allowed to dry. Since for some purposes it might be convenient to work with material stored in the dry state, a comparison was made of the rates of dissolution of silica from walls (a) dried in air, (b) dried in air and then in a vacuum desiccator over H_2SO_4 for 20 hr, (c) dried at 45°C for 23 hr and (d) heated to redness for 3 min in a platinum crucible. It was found that preparations (a), (b) and (c) dissolved at the same rate as wet walls, whereas the rate of dissolution of (d) was appreciably reduced (Fig. 5).

2. *Dissolution of silica from intact cells and from cleaned frustules*

When living cells were suspended in Tris buffer at pH 9·0 in darkness, silica went into solution only very slowly, and reached approximately 2 mg Si/l. after 50 days. After 30 days in the dark, suspensions streaked out on agar media and illuminated showed a high proportion of viable cells. The silica from heat-killed cells dissolved more rapidly, and reached 5–30 mg/l. in different experiments at the end of 50 days. Cleaned silica walls dissolved still more rapidly in Tris buffer at pH 9·0, until after 3–4 weeks the solution had reached saturation at 40–50 mg Si/l. (85–110 mg SiO_2/l.) (Fig. 6).

3. *Experiments to determine whether the agent retarding dissolution is of organic nature*

Since the silica of the walls dissolved more rapidly after the cells had been digested with nitric acid, it was considered possible that some organic component of the whole cells might be protecting the silica walls from dissolving. The following experiments to test this hypothesis were carried out.

Cells were treated with the following protein-denaturing or -solubilizing agents: (1) 0·5% pepsin, pH 2·0, 30°C, for 14 hr; (2) 0·5% trypsin, pH 7·9, 30°C, for 24 hr; (3) 40% urea, pH 3·0, for 3 days; (4) a combination of enzyme and urea treatments; (5) 5% bile salts, pH 6·4, for 3 days. In another experiment, cells were extracted overnight with the following organic solvents: ethanol, acetone, diethyl ether, methanol:benzene (1:3), glacial acetic acid and pyridine. None of these treatments affected the subsequent rate of dissolution of the silica walls, which in all cases parallelled that of heat-killed cells.

The possibility was next considered that a protective coat might cover only the "outer" surface of the valves, and that, if the cells were broken open, the "inner" surfaces of the silica walls might become exposed to rapid dissolution. Cells were ruptured by first compressing them to 28,000 lb/in^2 in a pressure chamber (French pressure cell, manufactured by the American Instrument Co.), and then extruding them through a small orifice. Although some cells remained apparently intact after this treatment, none of them proved viable. Most were broken open, and free silica walls could be seen floating among cellular debris in the suspension. Nevertheless, their rate of dissolution was unchanged, again parallelling that of heat-killed cells.

6

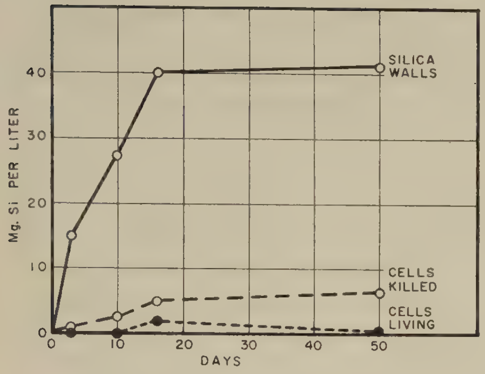

8

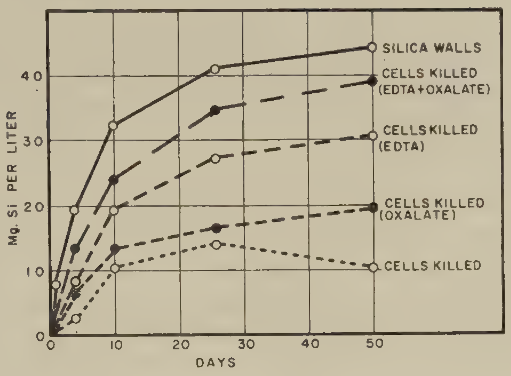

7

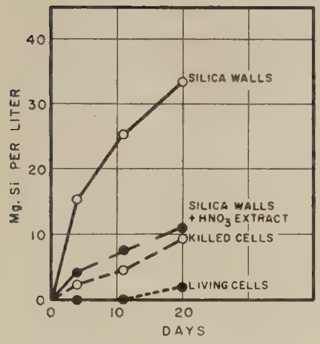

9

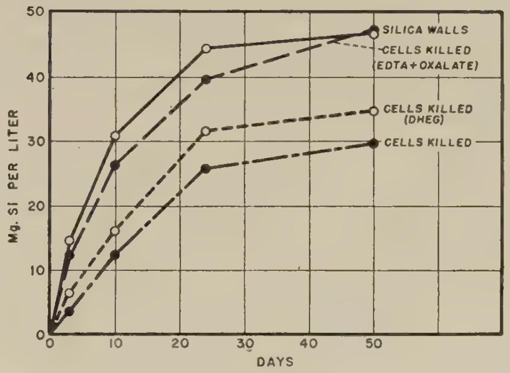

Fig. 6. Dissolution of silica in 0·01 M Tris buffer, pH 9·0–9·3, at 19°C, from whole cells (living and heat-killed), and from acid-cleaned valves.

Fig. 7. Dissolution of silica in 0·01 M Tris buffer, pH 9·0–9·3, at 19°C, from whole cells (living and heat-killed), from acid-cleaned valves, and from acid-cleaned valves subsequently treated with a nitric acid cell extract.

Fig. 8. Dissolution of silica in 0·01 M Tris buffer, pH 9·0–9·3, at 19°C, from silica valves, from heat-killed cells, and from heat-killed cells extracted with oxalate, EDTA, or EDTA + oxalate.

Fig. 9. Dissolution of silica in 0·01 M Tris buffer, pH 9·0–9·3, at 19°C, from silica valves, from heat-killed cells, and from heat-killed cells extracted with DHEG or with EDTA + oxalate.

It was concluded that whatever protective mechanism was responsible for retarding silica dissolution completely coated each valve of the frustule.

4. *Experiments to determine whether the agent retarding dissolution is of inorganic nature*

(a) *Tests with the nitric acid extract.* The nitric acid extract, obtained when the cells were cleaned, was evaporated to dryness, redissolved in water, and adjusted to pH 7·1 with NaOH. Cleaned silica walls, treated with this extract for 30 min and then thoroughly washed, subsequently dissolved at the same rate as heat-killed whole cells, i.e. considerably more slowly than the cleaned silica walls (see Fig. 7). Since all organic matter had presumably been destroyed by oxidation, this experiment implicated an inorganic element or elements, which could be removed from the cells by treatment with nitric acid, and which could be reassociated with the silica walls to reduce their rate of dissolution.

(b) *Effect of treating heat-killed cells with chelating agents, etc.* Attempts were then made to remove the inorganic factor by some means other than digestion with nitric acid.

Widely differing ions, such as Fe and Ca, could probably be removed from silica walls by EDTA and oxalate. Another chelating agent, N:N′- di(2-hydroxyethyl) glycine (DHEG or "Versene Fe-3 Specific") is said to complex Fe, Cu, Ni, Co, and Mn, but not Ca or Mg (Chaberek *et al.*, 1953). On the supposition that the factor was a polyvalent cation, cells were treated with EDTA, citrate, oxalate, EDTA *plus* citrate, EDTA *plus* oxalate and, in another experiment, with DHEG, all at 0·01 M adjusted to pH 6·8. They were then washed and suspended as usual in Tris buffer at pH 9·0. EDTA was more effective in accelerating the subsequent rate of dissolution of the silica than was either citrate or oxalate alone; EDTA *plus* citrate or oxalate was even more effective, although the rate of dissolution of the silica did not quite reach that of the acid-cleaned frustules (Fig. 8). DHEG was only slightly effective (Fig. 9).

5. *Rate of dissolution of cleaned silica walls after treatment with various ions*

It thus appeared that some cations, for which EDTA has a chelation affinity, either retarded the dissolution of the silica or changed its solubility by coating the frustules. In order to determine what ions could have this effect, cleaned silica walls were treated for 3 hr with salts of the following metals: divalent Ca, Mg, and Mn; trivalent Al, Be, Cr, Fe, Ga, Gd, La, Sc, Y, Yb; Ti^{4+} and Mo^{6+}. The divalent ions were used at a concentration of 0·01 M at pH values between 4·0 and 11·0 in 0·1 M acetate *plus* 0·01 M Tris buffer. All other salts were used at a concentration of 0·0037 M in the same buffer adjusted to pH values between 2·0 and 9·0. In those cases where an insoluble precipitate formed, this was removed by centrifugation, and only the supernatant was used for treating the silica frustules. At the end of the 3-hr treatment period, the frustules were washed thoroughly and suspended in Tris buffer at pH 9·0–9·3. Treatment of the silica walls with the buffer mixture alone at various pH values had no effect on the subsequent rate of dissolution of the silica walls.

La, Mo, Cr, Ca and Mg pretreatments were without significant effect on the subsequent rate of dissolution of the silica walls. The other ions retarded the dissolution of the silica to various degrees as illustrated in Figs. 10–19.

Since the results obtained with Al at 0·0037 M were the most striking, Al was also tested at concentrations of 0·00037 M and 0·037 M, with similar results (see Fig. 12). Above pH 8·0, Al in solution is presumably present in appreciable amounts as aluminate ion (Hutchinson, 1957), which in these experiments appeared to be as effective as the Al^{3+} ion in retarding the dissolution of the silica walls.

Freshly prepared $FeCl_3$ was only effective below pH 6, since above this pH all the Fe^{3+} ion had evidently been precipitated as $Fe(OH)_3$ before addition of the supernatant to the silica walls. Freshly prepared $FeSO_4 \cdot 7H_2O$ was most effective between pH 6 and pH 8·5, apparently due to slow atmospheric oxidation of the ferrous ion to the ferric state. At those pH values where Fe was effective, the silica walls assumed a rusty colour, which was not removed by washing. Above pH 8·5 neither source of Fe ions was effective in preventing the subsequent dissolution of silica walls. In an attempt to render the adsorption of iron more effective, an acid solution of $FeCl_3$ was added to a suspension of silica walls in acetate–Tris buffer. The final Fe concentration was 0·004 M and the pH was brought up to 5·2. After 3 hr in this medium, the cells were washed and resuspended in Tris buffer at pH 9. This pretreatment had no appreciable effect in decreasing the rate of dissolution of

10

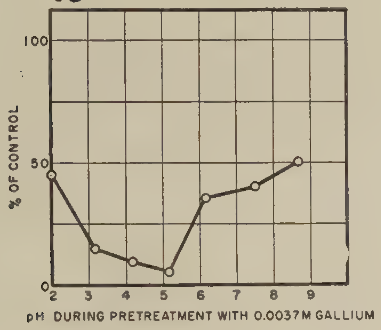

11

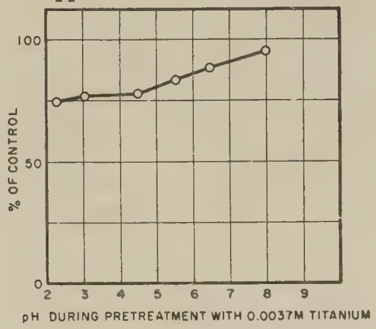

12

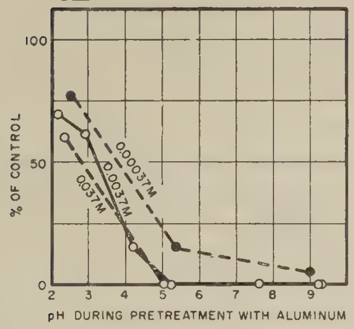

13

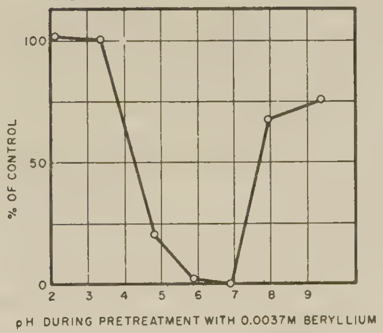

14

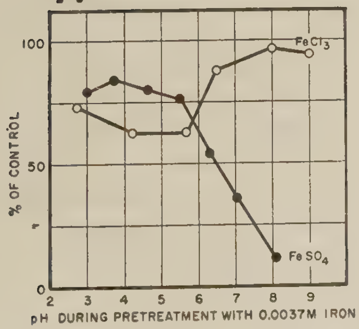

15

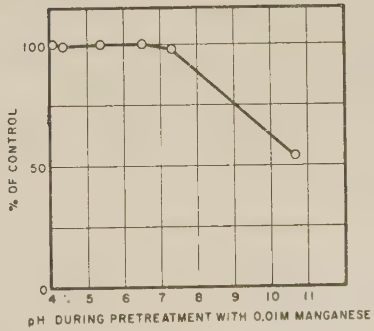

Figs. 10–19. Silicon in solution (per cent of the control) at the end of 10 days in Tris buffer, pH 9·0–9·3, at 19°C, plotted against the pH values at which acid-cleaned silica valves were pretreated for 3 hr with solutions of metal salts as indicated.

silica walls beyond that shown for $FeCl_3$ in Fig. 14. After 10 days the amount of silica which had gone into solution was 56 per cent of the control.

Aluminium, beryllium, gadolinium, gallium, iron and yttrium were of especial interest in that they were able to react with silica walls in the range of pH 8·0, which is the pH of sea water.

6. *A quantitative determination of* Al *combined with silica*

It is logical to assume that the reaction involved an adsorption of these cations on the cleaned silica surfaces. In order to test this assumption the following experiment with Al was carried out.

A known amount of acid-cleaned valves of *Navicula pelliculosa* was treated with a large excess of a clear solution of 0·0037 M Al in acetate–Tris buffer at pH 5·25 for 17 hr. At the end of this time the valves were thoroughly washed, and a quantitative analysis for adsorbed Al was carried out on the valves by D. P. KHARKAR, Scripps Institution of Oceanography, La Jolla,California, employing a micromethod devised by W. SACKETT. It was found that 5·5 mg of silica valves had adsorbed 57·4 μg of Al, equivalent to 1·04 per cent by weight.

7. *Rate of dissolution of silica from intact cells after pretreatment with aluminium*

Since Al ions could combine with cleaned silica walls at various pH values and retard their subsequent rate of dissolution in Tris buffer at pH 9·0, it was of interest to determine whether the silica surfaces of intact diatom cells were likewise available for combination with Al. Cells were first killed and treated for 10 min with EDTA *plus* oxalate (0·01 M, pH 7·3) to remove inorganic protective agents from the cell surfaces (as in Fig. 8).

After washing, such cells were treated with 0·0037 M $AlCl_3$ in buffer adjusted to various pH values. After 3 hr, the cells were again washed, and then transferred to Tris buffer at pH 9·0. The results after 10 days showed that treatment with EDTA *plus* oxalate had increased the subsequent rate of dissolution of the silica beyond that of heat-killed cells (as in Fig. 8). However, from those killed cells which had then been pretreated with Al, the silica dissolved at a greatly decreased rate (see Fig. 20). This indicated that Al could combine with the silica surfaces of intact cells, just as it could with cleaned silica walls, thereby retarding their subsequent rate of dissolution. Cleaned walls and intact cells differed in the extent to which the Al combined with silica walls at various pH values (compare Fig. 20 with Fig. 12).

8. *Dissolution of silica from fossil diatom walls*

Since such ions as Fe and Al may retard the rate of dissolution of silica walls, it was of interest to determine to what extent such metal ions might be responsible for the relative insolubility of fossil diatom walls.

Nine samples of diatomaceous earth, fresh-water and marine, ranging in age from Upper Cretaceous through Pliocene, were examined. The material was first powdered by grinding in a mortar and 5 mg samples of each earth were leached in 20 ml of Tris buffer at pH 9·3. In each case, after 35 days only a small amount of soluble silicon had appeared in the medium (approximately 1 mg Si/l. Similar samples first extracted with hot concentrated nitric acid before being placed in the Tris buffer gave off more soluble silicon to the medium than did the untreated walls, ranging

16

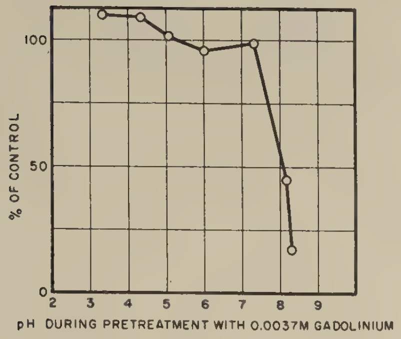

18

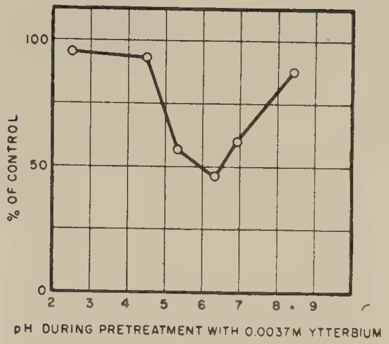

17

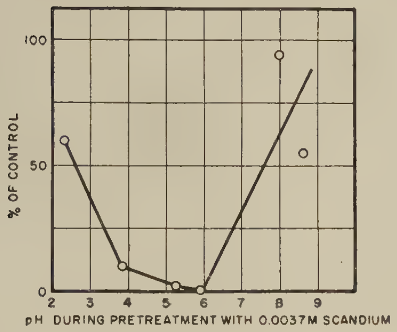

19

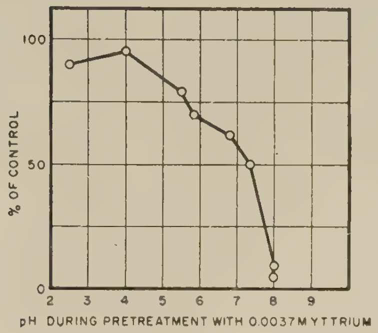

20

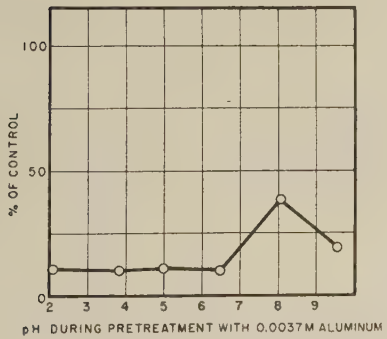

21

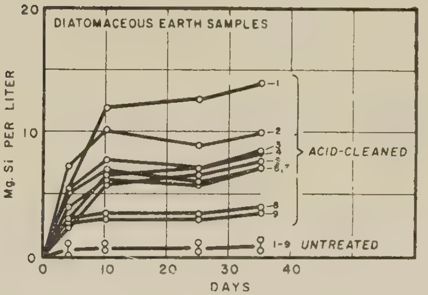

Fig. 20. Silicon in solution (per cent of the control) at the end of 10 days in Tris buffer, pH 9·0–9·3, at 19°C, plotted against the pH values at which whole heat-killed cells were pretreated with solutions of $AlCl_3$.

Fig. 21. Dissolution of silica in Tris buffer, pH 9·0–9·3, at 19°C, from diatomaceous earths, untreated and acid-cleaned.

(1) Terrebonne, Ore., 100,000–200,000 years (fresh-water).
(2) Sierra Vista Hill, Los Angeles, Calif., Upper Miocene.
(3) Shark Tooth Hill, Kern Co., Calif., Middle Miocene.
(4) Chico Martinez Creek, Kern Co., Calif., Upper Miocene.
(5) Walteria, Calif., Upper Miocene.
(6) Maria Madre, Mexico, Upper Miocene.
(7) Hat Creek Crossing, Shasta Co., Calif., Pliocene.
(8) Panoche Hills, Fresno Co., Calif., Upper Cretaceous
(9) Pit River, Calif., Pliocene (fresh-water).

from 3 to 13 mg Si/l. (Fig. 21). Since each sample contained considerably more silica than that required to saturate the solution, nitric acid treatment had served to free only a fraction of the silica for dissolution. The reduced solubility of silica from fossil diatom walls may be due to changes in microstructure of the silica with the passage of time. It is significant that the whitest sample (a fresh-water Pliocene diatomite from Pit River, California), which by X-ray diffraction showed no evidence of crystalline impurity even after preliminary acid digestion, showed only a low rate of dissolution in aqueous buffer, yielding in solution 3·5 p.p.m. Si after 35 days.

9. *Dissolution of silica from natural phytoplankton*

Phytoplankton consisting almost exclusively of diatoms (species of *Skeletonema*, *Chaetoceros* and *Rhizosolenia*) was collected with a No. 20 net from a wharf in Woods

22

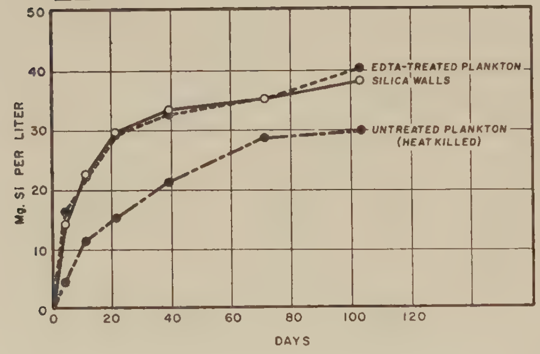

23

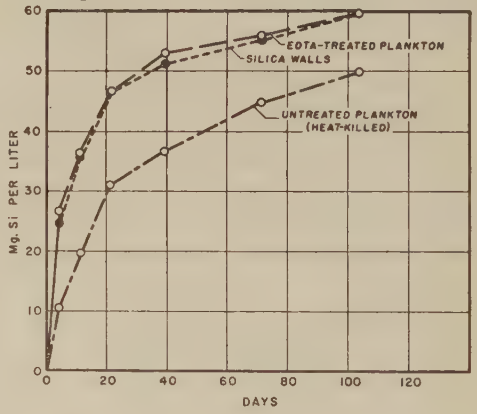

24

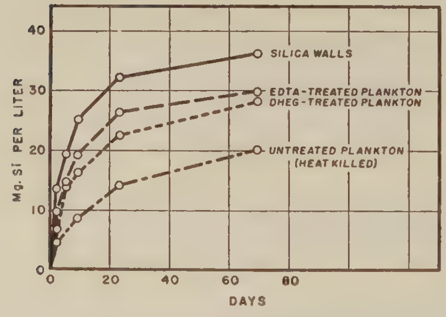

25

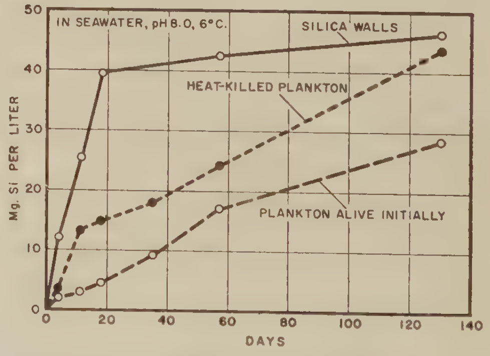

Fig. 22. Dissolution of silica in 0·01 M Tris buffer, pH 9·0–9·3, at 19°C, from killed plankton, from killed plankton extracted with EDTA, and from acid-cleaned valves.

Fig. 23. Conditions as in Fig. 22 but with twice as much plankton.

Fig. 24. Dissolution of silica in 0·01 M Tris buffer, pH 9·0–9·3, at 19°C, from acid-cleaned valves, from heat-killed plankton, and from heat-killed plankton extracted with EDTA and with DHEG.

Fig. 25. Dissolution of silica in sea water, pH 8·0, at 6°C, from acid-cleaned valves, from heat-killed plankton, and from plankton that was alive at the beginning of the experiment.

Hole in January 1959. Aliquots of the sample at two dilutions ($\times 1$, $\times \frac{1}{2}$) were (a) killed by immersion for 5 min in a boiling water bath, (b) killed and then extracted with a mixture of EDTA (0·01 M), oxalate (0·01 M) and Tris buffer (0·01 M) at pH 6·8, and (c) digested with hot concentrated nitric acid to destroy organic matter. The samples were then washed, and suspended in 20 ml Tris buffer (0·01 M) at pH 9·0 in polyethylene containers. At intervals over a period of 104 days, samples were removed, centrifuged, and the dissolved silicon in the supernatant determined.

The silica from plankton cells pretreated with EDTA *plus* oxalate dissolved at the same rate as that from acid-cleaned walls. On the other hand, the silica from killed, though otherwise untreated, plankton dissolved more slowly, initially at about half the rate of the cleaned walls. The greater part of the silica had dissolved from the EDTA-treated cells and the acid-cleaned walls after 30 days, but from the killed plankton only after 100 days (Figs. 22 and 23).

Another sample, from 70 miles offshore, consisting of an entirely different complement of diatoms (predominantly *Thalassionema nitzschioides* and *Coscinodiscus* sp.) was treated in a series similar to the previous sample, and exactly the same relationships were obtained. When pretreated with DHEG (0·01 M, in Tris buffer, pH 6·8), the silica from the diatom cells dissolved at the same rate as from cells pretreated with EDTA (Fig. 24).

Apparently some factor, presumably cations originally combined with the silica but removable by EDTA, DHEG or nitric acid, was instrumental in reducing the rate of dissolution of the silica from killed plankton.

The above experiments with naturally occurring phytoplankton were carried out in Tris buffer at pH 9·0 at 20°C. In order to approach more closely to natural conditions, another phytoplankton sample was set up in sea water, pH 8·0, at 6°C. Untreated cells, which were living at the outset, were also included for comparison. Glass flasks were used in this case, since commercial polyethylene vessels liberate some toxic substance into the medium. Nevertheless, such cells did not survive more than a few days, since the suspension was dense and was maintained in the dark to preclude photosynthesis. Correspondingly, during the first few days, silica dissolved more slowly from these untreated cells than from samples killed by heat, whereas later the rates of the two samples were similar (Fig. 25).

DISCUSSION

Living cells of fresh-water diatoms, grown in the laboratory and stored in darkness at pH 9·0 in a medium containing neither organic substrate nor nutrient salts, remained for the most part viable for several weeks. They released silicon into the medium at a much lower rate than cells which were initially dead. This difference could be attributed either to a vital suppression of the dissolution of the walls, or to the ability of the living cells to reabsorb silicic acid from the medium almost as fast as the silica dissolved. The latter possibility seems unlikely, since the uptake of soluble silicate by diatoms is a process requiring energy (LEWIN, 1955), whereas the cells used in these experiments were under starvation conditions and had no source of energy other than the respiration of depleted endogenous reserves. More probably, the silica in the walls of living cells was protected by some physicochemical system, which was disrupted as soon as they died.

Every treatment which killed the cells (heat, protein-denaturing agents, organic solvents, breakage) gave the same result, i.e. an increase in the rate of dissolution of the silica walls. However, this rate could be further accelerated by treatment with a chelating agent such as EDTA, which presumably removed a cationic inorganic factor retarding silica dissolution. Since iron was present in the original growth medium, this was probably the element concerned.

Aluminium is one of the most effective elements in combining with silica and thereby reducing its solubility and retarding its rate of dissolution (JEPHCOTT and JOHNSTON, 1950; GODBERT and HALPIN, 1955; GOTO, 1956; and OKAMOTO *et al.*, 1957). The hydrated Al^{3+} cation presumably reacts with free hydroxyl groups at the silica surface. ILER (1955, pp. 68–69) discussed in general terms the precipitation of polysilicic acid from solution by the addition of salts of various metals. Though the polysilicic acid of diatom walls is not in colloidal solution, similar chemical combinations would presumably occur at the surface in the presence of metal ions. The evidence indicates that "Combination with silicic acid does not occur much below the pH at which the metal hydroxide would be formed (either as a sol or as a precipitate) on prolonged standing." ILER suggested that the reaction could be considered as a combination between a silanol group ($\cdot$SiOH) and a basic metal ion (such as $Fe(OH)^{2+}$).

The results obtained in the present study indicate that certain metal ions under specific conditions may combine with the silica walls of diatoms and affect either their subsequent rate of dissolution or their final solubility. There is no direct information on the role of such combinations in nature. It should further be pointed out that the concentrations of cations employed for treatment of the silica walls in the experiments reported here were mostly in excess of those normally present dissolved in sea water. For instance, SIMONS *et al.* (1953) found that the soluble Al in sea water averaged 0·0025 mg/l. (approx. 10^{-7} M) and the soluble Fe averaged 0·0026 mg/l. (approx. 5×10^{-8} M), concentrations considerably below those employed here.

The amounts of Al, Be, Fe, Ga, Gd and Y, in sea water are too small to have any direct effect on the rate of dissolution of amorphous silica and, when cleaned walls of diatoms are suspended in sea water, the silica goes into solution. However, it is possible that, if the silica valves while a part of the intact living cell could be initially protected against solution by some other biophysical or biochemical means, there would be time later for colloidal ferric and aluminium hydroxides to be passively adsorbed and accumulated on the new surfaces and the system to be thereby stabilized. Observations on the adsorption of ferric hydroxide on diatom surfaces have been published by HARVEY (1937a,) GOLDBERG* (1952), GEISSLER (1958) and IVES (1959). It might be mentioned in this connexion that the true age of a diatom valve is not necessarily that of the cell which bears it, since, by the unique nature of diatom cell division, each daughter cell inherits one of the parental silica valves, which may already have been transmitted in this way for several generations. ROGALL (1939) analysed the walls of marine planktonic diatoms and found iron or aluminium oxides making up approximately 1·5 per cent of the ash weight. SPOONER (1949) showed that nearly all of the radioactive yttrium taken up by living or dead cells of a diatom (referred to simply as "Nitzschia") was adsorbed on the surface of the walls.

---

* GOLDBERG, in personal discussion, agreed that the high values published in his 1952 paper for the iron content of diatoms could be explained by a passive adsorption of particulate or colloidal iron upon the surfaces of the diatom cell, independent of the living activity of the cell. His use of the term "assimilation" was unfortunately misleading.

Investigations of the rates of dissolution of amorphous silica in water and of its solubility, i.e. equilibrium concentration under various conditions (ALEXANDER *et al.*, 1954; ILER 1955; KRAUSKOPF, 1956, 1959; WHITE *et al.*, 1956; GREENBERG, 1957; OKAMOTO *et al.*, 1957; SIEVER, 1957) indicate in some cases marked differences between the forms of amorphous silica, i.e. colloidal silica, silica gel, opal and silica glass. These observations, reviewed by KRAUSKOPF (1959), are of interest in relation to the differences in solubility between the amorphous silica from Recent (i.e. contemporary) diatoms and that from fossil diatoms. Recent diatom silica dissolves readily, at a rate similar to that of silica gel, whereas fossil diatomite dissolves very slowly. According to KRAUSKOPF (1959), WHITE has obtained values of 22 p.p.m. SiO_2 in fresh water and 34 p.p.m. SiO_2 in sea water in which diatomite has been dissolving for a period of 2 years. These values are in the same range as those reported here for diatomaceous earths which had been dissolving for 35 days, but in this case the material had first been cleaned with nitric acid to remove protective ions. One may ask what changes in the structure or chemical nature of the silica can have taken place to account for the differences in behaviour between Recent and fossil material. Measurements of the specific surface area (by the nitrogen adsorption method) of walls of the fresh-water species, *Navicula pelliculosa*, and of the marine species, *Coscinodiscus asteromphalus*, each grown in culture, gave values of 123 m^2/g and 89 m^2/g, respectively (LEWIN, unpublished). The average specific surface area of fossil diatomaceous earth was reported to be 22 m^2/g (ILER, 1955). These values indicate a reduction of specific surface area on ageing. Since the rate of solution (GREENBERG, 1957; GOTO, 1958) and the final solubility depend on the "available surface," i.e. the free silanol (SiOH) groups of the silica polymer (ALEXANDER, 1957), any loss of surface would be expected to result in a lower rate of solution.

The physical and chemical reactions involved in the fossilization of diatom walls, and the length of time required for the process, are unknown. ROGALL (1939) found that Recent, post-glacial, and interglacial diatom deposits, examined by X-ray diffraction methods, showed only amorphous structure, whereas in geologically older material he obtained some evidence for crystallinity. SWINEFORD and FRANKS (1959) published X-ray diffraction diagrams of a fossil diatomaceous marl showing that the diffraction pattern was distinctly different from the disordered low-cristobalite diagrams given by other forms of opal. The formation of diatom-type opal is thought to be a direct consequence of the chemical purity of the silica and the lack of cations necessary for the formation of a low-cristobalite structure disordered by incorporated tridymite. GEISSLER (1958) found that the walls of Recent diatom adsorbed dyes to the same degree as silica gel, whereas fossil walls were less reactive, being less strongly charged than Recent material.

Sporadic observations have been made on the dissolution of diatomaceous silica, some on recent cell material (KING and DAVIDSON, 1933; ATKINS, 1945; JØRGENSEN, 1955a, 1957; GOLTERMAN, 1960) and some on diatomaceous earths

(JEPHCOTT and JOHNSON, 1950; KRAUSKOPF, 1956; Hoss 1959). Since the silica of Recent diatoms differs from that of fossil materials, one would expect older samples to exhibit progressive degrees of fossilization, and thus different solubilities. The solvents, pH and temperatures employed in these studies were dissimilar, and therefore little can be gained from a comparison of the results.

The thickness of diatom walls varies considerably between species, in cells of different ages and conditions (LUND, 1950; JØRGENSEN, 1955b, 1957; LEWIN, 1957) For example, walls of *Coscinodiscus asteromphalus* may reach 25,000 Å in thickness whereas those of *Navicula pelliculosa* may range in average thickness from 200 Å to 600 Å (LEWIN, 1957). Obviously such variation in the average surface/volume ratio, as well as in the pattern of thickening and of microscopic pores, has a profound influence on the rate of solubility of the silica, as it may also have on the rate of fossilization. In many cases it has been observed that the specific composition of diatom skeletons in bottom deposits fails to reflect that of the living phytoplankton, apparently because the more delicate species tend to be eliminated and only the more resistant walls persist (HART, 1934, 1942; KOLBE, 1957). There may in addition be invisible differences in the submicroscopic constitution of the walls and in the distribution of the more soluble silanol groups. And we must now recognize the importance of adsorbed cations, such as Fe and Al, and perhaps also of organic protective coatings, in depressing the rate of solution of diatom walls. Nothing is known of the various conditions in the digestive tracts of diatom-eating planktonic animals and their predators which may have an appreciable influence on the degree of comminution and the rate of solution of silica walls. For all these reasons, no general statement of their solubility under natural conditions can be made. We cannot readily assess the factors involved in determining which skeletons of planktonic diatoms will dissolve, and which will persist to accumulate in bottom deposits, there to give rise to a diatomaceous ooze and, eventually, a diatomite.

Furthermore, those silica walls which persist long enough to reach the sediment, either associated with living cells or as empty frustules, are then subjected to a new set of physical and chemical factors peculiar to the particular sediment in question. For instance, ARRHENIUS (1952) observed that skeletons of diatoms and radiolarians were well preserved when associated with calcareous deposits in the Equatorial Pacific sediments and in several clays from the Central Pacific, whereas the siliceous structures associated with pelagic clays of the East Pacific were markedly corroded. RIEDEL (1959) pointed out that in areas of rapid sedimentation most siliceous skeletons are well preserved, whereas in areas of slow sedimentation many show partial dissolution. In the interstitial waters of some bottom sediments which may be already saturated with soluble silicic acid (BRUEVICH, 1953), as for example in beds of volcanic ash (see BRAMLETTE, 1946), the diatom frustules would tend to remain undissolved. OPPENHEIMER and KORNICKER (1958) described anaerobic marine sediments saturated with H_2S and CO_2, with pH values of from 5·4 to 7·6; under such reducing conditions, Fe associated with the walls might be removed as FeS, and the silica might then be free to dissolve. Its solubility would also be influenced by the solubility equilibria established by the mineral composition of the solid phase in the sediment (BRUEVICH, 1953).

REFERENCES

ALEXANDER G. B. (1957) The effect of particle size on the solubility of amorphous silica in water. *J. Phys. Chem.* **61,** 1563–1564.

ALEXANDER G. B., HESTON W. M. and ILER R. K. (1954) The solubility of amorphous silica in water. *J. Phys. Chem.* **58,** 453–455.

ARRHENIUS G. (1952) Sediment cores from the East Pacific. *Reps. Swed. Deep-Sea Exped.* **5,** No. 1, 1–127.

ATKINS W. R. G. (1945) Autotrophic flagellates as the major constituent of the oceanic phytoplankton. *Nature, Lond.* **156,** 446–447.

BRAMLETTE M. N. (1946) *The Monterey Formation of California and Origin of its Siliceous Rocks.* U.S. Geol. Survey Prof. Paper 212.

BRUEVICH S. V. (1953) Concerning the geochemistry of silicon in the sea. *Izv. Akad. Nauk SSSR, ser. geol.* No. 4, 67–79.

CHABEREK S., COURTNEY R. C. and MARTELL A. E. (1953) Stability of metal chelates V. N,N-Dihydroxyethylglycine. *J. Amer. Chem. Soc.* **75,** 2185–2190.

CONGER P. S. (1942) Accumulation of diatomaceous deposits. *J. Sediment. Petrol.* **12,** 55–66.

COOPER L. H. N. (1952) Factors affecting the distribution of silicate in the North Atlantic Ocean and the formation of North Atlantic deep water. *J. Mar. Biol. Ass.* U.K. **30,** 511–526.

DIÉNERT F. and WANDENBULCKE F. (1923) Sur le dosage de la silice dans les eaux. *C.R. Acad. Sci., Paris* **176,** 1478–1480.

GEISSLER U. (1958) Das Membranpotential einiger Diatomeen und seine Bedeutung für die lebende Kieselalgenzelle. *Mikroskopie* **13,** 145–172.

GODBERT A. L. and HALPIN R. K. (1955) The effect of aluminium salts on the solubility of quartz dust and its electrokinetic properties. *Research Report* No. 116, pp. 1–18, Safety in Mines Research Establishment.

GOLDBERG E. D. (1952) Iron assimilation by marine diatoms. *Biol. Bull.* **102,** 243–248.

GOLTERMAN H. L. (1960) Studies on the cycle of elements in fresh water. *Acta Botan. Neerlandica* **9,** 1–58.

GOTO K. (1956) Precipitation of silica in the presence of aluminum. *Bull. Chem. Soc. Japan* **29,** 741–742.

GOTO K. (1958) Estimation of specific surface area of particles in colloidal silica sols from the rate of dissolution. *Bull. Chem. Soc. Japan* **31,** 900–903.

GREENBERG S. A. (1957) The depolymerization of silica in sodium hydroxide solutions. *J. Phys. Chem.* **61,** 960–965.

HART T. J. (1934) On the phytoplankton of the south-west Atlantic and the Bellingshausen Sea, 1929–1931. *Discovery Reports* **8,** 1–268.

HART T. J. (1942) Phytoplankton periodicity in Antarctic surface waters. *Discovery Reports* **21,** 261–356.

HARVEY H. W. (1937a) The supply of iron to diatoms. *J. Mar. Biol. Ass. U.K.* **22,** 205–219.

HARVEY H. W. (1937b) Note on colloidal ferric hydroxide in sea water. *J. Mar. Biol. Ass. U.K.* **22,** 221–225.

HARVEY H. W. (1955) *The Chemistry and Fertility of Sea Waters.* Cambridge University Press.

HOSS H. (1959) Nachtrag zu den Untersuchungen über die Petrographie kulmischer Kieselschiefer. *Beitr. Mineral. u. Petrogr.* **6,** 248–260.

HUTCHINSON G. E. (1957) *A Treatise on Limnology* Vol. I. *Geography, Physics and Chemistry.* John Wiley, New York.

ILER R. K. (1955) *The Colloid Chemistry of Silica and Silicates.* Cornell University Press, Ithaca, New York.

IVES K. J. (1959) The significance of surface electrical charge on algae in water purification. *J. Biochem. Microbiol. Tech. Eng.* **1,** 37–47.

JEPHCOTT C. M. and JOHNSTON J. H. (1950) Solubility of silica and alumina. *Arch. Industr. Hyg. and Occupat. Med.* **1,** 323–340.

JØRGENSEN E. G. (1955a) Solubility of the silica in diatoms. *Physiol. Plantarum* **8,** 846–851.

JØRGENSEN E. G. (1955b) Variations in the silica content of diatoms. *Physiol. Plantarum* **8,** 840–845.

Jørgensen E. G. (1957) Diatom periodicity and silicon assimilation. *Dansk Botanisk Arkiv* **18,** 6–54.

King E. J. and Davidson V. (1933). The biochemistry of silicic acid. IV—Relation of silica to the growth of phytoplankton. *Biochem. J.* **27,** 1015–1021.

Kolbe R. W. (1957) Diatoms from Equatorial Indian Ocean cores. *Reps. Swed. Deep-Sea Exped.* **9,** No. 1, 1–50.

Krauskopf K. B. (1956) Dissolution and precipitation of silica at low temperatures. *Geochim. et Cosmochim. Acta* **10,** 1–26.

Krauskopf K. B. (1959) *The Geochemistry of Silica in Sedimentary Environments.* No. 7, pp. 80–91, Society of Economic Paleontologists and Mineralogists. Special Publication.

Lewin J. C. (1954) Silicon metabolism in diatoms. I—Evidence for the role of reduced sulfur compounds in silicon utilization. *J. Gen. Physiol.* **37,** 589–599.

Lewin J. C. (1955) Silicon metabolism in diatoms. III—Respiration and silicon uptake in *Navicula pelliculosa. J. Gen. Physiol.* **39,** 1–10.

Lewin J. C. (1957) Silicon metabolism in diatoms. IV—Growth and frustule formation in *Navicula pelliculosa. Canad. J. Microbiol.* **3,** 427–433.

Lund J. W. G. (1950) Studies on *Asterionella formosa* Hass. II—Nutrient depletion and the spring maximum. *J. Ecol.* **38,** 15–35.

Okamoto G., Okura T. and Goto K. (1957) Properties of silica in water. *Geochim. et Cosmochim. Acta* **12,** 123–132.

Oppenheimer C. H. and Kornicker L. S. (1958) Effect of the microbial production of hydrogen sulfide and carbon dioxide on the pH of Recent sediments. *Inst. Mar. Science* **5,** 5–15.

Riedel W. R. (1959) *Siliceous Organic Remains in Pelagic Sediments.* Special Publication No. 7, pp. 80–91, Society of Economic Paleontologists and Mineralogists.

Rogall E. (1939) Über den Feinbau der Kieselmembran der Diatomeen. *Planta* **29,** 279–291.

Siever R. (1957) The silica budget in the sedimentary cycle. *Amer. Min.* **42,** 821–841.

Simons L. H., Monaghan P. H. and Taggart M. S. (1953) Aluminium and iron in Atlantic and Gulf of Mexico surface waters. *Analyt. Chem.* **25,** 989–999.

Spooner G. M. (1949) Observations on the absorption of radioactive strontium and yttrium by marine algae. *J. Mar. Biol. Ass. U.K.* **28,** 587–626.

Swineford A. and Franks P. C. (1959) *Opal in the Ogallala Formation in Kansas.* Special Publication No. 7, pp. 111–120, Society of Economic Paleontologists and Mineralogists.

White D. E., Brannock W. W. and Murata K. J. (1956) Silica in hot-spring waters. *Geochim. et Cosmochim. Acta.* **10,** 27–59.

Contribution No. 1114

Made in United States of America
Reprinted from Limnology and Oceanography
Vol. 6, No. 2, April, 1961
pp. 154–164

FURTHER INVESTIGATIONS ON THE CARBOHYDRATE CONTENT OF MARINE ZOOPLANKTON

by J. E. G. Raymont and Robert J. Conover

FURTHER INVESTIGATIONS ON THE CARBOHYDRATE CONTENT OF MARINE ZOOPLANKTON[1]

J. E. G. Raymont and Robert J. Conover
University of Southampton, England, and
Woods Hole Oceanographic Institution

ABSTRACT

Studies on the carbohydrate content of 11 species of planktonic animals have been carried out. In the case of *Calanus finmarchicus*, *C. hyperboreus* and *Neomysis americana*, certain animals were fed laboratory phytoplankton cultures and comparisons were made between fed and starved groups. For *Calanus finmarchicus*, fed animals contained from 0.90–2.85 µg and starved animals from 0.68–1.50 µg carbohydrate/animal. As percent wet weight the carbohydrates ranged from 0.11–0.40 for fed and from 0.10–0.24 for starved *C. finmarchicus*. The carbohydrates in *C. hyperboreus* ranged from 0.14–0.29% wet weight and in *Neomysis* from 0.19–0.23%, but there was no significant difference between fed and starved animals. Feeding experiments were also attempted with the euphausids *Meganyctiphanes norvegica* and *Thysanoessa* sp. but feeding was poor and again no significant difference over the concentrations in starved animals could be detected. The concentration for all the euphausids was rather low: 0.05–0.08% wet weight for *Meganyctiphanes*, 0.09–0.11% for *Thysanoessa*, and 0.08–0.17 for *Nematoscelis megalops*. Carbohydrates were also low for the copepods *Paraeuchaeta norvegica* (0.06–0.11%) and *Pleuromamma* sp. (0.10%) and for *Hyperia galba* (0.15%). Another amphipod *Euthemisto* contained from 0.25–0.62% wet weight carbohydrate and an ostracod *Conchoecia* 0.31%. Respiratory measurements during periods of starvation were made for *Calanus hyperboreus*, *Nematoscelis megalops* and *Neomysis americana* which indicated that considerably more carbon was being oxidized than could be accounted for by changes in the carbohydrate content of the animals. Conversely, in certain feeding experiments with *Neomysis americana* and *C. finmarchicus* it seemed very doubtful that sufficient carbohydrate was obtained in the food consumed to meet the carbon requirements if carbohydrate was the principal energy source. It is concluded that the animals in question do not contain sufficient carbohydrate reserves to meet energy requirements, particularly during periods of food scarcity, and therefore, other metabolic substrates must be utilized as well.

INTRODUCTION

An understanding of the metabolism of the zooplankton is important to the study of food chains and energy flow in the sea. Although it is well known that the nature of the substance oxidized, whether carbohydrate, fat or protein, has a marked influence on the amount of oxygen used in the respiratory processes, very little work on the composition of the zooplankton organic matter has been carried out to date. Carbohydrates, in particular, are poorly known and the results of previous investigations have been widely divergent. The carbohydrate contents suggested by Brandt (1898) and Brandt and Raben (1919), for example, for mixed plankton are approximately ten times the values found in recent preliminary studies by Raymont and Krishnaswamy (1960) on selected species of zooplankton. These studies on zooplankton from the English Channel have been extended in the present investigation to some neritic species off the northeastern United States, and to several deep-water species. Since it had been shown also by Raymont and Krishnaswamy that starvation tended to lower carbohydrate levels in plankton, it was desirable to supplement the work on carbohydrate content with some investigations on respiration and feeding rates in the same species.

One of us, (J.E.G.R.) desires to express his thanks to the Director of the Woods Hole Oceanographic Institution for the invitation to work at the Institution and for a grant covering the period of the investiga-

---

[1] Contribution No. 1114 from the Woods Hole Oceanographic Institution. This research was supported in part by the National Science Foundation under Research Grants 3838, 8913 and 8339.

tion, and to Dr. George Clarke for his interest in the work.

Thanks are due Dr. John Barlow, Masateru Anraku, Michael Mullin, and Thomas Renshaw who aided in the collection of the experimental material. Dr. Robert Guillard kindly supplied the phytoplankton used in the feeding experiments. Constance Chadwick assisted in the identification of certain of the zooplankton species.

METHODS

The zooplankton used in the experiments were collected with a coarse plankton net (#00 or #000) in Cape Cod Bay, Gulf of Maine (42°10′N, 69°45′W) and also from the slope water off the eastern tip of Georges Bank (41°40′N, 65°05′W) and south of Woods Hole (39°N, 71°30′W). The catches were diluted and kept cool on board ship, and after being brought to the laboratory they were further diluted and kept in a cold room at 5°C. They were sorted as soon as possible into polyethylene vessels containing one to two liters of filtered sea water and maintained in a refrigerator at about 5°C.

Determinations in which comparisons were made on carbohydrate levels in fed and unfed animals were carried out on *Calanus finmarchicus*, and a few similar data were obtained for *Calanus hyperboreus* and *Neomysis americana*. The diatoms *Skeletonema costatum*, *Thalassiosira fluviatilis*, and *Rhizosolenia setigera* and an unidentified flagellate designated *Olisthodiscus* I, all from the Woods Hole Oceanographic culture collection, were used in the feeding experiments. Food concentrations were determined by cell counts using a Levy counting chamber with Fuchs Rosenthal rulings. In addition to changes in the cell numbers during the course of feeding experiments, the number of fecal pellets produced was also used as an index to the amount of feeding in some instances.

Feeding experiments were also attempted with two carnivorous forms, *Paraeuchaeta norvegica* and *Euthemisto compressa-bispinosa*[2] using living and dead copepods and portions of euphausids. However, feeding was limited for *Euthemisto* and *Paraeuchaeta* apparently did not eat any of the food offered it.

A few carbohydrate determinations were performed on other species of zooplankton, even though it was not possible to compare the effects of feeding and starvation satisfactorily. Included in this group were the euphausids *Thysanoessa* sp., *Meganyctiphanes norvegica, Nematoscelis megalops,* the amphipod *Hyperia galba,* the ostracod *Conchoecia* sp. and the copepod *Pleuromamma* sp.

Respiratory rates were determined for *Calanus hyperboreus, Nematoscelis megalops,* and *Neomysis americana* using the Winkler method as employed by Conover (1956, 1959) and from these rates, the amount of carbohydrate which could have been oxidized during the experiments was calculated.

For the determination of carbohydrates it was necessary to use about 100 *Calanus finmarchicus* (mostly stage V with a few females) for a single analysis, but much smaller numbers of larger zooplankton animals were required for a determination (e.g., only a single *Meganyctiphanes*). In each case the animals were rinsed briefly in distilled water, excess liquid removed with filter paper and then weighed. The methods of Mendel, Kemp and Myers (1954) and Kemp and Kits van Heijningen (1954) were used for the determination of carbohydrate, the animals being first ground with a mixture of 5% trichloracetic acid, containing 0.1% Ag_2SO_4, and the mixture then boiled for 15 min. After cooling and centrifuging, 1 ml of the supernatant liquid was boiled for 6½ min with 3 ml concentrated H_2SO_4 (1.84 specific gravity). The intensity of the resulting pink color was then determined by a Beckman D.U. spectrophotometer at 520 mμ, the readings be-

---

[2] Both *Euthemisto compressa* and *E. bispinosa* are found in the Gulf of Maine, often together (Bigelow 1925). The animals are quite similar in many respects and no attempt was made to distinguish between them in this study.

TABLE 1. *Carbohydrate content, grazing rate, and fecal pellet production of* Calanus finmarchicus *(mainly stage V copepodites)*

Date of haul	Date of analysis	Expt.	Number of animals	Carbohydrate content		Grazing rate ml/copepod day	No. fecal pellets produced	Remarks
				µg/copepod	% wet wt			
28.VII	29.VII	A_0	100 V	1.50	0.24	–	–	Initial, starved 24 hr
28.VII	30.VII	AT_1	99 V	1.26	0.18	–	2,200	Starved 24 hr, fed 20 hr
28.VII	30.VII	AT_2	97 V	1.39	0.20	–	1,932	Starved 24 hr, fed 21 hr
28.VII	30.VII	AS_1	98 V	1.89	0.29	–	4,730	Starved 24 hr, fed 22 hr
28.VII	30.VII	AS_2	94 V	1.70	0.24	–	6,110	Starved 24 hr, fed 23 hr
28.VII	30.VII	AC_1	82 V	1.22	0.18	–	281	Starved 38 hr
28.VII	30.VII	AC_2	c. 100 V	(1.10)*	0.16	–	318	Starved 39 hr
28.VII	30.VII	AC_3	84 V	1.07	0.14	–	390	Starved 41 hr
28.VII	30.VII	AC_4	c. 100 V	(0.85)*	0.14	–	252	Starved 42 hr
28.VII	3.VIII	B_1	200 V	1.23	0.18	6.9	9,160	Starved for 5 days, then fed 16 hr
28.VII	3.VIII	B_2	200 V	0.68	0.10	–	1,000	Starved for 6 days
3.VIII	4.VIII	$CR_{7\text{ and }8}$	100 V	1.45	0.19	–	1,000	Starved for 21 hr
3.VIII	4.VIII	$CR_{9\text{ and }10}$	100 V	2.45	0.28	29.8	6,760	Fed for 21 hr
3.VIII	6.VIII	$DR_{1\text{ and }2}$	100 V	2.70	0.38	–	5,760	Fed for 23 hr
3.VIII	7.VIII	$DR_{3\text{ and }4}$	100 V	2.85	0.40	–	9,360	Fed for 47 hr
3.VIII	7.VIII	$DR_{5\text{ and }6}$	106 V	(2.10)*	(0.26)	–	5,320	Fed for 23 hr, then accidentally killed
3.VIII	12.VIII	$ER_{4\text{ and }5}$	100 V	0.90	0.11	av. 15.6	3,041	Starved for 10 days, fed 18 hr
3.VIII	13.VIII	$ER_{1\text{ and }2}$	100 V	1.15	0.15	av. 17.0	2,680	Starved for 10 days, fed 45 hr
3.VIII	13.VIII	$ER_{3\text{ and }6}$	100 V	1.25	0.17	av. 17.0	1,998	Starved for 10 days, fed 24 hr, then starved 22 hr
25.VIII	26.VIII	F_3	117 IV & V	1.07	0.16	–	–	Starved for 1 day

* Values omitted from subsequent calculations

ing converted into units of glucose from a calibration curve. This method gave fairly accurate determinations for values from about 10 to about 110 µg glucose, but for higher amounts it was necessary first to dilute the supernatant fluid before boiling with H_2SO_4. In any case, several replicates were run for each sample and these generally agreed within one or two percent. Some difficulty was experienced on a few occasions owing to the necessity of using a different Beckman spectrophotometer with slightly variable sensitivity but a later check showed that the values were of the right order of magnitude and that apparently little error was introduced. For each analysis the amount of carbohydrate has been expressed as percentage of the wet body weight.

RESULTS

For *Calanus finmarchicus* the carbohydrate content of several sets of fed and starved animals were compared (Tables 1 and 2). The results show a considerable range of variability (0.11 – 0.40% for fed animals and 0.10 – 0.24% for starved), but for each set of experiments with one exception the data are reasonably consistent.

In series A (used almost immediately after capture on July 28, 1959, in Cape Cod Bay) there was a decided lowering of the carbohydrate levels in animals starved for 38 to 42 hr ($AC_1 – AC_4$) in comparison with the initial A_0. Among fed aminals AT_1, AT_2, AS_1 and AS_2 the levels remained high. Animals AT_1 and AT_2 received 2,190 cells/ml of *Thalassiosira fluviatilis* as food

TABLE 2. *Carbohydrate content of fed and starved* Calanus finmarchicus *(summary of data in Table 1)*

	All experiments on fed and unfed *Calanus* except $DR_{5 \text{ and } 6}$				Experiments on *Calanus* kept in laboratory not more than 7days *i.e.*, excluding series E			
	Carbohydrate % wet wt		Carbohydrate/ copepod (μg)		Carbohydrate % wet wt		Carbohydrate/ copepod (μg)	
	Range	Mean	Range	Mean	Range	Mean	Range	Mean
Fed	0.11–0.40	0.23	0.90–2.85	1.71	0.18–0.40	0.27	1.23–2.85	1.93
Starved	0.10–0.24	0.16	0.68–1.50	1.16	0.10–0.24	0.16	0.68–1.50	1.16

while animals AS_1 and AS_2 received 96,200 cells/ml of *Skeletonema costatum. Thalassiosira* is a substantially larger diatom than *Skeletonema* and the concentrations were adjusted to provide approximately the same biomass of cells per unit volume in each feeding culture. Nonetheless, *Calanus* produced twice as many fecal pellets when fed *Skeletonema* as when fed *Thalassiosira* and the carbohydrate levels in the AS_1 and AS_2 groups would seem to be significantly higher than in AT_1 and AT_2.

Fecal pellet production is not always a reliable index of the amount of food consumed unless some account is taken of the fact that pellets vary in size over a wide range. In the B series of experiments about 1,000 fecal pellets were produced by the starved B_2 animals. However, these pellets were very small and contained almost no particulate matter. On the other hand, the B_1 animals, which had a substantially higher carbohydrate content than the B_2 group, produced over 9,000 large, green pellets.

Both A and B animals were captured in the same tow-netting on July 28, 1959. If the A_0 group contains the initial concentration of carbohydrate at time zero, the amount of carbohydrate for starved animals in the groups AC_1, AC_3 and B_2 falls very roughly along a straight line when plotted on semi-logarithmic paper against time of starvation. Assuming that the loss of sugars is explained by a single logarithmic function, it can be calculated that the daily loss was about 13% for AC_1, 19% for AC_3 and 14% for B_2.

Three additional experiments, series C, D and E, were carried out with animals taken on August 3, 1959, in Cape Cod Bay. In series C, animals fed *Thalassiosira fluviatilis* ($CR_{9 \text{ and } 10}$) were compared with animals $CR_{7 \text{ and } 8}$ which were not fed (see Table 1). The D group was fed a mixture of the diatom *Th. fluviatilis* and a flagellate, possibly *Olisthodiscus* sp. In this experiment animals fed for varying periods of time were compared but unfortunately animals $DR_{5 \text{ and } 6}$, which were fed for one day and then starved, were accidentally killed by some contaminated water during the starvation period. Nonetheless, in both C and D experiments the carbohydrate content would seem to have increased as a result of feeding. The marked fecal pellet production in $CR_{9 \text{ and } 10}$, $DR_{1 \text{ and } 2}$, and $DR_{3 \text{ and } 4}$, indicating considerable feeding, is in agreement with the higher levels of carbohydrate observed.

The results from the experiments E are generally inconsistent. The animals used here had been kept under starvation conditions for 10 days and presumably they were in poor condition at the start of the run. Their carbohydrate content was lower than in most of the other experiments, even after two days of feeding. Fecal pellet production was not so great as in some other runs.

Another attempt to get *C. finmarchicus* from Cape Cod Bay on August 25 was largely unsuccessful. Only enough animals including some stage IV were obtained to run a single analysis F_3.

It is possible, since known numbers of *Calanus* were employed for the analyses, to calculate the carbohydrate content per copepod. The corrected values, omitting the experiments where animals were kept for more than one week, suggest substantially more carbohydrate in fed (mean 1.9 μg) as compared with starved copepods (mean 1.2 μg) (Table 2). These values may be compared with those obtained by Raymont and Krishnaswamy (1960) for *Calanus* from

TABLE 3. *Carbohydrate content and respiratory rate for* Calanus hyperboreus. *Copepods from haul 7.VIII.58, 42°10′N, 69°45′W*

Date of analysis	No. and stage of copepods	Carbohydrate content		Respiratory rate		Carbohydrate equivalent, μg glucose/animal day	Grazing rate ml/animal day	Remarks
		μg/copepod	% wet wt	μL/animal day	μL/mg wet wt day			
10.VIII	15 V	11.7	0.21	–	–	–	–	Not fed
15.VIII	20 V	8.2	0.16	–	–	–	–	Starved 7 days, fed 1 day
15.VIII	17 ♀	29.4	0.29	–	–	–	–	Starved 7 days, fed 1 day
17.VIII	20 V	9.2	0.18	–	–	–	3.71 (*Skeletonema*)	Starved 7 days, fed 3 days
17.VIII	20 V	12.7	0.20	–	–	–	2.57 (*Skeletonema*)	ditto
17.VIII	20 V	8.8	0.16	–	–	–	2.03 (*Skeletonema*)	ditto
17.VIII	18 ♀	15.8	0.18	–	–	–	4.25 (*Skeletonema*)	ditto
17.VIII	19 V	7.9	0.16	9.9	2.11	13.0	–	Starved 7 days, fed 1 day before expt., then starved 2 days
17.VIII	20 V	7.4	0.14	10.7	2.03	14.0	–	ditto
17.VIII	20 V	7.5	0.14	7.9	1.47	10.4	–	ditto
17.VIII	18 ♀	29.7	0.29	17.4	1.70	22.8	–	ditto

the English Channel. For freshly caught and for fed copepods they found a mean carbohydrate content of 1.30 μg; for starved *Calanus*, a value of 0.89 μg per copepod.

The data for *Calanus hyperboreus* (Table 3) suggest a carbohydrate content very similar to that for *C. finmarchicus.* Enough females of this species were taken to permit separate analysis. For experiments on stage V the mean carbohydrate value was 0.17% of the wet weight. For females, the result is more variable: two of the three determinations gave a value of 0.29% but one was much lower; the mean for all analyses was 0.25%. In any event the value suggested for female *C. hyperboreus* is of the same order as that for stage V and VI *C. finmarchicus.* Expressed as the amount of carbohydrate per copepod, the values for *C. hyperboreus* (stage V) ranged from 7.4 μg to 11.8 μg (mean 9.1 μg). For females the value is somewhat doubtful, as again one experiment gave much lower results than the other two, 15.8 μg as against 29.4 μg and 29.7 μg (Table 3). It is clear, however, that the larger female specimens have a considerably greater amount of carbohydrate than stage V copepodites but it would appear probable that the percentage of carbohydrate to body weight is also somewhat greater in females as compared with stage V of *C. hyperboreus.*

There appears to be little effect on carbohydrate level with feeding and starvation in *C. hyperboreus* but the data are few and uncertain. The mean level in fed stage V copepodites was 0.18% wet weight and for starved 0.15%. For the females, the starved animals appeared to contain more carbohydrate than the fed (Table 3). The grazing rate resulting from these experiments was very low. A mixture of *S. costatum* and *Th. fluviatilis* was given the animals but only the former was eaten. Subsequent work on *C. hyperboreus* has demonstrated that one to two weeks of exposure to laboratory conditions may be necessary before any consistent feeding occurs. Therefore, it is not surprising that differences in amount of sugar between fed and starved animals were not great. Since all animals had been starved for nearly a week before the experiments, the levels of carbohydrate were probably somewhat lower than in nature.

Some attempts were made to compare fed and starved euphausids, *Meganyctiphanes norvegica* and *Thysanoessa* sp., captured east of Georges Bank in the slope water. In the case of *Meganyctiphanes* the carbohydrate content was low in all analyses and there is no evidence that the level was affected by the food given (Table 4). All the experimental animals were kept without food for 5 days, but after feeding

TABLE 4. *Carbohydrate content, respiratory rate and grazing rate for some euphausids*

Animal	Date captured	Expt. date	Carbohydrate content		Respiratory rate		Carbohydrate equivalent, µg glucose/animal day	Grazing rate, ml/animal day	Remarks
			µg/animal	% wet wt	µl/animal day	µl/mg wet wt day			
Meganyctiphanes norvegica	6.VIII	14.VIII	153	0.05	–	–	–	–	Starved 5 days, fed 3 days
″	6.VIII	14.VIII	99	0.05	–	–	–	–	ditto
″	6.VIII	14.VIII	233	0.06	–	–	–	–	ditto
″	6.VIII	14.VIII	114	0.04*	–	–	–	–	ditto
″	6.VIII	14.VIII	213	0.04*	–	–	–	–	ditto
″	6.VIII	18.VIII	151	0.05	–	–	–	55.1 *Skeletonema*	Starved 5 days, fed 7 days
″	6.VIII	18.VIII	130	0.05	–	–	–	25.7 *Thalassiosira*	ditto
″	18.VIII	21.VIII	128	0.08	–	–	–	–	Starved 3 days
Thysanoessa sp.	6.VIII	18.VIII	72	0.11	–	–	–	62.3 *Skeletonema* 25.7 *Thalassiosira*	Fed 7 days
″	6.VIII	18.VIII	68	0.11	–	–	–	42.9 *Skeletonema* 38.3 *Thalassiosira*	Fed 7 days
″	18.VIII	21.VIII	16	0.09	–	–	–	–	Starved 3 days
Nematoscelis megalops	6.VIII	14.VIII	135	0.13	–	–	–	–	Starved 5 days, fed 3 days
″	18.VIII	18.VIII	53	0.12	–	–	–	–	–
″	18.VIII	18.VIII	–	0.17	–	–	–	–	–
″	18.VIII	18.VIII	50	0.15	–	–	–	–	–
″	18.VIII	18.VIII	82	0.13	–	–	–	–	–
″	18.VIII	18.VIII	50	0.13	–	–	–	–	–
″	18.VIII	18.VIII	56	0.15	–	–	–	–	–
″	18.VIII	18.VIII	51	0.11	–	–	–	–	–
″	18.VIII	19.VIII	46	0.13	93.5	2.54	122.8	–	No food 10°C
″	18.VIII	19.VIII	71	0.08	112.2	3.12	147.3	–	
″	18.VIII	19.VIII	50	0.14	140.5	2.63	184.5	–	
″	18.VIII	19.VIII	60	0.13	159.3	3.42	209.2	–	No food 4°C
″	18.VIII	19.VIII	45	0.13	116.8	3.23	153.4	–	
″	18.VIII	19.VIII	49	0.12	97.9	2.57	128.5	–	

* Animals dead before analysis

the monosaccharides and glycogen levels were still less than in one animal which was taken in a haul from slope water on August 18 and kept for 3 days without food (Table 4). A grazing rate computed for two animals kept in 900 ml of culture containing initially 6600 cells/ml of *Thalassiosira* and 119,900 cells/ml of *Skeletonema* was not particularly large when it is considered that the animals had an average wet weight of 285 mg, more than two orders of magnitude greater than *C. finmarchicus.* As in the experiment with *C. hyperboreus*, *Skeletonema* was favored over *Thalassiosira*, but it is probable that animal food is a necessary supplement to the diet of *Meganyctiphanes.*

The carbohydrate level in *Thysanoessa* was somewhat higher than in *Meganyctiphanes* and possibly affected to a greater extent by feeding on laboratory cultures of phytoplankton. A grazing rate was obtained for two groups; these specimens had only 25% of the biomass of *Meganyctiphanes* but had a similar filtration rate (Table 4). The carbohydrate content of these fed *Thysanoessa* was 0.11% of the wet weight. Another group of animals starved

TABLE 5. *Carbohydrate content, respiratory rate, and grazing rate for* Neomysis americana. *All animals obtained from Cape Cod Bay 25.VIII.1959*

Date of analysis	Expt.	No. of animals	Carbohydrate content		Respiratory rate		Carbohydrate equivalent, μg glucose/animal day	Grazing rate, ml/animal day	Remarks
			μg/animal	% wet wt	μl/animal day	μl/mg wet wt day			
26.VIII	M_1	15	16.7	0.23	–	–	–	–	Initial
26.VIII	M_2	15	17.3	0.22	–	–	–	–	Initial
27.VIII	M_3	14	15.0	0.20	47.8	6.37	62.8	–	No food, 4°C
27.VIII	M_4	14	14.3	0.20	46.0	7.01	60.4	–	No food, 4°C
27.VIII	M_5	14	12.5	0.21	54.9	9.25	72.1	–	No food, 10°C
27.VIII	M_6	14	13.9	0.20	60.0	8.47	78.8	–	No food, 10°C
27.VIII	M_7	15	13.0	0.19	–	–	–	7.7	Fed *Skeletonema costatum*, 4°C
27.VIII	M_8	15	11.7	0.22	–	–	–	43.0	Fed *Skeletonema costatum*, 4°C

over the same period had a carbohydrate content of only 0.06% wet weight. This latter value has, however, been omitted from Table 4, since the animals were dead or at least moribund before the analysis.

Additional analyses were performed on a few *Meganyctiphanes* and *Thysanoessa* taken in the slope water at about 39°N, 71°30′W on August 18. The animals had been without food for a few days so that the observed values were probably a little lower than expected for fresh material. It will be noted that these *Thysanoessa* were much smaller than the previous group and could have been juveniles or another species.

Despite the few determinations it is probable that the normal carbohydrate level for these two species of euphausids is probably in the vicinity of 0.10% of wet weight or somewhat lower than that observed for *C. finmarchicus* in Cape Cod Bay and in the English Channel (Raymont and Krishnaswamy 1960). The third species of euphausid studied, *Nematoscelis megalops* may contain somewhat more carbohydrate than the others tested (Table 4). The mean value of carbohydrate was 0.13% and the range was not excessively great (0.08 to 0.17%). To some extent this may reflect the fact that almost all determinations were made on one haul of *Nematoscelis* from the slope water south of Woods Hole and that the animals were kept only one day before analysis. Nevertheless, three groups of the animals were kept at a somewhat higher temperature (10°C) which might have been expected to deplete carbohydrate reserves, and one determination was made on a different group of animals which were kept for over one week and only received food for the last 3 days (Table 4). The carbohydrate content in both these experiments, however, was virtually the same as in the other analyses. Although carbohydrate is probably slightly higher in *Nematoscelis* than in the other two euphausids, it still appears to be somewhat below that of copepods such as *C. finmarchicus* from Cape Cod Bay. It would be of interest to learn whether in *Nematoscelis* the carbohydrate level fluctuates appreciably with food supply.

A few experiments made on the mysid *Neomysis americana*, taken in Cape Cod Bay, showed fairly constant carbohydrate values. The amount of glucose per mysid varied between 12 μg and 17 μg but the size of animal used differed considerably so that the values when expressed as percentage of wet weight varied only from 0.19% to 0.23% (Table 5). The mean for all determinations, including animals analyzed within one day of capture, as well as those fed and those starved in the laboratory was 0.21%. The results available suggest that there was practically no effect on carbohydrate level with feeding on phytoplankton for 20 hr or starvation over the

TABLE 6. *Carbohydrate content of certain zooplankton species*

			Carbohydrate content		
Date of capture	Date of analysis	No. of animals	µg per animal	% wet wt	Remarks
Paraeuchaeta					
7.VIII	13.VIII	11 V	3.2	0.07	Little, if any, food taken
7.VIII	13.VIII	12, mostly ♀	9.2	0.10	
7.VIII	20.VIII	30 V	3.7	0.07	
7.VIII	20.VIII	25 ♀	8.0	0.06	
18.VIII 7.VIII	20.VIII	15 ♀	13.3	0.11	
Euthemisto					
7.VIII	11.VIII	7	>110*	>0.25*	Some food consumed
7.VIII	12.VIII	4	128	0.33	
7.VIII	13.VIII	4	166	0.35	
18.VIII	21.VIII	10	28	0.62	
Pleuromamma					
18.VIII	21.VIII	94 V & VI	1.5	0.10	Not fed
Hyperia					
7.VIII	20.VIII	10	24	0.15	Not fed
Conchoecia					
18.VIII	21.VIII	50	7.5	0.31	Not fed

* Reading on spectrophotometer beyond limit of accuracy and sample lost before a dilution was measured.

same period. The mean carbohydrate percentage given for the species *N. americana* (0.21%) agrees well with that previously quoted by Raymont and Krishnaswamy (1960) for *Neomysis integer* from Plymouth, in which fed animals had a mean carbohydrate level of 0.26% of the wet body weight. Previous results with *N. integer,* however, suggested that on some occasions starvation reduced the carbohydrate reserves.

A number of additional observations on the carbohydrate content of other zooplankton animals is shown in Table 6. The carnivorous copepod, *Paraeuchaeta norvegica,* was not observed to eat during these experiments, though it has been observed to eat small copepods on other occasions. The amount of sugars expressed as a percentage of wet weight was among the lowest observed (mean for all experiments 0.08%). Whether a well fed *Paraeuchaeta* fresh from the sea would have an appreciably higher content cannot be stated at this time. A single analysis performed on a group of *Pleuromamma,* mostly stage V and adult, suggested a carbohydrate level near or slightly lower than that observed for *C. finmarchicus.* However, the animals had had no food for 3 days prior to extraction.

Two species of hyperid amphipod known to be carnivorous, *Euthemisto compressa-bispinosa* and *Hyperia galba* were also examined. *Euthemisto* was given some animal food which it appeared to eat. The results (Table 6) suggest a distinctly higher level of carbohydrate exceeding that for the copepods, euphausids and mysids investigated. The percentage of carbohydrate was about 0.34% for two sets of animals which had been in the laboratory for 5 to 6 days, but a higher carbohydrate level exceeding 0.6% of the wet body weight was observed in one group of *Euthemisto* which had been kept for only 3 days in the laboratory. The remarkable difference in the amount of carbohydrate per animal (28 – 166 µg) is explained by the fact that the size of the animals used showed an enormous range in the case of this species. Only a single analysis was made on *Hyperia* and the amount of carbohydrate was much lower (0.15% wet weight). These *Hyperia* had been kept more or less without food for nearly two weeks, however, and it is possible that a recently captured *Hyperia* would have shown a carbohydrate level nearer to that of *Euthemisto.*

The single analysis performed on *Conchoecia* gave a relatively high level of carbohydrate (0.31% of wet weight).

DISCUSSION

It is clear from the preceding data that, among the animals examined here, the presence of a considerable reserve of stored carbohydrate is unlikely. To be sure, some species such as *C. finmarchicus* have a carbohydrate content which varies over rather wide limits while in the case of the euphausids analyzed, the data though probably not conclusive, suggest very little variation. All the animals with the possible exception of *N. americana* are pelagic. It is well known that the distribution of planktonic communities is far from uniform in the sea, and there are marked seasonal variations so that the diets available to these animals probably vary from virtual starvation to vast excess. To some extent pelagic animals must be able to take advantage of the periods of excess to store up food reserves for survival during periods of food scarcity.

In some of these experiments, respiratory rates were obtained for the zooplankton under conditions of starvation at the same time that changes in the carbohydrate content were being determined. If the amount of oxygen taken up by the animals is converted to its carbohydrate equivalent (glucose), it is seen for *C. hyperboreus* (Table 3), *N. megalops* (Table 4) and *N. americana* (Table 5) that several times the total carbohydrate in the animal should have been oxidized assuming a respiratory quotient equal to one, but practically no change in total carbohydrate was observed. It is unfortunate that no respiratory data were obtained for *C. finmarchicus* which showed the greatest variability in carbohydrate reserves among the animals tested. However, if respiration values at 5°C are taken from Marshall and Orr (1958) and converted to carbohydrate oxidized, the amount burned is about 6 μg per day per animal. The average amount of glucose for fed animals is, however, less than 2 μg per copepod, so that once again the daily requirement for respiration is much greater than the total quantity of carbohydrate available. Further, in experiments with starving *Calanus* the greatest daily loss in carbohydrate amounted to about 0.10% of the wet weight. The measurements on Cape Cod Bay *Calanus* made during the past summer suggest an average wet weight of about 0.7 mg per individual. Hence, the maximum carbohydrate loss measured in these experiments is nearly an order of magnitude smaller than the amount predicted from respiration experiments.

In the present series of experiments the content of readily available carbohydrate of a mass culture of *Skeletonema costatum*, the most commonly eaten phytoplankton organism, was also determined to be about 6 μg per 10^6 cells. Hence, in the experiments in which grazing rates were computed it is possible to compare the amount of carbohydrate theoretically oxidized with the maximum carbohydrate which might have been acquired in feeding. The best combination of respiratory and grazing data was obtained for *N. americana.* It can be shown in the case of M_7 and M_8 (Table 5) that 28 × 10^4 and 120 × 10^4 cells respectively were consumed over a period of a day during which time roughly 60 – 80 μg of carbohydrate could have been burned ($M_3 - M_6$, Table 5). Even in the case of M_8, which had the higher grazing rate, the theoretical maximum carbohydrate which it could have acquired was 7.2 μg or one tenth of the amount oxidized.

Even the grazing rate observed for the mysids (43 ml/animal/day, Table 5), however, is not particularly large compared with values given in the literature for other animals. *N. americana* used for these studies was about 10 times as large on a wet weight basis as the *C. finmarchicus* used. Yet the grazing rate computed for *Calanus* in Table 1 was in one instance 70% that of the mysids and never as low as 10%. Grazing rates for *Calanus* from 70 ml to over 200 ml/day have been reported in the literature (Gauld 1951; Harvey 1937). Raymont and Krishnaswamy (1960) found that *N. integer* was cannibalistic in laboratory culture. Possibly *N. americana* would feed more readily if there was some animal protein available.

It is regrettable that grazing rates were not computed for the A *Calanus* series in Table 1 since the increase in carbohydrate with feeding on *Skeletonema* for AS_1 and AS_2 would seem to be significant if the level for A_0 is taken as a base line. However, the fecal pellet production can be used to give a rough estimate of the number of cells consumed. From the B series and E series where both cell counts and fecal pellet counts were made for *Calanus* feeding on *Skeletonema*, an average number of cells per fecal pellet can be determined. (The data for the C series could not be used as *Th. fluviatilis* was the food organism in this case.) The computed values varied from 7,600 cells/fecal pellet to 25,300 with a mean value of 15,800. Using this mean value it can be shown that the AS_1 animals consumed about 762×10^3 cells during the experiment and the AS_2 about $1{,}027 \times 10^3$ cells. With the carbohydrate content for *Skeletonema* mentioned above, carbohydrate income assuming 100% assimilation was about 4.5 μg for AS_1 and 6.2 μg for AS_2. For B_1 the carbohydrate uptake would have been around 5 μg and for the E series it ranged from 1.6 to 4.2 μg/day.

The error in the above calculations is certainly considerable, but it appears that under these experimental conditions, despite the low content of readily available carbohydrate in *Skeletonema*, the intake of food would just about fulfill the daily carbohydrate requirement. However, in the laboratory experiments the cell concentrations fed to the animals were one or two orders of magnitude greater than would be commonly found even in rich coastal waters.

In this study the 6 μg of carbohydrate found per million cells of *Skeletonema* would be equivalent to about 2.4 μg of carbon. Brand (1935) found 45 to 67 μg of carbon per 10^6 cells in *Skeletonema* which suggests that carbohydrate makes up a relatively small percentage of the total organic matter in this diatom. Clearly a *Calanus* could eat considerably fewer than a million *Skeletonema* cells and meet its food requirements, if it utilized the other forms of carbon available in addition to carbohydrate. Of course, when fat and protein in addition to carbohydrate are burned, the carbon requirement per milligram of oxygen used in respiration is also reduced.

There is considerable danger in extending the results of laboratory studies to the open ocean without qualification. However, judging from the existing data the amount of carbohydrate-rich food in the ocean available to the herbivorous zooplankton is not always very great. In 15 analyses of net catches of naturally occurring diatoms and dinoflagellates performed by Brandt and Raben (1919) there was a considerable range in carbohydrate from 0–46%.[3] Conversion of carbohydrate to fat by the zooplankton seems only likely when carbohydrate is very plentiful as it is an energy-consuming process. The reverse conversion of fat to carbohydrate which is then oxidized, or direct oxidation of fat, requires more oxygen than the direct oxidation of carbohydrate, but over twice as much energy is produced per gram of fat oxidized as per gram of carbohydrate. Since oxygen is seldom limiting in the sea whereas organic carbon may be, among the zooplankton in impoverished areas a considerable portion of the metabolic substrate might logically be expected to consist of fat.

It may be that carbohydrates acquired in the food are oxidized directly by the

[3] Brandt and Raben (1919) determined the fat, protein, chitin and ash in their catches and estimated carbohydrate by difference. Therefore, included in their estimates must be some stable polysaccharides such as cellulose and carbohydrates in other combinations. It is still uncertain whether the herbivorous zooplankton can make use of such material. Water and glycerine extracts of *Calanus finmarchicus* showed no evidence for presence of a cellulase (Marshall and Orr, 1955).

zooplankton or are stored briefly in the same chemical form when there is an excess. On the other hand, fats may be oxidized directly when needed or stored as the principal food reserve. Thus a more coastal organism such as *C. finmarchicus* generally living at shallower depths in regions of relatively high organic productivity might be expected to have a rather variable carbohydrate content, while an organism from deep water or the open ocean such as *C. hyperboreus* or *P. norvegica*, and many euphausids might be expected to have a relatively constant carbohydrate content, which would be a function of the rate of conversion of fat to carbohydrate rather than the amount of food consumed.

Certainly the assumption that R.Q. = 1, frequently made by ecologists in trophic calculations, ought to be qualified in the future. Analysis of both fat and carbohydrate content on the same species of zooplankton, together with measurement of oxygen consumption, carbon dioxide production, and nitrogen excretion are essential for a complete picture of zooplankton metabolism, but the present studies form a preliminary contribution to the over-all problem.

REFERENCES

BIGELOW, H. B. 1925. Plankton of the offshore waters of the Gulf of Maine. Bull. U. S. Bur. Fish. **401** pt. II: 509 pp.

BRAND, T. 1935. Methods for the determination of nitrogen and carbon in small amounts of plankton. Biol. Bull. Woods Hole, **69**: 221–232.

BRANDT, K. 1898. Beiträge zur Kenntniss der chemischen Zusammensetzung des Planktons. Wiss. Meeresuntersuch. Ab. Kiel. N. F., **3**: 43–90.

——— AND E. RABEN. 1919. Zur Kenntnis der chemischen Zusammensetzung des Planktons und einiger Bodenorganismen. Wiss. Meeresuntersuch. Ab. Kiel. N. F., **19**: 175–210.

CONOVER, R. J. 1956. Oceanography of Long Island Sound, 1952–1954. VI. Biology of *Acartia clausi* and *A. tonsa*. Bull. Bingham Oceanogr. Coll., **15**: 156–233.

———. 1959. Regional and seasonal variation in the respiratory rate of marine copepods. Limnol. and Oceanogr., **4**: 259–268.

GAULD, D. T. 1951. The grazing rate of planktonic copepods. J. Mar. Biol. Ass. U. K., **29**: 695–706.

HARVEY, H. W. 1937. Note on selective feeding by *Calanus*. J. Mar. Biol. Ass. U. K., **22**: 97–100.

KEMP, A. AND A. J. M. KITS VAN HEIJNINGEN. 1954. A colorimetric micromethod for the determination of glycogen in tissues. J. Biochem., **56**: 646–648.

MARSHALL, S. M. AND A. P. ORR. 1955. The biology of a marine copepod. Oliver and Boyd, Edinburgh. 188 pp.

——— AND ———. 1958. On the biology of *Calanus finmarchicus*. X. Seasonal changes in oxygen consumption. J. Mar. Biol. Ass. U. K., **37**: 459–472.

MENDEL, B., A. KEMP, AND D. K. MYERS. 1954. A colorimetric micromethod for the determination of glucose. J. Biochem., **56**: 639–646.

RAYMONT, J. E. G. AND S. KRISHNASWAMY. 1960. Carbohydrates in some marine plankton animals. J. Mar. Biol. Ass. U. K., **39**: 239–248.

Contribution No. 1118

Made in United States of America
Reprinted from Limnology and Oceanography
Vol. 6, No. 2, April, 1961
pp. 149–153

DIURNAL VARIATIONS IN SOME CHEMICAL AND BIOLOGICAL PROPERTIES OF THE SARGASSO SEA[1]

J. H. Ryther, D. W. Menzel and R. F. Vaccaro
Woods Hole Oceanographic Institution and Bermuda Biological Station

ABSTRACT

Periodic measurements were made during a 24-hr period in the surface layer (0–300 m) of the Sargasso Sea off Bermuda of the following variables: temperature, salinity, phosphate, nitrite, nitrate, chlorophyll, C^{14} assimilation and zooplankton standing crop. Nutrient concentrations, integrated from the surface to 150 m, increased at night and decreased during the day. Chlorophyll concentrations increased during the daylight hours and decreased at night. C^{14} assimilation over 24-hr periods was greater in experiments initiated at night than in those begun in the daytime. Thus changes in the C^{14}/chlorophyll relationship appear to have resulted from variations of both parameters. Zooplankton standing crop (0–200 m) increased markedly during the early evening but subsequently decreased throughout the rest of the night and following day.

Short-term diurnal variations in plant nutrients, phytoplankton chlorophyll, and photosynthetic potential have been reported by several investigators (Doty and Oguri 1957; Yentsch and Ryther 1957; Shimada 1958; Park *et al.* 1958; Bruce and Hood 1960). Seldom, however, have these different variables been observed simultaneously in such studies, and never in the open sea.

The reported variations in the photosynthetic potential were observed by the authors by measuring C^{14} uptake of surface samples taken at different times of the day and placed under constant artificial illumination. On an oceanographic cruise between Bermuda and the West Indies during January–February, 1960, a somewhat different type of photosynthetic periodicity was observed. Productivity measurements were made at 22 stations both by a simulated *in situ* C^{14} technique and by the chlorophyll-radiation method of Ryther and Yentsch (1957). By standard physical and chemical criteria, the surface waters of the area investigated were very similar and primary production, as determined by both methods showed little variability (Ryther and Menzel, *in press*). Nevertheless there was a strong indication that C^{14} uptake in experiments which were begun at night tended to be higher than in those initiated during the daylight hours, despite the fact that all of these measurements were made over a 24-hr period and under natural illumination. This is a rather different situation from that previously reported in which the instantaneous photosynthetic potential, under constant, artificial illumination, was found to vary diurnally. On the other hand, chlorophyll and hence the productivity values calculated from chlorophyll and radiation, were somewhat higher when the former was sampled during the day and lower when sampled at night.

These results, while suggestive, were far from conclusive. Not only did the ship cover a large area geographically, where conditions may have varied significantly, but the "day–night" interpretation is an oversimplification of the fact that most of the daytime stations were occupied in the early morning and most of the night stations early in the evening. To substantiate these findings, it was obviously necessary to make observations at the same location around the clock. To explain the behavior, if observed, corollary measurements of as many related environmental factors as possible were also clearly indicated.

On April 27–28 the authors spent 24-hr aboard the R. V. PANULIRUS at a location 15 miles southeast of Bermuda in 1500 fathoms of water. Earlier studies at this station (Station "S") indicated that conditions there were essentially those of the open Sargasso Sea (*cf.* Menzel and Ryther, 1960). Observations were made every 4 hr at selected depths to 300 m, and the following measurements were made: temperature, salinity (using a conductivity meter constructed at the British National Institute of Oceanography), phosphate (Murphy and Riley 1958), nitrite (Rider and Mellon 1946), nitrate (Mullin and Riley 1955) and chlorophyll, to 150 m only (Richards with Thompson 1952; Creitz and Richards 1955). Primary production was measured by the C^{14} technique (Steemann Nielsen 1952) on samples taken from the depths to which 100, 50, 25, 10 and 1% of the incident radiation penetrated. These samples, with C^{14} added, were incubated for 24 hr in a water-cooled box under neutral density filters transmitting the same fraction of the incident light to which the water was naturally exposed. Due to space limitation in the incubator, these measurements were made only four times, at 1330, 2100, 0030 and 0800 hr, respectively. Incident radiation was measured with an Epply pyrheliometer and this value and the chlorophyll data were used to calculate primary production by the method of Ryther and Yentsch (*loc. cit.*). Samples of zooplankton were obtained by making vertical hauls from 200 m to the surface with a #8 one-meter plankton net.

---

[1] Contribution No. 1118 of the Woods Hole Oceanographic Institution and Contribution No. 282 of the Bermuda Biological Station, under Contract AT(30–1)–2078 with the Atomic Energy Commission and with partial support of NSF Grants G 10693 and G 10709.

The complete results of our study, with the exception of the zooplankton data, are given in Table 1. The observations were

TABLE 1. *Physical, chemical and biological data, 0–300 m, in the Sargasso Sea off Bermuda at six times during a 24-hr period on April 27–28, 1960*

	Depth (m)	T (°C)	Sal. (‰)	σ_t	NO_2–N µg A/L	NO_3–N µg A/L	PO_4–P µg A/L	Chl *a* µg/L	Carbon/assim/m³/day	
									C^{14}	Chl–Rad.
Time: 1330	0	21.30	36.69	25.70	.010	.09	.08	.04	4.1	0.9
	15	20.36	36.62	25.92	.008	.29	.07	.05	3.7	1.6
	25	20.28	36.61	25.94	.008	.14	.05	.06	2.1	1.7
	50	19.58	36.60	26.11	.016	.07		.09	0.6	1.3
	75	19.25	36.59	26.19	.021	.17	.05	.31		
	100	18.82	36.58	26.29	.126	.10	.05	.54	0.4	0.6
	125	18.76	36.58	26.31	.024	.34	.09	.16		
	150	18.72	36.58	26.32	.010	.40	.11			
	200	18.54	36.57	26.36	.040	.31	.10			
	300	18.03	36.49	26.43	.016	.80	.18			
Time: 1600	0	21.06	36.64	25.74	.003	.27	.10	.13		3.0
	15	20.31	36.62	25.93	.010	.02	.07			
	25	20.23	36.62	25.95	.021	.08	.06			
	50	19.52	36.60	26.13	.008	.07	.07	.12		1.8
	75	19.37	36.58	26.15	.008	.16		.22		
	100	18.89	36.58	26.28	.024	.04	.06	.81		0.9
	125	18.76	36.60	26.32	.042	.34	.06	.10		
	150	18.70	36.59	26.33	.018	.45	.09	.07		
	200	18.60	36.58	26.35	.029	.60	.12			
	300	18.07	36.49	26.42	.005	1.73	.21			
Time: 2100	0	21.45	36.65	25.64	.021	.22	.07	.05	5.8	1.2
	15	20.39	36.61	25.90	.008	.09	.07	.05	4.2	1.6
	25	20.31	36.60	25.92	.008	.08	.06	.08	2.8	2.3
	50	19.74	36.60	26.06	.005	.08	.09	.08	0.6	1.2
	75	19.51	36.60	26.12	.003	.17	.07	.09		
	100	19.15	36.57	26.20	.008	.16	.07	.40	0.5	0.5
	125	18.76	36.57	26.30	.137	.20	.10	.65		
	150	18.69	36.57	26.32	.024	.54	.13	.12		
	200	18.53	36.56	26.36	.029	.98	.10			
	300	18.00	36.46	26.42	.021	.84	.25			

TABLE 1 (*Continued*)

	Depth (m)	T (°C)	Sal. (‰)	σ_t	NO_2–N µg A/L	NO_3–N µg A/L	PO_4–P µg A/L	Chl *a* µg/L	Carbon/assim/m³/day	
									C^{14}	Chl–Rad.
Time: 0030	0	21.54	36.62	25.59	.008	.08	.11	.04	4.3	0.9
	15	20.39	36.60	25.89	.003	.12	.07	.05	3.4	1.6
	25	19.87	36.59	26.02	.016	.25	.07	.05	2.8	1.4
	50	19.40	36.59	26.15	.003	.12	.07		1.9	
	75	19.01	36.58	26.24	.013	.09	.06	.24		
	100	18.84	36.58	26.29	.047	.28	.09	.54	0.6	0.6
	125	18.77	36.57	26.30	.032	.22	.09	.31		
	150	18.72	36.57	26.31	.024	.27	.14	.06		
	200	18.63	36.57	26.33	.024	.94	.09			
	300	18.15	36.49	26.40	.010	2.18	.11			
Time: 0400	0	21.00	36.62	25.74	.003	.09	.13	.04		0.9
	15	20.43	36.61	25.89	.003	.15	.09	.05		1.6
	25	20.22	36.63	25.96	.008	.07	.04	.04		1.1
	50	19.27	36.58	26.18	.003	.09	.09	.10		1.5
	75	19.00	36.58	26.25	.008	.11	.06	.41		
	100	18.84	36.58	26.29	.108	.30	.07	.45		0.5
	125	18.75	36.57	26.30	.029	.33	.10	.20		
	150	18.75	36.57	26.30	.023	.84	.14			
	200	18.65	36.57	26.34	.010	1.55	.11			
	300	18.40	36.53	26.36	.013	1.15	.13			
Time: 0800	0	20.98	36.61	25.74	.021	.12	.07	.07	5.0	1.7
	15	20.74	36.61	25.80	.008	.20	.06	.06	4.3	1.9
	25	20.02	36.60	25.99	.018	.30	.05	.06	1.5	1.7
	50	19.34	36.58	26.16	.010	.10		.12	0.9	0.8
	75	18.89	36.58	26.28	.042	.24	.06	.19		
	100	18.78	36.58	26.31	.016	.20		.27	0.9	0.3
	125	18.72	36.57	26.31	.029	.87	.09	.05		
	150	18.69	36.57	26.32	.008	.94	.10	.08		
	200	18.60 ?	36.56	26.34	.028	.33	.17			
	300	18.35 ?	36.53	26.37	.018	.53	.11			

made following the brief spring diatom flowering which is typical of the region (Hulburt *et al.* 1960). Summer conditions had just set in with the surface waters thermally stratified, nutrient impoverished, and sparsely populated with microorganisms. The greatest density of phytoplankton, as indicated by chlorophyll concentrations, occurred at about 100 m, at or near the compensation depth and at the point where the nutrient level begins to increase with depth. Again this situation is representative of summer conditions in the area (Menzel and Ryther *loc. cit.*).

It is under these impoverished conditions that one might expect the greatest response of organisms to daily changes in the environmental factors which critically limit their production. On the other hand, the concentrations of nutrients and phytoplankton and the level of primary production were all so low as to approach the limit of sensitivity of the various methods. For this reason it is difficult to detect and evaluate minor fluctuations in these variables. This is particularly true for individual measurements, but when the quantities and rates are integrated over the depth of the euphotic zone, within which several measurements were made, random errors tend to be cancelled out and a more reliable picture of changes with time is obtained.

Measurements of the extinction coefficient with a submarine photometer revealed that 1% of the incident radiation penetrated to approximately 100 m. We have integrated the nutrient and chlorophyll values to 150 m since the density remained al-

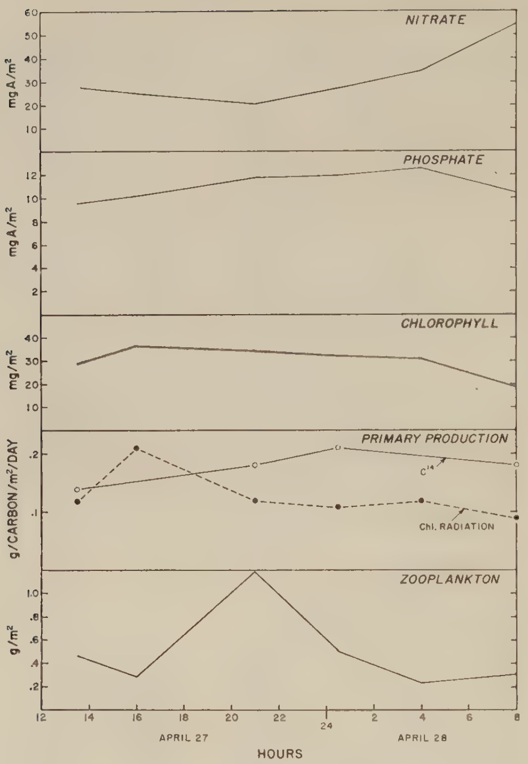

FIG. 1. Diurnal variations in nitrate, phosphate, chlorophyll, primary production and zooplankton standing crop at Station "S", April 27–28, 1960.

most constant at that depth (see Table 1) indicating that there were no appreciable effects of internal waves or other hydrodynamic features. Photosynthesis values were integrated to 100 m, below which our previous investigations have shown no detectable carbon assimilation. The zooplankton standing crop to 200 m was, of course, integrated over that depth by the method of collection. The results are shown in Figure 1.

Integrated nitrite variations were extremely small and irregular with time; hence they are not illustrated. It is noteworthy, however, that nitrite maxima were observed at 100–125 m ($\sigma_t = 26.29 - 26.30$) at the same depth as the chlorophyll maximum, confirming the observations of Vaccaro and Ryther (1960), who attribute this correlation to nitrate reduction by phytoplankton at low light intensities. This nitrite maximum varied from 0.042 to 0.137 μgA/L, but it is difficult to say whether these variations represent diurnal changes or whether the maximum occurs in such a narrow depth band that it was not sampled each time with the same precision.

The concentrations of nitrate and phosphate integrated over 150 m showed significant and systematic changes with time. Both nutrients were higher at night than during the day, but the nitrate reached its highest level at 0800, after increasing throughout the night, while phosphate began to increase in the afternoon, reached a peak at 0400 and decreased between 0400 and 0800 with a periodicity quite similar in time and magnitude to that described by Bruce and Hood (*loc. cit.*). Nitrate ranged from 20 – 55 mgA/m² within the depth studied while phosphate varied only from 9.6 – 12.6 mgA/m². The differences between the maximum and minimum concentrations of nitrate and phosphate were 35 mgA/m² NO_3–N and 3 mgA/m² PO_4–P respectively, a ratio of 12:1. If the phytoplankton assimilate carbon, nitrogen and phosphorus at a ratio of 100:15:1 by atoms (*cf.* Redfield 1934), the calculated daily rate of carbon fixation from the change in nitrate and phosphate would be 2.8 and 3.6 g/m² respectively, figures an order of magnitude higher than the observed production rates reported below. Apparently the exchange of these elements between organisms and water are far more rapid than and independent of the carbon cycle.

The chlorophyll increased during the day to a peak of 37 mg/m² at 1600 and then decreased during the night to a minimum of 19 mg/m² at 0800. Productivity calculated from these chlorophyll values and the radiation for the 24-hr period following the time of sampling, by the method of Ryther and Yentsch (1957) were therefore higher during the day when the chlorophyll concentrations were higher, and lower at night, ranging from 0.09–0.23 gC/m²/day. The C^{14} uptake values, on the other hand, behaved in the opposite way. Though fewer measurements were made, the lowest value (0.12 gC/m²/day) was obtained in the experiment initiated at midday, the highest (0.21 gC/m²/day) at midnight. These results, then, confirm those found by Ryther and Menzel (*loc. cit.*). Since the two methods of estimating production vary independently and oppositely, changes in their mutual interrelationship cannot be attributed to an inconsistency of either method alone. The diurnal increase and nocturnal decrease in chlorophyll is similar to that described in a small polluted estuary (Ryther *et al. loc. cit.*). The most likely explanation is a direct effect of light on the pigment or its synthesis. Why the daily uptake of C^{14} should depend upon the time within the 24-hr cycle that the experiment was started is more difficult to explain. It is clear that there is a daily cycle of available nutrients, but what role, if any, this plays remains obscure.

The standing crop of zooplankton was measured with the thought that the nocturnal migration of animals into the euphotic zone could influence the nutrient concentrations, by their excretions, or the phytoplankton populations, by their grazing activities. Such influences are nowhere obvious. The zooplankton behaved in a curious manner, increasing in abundance by fivefold in the upper 200 m between 1600 and 2000, but subsequently becoming less numerous throughout the night and showing no correlation with either nutrients or chlorophyll.

REFERENCES

Bruce, H. E. and D. W. Hood. 1960. Diurnal inorganic phosphate variations in Texas bays. Publ. Inst. Mar. Sci., **6**: 133–165.

Creitz, G. I. and F. A. Richards. 1955. The estimation and characterization of plankton populations by pigment analyses. III. A note on the use of "millipore" membrane filters in the estimation of plankton pigments. J. Mar. Res., **14**: 211–216.

Doty, M. S. and M. Oguri. 1957. Evidence for a photosynthetic daily periodicity. Limnol. and Oceanogr., **2**: 37–40.

Hulburt, E. M., J. H. Ryther and R. R. L. Guillard. 1960. The phytoplankton of the Sargasso Sea off Bermuda. J. Cons. Internat. Explor. Mer, **25**: 115–128.

Menzel, D. W. and J. H. Ryther. 1960. The annual cycle of primary production in the Sargasso Sea off Bermuda. Deep-Sea Res., (*in press*).

Mullin, J. P. and J. B. Riley. 1955. The spectrophotometric determination of nitrate in natural waters with particular reference to sea water. Analyt. Chim. Acta., **12**: 464–480.

Murphy, J. and J. P. Riley. 1958. Single solution method for determination of soluble phosphate in sea water. J. Mar. Biol. Assoc. U.K., **37**: 9–14.

Park, K., D. W. Hood and H. T. Odum. 1958. Diurnal pH variation in Texas bays, and its application to primary production estimation. Publ. Inst. Mar. Sci., **5**: 47–64.

Redfield, A. C. 1934. On the proportions of organic derivatives in sea water and their relation to the composition of plankton. James Johnstone Memorial Vol., Univ Press, Liverpool. pp. 176–192.

Richards, F. A. with T. G. Thompson. 1952. The estimation and characterization of plankton populations by pigment analyses. II. A spectrophotometric method for the estimation of plankton pigments. J. Mar. Res., **11**: 156–172.

Rider, B. F. and M. G. Mellon. 1946. Colorometric determination of nitrites. Ind. Engin. Chem. Anal. Edit., **18**: 96–99.

Ryther, J. H. and D. W. Menzel. Primary production in the Southwest Sargasso Sea, January–February, 1960. (*in press*).

———. and C. S. Yentsch. 1957. The estimation of phytoplankton production in the ocean from chlorophyll and light data. Limnol. and Oceanogr., **2**: 281–286.

———, ———, E. M. Hulburt and R. F. Vaccaro. 1958. The dynamics of a diatom bloom. Biol. Bull., **115**: 257–268.

Shimada, B. M. 1958. Diurnal fluctuations in photosynthetic rate and chlorophyll "a" content of phytoplankton from Eastern Pacific waters. Limnol. and Oceanogr., **3**: 336–339.

Steemann Nielsen, E. 1952. The use of radioactive carbon (C^{14}) for measuring organic production in the sea. J. Cons. Internat. Explor. Mer, **18**: 117–140.

Vaccaro, R. F. and J. H. Ryther. 1960. Marine phytoplankton and the distribution of nitrite in the sea. J. Cons. Internat. Explor. Mer, **25**: 260–271.

Yentsch, C .S. and J. H. Ryther. 1957. Short-term variations in phytoplankton chlorophyll and their significance. Limnol. and Oceanogr., **2**: 140–142.

Contribution No. 1119

Deep-Sea Research, 1961, Vol. 7, pp. 282 to 288. Pergamon Press Ltd., London. Printed in Great Britain

Annual variations in primary production of the Sargasso Sea off Bermuda*

D. W. MENZEL† and J. H. RYTHER‡

(*Received* 8 *July* 1960)

Abstract—Net and gross primary production, measured at two-week intervals over a period of three years, show annual variations during the winter period (November–April) which are directly related to the degree of mixing of the surface water and may be indirectly attributed to the severity of the winter as revealed by air temperature and wind strength. Seasonal and year-to-year changes were observed in the ratio net : gross production, as indicated by changes in the relationship between C^{14} assimilation and chlorophyll.

SINCE November, 1957 primary production has been measured at a standard oceanographic station (Station ' S ') 15 miles SE of Bermuda in the western Sargasso Sea. Measurements were made initially by means of *in situ* C^{14} experiments, since April, 1958 by a simulated *in situ* technique whereby samples from various depths are incubated on shipboard under neutral density filters which transmit the same fraction of the incident radiation as penetrates to the depths from which the samples were taken. Primary production was also determined from chlorophyll and radiation by the method of RYTHER and YENTSCH (1957), radiation having been established from KIMBALL'S (1928) tables until December, 1958, after which actual measurements were recorded at Bermuda with an Epply pyreheliometer. The annual cycle of primary production and the associated physical and chemical characteristics of the area were described for 1958 by MENZEL and RYTHER (1960), and a more detailed description of methods may be obtained from that publication. The purpose of this report will be to describe the annual cycle of primary production of the same region over two and a half years with emphasis upon variation observed during three winter periods and the conditions responsible for this variability.

C^{14} assimilation by marine plankton algae has been shown to be equivalent to net production (photosynthesis-respiration) while the plants are actively photosynthesizing (RYTHER, 1954). However, the C^{14} method, as conventionally used (cf. MENZEL and RYTHER, *loc. cit.*) includes no correction for night respiration. Only if the latter is small, relative to photosynthesis, do values approximate daily net production.

The chlorophyll-radiation method is based upon total photosynthesis and hence represents gross production, but recognized variability in the relationships between photosynthesis, radiation, and chlorophyll again preclude the possibility of any precise interpretation of the data.

---

*Contribution No. 1119 of the Woods Hole Oceanographic Institution and Contribution No. 275 of the Bermuda Biological Station jointly supported under Contract AT(30-1)–2078 with the Atomic Energy Commission and Contract Nonr–2196(00) with the U.S. Navy, and with partial support of National Science Foundation grant G3234.

†Bermuda Biological Station. ‡Woods Hole Oceanographic Institution.

While the two methods represent the best available experimental techniques for measuring oceanic productivity, at most they provide very rough quantitative estimates of net and gross production. A more reliable application is their use in describing the relative productivity of different oceanic regions or seasonal and geographical trends within a given area. It is primarily to this end that they have been applied in this investigation. Even here, however, inconsistencies in the relationships between variables confuse the picture. The simultaneous use of the two methods serves to demonstrate, if not explain, these inconsistencies, as will be shown. Data obtained by the respective methods will be referred to for convenience, but with the reservations stated above, as net and gross production.

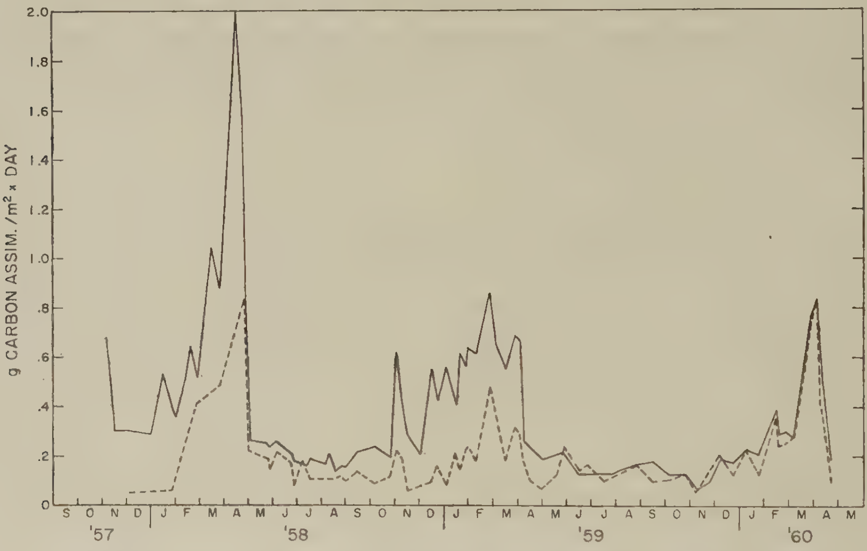

FIG. 1. Gross (solid line) and net (broken line) primary production at Station ' S,' 1957–1960.

Primary production as determined by the two above-mentioned methods from November, 1957 through April, 1960 is shown in Fig. 1. For the sake of consistency, the values obtained by the RYTHER and YENTSCH (*loc. cit.*) method have been based on radiation values taken from KIMBALL'S tables throughout. As previously mentioned solar radiation was recorded daily at Bermuda after December 1958. Values for the days when productivity measurements were made are shown in Fig. 2(A) together with the monthly mean values for the Bermuda latitude from KIMBALL. The latter appear to describe satisfactorily the average radiation but, as might be expected, there were large day-to-day departures from the mean. The effect of using actual radiation data for the day in question in the RYTHER and YENTSCH calculations, as compared to values obtained by using KIMBALL'S mean data, is shown in Fig. 2(B). Despite the relatively large differences in radiation and the resulting productivity calculations on individual days, the overall magnitude and seasonal trend is very nearly the same. Except where there is a need for precise photosynthesis measurements on a particular day, it would appear that the use of KIMBALL'S mean values are adequate for describing productivity within the limits of accuracy of the method.

Productivity during the summers of both 1958 and 1959 was equally low and undistinguished, ranging between about 0·10 and 0·20 g carbon/m²/day by both methods and characteristic of the magnitude of production encountered wherever and whenever surface waters are strongly stratified. It is during the winter period (i.e., November–April) that the greatest production occurs and that variations from year to year become obvious. As discussed in our earlier paper, the high winter levels result from mixing to depths as great as 300 metres and the resulting enrichment of the euphotic layer. Due to the high transparency of the water (k = *ca.* 0·05) and the relatively high incident radiation, the plants are not mixed below the ' critical depth,' the factor held responsible for low winter production further north (SVERDRUP, 1953). Annual production for the calendar years 1958 and 1959 by the chlorophyll-radiation method (gross) was 165 and 103 g carbon/m², by the C^{14} method (net), 77 and 58 g carbon/m² respectively. For the three winter periods (November–April) gross and net production, as so defined, in g carbon/m² were :

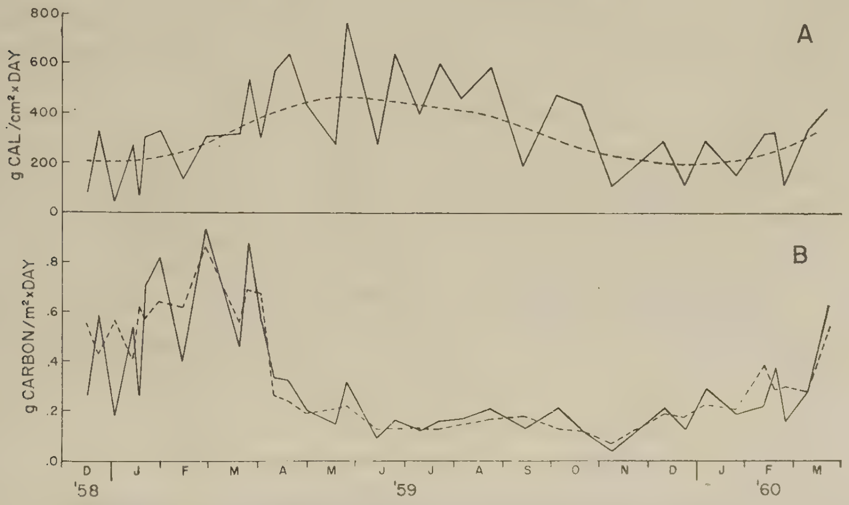

FIG. 2. (A) Incident solar radiation as measured on specific days (solid line) and from the monthly mean values of KIMBALL (1928) (broken line). (B) Gross primary production as calculated from radiation and chlorophyll by the method of RYTHER and YENTSCH (1957) using measured radiation (solid line) and KIMBALL's mean values (broken line).

Period	*Gross*	*Net*
1957–58	127	46
1958–59	90	37
1959–60	55	46

Thus the winter gross production varied in the three-year period by almost three-fold, while net production remained nearly constant. The former is clearly correlated with the degree of surface mixing as illustrated by the proximity to the surface of the wide band of relatively rich water of approximately 18° which overlies the permanent thermocline and underlies the seasonal thermocline (Fig. 3). In 1957–58, water of

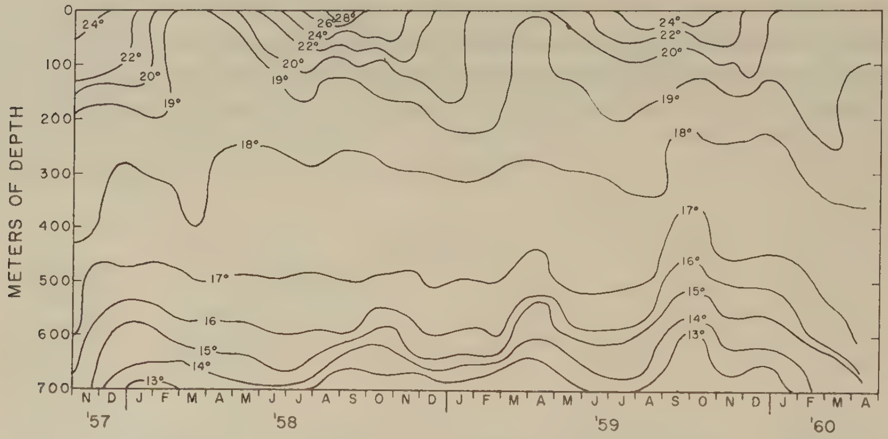

FIG. 3. Vertical profile of temperature in the upper 700 metres at Station 'S,' 1957–1960.

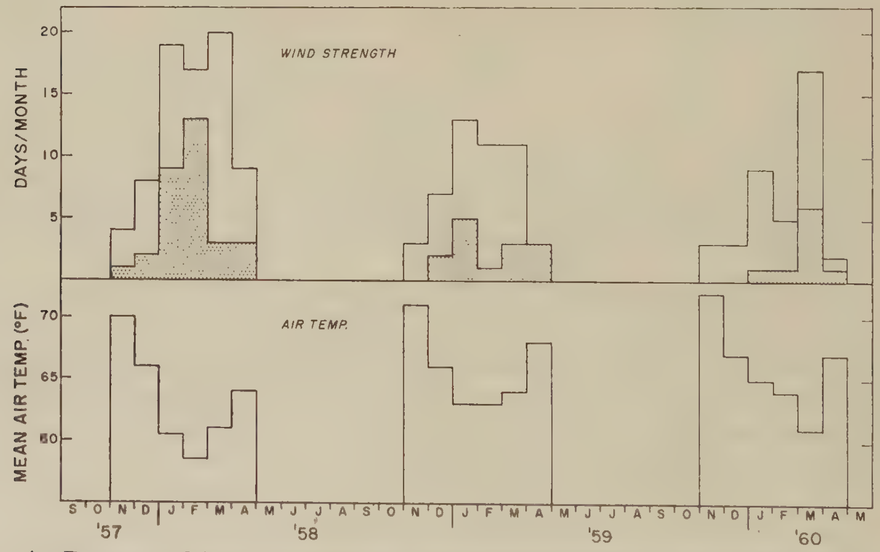

FIG. 4. Frequency of days with maximum wind strength greater than 30 knots (clear bars) and 40 knots (filled bars) and monthly mean temperatures at Bermuda from November through April, 1957–1960.

less than 19° outcropped at the surface, while in 1958–59 and 1959–60 warmer surface waters persisted throughout the winter. The mixing, in turn, appears to be directly related to the severity of the winter, as indicated by the mean air temperatures and maximum wind strengths recorded at U.S. Air Force meteorological station at Kindley Field, Bermuda (Fig. 4). The winter of 1957–58 was colder and had stronger winds than either of the two following winters. That of 1958–59, with relatively mild and uniform weather, had moderately high and uniform productivity. The winter of 1959–60 is particularly interesting since it was initially mild with high temperatures and moderate winds, but became quite severe during March. Not until then did productivity increase to values comparable to those encountered during the previous two winters.

One of the most interesting features of the productivity measurements during the three winter periods is the lack of agreement between the chlorophyll and C^{14} methods, by more than twofold, during 1957–58 and 1958–59 and the almost perfect agreement between them from May, 1959 through April 1960. The reasons for this are not obvious. Experimental techniques have not differed significantly throughout the investigation except for the change-over from *in situ* to simulated *in situ* C^{14} measurements in April, 1958. Chemical and physical characteristics of the water were essentially the same during the three winters. Samples were taken and C^{14} experiments initiated consistently at or near midday, thereby ruling out possible diurnal influences. The species composition of the phytoplankton during 1958, a predominantly coccolithophorid flora dominated by *Coccolithus huxleyi* throughout the winter giving way to a diatom flowering in April (see Hulburt, Ryther and Guillard, 1960) was repeated almost exactly in 1959–60.

To be consistent with our interpretation of the two methods, we would have to state that net production is less than half gross production during the first two winters while the two were nearly equal in 1959–60. While there is no apparent reason for this, an examination of the relationship between C^{14} assimilation and chlorophyll will perhaps shed some light on the problem.

Each value of net production shown in Fig. 1 was obtained by integrating measurements of daily C^{14} uptake at the five depths receiving 100, 50, 25, 10 and 1 per cent of the incident radiation. Chlorophyll measurements were made at the same depths for the calculation of gross production. It is therefore possible to express daily C^{14} uptake per unit of chlorophyll for five different intensities of solar radiation each day productivity measurements were made. When this is done for a single day, a smooth curve is obtained typical of the many photosynthesis-light intensity curves in the literature. However, when these values are compared for different seasons, strikingly different curves are obtained, and the reason why productivity measurements by the two methods agree at some times and not at others becomes at once obvious.

Clearly there was a transition from low ratios of C^{14}/chlorophyll during the winter of 1958–59 through intermediate levels in the spring of 1959 to high values in the summer of 1959 (Fig. 5(A)). Precisely the same seasonal trend has been described for the North Sea by Steele and Baird (in press). It is not difficult to find reasons for this change between summer and winter with variations in temperature, radiation, nutrient levels and phytoplankton species to fall back on as possible causative factors. Steemann Nielsen and Hansen (1959), among others, have pointed out the need to modify the assimilation number (photosynthesis/chlorophyll) for different water masses, populations, etc. Ryther and Menzel (1959) have shown that failure to consider light adaptation by the photoplankton in summer may result in the under-estimation of production as calculated from chlorophyll and radiation. However, it is more difficult to explain differences in the relationship between C^{14}/chlorophyll ratio on two successive winters when physical and chemical conditions and the phytoplankton populations were essentially the same (Fig. 5(B)).

The fact that the C^{14}/chlorophyll ratio does remain almost constant for long periods of time makes it appear that the changes, when they do occur, are not simply due to technical difficulties or errors of measurement. They are undoubtedly real and probably result from some environmental variable too subtle or too complex to be obvious.

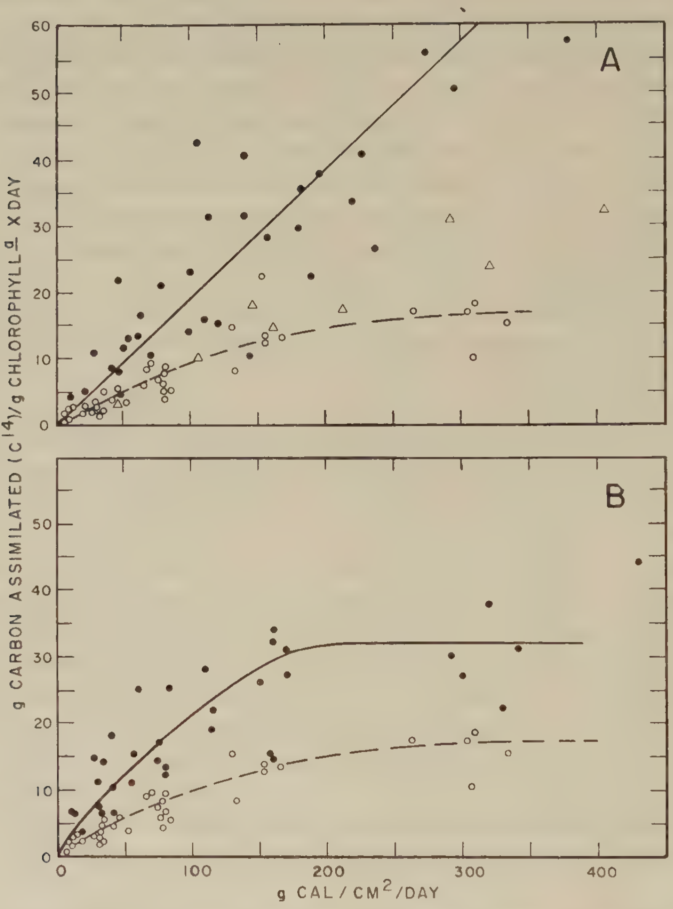

Fig. 5. (A) The ratio of C^{14} uptake/chlorophyll for different values of daily incident radiation during summer (filled circles), spring (triangles) and winter (open circles) for 1958–59. (B) The same for the winter of 1958–59 (open circles) and the winter of 1959–60 (filled circles).

We are left not only with that unanswered problem, but also with the question of whether these changes represent real differences in the relation between net and gross production or merely changes in the relationship between productivity and the criteria we have used to measure it.

REFERENCES

Hulburt E. M., Ryther J. H. and Guillard R. R. L. (1960) The Phytoplankton of the Sargasso Sea off Bermuda. *J. Cons. Internat. Explor. Mer.*, **25**, 115–128.

Kimball H. H. (1928) Amount of solar radiation that reaches the surface on the land and on the sea, and the methods by which it is measured. *Mon. Weath. Rev.*, **56**, 393–398.

Menzel D. W. and Ryther J. H. (1960) The annual cycle of primary production in the Sargasso Sea off Bermuda. *Deep-Sea Res.* **6**, 351–366.

RYTHER J. H. (1954) The ratio of photosynthesis to respiration in marine plankton algae and its effect upon the measurement of productivity. *Deep-Sea Res.* **2**, 134–139.

RYTHER J. H. and YENTSCH C. S. (1957) The estimation of phytoplankton production in the ocean from chlorophyll and light data. *Limnol. and Oceanogr.* **2**, 281–286.

RYTHER J. H. and MENZEL D. W. (1959) Light adaptation by marine phytoplankton. *Limnol. and Oceanogr.* **4**, 492–497.

STEELE J. H. and BAIRD I. E. Relations between production, chlorophyll, and particulate carbon in marine phytoplankton. *Limnol and Oceanogr.* (in press)

STEEMANN NIESLEN E. and HANSEN V. Kr. (1959) Measurements with the Carbon-14 technique of the respiration rates in natural populations of phytoplankton. *Deep-Sea Res.* **5**, 222–223.

SVERDRUP H. U. (1953) On conditions for the vernal blooming of phytoplankton. *J. Cons. Internat. Explor. Mer.*, **18**, 287–295.

Printed in Great Britain by The Salisbury Press Ltd., Publicity House, Wilton Road, Salisbury, Wilts. (27338)

Contribution No. 1120

Reprinted from
BULLETIN OF MARINE SCIENCE
OF THE GULF AND CARIBBEAN
Vol. 11, No. 3, pp. 381-388
SEPTEMBER, 1961

PRIMARY PRODUCTION IN THE SOUTHWEST SARGASSO SEA JANUARY-FEBRUARY, 1960[1]

JOHN H. RYTHER
Woods Hole Oceanographic Institution
AND
DAVID W. MENZEL
Bermuda Biological Station

ABSTRACT

Primary production was measured at 22 stations in the Sargasso Sea South of Bermuda during the winter of 1960. The mean rate of production was 0.05 g carbon assimilated/m^2/day as measured by C^{14} uptake and 0.09 as estimated from chlorophyll and radiation measurements. The low values appear to be typical of the tropical Atlantic and reflect nutrient impoverishment resulting from stratification of the surface layers.

Five-fold variations in solar radiation had little effect upon and showed no correlation with rates of primary production indicating that light is not a limiting or contributing factor at those latitudes.

There are indications of a diurnal periodicity in C^{14} uptake and chlorophyll concentrations, twenty-four hour C^{14} uptake experiments initiated in daytime giving lower values than those begun at night while lower chlorophyll values were measured at night than during daylight.

INTRODUCTION AND METHODS

During the winter of 1960 the authors participated in an oceanographic cruise (R. V. CRAWFORD 37) the primary purpose of which was the investigation of hydrographic conditions in the Sargasso Sea southwest of Bermuda. A total of 33 stations were occupied from Bermuda southeast to approximately 28°N, 48°W and thence southwest to the Windward Islands (Figure 1). Temperatures, salinity and dissolved oxygen (0-260 meters) were measured aboard ship and frozen samples were returned to the Bermuda Biological Station for analysis of nitrite, nitrate and phosphate. Daily incident radiation was measured with an Epply pyrheliometer throughout the cruise.

At 22 stations, including two where hydrographic measurements were not made, primary production was measured by a simulated *in situ* C^{14} technique. Water samples were collected with a non-metallic sampler from depths to which 100, 50, 25, 10 and 1 per cent of the incident radiation penetrated (as determined with a Weston submarine

---

[1] Contribution No. 1120 from the Woods Hole Oceanographic Institution and Contribution No. 293 of the Bermuda Biological Station, under Contract AT (30-1)-2078 and AT (30-1)-1918 with the Atomic Energy Commission, Contract Nonr-2196(00) with the U.S. Navy and with partial support of NSF. Grant B 8339.

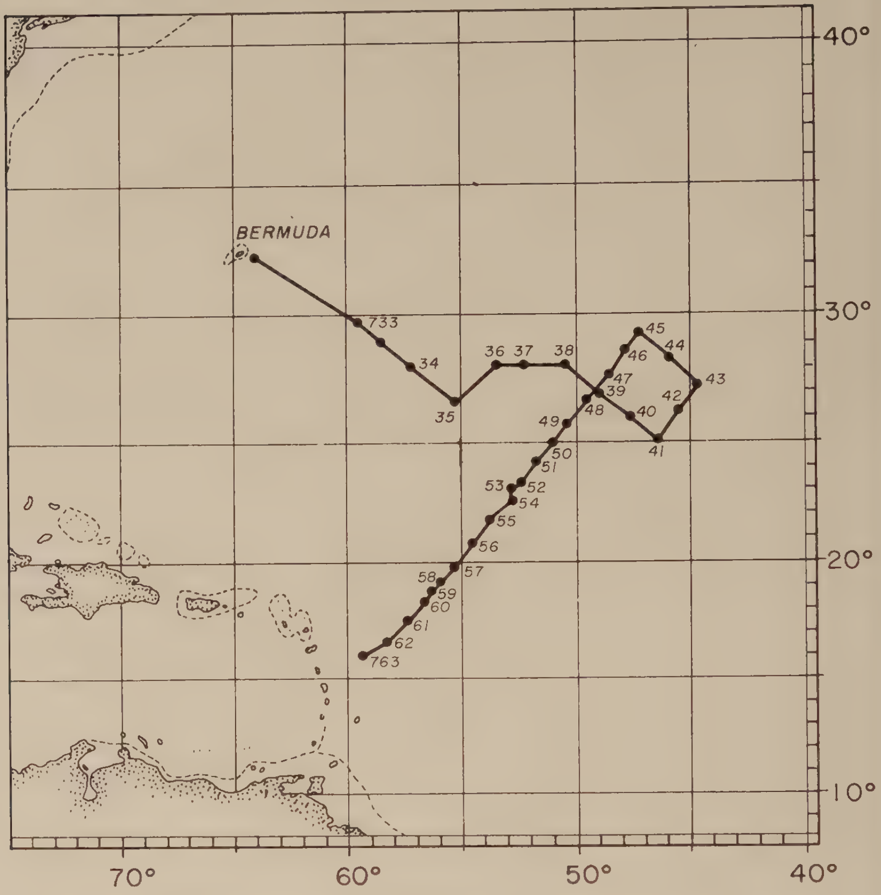
40°
30°
20°
10°
70°
60°
50°
40°
BERMUDA
733
34
35
36
37
38
39
40
41
42
43
44
45
46
47
48
49
50
51
52
53
54
55
56
57
58
59
60
61
62
763

FIGURE 1. Cruise plan of CRAWFORD 37 showing station locations.

photometer). These were dispensed into pyrex bottles, ca. 20μ curies $C^{14}O_3^{=}$ were added, and the bottles were placed in a water-cooled incubator and covered with Kodak wratten neutral density filters which transmitted the same fraction of sunlight to which the water had been naturally exposed. The bottles were so incubated for 24 hours after which treatment was essentially as described by Steemann Nielsen (1952). From the same depths four-liter water samples were collected and filtered for subsequent determination of chlorophyll *a* by the method of Richards with Thompson (1952) as modified by Creitz and Richards (1955). Production was then calculated from chlorophyll *a* concentration and radiation by the method of Ryther and Yentsch (1957). Productivity data by the C^{14} and cholorophyll methods are interpreted as measuring net and gross primary production respectively (Ryther and Yentsch, 1958).

Production in Relation to Latitude

The results of these studies are essentially the same as were found in March, 1959, on a short cruise from Bermuda south to latitude 25°, a distance of about 500 miles (Ryther and Menzel, 1960). At that time high production (ca. 1.00 g carbon/m^2/day by the C^{14} method) was observed near Bermuda where the waters were isothermal and mixed to depths well in excess of the euphotic zone. Just 150 miles south of Bermuda, however, the surface waters were stratified and net production was about 0.10 g carbon/m^2/day, an order of magnitude lower than that found in the Bermuda area.

The investigations made during CRAWFORD 37 were earlier in the winter, covered a much greater area, and were more intensive than those referred to above. On the whole, they confirm the hypothesis

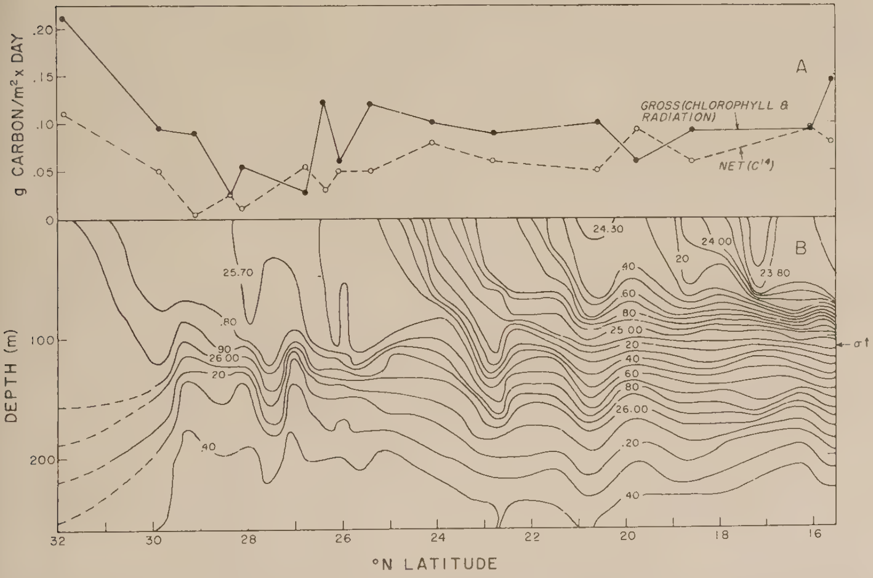

FIGURE 2. A. Gross (closed circles, solid line) and net (open circles, broken line) primary production. B. Vertical profile of density (σ_t) in the surface water as related to latitude on CRAWFORD 37.

that, due to stratification of the euphotic layer (0-100 meters), winter production in the tropical Atlantic is low and relatively constant.

The highest levels of net and gross production (0.12 and 0.21 g cargon /m²/day respectively) were observed just off Bermuda (32°N). South of this, from about 30°N to 15°N, production fell to appreciably lower values which showed minor fluctuations but did not vary latitudinally in any obvious systematic way (Figure 2 A). Mean net and gross production for all stations excluding the first were 0.05 and 0.09 g carbon/m²/day respectively.

The vertical density profile from 0-260 meters illustrates that the euphotic layer is unstratified in the Bermuda area, rather weakly stratified from 30° to about 25°, and very strongly stratified from there to the southern end of the section (Figure 2 B). Apparently the presence and not the degree of stratification is the important controlling factor since there appears to be little correlation between the intensity of stratification and productivity south of Bermuda.

The stratification of the sub-surface waters south of 25° is partly thermal but is also due in large part to the presence of a layer of high salinity water, often exceeding 37.00‰, centered at about 100 meters. This water is believed to be formed in winter at the surface roughly in the area described by 25-30°N, 45-50°W due to the combined effects of cooling and evaporation. This denser water sinks to about 100 meters and spreads to the south and west (L. V. Worthington, personal communication). The concerted effort made in that area (Figure 1) represented an unsuccessful attempt to observe this convergence in action, but some of the high salinity water had apparently been formed earlier in the season.

THE EFFECTS OF VARYING INTENSITIES OF INCIDENT RADIATION

Day-to-day changes in the weather caused incident radiation to vary during the cruise between 70 and 380 g cal/cm²/day. Within this five-fold range, net production as measured by C^{14} uptake showed very little change and no correlation with radiation. Gross production, determined from chlorophyll and radiation, necessarily showed some relation to the latter, but variation in chlorophyll concentration, quantitatively more important in the calculation, prevented a close correlation even here (Figure 3). These observations substantiate the hypotheses that, although light may be critical at higher latitudes, nutrients are the primary limiting factor in the tropics and almost completely obscure any minor effects of varying radiation (Steemann Nielsen and Jensen, 1957).

Diurnal Periodicity in Net and Gross Production

Excluding the first station off Bermuda, 21 productivity measurements were made, 12 during the daylight hours and 9 at night. Of the

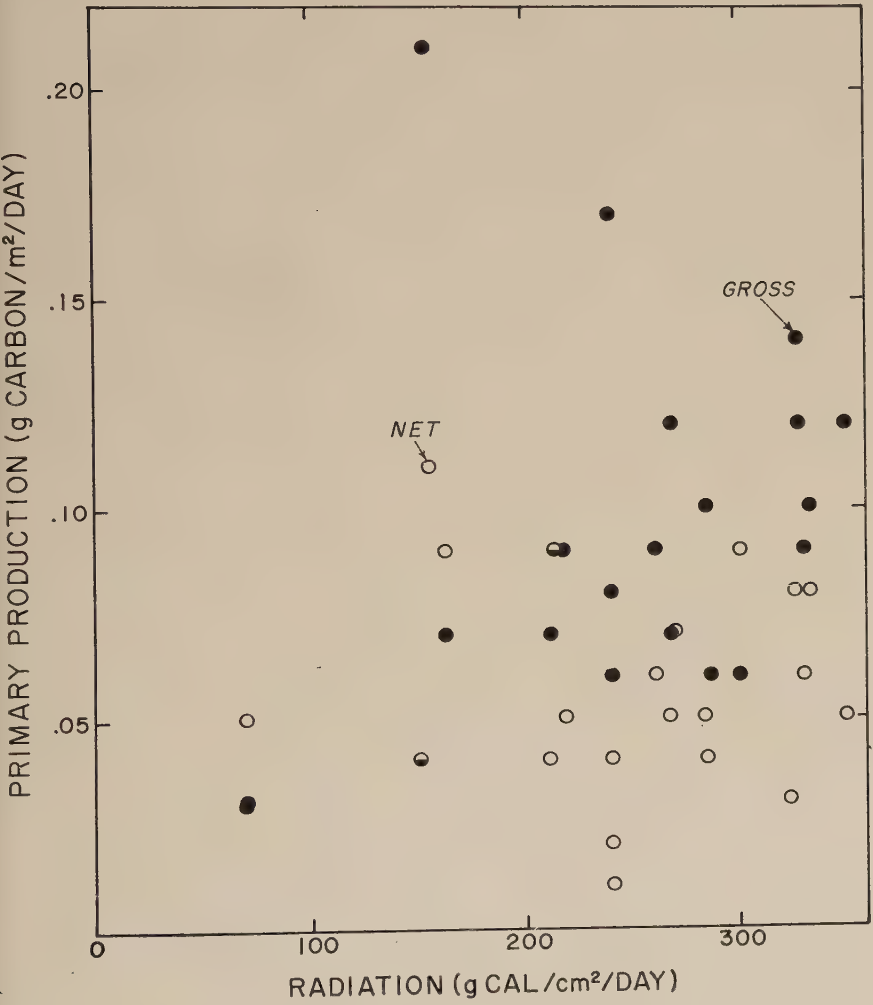

Figure 3. Gross (closed circles) and net (open circles) primary production as related to incident solar radiation.

12 daylight stations, 9 (75%) of the resulting C^{14} productivity values fell below the mean for all the stations, while 8 (67%) of the chlorophyll-based productivity values exceeded the mean. Of the 9 night stations, 6 (67%) of the C^{14} values exceeded the mean and 6 (67%) of the chlorophyll productivity values fell below the mean. While the quantitative aspects of these ratios are probably meaningless, the consistency of their trend suggests that C^{14} uptake is higher when experiments are begun at night than in the day while chlorophyll behaves in the opposite manner. It may be pointed out here that, although gross production is determined from the instantaneous concentration of chlorophyll at the time of sampling, net production is based upon C^{14} uptake over 24 hours. We had assumed that 24-hour measurements would avoid the problem of a diurnal periodicity in C^{14} uptake as described by Doty and Oguri (1957), Yentsch and Ryther (1957) and Shimada (1958). Apparently, however, daily C^{14} assimilation is dependent at least to some extent upon the time of day the measurements are initiated. This is one explanation for the minor variations in productivity in a region which appears to be otherwise homogeneous.

Since daily C^{14} uptake was measured at five intensities of radiation and we have chlorophyll concentrations from the corresponding depths at each productivity station, it is possible to plot C^{14} uptake per unit of chlorophyll for a wide range of light intensities. When this is done separately for all stations occupied at approximately 0800, 1200 and 2000 hours (Figure 4) it is clear, despite some unaccountable departures, that the majority of points describe a relationship between the two variables which varies appreciably throughout the day. This relationship was consistent from station-to-station with no indication of geographical variability. The six low carbon/chlorophyll ratios at high radiation values at 2000 were surface samples which may reflect the effects of light inhibition in those samples. Otherwise, no systematic variations with depth could be detected.

We have observed a similar change in the C^{14}/chlorophyll relationship from season to season and from year to year at a single station off Bermuda (Menzel and Ryther, 1960). Although this could not be explained, it was believed to have resulted from some systematic change in either C^{14} uptake or chlorophyll relative to the other. We are no nearer an explanation of this phenomenon now, but in view of what appears to be independent variations in C^{14} assimilation and chlorophyll at the same time but in opposite directions, inconsistencies in the

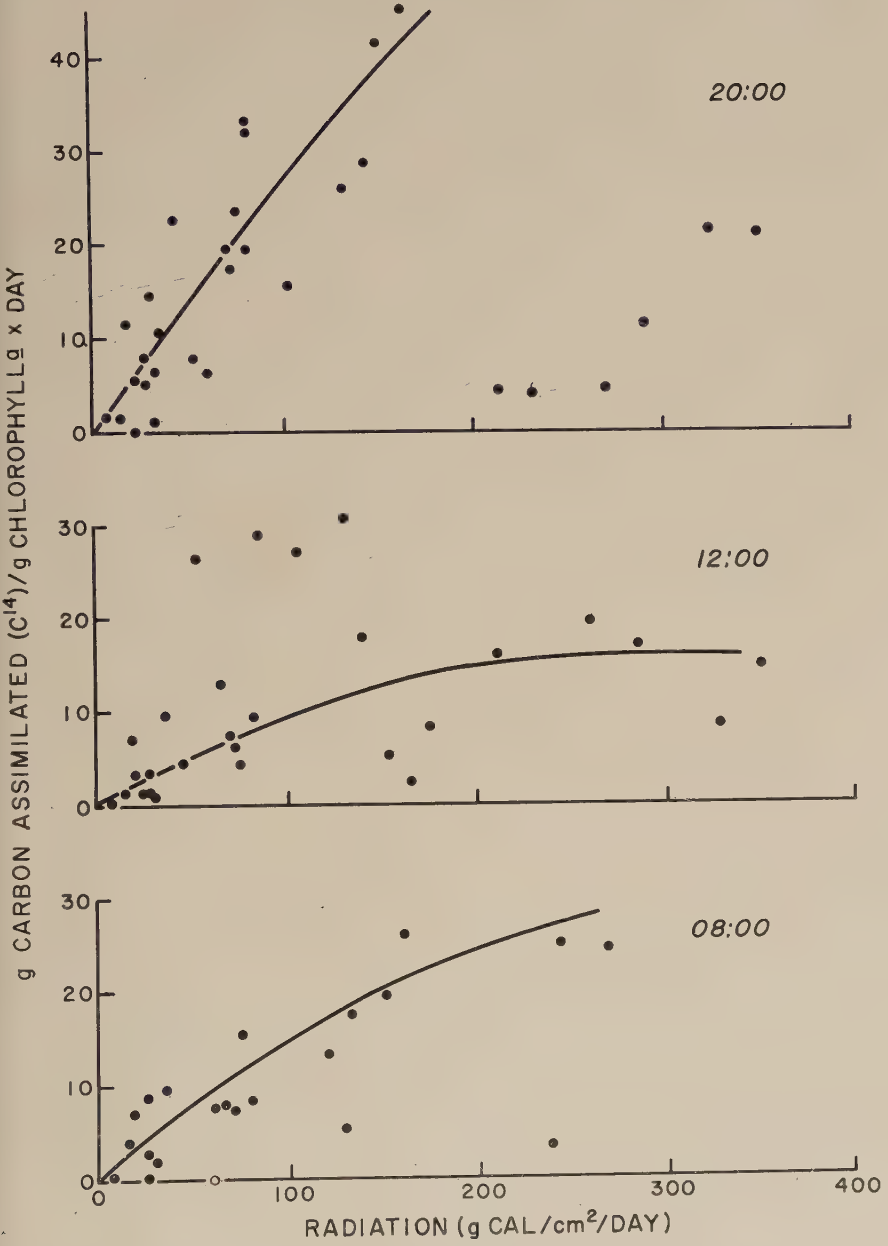

FIGURE 4. The ratio of C^{14} assimilation/chlorophyll as a function of the intensity of solar radiation in experiments initiated at different times of day.

relationship between net and gross production, as determined here, may result from changes in both chlorophyll and C^{14} uptake relative to each other. While these diurnal and seasonal irregularities in the criteria for determining productivity clearly warrant further investigation, the errors which they introduce appear to be of second order magnitude and are important only where very precise knowledge is required of the magnitude and variability of primary production.

LITERATURE CITED

CREITZ, G. I. AND F. A. RICHARDS
1955. The estimation and characterization of plankton populations by pigment analyses III. A note on the use of "millipore" membrane filters in the estimation of plankton pigments. J. Mar. Res., *14:* 211-216.

DOTY, M. S. AND M. OGURI
1957. Evidence for a photosynthetic daily periodicity. Limnol. and Oceanogr. 2: 37-40.

MENZEL, D. W. AND J. H. RYTHER
1960. Annual variations in primary production of the Sargasso Sea off Bermuda. Deep-Sea Res. 6: 351-367.

RICHARDS, F. A. WITH T. G. THOMPSON
1952. The estimation and characterization of plankton populations by pigment analyses II. A spectrophotometric method for the estimation of plankton pigments. J. Mar. Res., *11:* 156-172.

RYTHER, J. H. AND D. W. MENZEL
1960. The seasonal and geographical range of primary production in the Western Sargasso Sea. Deep-Sea Res., *6:* 235-238.

RYTHER, J. H. AND C. S. YENTSCH
1957. The estimation of phyto-plankton production in the ocean from chlorophyll and light data. Limnol. and Oceanogr., *2:* 281-286.

RYTHER, J. H. AND C. S. YENTSCH
1958. Primary production of continental shelf waters off New York. Limnol. and Oceanogr., *3:* 327-335.

SHIMADA, B. M.
1958. Diurnal fluctuations in photosynthetic rate and chlorophyll "a" content of phytoplankton from Eastern Pacific waters. Limnol. and Oceanogr., *3:* 336-339.

STEEMANN NIELSEN, E.
1952. The use of radioactive carbon (C^{14}) for measuring organic production in the sea. J. Cons. Internat. Explor. Mer., *18:* 117-140.

STEEMANN NIELSEN, E. AND E. A. JENSEN
1957. Primary oceanic production, the autotrophic production of organic matter in the oceans. Galathea Rept., *1:* 49-136.

YENTSCH, C. S. AND J. H. RYTHER
1957. Short-term variations in phytoplankton chlorophyll and their significance. Limnol. and Oceanogr., *2:* 140-142.

Contribution No. 1121

Zooplankton in the Sargasso Sea off Bermuda and its Relation to Organic Production[1])

By

David W. Menzel
Bermuda Biological Station

and

John H. Ryther
Woods Hole Oceanographic Institution

Introduction

Zooplankton studies in the Sargasso Sea have been largely restricted to such collections and observations as were possible during oceanographic cruises crossing the area. While they have provided information concerning the abundance of animals at scattered times and places (e.g., LEAVITT, 1935, 1938; CLARKE, 1940; RILEY and GORGY, 1948), these investigations were not adequate for the purpose of describing seasonal cycles or even for establishing the fact that such cycles exist. More intensive studies by MOORE (1949) suggest that maximum populations occur in the spring, but even they do not encompass a sufficiently long period of time to provide a complete picture of seasonal trends.

Data collected during a period of 30 months from a total of 52 plankton tows, as part of an investigation of the plankton ecology of the Sargasso Sea off Bermuda, has now made it possible to define more clearly the seasonal cycle of zooplankton of this region. Correlary studies (MENZEL and RYTHER, 1960) permit a comparison to be made between primary organic production and the abundance and metabolic requirements of the zooplankton populations. While it is our intention, with the assistance of specialists, to enumerate and describe separately at least the quantitatively important components of the zooplankton, work upon that aspect of the problem has not yet progressed to the point where it warrants discussion here. This report, then, will be limited to a consideration of dynamic aspects of the zooplankton as treated collectively in terms of volume and weight.

---

[1]) Contribution No. 288 of the Bermuda Biological Station and Contribution No. 1121 of the Woods Hole Oceanographic Institution supported under Contract AT (30–1)–2078 with the Atomic Energy Commission.

Methods

Collections were made routinely, at intervals of approximately two weeks, at a station located 15 miles SE of Bermuda in 1500 fathoms of water. Standard oblique tows were made from a depth of 500 m, using a 0·75 m No. 2 plankton net with a meter wheel mounted in its mouth. Depth was estimated from wire angle. From time to time special tows were made with opening and closing nets at selected depth intervals to 2000 m, and on other occasions the standard No. 2 net was towed together with No. 8 or No. 20 nets for comparative purposes.

The samples were first split, half being saved for taxonomic studies. Displacement volume, dry weight, and ash-free dry weight of the second half were determined as indices of standing crop. Volumes were determined by the method of YENTSCH and HEBARD (1957). After volume measurements the samples were dried to constant weight at 60°C and then combusted in a muffle furnace at 800°C for determinations of dry weight and ash content respectively.

Comparative tows with nets of different mesh size

A series of simultaneous oblique (500–0 m) tows were made to compare the catching ability of No. 2 nets (0·366 mm aperture) with No. 8 (0·203 mm aperture) and No. 20 (0·076 mm aperture) nets. The results are given in Figure 1 in terms of displacement volume and ash-free dry weight of the paired tows. In general the plankton volumes taken by the different nets were remarkably similar, with no consistent differences between Nos. 2, 8, and/or 20 mesh. The ash-free dry weights (i.e., organic content) of tows made with Nos. 2 and 8 nets also did not differ significantly, but the weights of samples taken by the No. 20 net averaged 60% greater than that obtained by the No. 2 net.

The species composition of the plankton taken by nets of different mesh size has not yet been studied, but superficial examination of No. 2 net and No. 20 net tows revealed obvious differences in the respective populations. The finer net consistently caught more smaller organisms, particularly crustacea, as would be expected, but at the same time it captured far less of the larger animals (e.g., chaetognaths, siphonophores, medusae, fish larvae, etc.). The reason for this is not clear. It may be related to differences in the turbulence at the mouth of the two nets. However, essentially the same volumes were filtered by Nos. 2 and 20 nets, at least as far as was indicated by the net flow meters. The greater proportion of water in the larger gelatinous organisms, as compared to microcrustacea for example, undoubtedly explains the greater ash-free dry weight of the samples taken with the No. 20 nets.

Vertical Distribution

All plankton tows made during this investigation were taken during daylight hours, usually near mid-day. While the effects of diurnal migration were thereby held more or less constant, migratory animals could be expected to be located at or near their maximum depths when the samples were obtained. The main scattering layer in the Bermuda area lies at 400–600 m in daytime and the deep scattering layers may extend to 1000 m or more (MOORE, 1950).

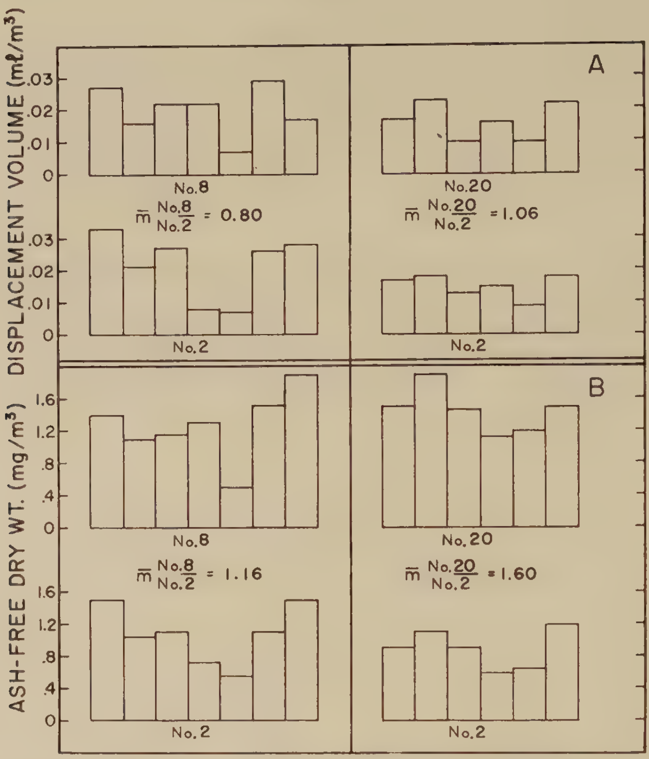

Figure 1. The comparison between (A) displacement volume and (B) ash-free dry weight of paired plankton tows with No. 2 versus No. 8 and No. 2 versus No. 20 mesh plankton nets.

Table 1

Vertical distribution of zooplankton

Depth interval (m)	Dry weight/depth interval (g)			Dry weight/m³ (mg)		
	June	Aug.	Feb.	June	Aug.	Feb.*
0– 100	0·49	0·19	0·17	4·92	1·90	1·16
100– 200	0·20	0·06	0·08	1·96	0·64	0·82
200– 300	0·12	0·06	0·15	1·22	0·61	1·46
300– 400	0·10	0·05	0·09	1·05	0·49	0·95
400– 500	0·09	0·15	0·09	0·93	1·54	0·93
500–1000*	0·77	0·35	0·90	1·55	0·69	1·21
1000–2000*	1·34	0·23	0·51	1·34	0·23	0·68
Total (g/m²)	3·11	1·09	1·99			
Mean (mg/m³)				1·85	0·87	1·03
% below 500 m	67·7	52·6	70·6			

---

* Depth intervals in February: 500 – 1250, 1250 – 2000 m.

To see whether our routine 500 m tows were missing a significant fraction of the zooplankton, and to investigate the vertical distribution of the organisms within discrete depth intervals, a series of tows were made with an opening and closing net, using essentially the same device as described by LEAVITT (1935), at depth intervals of 0–100, 100–200, 200–300, 300–400, 400–500, 500–1000, and 1000–2000 m. The results of three such series made in June and August 1959 and February 1960 (Table 1) reveal that an average of 63% of the zooplankton dry weight between 0 and 2000 m occurred below 500 m. The depth distribution of the zooplankton in terms of displacement volume and ash-free dry weight was almost idential to that found for dry weight, indicating that the major types of animals did not change greatly with depth.

The results of the three series were relatively consistent internally and in close agreement with LEAVITT (1938, Figure 4) who found an average of 59% of the plankton from 0–2000 m below 500 m in the Sargasso Sea north of Bermuda. Small to negligible fractions of the plankton were found by LEAVITT below 2000 m. Hence the values obtained by the standard 0–500 m tows may be increased by a factor of 2·75 to obtain an estimate of the total standing crop of zooplankton.

The Seasonal Cycle of Zooplankton Abundance

Zooplankton standing crops, in terms of displacement volume, dry weight, and ash-free dry weight beneath a square metre of surface as determined by the standard 0–500 m tows from November 1957 through April 1960 are reported in Table 2. The mean ratio for all the tows of displacement volume: dry weight: ash-free dry weight is 18:1·4:1.

For purposes of illustration, the seasonal cycle of zooplankton in terms of dry weight (0–500 m) is shown in Figure 2. It is clear that a spring maximum occurred during each of the three years. The magnitude and timing of these maxima paralleled to a close degree the spring flowering of phytoplankton, as will be discussed below. The spring maximum of 1958 (8·4 g/m^2) far exceeded those observed the following two years. Except for the spring period (March–June) the standing crop was low and almost constant, averaging less than 1·0 g/m^2, with no evidence of an autumn maximum.

Respiratory Requirement of the Zooplankton

Mixed zooplankton tows were diluted, dispensed in bottles and their oxygen consumption measured for periods of time ranging from 3 to 18 hours. A total of 55 measurements was made at eight times of the year (Table 3). Oxygen consumption was converted to carbon utilization assuming RQ = 1·0 and respiration is expressed as grammes carbon per gramme dry weight of zooplankton per day. There is considerable variability in the results, but no systematic variation with temperature was evident. The mean respiratory rate for 55 individual measurements was 0·125 g carbon/g zooplankton/day. The mean respiratory rate of a number of different marine zooplankton organisms, mainly copepods, reported in the literature is 0·103 g carbon/g zooplankton/day (Table 5), in good agreement with our results.

In view of the findings of CUSHING (1960) to the effect that the filtering rate

Table 2

Standing crop of zooplankton as determined from standard 0–500 m oblique tows with 0·75 m No. 2 net.

Date	Displacement volume (ml/m²)	Dry weight (g/m²)	Ash-free dry weight (g/m²)
1957			
Nov. 19	7·5	1·32	0·42
Dec. 3	8·0	0·47	0·13
1958			
Jan. 14	9·0	0·54	0·24
Jan. 30	8·5	0·94	0·32
Feb. 11	18·0	2·51	0·45
Feb. 22	12·0	0·89	0·18
Mar. 25	86·0	5·97	3·57
Apr. 21	106·5	8·43	5·84
Apr. 29	21·5	1·83	1·42
May 19	7·0	1·05	0·39
June 4	5·5	1·00	0·30
June 18	12·5	1·44	0·94
July 2	10·0	0·81	0·74
Aug. 5	7·0	0·46	0·41
Aug. 18	13·5	1·16	0·96
Aug. 30	8·5	0·61	0·52
Sept. 15	9·5	0·57	0·48
Oct. 2	9·5	0·59	0·53
Oct. 18	10·0	0·70	0·58
Nov. 1	5·0	0·43	0·36
Nov. 14	14·0	0·88	0·79
Dec. 2	6·0	0·37	0·34
1959			
Jan. 2	9·0	0·66	0·58
Jan. 30	7·0	0·55	0·50
Feb. 26	11·5	0·65	0·57
Mar. 25	23·5	1·95	1·75
Apr. 7	24·0	1·36	1·13
Apr. 17	12·0	0·88	0·78
Apr. 30	9·5	0·61	0·50
May 18	15·5	0·96	0·76
May 28	12·5	0·92	0·73
June 12	16·5	0·96	0·76
June 26	10·5	0·66	0·53
July 10	9·0	0·56	0·46
July 22	12·5	0·91	0·76
Aug. 5	18·5	0·74	0·55
Aug. 25	9·0	0·71	0·56
Sept. 14	6·5	0·55	0·45
Oct. 6	5·5	0·44	0·88
Oct. 27	4·0	0·37	0·34
Nov. 8	5·5	0·46	0·37
Nov. 24	4·5	0·35	0·28
Dec. 10	13·0	0·83	0·60
Dec. 21	8·0	0·61	0·46
1960			
Jan. 5	7·5	0·39	0·30
Jan. 27	4·5	0·41	0·32
Feb. 2	9·5	0·59	0·44
Feb. 25	14·0	0·95	0·76
Mar. 8	16·5	1·21	0·89
Mar. 24	12·5	0·96	0·74
Apr. 7	17·5	1·32	1·09
Apr. 20	13·5	0·98	0·78
Mean	14·0	1·08	0·75

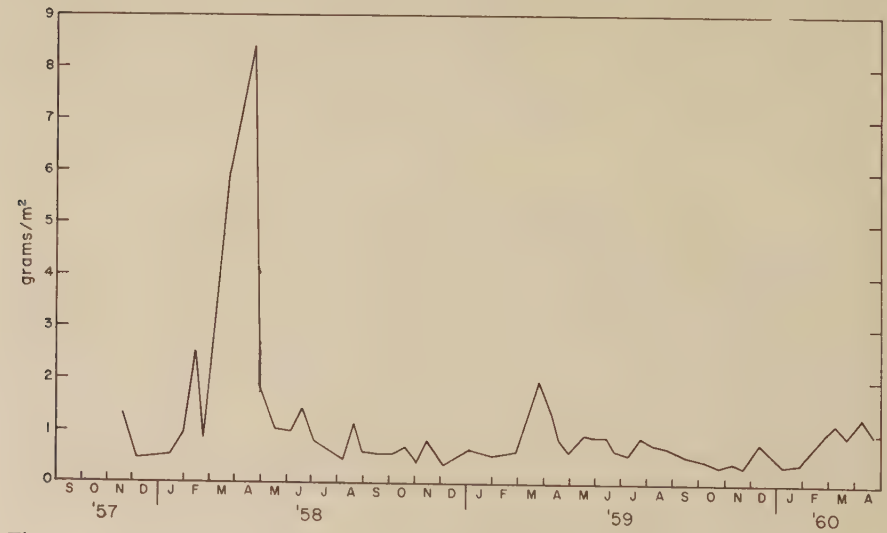

Figure 2. Dry weight of zooplankton from No. 2 mesh, 0·75 m, 0–500 m plankton tows, 1957–1960.

Table 3

Respiration of mixed zooplankton samples

Date	Temperature (°C)	Experiment length (hrs)	Number of measurements	Mean respiration (mgC/zooplankton/day)
1959				
Apr. 27	20·6	5	5	0·046
July 1	28·0	5	3	0·098
July 8	27·5	2	3	0·079
July 27	28·0	4	4	0·080
Aug.21	29·0	3·5	4	0·077
Oct. 28	25·0	5	4	0·123
Nov. 18	24·0	18	20	0·227
1960				
Apr. 19	20·0	3	12	0·087
			Mean	0·125

Table 4

Effect of the volume of container on the respiratory rate of mixed zooplankton, 18 hour experiment, 18. Nov. 1959, temperature 24·0°C

Volume container (ml)	Number of measurements	Mean respiration (mg C/mg zooplankton/day)
125	4	0·167
250	5	0·215
500	5	0·275
1000	3	0·239
2000	3	0·236

of marine zooplankton is proportional to the size of the experimental container, an experiment was carried out to determine whether respiration also is influenced by the volume of the experimental vessel (Table 4). For this experiment, individual copepods (*Paracalanus* sp. and *Labidocera* sp.) were selected out of a plankton tow and added to the vessels in numbers calculated to give the same density in every case. The density was lower than in the other experiments reported in Table 3, the experimental period considerably longer, and the resulting respiration rates appreciably higher. Below an experimental volume of 500 ml, there did appear to be reduction in the respiratory rates with the size of the vessel, but at 500 ml and above respiration remained relatively constant. The other measurements reported here were carried out in one litre containers.

It was intended that the experimental respiratory data be extrapolated to the environment in order to obtain an estimate of the metabolic requirement of natural zooplankton populations. In so doing, it seemed futile to attempt to correct respiration for temperature effects since the animals are distributed vertically within a temperature range which exceeds the seasonal range at the surface and migrate diurnally up and down within this range. The failure to observe any clear-cut temperature relation to respiration in our measurements, probably because of the crudity of the experiments, but possibly also due to temperature adaptation by the organisms, made it still easier to ignore this factor. We have therefore used a mean daily metabolic requirement in terms of carbon, of 12% of the dry weight of the zooplankton.

Table 5

Summary of reported respiratory rates of marine zooplankton
Carbon requirement calculated from oxygen consumption assuming RQ = 1·0

Organism	Reference	Respiration (g carbon/g zooplankton/day)
Calanus finmarchicus	MARSHALL *et al.* (1935)	0·026*
Centropages hamatus	ZEUTHEN (1947)	0·096*
Centropages hamatus	GAULD and RAYMONT (1953)	0·092*
Acartia clausi	CONOVER (1956)	0·116*
Acartia tonsa	CONOVER (1956)	0.154*
Marine copepods	ZEUTHEN (1947)	0·120*
Mixed zooplankton	RILEY and GORGY (1948)	0·120
	Mean	0·103

---

* Quoted from RICHMAN (1958) as recalculations of original data for 20°C assuming RQ = 1.

Net primary organic production and zooplankton metabolic requirements

Net primary organic production has been measured by the ^{14}C technique each time zooplankton tows were made, and has been discussed elsewhere (MENZEL and RYTHER, 1960, in press). The values are reproduced here (Figure 3), together with estimated values for zooplankton respiration (12% of the dry weight) based upon both measured standing crop (0–500 m) and estimated total standing crop (0–2000 m) obtained by multiplying the former by 2·75 as discussed above. It is assumed that the total respiratory requirement of the zooplankton populations falls within the range described by these two limits.

During most of the three-year period there was a striking agreement between net organic production and the metabolic requirement of the zooplankton. Clearly, the zooplankton is closely controlled by the availability of food during most of the year. The two high zooplankton values in March and April 1958, have been reported but are considered suspect since the volumes indicated by the net flow meter were exceptionally low. Without question there was a population maximum at that time but it is quite possible that gelatinous animals interfered with the turning of the meter, exaggerating the magnitude of the standing crop. Other than those values, the zooplankton appear to be closely controlled by the level of primary production, the spring flowerings of 1959 and 1960 being accompanied or closely followed by zooplankton maxima. The minor fluctuations in both zooplankton and primary production are probably no more than errors in measurement but may indicate short-term variations in both populations which are too rapid to be mutually influential. For example, there is the suggestion in the spring of 1960 that the short-lived high peak of primary production came and went too quickly to be reflected by the more slowly responding animal population.

In the relatively oligotrophic Sargasso Sea, then, there is little evidence of food surplus and wastage by the zooplankton, as has been proposed for more northern waters (e.g., HARVEY *et al.*, 1935; CUSHING, 1959). In the latter region, primary production is held in check by winter mixing and the resulting limitation of light. Nutrient levels within the euphotic zone far exceed anything observed in the Sargasso Sea. When stability of the surface layer permits phytoplankton growth, the spring bloom appears suddenly and the availability of algal food is

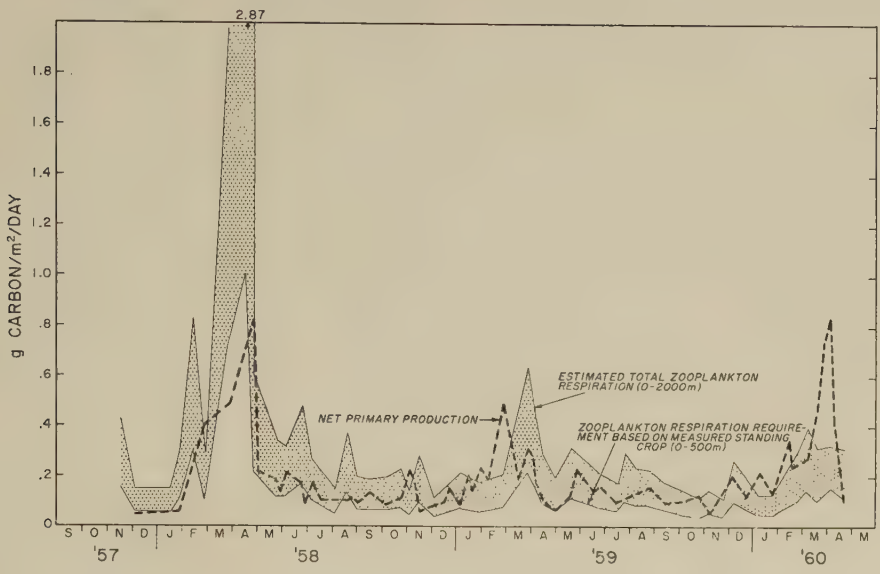

Figure 3. The relation between net primary production (broken line) and the metabolic requirement of the zooplankton represented as the stippled envelope. The lower limit being based on measured zooplankton populations 0–500 m and the upper limit based on the estimated total zooplankton population 0–2000 m.

greatly in excess of its demand by the lagging animal population. According to RILEY (1956) the zooplankton utilize no more than about 25% of the net primary production in Long Island Sound, the remainder sinking to the bottom or decomposing within the water in about equal proportions.

In the Sargasso Sea, by contrast, plant production proceeds throughout the winter unlimited by light but controlled in magnitude by the lower nutrient levels. The animals, by and large, keep up with the plants. Virtually 100% of the organic production is utilized by the relatively small and constant zooplankton populations. As CUSHING has pointed out, this is a highly efficient biological system and its efficiency is reflected in the small ranging populations of animals at the higher trophic levels. It is only in the inefficient eutrophic environments which irregularly produce large surpluses of basic food that large and dense populations of fishes can assemble and subsist.

Summary

1. Cycles in the abundance of zooplankton in the Sargasso Sea are characterized by maxima in the spring. Except for the spring period the standing crop is low and almost constant.

2. Experimental evidence indicates that the mean daily metabolic requirement in terms of carbon is 12% of the dry weight of the zooplankton.

3. There is striking agreement between net organic production and the metabolic requirement of the zooplankton. Clearly the zooplankton is closely controlled by the availability of food during most of the year. There is little evidence of food surplus and wastage.

References

CLARKE, G. L., 1940. "Comparative richness of zooplankton in the coastal and offshore areas of the Atlantic." Biol. Bull., Woods Hole, **78**: 226–55.

CONOVER, R. J., 1956. "Oceanography of Long Island Sound, 1952–1954. VI. Biology of *Acartia clausi* and *A. tonsa*." Bull. Bingham Oceanogr. Coll., **15**: 156–233.

CUSHING, D. H., 1959. "The control of primary production by grazing." Preprints of abstracts, Internat. Oceanogr. Congr., Aug.–Sept., 1959. Amer. Assoc. Adv. Sci., pp. 883–85.

GAULD, D. T., & RAYMONT, J. E. G., 1953. "The respiration of some planktonic copepods. II. The effect of temperature." J. mar. biol. Ass. U.K., **31**: 447–60.

HARVEY, H. W., COOPER, L. H. N., LEBOUR, M. V., & RUSSELL, F. S., 1935. "Plankton production and its control." J. mar. biol. Ass. U. K., **20**: 407–42.

LEAVITT, B. B., 1935. "A quantitative study of the vertical distribution of the larger zooplankton in deep water." Biol. Bull., Woods Hole, **68**: 115–30.

LEAVITT, B. B., 1938. "The quantitative vertical distribution of the macrozooplankton in the Atlantic Ocean basin." Biol. Bull., Woods Hole, **74**: 376–94.

MENZEL, D. W., & RYTHER, J. H., 1960. "The annual cycle of primary production in the Sargasso Sea off Bermuda." Deep-Sea Res., **6**: 351–67.

MENZEL, D. W., 1961. "Annual variations in primary production of the Sargasso Sea off Bermuda." Deep-Sea Res., **7**: 282–88.

MARSHALL, S. M., NICHOLLS, A. G., & ORR, A. P., 1935. "On the biology of *Calanus finmarchicus*. Part VI. Oxygen consumption in relation to environmental conditions." J. mar. biol. Ass. U.K., **20**: 1–25.

MOORE, H. B., 1949. "The zooplankton of the upper waters of the Bermuda area of the North Atlantic." Bull. Bingham Oceanogr. Coll., **12**: 1–97.

MOORE, H. B., 1950. "The relation between the scattering layer and the Euphausiacea." Biol. Bull., Woods Hole, **99**: 181–212.

RICHMAN, S., 1958. "The transformation of energy by *Daphnia pulex*." Ecol. Monogr., **28**: 273–91.

RILEY, G. A., 1956. "Oceanography of Long Island Sound, 1952–1954. IX. Production and utilization of organic matter." Bull. Bingham Oceanogr. Coll., **15**: 324–44.

RILEY, G. A., & GORGY, S., 1948. "Quantitative studies of summer plankton populations of the western North Atlantic." J. Mar. Res., **7**: 100–21.

YENTSCH, C. S., & HEBARD, J. F., 1957. "A gauge for determining plankton volume by the mercury immersion method." J. Cons. int. Explor. Mer, **22**: 184–90.

ZEUTHEN, E., 1947. "Body size and metabolic rate in the animal kingdom with special regard to the marine microfauna." C. R. Lab. Carlsberg, **26**: 17–61 (not seen by authors).

Contribution No. 1122

Deep-Sea Research, 1961, Vol. 8, pp. 152 to 153. Pergamon Press Ltd., London. Printed in Great Britain

LETTER TO THE EDITORS

Erratic Boulders from Great Meteor Seamount*

(*Received* 15 *June*, 1960)

Two cores, six dredge samples and a series of photographs were taken on Great Meteor Seamount (30°N, 28°W) by the U.S.N.S. *Chain* during its 1959 summer cruise. One of the dredge hauls (CD No. 1) constitutes a fifteen-minute haul in water that shoals from 713 m. (390 fms.) to 650 m. (355 fms.). Along with four boulders of continental-type rock it collected about a bushel of rock consisting of indurated foraminiferal limestone, boulders of reef material, dead coral, and a large slab of reef limestone, 20 × 18 in. in size†. The continental rock types are (1) a coarse-grained pink granite composed of orthoclase, quartz, biotite and plagioclase; (2) a garnet-bearing quartz-biotite schist; (3) a medium-grained diorite with plagioclase, biotite and hornblende and (4) a three-inch cobble of dense, thinly-laminated quartzite. These rocks differ markedly in appearance from the local foraminiferal and reef limestone (Fig. 1).

Dredge hauls from the flat top of the seamount brought up only fine-grained, uniform, calcareous sand and small, dead corals; hauls deep down the side returned with only calcareous mud and ooze and one round cobble of volcanic rock. A series of photographs taken down the south side of the seamount show zones of poorly sorted, sub-rounded cobbles and boulders (Fig. 2). The deeper slopes are massive rock with patches of white sand or ooze.

The erratic boulders and cobble of diverse rock types are apparently rather abundant on the upper slopes of Great Meteor Seamount. After examining the probability of human transportation, rafting by vegetation and local sources or origin, ice rafting seems to explain the presence of these erratic boulders most plausibly.

The Ice Atlas of the Northern Hemisphere (H. O. Pub. 550) and the Pilot Charts of the North Atlantic indicate that ice has infrequently been reported that far south. Thus in September 1883, it was reported at 36°N, 30°W; in May 1907, at 31°N, 38°W; in July 1926, at 30° 30′N, 63°W; and in 1934 at 31°N, 45°W. There are also several reports of ice near the Azores and one near Bermuda. However, the International Ice Patrol (personal communication) has suggested that some of the ice reported as drifting this far south may have been mistakenly identified. Despite such reports of southerly drifting ice, it seems improbable that a sufficient quantity of ice to carry erratic boulders to Great Meteor Seamount (30°N) has drifted that far south under present climatic conditions. Therefore, we must look to the Pleistocene ice advances for the source of the erratic-carrying ice. Assuming that the North Atlantic circulation was the same during the Pleistocene as it is at present, the origin of the erratics would most likely have been the North American Continent – indeed, probably the New England-Acadian Area. At the present time no ice is ever seen off the European coasts because of the effect of the warm Gulf Stream water. During the Pleistocene, however, ice could perhaps have been picked up from the seaward extension of the North American Continental ice sheet and transported across the Atlantic to Great Meteor Seamount.

---

*Contribution No. 1122 from the Woods Hole Oceanographic Institution.

†Glacial erratics and continental-derived rocks have been dredged from the North Atlantic by several other expeditions (Murray, 1891, p. 322; Ewing, 1949, p. 618; Heezen, 1959, p. 99).

Acknowledgements—The writer is indebted to the officers and crew of the U.S.N.S. *Chain* who made the dredging possible. Dr. J. B. Hersey and others at the Woods Hole Oceanographic Institution critically read the manuscript and made many helpful suggestions. The work was supported under Contract Nonr 1367 (00) with the Office of Naval Research, Department of the Navy.

R. M. Pratt

Woods Hole Oceanographic Institution,
Woods Hole, Massachusetts, U.S.A.,

REFERENCES

EWING, MAURICE (1949) New Discoveries on the Mid-Atlantic Ridge, *Nat. Geog. Mag.*, **96** (5).

HEEZEN, BRUCE (1959) The Floors of the Oceans, Part I, The North Atlantic, *Geol. Soc. Amer., Spec. Pap.* **65**, 122 pp.

MURRAY, JOHN and RENARD, A. F. (1891) Report on Deep Sea Deposits, *Challenger Repts.*, 525 pp.

UNITED STATES NAVY HYDROGRAPHIC OFFICE (1946) Ice Atlas of the Northern Hemisphere, *H.O. Pub.* **550**.

Printed in Great Britain by The Salisbury Press Ltd., Publicity House, Wilton Road, Salisbury, Wilts. (30319)

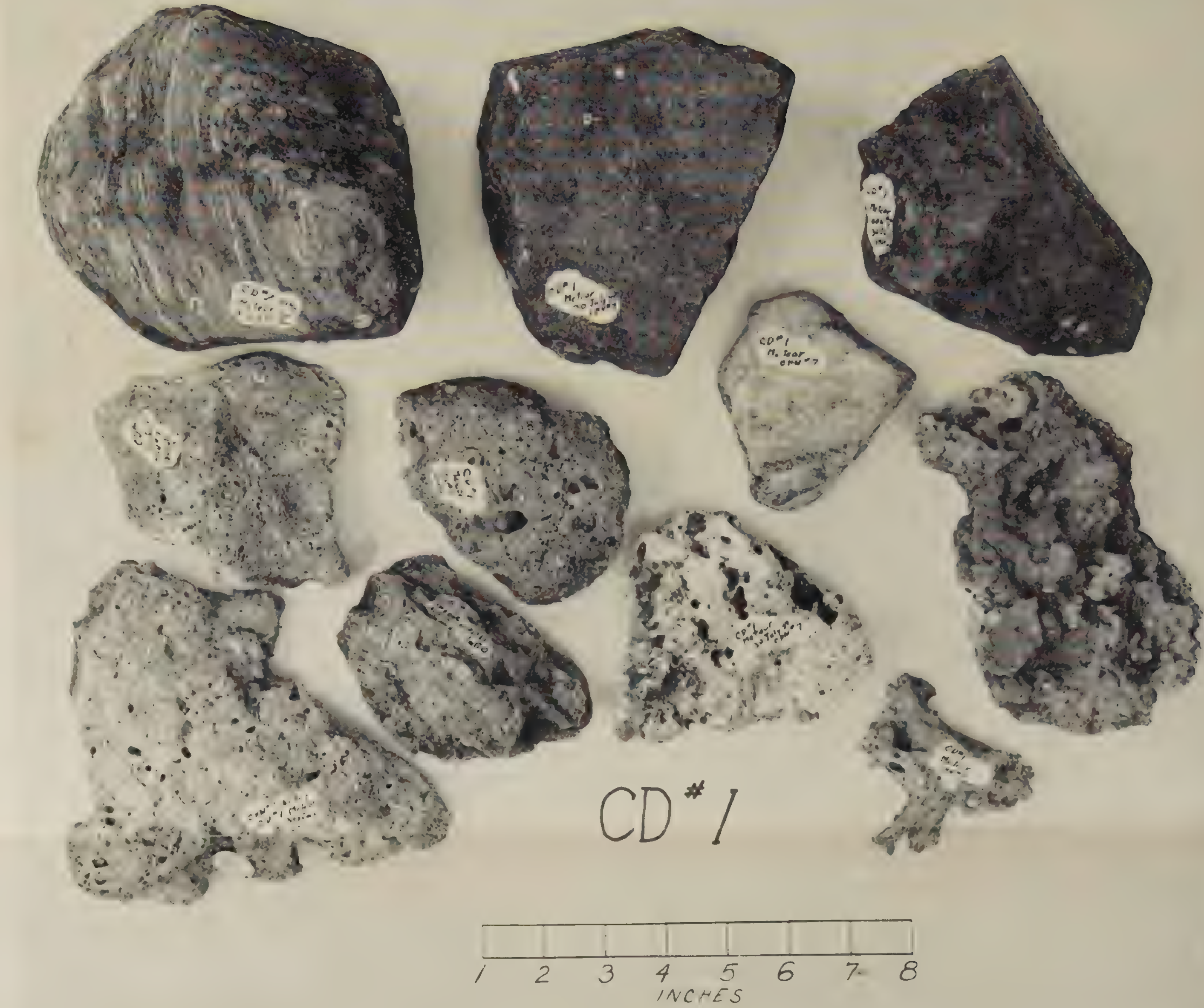

FIG. 1. Representative boulders and cobbles from dredge haul No. 1, 713 metres (390 fms). to 650 metres (355 fms.) on Great Meteor Seamount. The erratic rocks are at the top of the figure; reef types, probably of local origin, are on the lower portion.

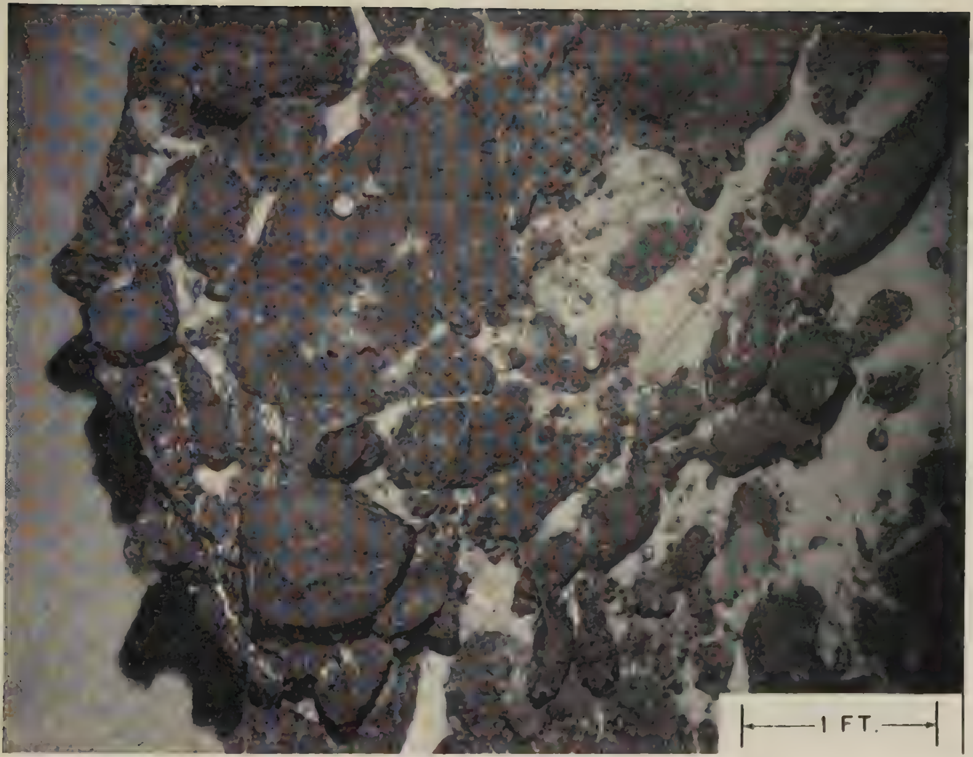

FIG. 2. Boulder and cobble deposit at 512 metres (280 fms.) on Great Meteor Seamount. Note the similarity of shape and size to the rocks shown in Fig. 1.

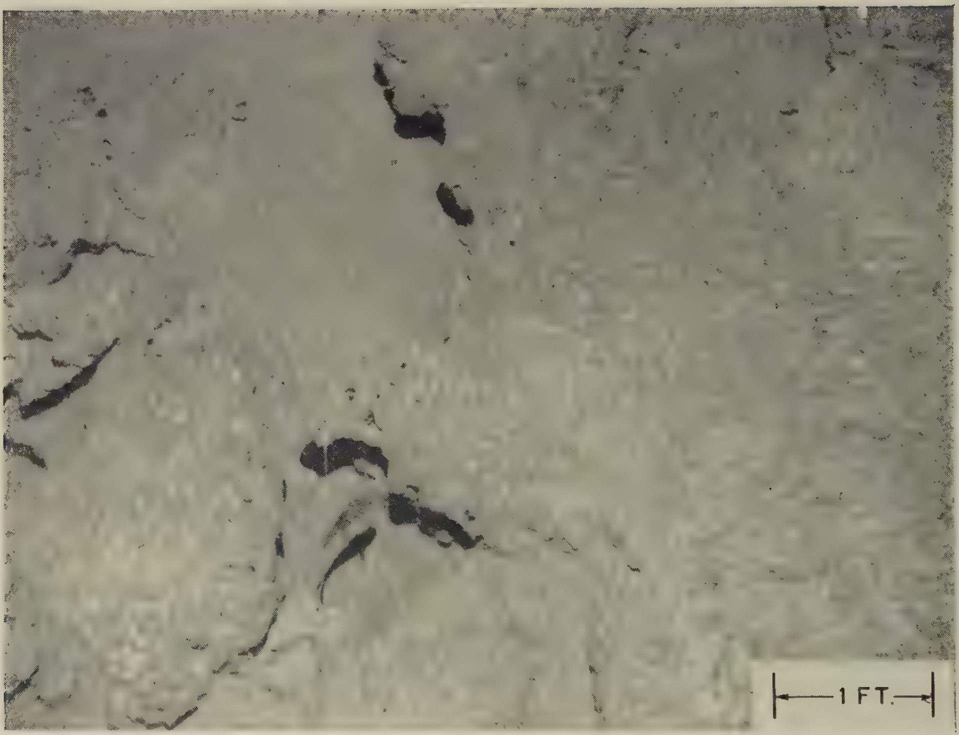

FIG. 3. A vertical photograph of the steep slope of the seamount at a depth of about 1280 metres (700 fms.). The jagged porous rock appears very similar to large slabs of calcareous reef rock brought up in the dredges.

Contribution No. 1123

Deep-Sea Research, 1961, Vol. 7, pp. 276 to 281. Pergamon Press Ltd., London. Printed in Great Britain

Nutrients limiting the production of Phytoplankton in the Sargasso Sea, with special reference to iron

D. W. MENZEL* and J. H. RYTHER†

(*Received* 8 *July* 1960)

Abstract—The effects of enriching surface water samples from the Sargasso Sea upon the rate of C^{14} assimilation was investigated. The addition of nitrate, phosphate and vitamins, added separately or in combination, had no stimulatory effect, while addition of a trace metal mixture increased C^{14} uptake by several-fold. The effective component of the trace metal mix was found to be iron, which alone enhanced C^{14} uptake for 24 hours but which required the addition of nitrogen and phosphorus to produce a comparable effect over a three-day period.

INTRODUCTION

CORRELATION between the nitrogen and phosphorus content of surface waters and the rate of organic synthesis has been demonstrated repeatedly in temperate seas (KETCHUM *et al,* 1958). This coupled with the fact that the large, central, relatively unproductive areas of the ocean often contain negligible quantities of these elements in their euphotic zone has led to the general belief that primary production is directly limited by supplies of nitrate and phosphate.

HARVEY (1926) first noted that nitrogen and phosphorus decreased together and at a constant ratio during the spring diatom maximum in the waters of the English Channel. He suggested that the two elements became limiting to plant production simultaneously . REDFIELD (1934) enlarged upon this theory extending it to the oceans as a whole. He observed that these elements are depleted from sea water in very nearly the same ratio as they occur in plankton (15 N : 1 P by atoms).

Statistically, over the oceans as a whole and at all depths, the concentrations of these elements occur at the same ratio, but values lower than this have consistently been recorded in surface waters. RILEY and CONOVER (1956), for example, reported a value of 8 : 1 in Long Island Sound, while repeated observations at Bermuda by the authors have shown an average value of 10 : 1. This has led to the belief that nitrogen rather than phosphorus is the more important limiting factor in these waters (KETCHUM et *al,* 1958).

Recent attempts by the authors (MENZEL and RYTHER, 1960) to correlate both the concentrations and rates of removal of nitrate and phosphate with plant growth in the Sargasso Sea have been unsuccessful. Accepting the thesis that these elements are truly limiting, two explanations may be offered for this lack of correlation : (1) the instantaneous concentration of their organic forms does not give an index as to their general availability, but rather the rate of their regeneration determines the level of production that may be attained, or (2) vertical diffusion accounts for the enrichment of surface waters. This enrichment however may never be reflected by changes in the absolute concentration of nitrate and phosphate since the nutrients

---

*Bermuda Biological Station, St. Georges West, Bermuda.
†Woods Hole Oceanographic Institution, Woods Hole, Mass.

may be utilized by plants as rapidly as they become available. Unfortunately little is known of the natural rate or quantitative significance of either of these processes and therefore their relative importance remains one of speculation.

A possible alternative explanation for lack of correlation between nitrogen and phosphorus and primary production is that these two elements are not in themselves primary limiting factors to production in these waters. Indications that this might actually be the case have been provided by HENTSCHEL (1932), STEEMANN NIELSEN and JENSEN (1957), CURRIE (1958), and RYTHER and GUILLARD (1959) when they, using the direct approach of enrichment procedure, found no increase in photosynthetic rates in samples of sea water to which nitrogen and phosphorus had been added. On the other hand, RYTHER and GUILLARD (loc. cit.) found that phytoplankton growth in the Sargasso Sea was enhanced by the addition of a combination of trace metals and iron. The problem remained then of attempting to isolate the critical element or elements within this mixture.

METHODS

The experiments described below were carried out during October, 1959 when the concentration of nutrients in the euphotic zone of the Sargasso Sea was minimal. Surface water was collected from a point 15 miles south of Bermuda. This was dispensed into a number of one-litre bottles and enriched with a combination of nutrients. These bottles were then placed in an incubator cooled with running sea water and exposed to a constant light source (fluorescent) of 1500 foot candles. At the end of the first 24 hours two aliquots of 150 ml each were withdrawn from each bottle and inoculated with approximately 15 μ curies of $C^{14}O_3$. One of these aliquots was then exposed to the same light source and the other placed in darkness for a period of four hours. After this time they were filtered through HA millipore filters, rinsed with ·01 N HCl, dried and the activity measured in a gas flow geiger counter. Additional aliquots were withdrawn after a period of 72 hours and treated in a similar manner. Results given in the following discussion were corrected for uptake in the dark.

*Table 1. Media used in enrichment experiments**

1. KNO_3	50 μ gA/L N
2. KH_2PO_4	5 μ gA/L P
3. Vitamin Mix	
Thiamin. HCl	0·2 mg/L
Biotin	1·0 μ g/L
B_{12}	1·0 μ g/L
4. Iron-trace Metal Mix	
FeNaEDTA	0·13 mg/L Fe
$CuSO_4 \cdot 5\,H_2O$	0·005 mg/L Cu
$ZnSO_4 \cdot 7\,H_2O$	0·010 mg/L Zn
$CoCl_2 \cdot 6\,H_2O$	0·005 mg/L Co
$MnCl_2 \cdot 4\,H_2O$	0·100 mg/L Mn
$Na_2MoO_4 \cdot 2\,H_2O$	0·005 mg/L Mo
5. $FeCl_3$	0·13 mg/L Fe
6. Na_2EDTA	1·0 mg/L

**Items 1–4 inclusive constitute complete media used except where indicated in the text.*

The nutrients used in these experiments are similar to those used routinely in the laboratory for the culture of marine phytoplankton. The complete media consisted of nitrate, phosphate, vitamins and trace metals with iron (Table 1). The experimental approach used was : (1) to enrich samples with the complete media lacking one or more of the major groups (i.e. N and P, metals, vitamins) thus permitting assay of the relative importance of groups of elements, (2) subtracting one element at a time ftom the larger group observed to directly affect the rate of photosynthesis, (3) adding the critical element or elements to samples singly or in combination until all controlling factors were isolated.

RESULTS

Table 2 shows the results of experiments that were concluded after phytoplankton had been exposed to enriched waters for a period of 24 hours. Although changes in relative photosynthesis were not large, values consistently higher than the control were demonstrated only in those samples to which metals had been added. The addition of nitrogen and phosphorus alone, or in combination with vitamins apparently had no effect on photosynthesis.

Table 2. Relative uptake of C^{14} (4-hour experiments) by enriched surface water after 24 hours. Values relative to C^{14} uptake in unenriched controls: i.e. *experimental/control*

	Experiment Number		
	(1)	(2)	(3)
Complete Media	1·8	1·6	2·0
Nitrate + Phosphate + Metals	2·0	1·7	2·7
Metals	2·0	1·7	2·4
Vitamins	1·0	1·0	—
Nitrate + Phosphate	0·7	1·0	0·9

When these experiments were extended for a period of 72 hours, however, the effect of adding the trace-metal iron complex alone was not apparent (Table 3). Here it became obvious that lacking nitrogen and phosphorus, enriched samples were not capable of any further growth than that shown at the end of 24 hours. The initial stages of this work, however, also exhibited the fact that the addition of nitrogen and phosphorus without the inclusion of the trace metal complex also had no apparent effect on growth. It seemed obvious then that growth was dependent upon nitrogen, phosphorus, and one or more elements of the trace-metal complex.

Table 3. Relative uptake of C^{14} (4-hour experiments) by enriched surface water after 72 hours. Values as in Table 2

	Experiment Number				
	(1)	(2)	(3)	(4)	(5)
Complete Media	18·7	13·6	14·3	—	—
Nitrate + Phosphate + Metals	16·1	12·6	11·5	12·7	11·6
Metals	1·2	1·0	1·3	—	—
Nitrate + Phosphate + Vitamins	1·2	1·1	1·2	—	—
Nitrate + Phosphate	0·9	0·8	1·3	1·5	1·0
Vitamins	1·1	0·9	—	—	—

The results of experiments designed to isolate the limiting factor from the mixture of metals are given in Table 4. They show clearly that little effect was evidenced except where iron was present in the media, and thus demonstrate that iron was critically limiting in these experiments. Nitrogen and phosphorus however very rapidly became limiting when iron was added in excess, as is evidenced from the fact that the effect of metal enrichment alone was measured only within the first 24 hours.

Table 4. Relative uptake of C^{14} (4-hour experiments) by surface water enriched with nitrate, phosphate and metals but omitting the metal indicated, after 72 hours. Values as in Table 2

	Experiment Number				
	(1)	(2)	(3)	(4)	(5)
Copper	13·0	9·2	—	—	—
Zinc	17·2	11·5	—	—	—
Manganese	8·8	19·6	—	—	—
Cobalt	1·9	12·0	11·9	11·5	10·9
Molybdate	10·0	18·1	—	—	—
Iron	1·0	1·1	1·1	1·1	1·1

Since iron was added as FeNaEDTA, the possibility remained that the chelating action of this compound and not its iron fraction was responsible for the results obtained. This was tested by (1) enriching samples with iron in the form of its chloride and (2) enriching samples with amounts of Na_2EDTA equivalent to that added when using FeNaEDTA. Table 5 provides evidence that iron and not the NaEDTA fraction of the molecule was responsible for increasing the rate of carbon uptake.

Table 5. Relative uptake of C^{14} (4-hour experiments) by surface water enriched with various forms of iron and EDTA *after 72 hours. Values as in Table 2*

	Experiment Number					
	(1)	(2)	(3)	(4)	(5)	(6)
Nitrate + Phosphate + FeNaEDTA	11·9	11·6	13·8	14·6	7·6	6·3
Nitrate + Phosphate + $FeCl_3$	7·8	6·9	10·2	10·4	—	—
Nitrate + Phosphate + Na_2EDTA	1·3	1·1	0·8	0·9	—	—

OBSERVATIONS BETWEEN BERMUDA AND THE WEST INDIES

To test whether iron is limiting in semi-tropical oceanic waters in general, a series of enrichment experiments were conducted on an oceanographic cruise (R.V. *Crawford* 37) between Bermuda and the West Indies. The technique used in this procedure was essentially the same as that described above except that enrichment was carried out only with nitrate plus phosphate alone and in combination with iron. In addition the samples were incubated in full daylight and not under constant artificial light.

Table 6. Relative uptake of C^{14} (4-hour experiments) by enriched surface water in passage from Bermuda to the West Indies. Values as in Table 2

Position	*Enrichment Media*	
	$NO_3 - N + PO_4 - P$	$NO_3 - N + PO_4 - P + Fe$
32 12′N 64 24′W	0·8	4·1
29 50·N 59 43′W	0·7	5·2
28 13·N 45 58′W	1·3	3·1
28 01′N 53 54′W	1·0	5·9
27 58′N 50 31′W 27 39′N 48 48′W	1·5 4·4	3·9 2·8
26 21′N 45 29′W	1·0	2·7
26 01′N 47 51′W	1·0	5·1
25 01′N 51 04′W	1·4	3·1
22 56′N 52 45′W	1·6	2·8
20 51′N 54 30′W	1·7	7·4
18 50′N 56 16′W	1·2	5·5
Mean	1·4	4·4

The results of this series of experiments show that with a single exception the addition of nitrate and phosphate to sea water had slight effect on photosynthesis, the values obtained averaging some 40 per cent above the control. However, when nitrogen, phosphorus and iron were added the photosynthetic rate was increased by an average of 440 per cent. This value is appreciably lower than that obtained in the work described above, possibly because of the different treatment with respect to light.

DISCUSSION

Observations on an annual basis have shown that approximately 0·5 μgA/L $NO_3 - N$ and 0·05 μ gA/L $PO_4 - P$ are always present in the surface waters of the Sargasso Sea (RILEY, 1957 ; MENZEL and RYTHER, 1960). Assuming that carbon, nitrogen and phosphorus are utilized in a ratio of 100 : 15 : 1 by atoms (REDFIELD, 1934), the average rate of plant production for the region, 3 mgC/m³/day, would require the daily utilization of ·04 μ gAN/L and ·003 μ gAP/L, indicating roughly a ten day supply of these nutrients at the normal rate of growth. Approaching this problem from the basis of standing crop, RILEY (1957) estimated that the level of nitrogen and phosphorus in Sargasso Sea water indicates a potential population 3 to 10 times larger than is actually measured.

The fact that these elements are never quite exhausted suggests another limiting factor. Enrichment experiments have indicated this to be iron. The influence of iron enrichment however was only measurable in one day experiments, at which time presumably all excess available nitrogen and phosphorus was utilized. Further growth then became dependent upon the additional enrichment with nitrogen and phosphorus.

The preceding conclusions appear to be applicable to the semi-tropical and tropical Western Atlantic and indicate that previous emphasis on the importance of nitrogen and phosphorus with respect to primary production has led to an over-simplification of the general problem. It is possible that in other oceanic regions nutrients other than or in addition to, iron, nitrogen and phosphorus may become critically limiting.

Contribution No. 1123 *from the Woods Hole Oceanographic Institution and Contribution No.* 256 *from the Bermuda Biological Station, under Contract* AT (30–1) – 2078 *with the Atomic Energy Commission. The work during* CRAWFORD 37 *was supported by* NSF *Grant* B 8339.

REFERENCES

CURRIE R. I. (1958) Some observations on organic production in the Northeast Atlantic. *Rapp. et Proc. Verb. Cons. Internat. Explor. Mer.* **144**, 96–102.
HARVEY, H. W. (1926) Nitrate in the sea. *J. Mar. Biol. Assoc., U.K.*, **14**, 71–88.
HENTSCHEL, E. (1932) Die biologischen Methoden und das biologische Beodachtungs material der *Meteor*—Expedition. *Wissench. Erg. d. Deutsch. Atl. Exp. auf d. Forsch. u. Vermessungssch. Meteor* 1925–1927, **10**, 1–274.
KETCHUM B. H., RYTHER J. H., YENTSCH C. S. and CORWIN N. (1958) Productivity in relation to nutrients. *Rapp. et Proc. Verb. Cons. Internat. Explor. Mer*, **144**, 132–140.
MENZEL D. W. and RYTHER J. H. The annual cycle of primary production in the Sargasso Sea off Bermuda. *Deep-Sea Res.* **6**, 351–367.
REDFIELD A. C. (1934) On the proportions of organic derivatives in sea water and their relation to the composition of plankton. In : James Johnstone Memorial Volume, Liverpool, pp. 176–192.
RILEY G. A. (1957) Phytoplankton of the north-central Sargasso Sea. *Limnol. and Oceanogr.* **2**, 252–270.
RILEY G. A. and CONOVER S. M. (1956) Oceanography of Long Island Sound 1952–1954. III. Chemical oceanography. *Bull. Bing. Oceanogr. Coll.*, **15**, 47–61.
RYTHER J. H. and GUILLARD R. R. L. (1959) Enrichment experiments as a means of studying nutrients limiting to phytoplankton populations. *Deep-Sea Res.*, **6**, 65–69.
STEEMAN NIELSEN E. and AABYE JENSEN E. (1957) Primary oceanic production. The autotrophic production of organic matter in the oceans. *Galathea Repts.*, **1**, 49–136.

Printed in Great Britain by The Salisbury Press Ltd., Publicity House Wilton Road, Salisbury, Wilts. (27337)

Contribution No. 1127

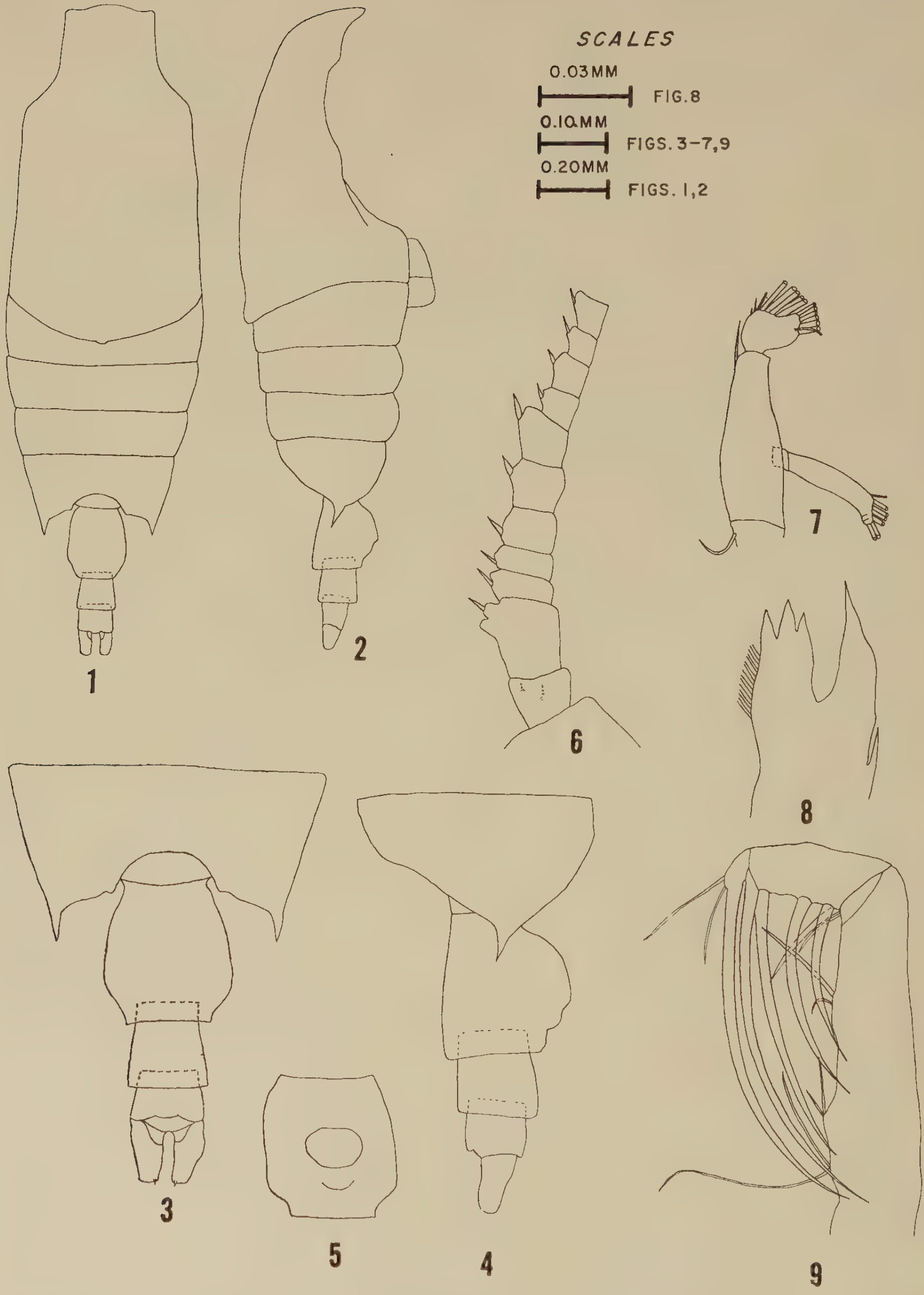
SCALES
0.03MM
FIG.8
0.10MM
FIGS. 3-7,9
0.20MM
FIGS. 1,2
1
2
6
7
8
3
5
4
9

Figs. 1-9. *Candacia ketchumi* n. sp. 1, female, dorsal view. — 2, lateral view. — 3, fourth and fifth thoracic segments and abdomen, dorsal view. — 4, fourth and fifth thoracic segments and abdomen, lateral view. — 5, genital segment, ventral view. — 6, proximal 11 segments of first antenna. — 7, second antenna. — 8, gnathal lobe of mandible. — 9, second maxilla.

There is a tricuspate basal tooth on the gnathal lobe of the mandible (fig. 8). The exopod has 5 and the endopod 6 setae.

The first maxilla is like that figured for *C. norvegica* (Boeck) by Grice and Jones (1960).

The second maxilla (fig. 9) is large and has 4 groups of small spines and setae on the first basipodal segment. There are 2 large spines on the second basipodal segment, the proximal one of which is shorter than the distal one. Three very large spines are present on the endopod. Of these the middle spine is the longest and the proximal spine is the shortest.

The maxilliped is small and similar to that found in other species of *Candacia*. The first basal segment is long and has 1 seta arising from the approximate mid-point and 1 long and 1 short seta arising from the disto-lateral corner. There are 3 setae near the distal end and a row of short hairs on the proximal end of the second basipodal segment. The endopod consists of 5 segments all of which have 2 setae excepting the first which has 3 setae.

The swimming feet have 3-segmented exopods and 2-segmented endopods (figs. 10-14). The lengths of the third exopodal segment of swimming feet 1 to 4 have the following relation to that of their respective terminal spines: 1 : 1.1, 1 : 0.8, 1 : 0.6, 1 : 0.8. The terminal spine on the third foot is bent at its tip and has small teeth-like structures extending onto the curved, distal portion (fig. 13).

The fifth pair of feet (fig. 15) are short and terminate in 2 sub-equal spine-like processes. Two small spine-like points are on the outer and 3 setae on the inner margin of the distal segment. There is a small seta on the outer, disto-lateral corner of the penultimate segment.

Male (figs. 16-21). The cephalothorax-abdomen ratio is 3.2 : 1 and the relative lengths of the abdominal segments and furca are as follows: 24, 20, 22, 13, 8, 13 = 100. These figures are based on measurements of the allotype, the total length of which is 1.75 mm.

The posterior lateral processes of the fifth thoracic segment are asymmetrical. The one on the right is pigmented, thickened and turned inward in dorsal view (fig. 16). In lateral view (fig. 17), the distal end is turned upward. The process on the left side resembles that of the female.

A small, elongate process is present on the right lateral margin of the genital segment (fig. 16). In lateral and oblique views (figs. 17, 18), the process appears to be diagonally oriented across part of the posterior end of the segment.

Segments 13 and 14 of the right first antenna have a small spine-like process on the distal margin, and segments 17, 18, and 19 have a row of teeth along the lateral margin (fig. 19). The teeth on segment 18 are coarse and extend for most of the length of the segment. Teeth on segment 17 are situated along the distal half of the segment, while those on segment 19 are limited to the proximal third of the segment. On these latter 2 segments the teeth are fine.

The right and left fifth feet are approximately equal in length (figs. 20, 21), the former being chelate. There are 2 small spines near the distal end of the finger of the chela and the raised internal margin has 1 long and 2 short spines.

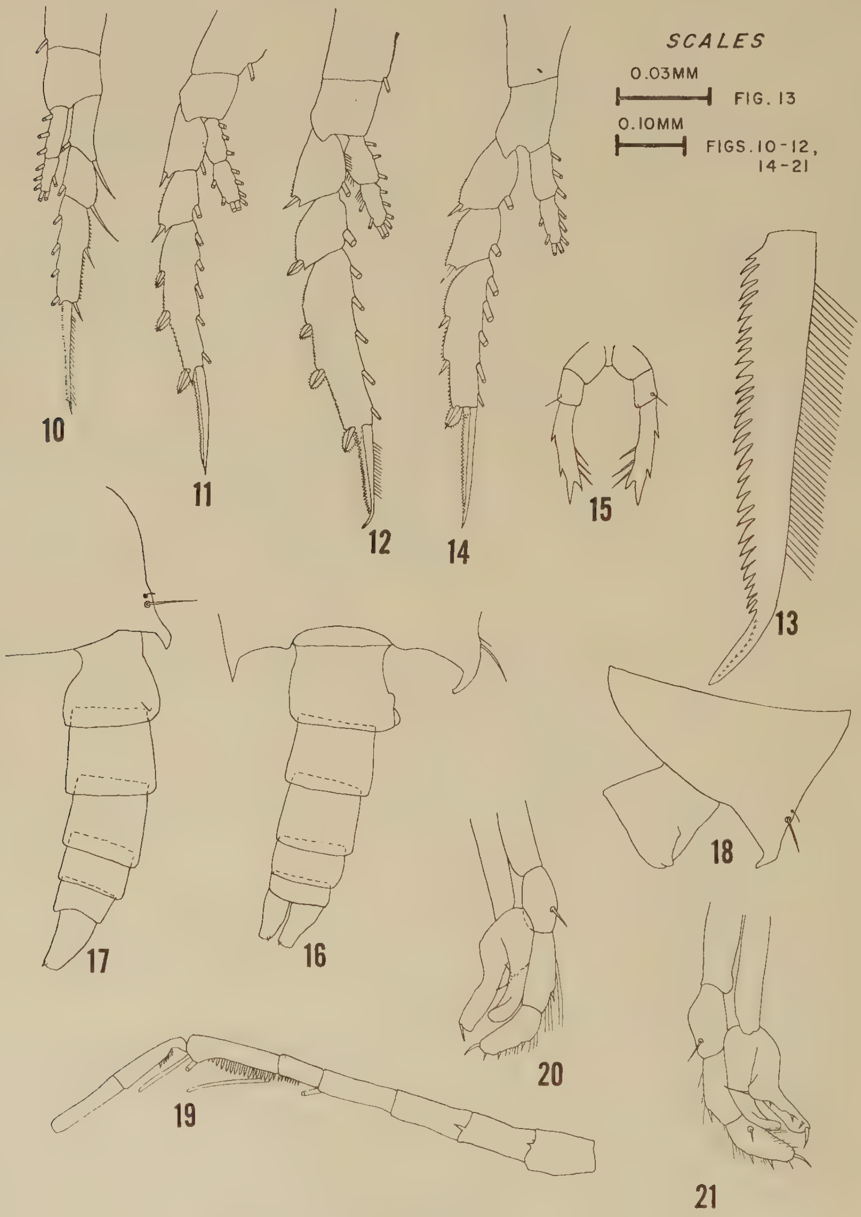
SCALES
0.03MM
FIG. 13
0.10MM
FIGS. 10-12, 14-21
10
11
12
14
15
13
17
16
18
20
19
21

Figs. 10-21. *Candacia ketchumi* n. sp. 10, female, first foot. — 11, second foot. — 12, third foot. — 13, terminal spine of third exopodal segment of third foot. — 14, fourth foot. — 15, fifth feet. — 16, male, abdomen, dorsal view. — 17, abdomen, lateral view. — 18, fourth and fifth thoracic segments and genital segment, oblique view. — 19, segments 13 to 20 of right first antenna. — 20, fifth feet. — 21, fifth feet, other side. Figs. 1-15 drawn from paratype; figs 16-21 drawn from allotype.

The thumb of the chela is short and naked. The terminal segment of the left fifth foot has 4 marginal and 1 surface spines.

Remarks — This species closely resembles *Candacia norvegica* (Boeck) but the two may be distinguished in a number of ways. In the female, *C. ketchumi* lacks the spines which are present on the sides of the genital segment of *C. norvegica.* The 2 spines on the second basipodal segment of the second maxilla of *C. norvegica* as figured by Sars (1903) and Grice and Jones (1960) are subequal, while in *C. ketchumi* the proximal one is distinctly shorter than the distal one. The fifth pair of feet of *C. ketchumi* lack the seta on the inner, disto-lateral corner of the penultimate segment.

In the male, the two species are most easily separated by the form of the process on the right side of the genital segment. In *C. norvegica* this process is quite large and has an irregular, lobiform tip. In *C. ketchumi* it is small and scarcely visible in dorsal view.

The two species also differ in size and probably in distribution. North Atlantic specimens of *C. norvegica* are approximately 3.2 mm in total length (Farran, 1948) whereas Sargasso Sea specimens of *C. ketchumi* are less than 1.90 mm. The former species apparently occurs in waters colder than those in which the latter species has so far been found (approximately 18°-22°C).

ZUSAMMENFASSUNG

Beschreibung der *Candacia ketchumi* n. sp. anhand von Exemplaren aus der nordwestlichen Sargasso See. Es ist bekannt, dass dreizehn andere Arten der Gattung *Candacia* im nordwestlichen Atlantik vorkommen.

LITERATURE CITED

BIGELOW, H. B., 1926. Plankton of the offshore waters of the Gulf of Maine. Bull. Bur. Fish., **40**, (2): 1-509.

FARRAN, G. P., 1948. Copepoda. Sub-order Calanoida. Family Candaciidae. Genus Candacia. Fiches Ident. Zooplancton, **13**. (Cons. perm. Internatl. pour l'Explor. de la Mer).

FLEMINGER, A. and T. E. BOWMAN, 1956. A new species of Candacia (Copepoda: Calanoida) from the western North Atlantic Ocean. Proc. U. S. Natl. Mus., **106** (3370): 331-337.

GRICE, G. D. and E. C. JONES, 1960. Two new species of Candacia (Copepoda: Calanoida) from the Central Pacific, with notes on two other species. Pacific Science, **14** (3): 280-291.

JESPERSEN, P., 1934. The Godthaab Expedition 1928 — Copepoda. Medd. Grønland, **79** (10): 1-166.

MOORE, H. B., 1949. The zooplankton of the upper waters of the Bermuda area of the north Atlantic. Bull. Bing. Oceanogr. Coll., **12** (2): 1-97.

SARS, G. O., 1903. Copepoda Calanoida. Crustacea of Norway, **4**: i-xiii, 1-171 (Bergen Museum, Bergen).

WILLEY, A., 1919. Report on the Copepoda obtained in the Gulf of St. Lawrence and adjacent waters. Canadian Fish. Exped. 1914-15: 173-220.

WILSON, C. B., 1932. Copepods of the Woods Hole region Massachusetts. U. S. Natl. Mus. Bull., **158**: 1-623.

——, 1936. Plankton of the Bermuda oceanographic expeditions, IV. Notes on Copepoda. Zoologica, New York, **21** (2): 89-93.

Received for publication: October 7, 1960

Contribution No. 1129

Deep-Sea Research, 1961, Vol. 8, pp. 1 to 19. Pergamon Press Ltd., London. Printed in Great Britain

An observation of a deep countercurrent in the Western North Atlantic

J. C. SWALLOW* and L. V. WORTHINGTON†

(*Received* 26 *May* 1960)

INTRODUCTION

THE DEPTH of the level of no motion under the Gulf Stream has been a matter of interest to oceanographers for many years, and widely-varying estimates of the volume-transport have been arrived at, according to the choice of reference level. DIETRICH (1936) used the oxygen-minimum as a reference surface, at a depth of about 800 metres, but it was pointed out by ROSSBY (1936) that this choice implied the existence of a deep counter-current with a transport more than double that in the upper layers. ISELIN (1936) in his study of the circulation of the western North Atlantic, presented currents calculated relative to the 2000-decibar surface, and from the observations available at that time it appeared that the dynamic topography in the deeper water was relatively weak. DEFANT (1941) chose a surface of no motion sloping downwards from west to east, at a depth of about 1500 m under the Gulf Stream off Cape Hatteras, and calculated southward velocities of the order of 3 to 6 cm/sec at 2000 m depth. The high oxygen content of the deep water in this region was recognized as being consistent with a southward flow (ISELIN, 1936) but the notion of a current increasing in velocity towards the bottom was rejected by many oceanographers as unlikely (SVERDRUP *et al.*, 1942, p. 456).

Three recent developments led to renewed interest in this problem and to the measurements described here. During the last few years the R.V. *Atlantis* of the Woods Hole Oceanographic Institution has made a number of more detailed hydrographic sections across the Gulf Stream, paying particular attention to the deep water, and it has become clear that the steep temperature gradients across the stream, already well known in the upper layers, persist all the way to the bottom (FIG. 1, Cape Romain Sect.). This implies, if the geostrophic equation is valid, a relatively strong narrow flow in the deep water, northward if the reference level is at the bottom, or southward below any mid-water reference level. No satisfactory choice could be made from considerations of continuity from one section to another, nor from the temperature-salinity relationship of the water masses themselves.

At the same time, STOMMEL (1956, 1957) devised a theoretical model of the circulation of the Atlantic Ocean which required, as an essential feature, the existence of a narrow southward current in the deep water at the western boundary.

A suitable instrument for making direct measurements of such a current was recently developed (SWALLOW, 1955, 1957) in the form of a neutrally-buoyant float, and it was arranged that the R.V. *Atlantis* should co-operate with the R.R.S. *Discovery*

---

*National Institute of Oceanography.
†Woods Hole Oceanographic Institution.

II of the British National Institute of Oceanography in current-measuring and water-sampling, in an attempt to detect the south-going current and to locate the level of no motion.

Parachute drogues (VOLKMANN, KNAUSS and VINE, 1956) were also available for current measurements at all depths, and a new method had been devised by A. S. LAUGHTON for measuring currents very near the bottom using an underwater camera.

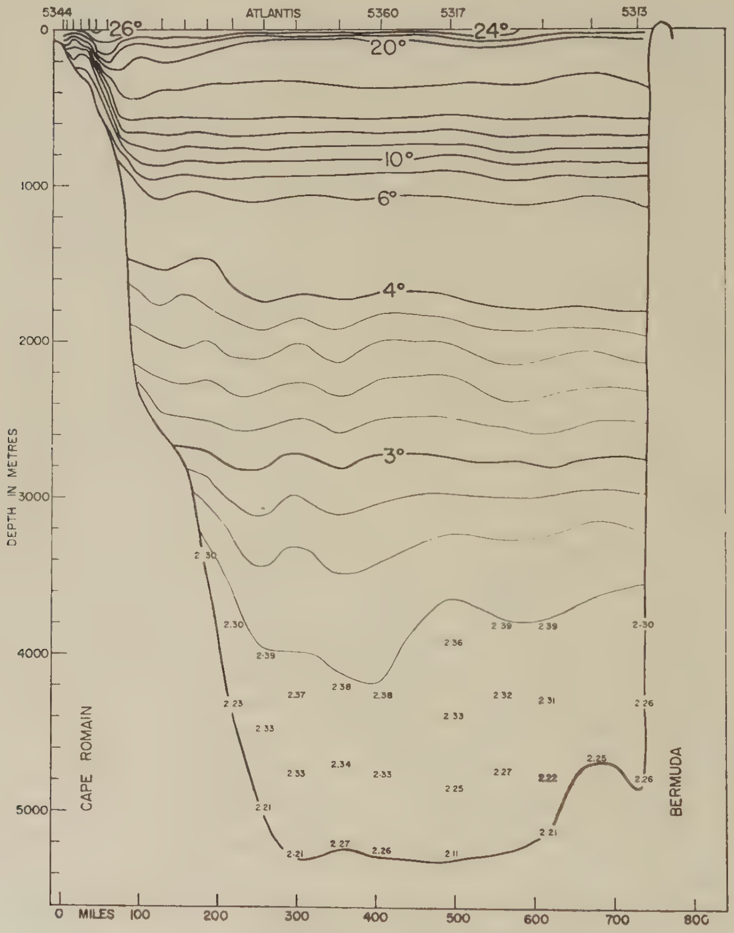

FIG. 1. Temperature Section, Cape Romain to Bermuda, made by *Atlantis* in June 1955.

It was planned that the *Atlantis* would first find the region of steep temperature gradients in the deep water, and then the *Discovery II* would make current measurements whilst the *Atlantis* occupied more hydrographic stations in the same area. Previous work had shown that, north of Cape Hatteras, the deep temperature gradients lay under the surface stream, and it was thought that surface currents of several knots would make deep current-measuring difficult. STOMMEL suggested that the most favourable area would be off Cape Romain, South Carolina, where the surface stream flows over the Blake Plateau, and the deep temperature gradients are found farther off-shore at the foot of the continental slope. Farther south, the deep temperature gradients become weaker, and it was decided to work as near as was practicable to the point of departure of the surface stream from the Blake Plateau.

METHODS OF MEASURING CURRENTS

In tracking neutrally-buoyant floats or parachute drogues, the accuracy of the measurement is limited by uncertainties in fixing the ship's position. The area chosen for the present measurements was within the ground-wave coverage of Loran stations 1H6 and 1H7, and good fixes could be obtained from them at most times. For the greater part of the work, the Loran readings were combined with radar fixes on an anchored buoy. This allowed averaging over groups of Loran readings, giving an improvement in accuracy and an estimate of the remaining uncertainty.

The parachute drogues, and their method of use, have been fully described by VOLKMANN, KNAUSS and VINE (1956), and the same technique was used in the present measurements, except that more use was made of radar in fixing the drogues. Although it seemed possible that a fairly strong deep countercurrent, of the order of 10 cm/sec, might be detected by this means, the results with the deep drogues were rendered uncertain by strong variable winds and surface currents, and only the measurements in the upper layers are considered reliable. Surface currents were measured occasionally by releasing fluorescein dye near the anchored buoy, and tracking it for a few hours.

One successful measurement of current near the bottom was made by the photographic method. A deep-sea camera (LAUGHTON, 1957) was mounted on a tripod looking vertically downward, and took a series of 60 photographs while on the bottom for 24 minutes. The orientation and tilt of the tripod were obtained from a combined compass and clinometer in the field of view. Two methods of current registration were used. First, drops of neutrally-buoyant aniline were ejected into the water from a spring-loaded hypodermic syringe. The velocities were higher than expected however, producing a large number of small drops (more than one per picture) so that only the direction and not the speed of the current could be obtained from them. The second method used was to observe the deflection from the vertical of a free-flooding ping-pong ball suspended on a thin thread. This angle could be calculated from the photographs, dimensions of the camera tripod and ball suspension being known. A calibration was made by towing a similar ball suspension in a tank at known velocities and measuring the deflection. Unfortunately, in an attempt to make another current measurement, the entire assembly was lost. The calibration could not therefore be made on the original ball, and one having the mean properties of six different makes was used instead.

The neutrally-buoyant floats, and the equipment used for receiving their sound signals, have already been described (SWALLOW, 1955, 1957). Only a brief account has been given previously of the method of operation, and some further details are given below.

First, the float has to be loaded to make it sink to the required depth. This load is calculated as follows. Each complete float is made neutrally-buoyant in a tank of salt water of known density and temperature. This adjustment is made to within 1 gm in a float weighing 10 kg, or 1 in 10^4. Suppose the density is ρ_0 at temperature T_0. Then the density of the float at depth D meters, where the temperature is T, will be approximately

$$\rho_0 (1 + kD - \alpha (T - T_0))$$

where k is the bulk compressibility of the float, per metre depth change, and α is the coefficient of volume expansion of the float material. For the tubes used, k was $15 (\pm 1) \times 10^{-7}$ per metre, and α was 69×10^{-6} per °C.

If the density of the sea water at the required depth D is ρ *(in situ)* obtained from observations of temperature and salinity, then the extra load needed to make the float sink to that depth is

$$\delta M = M \left(\frac{\rho \, (in\ situ)}{\rho_0 (1 + kD - \alpha (T - T_0))} - 1 \right)$$

where M is the mass of the float.

An allowance has to be made for movement of the rubber sealing rings in the end plugs, under pressure, and for the extra compressibility of the insulation on the transducer winding. Previous experience suggested that the calculated load should be reduced by 6 gms to allow for these effects.

Each float was tested for leaks, and for satisfactory working of its sound transmitter, by lowering it on a wire to more than the required working depth (usually 3000 m). If all was well when the float was recovered, the calculated load would be added and the float dropped over the side at a chosen position. They take three or four hours to sink to the stable depth, and usually no fixes were taken during that period.

Bearings could be obtained on the acoustic transmitter by stopping the ship head-to-wind and putting two hydrophones over the side, about 30 m apart. As the ship fell away from the wind direction, the path difference between the signals arriving at the two hydrophones was observed as a function of the bearing of the ship's head relative to north. FIG. 2 is a block diagram of the receiving equipment. The path difference was measured as a time delay on an oscilloscope. It was usually in the range 0 to 20 milliseconds and could be estimated with an accuracy of about $\frac{1}{2}$ milli-second. The amplifiers were tuned to 10 kc/s, with a bandwidth of about 500 c/s. In taking a bearing, a series of from six to ten readings of the time difference t was taken, while the ship's head swung through an arc of about 60°. If $t_{\max}$ is the time difference that would be observed with the ship heading directly towards the float, then

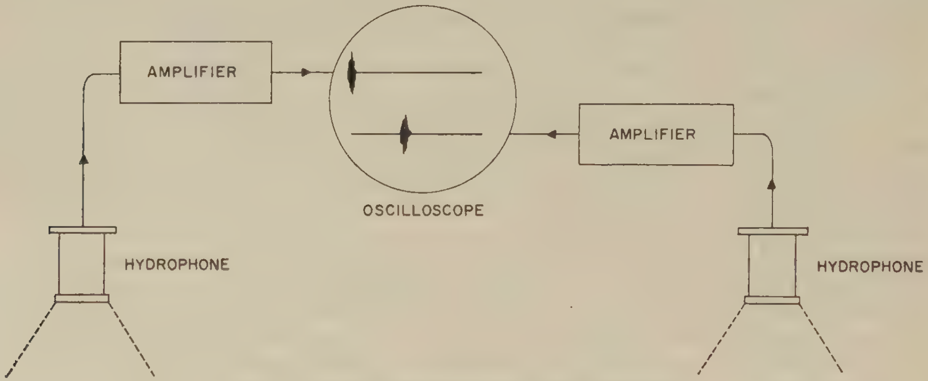

FIG. 2. Block diagram of receiving equipment.

$$t = t_{\max} \cos (\phi - \theta)$$

where ϕ is the heading of the ship, and θ is the bearing of the float, relative to north (FIG. 3). To determine θ and $t_{\max}$ from the series of observations of t and ϕ, rays were plotted at successive values of ϕ, and lines were drawn at right angles to them at distances from the centre proportional to the corresponding values of t. These lines should all pass through a point, at a distance proportional to $t_{\max}$ from the centre and on the ray making an angle θ with north (FIG. 4a).

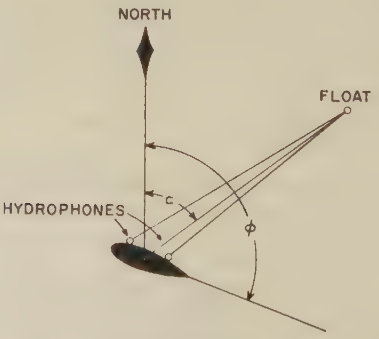

FIG. 3. Taking a bearing on a float.

Three or more bearings were taken in quick succession from different positions, their intersection defining the position of the float in a horizontal plane. It usually took about an hour to complete three bearings, in the R.R.S. *Discovery II*. To determine the ship's position, radar fixes and Loran readings were usually taken before and after each bearing. In most cases, the bearings intersected sufficiently well (Fig. 4b) for the position of the float to be determined relative to the anchored buoy with an error of less than 0·2 km, so that the six Loran fixes could be run together to give a mean Loran position for the float at the mean time of taking the bearings. To simplify the transferring of these fixes, a Loran plotting sheet for the area on a scale of 1 in. to the mile (1 cm to 0·73 km) was made by interpolation from Loran tables (USNHO Pub. 221). A minimum estimate of the uncertainty of the mean position could be obtained from the scatter of the individual Loran readings; this will be discussed below.

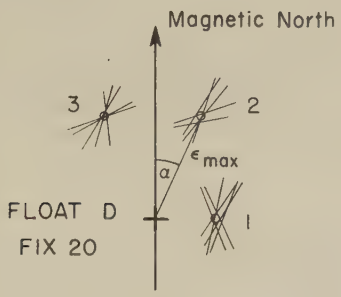
Magnetic North
3
2
ε max
α
FLOAT D
FIX 20
1

Fig. 4a. Part of laboratory plotting sheet.

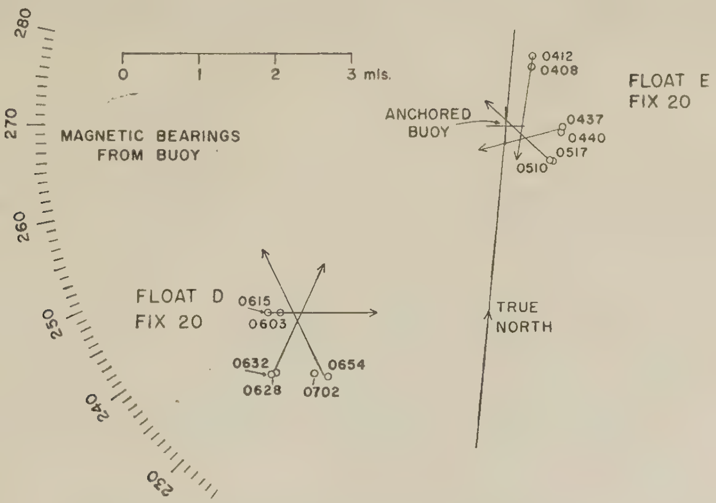
280
270
260
250
240
230
0
1
2
3 mls.
MAGNETIC BEARINGS
FROM BUOY
ANCHORED
BUOY
0412
0408
0437
0440
0517
0510
FLOAT E
FIX 20
FLOAT D
FIX 20
0615
0603
0632
0628
0654
0702
TRUE
NORTH

Fig. 4b. Part of a navigational plotting sheet.

When current-measurements were in progress, the deck officer on watch, assisted by one member of the scientific party, took the radar and Loran readings and kept a plot of the ship's movements relative to the anchored buoy on a 1 in. to the mile plotting sheet. At the same time, two others in the laboratory below took the oscilloscope readings and plotted them against ship's head to obtain bearings on the float, putting out hydrophones and recovering them as required. As each bearing was obtained, it was transferred to the navigational plotting sheet, and a suitable position was then chosen for taking the next bearing. FIG. 4a is an example of the laboratory plot for obtaining bearings, and FIG. 4b is part of a navigational plotting sheet.

Some of the floats moved quickly out of radar range of an anchored buoy and, instead of anchoring more buoys, tracking was continued using Loran only, the ship's positions being plotted directly on the large scale Loran plotting sheet.

The depth at which a float has stabilized itself can be estimated, each time a bearing is taken, from the observed value of t_{max} and the horizontal distance between the float and the ship. FIG. 5 is a vertical section showing the ship heading directly towards the float, when a time difference t_{max} will be observed. If l is the distance between the hydrophones, and the velocity of sound in the surface layer of water is V_0, then l/V_0 is the maximum time difference that would be observed if the float were at the surface, and when it is submerged the ratio $V_0\,t_{max}/l$ is the cosine of the angle between the horizontal and the rays arriving at the ship. Assuming that, below a relatively thin surface layer, sounds travel from the depth of the float with a uniform velocity V_m, the angle δ between the sound rays and the horizontal, over most of their path, will be given by

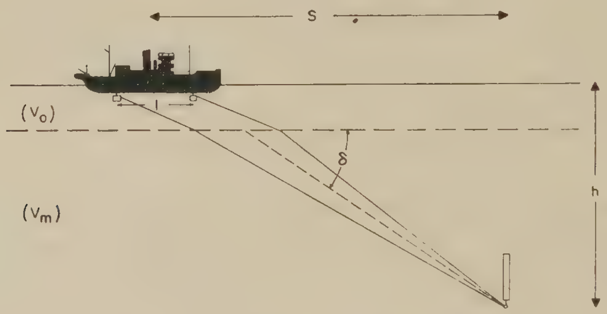

FIG. 5. Estimating the depth of a float.

$$\delta = \text{arc cos}\left(\frac{V_0\,t_{max}}{l} \times \frac{V_m}{V_0}\right), \quad \text{or} \quad \text{arc cos}\left(\frac{V_m\,t_{max}}{l}\right)$$

The horizontal range, s, is obtained from the radar plot of the ship's position as each bearing is taken (FIG. 4b) and the depth h is given by

$$h = s \tan \delta$$

The mean velocity V_m can be obtained from the vertical profile of temperature and salinity, using suitable tables (e.g. MATTHEWS, 1939). A value of the depth can thus be calculated for each bearing. The individual estimates show considerable scatter, but the mean value is usually within one or two hundred metres of the expected depth. Part of the scatter arises from uncertainties in the relative positions of the ship as determined by radar, and movements of the float and anchored buoy during a group of bearings. When Loran only was used, the uncertainties of relative positions were often too great for useful depth calculations to be made.

As a check on the validity of the assumption that a mean sound velocity may be used, the ray paths were calculated in detail in a few cases. The error introduced in the calculated depth by using the mean velocity was only a few tenths of one per cent and may be neglected.

To obtain the currents from the sequence of Loran fixes on the drifting floats, the positions were plotted on 1 in. to the mile scale. The north-south and east-west components were then plotted separately against time. Straight lines were then fitted by least squares to these displacement-time curves; in some cases where a change in the current seems to have occurred, the sequence was divided into two parts and separate lines fitted. The components of current derived from the slopes of these lines were then recombined to give the resultant velocities and directions of the mean currents.

ACCURACY OF NAVIGATION

Estimates of the r.m.s. error of a single Loran observation on the *Discovery II* were made from the scatter in the readings taken at each fix on a float. During the first part of the cruise, 82 pairs of Loran readings were taken during 20 fixes on a single float, and the r.m.s. error of a single Loran reading was 3·8 μs on 1H6 and 3·9 μs on 1H7. Some readings were missed because of poor reception, particularly on 1H7 at night. In the second part, 441 pairs of readings were taken during 73 fixes on floats; and the r.m.s. error of a single reading was 1·9 μs on 1H6 and 1·8 μs on 1H7. The decrease in scatter was due partly to improvements in the antenna system for the Loran receiver, and partly to increased operating experience. These correspond approximately to an r.m.s. error in position, for a single Loran reading, of 1·1 km in the first part and 0·6 km in the second part.

Systematic Loran errors due to fluctuations in propagation paths and lack of synchronism in transmitted pulses were unlikely to exceed 1 μs (PIERCE *et al.*, 1948) since we were within the normal ground-wave area for these stations. Systematic differences between receivers, of 1 or 2 microseconds, were found on a few occasions when simultaneous fixes were taken from the two ships and their relative positions were measured at the same time by radar. The *Atlantis* Loran positions were adjusted to make them consistent with those of the *Discovery II*, but the existence of these differences suggests that the instrumental contribution to the error of absolute position may be about 0·6 km.

A single Loran fix on the *Discovery II* would then have an r.m.s. error of approximately 1·3 km in the first part of the cruise, and 0·9 km in the second part.

Fixes on floats, being based on from 4 to 8 pairs of Loran readings, should be self-consistent to within about 0.6 km in the first part, and 0.3 km in the second part, assuming that the instrumental Loran errors are fixed. The observed residuals from fitted straight lines are slightly greater, 0·7 km for the first float (B) and 0·6 km for the remainder. The residuals were analyzed for periodicities, but nothing significant was found.

On board the *Atlantis*, Loran fixes were taken at the beginning and end of each hydrographic station, on a receiver on the bridge, and a fix was taken on another receiver in the laboratory when the deep cast was put down. The accuracy of fixes could not be estimated from the scatter of these readings, since the drift due to surface current and wind was insufficiently well known, and sometimes the ship was manoeuvered to reduce the hydrographic wire angle. It is assumed that the r.m.s. error of a station position is approximately 0·9 km, and the error relative to the float positions is approximately 0·6 km.

DIRECT CURRENT MEASUREMENTS

Durring the first part of the cruise, from March 4th to 11th, work was confined to a small area near 32° 29′N, 75° 21′W. The weather was poor, and both ships were hove-to for two of the eight days. Seven parachute drogues were laid, but some were never seen again and only three were tracked for a day or more. Three neutrally-buoyant floats were used but only one gave a useful measurement. The first one laid was abandoned after one fix, after the *Discovery II* had collided with the anchored buoy and spent one night lying-to, with the buoy and its floats wrapped round the screw. A new buoy was anchored 6 km west of the previous position and another float (B) was released near it, loaded for 2000 m depth (Table 2). This float was tracked for two days, and then the weather turned bad. When work was resumed two days later, a third float was launched, loaded for 700 m, since it seemed likely that float B's batteries would have run down. The new float could not be found at first fix, but the old one was heard giving a weak signal, and tracking was continued for another day, when the *Discovery II* had to leave the area in order to refuel at Charleston, S.C.

In the second part of the cruise an area 75 km to the north-west, closer to the surface Gulf Stream, was chosen, and current measurements were continued from March 17th to April 2nd. Six parachute drogues were laid, four of which were followed for periods up to 3½ days. Eight neutrally-buoyant floats were used, seven of which moved in directions between south and south-west at depths exceeding 2500 m. The first one laid, D, moved slowly south-west for three days, when a shallower one, E, was laid. Both floats were followed for another two days, the deeper one continuing south-west and the shallower one moving first north, then curving westwards. Both were abandoned on March 22nd and two more floats, F and G, were launched next day, loaded for 2500 m. They were 7 km apart in an east-west direction, and both moved slightly west of south at about one-sixth of a knot. Float G was the slower, and converged towards float F. Deeper measurements were started on March

26th, when floats H and I were launched, loaded for 2800 m. Again they were laid 7 km apart, and about 6 km north of the starting point for floats F and G. Both moved quickly south, H making about ⅓ knot and I about ¼ knot. Again, the slower eastern track converged towards the other. These two floats went quickly out of radar range of the anchored buoy, and tracking continued using Loran only. They were abandoned on March 29th, by which time float H had travelled 41 km, and had caught up with another float previously abandoned (probably F). In the afternoon of March 29th the bottom current was measured using the photographic method, near the beginning of the track of float I. The direction of flow was very close to south.

Two more floats (J and K) were launched early next day, loaded for 2800 m. One of them was intended to be in the track of the previous fast-moving float H, and the other was 7 km to the west. Another bottom-current measurement was attempted in the afternoon, but the camera and tripod were lost due to the wire parting when only 150 m remained to be recovered. Tracking continued on the two floats and a parachute drogue, float J being followed until a.m. April 2nd.

The results of the current measurements are summarized below. Table 1 gives all the measurements with parachute drogues and surface dye markers. The surface currents are seen to be variable in strength and direction, but generally of the order of half a knot to the north-east. The two drogue measurements at 10 m depth both show a current of the order of 35 cm/sec slightly south of east, though the direction may have been influenced by wind, which was from 330° in both cases. The measurements at 200 m and 700 m indicate a northward or north-eastward flow in the upper layers, the latter being particularly convincing since it moved upwind, though the observed current may be too small on this account.

The three deepest parachute drogues all moved approximately north-east at about 0·1 knot. Such small currents are hardly significant in view of the shear, which may be of the order of 50 cm/sec between surface and bottom. The drogues at 2700 m and 2800 m might have been expected to move south, but it is possible that the strong shear may have prevented the parachutes from reaching their full depth.

The neutrally-buoyant float results are presented in Table 2. The seven measurements at depths below 2000 m show southward movement, and although large variations were found at given depths, a general increase towards the bottom is indicated. It seems likely that the mean depths, of 2580 m for floats D, F and G, and 2840 m for H, I, J and K, are more reliable measures of the depths reached by these floats than the individual determinations are. The large scatter, from 2760 m to 2910 m at a nominal depth of 2800 m, is probably not genuine, in view of the close similarity of design of the floats and the accuracy of adjustment of densities. The very small mean current observed with float B, shows that, at that time and place, the level of no motion was very close to 2000 m in depth.

Table 3 shows the results obtained with the bottom-current meter. Fluctuations in direction, exceeding the uncertainty of measurement, were observed with both the suspended ball and the aniline drops. These may be genuine, but are more probably due to instability of the ball or to turbulence caused by the presence of the tripod framework. The velocity obtained from the deflection of the ball is comparable with that of float I nearby at 2800 m depth ; the lower velocity obtained from dispersal of the mud cloud, formed on touching the sea floor, may be due to diffusion upstream or to its being nearer the bottom.

THE METHOD OF COMPUTING THE VELOCITY PROFILES AND VOLUME TRANSPORT OF THE DEEP COUNTERCURRENT

All that has been described so far has been concerned with the direct current measurements themselves. In order to provide velocity profiles and estimates of the volume transport of the deep countercurrent, the physical data, consisting of temperature and salinity observations must be related to these direct measurements. This has been done by means of the classical geostrophic equation.

Atlantis made an initial oceanographic section to establish where the deep geostrophic gradients were strongest and subsequently made a number of sections intended to cross the deep countercurrent in such a way as to intercept the path of a drifting

Table 1. *Summary of current measurements with drogues and dye-markers, March–April* 1957

Time and date *from*	*to*	*Position* *(mean)*	*Nominal depth* (m)	*Mean current* cm/sec	*Bearing towards* °T	*Remarks*
2103/6	0130/7	*	10	33	115°	Wind 10–20 knots from 330 °T
1510/7	—	*	0	—	070°	Observation too short for speed to be estimated
0858/7	1500/9	*	1800	4·5	057°	Wind variable, 10–50 knots, 340°–240°. Exceeded 30 knots for 24 hours, from 240°–270°
1320/9	1404/9	*	0	4·5	075°	Wind 30 knots from 270 °T
0815/10	0654/11	*	700	4·5	343°	Wind decreasing 25 knots to 12 knots, from 320 °T
0900/11	0915/11	*	0	20 approx.	045°	Observation too short for reliable estimate
1738/17	1837/17	33° 08′N 75° 45′W	0	43	003°	Wind 14 knots, from 090 °T
1315/18	1410/18	33° 07′N 75° 44′W	0	20 approx.	015°	Approximate current from visual range estimate
2200/18	2200/19	33° 11′N 75° 45′W	2700	5·3	015°	Wind variable, 18 knots from 150 °T veering to 25 knots from 260 °T
1136/19	1339/19	33° 05′N 75° 45′W	0	13	295°	
1105/23	1756/23	33° 01′N 75° 43′W	10	36	129°	Wind 15 knots from 330 °T
0912/24	1453/24	33° 04′N 75° 42′W	0	9	108°	
2300/29	0400/1	33° 08′N 75° 41′W	2800	6·1	035°	Wind variable, 15 knots from 320 °T, then calm, then 15 knots from 090 °T
1015/1	1125/1	33° 05′N 75° 47′W	200	74	033°	Parachute was probably still sinking, observed current may represent average for upper 100 m

*All above observations were made in vicinity of 32° 29′N, 75° 21′W (within 2 mls.).

Table 2. Summary of current measurements with neutrally-buoyant floats, March–April, 1957

Float	*Launched* (*time and date*)	*Last fix* (*time and date*)	*Intended depth* (m)	*Mean observed depth* ((m) ± st. dev.)	*Mean velocity* (cm/sec ± st. dev.)	*Direction* (°T ± st. dev.)	*Remarks*
B	1000/6	0743/11	2000	2040 ± 70	0·33 ± 0·11	108 °T ± 18°	
D	1715/17	0718/22	2500	*2550 ± 40	4·27 ± 0·21 1·88 ± 0·11	201 °T ± 1·4° 235 °T ± 4°	2206/17–0320/19 0636/19–0718/22
E	1527/20	1717/22	1500	1480 ± 50	6·42 ± 0·47 6·50 ± 0·29	308 °T ± 4·7° 231 °T ± 2·3°	1825/20–2135/21 0010/22–1717/22
F	0954/23	0733/25	2500	*2620 ± 80	8·99 ± 0·53	190 °T ± 2·3°	
G	2050/23	1032/26	2500	*2600 ± 50	4·41 ± 0·26 7·08 ± 0·44	218 °T ± 3·3° 203 °T ± 2·3°	0002/24–0314/25 1110/25–1032/26
H	0815/26	0605/29	2800	†2910 ± 70	18·36 ± 0·28	182 °T ± 1·0°	
I	0854/26	1040/29	2800	†2760 ± 190	6·02 ± 0·27 12·62 ± 0·39	216 °T ± 2·6° 196 °T ± 1·3°	1424/26–0555/27 1715/27–1040/29
J	1110/30	1103/2	2800	†2900 ± 120	10·24 ± 0·18 9·42 ± 0·22	204 °T ± 1·7° 185 °T ± 11°	1347/30–0034/1 0858/1–1103/2
K	1156/30	0935/31	2800	†2770 ± 200	12·95 ± 0·59	207 °T ± 5·2°	

*Mean for D, F and G = 2580 m.
†Mean for H, I, J and K = 2840 m.

Table 3. *Results of measurements with photographic bottom-current meter*

Date	*Time*	*Position*	*Depth* (m)	*Mean current* (cm/sec)	*Bearing towards* °T	*Remarks*
29/3	1613–1636	33° 07′N 75° 42′W	3230	—	173° ± 11°	From movement of aniline drops
				11·5 ± 1·5	182° ± 6°	From deflection of ball, 40 cm above bottom
				5	ca. 180°	From dispersal of mud cloud, ca. 20 cm above bottom

float. When a section successfully crossed the path of a float, only one direct measurement was available. On the basis of this one measurement, the level of no motion between the pair of stations on either side of the float could be easily determined.

This was done by first computing the velocity between the two stations relative to an arbitrary level, usually 1500 m, and drawing a curve for velocity versus depth. The observed velocity (the component of the float's drift at right angles to the pair of stations) was plotted on the same graph at the depth of the float. Then the velocity depth curve was corrected at all levels by the difference between the observed velocity and the velocity given by the original curve at the float's depth. The depth at which the corrected curve crossed the 0 velocity line was taken to be the depth of the level of no motion.

So far, no assumptions had been made beyond those always made in dynamic computations, but in ascribing levels of no motion to other pairs of stations a further assumption was made. This was that the level of no motion between these stations fell at the same potential temperature surface as it did between stations where direct measurements were available.

The potential temperature/salinity relationship in this region is extremely reliable. The average deviation from the mean Θ/S curve is only 0·0035‰. In consequence, a potential temperature surface represents a potential density ($\sigma\Theta$) surface. These $\sigma\Theta$ surfaces sloped downwards in an offshore direction and the surfaces taken as levels of no motion in this work, always fell in a region of small vertical shear. They are in accord with Defant's (1941) requirements for the determination of the level of no motion. If one were to assume, for example, that the potential density surface at the position of the float was a constant velocity surface, the result would be that large volume transports would occur at the ends of the sections where little or no geostrophic gradients occurred.

The dynamic computations were performed according to Helland-Hansen's formula given in Proudman (1953, pp. 64 and 65), with one important exception. This was that instead of using the individual temperature and salinity, an average potential temperature vs. salinity curve was used to determine the specific volume anomaly ($10^5\ \delta$) at temperatures below the 4° isotherm, which lies at a depth of about 1500 metres in the region where the measurements were made. This was done because the Θ/S relationship is extremely reliable in this part of the Atlantic and also (since this was known beforehand) because salinity samples were not drawn on many of the stations.

The average deviation from a smooth Θ/S curve on this cruise was 0·0035‰ of salinity, (based on 538 observations below the 4° isotherm). Since this figure approaches that of the sensitivity of the Woods Hole salinometer (Schleicher and Bradshaw, 1956),* it seemed better to assume that the small irregularities which do occur are more likely to be caused by errors in the water sampling and analysis than by any real change in the Θ/S relationship in the ocean. Another reason why this method is preferred, is that error of analysis with the salinometer cannot be expected to be random. The instrument was standardized against Copenhagen Standard water at the beginning and end of each day's work, (about 125 samples). If one day's standardization differs by as little as 0·002‰ from that of the next day, a measurable difference in $10^5\ \delta$ can result; moreover, the instrument drifted during the course of a day's work by as much as 0·004‰ (average 0·003‰). Provided that this drift is at a constant rate no inaccuracy results, but it is by no means certain that the drift is constant.

---

*It can be appreciated that salinity values obtained by Knudsen titration would be entirely useless for dynamic computations of this kind since the errors of that method are about 7 times as large.

Both these sources of error are of the sort which would tend toward very small but systematic error in salinity. In North Atlantic deep water, an error of 0·003‰ in salinity (at constant temperature) results in an error of 0·23 in $10^5\ \delta$. This error is negligible if it is a random error, occurring on either side of the true Θ/S curve with more or less the same frequency, but if it is a systematic error occurring only on one side of the Θ/S curve it becomes serious. An error of 0·23 in $10^5\ \delta$ compounded over a 1000 metre water column causes an error in dynamic height of 0·0023 dynamic metres. In latitude 33°, where these observations were made, this would result in a systematic velocity error of 3 cm/sec if the stations concerned are 10 km apart ; this amount makes a considerable difference in determining the level of no motion. However, a random error remains even if the Θ/S curve is exact since there is an uncertainty of 0·01°C in each observation of temperature. This results in an uncertainty of velocity of 1 cm/sec, if the float is 1000 m below the reference level, and the stations are 10 km apart. An uncertainty of twice this amount (in addition to the systematic error) results if the individual temperature and salinity values are used.

Above the 4° isotherm the temperature/salinity relationship is less reliable and the values of $10^5\ \delta$ were obtained from the individual values of temperature and salinity at each Nansen bottle.

The volume transports were computed simply according to area x velocity. Transports were obtained for each standard depth interval between each pair of stations. The mean of the velocities at the top and bottom of each layer was used.

Since the observations were made across a sloping ocean floor, there were small areas adjacent to the bottom which fell below the greatest depth of observation at the inshore stations of each pair. In these cases, it was assumed that the velocity remained unchanged below the deepest standard depth. The size of these areas was determined by planimeter after the bottom contour had been drawn in. These areas were quite small since a 200 m standard depth interval was used and most of the stations extended almost to the bottom, (33 per cent of the stations extended to the bottom itself and 72 per cent to within 100 metres of the bottom).

THE ATLANTIS SECTIONS

2–4 *March*

The first section (stations 5476–5483) was made by *Atlantis* before the arrival of *Discovery II*. Its purpose was to establish where the strongest deep pressure gradients were to be found, so that the floats could be properly placed. The best spot seemed to be at about 32° 30′N 75° 20′W; here the slope of the deep isotherms was the steepest. The depth at this position is 3700 metres, which is well up the continental slope from the abyssal plain (5200 m) as had been expected from the Cape Romain section (FIG. 1).

6 *March*

The first successful float, B, was launched in this region and remained there, almost stationary, at a depth of 2070 metres for four and a half days.

6–7 *March*

While this float was drifting at this level, Section II (stations 5484–5489) was made across the position of the float, bracketing it between stations 5485 and 5486. The level of no motion was assumed to be 2070 metres between these stations as indicated by the float. A potential temperature of 3·44° was found at 2070 metres at the float (the average potential temperature of stations 5485 and 5486 at that depth) and this potential temperature surface was assumed to be motionless between the other pairs of stations on this section, as described in the previous chapter on methods of computation. The resulting velocity profile (Fig. 6) shows a consistent southerly current below the reference level. The volume transport of this current was 3·5 million m^3/sec. Most subsequent sections showed larger volume transports and it may be that the section was too short. This was the only section in the first part of the cruise which crossed the track of a float. However, two more sections (I and III) were made before both ships went into Charleston. Section I was the exploratory section already described and Section III was made at the conclusion of the first half of the cruise to see whether the deep gradients were any stronger to the north.

It seems reasonable to assign the same temperature to the reference level on these two sections, particularly since the first two sections made after leaving Charleston showed a potential temperature of 3·43° at the reference level, a change of only 0·01°. The velocity profile of Section I (Fig. 7) shows a stronger southerly current than that of Section II. The current seems to be divided into two halves with almost no transport taking place between stations 5479 and 5480. The total transport of the undercurrent in the section was 6·8 million m^3/sec. It is possible that the offshore half of the current is not the undercurrent proper (its salinities are slightly higher at the same potential temperature). If this is taken to be the case, the volume transport (stations 5479–5483) is reduced to 4·1 million m^3/sec, a figure in better agreement with those of subsequent sections. These were admittedly shorter.

11–12 *March*

Section III (Fig. 8) revealed that the gradients were indeed stronger to the north of the first working area and it was decided to move to the neighbourhood of this section for the second half of the work. The current was far narrower and swifter than before although roughly the same volume transport was computed; 4·4 million m^3/sec. The surface velocities of the Florida Current were much stronger as was to be expected but were not, as it turned out, sufficiently strong to hamper the deep measurements.

During the second half of the cruise, most of the stations consisted of one series of eleven bottles which extended from 1500 metres to the bottom in most cases. It was clearly desirable to make the stations as rapidly as possible, since in many cases two floats were adrift at the same time, and it was felt that the undercurrent lay wholly below the 1500 metre level. In retrospect, it would perhaps have been better to have extended these stations up to the 1200 metre level in order to include more of the northward flowing water but this would have decreased the density of the observations in the undercurrent itself.

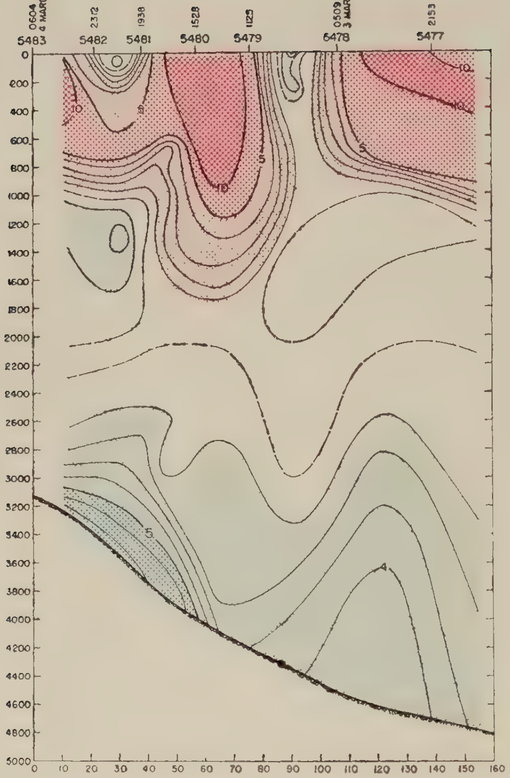

SECTION I, 2–4 MARCH

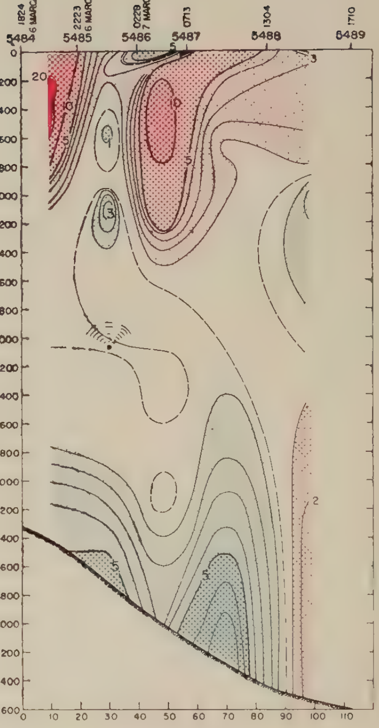

SECTION II, 6–7 MARCH

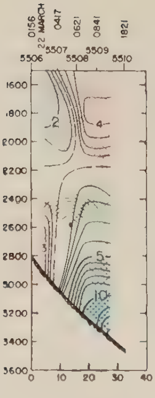

SECTION V MARCH 22

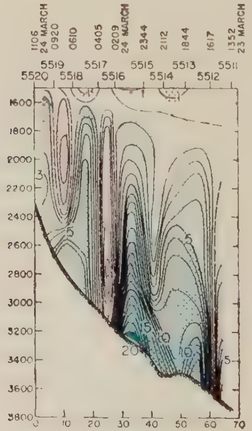

SECTION VI, 23–24 MARCH

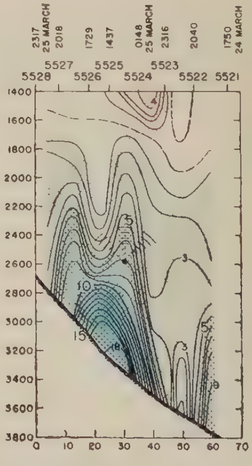

SECTION VII, 24–25 MARCH

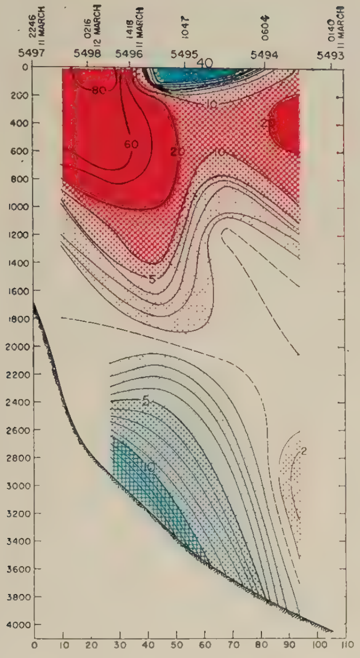

SECTION III, 11-12 MARCH

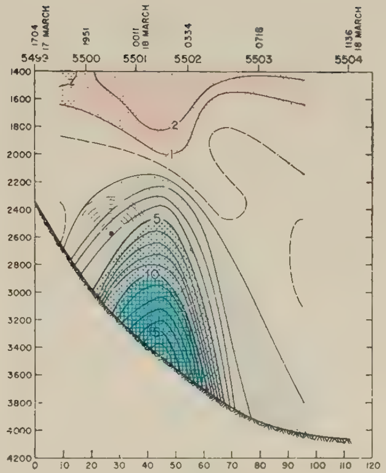

SECTION IV, 17-18 MARCH

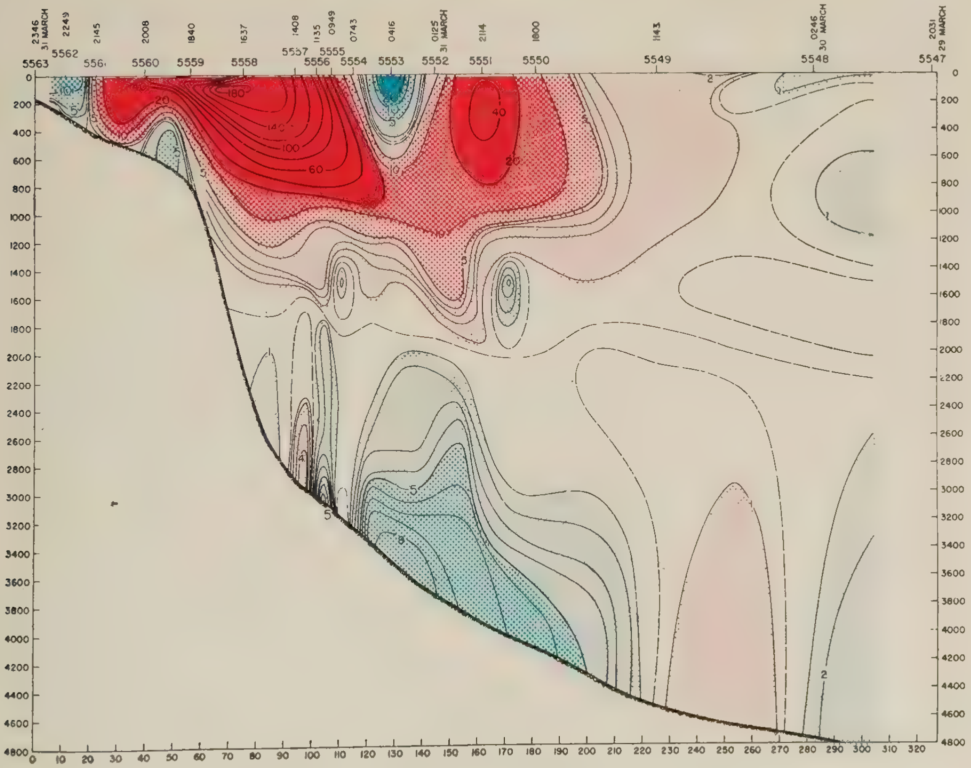

SECTION VIII, MARCH 29-31

16 *March*

After leaving Charleston, *Discovery II* preceded *Atlantis* to the new operating area which was centred at 33° 03′N, 75° 45′W. Section III had indicated that the strongest deep currents should be found above the 3150 metre depth contour.

17–18 *March*

Float D was launched at this contour and *Atlantis* made her fourth section (stations 5499–5504) across the path of this float, bracketing it between stations 5500 and 5501. The southerly component of velocity at right angles to these stations was measured by the float as 3·7 cm/sec at 2580 metres. The level of no motion between these two stations was 1950 metres and the potential temperature at that depth was 3·43°. The velocity section (Section IV, FIG. 9) shows a remarkably steady and symmetrical southerly current; this is probably due in part to the somewhat wider spacing of stations, (about 18 km). The volume transport of this current was computed at 4·1 million m^3/sec. The float was not in the swiftest part of the undercurrent which seemed to have meandered about 20 km offshore between the times of Section III and Section IV.

The next section was delayed partly by bad weather and partly because *Atlantis* took an injured scientist from *Discovery II* in to Morehead City for medical treatment. By this time, float D was still working but it was drifting much more slowly.

22 *March*

Atlantis made a short section (No. V, stations 5506–5510, FIG. 10) across the path of float D making no effort to cross the entire current but getting another estimate of the level of no motion. Float D's track was crossed between stations 5507 and 5508 and it showed a velocity component of 0·91 cm/sec at right angles to a line drawn between these stations. The computations gave a level of no motion at 2150 metres and the potential temperature surface used for this section was 3·43°, the same value as that of the previous section.

23–24 *March*

Following this *Atlantis* made two sections, one at 33° 10′N and the other at 33° 03′N. The intention was to cross the undercurrent both north and south of floats F and G, which had been launched on 23 March. However, insufficient allowance was made for the southerly drift of these floats which was double that of float D. Consequently, the northerly section of the two (stations 5511–5520) did not approach the track of either float closely enough to calculate a reference level from it. The reference level, therefore, was assumed to lie at the same potential temperature surface (3·68°), as the southerly section which immediately followed it.

The northerly section (No. VI, FIG. 11) is the most complicated. This is due in part to the close spacing of the stations, which averaged 8 kilometres, but there is no question about the reality of the streakiness in the crosscurrent pressure gradients. No navigational error can be expected to cause a reversal in the computed current direction such as appears between stations 5516 and 5517, and the highest velocity values are found between the most widely spaced pair of stations, 5516 and 5517, which is the reverse of what one would expect from a navigational error. The computed volume transport of this section was 4·4 million m^3/sec.

24–25 *March*

The southerly section (No. VII, stations 5521–5528, FIG. 12) is not so streaky although the station interval averaged only 9 km. For this section the drift of float G was used since F was already more than 11 km to the south before the section crossed its track. Float G passed between stations 5524 and 5525 at a depth of 2580 m with a velocity of 7·08 cm/sec at right angles to the stations. The calculated level of no motion was 1640 metres and the 3·68° potential isotherm was used as a reference level for the remainder of the section. The southerly volume transport of the undercurrent relative to that surface was 5·0 million m^3/sec. It is difficult to see any continuity of current between these two sections. The high velocity zone between stations 5515 and 5516 on Section VI can probably be connected with the high velocity zone between 5524 and 5525 on Section VII. Other highs and lows can be connected but with decreasing reliability.

26 *March*

On the morning of 26 March, *Discovery II* launched floats H and I loaded for 2800 metres and *Atlantis* began a square pattern of stations intended to cross the tracks of these floats. Bad weather forced her to stop after 4 stations, all to the east of these floats. Fortunately, two of these stations 5529 and 5532 crossed the path of float G, 6 km apart. It was consequently possible to get another estimate of the level of no motion, which fell at 1820 metres and at a potential temperature of 3·54° a figure well within the limits of the previous measurements.

27 *March*

A whole day was lost by *Atlantis*, hove to in heavy weather, but before midnight on 27 March she was able to resume work.

27–28 *March*

Three pairs of stations (5533–5534, 5535–5538 and 5536–5537) were made across the paths of floats H and I but unless the level of no motion lay much shallower than 1500 m the spacing of these stations was too wide to measure the true slopes of the isobaric surfaces and in consequence the computed currents are far slower than the observed. The narrowest spacing (13 km) was between stations 5533 and 5534 where the computed southward velocity (relative to the 3·68° potential isotherm) was 4 cm/sec at 2840 m the depth of floats H and I, whereas, the observed component of velocity at right angles to these stations was 17 cm/sec for float H and 12 cm/sec for float I. It can be seen from FIG. 12 that a station spacing of 13 km would result in diminished calculated velocities and a broader, slower flow.

28 *March*

Immediately following these stations, a section was made with an average station interval of 3 km, (stations 5538–5542). The southward computed velocities at 2840 m were 23 cm/sec between 5538 and 5539 and 12 cm/sec between 5539 and 5540. These velocities would go very well with floats H and I respectively, although the value of 23 cm/sec is rather too high for float H, but unfortunately both pairs of stations would have to be moved about 3 km to the west in order to cross the track of the floats. (These velocities were calculated relative to the 3·68° isotherm as before).

Float H was already 20 km to the south at the time the stations were made and float I was 4 km to the south since *Atlantis* again made insufficient allowance for the southerly drift of the floats. In consequence, all that the closely spaced section did establish was that geostrophic currents sufficiently strong to carry the floats at their maximum velocity could be calculated from the distribution of density. The high value of 23 cm/sec is possibly due to navigational error since stations 5538 and 5539 were only 1·9 km apart, the shortest station interval of the cruise.

Aboard *Atlantis* only rapid and rudimentary current calculations were made and the importance of bracketing the floats closely in time as well as in space was not properly appreciated. This apparently caused no great damage to the measurements involving the shallower floats, B to G, but the oceanographic observations on the deeper (2840 m) floats, H to K were not adequate since at that depth the pressure field evidently fluctuates more rapidly with time.

On the morning of 29 March, *Atlantis* left the working area in order to start the final oceanographic section. This section, it had been agreed, was to include the entire Florida Current as well as the deep undercurrent. The first station, 5547 was at 33° 01′N, 73° 30′W, about 220 km east of the working area. The stations consisted of two series except on the shelf and while crossing the tracks of floats J and K when only one series was made. Again, it seems, the oceanographic measurements were not adequate ; only half the velocity of these floats could be accounted for by the dynamic calculations unless the level of no motion were raised to 1000 m. While this could possibly have been the case, it seemed more sensible to assume that the true slopes of the isobaric surfaces were missed by *Atlantis* and that the level of no motion lay at some greater depth. The potential isothermal surface of 3·56°, a median value obtained from earlier measurements, was used as a reference level for this section.

On the basis of the existing stations, no satisfactory level of no motion could be obtained by using the deep floats, H-K. This is thought to be due mainly to the streakiness of the currents at 2840 m which required station intervals to be much closer than they were both in position and, particularly, timing.

30–31 *March*

This final section (No. VIII, FIG. 13) took two days to complete and gave a computed volume transport for the Florida Current (*above* the reference level) of 63·6 million m^3/sec, stations 5549–5561. The volume of the southerly undercurrent (stations 5549–5558) came to 6·7 million m^3/sec, and that of the shallow inshore countercurrent 0·5 million (stations 5561–5563). The net northerly transport through this section was, therefore, 56·4 million m^3/sec.

At first glance, it does not appear that an undercurrent of only 6·7 million m^3/sec can be of much importance to the water budget of the western North Atlantic, but it becomes extremely important when the net transport of 56·4 million m^3/sec is compared to the value obtained when the bottom is used as a reference surface.

If the direction of the southerly undercurrent is reversed by using the bottom as a reference surface, the northerly volume transport becomes 7·2 million m^3/sec (a slightly larger figure because the vertical shear is usually greater towards the bottom). In addition to this, between each pair of stations the transport above the intermediate reference level must be increased by an amount equal to the area included between the stations (above the reference level) times the velocity at the intermediate level. This comes to the more substantial figure of 16·2 million m³/sec.

Accordingly, the net transport relative to the bottom in this section is 63·6, + 7·2, + 16·2, − 0·5 (the inshore countercurrent), or 86·5 million m³/sec, an increase of 30·1 million. This increase is roughly equal to Montgomery's (1941) estimate of the total volume transport of the Florida Current between Key West and Havana. The establishment of the level of no motion can be seen to be of profound importance in estimating the water budget of the western North Atlantic in spite of the rather small volume of water transported by the deep countercurrent.

SUMMARY AND CONCLUSIONS

The direct measurements of currents, described above, show that southward velocities in the range 9–18 cm/sec can be found in the region of steep temperature gradients in the deep water off the Blake Plateau. The steadiness of these velocities, observed over periods of several days, and the consistent finding of a southward movement at depth, whether directly or indirectly observed, at each attempt during a period of a month, suggest that the southward flow may be a permanent feature of the circulation in that area.

In other regions, where weak temperature gradients are found, and where a few direct measurements of current at comparable depths have been made (Swallow, 1957, Swallow and Hamon, 1959) the observed velocities have been in the range 0–5 cm/sec, and variable in direction. The fast-moving southward deep currents off the Blake Plateau stand in a similar ratio to these weaker observations as does the surface Gulf Stream velocity to typical surface currents in the open ocean, and they may therefore perhaps, on account of their magnitude, be fairly described as a deep western boundary current.

Whether a continuous current can be traced in the deep water along a substantial part of the western Atlantic remains to be decided by further observations. Remarkably similar velocities have been computed by Wüst (1958) at the western boundary of the South Atlantic.

On the assumption that the flow is geostrophic, velocity profiles have been computed between pairs of hydrographic stations bracketing the tracks of the floats, using the directly-observed velocity as a reference, and hence estimates have been made of the depth of the level of no motion. On the further assumption that the surface of no motion is a surface of constant $\sigma\Theta$, velocities and volume transports have been computed between other pairs of hydrographic stations, leading to estimates of the total transport in the deep southward current and, in one case, of the transport in the Gulf Stream itself.

The level of no motion has been shown to lie at a depth of about 1900 m, off the Blake Plateau. This intermediate reference surface is consistent with that chosen by Defant (1941), but difficulties are encountered in extending the use of this reference surface to larger areas.

Stommel's (1957) thermohaline model of the Atlantic circulation, which inspired the measurements here described, is strongly supported by the demonstration that fast-moving southerly currents can exist in the deep water at the western boundary of the North Atlantic.

Contribution No. 1129 *from the Woods Hole Oceanographic Institution.*

REFERENCES

DEFANT A. (1941) Die absolute Topographie des physikalischen Meeresniveaus und der Druckflächen, sowie die Wasserbewegungen im Atlantischen Ozean. *Deutsche Atlantische Exped. Meteor* 1925–1927, *Wiss. Erg.*, **6** (2), 191–260.

DIETRICH G. (1936) Aufbau und Bewegung von Golfstrom und Agulhasstrom, eine vergleichende Betrachtung. *Die Naturwissenschaften*, **24** (15), 225–230.

ISELIN C. O'D. (1936) A study of the circulation of the Western North Atlantic. *Pap. Phys. Oceanogr. Meteor*, **4** (4), 1–101.

LAUGHTON A. S. (1957) A new deep-sea underwater camera. *Deep-Sea Res.* **4**, (2) 120–125.

MATTHEWS D. J. (1939) Tables of the velocity of sound in pure water and sea water. Hydrographic Department, Admiralty, London.

MONTGOMERY R. B. (1941) Transport of the Florida Current off Habana. *J. Mar. Res.*, **4** (3), 198–220.

PIERCE J. A., MCKENZIE A. A. and WOODWARD R. (1948) *Loran.* McGraw-Hill Book Co., Inc., New York. pp 000.

PROUDMAN J. (1953) Dynamical Oceanography. Methuen and Co., Ltd., London, 409 pp.

ROSSBY C-G. (1936) Dynamics of steady ocean currents in the light of experimental fluid mechanics. *Pap. Phys. Oceanogr. Meteor*, **5** (1), 1–43.

SCHLEICHER K. E. and BRADSHAW A. L. (1956) A conductivity bridge for measurements of the salinity of sea water. *J. Cons.* **22** (1), 9–20.

STOMMEL H. (1956) Oceanography. Washington conference on Theoretical Geophysics. *J. Geophys. Res.*, **61** (2.2), 320–323.

STOMMEL H. (1957) A survey of ocean current theory. *Deep Sea Res.* **4**, 149–184.

SVERDRUP H. U., JOHNSON M. W. and FLEMING R. H. (1942) *The Oceans.* Prentice Hall, New York, 1087 pp.

SWALLOW J. C. (1955) A neutral-buoyancy float for measuring deep currents. *Deep-Sea Res.*, **3**, 74–81.

SWALLOW J. C. (1957) Some further deep current measurements using neutrally-buoyant floats. *Deep-Sea Res.*, **4**, 93–104.

SWALLOW J. C. and HAMON B. V. (1959) Some measurements of deep currents in the Eastern North Atlantic. *Deep-Sea Res.* **6**, 155–168.

VOLKMANN G. H., KNAUSS J. A. and VINE A. C. (1956) The use of parachute drogues in the measurement of subsurface currents. *Trans. Amer. Geophys. Union*, **37** (5), 573–577.

WÜST G. (1958) Stromgeschwindigkeiten und Strommengen in den Tiefen des Atlantischen Ozeans. *Deutsche Atlantische Exped. Meteor* 1925–1927, *Wiss. Erg.*, **6**, 35–420.

Printed in Great Britain by The Salisbury Press Ltd., Publicity House, Wilton Road, Salisbury, Wilts. (29168)

Contribution No. 1131

CHAPTER 5

AN INSTRUMENTATION SYSTEM FOR WAVE MEASUREMENTS, RECORDING AND ANALYSIS

by

H. G. Farmer and D. D. Ketchum

Woods Hole Oceanographic Institution
Woods Hole, Massachusetts

ABSTRACT

For the instrumentation system to be described, it was required that the system detect the sea surface accurately, be flexible in dynamic range, be able to detect and record at least six wave records simultaneously, be able to record the data at a station remote from the detectors, and be able to convert the data from analogue to digital form for analysis by electronic computers. Two types of wave measurements were required, the wave elevation and the wave slope. Resistance wire detectors were used and the theory of their operation is presented. The data acquisition and reduction system utilize recently developed telemetry techniques. Raw data storage is on magnetic tape using an inexpensive tape recorder and the digital data storage utilizes punched paper tape. The resistance wires have proven most satisfactory for small and large waves. The data acquisition and reduction system is sufficiently general that it should have application to other type investigations.

INTRODUCTION

The instrumentation system to be described in this paper was developed for use with several research projects concerned with wind generated waves. It was developed at the Woods Hole Oceanographic Institution (WHOI) and has been in operation for the last year. These investigations required that the wave elevation be measured at several discrete points, these several channels of data to be recorded simultaneously as a function of time. A closely allied experiment required measurement of the instantaneous slope of the sea surface referred to two horizontal axes aligned parallel and perpendicular to the wind direction. To accomplish these aims it was necessary to develop a suitable measuring instrument, and because of the expected large quantity of data and extensive calculations to be done, an efficient and practical means for recording and data reduction was needed. It was assumed at the outset that nearly all of the calculations would be carried out on an electronic digital computer.

It was planned that a large number of the wave observations would be taken from a tower situated in Buzzards Bay, a line of sight distance of two miles from the Oceanographic Institution in Woods Hole.

---

*Contribution No. 1131 from the Woods Hole Oceanographic Institution.

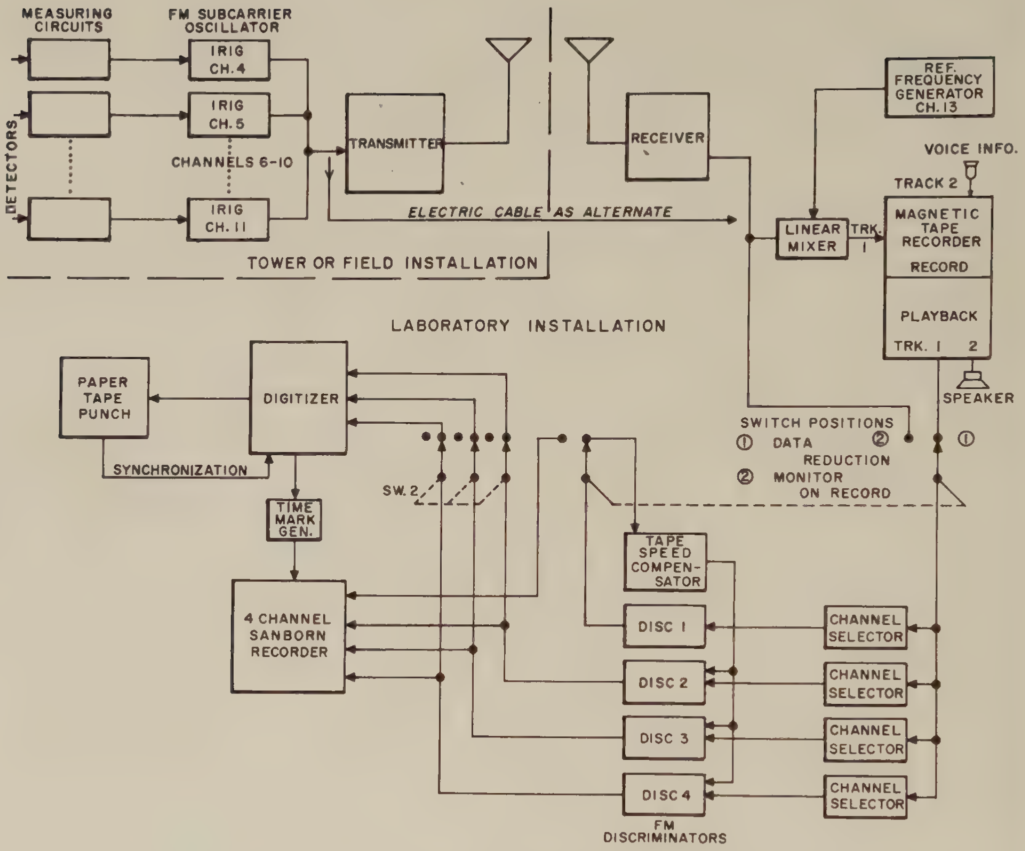
MEASURING CIRCUITS
FM SUBCARRIER OSCILLATOR
IRIG CH. 4
IRIG CH. 5
CHANNELS 6-10
IRIG CH. 11
DETECTORS
TRANSMITTER
RECEIVER
ELECTRIC CABLE AS ALTERNATE
TOWER OR FIELD INSTALLATION
REF. FREQUENCY GENERATOR CH. 13
VOICE INFO.
TRACK 2
LINEAR MIXER
TRK. 1
MAGNETIC TAPE RECORDER
RECORD
PLAYBACK
TRK. 1 2
SPEAKER
LABORATORY INSTALLATION
PAPER TAPE PUNCH
DIGITIZER
SYNCHRONIZATION
TIME MARK GEN.
SW. 2
SWITCH POSITIONS
① DATA REDUCTION
② MONITOR ON RECORD
②
①
TAPE SPEED COMPEN-SATOR
4 CHANNEL SANBORN RECORDER
DISC 1
DISC 2
DISC 3
DISC 4
FM DISCRIMINATORS
CHANNEL SELECTOR
CHANNEL SELECTOR
CHANNEL SELECTOR
CHANNEL SELECTOR

Fig. 1. WHOI multi-channel data acquisition and reduction system.

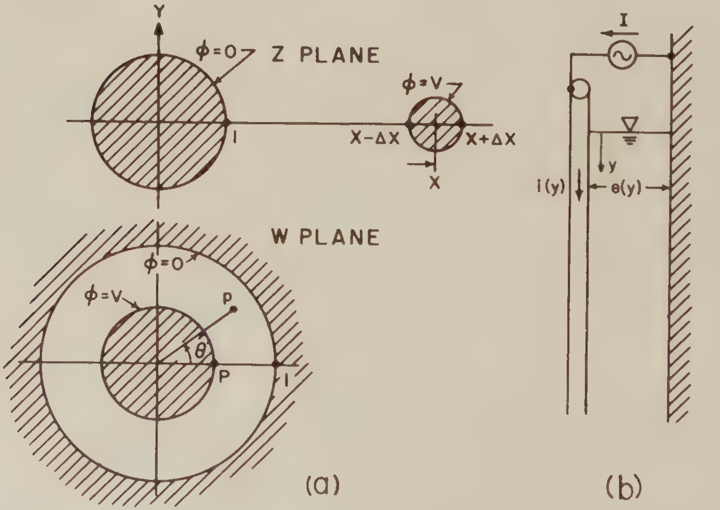
Y
$\phi=0$
Z PLANE
$\phi=V$
1
X-ΔX
X+ΔX
X
W PLANE
$\phi=0$
$\phi=V$
P
θ
P
1
I
y
i(y)
e(y)
(a)
(b)

Fig. 2. (a) Geometry of wire and ground conductor and their transformation, (b) Schematic diagram of single wire transmission line and parallel ground plane, constant current source.

Because of the physical conditions at the tower, only the necessary measuring circuits would be placed there and the several data channels, a total of eight, would be telemetered by radio to the laboratory, where they could be monitored and recorded. Furthermore, it was anticipated that observations would be made from other installations, and therefore the measuring and monitoring equipment should be kept portable.

An accurate measurement of the sea surface elevation immediately precluded any use of the well known pressure type wave recorder. Other techniques considered included the step-resistor type, Caldwell (1948), capacitance wire type, Tucker and Charnock (1955) and Whittenbury (1956) and the resistance wire type, Gerhardt, Jehn and Katz (1955). To take the difference in elevation of the sea surface between two points spaced close together, say approximately 6 inches, was considered adequate for the slope determination. This would require an accurate measure of the elevation at each point, and consequently the detectors must cause an absolute minimum disturbance to the water surface. It was hoped to make such measurements on waves up to six feet in height. For just the elevation observations, waves considerably higher than this were to be measured. The step-resistor gage was discarded as not having sufficient resolution, and the capacitance gage, although it was briefly investigated, was discarded as not being sufficiently reliable. The resistance wire gage had also been reported by Caldwell (1948), but was not rated favorably as a general purpose, durable, service instrument. The work of Gerhardt, Jehn, and Katz (1955), and also Clayton, Ivey and Teegardin (1954), suggested that this type of instrument, if properly designed and used, would be most satisfactory. A detailed analysis of this method of measurement was made for both the elevation and slope observations. An account of this analysis is given in a later section of this paper.

The complete multi-channel data acquisition and reduction system is illustrated in Fig. 1. In its most recent usage, the eight channels of data comprised six wave records, wind velocity and direction. With the provision of suitable measuring circuits there is no limit to the type of data that can be handled, except for the upper limit of the frequency content of the information. The system can easily accommodate up to twelve data channels, and, by eliminating the voice information, twenty-four data channels can be recorded. Data with frequencies up to 110 cps can be faithfully recorded. A maximum frequency limit of about 10 cps is imposed if the data is to be converted from analogue to digital form using the WHOI electronic digitizer. A 1% accuracy for the overall system was a desirable requirement. Rather than specify this, however, each component was selected for a 1% accuracy, or as close to this as practicable, so that the complete system might well be expected to have an accuracy of 3%. Data would be recorded for time intervals up to one half an hour. This system will also be discussed in detail. The Inter-Range Instrumentation Group (IRIG) Standards used in the system are briefly described in the text.

Finally, a brief description will be given of the field installation, a few practical considerations concerned with it and several examples of the type data collected.

Aside from the contribution this paper may make to the rather specialized subject of wave measurements, it is hoped that the telemetering and recording system will be of general interest since it is flexible enough to lend itself to a number of other uses without major modification. Although the techniques and most of the components involved are familiar to, and indeed were evolved largely be engineers in the missile industry, the authors are of the opinion that the subject is still sufficiently novel to oceanographers to warrant giving a description.

THE RESISTANCE WIRE WAVE MEASURING SYSTEM

The successful use of resistance wires for the measurement of waves requires careful design of the measuring circuits and a knowledge of the electrical behavior of the wires in the water. The wave height sensing devices consist of vertically supported stainless steel wires partly immersed in sea water. A constant current at audio frequency (4 kc/s) flowing in each wire and returning through the water path causes a voltage drop across the exposed portion of the wire proportional to the length of wire exposed. The voltage at the wire terminal after suitable amplification and detection is converted to a proper signal for telemetering to the laboratory for recording.

For the two types of measurements to be made, i.e., surface elevation and surface slope, the principal factors to be considered in the design are as follows:

a) The current and voltage distribution along the wire as a function of depth below the water surface;

b) The degree to which the generator feeding the wires must approximate an ideal current source;

c) The effect on the slope measuring circuits of the finite input impedance of the differential amplifiers;

d) The resolution of the wire in terms of the smallest measurable increment of the height of the surface.

In actual conditions of usage the resistance wire may be supported from quite different types of towers. At Woods Hole the wires were simply hung outboard of a light steel frame tower which served as the return path for the electrical current exciting the wire. This comprises a most complicated geometry to analyze in detail. Thus an analysis of (a) may best be performed by idealizing the geometry of the complete wire system. If the wire is considered to be supported parallel to a large vertical cylindrical conductor, partially immersed in a body of water of infinite extent, then it is possible to treat the immersed portion of the system as a transmission line with series resistance per unit length determined by the type of wire and shunt conductance per unit length determined by the geometry, the conductivity of the water and the polarization impedance at the wire-water interface.

In the following analysis, for the type of operation of the wire contemplated, it is found that for proper linearity of the voltage output with a constant current input it is necessary to maintain a certain minimum length of wire beneath the water surface at all times. For use in sea water with practical wire diameter and assumed geometry, the requirement for this minimum length of submerged wire may be easily met. This particular mode of operation of the wires proves impractical for use in fresh water. However, it is shown that a constant voltage system using a wire of very high conductivity should prove satisfactory. Further, for either the constant voltage or constant current system, it is shown that so long as certain minimum requirements are met, the exact current and voltage distribution along the subsurface portion of the wire are unimportant.

Since the specific resistance of the wire is known or can readily be measured, determination of the properties of the "transmission line" depends upon a knowledge of the shunt admittance existing between the wire and the ground plane. This admittance has two components in series: the polarization admittance arising from the electrochemical reaction at the surface of the wire electrode, and the admittance of the electrolyte, dependent upon the configuration of the electrodes and the physical properties of the water. Each of these admittances is complex, having a component of capacitive susceptance as well as conductance. However, it is well known to those familiar with the technique of sea water conductivity measurements that at frequencies above about 1 kc/s the effect of the capacitance becomes small enough to neglect, and the polarization admittance is essentially constant at a fixed frequency. It is for this reason that the 4 kc/s frequency was selected for the wire excitation. Therefore, although the polarization admittance accounts for a substantial part of the total effect, it can be regarded as a constant, which, since it is in series with the electrolyte admittance, reduces the total admittance to a value below that of the electrolyte admittance alone. In the case of the electrolyte admittance it is also true that the capacitance between the wire and the ground plane is small enough to be neglected at the operating frequency. Hence it only remains to calculate the real part of the electrolyte admittance, which will hereafter be simply termed the shunt conductance.

THE WIRE-GROUND CONDUCTOR FIELD PROBLEM

The determination of the shunt conductance requires the solution of the field problem associated with the configuration shown in Fig. 1a, where a wire of radius Δx is maintained at a potential V with respect to a parallel conductor of unit radius. If it is assumed that the immersed part of the system extends to infinite depth, then because of symmetry the solution for the potential may be found in two dimensions. Application of the following transformation, Churchill (1948), results in a coaxial configuration whose potential can easily be found:

$$w = \frac{z - a}{az - 1} \tag{1}$$

where

$$a = \frac{1 + (x + \Delta x)(x - \Delta x) + \sqrt{[(x + \Delta x)^2 - 1][(x - \Delta x)^2 - 1]}}{2x} \tag{2}$$

and the transformed radius is

$$P = \frac{(x + \Delta x)(x - \Delta x) - 1 - \sqrt{[(x + \Delta x)^2 - 1][(x - \Delta x)^2 - 1]}}{2x} \tag{3}$$

$$x - \Delta x < a < x + \Delta x \qquad 0 < P < 1 \quad \text{when } x - \Delta x < 1$$

The potential ϕ of the transformed system is

$$\phi = \frac{V}{\ln P} \ln p \tag{4}$$

and the total current per unit length flowing from the wire to the large conductor may be found as follows :

$$\vec{E} = \text{GRAD}\phi = -\frac{\partial\phi}{\partial p} \tag{5}$$

$$i = -\sigma \int_0^{2\pi} \vec{E}\, p\, d\theta = -\frac{2\pi\sigma V}{\ln P} \tag{6}$$

where σ = the conductivity of the water

$\vec{E}$ = the electric field vector

The shunt conductance per unit length is then

$$g = \frac{i}{V} = -\frac{2\pi\sigma}{\ln P} \tag{7}$$

In the practical case being considered the wire diameter is very small compared with the radius of the ground conductor, making the accurate computation of P tedious. The expression for P, eq. (3), may be simplified by replacing the square root term by the first two terms of its binominal expansion and neglecting the term in Δx to the fourth power. This approximation, eq. (8), is therefore valid for values of $\Delta x << x$.

$$P = \Delta x \left(\frac{1}{x^2 - 1} \right) \tag{8}$$

Rescaling the dimensions of the Z plane to the actual physical dimensions

$$P = \frac{k}{K} \left(\frac{1}{D^2/K^2 - 1} \right) \tag{9}$$

and from eq. (7) the shunt conductance becomes

$$g = \frac{2 \pi \sigma}{\ln \frac{K}{k} \left(\frac{D^2}{K^2} - 1 \right)} \tag{10}$$

where D = Distance between centers

K = Ground conductor radius

k = Wire radius

RESISTANCE WIRE ANALYSIS, CONSTANT CURRENT SOURCE

With the value of the shunt conductance established, the wire and ground conductor may now be regarded as a single wire transmission line parallel to a perfectly conducting ground plane (Fig. 2b). This last assumption is valid since the actual ground conductor is a pipe whose series resistance, because of its relatively great diameter, is negligible compared to the series resistance of the wire. If the original assumption of infinite immersed depth is for the moment maintained, the classic transmission line equations may be written, without, however, the complication of accounting for the reactive components, since the frequency of the wire current will be low enough to neglect series inductance, and the leakage, or shunt conductance, is so high in sea water that the effect of shunt capacitance will be negligible.

The general solution for the voltage with respect to the ground plane and the current in the wire as functions of distance along the wire are found by well-known methods, Guillemin, (1935), to be

$$e\ (y) = A\ e^{\sqrt{\rho g}\ y} + B\ e^{-\sqrt{\rho g}\ y} \qquad (11)$$

$$i\ (y) = \sqrt{g/\rho}\ \left[- A\ e^{\sqrt{\rho g}\ y} + B\ e^{-\sqrt{\rho g}\ y} \right], \qquad (12)$$

where ρ is the resistance per unit length of the wire,

and y is distance measured from water surface.

The constants are evaluated by applying the end conditions:

$$i\ (0) = I, \quad i\ (\infty) = 0 \qquad (13)$$

where I = the current in the wire above the water surface.

The voltage and current along the wire are seen to be simple exponential functions of depth.

$$i = I\ e^{-\sqrt{\rho g}\ y} \qquad (14)$$

$$e = I\ \sqrt{\rho/g}\ \ e^{-\sqrt{\rho g}\ y} \qquad (15)$$

Of interest is the depth at which the current decays to a negligible value. If this critical depth y_c is defined as the depth at which the current in the wire is reduced to 1% of I, then

$$y_c = \frac{4.60}{\sqrt{\rho g}} \qquad (16)$$

It therefore follows that so long as the wire is immersed at least to its critical depth, it will behave as though immersed to infinite depth, and the voltage drop from the wire to ground at the water surface will remain constant as the level of the water changes with respect to the wire. It is this fact that permits us to regard the instantaneous level of the water surface as the position of a short circuit to ground, since the constant voltage drop simply represents a constant zero shift which can be calibrated out.

Substituting the formula for the shunt conductance into eq. (16) and expressing ρ in terms of the wire radius shows how the critical depth depends upon the wire radius with all other parameters held constant. The result of this manipulation is

$$y_c = \frac{4.60\ k}{\sqrt{2\ \sigma\ \rho'}} \quad \sqrt{\ln \left[\frac{K}{k} \left(\frac{D^2}{K^2} - 1 \right) \right]} \qquad (17)$$

where ρ' is the resistivity of the metal used for the wire. The critical depth is found to be very nearly linear with respect to the wire radius as is seen in Fig. 3. This is a plot of eq. (17) for the case of stainless steel wire spaced 10 inches on centers from a pipe of one inch radius in sea water of conductivity 0.127 mhos per inch.

When the wire is immersed to a depth λ which is less than the critical depth, the behavior of current and voltage along the wire as a function of depth can be found by noting that the end conditions now become

$$i\ (0) = I,\ i\ (\lambda) = 0 \tag{18}$$

Thus:

$$i\ (y) = I\ \frac{\sinh \sqrt{\rho g}\ (\lambda - y)}{\sinh \sqrt{\rho g}\ \lambda} \tag{19}$$

$$e\ (y) = I\ \sqrt{\rho/g}\ \frac{\cosh \sqrt{\rho g}\ (\lambda - y)}{\sinh \sqrt{\rho g}\ \lambda} \tag{20}$$

Under these conditions the voltage at the water surface and the voltage at the end become respectively

$$e\ (0) = I\ \sqrt{\rho/g}\quad \coth \sqrt{\rho g}\ \lambda \tag{21}$$

$$e\ (L) = I\ \sqrt{\rho/g}\quad \operatorname{csch} \sqrt{\rho g}\ \lambda \tag{22}$$

The voltage at the surface was measured experimentally in a tank of sea water, using .015" stainless steel wire spaced 5.5 inches on centers from a 3/4" diameter stainless steel pipe. The curve from this experimental data was found to be similar in shape to eq. (22) but displaced from it. This discrepancy is expected to be due principally to the effect of the unknown but nonetheless real polarization admittance. For the manner in which the resistance wires were to be used an estimate of this polarization admittance was not required. However, an experiment of this sort could provide such an estimate.

In situations where it may be impractical to employ a wire of sufficient length to reach critical depth, terminating the wire in its characteristic impedance, $\sqrt{\rho/g}$, should, in theory, simulate an infinite length of wire below the surface. In this manner e (0) could be held constant for short lengths of wire.

In order for the voltage drop across the exposed portion of the wire to be proportional to the exposed length, the current I must be constant and independent of the position of the water surface. Indeed,

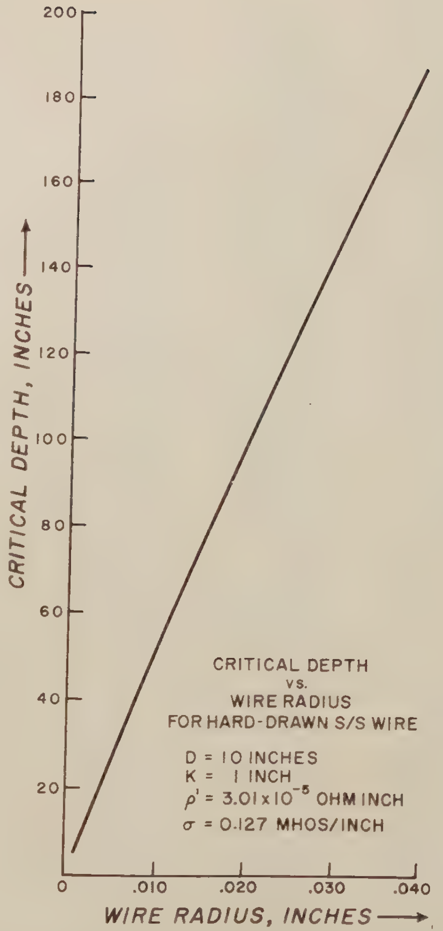

Fig. 3. Critical wire depth vs. wire radius, eq. 17.

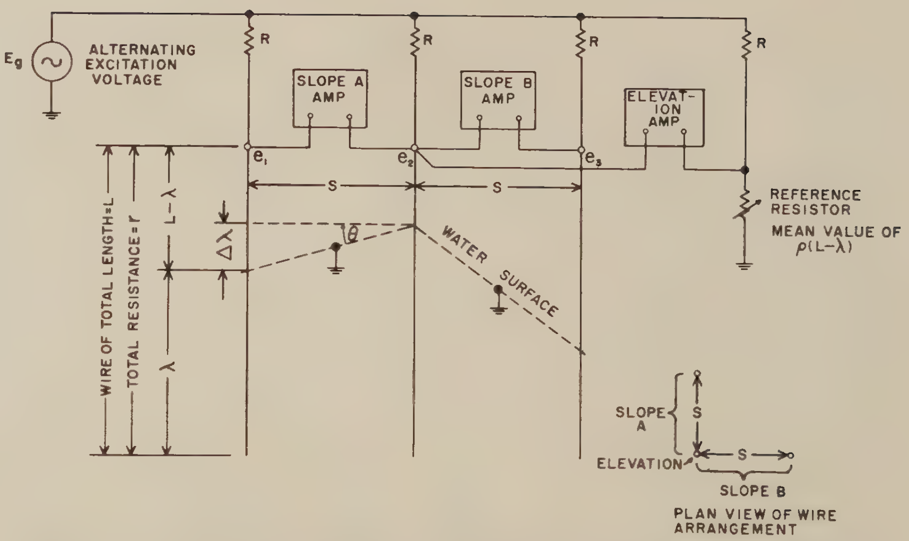
Eg
ALTERNATING EXCITATION VOLTAGE
R
SLOPE A AMP
SLOPE B AMP
ELEVATION AMP
e1
e2
e3
S
REFERENCE RESISTOR
MEAN VALUE OF ρ(L−λ)
WIRE OF TOTAL LENGTH=L
TOTAL RESISTANCE=r
L−λ
Δλ
λ
θ
WATER SURFACE
SLOPE A
ELEVATION
SLOPE B
PLAN VIEW OF WIRE ARRANGEMENT

Fig. 4. Schematic diagram of measuring circuits and wire detectors.

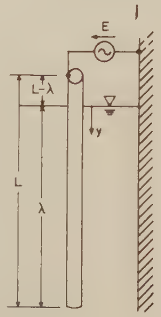

Fig. 5. Schematic diagram of single wire transmission line and parallel ground plane, constant voltage source.

the preceding analysis is based upon this assumption. The accuracy of the device is therefore dependent, among other things, upon two factors: namely, the degree to which the wire excitation source approximates a current source, and the degree to which the input impedance of the amplifiers associated with the wire approximates an open circuit.

The diagram in Fig. 4 shows how the equal current sources are approximated. Current regulation with respect to load variations is achieved by making the resistors R large compared to the sensing wire resistance r. The voltage source E_g is electronically regulated for stability. A simple calculation shows the ratio of series resistance to wire resistance required for a given percentage linearity of the output voltage appearing between one of the terminals and the water.

Assuming for the moment that the inputs of the amplifiers are open circuits, and for simplicity that the water surface is a short circuit, we will consider one individual wire. It is desired that the relation between the wire output voltage and the water height be linear within specified limits over the total range of interest. The output voltage is given by

$$e_2 (\lambda) = \frac{E_g \, r/L \, (L - \lambda)}{r/L \, (L - \lambda) + R} \tag{23}$$

The elevation sensitivity $d e_2/d \lambda$ must remain between specified limits to insure the desired linearity. (24)

Thus for 1% linearity,

$$\left.\frac{d e_2}{d \lambda}\right|_L - \left.\frac{d e_2}{d \lambda}\right|_0 = \frac{1}{100} \left.\frac{d e_2}{d \lambda}\right|_0 \tag{25}$$

Solution of (25) for R yields

$$R = 200 \, r \tag{26}$$

In the case of a slope determination the difference between the voltages at the terminals of two parallel wires whose spacing is known is measured by means of a differential amplifier. Analysis of the effect of the ratio R/r on the accuracy of this measurement shows that the voltage representing the slope is not nearly so sensitive to change in the elevation of the water surface as the elevation linearity. If we consider a pair of wires and assign the symbols e_1 and e_2 to the voltages at the terminals of the two wires, see Fig. 4, with respect to the water surface (considered as ground), then the slope of the water surface in the direction of a line connecting the two wires is proportional to e_{12}, the difference between e_1 and e_2. We must investigate how this difference varies for a constant slope over the length λ. Sufficient information for this purpose is given by comparing the expressions for the slope voltage at maximum and minimum elevation. Thus,

$$e_{12} = e_1 (\lambda) - e_2 (\lambda + \Delta\lambda) \tag{27}$$

and eq. (23) may be used for e_1 and e_2.

By taking the difference of e_{12} determined at $\lambda = L - \Delta\lambda$ and $\lambda = 0$, assuming $r \Delta\lambda << R L$, and allowing a maximum slope voltage variation of 1% over the range L, the following value of the resistance R is obtained

$$R = 1.58 r \tag{28}$$

Thus the requirement of eq. (26) more than fulfills the requirement for slope voltage accuracy over the length of the resistance wires.

The preceding discussion has been based on the assumption that the input impedance of the differential amplifiers is infinite. Although this is far from the actual case, it may be shown that if these impedances can be made high compared to the wire resistance, the above assumption is valid. Since the highest value of wire resistance contemplated in this design is about 20 ohms, it was possible to obtain an adequately high input impedance to the differential amplifiers which are of transistor design.

In the preceding analyses, the derived relations define the parameters of the sensing circuit and establish criteria for the sensitivity of the amplifier detector units and the output level of the stabilized voltage source. The maximum exposed wire resistance was chosen as nominally 20 ohms, which corresponds to about 10 feet of .015" diameter stainless steel wire. Thus, in providing the constant current source for the wire excitation, the series resistors R must be at least 4000 ohms according to eq. (26). Precision resistors with an accuracy ± .05% were used to insure that the currents flowing in each wire were identical.

RESISTANCE WIRE ANALYSIS, CONSTANT VOLTAGE SOURCE

An extension of the foregoing analysis shows how a wire may be used to measure waves in fresh water, where the conductivity is several orders of magnitude less than that of sea water. In this case a wire of very low specific resistance is driven with a voltage source E, as shown in

Fig. 5. Below the fresh water surface $y \geqq 0$ equations 11 and 12 hold, and for $y \leqq 0$:

$$e\,(y) = E - \rho\,(L - \lambda + y)\,i_0 \tag{29}$$

$$i\,(y) = i_0 = i\,(0) \tag{30}$$

Applying the end conditions

$$e\,(0) = A + B = E - \rho\,(L - \lambda)\,i_0 \tag{31}$$

$$i\,(\lambda) = 0 = - A\,e^{\sqrt{\rho g}\,\lambda} + B\,e^{-\sqrt{\rho g}\,\lambda} \tag{32}$$

and solving for i_0, we find the current in the exposed portion of the wire to be

$$i_0 = \frac{(1 - e^{-2\sqrt{\rho g}\,\lambda})\,\sqrt{g/\rho}\,E}{e^{-2\sqrt{\rho g}\,\lambda} + 1 + (1 - e^{-2\sqrt{\rho g}\,\lambda})\,\sqrt{\rho g}\,(L - \lambda)} \tag{33}$$

So long as $2\sqrt{\rho g}\,\lambda << 1$, equation (33) reduces to the approximation

$$i_0 = g\,E\,\lambda \tag{34}$$

showing that the current from the voltage source is directly proportional to the length of the immersed portion of the wire. For the range of conductivity encountered in most tap water it appears that the above criterion can be met by using copper wire of moderate diameter in lengths up to 10 feet. Calculation of the shunt capacitance of a typical system indicates that at low to medium audio frequencies the shunt susceptance is very small compared to the shunt conductance in fresh water. Hence as in the sea water system the analysis is valid without consideration of the reactive components.

VERIFICATION, MEASUREMENT RESOLUTION AND ADDITIONAL COMMENTS

It was found experimentally that the mean resolution of the current-driven wave measuring wire was limited to the order of 0.2 inch for a 12 foot length of wire. This result was demonstrated by an experiment where a pair of parallel wires was lowered and raised in a deep tank of sea water over a distance of 12 feet and maintained perpendicular to the calm surface. The output voltage from a single wire was measured for elevation. The output voltage from the differential amplifier fed from the two wire terminals, instead of remaining at zero, was observed to vary about its zero value in an erratic fashion. With a wire spacing of 6 inches the standard deviation from the mean value corresponded to 0.17 inch which was equivalent to a slope of 1.6°. Since careful attention had been devoted to the design of the differential amplifier, this effect could not be attributed to faulty common mode rejection or imperfect balance in the electronic circuits. The elevation measurements over the full range of immersion indicated the predicted linearity, but the difference measurements provided a measure of the resolution available.

The only plausible explanation for this "noise" appeared to be small random variations in the polarization admittance caused by surface contamination of the wire. Thus it was at least logical to assume that a thin but non-uniform layer of grease or contaminate could result in the admittance varying randomly with depth along the wire. Since the polarization admittance is a component of the shunt conductance, g, variations in the former would cause variations in e (0), upon whose constancy with surface height the system depends for its linearity. This thesis was partially supported by the fact that degreasing agents applied to the wires immediately prior to immersion caused changes in the effect, without, however, eliminating it.

In any case, since it would not be possible to maintain uncontaminated wires in field operation, a full-scale range of the order of two feet seems to be the practical limit where accuracy of one per cent of full scale is desired in an elevation wire, while the spacing of slope wires cannot be less than about six inches for angular accuracy of better than about 2^{o}.

In the equipment as it was actually built the signals from each of the elevation wires as well as the signals from the pairs of slope wires were amplified with differential amplifiers and detected with phase sensitive detectors. By adjustment of the various gain settings, the final output voltage was standardized to a 0-5 volt range for entry into the telemetering equipment. Differential amplifiers were used in the elevation circuits so that it would be possible to subtract from the wave wire signal another signal equivalent approximately to the mean length of unimmersed wire, refer to Fig. 4. This reference resistor is variable so that a proper adjustment may be made whatever the state of the tide. The total "swing" of the differential amplifier output is then primarily due to just the wave signal. The amplifier sensitivity is adjusted so that its full scale excursion in both directions is caused by the highest expected waves. The variable reference resistor may take the form of another wave wire which is supported in a tide tube. This tube would be designed so that the reference wire senses only tidal variation.

The design of the differential amplifier, particularly those for the slope measurements, required great care to be taken to insure high common mode rejection. The common mode rejection ratio of the amplifiers is determined by measuring the differential gain, the ratio of output voltage to the difference between the two input voltages. The two input voltages are made equal by tying the two input terminals together and the ratio of the output voltage to the common input voltage, or common mode gain, is measured. The common mode rejection ratio obtained was in the order of 10,000.

The 4 kc/s outputs of the differential amplifiers are detected in phase sensitive detectors, the magnitude of whose D.C. output is proportional to the amplified difference voltage applied. The polarity of each phase detector output is dependent upon the phase of the input compared to that of the fixed reference phase of the wire drive supply. Since the difference voltage undergoes a phase reversal at the point where the voltage difference input to the amplifier becomes zero, the sense of the instantaneous water level is preserved.

WHOI MULTI CHANNEL DATA ACQUISITION AND REDUCTION SYSTEM

The complete system in its present operational form is illustrated in Fig. 1. Two main divisions of the equipment have been made, the field installation and the laboratory installation. The means for telemetering the information between these two stations may be either by radio or electrical cable with each method requiring its own special terminal equipment. All of the data received at the laboratory in its full analogue form is recorded on magnetic tape, which serves as the raw data storage. Upon playback the data may be monitored, edited, digitized, or otherwise operated upon without altering the original data recording. Since the analysis was to be carried out on an electronic digital computer it was necessary to provide an analogue-to-digital converter and a means of storage, punched paper tape, for the digital information.

Besides the accuracy requirement of 1% for each component it was considered important to keep the system as adaptable as possible to a wide variety of applications and problems. As always it was necessary to keep the overall cost at a minimum.

The design of the telemetering apparatus was fortunately much simplified by the fact that the art of FM/FM telemetry has reached the advanced state where standard components are available from commercial manufacturers. Standard subcarrier frequencies, channel spacings and bandwidths, designed to permit optimum use of the available spectrum consistent with the requirements of bandwidth and signal-to-noise ratio have for some years been promulgated by the Inter-Range Instrumentation Group (IRIG) and are widely accepted by the industry. Nichols and Rauch (1957) give a comprehensive introduction to the theory and practice in the field of radio telemetry. When analogue information is to be transmitted any distance by radio, it is well known that frequency modulation best preserves the information against distortion by extraneous noise. Similarly, for magnetic tape recording as well as for radio transmission when the information data frequencies extend down to zero it is necessary to utilize frequency modulation (FM) to preserve this information. To obtain a number of data channels for transmission over a single radio frequency carrier or for recording on a single track magnetic tape recorder, the range of frequencies extending from about .4 kc to 70 kc has been divided up into a number of bands each of which is assigned a center frequency. See Table I. The information signal is then used to frequency modulate this center frequency, the maximum deviation for each band being ± 7 1/2% of its center frequency. From the table it will be seen that the maximum intelligence frequency depends on the subcarrier band selected. The WHOI system utilizes the IRIG data channels 4 through 11 but can accommodate channels 1 through 12.

A most satisfactory means for recording these several channels of data is on magnetic tape. It is significant to note that an expensive instrumentation recorder is not required. A relatively inexpensive, portable, hi-fidelity, dual track tape recorder has proven adequate for the job. One track is used for data recording, and voice information is put on the second track. In this manner the data may be documented with whatever additional information is needed while it is being recorded. Because of slight irregularities in the motion of the tape on both record and playback, occurring in all tape recorders, FM recorded data may be very seriously distorted. This difficulty can be virtually eliminated, however, by recording along with the data a stable reference or control frequency. Upon playback the variations in this frequency are used to correct the data restoring it to its original form well within the accuracy limits of the overall system. This correction process is referred to as tape speed compensation.

The field installation comprises the detectors, measuring circuits, FM subcarrier oscillators and, if required, a radio transmitter. The FM subcarrier oscillators are voltage controlled, a 0 to 5 volt swing at the input causing the output frequency to range from its lower to its upper limit. In order effectively to utilize the accuracy available in this telemetering and recording system, the sensitivity of the measuring circuits should be so adjusted that full scale of the information corresponds to the full 0-5 volt range of the subcarrier oscillator. Generally this can be easily done. The outputs of the oscillators are then linearly mixed and the combined signal is fed to the FM transmitter. It is by virtue of the information frequency modulating the subcarriers, and the several subcarriers frequency modulating the radio frequency carrier that the system is referred to as FM/FM telemetry. In those field installations where electrical power is primarily supplied by batteries, it is desirable to use as much transistorized circuitry as possible in order to prolong battery life and reduce the number of batteries required. Transistorized subcarrier oscillators are commercially available and are extremely rugged and highly dependable. The measuring circuits designed and built at WHOI for the wave observations were also transistorized.

TABLE I

IRIG STANDARD SUBCARRIER BANDS

Channel	Center Frequency (cps)	Deviation (cps)	Lower Limit (cps)	Upper Limit (cps)	Maximum Intelligence Frequency (Modulation Index 5) (cps)
		± 7 1/2% Deviation Channels			
1	400	± 30	370	430	6.0
2	560	42	518	602	8.4
3	730	55	675	785	11
4	960	72	888	1,032	14
5	1.3 kc/s	98	1,202	1,398	20
6	1.7	128	1,572	1,828	25
7	2.3	173	2,127	2,473	35
8	3.0	225	2,775	3,225	45
9	3.9	293	3,607	4,193	59
10	5.4	405	4,995	5,805	81
11	7.35	551	6,799	7,901	110
12	10.5	788	9,712	11,288	160
13	14.5	1,088	13,412	15,588	220
14	22.0	1,650	20,350	23,650	330
15	30.0	2,250	27,750	32,250	450
16	40.0	3,000	37,000	43,000	600
17	52.5	3,940	48,560	56,440	790
18	70.0	5,250	64,750	75,250	1,050

In choosing the means for telemetering the information from the field to the laboratory installation several factors must be considered. Among these are the total number of data channels, the channel center frequencies, the range of transmission, whether or not line of sight communication exists, etc. Generally if a large number of data channels are required and IRIG channel 7 or greater is used, the total band width of these data channels will require for radio transmission a VHF (say 230 mc) carrier with frequency modulation. This VHF-FM radio link will provide high quality telemetry, but the line of sight transmission may introduce a range limitation. With fewer data channels, IRIG 1 thru 6, the total band width of the several channels will permit use of an HF (2-6 mc) carrier but with amplitude modulation. In this case, the range of transmission will be greatly increased but there may also be some sacrifice in quality.

Electrical cables may also be used for the telemetering link. In this case the subcarrier signals are fed directly to the cable. Here again the band width and frequencies of the transmitted signals will dictate the selection of the cable. Generally if the band width is large and the higher frequency data channels are used a coaxial cable will be required.

At the laboratory the output of the FM receiver is linearly mixed with the reference frequency, 14.5 kc/s the center frequency of IRIG channel 13, and recorded with the magnetic tape recorder. At the same time, with switch 1 in position 2 any four of the data channels may be selected, using the appropriate channel selectors, sharp cut off band pass filters, discriminated and recorded on the four channel Sanborn recorder. This ability to monitor the data while it is being recorded is considered an important function of the system.

In the data reduction phase, one, two or three data channels may be arbitrarily chosen using the channel selectors. The fourth discriminator is used in conjunction with the tape speed compensator. The graphic recorder and the digitizer are both fed directly from the discriminator outputs, which are faithful reproductions of the original data.

The paper tape punch is driven by a 3600 rpm synchronous motor and contact closures operated by the motor provide timing signals and synchronization to the digitizer. The digitizer accepts a maximum of three data channels and digitizes them sequentially. Each channel is switched in, a sample is taken, converted to a seven level binary number and punched out on the paper tape, all in 1/60 second. The same sequence of events follows for the next two channels, a total of 1/20 of a second being required for the complete operation on all three channels. Following this sequence the paper tape is advanced with no punch, thus providing a space, i.e., a fourth channel with zero punch, to separate this data group from the next data group to be punched. Preselected sample rates of 15, 10, 5, 3, 2, 1 per second are provided. A time mark generator controlled by the digitizer provides a tick mark on the graphic record at each time a group is sampled.

A seven level binary code was selected for the digital format for two reasons. First, the seven level binary code provides for any number from 0 to 127 thus permitting a digitizing accuracy of better than 1%. The second reason is that with the straight binary code the Teletype tape punch can punch any number up to 127 in a single operation, thus permitting a rapid digitizing rate and also the optimum packing density of information on the paper tape. The relatively fast operation approximates simultaneous digitization of the three data channels if their signals do not vary rapidly. This scanning rate was a specific requirement in setting forth the specifications for the digitizer and tape punch. In any event the time difference between adjacent channels is 1/60 second plus or minus approximately 3/4 millisecond on the average.

There is one disadvantage to the use of the seven level binary code which should be clearly emphasized. No electronic computer known to the authors or their associates uses this particular code for normal entry of data. However, data entry has been easily accomplished in two cases using available paper tape readers. The IBM 46 tape-to-card punch has been used to transfer the data to IBM cards. This IBM 46 has been more effectively used, however, as a tape reader for direct entry of the data into an IBM 650 computer. A tape reader has also been provided for entry of the data directly into the Autonetics Recomp II computer. In both of these computers, through programming, the data is then put into proper format for subsequent calculation. Mr. R. G. Stevens of the WHOI has done all the work pertaining to the entry of the punched paper tape data into these two computers.

The digitizer was specially built because of its particular operating characteristics. The only other piece of equipment which required any special attention in its selection was the tape recorder. Because of the recording of FM signals, in selecting the tape recorder it was necessary to specify that the intermodulation distortion be kept as low as practicable. This was satisfied with the installation of a higher quality recording-reproducing head than normally supplied. However, in so doing, the frequency response of the recorder was reduced to 15 kc/s at 15 inches/second. It is for this reason that the total number of data channels that could be recorded on each track of the tape was limited to the first twelve, the thirteenth channel being required for tape speed compensation. The recorder has three standard operating speeds, 15, 7 1/2 and 3 3/4 inches/second, and with a small modification 1 7/8 inches/second. At this lowest tape speed using standard 1.5 mil magnetic

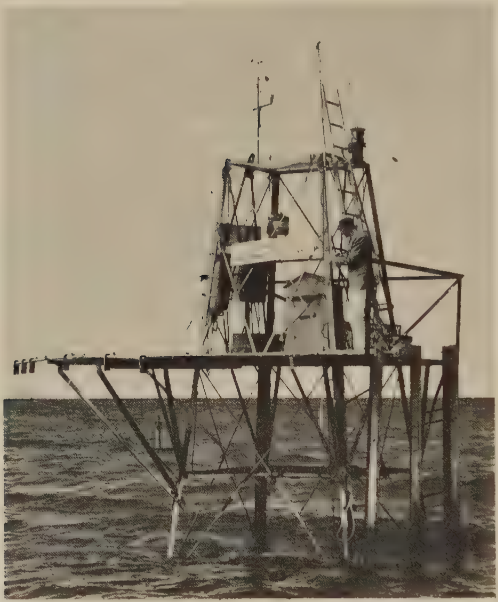

Fig. 6. WHOI tower situated in Buzzards Bay, Mass., water depth 42 feet. 0.015 inch diameter SS wire detectors hang from coaxial cables supported off left edge of tower.

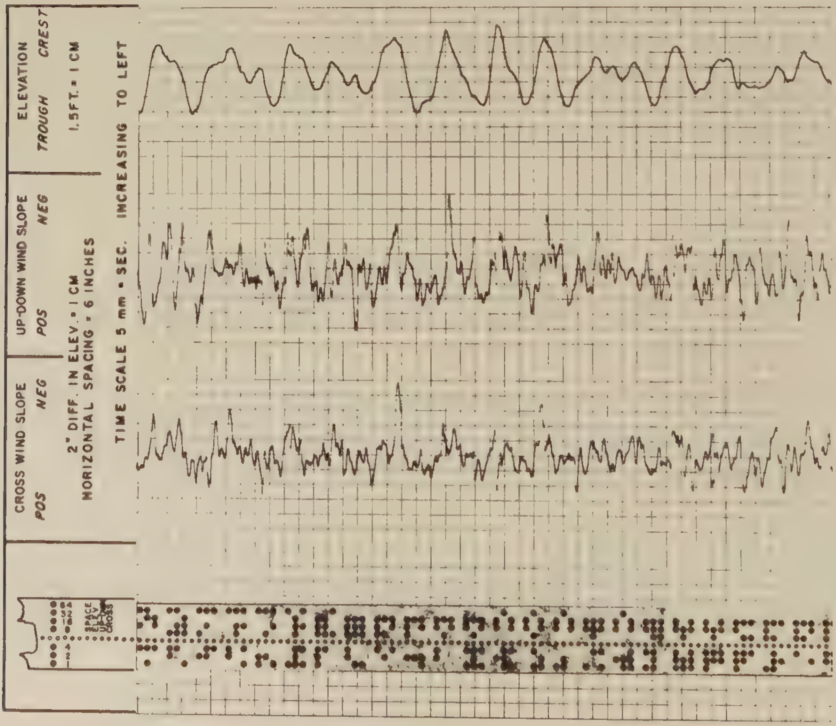

Fig. 7. Sample data obtained with resistance wire detectors. The heave lines are at 5 mm spacing. Bottom figure is sample of punched paper tape digitized at 10 groups per second. Tape is unrelated to data above.

tape, recordings of eight hours in duration can be made using the first five data channels. By in large, the intelligence frequencies present in oceanographic data are very low. For the wave studies carried out at WHOI it was necessary, however, to be able to record faithfully frequencies up to 10 cps. As is apparent in Table I, the system can record intelligence frequencies up to 110 cps. Thus, with faster digitizing equipment, the system may have a much wider range of application in other types of research. For the WHOI or similar type system further applications more directly related to the field of oceanography have been discussed briefly in Ref. 10.

In this section the intent has been to describe the data acquisition and reduction system through a rather general description, but of sufficient detail that its operating characteristics are clearly understood. Several practical features of the system have been emphasized because of their versatile and practical aspects. Finally, it is believed that the system presents a unified and logical concept in data handling.

THE FIELD INSTALLATION AND RECENT OBSERVATIONS

An extensive program of wave observations has been carried out using the equipment described in the preceding sections. A tower was placed in Buzzards Bay in water 42 feet deep and at a location 2 miles line of sight distance from the laboratory in Woods Hole. The tower, which is of light steel frame construction and 60 feet in height, was originally designed as a wind mill structure. The bottom of each leg is fitted with a large box shaped foot to provide a bearing surface. The lower sections of the tower were reinforced so as to support an additional 6 ton weight to "anchor" the tower to the bottom. A large cast concrete and scrap iron anchor had been previously placed at the proper site. The tower is placed over the anchor and attached to it with an hydraulic cylinder. By pumping oil into the cylinder the tower is anchored to the bottom with a predetermined part of the anchor weight. This manner of installation has proven most satisfactory and the tower has withstood winds in excess of 60 knots and waves up to 6 feet in height. The tower is disconnected from its anchor, picked up and carried to shore and stored during the winter months when heavy icing conditions may prevail. A detailed description of this facility is given by Carver, (1958), and an illustration of the tower is given in Fig. 6.

The wave wires are electrically connected to the input of the measuring circuits with a relatively inexpensive coaxial cable, RG-58AU. Equal lengths of coaxial cable were used for each wave wire detector. The simplest, most expedient and satisfactory means for holding the resistance wire in place was to hang each wire by means of a clamp on the coaxial cable with a small lead ball of about 3 pounds weight tied on the end of the wire. The submerged length of wire was about 20 feet so that the small lead ball was not subjected to any appreciable fluid velocities resulting from the wave field. The estimated critical length of the 0.015 inch stainless steel wire was about 3.5 to 4 feet. At no time were the wires observed to move because of wave motion or wind.

Referring to Fig. 6 there may be seen the wooden box in the shape of a dog house which encloses all the necessary electronics for obtaining the wave and wind data and telemetering it to the laboratory. Mounted on masts above the tower are the anemometer and wind direction indicator and the 230 mc tuned ground plane antenna. At the laboratory a corner reflector and antenna were mounted above the roof from which sufficient signal strength was obtained for reliable operation. The accumulator and oil tank for the hydraulic anchoring system are also visible.

On another occasion these same type resistance wires were used from a much larger tower installation. Approximately 40 foot lengths of 0.015 inch resistance wire were used and approximately 25 to 30 feet of this was below water level. Satisfactory wave records were obtained in winds in excess of 40 knots and waves 20 to 25 feet in height. The wires were observed to be in some motion dependent upon the size waves encountered. The maximum horizontal motion of the wire was about 1 foot for the highest and longest waves observed.

A sample record of elevation, up-down wind slope and crosswind slope is shown in Fig. 7. The wind speed at the time of recording was 16 knots, having been this speed for the previous hour and before that time the wind had been blowing at about 10 knots. For the up-down wind slope record the negative sign refers to the slope found, on the average, on the side of the wave facing the direction in which it is propagating. The same rule holds for the crosswind slopes if the wave were traveling from left to right when looking into the wind. To obtain the actual slope it is necessary to divide the indicated differences in elevation by the wire spacing which was 6 inches.

At the bottom of Fig. 7 there is reproduced a sample of the punched paper tape for a record similar to that above it. The four channels, crosswind slope, up-down wind slope, elevation and space are indicated in the figure. The group punching rate was 10 times/second.

ACKNOWLEDGMENTS

The developments reported in this paper were made possible through a grant to the Woods Hole Oceanographic Institution from the National Science Foundation of the National Academy of Sciences and in part through a contract with the U. S. Navy Office of Naval Research.

AN INSTRUMENTATION SYSTEM FOR WAVE MEASUREMENTS, RECORDING AND ANALYSIS

REFERENCES

1. Caldwell, J. M. (1948). An ocean wave measuring instrument: Tech. Memo. No. 6, U. S. Army Corps of Engineers, Washington, D. C.

2. Carver, C. E. Jr. (1958). The WHOI wave tower research facility: Ref. No. 58-51, Woods Hole Oceanographic Institution, Woods Hole, Mass. (Unpublished manuscript)

3. Churchill, R. V. (1948). Introduction to complex variables and applications: McGraw-Hill Book Co., New York

4. Clayton, L., Ivey, H. D. and Teegardin, H. H. (1954). Preliminary study for the development of a sea state meter: Tech. Report No. 6 Engineering Experiment Station Proj. No. 157-96, Georgia Inst. of Tech.

5. Gerhardt, J. R., Jehn, K. H. and Katz, D. (1955). A comparison of step-, pressure- and continuous wire-gage wave recordings in the Golden Gate Channel: Trans. Amer. Geophys. Union Vol. 36, No. 2

6. Guillemin, E. A. (1935). Communication networks: John Wiley and Sons, Inc., New York, Vol. II

7. Nichols, M. H. and Rauch, L. L. (1957). Radio telemetry: John Wiley and Sons, Inc., New York

8. Tucker, M. J. and Charnock, H. (1955). A capacitance-wire recorder for small waves: Proc. 5th Conf. Coastal Eng. Council Wave Res. Univ. of Calif. Berkeley

9. Whittenbury, C. G. (1956). A capacitance probe for recording water waves: Report No. R-84, Control Systems Lab. Univ. of Ill. Urbana, Ill.

10. Proceedings of the conference on automatic data handling for oceanographic observations (1959) Ref. No. 60-10, Woods Hole Oceanographic Institution, Woods Hole, Mass. (Unpublished manuscript)

Contribution No. 1132

Reprinted from BIOLOGICAL BULLETIN, Vol. 120, No. 1, pp. 92–109, February, 1961
Printed in U. S. A.

METAMORPHOSIS OF THE VELIGER LARVAE OF NASSARIUS OBSOLETUS (GASTROPODA) IN RESPONSE TO BOTTOM SEDIMENT

RUDOLF S. SCHELTEMA

Woods Hole Oceanographic Institution, Woods Hole, Massachusetts

METAMORPHOSIS OF THE VELIGER LARVAE OF NASSARIUS OBSOLETUS (GASTROPODA) IN RESPONSE TO BOTTOM SEDIMENT[1]

RUDOLF S. SCHELTEMA[2]

Woods Hole Oceanographic Institution, Woods Hole, Massachusetts

Characteristic of most marine organisms is propagation of their kind by the production of great numbers of pelagic larvae. As a consequence, the dispersion of such organisms over large areas is possible. Success of benthic organisms is dependent, however, upon the metamorphosis of their larvae onto a substratum which meets their special adaptations and requirements. The metamorphosis of marine larvae upon a favorable substratum, if left to chance alone, would be indeed remote.

This hazard is apparently not as great as was once supposed, since many marine invertebrate organisms delay metamorphosis until they encounter a favorable substratum. Metamorphosis occurs as the response to a stimulus received from the desirable environment. Inasmuch as the evidence has been reviewed in a recent paper by Wilson (1952), it is necessary to relate only briefly the facts which lead to this conclusion.

The earliest laboratory observations which indicated that the substratum played a role in stimulating metamorphosis were those of Mortensen (1921) on the echinoid *Mellita sexiesperforata.* Mortensen made the casual observation that when larvae which were ready to metamorphose were placed in a culture jar with sand, metamorphosis ensued within a few days, while similar larvae from the same original culture placed in a jar without sand showed "hardly any further advance in the process of metamorphosis." This observation was later confirmed on three other species (Mortensen, 1938).

Harrington (1921) observed that shipworm larvae (*Teredo norvegica*) were positively chemotactic to a substance which he extracted from wood and which he believed was malic acid. Wilson (1952) has extended this observation and has shown that in the absence of the wood, shipworm larvae do not metamorphose. Settlement may be postponed for about one week.

Wilson (1932, 1937, 1948) and Day and Wilson (1934) observed the response of larvae of several polychaetous worms to the presence of their natural substratum. In all cases the settlement of the larvae was brought on by the addition of small quantities of substratum collected from their normal habitat. Substrata from other areas either were less effective or appeared to inhibit metamorphosis. Wilson chose *Ophelia bicornis* for a more detailed study and the results of this work have been reported in a series of papers (Wilson, 1948, 1951, 1952, 1953a, 1953b, 1954,

---

[1] Contribution No. 1132, Woods Hole Oceanographic Institution.

[2] This paper is based on part of a dissertation presented to the University of North Carolina, Chapel Hill, N. C., in partial fulfillment of the requirements for the degree of Doctor of Philosophy.

1955). While size and shape of grains seemed to have some bearing on the metamorphosis-inducing quality of the substratum, Wilson (1955) finally concluded that (p. 537) "the factor most active in inducing metamorphosis and settlement of *Ophelia bicornis* larvae is the presence on sand grains of living organisms, such as bacteria, and that these should be neither too few nor too abundant. . . . Certain species are more effective in promoting settlement than are others. . . . "

Two other species of polychaetes have shown a settlement response to the presence of substratum. Nyholm (1950) found that *Melinna cristata* (p. 88) "tended to metamorphose only in the presence of a suitable substratum rich in detritus and never when merely supplied with clear water." Smidt (1951) observed that (p. 60) "the lack of substratum will prolong larval life [of *Pygospio elegans*] while settling is furthered by the presence of a substratum." Moreover, "sterile sand and naturally occurring pebbles have an impeding effect" on metamorphosis.

In a careful study, settling of the actinotroch larvae of *Actinotrocha branchiata* [= *Phoronis mülleri*] is described by Silén (1954, p. 234): "The metamorphosis is easily and infallibly brought about by introducing some of the clay-mixed sand in which the adults are found, to a bowl containing a mature specimen." The metamorphosis which occurs "within a few usually about ten minutes" is described in great detail and involves the testing of the substratum by the larvae.

The study of Jägersten (1940) on the metamorphosis of the archiannelid *Protodrilus rubropharyngeus* is especially interesting because it describes the characteristics of a metamorphosis-inducing material. In nature *P. rubropharyngeus* has positively phototactic mature swimming larvae which, on reversing their photic response, sink to the bottom and metamorphose in a limited littoral zone with a shell or shell and pebble bottom. In the laboratory swimming larvae usually do not metamorphose but may live for two weeks without signs of transformation. If a shell or pebble from the normal habitat is included in the culture vessel, the larvae metamorphose within twenty-four hours. The material which induces this metamorphosis may be transferred to the water. It is resistant to heat, acids, and alkalis and is apparently associated with suspended material which may be removed either by centrifugation or filtration. Jägersten concluded that some non-living inorganic material is responsible for the settling response.

Wilson (1952) has concluded (p. 53 ff.): "It is evident that larvae do not settle just anywhere and that many of them have some power of selection. Over what period of time this power can be exercised is not always so clear; neither is the mechanism whereby larvae are enabled to make the selection, whether by touch, smell or other means. . . . It has proved easier to establish the facts that metamorphosis can be delayed and that larvae can choose their substratum . . . than to determine the actual features of the environment, physical, chemical or biological, perceived by the larvae and to which they react."

One of the more conspicuous organisms on intertidal flats along the Atlantic coast from the Gulf of St. Lawrence to northern Florida is *Nassarius obsoletus* Say. This prosobranch gastropod is extremely abundant in its preferred habitat. Newly metamorphosed snails, during favorable years, occur in large aggregations which reach densities of 23,000 individuals per square meter. A patch of newly metamorphosed snails, while usually not uniform in density, may exceed 100 square meters in area. Apparently success of the species is due to the settlement of the larvae in a favorable environment; an explanation may be that the larvae metamorphose in response to some clue provided by the environment.

The experiments which are described in the following pages are offered in support of such a hypothesis. They show that in the laboratory, the larvae of the gastropod mollusk *N. obsoletus* are able to recognize a favorable substratum and can, to a considerable degree, delay metamorphosis until a suitable substratum is come upon. Hence the "power of selection" in choosing a place for settlement is proven to exist in yet another group of invertebrate animals. The experiments also suggest the singular manner by which the larvae achieve this end.

I should like to acknowledge with gratitude the financial assistance afforded through a fellowship from the Woods Hole Oceanographic Institution during the summers of 1956, 1957, and 1958, and the encouragement offered by Dr. Bostwick H. Ketchum of that institution.

Mr. Harry J. Turner has been most generous in making available all the facilities of his laboratory. At various times during the course of the research he offered comments and suggestions which were helpful and for which I am indebted.

I am grateful to Dr. Charles E. Jenner for his suggestions and advice at certain critical points of the research and for his careful reading of the manuscript.

With Amelie, my wife, I have shared some exciting moments of discovery, but also many evenings counting over larvae and editing the manuscript.

Experimental Procedures

The experiments that have demonstrated the relationship between the substratum and metamorphosis in *Nassarius obsoletus* have been simple in their design. Inasmuch as all of these experiments involved quite similar methods, the general procedure used will be described here; the details are presented later together with the results.

All experiments entailed the use of at least one control and one experimental container, each with twenty veliger larvae. The containers, which were of translucent polyethylene,[3] were filled with one-half liter of sea water that had been filtered through glass or dacron wool.

The bottom sediment to be tested was placed in the experimental dishes. About 5 cc. of substrate material were required to just cover the bottom of a container. The substratum, unless otherwise indicated, was screened before use by passing it through either a Number 60 (240 μ) or 100 (140 μ) stainless steel screen, or a Number 2 (316 μ) bolting cloth. This removed all organisms larger than *ca.* 0.3 mm, which interfered with the conduct of the experiment. The substratum usually was composed of a very fine sand and included a considerable amount of organic material.

The controls consisted of containers with filtered sea water only; in some cases, when the substratum was treated in a manner to be explained later, additional controls with untreated substratum were added to the series.

---

[3] Manufactured by the Kordite Corporation, Macedon, N. Y. Polyethylene to which coloring matter has been added is unsuitable, presumably because of the toxic effect of the dye.

Control and experimental containers were started simultaneously with larvae grown in and picked at random from the same culture. The larvae at the beginning of the experiment were at a stage of development which precedes metamorphosis, *viz.*, the creeping-swimming stage, attained about 3 weeks after emergence from the egg capsule. Subsequently both experimental and control containers were placed together on a sea table or nearby shelf. Hence the larvae are presumed to have been maintained under similar but not necessarily constant or uniform conditions throughout the course of their growth previous to the experiments and also, except for the conditions being tested, throughout the duration of the experiments. Temperature throughout the experiments ranged from 22° to 24° C.

Most experiments were terminated after 24 hours; some ran only 12 hours and others lasted up to four days.The larvae or recently metamorphosed young were removed from the plastic containers either by pipetting them directly from the containers or by carefully screening the contents of the containers so as to permit the substratum to pass through, leaving the organisms behind. The number of larvae that had metamorphosed was then determined by inspecting each larva under a dissecting miscroscope. The criterion used to determine metamorphosis was the loss of the velum.

A concise description of the method used in rearing the larvae will suffice, inasmuch as a more complete account will be given elsewhere, together with the external morphology of the larvae. Egg capsules were obtained in the field or from snails held in the laboratory. After emergence from the egg capsules the larvae were collected on a fine mesh screen, placed into 15-liter rearing vessels, and aerated. Water in the rearing vessels was changed every second or third day by passing the entire contents of the vessel through a fine mesh screen which retained the larvae. *Phaeodactylum tricornutum* Bohlin (Ehr.) W. Sm. at a concentration of 2×10^5 cells/ml. was used as a source of food. This diatom may be readily grown in mass culture.

A brief explanation of the experimental data given in the tables is required. Since the age of the larvae, as well as previous cultural conditions, was of necessity not identical from one group of experiments to the next, any set of experiments performed at one time are not strictly identical to those of another. The past history of the culture and the difference in the age of the creeping-swimming larvae explain much of the variability observed in the data. It is clearly valid, however, to compare the results from a series of experimental containers with those derived from their respective controls. The statistical significance of the difference between such means has been determined by the Student t-test. The percentages metamorphosed were corrected for mortality, and all statistical computations are based on the number of living organisms recovered at the end of the experiments.

Reaction of Nassarius obsoletus to the Substratum

a. *Metamorphosis in the presence of natural substratum*

The importance of the substratum to onset of metamorphosis in *Nassarius obsoletus* is readily demonstrated. In the presence of a bottom sediment on which

TABLE I

Percentage metamorphosis of Nassarius obsoletus *in the presence of of natural substratum (results from ninety-four experiments)*

Experimental condition	Per cent mortality	Mean per cent metamorphosed*
Natural substratum	2.1	70.0 ± 2.4
Without substratum	1.4	18.9 ± 1.4

* One standard error is indicated on all values throughout this paper.

juvenile *N. obsoletus* are found in nature, the percentage metamorphosis is very significantly greater than in controls without such natural substratum. The results of 94 experiments show that with a natural substratum 70.0% of the larvae ended their planktonic existence, whereas in controls of filtered sea water only, 18.9% of the larvae metamorphosed. The value of P in these experiments equals less than 0.001. Moreover, in not one of the above experiments did the percentage of metamorphosis in the control ever exceed that in the experimental culture. The results of the experiments are summarized in Table I. The larvae at the end of

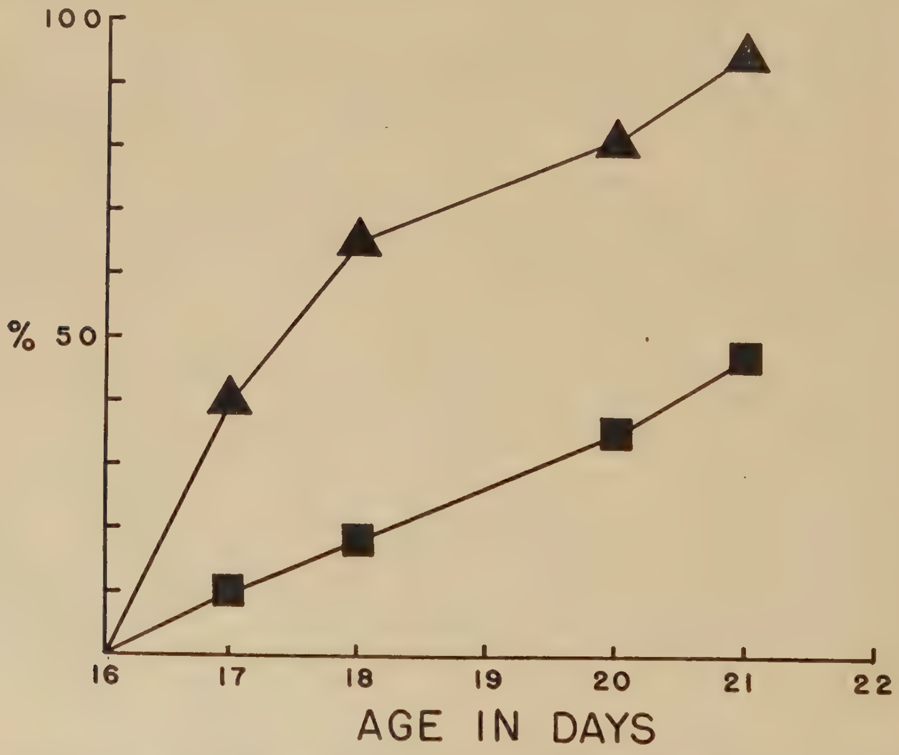

FIGURE 1. Percentage metamorphosis with (▲) and without (■) natural substratum in *Nassarius obsoletus*. Fifty larvae, 16 days after emergence from egg capsules, were placed in each of two 2-liter containers. In the bottom of one was placed freshly collected substratum; no substratum was placed in the control. The percentage metamorphosis in each container is shown at the times indicated on the abscissa.

the experiments ranged in age from 16 to 35 days (mean 25.7) after emergence from the capsule. The eggs were obtained from snail populations in the vicinities of Woods Hole, Massachusetts, and Beaufort, North Carolina.

Apparently metamorphosis cannot be indefinitely delayed. In the absence of bottom sediment the tendency to metamorphose is a simple linear function of age (Fig. 1). The maximum delay which was demonstrated was 20 days after the creeping-swimming stage had been attained. In the presence of bottom sediment the tendency to metamorphose is also a function of age; however, this tendency increases very rapidly and is not a simple linear function. In a series of experiments (Scheltema, 1956), it was shown that when 20-day-old larvae were used, 17% metamorphosed in response to bottom sediment, whereas in similar experiments using 31-day-old larvae 90% metamorphosis resulted.

TABLE II

Mechanical analyses of substrata from three areas used in metamorphosis experiments*

Mesh no.	Openings in mm.	Per cent passing through sieve		
		Substratum #1	Substratum #2	Substratum #3
5	4.000	82.8	—	—
10	2.000	75.4	—	—
18	1.000	57.5	100.0	100.0
35	0.500	24.3	99.6	97.7
60	0.250	6.3	94.4	92.0
120	0.125	0.5	66.2	84.1
230	0.062	—	7.3	77.3
Median diameter		0.9 mm.	0.1 mm.	<0.06 mm.

* Substratum #1: Head of Great Pond (off mouth of Perch Pond), East Falmouth, Cape Cod, Massachusetts (see Hulburt, 1956). "Favorable" substratum in preférence experiments.

Substratum #2: Experimental area of Woods Hole Oceanographic Institution, Barnstable Harbor, Cape Cod, Massachusetts (see Ayers, 1959).

Substratum #3: Mouth of Great Pond (west shore), East Falmouth, Cape Cod, Massachusetts (see Hulburt, 1956). "Unfavorable" substratum in preference experiments.

b. *Preference for a favorable substratum*

Certain natural substrata are apparently preferred over others, inasmuch as a significant difference in the response of *Nassarius obsoletus* larvae to different substrata may be demonstrated experimentally. A sustratum sample obtained from a location shown to be very favorable for metamorphosis of *N. obsoletus* (#1, Table II), as indicated by the large number of snails observed to have metamorphosed there in the previous two years, was compared with another sample collected from a region believed to be unfavorable for metamorphosis (#3, Table II), as demonstrated by the complete absence of recently metamorphosed snails during the same two-year period. The latter region, although unfavorable for metamorphosis, was not inimical to the existence of the species, since older snails of three years or over regularly were found to inhabit this flat. Plankton tows revealed great numbers of larvae during the months of July in the waters over both regions from which the substratum samples were obtained.

The two substrata differed markedly. That taken from the area where juvenile snails were abundant was composed largely of coarse sand and fine gravel. It was poorly sorted, with a median grain size of 0.9 mm. An abundance of living diatoms was present in this substratum. The other substratum was rich black and probably somewhat anaerobic since a trace of hydrogen sulfide odor could be detected. This material was less than 0.06 mm. in median diameter and may be characterized as silt. Viewed under the microscope it appeared to contain large amounts of organic detritus. The mechanical analyses of the substrata are summarized in Table II. The substrata used in the experiments were not screened, but all larger organisms were removed from them with forceps under a dissecting microscope.

Table III

The preference of Nassarius obsoletus *for a favorable substratum for metamorphosis (results from seven experiments)*

Experimental condition	Per cent mortality	Mean per cent metamorphosed
Favorable substratum (#1, Table II)	0.0	84.4 ± 8.3
Unfavorable substratum (#3, Table II)	0.0	51.6 ± 7.6
Without substratum	0.0	30.2 ± 11.0

The percentage metamorphosis on the two substrata may be compared in Table III. In the coarse substratum 84.4% of the larvae metamorphosed, whereas on the fine black organic substratum 51.6% ended their planktonic existence. This difference is statistically significant (P equals less than 0.025). The difference between the fine black substratum and the control without substratum was not significant (P equals 0.20). The mean age of the larvae at the beginning of the experiment was 25.0 days.

The experiments show that substrata favored in the laboratory are similar to those preferred under natural conditions, and that there is a correspondence between experimental results and field observations. The general application of these results should be viewed with considerable reservation, however, pending further experiments using other favorable and unfavorable bottom sediments.

Properties of the Substratum Which Induce Metamorphosis

Numerous experiments indicate that the induction of metamorphosis by a favorable substratum is not a direct function of its physical character, but rather the result of its biological and chemical properties. Two lines of evidence support this conclusion.

a. *Physical properties of the substratum*

During the course of many experiments, sediments have been used from widely diverse regions. Mean grain size and sorting have differed greatly. Of those substrata that have been tested experimentally and proven effective in inducing metamorphosis, the greatest extremes in physical properties are to be found in substrata #1 and #2 in Table II. The former, from the head of Great Pond, East Falmouth, Massachusetts, is poorly sorted gravel and sand. The latter, from Barnstable Harbor, Cape Cod, Massachusetts, is well sorted and consists primarily of fine reworked glacial sand. For the purpose of the experiments, the Barnstable Harbor substratum was passed through a Number 2 (316 μ) bolting cloth. This sieving had little effect on the physical character of the sediment, removing at most perhaps 2% of the total sample, *i.e.,* that portion exceeding 0.3 mm., in diameter. The Great Pond sample was not screened, but mollusks and annelids were removed. Table IV shows the results obtained with these substrata: in the Great Pond sample 84.4% of the larvae metamorphosed, while in the Barnstable substrate 88.7% completed their planktonic existence. Although experiments with the Barnstable and Great Pond sediments were conducted at different times and with larvae from different cultures, it seems justifiable in this instance to compare results and to conclude that the wide difference in physical character of the substrata had no effect on their ability to influence metamorphosis. The experimental results are completely in accord with the observations in nature that the larvae in fact do metamorphose in large numbers on these two substrata.

TABLE IV

The effect of two substrata, differing widely in physical properties, on the percentage metamorphosis of Nassarius obsoletus

Substratum used	Character of substratum	No. of expts.	Mean per cent metamorphosed with substratum	Mean per cent metamorphosed without substratum
Great Pond, Falmouth, Mass. #1, Table II	0.9 mm. median diameter, poorly sorted sand and gravel	7	84.4 ± 8.3	30.2 ± 11.0
Barnstable Harbor, Mass. #2, Table II	0.1 mm. median diameter, well sorted fine sand	18	88.7 ± 3.3	21.0 ± 4.8

It may be concluded from this evidence that, within wide limits, mean particle size and sorting have no direct effect on metamorphosis. There are, however, certain indirect effects of particle size on the biological properties of the substratum as a consequence of decreased surface with increasing particle size. ZoBell (1946) has shown, for example, that the size of bacteria populations may be related to particle size.

b. *Biological and chemical properties of the substratum*

Response of larvae to the biological and chemical attributes of the substratum was tested in a series of experiments. It was intended to alter the sediment biologically and chemically without changing its physical properties.

Treating a substratum sample by (1) incinerating, (2) oven-heating, (3) washing, (4) heating in a water bath, or (5) irradiating with ultraviolet light results in each case in a significant reduction of the metamorphosis-inducing properties of the substratum.

Incineration was accomplished by first washing and boiling the sediment in distilled water several times to remove most of the organic material, and then placing the cleaned sediment in a crucible and heating it above the high flame of a bunsen burner for one hour. The result of this treatment was to render the substratum abiotic and to free it of all traces of organic matter.

Oven-heating the sediment was done at 210° C. for 15 to 30 hours. The dried sample when removed from the oven had a dark brown appearance and a slightly pungent odor. This substratum also was abiotic, but differed from the incinerated substratum in probably having some organic material still present.

Washing the sediment consisted of boiling it in sea water and then in distilled water for several minutes, stirring vigorously, and finally decanting the surplus fine organic material. This process was repeated until the sample appeared essentially clean, *i.e.,* until it assumed a more or less light gray color and lacked any apparent suspended material when stirred. This treatment resulted in removal of part of the organic material and perhaps much of the natural microflora.

Heating the sediment was done by placing a small flask containing some sea water and the sediment sample into a beaker of water and raising the temperature to 70° to 90° C. for five to fifteen minutes. When the experiments were performed, the sea water heated inside the flask with the substratum was used along with new sea water added to make up a volume of one-half liter. Hence no part of the original substratum could have been lost, even if some material is assumed to have gone into solution as a result of the treatment. It was hoped that as a result of this treatment most of the micro-organisms would be killed without substantially affecting the organic material in the sediment. Actually this manipulation resulted, after a period of 24 hours, in a greater total number of micro-organisms than found in the natural substratum, presumably owing to the increased growth of saprophytic bacteria on dead micro-benthos. The difference amounted to two orders of magnitude as determined by plate counts, using ZoBell's marine medium No. 2216 (ZoBell, 1946). The resulting micro-flora was also qualitatively different. The treatment did not appear to cause anaerobic conditions and no fouling of water occurred.

Irradiation with ultra-violet light was done by placing, under a 15-watt germicidal lamp, containers with sediment covered by sea water to a depth of $1\frac{1}{2}$ cm. The treatment was continued 18 hours, the containers being occasionally agitated. After treatment additional sea water was added to each container. Preliminary studies showed that UV treatment reduced the number of bacteria culturable in a marine medium (ZoBell's 2216) by two orders of magnitude if plated after two hours of treatment. The results of the UV treatment were not entirely successful in that complete sterilization is not possible. There is a minimum bacterial count below which further treatment is ineffective even with frequent agitation. Moreover, subsequent to irradiation, growth of saprophytic bacteria is probably very great because of the increase in decomposable material (dead micro-benthos).

The five treatments, as is shown in Table V, all resulted in a significant reduction in the attractiveness of the substrata, as determined by their effectiveness in promoting metamorphosis. Comparison of the experimental groups with their

TABLE V

The effect of various treatments on the metamorphosis-inducing property of the substratum

Treatment of substratum	No. of expts.	Mean age of larvae at start	Mean per cent metamorphosis in treated substratum	Mean per cent metamorphosis in control (untreated substratum)	Difference between treated substratum and control
Incineration	14	24.6	7.2 ± 1.5	71.2 ± 5.3	64.0
Oven-heating (210° C.)	11	26.8	19.0 ± 4.5	69.7 ± 5.0	50.7
Washing	10	22.8	4.6 ± 1.2	51.5 ± 3.9	46.9
Heating in water bath (70°–90° C.)	24	28.4	40.0 ± 4.7	81.2 ± 3.8	41.2
UV irradiation (18 hrs.)	5	28.0	70.4 ± 6.7	91.4 ± 3.4	21.0

untreated controls gives values of P less than 0.001 in all cases except that of the UV irradiation, in which a value of 0.05 was obtained.

Inasmuch as all the treatments shown in Table V have in common the fact that they drastically affected the biological properties and to varying degrees the chemical properties of the substrata, without greatly affecting the physical properties, one may conclude that biological and chemical attributes of the substrata are responsible for their metamorphosis-inducing property.

The various treatments of the substrata in these experiments (Table V) cannot be directly compared with one another because the experiments were conducted with different samples of sediment and with larvae of different ages from different cultures. Nevertheless, the differences between the treated and the control substrata (right-hand column) give some suggestion as to the relative effectiveness of each treatment in destroying the metamorphosis-inducing property of the substrata.

Further experiments have confirmed that a statistically significant difference does indeed exist between the various treatments of the substrata and their attractiveness in inducing metamorphosis. The experiments shown in Table VI were performed with larvae from the same culture and with substratum from a single source. Their only differences were the experimental conditions indicated in the left-hand column. Heating of the substratum in a water bath to 90° C. for

TABLE VI

Relative effect of two treatments of the substratum on its metamorphosis-inducing property (results from fourteen experiments)

Experimental condition	Per cent mortality	Mean per cent metamorphosed
Untreated substratum	1.5	71.2 ± 5.3
Substratum heated in water bath to 90° C.	3.4	33.3 ± 4.8
Incinerated substratum	0.0	7.2 ± 1.5
Without substratum	1.6	13.9 ± 2.6

15 minutes rendered it very significantly less attractive than the normal substratum; however, it also remained very significantly more attractive than incinerated substratum or the controls without substratum (P equals less than 0.001 in both instances). No significant difference resulted between incinerated substratum and the controls without substratum (P equals approximately 0.10).

These experiments show that the treatment of heating the substratum in a water bath at 90° C. yielded results which fall approximately midway between those using the natural substratum and the incinerated substratum.

The experiments on the effects of various treatments of the substratum indicated that: (1) complete removal of the micro-flora and -fauna and of all organic material rendered the substratum unsuitable for stimulating metamorphosis of veliger larvae; (2) qualitative and quantitative changes in the bacterial flora, accompanied by (a) the removal of living microscopic algae and micro-fauna and (b) the alterations in the organic material, owing to heat and addition of decomposition products from the micro-benthos, made the substratum less attractive in inducing metamorphosis; (3) the biological and possibly the chemical character of the substratum was the determining factor in making the substratum suitable for metamorphosis.

A micro-benthic community cannot be separated from the organic material in a sediment. Therefore there is no experimental procedure by which to measure the effect of a micro-benthic community as a whole upon the metamorphosis-inducing property of the substratum. Single species isolated from the substratum may be tested if members of the micro-benthos can be isolated. Preliminary experiments on the effects of benthic marine bacteria isolated from favorable substrata have not yielded consistent results. The effect of the organic material on the suitability of the substratum theoretically may be tested, but no satisfactory method is available to sterilize a substratum without altering the organic material present.

NATURE OF THE METAMORPHOSIS RESPONSE: EXPERIMENTAL EVIDENCE FOR THE PRESENCE OF A SOLUBLE, BIOLOGICALLY ACTIVE, SUBSTRATUM FACTOR

How do the larvae perceive a favorable substratum? Is actual contact with the substratum necessary or can the larvae distinguish a favorable place for metamorphosis by some sensory clue received from material liberated into the water? Is some biologically active substance or perhaps ectocrine (see Lucas, 1955) responsible for the response to the substratum? The experiments which follow were designed to answer these questions.

a. *Transfer of the metamorphosis-inducing factor from the substratum to adjacent water*

When sea water is permitted to stand over a substratum favorable for inducing metamorphosis of veliger larvae, it soon acquires some of the metamorphosis-inducing property. Evidently some of the qualities of the substratum are transferred to the sea water.

The water was conditioned by filling a large fingerbowl to 2 cm. in depth with a sediment favorable for metamorphosis. The remainder of the bowl was then filled with fresh, filtered sea water and allowed to stand in a south window for several days to a week. Carefully the sea water was then siphoned off, particular care being taken to exclude particles of the sediment. Filtered sea water not treated with substratum was used as control. A total of ten different substratum samples was used. In some cases, because of the time involved in treatment, the conditioned sea water was re-used. The results of the experiments are shown in Table VII.

The mean percentage metamorphosis in the substrate-conditioned sea water was 48.5 and differed significantly from the untreated control in which only 11.2% of the larvae metamorphosed (P equals less than 0.001).

The results showed that a metamorphosis-inducing factor could be transferred from the substratum into the water to a significant degree, and that larvae were able to discriminate between water recently exposed to a favorable substratum and water not recently in contact with such a substratum.

TABLE VII

The effect of sea water conditioned with substratum on the percentage metamorphosis of Nassarius obsoletus *(results from twenty-four experiments)*

Experimental condition	Per cent mortality	Mean per cent metamorphosed
Substrate-conditioned sea water	1.1	48.5 ± 4.9
Untreated sea water control	1.2	11.2 ± 2.5

b. *Filterability of the substrate factor through membrane filters*

The metamorphosis-inducing substrate factor, if soluble, should pass through a molecular filter unaltered. An experiment was performed similar to those just described except that the substrate-conditioned sea water was divided into two equal parts. One half was filtered through a molecular filter[4] with a pore size of 0.8 μ; the other half was retained as a control. Both water samples were then tested for their metamorphosis-inducing property against a sample of untreated sea water. The resulting metamorphosis of larvae in the unfiltered, substrate-conditioned sea water and the filtered, substrate-conditioned sea water is shown in Table VIII. The mean age of the larvae at the beginning of the experiments was 28.8 days. Twelve and three-tenths per cent of the larvae in the untreated, 46.9% of the larvae in the substrate-conditioned, and 33.0% of the larvae in the filtered, substrate-conditioned sea water metamorphosed within a period of 48 hours. The difference in results between the filtered, substrate-conditioned water and the untreated sea water was significantly different (P equal to less than 0.001). The difference between the filtered, substrate-conditioned sea water and unfiltered, substrate-conditioned sea water was not significant since the value of P was approximately 0.10.

The experiments showed that the metamorphosis-inducing property of the substratum was at least in part a water-soluble substance; previous evidence has already indicated that it must be relatively stable at temperatures likely to be encountered in nature. One may speculate that the metamorphosis-inducing factor can be adsorbed by the sediment since experiments using the substratum showed a consistently higher per cent metamorphosis over those with substrate-conditioned sea water. Such a comparison is not valid, however, without further experiment using similar larvae and sediments. The difference between the mean percentage metamorphosis in the filtered and unfiltered substratum-conditioned sea water, though not statistically significant, may perhaps indicate that under certain circumstances some adsorption may occur either on fine suspended or colloidal particles, which are removed on filtration, or on the filter itself.

---

[4] Millipore Filter Corporation, Watertown, Massachusetts.

c. *Implications of the experiments using substrate-conditioned sea water*

The two series of experiments using substrate-conditioned sea water supply the evidence which makes possible a reasonable hypothesis to explain the nature of the response to the substratum. The experiments suggest that the metamorphosis response of *Nassarius obsoletus* larvae is due to a soluble substance, which is relatively stable, and of biological origin. Such a substance may justifiably be termed a "biologically active" substance. Apparently the larvae perceive this substance without contact with the substratum. The latter conclusion presupposes that the veligers must have chemoreceptors sensitive enough to discriminate between the presence or absence of the metamorphosis-inducing factor in the water.

Table VIII

The effect of filtrating the metamorphosis-inducing property oj the substratum through a molecular filter (results from eighteen experiments)

Experimental condition	Per cent mortality	Mean per cent metamorphosed
Substrate-conditioned sea water	1.2	46.9 ± 6.5
Molecular filtered substrate-conditioned sea water (0.8 μ pore diameter)	0.3	33.0 ± 5.6
Untreated sea water	0.3	12.3 ± 3.0

Observations on adult *N. obsoletus* under both laboratory and field conditions indicate a high degree of chemoreception. For example, snails placed in a tank with a small piece of clam meat are able to locate such food very rapidly by testing water through their siphons. Chemical sensitivity has been demonstrated on two European species of the same genus (Henschel, 1932; Weber, 1924). In view of these well-developed chemical sense organs observed in the adults of the genus, it is not too surprising to encounter a well-developed chemoreception in the creeping-swimming stage of *N. obsoletus*.

Two types of chemoreception may be distinguished (Carthy, 1958) : a contact chemical sense and an olfactory sense. The distinction is largely that of the concentration required to stimulate. Inasmuch as contact with the substratum by *N. obsoletus* is unnecessary, olfaction, the more sensitive chemical sense, is probably involved in the initial response.

Once the creeping-swimming larva descends to the bottom, further testing of the substratum is possible by contact chemoreceptors. This may provide an explanation for the relatively higher percentage of metamorphosis in those experiments using a substratum over those in which substrate-conditioned water was used.

Biologically active substances encompass a wide variety of materials and have been demonstrated to be of importance in a great diversity of biological activities. The subject has recently been extensively reviewed by Collier (1953) and Lucas (1955). We shall therefore not attempt an extensive summary here. It will suffice to say that the regulation of many marine animal relationships, including commensalism, antibiosis, and predation, have been explained by the demonstration of a biologically active substance.

A large diversity of organic compounds are apparently to be found in the ocean. Collier in 1953 reviewed the types of organic substances which had been found up to that time. Among these he listed N-ethylcarbazol substances ("carbohydrates"), tryosine, tryptophane, rhamnoside, ascorbic acid, and certain other unknown materials, among these a yellow lipoid substance. To these may now be added many other materials which have recently been discovered such as B_{12}-active substances (Burkholder and Burkholder, 1956; Starr *et al.*, 1957), organic acids (Koyama and Thompson, 1959; Slowey *et al.*, 1959), and various algal (Proctor, 1957) and bacterial (Sieburth, 1959) antibiotics.

Clearly, biologically active substances must encompass a wide variety of materials. Collier (1953) believes that organic compounds may originate (1) as degradation products of dead or dying animals and plants, (2) as excretory products, (3) as diffusible metabolites, and (4) from microbial activity. In the case of the metamorphosis response of *Nassarius obsoletus* to bottom sediment we do not yet know the chemical identity nor the exact source of the biologically active material. "A mud or soil with an abundant and varied microflora should contain very nearly the gamut of microbial metabolites . . ." (Hutner and Provasoli, 1951). Moreover, it is not apparent whether more than one substance may be involved in the response of the larvae. The evidence shows no discrete threshold at which metamorphosis occurs, inasmuch as the response of a group of experimental larvae to the metamorphosis-inducing factor is not "all or none." Hence not all creeping-swimming larvae metamorphose after 24 hours, despite the presence of a suitable substratum. Obviously the metamorphosis response to the substratum is not a simple one, nor should simplicity in behavior be expected from larvae, inasmuch as they are in most anatomical and physiological respects fully as complex as adults.

FUNCTION AND ECOLOGICAL SIGNIFICANCE OF THE SUBSTRATUM IN INDUCING METAMORPHOSIS IN NASSARIUS OBSOLETUS AND NASSARIUS VIBEX

a. *Adaptive value of the response of larvae to the substratum*

Nassarius obsoletus, which ingests large quantities of bottom material by means of its proboscis, is a deposit feeder. The evidence for this comes from the examination of fecal material and digestive tract contents. Since a crystalline style is present (Jenner, 1956), it is presumed that large amounts of carbohydrates are digested from the microflora within the sediment. Living bivalves of any size or species which have been tried in the laboratory are consistently refused, including those which are frequently associated with *N. obsoletus* (*e.g.,* recently metamorphosed *Venus mercenaria* and juvenile *Gemma gemma*). Subsistence from dead mollusks or Crustacea is possible; indeed, on intertidal flats one frequently encounters aggregations of several hundred *N. obsoletus* feeding on some dead marine organism. Such dead organisms cannot, however, form a principal item of diet because of the large size of the *N. obsoletus* populations found on the intertidal flats.

Observations on another species of the genus *Nassarius* suggest that there is a correspondence between the metamorphosis response to bottom sediment and the adaptive value of such a response. *Nassarius vibex,* which is sometimes found sympatrically with *N. obsoletus,* is a scavenger. It is found much less abundantly than *N. obsoletus,* as would be expected by its trophic position in the community in which it lives. Experimentally we have shown that *N. vibex* does not metamorphose in response to a bottom sediment. A series of eleven experiments resulted in 67.4 ± 11.8% metamorphosis when sediment was present on the bottom of the experimental containers, whereas 62.9 ± 11.5% metamorphosed without the presence of sediment. Hence the complex behavior pattern of *N. obsoletus,* which results in the metamorphosis of larvae on a favorable substratum, has considerable adaptive value; such a response seemingly would be of no marked advantage to *N. vibex.*

b. *Ecological significance of the response of* Nassarius obsoletus *to the substratum*

"The continued presence of an animal in an environment depends upon the developmental stage in which it has the least adaptability and this stage, the weakest link of the chain, will normally be found during the breeding period and larval development." (Thorson, 1957, p. 472.) Hence, less stability should be expected of populations of organisms which have long pelagic larval stages. A comparison of arctic bottom communities, where almost all benthic organisms have direct development, with tropical benthic communities, where 75 to 80% of all bottom forms have pelagic larvae, displays no marked difference in the stability of the two (Thorson, 1957). There must exist a means, aside from chance, by which tropical benthic communities maintain their relative stability. Indeed the stability of any bottom community which depends largely on recruitment of pelagic larvae needs explanation.

One interpretation of the relative stability of large benthic populations may be found in the response of larvae to a metamorphosis-inducing factor in the substratum or, more accurately, to a very complex behavior pattern which consists of (1) recognition of a favorable substratum or environment and (2) a response to this favorable substratum, terminating in metamorphosis. This type of response may be expected in benthic forms which are deposit feeders. Our experiments have shown that under optimum laboratory conditions larvae of *N. obsoletus* may metamorphose as early as 17 days after their emergence from the egg capsule, while in the absence of a favorable substratum the termination of planktonic existence may be delayed for as long as 20 days after the creeping-swimming stage has been attained. Although the favorable substratum is come upon accidentally, the larvae may delay their metamorphosis over a period of sufficient time so as to make such an encounter very highly probable. Estuaries, which form the chief habitat for *N. obsoletus,* often have circulations of the type which will carry swimming larvae over long distances upstream along the bottom (Pritchard, 1951). Larvae as they are carried by bottom currents over a particularly suitable region will metamorphose.

SUMMARY

1. Experimental evidence shows that the presence of a favorable substratum has a marked effect on the metamorphosis of *Nassarius obsoletus* larvae. In the presence of a natural substratum the percentage metamorphosis was very significantly greater than in controls without such natural substratum. Larvae postponed metamorphosis for over two weeks when a desirable substratum was not encountered.

2. Certain substrata were preferred over others; a significant difference in the response of *N. obsoletus* larvae to different sediments was demonstrated experimentally. A correspondence exists between substrata preferred under natural conditions and those favored in experiments in the laboratory.

3. The physical properties of a substratum, such as median grain size and sorting, do not directly influence the metamorphosis of *N. obsoletus* veliger larvae. This was demonstrated both experimentally and by field observations.

4. Certain biological properties are important in making the substratum attractive for the metamorphosis of *N. obsoletus* veligers. This was shown by the differences in settlement obtained experimentally when the sediment was treated in various ways. When a sediment was rendered completely abiotic by incineration, no significant difference existed between the percentage metamorphosis on such a substratum and in controls without substratum. If the biological characteristics of the sediment were drastically altered by heating in sea water, the attractiveness of the substratum to metamorphosis by veliger larvae was significantly reduced, but it remained nevertheless significantly more attractive for metamorphosis than a substratum which had been made completely abiotic.

5. The metamorphosis-inducing properties of a substratum may be transferred to the adjacent water, as was demonstrated experimentally.

6. Experimental evidence showed that the metamorphosis-inducing factor from the substratum is probably a water-soluble substance.

7. Inasmuch as the response to a metamorphosis-inducing factor is possible without contact with the substratum, a rather sensitive chemoreception by *N. obsoletus* larvae must be involved. Stimulation may be followed by a complex behavior pattern which includes further testing of the substratum and subsequent metamorphosis.

8 Since *N. obsoletus* is primarily a deposit feeder, the selection of a favorable substratum has considerable adaptive value.

9. The ability to delay metamorphosis and the response to a favorable substratum greatly increase the probability that the larvae of *N. obsoletus* will terminate their pelagic existence in a favorable habitat.

LITERATURE CITED

AYERS, J. C., 1959. The hydrography of Barnstable Harbor, Massachusetts. *Limnol. Oceanogr.*, **4**: 448–462.

BURKHOLDER, P. R., AND L. M. BURKHOLDER, 1956. Vitamin B_{12} in suspended solids and marsh muds collected along the coast of Georgia. *Limnol. Oceanogr.*, **1**: 202–208.

CARTHY, J. D., 1958. An Introduction to the Behavior of Invertebrates. George Allen and Unwin, Ltd., London. xiv + 380 pp.

COLLIER, A., 1953. On the significance of organic compounds in sea water. *Proc. Eighteenth N. A. Wildlife Conf.*, pp. 463–468.

DAY, J. H., AND D. P. WILSON, 1934. On the relation of the substratum to the metamorphosis of *Scolecolepis fuliginosa* (Claparède). *J. Mar. Biol. Assoc.*, **19**: 655–662.

HARRINGTON, C. R., 1921. A note on the physiology of the ship-worm (*Teredo norvegica*). *Biochem. J.*, **15**: 736–741.

HENSCHEL, J., 1932. Untersuchungen über den chemischen Sinn von *Nassarius reticulata*. *Wiss. Meeresunters., Abtl. Kiel*, **21**: 133–158.

HULBURT, E. M., 1956. The phytoplankton of Great Pond, Massachusetts. *Biol. Bull.*, **110**: 157–168.

HUTNER, S. H., AND L. PROVASOLI, 1951. The phytoflagellates. pp. 27–128. *In:* Biochemistry and Physiology of Protozoa, Vol. I, ed. by A. Lwoff. Academic Press, New York.

JÄGERSTEN, G., 1940. Die Abhängigkeit der Metamorphose vom Substrat des Biotops bei Protodrilus. *Arkiv f. Zool.*, **32A** (No. 17) : 1–12.

JENNER, C. E., 1956. The occurrence of a crystalline style in the marine snail, *Nassarius obsoletus*. *Biol. Bull.*, **111**: 304.

KOYAMA, T., AND T. G. THOMPSON, 1959. Organic acids in sea water. *Preprints Internat. Oceanogr. Congr.* 1959 [New York], AAAS, Washington, D. C., p. 925.

LUCAS, C. E., 1955. External metabolites in the sea. Pap. Mar. Biol. and Oceanogr., *Deep-Sea Res.*, Suppl. to Vol. **3**: 139–148.

MORTENSEN, TH., 1921. Studies of the Development and Larval Forms of Echinoderms. Gad, København (Copenhagen). 266 pp.

MORTENSEN, TH., 1938. Contributions to the study of the development and larval forms of Echinoderms. IV Kgl. *Danske Vidensk. Selsk. Skrifter, Naturv. og Math. Afd. Raekke* 9, **7**: 1–59.

NYHOLM, K., 1950. Contributions to the life-history of the Ampharetid, *Melinna cristata*. *Zool. Bid. Uppsala*, **29**: 79–91.

PRITCHARD, D. W., 1951. The physical hydrography of estuaries and some applications to biological problems. *Proc. Sixteenth N. A. Wildlife Conf.*, pp. 368–376.

PROCTOR, V. W., 1957. Studies of algal antibiosis using *Hematococcus* and *Chlamydomonas*. *Limnol. Oceanogr.*, **2**: 125–139.

SCHELTEMA, R. S., 1956. The effect of substrate on the length of planktonic existence in *Nassarius obsoletus*. *Biol. Bull.*, **111**: 312.

SIEBURTH, J. M., 1959. Antibacterial activity of Antarctic marine phytoplankton. *Limnol. Oceanogr.*, **4**: 419–424.

SILÉN, L., 1954. Developmental biology of Phoronidae of the Gullmar Fiord area (west coast of Sweden). *Acta Zoologica*, **35**: 215–257.

SLOWEY, J. F., L. M. JEFFREY AND D. W. HOOD, 1959. Characterization of the ethyl acetate extractable organic material of sea water. *Preprints Internat. Oceanogr. Congr.* 1959 [New York], AAAS, Washington, D. C., p. 935.

SMIDT, E. L. B., 1951. Animal production in the Danish Waddensea. *Medd. Komm. Danmarks Fisk. Havunders., Ser. Fiskeri*, **11**(6) : 1–151.

STARR, T. J., M. E. JONES AND D. MARTINEZ, 1957. The production of vitamin B_{12}-active substances by marine bacteria. *Limnol. Oceanogr.*, **2**: 114–119.

THORSON, G., 1957. Bottom communities (sublittoral or shallow shelf). pp. 461–534. *In:* Treatise on marine ecology and paleoecology, Vol. I: Ecology, ed. J. W. Hedgpeth. *Geol. Soc. Amer., Mem.* **67**. viii + 1296 pp.

WEBER, H., 1924. Ein Umdreh und ein Fluchtreflex bei *Nassa mutabilis*. *Zool. Anz.*, **60**: 261–269.

WILSON, D. P., 1932. On the mitraria larvae of *Owenia fusiformis* Delle Chiaje. *Phil. Trans. Roy. Soc. London, Ser. B*, **221**: 231–334.

WILSON, D. P., 1937. The influence of the substratum on the metamorphosis of Notomastus larvae. *J. Mar. Biol. Assoc.*, **22**: 227–243.

WILSON, D. P., 1948. The relation of the substratum to the metamorphosis of Ophelia larvae. *J. Mar. Biol. Assoc.*, **27**: 723–760.

WILSON, D. P., 1951. Larval metamorphosis and the substratum. *Ann. Biol. (Paris)*, **27**: 259–269.

WILSON, D. P., 1952. The influence of the nature of the substratum on the metamorphosis of the larvae of marine animals, especially the larvae of *Ophelia bicornis* Savigny. *Ann. Inst. Oceanogr. (Monaco)*, **27**: 49–156.

WILSON, D. P., 1953a. The settlement of *Ophelia bicornis* Savigny larvae. The 1951 experiments. *J. Mar. Biol. Assoc.*, **31**: 413–438.

WILSON, D. P., 1953b. The settlement of *Ophelia bicornis* Savigny larvae. The 1952 experiments. *J. Mar. Biol. Assoc.*, **32**: 209–233.

WILSON, D. P., 1954. The attractive factor in the settlement of *Ophelia bicornis* Savigny. *J. Mar. Biol. Assoc.*, **33**: 361–380.

WILSON, D. P., 1955. The role of micro-organisms in the settlement of *Ophelia bicornis* Savigny. *J. Mar. Biol. Assoc.*, **34**: 513–543.

ZOBELL, C. E., 1946. Marine Microbiology. Chronica Botanica Co., Waltham, Massachusetts. 240 pp.

Contribution No. 1135

Särtryck ur Tellus nr 1, 1961

Experimentally Observed Instability of a Laminar Ekman Flow in a Rotating Basin[1, 2]

By A. B. ARONS, A. P. INGERSOLL, T. GREEN III
Amherst College and Woods Hole Oceanographic Institution

(Manuscript received August 18, 1960)

Abstract

In studying the axi-symmetric flow induced by source-sink distributions in a rotating cylindrical basin in the absence of radial barriers, a highly organized pattern of instability has been observed in the laminar Ekman layer along the bottom of the basin. The instability manifests itself in the form of almost perfectly concentric cylindrical sheets or curtains of water which rise as sharply defined vertical jets from the Ekman layer and penetrate the entire depth of fluid. A less sharply defined downward motion between the curtains completes the circulation cells thus developed. At some maximum critical radius, the curtains usually disappear, and the flow at larger radii is a stable, laminar Ekman flow. Quantitative observations of ring spacing and critical radius are reported for experiments in which angular velocity, flow rate, viscosity and total depth of water were varied over experimentally available ranges.

Introduction

It has been shown in an earlier paper in this journal (Stommel, Arons, and Faller, 1959) that it is possible to drive systematic circulations in a rotating basin by means of suitably distributed sources and sinks of fluid. This technique offers the possibility of studying flows in a homogenous system, without the complexities introduced by density gradients and convection phenomena in the presence of temperature fields.

In studying the axi-symmetric flows induced by source-sink distributions in an "open" cylindrical basin (i. e. in the absence of radial barriers), we have observed a highly organized pattern of instablity in the laminar Ekman flow which forms a boundary layer in contact with the bottom of the basin. It is within this Ek-

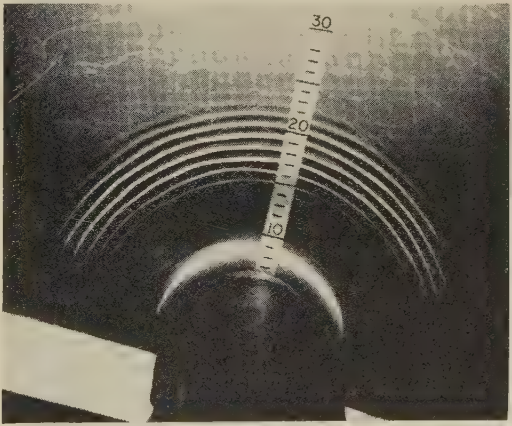

Fig. 1. Top view of tank showing concentric curtains of fluorescein dyed fluid rising from Ekman layer. Source at center of tank near bottom of photograph; rotation counter clockwise; relative zonal velocity ν_ϕ clockwise; Ekman layer spreading radially outwards. (Scale markings in cm.)

---

[1] Contribution No. 1135 of the Woods Hole Oceanographic Institution.

[2] The rotating tank facility was constructed and operated under a grant from the Research Corporation,

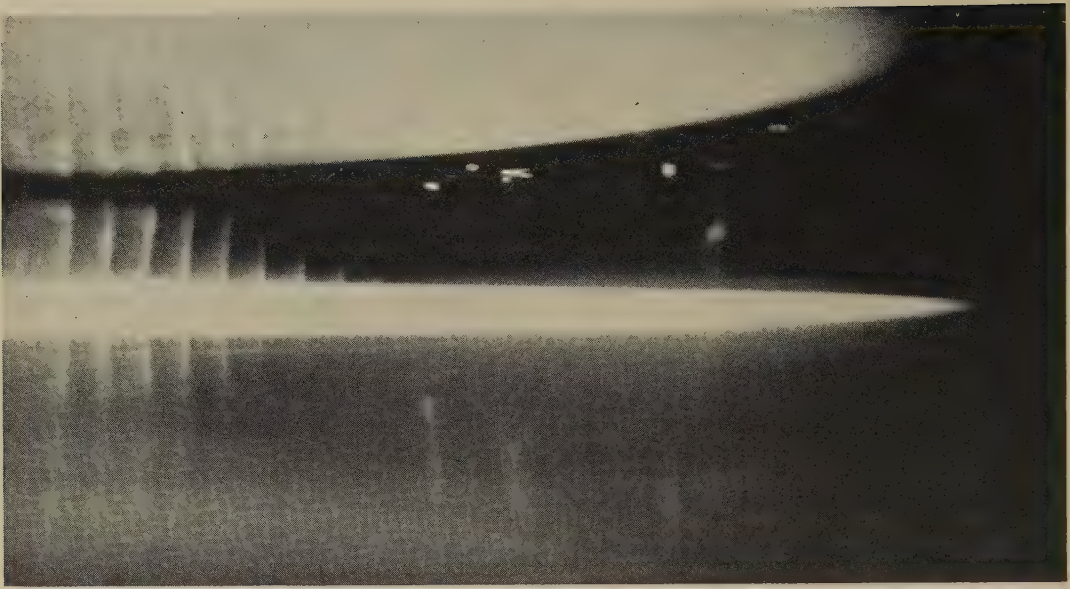

Fig. 2. Side view through wall of tank, showing sharpness of rising curtains and Ekman layer along bottom. Center of tank is to left of photograph; dyed region spread from left to right. Jets at right look lower than those at left because upward velocities are smaller at radii approaching the critical radius. Multiple images are present because of reflections at bottom and at water surface, i.e. colored region, circles, and downward jets appearing in upper part of photograph are surface reflections of the interior flow. Upward velocity of curtains is about 0.7 cm/min.

man layer that fluid is transported radially, either inward or outward, across isobars of the essentially geostrophic bulk flow in the interior of the basin.

The instability manifests itself in the form of almost perfectly concentric cylindrical sheets or curtains of fluid which rise as sharply defined vertical jets from the Ekman layer and penetrate the entire depth of fluid (Figures 1, 2) forming circulation cells with less sharply defined downward motions in the regions between the upward rising curtains. The radial spacing between the rising curtains is highly regular and is a function of angular velocity, viscosity, and total depth of fluid in the tank, i.e. it is indicated to be a function of the Taylor or of the Ekman number. At some maximum critical radius the curtains usually disappear, and the flow at larger radii is a stable, laminar Ekman flow; this points to the existence of a critical Reynolds number for the development and maintenance of the instability.

Stern (1960) has examined, theoretically, the stability of Ekman flows in a somewhat simpler geometry. His analysis predicts, at least qualitatively, the principal features of the instability we describe in this paper.

Method of observation

The experimental system consists of a cylindrical lucite tank, 130 cm diameter and about 30 cm deep, mounted on a carefully levelled rotating platform, driven by a synchronous motor through a Graham variable speed transmission. During experiments, a transparent cover was placed over the tank to prevent the development of "wind driven" circulations. The "source" consisted of a measured flow of water supplied to a funnel mounted at the center of the tank. To reduce turbulence in the source region, this water entered a vertical cylinder with a diameter of twelve centimeters, mounted at the center of the basin in such a way that the source water could run radially outward around the bottom of the cylinder.

The flow within the system was made visible by using potassium permanganate or fluorescein dye in the source water. Photographs could be taken from above or through the side of the tank. Observations of the velocity of the zonal geostrophic flow in the interior of the basin were made by periodically photographing the displacement of small particles or bits of paper moving with the water (at the surface).

Thermal circulations were minimized by performing experiments when tank water and source water were in equilibrium with room temperature. The latter was changed in order to change the temperature (and, therefore, the viscosity of the water) in certain series of experiments. Check runs at zero source strength showed no systematic circulations of the kind observed at non-zero source strengths; no local velocity noted at zero source strength exceeded 0.09 cm/sec.

In several runs, where the temperature of the source water was 1—2°C lower than that of the water in the tank, rings were observed as usual; in other words, the pattern occurred in spite of the thermal stability induced by the denser Ekman layer water.

Experiments were performed at angular velocities of 1 to 2 radians/sec., source strength of 1 to 5 cm^3/sec., kinematic viscosities in the range of 0.007 to 0.012 cm^2/sec., and water depths of about 2 to 12 cm. The laminar Ekman layer under these circumstances has a depth of the order of 1 mm.

In all cases, quantitative observations were made only after the system had had a period of the order of one hour in which to arrive at a steady state.

Equations of the basic flow

Using cylindrical coordinates r, ϕ, z and taking ϕ positive in the same sense as ω, the angular velocity of the tank, we have:

For the depth of water when the tank is rotating in static equilibrium:

$$\begin{aligned} h &= h_0 + \frac{\omega^2 r^2}{2g} \\ &= D_0 - \frac{\omega^2}{2g}\left(\frac{a^2}{2} - r^2\right) \end{aligned} \qquad (1)$$

where h_0 is the depth at $r = 0$; D_0 is the depth of water when the tank is not rotating, and a is the radius of the tank.

For the equations of motion:

$$-2\omega v_\phi = -g\frac{d\eta}{dr} + \nu\frac{\partial^2 v_r}{\partial z^2} \qquad (2)$$

$$2\omega v_r = \nu\frac{\partial^2 v_\phi}{\partial z^2} \qquad (3)$$

where v_r and v_ϕ are the respective components of velocity relative to the tank, η is the perturbation in the height of the free surface, and ν is the kinematic viscosity.

These equations assume: (a) steady flow with negligibly small inertial terms, (b) hydrostatic equilibrium in the vertical direction, (c) axial symmetry, i.e. no ϕ dependence of $\vec{v}$ or η, (d) negligible lateral friction, i.e. negligible contribution from the lateral Navier-Stokes term $\nu\nabla_H^2\vec{v}$ where ∇_H^2 is the horizontal Laplacian. (As will be shown subsequently, $\nu\nabla_H^2\vec{v}$ turns out to be identically zero for the solution obtained, which is therefore in reality a complete solution for the linearized Navier-Stokes equation in this case).

The vertical boundary conditions are

$$v_r = v_\phi = 0 \qquad (4)$$

along $z = 0$, the bottom of the tank, and

$$\frac{\partial v_r}{\partial z} = \frac{\partial v_\phi}{\partial z} = 0 \qquad (5)$$

along $z = h$, the free surface.

The quantity $\frac{d\eta}{dr}$ is carried as a parameter and is ultimately determined by the source and sink conditions at $r = 0$ and $r = a$ and the requirements of continuity.

It is convenient to introduce the notation

$$d \equiv \left(\frac{\nu}{\omega}\right)^{\frac{1}{2}}; \quad \mu \equiv \frac{h}{d}; \quad \zeta \equiv \frac{z}{d}$$

The solutions of equations (2), (3), (4), (5) are then found by standard methods:

$$v_r = -\frac{g}{2\omega}\frac{d\eta}{dr}\cdot \left[\frac{\sinh(2\mu-\zeta)\sin\zeta + \sin(2\mu-\zeta)\sinh\zeta}{\cosh 2\mu + \cos 2\mu}\right] \qquad (6)$$

$$v_\phi = \frac{g}{2\omega}\frac{d\eta}{dr}\cdot \left[1 - \frac{\cosh(2\mu-\zeta)\cos\zeta + \cos(2\mu-\zeta)\cosh\zeta}{\cosh 2\mu + \cos 2\mu}\right] \qquad (7)$$

In these experiments μ is of the order of 10 to 50, and equations (6) and (7) reduce to the simpler forms with the familiar laminar Ekman spiral in the neighborhood of the bottom of the tank:

$$v_r = -\frac{g}{2\omega}\frac{d\eta}{dr}\varepsilon^{-\zeta}\sin\zeta \qquad (8)$$

$$v_\phi = \frac{g}{2\omega}\frac{d\eta}{dr}[1-\varepsilon^{-\zeta}\cos\zeta] \qquad (9)$$

The vertically integrated radial and zonal volume transports V_r and V_ϕ become, respectively:

$$V_r = -\frac{g}{2\omega}\frac{d\eta}{dr}\frac{d}{2}\ \text{cm}^3/\text{sec., cm} \qquad (10)$$

$$V_\phi = \frac{gh}{2\omega}\frac{d\eta}{dr}\left[1-\frac{d}{2h}\right]\ \text{cm}^3/\text{sec., cm} \qquad (11)$$

For particular cases, $\frac{d\eta}{dr}$ is determined by continuity and source-sink conditions:

(a) Source of S_0 cm³/sec. at $r = 0$, and sink of equal intensity uniformly distributed around the periphery at $r = a$. Free surface neither rises nor falls, i.e. vertical velocity $\dot{\eta}_0 = 0$. Continuity requires:

$$2\pi r V_r = S_0 \qquad (12)$$

and combination of equations (10) and (12) gives

$$\frac{d\eta}{dr} = -\frac{2\omega S_0}{\pi g d r} \qquad (13)$$

then

$$V_r = \frac{S_0}{2\pi r} \qquad (14)$$

$$V_\phi = -\frac{hS_0}{\pi d}\frac{1}{r}\left[1-\frac{d}{2h}\right] \qquad (15)$$

and v_ϕ becomes essentially a $1/r$ vortex above the Ekman layer.

(b) If the surface is allowed to rise or fall (i.e. the basin fill or empty because of the source-sink distribution), $\dot{\eta}_0 \neq 0$, and the equation of continuity requires:

$$\frac{1}{r}\frac{\partial(rV_r)}{\partial r} = -\dot{\eta}_0 \qquad (16)$$

Combination of (16) and (10) and integration give:

$$\frac{d\eta}{dr} = \frac{2\omega\dot{\eta}_0}{gd}r + \frac{C}{r} \qquad (17$$

where C is the constant of integration.

(c) If a source S_0 is uniformly distribute around the periphery, and $V_r = 0$ at $r =$ we have:

$$\dot{\eta}_0 = \frac{S_0}{\pi a^2};\quad C = 0$$

$$V_r = -\frac{S_0}{2\pi a^2}r \qquad (18$$

$$V_\phi = \frac{S_0}{\pi a^2}\frac{h}{d}\left[1-\frac{d}{2h}\right]r \qquad (19$$

Here v_ϕ represents a "solid rotation" abov the Ekman layer. v_ϕ is cyclonic and the Ekma transport, V_r, is radially inward for positive S_0

(d) If there is a point source S_0 at $r = 0$ an $V_r = 0$ at $r = a$, we have:

$$C = -\frac{2\omega S_0}{\pi g d}$$

$$V_r = \frac{S_0}{2\pi a}\left(\frac{a}{r}-\frac{r}{a}\right) \qquad (20$$

$$v_r = \frac{S_0}{\pi a d}\left(\frac{a}{r}-\frac{r}{a}\right)\varepsilon^{-\zeta}\sin\zeta \qquad (21$$

$$V_\phi = -\frac{S_0 h}{\pi a d}\left(\frac{a}{r}-\frac{r}{a}\right)\left[1-\frac{d}{2h}\right] \qquad (22$$

$$v_\phi = -\frac{S_0}{\pi a d}\left(\frac{a}{r}-\frac{r}{a}\right)[1-\varepsilon^{-\zeta}\cos\zeta] \qquad (23$$

Here v_ϕ above the Ekman layer is determined by the superposition of a $1/r$ vortex an a solid rotation in the opposite sense in such way as to give $v_\phi = 0$ at $r = a$.

One experiment has been performed with peripherally distributed source (case (c)) t verify the prediction of eq. (19) that the zona flow will be a solid rotation. A solid rotatio was observed under these circumstances.

All the observations of instability of the Ek man flow were made with a central sourc (case (d)) for the situation described by eqs (20)—(23). The physical interpretation or de scription of this situation is as follows: Th presence of a central source (positive S_0) mus produce a uniform vertical velocity throughout the fluid as the surface rises. Water must be transported radially outward from the central source, and such transport can occur only in the frictional boundary layer. The source therefore induces a general anticyclonic zonal geostrophic flow with an Ekman layer at the bottom. A net cross-isobar transport of water radially outward (to the left of the zonal flow) takes place in the Ekman layer, the zonal geostrophic velocities adjusting themselves to produce the required transport and horizontal divergence in the Ekman layer.

If the equations of motion were written to include the effect of lateral friction, eq. (2) would have on the right hand side the added term

$$\nu\left[\frac{1}{r}\frac{\partial}{\partial r}\left(r\frac{\partial v_r}{\partial r}\right)-\frac{v_r}{r^2}\right] \qquad (23\,a)$$

and eq. (3) would have a similar one in v_ϕ. Solutions with radial dependence of the form r or $1/r$ make this term identically zero. Thus the basic field solutions developed above are actually solutions to the complete, linearized Navier-Stokes equations applicable to this problem.

Quantitative verification of the basic flow

The basic flow as described by eqs. (20)—(23) was verified quantitatively in two ways:

(a) by direct observation of the zonal surface velocity v_ϕ for various values of ω and S_0.

(b) by direct observation of the rate of radial spread of the colored Ekman layer when dye was introduced into the source.

A comparison of observed and predicted zonal surface velocities is shown in Figure 3. Each set of points, denoted by a particular symbol, represents the results at different radii for a particular run at some value of ω, ν, and S_0. Instability of the Ekman layer was present in each run. Under the existing circumstances, however, the scatter of the data is within the range of experimental uncertainty. We are led to say that in these experiments the zonal surface velocities agree, within experimental error, with the predicted basic field values, and it is not possible to assert a significant effect of the Ekman instability on the basic flow.

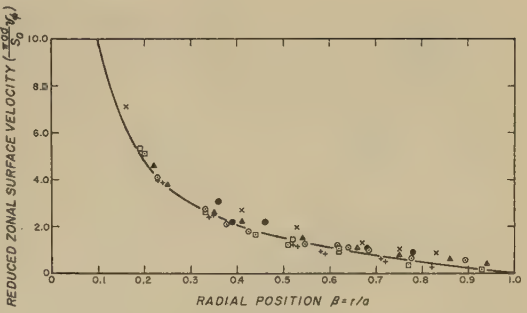

Fig. 3. Scaled zonal velocity v_ϕ vs. radial position, for various combinations of source strength and angular velocity.

Theoretical curve: $-\frac{\Pi a d}{S_0} v_\phi = \frac{1}{\beta} - \beta$

Experimental Runs

Symbol	S_0 (cm^3/sec)	ω radians/sec
⊙	2.71	1.02
×	3.32	2.01
●	3.39	1.02
△	3.30	2.01
⊡	3.65	2.02
+	3.74	1.00

A similar result is obtained for observations of the radial spread of the Ekman layer. Assuming that the visible radial spread will be determined by the maximum value of v_r in the Ekman layer, eq. (21) gives:

$$v_{r\,\max} = \frac{0.322\, S_0}{\pi a d}\left(\frac{1}{\beta} - \beta\right) \qquad (24)$$

where $\beta \equiv r/a$. Integration of eq. (24) gives:

$$t = 1.553\, \frac{\pi a^2 d}{S_0} \ln(1 - \beta^2) \qquad (25)$$

where $t = 0$ when $r = 0$, and t is the time taken for a particle to reach radial position β.

Figure 4 shows a semilogarithmic plot of $(1 - \beta^2)$ vs. t. Only one run of this kind was made, and the scatter of results from run to run is therefore not established, but the observed values are considered to be in good agreement with predictions, especially at values of β of about 0.3 to 0.5 where the instabilities and their critical limit were usually observed. The uncertainty indicated for the experimental points in Figure 4 stems from the fact that the outer boundary of the colored ring was not perfectly circular.

We thus conclude that the basic flow field obtained in these experiments is in good agree-

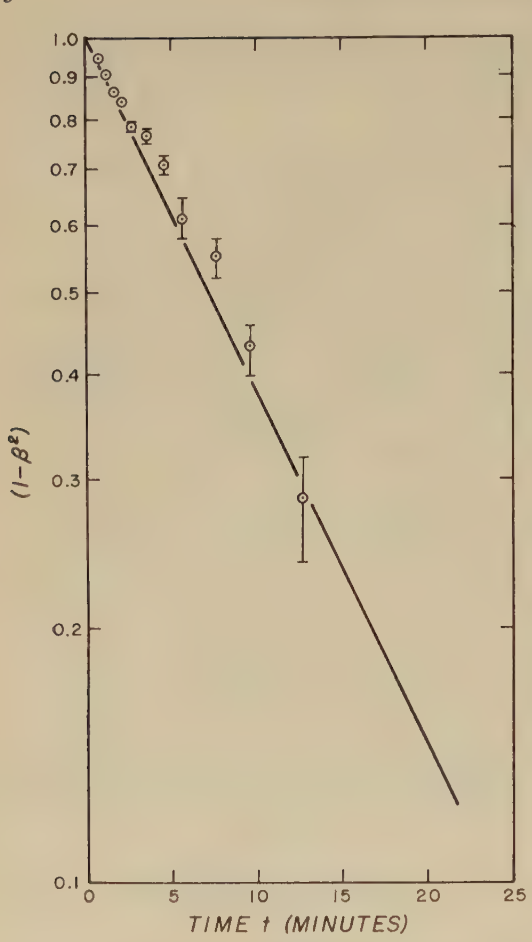

Fig. 4. Radial spread of Ekman layer vs. time

Theoretical curve: eq. (25)
Experimental observations:

ω = 1.79 radians/sec.; S_0 = 2.42 cm³/sec.
a = 65 cm.

Range of uncertainty indicates out of roundness of spreading Ekman layer.

ment with the values predicted by the analysis of the preceding section. Noticeable departures from simple laminar flow are, however, invariably observed in two regions: (1) a turbulent region within a few centimeters of the center of the tank (2) a turbulent band several centimeters wide at the outer rim. In these regions the laminar flow is unstable, and turbulence penetrates the entire depth of fluid. Apparently the presence of these two turbulent regions does not seriously affect the basic flow regime in the interior of the basin.

Observed instability of the Ekman flow

Figures 1 and 2 show typical top and side views, respectively, of the curtains of fluid which originate in the Ekman layer and penetrate the entire depth of flow, The phenomenon is characterized by a "wave length", λ, or spacing between the curtains, of the order of 1 to 2 cm. and by a critical radius r_c beyond which the curtains do not occur. All the accumulated values of λ and r_c for various combinations of S_0, ω, h, and are ν summarized in Table I together with accompanying values of Ekman, Taylor, Reynolds, Rossby, and Froude numbers. The specific definitions for the various numbers in the present context are indicated in Table I.

STERN's (1960) assymptotic analysis in Cartesian coordinates predicts an instability of essentially the type observed in these experiments—a flow drawing its energy from the Ekman layer and penetrating the entire depth of fluid. He further predicts that the wave length of the resulting cells will be a function of the Taylor number, E (see Table I):

$$\frac{\lambda}{d} \sim 6 E^{\frac{1}{4}} \qquad (26)$$

Figure 5 shows a plot of observed values of

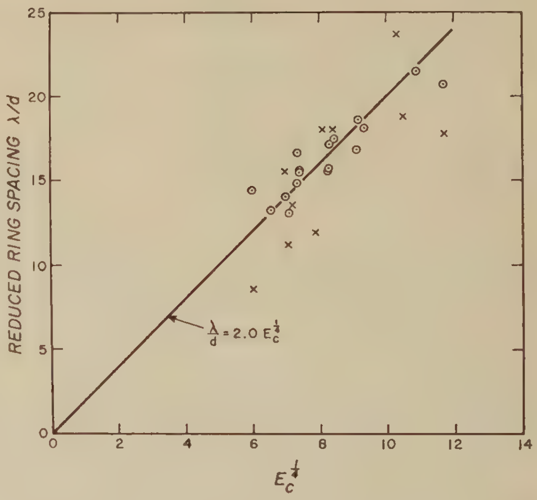

Fig. 5. Reduced ring spacing, λ/d vs. fourth root of Taylor number, $E_c^{1/4}$.

- ○ Points from Table I for cases in which r_c was reasonably well defined.
- × Points marked (?) in Table I for cases in which r_c was very poorly defined.

Table 1. **Observed ring spacing and critical radii.**

Angular Velocity ω rad./sec.	Source Strength S_0 cm³/sec.	Kinematic Viscosity $\nu \times 10^2$ cm²/sec.	Average Ring Spacing λ cm.	Critical Radius r_c cm.	Depth At r_c h_c cm.	Reduced Ring Spacing λ/d	Dimensionless Parameters Applicable to flow at r_c						
							E_c	$R_{\cdot c}$	R_{IC}	ε_c	F_c	$R_C \times 10^3$	$R_{E(19)}$
2.18	2.87	.983	0.87	27	3.40	13.0	2570	2.80	141	.0197	1.04	7.0	4.48
2.18	2.77	.971	1.38	38	9.20	20.7	19000	1.59	221	.0072	0.76	2.8	4.37
2.18	2.82	.915	1.20	29	5.40	18.6	6940	2.70	225	.0120	0.75	6.0	4.73
2.18	2.83	.983	1.21	28	4.40	18.0	4330	2.65	174	.0152	0.86	6.3	4.42
1.57	2.83	.925	1.65	34(?)	9.15	21.5	14200	2.06	245	.0084	0.32	4.6	4.70
1.57	2.80	.947	1.40	32	5.45	18.0	4890	2.24	157	.0143	0.48	5.5	4.54
2.18	2.76	1.140	1.20	22	3.90	16.6	2920	3.10	168	.0185	0.60	10.2	3.71
2.18	2.76	.893	1.09	28	4.40	17.1	4750	2.91	201	.0145	0.86	6.6	4.74
1.57	2.85	.947	1.40	27(?)	5.05	18.0	4210	2.89	188	.0154	.037	8.3	4.62
1.92	2.76	.900	1.20	25	4.90	17.5	5110	3.40	243	.0140	0.48	9.3	4.70
1.64	2.75	.906	1.40	50(?)	8.20	18.8	12100	0.80	89	.0091	0.84	1.2	4.65
2.18	2.82	.901	0.70	30(?)	4.05	10.9	3960	2.62	165	.0159	1.07	5.6	4.80
1.92	2.81	.932	1.08	24	3.80	15.5	2980	3.46	189	.0183	0.57	10.0	4.63
1.04	2.78	1.130	1.50	19	3.75	14.4	1290	3.65	131	.0278	0.11	20.0	3.77
2.18	2.87	.990	1.20	44(?)	9.20	17.8	18800	1.10	151	.0073	1.02	1.7	4.45
1.04	2.85	.893	1.20	32	3.90	13.2	1840	2.37	102	.0233	0.29	6.7	4.90
1.32	2.81	.902	1.16	32	4.05	14.0	2400	2.35	115	.0204	0.45	6.1	4.78
1.64	2.80	.893	1.12	29	4.15	15.2	3160	2.75	154	.0178	0.56	7.0	4.81
1.64	2.13	.904	1.10	28	4.00	14.8	2920	2.20	119	.0185	0.54	5.8	3.62
1.64	1.52	.897	1.16	27	4.05	15.7	3020	1.67	92	.0182	0.49	4.6	2.60
1.64	3.52	.897	1.16	34	5.05	15.7	4630	2.67	181	.0147	0.63	7.8	6.02
1.64	4.25	.913	1.16	36	5.05	15.5	4570	2.85	193	.0148	0.70	5.9	7.14
1.04	2.67	1.165	0.9(?)	28(?)	3.85	8.5	1320	2.13	77	.0275	0.22	8.0	3.52
1.04	2.75	1.205	1.2(?)	26(?)	5.10	11.2	2240	2.33	110	.0211	0.15	9.6	3.50
2.18	2.73	1.205	1.0(?)	20(?)	3.85	13.5	2680	3.25	168	.0193	0.50	12.1	3.47
1.00	4.00	1.060	1.6	27(?)	5.05	15.5	2400	3.71	182	.0204	0.15	14.2	5.80
1.25	4.90	.960	2.1(?)	50(?)	9.30	23.7	11300	1.32	140	.0094	0.43	2.3	7.83
2.18	2.65	.810	1.1	33	5.27	18.1	7560	2.49	216	.0115	1.00	3.0	5.02
2.18	2.82	.716	0.96	30	4.76	16.8	6940	3.23	269	.0120	0.92	6.2	6.04

Dimensionless parameters at r_c:

Taylor no. $E_c \equiv \frac{\omega h_c^2}{\nu}$

Ekman no. $\varepsilon_c \equiv \frac{1}{h_c}\left(\frac{\nu}{\omega}\right)^{\frac{1}{2}}$

Reynolds no. for Ekman layer:

$$R_{EC} \equiv \frac{v_c d}{\nu} = \frac{S_0}{\nu \pi a}\left(\frac{a \qquad r_c}{r_c \qquad a}\right)$$

$R_{E(19)}$ = Reynolds no. at $r = 19$ cm.

Reynolds no. for interior flow:

$$R_{IC} \equiv \frac{v_c h_c}{\nu} = \frac{R_{EC}}{\varepsilon_c}$$

Froude no. $F_c \equiv \frac{(r_c\omega)^2}{g h_c}$

Rossby no. $R_c = \frac{v_c}{r_c\omega} = \frac{R_{EC}}{r_c}\left(\frac{\nu}{\omega}\right)^{\frac{1}{2}}$

(?) denotes poorly defined values

$\frac{\lambda}{d}$ versus $E_c^{1/4}$, taken from Table I. (The local Taylor number of the flow varies with r, but λ is uniform within a few percent in the region where the rings occur. It seems reasonable to take as the characteristic Taylor number for any given case that value which obtains at the critical radius r_c).

We do not have enough data or attempts at identical repetition of experiments to state positively whether the scatter of points in Figure 5 contains systematic dependence on other parameters or represents the intrinsic variability of the observations. Assuming the latter, the observations scatter about a straight line represented approximately by

$$\frac{\lambda}{d} = 2.0\, E_c^{1/4} \qquad (27)$$

This is consistent with Stern's asymptotic

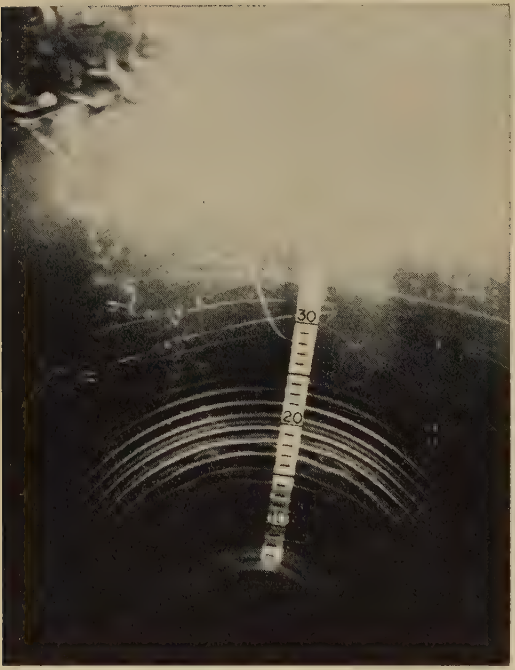

Fig. 6. Downward circulation between rising curtains: Intense rings are the rising jets; fainter rings at 19 and 20 cm. marks, between the more intense rings, mark downward circulation of dye shortly after it reached the water surface. Marks of downward circulation between rings closer to center have become more diffuse since dye reached these regions several minutes before instant of photograph. Upper left hand corner of photograph shows band of turbulence along outer rim of tank.

result for the simpler geometry. Two Reynolds numbers at the critical radius r_c have been tabulated in Table I. The Reynolds number R_{IC} of the interior geostrophic flow varies widely and shows no discernable correlation with other parameters. The Reynolds number R_{EC} of the Ekman flow, when questionable values of r_c are omitted, lies in the relatively narrow range between 1.6 and 3.6, (the extreme range of values of this number for various radial positions in these experiments is of the order of 0 to 10). The apparent correlation of the onset of rings with a narrow range of values of R_{EC} implies that the instability draws its energy from the Ekman layer rather than from the geostrophic flow, and this view is also consistent with Stern's analysis.

The last column in Table I gives values of the Reynolds number of the Ekman layer at a radius of 19 cm, which was usually about the mid-region for the occurrence of the vertical sheets. Comparison of values of $R_{E(19)}$ with R_{EC} will indicate the extent to which the Reynolds number at the critical radius is exceeded in the interior of the region of instability; this might be an index to the importance of finite amplitude effects in this region.

In general, downward circulation between the rising curtains was considerably less sharp and intense than that of the rising phase. A top view, showing evidence of the downward motions, is shown in Figure 6. The fainter rings, when observed from the side of the tank, were seen to be moving downward, and do not represent a rising mode of smaller wavelength. Both upward and downward motions were also observed when dye was injected very slowly from capillary probes inserted at various points in the body of the flow.

The upward velocities of the curtains are roughly 0.7 cm/min., i.e. an order of magnitude of about 1 % of the basic zonal velocity.

On some occasions a fairly regular, small scale, zonal wave or vortex structure was formed on the rising curtains. An illustration of this effect is shown in Figure 7. This phenomenon did not seem to correlate with systematically outlying values of either of the calculated Reynolds numbers; in a substantial number of cases the waves did not form in experiments conducted at Reynolds numbers higher than those in which waves were observed. The waves appeared to occur somewhat more frequently however in experiments at

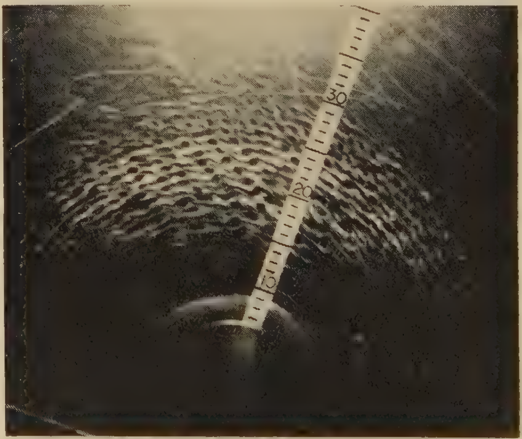

Fig. 7. Illustration of small scale zonal disturbances which were occasionally observed. Although these waves could not be unequivocally correlated with relatively high Reynolds numbers, they seemed to occur somewhat more frequently at high source rates and low viscosities.

gher source strengths or at lower viscosities. o rings or curtains were observed to form several experiments performed at tempera-ures below 13°C., i.e. at kinematic viscosities reater than about 0.012 cm^2/sec.; in these ases the Ekman flow was laminar and stable.

Since the ranges of variation of ω and h e limited by the design of the existing equip-ent, it has not been possible to vary these arameters over a wide enough range to test the xpectation that the cut-off of the ring pheno-enon depends on a dimensionless parameter nd is not determined solely by the higher iscosity of the water at the lower temperatures very effort, however, has been made to erform the experiments under conditions of mperature homogenity throughout the tank nd at temperature equilibrium between the nk and the room. The tank was carefully overed to minimize both wind and evapora-on effects. The experiments were performed the winter time, and when low temperature runs were underway, the room itself was cooled to the temperature of the run by turning off the heat. If any error in maintainance of inhomogeneity existed, it was more probably in the direction of allowing the existence of vertical *stability* in the body of water in the tank.

In a few instances, rings did not form under conditions in which they normally occurred. Disturbances such as jarring the tank and briefly interrupting the source flow then led to the formation of rings—sometimes in competing sets at different radii, the competing sets then shifted and wandered somewhat until they interlocked into a normal pattern.

REFERENCES

Stern, M. E., 1960; Instability of Ekman Flows at Large Taylor Numbers. *Tellus* **12**, pp. 399—417.

Stommel, H., Arons, A. B.; Faller, A. J.; 1958: Some Examples of Stationary Planetary Flow Patterns in Bounded Basins. *Tellus* **10**, pp. 179—187.

PRINTED IN SWEDEN
ESSELTE, STHLM 61

Contribution No. 1136

RADIOACTIVE RARE EARTHS FROM FALLOUT FOR STUDY OF PARTICLE MOVEMENT IN THE SEA

Thomas T. Sugihara
Clark University, Worcester, Mass.
and
Vaughan T. Bowen
Woods Hole Oceanographic Institution, Woods Hole, Mass.
United States of America

Abstract — Résumé — Аннотация — Resumen

Radioactive rare earths from fallout for study of particle movement in the sea. As part of an extensive study of the distribution of long-lived radionuclides from fallout in the Atlantic Ocean, a large number of measurements of cerium-144 and promethium-147 concentration have been made. Comparison of these concentrations as they vary both horizontally and vertically, with simultaneously measured concentrations of strontium-90, indicates that the rare earths are generally depleted in surface water, by comparison with the nuclides known to be soluble. This observation, coupled with frequent observation of rare-earth enrichment at depth, leads us to postulate rapid vertical transport of rare earths by attachment to particles undergoing sedimentation. This is completely plausible in terms of the "radiocolloid" behaviour generally observed for rare earths at sea-water pH.

An attempt is made to interpret this study in the overall picture of the marine geochemistry of the trivalent cations, as well as to emphasize the unique and generally useful aspects of the fallout tracer experiment.

Etude du mouvement des particules dans la mer à l'aide de terres rares radioactives provenant de retombées. Dans le cadre d'une vaste étude sur la répartition dans l'Océan Atlantique des radionuclides de longue période provenant de retombées, on a procédé à de nombreuses mesures de la concentration du cérium-144 et du prométhéum-147. En comprenant les variations horizontales et verticales de ces concentrations avec les concentrations, mesurées simultanément, du strontium-90, on constate que les terres rares sont en général moins abondantes en surface que les nuclides connus pour être solubles. Cette observation, jointe au fait que l'on a souvent constaté un enrichissement des eaux profondes en terres rares, amène les auteurs à considérer qu'il s'effectue un transport vertical rapide des terres rares, par adhésion aux particules qui subissent une sédimentation. Cette hypothèse est entièrement compatible avec le comportement «radiocolloïdal» que les terres rares ont généralement dans un milieu ayant le pH de l'eau de mer.

Les auteurs du mémoire essaient d'interpréter les résultats de cette étude dans le cadre général de la géochimie marine des cations trivalents, et de mettre en évidence les aspects particuliers et l'utilité générale de cet essai d'utilisation des retombées comme indicateurs.

Использование осаждающихся при выпадении радиоактивных редких земель для исследования движения частиц в море. В качестве части подробного исследования распределения долгоживущих радиоизотопов, осевших при выпадении в Атлантическом океане, было проделано значительное число замеров концентрации церия-144 и прометия-147. Сопоставление этих концентраций по мере их изменения как в горизонтальном, так и в вертикальном направлениях с одновременно замеренными концентрациями стронция-90 показывает, что редкие земли находятся обычно в меньших количествах на поверхности воды, чем изотопы, известные как растворимые. Это замечание совместно с частым наблюдением обогащения редкими землями на глубине приводит нас к предположению, что редкие земли быстро переносятся в вертикальном направлении, благодаря прилипанию к оседающим частицам. Это предположение вполне вероятно в свете „радиоколлоидального“ поведения, обычно наблюдаемого для редких земель при pH морской воды.

Делается попытка истолковать настоящее исследование в связи с общей картиной морской геохимии тривалентных катионов, а также подчеркнуть исключительные и обычно полезные аспекты опытов изучения выпадения при помощи радиоактивных индикаторов.

Estudio del movimiento de las particulas en el mar con ayuda de tierras raras radiactivas procedentes de las precipitaciones. En el marco de un vasto estudio sobre la distribución en el océano Atlántico de los radionúclidos de período largo procedentes de precipitaciones radiactivas, se han efectuado numerosas mediciones de la concentración del cerio-144 y del promecio-147. Una comporación de las variaciones horizontales y verticales de estas concentraciones con las concentraciones del estroncio-90, que fueron medidas al mismo al mismo tiempo, demuestra que las tierras rasas suelen abundar menos en las aguas superficiales que los núclidos que se sabe son solubles. Esta observación, unida al hecho de que se ha observado a menudo un enriquecimiento de las aguas profundas en tierras raras, permite afirmar que esos elementos experimentan un rápido transporte vertical al fijarse a partículas en vías de sedimentación. Esta hipótesis es perfectamente compatible con el comportamiento "radiocoloidal" característico de las tierras raras al pH del agua de mar.

En la memoria se procura interpretar este estudio en el contexto de las propiedades generales de los cationes trivalentes en geoquímica marina; asimismo, se ponen de manifiesto los aspectos característicos y la utilidad general de este ensayo de utilización de las precipitaciones como indicadores radiactivos.

Introduction

In earlier reports [1—3] we have outlined the basis for drawing geochemical and hydrodynamic conclusions from the study of vertical and horizontal distributions of long-lived fission-product radioactivities in the Atlantic Ocean. Most of the earlier discussions have dealt primarily with strontium-90, although the outlines of a rationale for interpreting cerium-144 and promethium-147 analyses have been worked out provisionally [2]. The present report will deal primarily with analyses of these two rare-earth radioisotopes.

The analytical procedures used in previous years have been reported [4]. Some changes have been made, resulting in improved precision and yields, as well as a saving in time. These will be reported in a manuscript now being prepared. The data reported here have been obtained by using all our various methods. During the past year, it has been possible to run several series of very detailed blank determinations, as well as of careful, step-wise, measurements of recovery. These have justified making estimates of the probable confidence limits of the rare-earth determinations, including both chemical uncertainties and counting statistics. Numbers subject to this qualification are marked with asterisks in the following tables; those not marked show only the variation to be expected from counting statistics.

In the discussion below, only the lanthanide radioactivities are known and discussed, even when the element name alone is used. This is generally true of strontium as well.

TABLE I

FALLOUT RARE EARTH RADIOACTIVITY IN SURFACE OCEAN

Sta.	Collection Date	Lat.	Long.	Radioactivity (dpm/100 l)		Ce/Pm	Ce/Sr^{90}	Notes:
				Ce^{144}	Pm^{147}			
	9–XII–56	17° 49′ N	60° 07′ W	31.0 ± 0.9	3.5 ± 0.5	8.9	3.0	
	12–XII–56	24° 50′ N	61° 55′ W	91.1 ± 1.8	11.6 ± 0.8	7.8	7.6	
80A	13–II –57	21° 08′ N	33° 20′ W	14.7 ± 1.2*	2.20 ± 0.26*	6.7	3.1	
	16–II –57	36° 26′ N	72° 10′ W	25.8 ± 0.7	7.1 ± 0.9	3.6	2.5	
	7–III –57	8° 18′ S	7° 43′ W	9.5 ± 0.4	2.1 ± 0.2	4.5	1.9	
	20–III –57	8° 18′ S	31° 17′ W	8.8 ± 0.5	2.2 ± 0.5	4.0	2.6	
176	17–V –57	8° 17′ N	49° 15′ W	18.1 ± 1.3*	2.03 ± 0.24*	8.9	3.3	
	23–VII–57	36° 23′ N	70° 33′ W	42.2 ± 1.2	8.8 ± 0.9	4.8	4.0	
	15–XI –57	15° 26′ N	68° 30′ W	18.1 ± 0.5	3.7 ± 0.6	4.9	3.1	
	18–XI –57	15° 23′ N	70° 48′ W	20.5 ± 0.5	5.5 ± 0.6	3.7	3.4	
	20–XI –57	17° 38′ N	76° 02′ W	14.1 ± 0.5	6.2 ± 0.5	2.3	1.3	
297	23–XI –57	16° 14′ N	45° 01′ W	33.3 ± 2.8*	6.5 ± 1.0*	5.1	5.3	
311	8–XII–57	31° 15′ N	68° 10′ W	107 ± 13*	—	—	9.8	
	10–XII–57	36° 51′ N	69° 30.5′ W	29.0 ± 2.2	12.3 ± 2.2	2.4	2.0	
Bimini	30–XII–57	25° 30′ N	78° W	11.0 ± 0.9*	1.22 ± 0.17*	9.0	1.4	Mangrove Cove-Bimini
	30–XII–57	25° 30′ N	78° W	44.5 ± 3.6*	3.30 ± 0.46*	13.5	4.0	N. E. Well-Bimini
	12–VII–58	34° 30′ N	65° 42′ W	51.2 ± 1.0*	—	—	6.7	
	16–VII–58	34° 39′ N	67° 24′ W	54.4 ± 1.0	7.2 ± 0.7	7.5	6.0	
	17–VII–58	36° 20′ N	70° 18′ W	71.8 ± 5.0*	9.4 ± 0.8*	7.6	1.5	Surf. Sal. 31.35-near Gulf Stream
	6–IX –58	39° 47.7′ N	71° 13′ W	144 ± 9*	31 ± 3*	4.7	5.1	

* Standard error includes uncertainty from chemical separations; **cf. Introduction**

Results

The analyses which we wish to discuss here are set out in three tables: Table I containing analyses of surface samples of sea-water obtained on various cruises from late 1956 to late 1958; Table II containing analyses taken during 1957 from five stations which yielded analysable samples of deep water; and Table III containing analyses taken during 1958 from four similar stations. In all cases the activity reported for cerium-144 and for promethium-147 has been adjusted to allow for radioactive decay since the date of collection. Such correction has not been applied to the strontium-90 data with which these numbers are compared.

The data reported for deep samples are always for samples on which salinity determination showed proper operation of the sampling devices.

Discussion

The ratios Ce: Pm and Ce: Sr are interpretable in relation to these same ratios as inferred for production in nuclear fission explosions [2], and subject to certain assumptions, can be employed to indicate the age of the fission-product mixture in question. In this application, of course, the critical assumption is that no chemical separation of the fission products has occurred in their atmospheric or marine geochemistry. Initially this assumption was held to be valid for the pair cerium-promethium, and not valid for the pair cerium-strontium.

From recently released data presented by Dunham [5], we can obtain roughly the pattern over time of radioactivity production by fission. These estimates run as follows: during 1945—1951, 760 kt equivalent; during 1952—1954, 60000 kt; during 1955—1956, 28000 kt; and during 1957—1958, 85000 kt. Making the simplest possible assumptions about fallout mechanisms and rates, we may infer from this that for sea-water samples taken in 1956 and early 1957, some two-thirds of the fission mixture, at least, should be two years old; for late 1957 and the first half of 1958, at least one-half the fission mixture should be three years old. In addition to suiting present theories of the rate of removal of fallout from the stratosphere [6], this short stratospheric residence time is supported by the Ce^{144}: Sr^{90} ratios in upper air [7]. These reported ratios rarely fall below 9 and rarely rise above 18. Unfortunately, promethium-147 is not measured as a part of this or of any other publicized program.

Turning now to Tables I, II and III, we see that both the given Ce: Sr ratios and the Pm: Sr ratios, which are easily obtainable, but have been omitted to save space, indicate general depletion of the two rare earths with respect to strontium. This is as expected, since strontium, as we have emphasized [2] [3], moves in the sea only as a solute, while the lanthanides, in the very low concentrations which occur in sea-water, should be present very largely as radiocolloids [8] and rapidly become associated with any solid surfaces available. It is evident from our data, however, that promethium has been depleted in comparison with cerium. Most of the Ce: Pm ratios are higher than would be reasonable even for fresh fission mixtures. The mechanism for this depletion has yet to be established. We believe it to lie in the marine geochemistry of cerium, and suspect it to relate to our observation that at pH values not far removed from neutrality, tracer amounts of cerium undergo rapid air oxidation to the four-valent state. This is a common observation in our ion-exchange separations, and if extrapolated to sea-water and combined with radiocolloid

TABLE II

FALLOUT RARE EARTH RADIOACTIVITY PENETRATION TO DEPTH IN ATLANTIC OCEAN—I

Station	Collection Date	Lat.	Long.	Sample depth (m)	Radioactivity (dpm/100 l)		Ce/Pm	Ce/Sr^{90}
					Ce^{144}	Pm^{147}		
86	1– III–57	8° 26′ S	7° 45′ E	~0	(9.0 ± 1.0)	(2.1 ± 0.5)	4.3	1.8
				295	4.6 ± 0.4	1.7 ± 0.5	2.7	1.9
				795	2.4 ± 0.8	2.5 ± 0.5	1.0	8
116	20– III–57	8° 18′ S	31° 17′ W	10	8.8 ± 0.5	2.2 ± 0.5	4.0	2.6
				985	4.1 ± 0.5	0.9 ± 0.5	4.5	6.8
124	2– IV–57	15° 49′ S	35° 50′ W	30				
				910	7.3 ± 0.9*	0.63 ± 0.38*	11.5	4.8
296	22– XI–57	16° 15′ N	43° 37.5′ W	~0	(33.3 ± 2.8)*	(6.5 ± 1.0)*	5.1	5.3
				90	20.0 ± 1.0*	5.3 ± 1.3*	3.8	3.7
				350	25.6 ± 2.4*	2.6 ± 1.2*	9.8	11.6
				1100	—	2.9 ± 1.0*		
311	8–XII–57	31° 15′ N	68° 10′ W	0	107 ± 13*	—	—	9.8
				97	31.3 ± 1.0*	8.6 ± 1.7*	3.6	4.1
				400	11.7 ± 0.6*	3.5 ± 0.9*	3.3	3.4

* Standard error includes uncertainty from chemical separations; cf. **Introduction**

TABLE III

FALLOUT RARE EARTH RADIOACTIVITY PENETRATION TO DEPTH IN ATLANTIC OCEAN—II

Station	Collection Date	Lat.	Long.	Sample depth (m)	Radioactivity (dpm/100 l)		Ce/Pm	Ce/Sr^{90}
					Ce^{144}	Pm^{147}		
408	11/12–VII–58	34° 30′ N	65° 42′ W	0	51.2 ± 5.1*	—	—	6.7
				300	39.4 ± 2.0*	6.8 ± 0.6*	5.8	3.3
				500	23.3 ± 1.0*	2.4 ± 1.2*	9.7	3.2
				675	10.9 ± 0.7*	2.0 ± 0.7*	5.5	3.0
				975	14.9 ± 1.2*	1.6 ± 0.6*	9.3	16.5
	15/16–VII–58	34° 39′ N	67° 24′ W	0	54.4 ± 1.0	7.2 ± 0.7	7.5	6.0
				98	32.8 ± 0.7	6.0 ± 0.7	4.0	5.5
				300	21.4 ± 0.7	3.0 ± 0.7	7.1	3.9
				700	7.2 ± 0.2	—	—	2.1
				1000	38.7 ± 1.0	—	—	22.8
	17–VII–58	36° 20′ N	70° 12′ W	0	71.8 ± 5.0*	9.4 ± 0.8*	7.6	1.5
				80	24.8 ± 2.2*	5.4 ± 0.5*	4.6	1.7
				250	7.3 ± 0.7*	2.7 ± 0.3*	2.5	1.9
				420	6.1 ± 0.7*	1.2 ± 0.2*	4.9	4.0
533	6– IX–58	39° 47.7′ N	71° 13′ W	0	144 ± 9.0*	31 ± 3*	4.7	5.1
				75	14.3 ± 0.8*	2.3 ± 0.3*	6.2	4.0
				100	15.1 ± 0.9*	1.7 ± 0.4*	8.9	4.4
				200	16.0 ± 1.0*	4.0 ± 0.6*	4.0	4.6

* Standard error includes uncertainty from chemical separations; cf. **Introduction.**

behaviour of the trivalent lanthanides, offers a sufficient explanation of the ratios observed.

We take the low Pm:Sr values of the two Bimini samples as further supporting evidence. The Great Bahama's Bank, from which these came, is an area of great biological activity, and also of extensive wave-reworking of the oölitic sediments covering the bank. From the Mangrove Cove sample, which is reasonably accepted as being the most thoroughly particle-swept, we reported a Sr^{90} value of 7.6 disintegrations/min per 100 l (in the range of most surface sea-water for late 1957). The Ce:Sr ratio, however, is only 1.4, and the Pm:Sr value is 0.15: this is the greatest lanthanide depletion we have observed. The Ce:Pm ratio of 9.0 is one of the highest we have seen, confirming that even with very efficient lanthanide removal, preferential retention of cerium occurs in the water. The other Bimini sample, from a more open well on the reef, again showed normal Sr^{90}, and not unusually low Ce^{144}, but the third lowest Pm:Sr (0.3) that we have observed.

The Pm:Sr ratios in deeper water from the first four 1957 stations (Table II) are consistent, being highest in the 800 to 1100-m samples, intermediate at 300 and 350 m, and lowest at the surface. The cerium values, in relation to the others, do not show comparable regularity; only in the two southerly stations from March 1957 do we see Ce:Sr ratios increasing with depth, and even here the Ce:Pm ratio increases slightly with depth at one station, while decreasing at the other. The only other station showing this pattern of increase with depth of both lanthanides, relative to strontium, is the third station (Table III) from July 1958. This was an attempt to obtain a profile in the Gulf Stream, and not a wholly successful one: most of the column, although moving at Gulf Stream velocities, was shelf water with a rather low surface salinity. It appears to show the effects both of silt and biological purging of lanthanides. Here too, the Ce:Pm ratio, though diminishing regularly as anticipated in the upper three samples, is high at 400 m.

In the late 1957 and 1958 stations, with the one exception noted, two tendencies appear: high Ce:Sr ratios at the surface, diminishing with increasing depth; and secondary maxima, at depth, of Ce^{144} or Pm^{147} or both, generally resulting in the highest Ce:Sr ratio occurring at this depth. In these stations a tendency is also seen for a minimum in Pm:Sr ratio at intermediate depths, but not coinciding with the highest cerium radioactivity. If these maxima at depth are real, which is our provisional assumption, then some are quite narrow bands: a sample from the first station of Table III, but about 960 m deep, shows 4.2 disintegrations/min Ce^{144} and 0.7 disintegrations/min Pm^{147}. Unfortunately, none have so far been observed from stations from which replicate aliquots are available for analysis.

To us, it seems likely however, that these double maxima, at surface and at depth in late 1957 and 1958 and at mid-northern latitudes, are related to the very high injection of fission material which occurred in early 1957 [7]. This appeared as an extremely high monthly amount of Sr^{90} over New York City in April of that year, and may reasonably be expected to account for the high Ce^{144} and Pm^{147} in the 30° to 40° N surface samples collected subsequently. Such an addition should have resulted, as it appears likely to have done, in a reversal of the direction of the gradient of lanthanide: strontium ratios. Although striking a balance for Ce^{144} or Pm^{147} is even more difficult than for Sr^{90}, the increase in surface ratios is generally not so high as might have been expected, nor does the content in the water columns appear to correspond to the total that might have been added. This line of argument includes the assumption that the injection of fission material which produced the high New York City values of April, May and June 1958 had not yet appeared in the three ocean stations of July 1958, although it is thought to have contributed to that of September 1958.

Given then the assumption of high surface fallout of relatively fresh fission mixture sometime between June and August 1957, and its direct relation to secondary maxima of lanthanide radioactivity at depth, we can discern, dimly, the progress of populations of labelled surfaces downward through the sea. Some particles, labelled with Ce^{144}, appear to have sunk some 300 m in about four months at 16° N (Table II). Others, at about 34° N (Table III) appear to have sunk 1000 m in about a year. The very high Pm:Sr ratio at 1100 m at 16° N (Table II) may indicate a more rapid sinking for promethium-labelled particles. This is supported by the much-more-distinct Pm maximum at 200 m from the fourth station of Table III, as well as by the general promethium depletion shown by all the water columns.

The high lanthanide: strontium ratios at 800 to 1000 m from the 8° S stations (Table II) may be taken to indicate a residue of very slowly sinking particles labelled during 1954, and representing a vertical velocity of about 2.5 yr/1000 m.

On the basis of our earlier discussion, it is not unreasonable to assume that promethium should associate preferentially with the more rapidly sinking particle populations. Should Ce (IV) require to be reduced before adsorption of cerium, this may well occur in the neighbourhood of organic debris of lower density, whereas promethium should associate with all types of surface, in proportion only to the areas represented by each. JERLOV [9] has shown that ocean water masses can be characterized by their particle content; in other words, that measurable populations of particles have vertical velocities no different from that of the water in which they lie. Ultimately, we hope to ascertain whether, as anticipated, a residue of promethium is associated with these; and if this proves indeed true, to be able from its magnitude to estimate the relative surface per m^3 represented by sinking and non-sinking particles.

Thus far our analyses show that the surfaces of large zooplankton, even filter feeders, are rarely of immediate significance in lanthanide sinking. These organisms—0.1 mm or larger—are easily separable, by netting, from detritus, phytoplankton or smaller animals. In the dozen or so samples thus far examined, less than 0.1% of the cerium-144 has been removed in this fraction. Unfortunately the Pm^{147} has not been carefully examined, but we can set an upper limit of no more than a few per cent of this nuclide.

Satisfactory division of fine-particle samples into detritus, phyto- and zooplankton fractions has not yet been achieved in radiochemically useful amounts. This problem looms large on our horizon.

Conclusions

In addition to demonstrating that in the sea considerable discrimination takes place between cerium and promethium tracers, we have presented data consistent with the idea that these elements are removed from surface seawater by becoming associated with sinking particles. It appears likely that most promethium is removed on particles sinking faster than 100 m/month, whereas most cerium is removed on particles sinking at about 100 m/month or a little slower. It has been reported that there are indications of another, still significant, particle population sinking at no more than 50 m/month. Should nuclear weapons testing be resumed at any future date, these studies provide a basis for the use of other, shorter-lived lanthanides to examine particle sinking rates in much greater detail.

ACKNOWLEDGEMENTS

These studies form contribution No. 1136 from the Woods Hole Oceanographic Institution, and have been supported by the United States Atomic Energy Commission under contracts AT (30-1)-1930, AT (30-1)-1918, AT (30-1)-2174 and AT (30-1)-2078; by the United States Office of Naval Research under contracts NONR-2196 and NONR-1238; by the National Science Foundation; and by the United States Program for the International Geophysical Year under grant NSF Y/9.12/143.

It is a real pleasure to express our best thanks to the many collaborators on whose efforts this study has depended.

REFERENCES

[1] BOWEN, V. T. and SUGIHARA, T. T., "Strontium-90 in North Atlantic Surface Water", *Proc. Natl. Acad. Sci.* **43** (1957) 576—580.
[2] BOWEN, V. T. and SUGIHARA, T. T., "Marine geochemical studies with fallout radioisotopes", Proc. 2nd UN Int. Conf. PUAE, **18** (1958) 434.
[3] BOWEN, V. T. and SUGIHARA, T. T., "Strontium-90 in the 'mixed-layer' of the Atlantic Ocean", *Nature* **186** (1960) 71—72.
[4] SUGIHARA, T. T., JAMES, H. I., TROIANELLO, E. J. and BOWEN, V. T., "Radiochemical separation of fission products from large volumes of sea water", *Anal. Chem.* **31** (1959) 44—49.
[5] DUNHAM, C. L., *Fallout from Nuclear Weapons Tests* **1** United States Govt. Printing Office (1959) 23.
[6] ALEXANDER, L. T., JORDAN, R. H., DEVER, R. F., HARDY, E. P., JR., HAMODA, G. H., MACHTA, L. and LIST, R. J., "Strontium-90 on the earth's surface", *Science*, to be published (1960).
[7] HARDY, E. P. JR. and KLEIN, S., "Fallout Program", Quarterly Summary Report, USAEC, bulletin HASL **84** and **88** (1960).
[8] SCHWEITZER, G. K., "The radiocolloidal properties of the rare-earth elements". ORINS—**12** (1956) 31—34.
[9] JERLOV, N. G., "The particulate matter of the sea as determined by means of the Tyndall meter". *Tellus* **7** (1955) 218—225.

Contribution No. 1137

GEOPHYSICAL INVESTIGATION OF CAPE COD BAY, MASSACHUSETTS, USING THE CONTINUOUS SEISMIC PROFILER

HARTLEY HOSKINS AND S. T. KNOTT

Reprinted for private circulation from
THE JOURNAL OF GEOLOGY
Vol. 69, No. 3, May 1961
Copyright 1961 by the University of Chicago
PRINTED IN U.S.A.

GEOPHYSICAL INVESTIGATION OF CAPE COD BAY, MASSACHUSETTS, USING THE CONTINUOUS SEISMIC PROFILER[1]

HARTLEY HOSKINS AND S. T. KNOTT
Woods Hole Oceanographic Institution, Woods Hole, Massachusetts

ABSTRACT

The Woods Hole Oceanographic Institution's continuous seismic profiler was used in Cape Cod Bay to make two hundred miles of reflection profiles and eight oblique reflection-refraction stations. From these the areal extent and velocities of the principal seismic layers were determined.

The deepest layer found (having a compressional wave velocity of 15,000–16,500 feet per second; 4.6–5.0 kilometers per second) is interpreted as Paleozoic in age. Its top surface forms an open-ended basin which deepens northeastward from the northeast entrance of Cape Cod Canal. Overlying it are patches of material (10,000–13,000 feet per second; 3.0–4.0 kmps) which are interpreted as erosional remnants of Cretaceous sediments. Of still younger age are three horizons with material having a compressional wave velocity in the 6,000–8,000 feet per second (1.8–2.4 kmps) range. The deepest seems likely to be marine Tertiary. The intermediate one is believed to be glacial till, and the shallowest a thin covering of postglacial sediments.

INSTRUMENTATION

The continuous seismic profiler (Knott and Hersey, 1956; Hersey, 1956; Luskin *et al.*, 1958; Beckman *et al.*, 1959; Officer, 1959; Stetson, 1960; and unpublished reports by Hersey [in press], and Fink, 1958) can be used on a moving ship to collect information about buried geological structures. It consists of (figs. 1, 2, and 3):

a) A repetitive broad-band sound source which emits complex pulses of short duration at rates up to 2 per second. The pulse is generated by discharging a capacitor bank through an electrode towed in the water (underwater spark or "Sparker," Woods Hole Oceanographic Institution) or through a coil mounted against a spring-loaded plate ("Thumper," Edgerton, Germeshausen & Grier, Inc.). The energy produced in compressional waves is equivalent to that of about 0.1 gram of TNT and has its greatest spectrum component in the range 200–600 cycles per second.

b) A precision graphic recorder (Knott and Hersey, 1956; Knott and Witzell, 1960), which gives a plot of the travel times of acoustic pulses that originate at the surface, penetrate to the reflecting bottom and subbottom surfaces and return to a receiver towed from the observing vessel. These arrivals are recorded as a darkening proportional to the signal amplitude on a rectilinear sweep across a continually advancing strip of electrosensitized paper. The outgoing pulses appear along a line at a fixed distance from the edge of the paper. The paper advances slowly; consecutive pulses and echoes are recorded side by side. Consequently, a reflecting horizon appears as a coherent sequence of traces along the strip. This method of display is remarkably helpful in detecting a steady succession of low-energy returns against background noise.

c) A broad-band hydrophone with a sensitivity of approximately 80 decibels below a reference of 1 volt for a sound field of one microbar, a broad-band amplifier (Dow, 1952), and variable band-pass filters.

The ability of the profiler to resolve two reflecting horizons that differ slightly in depth is determined partly by the length (approximately 2 milliseconds) and shape of the complex pulse and more importantly by the towing depth of the source and of the receiving hydrophone. Because the sea surface acts as a sound mirror, the down-going and returning pulses are made complicated by the addition of surface-reflected waves that are phase-inverted and displaced in time. A *single* reflecting interface thus appears as a group of parallel traces; these should not be regarded as representing *many* reflecting interfaces. It follows that the resolution between two reflecting horizons depends mainly on the depths of the source and of the receiver; in this survey it

---

[1] Contribution No. 1137 of the Woods Hole Oceanographic Institution. Manuscript received October 10, 1960.

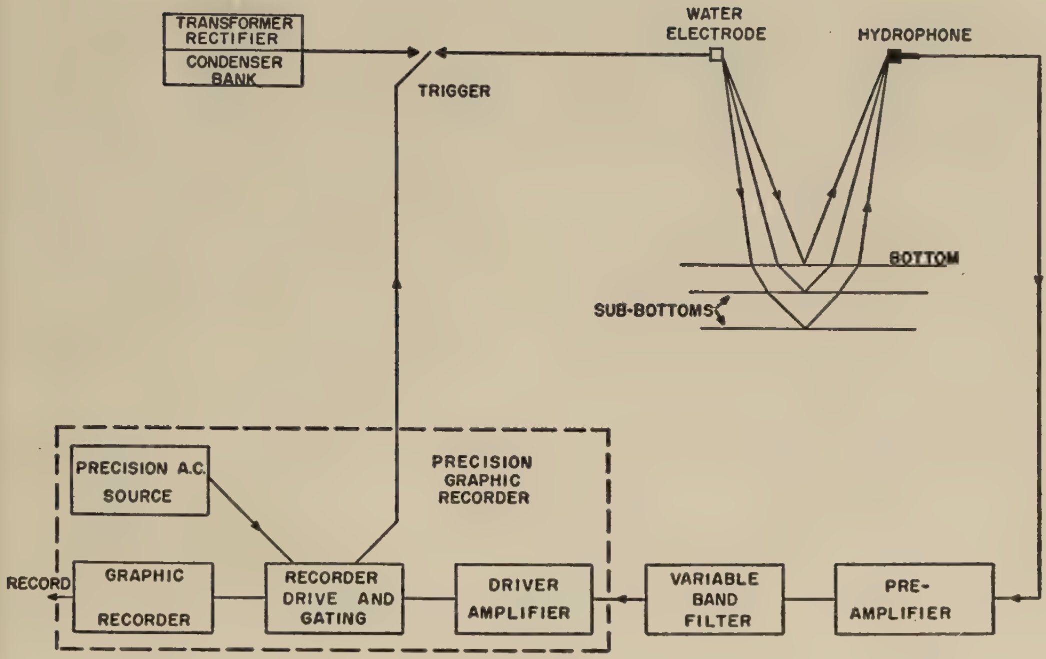
TRANSFORMER RECTIFIER
CONDENSER BANK
TRIGGER
WATER ELECTRODE
HYDROPHONE
BOTTOM
SUB-BOTTOMS
PRECISION A.C. SOURCE
PRECISION GRAPHIC RECORDER
RECORD
GRAPHIC RECORDER
RECORDER DRIVE AND GATING
DRIVER AMPLIFIER
VARIABLE BAND FILTER
PRE-AMPLIFIER

FIG. 1.—Block diagram of the continuous seismic profiler

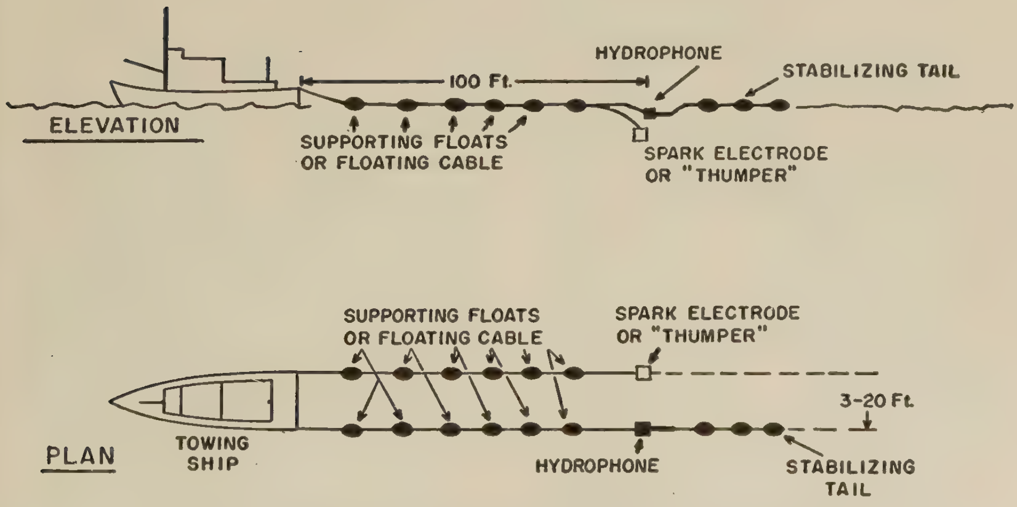
HYDROPHONE
STABILIZING TAIL
100 Ft.
ELEVATION
SUPPORTING FLOATS OR FLOATING CABLE
SPARK ELECTRODE OR "THUMPER"
SUPPORTING FLOATS OR FLOATING CABLE
SPARK ELECTRODE OR "THUMPER"
3-20 Ft.
PLAN
TOWING SHIP
HYDROPHONE
STABILIZING TAIL

FIG. 2.—Typical towing arrangement for continuous reflection profiling

was generally about 15 feet. The choice of source and receiver depths calls for a compromise between the requirements of radiating and receiving effectiveness and of resolution.

FIELD TECHNIQUES

The field techniques and methods of record analysis have been discussed by Hoskins (1960), and specifications of equipment by Knott and Witzell (1960); these reports are available upon request to the Institution. Navigation by radar and by visual three-arm protractor fixes on shore points was accurate to within a quarter of a mile. The reflection profiles and oblique reflection-refraction stations are plotted in figure 4. Agreement between records was obtained on repeated tracks and at points where tracks crossed one another.

In the interpretation of these records special consideration must be given to the fact that the source and receiver, unless arrays are used, are non-directional and that reflections may be received from any direction. As a consequence, it is possible for a reflector not directly below the observing equipment to return an echo that arrives either earlier or later than those from surfaces which are directly below. In some cases these ambiguities may be resolved by the study of the influence of low (100–600 cps) and high (> 1,000 cps) frequency bandpass filters: characteristically, the higher frequencies are preferentially attenuated in their passage through sediments.

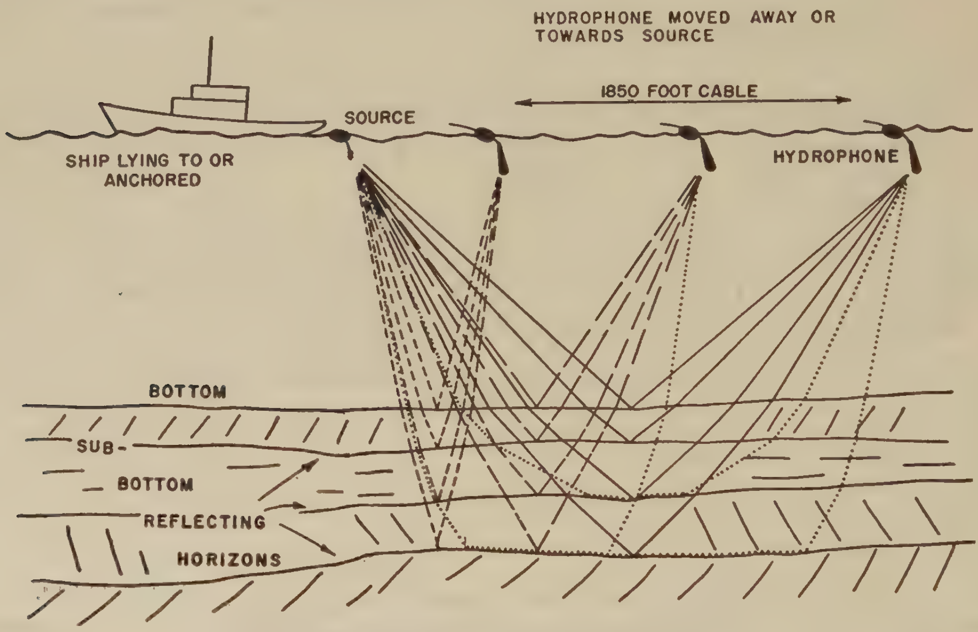

FIG. 3.—Oblique reflection-refraction station technique

Figure 3 illustrates the technique used for oblique reflection-refraction stations. Owing to difficulties in relocating the initial source and receiver positions, none of these stations were reversed. A reflection profile along the station will indicate the necessary slope correction. About two hundred miles of profile were taken in fifty hours. Areas near shore, especially on the southeast side of Cape Cod Bay, were not explored because of ship-handling problems.

SUMMARY OF DATA

The term "horizon" is here employed to mean the interface or zone of contact between two masses of material of differing elastic impedance.

The deepest horizon is underlain by material having a compressional wave velocity of 15,000–16,500 feet per second, measured at four stations. This horizon can be followed continuously on most of the records. Figure 5 gives a generalized contour map of the computed depth of this horizon below sea level and shows adjoining outcrops of Paleozoic rocks. This map is based on continuous seismic profiler data and other published information (Emerson, 1917; Woodworth and Wigglesworth, 1934). Relief of a hundred feet or more is found on an open-ended basin which deepens northeastward from the northeast entrance of Cape Cod Canal at an average slope of thirty feet per mile.

A crude isopachous map of the overlying layer which has a compressional wave velocity of 10,000–13,000 feet per second is presented in figure 6*a*. Figure 6*b* shows a comparison of the areal distribution of this material with sea-floor topography. The thickness of this material exceeds 450 feet at Fishing Ledge. A minimum thickness of 400 feet, possibly of this same material, is found under the southern tip of Stellwagen Bank. Because this material is patchy, considerably more profiling would be required to determine its distribution adequately. Few reflecting horizons were detected within this material. An angular unconformity between this material and the overlying lower velocity material is shown in figure 11.

The shallowest group of layers, having velocities in the range 6,000–8,000 feet per second, can be divided into three members on the basis of the appearance of the records. The distribution of the deepest member of the group is indicated in figure 7. On the recording it appears as a layered sequence,

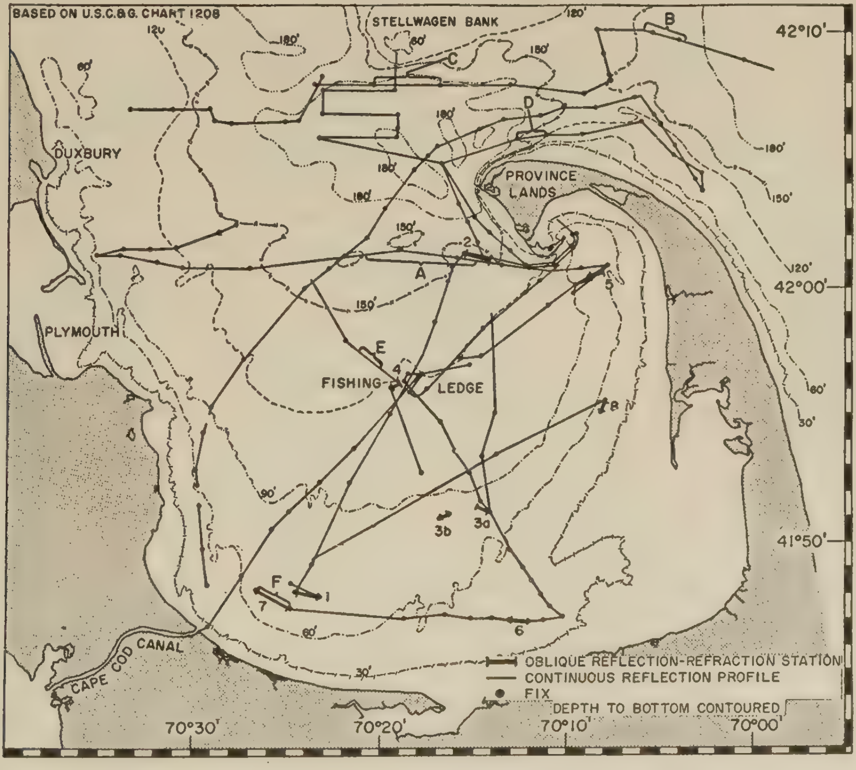
BASED ON U.S.C.&G. CHART 1208
STELLWAGEN BANK
B
C
D
A
E
F
42°10'
42°00'
41°50'
DUXBURY
PROVINCE LANDS
PLYMOUTH
FISHING LEDGE
CAPE COD CANAL
1
2
3
3a
3b
4
5
6
7
8
120'
180'
150'
90'
60'
30'
OBLIQUE REFLECTION-REFRACTION STATION
CONTINUOUS REFLECTION PROFILE
FIX
DEPTH TO BOTTOM CONTOURED
70°30'
70°20'
70°10'
70°00'

FIG. 4.—Track chart. The letters designate the location of sections of the record illustrated in the following figures: *A* = fig. 8; *B* = fig. 10; *C* = fig. 11; *D* = fig. 12; *E* = fig. 13; *F* = fig. 14.

some layers of which can be traced almost continuously within the restricted area shown in figure 7. The middle and top members can be found on most of the records taken in Cape Cod Bay. The middle member, recognized by its content of numerous objects of high acoustic reflectivity and indications of very local stratification (see fig. 8 for detail), increases in thickness from northwest to southeast, as shown in figure 9. Its thickness closely reflects the underlying topography. The top member is uniformly less than fifty feet in thickness and fills small depressions in the underlying layer.

North of the Provincelands there is a distinctive area (sketched in fig. 7) where the reflectivity of the bottom and a shallow subbottom horizon is so great that little penetration is achieved; instead, the pulses reverberate several times in the water column. A short distance to the east of this area, good penetration to what is believed to be Paleozoic rock at more than 900 feet below sea level was obtained on one profile.

Detailed features of the records are shown, with interpretation, in figures 10, 11, 12, 13, and 14. The vertical exaggeration varies inversely with the compressional wave velocity of the horizon.

Overlays of three profiles are given in

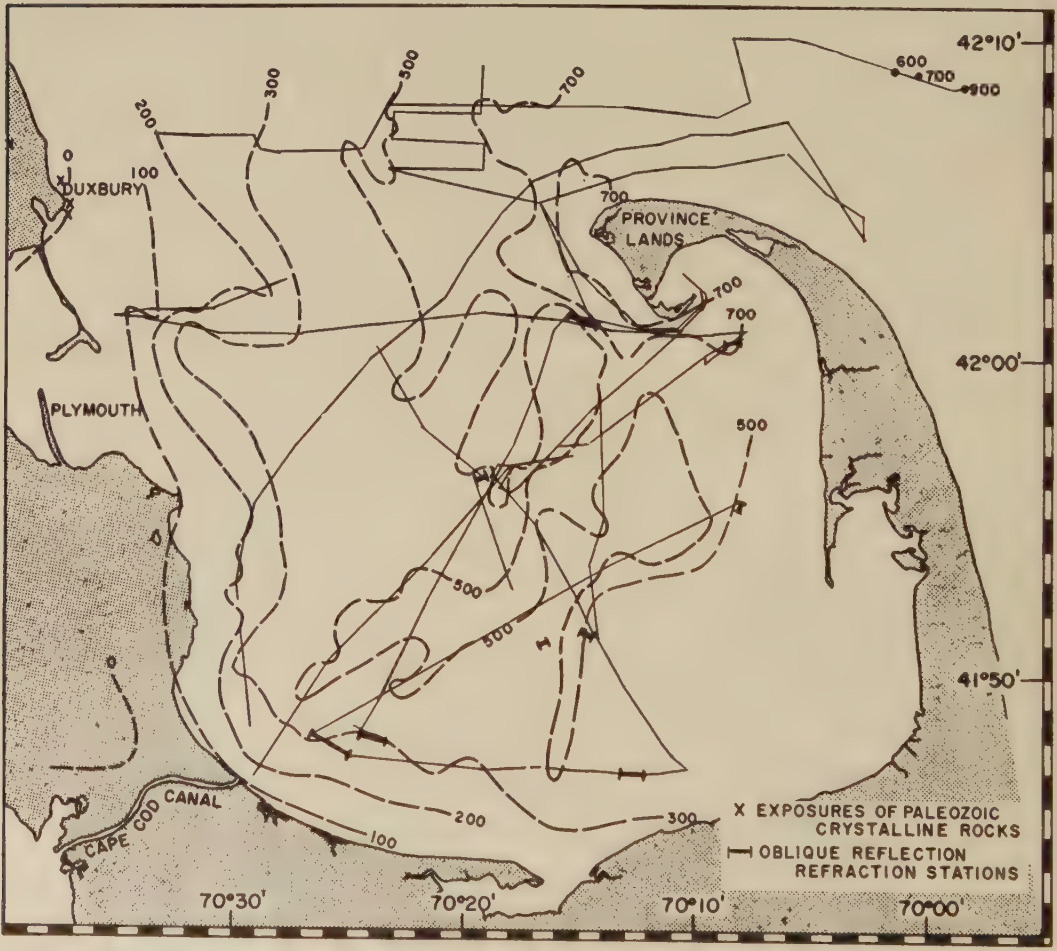
42°10'
600
700
900
300
500
700
200
0
100
DUXBURY
700
PROVINCE LANDS
700
700
42°00'
PLYMOUTH
500
500
500
41°50'
CANAL
CAPE COD
200
100
300
X EXPOSURES OF PALEOZOIC CRYSTALLINE ROCKS
OBLIQUE REFLECTION REFRACTION STATIONS
70°30'
70°20'
70°10'
70°00'

FIG. 5.—Contour chart of topography (in feet below sea level) of the horizon underlain by material with compressional wave velocity 15,000–20,000 feet per second (pre-Mesozoic rocks), showing land outcrops.

figure 15. The velocities as extrapolated from oblique reflection-refraction stations were used to compute depths to each reflecting interface. It should be noted that the recordings are made on a fixed-time base; therefore, the superimposed depth scale is *variable.*

The compressional wave velocities determined at the stations indicated in figure 3 are given in table 1.

DISCUSSION AND CONCLUSIONS

The deepest rock unit (velocity 15,000–16,500 feet per second) observed is considered to be an eastward submarine extension of the Paleozoic rocks (basement) which outcrops in Plymouth County and the Boston Basin (fig. 5). This conclusion is based on (1) the measured compressional wave velocity and its coincidence with velocities of crystalline and metamorphic rocks of the Boston Basin (Birch, 1960); (2) extrapolation to land outcrops in Plymouth County; (3) topographic relief comparable to adjacent land surfaces. Pre-Mesozoic sedimentary, metamorphic, and igneous rocks are located in the area west and northwest of Cape Cod Bay (Emerson, 1917; Billings,

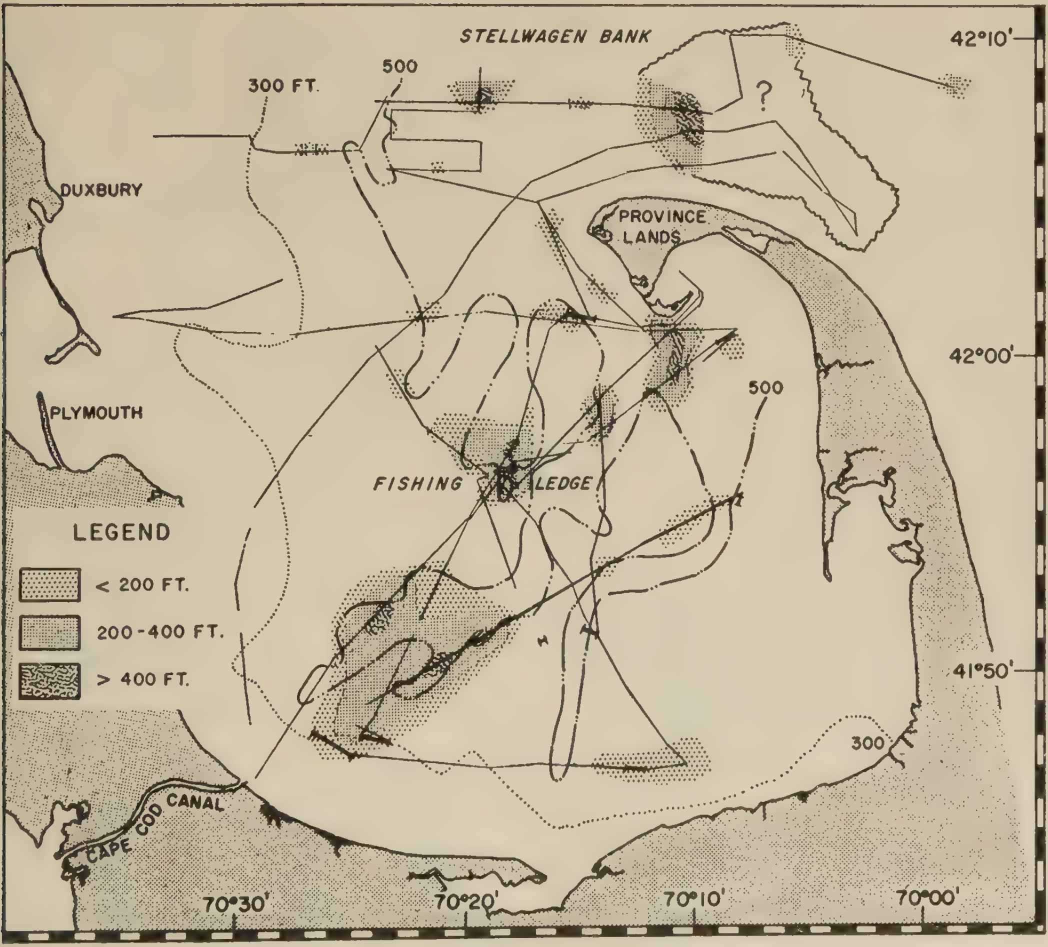
STELLWAGEN BANK
42°10'
300 FT.
500
?
DUXBURY
PROVINCE LANDS
42°00'
PLYMOUTH
500
FISHING LEDGE
LEGEND
< 200 FT.
200-400 FT.
> 400 FT.
41°50'
300
CAPE COD CANAL
70°30'
70°20'
70°10'
70°00'

FIG. 6*a*.—Areal distribution of material with compressional wave velocity 10,000–13,000 feet per second (possibly Cretaceous sediments). Thickness indicated by stippled patterns. Depth to basement below sea level contoured.

1929; LaForge, 1932). Seismic measurements some thirty miles to the southwest, in the Rhode Island formation (Curtis R. Tuttle, oral communication), a well-consolidated Carboniferous sedimentary sequence, give 14,000 feet per second as a representative velocity. The data on which figure 5 is based are consistent with the supposition that the ancient Cape Cod Basin drained to the northeast.

The layer of intermediate velocity is patchy in its distribution. A compressional wave velocity of 10,000–12,500 feet per second is representative of "semi-consolidated sediments" (Ewing *et al.*, 1939). Local occurrence of a horizon with a velocity 10,000–13,000 feet per second has been detected on Cape Cod (Linehan, oral communication). The correlation indicated between bottom topography and areal distribution of this material in figure 6*b* may be explained in part by assuming that the older, higher-velocity material is more compact than the overlying material. Because of differential compaction of the older and younger sediment, the present sea-floor topography indicates the location of older buried relief. Examples of this phenomenon are cited in

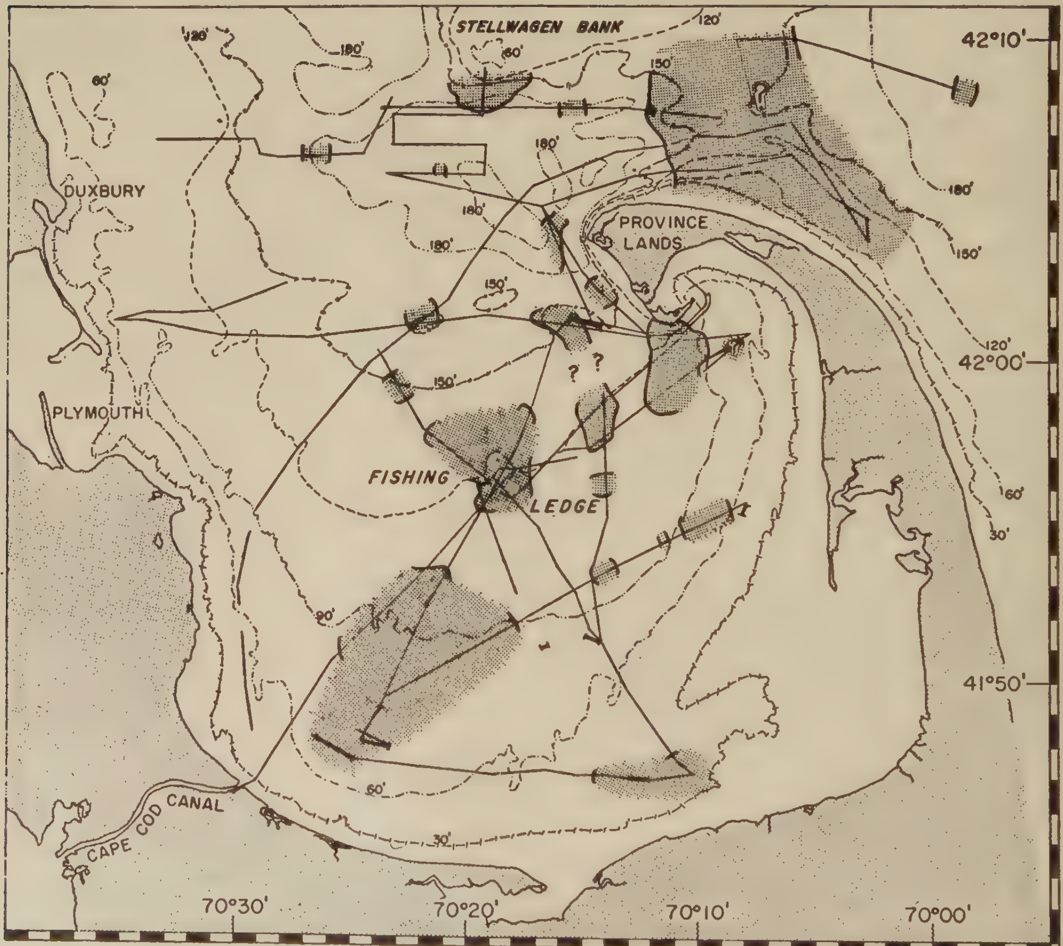

FIG. 6*b*.—Areal distribution of material with compressional wave velocity 10,000–13,000 feet per second and sea-floor topography.

TABLE 1

Summary of Apparent Compressional Wave Velocities*

Station No.	Bottom (Ft/sec)	Depth (Ft.)	Subbottom Horizons (Ft/sec)	Depth (Ft.)	Basement (Ft/sec)	Depth (Ft.)
1..........	5,800	72	......	...	16,300	300
2..........	6,500	138	8,000	333	......	...
3a and b....	6,000	78	......	...	......	...
4..........	5,800	78	9,100	188	16,300	540
			12,900	492	......	...
5..........	5,800	78	7,800	344	......	...
			8,900	375	......	...
			11,000	475	......	...
6..........	5,200	60	8,700	124	16,300	466
			12,900	385	......	...
7..........	7,200	78	12,200	96	14,900	300
8..........	4,850	50	6,000	75	......	...

* Velocity determinations: ± 300 ft/sec; depth determination: ± 15 feet.

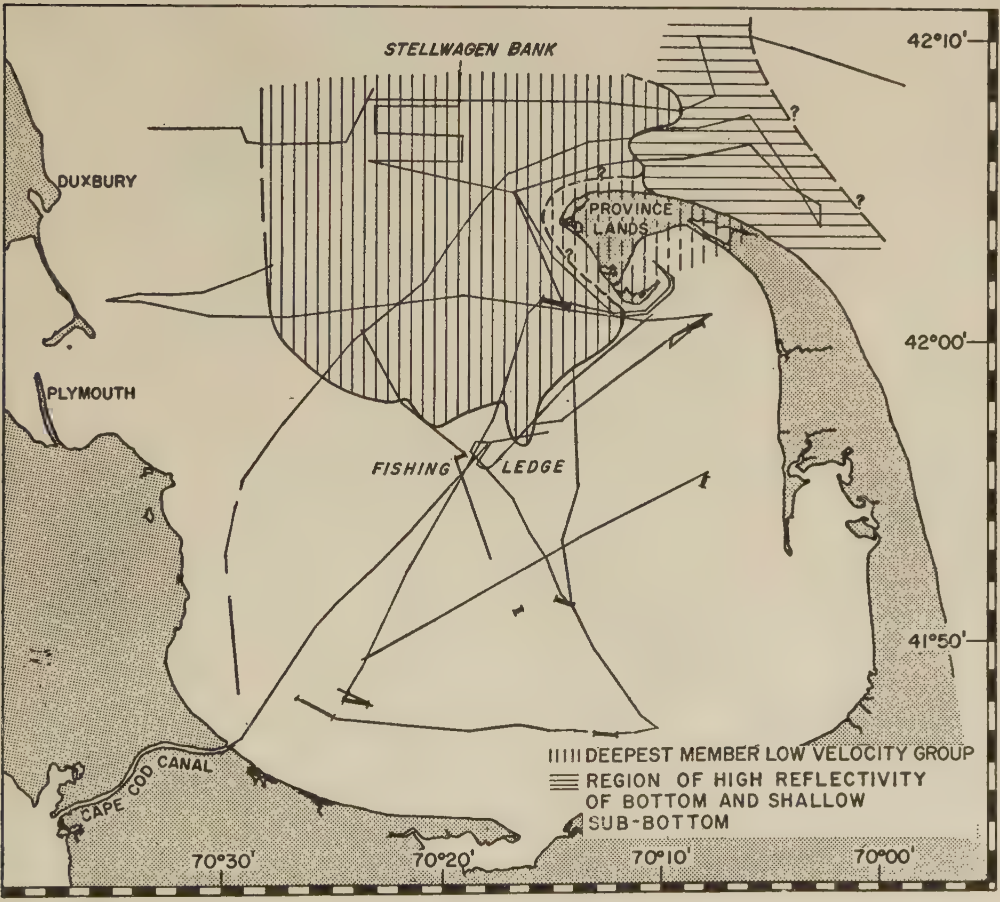
STELLWAGEN BANK
42°10'
DUXBURY
PROVINCE LANDS
?
42°00'
PLYMOUTH
FISHING LEDGE
41°50'
CAPE COD CANAL
IIIII DEEPEST MEMBER LOW VELOCITY GROUP
≡ REGION OF HIGH REFLECTIVITY OF BOTTOM AND SHALLOW SUB-BOTTOM
70°30'
70°20'
70°10'
70°00'

FIG. 7.—Areal distribution of deepest layer of low-velocity group (6,000–8,000 feet per second Tertiary sediments) and region of high reflectivity of bottom and shallow subbottom.

Moore (1920), Lalicker (1949), and Krumbein and Sloss (1955). No Triassic or Jurassic sediments are known nearer than the Connecticut Valley (Fenneman, 1938). Woodworth and Wigglesworth (1934) report terrestrial Cretaceous sediments about thirty-five miles to the south at Gay Head on Martha's Vineyard and on Nonamesset in the Elizabeth Islands, Massachusetts. Seismic measurements near Nonamesset (Hoskins, 1960) indicate that sediments of possible Cretaceous age have acoustic velocities of 9.100 feet per second. Cretaceous sediments have been found in submarine canyons on the south side of Georges Bank 125 miles to the east (Cushman, 1936). Taken together, these observations lead to the inference that the patches of intermediate velocity material overlying the Paleozoic rocks are Cretaceous sediments.

The distinctive area of limited penetration north of the Provincelands (fig. 7) is a topographic saddle; possibly it represents a broad channel cutting the material which forms the subsurface of the Outer Cape and Stellwagen Bank. It is reasonable that this is an area of exposed or thinly covered Cretaceous sediments, but there are no velocity data to support this view. Long cores were attempted in this area and on Stellwagen

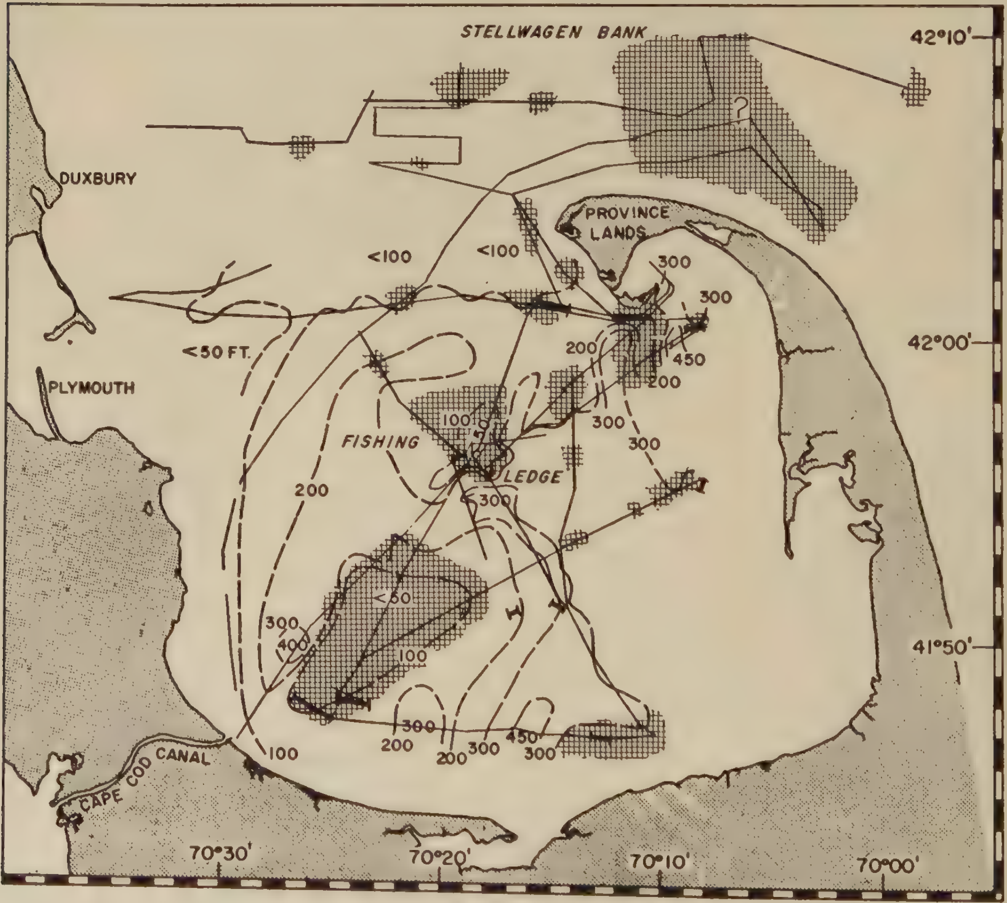
STELLWAGEN BANK
42°10'
?
DUXBURY
PROVINCE LANDS
<100
<100
300
300
<50 FT.
200
450
200
42°00'
PLYMOUTH
100
300
300
FISHING
LEDGE
200
300
<50
300
400
100
41°50'
CANAL
CAPE COD
100
200
300
200
300
450
300
70°30'
70°20'
70°10'
70°00'

FIG. 9.—Isopachous map of middle layer of group with average velocity 6,000–8,000 feet per second (Pleistocene glacial material). Hatching indicates areal distribution of underlying material with compressional wave velocity 10,000–13,000 feet per second.

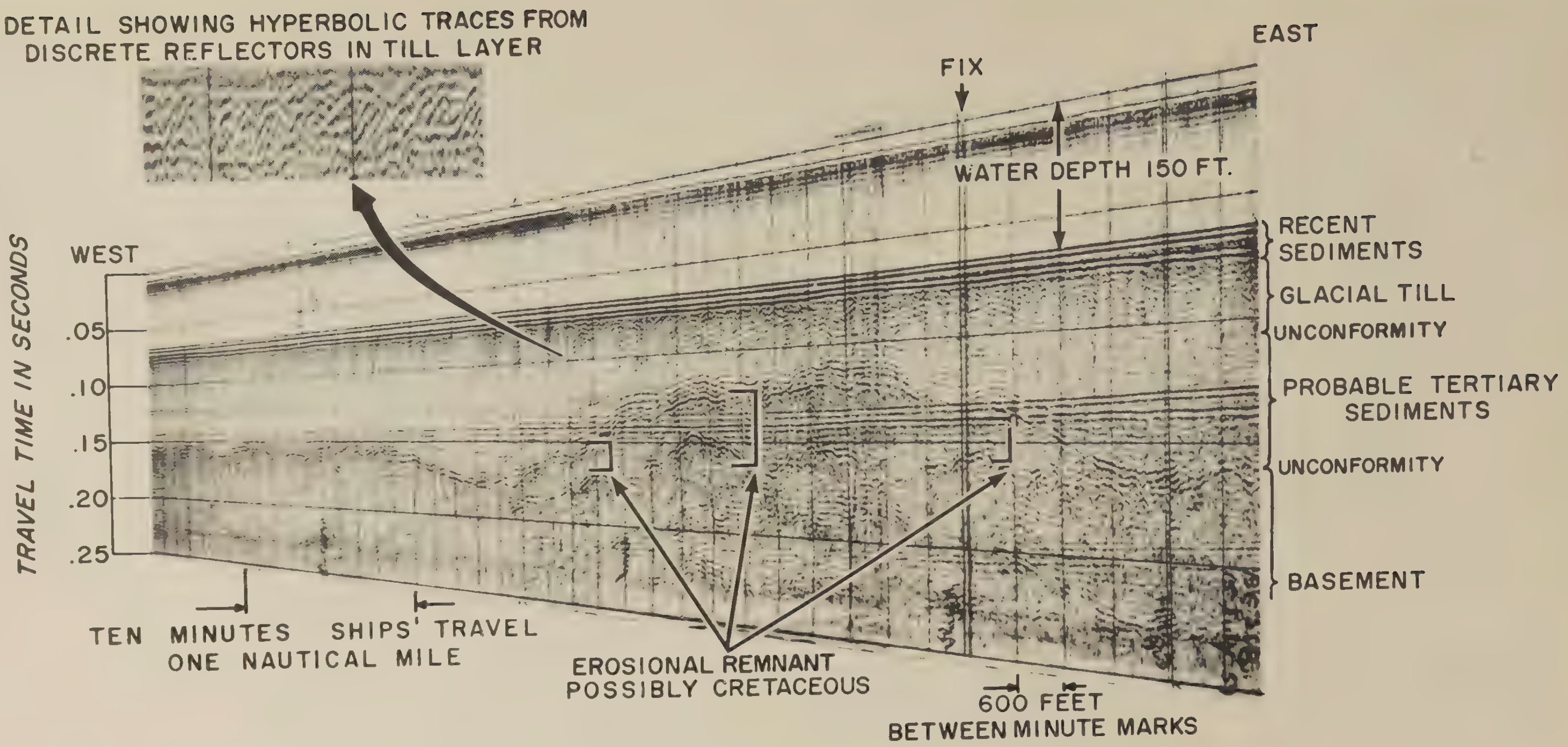

Fig. 8.—Oblique photograph of record showing stratigraphic sequence. Note that a single reflecting horizon appears on the record as a group of parallel traces. Vertical time exaggeration, ≈ 2,200; vertical distance exaggeration, 3–9.5.

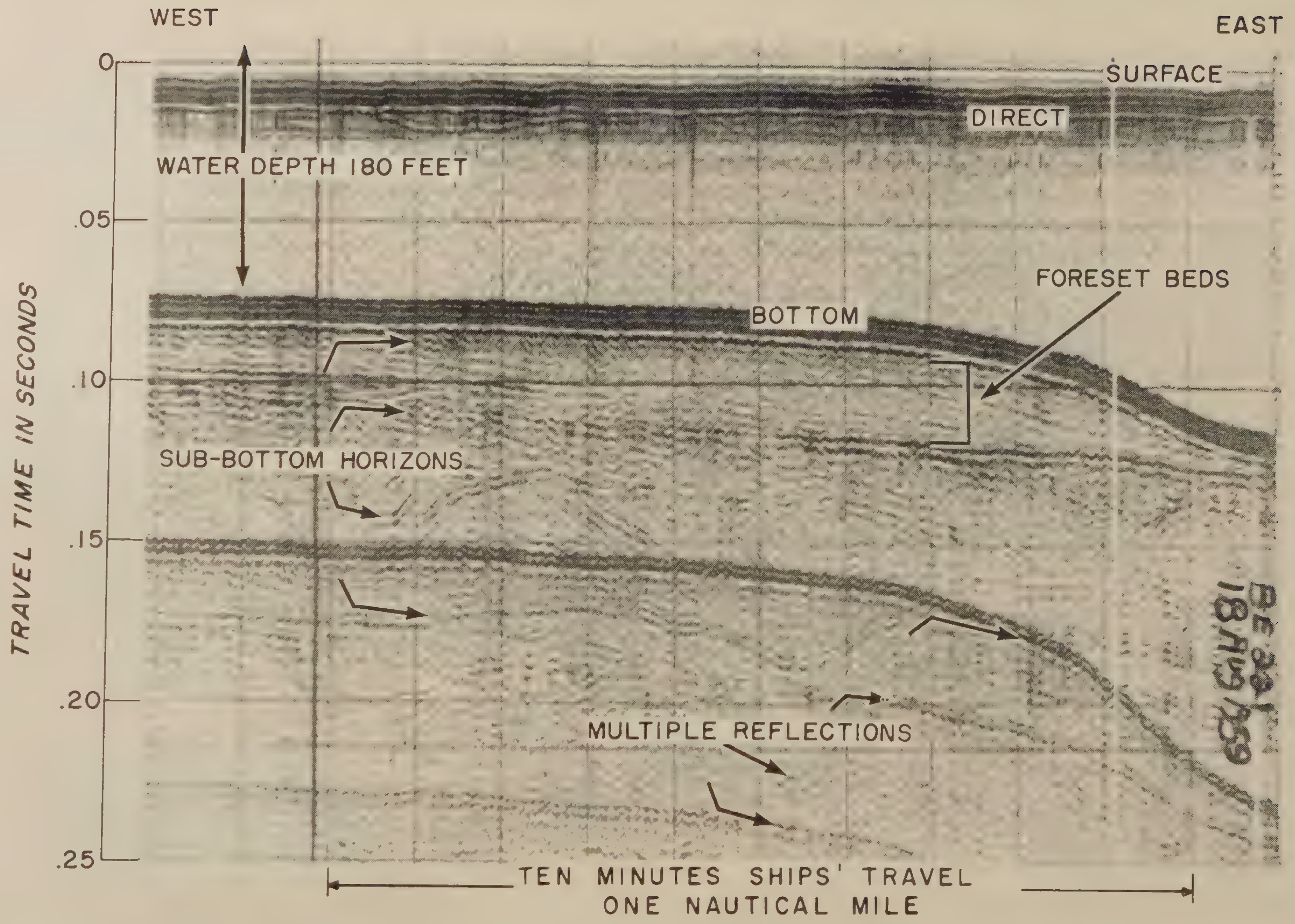

Fig. 10.—Record showing possible deltaic structure. Vertical time exaggeration, ≈ 2,200; vertical distance exaggeration 3–9.5

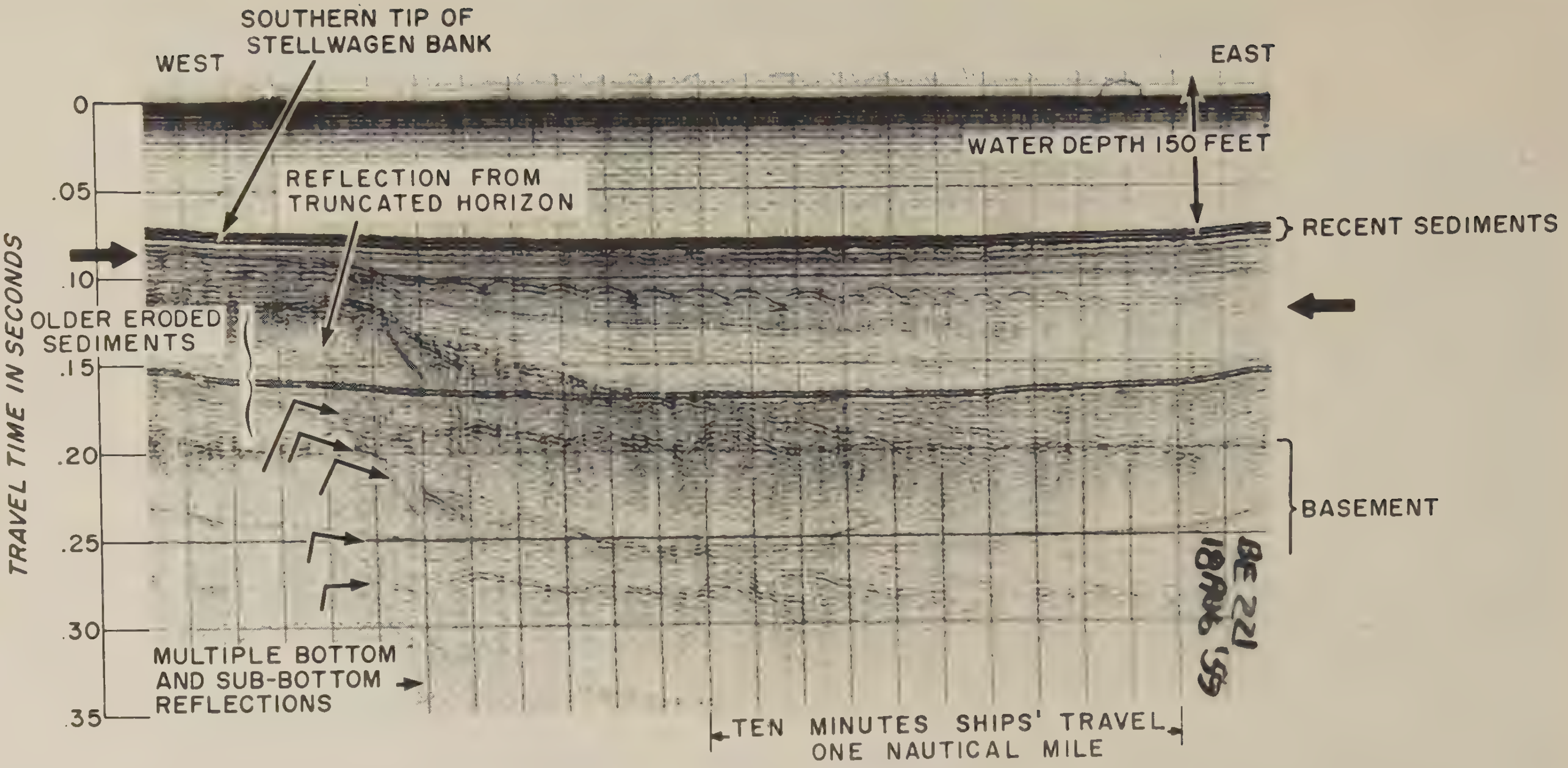

FIG. 11.—Record showing periodic thickening and thinning of sediment layer (*large arrows*). Vertical time exaggeration, ≈ 2,200: vertical distance exaggeration, 3–9.5

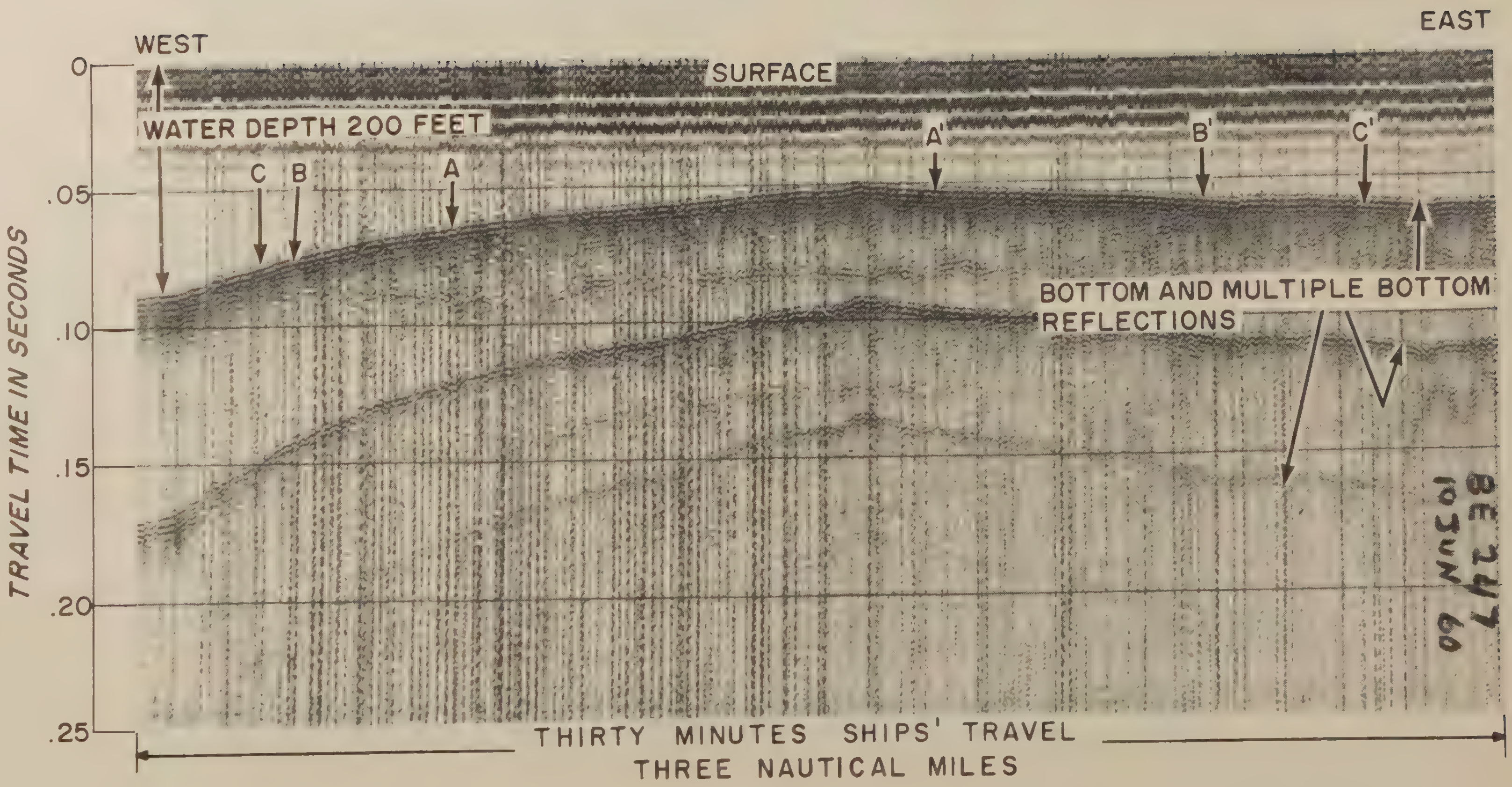

FIG. 12.—Record showing erosional truncation of three layers, *AA'*, *BB'*, and *CC'*. Vertical time exaggeration, ≈ 2,200; vertical distance exaggeration, 3–9.5

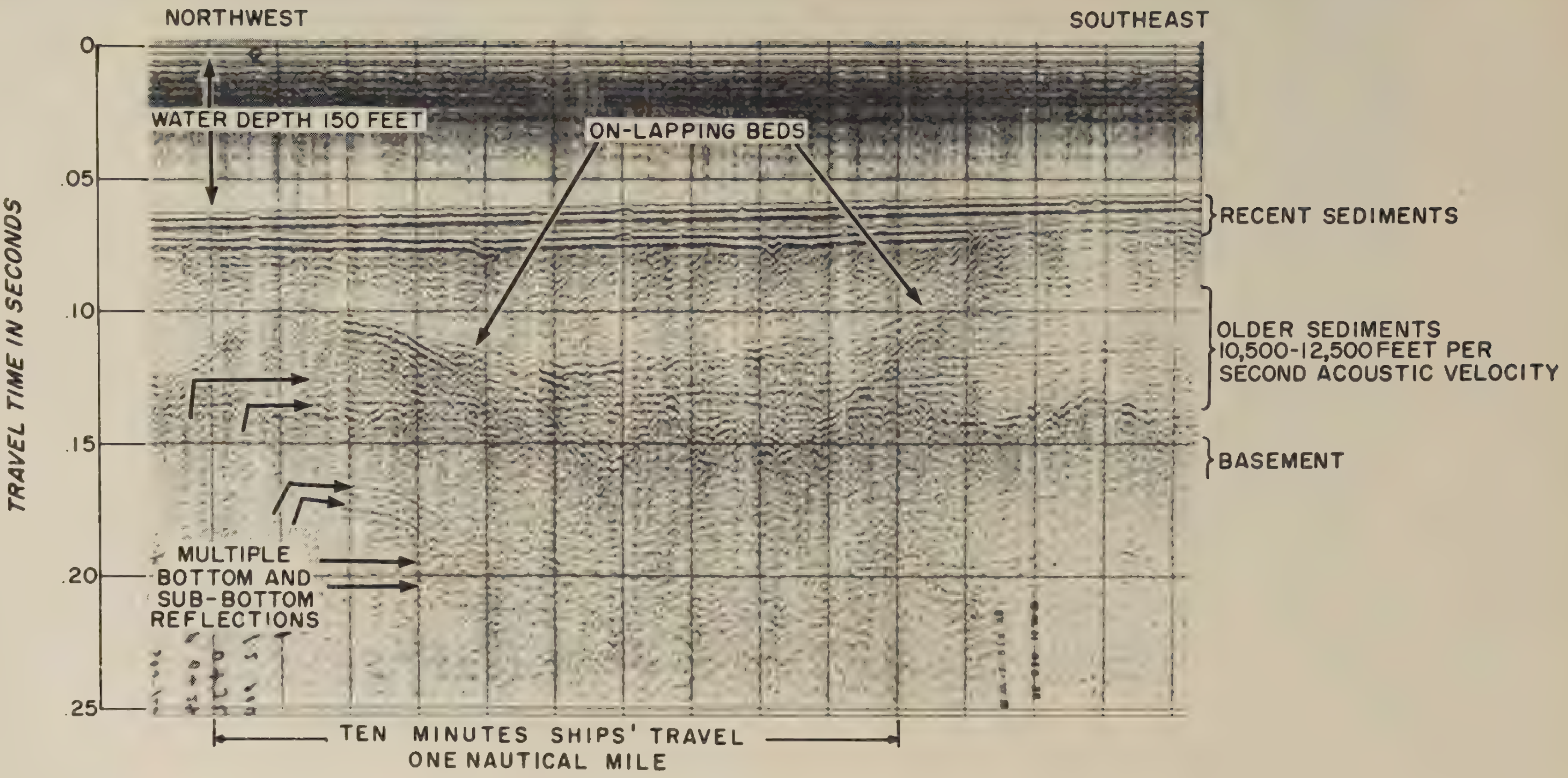

FIG. 13.—Record showing buried depression filled with sediment. Vertical time exaggeration, ≈ 2,200; vertical distance exaggeration, 3–9.5

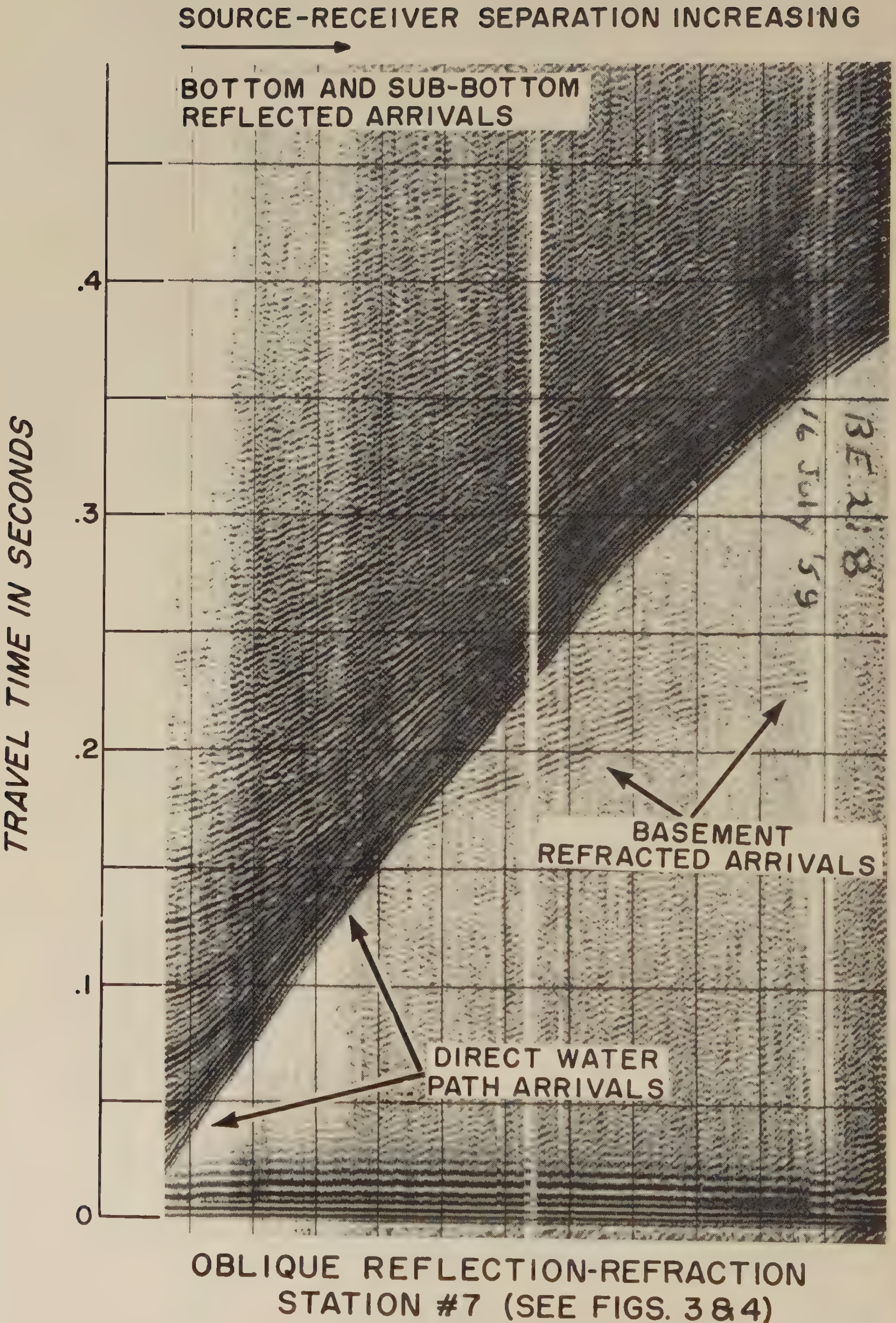

Fig. 14.—Oblique reflection-refraction station No. 7 showing strong basement-refraction arrival (see figs. 3 and 4).

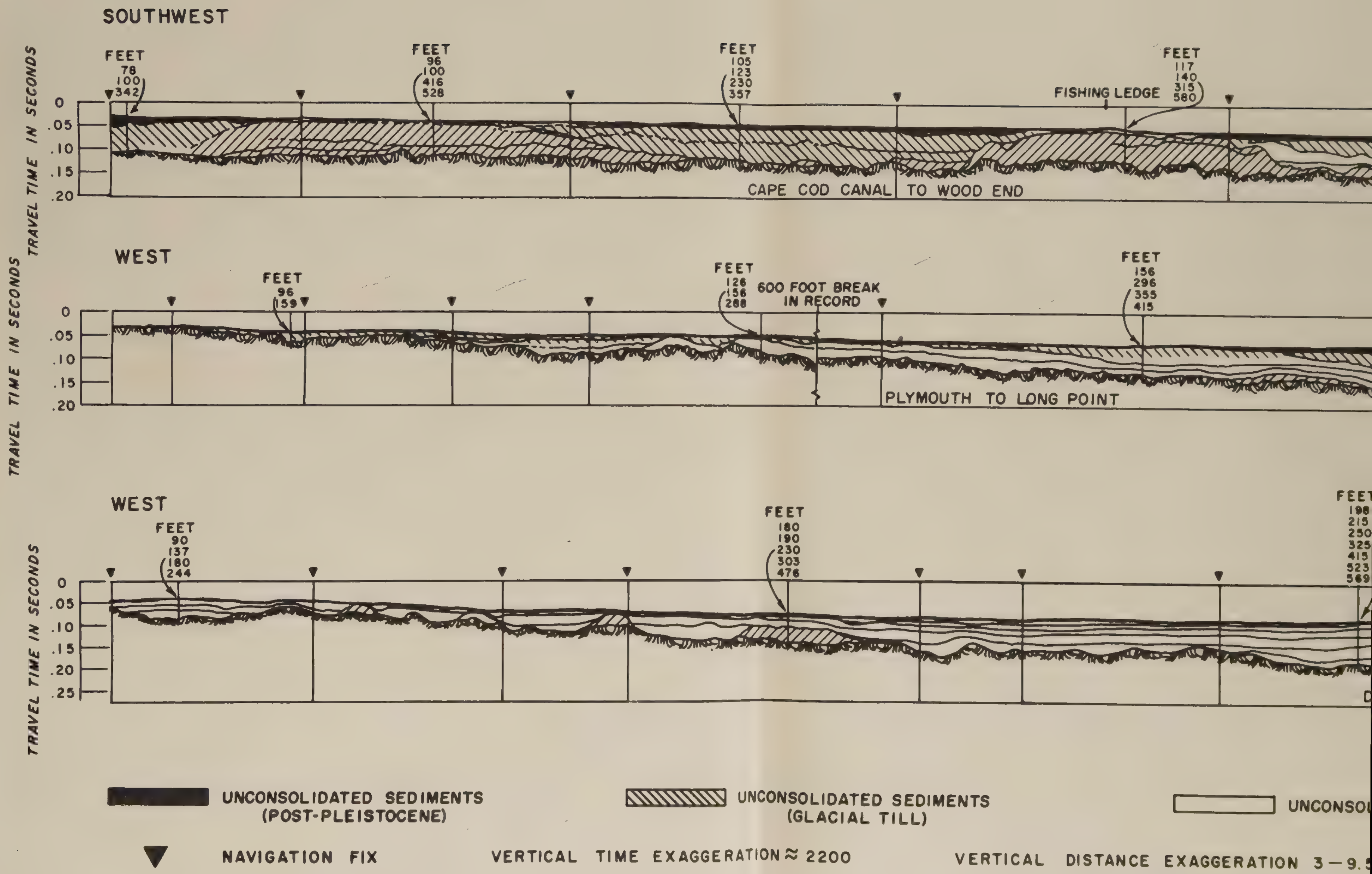

FIG. 15.—Continuous seismic reflection profiles (travel time vers

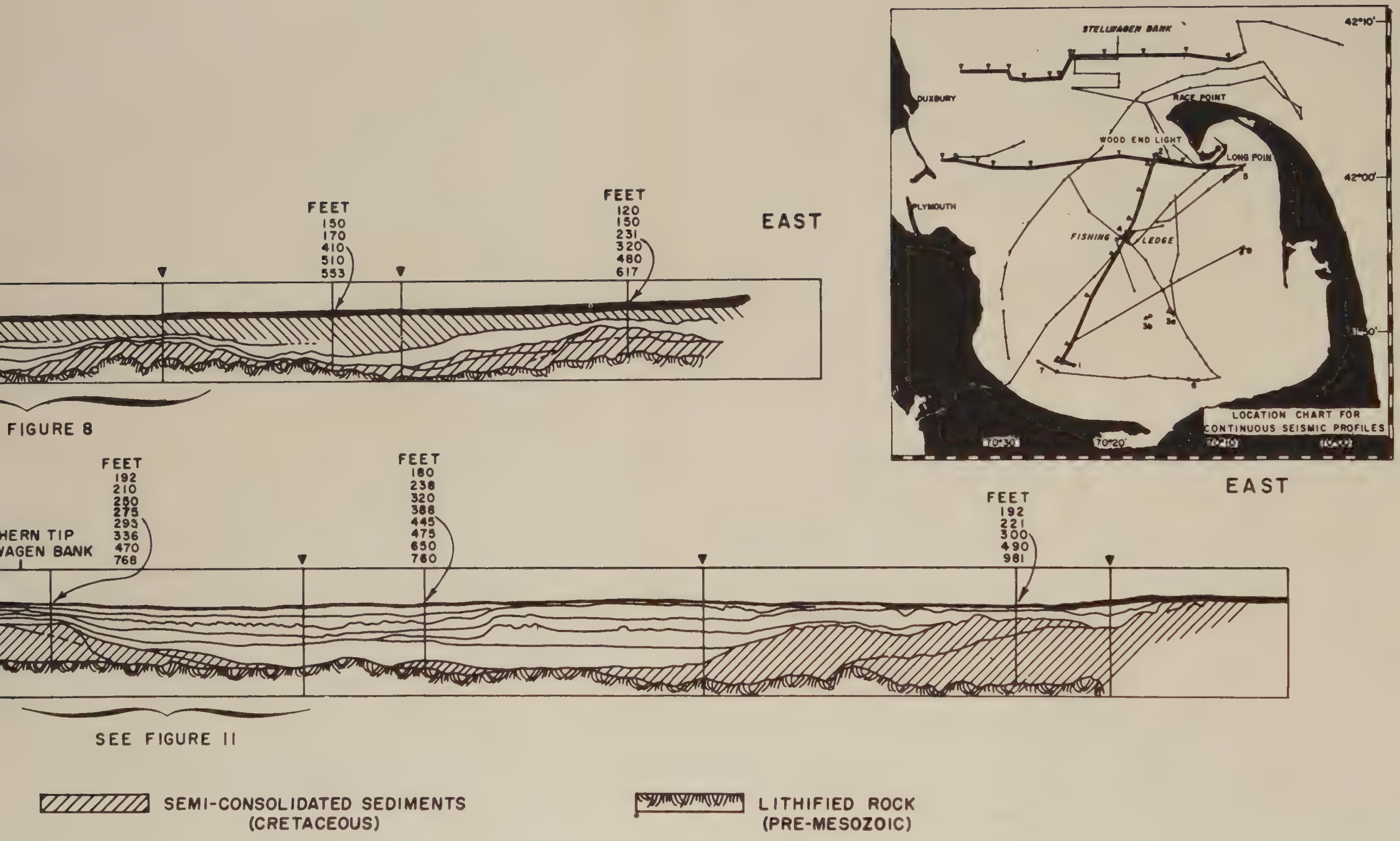

STELLWAGEN BANK
DUXBURY
RACE POINT
WOOD END LIGHT
LONG POIN
PLYMOUTH
FISHING
LEDGE
42°10'
42°00'
41°50'
70°30'
70°20'
70°10'
70°00'
LOCATION CHART FOR CONTINUOUS SEISMIC PROFILES
FEET 150 170 410 510 553
FEET 120 150 231 320 480 617
EAST
FIGURE 8
FEET 192 210 280 275 293 336 470 768
HERN TIP
WAGEN BANK
FEET 180 238 320 388 445 475 650 760
FEET 192 221 300 490 981
EAST
SEE FIGURE 11
SEMI-CONSOLIDATED SEDIMENTS (CRETACEOUS)
LITHIFIED ROCK (PRE-MESOZOIC)

. Computed depths in feet indicated at selected points

Bank, but they were not able to penetrate the sandy bottom.

A velocity of 6,000–8,000 feet per second is representative of unconsolidated sediments (Ewing *et al.*, 1939). Unique age assignment of the deepest subdivision cannot be based on present observations alone. It seems, however, that they are probably of early Tertiary age, since Eocene marine sediments have been found in wells in the Provincelands (Zeigler *et al.*, 1960), and Miocene sediments have been reported in Duxbury, Martha's Vineyard, and the Elizabeth Islands (Woodworth and Wigglesworth, 1934). Well logs on file at the Boston office of the Ground Water Division of the United States Geological Survey contain several notations suggesting the presence of marine facies lying below till in the area of Cape Cod and along the mainland shore to the west of the Bay. Since the extensive individual layers of this subdivision appear continuous across thickenings of the Cretaceous sediments (see fig. 8), it is probable that these younger sediments were not derived from erosion of the Cretaceous in the immediate area and are probably marine in origin. There are indications of shallow disturbances of these sediments, possibly due to the advance of the Pleistocene ice sheet. That the middle subdivision is glacial till or morainal deposit carrying occasional large boulders is inferred from the presence of numerous discrete, intense reflectors. It should be noted that, whereas the layered marine sediments pinch out to the south, the thickness of the glacial deposits increases in that direction. No faults or folds with vertical displacement greater than the resolution of the technique were detected in the low-velocity sediments in this area.

The uppermost low-velocity subdivision is generally thin. It may represent the reworking of the glacial deposit by the transgressing post-Pleistocene sea and Recent sedimentation.

INFERRED GEOLOGICAL HISTORY OF CAPE COD BAY

The Paleozoic rocks were eroded to form an open-ended basin. Cretaceous sediments were deposited on this erosional surface and later were largely removed except for local patches. The sea transgressed during the early Tertiary, and the first group of unconsolidated, layered sediments was laid down. Glaciation followed and was extensive over the area. The post-Pleistocene sea transgressed, reworked the glacial deposits in part, and formed the present bottom material.

Acknowledgments.—The investigation was supported by the Woods Hole Oceanographic Institution under U.S. Navy Bureau of Ships Contract NObsr 72521. Observations were made aboard the research vessel "Bear," of the Woods Hole Oceanographic Institution, during the summers of 1959 and 1960. The co-operation of Captains Eugene J. Mysona and Harry H. Seibert and their crew is gratefully acknowledged.

In addition to the authors, those participating in the cruises were Richard A. Allen, Anthony M. Hauck, III, Matts A. Myrhmann, Thomas R. Stetson, and Warren E. Witzell. The advice and assistance of the following are gratefully acknowledged: Elizabeth T. Bunce, Susan A. deRopp, Richard S. Edwards, Davis A. Fahlquist, John W. Graham, J. B. Hersey, Charles S. Innis, John W. Kanwisher, Andrew J. Nalwalk, and John M. Zeigler. The co-operation of the Rev. Daniel Linehan, S.J., of Weston Seismological Observatory, and Richard G. Petersen and Curtis R. Tuttle, of the United States Geological Survey is greatly appreciated.

REFERENCES CITED

Beckmann, Walter C., Roberts, Archie C., and Luskin, Bernard, 1959, Sub-bottom depth recorder: Geophysics, v. 24, p. 749–760.

Billings, Marland P., 1929, Structural geology of the eastern part of the Boston Basin: Am. Jour. Sci., 5th ser., v. 18, p. 97–137.

Birch, Francis, 1960, The velocity of compressional waves in rocks to 10 kilobars. Part I: Jour. Geophys. Research, v. 65, p. 1083–1112.

Cushman, Joseph A., 1936, Geology and paleontology of the Georges Bank Canyons. Part IV. Cretaceous and late Tertiary Foraminifera: Geol. Soc. America Bull., v. 47, p. 413–440.

Dow, Willard, 1952. An experimental portable listening device for detection, measurement and recording underwater sound: Woods Hole, Mass., Woods Hole Oceanographic Institution, ref. no. 52-10.

Emerson, B. K., 1917, Geology of Massachusetts and Rhode Island: U.S. Geol. Survey Bull. 597.

Ewing, Maurice, Woollard, George P., and Vine, A. C., 1939, Geophysical investigation in the emerged and submerged Atlantic Coastal Plain. Part III: Geol. Soc. America Bull., v. 50, p. 257–296.

Fenneman, Nevin M., 1938, Physiography of eastern United States: New York, McGraw-Hill Book Co., chap. i and vi.

Fink, Don R., 1958, Sub-bottom reflection survey, southern Narragansett Bay, Rhode Island (preliminary report): Woods Hole, Mass., Woods Hole Oceanographic Institution.

Hersey, J. B., Continuous seismic profiling, *in* The Sea: Ideas and observations: New York, Interscience Publishers (in press).

Hoskins, Hartley, 1960, Analysis of reflection and refraction records taken with the continuous seismic profiler: Woods Hole, Mass., Woods Hole Oceanographic Institution, ref. no. 60-37.

Knott, S. T., and Hersey, J. B., 1956, Interpretation of high-resolution echo-sound techniques and their use in bathymetry, marine geophysics and biology: Deep-Sea Research, v. 4, p. 36–44.

——— and Witzell, W. E., 1960, Instruction manual for precision graphic recorder (PGR): Woods Hole, Mass., Woods Hole Oceanographic Institution, ref. no. 60–38.

Krumbein, W. C., and Sloss, L. L., 1955, Stratigraphy and sedimentation: San Francisco, W. H. Freeman & Co., p. 345–347.

LaForge, Laurence, 1932, Geology of the Boston area, Massachusetts: U.S. Geol. Survey Bull. 839.

Lalicker, Cecil G., 1949, Principles of petroleum geology: New York, Appleton-Century-Croft, Inc., p. 120–123.

Linehan, Rev. Daniel, S.J., oral communications.

Luskin, Bernard, Roberts, Archie C., and Beckmann, Walter C., 1958, Sub-bottom depth recorder: Palisades, N.Y., Lamont Geological Observatory, Columbia University, Tech. Rept. 16, CU-44-58.

Moore, Raymond C., 1920, The relation of the buried granite in Kansas to oil production: Am. Assoc. Petroleum Geologists Bull., v. 4, p. 255–261.

Officer, Charles B., 1959, Continuous seismic profiler aids marine exploration: World Oil, April, 1959.

——— and Weber, J. H., 1959, Use of continuous seismic profiler in offshore exploration and engineering: Offshore, July, 1959.

Stetson, Thomas R., 1960, Seismic profiler recordings on the Blake plateau: Woods Hole, Mass., Woods Hole Oceanographic Institution, Tech. Memo. 3-60.

Tuttle, Curtis R., 1960, oral communications.

Woodworth, J. B., and Wigglesworth, E., 1934, Geography and geology of the region including Cape Cod, the Elizabeth Islands, Nantucket, Martha's Vineyard, No Mans Land and Block Island: Cambridge, Mass., Mus. Comp. Zoölogy, Harvard Coll., Mem. 52.

Zeigler, John M., Hoffmeister, W. S., Geise, Graham, and Tasha, Herman, 1960, A discovery of Eocene sediments in the sub-surface of Cape Cod, Massachusetts: Science, v. 132, p. 1397–1398.

Contribution No. 1138

rinted from
E PHYSICS OF FLUIDS VOLUME 4, NUMBER 1 JANUARY, 1961
Printed in U.S.A.

Surface Electroconvection

W. V. R. Malkus and G. Veronis
Woods Hole Oceanographic Institution, Woods Hole, Massachusetts

(Received August 15, 1960)

An electric field can produce steady cellular motions in the interface region of two immiscible semiconducting fluids. The theory of this instability is explored. The characteristic parameter is found to depend upon the difference in conductivity of the fluids and the curvature of the interface. Quantitative finite amplitude experiments established that the electric current produced by the cellular motions is proportional to the characteristic parameter minus the critical value of this parameter.

I. INTRODUCTION

LECTROCONVECTION is the name given to those macroscopic motions produced in a fluid externally imposed electric fields. Vettin[1] appears be the first one to experiment with electrocon- tion. He introduced tobacco smoke between allel electrodes and described the various types transient motions produced. The first report of ady electroconvection was made by Avsec and ntz.[2-4] Using fields strengths up to 10^7 v/m, y generated and photographed steady cellular terns of motion in light oils.

The fluids in which electroconvection has been served have very small electrical conductivity. erefore, it seemed plausible to us that neither ating effects nor magnetic effects could be respon- le for the motions. In magnetohydrodynamics one dies that extreme situation in which the signifi- t body force is due to the cross product of the rent and magnetic field. It seems worthwhile to ntify as "electrohydrodynamics" that extreme which the only significant body force is the duct of electric field and charge density.

This study was primarily motivated by our in- est in these unanalyzed laboratory observations. wever, we believe that these same electrocon- tive process might play an important role in eral geophysical phenomena. The transition be- en the ionosphere and the atmosphere of the th is a region where electrical forces can dominate driving the fluid. The electrical forces in thunder- rms also appear to be at least as important as rmal forces at some stages of their development. inal reason for our interest in electroconvection hat experimental studies of finite-amplitude and turbulent fluid processes may be facilitated because the measurement of electrical quantities is often simpler than the corresponding measurement of thermal or hydrodynamical variables.

Electroconvective phenomena can be divided into two types: those which occur in the body of a single fluid, and those which occur in the vicinity of the interface of two fluids with different electrical properties. Our experimental endeavors have been aimed principally at reproducing the interesting fields of motion reported by Avsec and Luntz in order to add quantitative information to the largely qualitative results which they have reported.[5] We shall briefly describe these observations.[4]

(a) The gap between two concentric metallic cylinders is filled with dielectric fluid, and the electrical potential of the inner cylinder has a value ϕ with the outer cylinder grounded. When ϕ reaches some critical value ϕ_c the fluid between the two cylinders is set into motion. Figure 1 is a reproduction from Avsec and Luntz[4] where the outer cylinder is glass with a semitransparent coating of silver and the fluid is some unspecified oil. The motion seems to be two-dimensional and toroidal. The critical value ϕ_c is not given by Avsec and Luntz, but Luntz (private communication) reported that a field strength of approximately 10^7 v/m was necessary to generate the motion.

(b) The gap (of width d) between two vertical parallel metallic plates is filled to some depth h with a dielectric fluid. One of the plates has a

---

F. Vettin, Meteor. Z. **3**, 38 (1886).

D. Avsec and M. Luntz, Compt. rend. **203**, 1140 (1936).

D. Avsec and M. Luntz, Compt. rend. **204**, 470 (1937).

D. Avsec and M. Luntz, Compt. rend. **204**, 757 (1937).

[5] Recently Ostroumov [G. A. Ostroumov, Zhur. Eksptl. i Teoret. Fiz. **30**, 282 (1956)] has reported observations of electroconvection. He first heated a fluid from the top so that the resulting very small density gradients could be observed optically and then he applied an electric field to show the types of transient motions which occur in the fluid. Also Stuetzer[6] has described a one-dimensional electrohydrodynamic instability produced by injecting ions into a parallel flow.

[6] O. M. Stuetzer, Phys. Fluids **2**, 642 (1959).

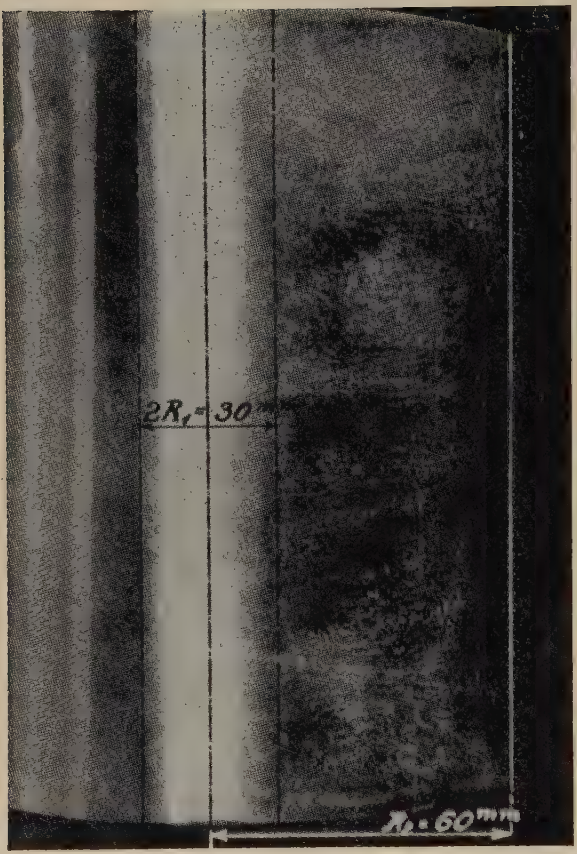

FIG. 1. Toridal cells produced between cylindrical electrodes.

potential ϕ relative to the other. At some critical value ϕ_c the fluid in the vicinity of the surface begins to move in a pattern of regular steady cells. Figure 2 shows one of the patterns (on the surface of the fluid). In our observation of turpentine, where h equaled 3 cm and d equaled 1 cm, the critical potential difference was approximately 200 v.

In addition to the surface motion some fluids exhibit a slower, quasi-cellular, body motion throughout the fluid. This latter motion was unsteady and disordered, unlike the body motion described in (a). The critical field strength has about the same value as that for the surface motions.

(c) A layer of dielectric fluid covers the metallic bottom of a container. The walls are made of glass or some other insulating material. A pointed electrode is then placed above the surface of the flui and raised to a potential of 10^5 v. The air in th vicinity of the electrode is ionized and this ionizatio causes a cellular distortion of the free surface the fluid whose amplitude is of the order of th depth. The surface distortion is accompanied b fluid motions in the cells similar to cellular therm convection. The fluid at the center of the cel ascends in some cases and descends in other Figure 3 is a photograph (from Avsec and Luntz of a distorted surface with fluid descending in th center of the cell.

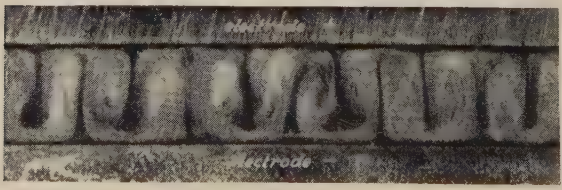

FIG. 2. Surface cells between parallel electrodes.

Several other types of motions are reported b Avsec[7,8] and Luntz.[9] However, the latter phenomen are concerned with an initial introduction of ior into a system and are transient, i.e., when the ior are swept out of, or redistributed in, the system the fluid motions stop.

In our attempts to analyze the body motions whic occur in the first two experiments described in th foregoing, it became evident at a very early stag that in order for electroconvection to occur it necessary that the effective electrical conductivit be a function of the field or of the space coordinate This was further borne out by the fact that nor of the fluids satisfied Ohm's law in its simple forn

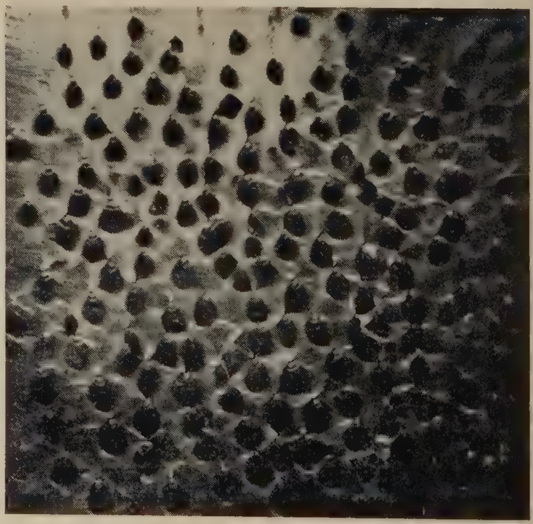

FIG. 3. Surface cells due to a point electrode above the surfac

It therefore appears that one must understand th conduction mechanism at the molecular level mo completely than it is known at present or that ne

---

[7] D. Avsec, Compt. rend. **208**, 1886 (1939a).
[8] D. Avsec, Compt. rend. **209**, 869 (1939b).
[9] M. Luntz, Compt. rend. **210**, 76 (1940).

erminable parameters must be introduced into e analysis.

The surface phenomena, on the other hand, are ite clearly based on the different physical proper- s of two adjacent fluids, viz., air and the dielectric id of the experiment. Although motions of the dy-type frequently accompany these surface tions, the amplitudes of the latter are often an der of magnitude or so greater than the amplitudes the body motion so that to a first approximation e can neglect the body motions.

We shall, therefore, confine our analyses to that pe of surface motion described in the first para- ph listed under (b). We feel that this process presents the most straightforward example of ctroconvection and that an understanding of the ture of the destabilizing mechanism which gives e to these surface motions may be an aid toward understanding of the more complicated body enomena.

II. EQUATIONS FOR SURFACE ELECTROCONVECTION

The physical model which we shall consider is e following: The gap between two infinite parallel tes contains two dielectric fluids which are im- scible and separated by an interface $z = z(x)$ ig. 4). The interface is distorted by forces which e not electrical in origin, e.g., cohesion between e fluids and the plates and surface tension. The te at $x = 0$ is grounded and the plate at $x = d$ s an electric potential of ϕ_d. What are the condi- ns under which motion can occur in the vicinity the interface between the fluids?

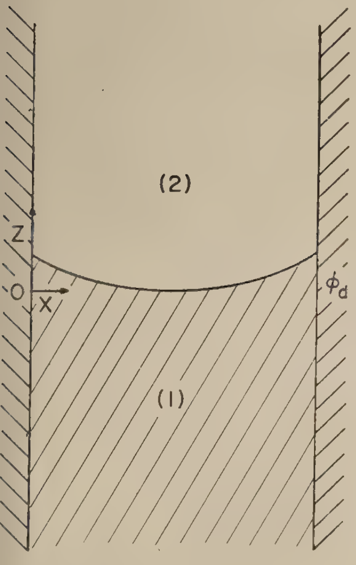

FIG. 4. Idealized geometry for surface electroconvection.

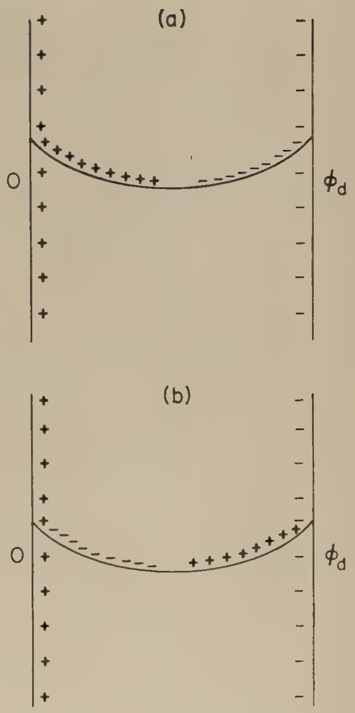

FIG. 5. Charge distribution at interface as a cause of (a) instability, and (b) stability.

Before deriving the mathematical equations which describe this system we give first a brief qualitative description of the nature of the destabilizing mechanism.

When the plate at $x = d$ has a potential ϕ_d, the potential in the fluid far from the interface ($|z| \gg d$) increases linearly from $\phi = 0$ at $x = 0$ to $\phi = \phi_d$ at $x = d$. However, in the vicinity of the interface the electric field is distorted. The ratio of the normal components of the electric field is $E_{1n}/E_{2n} = \sigma_2/\sigma_1$, since the divergence of the current at the surface must vanish in the steady state. If the ratio of the conductivities σ_1/σ_2 is much greater than the ratio of the dielectric constants, i.e., the larger of the ratios ϵ_1/ϵ_2 or ϵ_2/ϵ_1, the distortion of the electric field is determined primarily by the difference in conductivities.

However, the change in the normal component of field strength must be accompanied by a (true) charge at the interface. Therefore, the distribution of charge on the interface will be such that either positive charges accumulate near the positive plate and negative charges near the negative plate [Fig. 5(a)] or negative charges accumulate near the positive plate and positive charges near the negative plate [Fig. 5(b)].

It is clear that the first of these configurations can be unstable to disturbances which are periodic in y since positive charges are displaced toward the negative plate and vice versa, so that a regime of lower potential energy can be achieved. The second configuration is stable. The field strength must achieve some finite value before instability can occur because the redistribution of charge through fluid motion is accompanied by viscous and electrical dissipation. The rate of release of potential energy must be sufficiently large to balance these dissipation rates in order that the motion be sustained.

We now return to the task of formulating the problem mathematically. Each of the fluids is taken to be homogeneous with constant microscopic parameter. We shall denote the quantities in the lower fluid by the subscript "1" and those of the upper fluid by subscript "2." Electrical conductivity, dielectric constant and viscosity are, respectively, denoted by σ, ϵ, and μ. Then the equations which determine the dynamic and electrical behavior of the fluids are the Navier-Stokes equations

$$\frac{\partial v_i}{\partial t} + v_k v_{i,k} = \frac{1}{\rho_f}\left(S^m_{ki,k} + S^e_{ki,k}\right) + F_i; \qquad (1)$$

the equation of mass conservation for an incompressible fluid

$$v_{i,i} = 0; \qquad (2)$$

the electrical divergence relation

$$\epsilon E_{i,i} = \rho; \qquad (3)$$

the conservation of charge

$$(\partial\rho/\partial t) + j_{i,i} = 0; \qquad (4)$$

a modified Ohm's law which includes the macroscopic convection of charge

$$j_i = \sigma E_i + \rho v_i; \qquad (5)$$

and the irrotational property of the electrical field intensity E_i, i.e., E_i can be expressed as the gradient of a potential

$$E_i = -\phi_{,i}. \qquad (6)$$

The equations have been written in Cartesian tensor notation because we shall work directly with the stress tensors S^m_{ki} and S^e_{ki} (the superscripts refer, respectively, to "mechanical" and "electrical" quantities). The usual tensor notation obtains: A subscript following a comma denotes differentiation with respect to that coordinate and a repeated index corresponds to a sum over all three values. The quantity v_i is the ith velocity component; ρ_f is the fluid density; F_i is the ith component of the forces such as gravitational and surface distorting forces; ρ is the (volume) charge density; and, j_i is the component of the current densit
We use mks units.

The mechanical stress tensor is given by

$$S^m_{ki} = S^m_{ik} = -p\,\delta_{ik} + \mu(v_{i,k} + v_{k,i}), \qquad (7$$

where p is the fluid pressure and δ_{ik} is the Kronecke delta; and, the electrical stress tensor is

$$S^e_{ki} = S^e_{ik} = \epsilon E_i E_k + S E_l E_l\,\delta_{ik}, \qquad (8$$

where S is a function of ϵ and ρ_f and contains th electrostrictive terms.

It will be noted that we have neglected magneti effects in the electrodynamic equations, Eqs. (3) t (6). The magnetic stress tensor in the Navier-Stoke equations has also been neglected. These approxima tions are in accord with our remarks in the Intr duction.

Rather than specify the forces for a particula problem we shall proceed to derive the genera relations for the stable configuration (Sec. III) an the stability problem (Sec. IV). When these hav been derived we shall then consider the particula problem which is to be analyzed in detail.

III. STABLE CONFIGURATION

Our first task is to find the distribution of electric properties in the absence of macroscopic motion.

Equation (5) is now Ohm's law

$$j_i = \sigma E_i \qquad ($$

and Eq. (4) becomes

$$\frac{\partial\rho}{\partial t} + \sigma E_{i,i} = \frac{\partial\rho}{\partial t} + \frac{\sigma}{\epsilon}\rho = 0, \qquad (1$$

where we have used Eq. (3) to derive the righ hand side of Eq. (10). This means that for fixe boundary conditions the charge density in the flui must vanish. Hence, in the absence of motion, wit fixed boundary conditions

$$\rho^1 = \rho^2 = 0, \qquad (1$$

where the superscript denotes the upper or low fluid. From Eqs. (3) and (6) we have, therefor

$$\phi_{,kk} \equiv \nabla^2\phi = 0 \qquad (1$$

in each fluid.

In this steady field the divergence of Eq. (vanishes. Hence we must also have

$$\frac{\partial\phi^1}{\partial n}\bigg/\frac{\partial\phi^2}{\partial n} = -\frac{\sigma_2}{\sigma_1} \quad \text{on} \quad z = z_0, \qquad (1$$

as well as the continuity of ϕ. i.e.,

$$\phi^1 = \phi^2 \quad \text{on} \quad z = z_0. \qquad (13$$

The remaining boundary conditions are

$$\begin{aligned} \phi &= 0 \quad \text{on} \quad x = 0 \\ \phi &= \phi_d \quad \text{on} \quad x = d \\ \phi^2 &\to \phi_d \frac{x}{d} \quad \text{as} \quad z \to \infty \\ \phi^1 &\to \phi_d \frac{x}{d} \quad \text{as} \quad z \to -\infty. \end{aligned} \tag{14}$$

The Navier-Stokes equations, Eqs. (1), become

$$\frac{1}{\rho}(S^m_{ki,k} + S^e_{ki,k}) + F_i = 0 \tag{15}$$

., there is a balance between mechanical, electrical, d external forces.

Suppose we have a solution to Eqs. (12) to (14) that the steady-state field distribution and inter-ce distortion are known. We shall denote these φ $= \bar{\phi}^1(x, z)$ for the lower layer, $\phi = \bar{\phi}^2(x, z)$ r the upper layer and $z = z_0(x)$ at the interface. en by the divergence relation,

$$\epsilon_1 \frac{\partial \bar{\phi}^2}{\partial n} - \epsilon_2 \frac{\partial \bar{\phi}^2}{\partial n} = \omega, \quad \text{on} \quad z = z_0(x), \tag{16}$$

e can determine the induced surface charge distri-ution ω on the interface.

Is this configuration stable? If it is not, what are e conditions which determine instability?

IV. EQUATIONS FOR THE STABILITY ANALYSIS

Following the customary procedure for stability oblems, we shall separate the field variables into mean contribution (corresponding to the steady ate deduced in Sec. III) and a perturbation. Thus,

$$\begin{aligned} j_i &= \bar{j}_i + j'_i, \qquad & \rho &= \bar{\rho} + \rho' \\ \phi &= \bar{\phi} + \phi', \qquad & E_i &= \bar{E}_i + E'_i \\ \omega &= \bar{\omega} + \omega', \qquad & z_0 &= \bar{z}_0 + z'_0, \end{aligned} \tag{17}$$

ere the bar denotes the mean quantity and the imed variables are the infinitesimal perturbations. nce there is no velocity in the basic state, the locities are only perturbation quantities. We sub-tute Eqs. (17) into the basic equations, Eqs.) to (6), and neglect products of the infinitesimal rturbations.

In the body of each of the fluids $\bar{\rho} = 0$. Hence, s. (3), (4), and (5) take the form

$$\epsilon E'_{k,k} = \rho' \tag{18}$$

$$\frac{\partial \rho'}{\partial t} + j'_{i,i} = 0 \tag{19}$$

$$j'_i = \sigma E'_i. \tag{20}$$

Thus following the argument given in Sec. III, we note that ρ' must vanish in the body of each fluid (in fact, there can be a transient perturbation charge but the decay rate is given by $e^{-(\sigma/\epsilon)t}$ which can be considered instantaneous in the present problem) and the electric field is determined by

$$\phi'_{,ii} \equiv \nabla^2 \phi' = 0 \tag{21}$$

in each fluid. The boundary conditions on ϕ' are

$$\begin{aligned} \phi' &= 0 \quad \text{on} \quad x = 0, d \\ \phi' &\to 0 \quad \text{as} \quad |z| \to \infty \\ \phi^{1\prime} &= \phi^{2\prime} \quad \text{on} \quad z = \bar{z}_0. \end{aligned} \tag{22}$$

The divergence of the stress tensors $S^{m\prime}_{ki,k}$ and $S^{e\prime}_{ki,k}$ in each fluid can be written explicitly. Thus

$$S^{m\prime}_{ki,k} = -P'_{,i} + \mu v_{i,kk}. \tag{23}$$

The electric stress tensor can be simplified in view of the fact that there is no free charge in the fluid. In particular, we note that the derivative of the first term on the right-hand side of Eq. (8) is

$$(\epsilon E_i E_k)_{,k} = \epsilon E_k E_{i,k} + \epsilon E_i E_{k,k}. \tag{24}$$

But the term $E_{k,k}$ must vanish for both the steady field and the perturbation field since no charge distribution exists in the fluid. We can take advantage of the irrotational character of the field intensity to write

$$\epsilon E_k E_{i,k} = \tfrac{1}{2}\epsilon (E_k E_k)_{,i}. \tag{25}$$

Hence in the body of each fluid the entire electrical force can be written as a gradient and incorporated into the pressure term. (The perturbation force F'_i contributes only at the interface and thus vanishes in the body of each fluid.) We have, therefore, for the perturbation Navier-Stokes equations

$$\frac{\partial v_i}{\partial t} = -\frac{1}{\rho}\tilde{p}'_{,i} + \nu v_{i,kk}, \tag{26}$$

where

$$\tilde{p} = p + \left(S + \frac{\epsilon}{2}\right)E_{kk}, \qquad \nu = \mu/\rho_F \tag{27}$$

and

$$v_{i,i} = 0.$$

Taking the curl of (26) two successive times and using Eqs. (27), we arrive at

$$\partial v_{i,kk}/\partial t = \nu v_{i,kkmm} \tag{28}$$

or

$$(\partial/\partial t)\nabla^2 v_i = \nu\nabla^4 v_i$$

for each fluid.

The boundary conditions on v_i are

$$\begin{aligned} v_i &= 0 \quad \text{on} \quad x = 0, d \\ v_s^1 &= v_s^2 \quad \text{on} \quad z = \bar{z}_0 \qquad (29) \\ v_n^1 &= \partial z_0'/\partial t = v_n^2 \quad \text{on} \quad z = \bar{z}_0, \end{aligned}$$

where the subscripts s and n correspond to the velocity components tangential and normal to the surface.

We must finally satisfy certain conditions across the interface. If we take a small element of volume with the base parallel and the height normal to the interface, then the stresses acting on the surface of the volume element must be balanced by the integrated momentum flux through the volume. If we then allow the dimensions of the volume element to become vanishingly small, the stresses on the lateral faces must also become vanishingly small. However, the stresses on the faces parallel to the boundary may have a finite contribution, since the stresses can be discontinuous across the interface. If the height of the volume element is $2\Delta h$, we thus have

$$\lim_{h\to 0}\int_{-h}^{h}\frac{\partial v_n}{\partial t}\,dx_n = \{S^{e\prime}_{ki}n_k + S^{m\prime}_{ki}n_k\}_1^2, \qquad (30)$$

where $\{\ \}_1^2$ corresponds to the difference of the values of the bracketed quantity on the two sides of the interface and the primes correspond to the first-order contributions to the stress terms.

The other condition which must be satisfied across the interface is the condition that in a small volume element the rate of change of charge (i.e., the current) must be balanced by the macroscopic convection of charge and by the molecular conduction of charge through the volume element. Again letting the sides of the volume element become vanishingly small, we have contributions to the molecular flux of charge only from the sides whose faces are parallel to the boundary. Since the total charge concentration is at the interface, the first-order convective contribution to the charge flux is given by

$$(\partial/\partial x_s)(v_s\bar{\omega}),$$

where x_S and v_S are the horizontal components of the coordinate vector and the velocity, respectively. If we note that

$$\lim_{h\to 0}\int_{-h}^{h}\rho'\,dx_n = \omega',$$

we conclude that

$$\begin{aligned} \frac{\partial\omega'}{\partial t} &= \{\sigma E_n'\}_1^2 + \frac{\partial}{\partial x_s}(v_s\bar{\omega}) \\ &= \{\sigma E_n'\}_1^2 + v_s\frac{\partial\bar{\omega}}{\partial x_s} + \bar{\omega}\frac{\partial v_s}{\partial x_s}. \qquad (31 \end{aligned}$$

Thus the stability problem is reduced to the tas of finding the eigenvalues and eigenfunctions o the system of equations given by Eqs. (21), (22 and (28) through (31).

V. ANALYSIS FOR STEADY-STATE CONFIGURATION

Some of the difficulties which one encounters i attempting to solve the general problem becom apparent even in the analysis for the steady-stat configuration; e.g., the position of the interface a which the boundary conditions must be satisfied i implicitly contained in the boundary condition We shall therefore make several restrictions an simplifications which will reduce the problem to more tractable form.

In the first place, the surface-distorting force in the experimental arrangement are restricted t surface tension and gravity. We would like to consider the case where the slope of the free surface i small so that the boundary conditions can be satisfied on the x, y plane to first order in the slopes Most of the experimental fluids, however, have contact angle with the glass surface which is ver small so that the slope of the surface is very larg near the boundary. We shall, therefore, alter th experimental arrangement slightly.

The two horizontal plates are cut along the line $x = 0$, $z = 0$ and $x = d$, $z = 0$ (Fig. 6). The heigh of the cut is very small so that for all practica purposes the electric field is unaltered by the cut Now as the liquid is poured into the system, th small contact angle between the liquid and the plat will be maintained until the edges of the liqui

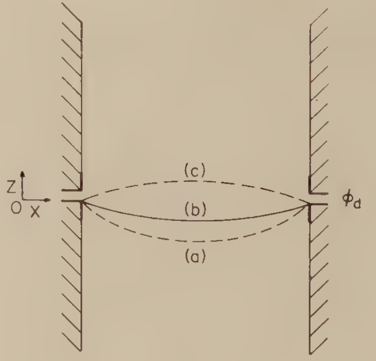

FIG. 6. Idealize experimental arrangement to control surface curvature.

h the gap [dotted line (a), Fig. 6]. If more fluid dded, the liquid level between the plates will , but the level of the contact point remains ltered, until the liquid level away from the walls ually exceeds the boundary level [dotted line (c), . 6]. In this way one can produce as small a e as desired for the surface.

he second simplification which we shall make ased on the observation that the position of the id level is not discernably affected by the electric l before instability. Therefore, the position of interface will be taken as that which is deter- ed by the mechanical forces alone before the tric field is applied.

hese two simplifications plus a sufficiently small width enable us to represent the interface by mple parabolic curve,

$$z_0 = \beta[x - (d/2)]^2, \tag{32}$$

ere $\beta d \ll 1$, i.e., the surface slope is small. Now small slopes we can write to first order in the e

$$\Big|_{z=z_0} = \frac{\partial x}{\partial n}\frac{\partial}{\partial x} + \frac{\partial z}{\partial n}\frac{\partial}{\partial z} \approx -\frac{\partial z_0}{\partial x}\frac{\partial}{\partial x} + \frac{\partial}{\partial z}. \tag{33}$$

uations (32) and (33) will be used in the remainder his analysis.

n all our experiments the liquid dielectric was ch more conductive than air. Indeed, the condi- n $\sigma_2/\sigma_1 \le 10^{-3}$ was always satisfied. Therefore m Eq. (13) it can be seen that the normal com- ent of the electric intensity in the liquid is remely small as compared to that of the air at interface. Hence, to a good approximation we write

$$\frac{\partial\phi^1}{\partial n} = -\frac{\partial z_0}{\partial x}\frac{\partial\phi^1}{\partial x} + \frac{\partial\phi^1}{\partial z} = 0. \tag{34}$$

Ve arrive, therefore, at a boundary-value problem the lower fluid defined by Eqs. (12), (14), (32), l (34). The boundary condition, Eq. (34), contains effects of the distorted interface $z = z_0$, but it be satisfied on the surface $z = 0$. For the zero- er approximation we can neglect the term $_0/\partial x)(\partial\phi^1/\partial x)$ in Eq. (34) and have simply $/\partial z = 0$ on $z = 0$. The solution to this problem n becomes

$$\phi^1 = \phi_d(x/d). \tag{35}$$

e corresponding problem for the upper layer is ined by Eqs. (12), (13a) and (14) with Eq. (13a) isfied on $z = 0$. The solution is again

$$\phi^2 = \phi_d(x/d). \tag{36}$$

If we put Eq. (35) into the term $\partial\phi^1/\partial x$ in Eq. (34), we can arrive at the first-order (in the slope) approximation to the electrical boundary-value problem. Because the boundary condition now has nonconstant coefficients, we must expand the first-order solution in a Fourier series, i.e.,

$$\frac{\partial z_0}{\partial x} = 2\beta\left(x - \frac{d}{2}\right) = \sum_1^\infty f_m \sin\frac{m\pi x}{d}, \tag{37}$$

where $f_m = -4\beta d/m\pi$ for even m and $f_m = 0$ for odd m. The first-order problem for ϕ^1 is

$$\nabla^2\phi^1 = 0$$

$$\phi^1 = 0 \quad \text{on} \quad x = 0, d$$

$$\frac{\partial\phi^1}{\partial z} = \frac{\phi_d}{d}\sum_1^\infty f_m \sin\frac{m\pi x}{d} \quad \text{on} \quad z = 0 \tag{38}$$

$$\phi^1 \to 0 \quad \text{as} \quad z \to -\infty.$$

This first-order solution can be easily shown to have the form

$$\phi^1 = \frac{\phi_d}{d}\sum_1^\infty \frac{f_m}{m}\sin\frac{m\pi x}{d}\, e^{m\pi z/d}. \tag{39}$$

Using Eq. (13a) on $z = 0$ as the matching condition across the interface, we find for the first-order upper-layer solution

$$\phi^2 = \frac{\phi_d}{d}\sum_1^\infty \frac{f_m}{m}\sin\frac{m\pi x}{d}\, e^{-m\pi z/d}. \tag{40}$$

Now by the divergence relation, Eq. (16), we can determine ω. We note that to first order in the slope

$$\omega = \frac{2\phi_d}{d}\sum_1^\infty f_m \sin\frac{m\pi x}{d} \equiv 2\frac{\phi_d}{d}\epsilon_2\frac{\partial z_0}{\partial x}. \tag{41}$$

(It can be shown also that ω is proportional to the slope of the interface for more complex forms of z_0.) It is clear from Eq. (41) that if the interface is horizontal, i.e., if $\beta = 0$, there is no surface-charge distribution. One can easily check this result since Eqs. (35) and (36) then satisfy the equations and boundary conditions exactly.

Thus we arrive at an approximate steady-state solution on the basis of four simplifications: First, the gap width is small; second, the slope of the interface is small and is determined by mechanical forces only; third, the conductivity of the dielectric liquid is much greater than that of air; fourth, the solution is found to first order in the slope. The first three are easily arranged experimentally. The last is a mathematical approximation which can be extended to higher order.

VI. STABILITY ANALYSIS

We encounter mathematical difficulties also in the analysis for the stability problem. However, since our purpose here is to demonstrate electroconvective instability, we shall make certain simplifications which allow us to keep the essential physical features in the system.

Our first assumption is that the principle of exchange of stabilities is valid, i.e., that $\partial/\partial t \equiv 0$ everywhere in the problem. This assumption is consistent with the fact that we observe steady cells experimentally. Next, we consider an idealized system in which the lateral walls (electrodes) are boundaries which do not retard the fluid; these are so-called "slip" or "free" boundaries. Although we cannot hope to achieve this situation experimentally, it simplifies the analysis and provides an extremum for the eigenvalue. (In reality, of course, the energy releasing mechanism in the fluid must be such as to overcome the frictional retardation at the walls as well as in the body of the fluid.)

Also, as a first approximation we neglect the deviation of the interface from the plane $z = 0$. The effect of the sloping boundary is contained in the presence of the surface charge ω. We still have the possibility of improving on this approximation by an iteration procedure.

We now turn to the formal analysis. The functional dependence in the y direction is taken to be periodic. By Fourier's theorem we can then extend the analysis to more complex y dependence. Therefore, we write

$$\nabla^2 g \equiv \left(\frac{\partial^2}{\partial x^2} + \frac{\partial^2}{\partial y^2} + \frac{\partial^2}{\partial z^2}\right) g = \left(\frac{\partial^2}{\partial x^2} - \frac{\pi^2\alpha^2}{d^2} + \frac{\partial^2}{\partial z^2}\right) g,$$

where α is the wave number in the y direction.

The solution to Eqs. (21) and (22) for the electric potential is then easily written down.

$$\phi^{1\prime} = \sum_1^\infty C^n \sin\frac{n\pi x}{d}\cos\frac{\pi\alpha y}{d}\exp\left[(\alpha^2 + n^2)^{\frac{1}{2}}\frac{\pi z}{d}\right]$$

$$\phi^{2\prime} = \sum_1^\infty C^n \sin\frac{n\pi x}{d}\cos\frac{\pi\alpha y}{d}\exp\left[-(\alpha^2 + n^2)^{\frac{1}{2}}\frac{\pi z}{d}\right], \tag{42}$$

where the C^n are as yet undetermined amplitudes.

One can verify also that the solution to Eqs. (28) and (29) with $\partial v_i/\partial t \equiv 0$ and with $\partial v_S/\partial n$ on $x = 0, d$ instead of the first condition of Eq. (29) is

$$u^1 = \sum_1^\infty \left(-\frac{\pi z}{d} A^n + B^n\right)\sin\frac{n\pi x}{d}$$
$$\cdot\cos\frac{\pi\alpha y}{d}\exp\left[(\alpha^2 + n^2)^{\frac{1}{2}}\frac{\pi z}{d}\right]$$

$$u^2 = \sum_1^\infty \left(\frac{\pi z}{d} A^n + B^n\right)\sin\frac{n\pi x}{d}$$
$$\cdot\cos\frac{\pi\alpha y}{d}\exp\left[-(\alpha^2 + n^2)^{\frac{1}{2}}\frac{\pi z}{d}\right]$$

$$v^1 = \sum_1^\infty \left\{-\frac{\pi z}{d}\frac{\alpha}{n} A^n - \frac{1}{n\alpha}[n^2B^n + (\alpha^2 + n^2)^{\frac{1}{2}}A^n]\right.$$
$$\cdot\cos\frac{n\pi x}{d}\sin\frac{\pi\alpha y}{d}\exp\left[(\alpha^2 + n^2)^{\frac{1}{2}}\frac{\pi z}{d}\right]$$

$$v^2 = \sum_1^\infty \left\{\frac{\pi z}{d}\frac{\alpha}{n} A^n - \frac{1}{n\alpha}[n^2B^n + (\alpha^2 + n^2)^{\frac{1}{2}}A^n]\right\}$$
$$\cdot\cos\frac{n\pi x}{d}\sin\frac{\pi\alpha y}{d}\exp\left[-(\alpha^2 + n^2)^{\frac{1}{2}}\frac{\pi z}{d}\right]$$

$$w^1 = \sum_1^\infty \frac{\pi z}{d}\frac{(\alpha^2 + n^2)^{\frac{1}{2}}}{n} A^n \cos\frac{n\pi x}{d}$$
$$\cdot\cos\frac{\pi\alpha y}{d}\exp\left[(\alpha^2 + n^2)^{\frac{1}{2}}\frac{\pi z}{d}\right]$$

$$w^2 = \sum_1^\infty \frac{\pi z}{d}\frac{(\alpha^2 + n^2)^{\frac{1}{2}}}{n} A^n \cos\frac{n\pi x}{d}$$
$$\cdot\cos\frac{\pi\alpha y}{d}\exp\left[-(\alpha^2 + n^2)^{\frac{1}{2}}\frac{\pi z}{d}\right], \qquad (4$$

where we impose the conditions $w^1 = 0 =$ $u^1 = u^2$, $v^1 = v^2$ at the interface $z = 0$. The fre boundary conditions at $x = 0, d$ are automatica satisfied by sin $(n\pi x/d)$ for u and cos $(n\pi x/d)$ f v and w.

To satisfy the stress condition, Eq. (30), acro the interface we note that, upon neglecting ter which depend on the slope, we have in compone form

$$\left\{\epsilon\bar{E}_x E_z' + \mu\frac{\partial u}{\partial z}\right\}_1^2 = 0 \qquad (44$$

$$\left\{\mu\frac{\partial v}{\partial z}\right\}_1^2 = 0 \qquad (44$$

$$\left\{-\tilde{p} + 2\mu\frac{\partial w}{\partial z}\right\}_1^2 = 0. \qquad (44$$

The terms F' and $\epsilon E_z E_z'$ which occur in Eq. (44 as well as the remaining terms containing $\bar{E}_z$ Eqs. (44a) and (44b) are all proportional to t slope and therefore have been neglected.

Equation (44c) is satisfied identically. From E (44b) we deduce

$$B^n = -(2\alpha^2 + n^2)/n^2(\alpha^2 + n^2)^{\frac{1}{2}}A^n. \qquad (4$$

Condition (44a) yields

$$C^n = -\frac{2(\mu_1 + \mu_2)}{\bar{E}_z(\epsilon_1 + \epsilon_2)}\frac{(\alpha^2 + n^2)^{\frac{1}{2}}}{n^2}A^n. \qquad (4$$

inally, the conditions for the current across the
rface, Eq. (31) with $\partial\omega'/\partial t \equiv 0$, can be written

$$\{\sigma E'_z\}_1^2 + u \frac{\partial \bar{\omega}}{\partial x} - \bar{\omega} \frac{\partial w}{\partial z} = 0 \tag{47}$$

this yields

$$+ \sigma_2) \sum_1^\infty \frac{\pi}{d} (\alpha^2 + n^2)^{\frac{1}{2}} C^n \sin \frac{n\pi x}{d} - \frac{2\phi_d}{d} \epsilon_2$$

$$\cdot \sum_1^\infty f_m \sin \frac{m\pi x}{d} \sum_1^\infty \frac{\pi}{jd} (\alpha^2 + j^2)^{\frac{1}{2}} A^i \cos \frac{j\pi x}{d}$$

$$\frac{4\phi_d \beta \epsilon_2}{d} \sum_1^\infty B^n \sin \frac{n\pi x}{d} = 0, \tag{48}$$

ere Eq. (41) has been substituted for ω.
ubstituting Eqs. (45) and (46) into Eq. (48),
find that

$$\frac{(\sigma_1 + \sigma_2)(\mu_1 + \mu_2)}{\bar{E}_z(\epsilon_1 + \epsilon_2)} \sum_1^\infty \frac{\alpha^2 + n^2}{n^2} A^n \sin \frac{n\pi x}{d}$$

$$- \frac{2\phi_d}{\pi} \epsilon_2 \sum_1^\infty f_m \sin \frac{m\pi x}{d}$$

$$\cdot \sum_1^\infty \frac{\pi}{jd} (\alpha^2 + j^2)^{\frac{1}{2}} A^i \cos \frac{j\pi x}{d}$$

$$- \frac{4\phi_d \beta \epsilon_2}{\pi} \sum_1^\infty \frac{2\alpha^2 + n^2}{n^2(\alpha^2 + n^2)^{\frac{1}{2}}} A^n \sin \frac{n\pi x}{d} = 0. \tag{49}$$

e product of the sums can be rewritten and we
lly have

$$\sum_{n=1}^\infty \Bigg\{ -\frac{\alpha^2 + n^2}{n^2} A^n - \lambda \sum_{m=1}^{n} f'_m \frac{[\alpha^2 + (n - m + 1)^2]^{\frac{1}{2}}}{n - m + 1} A^{n-m+1} + \lambda \frac{2\alpha^2 + n^2}{n^2(\alpha^2 + n^2)^{\frac{1}{2}}} A^n + \lambda \sum_{m=n+1}^\infty \Bigg[f'_m \frac{[\alpha^2 + (m - n)^2]^{\frac{1}{2}}}{m - n} A^{m-n} - f'_{m-n} \frac{(\alpha^2 + m^2)^{\frac{1}{2}}}{m} A^m \Bigg] \Bigg\} \sin \frac{n\pi x}{d} = 0,$$

where

$$\begin{aligned} f'_m &= 1/m \quad \text{for} \quad m \quad \text{even} \\ &= 0 \quad \text{for} \quad m \quad \text{odd} \end{aligned} \tag{50}$$

and

$$\lambda = -\frac{2\beta\phi_d}{\pi} \bar{E}_z \frac{\epsilon_2(\epsilon_1 + \epsilon_2)}{(\sigma_1 + \sigma_2)(\mu_1 + \mu_2)}.$$

Since the coefficients of $\sin n\pi x/d$ must vanish for each n, the resulting infinite determinant provides a relation between λ and α which must be satisfied for a nontrivial solution. The first few terms of this determinant are written, as follows, with the columns denoting the coefficients of the respective A^n and the rows the coefficients of the respective $\sin n\pi x/d$.

$$\begin{vmatrix} -(\alpha^2 + 1) + \dfrac{5\alpha^2 + 3}{2(\alpha^2 + 1)^{\frac{1}{2}}} \lambda & 0 & -\dfrac{(\alpha^2 + 9)^{\frac{1}{2}}}{12} \lambda \\ -\dfrac{(\alpha^2 + 1)^{\frac{1}{2}}}{2} \lambda & -\dfrac{\alpha^2 + 4}{4} + \dfrac{5\alpha^2 + 12}{8(\alpha^2 + 4)^{\frac{1}{2}}} \lambda & 0 \\ \dfrac{(\alpha^2 + 1)^{\frac{1}{2}}}{4} \lambda & -\dfrac{(\alpha^2 + 4)^{\frac{1}{2}}}{4} \lambda & -\dfrac{\alpha^2 + 9}{9} + \dfrac{5\alpha^2 + 27}{18(\alpha^2 + 9)^{\frac{1}{2}}} \lambda \\ \cdots & \cdots & \cdots \end{vmatrix} = 0. \tag{51}$$

---

quation (51) can be solved approximately by
ing successively larger portions of the determi-
nt and observing the convergence of the successive
tions. It is fortunate in this instance that the
diagonal terms are quite small (at no point is
total correction to any of the coefficients of the
in excess of 3% of the coefficients due to the
gonal terms). We therefore derive an exceedingly
d approximation to the relation which provides
minimum λ by considering the first term alone:

$$\lambda = 2(\alpha^2 + 1)^{\frac{1}{2}}/(5\alpha^2 + 3). \tag{52}$$

minimum occurs for $\alpha^2 = \frac{1}{5}$ and is

$$\lambda_m = 0.66. \tag{53}$$

By analogy with the analysis of thermal convection cells one would expect the rigid boundary conditions to yield a smaller cell size (larger α^2) and a larger value of λ_m.

It is worthwhile to look at the eigenparameter in a little more detail. From Eq. (50)

$$\begin{aligned} \lambda &= -\frac{2\beta\phi_d}{\pi} \bar{E}_z \frac{\epsilon_2(\epsilon_1 + \epsilon_2)}{(\sigma_1 + \sigma_2)(\mu_1 + \mu_2)} \\ &= \frac{2\beta\phi_d^2}{\pi d} \frac{\epsilon_2(\epsilon_1 + \epsilon_2)}{(\sigma_1 + \sigma_2)(\mu_1 + \mu_2)} \\ &= \frac{2\beta\bar{E}_z^2 d}{\pi} \frac{\epsilon_2(\epsilon_1 + \epsilon_2)}{(\sigma_1 + \sigma_2)(\mu_1 + \mu_2)}, \end{aligned} \tag{54}$$

and one can see immediately that it is necessary that $\beta > 0$ for instability to occur. If $\sigma_2 > \sigma_1$, it would be necessary that $\beta < 0$, since in that case $\bar{\omega}/\beta$ would have the opposite sign to that deduced.

The numerator of λ corresponds to the energy releasing mechanism and the denominator contains the two dissipative mechanisms (viscosity and conductivity).

VII. COMPARISON WITH EXPERIMENT

The design of an experiment to test the conclusions we have reached presents several difficulties. Clearly the initiation of the motion is not detectable. One observes the finite amplitude motion beyond the point of instability. If we were to measure the increase in the electrical current which must accompany the advent of motion, the change in slope of the voltage-current curve could be used to determine the point of instability. Unfortunately so little additional current flows to drive the cellular motions that it is barely detectable. An alternative, which is not entirely satisfactory, is to add some tracer to the fluid and measure its velocity as a function of field strength. We have found th a small amount of aluminum powder may be add to many dielectric fluids without altering th conductivities. However, in most of these flu many of the aluminum particles dash back a forth, as do pith balls, rather than achieve a lo electrical equilibrium. Several turpenes do not exhi this failing. Hence we have used purified pine for most of the quantitative work to be describ (Pinene is the principal constituent of commerc turpentine.)

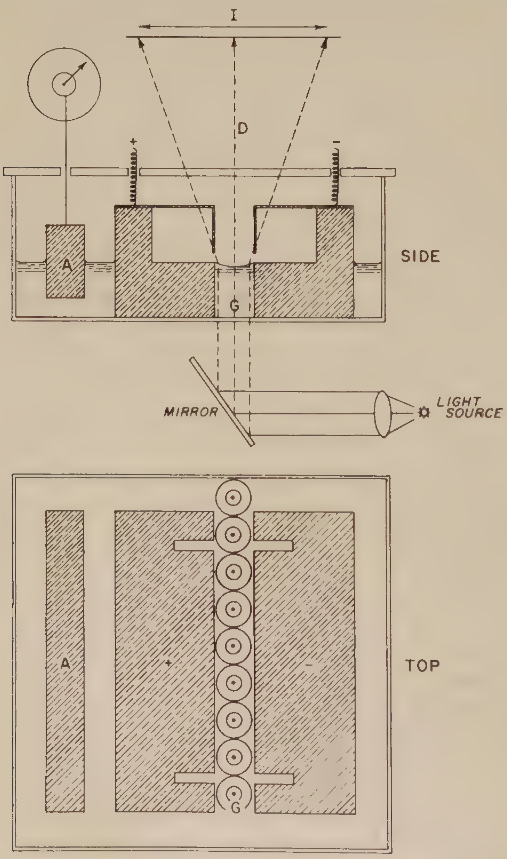

Fig. 7. Experimental arrangement for surface electroconvection.

Figure 7 is a schematic diagram of the expe mental arrangement used to test the validity the theory. The two electrodes, Q_+ and Q_-, bou the fluid in the gap G (as in Fig. 6). The shape the free surface in the gap is controlled by t calibrated plunger, A. For small curvatures of t free surface it acts as a thin cylindrical lens. Th curvature and its constancy along the gap a measured by the spread I of an initially paral beam of light passing through the fluid from belo The slope parameter β is given by the expressi

$$\beta = \frac{I - d}{2(n - 1)\, dD} = \frac{1}{2R}, \qquad (5$$

where n is the index of refraction of the fluid, is the distance from the fluid surface to the surfa on which the illumination is measured, and R the radius of curvature of the fluid surface.

Though the cellular electroconvection is mu more dramatic with large gap spacing, the surfa shape Eq. (32) can be retained only for gap spacin smaller than $2(\alpha/\rho_F g)^{\frac{1}{2}}$, where α is the surfa tension and g the acceleration of gravity. Hence usual gap spacing was 4×10^{-3} m, though th is exaggerated for clarity in the figure. The clearan between an electrode and its extension beyond t free surface was kept below 4×10^{-4} m. The dep of the fluid layer was 2×10^{-2} m.

The electrical equipment consisted of a voltmet a dc electronic microammeter and a 0-to 12 000-v power supply. (A 0-to 1000-v power supply w adequate for most of the study.)

The motion of the particles of the aluminum d in the cells was observed by eye and through a lo power binocular microscope. At each voltage a curvature six measurements were made of the ti required for 10 complete revolutions of a parti near the center of a cell.

Figure 8 is a graph of the results for pine Each point on the graph is an average of the time measurements and has a probable error about ±5%. However the absolute value of t

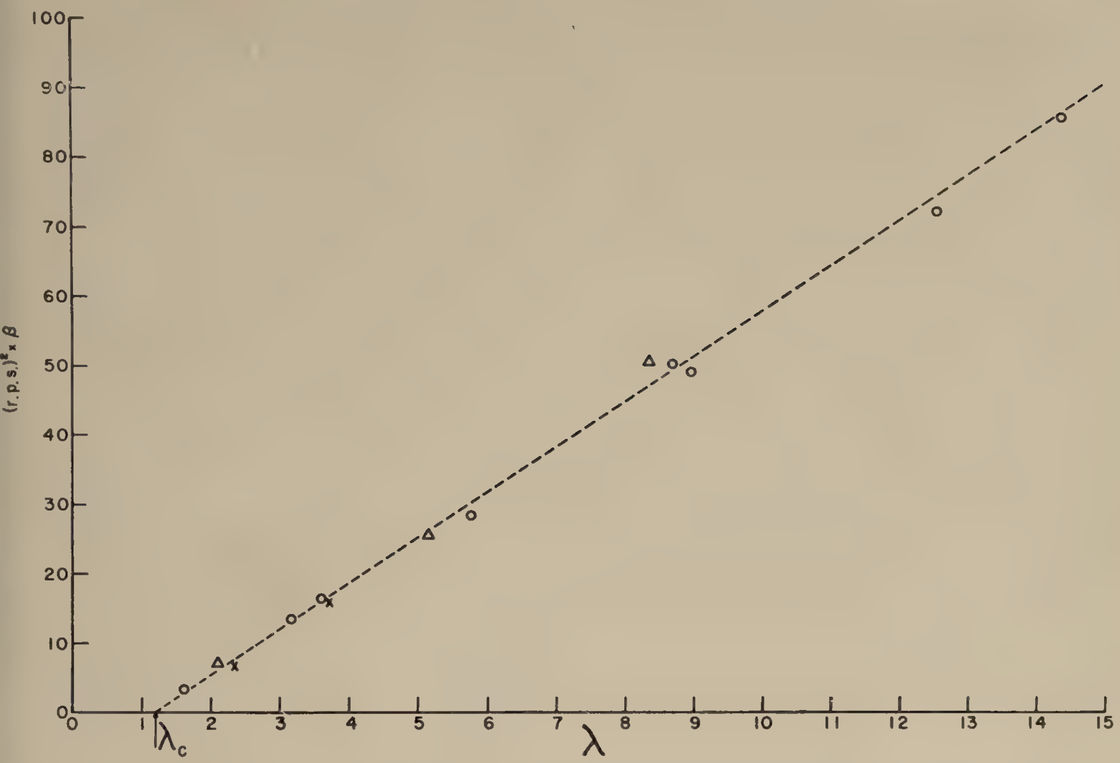

IG. 8. Determination of the critical eigenvalue for surface electroconvection. The ordinate is the square of the revolutions econd of a cell times the curvature parameter β. The abscissa is the eigenparameter, Eq. (54). The data points with a circle or $\beta = 71.4$ m^{-1}, with a triangle $\beta = 47.6$ m^{-1}, and with a square $\beta = 23.8$ m^{-1}.

e on the abscissa is probably in error ±20% ause it involves the separate determinations of luctivity, viscosity, dielectric constant, and index efraction of the fluid.

he coordinates of the graph were suggested by evious study of the authors[10]: In finite-amplitude rmal convection the amplitude of the heat trans- t due to motion just beyond the critical eigen- ameter is proportional to the square root of the nparameter minus the critical eigenparameter. he analog to heat transport in the electrocon- ive cell is the electrical current which flows due advection of the surface charge. In the first- r solution found here this surface current is portional to the square of the surface velocity es the curvature parameter. The revolutions per nd of a tracer near the center of a cell is pro- ional to amplitude of the velocity, hence the e of the ordinate is proportional to the surface ent. The extrapolation of the observed curve the abscissa determines a critical value for ability.

he existence of this common curve for the several rent curvatures and field strengths is the best evidence we can offer that the physics of this process has been successfully isolated. As anticipated, however, both the observed critical eigenvalue and cell size differ from the results of the simplified mathematical model. The observed $\lambda_c = 1.20$. The observed $\alpha^2 = 1.06$ near the point of instability and increases with increasing λ. Both differ in the correct direction from the free-surface model and by an amount which is similar to the difference found in thermal convection.

Several other fluids have been investigated, but with considerably less accuracy. Benzene, many paraffin-based oils and the Silicone oils exhibit well-defined electroconvective cells. The range of voltages which first produce motion is from approximately 5×10^3 v/m (for Shell oil 8232, $\mu = 0.82$ cs) to approximately 10^5 v/m (Silicone 200, $\mu = 100$ cs). Critical values for λ differed from the theoretical free-surface value by about two to one, as in the case of pinene.

ACKNOWLEDGMENTS

This study constitutes Woods Hole Oceanographic Institution Contribution No. 1138. This work was supported by the Office of Naval Research.

W. V. R. Malkus and G. Veronis, J. Fluid Mech. 4, 1958).

Contribution No. 1139

A Spherical Vortex Model of the Buoyant Thermal in Cumulus and Dry Convection[1, 2]

By Joseph Levine, Woods Hole Oceanographic Institution

Presented at the 8th OSTIV Congress, Cologne, Germany, June 1960

Within the last few years, laboratory experiments and observations have led to a spherical or ring-vortex conception of the buoyant element in atmospheric convection. Recently I have had an opportunity to witness laboratory experiments by Schaefer in which buoyant jets broke up into elements that looked very much like spherical vortices. Therefore turbulent convection probably does tend to consist of such vortex elements. Very likely even turbulent steady state jets consist of a conglomeration of overlapping vortex elements.

In my paper (1959), I combined Stommel's entrainment ideas (1947) with a spherical vortex model. Actually my adaptation of Stommel's ideas may be applied to any dynamic model. The spherical vortex was used only to obtain an approximate description of the internal motion of a bubble-like thermal and its effect on the surrounding air.

The problem may be treated very simply by divesting it of any explicit introduction of the spherical vortex aspect. The behavior of a thermal is grossly described in terms of equations for the conservation of mass, momentum, potential temperature, and specific humidity. The potential temperature and specific humidity conservation equations may easily be combined in an equation for the conservation of equivalent potential temperature.

Table of conservation equations

Mass:

$$\frac{dM}{dt} = \left(\frac{dM}{dt}\right)_+ - \left(\frac{dM}{dt}\right)_- \qquad (1)$$

Momentum:

$$\frac{dMW}{dt} = Mg\left[\frac{\rho_0 - \rho}{\rho} - \frac{\rho_1}{\rho}\right] - \left[\left(\frac{dM}{dt}\right)_+ + \left(\frac{dM}{dt}\right)_-\right]W \qquad (2)$$

$$-\frac{1}{2}\, C_D S a^2 \rho\, W^2$$

Specific humidity:

$$\frac{dMx}{dt} = x_0\left(\frac{dM}{dt}\right)_+ - x\left(\frac{dM}{dt}\right)_- - M\left(\frac{dx}{dt}\right)_c \qquad (3)$$

Potential temperature:

$$\frac{dM\Theta}{dt} = \Theta_0\left(\frac{dM}{dt}\right)_+ - \Theta\left(\frac{dM}{dt}\right)_- + M\left(\frac{d\Theta}{dt}\right)_c \qquad (4)$$

where M is the mass of the thermal, ρ the air density, ρ_1 the liquid water density, x the specific humidity, a the radius (or some similar characteristic dimension) of the thermal, C_D the aerodynamic drag coefficient, and S a shape factor (such as π for a spherical thermal). The subscript 0 is used to denote variables in the thermal's immediate environment. The quantities

$$\left(\frac{dM}{dt}\right)_+ \text{ and } \left(\frac{dM}{dt}\right)_-$$

indicate symbolically the instantaneous rate of addition of environment air to the thermal and the rate of removal of thermal air, respectively.

The above equations are exact in principal. Difficulties arise in defining the precise extent of the thermal element and in the quantitative definition of

$$\left(\frac{dM}{dt}\right)_+ \text{ and } \left(\frac{dM}{dt}\right)_-$$

If there is any marked coherence of behavior of a given thermal element, the former may be reasonably well defined. The latter can be shown to have a rather finite range of variation.

Page 101

The lower limit of both

$$\left(\frac{dM}{dt}\right)_+ \text{ and } \left(\frac{dM}{dt}\right)_-$$

is zero for a thermal not mixing with the environment. The upper limit may be defined in terms of a complete exchange of mass when the thermal moves through a distance of order a. If we imagine the surface of a thermal to behave like a wire mesh through which the air can flow unimpeded, the upper limit becomes quite definite and intelligible. The drag coefficient C_D likewise has definite upper and lower limits. Thus by introducing in addition to C_D the arbitrary parameters K_1 and K_2 defined by

$$\frac{1}{M}\left(\frac{dM}{dt}\right)_- = K_1 \frac{W}{a} \qquad (5)$$

and

$$\frac{1}{M}\left(\frac{dM}{dt}\right)_+ = K_2 \frac{W}{a} \qquad (6)$$

the problem of determining the motion of a thermal of given size in a given environment is completely determined by the conservation equations (1) to (4) and the knowledge of the saturation specific humidity as a function of potential temperature and pressure contained in thermodynamic charts except for the arbitrariness of the parameters K_1, K_2, C_D. Computations of this sort have been made and are illustrated in my paper (1959).

The behavior of the arbitrary parameters K_1, K_2, and C_D into which I have concentrated our ignorance may be possibly further limited by some semi-quantitative argument. However these parameters may be empirically evaluated from actual observations.

The above records were obtained by a DC-3 aircraft making a pass through a cloud tower at about 5000′ with cloud base at about 2000′ and with an indicated air speed of 100 knots in the neighborhood of Trinidad. The zero lines represent values just before entering cloud as references. Note the definitely buoyant thermal centered at 5.8 secs and approximately 2 secs in extent (100 meters). Also note the relatively cool portion just to the left of the thermal and to-

---

[1] The research done for this paper has been carried out under a National Science Foundation grant (NSF 7368).

[2] Contribution No. 1139 from the Woods Hole Oceanographic Institution.

wards the end of the pass. There are distinct maxima in liquid water content and vertical velocity coinciding with the abovementioned thermal. The vertical velocity profile of the thermal appears remarkably similar to that of a spherical vortex.

Temperature, liquid water content, and vertical velocity measurements from aircraft flights through cumulus appear to indicate that the major portion of visible cloud consists of turbulent air cool with respect to the environment and relatively small positively buoyant elements. The positively buoyant elements apparently are consistently quite uniform and relatively high in liquid water content and temperature with vertical velocity profiles very much like that of a spherical vortex. But it must be realized that an elongated thermal or jet might have the same sort of velocity profile.

Eventually I hope to determine the behavior of K_1, K_2, and C_D by working backwards from the observations of temperature, cloud liquid water content, and vertical velocity in buoyant thermals. The relatively high liquid water contents of buoyant thermals lead me to believe that radar might be a very useful additional tool for exploring the extent and shape of buoyant thermals in clouds.

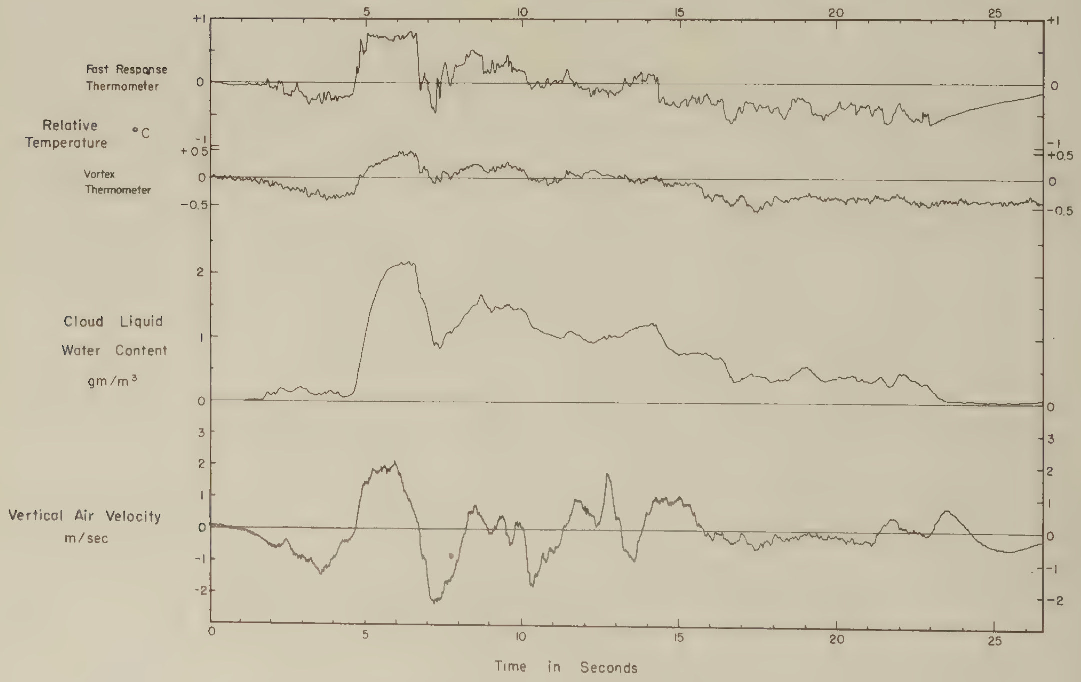

References

Levine, J., 1959: Spherical vortex theory of bubble-like motion in cumulus clouds. J. Meteor. 16, 653–662.

Stommel, H., 1947: Entrainment of air into a cumulus cloud. J. Meteor. 4, 91–94.

Reprinted from:
Aero-Revue, Schweizer Aero-Revue, Zurich, 36(2):100-101.

Contribution No. 1144

SEDIMENTATION IN A MODERN GEOSYNCLINE OFF THE ARID COAST OF PERU AND NORTHERN CHILE*

By PARKER D. TRASK
U.S.A.

ABSTRACT

A relatively deep and narrow trench lies off the coast of Peru and northern Chile. Its sediments are derived from an arid mountainous hinterland practically devoid of vegetation. The deep trough is favorable to the deposition of geosynclinal sediments, provided the rate of sedimentation equals or exceeds the rate of sinking. At present the supply of debris apparently is not sufficient to cause sedimentation to keep up with rate of sinking. The sediments in general are coarser than those found at similar distances off humid coasts. The average (median) grain size of deposits in the deep trough ranges from 2 to 8 microns. The sorting of the sediments on the whole is about normal except for those near shore where the coefficient of sorting is near 4.0. The size distribution in general is skewed with the mode lying on the coarse side of the median. The calcium carbonate content is low, 0–3 percent, except for samples rich in shell fragments near shore. The organic content of the deposits is high. Most of the deposits within 50 kilometers of the coast contain from 2 to 4 percent carbon. Occasional samples contain more than 10 percent carbon. This high organic content reflects the high productivity of organic matter in the ocean, resulting from upwelling. A maximum hydrocarbon content of 171 parts per million occurs in a sample at a depth of burial of one meter in a core obtained in 6000 meters of water near the bottom of the Peru-Chile trench off the coast of northern Chile. Within 25 kilometers of shore the grain-size distribution, calcium carbonate and organic content vary considerably with depth of burial. Elsewhere the sediments do not change greatly in character with depth of burial. The variation at depth presumably reflects changes in configuration of the sea floor during the course of deposition of the sediments.

INTRODUCTION

Woods Hole Oceanographic Institution in the fall of 1955 sent the ship ATLANTIS to investigate the conditions of sedimentation in the deep Peru-Chile Trench, which lies a short distance off the coast of Peru and northern Chile. The late Henry C. Stetson planned the expedition and was the leader until his unfortunate death off northern Chile. After his passing I was designated Chief Scientist of the expedition and was assigned the task of investigating the samples collected.

Acknowledgements are due Captain Bray of the ATLANTIS, William Ahern, Bernhard Kummel and John Zeigler, geologists who participated in the expedition.

The primary purpose of the expedition was to study the nature of the sediments accumulating in and near this deep trough, which lies off the coast of an arid and mountainous region. The area studied is more than 1500 kilometers in length. The adjacent land is almost completely devoid of vegetation and contains little or no soil. Rain comes in sudden and intense storms at intervals of several years. The total supply of sediment to the ocean is relatively little, but occasional storms can supply much debris to the ocean.

The trough that was the principal object of study ranges in depth from 4000 meters at the north to more than 7500 meters at the south. It is 150 kilometers from shore at the north and 75 miles at the south. The trough continues with varying depth for several hundred kilometers to the north and the south of the area shown on Figure 1, which indicates the course taken by the ATLANTIS during the expedition.

---

* Contribution No. 1144 . Woods Hole Oceanographic Institution.

The present report is a preliminary report describing the general aspects of the conditions of sedimentation in the area studied. More detailed accounts will be published subsequently in other journals. The report presents figures showing (1) the areal distribution of median diameter, sorting, calcium carbonate and organic carbon in the samples collected, and (2) the vertical distribution of these parameters along two of the profiles occupied. One profile is west of Antogafasta, Chile, across the deepest part of the Peru-Chile Trench and the other off Arica, 500 kilometers to the north. The configuration of the sea bottom along these and other profiles that were occupied have previously been reported by Zeigler, et al., (1957).

METHODS OF STUDY

The method of study was to take core samples at intervals of 5 to 20 kilometers along transverse profiles 150 to 250 kilometers length. The profiles are indicated by letters FF', JJ', etc., on Figure 1. A few short profiles 15 to 25 kilometers long, not designated by letters, were occupied close to the coast between Arica and Callao. In all 100 core samples, ranging in length from 10 to 250 centimeters were taken.

The cores were collected with the Stetson sampler, which is a modified Ekman sampler supplied with a coring tube 3 meters long and 10 centimeters wide and supplied with a load of 500 kilograms to aid penetration (Trask, 1955, pp. xiv–xvi). The device is lowered slowly by means of a winch and when 15 meters from the bottom is tripped by a lever arm that is released when a weight suspended from the lever arm strikes the mud. The device then falls under its own momentum. The weight used to trip sampler is a Phleger sampler weighing about 25 kilograms. This sampler is a miniature Stetson tube sampler having a core barrel 60 centimeters long and 3 centimeters diameter.

The ends of both samplers are supplied with removal bits and core catchers. The sediments are collected in removable plastic tubes in both samplers. In a few places one or both samplers failed to recover a sample either due to rocky bottom or non-cohesive material, such as sand.

The analytical procedures consisted of analyzing the grain-size distribution and total carbon, carbonate carbon, and nitrogen content of the sediments. The size distribution was determined by mechanical analyses for particles larger than 75 microns in diameter and by hydrometer analyses for fractions smaller than 75 microns. Calcium carbonate was computed from carbonate carbon, and organic carbon from the difference between total carbon and carbonate carbon. Nitrogen was determined directly.

The mechanical analyses were made by James Close, Henry Klehn, and Sigrid Snider of the Waves Research Laboratory of the University of California. The carbon and nitrogen analyses were made by James W. Kerrigan and Gerald Klein of the Sanitary Engineering Laboratory of the University of California.

In the present paper the results of the mechanical analyses are presented in terms of the median diameter, sorting and skewness. The median diameter is the mid-point

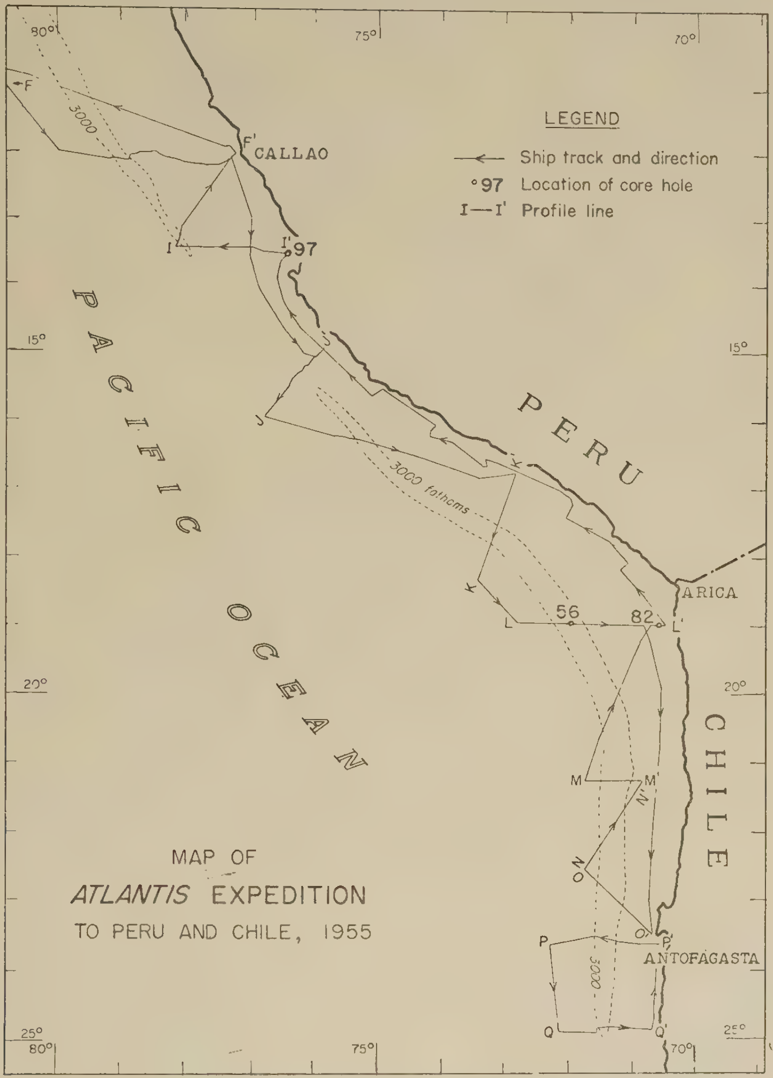
LEGEND
Ship track and direction
°97 Location of core hole
I—I' Profile line
80°
75°
70°
15°
20°
25°
CALLAO
ARICA
ANTOFAGASTA
PERU
CHILE
PACIFIC OCEAN
3000 fathoms
97
56
82
F
F'
I
I'
J
K
L
L'
M
M'
N
N'
O
O'
P
P'
Q
Q'
MAP OF
ATLANTIS EXPEDITION
TO PERU AND CHILE, 1955

Fig. 1.—*Map of area investigated by the ATLANTIS expedition to Peru and Chile,* 1955.

or 50 percentile on the weight accumulation or grading curve of the sediments (Trask, 1932, pp. 70–74). The sorting and skewness are based on the quartiles, that is the diameters representing the 25 and 75 percentiles. Calcium carbonate and organic carbon are reported in percent. Data for nitrogen results are not given in the present paper.

RESULTS

Description of figures.

The results are presented in Figures 2 to 11. These figures are arranged according to the various parameters studied. For each parameter two sets of figures are shown.

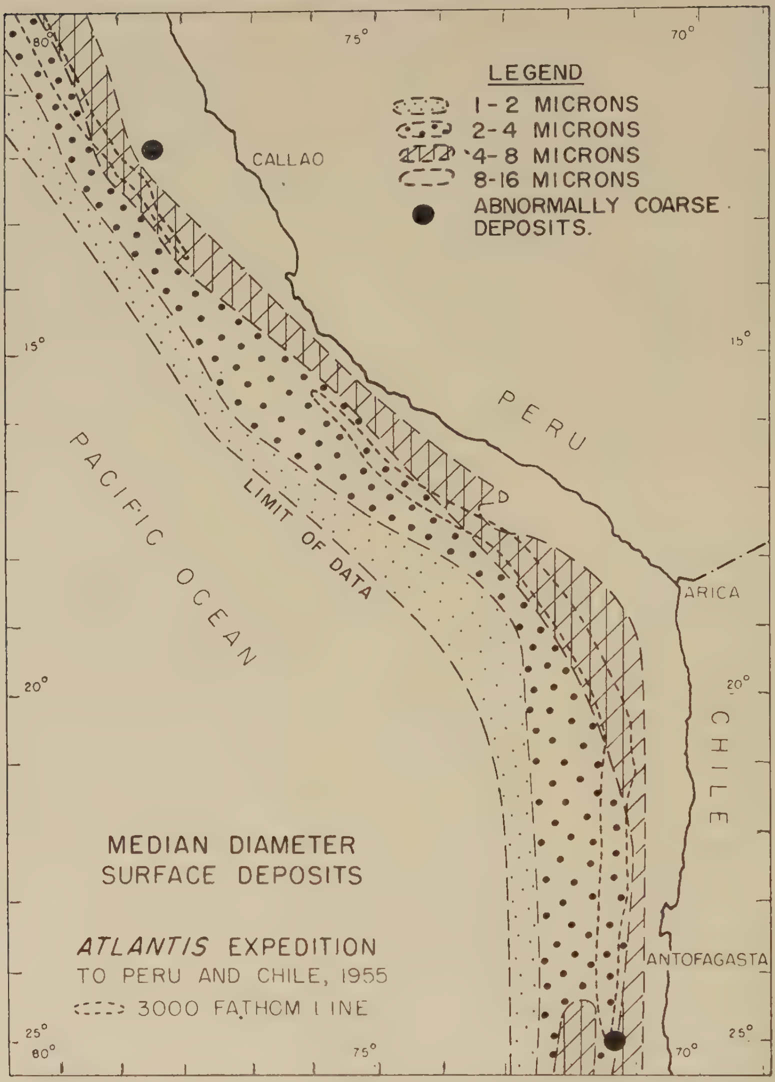
LEGEND
1-2 MICRONS
2-4 MICRONS
4-8 MICRONS
8-16 MICRONS
ABNORMALLY COARSE DEPOSITS.
CALLAO
PERU
ARICA
CHILE
ANTOFAGASTA
PACIFIC OCEAN
LIMIT OF DATA
MEDIAN DIAMETER
SURFACE DEPOSITS
ATLANTIS EXPEDITION
TO PERU AND CHILE, 1955
3000 FATHOM LINE
80°
75°
70°
15°
20°
25°

FIG. 2.—*Median diameter of surface deposits off the coast of Peru and northern Chile.*

One represents the areal distribution of the surface deposits as indicated by the top parts of the Phleger core samples collected along the different profiles that were occupied. The other set shows the variation of each parameter with depth of burial. In the latter series of tables, two profiles are shown. Both these profiles lie off the coast of northern Chile where the Peru-Chile Trench is relatively deep. One is Profile 5 off Arica and the other is Profile 6 off Antofagasta. These profiles are designated LL' and PP', respectively, on Figure 1.

The figures showing the areal distribution are generalized, owing to the relatively great distance between profiles and to local variations in grain size along the profile lines. The data for the various parameters as plotted on maps, however, are remark-

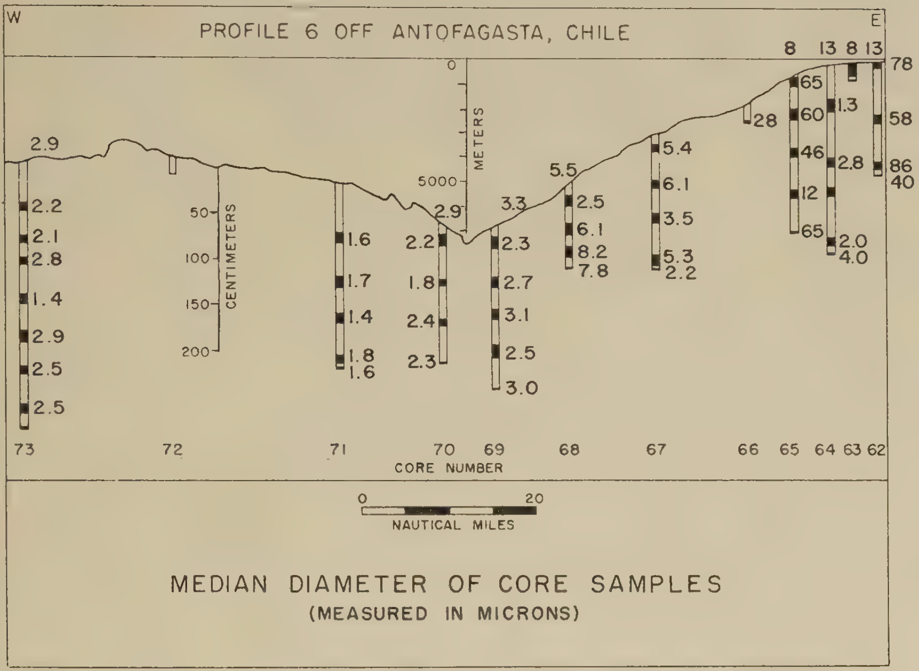

FIG. 3.—*Median diameter of core samples along Profile* 6 *off Antofagasta, Chile*

ably consistant and permit the drawing of the boundaries between the various size groups shown on each areal chart. Special symbols indicate marked deviations from the general trends.

Grain-size.

The median diameter of the sediments as shown on Figure 2 decreases in size progressively away from shore. In general the deep trough has little effect upon grain size, though profiles 5 and 6 (Figures 3 and 4) show local irregularities, some of which are related to changes in slope of the sea bottom. The sediments at the first sampling station, which was 5 to 20 kilometers, but generally about 10 kilometers from the shore, are of silt size. The median diameter of these samples is 8 to 16 microns (6.0 to 7.0 Phi units). The 84 percentile is commonly coarse silt in the very fine size (32 to 125 microns—3.0 to 5.0 Phi units). The median of the sediments in the trough ranges from 2 to 8 microns (7.0 to 9.0 Phi units). The most fine-grained sediments are found midway between Arica and Callao and off Antofagasta where the rate of change in grain size with distance is relatively high, and the trough is comparatively near the coast. The sediments seaward from the trough become decreasingly finer with distance. In general the median ranges from 1.5 to 2 microns at the seaward end of the profiles.

The variations in average grain size are more clearly shown on Figures 3 and 4 which show the vertical distribution of median diameter along two of the profiles. As a rule the grain size does not vary greatly with depth, but there are numerous

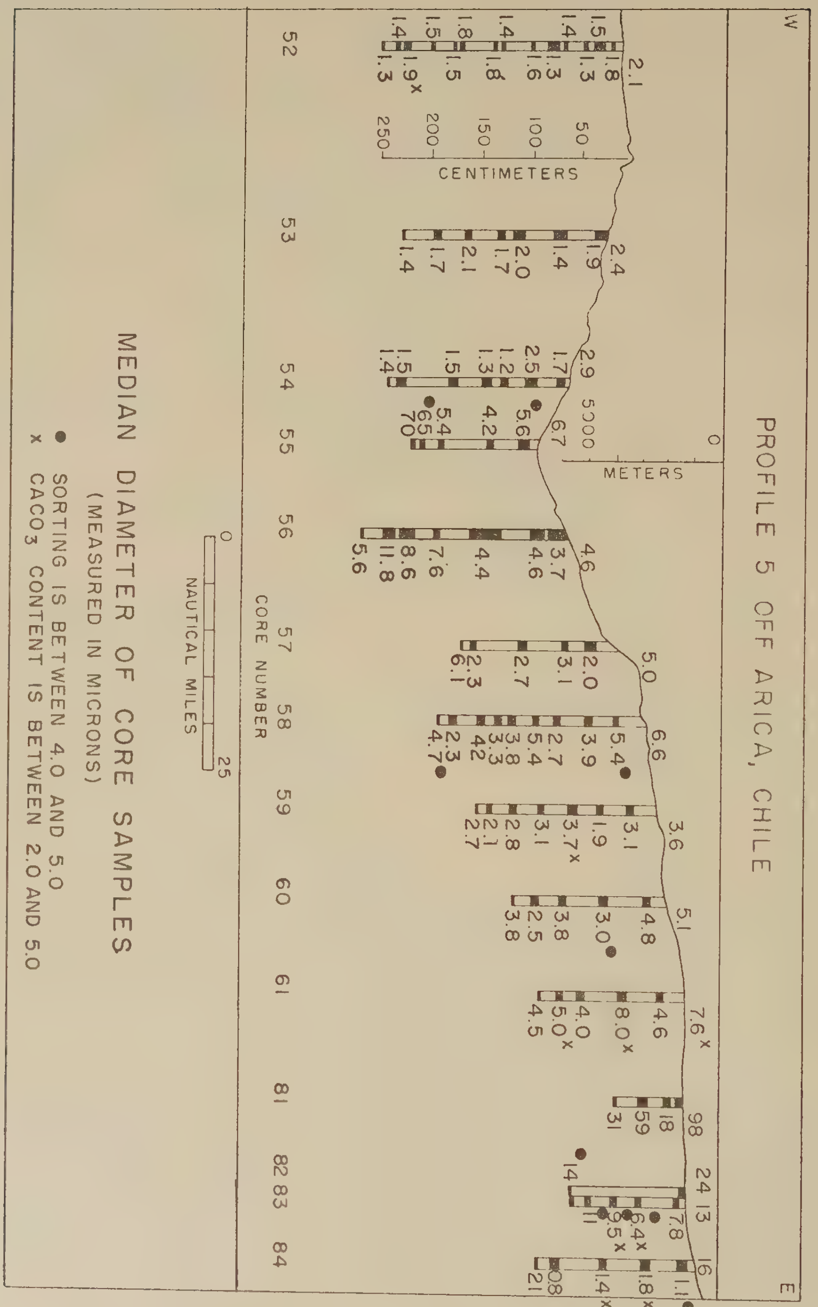

FIG. 4.—*Median diameter of core samples along Profile 5 off Arica, Chile.*

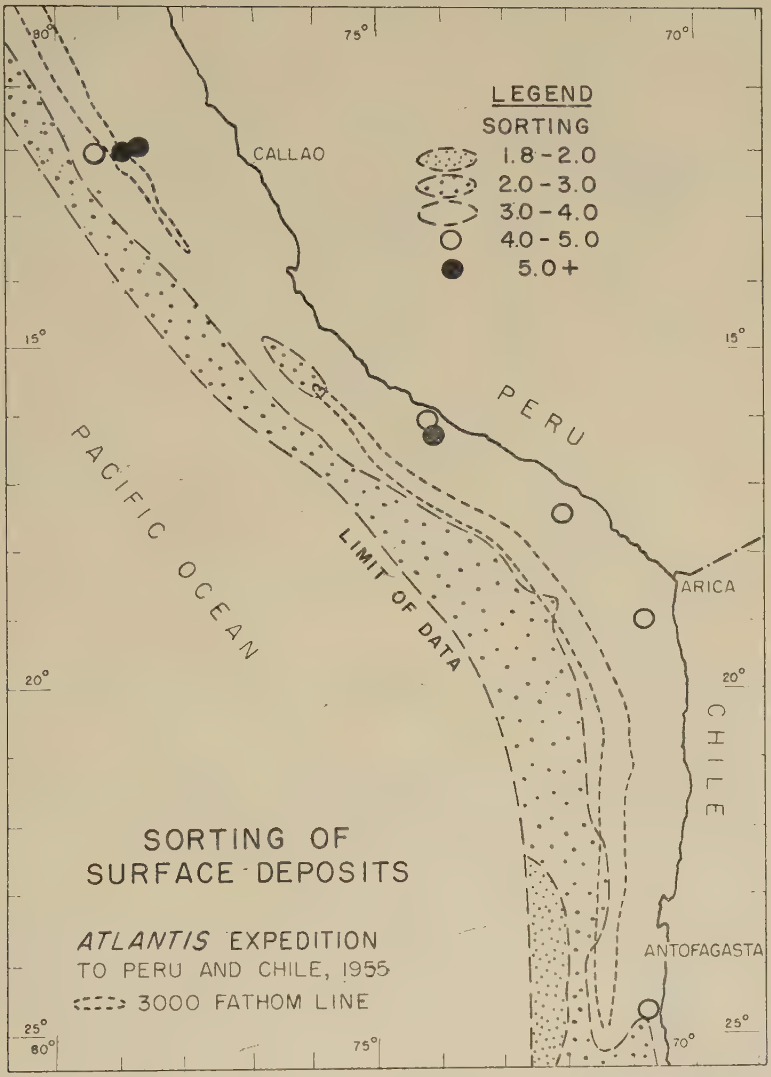
80°
75°
70°
15°
20°
25°
LEGEND
SORTING
1.8 - 2.0
2.0 - 3.0
3.0 - 4.0
4.0 - 5.0
5.0 +
CALLAO
PERU
PACIFIC OCEAN
LIMIT OF DATA
ARICA
CHILE
ANTOFAGASTA
SORTING OF SURFACE DEPOSITS
ATLANTIS EXPEDITION TO PERU AND CHILE, 1955
3000 FATHOM LINE

FIG. 5.—*Sorting of surface sediments off the coast of Peru and northern Chile.*

exceptions to this rule. A notable example is core 65, some 25 kilometers off the coast at Antofagasta, where the median diameter of the surface sediments is 8 microns and at depth in the core it ranges between 12 and 65 microns. Variations in grain size between 2.5 and 8.2 microns occur in core 68 on the same profile. Notable changes in depth are also observed in cores 81 to 84 along Profile 5 (Figure 4). In core 55 in 7000 meters of water near the bottom of the trench the grain size increases abruptly from about 5 microns to 65 microns at a depth of burial of 125 centimeters. Lesser variations with depth of burial are observed in other cores. However the cores at the seaward end of Profile 6 are essentially constant in median diameter with

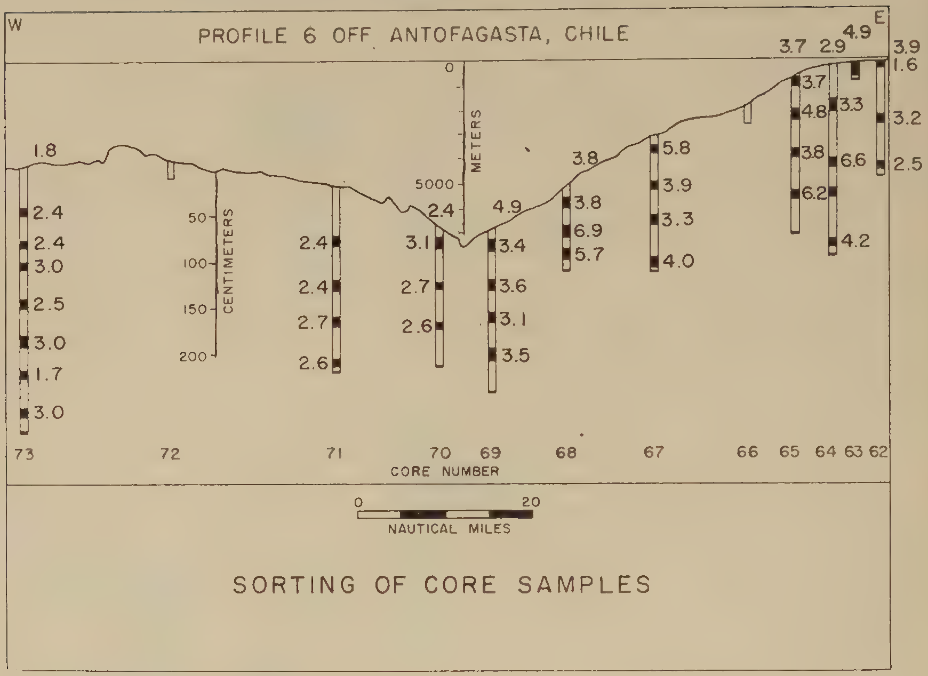

FIG. 6.—*Sorting of core samples along Profile* 6, *off Antofagasta, Chile.*

depth of burial, particularly core 52 which ranges in median mostly between 1.5 and 2.0 microns throughout a vertical distance of 250 centimeters.

Sorting.

The coefficient of sorting is illustrated by Figures 5 and 6. The sorting is the square root of the quotient of the third and first quartiles. In a symmetrical or normal size distitution the third quartile is the product of the median and the coefficient of sorting. Thus the third quartile can be estimated roughly by multiplying the median by the coefficient of sorting.

The coefficient of sorting in general decreases seaward from about 4.0 near shore to 2.0 at the outer ends of the profiles. Off Antofagasta it decreases to about 1.8 seaward. This decrease in coefficient of sorting indicates that the sediments become progressively better sorted offshore. Thus, the range in grain size between the first and third quartiles becomes progressively less seaward. Or in other words, near shore there is a much wider range in grain size in the sediments than in deeper water and in areas away from shore. Along profile QQ' south of Antofagasta the sediments are much better sorted near shore than in other nearshore areas. Also in sporadic samples located in several different areas as shown by the black and white circular symbols on Figure 5, the sediments are much more poorly sorted than in other places. Some of these sediments have coefficients of sorting greater than 5.

The sorting of the sediments in general does not vary greatly with depth of burial as indicated by Figure 6 representing the profile off Antofagasta. However in cores

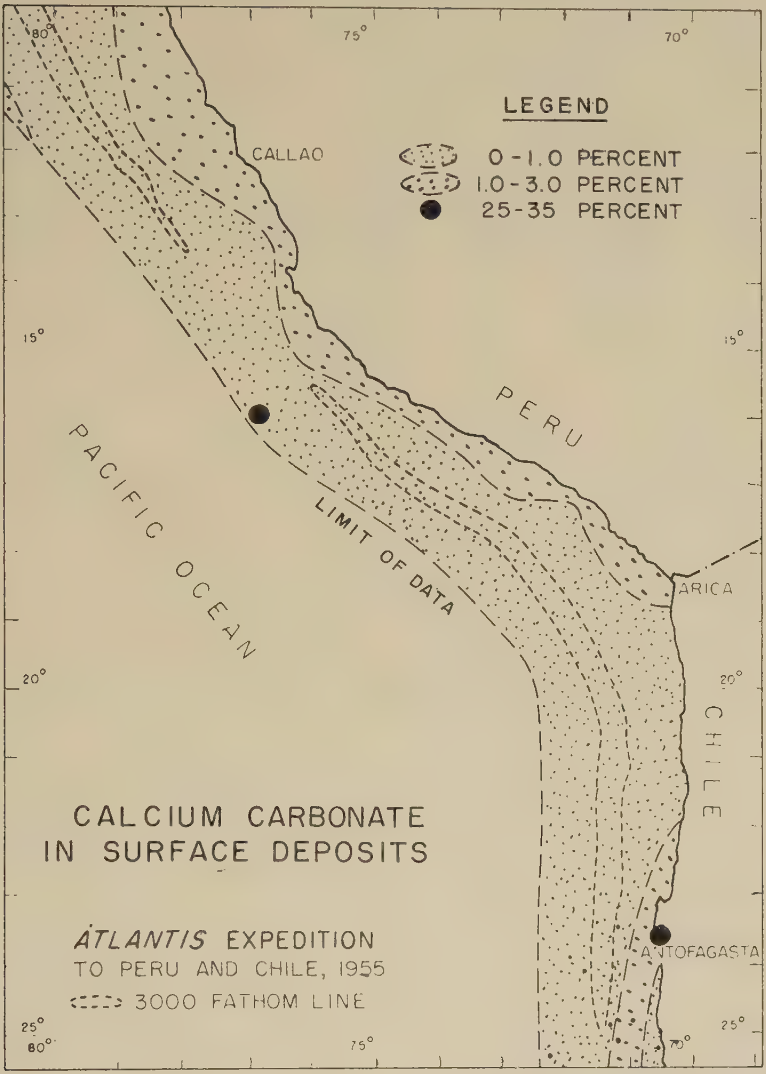
LEGEND
0-1.0 PERCENT
1.0-3.0 PERCENT
● 25-35 PERCENT
CALLAO
PERU
PACIFIC OCEAN
LIMIT OF DATA
ARICA
CHILE
ANTOFAGASTA
CALCIUM CARBONATE IN SURFACE DEPOSITS
ATLANTIS EXPEDITION TO PERU AND CHILE, 1955
3000 FATHOM LINE
80°
75°
70°
15°
20°
25°

FIG. 7.—*Calcium carbonate content of surface sediments off the coast of Peru and northern Chile.*

62 to 65, close to shore on this section, the sorting varies greatly with depth. At some depths, the coefficient is greater than 6, which indicates a very poor degree of sorting.

Calcium carbonate.

The calcium carbonate content of the sediments in general is low, as is illustrated by Figures 7 and 8. Near shore it ranges mainly between one and three percent, but beyond about 50 kilometers from the coast it is almost invariably less than one percent. At the seaward end of a profile taken off the Peruvian Coast west of Talara, 750 kilometers northwest of Lima the calcium carbonate content increases to almost

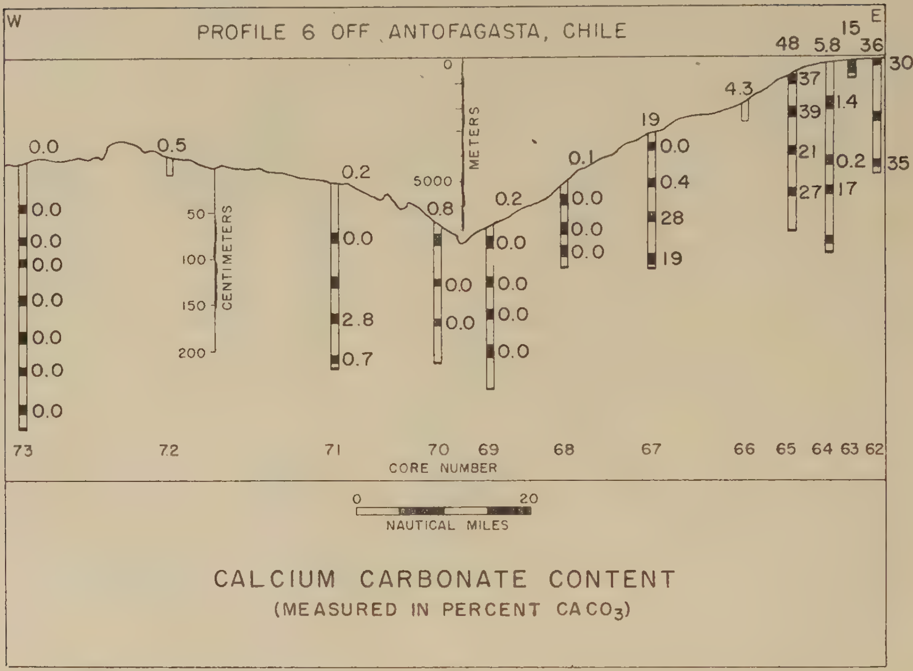
W
PROFILE 6 OFF ANTOFAGASTA, CHILE
E
48 5.8 15 36
30
37
39
1.4
21
0.2
35
27
17
4.3
19
0.0
0.4
28
19
0.1
0.0
0.0
0.0
METERS
0
5000
0.2
0.8
0.0
0.0
0.0
0.0
0.0
0.0
0.2
0.0
2.8
0.7
0.0
0.5
50
100
150
200
CENTIMETERS
0.0
0.0
0.0
0.0
0.0
0.0
0.0
0.0
73
72
71
70
69
68
67
66
65
64
63
62
CORE NUMBER
0
20
NAUTICAL MILES
CALCIUM CARBONATE CONTENT
(MEASURED IN PERCENT CACO3)

FIG. 8.—*Calcium carbonate content of core samples along Profile 6 off Antofagasta, Chile.*

20 percent. A small wedge at the northwest end of the map area shown on Figure 7 portrays the beginning of this enrichment in calcium carbonate seaward. At a few places indicated by black dots the calcium carbonate content is in excess of 25 percent. One of these localities is close to shore at Antofagasta, where shell fragments accounted for most of the carbonate.

The calcium carbonate content of the off-shore samples is essentially constant with depth; but in cores 62 to 65 on Profile 6 near Antofagasta the carbonate content, like both the median diameter and sorting, varies greatly with depth. Also core 67 in water 3500 meters deep varies in carbonate content with depth, having 19 percent at the surface, little or none at depths of 20 to 60 centimeters and 19 percent or more at depths of 100 to 159 centimeters.

Organic content.

The organic content of the sediments is relatively high, as shown on Figures 9 to 11. The organic carbon content is 2 to 4 percent near shore and decreases to one percent or less at the seaward ends of the profiles. The organic content shows no tendency to increase in the bottoms of the troughs except along profile 5 off Arica where the organic carbon is 1.9 percent at the bottom of the trench and 0.5 percent in adjacent shallower water. The sediments are rich in organic matter for a greater distance off shore in the vicinity of Callao than they are off the coast of Chile. In fact the organic content of the sediments in general decreases southward from Callao.

The organic carbon content, like the other parameters of the sediments, as a rule

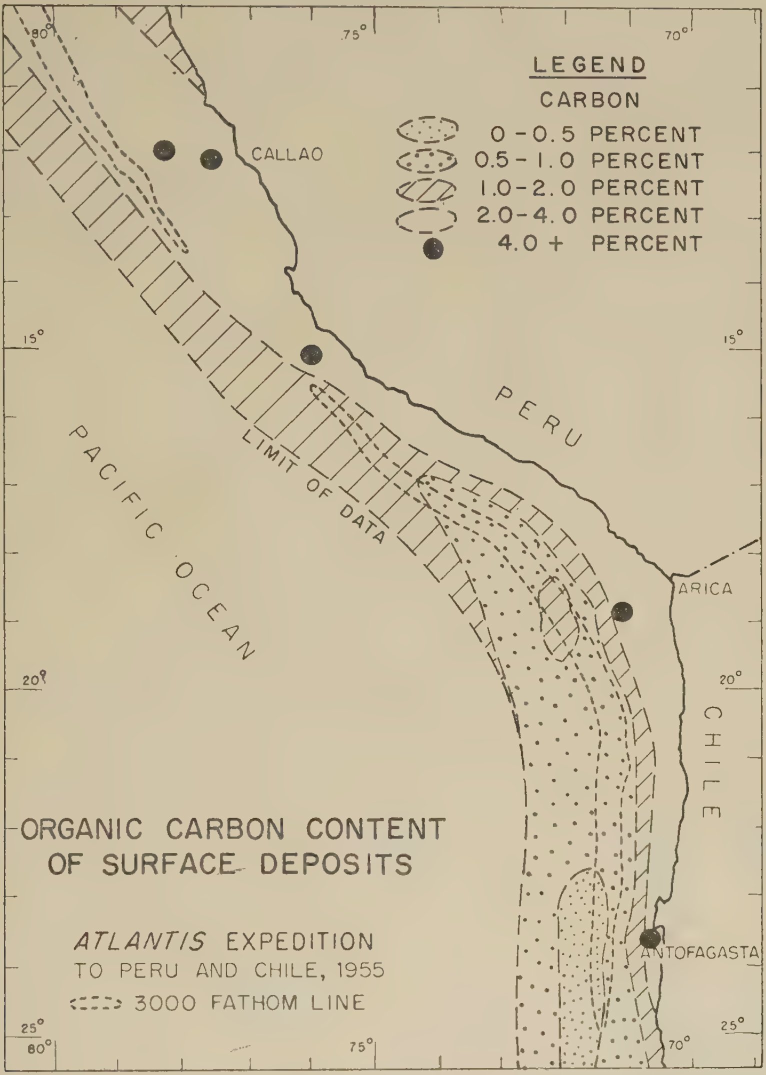
80°
75°
70°
LEGEND
CARBON
0 - 0.5 PERCENT
0.5 - 1.0 PERCENT
1.0 - 2.0 PERCENT
2.0 - 4.0 PERCENT
4.0 + PERCENT
CALLAO
15°
PERU
PACIFIC OCEAN
LIMIT OF DATA
ARICA
20°
CHILE
ORGANIC CARBON CONTENT OF SURFACE DEPOSITS
ATLANTIS EXPEDITION TO PERU AND CHILE, 1955
3000 FATHOM LINE
ANTOFAGASTA
25°
80°
75°
70°

FIG. 9.—*Organic carbon content of surface deposits off the coast of Peru and northern Chile.*

is essentially constant with depth, except in the cores near shore, represented by cores 62 to 65 on Figure 10 and cores 81 to 84 on Figure 11. The samples on profiles 5 and 6 show some tendency to decrease in organic matter with depth of burial. A preliminary compilation of the data on the upper and lower parts of the samples collected in Phleger core samples indicates a slight decrease in organic content in the upper 25 centimeters of sediment. Such a decrease in organic content with depth of burial in marine sediments seems to be of general occurrence (Trask, 1932, pp. 205–218).

As nitrogen varies in a similar manner to carbon the results of the nitrogen analyses are not presented. The average carbon-nitrogen ratio of the surface sed-

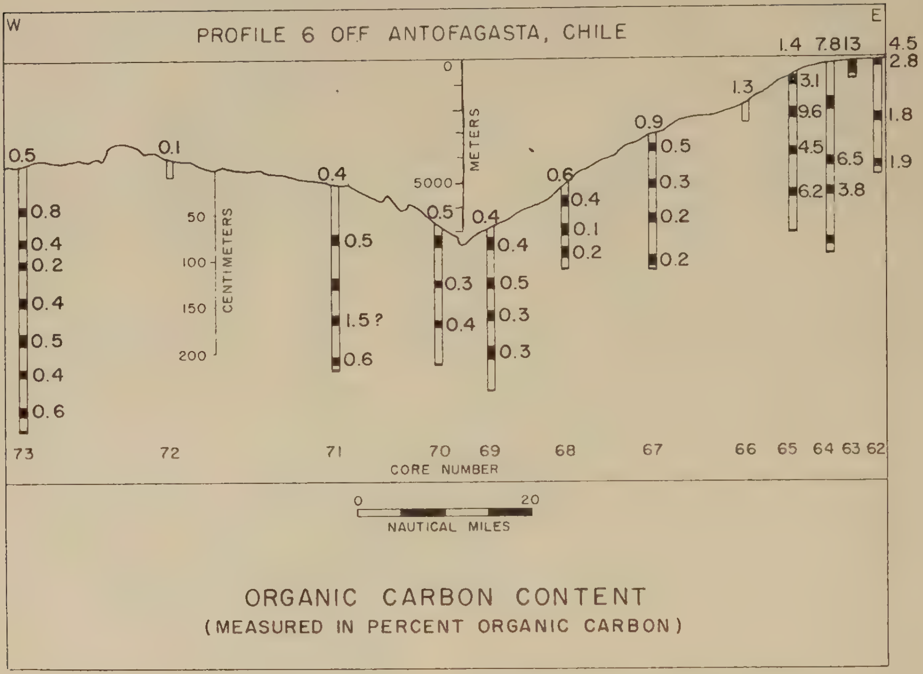
W
PROFILE 6 OFF ANTOFAGASTA, CHILE
E
1.4 7.8 13
4.5
2.8
3.1
9.6
4.5
6.2
6.5
3.8
1.8
1.9
1.3
0.9
0.5
0.3
0.2
0.2
0.6
0.4
0.1
0.2
0.5
0.1
0.4
0.8
0.4
0.2
0.4
0.5
0.4
0.6
0.5
1.5 ?
0.6
0.5
0.3
0.4
0.4
0.4
0.5
0.3
0.3
0
METERS
5000
50
100
150
200
CENTIMETERS
73
72
71
70
69
68
67
66
65
64
63
62
CORE NUMBER
0
20
NAUTICAL MILES
ORGANIC CARBON CONTENT
(MEASURED IN PERCENT ORGANIC CARBON)

FIG. 10.—*Organic carbon content of core samples along Profile 6 off Antofagasta, Chile.*

iments is about 8.4, which is essentially the same average found in the author's previous study of marine sediments. (Trask 1932, p. 22). The carbon-nitrogen ratio seems to increase with depth of burial, but at the time of writing this report a critical study of variations in this ratio has not been made.

Skewness.

The results of skewness, which is a measure of the relative concentration of grain size of approximately the median diameter, are not reported, as no areal or vertical trends in skewness are indicated by the data obtained. As a rule the quartile skewness in the present samples is less than one, which means that the ratio of the third quartile to the median diameter is less than the ratio of the median to the first quartile. That is, the main mode lies on the coarse side of the median. This position of the main mode represents a concentration of grain size in the size interval between the median diameter and the third or larger quartile. Thus, the weight percent of grains of similar coarse size is greater than the weight percent of similar fine size. "Similar" is used in the sense of similar Phi-unit size. Or to put it another way, a skewed size distribution of the type generally found in the present sediments indicates the presence of two size distributions one superimposed upon the other. The major one, which forms the greater proportion of the weight of the sediments is relatively coarse in size. The other, which forms a minor part of the total sediment is relatively fine in size. In some samples the reverse is true, but these will be discussed in a later report.

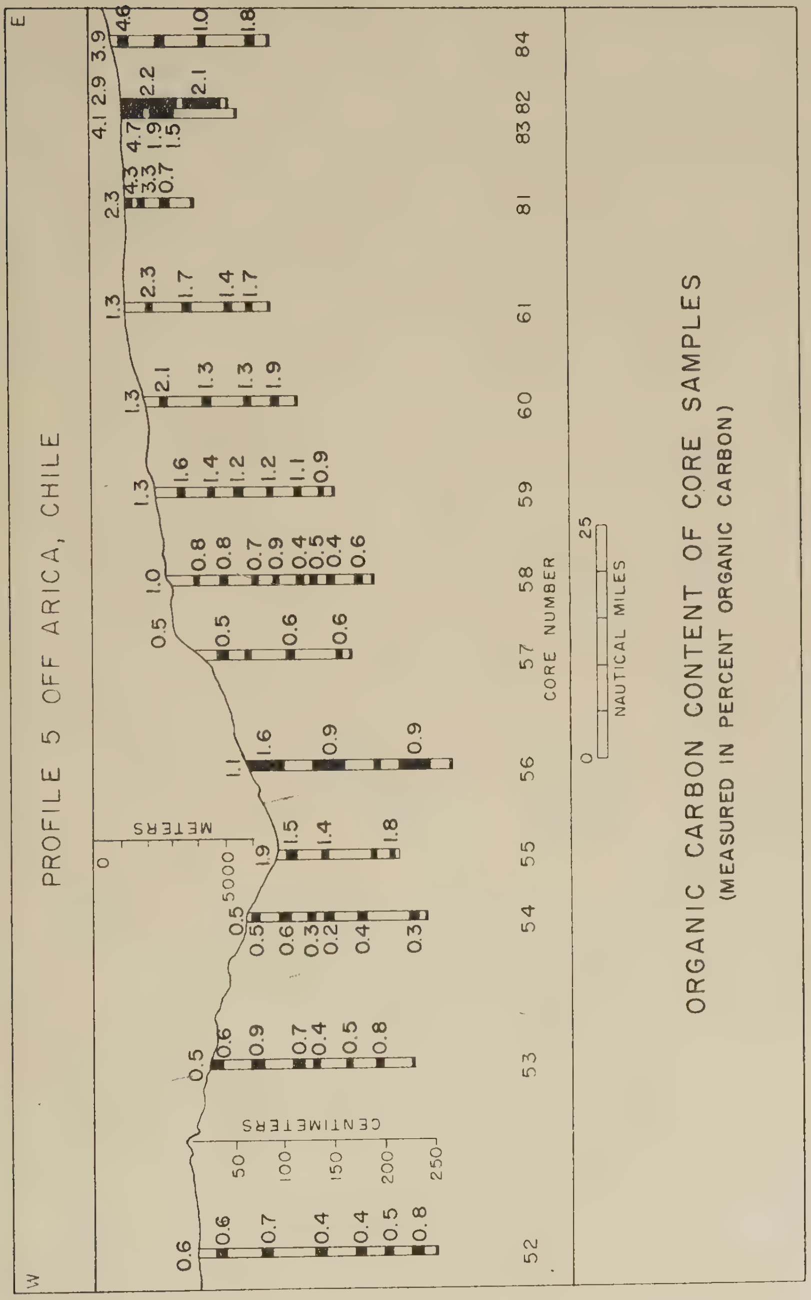

FIG. 11.—*Organic carbon content of core samples along Profile 5 off Arica, Chile.*

SIGNIFICANCE OF RESULTS

The deep trough off the coast of Peru and northern Chile almost certainly is a geosyncline in the making. At present the trough is deepening at a more rapid rate than it is filling. Likewise the adjacent mountains are rising faster than they are eroding. The difference in altitude between the deepest part of the trough and the crest of the adjacent mountains is more than 13,000 meters in some areas. In places this change in altitude lies within a distance of 150 kilometers. The region is very arid. Little or no soil is found, because most of the soil that is formed is eroded by the infrequent but heavy rains. Few intense storms or high waves pound the shore line. Consequently debris supplied the sea either from land or the sea cliffs is relatively small. Along much of the coast, particularly for a few hundred kilometers north and south of Callao, sand is being blown inward from the coast line. Hence, a significant proportion of the debris supplied the sea is recycled on land to be in part again transported to the ocean.

The sediments in the deep trough are relatively coarse, as most of the median diameters are between 2 and 8 microns. As has been pointed out above such a phenomenon seems to be characteristic of deposits that accumulate off arid or semi-arid coasts.

The grain size seems to be independent of the trough. The trough however in places has steep sides. The fathometer record taken while the ship was underway indicated some slopes that might be as steep as 35 to 45 degrees. In fact the fathometer trace along some of the profiles showed sudden steepenings in slope that suggested a series of down-thrown blocks one after the other, with the deepest occupying a graben in the bottom of the trough. Some of the sediments collected on these steeper parts of the bottom were coarser than adjacent sediments, suggesting an effect of the configuration of the sea bottom on the bottom sediments, just as the author has previously reported (Trask, 1932, p. 135). However, the samples were not collected at close enough intervals to indicate whether such a change in grain size is definitely related to bottom profile.

The sorting averages a little more than 3.0, which is about normal for fine-grained marine near-shore sediments, such as are encountered in the present investigation. The relatively high coefficient of sorting of the sediments near shore, with its accompanying skewed size distribution, indicates the presence of two or more populations of grain size of different origin superimposed upon one another. One might think that the major population reflected the normal seaward transport of terrigenous debris and the minor population as representing the effect of subsurface or bottom currents. Persons who take comfort in turbidity currents to explain abnormal size distributions may wish to consider them as factors in the origin of some of these sediments. It is beyond the scope of this paper, however, to discuss turbidity currents as applied to this region.

Over most of the seaward area considered in the present report conditions of sedimentation down to a depth of burial one or two meters have not changed much in the course of the time during which these sediments were being deposited. However, here and there markedly different sediments have been deposited in some places, especially within 25 kilometers of the shore line off the coast of northern Chile. These near-shore sediments vary greatly with depth of burial. As the general region is active orogenically, blocks of the earth's crust in this near-shore area may have been displaced by faulting during the course of time represented by cores. If there is anything to the concept that shape of the sea bottom influences deep currents and thus affects the nature of the sediments, these changes in grain size could be caused by such a situation.

The calcium carbonate content is low. Near shore the carbonate presumably is due to broken shells. If such is the source of the carbonate, one would expect to find small amounts of carbonate along the seaward parts of the profiles where the sediments are of terrigenous origin. But many of the samples contain no measurable carbonate. Perhaps the carbonate particles of the seaward samples dissolve as they settle down through the deep water. The increase in carbonate off shore on the seaward side of the north end of the Peru-Chile Trench presumably reflects a trend toward the development of Globigerina ooze, such as is commonly found off-shore in deep water. The greater content of carbonate in the northern part of the area studied compared with the southern part, thus might reflect greater saturation of the water, especially the deep water, with respect to calcium carbonate (Trask, 1937).

The sediments are rich in organic matter. The region is a well known area of upwelling and produces a large amount of plankton and sea life, as is reflected by the millions of guano birds one sees while cruising in the area. These birds are more plentiful in the vicinity of Callao than near Chile. As their abundance reflects richness of food supply, the productivity of organic matter in the sea must be greater to the north than to the south. Also the productivity likewise must be greater nearer shore than seaward, as is reflected by the greater content of organic matter near shore. This greater productivity near shore is more than indicated by the proportionate increase in organic content, because the rate of sedimentation must be greater near shore where the supply of terrigenous material is greater. Hence each centimeter of deposition near shore represents a shorter interval of time than off shore; so if the organic matter is greater per unit volume of sediment, then the production of organic source material must be correspondingly greater than indicated by the weight-percent increase.

The sediments in this area almost certainly represent potential future source beds of petroleum. Cores 56, 82 and 97, collected from Profiles II' and LL' indicated on Figure 1, according to analyses made by Maxine Brenneman of the Esso Research Laboratory at Linden, New Jersey, on samples kept frozen from the time they were collected until the time they were analyzed, contained hydrocarbons to the extent of 55 to 171 parts per million. The results of these chemical analyses will be reported later in an article by Brenneman and Trask. However, the relatively large amount of hydrocarbons in such sediments is most significant with respect to the origin of oil. The greatest content of hydrocarbons, 171 parts per million of the dried weight of the sediment, was found at a depth burial of one meter in core 56 collected in 6000 meters of water near the bottom of the Peru-Chile Trench off the northern coast of Chile near Arica.

The average carbon nitrogen ratio of 8.4 for the surface sediments indicates that the conditions of accumulation of organic matter are similar to marine sediments in general, which would indicate no special set of conditions of accumulation of organic matter in these sediments. As pointed out earlier the carbon-nitrogen ratio tends to increase with depth. This increase with depth reflects the greater susceptibility of nitrogen to microbial decay than carbon.

As a final conclusion the remark might be made that other than (1) an abnormally high organic content, (2) relatively coarse-grain size of the constituent minerals, and (3) a skewed size distribution the sediments deposited off this arid and mountainous area of South America are similar to near-shore sediments of terrigenous origin in other parts of the world.

REFERENCES

Trask, Parker D. (1932): Origin and environment of source beds of petroleum. Gulf Publishing Co., Houston, Texas, 323 pp.

Trask, Parker D. (1937): Relation of salinity to calcium carbonate content of sediments, *U.S. Geol. Survey, Prof. Paper,* 186-N, pp. 293–299.

Trask, Parker D. (1955): Statement of progress in studies of recent marine sediments, 1939–1954. Recent Marine Sediments, second edition, *Soc. Econ. Paleontologists and Mineralogists,* Tulsa, Oklahoma, pp. xi to lvi.

Zeigler, John, W. D. Athearn, and H. Small (1957): Profiles across the Peru-Chile Trench, *Deep-sea Research,* vol. 4, pp. 238–249.

[*Manuscript received November 2nd,* 1960]

Contribution No. 1145

Särtryck ur Tellus nr 1, 1961

Cloud Patterns in Hurricane Daisy, 1958[1]

By JOANNE S. MALKUS, CLAUDE RONNE and MARGARET CHAFFEE,
Woods Hole Oceanographic Institution, Massachusetts

(Manuscript received November 8, 1960)

Abstract

Maps of clouds in Hurricane Daisy, 1958, have been constructed from aerial ciné photographs made by the aircraft of the National Hurricane Research Project of the U.S. Weather Bureau. Films suitable for quantitative analysis were available for four flights on three separate days during the formation, deepening, and maturity of this small but intense Atlantic hurricane which moved slowly over the ocean in the vicinity of 30° N, 76° W. Clouds were located within 5—10 nautical miles relative to the known aircraft path (in coordinates with origin at hurricane center) by a modified method of aerial photogrammetry using the accurately known times for the image to cross a frame. Horizontal and vertical dimensions of important clouds and cloud forms have been measured to within about 10 %.

The photographic maps are compared to radar analyses made from the same and also different aircraft (U.S. Navy WV-4). The most significant results are first the remarkable persistence of recognizable cloud patterns throughout the three days studied, during which the storm deepened and moved about 200 nautical miles and second, the concentration of convective activity into a few lines of cumulonimbus towers which even on the mature day occupied only about 4 % of the rain area (radius within about 200 nautical miles).

Introduction

Hurricane Daisy, 1958, afforded the first opportunity for a quantitative study of cloud structures during the formation and deepening of a tropical hurricane. The instrumented aircraft of the National Hurricane Research Project of the U.S. Weather Bureau (hereinafter referred to as NHRP) successfully obtained data from several flight levels on August 25, 26, 27, and 28, 1958, in the incipient, deepening, mature, and decay phases of the storm, respectively. The basic measurements were of winds, temperature, and humidity as functions of position as the aircraft executed their prescribed flight patterns. Time-lapse motion pictures (in kodachrome) were made from ciné cameras mounted in the nose of each aircraft; some of the footage was suitable for cloud measurements and mapping. We have undertaken this extensive labor for two main motives: first to provide a quantitative description of the cloud patterns; and second as a test and supplement to numerous calculations concerning individual clouds and their role in the processes of the storm (Malkus, 1960).

Recent hurricane models (see, in particular, Malkus and Riehl, 1960) suggest the important function of convection. The furious winds are driven by latent heat released by giant clouds; their concentrated and highly buoyant character is also apparently essential in the heat and mass transports of the storm. The models envisage that the ascent in the core occurs in extremely restricted regions of undilute, rapidly rising cumulonimbus towers, which only come to occupy a significant fraction of the rain area as the eye wall is approached (MALKUS, 1958). This latter concept has been informally christened the "hot tower hypothesis". Suggested originally by an equatorial trough study (RIEHL and MALKUS, 1958), it is currently being evolved and tested in the hurricane context (RIEHL and MALKUS, 1961). This paper lays a part of the background by presenting results of the cloud mapping.

---

[1] Contribution No. 1145 from the Woods Hole Oceanographic Institution.

The questions we hoped to answer were thus largely focussed on convective clouds. Are there orderly patterns or lines of cumulonimbus, and if so how are these oriented and how persistent are they? How many large cumulonimbus towers occur and are they clustered in particular quadrants or regions of the storm? Is penetrative convection occurring randomly throughout the rain area or is it highly concentrated in small regions separated by wide suppressed zones? What is the origin and distribution of the "cirrus shield" and stratus layers? And finally, how does a picture of the storm we see on a radarscope correspond with that which the eye or camera would behold?

2. The data and method of study

The basic data from which our measurements were made were the NHRP aircraft nose camera films. The most attention was concentrated on the flights of August 25 and 27, the formation and mature days of the storm. These are the days for which extensive budget, dynamic, and energetic calculations have been carried out (RIEHL and MALKUS, 1961) for the storm as a whole and can be used in comparison with the cloud study. On August 25th, three flight levels were flown, but only the upper, or C-level film, had time marks permitting detailed reduction. On August 27th, upper and middle-level flights were made and both have been analyzed herein. A somewhat rougher analysis of the high level flight on the 26th has been included for continuity.

The method of film reduction was adapted to the observational procedures of NHRP and designed to take advantage of the accurate Doppler navigation of their aircraft. Absolute geographic positions were known at all times to within 3—4 nautical miles. The position of the storm center was defined from radar photographs; it was found as a function of time using these, together with a preliminary temperature and wind analysis. All data were then repositioned in terms of coordinates relative to the moving center. The base maps for our cloud study consisted of "plot-outs" for each flight provided by NHRP showing the aircraft track in these coordinates with times entered thereon. Aircraft positions relative to defined storm center are accurate within 1—2 nautical miles.

The detailed procedures of cloud measurement and mapping from the films have been described elsewhere by RONNE (1959) and therefore will be summarized only briefly here. A simplified version of aerial photogrammetry was employed whereby clouds are located relative to the aircraft by measuring the time required to traverse the picture or fixed portions thereof, since the interval between frames was accurately determined. On the three upper-level flights, frames were exposed at an average rate of 50 per minute. A clock appeared continuously in the photographs, permitting the exact rate to be found at each measurement; synchronization with the plot-out was achievable within 30 seconds. Since the aircraft made a ground speed ranging between 6.8 and 7.5 nautical miles per minute, errors in cloud positions (in relative coordinates) did not exceed 4 nautical miles due to this cause. On the one mid-level flight analyzed, intermittent appearances of a watch were supplemented by frame counts from recognized turns in the flight pattern. The frame interval here was electrically fixed at 30 per minute throughout. Although synchronization of film to plot-out may have been off as much as 50 seconds, the slower ground speed of the aircraft (3.4—4.5 n.m. per min.) compensated, and again the resulting error in relative coordinates was never more than 4 nautical miles.

In general, a point on a selected cloud was located on the map by two or more separate fixes upon it from aircraft positions several minutes apart. A large-sized cloud usually required several points to locate it on the map. Horizontal dimensions of smaller ones were readily obtained from distance away, image size, and lens properties. These photogrammetric calculations can be shown to be accurate to about 5 %. Altogether, then, clouds within 50 n.m. of the flight path have been mapped to within about 5 n.m. of their actual (relative to storm center) positions, while those between 50—100 n.m. of the flight path are located within 10 n.m.

The vertical extent of a cloud presented a greater problem, as few were visible in their entirety from base to top. A horizon had therefore to be determined on the film. On August 25 this was not difficult; the actual horizon was visible during large portions of the flight and the aircraft attitude remained steady. Furthermore, an independent height-size relationship from dynamic computations (Malkus, 1960) was available as a test. The top heights for the 25th are thus correct to within about 1000 ft. On the 27th, the horizon was visible less often and the aircraft wobbled more. The heights are thus only accurate to about 2000 ft for those clouds measured precisely. Many others have been indicated as approximately determined. Checks on the horizon were provided by the internal consistency of tower tops at varying distances, several cases of clouds visible from base to top, and one case of distance determination on a cloud whose base was exactly at the bottom of the frame, all with excellent results. A correction for the earth's curvature and atmospheric refraction was introduced for all clouds at distances greater than 10 nautical miles (see Riehl, Gray, Malkus, and Ronne, 1959). Retrospectively, the greatest disadvantage in such a study is not the problem of accuracy, which proved adequate for the purposes desired, but the fantastic labor involved. The maps presented

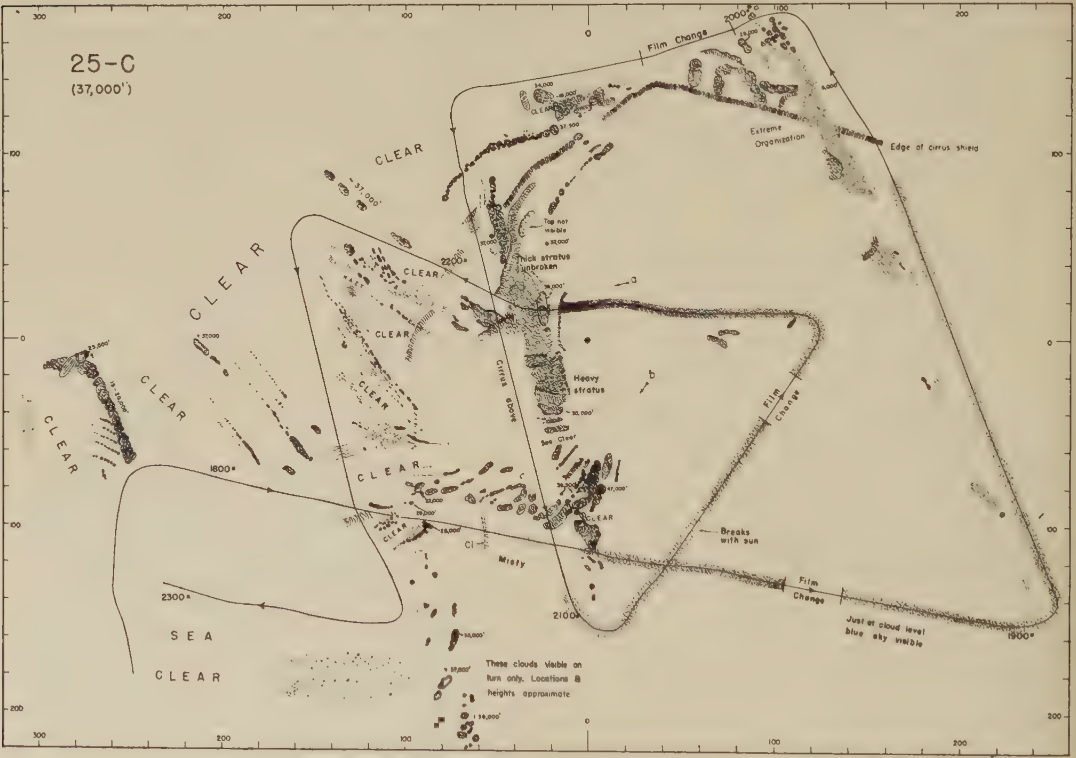
25-C
(37,000')
300
200
100
0
100
200
CLEAR
37,000'
CLEAR
CLEAR
CLEAR
CLEAR
CLEAR
CLEAR
CLEAR
CLEAR R...
25,000'
15-20,000'
37,000
1800
2200
2000
2100
2300
1900
Film Change
Film Change
Film Change
34,000
CLEAR
37,500
Extreme Organization
Edge of cirrus shield
Top not visible
37,000'
32,000
Thick stratus unbroken
38,000'
a
b
Cirrus above
Heavy stratus
~30,000'
Sea Clear
47,000'
CLEAR
22,000
29,000'
28,000'
Ci
Misty
Breaks with sun
Just at cloud level blue sky visible
SEA
CLEAR
These clouds visible on turn only. Locations & heights approximate
34,000'

Fig. 1. Photographic cloud map for Daisy August 25, 1958, constructed from C-level (37,000 ft) NHRP nose camera film. Camera axis aimed 50° to left of flight path, horizontal view angle is about 53°. Coordinates are in nautical miles relative to origin at storm center. Solid line with arrows is flight path, with times (Greenwich or Z) noted every hour. Stippled portion of path denotes "in cloud" and relative darkness is indicated by dot density. Edge of cirrus shield (when above aircraft) denoted by dashed line with perpendicular hatching. Heights of tops of most penetrative cumulonimbi (tops > 37,000 ft) noted. Dotted regions to left of east flight leg are rows of suppressed small cumuli. Arrows marked "a" and "b" are locations and directions of corresponding still photographs shown in Fig. 5, made from mid-level (15,600 ft) flight during same period.

herein required six months full-time effort on the part of three experienced persons; in the future, the reduction time could conceivably be cut in half if the original photographs were taken with this use in mind.

3. Discussion of the cloud maps

The resulting cloud maps for the high-level flights (altitude about 37,000 ft) for August 25, 26, and 27 are shown in Figs. 1—3. The middle-level flight for the 27th (altitude 13,000 ft) is shown by itself in Fig. 4 and in red superposed on the corresponding upper flight in Fig. 6. Fig. 5 shows selected still photographs from the 25th and 27th; their locations and directions are indicated by arrows in Figs. 1, 3, and 4. Pertinent general information concerning hurricane Daisy on these days is summarized in Table I. A detailed presentation of analyses of the NHRP Daisy wind, temperature, and humidity data has been prepared by COLÓN ET AL. (1961).

August 25—Formation Day

The flights on August 25, 1958, explored hurricane Daisy between the hours of 1800—2300 Z or Greenwich Civil Time (1300—1800 EST). The storm was centered near 27° 30′ N, 76° W and was moving northwestward at 7 knots. The central pressure had achieved 997 mb and was thus at the transition point between "tropical storm" and "hurricane"; correspondingly the maximum wind strength had reached 60 knots, just short of hurricane force.

The cloud map is shown in Fig. 1. In studying it, the sampling problem should be brought to mind. On all the upper level flights, the

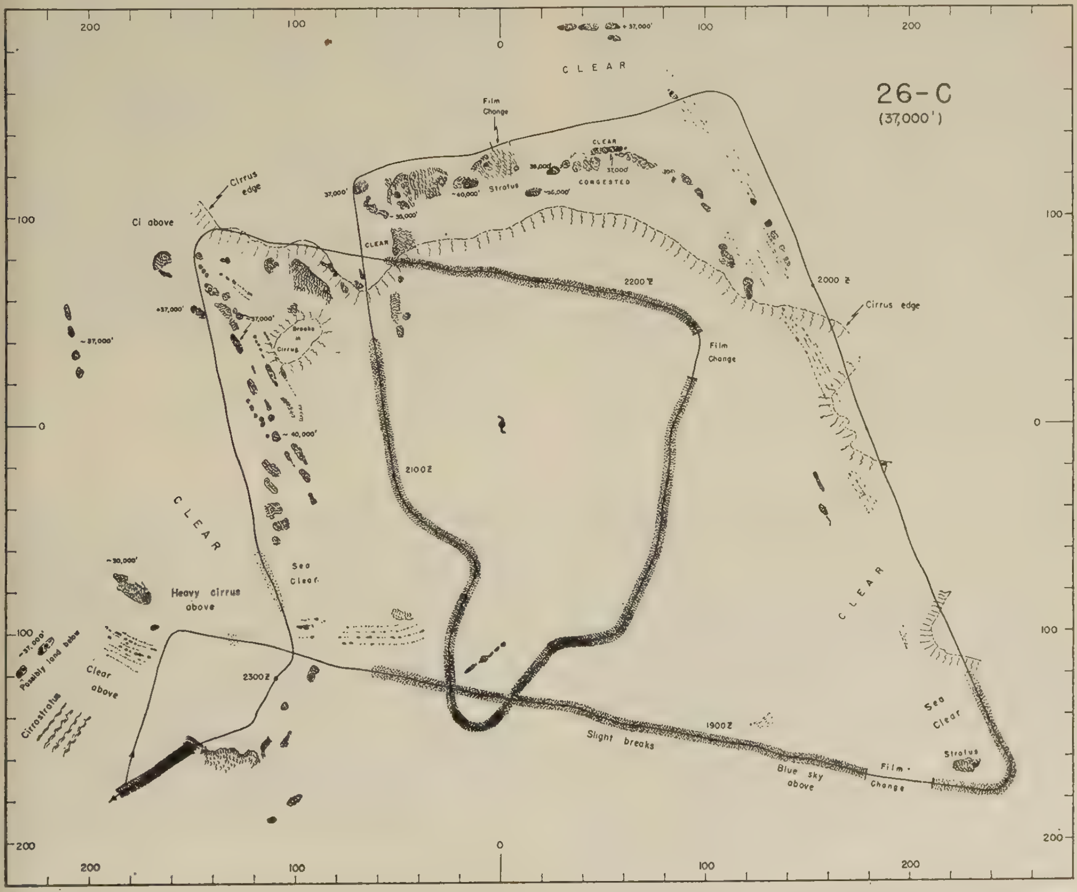
200
100
0
100
200
+37,000'
CLEAR
26-C
(37,000')
Film Change
Cirrus edge
Ci above
37,000'
Stratus
~40,000'
~30,000'
CLEAR
37,000
CONGESTED
~36,000'
2200 Z
2000 Z
Cirrus edge
Film Change
+37,000'
~37,000'
~37,000'
Breaks in Cirrus
~40,000'
2100 Z
CLEAR
Sea Clear
~30,000'
Heavy cirrus above
~37,000'
Possibly land base
Clear above
Cirrostratus
2300 Z
1900 Z
Slight breaks
Blue sky above
Film Change
Stratus
Sea clear
CLEAR

Fig. 2. Photographic cloud map for Daisy August 26, 1958, constructed from C-level (37,000 ft) NHRP nose camera film. Notation, coordinates, and procedure same as Fig. 1.

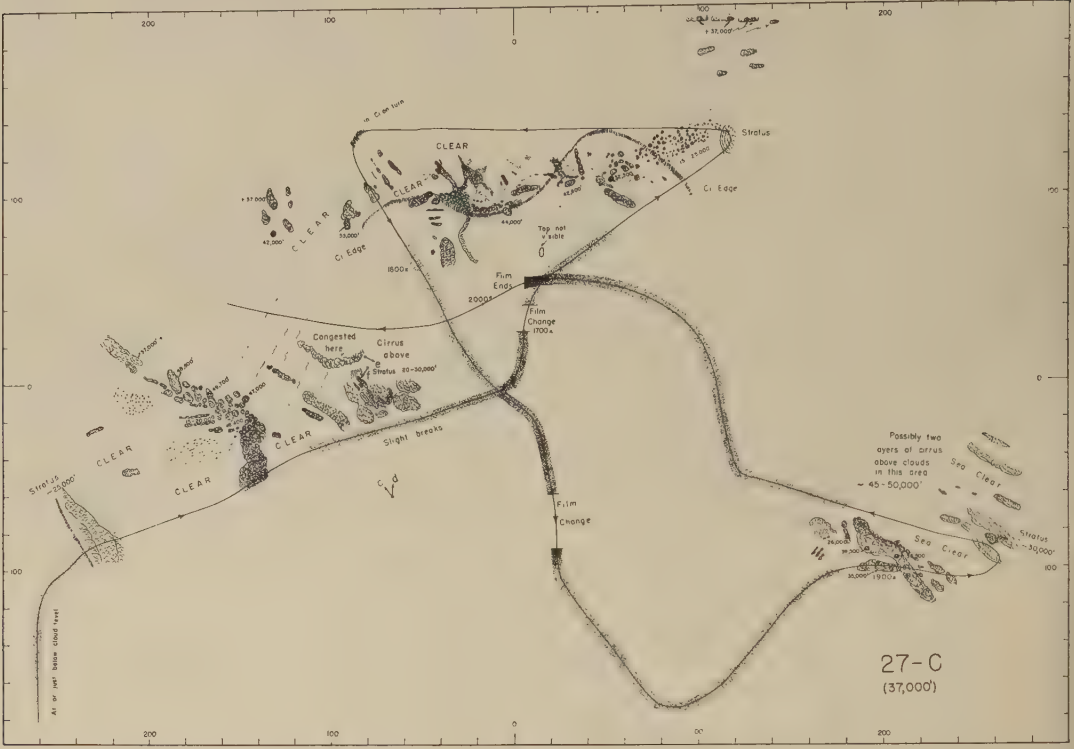
200
100
0
100
200
100
0
100
in Ci on turn
CLEAR
CLEAR
Stratus
25,000
Ci Edge
+37,000'
42,000'
CLEAR
53,000'
Ci Edge
44,000'
42,800
Top not visible
1800z
Film Ends
2000z
Film Change 1700z
Congested here
Cirrus above
e
f
Stratus 20-30,000'
37,000'
49,700
47,000
CLEAR
CLEAR
CLEAR
Slight breaks
Stratus ~25,000'
c
d
At or just below cloud level
Film Change
Possibly two ayers of cirrus above clouds in this area ~ 45-50,000'
Sea Clear
Sea Clear
Stratus ~30,000'
26,000
35,000'
1900z
27-C
(37,000')

Fig. 3. Photographic cloud map for Daisy August 27, 1958, constructed from C-level (37,000 ft) NHRP nose camera film. Notation, coordinates and procedure same as Fig. 1. Arrows marked "c", "d", "e" and "f" are locations and directions of corresponding still photographs shown in Fig. 5, made from mid-level (c and d at 13,000 ft; e and f at 20,000 ft) flight during same period.

camera was pointed 50° to left of straight ahead so that very few clouds to the right of the aircraft's path could be seen. Secondly, the enormous labor of cloud plotting makes it inevitable that the coverage is less than complete, so that the actual cloudiness is always greater than the map suggests. Furthermore, the aircraft was "socked in" by cirrus during approximately 40 % of the time spent in the storm area; actually the lower flights and other evidence suggest that the region covered by cirrus (somewhat more than the southeast quadrant) was the most active portion of the storm, in terms of convective activity, precipitation, and wind speeds. These reservations must be kept in mind in drawing conclusions from our results. Our procedure in mapping was to concentrate on accurate locations of all visible well-delineated cumulonimbus towers reaching flight level and above, and upon accurate mapping of the cirrus shield. Samplings and height ranges of groups of middle level cumulus were taken wherever possible, and the organization of smaller suppressed cumuliform clouds was noted schematically in the proper locations. Stratus decks were entered schematically wherever these were prominent.

Cumulonimbus structure

The highest cumulonimbus tower seen was at 47,000 ft; it had an active, rounded top, 6 km across, located 80 n.m. due south of the center. About fourteen penetrative towers reaching above flight altitude (tops above 37,000 ft) were mapped. This sample permits us to estimate roughly the total number of towering cumulonimbi in the rain area. One-third of the rain area (radius 200 n.m.) was rendered invisible by cirrus. About one-half of the remaining two thirds was sampled by the camera. Therefore, if the unsampled portions were no more productive of cumulonimbi than the sampled portions, about forty towers in the active or just dying phase might be ex-

Fig. 5. Series of still photographs illustrating visual character of hurricane Daisy, a and b for August 25, remainder for August 27.

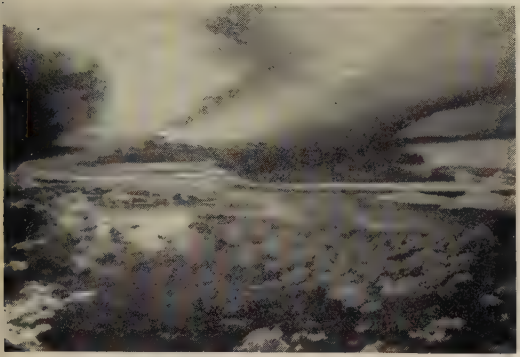

a. Still photograph, located and oriented as shown by arrow in Fig. 1. Time: 2143 Z, August 25, 1958. Made from mid-level aircraft at 15,600 ft.

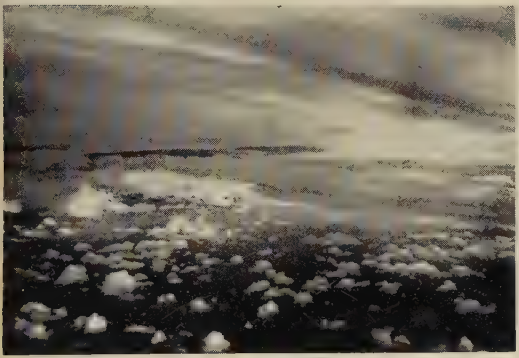

b. Still photograph, located and oriented (approximately) as shown by arrow in Fig. 1. Time: About 2330 Z, August 25, 1958. Made from mid-level aircraft at 15,600 ft.

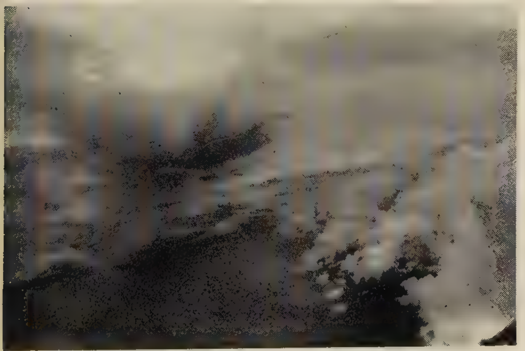

c. Still photograph, located and oriented as shown by arrows in Figs. 3 and 4. Time: 1544 Z, August 27, 1958. Made from mid-level aircraft at 13,000 ft.

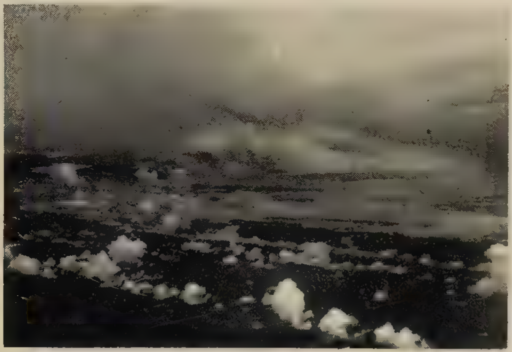

d. Still photograph, located and oriented as shown by arrows in Figs. 3 and 4. Time: 1544 Z, August 27, 1958. Made from mid-level aircraft at 13,000 ft.

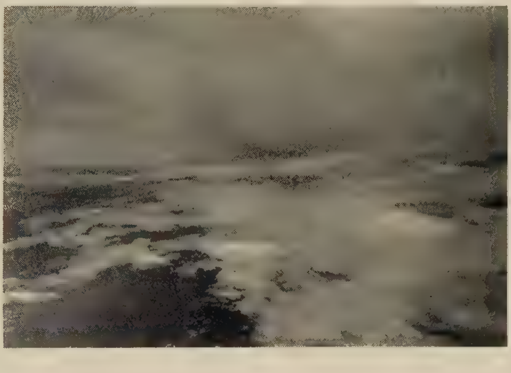

e. Still photograph, located and oriented as shown by arrows in Figs. 3 and 4. Time: 2048 Z, August 27, 1958. Made from continuation of mid-level flight at 20,000 ft.

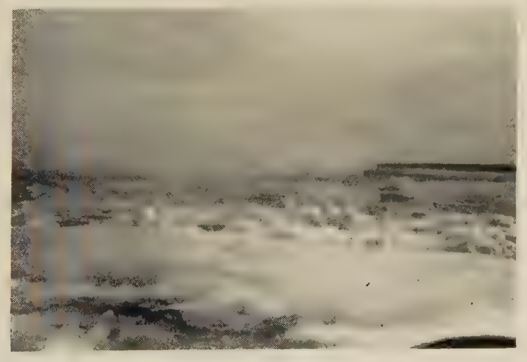

f. Still photograph, located and oriented as shown by arrows in Figs. 3 and 4. Time: 2050 Z, August 27, 1958. Made from continuation of mid-level flight at 20,000 ft.

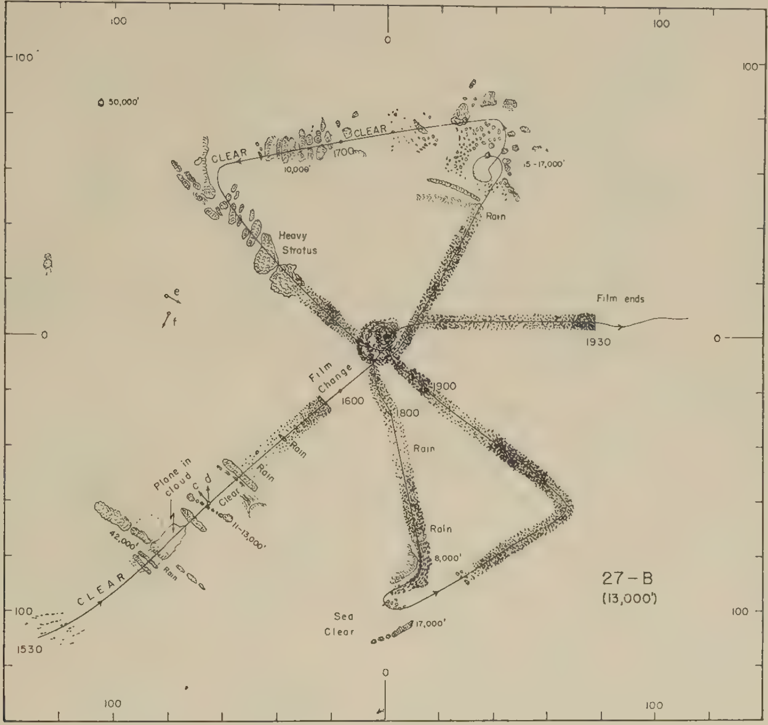

Fig. 4. Photographic cloud map for Daisy August 27, 1958, constructed from the B-level (13,000 ft) NHRP nose camera film. Notation, scale, coordinates and procedure same as Figs. 1—3, except for difference in aircraft, flight path, altitude, and camera orientation. The mid-level nose camera was aimed straight ahead. Arrows marked "c" and "d" denote corresponding still photographs in Fig. 5 taken on this flight, arrows marked "e" and "f" denote last two stills in Fig. 5 which were taken from a higher-level (20,000 ft) continuation of this flight not covered by the ciné film.

pected. Actually, since the eye wall and most active third of the rain area were those parts not sampled, we estimate the number as nearer sixty, since the lower level films suggest that the actively convecting regions were about twice as close together in the cirrus-covered region.

The cumulonimbus towers were clearly concentrated in widely separated rows, approximately parallel to the low-level flow, although the continuous "spiral band" character was both much less than ideal and less pronounced than that observed in hurricane Cleo a week previous (now being studied). The main row visible to the camera was found just south of the northern flight leg. Along this leg its distance from the center decreased from about 160 n.m. at the eastern end to 120 n.m. at the western. Later the radar comparison will suggest that this band spiralled into the eye wall on its west side, with a break to more suppressed cloud material occurring between 80 and 40 n.m. north-northwest of the center. The highly congested region 80 n.m. to the south of the center which contained the tallest (47,000 ft) tower was apparently a fragment of a second band which may have spiralled in to the eye wall on the east side. With the exception of an interrupted line of widely separated towers oriented northwest—southeast about 160 n.m. out in the southwest quadrant, and a faint suggestion of what could have been another distant partial band more than 200 n.m. to the north, these were all the "hot towers" which were visible on the film. We may therefore conclude that penetrative convection was extremely highly concentrated into very restricted regions, which in

Table 1. Hurricane Daisy

Date	Time of C Flight	Location of Center	Central Pressure	Maximum Wind	Movement of Storm Center
Aug. 25	1800—2300 Z	27°30′N; 76°W	997 mb	60 kt	7 kt, to NW
Aug. 26	1800—2300 Z	28°30′N; 76°50′W	972 mb	90 kt	3 kt, to NNE
Aug. 27	1600—2100 Z	29°30′N; 75°20′W	950 mb	115 kt	8 kt, to NE

turn were lined up with the low-level flow in widely separated rows; altogether not more than 1 % of the rain area within 200 n.m. can have been occupied with active towers at this level and at this time.

A remarkable and unexpected feature of the penetrative cloud structure on this flight was its persistence. For example, the group of cumulonimbi to the south of the center containing the 47,000 ft buildup and at least one more up to flight level was first observed on the entering leg at about 1830 Z although the aircraft went into cirrus too soon for a measurement on them at that time. The measurements were actually made on the southward leg (which terminated at 2100 Z) 2½ hours later, when remarkably enough, the cloud group had very nearly the same appearance, including a giant buildup! It will be recalled that the storm had moved some 12—13 n.m. in that time and thus this persistent cloud feature cannot be attributed to any fixed oceanic or geographic influence. Furthermore, the nearest Bahama Islands were 40—50 n.m. from this locality (see Fig. 7). From our knowledge of the life spans of non-hurricane cumulonimbi (Malkus and Ronne, 1954), it is questionable whether the same cloud was seen on both legs; alternatively this spot, relative to storm center, may have been a preferred one for cumulonimbus production.

Another apparently persistent cumulonimbus was the 38,000 ft one passed through by the aircraft just northwest of the eye at 2155 Z, which was also located and measured on the southward leg at 2030 Z, or nearly 1½ hours earlier. This cloud apparently moved 10—15 n.m. toward the south in the interval and it is therefore not certain whether it was the same cumulonimbus, moving downwind at about one-third the low-level wind speed, or a new one regenerated in nearly the same spot, relative to storm coordinates. However, the appearance of the cloud in this location shown in the still photograph (Fig. 5a) from the mid-level flight at 2143 Z is recognizably similar to that on the nose camera film at 2030 Z, except for aging of the top and spreading out of the anvil.

If, in fact, it turns out upon further study that there are preferred spots for tower generation which remain relatively fixed in storm coordinates, this is a significant matter. It may be related to meso-scale wind and temperature streakiness and may further hold the key to interaction between the convective structure and the large-scale dynamics of the storm.

Eye

The high-level flight made no eye traverses on this day, although the lower flights and observers' reports record that throughout Daisy's history it was very small (about 10—15 n.m. diameter), and cloudy. The eye and wall cloud will be discussed later in connection with the radar.

Cirrus

Cirrus was first encountered by the aircraft on the entrance leg 160 n.m. from the storm center. It was in the form of streamers, oriented approximately north-south. Where the stippled region on the map begins, the plane entered cirrus at flight level and remained "socked in" almost to the northeast corner of the pattern. The edge of the cirrus (above flight level) is marked along that leg; it continued, in a banded and broken manner to the west of the storm center where it ended less than 100 n.m. from the eye wall, in contrast to its greater than 200 n.m. extent on the east side. In addition to its pronounced asymmetry on the 25th, the cirrus was not generally well organized into a uniform "shield" but was frequently in the form of streamers apparently emanating from the eye wall and congested regions of cumulonimbus such as the one 80

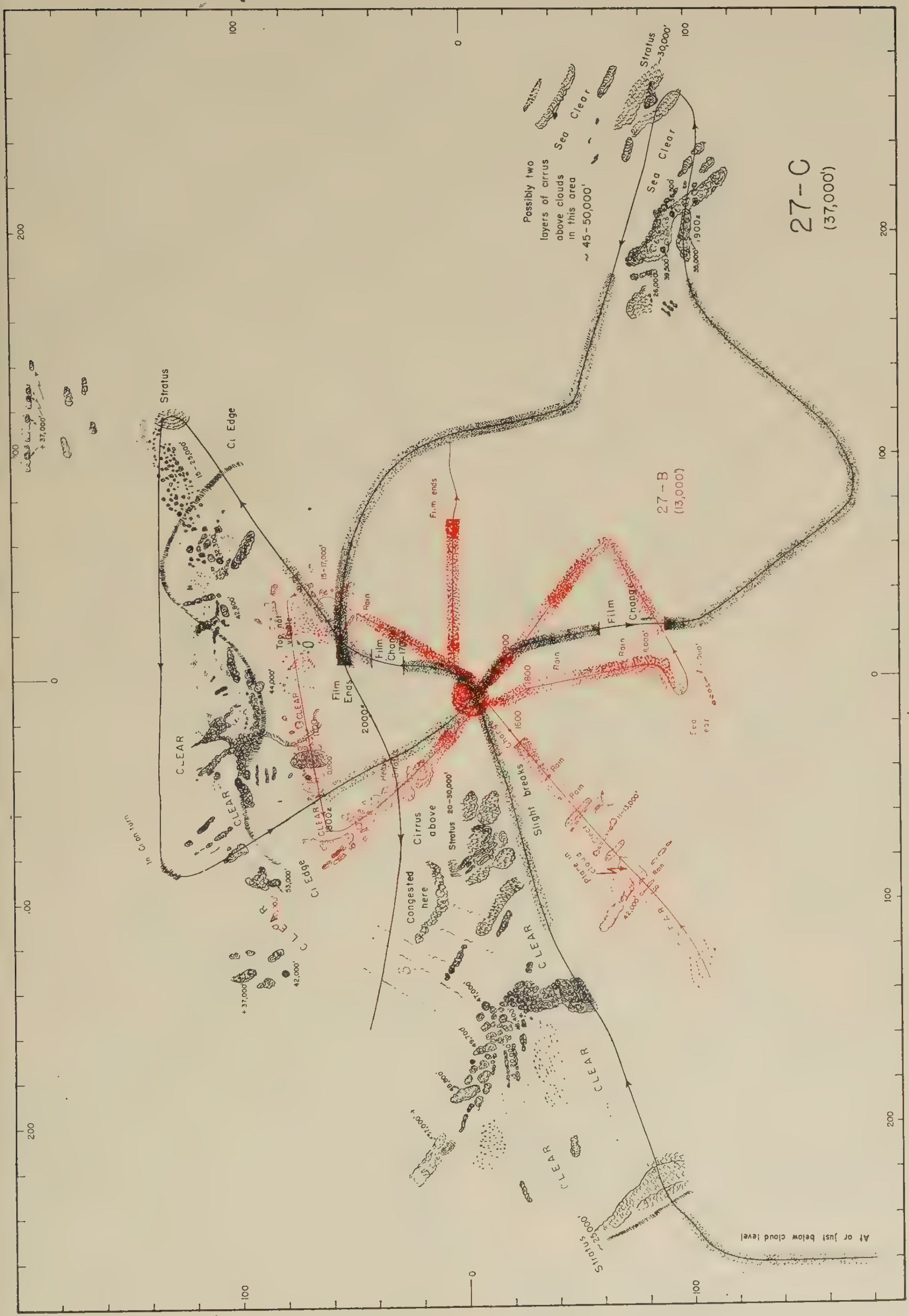
27-C
(37,000')
27-B
(13,000')
Possibly two layers of cirrus above clouds in this area ~45-50,000'
Sea Clear
Sea Clear
Stratus
Stratus
Ci Edge
Ci Edge
CLEAR
CLEAR
CLEAR
CLEAR
CLEAR
Film Ends
Film ends
Film Change
Film Change
Rain
Rain
Rain
Rain
Top not visible
Cirrus above Stratus 20-30,000'
Congested here
Slight breaks
In Ci on turn
At or just below cloud level
+37,000'
42,000'
53,000'
44,000'
15-17,000'
15-25,000'
0
100
200

Fig. 6. Mid-level cloud map (red) for Daisy, August 27 (previous Fig. 4) superimposed on high-level cloud map for August 27 (previous Fig. 3).

n.m. to the south of the center (contrast Figs. 5a and b with 5f made two days later on August 27th).

Summary of cloud features on August 25

The cloud configuration on the 25th was apparently in a transitional stage from the deep easterly wave type (examples mapped elsewhere by this group, i.e. report by Riehl, Gray, Malkus, and Ronne, 1959) which is extremely asymmetrical, with the huge buildups and cirrus confined to a convection zone to the rear side (generally the east) and the full hurricane in which the distributions are generally more symmetrical about the center. It will be seen, however, that even on Daisy 25, the cloud patterns far more closely resembled those of Daisy 26th and 27th, than they did either the deep easterly wave or any other disturbance so far studied.

Visible cumulus congestus (tops 10—25,000 ft) were considerably rarer than in the easterly wave, although on Daisy 25 they were more common than later on in the storm. They were not seen inward of 100 n.m. except in the neighborhood of cumulonimbi. The visible parts of the inner rain area ($r < 100$ n.m.) were characterized by alternation between very restricted regions of huge buildups and much wider suppressed regions with two or more stratus layers (often very broken) showing scud and intermittent lines of suppressed cumuli below, as contrasted by the photographs in Figs. 5a and 5b. The stunted cumuli were particularly pronounced throughout the eastern flight leg; wherever one could see downward, the sea surface was obscured by small highly-organized rows of them lined up approximately from south-southeast to north-northwest, or parallel to the low-level flow.

The western portion of the "rain area" was very much freer of cloud than the eastern, with little or no precipitation beyond 40 n.m. from the center, except for a line of showering congestus nearly 260 n.m. out. This region contained mainly streaky cirrus aloft and rows of suppressed cumuli below, with wide patches of visible blue sea and sky.

August 26—Deepening Day

The high-level flight on August 26th took place just 24 hours after that of the 25th. The flight patterns flown were very similar. The storm had moved 95 n.m. to the northwest and was just at the re-curvature point, with a travel velocity of 3 knots to the north-northeast. It had deepened to show a central pressure of 972 mb; the flights on the 26th were made very close to the time of most rapid deepening. The maximum wind was now 90 knots, but speeds in excess of hurricane force covered only a very small region in the eye wall.

The cloud map constructed from the upper level flight is shown in Fig. 2. It was made with somewhat less detail and precision in height measurements than those of the 25th and 27th for the two reasons that a) nearly 60 % of the flight time was spent socked in by cirrus and b) this day has not been used (as yet) for overall storm computations and hence soundings, budgets, and plots of other important variables were less accessible for checks and comparisons.

Cumulonimbus structure

Despite the very small sampling by the camera (about 20 % of the area wherein $r < 200$ n.m., almost none of this in the inner rain area, where $r < 100$ n.m.) on the 26th, the resemblance of what can be seen of the cumulonimbus structure to that of the 25th is striking. In particular the line of cumulonimbus just south of the north flight leg is present twenty-four hours later at identical radius from the storm center. The changes in cumulonimbus structure are twofold: toward more and bigger buildups and toward a more symmetrical distribution about the storm center. There are now 16 towers visible above flight level. Taking into account the proportion of area sampled, we estimate a total of 80 buildups by pure extrapolation, or 144 if we assume that the unsampled inner area is twice as productive as that sampled. The main visible line of cumulonimbi contains at least twice as many penetrative ($>$ 37,000 ft) towers as on the 25th and has extended itself (in relative coordinates) westward, with a 37,000 ft tower just at the western turn which was definitely not present on the 25th. The final (westernmost, flying southward) flight leg revealed 8 towers above flight level, as indicated, in a region which had only suppressed lines of cumulus previously, indicating a symmetrizing of the storm's convection with time by developments in the western quadrants. Finally, a line of at

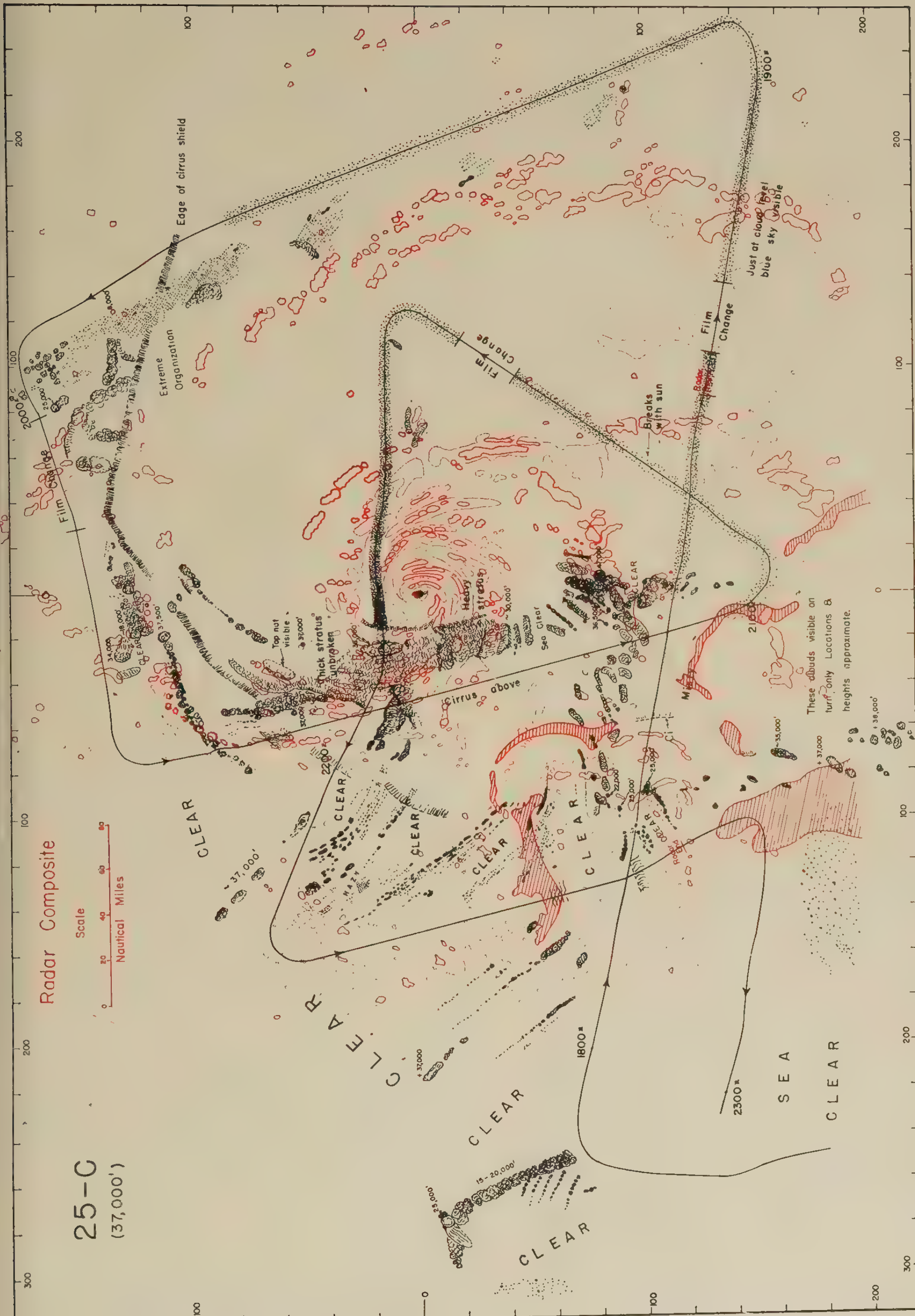
Radar Composite
Scale
Nautical Miles
0
20
40
60
80
25-C
(37,000')
Edge of cirrus shield
Extreme Organization
Film Change
Film Change
Film Change
Just at cloud level blue sky visible
1900Z
2000Z
2100Z
2200Z
1800Z
2300Z
Breaks with sun
Heavy stratus
Thick stratus unbroken
Top not visible
Cirrus above
Clear Sea
These clouds visible on turn only Locations & heights approximate.
CLEAR
HAZE
SEA
37,000'
15-20,000'
25,000'
34,000'
35,000'
36,000'
38,000'
100
200
300

Fig. 7. Radar composite for Daisy August 25 in red superimposed on high-level cloud map (previous Fig. 1). The radar composite was prepared by W. S. Gray from the same NHRP C-level flight (using APS-64 3 cm radar) as was the cloud map; it was constructed by tracing a projected enlargement of successive frames of the radarscope movie film. Regions outlined by solid lines are "hard core" echoes, while those outlined by lighter dotted lines were more diffuse or fainter. The hatched regions are the Bahama Islands.

007469 Sep.

least four towers above flight level was now seen far (≥ 200 n.m. from center) to the north of the north leg, suggesting that expansion of the active convection zone was also occurring. Using the figure of 144 penetrative clouds within $r < 200$ n.m. we compute that the area coverage by hot towers is now approximately 2 ½ % at this level.

Cirrus

On the whole, the cirrus distribution on the 26th was remarkably similar to that on the 25th; it dominated the flight in the southeastern portion and showed the same lowering or thinning just as the aircraft approached the southeastern turn. The main changes were toward greater symmetry about the storm center and consolidation into a more uniform "shield" in contrast to the somewhat streaky or banded structure frequently encountered on the formation day.

The shield had actually retreated somewhat on the east leg, which was no longer truly socked in, and on the north leg also, where its outer boundary was 20—30 n.m. nearer storm center. On the west side, on the other hand, it had markedly spread and consolidated. The inner western leg ($\sim$ 40 n.m. west of center) was now wholly socked in, and the outer western leg had banded and broken cirrus above the plane. The cirrostratus and cirrus in the extreme southwestern corner of the map was separated from the main hurricane cirrus by a band of blue sky above, at least 20 n.m. across. This "clear ring" to the southwest persisted throughout the three days at a radius of about 200 n.m. and may have marked the outer boundary of the storm convergence.

Summary of cloud features on August 26

Hurricane Daisy appeared to retain her individual cloud characteristics on the deepening day; these, however, showed further development from tropical wave to true hurricane by becoming a) more symmetrical, b) more productive of penetrative towers, both where found previously and in new places, particularly spreading into the previously inactive western quadrants and outward, at least to the north and c) more organized in both cirrus and convective structure. By the latter, we mean that fewer groups of cumulus congestus were seen scattered in the rain area; the upmotions appeared more concentrated in hot towers, separated by spreading layers of alto-stratus (now increasingly predominant on the north leg), below which were found either scud or organized rows of suppressed cumuli. This type of organization was also found on our previous Pacific study (Riehl, Gray, Malkus, and Ronne, 1959, see cloud code types 13—16) characterizing severely disturbed or typhoon situations.

August 27—Mature Day

The middle and high-level flights on the 27th occurred between about 1600—2100 Z. The storm was located at 29° 30′ N, 75° 20′ W. In the 22 hour interval since the flights on the 26th, the center had moved 115 n.m. toward the northeast; it was now travelling in this direction at 8 knots, having accelerated somewhat after recurvature. The flights on the 27th encountered hurricane Daisy at her maximum development. The central pressure attained its minimal value of about 950 mb at this time, although the strongest winds did not appear to match this low pressure, since they exceed 100 knots only in a narrow region in the southeastern segment of the eye wall. On this day the upper flight performed a fairly similar pattern to the previous two, but unfortunately the exit leg was lost due to the film having ended just before 2000 Z. The aircraft was socked in by cirrus about 50 % of its time in the storm area. The results of the upper flight are shown in Fig. 3. Fortunately on this day the middle level flight had adequate time checks for reduction; its map is shown separately in Fig. 4 and superposed (in red) on the upper level flight map in Fig. 6.

Cumulonimbus Structure

Again the striking feature of the cumulonimbus structure is its pronounced resemblance, with gradual evolution, to that of the preceding two days. On the day of maximum intensity, hurricane Daisy showed a row of cumulonimbus towers just to the south of the northern flight leg, a highly congested active precipitation zone 80 n.m. due south of the center (see Fig. 4), and another row of active towers 150 miles west-southwest of the center. The first two of these features had persisted in nearly the same location relative to the storm center from the formation day on the 25th! The row of cumulonimbi in the western sector had only one member on the 25th, showed two or three on the 26th and now on the 27th had at least five towers with tops above 37,000 ft.

Development toward greater symmetry and more buildups was also apparent in the north line, which had extended further into the northwest quadrant and was slightly closer to storm center than previously. This line contained the tallest tower measured, which from the B flight (13,000 ft) came out to be 50,000 ft at 1700 Z, and from the C flight was topped at 53,000 ft about a half hour later. Whether the change was due to growth or errors in one or both measurements is not possible to say, although the tower appeared to be still rounded and rising at 1700 Z. The northernmost line was also still visible on the 27th, in about the same relative location and state of development as on the 26th. In addition, part of another cumulonimbus line was now visible about 200 n.m. out from center in the southeast quadrant; this was a region in which the aircraft had been socked in by cirrus on the previous two days.

Not more than 20 % of the rain area ($r <$ 200 n.m.) was seen by the camera on the mature day. We can furthermore be confident that on this day the "socked in" regions of the C flight were, in fact, the most convectively active portions of the rain area. The B flight (Figs. 4 and 6) shows clearly that the very black, rainiest, and bumpy portions of the storm were in the eye wall region and the southeast quadrant, and that therein these were spaced about twice as closely together as the visible cumulonimbus rows in the outer portions mapped. Since we counted 22 cumulonimbus towers above flight level on the C flight, we therefore estimate the total number of penetrative hot towers to be not less than 200. Hot towers may therefore cover about 4 % of the rain area at this level on the mature day of hurricane Daisy.

Cirrus

The cirrus shield also showed the same general character and distribution as previously, with gradual evolution toward consolidation and symmetrization, which were presumably at a maximum on the 27th. After that the storm began to accelerate northward and out of the tropics.

The cirrus shield at flight level had retreated on the east leg somewhat farther toward the center than on the 26th, but above the aircraft cirrus extended outward to at least a radius of 300 n.m. (where visible on the southeast turn). There was a real indication of a higher cirrus layer (55—60,000 ft) above the extension of the main shield which rose from flight level to about 45,000 ft on the corner.

To the north of storm center, the cirrus shield had shown little change in the three days and was on the 27th of about the same extent as on the 25th; however it had spread considerably to westward, now overlying the entire northwest quadrant in a continuous sheet reaching a radius of 100 n.m. (see Figs. 5e and f). Outward of that, banded cirrus extended about another 40 miles, with the bands aligned roughly north—south. Still, however, the entire western cirrus structure was less dense and less well developed than that in the southeast quadrant.

Other cloud features on August 27

The B-level map (13,000 ft. Fig. 4) provided a valuable supplementation; in particular it showed what was below the cirrus in the active southeast quadrant. The mid-level aircraft also performed numerous circles in the eye wall. The photographs showed there the blackest, most turbulent and rainy conditions encountered. That extraordinarily intense and penetrative convection, even for a hurricane, was occurring there was substantiated by the August 27th radar (see Jordan, Hurt and Lowrey, 1960) which shows that the eye wall contained cumulonimbus towers up to at least 60,000 ft. We may therefore use the pictures there as a rough calibration for the remaining B film. The next blackest, rainiest, and most convectively active region was found about 80 n.m. south of the center, in nearly the same relative location as the huge towers on the 25th. The photographic and radar evidence suggest this was a part of a well-developed line which in the southeast quadrant had a radius of 45 n.m. and spiralled gradually into the eye wall from the northwest.

More stratus layers were now present than previously; the northern flight leg on the B flight ($r \sim 65$ n.m.) passed between two of these in a convectively inactive region. Concentration of convection was a maximum on this day, with the eye wall and a few pronounced bands in the rain area accomplishing all of it; no congesti were found except in the close vicinity of these bands.

The photographs shown in Figs. 5c and d were made on the entrance leg of this flight (see Fig. 4 for location) and 5e and f were made on its continuation at 20,000 ft altitude after the movie film had ended. These stills were all made in the western sector of the storm, which was relatively cloud-free on the 25th, emphasizing the trend toward symmetrization. The generally blacker appearance, heavier stratus layers, and more suppressed low-level convection are obvious in contrast with Figs. 5a and b from the 25th. At the B-level on the 27th, individual hot towers were largely obscured by stratus and rain, and with one or two exceptions, could only be picked out clearly on the high-level flight.

Summary of Daisy's Visual Cloud Distributions on the Three Days

By far the outstanding result of the photographic mapping of Daisy's visible cloud distribution was the persistence, in the same relative locations, of definite cloud patterns. This persistence was notable both between legs on the same flight, separated by hours, and, even more remarkably, over the entire three days. While these cloud patterns showed gradual evolution during the period studied from those resembling a deep easterly wave to those characteristic of a member of the species hurricane, persons who have looked at films from several hurricanes would never have confused Daisy with any of the others; her aspect remained as peculiarly her own as does a human's physical appearance.

Of significance in particular is the persistence of the lines or spiral bands of cumulonimbus in the same relative coordinate position over 48 hours, despite a travel of the storm some 200 n.m. If this feature proves characteristic of many hurricanes it may be one of the most potentially important revealed to date. The implication is that some kind of stable interaction between convective and hurricane scale motions is taking place such that clouds are continually regenerated in a few relative coordinate locations and suppressed elsewhere.

A puzzling outcome of this first endeavor of quantitative mapping of clouds in a hurricane over days is the quite different impression produced by our results from that discussed by most radar meteorologists concerning persistence versus fluctuations in patterns. The common impression among radar experts who have studied hurricanes seems to be the transience in both the life of individual echoes and their arrangement. We believe that an urgent need in future hurricane studies is a systematic comparison between radar and photographic maps, both at single instants and over periods of time. In the next section we have made a preliminary effort to make such a comparison for Daisy.

4. Comparison of the photographic maps with radar pictures

The radar data which will be compared with our maps herein have been taken primarily from a fine study by JORDAN, HURT, and LOWREY (1960) who participated in an operational reconnaissance flight into Daisy on August 27th in a radar Constellation of the U.S. Navy Airborne Early Warning Squadron Four (WV-4). Their paper shows selected photographs of its radarscope and also a few from the radar of the upper-level NHRP aircraft on the same day, for which our photographic map is Fig. 3. Fortunately, we also had one radar map available from August 25th, composited by W. S. Gray from the radar of the high-level NHRP aircraft, whose nose camera film was used to prepare Fig. 1. We should like to emphasize that our presentation in this section is only a fraction of what could and should be done with radar analysis on Daisy; many more thousands of feet of radar film are on file at NHRP and, in particular, August 26th has not yet been worked up.

Comparison for August 25th

Fig. 7 shows Gray's radar composite (in red) superposed upon our cloud map shown previously in Fig. 1. Unfortunately there was a synchronization problem, since the clock in the radar frames was running 30 seconds behind the plot-out at the start and 60 seconds behind it at the end of the flight portion mapped. Resulting relative coordinate errors in the radar chart would thus grow from about 3 n.m. to 6 n.m. by the later flight legs. We have corrected some but not all of these errors in positions of large clouds after 2020 Z (final turn on north leg).

The radar in the C-level aircraft was a 3 cm set (APS-64) which operates at a fairly low power output. According to JORDAN ET AL., the energy from this installation "is sent out in a very broad beam below the aircraft but because of the location of the radome, none of the energy is sent out above the horizontal. Therefore the echoes shown can be considered as the integrated effect of the return from hydrometeors in the surface to 37,000 ft layer."

The comparison in Fig. 7 is extremely illuminating and valuably supplements the photographic map. We see that even on the 25th, the cumulonimbus-producing region 80 n.m. south of the center is the outer edge of a band spiralling into the eye wall on the northwest side. We also learn that the cumulonimbus line to the north, which the photography located on all three days, is part of a very long spiral arm extending roughly north-south slightly west of the eastern flight leg and crossing the south leg just inward of the southeast corner. Interestingly enough, this is exactly where the cumulonimbus towers were revealed by retreat of the cirrus on the 27th (Fig. 3), supporting our supposition that this, too, was a persistent feature. There is a relative scarcity of echoes on the western side, as already suggested by the pictures.

On the whole, the correspondence between hard core echoes and penetrative cumulus is good, but by no means perfect. There were a few visual penetrative buildups, even some reaching above 37,000 ft, which do not appear on the radar map. Conversely, in the well-sampled areas there were occasional hard cores with which cumulus towers were apparently not associated, although the later non-correspondence is less certain than the former due to obscuring of the field of view on the film by stratus, nearer clouds, etc. It appears likely, in close examination of the region just west of the eye (from about 100 n.m. north to 100 n.m. south) that some echoes coded as "hard core" may have had their origin from hydrometeors in heavy stratus. However, since this region was generously larded with penetrative towers, a conclusion that this type of echo came from "stratus precipitation" might be quite false.

The echoes delineated by lighter dotted red lines were dimmer and more diffuse than those called "hard core". The shape and distribution of these near the hard core echoes makes it likely that they were also convective in origin (shorter, older, less wet clouds, or smaller drop sizes, perhaps). Thus precipitation from stratus (without nearby convection) either was predominantly absent on the 25th, or so undeveloped that this radar set did not detect it. The nose camera film supports this; stratus sheets were rarer, less murky, and less extensive on the 25th than on the succeeding two days.

A calculation by Mr. R. H. Simpson[1] of the fraction of the rain area covered by all radar echoes on this day gave 22 %, over equal area radial intervals out to 55 n.m. The fraction so covered by hard core echoes was a uniform 6 %. It is interesting to note that the latter figure is six times greater than our maximum estimate from the photographic map of area covered by penetrative cumulonimbus (tops above 37,000) towers.

Comparison for August 27th

The PPI presentations on the paper of JORDAN ET AL. were from two different radar sets and installations, one being that of the NHRP described above. The others were from an APS-20E set mounted in the U.S. Navy WV-4 (Lockheed Super-Constellation radar reconnaissance aircraft). The latter is, according to them, "a very high-powered set which operates at a wavelength near 10 cm with a maximum range of 250 miles" and is much less affected by attenuation than sets of shorter wavelengths. The vertical width of the beam is 6° and variable gain, antenna tilt and position of aircraft result in the fact that different layers, intensities of echoes, and portions of the storm are seen as these are varied. JORDAN ET AL. have presented an excellent critique of these in each scope photograph they reproduced, which will be accepted without modification here.

Perusal of the radar photographs of JORDAN ET AL. might lead the casual reader to conclude

---

[1] During a graduate class analysis of Daisy conducted at the University of Chicago in January 1959 by Professor Herbert Riehl.

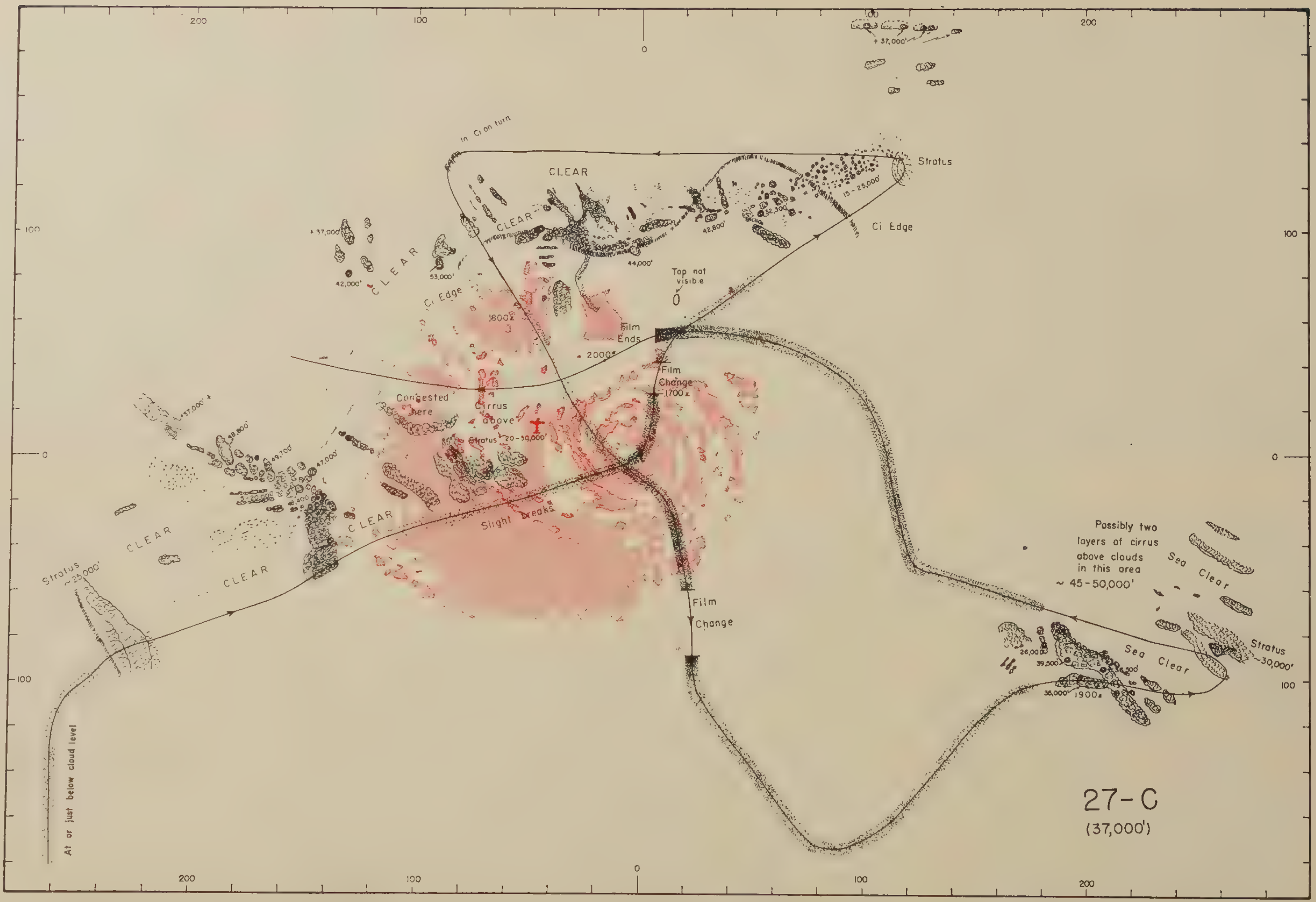
27-C
(37,000')
200
100
0
100
200
Stratus
Ci Edge
CLEAR
In Ci on turn
15-25,000'
32,300'
42,800'
44,000'
Top not visible
Film Ends
2000z
1800z
Film Change 1700z
+37,000'
42,000'
53,000'
Ci Edge
Contested here
Cirrus above
Stratus 20-30,000'
47,000'
49,700'
Slight breaks
Stratus ~25,000'
At or just below cloud level
Film Change
Possibly two layers of cirrus above clouds in this area ~ 45-50,000'
Sea Clear
Stratus ~30,000'
26,000'
39,500'
38,000'
1900z

Fig. 8. Radar map (red) constructed from single-frame photograph of radar Constellation's (WV-4, U.S. Navy) APS-20E scope at 1511 Z August 27th (after Fig. 2 from Jordan et al., 1960) superimposed on C-flight cloud map (previous Fig. 3). The Constellation at the time of this frame was at 8500 ft altitude about 45 n.m. west-north-west of storm center. The coding into "hard core" echoes (hatched) and fainter or more diffuse echoes (shaded) was introduced subjectively by us from the photograph provided by Jordan et al.

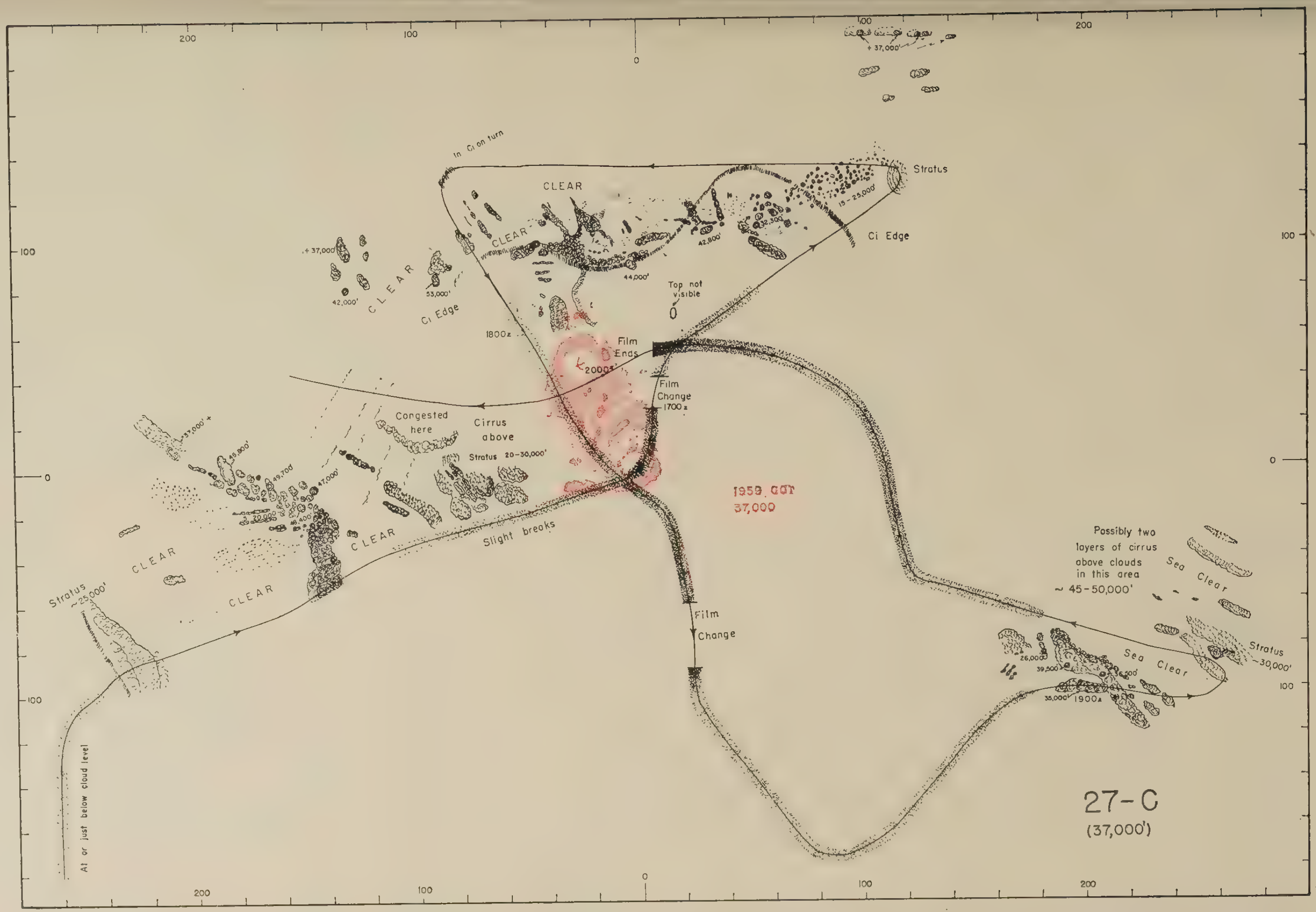
27-C
(37,000')
1959 GCT
37,000
Stratus
15-25,000'
Ci Edge
CLEAR
In Ci on turn
42,800'
32,300
44,000'
Top not visible
Film Ends
2000z
Film Change
1700z
1800z
+37,000'
42,000'
53,000'
CLEAR
Ci Edge
Congested here
Cirrus above
Stratus 20-30,000'
37,000'+
45,800'
49,700'
47,000'
CLEAR
Slight breaks
CLEAR
CLEAR
Stratus ~25,000'
At or just below cloud level
Film Change
Possibly two layers of cirrus above clouds in this area ~ 45-50,000'
Sea Clear
Sea Clear
Stratus ~30,000'
26,000'
39,500'
35,000'
1900z
200
100
0
100
200

Fig. 9. Radar map from single frame of NHRP APS-64 set (after Jordan et al. Fig. 10) superimposed upon our August 27 C-level cloud map. Radar frame was take from same flight as photography but on exit leg at 1959 Z just after nose camera film had ended.

that Daisy's echo patterns were chaotic, confusing, and highly variable from one time, location of aircraft, and type of radar set to the next. On some of the pictures a spiral band wound around the north of the center and none to the south; on others, a band wound around on the south but not the north, and on still a third no spiral bands at all were detectable but only a concentric ring of echoes around the eye. With the possible exception of the last problem (largely resolved in the discussion by JORDAN ET AL.), most of the apparent inconsistencies are removed by reproducing all radar pictures on the same distance scale (we chose that of our photographic maps) and superimposing them on each other. The remaining problems in interpretation are then greatly illuminated by using the radar pictures as overlays for the cloud maps, aided by the analysis of JORDAN ET AL. concerning what layers were seen by the radar. It should be kept in mind that all the radar figures to be shown for August 27th are photographs of single frames and not composites.

Fig. 8 shows a map we made from an APS-20E radarscope photograph (after Fig. 2 in JORDAN ET AL.) superposed on our C-level cloud map, shown earlier by itself in Fig. 3. The scope photograph was made at 1511 Z when the radar Constellation was flying at 8500 ft and was located, as shown, about 45 n.m. west-northwest of the eye center. It is thus within 1 ½—2 hours synoptic with the corresponding patterns of the photographic map. According to Jordan et al., since the antenna tilt was kept at about 4 degrees above horizontal during most of the Constellation flight on the 27th, the patterns shown result primarily from returns in a layer from about 12,000—35,000 ft.

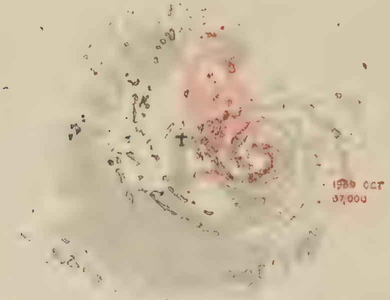

Fig. 10. NHRP APS-64 radar frame (red) from Fig. 9 superimposed on radar Constellation's APS-20E frame shown in Fig. 8. Note similarities despite nearly five hours time difference (APS-20E frame earlier), difference in equipment, and aircraft altitudes.

Fig. 9 shows a superposition of an APS-64 radarscope frame (after JORDAN ET AL. Fig. 10) upon the same cloud map. This was taken from the C-level NHRP flight on the exit leg at 1959 Z just after the photographic film had ended. It shows echoes from hydrometeors extending from the surface to flight level in the vicinity of the aircraft's location at 1959 Z.

Fig. 10 consists of the NHRP APS-64 radar map (red) superimposed on the Constellation's APS-20E map of Fig. 8.

Fig. 11 shows a much later (2345 Z, 3 hours after the NHRP aircraft had left the storm) map made from the APS-20E (after JORDAN ET AL., Fig. 11) as overlay on the C-flight cloud map. The Constellation was now 200 n.m. to the west of the storm center and saw a bigger portion of the rain area, but presumably with more effect of attenuation.

Fig. 12 superposes the two APS-20E radar maps (1511 Z in red, 2345 Z in black), and finally Fig. 13 shows the 1511 Z APS-20E map in red upon the B-level photographic map.

The results of the superpositions in Figs. 8—13 are both gratifying and illuminating. Allowing for different radar sets, gains, times, aircraft locations, etc., we find the radar maps in good agreement with each other and a valuable supplementation of the photography (or vice versa). The main conclusion now becomes not chaos or transience, but a remarkable persistence in pattern throughout all observations. Figure 8 shows that the much-photographed cumulonimbus line to the north spiralled into the eye wall from west and southwest. It also shows that the line of near 50,000 ft buildups 160 n.m. west-southwest of center which crossed into the "blind" region of the nose camera, was part of the spiral band containing the big buildups 70—80 n.m. south of the eye. It continued (more weakly) spiralling toward the center, joining the eye wall from the north. As we have seen, these two main spiral bands were characteristic of Daisy throughout her observed lifetime. It is not clear whether the more diffuse echoes are from stratus or cirrus, although the marked increase and spreading of such echoes between the two NHRP radar maps of the 25th and 27th, together with the photographically recorded

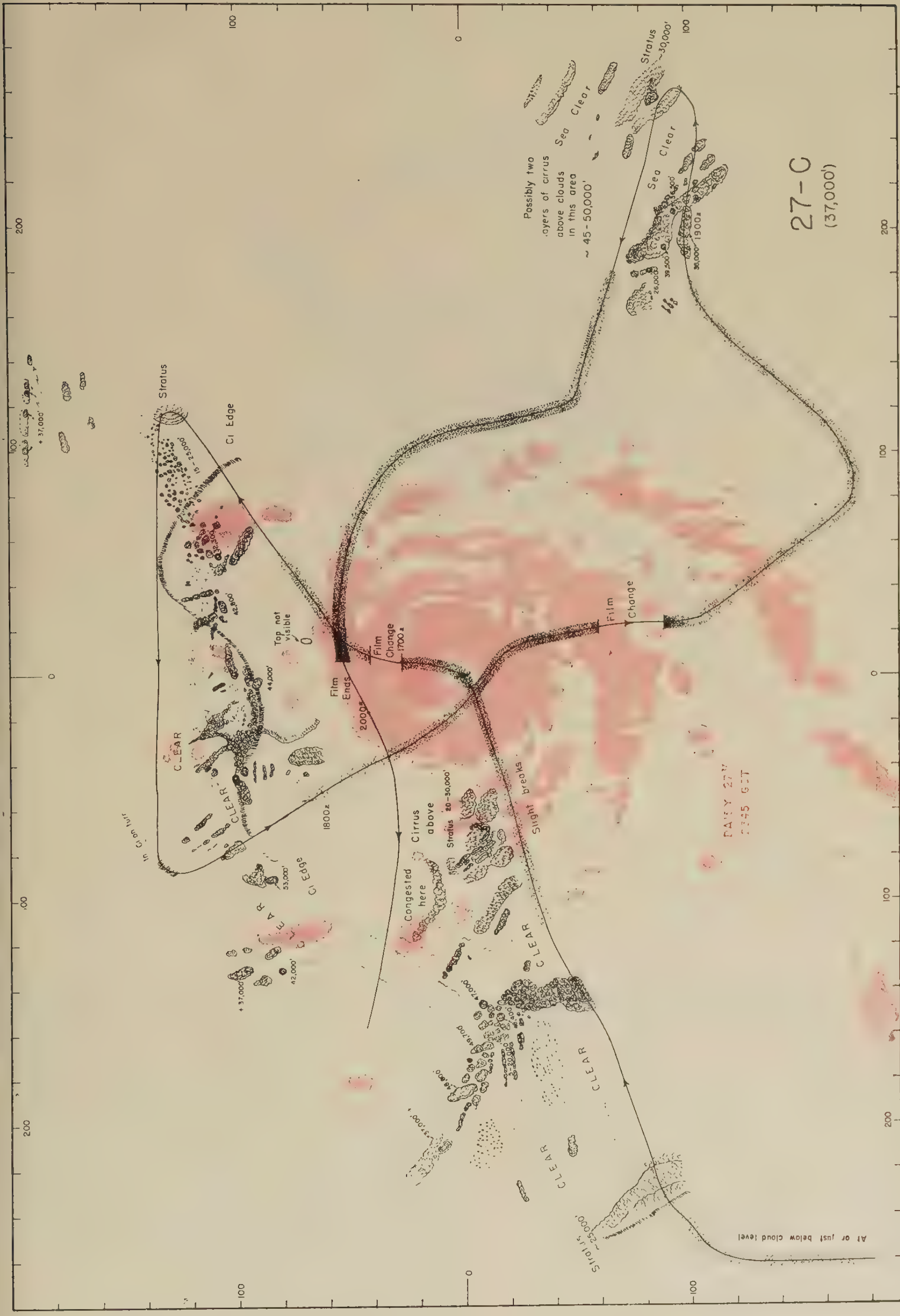
27-C
(37,000')
Possibly two layers of cirrus above clouds in this area ~ 45-50,000'
Sea Clear
Sea Clear
Stratus ~30,000'
1900z
26,000'
39,500'
30,000'
Film Change
Film Change 1700z
Film Ends
2000z
1800z
Top not visible
44,000'
42,800'
15-25,000'
Ci Edge
Stratus
CLEAR
CLEAR
CLEAR
CLEAR
CLEAR
in Ci on turn
53,000'
42,000'
+37,000'
Ci Edge
Congested here
Cirrus above
Stratus 20-30,000'
Slight breaks
Stratus ~25,000'
At or just below cloud level
DAISY 27
2345 GMT
100
200
0

Fig. 11. Much later radar Constellation frame (2345 Z, after Fig. 11 Jordan et al.) in red, superimposed on Fig. 3 photographic cloud map. Constellation was now 200 n.m. to west of storm center at an altitude of 7000 ft. Shading has been designed (subjectively) to correspond to brightness on radar print.

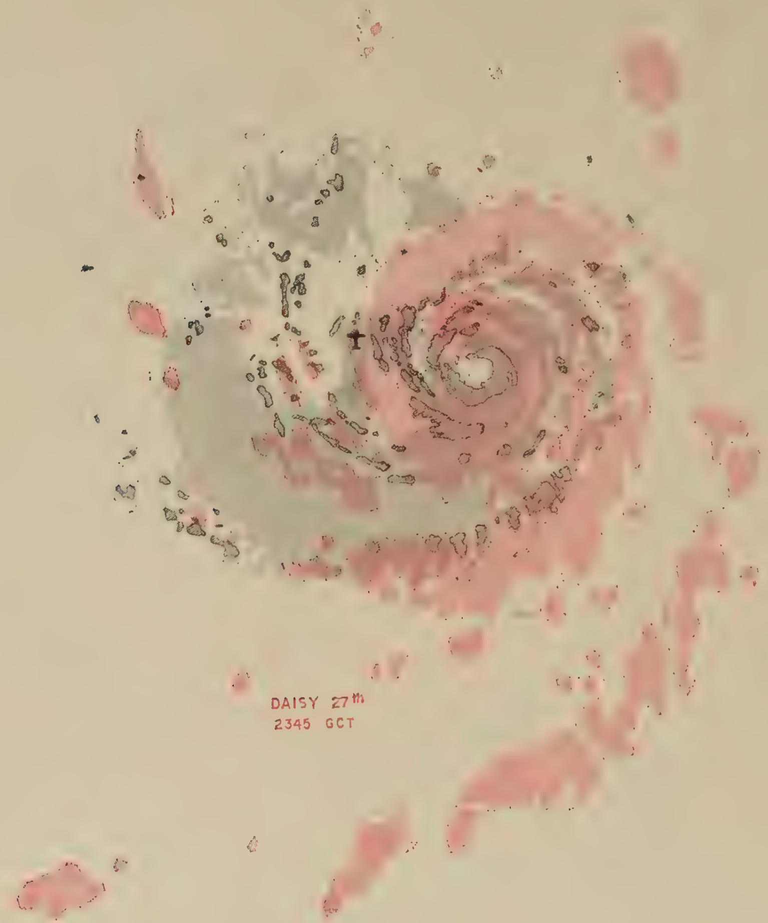

Fig. 12. Superposition of radar frame in Fig. 11 (red) upon that in Fig. 8. Both from Constellation's APS-20E set, comparable altitudes (7000 and 8500 ft, respectively) but at different times and aircraft locations. The red chart is from a frame nearly nine hours after the black with aircraft at a far greater distance from storm center.

increase and darkening of stratus decks, suggests the former. This is confirmed if, as stated by JORDAN ET AL., the radar saw little above flight level; much or most of the cirrus was at or above 37,000 ft.

Figure 11 shows little change in the main radar features from Fig. 8, despite a nearly nine-hour time difference. It also gives us a look, albeit probably attenuated, into the cirrus-covered southeastern quadrant. This further validates our photographically-deduced conclusion that this was the most convectively active portion of the rain area. Figure 11 shows another spiral band of echoes crossing the C-flight track about 120 n.m. south-southeast of the center. This may be identified with a fragmentary band only about 10 n.m. farther from storm center on the 25th NHRP radar (Fig. 7) and is almost surely also convective in origin, being so similar to others now positively shown to be such. Since the photographs showed still another cumulonimbus row about 220 n.m. out to the southeast, we have about three major bands (exclusive of eye wall) in the southeastern quadrant, compared to about one and a half in the same radial coverage to the north, west, and southwest.

Superposition of the APS-20E 1511 Z radar map on the B-flight cloud map (Fig. 13) gives equally agreeable and consistent results. It

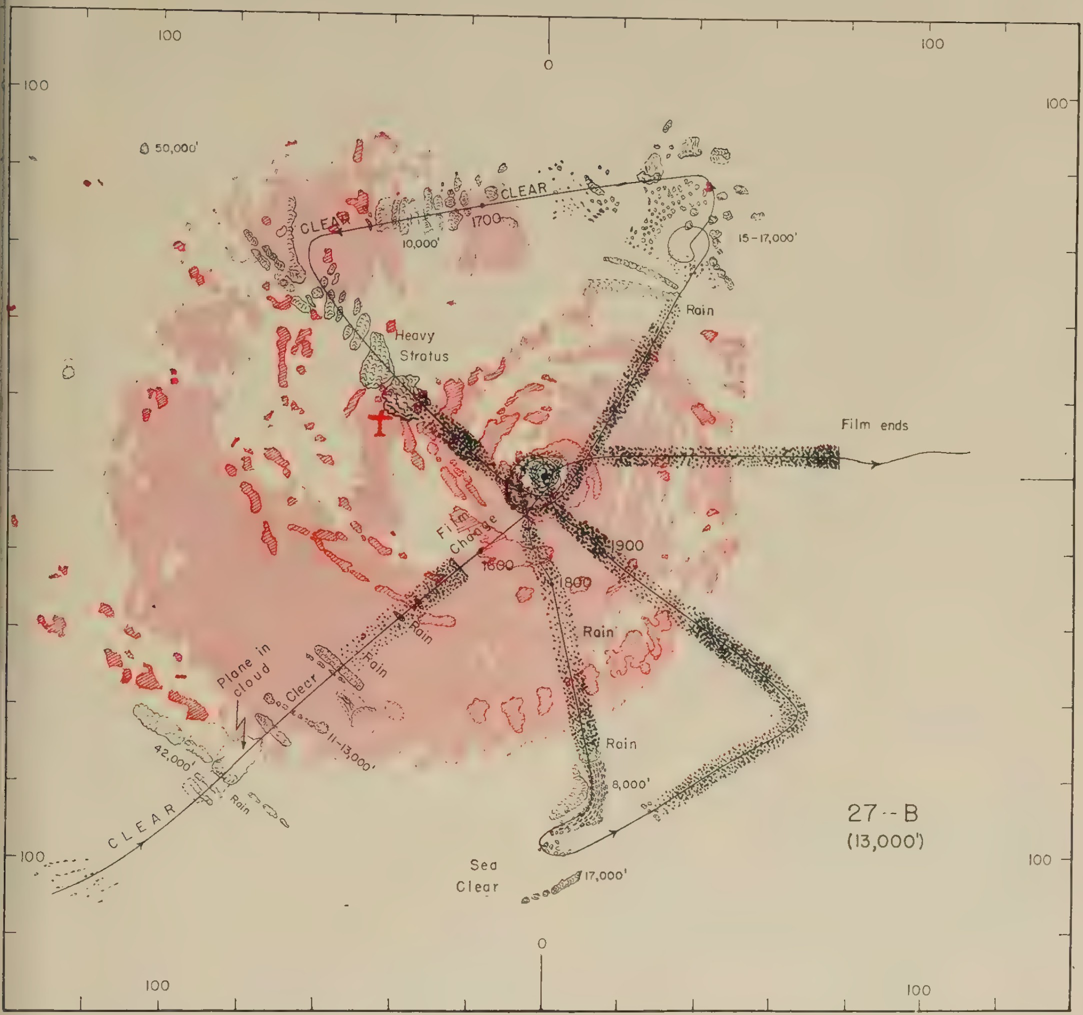
100
0
100
100
100
50,000'
CLEAR
CLEAR
1700
10,000'
15-17,000'
Rain
Heavy Stratus
Film ends
Film Change
1600
1900
1800
Rain
Rain
Rain
Plane in cloud
Clear
11-13,000'
42,000'
Rain
CLEAR
Rain
8,000'
27 - B
(13,000')
100
100
Sea Clear
17,000'
0
100
100

Fig. 13. Radar chart from Constellation's APS-20E 1511 Z frame (red, formerly in Fig. 8) superimposed on our B-level photographic cloud map (previously Fig. 4).

further confirms our operational conclusion that generally very black, rainy, heavily "socked in" portions of mid-level nose camera films would coincide with relatively strong radar echoes, and that maps constructed showing regions of "equal blackness" from film records would be in pretty good agreement with radar maps.[1] Outside the eye wall itself, the film's blackest, most rainy portion was that convective area, previously discussed, 70—80 n.m. to the south, which shows here also the hardest core radar echoes, despite being more than 100 miles away from the aircraft.

An important point brought out by this figure is the difference in convective activity between the northern cloverleaf and southern cloverleaf of the B-flight. Further consequences of this and its relevance to the averaging and sampling problems are brought out in Section 5.

Finally, we may compare the radar patterns on the 25th (Fig. 7) with those of the 27th (Figs. 8—13). Especially with allowances for different sets, gains, altitudes, etc., and for the fact that the 25th map is a composite while those for the 27th are single frames, we are more impressed with the similarities between the pictures than the differences, which themselves may now largely be explained in a logical manner. The arrangement of echoes into essentially the same (in pattern and in relative storm coordinates) broken spiral bands is obvious, and even the breaks (along themselves) in the bands occur at roughly the same distance and direction from storm center. The main differences on the 27th radar from the 25th are: 1) greater symmetrization in echo distribution; in particular, more echoes in western quadrants, 2) the weaker and diffuse echoes are more spread out and extensive, suggesting stratus decks, rather than isolated, smaller convective towers, as on the 25th, and 3) the two main bands are 10—20 n.m. radially closer to the center. It is not likely that the latter change had anything to do with the presence of the Bahama Islands on the 25th, since the 26th map put them in the same relative locations as the 25th. All these differences were independently suggested by the photographic maps, and we believe they had little, if any, origin in differences in radar instrumentation or usage.

---

[1] Our currently undertaken study of hurricane Cleo (August 18, 1958), mapping from films and radar, is showing this general agreement also.

We conclude this section in strong support of the advocacy by JORDAN ET AL. of the usefulness of careful radar analysis in hurricane studies, with the further recommendation that the addition of synoptic photographic analyses would multiply the usefulness of radar many times.

5. Asymmetries of convective structure in hurricane Daisy

We have seen from all the cloud and radar maps studied herein that the southeast quadrant of Daisy was, throughout the three days, her most convectively active portion. Marked asymmetries in other variables, such as winds, temperatures, and humidities might be sought in consequence of this concentration of active convection. In this section, we present a preliminary attempt to relate the observed temperature field to the convective structure of the storm as depicted by our cloud maps.

In Daisy, the asymmetry should be particularly pronounced in the case of the 27th B flight (Figs. 4 and 13). Here the southern cloverleaf traversed an intensely active part of the storm, twice crossing the southeastern spiral cumulonimbus band, and the northern cloverleaf passed through a suppressed zone. The northernmost leg, in fact, passed largely between two stratus decks, with good visibility and little precipitation throughout.

In Fig. 14 we compare the small-scale temperature structure on the suppressed northern leg and the active southeastern cloverleaf of this flight, using the records of the NHRP vortex thermometer, adjusted for altitude fluctuations. The top graph gives temperature (plotted every two seconds) as a function of time in the vicinity of 1700 Z, when the aircraft was passing from a relatively clear region (cirrus shield above) into a zone of broken stratus undercast. The temperature fluctuates less than ± 0.5° C on each side of its average of about 3.5° C. The lower graph similarly gives temperature as a function of time on rounding the end turn (from northeast to northwest heading) of the southeastern cloverleaf, continuing into the heart of the main rainband (dark region at 1850 Z on cloud map in Fig. 13; hard core echoes on superposed red radar map).

In the first place, it is obvious that the convectively active southern leg averaged 2—2.5° C colder than the suppressed leg. This is in good agreement with Woods Hole aircraft observations (MALKUS, 1958a) in normal trade winds and weak-to-moderate tropical storms, where it was found that cloud areas are consistently cooler than the intervening clear or suppressed regions, by 0.2—0.5° C in the normal situations and by as much as 1—2° C under disturbed conditions. However, this by no means implies that active convection elements are virtually cooler than their *immediate* environment; that the very small fraction of visible cloud matter which is actively rising is usually also buoyant has been demonstrated by other Woods Hole observations (for example, BUNKER, 1959). Fig. 14 suggests that the hurricane rain area is qualitatively similar.

On the active leg shown in the lower graph, which was all within cloud, relative darkness of the film is indicated below the temperature trace. We see that blackest portion of the rainband (1849 Z to end) averaged 1.5° C warmer than the surroundings, with a peak value of 3° C warmer at the edge closest to storm center. The clearly buoyant region ap-

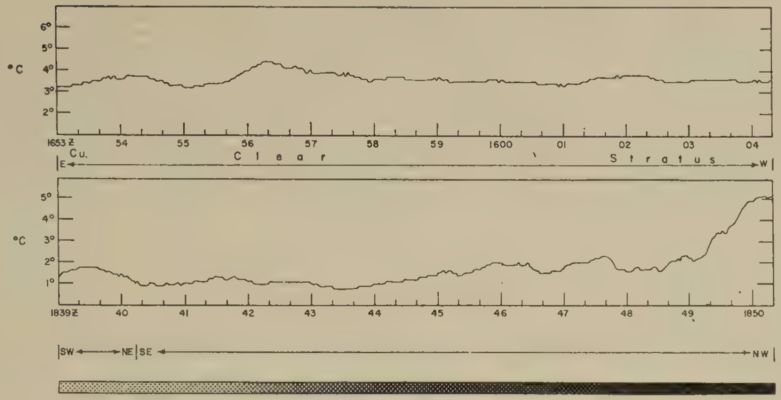

Fig. 14. Upper graph shows temperature as a function of time (altitude-adjusted vortex readings plotted at 2-minute intervals) on northern leg of northern cloverleaf of August 27th B-flight (Fig. 4, region around 1700 Z). Lower graph similarly shows temperature as a function of time for portion of southern cloverleaf on same flight near southeastern turn, where flight heading changes from northeast to northwest. The shaded region below denotes degree of blackness on film, which darkened markedly as heart of convective band was penetrated. Note pronounced difference in character, mean tempera ture, and fluctuations between upper (convectively inactive or suppressed region) and lower (convectively active region) temperature graphs.

peared about 8 n.m. across, although the lag of the vortex thermometer (about 10 seconds) precludes its accurate definition or recognition of individual convection elements.

These fragments in Fig. 14 are typical of the character of Daisy's temperature structure and its relation to the cloud patterns. Suppressed flight legs were warm and showed little or no spatial fluctuations, while convective legs were cool, with marked hot and cold spots of 1.5—3° C amplitude. We conclude that radial averages of temperature from limited and necessarily arbitrary flight paths must be interpreted with caution. The cloud maps provide a tool to investigate the sampling problem and to relate the convective structure to the thermal and dynamic features of the storm.

6. Conclusions

The primary conclusions to be drawn are four in number:

1) The patterns of clouds associated with hurricane Daisy were remarkably persistent over the three days studied, in that the major cumulonimbus rows and cirrus shield were found *in nearly the same coordinates relative to storm center* over more than 48 hours and 200 n.m. travel of the center.

2) While persistence was the major feature of Daisy's cloud patterns, they also showed a slow and gradual evolution toward a symmetrical distribution about the center, consistent with the maturing of the storm circulation. On the first day studied (August 25, 1958) Daisy's cloud patterns appeared transitional between those we have mapped in easterly-wave type, sub-hurricane disturbances (Riehl, Gray, Malkus, and Ronne, 1959) and those characteristic of the full hurricane or typhoon, in that the forward quadrants were significantly less convectively active than the rear (particularly the southeast). Symmetrization was achieved by gradual extension of the cumulonimbus rows and cirrus shield into the forward quadrants, with amazingly small changes elsewhere, except toward more buildups per line and extension of the convective area by appearance of an additional row at a larger radius.

3) Penetrative convection was extremely restricted in area and occurred only in the major lines of cumulonimbus. On the formation day about 1 % of the rain area ($r < 200$ n.m.) was covered with "hot towers", defined here as photographically well-defined cumulonimbi with tops above 37,000 ft. This figure had increased to 2½ % on the

deepening day, and 4 % on the mature day, on which a total of about 200 hot towers was estimated from our sample.

4) On all three days, we can fairly safely infer that the southeast quadrant of the storm contained roughly twice as many cumulonimbi as did the remaining quadrants. This concentration is reflected in the temperature field. In addition to posing a sampling problem, such asymmetry in convective activity may be of importance in hurricane dynamics and movement.

These hurricane cloud maps, taken in context with our similar analyses of sub-hurricane perturbations (Riehl, Gray, Malkus, and Ronne, 1959) begin to suggest that each type of tropical disturbance has a characteristic arrangement of cloud forms which identifies it as a member of a species. Our study of Daisy raises the further possibility that, within the species, each storm may show a relatively persistent or slowly evolving character of its own which distinguishes it from other members of the same species, in a similar manner as do the physical features of a human being. If it proves sound, "fingerprinting" of atmospheric disturbances by cloud patterns may be valuable in interpretation of satellite photographs, which can be used to develop and test our suggestion further, and to explore its dynamic implications.

Acknowledgments

The writers acknowledge with deep gratitude the assistance provided by the Director and Staff of the National Hurricane Project of the U.S. Weather Bureau, who have generously made available their data, facilities, and vast experience in hurricane research. In particular, we thank Mr. Harry Hawkins, the Acting Director, without whose constant help and encouragement this labor could not have been completed.

Much of the work on hurricane Daisy was carried out at the University of Chicago in a graduate class and program under the direction of Prof. Herbert Riehl, whose participation has been invaluable. In an effort as extensive as this, it is difficult to sort out the contributions of individuals and groups, of which there have been many. This phase of the study is intended as a part of an overall analysis of hurricane Daisy going on at several institutions. The radar maps herein have been reproduced with the kind permission of Mr. W. S. Gray and Prof. Charles L. Jordan. Mrs. Mary C. Thayer was responsible for preparations of the manuscript.

This study was supported jointly by the National Science Foundation, the U.S. Office of Naval Research, and the U.S. Weather Bureau under research grants to the Woods Hole Oceanographic Institution.

REFERENCES

Bunker, A. F., 1959: *Cloud and environment vertical velocities, temperatures, humidities, and water contents associated with a shear zone in the trade winds.* Unpublished. Woods Hole Oceanographic Inst. Ref. No. 59—42.

Colón, J., et al., 1961: *Hurricane Daisy, 1958.* Manuscript to appear in preprint series of National Hurricane Project, U.S. Weather Bureau, Department of Commerce, Washington, D.C.

Jordan, C. L., Lt. Comdr. D. A. Hurt, Jr., USN, and Lt. C. A. Lowrey, USN, 1960: On the structure of hurricane Daisy on August 27, 1958. *J. Meteor.*, **17**, pp. 337—348.

Malkus, J. S., 1958: On the thermal structure of the hurricane core. Proc. Tech. Conf. on Hurricanes, Miami, Florida, Nov. 1958. *Amer. Met. Soc.*, D**3**, pp. 1—2.

Malkus, J. S., 1958a: On the structure of the trade-wind moist layer. Papers in *Phys. Oceanog. and Meteor.*, Mass. Inst. of Tech. and Woods Hole Oceanog. Inst., **13**, No. 2, 47 pp.

Malkus, J. S., 1960: *Recent developments in the study of penetrative convection and an application to hurricane cumulonimbus towers.* Cumulus Dynamics, pp. 65—83, Pergamon Press.

Malkus, J. S., and Riehl, H., 1960: On the dynamics and energy transformations in steady-state hurricanes. *Tellus.* **12**, pp. 1—20.

Malkus, J. S., and Ronne, C., 1954: On the structure of some cumulonimbus clouds which penetrated the high tropical troposhere. *Tellus*, **6**, pp. 351—366.

Riehl, H., Gray, W. S., Malkus, J. S., and Ronne, C., 1959: *Cloud structures and distributions over the tropical Pacific, Part I.* Unpublished. Woods Hole Oceanographic Inst. Ref. No. 58—62.

Riehl, H., and Malkus, J. S., 1961: *Some aspects of Hurricane Daisy, 1958.* Tellus, in press.

Ronne, C., 1959: *On a method of cloud measurement from aircraft motion picture films.* Unpublished. Woods Hole Oceanographic Inst., Ref. No. 59—29.

PRINTED IN SWEDEN
ESSELTE, STHLM 61

Contribution No. 1147

Reprinted from THE JOURNAL OF THE ACOUSTICAL SOCIETY OF AMERICA, Vol. 33, No. 4, 452–456, April, 1961
Copyright, 1961 by the Acoustical Society of America.
Printed in U. S. A.

efraction of Underwater Explosion Shock Waves by a Strong Velocity Gradient*

R. R. BROCKHURST AND J. G. BRUCE, JR.
Woods Hole Oceanographic Institution, Woods Hole, Massachusetts

AND

A. B. ARONS
Woods Hole Oceanographic Institution, Woods Hole, Massachusetts, and Amherst College, Amherst, Massachusetts

(Received December 5, 1960)

The effects of a strongly refracting summer thermocline on the initial pressure pulse from an underwater explosion were accurately measured in a flooded quarry. The familiar exponentially decaying pulse shape was observed to be drastically altered in highly divergent regions of the field. Closely spaced measurements permitted these shape changes, as well as the increased amplitude and decreased time constant in a caustic region, to be followed continuously from the source. It is presently impossible to compute the observed pulse shapes although measured shock pressures agreed well with ray-theory predictions except near the caustic. Measured travel time differences between initial arrivals and both second direct arrivals and surface reflections agreed quite exactly with predictions.

1. INTRODUCTION

SERIES of experimental measurements in a flooded quarry accurately determined the re- e effects of a strong velocity gradient on under- explosion shock waves. Data were obtained at smaller intervals of range and depth than were usly practical. The resulting detail made it pos- or the first time to continuously follow changes shock wave with increasing range and permitted sive evaluation of theoretical predictions. The ic structure in the quarry provided a model for ely common oceanic conditions. For example, aximum range of 350 ft in the quarry is roughly lent to a range of 5000 yd in the central Caribbean

2. EXPERIMENTAL METHODS

experimental data reported in this paper were ed in a flooded limestone quarry (Blackington near Rockland, Main) during the summers of and 1955. Charges and gauges were suspended a network of cables strung above the quarry to fy the determination of range within 6 in. and within 3 in.

a were obtained from oscillographically recorded re-time curves using standard explosive research ques[2] with tourmaline gauges[2,3]. Rotating drum as recorded for about 19 msec with a film speed roximately 1 in./msec. That portion of the quarry as used was approximately 200 ft deep and over wide. Therefore, all wall and bottom reflections d long after the shock waves had been recorded.

The most complete demonstration of refractive effects was obtained in 1954 with 56-lb cast TNT charges at a depth of 50 ft. Two independent eight-channel systems were used to record, for each shot, the output of two vertical strings of eight gauges 2 ft apart, spaced 25 ft apart in range. Each shot was thus recorded at 16 points covering two ranges over a depth interval of 14 ft. The initial pressure pulse from a charge at a depth of 50 ft was measured between the ranges of 125 and 350 ft at 25-ft intervals from the surface to a depth of 70 ft at 2-ft intervals with some small gaps and some overlapping. Results at a range of 125 ft and at depths of 70 ft for all ranges agreed well with values computed for isovelocity water. Most of the significant refraction effects, including strong divergence and convergence, a caustic and second arrivals, were observed between 200 and 350 ft in range from the surface to a depth of 50 ft.

Shock wave parameters in isovelocity water were measured in the quarry with the same system in 1955. TNT charges of 2- to 12-lb were fired at a depth of 80 ft and recorded between 58 and 94 ft in depth at ranges from 20 to 225 ft. Charges of 12 lb. were also fired at 135 ft and recorded from 77 to 142 ft in depth at the same ranges.

The thermal structure of the water was measured frequently with thermistors and with horizontally suspended, hand lowered bathythermographs. The acoustic structure was obtained from the measured temperatures using graphical tables by Del Grosso.[4] Several thermistor lowerings indicated a very high gradient layer, no more than a few inches thick, at about 17 ft in depth. This layer was so thin that it was impossible to resolve with a horizontally suspended bathythermograph. It was difficult, and not always possible to locate it with a thermistor. The significance of this thin layer was not recognized at the time and it was not included in the machine computations. Later com-

---

tribution No. 1147, Woods Hole Oceanographic Institu- xperimental work was performed under contract with avy Department, Bureau of Ordnance. Machine computa- s developed under contract with the Office of Naval h.

S. Rutstein, Trans. Am. Geophys. Union **38**, 688 (1957).

H. Cole, *Underwater Explosions* (Princeton University rinceton, New Jersey, 1948).

B. Arons and R. H. Cole, Rev. Sci. Instr. **21**, 31 (1950).

[4] V. A. Del Grosso, NRL Rept. 4002 (June, 1952).

parison between observed and computed second arrivals indicated that this layer was indeed present and must have approached a velocity discontinuity.

3. THEORETICAL METHODS

The theoretical results used in this paper are based on machine computations using conventional acoustic analysis of energy flux in terms of the solid angle subtended at the source by a group of rays in the neighborhood of the point of observation. The velocity structure is approximated by a series of layers, in each of which the velocity is a linear function of depth. Amplitude ratios to a standard range of one foot are taken as the square roots of the intensity ratios computed along each ray.[5,6] The resulting amplitudes are multiplied by the reciprocal path length raised to the 0.13 power to correct for the observed slope of the empirical pressure similarity equation[2,7] for isovelocity water.

This conventional ray-theory treatment neglects diffraction and so assumes that the pulse shape remains exponential for an exponential source. The similarity equations correct for the small changes in the exponential pulse with range that are observed in isovelocity water. The greater diffraction effects of a highly refractive medium can not be computed at present, so that it remains impossible to predict pulse shapes in a divergent region and in the neighborhood of a caustic. Pekeris[8] and others have devised analytical methods that apply to divergent and shadow regions in principle. Unfortunately, the computations become numerically intractable[9] in just the frequency range of primary interest.

The computed intensity can not be used directly to predict impulse and energy flux since it does not include the effects of the surface reflection. Impulse and energy flux were therefore predicted by integrating an exponential pulse, having the ray-theory amplitude and similarity time constant, from the initial shock to the predicted time of arrival of the surface reflection.

Machine-computed second arrivals proved to be more intense than those observed. Observed amplitudes required the assumption of partial positive-phase reflection from a velocity discontinuity at a depth of 17 ft. Hand computations which confirmed this assumption were not sufficiently complete to be included.

4. ISOVELOCITY PARAMETERS

Measurements in the deep isothermal water o quarry established the following similarity equati

$$P=2.33\ (10^4)\ (W^{\frac{1}{3}}/R)^{1.13}$$

$$E/W^{\frac{1}{3}}=3.34\ (10^3)\ (W^{\frac{1}{3}}/R)^{2.06}$$

$$I/W^{\frac{1}{3}}=1.70\ (W^{\frac{1}{3}}/R)^{0.94}$$

$$\theta/W^{\frac{1}{3}}=57\ (W^{\frac{1}{3}}/R)^{-0.19}$$

where P is the initial shock pressure in pounds square inch, W the weight of TNT in pounds, range in feet, E the energy flux in inch-pounds square inch, I the impulse in pound-seconds per sq inch, and θ the time constant of the exponential sure pulse in microseconds.

These equations are in good agreement with t obtained in the ocean over greater ranges by Ar The pressure is about 8% higher, the energy flux a 14% higher, the impulse about 5% lower and the constant essentially the same.

5. REFRACTING CONDITIONS

The data reported here were obtained in the summer when the thermal structure of the qu water remained quite constant for a period of se weeks. Figure 1 shows the approximate limits of structure, with the resulting velocity profiles use the machine computations. The velocity disconti believed to exist at about 17 ft is not included a plained above.

The conventional ray diagram for the solid cur Fig. 1 is shown in Fig. 2. Results for the dotted c of Fig. 1 differed only in minor details. Rays are la with the angle each made with the horizontal a source so that equal intervals represent equal e flux. Regions of high divergence, of caustic, an multiple arrivals are clearly delineated. Plus and m signs indicate respectively the depths of maximum minimum shock pressures observed at each range.

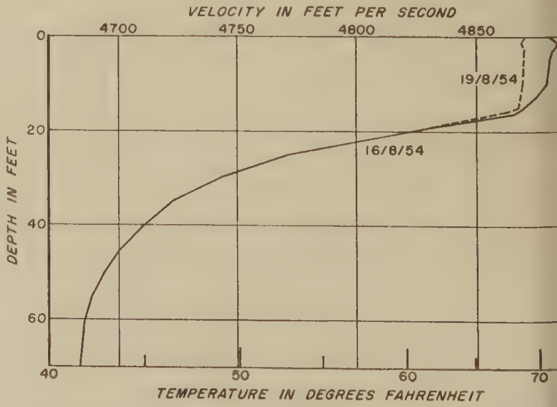

FIG. 1. Velocity (temperature) vs depth. Two profiles for computation are close to the limits observed during the when most of the data were obtained.

---

[5] P. G. Bergmann, L. Spitzer, Jr., P. G. Frank, A. Yaspan, and C. Herring, "Physics of sound in the sea. I. Transmission," Div. 6, Vol. 8, NDRC Summary Tech. Rept.

[6] Maurice Ewing, "Instruction manual for the refraction slide rule" (unpublished, WHOI, October 1942).

[7] A. B. Arons, J. Acoust. Soc. Am. **26**, 343 (1954).

[8] C. L. Pekeris, J. Acoust. Soc. Am. **18**, 295 (1946).

[9] D. H. Towne and K. G. Wilson, "Refraction and diffraction of explosive pressure pulses by gradients in the propagation velocity. II. Status of application of mathematical analysis to the problem of calculation of pulse shapes," WHOI reference 57–45 (July, 1957).

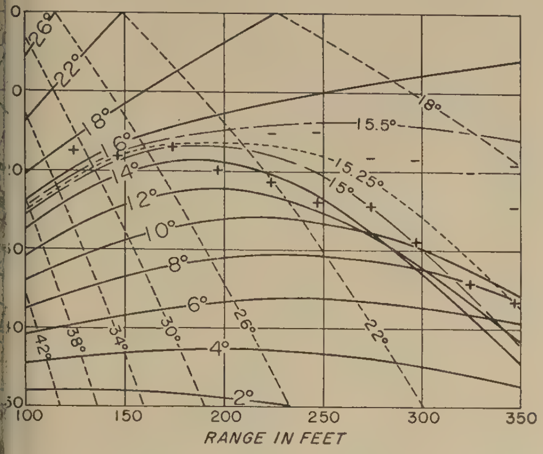

. 2. Ray diagram for source at 50 ft. Angles are with the ntal at the source at a depth of 50 ft for solid profile of . Surface reflected rays are dashed. Plus and minus signs te, respectively, the depths of maximum and minimum res observed at each range.

6. PULSE SHAPES

lse shapes at ranges of 200 ft and less were essen- the same as the exponential source. Figure 3 s the shapes observed at ranges of 250, 300, and ft. Intermediate results follow the same pattern. composite observed pulse (solid curve) is com- d with that computed for isovelocity water at the point. The most drastic alteration in shape is rved in the highly divergent region of the field e the initial shock pressures are very much re- d. The pulses along the caustic are again essentially exponential, but with markedly shorter time constants as well as increased amplitudes. Clearly defined second arrivals are apparent below the caustic. These second arrivals are observed much deeper than predicted by the ray diagram of Fig. 2 which does not include the effects of a velocity discontinuity at 17 ft. Rays partially reflected from such a discontinuity explain both the extent and the amplitudes of the second arrivals. It is obvious, particularly at a range of 350 ft, that extra energy arrives at all times between the first and second positive arrivals. This energy results from diffraction and is not accounted for by ray-theory refraction.

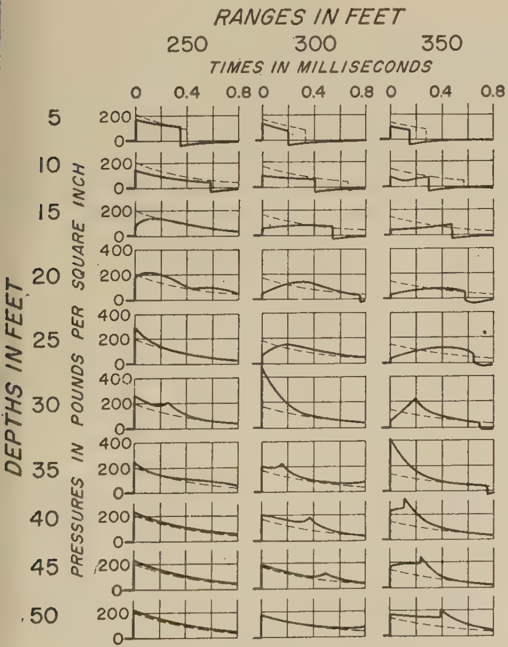

. 3. Pulse shapes for a 56-lb TNT charge at a depth of 50 served pulses (solid) are compared with isovelocity expecta- (dotted) at selected points.

7. ARRIVAL TIMES

Figure 4 illustrates the effect of refraction on the travel time differences between the initial pressure rise and both surface reflected and second positive arrivals at a range of 350 ft, and demonstrates the precision of ray theory predictions. The positive phase duration, or time difference to the negative surface reflection which cuts off the positive pulse, is very substantially less than that obtained under isovelocity conditions. Most of this reduction is of course due to the refraction of the direct arrival since the surface reflection is associated with higher angle rays showing correspondingly less refraction. Above the caustic, the single direct arrival is associated with relatively high-angle rays. Near the caustic (35 ft in depth at 350 ft range) two direct arrivals are nearly superposed. Below the caustic, the first direct arrival is along low-angle rays, while the second peak is associated with higher angle refracted rays and rays partially reflected from the velocity discontinuity at 17 ft. The times of these reflected rays are included in the dotted-line prediction of second

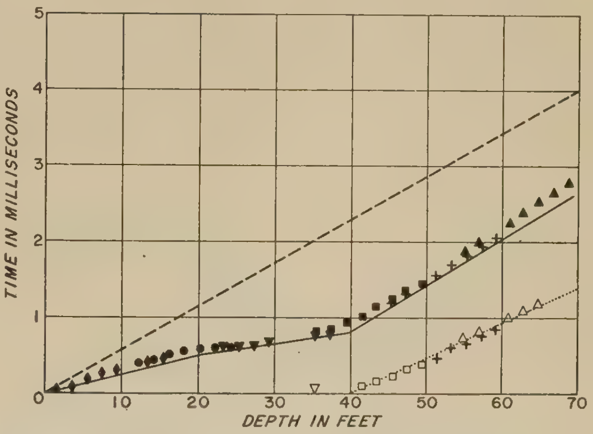

Fig. 4. Relative arrival time vs depth at a range of 350 ft for a 56-lb. TNT charge at a depth of 50 ft. Observed times, following initial pressure rise, of second arrivals (open symbols) and surface reflections (solid symbols) are compared with ray-theory values (dotted and solid lines respectively). Dashed line gives isovelocity surface reflection times.

arrivals since they were easy to compute by hand from machine computed components.

8. SHOCK PRESSURES

Figure 5 compares the observed amplitudes of the initial sharp rise in pressure at the 350 ft range with the computed results. Agreement is reasonably satisfactory in all regions where ray-theory applies. Infinite discontinuities make ray-theory completely useless near the caustic. Ray-theory predicts no shape changes so that these initial pressures would be the predicted maxima. This is essentially correct near the surface and below the caustic, but maximum amplitudes in the divergent region above the caustic are up to four times the shock values of Fig. 5. Our inability to include diffraction in the computations prevents the prediction of these maximum amplitudes. The largest percentage disagreement in initial shock pressures also occurs in the divergent region between 15 and 25 ft in depth. This region is covered by rays that would be partially reflected by a discontinuity at 17 ft. The use of such a discontinuity would improve agreement between 15 and 25 ft without affecting other depths.

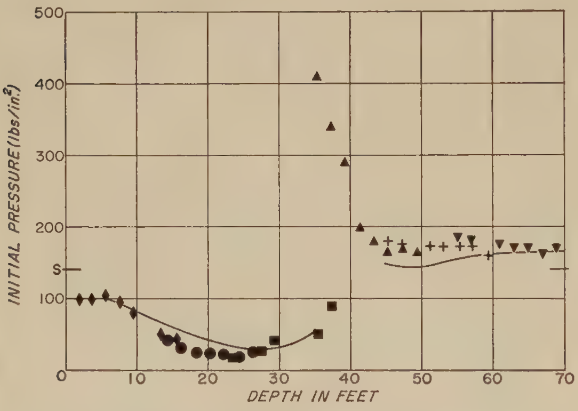

FIG. 5. Initial pressures vs depth at a range of 350 ft for a 56-lb TNT charge at a depth of 50 ft. Observed points obtained between August 10 and 25, 1954 and are compared with computed values (solid lines). Each symbol represents results from a single shot. Marginal mark (*S*) indicates isovelocity similarity value.

9. IMPULSE AND ENERGY FLUX

Experimental values of impulse and energy flux are compared with theoretical values at a range of 350 ft in Figs. 6 and 7. Agreement is good only near the surface and in deep water where the pressure pulse retains the exponentially decaying shape of the source. In the divergent region, the increasing amplitude following the initial shock drastically increases both the impulse and energy flux over the values expected with unchanged pulse shapes. Near the caustic, the decreased time constant compensates for the higher amplitude to give an impulse essentially the same as the similarity value. The energy flux, depending primarily on the maximum amplitude, increases significa near the caustic in spite of the decreased time stant. The predicted energy flux below the caust significantly below observed values since comp second arrivals are not included. The second arri have almost negligible effect on the impulse, but sufficient amplitude to significantly increase the en flux. They could not be conveniently separated the measured values. Hand computations includi velocity discontinuity at 17 ft gave a range of va depending on the magnitude of the discontinuity, w included the observed values. These results were included because precise measurement of the dis tinuity had proved impossible.

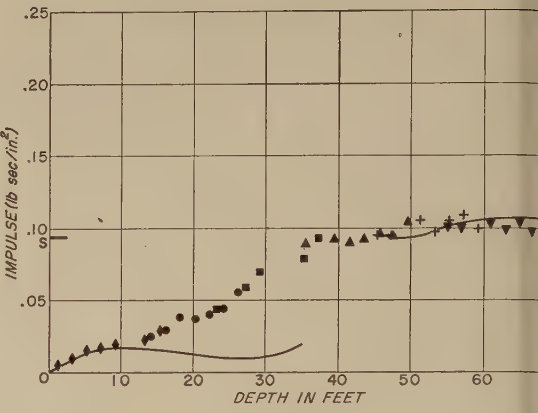

FIG. 6. Impulse vs depth at a range of 350 ft for a 56-lb charge at a depth of 50 ft. Symbols correspond to Fig. 5

10. SUMMARY

Conventional ray-theory, modified by the explo similarity equations, is very effective in predic some refractive effects. When the acoustic structu accurately known, ray-theory permits excellent pr tions of arrival times and initial shock pressures u refracting conditions, except in the neighborhood caustic. Both of these parameters depend primaril

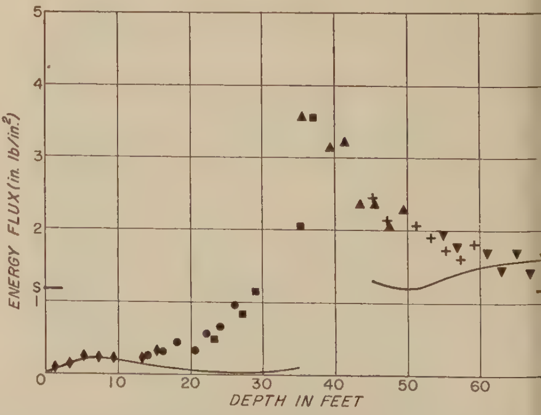

FIG. 7. Energy flux vs depth at a range of 350 ft for a 56-lb charge at a depth of 50 ft. Symbols correspond to Fig. 5

gh frequency end of the pulse spectrum. Ray- does not include diffraction effects and is there- capable of dealing with wave shapes wherever re significantly different from isovelocity shapes. ntional ray-theory is therefore not adequate to t impulse and energy in highly divergent areas. sophisticated theories presently available are not for detailed predictions because computation in quired frequency range proves impossible.

ACKNOWLEDGMENTS

authors wish to acknowledge the valuable as- e of many staff members of the Woods Hole ographic Institution that space prohibits listing ually. Of particular importance were the con- ons of Paul E. Bennett for equipment design nstruction, Allyn C. Vine and Milton S. Rutstein for experimental installation, Mrs. Nellie E. Andersen for gauge mounting, and Mrs. Maxine M. Jones and Fred H. Beck for data reduction and computation. The field parties included J. Avard Elmgren, William M. Moss, Donald A. Norman, Leonard S. Perry, and Kenneth F. Simpson, Jr.

The Naval Ordnance Laboratory rendered valuable assistance in planning, and provided standard charges for field calibration of the equipment.

The authors are indebted to Mr. Audrey E. Orff, President of the Rockland-Rockport Lime Company, for permission to use the flooded Blackington Farm Quarry near Rockland, Maine. The Bicknell Manufacturing Company, of Rockland, and the Dragon Cement Company of Thomaston, Maine provided invaluable assistance in transporting and storing the required explosives.

Contribution No. 1150

THE EFFECT OF SALINITY ON GROWTH AND CHLOROPHYLL CONTENT IN REPRESENTATIVE CLASSES OF UNICELLULAR MARINE ALGAE[1]

JACK McLACHLAN[2]

Abstract

Growth and relative chlorophyll content per cell of *Platymonas* sp., *Syracosphaera carterae*, *Monochrysis lutheri*, *Olisthodiscus* sp., *Thalassiosira decipiens*, *Cyclotella* sp., *Cryptomonas* sp., *Amphidinium carteri*, and *Porphyridium* sp. were determined at various salinities from 2.5 to 35 parts per thousand in an enriched sea-water medium.

All of these organisms grew well in a wide range of salinities, and when growth was completely suppressed it was at the lower salinities. *Thalassiosira*, *Cyclotella*, *Syracosphaera*, *Cryptomonas*, and *Monochrysis* did not show a definite salinity optimum for growth, and the chlorophyll content per cell was approximately the same at all salinities. *Olisthodiscus* and *Amphidinium* showed a salinity optimum for growth, and the chlorophyll content per cell was also higher at the optimum salinity for growth. Growth of *Platymonas* and *Porphyridium* was little influenced by changes in salinity, but the chlorophyll content per cell was affected by changes in salinity.

Introduction

Salinity is considered an important ecological variable in the marine environment, particularly in inshore areas (11, 14). Completely euryhaline organisms (i.e. organisms which are capable of moving from fresh water to full strength sea water) are relatively uncommon (10). Blinks (1) mentions observations of marine algae growing on the hulls of ships which move daily from fresh water to salt water. However, most of the larger marine algal species cannot tolerate dilutions below 0.5× or concentrations of more than 1.5× sea water. Laboratory studies with unicellular marine algae (cf. 2, 3, 4, 12, 13) have shown that most species in culture are tolerant of a wide range of salinities, although generally these organisms show a preference for lower salinities.

In a previous report (7), *Dunaliella* was shown to have a broad salinity tolerance as determined by cell concentrations. However, an empirical estimation of the chlorophyll content indicated that a narrower range of salinities was necessary for maximum synthesis of this pigment. Also, Kim (5) working with higher plants, showed that, in general, there was an inverse relationship between the chlorophyll content and the salt concentration of the culture solutions. In studies of fresh-water algae, pigment changes have been noted with variations in the nutrients of the medium (cf. 8, 9). The purpose of the present study was to ascertain if, in unicellular marine algae, a general relationship exists between the relative amount of chlorophyll per cell and growth at various salinities.

---

[1] Manuscript received November 25, 1960.
Contribution No. 1150 from the Woods Hole Oceanographic Institution, Woods Hole, Massachusetts, U.S.A.

[2] Public Health Service Research Fellow of the National Institutes of Health. Present address: Atlantic Regional Laboratory, National Research Council, Halifax, Canada.

Materials and Methods

Nine different cultures of unicellular marine algae representative of various algal groups were used in this study. A listing of these cultures together with information on the original isolation is presented in Table I. With the exception of *Porphyridium* sp., all cultures were considered axenic (R. Guillard, personal communication).

TABLE I

Cultures of algae used.* Information regarding original isolation (i.e. person, place, and time) is given when known. The initial concentration of cells in the inoculated cultures (N_0) and the duration of the incubation period are also presented

Organism	Isolation	Initial no. cells/ml $\times 10^4$	Days of growth
Chlorophyte flagellate			
Platymonas sp.	R. Guillard, Great Pond, Falmouth, Mass., 1954	4.20	7
Chrysophyte flagellates			
Syracosphaera carterae Braarud & Fagerland	I. Pintner, Woods Hole, Mass., 1958	4.18	6
Monochrysis lutheri Droop	M. Droop	4.50	8
Olisthodiscus sp.	R. Guillard, Milford, Conn., 1957	0.94	9
Concentric diatoms			
Thalassiosira decipiens (Grunow) Jørgensen	R. Guillard, Milford, Conn., 1957	0.035	15
Cyclotella sp.	R. Guillard, West Tisbury, Great Pond, Martha's Vineyard, Mass., 1956	0.58	8
Cryptomonad			
Cryptomonas sp.	R. Guillard, Milford, Conn., 1957	4.22	6
Dinoflagellate			
Amphidinium carteri Hulburt	R. Guillard, Great Pond, Falmouth, Mass., 1954	0.30	9
Rhodophyte			
Porphyridium sp.	R. Lewin	3.60	8

*All cultures were obtained from Dr. R. R. L. Guillard, Woods Hole Oceanographic Institution.

The cultures were grown in an enriched sea-water medium. The sea water was collected from the Sargasso Sea,[3] and was passed through a membrane filter (Millipore AA). Glass-distilled water was used to dilute the sea water to the desired salinities varying from 2.5 to $35^0/_{00}$ (parts per thousand). The following enrichments in mmoles/liter were added to the sea-water base: potassium nitrate 1.00, potassium monohydrogen phosphate 0.10, sodium silicate 0.10, disodium ethylenediaminetetraacetate 0.03, tris(hydroxymethyl)-aminomethane 5.00, and micronutrients at the concentration previously used (7). As some of the organisms selected are known to be auxotrophs (11), the following vitamins also were added: thiamine:hydrochloride 0.2 mg/liter, biotin 1.0 μg/liter, and B_{12} 1.0 μg/liter.

---

[3] R/V Crawford Cruise 27. Station 553 (May 1959).

The algae were cultured in 125-ml Erlenmeyer flasks containing 35 ml of medium. The cultures were incubated at about 18° C under approximately 3500 meter-candles illumination provided by cool-white fluorescent lights. It was necessary, however, to grow *Porphyridium* sp. in dim, indirect illumination. Growth was estimated by cell counts using a Levy hemocytometer counting chamber, and the results are expressed as $\log_2 N_t/N_0$, which gives the number of times the population has doubled (7). The length of the incubation period and the initial concentration of cells (N_0) in the inoculated cultures are also given in Table I. The concentration of chlorophyll *a* was estimated by the non-extractive method of Yentsch (15), but expressed in arbitrary units giving relative values for each organism. These values should not be compared, since the absolute amounts were quite different for each organism. Measurements were made with a model DU Beckman spectrophotometer at 670 mμ. Some interference with other chlorophylls may be expected at this wave length but probably does not exceed 5% of chlorophyll *a*.

Results

Monochrysis lutheri, *Syracosphaera carterae*, *Cyclotella* sp., *Thalassiosira decipiens*, and *Cryptomonas* sp. did not show a distinct salinity optimum with regard to growth, nor was there a significant difference in the concentration of chlorophyll per cell at the various salinities.

Growth of *Monochrysis* at 2.5‰ was not as dense as at the higher salinities, and the chlorophyll concentration per cell was also low at this salinity. *Syracosphaera* failed to grow at 2.5‰, but growth and chlorophyll concentration per cell at the other salinities were essentially the same. Growth and the chlorophyll concentration of *Cyclotella* were approximately the same from 2.5 to 35‰. *Thalassiosira* did not grow at salinities below 15‰, but growth and the chlorophyll concentration per cell were essentially the same at the higher salinities. *Cryptomonas* grew about equally well at all salinities, and there was no significant change in the concentration of chlorophyll per cell throughout the salinity range.

Growth of *Olisthodiscus* was completely suppressed at 2.5 and 5.0‰ (Fig. 1*a*). Maximum growth occurred at 15‰, and from 20 to 35‰, growth was essentially the same. A maximum concentration of chlorophyll per cell was also found at 15‰. Therefore, both the cell concentration and chlorophyll per cell content indicate an optimum salinity of 15‰ for this organism.

Maximum growth and chlorophyll concentration per cell occurred at 25‰ for *Amphidinium* (Fig. 1*b*). There was no growth at salinities from 2.5 to 10‰. The chlorophyll maximum at 25‰, though, was not as well defined in this alga as in *Olisthodiscus*.

Growth of *Porphyridium* sp. occurred at all salinities from 2.5 to 35‰ (Fig. 2*a*). Growth at 2.5‰ was slightly depressed, but from 5 to 35‰ growth was essentially the same. The concentration of chlorophyll per cell showed a maximum at 25‰.

Platymonas sp. grew at salinities from 2.5 to 35‰; growth from 15 to 35‰ was approximately the same (Fig. 2*b*). Growth at 2.5‰ was very much reduced, and increased with increasing salinity to 15‰. Maximum chlorophyll

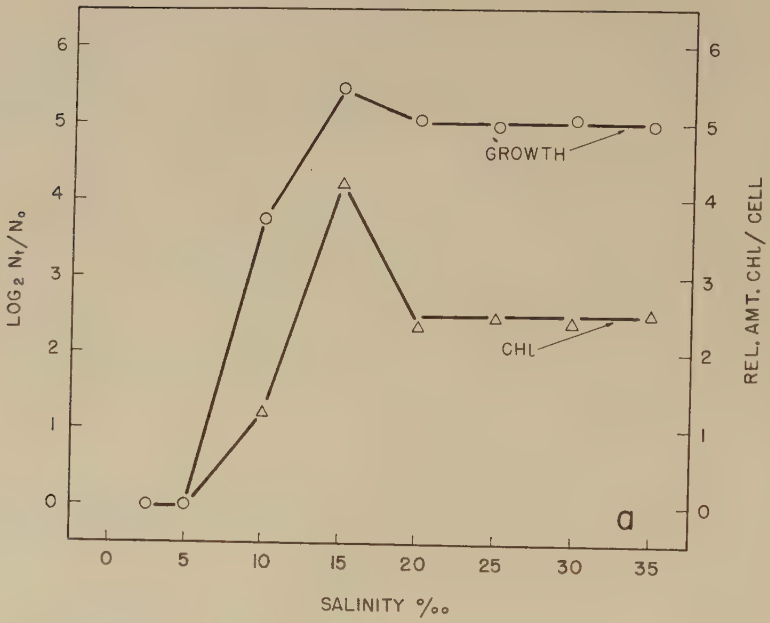

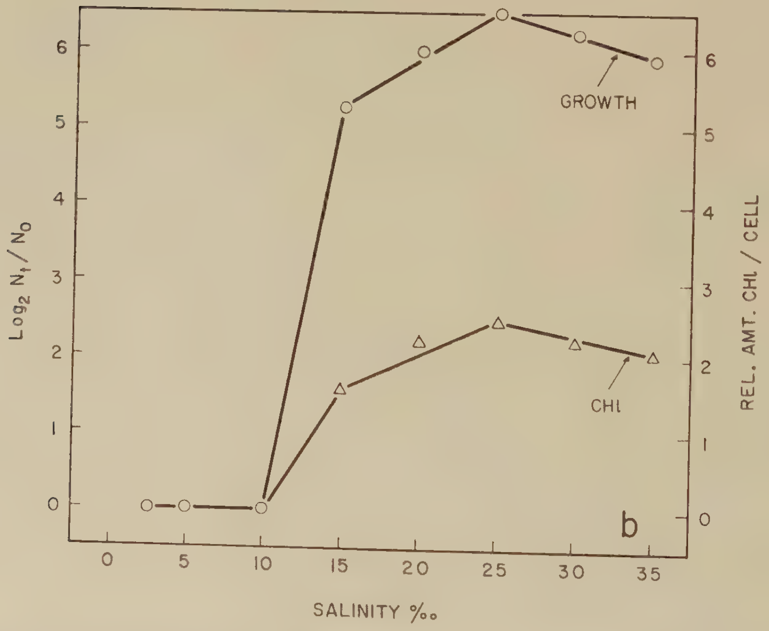

FIG. 1*a*. Growth and relative amount (see text) of chlorophyll per cell at the various salinities in *Olisthodiscus* sp.

FIG. 1*b*. Growth and relative amount of chlorophyll per cell at the various salinities in *Amphidinium carteri*.

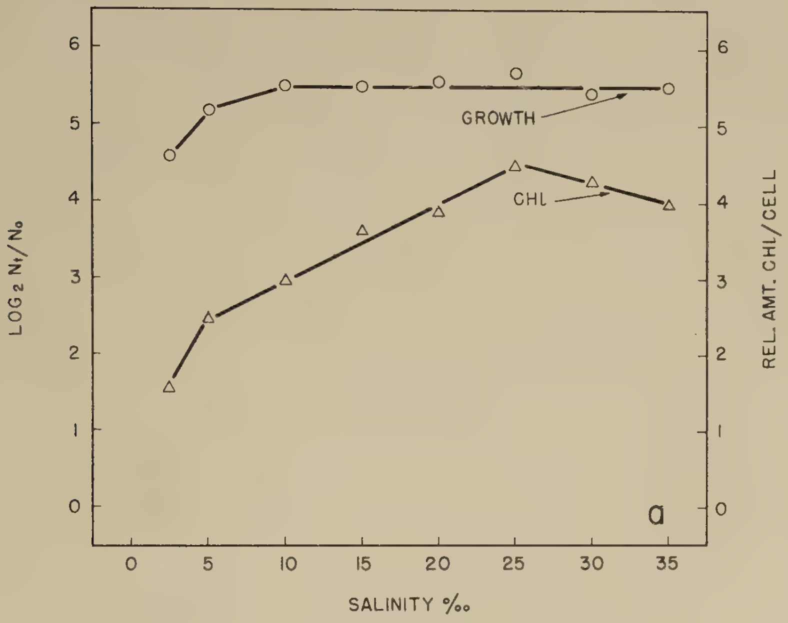

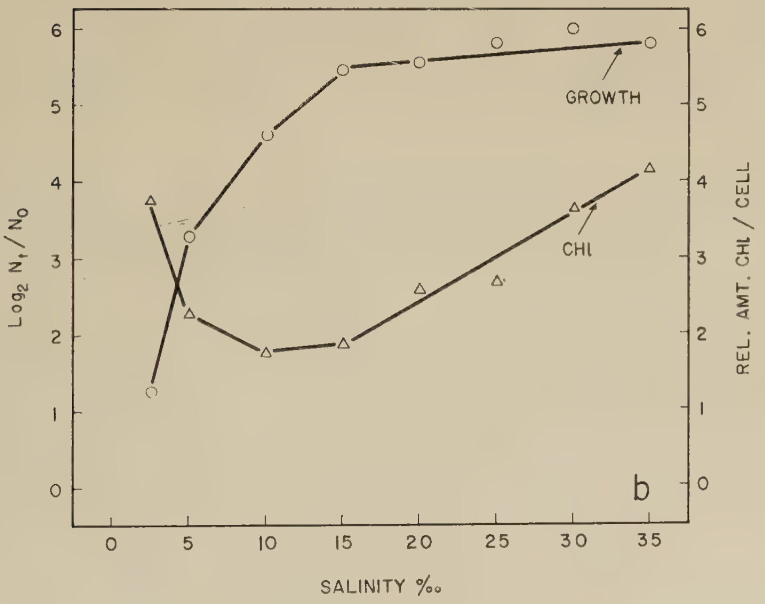

FIG. 2*a*. Growth and relative amount of chlorophyll per cell at the various salinities in *Porphyridium* sp.

FIG. 2*b*. Growth and relative amount of chlorophyll per cell at the various salinities in *Platymonas* sp.

concentrations per cell occurred at 2.5 and 35‰. Minimum concentrations of chlorophyll per cell were recorded at 10 to 15‰. However, the chlorophyll concentration per unit volume of culture medium can be directly related to salinity (Fig. 3). These results indicate an optimum salinity for chlorophyll synthesis in this alga to be 35‰ or greater.

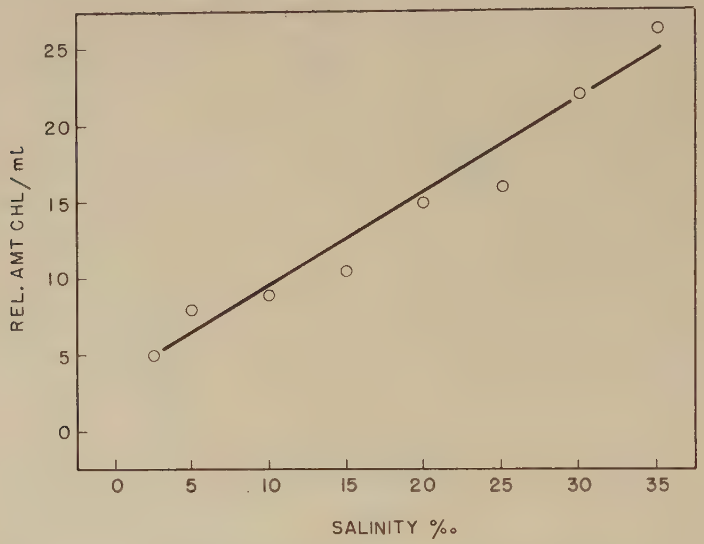

FIG. 3. Relationship between the relative amount of chlorophyll per ml of culture medium and salinity in *Platymonas*.

Discussion

All of the organisms investigated showed a wide salinity tolerance. Two of these algae showed salinity optima; generally there was an optimum salinity range for growth. Where an optimum was demonstrated, this was at a salinity lower than that of full strength sea water (ca. 34–35‰). The chlorophyll results for *Platymonas* do, however, suggest a salinity optimum greater than that of full strength sea water for this organism.

Some organisms are known to be osmotically adaptive and perform little actual work in adjusting to the external environment (10). Most of the osmotic pressure of algal cell sap is due to inorganic salts. The internal concentration of these salts passively changes with the salinity of the environment, and little or no injury occurs (1). In other groups of algae, respiration is affected by changes in salinity (1, 6). Blinks (1) has also cited a case in which photosynthesis was influenced by changes in salinity. Either an increase in respiration or a decrease in photosynthesis means that the supply of compounds produced by photosynthesis and which ordinarily would be available for growth and cellular synthesis is reduced. With multicellular algae, this results in a decrease in size (6), and with unicellular algae there is a decrease in cell concentration. Most of the species investigated in the present study are apparently osmotically labile, but several show a preference for a restricted salinity range, and hence an increase in growth within this range. It is not known, though, whether this increase in growth is the result of a lower respiratory rate or perhaps an increase in the photosynthetic rate. However, even more direct effects upon the growth process may be involved.

In some organisms, chlorophyll synthesis seems to be affected before cell division within a particular salinity range. *Porphyridium* and *Platymonas* developed a maximum chlorophyll concentration per cell at a certain salinity, although maximum cell concentrations occurred over a broad range of salinities. Contrariwise, *Olisthodiscus* and *Amphidinium* to a lesser extent show the maximum chlorophyll per cell to correspond with the maximum cell concentration.

Platymonas seems to present, in part, an anomalous situation. The maximum concentrations of chlorophyll per cell were obtained at the extremes of the salinity range, the minimum chlorophyll concentrations being at the intermediate salinities. Provasoli *et al.* (12) found that one of their organisms was unable to undergo cell division at unfavorable salinities, but the alga remained viable under these conditions. It would seem that low salinities restrict cell division of *Platymonas* whereas chlorophyll synthesis is not affected to the same degree. There is, however, a direct relationship between the relative chlorophyll concentration per unit volume of culture medium and salinity (Fig. 3). Therefore, at the intermediate salinities, the total chlorophyll content in the culture was greater than at the lower salinities, but was distributed throughout many more cells.

The results obtained in this investigation suggest that salinity is an important factor in controlling the distribution of organisms in the marine environment, especially in areas of low salinity.

Acknowledgments

Dr. Paul R. Gorham and Dr. Bostwick H. Ketchum have read the manuscript and offered valuable suggestions. Appreciation also is extended to Dr. R. R. L. Guillard, who made cultures available for this study.

References

1. Blinks, L. R. Physiology and biochemistry of algae. *In* Manual of phycology. *Edited by* G. M. Smith. Chronica Botanica, Waltham, Mass. 1951. pp. 263–291.
2. Braarud, T. Salinity as an ecological factor in marine phytoplankton. Physiol. Plantarum, **4**, 28–34 (1951).
3. Droop, M. R. Optimum, relative and actual ionic concentrations for growth of some euryhaline algae. Verhandel. Intern. Ver. Limnol. **23**, 722–730 (1958).
4. Gibor, A. The culture of brine algae. Biol. Bull. **111**, 223–229 (1956).
5. Kim, C. M. Effect of saline and alkaline salts on the growth and internal components of selected vegetable plants. Physiol. Plantarum, **11**, 441–480 (1958).
6. Levring, T. Some modern aspects of growth and reproduction in marine algae in different regions. Ann. Biol. **33**, 57–65 (1957).
7. McLachlan, J. The culture of *Dunaliella tertiolecta* Butcher—a euryhaline organism. Can. J. Microbiol. **6**, 367–379 (1960).
8. Miller, J. D. A. and Fogg, G. E. Studies on the growth of Xanthophyceae in pure culture. I. The mineral nutrition of *Monodus subterraneus* Petersen. Arch. Mikrobiol. **28**, 1–17 (1957).
9. Myers, J. and Kratz, W. A. Relations between pigment content and photosynthetic characteristics in a blue-green alga. J. Gen. Physiol. **39**, 11–22 (1956).

10. Pearse, A. S. and Gunter, G. Salinity. *In* Treatise on marine ecology and paleoecology. Vol. I. Ecology. *Edited by* J. W. Hedgpeth. Geol. Soc. Am. Mem. No. 67. 1957. pp. 129–158.
11. Provasoli, L. Nutrition and ecology of protozoa and algae. Ann. Rev. Microbiol. **12**, 279–308 (1958).
12. Provasoli, L. McLaughlin, J. J. A., and Pintner, I. J. Relative and limiting concentrations of major mineral constituents for the growth of algal flagellates. Trans. N. Y. Acad. Sci., Ser. II, **16**, 412–417 (1954).
13. Ryther, J. H. The ecology of phytoplankton blooms in Moriches Bay and Great South Bay, Long Island, New York. Biol. Bull. **106**, 198–209 (1954).
14. Smayda, T. Biogeographical studies of marine phytoplankton. Oikos, **9**, 158–191 (1958).
15. Yentsch, C. S. A non-extractive method for the quantitative estimation of chlorophyll in algal cultures. Nature, **179**, 1302–1304 (1957).

Contribution No. 1152

(Reprinted from the Journal of Meteorology, Vol. 18, No. 4. pp 451-467)

AN OBSERVATIONAL STUDY OF CUMULUS[1,2]

Peter M. Saunders

Woods Hole Oceanographic Institution

(Original manuscript received 11 November 1960; revised manuscript received 9 January 1961)

ABSTRACT

An observational study of cumulus is made from time-lapse film records, and laws describing the growth of cloud thermals (discrete masses of buoyant air) are deduced.

The *diameter* of isolated thermals emerging from the summits or on the flanks of a cumulus is found to have a well-defined upper limit which is a simple linear function of height. It is inferred that, in the saturated interior of a cloud, thermals broaden linearly with height incorporating into themselves the residues of earlier (now decaying) thermals. Their rate of broadening with height, 0.40 ± .04, is found insensitive to variations of the stability and humidity of the cloud layer and to the presence or absence of precipitation.

From the observed broadening, the *buoyancy* of cloud thermals can be deduced if a knowledge of the properties of decaying thermal residues is given. A probable upper limit to thermal buoyancy is computed and is found to be some fraction of the adiabatic value.

Observations of the *rate of rise* and the diameter of the most vigorous thermals emerging from the cloud interior and estimates of their buoyancy permit a test of a proposed simple relationship between these properties. Fair agreement is obtained in the statically unstable part of the cloud layer. Thermals with smaller rates of rise are deduced to have smaller buoyancy due to their growth in less favorable environment.

The relation between the properties of cloud thermals and the history of the cloud is indicated.

Both the quantitative and qualitative results of the investigation establish the 'thermal theory' of cumulus convection on a firmer basis than hitherto.

1. Introduction

In a recent paper on the generation of large hail in convective clouds, Ludlam [1] put forward views which differed in certain important respects from earlier versions of the bubble or thermal[3] theory of cumulus. We may recall that this theory emphasizes the discrete unsteady nature of the movement of buoyant air within cloud [2; 3]. In these earlier accounts, the general increase in the horizontal scale of cloud thermals with increasing depth of cloud was supposed due to amalgamation processes in which large thermals aggregate from the wakes and residues of smaller ones. In the hail paper [1], it was pointed out that individual thermals can also grow *continuously in size* by mixing into themselves some of the environment through which they pass; large thermal size is thus a consequence of large vertical penetration. In this idea, Ludlam was strongly influenced by the laboratory experiments of Scorer [4] and Woodward [5] which had revealed the mechanism of the mixing or entrainment process hypothesized much earlier by Stommel [6; 7]. With the model of a thermal as a discrete entraining mass, it became possible to predict the buoyancy, liquid-water content and rate of rise of cloud thermals *with the aid of simple general hypotheses*. Levine [8] considered a model similar in a number of important respects to Ludlam's but lacking its simplicity; for this reason, Ludlam's treatment is preferred here.

In Ludlam's paper, the derivation of the properties of a thermal traversing the interior of a cumulus rests on two assumptions, (i) that the size of the thermal increases linearly with the distance that it penetrates and (ii) that the air entrained has zero liquid-water content and the same virtual temperature as the clear-air environment of the cloud; given the clear-air sounding, the thermodynamic characteristics of the thermal are then determined. For example, away from the region of the cloud base, the mean liquid-water content in the thermal is found to be 1/3 to 1/4 of the adiabatic value. In addition, by employing a relationship found valid in laboratory studies [4], the rate of rise of a cloud thermal is shown to be related to the clear-air sounding.

A small quantity of observational data furnished from aircraft traverses of cumulus was advanced in

---

[1] Contribution No. 1152 from the Woods Hole Oceanographic Institution.

[2] The research reported in this paper is part of the author's thesis for the degree of Doctor of Philosophy in the University of London. It was completed during the author's tenure of the Rossby Memorial Fellowship at Woods Hole Oceanographic Institution. This fellowship was awarded him by the American Meteorological Society.

[3] The term "thermal" is preferred to "bubble" and is used throughout this paper.

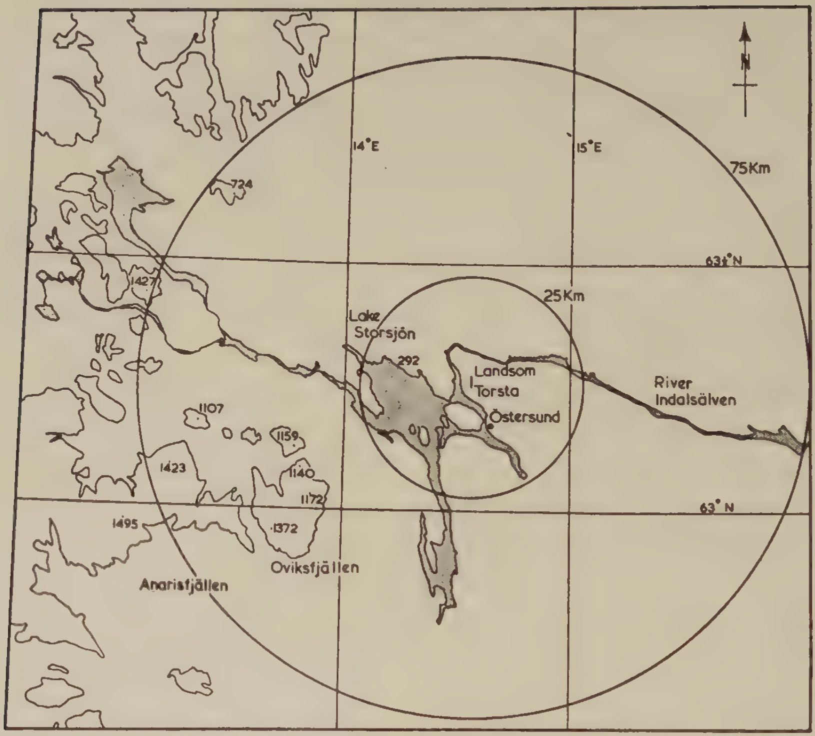

FIG. 1. Location and surroundings of observing station, central Sweden. The treeline (about 600 m above sea level) is marked, and peak heights are given in meters.

support of the analysis, but these give the arguments plausibility rather than solid substantiation. Now, observations of the outline of clouds, *yielding measurements of the height, diameter and rate of rise of cumulus thermals* also provide material for examining Ludlam's treatment and determining its limitations: we thought it worthwhile to make measurements of these quantities from time-lapse films, and the results of this study are presented below.

2. The nature, selection and treatment of the data

The data employed in this study were obtained from 16-mm time-lapse films which had been exposed during a field investigation of showers in Central Sweden. The operations were conducted during the summers of 1954 and 1955 under the leadership of F. H. Ludlam. A number of papers describing the work have already been published [9; 10; 11]. The film records were supplemented by a host of other information (described in detail in one of these papers [10]) namely, double-theodolite measurements of the height of the top and base of selected cumulus, observations of the onset of showers, data from special and routine radiosonde ascents made within 10 km of the observing site, and a limited number of aircraft soundings.

The field site is situated a few kilometers north of the town of Östersund on a hill overlooking Lake Storsjön (fig. 1). To the west, beyond the lake, the countryside is mountainous with a number of peaks over 1000 m, and to the east the ground undulates gently between 300 and 400 m above sea-level; it is forest-covered with clearings beside numerous small lakes and rivers. In the mornings, the largest cumulus are generally over the mountains, but by afternoon the principal cloud development is frequently over the lower ground to the east. The great majority of the clouds examined here occurred in the latter location at distances ranging from 15 to 75 km.

In selecting the data from nearly 1000 ft or 40,000 frames of film, we searched out cumulus which contained *large isolated* thermals and made our measurements on these. Since Ludlam's theory relates to the behavior of separate, *isolated* thermals, the selection of such for measurement requires no further comment. The choice of large thermals is justified as follows: in a given cumulus it may be that no one thermal is strictly isolated; however, since large thermals are less influenced by the presence of nearby small thermals than small ones are influenced by the presence of nearby large ones, large cloud thermals approach more closely to the required condition of isolation. In addition, the choice of large thermals is made on the grounds that they contribute most to the sheer volume of a cloud and that they are probably the most active regions for the development of precipitation. The nature of the selection should be borne in mind in the following discussion, since it will clearly restrict the conclusions which are reached.

The dimensions of clouds and cloud thermals were determined from measurements made on a projected image of the film. An enlargement of the film (whose frame size is only 7.5 × 10.5 mm) 80 times was found convenient. These measurements were converted to a true scale by using the height of the cloud base; this quantity was known, determined from double-theodolite observations, on all occasions when film was exposed. In the region defined in fig. 1, we frequently observed a systematic difference between the height of the base of clouds growing over the high ground to the southwest of the station and the height of the base of those growing over the low ground to the east. This difference which never exceeded 500 m was a maximum in the early morning and generally vanished by mid-afternoon. In either sector of the sky and at any given time, however, the base height was rather uniform: the variation was 100 to 200 m in the absence of showers and 300 to 400 m in their presence [10]. Thus, even when the base height appropriate to the region and time are employed, cloud dimensions deduced here have an uncertainty of up to ±10 per cent. A small number of the clouds had also been chosen for double-thedolite measurement, and their height and diameter determinations are more reliable.

Systematic errors in the measurements arise from perspective distortions produced during photography and enlargement; these are considered in detail in a paper which is currently being prepared. The most important resulted from the tilting of the camera during photography, a practice ensuring the maximum amount of sky within the field of view. The nature and magnitude of the errors produced thereby are summarized in table 1, and we note that the shorter focal-length lens, allowing greater camera tilt while retaining the horizon as reference, generates the larger errors. Inspection of table 1 also reveals that the magnitude of these errors is small compared with ±10 per cent uncertainty resulting from the variability of the height of cloud base, and because of this we are able to neglect them.

Occasionally, in calculating the rate of rise of a cloud top, it was necessary to correct for the motion of the cloud top relative to the cloud base. (Recall that, by constructing the top/base ratio for all our measurements, changes in the distance of the cloud base from the camera were accounted for.) The required correction is $-V\cos\alpha\tan\theta$ where V is the relative wind between top and base, α is the difference between the azimuth of the cloud top and that of the

Table 1. Summary of errors in measurements of the diameter, height and rate of rise of cumulus thermals.

				Lens focal length	16 mm		10 mm	
				Tilt angle	10°		17°	
				Frequency of use	80%		20%	
Thermal property	Cause of error	Whether due to camera tilt	Error characteristics	Magnitude of error per cent	Mean	Max.	Mean	Max.
Diameter	Use of base height to give scale	No			±10		±10	
	Axially symmetric nature	No	Zero on meridian plane, maximum at vertical edges of film		+1.4	+4	+3.5	+8
	Convergence of verticals	Yes	Zero at horizon, maximum at film top		−3.5	−6.5	−4.3	−10
Height	Use of base height to give scale	No			±10		±10	
	Top/base distortion	Yes	Proportional to difference in angular elevations of cloud top and base		−2.0	−3	−2.0	−3
Rate of Rise	Use of base height to give scale	No			±10		±10	
	Top/base distortion	Yes	Generally increases with angular size of cloud		−4.0	−7	−7.0	−12

Note extreme values are those which are appropriate to the data presented here. They are generally much smaller than could occur with the same procedures and equipment.

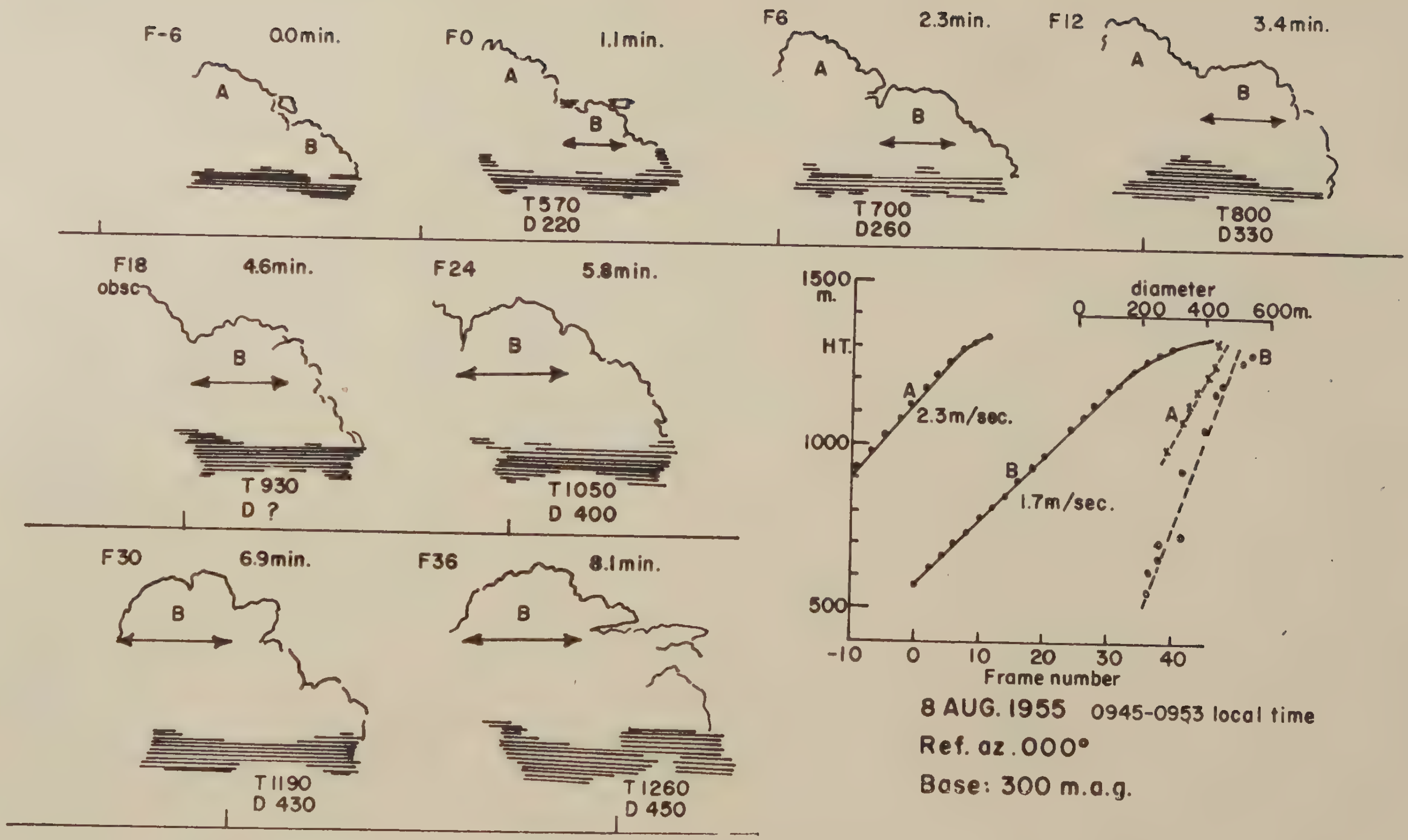

FIG. 2. A sequence of drawings traced from films showing the emergence of cloud thermals on the flanks and in the summits of cumulus. Estimates of the diameter of individual thermals, which are lettered A, B, C, *etc.*, are denoted by double-ended arrows. The height of the cap of a thermal above ground follows the letter T, its diameter follows the letter D; both values are given in meters.

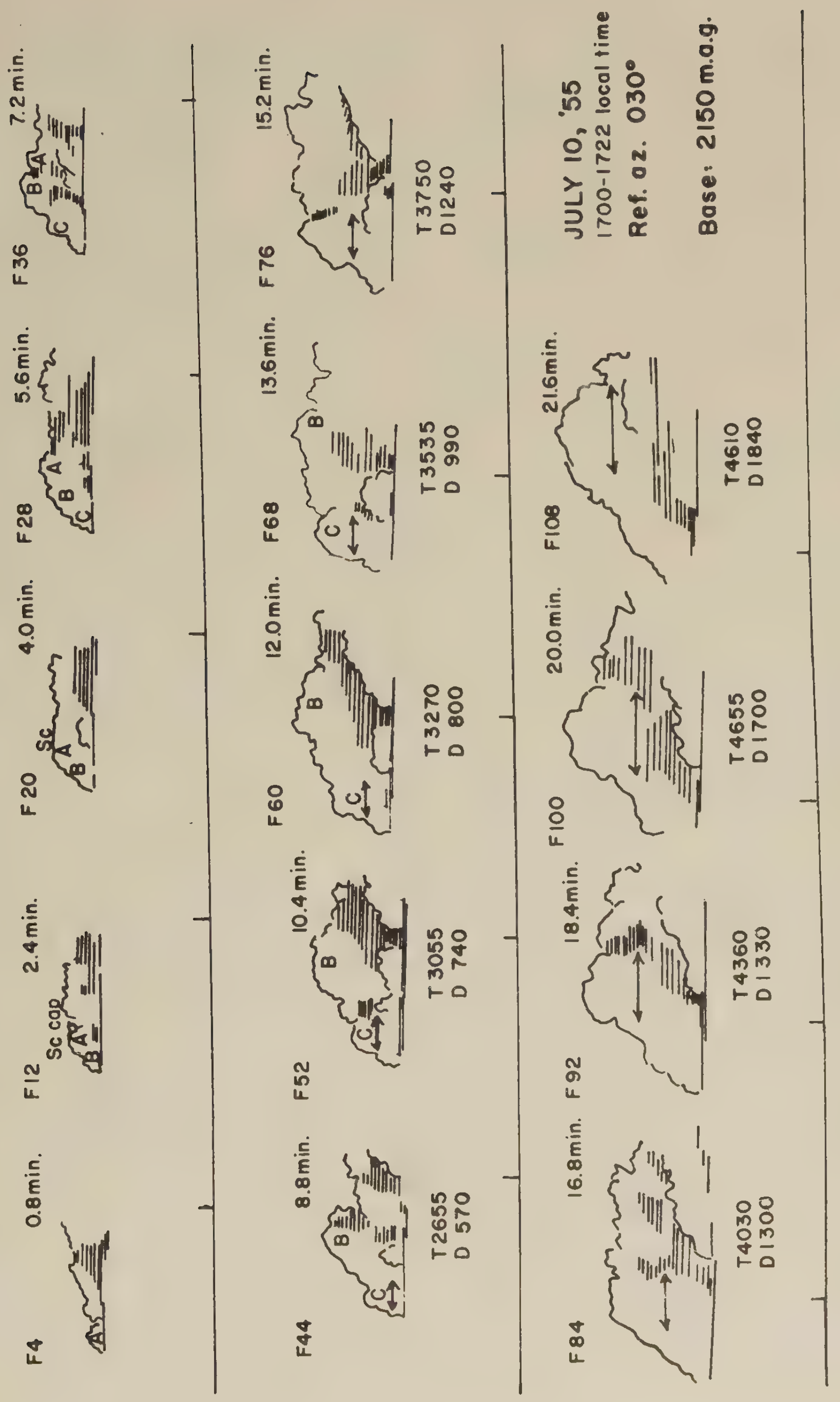
F4
0.8min.
A
F12
2.4min.
Sc cap
A
B
F20
4.0min.
Sc
A
B
F28
5.6min.
A
B
C
F36
7.2min.
A
B
C
F44
8.8min.
B
C
T2655
D 570
F52
10.4min.
B
C
T3055
D 740
F60
12.0min.
B
C
T3270
D 800
F68
13.6min.
B
C
T3535
D 990
F76
15.2min.
T3750
D1240
F84
16.8min.
T4030
D1300
F92
18.4min.
T4360
D1330
F100
20.0min.
T4655
D1700
F108
21.6min.
T4610
D1840
JULY 10, '55
1700-1722 local time
Ref. az. 030°
Base: 2150 m.a.g.

FIG. 3. See fig. 2.

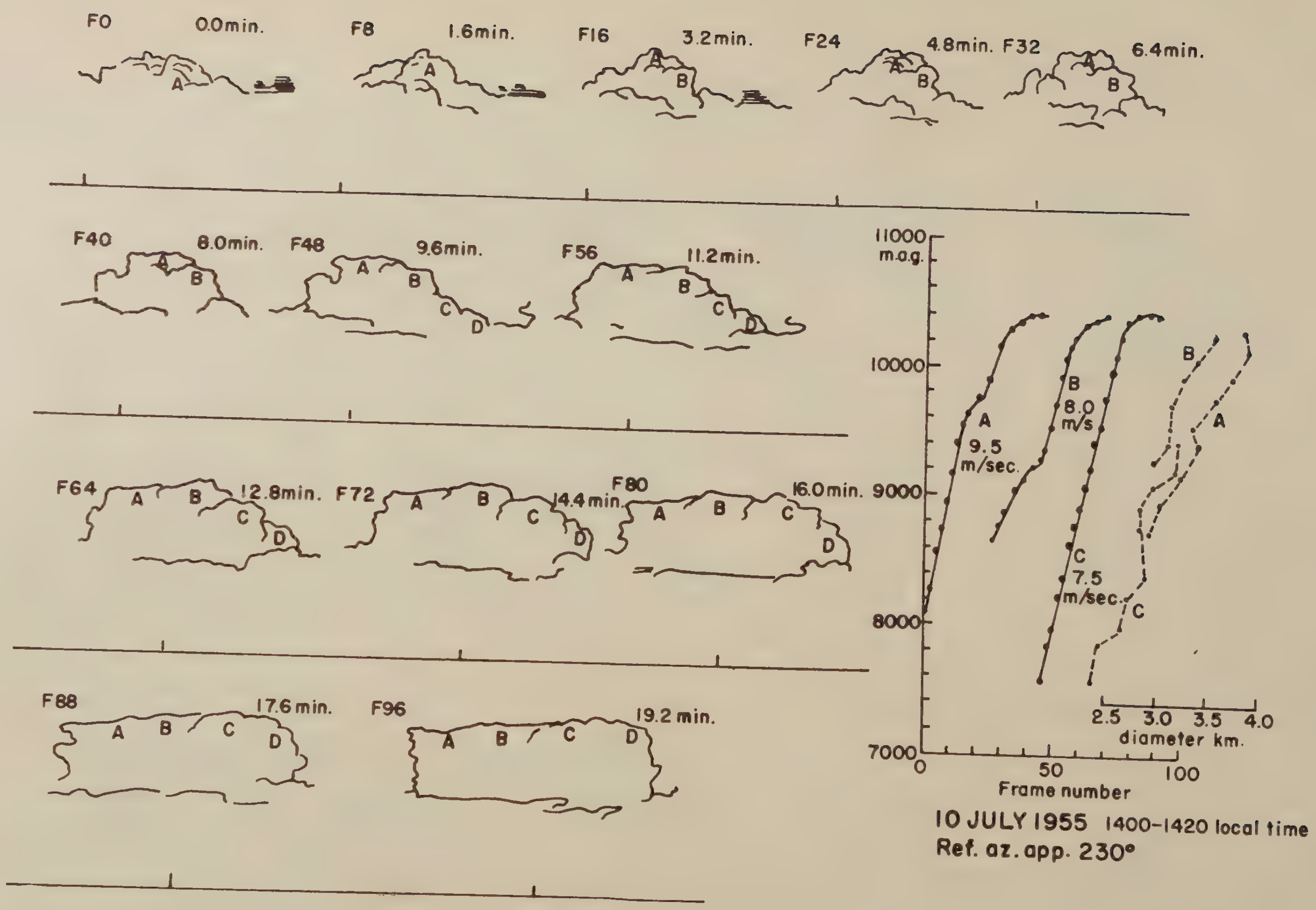

FIG. 4. See fig. 2.

relative wind, and θ is the mean elevation of the top for the interval employed. Since, for the occasions studied here, the winds in the lower troposphere were generally less than 10kn and the shear was therefore correspondingly weak, this correction was generally employed only for massive clouds.

3. The diameter of cumulus thermals

Consider first observations of the horizontal dimensions or *diameter* of cloud thermals. Our principal concern is for diameter measurements which are made as thermals emerge at the cloud summits or on the cloud flanks, because after emergence they mix with the unsaturated air surrounding the cloud and as a result lose buoyancy; they suffer erosion [12], and the simple linear relationship predicted for thermals traversing the saturated interior of the cloud [1] no longer holds.

Early in the course of our examination, it became apparent that large thermals emerge only from deep clouds, while shallow clouds produce only small thermals; see the drawings traced from the films in figs. 2 to 4. In addition, it became apparent that the concept of a cumulus as containing a *small* number of thermals is useful for clouds ranging in size from humilis to the massive cumulonimbus; the deeper the cloud, the larger the 'bricks' from which it is constructed. Consequently, we can expect that an improved description of the behavior of individual thermals will benefit our understanding of both small and large cumulus.

At this point, it seems appropriate to describe the procedure by which the 'diameter' of a thermal is measured. As thermals first emerge from the residues of earlier colleagues, we make use of the observation that they have a roughly hemispherical upper cap; the first estimate of thermal diameter is thus obtained by fitting an imaginary semi-circle to the cloud outline (fig. 5a). We continue to make diameter measurements as the cloud thermal grows, generally at 20- to 40-sec intervals, until it has risen well above the inactive cloud when its diameter is commonly unequivocally defined (fig. 5b). Here the diameter (=width) measurement is made at a distance between $D/2$ and D below the peak. The continuity which must exist between these two methods of estimation is found to lead to a considerable reduction in the uncertainty of the early emergent values; nevertheless, even with this check, a simple test showed estimates varied by 5 to 15 per cent. Because of the confirmation afforded by the successive diameter measurements, they (together with the emergent values) will generally be found here.

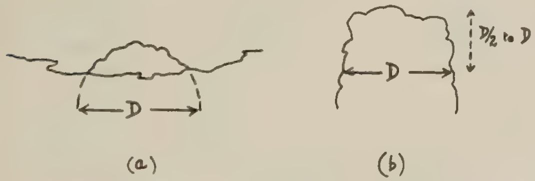

FIG. 5. Estimating cloud-thermal diameter.

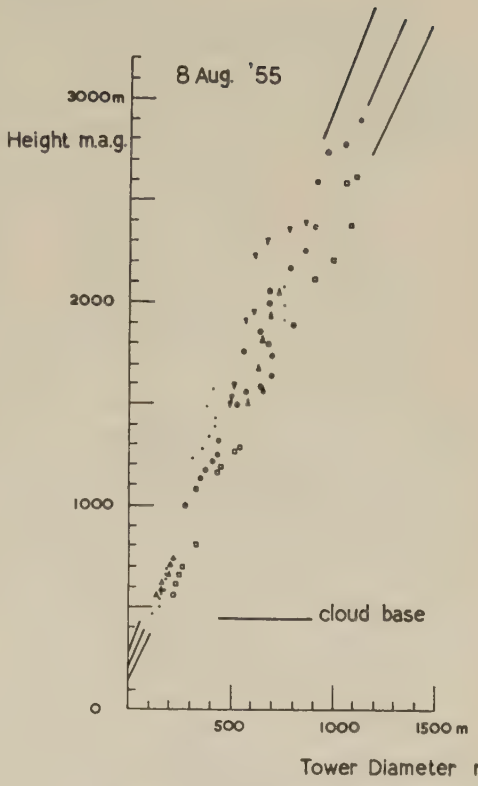

FIG. 6. The diameter of active isolated cloud thermals as a function of height. Measurements made on the same thermal are given the same symbol: the emergent diameter value is thus represented by the lowest in each group. (The abbreviation m.a.g. is meters above ground.)

The height-diameter relationships of the individual 10 to 25 thermals studied on each of ten days have been plotted, and specimen results are shown in figs. 6 to 8. The same symbol is used to denote measurements made on the same thermal, generally with the smallest value representing the diameter of the emerging cumulus thermal. From these diagrams, two significant conclusions are drawn — namely, that at a given height there is a well defined upper limit to the diameter of a thermal emerging from a cumulus, and that this limiting diameter increases linearly with height. If D denotes the upper limit to the diameter of cloud thermals whose caps are at a height Z_{cap},

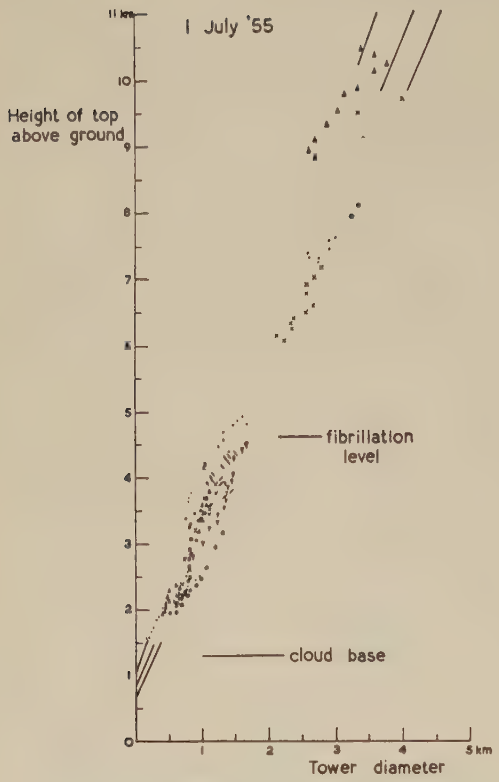

FIG. 7. See fig. 6.

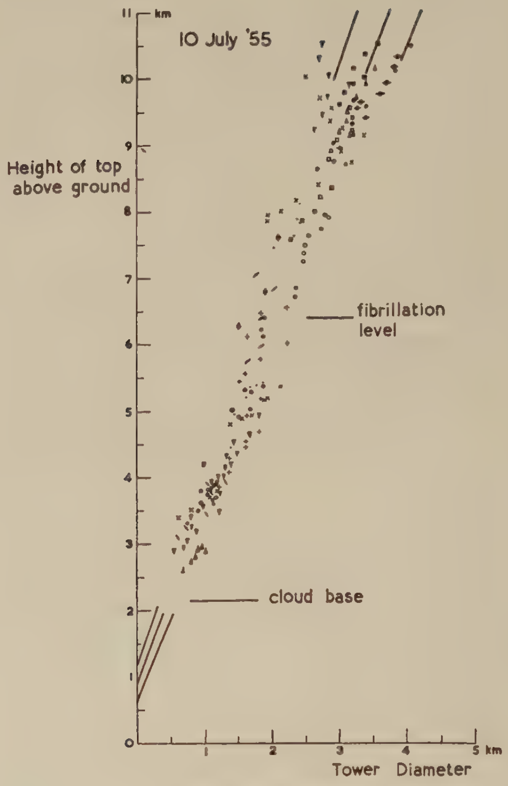

FIG. 8. See fig. 6.

then

$$D = m(Z_{\text{cap}} - Z_0) \tag{1}$$

where we term m the broadening coefficient and Z_0 the height of the thermal virtual origin. m and Z_0 were determined from the data for each day's observations by drawing a line by eye through the scatter of points. Two further lines were drawn on each figure to contain about 90 per cent of the estimates of the diameter of the emerging thermals. Thus, from fig. 6, we obtain $m = 0.41 \pm 0.04$ and $Z_0 = 200 \mp 70$ m. The lower limit on this spread probably has little significance because of the selection of the largest cloud thermals present at any height. On the other hand, the upper limit is about what would be expected from the uncertainty of the diameter estimate if relation (1) were precise.

It will be recalled from a previous paper [10] that when cloud thermals appreciably surpass a certain height, termed the fibrillation level, they become glaciated and charged with precipitation. It is noteworthy that the emergent diameter-*versus*-height relationship for these glaciated thermals is not different from that for the smaller thermals of non-precipitating clouds; for the days of figs. 7 and 8, for example, the values of m are 0.38 ± 0.04 and 0.41 ± 0.04 respectively. Indeed, the total range of values of the broadening coefficient for all the days of observation is small, from 0.35–0.42 (see table 2). Because of the uncertainty in deducing the value of m this variation is not considered significant.

The mean value of the broadening coefficient has been derived in a number of different ways: (1) by giving each day's value of m equal weight, and by weighting each day's value of m by (2) the number of thermals measured and (3) the total height range. All methods give the same value of $\bar{m} = 0.40 \pm 0.04$.

Aerological data for the occasions studied were obtained from the 1500 local time radiosonde ascent made at Frösön, only 10 km south of the observing site. From this data, we have computed the average relative humidity for the cloud layer; values are presented in table 2. On the assumption that these values are representative of an area with 75 km radius and for a period of up to 6 hr before and after the release of the sonde, we would conclude that the

TABLE 2. Values of the broadening coefficient and height of the virtual origin for ten days of scattered cumulus.

Date	m	Z_0 (m)	$Z_{c.b}$ (m)	Mean approp. relative humidity (%)	Rate of rise (m/sec)	Height range studied (km)	No. of towers studied
9 Aug. 54	0.37±0.04	410∓40	750	80±20	1–3	0.9–3.0	11
19 Aug. 54(1)	0.42±0.03	1150∓200	1400	70±15	1–3	1.5–4.5	13
1 Jul. 55(5)	0.41±0.04	800∓150	1300	75±10	2–8	1.5–10.5	26
10 Jul. 55(6)	0.38±0.04	950∓250	2150	85±15	4–10	2.5–10.5	24
11 Jul. 55(7)	0.42±0.05	1300∓200	2100	50±10	4–9	2.7–9.8	15
12 Jul. 55(8)	0.42±0.03	1400∓350	2000	40±10	2–6	2.5–7.3	14
14 Jul. 55(10)	0.35±0.06	1050∓250	1600	70±10	3–7	2.3–6.8	25
8 Aug. 55(11)	0.41±0.04	200∓70	450	80±10	1–4	0.5–3.0	15
15 Aug. 55(13)	0.42±0.04	1300∓150	1850	65±10	1–3	2.2–4.3	17
16 Aug. 55(14)	0.36±0.03	1100∓150	1900	65±10	2–5	2.2–4.7	7
Mean:	0.40±0.04		Range:	40–80%	1–10 m/sec	0.5–10.5 km	Total: 167.

The numbers in brackets identify the occasions.
$Z_{c.b}$ is the height of the cloud base above ground at 1500 local time.

broadening coefficient was insensitive to variations in the mean relative humidity of the cloud layer for the range 40 to 80 per cent. There is some direct support for this assumption in the measurements made from an aircraft flying at the time of the radiosonde ascents and within 5 to 30 km of their release point; these observations showed close agreement in temperature and humidity values and therefore relatively weak horizontal gradients in these quantities [11]. Moreover, the reports in previous papers [9; 10] of the remarkably uniform characteristics of the air-mass convection observed in this entire area implies that the uniformity in the air-mass properties has a scale larger than the observations cited. Presumably, the occurrence of layer cloud at a number of levels between the cumulus is an indication of high humidity in the cloud layer; such clouds were abundant throughout the day on 9 August 1954 and 8 August 1955 when the measured mean humidity was 80 per cent but were almost completely absent on 15 and 16 August 1955 when the measured mean humidity was 65 per cent. Thus, there is both direct and indirect support for the assertion that, on the occasions when the broadening coefficient was measured, there were significant differences in the mean relative humidity of the cloud layer whereas there were no significant differences in the value of the broadening coefficient itself. Such a result is seen to be consistent with the argument that the processes which are responsible for the dimensions of the *emerging* thermal operate within the saturated interior of the cloud. Once the thermal has emerged into the clear air, however, the relative humidity can be expected to influence its further horizontal and vertical growth.

An unexpected and also surprising result is that the broadening coefficient m is insensitive to changes in the vertical distribution of temperature or stability in the cloud layer. This conclusion is commented on later.

A few measurements of the diameter of isolated cumulus thermals have been made by other authors. Malkus and Scorer [12] studied small clouds growing over islands in eastern Massachusetts and in the West Indies, and from their observations the diameter-height ratio for 12 thermals is found to be 0.18–0.34 (the height of the cloud virtual origin was assumed to be the same as that given in our data). In other studies of deep tropical convection [13; 14], ratios of 0.1–0.43 have been found, the largest values associated with towers penetrating the high tropical stratosphere at a height of 17 km. Estimates of the diameter of cloud thermals may also be made from aircraft traverses of a cloud; generally, however, it is not known whether the passes are made through an isolated thermal or two or more adjacent thermals, nor is the height of the cap of the thermal known.[4]

Let us recall that the broadening coefficient m defined in eq (1) relates the diameter of the largest cloud thermals to their height; thus, the value of $m = 0.4$ represents only the upper limit to the ratio between the *emergent* diameter and height. Let us also note that the reported values [12; 13; 14] are a few individual measurements made on thermals which have generally penetrated some distance into the clear air above cloud; there they suffer erosion which diminishes their diameter-height ratio (see next section). For these reasons, we conclude that the observations of other authors are consistent with the data presented here, though they do not permit us to exclude the possibility that real differences may exist.

---

[4] If we suppose a cloud thermal is roughly spherical in shape, then the height of its widest part (or center of mass) Z_G is related to the height of its cap by the expression

$$Z_G = Z_{\mathrm{cap}} - D/2.$$

In terms of Z_G, eq (1) becomes

$$D = \frac{m}{1 - m/2}(Z_G - Z_0), \tag{2}$$

and, for $m = 0.4$, $m/(1 - m/2) = 0.5$. Consequently, the diameter-height ratio conveniently measured on aircraft traverses can have a somewhat higher value than that conveniently determined from ground measurements.

4. The broadening of cumulus thermals

Only one estimate of the diameter of a thermal growing in the interior of a cumulus is provided by observations of the external features of a cloud; this is the thermal diameter just prior to its emergence into the clear air. Consequently, from these observations alone, no direct test can be made of the hypothesis that in the interior of the cloud the diameter of *individual* thermals increases linearly with height. However, the principal result of the previous section — namely, that the upper limit to the diameter of the emerging cumulus thermal is a linear function of height, with a coefficient of proportionality 0.40 ± 0.04 close to the value of 0.5 found in Scorer's experimental studies — strongly supports this notion.

Further confirmatory evidence is furnished by the behavior of isolated cloud thermals *in clear air*. Measurements of the diameter of cloud thermals growing in clear air show that here too the thermal *may* broaden as it grows; see figs. 2 to 4, 6 to 8, and especially figs. 9 and 10. These latter figures have been constructed from film sequences on near clouds which remained at the same distance from the camera and were not subject to shear. The broadening of cloud thermals in the clear air, a common but by no means invariable behavior, is also found in photographs published by other authors; we may instance examples by Malkus and Bunker [15], Scorer and Ludlam [3] and Koldovský [16]. However, the superimposition technique shown in figs. 9 and 10 reveals this phenomenon in a striking fashion.[5]

As is mentioned earlier, when a cloud thermal emerges from the interior of a cloud, evaporative chilling takes place on its periphery; the volume of buoyant air comprising the thermal may then diminish due to the shedding of mixed material into a wake. Because of this process, first described by Malkus and Scorer [12], the proposed linear diameter-height relationship breaks down. These ideas seem supported in the laboratory studies of Scorer and Rönne [17] who released isolated masses of buoyant fluid into fluid at rest and possessing a stable density stratification. The equilibrium level of the buoyant fluid released then varies according to the amount of dilution it suffers. Thus, fluid which is strongly diluted rapidly reaches its equilibrium level and is shed into a wake behind the less diluted fluid of which the advancing mass is composed. Depending on the balance between this shedding and the incorporation of new fluid, the diameter of the mass may now increase or decrease with height. Certainly, however, its diameter increases less rapidly than that observed in the presence of neutral stratification. Probably evaporative erosion in cumulus thermals has the same characteristics, so that when a cloud thermal passes from the interior of a cloud to the exterior its rate of broadening decreases.

Thus, the fact that individual cloud thermals are commonly observed to broaden with height in clear air lends added confidence to the assertion of the broadening of individual thermals in the cloud interior.

5. The rate of rise of cloud thermals

There is nothing in this study which provides information about the vertical extent of the buoyant air within a thermal. In what follows, we shall assume a roughly spherical shape with vertical extent equal to its diameter.

By appeal to dimensional arguments, an expression can be derived for the rate of rise of such a buoyant mass [4; 18]. Calling the mean buoyancy of the mass $g\bar{B}$, where $\bar{B} = \overline{\Delta\rho}/\rho$ with $\overline{\Delta\rho}$ the mean density difference between the mass and its exterior (of density ρ), and r the radius of the mass, the ascent rate W is given by the expression

$$W = C(g\bar{B}r)^{\frac{1}{2}} \qquad (3)$$

where C is a constant. Relation (3) was well confirmed in the experimental studies of Scorer [4] in an environment with neutral stratification, and a value of $C = 1.2$ was obtained.

Elsewhere [18; 19], it was pointed out that the relation for the rate of rise of the buoyant mass changed when its surroundings are stratified; the value of C is no longer generally constant but is some complex function of the stratification. Ludlam [1], however, employed eq (3) to predict the rate of rise of cloud thermals in an unstable environment by assuming that the stratification was sufficiently close to neutral for the value of C to be close to 1.2. The application of eq (3) is clearly seen to be restricted, for it does not permit the penetration of a thermal beyond its equilibrium level, when $g\bar{B} \rightarrow 0$, $W \rightarrow 0$, whereas 'overshoot' is known to occur [14; 20].

In examining the validity of eq (3) for cloud thermals, we again suppose that only measurements on emergent thermals approximate to their properties

---

[5] The motion of the nodules or details which appear on the upper cap of cloud thermals growing in clear air is also shown in figs. 9 and 10. From a total number of seven cases in which thermal diameters ranged from 200 to 2,000 m and detail sizes from 25 to 300 m, two conclusions were reached:

(i) The clear air adjacent to the cap of the growing thermal is pushed upwards and outwards with horizontal velocities reaching 0.6 to 0.8 of the rate of rise of the cap. The existence of such horizontal motions in convection has often been assumed; here they are demonstrated.

(ii) Details which initially appear on the central parts of the thermal cap may later arrive in the vertical cloud walls. Since the cap of the growing thermal is a region of pronounced mixing, the material in the cloud wall is considerably diluted; it is not necessary to postulate lateral mixing at the cloud wall to account for the dilution observed there.

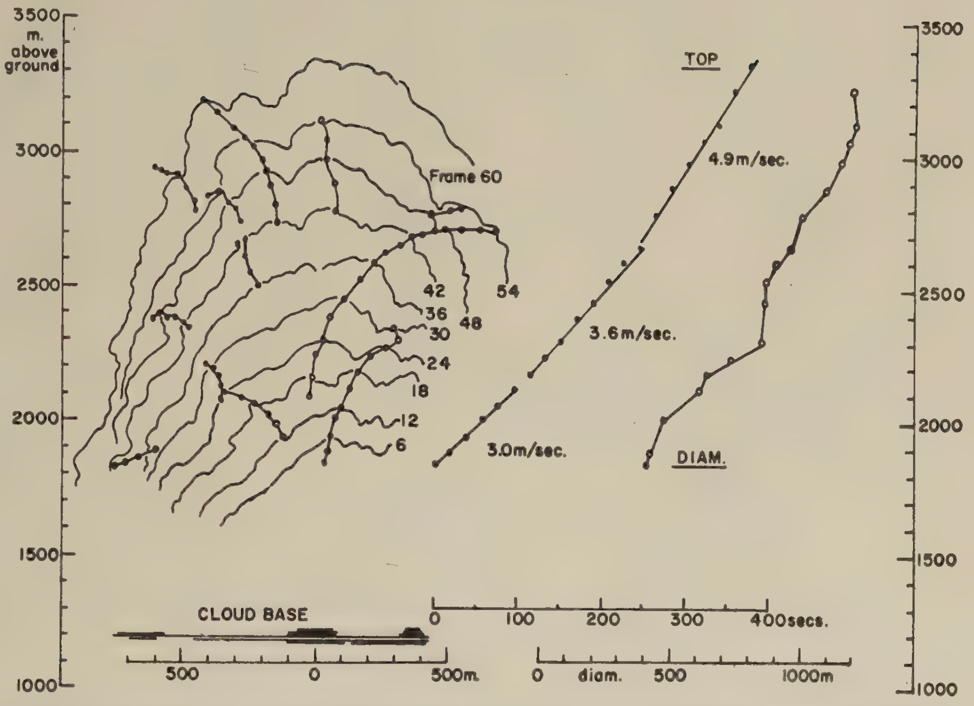

FIG. 9. The broadening of a cumulus thermal with height in the clear air; the growth of a congestus of 1348–1354 local time, Östersund, 10 August 1955: the outline of the thermal is shown superimposed at intervals of 37 sec. The motions of protuberances and nodules on its surface are also indicated.

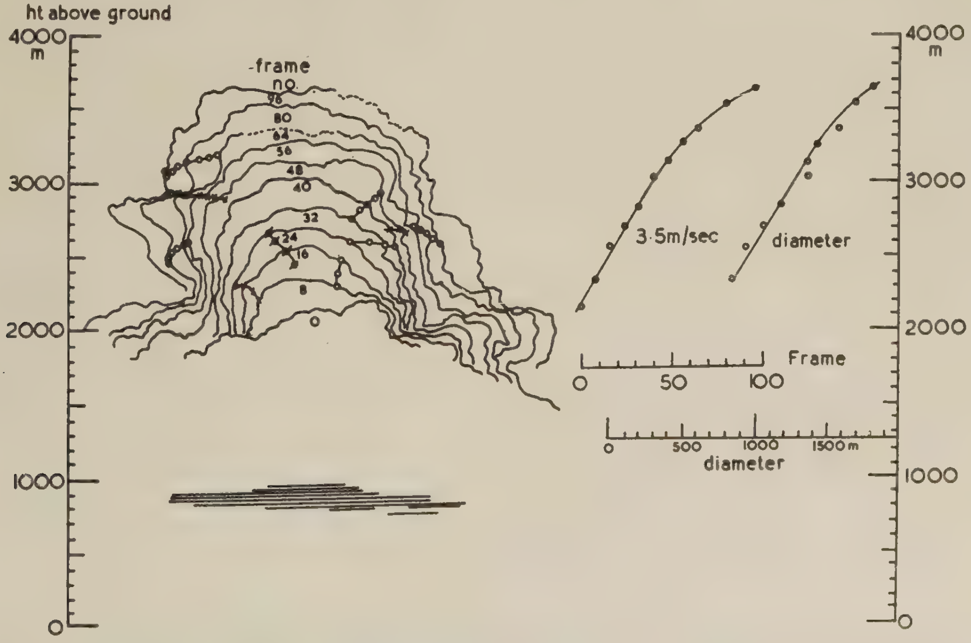

FIG. 10. The growth of a congestus thermal of 1750–1800 local time, Östersund, 1 July 1955. The outline is shown superimposed at intervals of 57 sec.

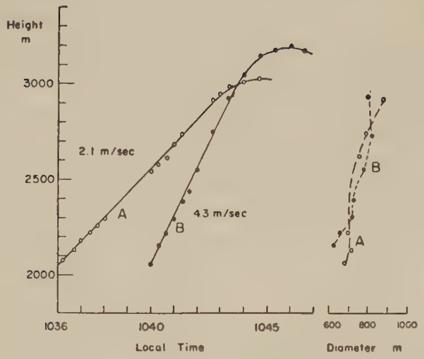

FIG. 11. The diameter-height and height-time relationships for pairs of contemporary cumulus thermals. Östersund, 9 August 1954.

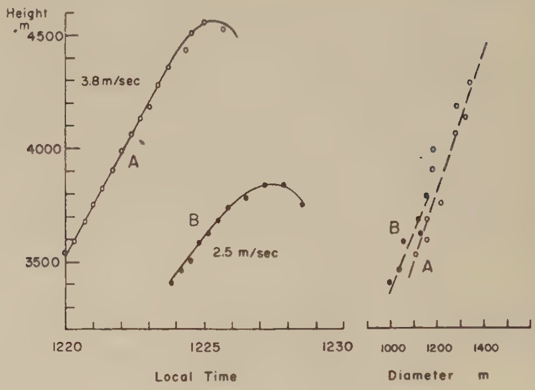

FIG. 12. See fig. 11. 19 August 1954.

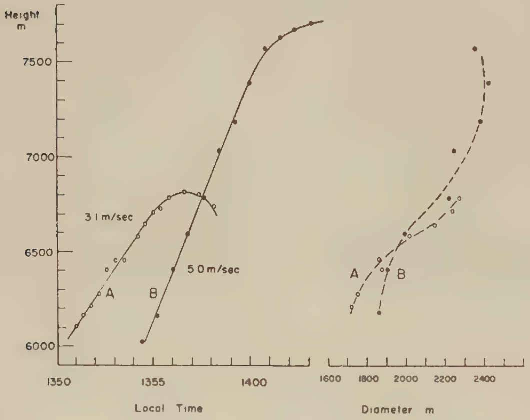

FIG. 13. See fig. 11. 12 July 1955.

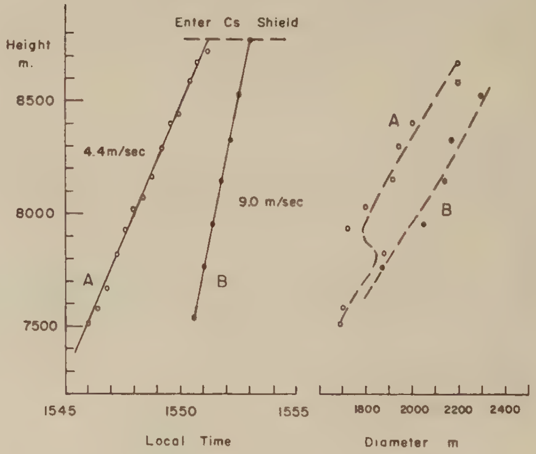

FIG. 14. See fig. 11. 11 July 1955.

in the cloud interior. Measurements were made of the height of the top of the thermal at 20- to 40-sec intervals (sufficient to obtain a displacement of at least 2 or 3 mm on the projection screen) from the moment of emergence up to the cessation of its vertical growth. Figs. 2, 4 and 9 through 14 illustrate these measurements and indicate the facility with which the emergent rate of rise is estimated.

Figs. 11 through 14 show the diameter-height and height-time relationships for pairs of cumulus thermals which emerged at the same height and time in the summits of adjacent clouds (nearer than 5 km). These examples were selected to demonstrate that thermals may have widely different rates of rise although they are contemporary and have approximately the same lateral dimensions. On the basis of eq (3), we conclude that in each pair the thermals have different buoyancies. If we examine the data for all the days of cumulus, we find that at any height the scatter in the values of emergent diameters (±15 per cent about a mean) can produce only a small part of the scatter found in the rate-of-rise values (greater than ±50 per cent about a mean); see eq (3). We thus conclude that, at a given height, differences in the rate of rise of cloud thermals are principally due to difference in their buoyancy and that the most rapidly ascending thermals have the greatest buoyancy.

According to the view of a thermal as an entraining mass, the buoyancy of a thermal at any height is strongly influenced or even largely determined by the character of the environment through which it has passed. Now the immediate environment of rising thermals, we may recall, is composed of the slowly evaporating residues and wakes of previous thermals. Ludlam (*loc. cit.*) thus argues that, when thermals are generated in cloud at wide intervals and therefore ascend widely separated from one another, their residues can partially evaporate into the clear air around the cloud; the cloud may thus dissipate despite the generation of new thermals. Furthermore, the diminishing volume of cloud air in which these new thermals grow may be colder than the clear air surrounding the cloud. As the rate of thermal generation increases, however, thermals follow one another more closely and their residues may accumulate; the cloud volume thus increases, but more importantly here the buoyancy of the thermal residues may now approach that of the clear-air environment. If the rate of thermal generation is sufficiently high, the buoyancy of the thermal residues may even exceed that of the clear air. Great emphasis is thereby placed on the history of the cloud preceeding a particular instant for the properties observed at that time.

We now make the assumption that the rate of generation of thermals in the clouds studied here is such that the virtual temperature of the thermal residues can approach but not exceed that of the clear air around the cloud; in addition, we shall suppose the liquid-water content of the thermal residues is zero. Since observations of the internal properties of cumulus do not permit us to claim more than plausibility for the assumption [21], the only justification which can be advanced for this hypothesis is that it is simple and avoids the use of arbitrary and adjustable constants. We note that, with this tentative hypothesis, we are only able to calculate an upper limit to the mean buoyancy of cloud thermals; any individual thermal we observe will have a buoyancy less than this value — and less by an unknown amount.

In a previous paragraph, we showed that those emerging thermals which have the greatest ascent rates have the greatest buoyancy. Since we can only calculate the upper limit to the buoyancy in a thermal in order to test relation (3), we must employ the maximum rates of rise that are observed. Profiles of this quantity have been constructed by drawing an envelope to the scatter of values of (emergent) rates of rise, and these are presented in fig. 15. For reasons which will become apparent later, only observations derived from thermals which contain no precipitation and which do not glaciate are considered; that is, we restrict attention to thermals at heights between cloud base and the fibrillation level [10]. Within this range, the *upper limit* to the ascent rates varies from 1 to 8 m per sec (fig. 15).

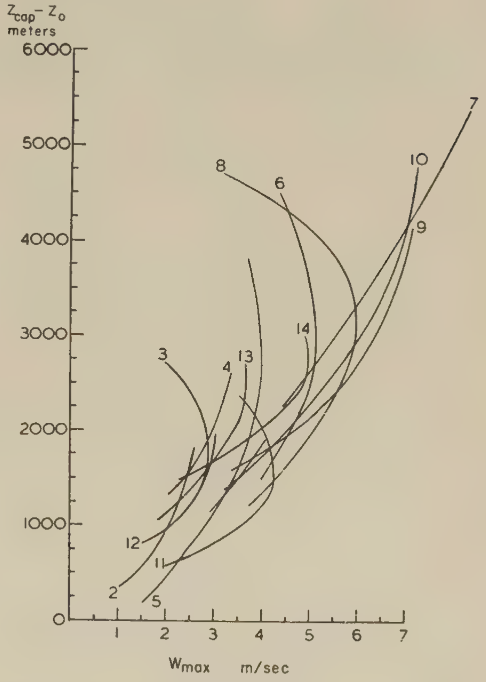

FIG. 15. Maximum rates of rise of emergent cloud thermals on the occasions numbered in table 4, as a function of height above thermal virtual origin, from near cloud base to the level of shower formation.

6. The maximum buoyancy in cloud thermals

The manner in which the upper limit to the average thermal buoyancy is deduced has been demonstrated by Ludlam [1]; here we follow him closely but derive a more general result. A cloud thermal is assumed to have a roughly spherical *shape* which does not change during its growth in the cloud interior; the thermal *size* is also assumed to increase linearly with height. Then its mass $M(\zeta)$ is written

$$M = A\rho\zeta^3 \tag{4}$$

where ρ is the air density averaged throughout the thermal and $\zeta = Z_G - Z_0$ is the height of the center of mass of the thermal above its virtual origin. A is determined by the actual geometrical shape of the thermal and by the broadening coefficient m; as we shall see, its value does not enter the analysis as long as both these factors remain unchanged.

The properties of the thermal at height ζ_1 are then calculated in the following way. The level of origin of an increment of its mass $dM = d(A\rho\zeta^3)$ is the height ζ. In being lifted from the height ζ to the height ζ_1, the mass increment is assumed to undergo a (saturation) adiabatic expansion and upon its arrival at ζ_1 to mix uniformly with other incremental masses originating at other heights. To fix ideas, consider the argument for the average *buoyancy* of a cloud thermal. This quantity is measured by the difference between the cloud virtual temperature of the thermal and that of the clear-air environment; the cloud virtual temperature is the virtual temperature corrected for the weight of liquid water [22].

Let $\Delta T(\zeta \rightarrow \zeta_1)$ be the cloud virtual-temperature excess of saturated air lifted adiabatically from the height ζ to the height ζ_1; by the above argument, the average cloud virtual-temperature excess of the thermal $\Delta\bar{T}$ at height ζ_1 is then

$$M(\zeta_1)\cdot\Delta\bar{T} = \int_{\zeta_{c.b}}^{\zeta_1} \Delta T(\zeta \rightarrow \zeta_1)\cdot dM + M(\zeta_{c.b})\cdot\Delta T(\zeta_{c.b} \rightarrow \zeta_1) \quad (5)$$

where $\zeta_{c.b}$ is the height of the base of the cumulus. This derivation, we note, neglects any slight change in temperature resulting from an adjustment of the vapor content of the mixture to its saturation value. By making a further approximation,

$$\Delta T(\zeta \rightarrow \zeta_1) = \Delta T(\zeta_{c.b} \rightarrow \zeta_1) - \Delta T(\zeta_{c.b} \rightarrow \zeta), \quad (6)$$

which is approximately equivalent to assuming that on an aerological diagram adjacent saturation adiabats are parallel, we arrive at the result

$$\Delta\bar{T} = \Delta T(\zeta_{c.b} \rightarrow \zeta_1) - \frac{1}{M(\zeta_1)} \int_{\zeta_{c.b}}^{\zeta_1} \Delta T(\zeta_{c.b} \rightarrow \zeta)\cdot dM. \quad (7)$$

When one recalls that $\Delta T(\zeta_{c.b} \rightarrow \zeta)$ represents the cloud virtual-temperature excess of air lifted adiabatically from cloud-base level to height ζ, it is evident from eq (7) that, if the clear-air sounding is known, the average buoyancy of the most vigorous thermals can be computed.

By inspection of eq (7), we see that at any height ζ_1 the thermal buoyancy depends on the profile of the sounding at all heights up to ζ_1; in this respect, it differs from the parcel model ($dM = 0$) which gives the buoyancy of a rising element at height ζ_1 as $\Delta T(\zeta_{c.b} \rightarrow \zeta_1)$.

In order to evaluate the integral in eq (7), the local 1500 radiosonde ascent was plotted and the cloud base for that time located on it. By 1500 hr local time, the surface wet-bulb potential temperature and the cloud-base wet-bulb potential temperature have generally reached their maximum values. Accordingly, in the cloud layer, the difference between the clear-air temperature and the saturation adiabat through the cloud base has also reached a maximum by this time; that is, by mid-afternoon, the atmosphere has reached a state of maximum instability for the day. (Again, horizontal uniformity of the air mass is assumed.) Consequently, calculations of thermal buoyancies based on the 1500 sounding should indeed represent their upper limit. Initially, we assumed that the temperature excess of air reaching the level of cloud base and generating cloud thermals was zero. Then, with the aid of computations presented elsewhere [22], $\Delta T(\zeta_{c.b} \rightarrow \zeta)$ was obtained at 500-m intervals.

Values for the height of the virtual origin were taken from table 2 and the expression

$$\rho = \rho_0(1 - \zeta/H)$$

with $H = 13.5$ km was used to approximate the variation of density with height in the height range 1 to 7 km. The upper limit to the mean thermal buoyancy was then determined at 500-m intervals from cloud base to the fibrillation level. A trial numerical integration with $\Delta T(\zeta_{c.b} \rightarrow \zeta) = a\cdot\zeta$ for which the exact analytical result is readily obtained showed that the trapezium rule gave poor results, especially for small ζ. Simpson's rule gave very good results and was employed throughout these calculations.

In table 3, a specimen evaluation of the buoyancy in cloud thermals is presented, and in figs. 16 to 18 are shown both the *adiabatic* cloud virtual-temperature excess (solid line) and the mean *thermal* cloud virtual-temperature excess (pecked line) for three of the days studied.

The most striking result of the calculations is that thermals growing in cloud in the lower 2/3 to 3/4 of

TABLE 3. Evaluation of buoyancy of thermals growing in cloud on 11 July 1955 (day 7); also evaluation of C.
$Z_0 = 1300$ m $\zeta_{c.b} = 800$ m Cloud wet-bulb potential temperature 19.4C

Z m	ζ m	ΔT_1 °C	ΔT_2 °C	ΔT_3 °C	ΔT_4 °C	Integral of eq (7)	$\Delta\bar{T}$ °C	$\Delta\bar{T}/\Delta T_4$	$D/2$ m	$\left(g\frac{\Delta\bar{T}}{T}\frac{D}{2}\right)^{\frac{1}{2}}$ m/sec	W_{max} m/sec	C
2100	800	0	0.6	0	0.6	0	0.6	1.0	200	0.65	—	—
2600	1300	1.4	0.7	−0.3	1.8	0.93	0.87	0.48	325	3.15	4.1	1.30
3100	1800	2.0	0.6	−0.5	2.1	1.63	0.47	0.22	450	2.72	5.2	1.91
3600	2300	3.0	0.5	−0.7	2.8	1.99	0.81	0.29	575	4.04	5.9	1.46
4100	2800	3.8	0.3	−0.9	3.2	2.46	0.74	0.23	700	4.25	6.3	1.48
4600	3300	3.7	0.2	−1.1	2.8	2.65	0.15	0.05	825	2.08	6.2	2.98
5100	3800	3.4	0.2	−1.3	2.3	2.61	−0.31	—	950	—	7.0	—
5600	4300	3.5	0.1	−1.4	2.2	2.50	−0.30	—	1075	—	8.3	—

Cloud base $Z_{c.b} = 2100$ m.

Fibrillation level-thermal cap $\begin{cases} Z_{cap} = 6400 \text{ m} \\ \zeta_{cap} = 5100 \text{ m} \end{cases}$ thermal center of mass $\begin{cases} Z_G = 5380 \text{ m} \\ \zeta_G = 4080 \text{ m.} \end{cases}$

ΔT_1 = difference between clear air temperature and saturation pseudo-adiabat.
ΔT_2 = virtual temperature increment.
ΔT_3 = cloud virtual temperature increment (Reference [22], fig. 6).
$\Delta T_4 = \Delta T_1 + \Delta T_2 + \Delta T_3 = \Delta T(\zeta_{c.b} \rightarrow \zeta)$.

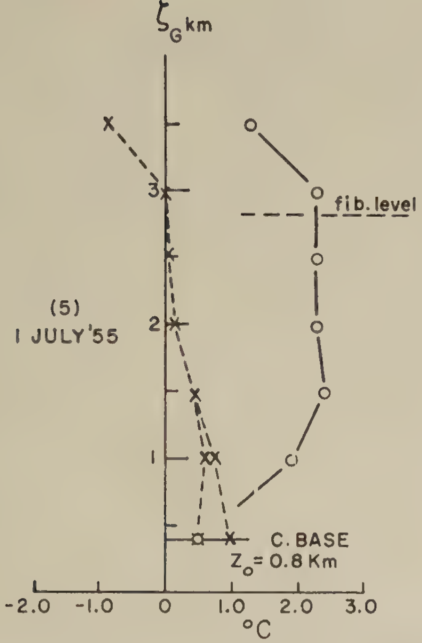

FIG. 16. The buoyancy in cloud thermals as a function of height above thermal virtual origin. The solid line represents the adiabatic cloud virtual-temperature excess, the pecked lines represent upper limits to the average cloud temperature excess in thermals with an initial temperature excess of (a) zero and (b) 0.5C.

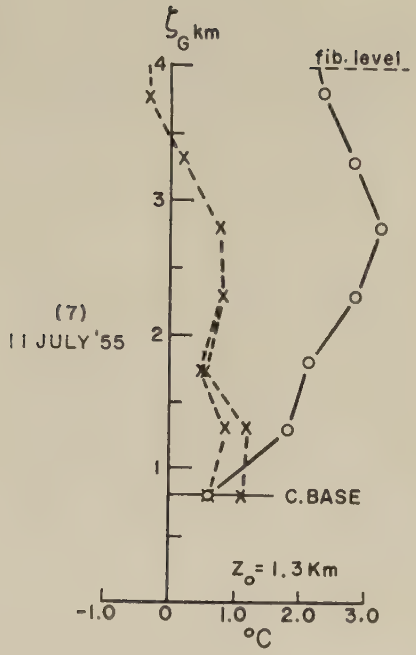

FIG. 17. See fig. 16.

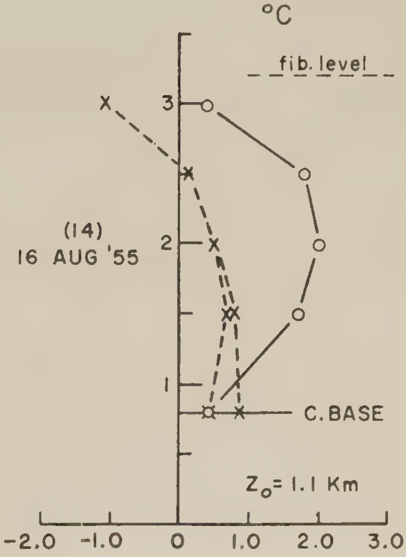

FIG. 18. See fig. 16.

the layer extending from cloud base up to the level of shower formation can have positive buoyancy, while in the upper 1/3 to 1/4 of this layer, however, they are negatively buoyant with respect to their surroundings. Secondly, as expected from the earlier studies of Ludlam [1], where the cloud thermal has positive buoyancy it is less than the adiabatic value. Characteristically, where the adiabatic cloud virtual-temperature excess is 2C to 3C, the corresponding mean thermal excess in the most buoyant thermals is only $\frac{1}{2}$C to 1C.

Above the level where the adiabatic buoyancy reaches its maximum value, the average buoyancy in the cloud thermal rapidly falls to zero, within 500 to 800 m in our data, and then becomes negative. As indicated above, this disappearance of buoyancy generally takes place in thermals before they can attain the height of the fibrillation level. Since we observe clouds to grow up to and even well beyond this level, we conclude that thermals in such clouds overshot their equilibrium level. When we compute for each day how far the level of zero buoyancy is below the fibrillation level, we obtain values closely comparable with the diameter of cloud thermals at the level of zero buoyancy (see table 4). Thus, we conclude that the most buoyant thermals need only overshoot their equilibrium level by a distance equal to their diameter in order to reach the fibrillation level. We may note here that, once the fibrillation level is surpassed, fresh sources of buoyancy become available to the thermal (as is discussed below) so that the further growth of cloud is possible without

TABLE 4. Some properties of the cloud layer between base height and the fibrillation level.

Day	Total cloud depth base to fibrillation level	Distance of cap of thermal below fibrillation level when mean buoyancy disappears	Diameter of thermal at level where buoyancy disappears	Depth of unstable cloud layer	Extreme values of C in unstable cloud layer
2	2000 m	450 m	800 m	1100 m	0.87–1.83
3	2600	600	1100	1350	0.77–1.71
4	3100	850	1250	2050	1.36–2.38
5	3500	(200 m above)	—	1400	1.28–1.63
6	4300	1500	1150	1900	1.03–1.99
7	4300	650	1750	2500	1.3 –1.91
8	4400	150	1900	650	0.73–1.46
9	4000	1150	1300	2500	1.46–1.93
10	4600	1850	1100	1700	1.28–1.81
11	3300	1200	950	2000	0.9 –2.06
13	3300	1900	750	850	1.16–1.25
14	3300	850	1150	1600	1.36–1.87

further overshoot. That cloud thermals can overshoot a distance equal to their diameter does not seem unreasonable in view of the observed penetration of the stratosphere by cumulonimbus towers where the tropopause can be taken as the thermal equilibrium level [14; 20].

If we suppose that the mass of air from which the cloud thermal originates has a temperature excess of 0.5C over that of the air surrounding it at the cloud base (as against a zero value assumed above), the conclusions of the previous paragraphs are unaltered. Because the original mass of the thermal is small, the influence of its original temperature excess falls off rather rapidly (see figs. 16 to 18); indeed, at a height of 1 km above cloud base, its effect is already negligible.

Now it is readily demonstrated that only moderate amounts of liquid water when either precipitated from or frozen in a cloud thermal can add significantly to the thermal buoyancy. Thus, if 1 g of liquid water is removed from 1 kg of air, the buoyancy gain is equivalent to a warming of 0.25C: if this amount of liquid water freezes (but is retained), the warming is 0.3C. These figures are comparable with the mean buoyancy we calculate thermals to possess, so that both processes can add significantly to the buoyancy of thermals growing in showering clouds. Because eq (5) to (7) do not take into account either of these processes, we have been restricted in our calculations to levels up to but not beyond the stage of fibrillation. In order to estimate thermal buoyancy in the more massive clouds, it is necessary to make hypotheses about the details of the fall-out and glaciation processes, and, because of our ignorance of these details and also because of the already tentative nature of the buoyancy calculations, we have not yet attempted it.

7. The dependence of thermal rate of rise on buoyancy and diameter

If the measurements of thermal diameter (section 3) and the estimates of the upper limit of thermal ascent rate (section 5) and of thermal buoyancy (section 6) are given, it is possible to construct values of the quantity

$$\frac{W_{\max}}{\left(g\,\dfrac{\overline{\Delta T}}{T}\,\dfrac{D}{2}\right)^{\frac{1}{2}}}$$

which from eq (3) should be equal to the constant C. Because of the finite vertical extent of the thermal, the emergent rate of rise measured at height Z_{cap} is to be associated with the calculated buoyancy at height $Z_{\text{cap}} - D/2$ rather than with that at height Z_{cap} itself. This procedure is consistent with the assumption that the thermal is roughly spherical. The ratio above can only be determined for positive values of $\overline{\Delta T}$, and as concluded earlier these are closely related to the layer within which the lapse of temperature exceeds the saturation adiabatic. Consequently, eq (3) can only be expected to be valid within the statically unstable region of the cloud layer and can only be tested there.

Values of C have been determined at 500-m intervals above cloud base for twelve days of observations, and their range is presented in table 4. A wide scatter of values results, although no systematic trend of C with height is apparent; the mean value for C is 1.5 with a standard deviation of 0.5. Evidently, C is not defined with great precision from these observations but can be said to lie close to the value of 1.2 found in laboratory experiments [4]. In view of the tentative nature of buoyancy estimates in thermals and the uncertainty of the validity of a constant C in a statically unstable atmosphere, this agreement is considered remarkable.

8. Summary and conclusions

Further descriptive evidence has been advanced for the 'thermal' theory of cumulus convection, but more significantly steps have been taken to set the theory on a firmer quantitative basis than hitherto. Because cumulus dynamics are dominated by the latent heat released in the condensation process, the principal results obtained here should have wide generality. These results are summarized below.

a. From measurements of the diameter of cumulus thermals emerging on the flanks and in the summits of cloud, it is concluded that in the cloud interior the vertical growth of a thermal is always accompanied by growth in its lateral dimensions; a linear relationship is found between diameter and distance penetrated with a coefficient of proportionality 0.40.

b. The broadening of a cloud thermal results from the entrainment of the wakes and residues of earlier thermals which lie in its path; by hypothesizing that the virtual temperature of the entrained air approaches (as an upper limit) the virtual temperature of the clear-air environment, the buoyancy in the most vigorous thermals is deduced. Characteristically, the buoyancies here are only ½C to 1C, much smaller than the adiabatic values. Once a cloud is large enough to shower, fall-out and glaciation augment its buoyancy sufficiently to permit further growth.

c. A relation between rate of rise, buoyancy and diameter (eq 3) found valid in experimental studies is shown to describe the behavior of thermals emerging from cumulus; the use of the relation, however, is restricted to the statically unstable fraction of the cloud layer.

Further studies are desirable to generalize relation (3) for conditions in which the environment is statically stable and 'overshoot' can occur; the area in which the thermal theory can be tested will be extended thereby. It is hoped that experimental studies currently being performed by the author will help in this matter and will also clarify the observations of the insensitivity of broadening coefficient to stability.

In the discussion of the evaluation of the buoyancy of cloud thermals, the importance of the entire history of a cloud for the properties of thermals growing within it is emphasized. We have argued with Ludlam [1] that the rate of generation of thermals within cloud determines whether a cloud dissipates or builds and also controls the character of the environment through which new thermals must rise. Thus, we must establish the factors that determine the rate of generation of thermals in cloud and link the generation rate to the resulting character of the environment. With such information, we can hope to proceed further towards an understanding of the changing balance in which a cumulus is maintained.

Acknowledgements. The writer would like to acknowledge the generous support, friendly encouragement and guidance of F. H. Ludlam and the helpful discussions with R. S. Scorer and J. S. Malkus. The writer wishes to acknowledge the financial support of the Department of Scientific and Industrial Research in the United Kingdom, the Statens Tekniska Forskningsråd, Sweden, and the Munitalp Foundation, U.S.A.; these latter organizations made possible the field work.

REFERENCES

1. Ludlam, F. H., 1958: The hail problem. *Nubila*, **1**, 13–96.
2. Ludlam, F. H., and R. S. Scorer, 1953: Convection in the atmosphere. *Quart. J. r. meteor. Soc.*, **79**, 317–341.
3. Scorer, R. S., and F. H. Ludlam, 1953: Bubble theory of penetrative convection. *Quart. J. r. meteor. Soc.*, **79**, 94–103.
4. Scorer, R. S., 1957: Experiments on convection of isolated masses of buoyant fluid. *J. Fluid Mech.*, **2**, 583–594.
5. Woodward, E. W., 1959: The motion in and around isolated thermals. *Quart. J. r. meteor. Soc.*, **85**, 144–151.
6. Stommel, H., 1947: Entrainment of air into cumulus cloud. *J. Meteor.*, **4**, 91–94.
7. Stommel, H., 1951: Entrainment of air into cumulus cloud II. *J. Meteor.*, **8**, 127–129.
8. Levine, J., 1959: Spherical vortex theory of bubble-like motion in cumulus clouds. *J. Meteor.*, **16**, 653–662.
9. Ludlam, F. H., 1955: Planning cloud seeding research. *Archiv. Meteor. Geophys. Bioklim.*, **A8**, 283–292.
10. Ludlam, F. H., and P. M. Saunders, 1956: Shower formation in large cumulus. *Tellus*, **8**, 424–442.
11. Ludlam, F. H., and P. M. Saunders, 1957: Comparison of aerological soundings made simultaneously by radiosonde and aircraft. *Tellus*, **10**, 83–87.
12. Malkus, J. S., and R. S. Scorer, 1955: The erosion of cumulus towers. *J. Meteor.*, **12**, 43–57.
13. Malkus, J. S., and C. Rönne, 1954: On the structure of some cumulus clouds which penetrated the high tropical troposphere. *Tellus*, **6**, 351–356.
14. Malkus, J. S., 1959: *Recent developments in studies of penetrative convection and an application to hurricane cumulonimbus towers.* Unpubl. ms., Woods Hole Oceanog. Inst.
15. Malkus, J. S., and A. F. Bunker, 1952: *Observational studies of the air flow over Nantucket Island during the summer of 1950.* Pap. in Phys. Oceanog. and Meteor., *XII*, No. 2, Mass. Inst. Tech. and Woods Hole Oceanog. Inst.
16. Koldovský, M., 1959: Photographic observation of the development of a thunderstorm cloud. *Studia geoph. et geod.*, **3**, 93–97.
17. Scorer, R. S., and C. Rönne, 1956: Experiments with convection bubbles. *Weather*, **11**, 151–154.
18. Batchelor, G. K., 1954: Heat convection and buoyancy effects in fluids. *Quart. J. r. meteor. Soc.*, **80**, 339–358.
19. Scorer, R. S., 1958: *Natural aerodynamics.* London, Pergamon Press.
20. Ludlam, F. H., 1959: Hailstorm studies, 1958. *Nubila*, **2**, 7–27.
21. Cunningham, R. M., V. G. Plank, and C. F. Campen, 1956: *Cloud refractive index studies.* Geophys. Res. Pap. 51, Geophys. Res. Dir., Cambridge, Mass.
22. Saunders, P. M., 1957: The thermodynamics of saturated air: a contribution to the classical theory. *Quart. J. r. meteor. Soc.*, **83**, 342–350.

Contribution No. 1153

Deep-Sea Research, 1961, Vol. 7, pp. 237 to 253. Pergamon Press Ltd., n. Printed in Great Britain

Nitrogen/argon and nitrogen isotope ratios in aerobic* sea water

BRUCE B. BENSON† and PETER D. M. PARKER†

(*Received* 29 *November* 1960)

Abstract—Various factors which influence the concentrations of gases dissolved in sea water are discussed. A surface equilibrium model is proposed, and results presented to test the model and to ascertain whether or not nitrogen dissolved in sea water is biologically and chemically inert. The method utilized argon as a reference gas, with a mass spectrometer as the primary analytical tool. The conclusion is reached that within ± 1 per cent the model is applicable and nitrogen is 'conservative.' The possible implications of apparent small differences between the predictions of the model and the experimental results are discussed. There is some evidence that the nitrogen 29/28 relative abundance in the dissolved gas may be greater than that in the atmosphere by approximately one part in 10,000.

INTRODUCTION

VARIATIONS in the percentage saturations** of nitrogen and the inert gases dissolved in sea water have been reported by several workers. BUCH (1929) found a range of 93 to 111 per cent for the combined nitrogen and inert gas content.†† Nitrogen and 'crude argon' (which included all the residual gases after the removal of carbon dioxide, oxygen and nitrogen) were analyzed separately by RAKESTRAW and EMMEL (1938). Their results for nitrogen varied from 95 to 108 per cent and for the crude argon from 94 to 124 per cent. They ascribed the larger variation for the latter to less accurate measurements and to the possibility that traces of hydrogen or hydrocarbons were present in the crude argon. HAMM and THOMPSON (1941) found a range, for the combined nitrogen and inert gas content, of 93·7 to 109·1 per cent in surface waters, and of 91 to 102 per cent in Pacific Ocean waters.

Despite the variations described above, nitrogen gas dissolved in sea water is usually assumed to be conservative, i.e., the nitrogen concentration is assumed to be unaltered by biological and chemical activity (SVERDRUP, JOHNSON and FLEMING, 1942, pp. 186, 188; RICHARDS, 1957, p. 102). BUCH based a technique for determining the 'biologisch unbeeinflussten Sauerstoffs' (or, in the nomenclature of this paper, the 'initial oxygen concentration'), and the consumption of oxygen, partly upon the assumption that the combined nitrogen and crude argon content is conservative. In a refinement of BUCH's method, RAKESTRAW and EMMEL assumed nitrogen and crude argon were *each* biologically and chemically inert.

---

*As used here, the word 'aerobic' is a misnomer. (See the authors' note in the following paper by RICHARDS and BENSON (1961)). We propose that in the future the word 'oxic' be used to convey the idea intended here, i.e., that the water contains dissolved oxygen.

†Department of Physics, Amherst College, Amherst, Massachusetts, U.S.A. and Woods Hole Oceanographic Institution, Woods Hole, Massachusetts, U.S.A.

**The percentage saturation of a particular dissolved gas is defined to be the ratio of the concentration of the gas to the solubility of that gas in water of the observed *in situ* temperature and salinity, which is in equilibrium with a normal atmosphere at a pressure of 760 mm of mercury. As used, the pressure refers sometimes to 760 mm of mercury exclusive of the partial pressure of water vapour ('dry' atmosphere), and sometimes to a total pressure of 760 mm of mercury including that of water vapour ('wet' atmosphere).

††The term 'atmospheric nitrogen' is avoided because in this paper it will be used in its literal sense to mean nitrogen gas in or from the atmosphere.

If nitrogen is conservative, it is evident that one or more physical effects must be responsible for the observed variations in the percentage saturation of nitrogen. Both BUCH, and RAKESTRAW and EMMEL, assumed that 'the apparent changes in "percentage saturations" are only the result of temperature and salinity variations in the water . . . . ' (RAKESTRAW and EMMEL). The data of RAKESTRAW and EMMEL were re-examined by CARRITT (1954), who pointed out that the majority of the variations in the percentage saturation of nitrogen could have been due to atmospheric pressure fluctuations over the sea surface.*

From the discussion above it is clearly desirable to determine the physical and/or biological causes responsible for the observed variations in the percentage saturation of nitrogen. The approach used in the research reported here was in some respects similar to that of BUCH and RAKESTRAW and EMMEL. The concentration of argon, a gas influenced only by physical effects, was compared with the concentration of nitrogen. The analyses were carried out with a mass spectrometer, instead of by gasometric techniques.

THEORETICAL CONSIDERATIONS

The fact that the percentage saturations of gases dissolved in surface sea water do not differ greatly from 100 per cent suggests that the gases in the atmosphere are approximately in thermodynamic equilibrium with the sea surface, i.e., to a first approximation the concentration of each gas is predictable from its solubility coefficient, its partial pressure in the atmosphere, and Henry's law. Stated more accurately : the atmosphere and the oceans are in an approximately steady state such that essentially equilibrium conditions exist at the interface between them, even though within the bodies of the atmosphere and the oceans the conditions are very far from equilibrium. This situation results from the relative kinetics of surface exchange mechanisms and body mixing mechanisms, coupled with the vastly different distances over which they must act. The point is illustrated by noting that the converse situation usually exists in laboratory experiments on the solubilities of gases, where it is much easier to keep the liquid uniformly mixed than it is to ensure that equilibrium is achieved between the liquid and gas phases.

Two questions arise from the above: (1) How closely do conditions at the sea–air interface correspond to equilibrium ? (2) If deviations from equilibrium exist, how can they be utilized to deduce information about the exchange processes ? The first of these, and the question of whether free dissolved nitrogen is conserved within the body of the oceans, are the primary subjects of this paper. As will be seen, some qualitative comments on question (2) can be made, but at the time these experiments were performed, the analytical precision and, particularly, the sampling techniques, were not reliable enough to draw quantitative conclusions. The method of approach will be to propose a theoretical model which assumes both surface equilibrium and conservation of dissolved nitrogen and which can be tested.

Before proceeding to the model it is useful to list the physical factors which may, and presumably do, influence the concentrations of gases dissolved in sea water. They may be separated into two categories :

---

*CARRITT (private communication) has discovered that some of his numbers were incorrect, but his main thesis is not invalidated.

A. Surface factors :
  1. Water temperature.
  2. Salinity.
  3. Atmospheric pressure.
  4. Atmospheric humidity.
  5. Air temperature.
  6. Surface conditions.
  7. Kinetics of near-surface mechanisms.

B. Body factors :
  1. Radioactive decay.
  2. Influx (or efflux) through the sea floor.
  3. Mixing.
  4. Radiative heating or heating from below. (Although this would not alter the concentration, it would affect the number obtained for the percentage saturation or for any other quantity deduced from the measured temperature).
  5. Hydrostatic pressure.

To introduce the model, suppose that in a ‘ thought experiment ’ an element of water at the surface and the element of atmosphere immediately above it, were isolated and found to be in thermodynamic equilibrium. This would mean that the water and air temperatures were identical, that the relative humidity was 100 per cent, and that the concentration of each gas dissolved in the liquid was given by

$$C_i = S' \frac{P_a - P_w}{760} \tag{1}$$

where the symbols have the following meanings :

C_i = initial concentration of the gas in cm^3 per litre (‘ initial concentration ’ in the sense that later we shall assume the element of water sinks and becomes isolated from the atmosphere).

S' = the solubility of the gas, i.e., the number of cm^3 of dissolved gas per litre when the liquid is in equilibrium with a ‘ normal ’ atmosphere whose total pressure, excluding water vapour, is 760 mm of mercury. This is the ‘ dry ’ solubility, like that discussed by FOX (1909) or BENSON and PARKER (1961). For all surface phenomena we may consider S' to be a function of temperature and salinity only [KLOTS (1961)].

P_a = atmospheric pressure.

P_w = saturated vapour pressure of water at the temperature and salinity of the water.

It is obvious that the hypothetical situation just described idealizes the real ones in several respects. The relative humidity cannot be 100 per cent – at least on the average – for otherwise evaporation from the sea surface could not occur.* On the other hand, it is quite certain that the relative humidity cannot be zero near the sea surface. If the water and air were not in true thermodynamic equilibrium but in a kind of quasi-equilibrium, i.e., an equilibrium with respect to dissolved gas but not water vapour, equation (1) would take the form :

---

*It should be noted, however, that the relative humidity at the interface need be only infinitesimally less than 100 per cent to permit evaporation, with air currents continually supplying slightly less saturated air to the surface.

$$C_i = S' \frac{P_a - RH(P_w)}{760}, \tag{1a}$$

where RH is the relative humidity in the layer of air at the interface. Equations (1) or (1a) implicitly express, in analytical form, CARRITT'S (1954) suggested explanation for the variation of percentage saturation in terms of atmospheric pressure, but they go further in that they clarify the role of relative humidity. Because it is impossible to know either the P_a or the RH appropriate to a sample taken from depth, it is evident that the concept of percentage saturation offers only a gross kind of parameter for any gas.

It is difficult to assess the effect on C_i due to a difference in temperature between the air and the water. One might guess that an air temperature greater than the water temperature would cause C_i to be greater than predicted by equations (1) or (1a), with low molecular weight gases affected more than heavier ones. The effect should be small, however, compared to those to be discussed next, and it will be neglected.

Surface conditions and the kinetics of the various mechanisms near the surface probably play significant, interrelated and complicated roles in controlling the dissolved gas concentrations. Two examples will illustrate the problem. At first glance one might expect that the equilibrium situation described above would be most likely to occur with a placid surface across which molecular exchange equilibrium could take place without the complications of surface trapping of air bubbles, etc. Suppose, however, that sub-surface waters were either under- or over-saturated relative to the surface. If internal mixing or molecular diffusion, or both, were more rapid than molecular exchange through the interface, the surface might never have sufficient time to achieve equilibrium. In this case bubbles of air within the liquid, and the bursting of bubbles at the surface (BLANCHARD and WOODCOCK, 1957), might aid in achieving equilibrium through the provision of greater effective surface area.

On the other hand, turbulent surface conditions, especially during violent storms, can cause very extensive trapping of air bubbles which penetrate to depths of many metres (J. KANWISHER, private communication). The solution, partial or complete, of these bubbles would tend to supersaturate the water.

The latter would be accompanied by a most interesting two-sided phenomenon. Consider an air bubble which has been trapped and carried a few metres below the surface. As it descends the partial pressure of each of the gases within the bubble will increase and the gases will tend to go into solution. Assuming that the kinetics of solution of the various gases are not too different, argon and oxygen will be preferentially dissolved relative to nitrogen because the solubility coefficient of the latter is only approximately one-half that of the other two. [The situation is like that in the closed system absorptiometric method of studying gas solubilities. It was FOX (1909) who first recognized the problem arising from the differing solubility coefficients of nitrogen and argon]. Consequently, if one could sample the water alone, without the undissolved bubbles, one would expect to find a greater excess of oxygen and argon than of nitrogen. But if the sampling captured both water and undissolved bubbles

– and this normally would be the case – just the opposite would be observed, because the ratio of nitrogen to argon in the atmosphere is about 83 to 1, whereas the ratio of their solubilities is approximately 39 to 1.

Despite the several possible difficulties with the surface equilibrium model, let us tentatively adopt it and examine its consequences when applied to surface waters in general, and especially those which are ' sources ' for deep water. When the surface water sinks and becomes isolated from the atmosphere, the initial concentrations of nitrogen and argon will each be given by equations of the form of either equation (1) or equation (1a). For our purposes, we shall write down only the expression for the initial *ratio* of the concentrations of the two gases :

$$\frac{N_{2_i}}{A_i} = \frac{N_2'}{A'}, \tag{2}$$

where the symbols have obvious meanings from equation (1). It is evident that atmospheric pressure and relative humidity cancel out, so that variations in either are unimportant. Equation (2) states that if the surface equilibrium model is correct, the initial percentage saturations of the two gases will be equal.

In considering effects within the body of the oceans we shall not assume initially that nitrogen is biologically and chemically inert. In this way the arguments developed will apply to more general situations, for example, to oxygen/argon analyses. The only assumption which will be added to the surface equilibrium model is that the argon concentration remains unchanged during the history of an element of water after it leaves the surface. Stated analytically :

$$A = A_i \tag{3}$$

Where A is the *in situ* concentration of argon at the time of sampling.

Equations (2) and (3) can be combined and manipulated to yield several fruitful formulations :

$$N_{2_i} = \frac{N_2'}{A'} A \tag{4a}$$

$$N_{2_i} = \left(\frac{N_2'}{A'}\right)\left(\frac{A}{N_2}\right) N_2 \tag{4b}$$

$$\frac{N_2}{N_{2_i}} = \left(\frac{N_2}{A}\right)\left(\frac{A'}{N_2'}\right) \tag{5}$$

$$\Delta N_2 = N_2 - N_{2_i} = \left[\frac{N_2}{A} - \frac{N_2'}{A'}\right] A \tag{6}$$

In each case N_2/A is the measured ratio of nitrogen to argon in the gas extracted from a sample of water. The values for N_2'/A' are obtained from measurements of the *in situ* temperature and salinity of the water sample and from laboratory measurements of N_2'/A' vs. temperature and salinity [BENSON and PARKER (1961)].

Equation 4(a) states that the initial concentration of nitrogen may be calculated from the measurement of the *in situ* temperature and salinity of the water sample and the concentration of argon in the sample. If it were more convenient to determine the concentration of nitrogen in the sample, equation (4b) would be more useful, but would necessitate the measurement of N_2/A. If the only quantity desired is the percentage of the initial nitrogen remaining, i.e., N_2/N_{2_i}, equation (5) states that it is unnecessary to determine anything other than the temperature, salinity and the nitrogen/argon ratio in the gas extracted from the sample.

From equation (6) one can calculate the increase in the concentration of nitrogen which has occurred during the history of the sample of water. It is interesting to compare the decrease in nitrogen concentration, $-\Delta N_2 = N_{2_i} - N_2$, given by equation (6), with what, by analogy with oxygen, would be called the 'apparent nitrogen utilization,' A.N.U. $= N_2' - N_2$.

If the assumption is made that nitrogen is conserved within the body of the oceans, i.e., $N_2 = N_{2_i}$, any one of the equations predicts that

$$\frac{N_2}{A}\bigg/\frac{N_2'}{A'} = 1 \quad (\text{or } 100\%). \tag{7}$$

Alternatively, a plot of N_2/A vs. N_2'/A' should yield a straight line with a slope of unity. The data from this research will be presented in these forms, but before turning to the experimental results, we shall discuss briefly the physical body factors listed earlier, which might cause changes, either real or apparent, in the nitrogen and argon concentrations.

Radioactivity and influx through the sea floor could affect the argon concentration. One possibility for the genesis of argon 40 (the most abundant isotope) in the atmosphere is that it has been released to the atmosphere from the geosphere and hydrosphere through the radioactive decay of potassium 40. (See, for example, Damon and Kulp, 1958). Calculation shows, however, that for any conceivable turn-over time for the oceans, the increase in the argon concentration should have been undetectable in these experiments.

If two volumes of sea water, individually equilibrated with the atmosphere at two different temperatures, are mixed together, it is well-known that the resulting concentrations of the dissolved gases will be greater than the concentrations obtained by equilibrating the water with the atmosphere at the temperature of the mixture. For example, using the Fox plus Benson and Parker data for nitrogen and argon (Benson and Parker 1961), and taking the extreme case of mixing equal volumes of water at 0 °C and 30 °C (salinities equal 36·13 ‰), the concentrations of nitrogen and argon in the mixture will be 11·51 cm^3/litre and 0·3025 cm^3/litre, respectively, compared to the corresponding values 10·78 and 0·282 for water equilibrated at the 15 °C temperature of the mixture. For two equal samples at 10 °C and 20 °C, the mixture will contain 10·85 cm^3/litre of nitrogen and 0·284 cm^3/litre of argon, compared to the 10·78 and 0·282 for 15 °C as above.

A similar effect would result from heating. Water in equilibrium with the atmosphere at 0 °C would contain 14·04 cm^3/litre of nitrogen and 0·375 cm^3/litre of argon. If, while isolated from the atmosphere, it were heated to 5 °C the actual concentrations would remain unchanged, but the corresponding concentrations deduced from the new temperature would be 12·65 and 0·335.

It is clear that mixing and heating could have significant effects on the concentrations relative to the values deduced from the temperature and salinity. It was these effects which Buch and Rakestraw and Emmel took to be the primary causes of the observed variations in percentage saturation of the gases.

The *ratios* of the concentrations of nitrogen to argon, unlike the concentrations *per se*, are affected very little by either mixing or heating. For the case of mixing two samples at 10 °C and 20 °C the ratio in the mixture is 38·20 compared to the value 38·26 deduced from the temperature. The difference is only 0·16 per cent. In the heating example, the actual ratio would be 37·48, whereas the number obtained from the temperature would be 37·74, a difference of 0·7 per cent. It should be noted that in both cases the tendency is to make the measured ratio, N_2/A, smaller than N_2'/A'.

KLOTS (1961) has pointed out that the increased hydrostatic pressure to which an element of water is subjected when it sinks from the surface to depth, causes the water to become thermodynamically supersaturated, i.e., the solubility coefficient decreases with increased hydrostatic pressure. Although the hydrostatic pressure prevents bubble formation, there will be a tendency for molecular diffusion of the dissolved gases to take place toward regions of lower supersaturation, that is, upward. Because it depends upon molecular diffusion the effect of this factor on the N_2/A ratio is probably negligible compared to even the small effects of mixing and heating, but it should be borne in mind.

EXPERIMENTAL PROCEDURES

Samples were taken during the 1956–57 cruise V12 of the R.V. *Vema* of the Lamont Geological Observatory of Columbia University, and during the August, 1957 cruise of the R.V. *Atlantis* of the Woods Hole Oceanographic Institution.

Nansen bottles were employed as in standard hydrographic work. As soon as possible after the Nansen bottles reached the surface, portions of their contents were transferred to 400 cm^3 glass water sample bottles (Fig. 1). The essential features of the bottle were that once filled, with the double ‘ O-ring ’ piston in place and with the stopcock closed, the water was completely isolated from the air, with provision for expansion without excessive danger of breaking the bottle. The pistons were nickel-plated brass. The idea of developing a piston-cylinder type of bottle was suggested by Professor MAURICE EWING. The final design was due to Professor ARNOLD B. ARONS and the first author. The procedure for transferring water to the glass bottles consisted of the following steps :

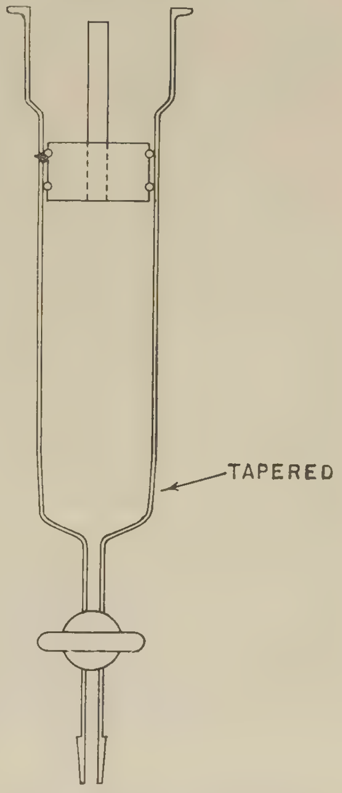

FIG. 1. Glass water sample bottle with ‘ O-ring ’ nickel-plated brass piston. Pressure-type stopcock has 6 mm bore. Main cylinder is made of 60 mm heavy wall glass approximately 175 mm long.

1. One end of a tube was attached to the Nansen bottle petcock and the other end inserted through the large end of the glass bottle to a point close to the stopcock at the bottom.

2. With the stopcock closed, water was flowed gently into the glass bottle, displacing air until the water surface rose to approximately the center of the largest tubing. If the bottle had been carefully cleaned, no difficulty was encountered with trapping air at the glass walls. Only the initial water and the water surface came into direct contact with the air, and this water was discarded as described below.
3. The bottle was tipped to an appropriate angle and the piston inserted with a turning motion to prevent trapping of air bubbles near the first ' O-ring.'
4. With the first ' O-ring ' fully immersed the piston was pushed in until a seal was made with the main glass cylinder. Then the bottle was inverted, draining the excess water at the top, the stopcock opened, and the piston pushed in to the position shown.

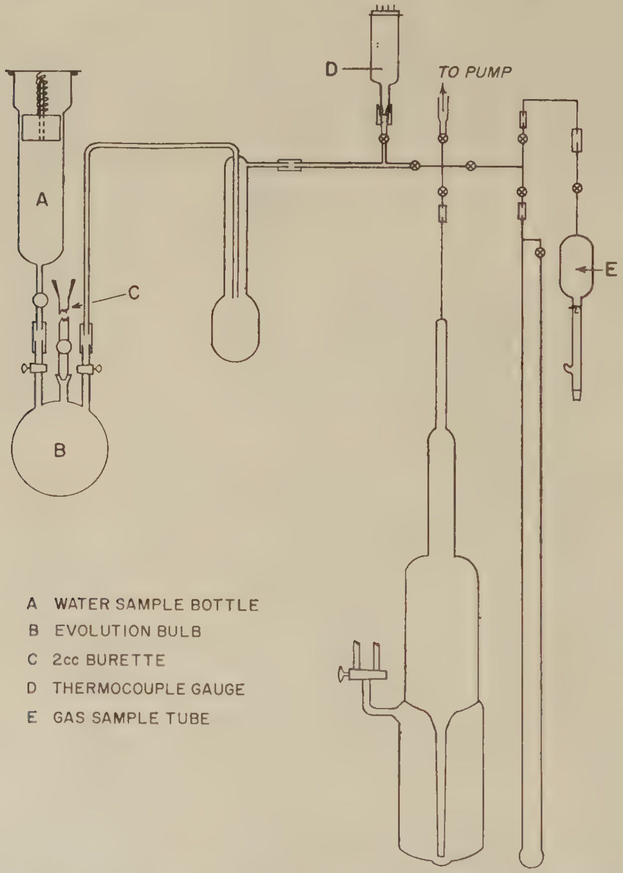

FIG. 2. Toepler pump vacuum manifold for extraction at sea of gases dissolved in water.

5. After closing the stopcock, a spring and clamp assembly was attached to the flange at the top of the bottle to allow small controlled movement of the piston as a presssure release.
6. The samples were stored in a cold dark place until extraction of the dissolved gases, which usually took place within twenty-four hours.

To extract the gases a bottle was attached to a vacuum manifold similar to the one shown in Fig. 2.* The system was made of heavy wall glass except for the thermocouple gauge and the valve manifold above the Toepler pump. The valves were ‘ Monel ’ high vacuum ‘ Sylphon ’ bellows valves made by ‘ Hoke.’ Extra heavy rubber vacuum tubing was used at several points not only for connecting metal to glass, but also to absorb shock. The unit was attached to a heavily-braced frame mounted on a shock-mounted table.

The system up to the stopcock on the water sample bottle was evacuated by means of a ballast type mechanical pump designed to handle water vapour, to a pressure less than 100 microns (limited primarily by residual water vapour). After closing the pump and thermocouple valves the water was drawn into the evolution bulb. The vacuum tight piston descended slowly during this process and came to rest in a tight seal against the tapered lower portion of the water bottle.

The burette permitted the insertion of approximately 2 cm³ of concentrated hydrochloric acid to release the dissolved bicarbonate as carbon dioxide. The salt-ice trap served to condense most of the water evaporated while the gas was being Toepler-pumped into the ‘ break-seal ’ gas sample tubes. The tubes had been evacuated and outgassed before they were put on shipboard, to reduce the time required to evacuate the system at sea. Four to six Toepler-pumping cycles extracted essentially all of the dissolved gases as indicated by no further change in the manometer. Laboratory tests had shown that, even without the hydrochloric acid, at least 97 to 99 per cent of the gas was evolved, and the addition of the acid made the evolution process even more efficient. In any case, for ratio determinations the errors introduced by imperfect extraction were probably not significant. The gas sample tubes were sealed with a glass-blowing torch and stored in crates until the end of the cruise.

At Amherst the gas samples were further processed to eliminate all water vapour and to separate vapours like carbon dioxide, which are condensable in liquid air, from the nitrogen, oxygen and argon. For reasons explained by BENSON and PARKER (1961), the oxygen was then removed by cycling the gas through a ‘ Vycor ’ furnace filled with copper turnings at 700 °C, followed by a liquid air trap. The procedure for carrying out the N_2/A analyses with the mass spectrometer were identical with those described by BENSON and PARKER.

In addition to the determination of the ratio of nitrogen to argon in each sample, measurements were made on the *Atlantis* samples of the ratio of the abundances of the two stable nitrogen isotopes with masses 14 and 15, relative to their ratio in atmospheric nitrogen. Precision ‘ double collection ’ techniques (McKINNEY, *et al.* 1950) were employed for this purpose.

DATA AND RESULTS

The data from 74 samples taken at stations in the North Atlantic Ocean and the South Atlantic Ocean are shown in Table 1. The hydrographic data were supplied by the Lamont Geological Observatory and the Woods Hole Oceanographic Institution. Salinities given to only three significant figures were taken from WÜST profiles and are approximate. Because the N_2'/A' ratio is almost independent of salinity, values for the latter are given only to indicate that they were in the range of 33 to

---

*The manifold shown was employed on the *Atlantis*. A more complicated manifold, which was a modification of one reported by RAKESTRAW and EMMEL (1937), was used on the *Vema*.

Table 1. *Nitrogen/argon and nitrogen isotope data from* Vema *V12 cruise and R.V.* Atlantis *stations 5590 and 5594*

	Sample	Date	Latitude	Longitude	Sonic Depth (m)	Sample Depth (m)	Salinity (‰)	Potential Temperature (°C)	$\frac{N_2}{A}$	$\frac{N_2'}{A'}$	$\frac{N_2}{N_{2i}}$ (%)	$\delta_{29/28}$ (‰)
	V-12											
Faukland Current	3	7-3-57	41° 44·5′ S	60° 59′ W	ca 59	0	34·566	13·61	38·46	38·19	100·7	
	6	14-3-57	41° 02·5′ S	60° 48·5′ W	59	55	33·391	13·08	38·04	38·16	99·7	
	8	16-3-57	45° 43′ S	66° 20′ W	91	82	33·297	7·61	37·62	37·88	99·3	
	7	16-3-57	45° 34′ S	65° 50′ W	95	91	33·237	8·15	37·96	37·91	100·1	
	9	3-4-57	41° 12·3′ S	51° 18′ W	5545	0	34·688	16·60	38·29	38·35	99·8	
	10	7-4-57	38° 55·5′ S	40° 04′ W	5092	1065	34·356	2·78	37·28	37·63	99·1	
	12	17-4-57	39° 21·2′ S	01° 08·5′ E	5101	45	34·672	13·90	37·94	38·20	99·3	
South of Walvis Ridge	13	18-4-57	36° 56·5′ S	04° 39′ E	5101	0	—	15·10	38·69	38·27	101·1	
	14	"	"	"	5101	ca 2900	34·860	1·88	37·44	37·57	99·6	
	16	"	"	"	5101	ca 3800	35·5	? 2·83	37·76	37·63	100·3	
	15	"	"	"	5101	ca 4800	? 35·487	? 0·96	38·27	37·53	102·0	
	17	19-4-57	34° 42′ S	06° 30′ E	5298	ca 1200	? 34·802	2·83	37·97	37·63	100·9	
	19	"	"	"	5298	ca 2377	34·8	(2·42)	37·47	37·60	99·6	
	20	"	"	"	5298	ca 4300	34·8	0·75	37·48	37·52	99·9	
	18	"	"	"	5298	ca 4500	34·7	0·77	37·41	37·52	99·7	
	*22	29-4-57	32° 13′ S	16° 15·5′ E	448	0	35·1	20·11	38·51	38·53	99·9	
	21	"	"	"	448	137	35·0	10·96	37·95	38·05	99·7	
	23	30-4-57	30° 14·9′ S	13° 03′ E	3063	988	34·4	3·02	37·57	37·64	99·8	
	24	"	"	"	3063	1966	34·9	2·81	37·53	37·63	99·7	
	25	"	"	"	3063	2980	34·9	2·28	37·09	37·60	98·6	
Benguela Current	28	4-5-57	24° 17′ S	14° 07·5′ E	130	0	35·3	14·17	38·63	38·22	101·1	
	29	"	"	"	130	? 64	35·5	11·89	38·28	38·10	100·5	
	30	5-5-57	22° 31·5′ S	14° 14·5′ E	75	0	35·2	12·7	38·34	38·15	100·5	
	31	"	"	"	75	64	35·2	12·06	38·53	38·11	101·1	
	**34	6-5-57	22° 53′ S	10° 17·5′ E	—	0	—	20·44	38·49	38·55	99·8	
	**35	"	"	"	—	0	—	20·44	38·63	38·55	100·2	
	**36	"	"	"	—	0	—	20·44	38·46	38·55	99·8	
	38	8-5-57	22° 56′ S	04° 50′ E	2740	? 54	35·6	21·07	39·11	38·58	101·4	
	40	"	"	"	2740	? 265	35·0	ca 12·56	37·75	38·14	99·0	
	41	"	22° 41′ S	03° 16′ E	5030	493	34·5	7·01	37·71	37·85	99·6	
	42	"	"	"	5030	988	34·5	3·69	37·50	37·68	99·5	
	43	"	"	"	5030	1500	34·8	3·46	37·15	37·66	98·6	
	44	"	"	"	5030	2012	34·9	2·88	37·47	37·63	99·6	
	45	"	"	"	5030	3144	34·9	2·31	37·88	37·60	100·7	
	46	"	"	"	5030	4150	34·9	2·07	37·09	37·58	98·7	
	48	12-5-57	15° 16·5′ S	07° 00′ E	5038	4938	34·9	2·14	37·64	37·59	100·1	
	49	20-5-57	5° 54·9′ S	10° 33′ E	2140	0	ca35·8	27·56	39·44	38·92	101·3	
	50	"	"	"	2440	2002	36·0	3·50	37·60	37·66	99·8	

Table 1 (contd.)

Sample	Date	Latitude	Longitude	Sonic Depth (m)	Sample Depth (m)	Salinity (‰)	Potential Temperature (°C)	$\frac{N_2}{A}$	$\frac{N_2'}{A'}$	$\frac{N_2}{N_{2i}}$	$\delta_{29/28}$ (‰)
V-12											
54	26-5-57	04° 49·0′ S	02° 37·5′ E	5500	256	35·6	11·55	37·99	38·08	99·8	
51	,,	,,	,,	5500	2950	36·3	2·51	37·55	37·61	99·8	
52	,,	,,	,,	5500	3930	34·9	2·10	37·61	37·59	100·0	
56	27-5-57	04° 23·9′ S	00° 14′ W	4755	475	34·7	7·96	38·03	37·90	100·3	
57	,,	,,	,,	4755	1024	34·6	4·16	37·83	37·70	100·3	
58	,,	,,	,,	4755	2012	34·9	3·31	37·36	37·66	99·2	
59	,,	,,	,,	4755	? 4572	34·9	2·00	36·62	37·58	97·4	
60	1-6-57	01° 52′ N	16° 04·5′ W	4800	ca 3600	34·72	1·96	37·68	37·58	100·3	
61	2-6-57	00° 18·5′ N	18° 49′ W	—	0	—	25·22	38·79	38·79	100·0	
*62	5-6-57	32° 13′ S	16° 15·5′ E	448	0	35·1	20·11	38·70	38·53	100·4	
A-5590											
13	13-8-57	32° 04′ N	61° 02′ W	4645	1	36·30	26·64	39·20	38·87	100·8	+ 0·24
14	,,	,,	,,	,,	49	36·41	23·26	39·27	38·69	101·5	0·17
15	,,	,,	,,	,,	98	36·59	20·52	38·86	38·55	100·8	0·25
16	,,	,,	,,	,,	584	36·33	16·87	—	38·36	—	—
17	,,	,,	,,	,,	779	35·80	13·19	38·22	38·17	100·1	0·15
18	,,	,,	,,	,,	877	35·34	10·70	38·07	38·04	100·1	0·23
19	,,	,,	,,	,,	975	35·26	8·64	37·96	37·93	100·1	0·19
20	,,	,,	,,	,,	1243	35·14	5·40	38·57*	37·76	—	0·04
21	,,	,,	,,	,,	1757	35·08	3·92	38·85*	37·69	—	0·18
22	,,	,,	,,	,,	2823	35·00	2·84	37·57	37·63	99·8	0·46
23	,,	,,	,,	,,	3552	34·87	2·20	37·50	37·59	99·8	0·04
24	,,	,,	,,	,,	3925	34·96	? 2·05	36·69	37·58	97·6	0·19
25	,,	,,	,,	,,	4396	34·84	? 1·89	36·93	37·57	98·3	0·07
A-5594											
64	18-8-57	31° 55′ N	42° 20′ W	3813 to 3840	1	36·21	26·47	38·79	38·86	99·8	− 0·06
75	,,	,,	,,	,,	43	—	—	—	—	—	+ 0·07
65	,,	,,	,,	,,	87	36·59	19·39	38·37	38·49	99·7	− 0·06
66	,,	,,	,,	,,	430	36·00	15·24	38·11	38·28	99·6	− 0·16
67	,,	,,	,,	,,	523	35·89	14·61	37·89	38·24	99·1	+ 0·05
68	,,	,,	,,	,,	617	35·69	13·61	37·94	38·19	99·3	0·11
69	,,	,,	,,	,,	942	35·26	7·82	37·63	37·89	99·3	0·19
70	,,	,,	,,	,,	1644	34·96	4·17	37·20	37·70	98·7	0·05
71	,,	,,	,,	,,	2186	34·98	3·37	37·26	37·66	98·9	0·10
72	,,	,,	,,	,,	2737	34·98	2·84	37·24	37·63	99·0	0·12
76	,,	,,	,,	,,	3104	34·91	2·54	—	37·61	—	0·31
73	,,	,,	,,	,,	3471	34·88	2·34	—	37·60	—	0·25
74	,,	,,	,,	,,	3838	34·93	2·15	—	37·59	—	0·14

36 per mille for which the BENSON and PARKER N_2'/A' values are valid. Dissolved oxygen was present in all samples.

Samples V12–22 and V12–62 were identical samples taken at the same time. Sample V12–22 was processed immediately, and sample V12–62 was deliberately stored in the dark for approximately five weeks before extraction of the dissolved gases. Samples V12–34, 35 and 36 were identical. The first was processed immediately, whereas the second was stored in the dark for seven hours and the third in sunlight for seven hours before extractions of the gases.

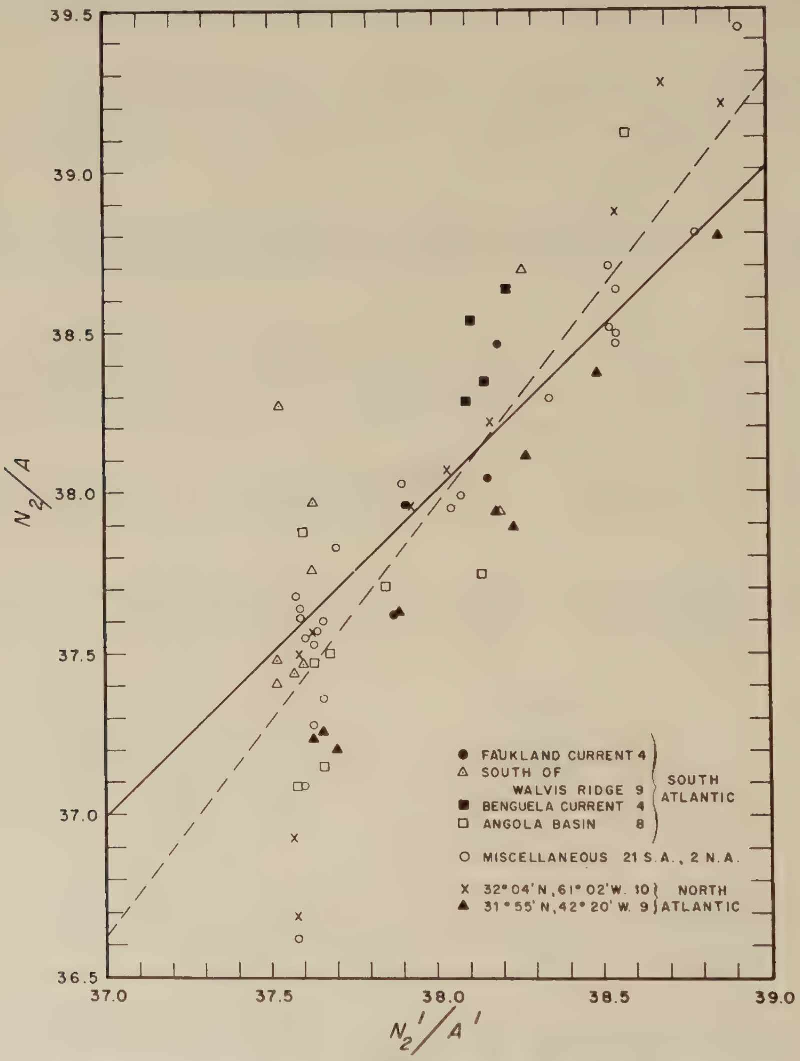

FIG. 3. Expanded graph of N_2/A vs. N_2'/A' for all data. Dashed line is linear least squares fit of all data. Solid line represents $N_2/A = N_2'/A'$.

Sample A5590–16 was lost. The values of N_2/A for samples A5590–20 and 21 were in error because of contamination through a crack in one of the sample system manifolds on the mass spectrometer. Fortunately, the isotope ratio measurements had already been made before the contamination. Samples A5594–73 to 76 were not analyzed for N_2/A because of a major break in one of the manifolds on the mass spectrometer. The measurements had to be terminated before the break could be repaired and high vacuum again achieved.

It is clear from the earlier discussion that it is most appropriate to use the potential temperature for determination of the values of N_2'/A' from the table given by BENSON and PARKER. Accordingly, the measured temperatures were converted to potential temperatures, although the precision of the measurements was not high enough to necessitate it.

The corresponding values for N_2/A and N_2'/A' were used to calculate N_2/N_2 from equation (5). The results are given in per cent in the second-to-last column in Table 1. Of the 67 values for N_2/N_{2_i}, 38 (or 57 per cent) lie within the range 100 ± 0·5 per cent, 52 (or 78 per cent) within 100 ± 1·0 per cent, and all but two values within 100 ± 2·0 per cent. The standard deviation of all values from 100 per cent is 0·86 per cent, and if samples V12–15, V12–59 and A5590–24 are disregarded, the standard deviation is 0·71 per cent. The average of all values is 99·84 per cent.

The estimated precision of the mass spectrometer measurements alone, as determined from the standard deviation of repeated measurements, was approximately 0·2 per cent. In addition, errors of unknown magnitude were certainly possible in the techniques used for sampling the water and processing to remove the gases. Any possible systematic error in the values of N_2'/A', associated with the calibration of the spectrometer (BENSON and PARKER, 1961), would have caused no error in the present work. Because the same calibration was used, the solubility samples and the ocean samples were effectively compared directly with one another. Small random or systematic errors from other sources in the N_2'/A' vs. temperature measurements cannot be ruled out.

After a consideration of the possible errors involved, we believe that within ± 1 per cent, and perhaps more closely, the experimental results in the present work verify the applicability* of the surface equilibrium model, and show that nitrogen is biologically and chemically inert in the waters studied. The N_2/A results are also represented in the highly expanded graph of Fig. 3, where values for N_2/A are plotted against the corresponding values for N_2'/A'. The solid line is the straight line to be expected if $N_2/A = N_2'/A'$. The dashed line is a linear least squares fit for all the experimental points. At $N_2'/A' = 37{\cdot}50$, which corresponds to 0·5 °C, the two curves differ only by 0·53 per cent, and at $N_2'/A' = 38{\cdot}89$, which corresponds to 27 °C, they differ by 0·64 per cent.

Having established in ‘ gross ’ terms the conclusions stated above, we are tempted to interpret the fine detail in the last paragraph. It is quite possible, and perhaps likely, considering the spread in the points at low temperatures, that the difference between the solid and dashed lines is a result simply of small random or systematic errors. Nevertheless, it is interesting to note that the experimental curve lies above the theoretical curve at high temperatures where most surface waters are represented. This is what would be expected if trapping of air bubbles from surface turbulence were significant. Furthermore, at the lower temperatures (deep samples) the difference is in the direction to be expected from mixing or heating. Examination of these possibilities must await more precise techniques.

---

*The word ‘applicability’ is chosen advisedly, for it has not been proven that the observed variations in the percentage saturation of nitrogen are due to surface effects, but only that the surface equilibrium model is consistent with the N_2/A results.

Fig. 4 contains expanded graphs of the experimental results for N_2/A vs. depth for four stations. The solid line in each case is a plot of N_2'/A' vs. depth. The rather large random deviations in the Angola Basin graph may have been due to sampling or processing difficulties. A similar explanation would seem to apply to the two deepest samples at 32° 04′ N, 61° 02′ W. The smooth pattern of points for 31° 55′ N, 42° 20′ W, suggests that the differences of N_2/A from N_2'/A' may be significant. If they are, the results might be interpreted to mean that a general rise of older, mixed or heated water, was occurring in that region. This, of course, is highly speculative, but further study seems warranted.

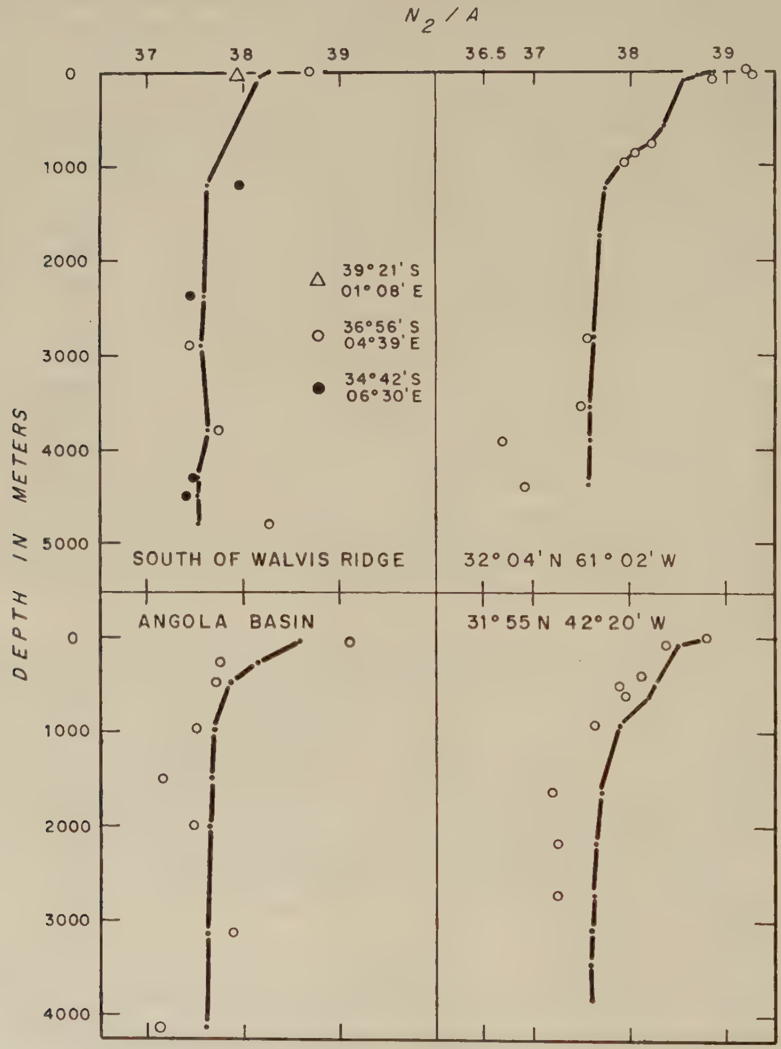

FIG. 4. Expanded graph of data for N_2/A vs. depth for two stations in the North Atlantic and two stations in the South Atlantic. Curves are graphs of N_2'/A' vs. depth.

The results of the nitrogen isotope determinations on the *Atlantis* samples are presented in the last column of Table 1. The quantity measured with the mass spectrometer was the per mille difference between the ratio of molecular nitrogen 29 to molecular nitrogen 28 for each sample, and the corresponding ratio for atmospheric nitrogen.

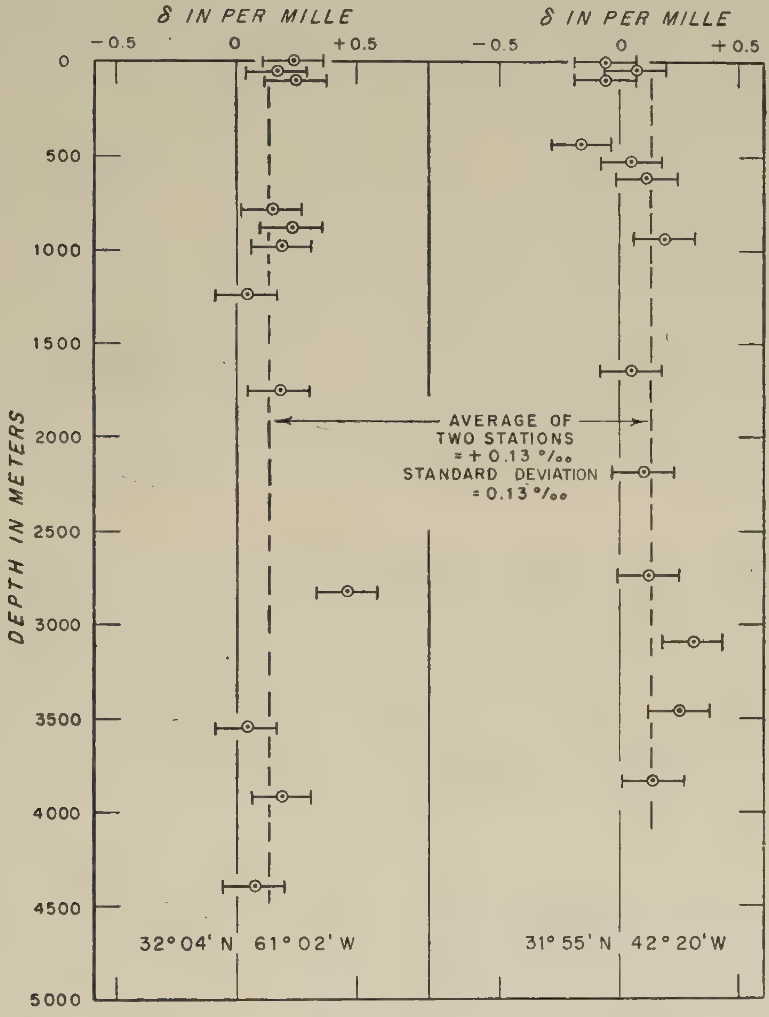

FIG. 5. Graphs of $\delta_{29/28}$ vs. depth for two North Atlantic stations.

$$\delta_{29/28} = \frac{\left(\frac{^{14}N\,^{15}N}{^{14}N\,^{14}N}\right)_x - \left(\frac{^{14}N\,^{15}N}{^{14}N\,^{14}N}\right)_{\text{air}}}{\left(\frac{^{14}N\,^{15}N}{^{14}N\,^{14}N}\right)_{\text{air}}} \times 10^3.$$

The values for δ for the two stations are plotted vs. depth in Fig. 5. Because visual examination of the results suggests that the isotope ratio is uniform with depth, a simple numerical average of all the values has been calculated and found to be + 0·13 per mille, with a standard deviation of 0·13 per mille. Although a small correction was necessary for a systematic difference between the two sample systems on the mass spectrometer,* we believe that the difference between the dissolved nitrogen and atmospheric nitrogen may be significant, If it is, the results indicate that the solution of nitrogen in sea water, under conditions at sea, is accomplished by a small fractionation of the isotopes with the dissolved molecular ratio being larger by approximately one part in 10,000.

Acknowledgements—Special thanks are due Professor ARNOLD B. ARONS who participated in some aspects of the early experimental work and who has made his counsel available throughout. In addition, it was his suggestion that generated our original interest in applying mass spectrometric techniques to problems in oceanography. We acknowledge the generous co-operation of the staffs at Lamont Geological Observatory, particularly Professor MAURICE EWING and Mr. ROBERT GERARD, and of the Woods Hole Oceanographic Institution, particularly Dr. FRANCIS A. RICHARDS (now at the University of Washington, Seattle) and Mr. ARTHUR R. MILLER. The sampling and gas extractions were carried out on the R.V. *Vema* by Mr. CLYDE BUCHANAN, and on the R.V. *Atlantis* by Mr. WINTHROP W. SMITH and Mr. ANDREW P. INGERSOLL. Part of the sample preparation and mass spectrometric analyses were done by Dr. EVA KUHN HILFER, Mr. JOHN D. STACKPOLE, Mr. JOHN B. HOPKINS, Mr. ROBERT A. R. PARKER and Mr. NOEL S. BARTLETT. We have benefited from discussions with Professor DAYTON E. CARRITT and Dr. CORNELIUS E. KLOTS, who also has read the manuscript critically.

Contribution No. 1153 *from the Woods Hole Oceanographic Institution. This research was supported in part by United States Atomic Energy Commission Contract AT* (30–1)–1794 *with the Woods Hole Oceanographic Institution, and in part by National Science Foundation grant G*4650 *to Amherst College. A major part of the preparation of the material for the manuscript was carried out during* 1959, *when one of the authors, B.B.B., was the recipient of a John Simon Guggenheim Memorial Fellowship. The second author, P.D.M.P. is now National Science Foundation Fellow and Danforth Fellow, Department of Physics, California Institute of Technology, Pasadena, California.*

REFERENCES

BENSON, B. B. and PARKER, P. D. M. (1961) Relations among the solubilities of nitrogen, argon and oxygen in distilled water and sea water. (To be published).

BLANCHARD, D. C. and WOODCOCK A. H. (1957) Bubble formation and modification in the sea and its meteorological significance. *Tellus*, **9**, 145–158.

BUCH, K. (1929) Die Verwendung von Stickstoff-Sauerstoffanalysen in der Meeresforschung. *J. du Conseil*, **4**, 162–191.

CARRITT, D. E. (1954) Atmospheric pressure changes and gas solubility. *Deep Sea Res.* **2**, 59–62.

DAMON, P. E. and KULP, J. L. (1958) Inert gases and the evolution of the atmosphere. *Geochimica et Cosmochimica Acta* **13**, 280–292.

FOX, C. J. J. (1909) On the coefficients of absorption of nitrogen and oxygen in distilled water and sea-water, and of atmospheric carbonic acid in sea water. *Trans. Faraday Soc.* **5**, 68–87.

HAMM, R. E. and THOMPSON, T. G. (1941) Dissolved nitrogen in the sea water of the northeast Pacific with notes on the total carbon dioxide and the dissolved oxygen. *J. Mar. Res.* **4** (1) 11–26.

KLOTS, C. E. (1961) Effect of the hydrostatic pressure in natural settings upon the solubility of gases. (To be published).

---

*This correction was made by periodically determining the ‘ apparent ’ δ, when the same sample, atmospheric nitrogen, was put in both sample systems.

McKinney, C. R., McCrea, J. M., Epstein, S., Allen, H. A. and Urey, H. C. (1950) Improvements in mass spectrometers for the measurement of small differences in isotope abundance ratios. *Rev. Sci. Instr.* **21**, 724–730.

Rakestraw, N. W. and Emmel, V. M. (1938) The relation of dissolved oxygen to nitrogen in some Atlantic waters. *J. Mar. Res.* **1**, 207–216.

Rakestraw, N. W. and Emmel, V. M. (1937) The determination of dissolved nitrogen in sea water. *Ind. Eng. Chem., Anal. Ed.* **9**, 344.

Richards, F. A. (1957) Some current aspects of chemical oceanography. In: *Progress in Physics and Chemistry of the Earth, Vol.* 2, 77–128.

Richards, F. A. and Benson, B. B. (1961) Nitrogen/argon and nitrogen isotope ratios in two anaerobic environments, the Cariaco Trench in the Caribbean Sea and Dramsfjord, Norway. *Deep Sea Res.* **7**, 4. 254–264.

Sverdrup, H. U., Johnson, M. W. and Fleming, R. H. (1942) *The Oceans.* Prentice-Hall, New York, 1087 pp.

Printed in Great Britain by The Salisbury Press Ltd., Publicity House, Wilton Road, Salisbury, Wilts. (27334)

Contribution No. 1154

[Reprinted from the Journal of Physical Chemistry, 65, 1489 (1961).]
Copyright 1961 by the American Chemical Society and reprinted by permission of the copyright owner.

RELATIONS AMONG THE SOLUBILITIES OF NITROGEN, ARGON AND OXYGEN IN DISTILLED WATER AND SEA WATER[1]

By Bruce B. Benson and Peter D. M. Parker[2]

Department of Physics, Amherst College, Amherst, Massachusetts, and Woods Hole Oceanographic Institution, Woods Hole, Massachusetts

Received December 12, 1960

Experiments have been carried out with a mass spectrometer to determine the *ratio* of the solubilities of nitrogen and argon in distilled water and sea water as a function of temperature. The literature on the solubilities of nitrogen, oxygen and argon has been examined critically in an attempt to clarify a generally confusing situation. The nitrogen/argon ratios, together with the results from somewhat less precise nitrogen/oxygen solubility ratio measurements reported here, have been used to intercompare the solubility determinations on the three gases as made by various workers. For distilled water seven independent lines of evidence are internally consistent, and it is suggested that the most reliable results are oxygen solubility coefficients from Elmore and Hayes, "atmospheric nitrogen" solubility coefficients from Hamberg, and the ratios of the solubility coefficients for nitrogen and argon from this research. From these, all the solubility coefficients for distilled water can be calculated. For sea water the situation is less clear cut, but it is suggested that the best data available are oxygen solubilities from Fox, Rakestraw and Emmel nitrogen solubilities corrected to dry air, and nitrogen to argon solubility ratios from this research. A combination of the last two provides the first information available on the solubility of pure argon in sea water.

Introduction

During the course of experiments by Benson and Parker,[3] and Richards and Benson,[4] on gaseous nitrogen and argon dissolved in sea water, it became desirable to know with an accuracy approaching 0.1%, the ratio of the saturated solubilities of the two gases in sea water equilibrated with atmospheric air.

Values for the solubility of nitrogen in sea water have been given by Fox[5] and Rakestraw and Emmel.[6] Their results disagreed markedly with one another. For example, at 0° Rakestraw and Emmel reported values approximately 1.2% higher than Fox (after correction for argon), while at 25° their values were lower than those of Fox by 7.5%. The only available data for argon were those of Rakestraw and Emmel,[6] which they have stated[7] to be "probably no more accurate than to about 5% . . . ." Furthermore, the "argon" to which they referred was the total residual gas after removal of carbon dioxide, oxygen and nitrogen.

Because the uncertainties in the nitrogen and argon solubilities were considerably greater than the accuracy required for our work, new experiments employing a mass spectrometer were undertaken to determine the ratio of the two solubilities in sea water as a function of temperature and salinity, and in distilled water as a function of temperature.

---

[1] Contribution No. 1154 from the Woods Hole Oceanographic Institution. This research was supported in part by National Science Foundation grant G4650 to Amherst College. A major part of the preparation of the material for the manuscript was carried out during 1959, when B.B.B. was the recipient of a John Simon Guggenheim Memorial Fellowship.

[2] Now National Science Foundation Fellow and Danforth Fellow, Department of Physics, California Institute of Technology, Pasadena, California.

[3] B. B. Benson and P. D. M. Parker, *Deep-Sea Res.*, **7**, 237 (1961).

[4] F. A. Richards and B. B. Benson, *ibid.*, **7**, 254 (1961).

[5] C. J. J. Fox, *Trans. Faraday Soc.*, **5**, 68 (1909).

[6] N. W. Rakestraw and V. M. Emmel, *J. Phys. Chem.*, **42**, 1211 (1938).

[7] N. W. Rakestraw and V. M. Emmel, *J. Marine Res.*, **1**, 207 (1938).

In addition an attempt was made to obtain the individual solubilities of nitrogen and argon. The procedure involved gasometric determinations of the total nitrogen, oxygen and argon extracted from water equilibrated with air, together with measurements of the ratio of nitrogen to oxygen and the ratio of nitrogen to argon. Unfortunately, the volumetric results were not reliable and they are not reported here, but it was realized that the two kinds of ratio measurements, alone, provided a means for at least a partial clarification of the generally confusing situation with respect to gas solubilities. Recently, for example, the solubility of oxygen has been a subject of particular controversy.[8-11]

In general, it probably is correct to state that although the precision of solubility measurements—gauged by the gross amplitude of scatter of repeated measurements—has ranged approximately from 1 to 0.5%, the results from various workers have differed by as much as 3%, even for a gas as extensively studied as oxygen. Stated in another way: gas solubility measurements have been subject to small random errors but large systematic errors.

In the absence of demonstrable sources of systematic error, the only basis for choosing one set of results as probably the most reliable for a particular gas has been substantiation by several workers on that single gas. For example, the fact that the values for oxygen in distilled water found by Elmore and Hayes,[11] Morris,[10] Fox,[5] and Winkler[12] are in essential agreement (0 to 1%, depending upon temperature), justifies the conclusion that some average of these values *probably* is more accurate than the values of Truesdale, *et al.*[8] (The fact that Elmore and Hayes carried out more experiments than anyone else, and found excellent "consistency," indicates only that their precision was very good, not that they had a smaller systematic error than, for example, Fox.) Nevertheless, the odds of 4 to 1 against Truesdale, *et al.*, are not overwhelming, and it is of interest to obtain further evidence on the question. With respect to nitrogen and argon, and to oxygen in sea water, the situation is still cloudier, because fewer measurements have been made and, as indicated earlier, the differences among workers are larger.

Direct measurements of the ratios of solubilities are of particular interest, because they permit *intercomparisons* of measurements of various workers on *different* gases, in addition to comparisons of determinations on a single gas. The procedure is an extension of the idea above—an attempt is made to find internally consistent sets of solubility and solubility ratio results for two or more gases. Alternatively, if the solubilities of one gas have been established accurately, ratio measurements can yield the solubilities of other gases. In either case, it is customary to make the tacit assumption that the solubility of a gas under normal atmospheric conditions is independent of the other gases present. In the absence of evidence to the contrary, we shall in this paper take this assumption to be valid.

Ratio measurements with a mass spectrometer have certain inherent advantages for attacking the question of systematic errors in gas solubility determinations. Lack of achievement of "true" equilibrium, variation of atmospheric pressure, incomplete extraction of the dissolved gases, uncertainties in relative humidity, and gas impurities, cause either no effect or, at worst, second-order effects due to differences in rates of solution. The only serious source of systematic error in the measurement of solubility ratios is in the preparation of standards for calibrating the mass spectrometer.

The results reported here should be considered preliminary, and some of the conclusions tentative. Nevertheless, we believe that certain of the values are more reliable than those previously available, and that partial clarification of the issue regarding gas solubilities has been achieved. Further experiments are now in progress for very accurate determinations of both solubilities and solubility ratios.

Experimental Procedures

For purposes of discussion, the procedures employed can be divided into three parts: (A) water-air equilibration; (B) extraction of the dissolved gases; and (C) mass spectrometric analyses of the gases.

A. The procedure for equilibration was suggested by the work of Rakestraw and Emmel.[6] Four flasks, open to the atmosphere, were almost completely immersed in a constant temperature bath. One of the flasks contained distilled water and the other three contained natural, untreated sea water with salinities of approximately 32, 34 and 36‰, respectively. The 32 and 34‰ waters were made by diluting the 36‰ water with distilled water. The partially submerged flasks were suspended in such a way that they were subject to a constant but gentle agitation from the motion of the water in the bath. The bath was maintained at a given temperature to within ± 0.05°. At the time the measurements were made no standard thermometer was available. Since then, however, the thermometer which was used has been checked and found to be sufficiently accurate (maximum error 0.15°) for these preliminary solubility ratio determinations.

After equilibrating a set of samples for at least sixty hours, each sample was transferred to a glass sample bulb, which had been brought to the temperature of the bath by partial immersion. A six millimeter T-bore, pressure type, precision grade stopcock attached to the bulb permitted a thistle tube to be inserted through it to the bottom of the bulb. In this way the air in the bulb could be displaced gently without trapping air bubbles. After flowing the water up through the stopcock, the stopcock was closed, thereby isolating the water sample which completely filled the bulb. The bulbs had volumes of approximately 200 cc. Samples of water from each flask also were put in small bottles, sealed, and sent to the Woods Hole Oceanographic Institution where the salinity of each was determined.

B. For extraction of the dissolved gases, a water sample bulb was attached by means of a standard taper joint to a vacuum system consisting of a one liter "extraction bulb," a Dry-Ice–acetone trap for water vapor, a liquid air trap for other condensable vapors, particularly carbon dioxide, and a mercury Toepler pump and gasometric system.

---

[8] G. A. Truesdale, A. L. Downing and G. F. Lowden, *J. Appl. Chem.*, **5**, 53 (1955).

[9] H. Steen, *Limnology and Oceanography*, **3**, 423 (1958).

[10] J. C. Morris, Final Report, Contract No. SAph 69705, Department of Health, Education and Welfare with Harvard University, 5/1/58 to 1/31/59.

[11] H. L. Elmore and T. W. Hayes, *Proc. ASCE*, **86**, 2556 (1960).

[12] L. W. Winkler, *Ber. Deutsch. Chem. Ges.*, **22**, 1764 (1889); Winkler, *ibid.*, **24**, 3602 (1891).

After pumping down the system (including the T-bore stopcock on the water sample bulb) to approximately one micron, the sample was admitted to the system and the dissolved gases Toepler-pumped off. To ensure complete extraction of the dissolved gases the procedure of Cook and Hanson[13] was followed. They reported complete extraction when 10 to 20% of the solvent was boiled off over a period of one to two hours. In our case between 40 and 90% (on the average approximately 70%) of the water in the extraction bulb was evaporated, and retrapped in the Dry Ice–acetone trap, over a period of one hour. With the condensable vapors removed, gas was transferred to a gas sample tube for analysis on the mass spectrometer. (Procedures carried out for the attempt at solubility determinations have not been included in this description.)

C. With the exception of the electronic circuitry, the mass spectrometer is like the 60° magnetic sector, single-focusing machine described by Nier.[14] In addition the instrument is equipped with a dual sample system [McKinney, *et al.*[15]] for precision isotope ratio analysis.

Employing "single collection" techniques with the mass spectrometer, the relative sizes of the beams for m/q = 28, 32 and 40 (molecular nitrogen, oxygen and argon, respectively) were determined for each extracted gas sample and for carbon dioxide-free air used as a standard gas to calibrate the spectrometer. From these measurements the ratio of nitrogen to oxygen, and a tentative value for the ratio of nitrogen to argon, could be calculated with accuracies of approximately 1%.

"Standard air" samples were taken outdoors by opening an evacuated and outgassed sample tube while holding it at arm's length and approximately five feet above the ground. Within the precision of our measurements, no differences in the nitrogen/oxygen/argon ratios were apparent between winter and summer. Carbon dioxide (and water vapor) were removed by immersing the tube in liquid air and transferring the uncondensed gases to another evacuated tube. The percentages of the gases in air were taken to be nitrogen 78.08%, oxygen 20.94%, argon 0.93%, carbon dioxide 0.032%, and traces of the rarer gases. The figure for oxygen is the mean of the values from P. F. Scholander as quoted by Richards,[16] and the figure for nitrogen was chosen to be consistent with the oxygen value. The percentage for argon is from Paneth.[17]

For more accurate analysis of the ratio of nitrogen to argon, another portion of the extracted gas was processed to remove the oxygen by cycling the gas through a manifold consisting of a "Vycor" furnace filled with copper turnings at 700°, in series with a liquid air trap. This procedure is necessary for precise analyses of nitrogen, because when oxygen is present in a gas sample, the high temperature conditions in the mass spectrometer ion source cause a small part of the oxygen to combine with carbon impurities to form carbon monoxide. Since carbon monoxide also has a molecular weight of 28 for the most abundant isotopes, the 28/40 ion beam ratio will not be a measure of the true nitrogen to argon ratio. With a "clean" mass spectrometer the effect is small enough so that when both the sample and the standard gases contain oxygen, and when appropriate corrections are made, an accuracy of 1% is possible for the nitrogen/argon ratio, but higher accuracy requires removal of the oxygen in both samples. It is evident that analyses of nitrogen should not be carried out on a mass spectrometer used for analyses of organic materials. Tests have shown that when a pure nitrogen and argon mixture is processed in the "Vycor" furnace, the ratio of nitrogen to argon is unaffected.

After processing, the samples were reanalyzed on the spectrometer. In these measurements the amplifier system was made more sensitive by inserting a "bucking" potential so that the recorded signal was the difference between the beam signal and the bucking potential. In addition the effect of spectrometer drift was reduced by a magnetic field switching arrangement which permitted rapid switching from one beam to the other. The gross scatter of these measurements of the nitrogen to argon ratio was approximately ± 0.3% (± 0.15% each, for the sample and standard).

In order to avoid any possible dependence of mass spectrometer ion source "discrimination" upon the nitrogen to argon ratio (this was a significant question because the ratio in the dissolved gases is approximately 39 to 1, whereas in air it is 84 to 1), standard samples were made up from tank nitrogen and tank argon with ratios comparable to those for the dissolved gases. Appropriate corrections were made for impurities in the tank gases.

As a check an air standard, with the oxygen removed, also was analyzed. The spectrometer correction factor (*i.e.*, the number by which the 28/40 beam ratio was multiplied to give the nitrogen to argon ratio) obtained was somewhat smaller than with the artificial standards. Unfortunately, the experiments had to be terminated before it could be established definitely that this result was caused by a difference in discrimination and was not the result of a systematic error in the volumetric preparation of the standards. For this reason we must assign a possible systematic error of −0, +1.5% to the absolute values for the nitrogen/argon ratios. The ratios given are based on the artificial standards. This possible systematic error would not apply, however, to the results on gases dissolved in the oceans reported in (3) and (4), because the same spectrometer correction factor was used in that work as in these solubility measurements.

Experimental Results and Discussion

As used throughout this paper, the solubility of a particular gas is defined to be the number of cc. of gas, measured at standard temperature and pressure, dissolved in one liter of water in equilibrium with a normal, free, dry atmosphere with total pressure 760 mm. of mercury. As stated earlier, a "normal" atmosphere was assumed to have a composition by volume of 78.08% nitrogen, 20.94% oxygen, 0.93% argon, 0.032% carbon dioxide, and traces of rarer gases. By "dry" is meant that the total partial pressure of the atmospheric gases, excluding water vapor, is 760 mm. of mercury. The symbols N_2', O_2' and A' denote the respective solubilities.

The solubility coefficient α for a particular gas is the number of cc. of gas, measured at standard temperature and pressure, dissolved in one liter of water in equilibrium with the gas when its partial pressure is 760 mm. of mercury. We shall use solubility coefficients when discussing pure water, and solubilities when referring to sea water.

Following Fox,[5] "atmospheric nitrogen"[18] is defined in this paper to be a mixture of nitrogen and argon, although, of course, as measured by him and others it is truly a mixture of nitrogen, argon, helium and the other inert gases, and perhaps nitrous oxide, etc. (depending upon the techniques used to prepare the gas). A moment's reflection reveals that neglecting the gases other than nitrogen and argon introduces a negligible error in the calculations of both nitrogen *and* argon, when the "true" nitrogen/argon ratio is combined with the "atmospheric nitrogen" solubility.

Table I gives the experimental data for the ratios

---

[13] M. W. Cook and D. N. Hanson, *Rev. Sci. Instr.*, **28**, 370 (1957).

[14] A. O. Nier, *Rev. Sci. Instr.*, **18**, 398 (1947).

[15] C. R. McKinney, J. M. McCrea, S. Epstein, H. A. Allen and H. C. Urey, *ibid.*, **21**, 724 (1950).

[16] F. A. Richards, "Some Current Aspects of Chemical Oceanography," in "Physics and Chemistry of the Earth," Vol. 2, page 103, Pergamon Press, New York, N. Y., 1957.

[17] F. A. Paneth, *Quart. J. Roy. Meteorol. Soc.*, **63**, 433 (1937).

[18] With the availability of various modern analytical techniques, we suggest that in the future this use of the phrase "atmospheric nitrogen" be dropped. It would seem to make more sense to have it mean literally "nitrogen in or from the atmosphere," so that, for instance, one could distinguish clearly and easily between dissolved nitrogen whose source was the atmosphere and dissolved nitrogen from other sources such as biochemical activity.[4]

N_2'/A' and N_2'/O_2' at various temperatures and salinities. It may be noted that the measured salinities for the sea water measurements at 30° are slightly higher than for the lower temperatures. This presumably resulted from partial net evaporation of water from the samples in the open flasks. The standard deviation of the N_2'/A' mass spectrometric determinations was approximately 0.2%. As indicated above, less care was taken with the N_2'/O_2' measurements, and the analytical precision was approximately ± 1%. The fourth figure, therefore, is not significant.

Table I

Experimental Data for N_2'/A' and N_2'/O_2' as Functions of Temperature and Salinity

Salinity, ‰	Temp., °C.	N_2'/A'	N_2'/O_2'
0.066	0.0	37.92	1.836
.066	5.0	38.29	1.825
.48	10.0	38.42	1.826
.066	15.0	38.66	1.859
.084	20.0	39.03	1.887
.11	25.0	39.43	1.941
.102	30.0	39.71	1.987
32.59	0.0	37.78	1.833
32.565	5.0	37.78	1.803
32.60	10.0	38.00	1.830
32.65	15.0	37.51[a]	1.821[a]
32.58	20.0	38.47	1.907
32.65	25.0	38.78	1.934
32.97	30.0	39.25	1.954
34.70	0.0	37.52	1.845
34.70	5.0	37.64	1.816
34.71	10.0	38.05	1.828
34.67	15.0	37.96	1.833
34.695	20.0	38.28	1.858
34.65	25.0	38.89	1.947
35.11	30.0	39.23	1.926
36.12	0.0	37.74	1.860
36.14	5.0	37.72	1.821
36.17	10.0	37.80	1.803
36.16	15.0	37.96	1.830
36.17	20.0	38.45	1.870
36.23	25.0	38.73	1.914
36.61	30.0	39.24	1.918

[a] These two values were rejected.

A. Distilled Water.—A plot of the values for N_2'/A' *vs.* temperature in distilled water yields a straight line within the analytical precision of ±0.2%. The least squares fit for the data is

$$N_2'/A' = 37.90 + 0.0590t$$

with a standard deviation of 0.076 or approximately 0.2% of the mean N_2'/A'. Values calculated from this equation are tabulated in Table II. As stated previously, they may be systematically high by approximately 1.5%.

In Table III the ratios of the solubility coefficients have been calculated from the expression

$$\frac{\alpha_{N_2}}{\alpha_A} = \frac{0.93N_2'}{78.08A'}$$

using our values for N_2'/A'. The values for $\alpha_{N_2Atm.}$ from the work of Hamberg,[19] Winkler[12] and Fox[5] have been taken from Coste,[20,21] who included corrections (first suggested by Fox) to the Winkler and Fox results, required because of the effect of differences in the solubilities of nitrogen and argon in the closed system absorptiometric type of experiment. Since $\alpha_{N_2Atm.} = 0.98823\alpha_{N_2} + 0.01177\alpha_A$, it can be shown that

$$\alpha_{N_2} = \frac{\alpha_{N_2Atm.}}{0.98823 + \dfrac{0.01177}{(\alpha_{N_2}/\alpha_A)}}$$

$$\alpha_A = \alpha_{N_2}/(\alpha_{N_2}/\alpha_A)$$

Using our values for α_{N_2}/α_A and the values of $\alpha_{N_2Atm.}$ from Hamberg, Winkler, and Fox, respectively, these equations have been used to calculate the values for α_{N_2} and α_A shown in Table III.

The values for α_{N_2} differ slightly from the values calculated by Coste, who apparently used values for α_A from Estreicher, which we believe to be less reliable than our α_{N_2}/α_A values. This implies, further, that the corrected values given by Coste for $\alpha_{N_2Atm.}$ also are slightly in error, but the error probably is not large enough to warrant a complete recalculation of all the original data.

The final three rows in Table III show values for α_A obtained by Estreicher,[22] Winkler,[23] and Lannung,[24] as given by Lannung, and by Åkerlöf.[25] Åkerloff found $\alpha_A = 33.2$ at 25°. A comparison of the six sets of values for α_A is fruitful. The Hamberg plus B. P values agree very well with the Fox plus B.P. results at the higher temperatures, but at lower temperatures the difference is 2.5%. The Winkler plus B.P. value for 25° is lower than the previous two by 4%, but in essential agreement with the Fox plus B.P. value at 0°. The agreement between the Hamberg plus B.P. results and those of Lannung is particularly evident. It is unfortunate that Lannung did not extend his measurements to lower temperatures. Nevertheless, the results at 10° suggest that Lannung and Hamberg plus B.P. agree better at lower temperatures than do Lannung and Fox plus B.P. The values for α_A from Estreicher and Winkler, especially the former, are distinctly higher than the others and not in agreement with each other.

From the above discussion and the fact that our α_{N_2}/α_A values are high, if anything, we form the tentative conclusion that the results of Hamberg, Fox, Lannung, and Benson and Parker are probably the most reliable, with the Hamberg, Lannung, and Benson and Parker results in best agreement for the solubility coefficients of argon, and therefore for nitrogen as well. Coste reached the conclusion in 1927 that the Hamberg and Fox "atmospheric nitrogen" results were the most reliable. It is surprising to note that the Winkler values still persist in the "Handbook of Chemistry and Physics." In essence, the inclusion of our results and those of Lannung doubles the probability

---

[19] Hamberg, *J. prakt. Chem.*, **33**, 433 (1886).

[20] J. H. Coste, *J. Phys. Chem.*, **31**, 81 (1927).

[21] In this discussion, and in the discussions to follow, we have not attempted to include values from all the sources quoted by Coste or others, but only those which seem to be customarily considered as among the most reliable.

[22] T. Estreicher, *Z. physik. Chem.*, **31**, 176 (1899).

[23] L. W. Winkler, *ibid.*, **55**, 344 (1906).

[24] A. Lannung, *J. Am. Chem. Soc.*, **52**, 68 (1930).

[25] G. Åkerlöf, *ibid.*, **57**, 1196 (1935).

TABLE II

ADOPTED VALUES FOR N_2'/A' *vs.* TEMPERATURE IN DISTILLED WATER, CALCULATED FROM THE LEAST SQUARES EQUATION

$$N_2'/A' = 37.90 + 0.0590t$$

°C.	0	1	2	3	4	5	6	7	8	9
0	37.90	37.96	38.02	38.08	38.14	38.20	38.25	38.31	38.37	38.43
10	38.49	38.55	38.61	38.67	38.73	38.78	38.84	38.90	38.96	39.02
20	39.08	39.14	39.20	39.26	39.32	39.38	39.43	39.49	39.55	39.61
30	39.67									

TABLE III

Results of combining the ratios of nitrogen and argon solubility coefficients from this research, with the solubility coefficients for "atmospheric nitrogen" found by Hamberg, Winkler and Fox, to obtain the individual solubility coefficients for nitrogen and argon. For comparison, values for the solubility coefficients for argon from Estreicher, Winkler and Lannung are included.

	Temp., °C.	0	5	10	15	20	25	30
Benson and Parker	N_2'/A'	37.90	38.20	38.49	38.78	39.08	39.38	39.67
	α_{N_2}/α_A	0.4514	0.4550	0.4584	0.4619	0.4655	0.4690	0.4725
Hamberg	$\alpha_{N_2 Atm.}$	24.21	21.42	19.15	17.37	15.98	14.94	...
Winkler	$\alpha_{N_2 Atm.}$	23.54	20.86	18.61	16.85	15.45	14.34	13.42
Fox	$\alpha_{N_2 Atm.}$	23.59	21.03	18.95	17.31	15.98	14.89	...
Hamberg + B. and P.	α_{N_2}	23.87	21.12	18.89	17.14	15.77	14.74	...
Winkler + B. and P.	α_{N_2}	23.21	20.57	18.35	16.62	15.24	14.15	13.25
Fox + B. and P.	α_{N_2}	23.26	20.74	18.69	17.08	15.77	14.69	...
Hamberg + B. and P.	α_A	52.88	46.42	41.21	37.11	33.88	31.43	...
Winkler + B. and P.	α_A	51.42	45.21	40.03	35.98	32.74	30.17	28.04
Fox + B. and P.	α_A	51.53	45.58	40.77	36.98	33.88	31.32	...
Estreicher	α_A	...	...	45.2	...	37.9	...	32.5
Winkler	α_A	...	...	42.0	...	35.0	32.6	30.0
Lannung	α_A	...	...	41.1	37.1	33.6	31.4	28.9

that Coste's conclusion was correct, and suggests that the Hamberg plus B.P. values for α_{N_2} and α_A (or those of Lannung for α_A) are to be preferred over those obtained from Fox's data. This will be discussed further below.

A graph of the data for N_2'/O_2' *vs.* temperature in distilled water suggests the possibility that the temperature gradient of the ratio may increase with an increase in temperature. This, however, may be an artifact of the measurements, since no attempt was made to prevent B.O.D. (biochemical oxygen demand), as our original interest was not in oxygen. The water samples were not stored very long before gas extraction, but it is possible that B.O.D. has made the N_2'/O_2' results systematically high and subject to greater random fluctuations. In view of the uncertainties it was decided that the most objective manner of treating the data was to obtain a linear least squares fit, as was done with N_2'/A'. The result is

$$N_2'/O_2' = 1.800 + 0.00533t$$

with the standard deviation of the experimental points from the least squares fit equal to 0.025 or approximately 1.3% of the mean N_2'/O_2'.

Values for N_2'/O_2' calculated from the least squares solution are shown in Table IV. The values for $\alpha_{N_2}/\alpha_{O_2}$ were calculated from the equation

$$\frac{\alpha_{N_2}}{\alpha_{O_2}} = \frac{20.94 N_2'}{78.08 O_2'}$$

The next four rows list the results for α_{O_2} from Winkler,[12] Fox,[5] Truesdale, Downing and Lowden,[8] and Elmore and Hayes.[11] The Winkler values actually were taken from the "Handbook of Chemistry and Physics," 33rd Edition, 1951–1952, and the Truesdale, *et al.*, and Elmore and Hayes numbers were obtained by converting their solubility values, in parts per million from a "wet" atmosphere, to solubility coefficients.

The values for α_{N_2} shown in the next four rows were calculated by multiplying each of the oxygen solubility coefficients from the four sources by our solubility coefficient ratios. The last three rows consist of α_{N_2} values obtained in Table III from independent evidence.

There is striking agreement among the values for α_{N_2} from the Elmore and Hayes plus B.P. results for α_{O_2} and $\alpha_{N_2}/\alpha_{O_2}$, the Winkler plus B.P. results for α_{O_2} and $\alpha_{N_2}/\alpha_{O_2}$, the Fox plus B.P. results for α_{O_2} and $\alpha_{N_2}/\alpha_{O_2}$, and the Hamberg plus B.P. results for $\alpha_{N_2 Atm}$ and α_{N_2}/α_A. The first and last show the best agreement, differing by less than 0.5% except at 25° where the difference is still only 0.7%. Recall, also, the excellent correspondence between the Lannung α_A and the Hamberg plus B.P. values from $\alpha_{N_2 Atm}$ and α_{N_2}/α_A.

It is possible that the consistency of the whole scheme is fortuitous. Indeed, we might expect it to be, in view of the fact that there are possible systematic errors of 1.5% in each of our measurements alone, not to mention unknown systematic errors in all the other determinations. Nevertheless, one cannot remain unimpressed when seven independent sets of measurements (Winkler, Fox, and Elmore and Hayes oxygen solubilities, Benson and Parker N_2'/A' and N_2'/O_2' solubility ratios, Hamberg "atmospheric nitrogen" solubilities, and Lannung argon solubilities) by different workers, on three gases, using a wide variety of methods, all lead to an internally consistent scheme to within approximately 1%. Still further support for this

TABLE IV

Results of combining the ratios of nitrogen and oxygen solubility coefficients from this research, with solubility coefficients for oxygen found by Winkler, Fox, Truesdale, Downing and Lowden, and Elmore and Hayes, to obtain the individual solubility coefficients for nitrogen. For comparison, the independently determined values for α_{N_2} from Table III are included.

		Temp., °C.	0	5	10	15	20	25	30
	Benson and Parker	N_2'/O_2'	1.800	1.827	1.853	1.880	1.907	1.933	1.960
		$\alpha_{N_2}/\alpha_{O_2}$	0.4827	0.4900	0.4970	0.5042	0.5114	0.5184	0.5257
	Winkler	α_{O_2}	48.89	42.87	38.02	34.15	31.02	28.31	26.08
	Fox	α_{O_2}	49.24	43.21	38.37	34.55	31.44	28.90	26.65
	Truesdale, D. and L.	α_{O_2}	47.65	41.74	36.98	33.20	30.27	28.00	26.28
	Elmore and Hayes	α_{O_2}	49.30	43.16	38.16	34.13	30.88	28.25	25.97
	Winkler + B. and P.	α_{N_2}	23.60	21.01	18.90	17.22	15.86	14.68	13.71
	Fox + B. and P.	α_{N_2}	23.77	21.17	19.07	17.42	16.08	14.98	14 01
	T.,D. and L. + B. and P.	α_{N_2}	23.00	20.45	18.38	16.74	15.48	14.52	13.82
	E. and H. + B. and P.	α_{N_2}	23.80	21.15	18.97	17.21	15.79	14.64	13.65
From Table III	Hamberg + B. and P.	α_{N_2}	23.87	21.12	18.89	17.14	15.77	14.74	...
	Winkler + B. and P.	α_{N_2}	23.21	20.57	18.35	16.62	15.24	14.15	13.25
	Fox + B. and P.	α_{N_2}	23.26	20.74	18.69	17.08	15.77	14.69	...

impression is provided by still incomplete and unpublished determinations of the solubility coefficients for pure nitrogen by Klots and Benson. These new results are higher than those of Hamberg plus B.P. by only 0.2% at 5° and 0.7% at 15°, and lower by 0.5% at 25°.

The agreement between Truesdale, Downing and Lowden plus B.P. results and the Fox ($\alpha_{N_2\text{Atm.}}$) plus B.P. values, is good, though not as satisfactory as the above, but they do not have the support of several other lines of investigation.

Incidentally, there was a potential source of systematic error in the measurements of Truesdale, *et al.*, which they apparently did not correct for, and which no one else seems to have recognized. In order to maintain gas flow in their apparatus a negative pressure gradient was required in the direction of gas flow. Consequently, the actual pressure inside the vessel must have been greater than, rather than equal to, barometric pressure. With a small flow tube, which their drawing suggests, the error might be considerable. Unfortunately, this does not explain why their values are lower than those of other workers, because a correction for the effect would lower their results still further.

To summarize our conclusions for distilled water, we suggest on the basis of present evidence that the most reliable results are the Elmore and Hayes oxygen solubility coefficients, the Hamberg "atmospheric nitrogen" solubility coefficients, and the Benson and Parker nitrogen to argon solubility coefficient ratios, from which all the solubility coefficients, solubilities and solubility ratios for the three gases can be calculated as illustrated above.

B. Sea Water.—When the N_2'/A' data are plotted against the temperature, it is evident that the random errors in the data preclude the possibility of deducing the dependence of the solubility ratio upon salinity for the range of salinities studied. (There is a small variation of N_2'/A' with salinity, however, as can be seen from a comparison of Table II and Table V.) Furthermore, such a graph indicates a possible small non-linear dependence of the ratio upon temperature. These fluctuations and the apparent non-linearity may have been the result of experimental difficulties, but perhaps for a different reason. The gasometric measurements, although unreliable, indicated a smaller amount of total gas extracted from the samples at 0° and 5° than would have been expected from the measurements at the higher temperatures. This could have resulted from a greater B.O.D., or from incomplete equilibrations. The former would not have influenced the N_2'/A' ratios, but the latter could have caused an error in them. For reasons implied in the introduction, this error would have been small, but at the sensitivity of these measurements it might show up.

On the basis of the above it was deemed preferable to consider all the data applying to an average salinity of 34.5‰, and to obtain a linear least squares fit as in the previous cases. The resulting dependence of the ratio upon temperature is given by

$$N_2'/A' = 37.48 + 0.0522t$$

for a salinity of 34.5‰, with a standard deviation of 0.175 or approximately 0.46%—over twice as large as the estimated error due to the spectrometer measurements alone. The adopted values for N_2'/A', calculated from the least squares equation, are shown in Table V. The possible error in the mass spectrometer calibration could have made these solubility ratios systematically too high by approximately 1.5%.

In Table VI the values for $N_2'_{\text{Atm.}}$ were calculated from Fox's equation. The Fox plus B.P. values for N_2' and A' were obtained by combining N_2'/A' with the relation $N_2'_{\text{Atm.}} = N_2' + A'$. The Rakestraw and Emmel $N_2'^*$ and A'^* results were taken from their paper.[6] (The reason for the asterisks will appear below.) The numbers in parentheses were found by extrapolation. Table VI includes values for only one salinity because these are sufficient for the purpose of this discussion.

On the basis of the fact that Rakestraw and Emmel had found sea water from nearly all sources to be unsaturated relative to Fox's solubilities, they "suspected that his [Fox] systems might have been supersaturated." Another interpretation is

TABLE V

Adopted values for N_2'/A' *vs.* temperature in sea water of mean salinity 34.5‰. Calculated from the least squares equation $N_2'/A' = 37.48 + 0.0522t$.

°C.	0	1	2	3	4	7	6	7	8	9
0	37.48	37.53	37.58	37.64	37.69	37.74	37.79	37.85	37.90	37.95
10	38.00	38.05	38.11	38.16	38.21	38.26	38.32	38.37	38.42	38.47
20	38.52	38.58	38.63	38.68	38.73	38.78	38.84	38.89	38.94	38.99
30	39.05									

TABLE VI

Values for N_2' and A' in sea water with chlorinity 20‰ or salinity 36.13‰, obtained from our N_2'/A' values, Fox's $N_2'_{Atm}$ results, and nitrogen and argon data from Rakestraw and Emmel.

	Temp., °C.	0	5	10	15	20	25	30
Benson and Parker	N_2'/A'	37.48	37.74	38.00	38.26	38.52	38.78	39.05
Fox	N_2' atm.	14.30	12.99	11.93	11.06	10.34	9.74	9.21
Fox + B. and P.	N_2'	13.93	12.65	11.62	10.78	10.08	9.50	8.98
Rakestraw and Emmel	N_2'	14.30	12.73	11.56	10.57	9.77	9.10	(8.57)
Rakestraw and Emmel	$N_2'^*$	14.21	12.62	11.42	10.39	9.54	8.82	(8.21)
Fox + B. and P.	A'	0.375	0.335	0.306	0.282	0.262	0.245	0.230
Rakestraw and Emmel + B. and P.	A'	.382	.337	.304	.276	.254	.235	(.219)
Rakestraw and Emmel	A'	(.405)	.352	.314	.283	.259	.238	(.217)
Rakestraw and Emmel	A'^*	(.403)	.349	.310	.278	.253	.231	(.208)

TABLE VII

Values for N_2' in sea water with chlorinity 20‰ or salinity 36.13‰, obtained from a combination of N_2'/O_2' from this research with oxygen solubility data from Fox and from Truesdale, Downing and Lowden. The results for N_2' from Table VI are included for comparison.

		Temp., °C.	0	5	10	15	20	25	30
	Benson and Parker	N_2'/O_2'	1.807	1.827	1.847	1.866	1.886	1.906	1.926
	Fox	O_2'	7.97	7.07	6.36	5.79	5.31	4.89	4.46
	Truesdale, D. and L.	O_2'	7.84	6.90	6.14	5.56	5.10	4.73	4.43
	Fox + B. and P.	N_2'	14.40	12.92	11.75	10.80	10.01	9.32	8.59
	T.D. and L. + B. and P.	N_2'	14.17	12.61	11.34	10.37	9.62	9.02	8.53
From Table VI	Fox + B. and P.	N_2'	13.93	12.65	11.62	10.78	10.08	9.50	8.98
	Rakestraw and Emmel	N_2'	14.30	12.73	11.56	10.57	9.77	9.10	(8.57)

possible as at least a partial explanation of this apparent unsaturation in sea water. The solution of atmospheric gases in the sea probably occurs under conditions in which the air just above the surface is nearly saturated with water vapor. Therefore in determining the percentage saturation of any gas in sea water, "wet" solubilities probably should be used. But Fox's results were presented as "dry" solubilities (he performed his measurements under conditions in which his gas was almost certainly saturated with water vapor, and then corrected the data to "dry" solubilities), so that an apparent undersaturation would be expected when using them as a basis for sea measurements.

A similar reason would appear to explain part of the large differences (7.5% for nitrogen at 25°) between the Fox plus B.P. and Rakestraw and Emmel asterisked values for both nitrogen and argon shown in Table VI. Rakestraw and Emmel carried out their solubility measurements under circumstances which would have corresponded to a state between a "dry" and a " wet" atmosphere, probably nearer the latter. If this was the case, the Rakestraw and Emmel values are not "true" N_2' values (*i.e.*, "dry") as defined in this paper. This is the reason for marking them with asterisks. If it is assumed that they represent "wet" solubilities, the corresponding "dry" solubilities can be calculated, and these are given in Table VI without asterisks. Comparing them for nitrogen with those of Fox plus B.P. the agreement is seen to be better, with the former higher by 2.6% at 0°, in essential agreement (within 1%) at 5° and and 10°, and lower by 4.3% at 25°. It should be noted that although we equilibrated in a manner similar to Rakestraw and Emmel, the *ratio* N_2'/A' would not have been influenced by the relative humidity.

Because the Rakestraw and Emmel "argon" actually consisted of all the residual gases after the removal of carbon dioxide, oxygen and nitrogen, values for A' calculated from their N_2' ("dry") values and our N_2'/A' ratios also are shown in Table VI.

The random errors in the N_2'/O_2' data for sea water masked the small variation of the ratio with salinity over the range of salinities examined. The remarks made with respect to the data for N_2'/O_2' in distilled water and N_2'/A' in sea water concerning the possible sources of these fluctuations and of the apparent non-linear dependence of the ratio upon temperature apply here as well. Therefore, all the data were considered to correspond to a salinity of 34.5‰, and a linear least squares fit was obtained with the result

$$N_2'/O_2' = 1.807 + 0.00396t$$

The standard deviation of the experimental points from the least squares fit was 0.028 or approximately 1.5% of the mean ratio.

Table VII shows values for N_2'/O_2' obtained from the equation above, together with values of O_2' calculated from Fox's equation and the O_2' results of Truesdale, Downing and Lowden corrected to dry solubilities. The last section of the table gives the results for N_2' calculated from the N_2'/O_2' values and the respective oxygen solubilities. The final two lines show the N_2' results from Table VI, which were derived from independent measurements.

The recalculated "dry" N_2' Rakestraw and Emmel values at each temperature are very nearly equal to the mean of the Fox plus B.P. oxygen-derived values and the Truesdale, *et al.*, plus B.P. values. The Fox plus B.P. nitrogen-derived results show the poorest agreement with a distinctly different slope from the other three. This could not have resulted from a possible error in our N_2'/A' measurements due to incomplete equilibrium at low temperatures, because the ratio determinations influence the calculated N_2' values very little.

Choosing among the other three sets of results is more difficult. If it is assumed that incomplete equilibration was a negligible source of error in the N_2'/O_2' measurements, we would be inclined to prefer the Fox oxygen results in sea water for two reasons: (1) The Truesdale, *et al.*, sea water results might be expected to be too low—especially at low temperatures—on the basis of their oxygen results in distilled water. (This is not a very convincing argument since the Fox nitrogen solubilities are taken to be in error even though his oxygen results will be considered the best. It has some validity, however, on the basis that Fox and Truesdale, *et al.*, are each internally consistent with respect to oxygen in distilled water and sea water.) (2) Any possible B.O.D. effects on our N_2'/O_2' determinations would tend to make the ratios and, consequently, the two oxygen derived sets for N_2', too high. Correction for this would improve the agreement between the Fox plus B.P. results and the Rakestraw and Emmel N_2' results and have the opposite effect on the Truesdale, *et al.*, plus B.P. results. If incomplete equilibration was a source of error in our measurements, the nature of the nonlinear dependence of both N_2'/A' and N_2'/O_2' on temperature would indicate that either our nitrogen concentrations were too high at low temperatures or oxygen and argon too low. Correction for this would again favor the Fox values over Truesdale, *et al.*

In summarizing the situation for sea water, it is suggested—although with much less confidence than indicated earlier for distilled water—that possibly the most reliable data are the Fox oxygen solubilities, the Rakestraw and Emmel corrected nitrogen solubilities, and the N_2'/A' ratios from this research. The argon solubilities obtained from a combination of the latter two sets of results are the first information available on the solubility of pure argon in sea water. Although we have chosen to consider dry solubilities in this paper, it is suggested that for comparisons with oceanographic measurements wet solubilities probably are preferable. Finally, it is clear that much further work needs to be done on the solubilities of all the gases in sea water.

Acknowledgments.—We wish to express our appreciation to Mr. Nathaniel Corwin for obtaining the sea water, to Mr. Dean Bumpus for the salinity determinations, to Dr. Eva Kuhn Hilfer, Mr. Robert A. R. Parker and Mr. Noel S. Bartlett, who carried out part of the gas sample processing and mass spectrometer measurements, and to Dr. Mary Sears for her patience and help in preparing the manuscript for publication. Thanks are due Professor Arnold B. Arons and Dr. Cornelius E. Klots for critical reading of the manuscript. Conversations with Dr. Klots, Dr. James H. Carpenter, Professor Francis A. Richards and Dr. Leslie H. N. Cooper have been very helpful.

Contribution No. 1155

Geochimica et Cosmochimica Acta, 1961, Vol. 25, pp. 81 to 90. Pergamon Press Ltd. Printed in Northern Ireland

Fossil porphyrins: uncomplexed chlorins in a triassic sediment*

M. Blumer and G. S. Omenn
Woods Hole Oceanographic Institution, Woods Hole, Massachusetts, U.S.A.

(*Received* 9 *March* 1961)

Abstract—The Triassic oil shale of Serpiano (Switzerland) contains, besides the well-known tetrapyrrole pigments of the porphyrin class, some small amounts of chlorins. These pigments have now been isolated and identified as desoxomesoetiopyropheophorbide *a* and etiochlorin III, with their structure confirmed both by dehydrogenation to the corresponding porphyrins and by synthesis. These ancient chlorins are not direct descendants of chlorophyll; rather, they are secondary, synthetic chlorins, formed by hydrogenation of meso- and desoxophyllerythroetioporphyrin under extreme reducing conditions, probably in a late diagenetic stage in the sediment.

INTRODUCTION

THE discovery of porphyrins in geological materials (DHÉRÉ and HRADIL, 1934; TREIBS, 1934) marked a most decisive step in the development of the present thought on the transformation of organic matter in the sediments and on the genesis of petroleum, oil shales and coal. TREIBS, in his pioneering investigations (summarized by TREIBS, 1936), identified several fossil chlorophyll and haemin derivatives, some common to petroleum, oil shales and bituminous coals (mesoporphyrin (MP), desoxophyllerythrin (DP) and their etioporphyrins (MEP, DPEP)), and others restricted to coal (deutero- and deuteroetio-porphyrin). Occasionally, these pigments are found in their free state; usually, however, they are complexed with metals such as vanadium and nickel. TREIBS also reported spectroscopic evidence for the frequent occurrence of small quantities of related pigments, including some green chlorophyll derivatives, in sediments of a wide age range. These green pigments, recognized by their characteristic absorption band at 640 mμ, were later found throughout the entire stratigraphic sequence of the Triassic oil shales of Serpiano, Switzerland (BLUMER, 1950b). Because of their high pigment content, these shales have now been chosen for an attempt to isolate the ancient green pigments.†

Isolation

Uncomplexed tetrapyrrole pigments, due to their basic nature, are extracted from solvents such as ether into aqueous acids; this property is frequently utilized for the isolation of porphyrins and the resolution of pigments differing in their basicity. However, when applied to extracts from bituminous materials, solvent partitioning often fails to achieve the expected separation. This is caused by the presence of certain ether-soluble materials which alter the partition coefficients in favour of the organic phase. This difficulty can be overcome by using a poorer solvent (e.g. *iso*propyl ether (BLUMER, 1950b)) or by first precipitating these compounds with a paraffin hydrocarbon. In either case, although some of the desired pigment is lost in the insoluble fraction, recovery by repeated extraction or precipitation is often possible.

---

* Contribution no. 1155 of the Woods Hole Oceanographic Institution.

† A brief report of this investigation appeared earlier (BLUMER and OMENN, 1961).

For the isolation of the green pigment, the benzene–methanol extract of the oil shale is evaporated, redissolved in chloroform, and precipitated with an excess of *iso*octane; the asphaltenes are reprecipitated if spectroscopic examination indicates the necessity. The soluble fraction is transferred into ether and extracted with 2·5 and 5–6 N HCl. The first acid extract contains most of the free DPEP and MEP, while the less basic green pigments accumulate in the second extract. Some vanadium complex also enters the acid phase and must be removed by further partitioning of the pigments between ether and HCl (see experimental part).

Repetitive chromatography over alumina serves for the final purification of the pigments. A moderately active adsorbent (Brockmann II) is best suited for the initial separation of the pigment from hydrocarbons and coloured, high molecular weight materials. Rechromatography on alumina of lower activity (Brockmann III) then resolves the pigment mixture, eluting the green pigments ahead of the more strongly retained DPEP/MEP-fraction.

Structural evidence from spectroscopy and chromatography

The pigment exhibits a typical chlorin spectrum (Stern and Wenderlein, 1936) (Fig. 1a), characterizing it as a tetrapyrrole compound of the chlorophyll *a* series with one hydrogenated pyrrole ring. The high chromatographic mobility of the pigment on alumina and on paper (r_f-value of 0·75 on Whatman no. 3 paper, CCl_4-*iso*octane, 7:3, v/v) indicates the absence of polar groups such as —COOH, —COOR, —OH, —CO and —COH. The presence of a minor band (Ia) at 613 mμ, together with the partial resolution of the band V into two bands at 486 and 494 mμ is typical of mesochlorins (Stern and Pruckner, 1937), chlorophyll derivatives in which the 2-vinyl group has been hydrogenated to an ethyl group. Few chlorins have their main band (I) at a wavelength so low as 640 mμ; this again agrees with the assumption that the fossil pigment has a mesochlorin structure and lacks polar substitution.

Thus, the range of probable pigment structures is reduced to those of a small group of mesoetiochlorins, including etiochlorin, mesopyrro and mesophylloetiochlorin, as well as the unknown chlorin analogue of DPEP. Mesopyrroetiochlorin, with band I at a slightly higher wavelength (645 mμ), is not likely to be the major pigment component. Also, in contrast to the fossil chlorin, its band Ia has an extinction equal to that of band II; this is also the case for etiochlorin III. The spectrum of the fossil pigment resembles much more closely that of mesophyllochlorin or mesophylloetiochlorin (Pruckner, 1940).* The unknown chlorin analogue of DPEP differs from mesophylloetiochlorin only in the presence of an additional CH_2-group (in the isocyclic ring between the 8- and 6-carbon atoms); its spectrum, therefore, must be very similar.

Dehydrogenation of chlorins to porphyrins

Several reactions may be used for the conversion of chlorins into the more easily identified porphyrins. Fischer's technique (Fischer and Stern, 1940), using boiling formic acid and iron powder, was unsuccessful, when applied to the fossil pigment; however, the dehydrogenation was found to take place rapidly with chloranil in refluxing xylene. The strongly basic dehydrogenation products are

---

* Pruckner's paper contains two spectral plots for mesophyllochlorin in dioxane, showing the 490 mμ band resolved in one and unresolved in the other.

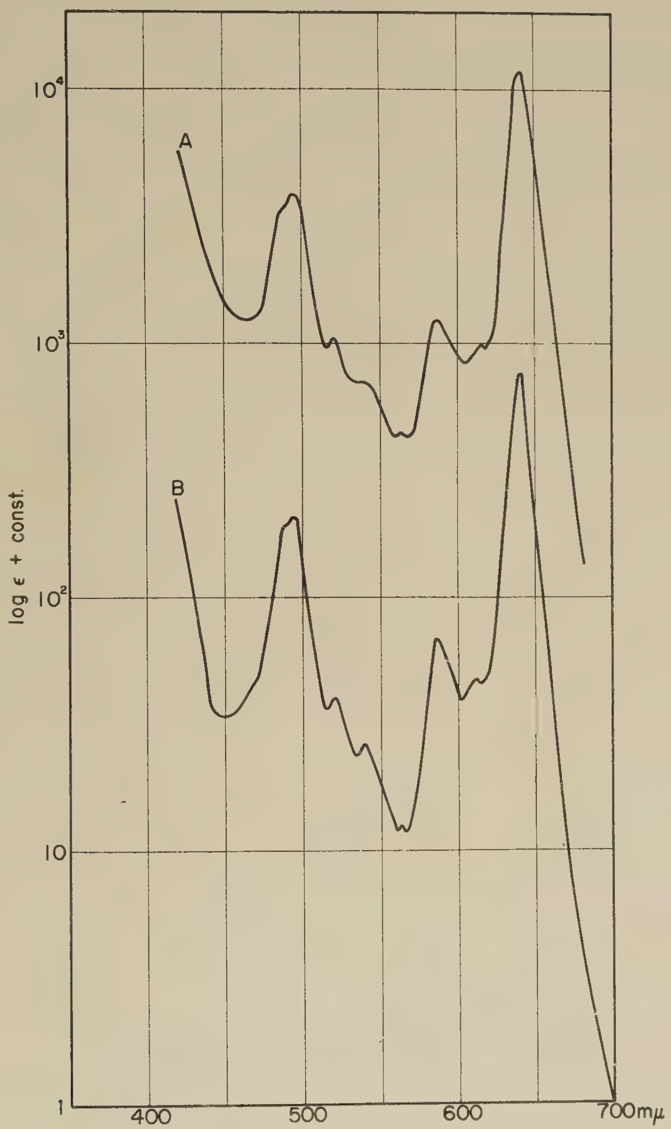

Fig. 1. (a) Natural desoxomesoetiopyropheophorbide *a*.
(b) Synthetic desoxomesoetiopyropheophorbide *a*.

easily separated from excess chloranil and any remaining chlorin. The products have a typical porphyrin spectrum (Fig. 2b), intermediate between those of DPEP and of MEP and identical with the spectrum of the DPEP/MEP-fraction of the same sediment. Chromatography over alumina (Brockmann III) partially resolves the dehydrogenated pigments. The fractions show a gradual change from the etiospectrum of MEP to the phyllo spectrum of DPEP, accompanied by a corresponding increase in the ratio of band II to band III and a shift in the position of band III from 524 to 530 mμ. Paper chromatography confirms these spectroscopic findings: the early eluates produce two distinct spots at the location of MEP ($r_f = 0{\cdot}64$) and of DPEP ($r_f = 0{\cdot}48$) with only the latter present in the succeeding fractions.

It should be pointed out that mesochlorins are much more strongly reducing and more easily converted into porphyrins than the natural 2-vinyl-chlorins. The fossil chlorins, for instance, are dehydrogenated even by some rather strongly reducing media; thus, it was found that vanadyl sulfate in boiling acetic acid–pyridine (3 : 1, v/v) oxidized the chlorins to porphyrins at a rate far exceeding that of complex formation. Also, the pigments are quite unstable and are destroyed rapidly, even when stored in darkness and under refrigeration.

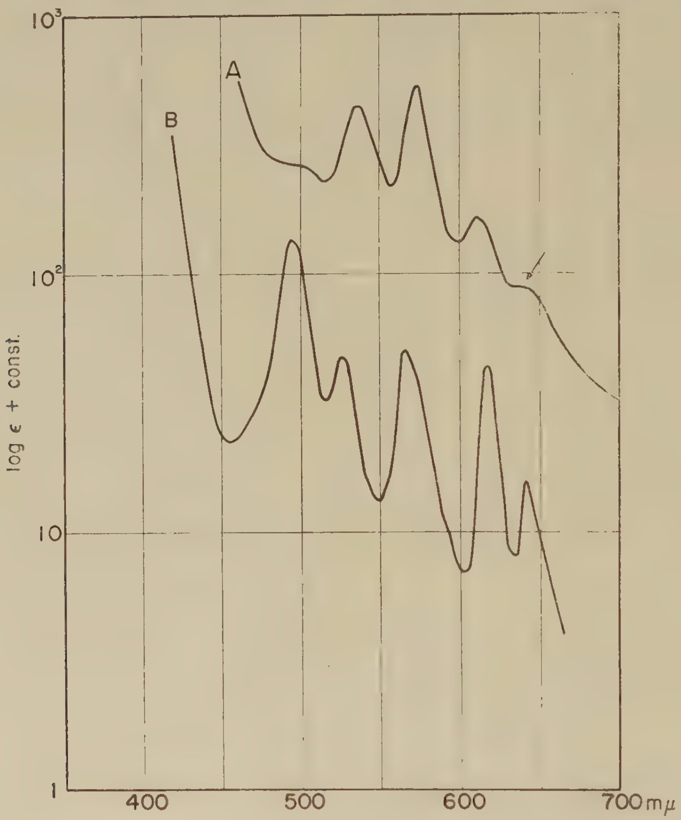

Fig. 2. (a) Benzene–methanol extract of Serpiano oil shale.
(b) Porphyrins obtained by dehydrogenation; the small peak at 641 mμ is due to a trace of residual chlorin.

Synthesis of dihydro-DPEP (*desoxomesoetiopyropheophorbide* a)

The dehydrogenation experiments characterize the fossil pigment as a mixture of a small amount of dihydro-MEP (etiochlorin III) with dihydro-DPEP (desoxomesoetiopyropheophorbide *a**). The presence of mesophylloetiochlorin is clearly excluded, since band I of phylloetioporphyrin (627 mμ) is not found in the dehydrogenated pigments. In order to substantiate this structural identification, dihydro-DPEP was synthesized. For that purpose, a mixture of DPEP and MEP was isolated from the Serpiano oil shale and resolved by chromatography. The fraction with the highest DPEP/MEP-ratio (extinction ratio of band II/band III = 1·47) was converted into the zinc complex and hydrogenated in boiling ethanol with Raney nickel as catalyst. The zinc chlorin complex was split with acid, and the chlorin was separated from unreacted porphyrins by acid fractionation and chromatography.

The spectrum of the synthetic dihydro-DPEP agrees very well with that of the natural pigment (Fig. 1b); the higher relative extinction of the latter in the regions of the 460 and 560 mμ minima indicates the presence of some residual contamination. The r_f value (Whatman no. 3, CCl_4–*iso*octane, 7 : 3, v/v) of the natural chlorin is slightly higher than that of the synthetic pigment (0·75 vs. 0·68), because of a higher proportion of the more rapidly moving etiochlorin III.

The geochemical history of the fossil chlorins

When Treibs first noted the presence of green pigments in some ancient sediments, he assumed that they stood in a close genetic relationship to the chlorophylls. With the isolation and structural identification of two of these pigments, his hypothesis can now be re-examined. In the case of etiochlorin III, a haemin derivative, it is obvious that the chlorin structure is of secondary origin. The porphyrin structure of MEP was converted, in a strongly reducing sedimentary environment, into the corresponding chlorin structure. The situation in the case of dihydro-DPEP is ambiguous; again, the chlorin structure might be of a secondary nature, or it might have been retained ever since the deposition of the sediment. A comparison of the parallel and competing redox pathways between chlorophyll and dihydro-DPEP shows that the former alternative is the more probable one.

One of the first geochemical reactions in this sequence—apart from the removal of magnesium and the hydrolysis of the esters—is the conversion of the vinyl into ethyl groups with formation of a meso pigment:

$$\text{vinylchlorin} + H_2 \rightarrow \text{mesochlorin} \qquad (1)$$

$$\text{vinylporphyrin} + H_2 \rightarrow \text{mesoporphyrin} \qquad (2)$$

In the chlorophyll series, reaction (1) probably competes with the isomerization of the vinylchlorins:

$$\text{vinylchlorin} \rightarrow \text{mesoporphyrin} \qquad (3)$$

It has long been known that vinyl groups in side chains of the tetrapyrrole system stabilize the reduced (chlorin) state of the pigments. This is revealed by the much greater ease of dehydrogenation of the mesochlorins by air and other oxidants.

---

* Formally, the pigment belongs to the chlorophyll *a* series; however, this must not be taken to imply necessarily a genetic relationship. Under the strongly reducing conditions in the subsurface, chlorophyll *b* and bacteriochlorophyll may also be converted to the same pigment.

The carbonyl group (of the isocyclic ring and of the formyl and acetyl groups) is also rather easily attacked by the reducing enviroment of the sediments; here, the influence of the reduction state of the side chain on the redox potential of the tetrapyrrole system is less pronounced.

$$\mathrm{R{-}CO{-}R} + 2\mathrm{H_2} \rightarrow \mathrm{R{-}CH_2{-}R} + \mathrm{H_2O} \tag{4}$$

$$\mathrm{R{-}COH} + 2\mathrm{H_2} \rightarrow \mathrm{R{-}CH_3} + \mathrm{H_2O} \tag{5}$$

$$\mathrm{R{-}CO{-}CH_3} + 2\mathrm{H_2} \rightarrow \mathrm{R{-}CH_2{-}CH_3} + \mathrm{H_2O} \tag{6}$$

Reactions (1) to (6) proceed easily in the direction indicated. The rates of the reverse reactions are infinitely small; high redox potentials in the environment will much more readily lead to the complete destruction of the tetrapyrrole ring system than bring about the specific reverse reaction. Therefore, we can consider these reactions as entirely irreversible, even for geological time spans of 10^8–10^9 years. In contrast, the redox reactions, which involve the conjugated tetrapyrrole system, proceed rapidly enough in either direction to be considered *geochemically* reversible:

$$\text{vinylporphyrin} + \mathrm{H_2} \rightleftharpoons \text{vinylchlorin} \tag{7}$$

$$\text{mesoporphyrin} + \mathrm{H_2} \rightleftharpoons \text{mesochlorin} \tag{8}$$

The equilibria (7) and (8) are most important at intermediate and low redox potentials; an additional one of the four pyrrole rings can enter into the equilibrium at very low potentials, though it is still questionable whether the sedimentary environment ever reaches the low reduction state necessary:

$$\text{mesochlorin} + \mathrm{H_2} \rightleftharpoons \text{tetrahydromesoporphyrin} \tag{9}$$

The standard potentials of these "semi-reversible" redox systems are not easily measured, but we know—as already mentioned—that the redox potential of the meso pigments is considerably lower than that of the vinyl pigments. This is expressed in the semiquantitative diagram of Fig. 3, with which we can now trace the geochemical fate of a pigment of the type of chlorophyll *a*. Hydrolytic processes, such as the exchange of H^+ for Mg^{2+} and the saponification of the esters with the consecutive decarboxylation in 10-position, rapidly transform chlorophyll *a* into pyropheophorbide *a*, which is subsequently reduced. Most organic-rich sediments, immediately upon deposition or shortly thereafter, acquire a negative redox potential which is gradually lowered with increasing age of the sediment (ZoBell, 1946). Under these conditions, the reduction of the vinyl and of the carbonyl groups can take place. As irreversible reactions they will immediately proceed to completion; the ratio of starting-to-end product is independent of the potential of the environment. This explains why vinyl and carbonyl pigments have never been found in sediments of appreciable age. In contrast, reactions between chlorins and porphyrins lead to an equilibrium, and the potential of the environment determines the ratio of the two forms.

Thus, any mesochlorins, formed by the reduction of vinylchlorins during early diagenesis and at relatively high potential, will be largely reoxidized to mesoporphyrins, the overall effect being that of an isomerization. The mesochlorins reappear in appreciable quantities only much later, when the potential of the environment drops far below the values required for the reduction of vinyl and carbonyl groups.

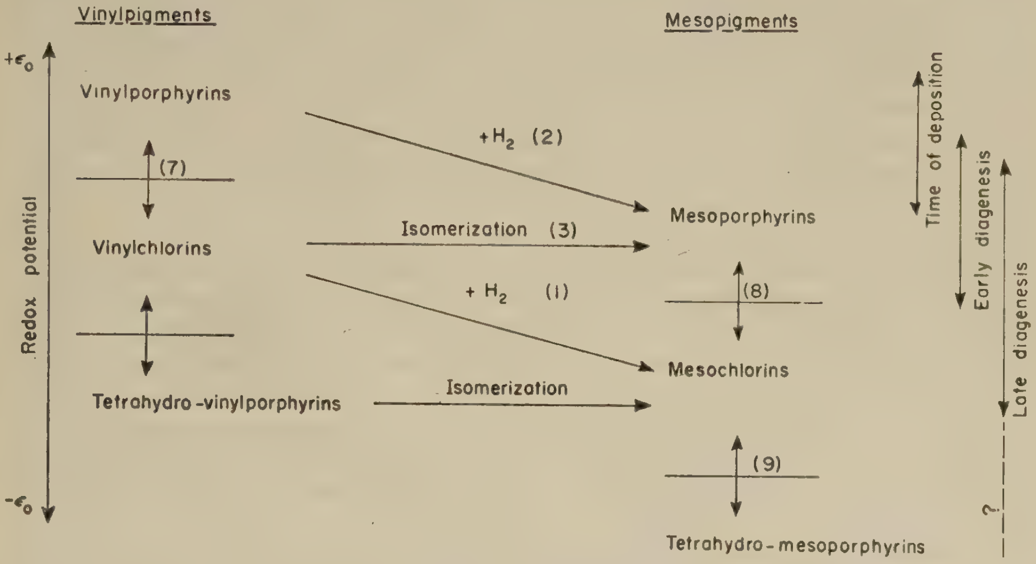
Vinylpigments
Mesopigments
$+\epsilon_0$
$-\epsilon_0$
Redox potential
Vinylporphyrins
(7)
Vinylchlorins
Tetrahydro-vinylporphyrins
$+H_2$ (2)
Isomerization (3)
$+H_2$ (1)
Isomerization
Mesoporphyrins
(8)
Mesochlorins
(9)
Tetrahydro-mesoporphyrins
Time of deposition
Early diagenesis
Late diagenesis
?

Fig. 3. Some redox processes of tetrapyrrole pigments. Under geochemical conditions, reactions occurring in a vertical direction are reversible, those in a horizontal direction are irreversible.

An earlier paper indicated (BLUMER, 1950a) that the redox potential of the vanadium (III)–vanadium (IV) system nearly coincides with the lower potential limit reached by water-wet sediments. The presence in a sediment of fossil chlorins—capable of reducing V (IV)—therefore indicates extremely strong reducing conditions.

We can conclude that both the fossil etiochlorin III and the desoxomesoetiopyropheophorbide *a* are *secondary* chlorins, formed by the reduction of mesoetioporphyrins, in the extremely reducing environment of the oil shale of Serpiano, probably during a late diagenetic stage.

The sediments of Serpiano have been raised above the ground water table for a very considerable length of time. The fact that the chlorins survived this long exposure of the sediment to an oxidizing environment indicates that they are well protected—either by the low permeability of the oil shale or by the presence of protective agents which are preferentially oxidized. Any effect of the exposure since sampling is negligible compared to that of the exposure *in situ*.

EXPERIMENTAL

The oil shale used for this investigation was collected in the most recently worked section of the abandoned mine at Serpiano, Switzerland, during the autumn of 1959. All samples originated at horizon S XVIII of the "Grenzbitumen" (Anisien-Ladinien, Triassic). They were stored air-dry until summer, 1960, when they were crushed and ground in a ball mill just prior to extraction.

The lability of the fossil chlorins requires considerable care and rapid work. Our initial experiments, which led to the isolation and tentative identification of the pigments, were spread out over a 6-week period; during that time most of the chlorin was lost by air-oxidation in spite of careful handling in near darkness. The important steps of the purification procedure and the characterization were therefore repeated within just 6 days; all fractions were stored at −20°C in order to retard air oxidation.

Continuous spectrophotometric control, using a Cary model 14 spectrophotometer, was maintained during the entire experimental sequence.

Isolation of the pigments

The extraction and isolation of the pigments was carried out in several batches, using a total of 1·6 kg of the oil shale. The following data are representative for a single 10-g sample of the sediment. After exhaustive extraction with benzene–methanol (1:1, v/v), using a Soxhlet extractor, the spectrum (Fig. 2a) indicated the presence in the extract of 37 mg (or 0·37 per cent by weight of sediment) of porphyrin vanadium complex and 250 μg (or 25 p.p.m.) of chlorin. Both values are approximate because of the need for a large background correction; also, the extinction coefficient may be somewhat inaccurate (Treibs' value for DPEP-V was used in the first case and the extinction coefficient for mesophyllochlorin at 640 mμ (Pruckner, 1940) in the second).

The dried extract was redissolved in 3 ml of chloroform and the asphaltenes were precipitated by adding 27 ml hot *iso*octane. The precipitate was filtered and washed with a mixture of chloroform and *iso*octane. The filtrate, containing 14 mg of vanadium complex and most of the chlorin, was evaporated, redissolved in warm diethyl ether, and extracted twice with 5 ml of 2·4 N HCl, three times with 5 ml of 4·9 N HCl and once with 5 ml of 6·1 N HCl. The 2·4 N extracts were diluted with water, neutralized with sodium acetate, and the pigments extracted with ether. This fraction contained only a little green pigment in addition to 1·8 mg of free DPEP and MEP. The 4·9 and 6·1 N extracts were diluted to 1·0 N acidity and the chlorins (210 μg) were recovered by ether extraction. They were further purified by re-extracting the ether solution first with 1·2 and then with 4·9 N HCl. The first extract (mainly DPEP/MEP) and the residual ether (containing DPEP-V) were discarded and the chlorins were recovered from the 4·9 N extract by dilution and extraction.

For final purification, the pigment, dissolved in benzene–*iso*octane (1:1), was adsorbed on an alumina (Brockmann II) column packed in *iso*octane. The elution was carried out with *iso*octane of increasing benzene content. The first eluates (up to 50–60 per cent benzene) contained non-pigment impurities. Relatively pure chlorin was recovered from the 70–80 per cent benzene eluates, while the succeeding fractions again were contaminated (with an unknown pigment, absorbing at 630 mμ and with much DPEP/MEP). Rechromatography of these last fractions yielded some additional chlorin. All equivalent fractions were combined and again chromatographed, this time over a less active adsorbent (alumina, Brockmann III), using *cyclo*pentane as solvent for the pigments. Impurities were now eluted in the 5–10 per cent benzene fractions. The pure chlorin in the 15 per cent benzene fraction was followed by some contaminated material from which more chlorin was recovered upon rechromatography.

Dehydrogenation

The dehydrogenation of the fossil chlorin by chloranil takes place rapidly and with good yield only if the pigment has been highly purified. Impurities from the oil shale, if not completely removed, use up much chloranil; this retards the reaction and leads to excessive decomposition of the pigment.

In a successful dehydrogenation experiment, 23 μg of the natural pigment in 0·5 ml ether was added to 10 ml xylene and 5 mg chloranil. The solution was refluxed under intermittent spectrophotometric control. The 640 mμ chlorin peak decreased to 18 per cent of its initial extinction within 15 min. The reaction was then terminated and the product, dissolved in 50 ml, ether, was extracted twice with 10-ml fractions of 2·4 and 4·9 N HCl. The porphyrins in the 2·4 N HCl fraction and the unreacted chlorins in both fractions amounted to 10 μg and 2·4 μg, respectively.

The porphyrin fraction was adsorbed from its *cyclo*pentane solution on a 5-ml alumina (Brockmann III) column in *iso*octane and developed with mixtures of *iso*octane and benzene. Some chlorin was eluted in the early fractions. Mesoetioporphyrin with its typical etio spectrum, appeared in the fraction containing 50 per cent benzene and was followed immediately by DPEP. Four porphyrin fractions were collected and aliquots spotted on Whatman no. 3 paper. Development with CCl_4–*iso*octane (7:3, v/v) produced the results shown in Table 1.

Table 1. Paperchromatography of the dehydrogenated pigments

	r_f values					
	Chromatogram no. 1		Chromatogram no. 2		Average value	
Eluate no. 1	0·48	0·63	0·47	0·64	0·48	0·64
Eluate no. 2	0·49	0·65 (weak)	0·47		0·48	0·65
Eluate no. 3	0·46		0·47		0·47	
Eluate no. 4	0·46		0·47		0·47	

Literature value (Blumer, 1956): DPEP: $r_f = 0{\cdot}46$ MEP: $r_f = 0{\cdot}63$.

Synthesis of desoxomesoetiopyropheophorbide a

A DPEP concentrate was prepared from fossil DPEP-V/MEP-V by breaking the complex with HBr-acetic acid followed by solvent partitioning and chromatography. The fraction with the most pronounced phyllo spectrum (ratio of band II/band III = 1·47) was quantitatively converted into its zinc complex by boiling it briefly with zinc acetate in glacial acetic acid. It was then hydrogenated by refluxing for 3 hr in ethanol with Raney nickel as catalyst. The complexes in the filtrate and pyridine washings of the catalyst were split with 3·7 N HCl. The free pigments, after transfer into ether, were separated by acid extraction, and the weakly basic chlorin was further purified by chromatography. Elution occurred under the same conditions and in the same fractions as described above for the natural pigment. Spectrum and paper chromatographic r_f values provide further support for the identity of the natural and synthetic pigments.

Acknowledgements—This investigation has been supported by a research contract with the United States Office of Naval Research (Contract NONR-2196 (00)) and the grant of a Woods Hole Oceanographic Institution summer student fellowship to one of us (G. O.).

References

Blumer M. (1950a) Die Existenzgrenzen anorganischer Ionen bei der Bildung von Sedimentgesteinen. *Helv. Chim. Acta* **33,** 1568–81.

Blumer M. (1950b) Porphyrinfarbstoffe und Porphyrin-Metallkomplexe in schweizerischen Bituhina. *Helv. Chim. Acta* **33,** 1627–37.

Blumer M. (1956) Separation of porphyrins by paper chromatography. *Analyt. Chem.* **28,** 1640–44.

Blumer M. and Omenn G. S. (1961) Fossil chlorins in a triassic sediment. *Nature, Lond.* **189,** In press.

Dhéré C. and Hradil G. (1934) Spectroscopic investigation of the fluorescence of oil shales. *Schweiz. min.-petr. Mittlg.* **14,** 279–95.

Fischer H. and Stern A. (1940) *Die Chemie des Pyrrols* Vol. II. Akad. Verlag., Leipzig.

Pruckner F. (1940) Lichtabsorption und Konstitution der Chlorophyll derivate—II. *Z. phys. Chem.* A **187,** 257–75.

Stern A. and Wenderlein H. (1936) Ueber die Lichtabsorption der Porphyrine—V. *Z. phys. Chem.* A **176,** 81–124.

Stern A. and Pruckner F. (1937) Lichtabsorption und Konstitution einiger Derivate der Chlorophylle. *Z. phys. Chem.* A **180,** 321–58.

Treibs A. (1934) Ueber das Vorkommen von Chlorophyllderivaten in einem Oelschiefer der oberen Trias. *Liebigs Ann.* **509,** 103–14.

Treibs A. (1936) Chlorophyll- und Haeminderivate in organischen Mineral-stoffen. *Angew. Chem.* **49,** 682–86.

ZoBell C. E. (1946) Studies on redox potential of marine sediments. *Bull. Amer. Ass. Petr Geol.* **30,** 477–513.

Contribution No. 1156

Särtryck ur Tellus nr 2, 1961

Some Aspects of Hurricane Daisy, 1958[1]

By HERBERT RIEHL, Colorado State University

and

JOANNE MALKUS, Woods Hole Oceanographic Institution

(Manuscript received January 4, 1961)

Abstract

Observations from research flight missions into hurricane Daisy (1958) are utilized to compute the budgets of heat, moisture, kinetic energy, and momentum. Calculations are performed for a period when the cyclone was just becoming a hurricane, and for a second period, two days later, when it had attained maturity.

The level of non-divergence separating lower inflow from upper outflow was quite high, near 500 mb. Mass flow increased considerably between the two days, but rainfall remained quite moderate for a severe hurricane. The radiation heat sink was small compared to the oceanic source so that the system was "open" within the confines of the study. If all ascent took place in the hard radar echoes, the mean vertical speed there was about 7 meters per sec. Without such localized ascent, heat balance could not be achieved. Heat budget computations permitted assessing the fraction of mass flow reaching upper levels in undilute "hot" cumulonimbus towers and estimation of the number of such towers required, to compare with previous photographic studies. Hot towers proved to be the dominant mechanism of raising warm air to upper levels, particularly in the inner core. However, because of the high level of non-divergence the constraint known as ventilation was active. It is shown not to have been a severe deterrent upon Daisy, nor was it the reason she did not become an extreme storm.

Kinetic energy balance is obtained readily on the first day. Import of kinetic energy through the outermost radius was small, so that most of the energy dissipated in the interior was also produced there by the pressure forces. Ground and internal friction were about equal. The kinetic energy source shifted outward as the storm grew, so that on the day of maturity large inward transport took place. The internal source also increased but wind speeds failed to rise correspondingly. Hence ground friction was inadequate to balance production plus import, and large internal dissipation had to be invoked. This dissipation must be assigned largely to vertical eddies. If ascribed to horizontal eddies, the coefficient of lateral exchange becomes so large that momentum budget requirements cannot be fulfilled by a large amount.

It is concluded from the study that the important mechanisms of the hurricane core can be well represented in a two-dimensional framework, provided the essential effects of the buoyant cumulonimbus towers are properly introduced or parameterized therein. The two-dimensional flow of mass is shown in relation to the fields of heat, momentum, and vorticity. The law of conservation of potential vorticity appears to be well satisfied along the stream tubes of the mean motion.

. Introduction

In a previous study Palmén and Riehl (1957) alculated the budgets of angular momentum, inetic energy, and heat for a hurricane possessing a mean structure as determined by Hughes (1952) and E. Jordan (1952) from Pacific Ocean data. Due to sparse and uneven distribution of observations, which were usually almost entirely lacking in the innermost 100 nautical miles, analyses were confined to the peripheral regions of a composited "mean hurricane". It has been of much interest to repeat this experiment in the core of an individual hurricane in various stages of development; the aircraft program of the National Hurricane Research Project of the U.S. Weather Bureau (hereinafter referred to as NHRP) was designed with this as a major part of its purpose. Here we carry out, from their data, a budget study of the core of hurricane Daisy, 1958, with several definite objectives in mind.

---

[1] Contribution No. 1156 from the Woods Hole Oceanographic Institution.

Preliminary results from the NHRP program pointed to the vital importance of the core region, and in particular to highly concentrated convective processes within it, in the development and maintenance of the hurricane engine. It is commonly within the inmost 50—100 n.mi. that the extreme pressure gradients are generated which are responsible for the furious winds. In a semi-theoretical model, the writers (Malkus and Riehl, 1960) showed that establishment of these pressure gradients requires both an enhanced oceanic heat source and concomitantly a means to raise surface air of increased heat content to great heights; the latter condition apparently is the difficult one to meet. To achieve this, a selective buoyancy or "hot tower" mechanism was suggested (Malkus, 1958), which has received support from cumulonimbus dynamics and photographic cloud measurements in hurricane Daisy (Malkus, 1960; Malkus, Ronne, and Chaffee, 1961). We postulated that all, or nearly all the mass reaching great heights in the core ascends rapidly in a few nearly undilute convective "hot" towers, rather than by a uniform and gradual "mass circulation". Now we wish to inquire whether these processes are consistent with and deducible from the azimuth-averaged thermal, motion, and energy structure of the actual storm core, and to test the predicted relationships of the model in the framework of the overall storm budgets computed from the NHRP wind, temperature, and moisture data. What are the roles of the various scales of motion in establishing the budgets of the core? If the important processes are in fact concentrated into restricted convective regions, how much usefulness or meaning does an azimuth-averaged picture possess? Can it serve as a basis for developing numerical or theoretical models of predictive ability?

The rarity of the hurricane phenomenon and its development only under specialized synoptic conditions also suggests critical relationships to be sought between the core of an incipient storm, its periphery, and the surrounding large-scale circulations, both normally as brakes and exceptionally as brake releasers or vortex initiators. "Ventilation" by cooler, drier outside air has been postulated (Simpson and Riehl, 1958) as a brake; tropical disturbances which fail to make hurricane are frequently found to suffer cross-flow of mid-tropospheric air of low heat content. Whether removal of critical brakes is adequate to start a hurricane, or whether one or more specific destabilizing mechanisms are also necessary has remained conspicuously unclarified, although forcing by external circulations appears indicated in a majority of cases. Some workers, for example, have advocated the possible importance of lateral eddy momentum transports in the deepening process. A basic question is whether or not these, or other, asymmetrical interactions are vital and at what stages, or whether the key features may be modelled in simplified symmetrical coordinates through all or a major part of the storm's life cycle.

Fully adequate data to resolve these questions are not yet available. Nevertheless, in spite of many shortcomings, it is considered worthwhile to present computations from the NHRP's Daisy flights as a "lead off" in the quantitative description of a hurricane's internal mechanisms. Several successive days of multi-level records on a single storm, from incipience to maturity, is a monumental and not readily reproducible observational undertaking. Our aim is to make the most of this achievement by treating those aspects of the questions to which the data are best suited; we can thereby assess the magnitudes of some of the interacting processes and scales of motion at more than one stage in a single hurricane's life cycle, with the hope of determining which are most vital and which may be parameterized or possibly ignored. Although it must be stated clearly at the outset that these results are tentative, and subject to revisions by future measurements, their very inadequacies may lead to more fruitful and penetrating questions to be pursued with improved observational facilities as they become available.

Hurricane Daisy began to develop in the Bahamas on August 23—24, 1958, and had

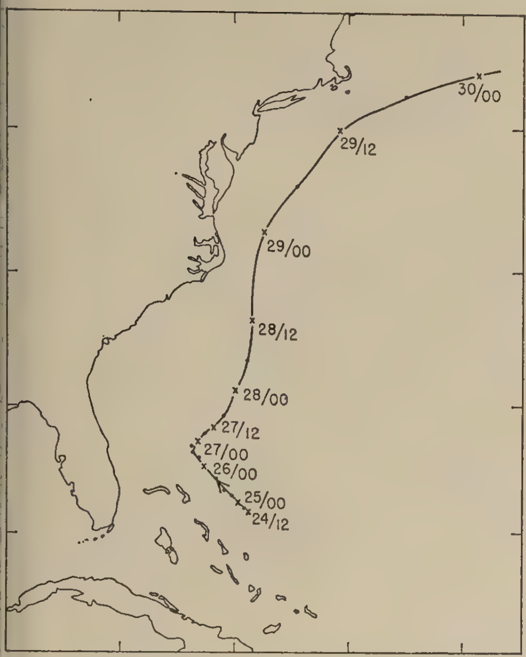

Fig. 1. Track of hurricane Daisy, August 24—28, 1958. Time in GMT.

not quite attained hurricane intensity when it was first penetrated by NHRP aircraft on August 25. During this and subsequent days numerous research flights were conducted; Daisy's track is shown in Fig. 1. Here we shall treat August 25 when the hurricane was immature and growing, and August 27 when the winds reached their peak of about 115 knots in the middle troposphere, when the surface pressure was below 950 mb, and when steady state was attained as nearly as can be expected in actuality.

The research aircraft of NHRP and their instrumentation have been described elsewhere (U.S. WEATHER BUREAU, 1956). Prescribed flight patterns, in a form resembling boxes about the storm center, or leaves of a clover radiating therefrom were executed. The data are presented by NHRP as a function of coordinates relative to the moving storm center, from its radar location, as well as in latitude and longitude. Analyses of the Daisy wind, temperature, and humidity data have been prepared by COLÓN ET AL. (1961). Cloud maps were constructed from the aircraft nose camera films by MALKUS ET AL. (1961), who have discussed the sampling problem posed by the relation between the flight paths and the cloud patterns. Studies of the airborne radar in Daisy were made by those authors and also by JORDAN ET AL. (1960). In this article we shall be concerned mainly with the three-dimensional distribution of wind, temperature, moisture and height of isobaric surfaces. At each flight level, averages are constructed of each property to determine its mean distribution with radial distance and azimuthal departures from this mean. On August 25 extensive tracks were flown at 830, 570, and 237 mb, with additional legs at 960 and 915 mb, so that distributions throughout the troposphere were readily constructed for the inner 100 n.mi. On August 27, the flight altitudes were 620 and 237 mb, so that more extrapolation was required. Surface ship observations, composited with respect to the center over 12-hour intervals, supplemented the aircraft data; however, on August 27 no ships were situated, reasonably enough, inside the 100-mile radius.

2. The mass budget

In an analysis of hurricanes it is logical to determine the flux of any property through cylindrical walls concentric about the core. We shall adopt a quasi-cylindrical coordinate system Θ, r, p, centered on Daisy, with velocity components u, v, w. The radius r is taken positive outward and Θ, the azimuth angle, positive counterclockwise. Flux of any property through the vertical walls of the cylinder may be brought about by the net mass circulation flowing in at low levels and out at high levels, and by asymmetries of property around the cylinder acted on by the radial wind components. As a first step in flux calculations, mass balance must be computed.

For this purpose it should be noted that even in strongly deepening cyclones the change of mass inside a given cylinder is so small that it is fully within range of error of the wind measurements and must be neglected. Hence mass balance must be obtained by setting

$$\int_{p_0}^{p_H} v\,dp = 0 \qquad (1)$$

where p_0 is the surface pressure and $p_H = 0$, alternately the pressure at the top of the storm, if such a place can be found. In practice p_H does exist and may be defined as the lowest pressure to which buoyant clouds will mainly penetrate from the surface layer. From cloud observations (MALKUS ET AL., 1961) and buoyancy calculations $p_H \sim 150$ mb (about 47,000 ft) on 25 August and $p_H \sim 100$ mb (about 54,000 ft) on 27 August. Above p_H the circulation should be quasi-steady. That this is likely to be the case has been shown by many radio-wind ascents in tropical storms in several oceans. The stratospheric easterlies remain undisturbed as far as one can tell (RIEHL, 1954). GROENING (1960) has demonstrated this steady stratospheric flow field for 25 August in the periphery of Daisy. No radio-wind data, of course, existed in the central region. There p_H must be assumed, but the cloud observations strongly support the validity of the assumption.

The procedure for determining mass balance is as follows:

1) The v-field is analyzed at all available flight levels.
2) The analysis is tabulated on a polar grid (Fig. 2).
3) $\bar{v}$ is computed at each radius, where the bar denotes averaging with respect to the azimuth angle.
4) $\bar{v}$ is plotted against pressure on each radius and a profile is drawn. From this profile values of $\bar{v}$ are determined for layers of 50-mb or 100-mb thickness and summed from p_0 to p_H.

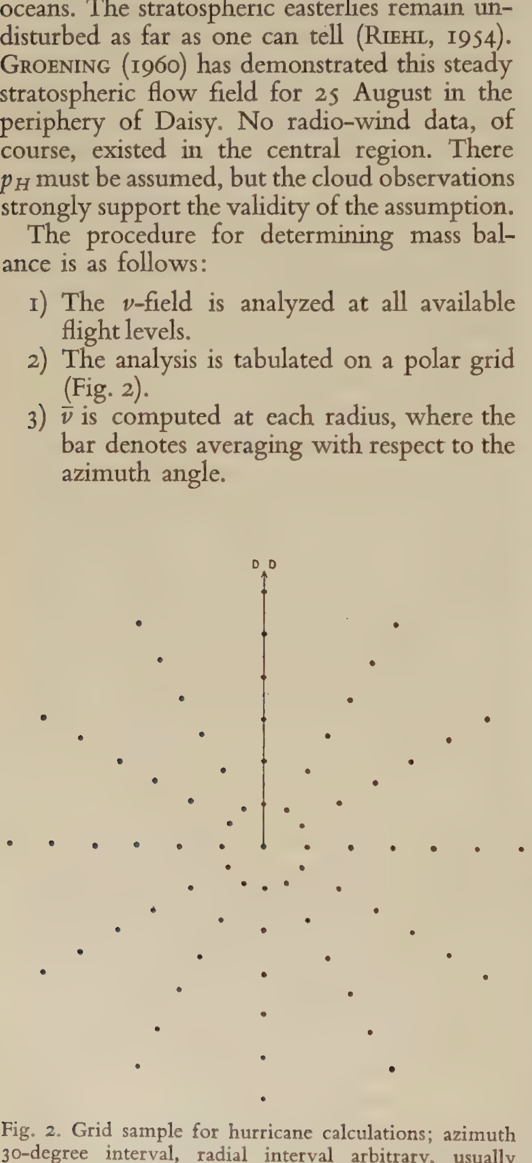

Fig. 2. Grid sample for hurricane calculations; azimuth 30-degree interval, radial interval arbitrary, usually taken as 10 n.mi.

According to equation 1 the sum must vanish.

Given enough flight levels and reliable data, there should be no problem in satisfying equation 1. In actuality, analysis of the v-fields turned out to be a difficult task so that the $\bar{v}$-values are not stable. Contrary to early expectations the v-fields have not always shown consistent patterns along individual flight legs, triangles, or boxes. Further, an aircraft recrossing a point where it had been earlier, often yielded a v-value different from the first one, at times even with opposite sign. Several possible reasons may be cited for these difficulties:

a) Errors in wind measuring equipment or evaluation. Since the v-component is the weak flow component it is sensitive to such errors.

b) Errors in center fixing. Unfortunately a hurricane seldom yields a precise point which may be taken as the center, but there is a flat area to which a center must be assigned. This will affect v, especially at small radii.

c) Errors in estimating storm propagation. In order to obtain a "synoptic" picture, the information gathered on successive flight legs must be "composited" with respect to the moving center. Hence its propagation rate must be known. While the mean 24-hour motion can be estimated quite accurately, this does not always hold for small time intervals such as one or two hours.

d) Travelling micropatterns within the general envelope. Motions with the scale of the convective bands are quite active, and this motion may be unsteady in time and space. Compositing of flight legs which are successive in time, cannot readily take account of such transient small scale features.

e) Time changes of the whole vortex. On 25 August, for instance, Daisy was deepening while the aircraft remained in the storm for eight hours or more.

In view of these data problems it was necessary at times to make considerable compromises in analyzing the v-field; at other times a good fit could be obtained quite readily.

Surface inflow: For the purpose of determining the surface mass flow, ship reports were composited for 12-hour periods with respect to the moving center, i.e. three six-hourly charts plus intermediate data were combined. These reports, also far from homogeneous, were first averaged over areas with radial length of 60 n.mi. (one degree latitude) and arc length of 30 degrees. Inside the one-degree radius an attempt was made to average over shorter radial lengths, where data were sufficient to permit this. On 25 August, flight data at 960 mb were used for this purpose. Then an analysis was performed with smoothing and $\bar{v}$ was computed for different radii. Next the quantity $\bar{v}\ x\ r$, which is proportional to mass flow, was plotted on graph paper and smooth curves were drawn.

Fig. 3 portrays the rise of surface mass inflow from the early stages of Daisy up to the time of maturity. An orderly increase took place day by day as the storm deepened. Central pressure and maximum inflow thus were inversely correlated; the regression found by KRUEGER (1958) on six previous Atlantic hurricanes held well. The size of the storm increased with its intensity. On 24 and 25 August the limit of mass flow was situated near the 5-degree radius, and average convergence was confined to a belt about 100 n. mi. wide around the center. On the last two days tremendous expansion took place. The hurricane boundary could no longer be ascertained; maximum inflow occurred 200—300 n.mi. from the center just as in the hurricanes treated by Krueger. Hence the mass flow was convergent over the entire inner area (cf. also MALKUS and RIEHL, 1960). On 26 August ships were still travelling near the cyclone center, but on the 27th the innermost point to be obtained was at the 2-degree radius. From there the mass flow profile had to be extrapolated inward. While the precise course of this curve is uncertain, its general character probably is reliable.

Mass transport diagrams: The $\bar{v}$-values for the surface and the flight levels were entered on diagrams of $\bar{v}\ x\ r$ against pressure on a linear scale, and curves were drawn as illustrated in Fig. 4 for 25 August. Then $\bar{v}\ x\ r$ was tabulated over layers of 100-mb thickness up to 200 mb and in 50-mb steps higher up at each radius; mass at pressures higher than 1,000 mb was neglected. As pointed out, the sum of these values should vanish after proper weighting. This condition was closely met by the curves at the 20 and 40 n. mi. radii in Fig. 4. At the three outer radii inflow exceeded outflow, and some downward revision of the inflow was made. It is probable that the 830-mb level gave too much indraft. At 560 mb, all values were so close together that a band rather than a series of five points has been

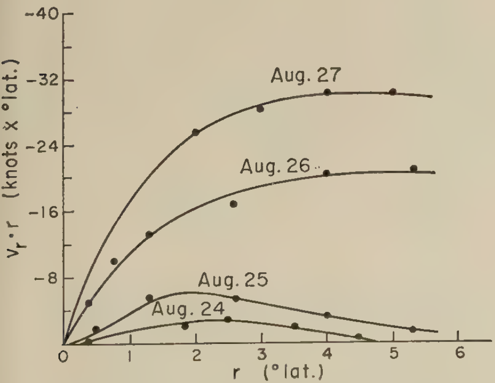

Fig. 3. Growth of mass circulation in Daisy. Values at surface, constructed from ship reports.

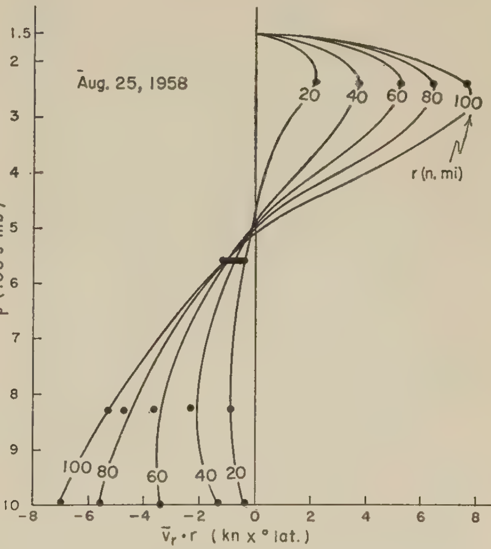

Fig. 4. Profiles of mass flux against pressure for different radii, August 25.

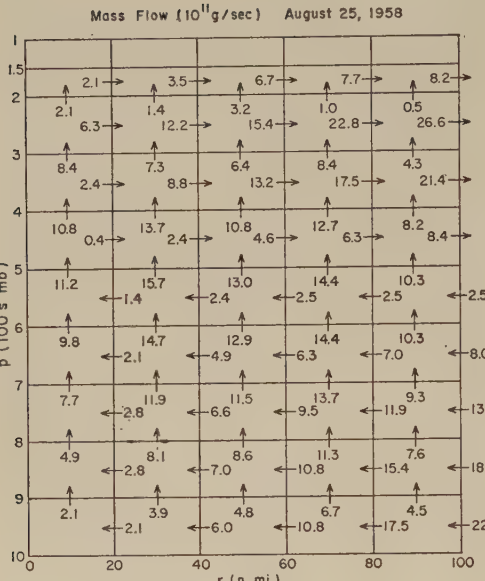

Fig. 5. Mass flow on August 25.

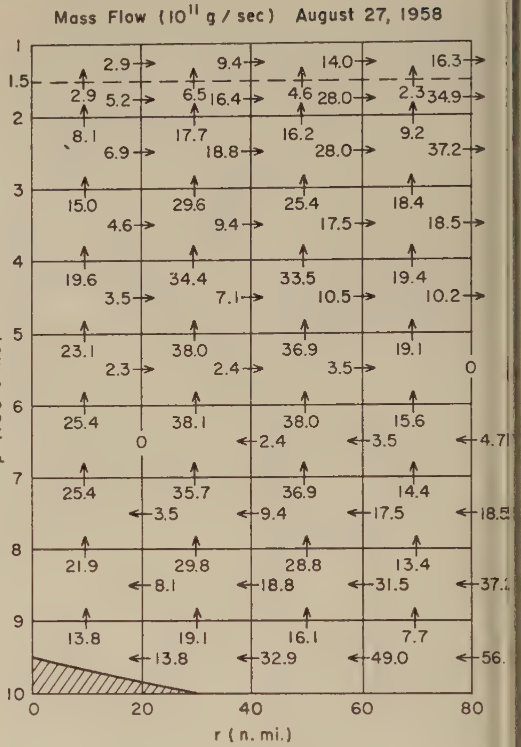

Fig. 6. Mass flow on August 27.

entered in Fig. 4. Analysis at this level was particularly difficult but the net result, as also on other occasions, was that light inflow prevailed. Thus the level of non-divergence was located near 500 mb, a higher altitude than previously expected.

From curves as illustrated in Fig. 4 mass flow diagrams were constructed (Figs. 5—6). A few irregularities remain, but in general vertical and lateral consistency is good. On 27 August the inflow extended upward to about 500 mb as on 25 August, but the percentage of the inflow taking place in the surface layer increased from one-third to one-half. Thus, while the middle troposphere is revealed as a constraint upon the hurricane by means of the "ventilating" mechanism, the basic statement still stands that the principal inflow must occur in the surface layer in order for a hurricane to happen (see end of Section 6).

Figs. 5 and 6 are not meant to imply uniform radial and vertical mass flow in each of the rings. It has long been known that the radial velocity component at the surface is not symmetrical at any radius. In a statistical treatment of North Atlantic hurricanes of 1954—55 AUSMAN (1959) demonstrated that a large sector with outflow usually exists, even in quasi-stationary cases. Most flight data contain similar asymmetries. Further, from radar observations and cloud photography, the mass ascends in rather narrow bands covering only a small fraction of a hurricane's area. MALKUS ET AL. (1961) pointed out that the area covered by "hard" radar echoes on 25 August was six per cent as far out as the 55 n.mi. radius. If all ascent at the level of non-divergence (500 mb) took place in an area of the size of the hard echoes, the average vertical velocity in the bands was 7.2 m/sec inside the 20-mile radius, 3.2 m/sec from 20 to 40 miles, and 1.6 m/sec from 40 to 60 miles, a quasi-logarithmic decrease illustrated in Fig. 7.

3. The total heat budget and air-sea exchange

Introductory comments

The heat export from any cylindrical volume is closely given by

$$\operatorname{div}(H) = \iint (gz + c_p T + Lq)\, c_n\, d\sigma \frac{dp}{g}.$$

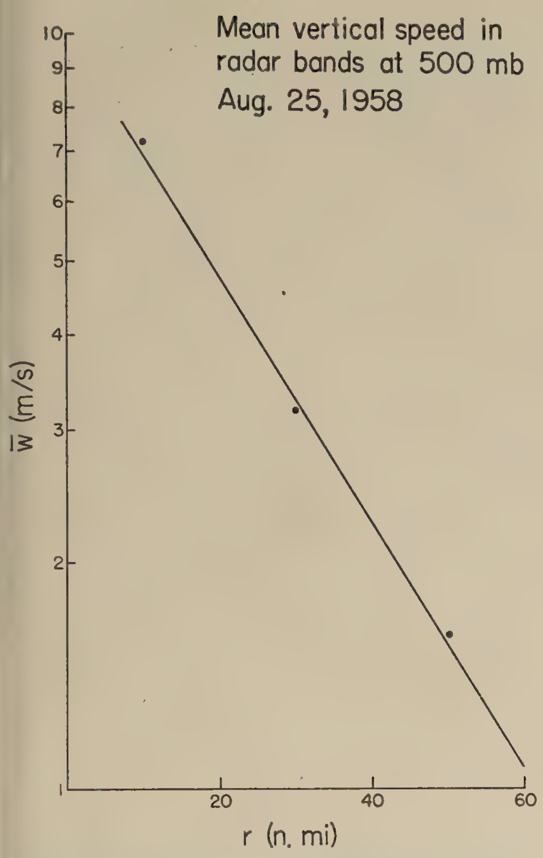

Fig. 7. Distribution of mean vertical velocity with radius, assuming that all ascent takes place in an area comparable to that of the radar bands. Note this special definition of the bar over the 'ω'.

Here div(H) is the divergence of heat transport, g the acceleration of gravity, z height, c_p specific heat at constant pressure, L latent heat of condensation, q specific humidity, T temperature, c_n the wind component normal to the boundary and σ the surface of the cylinder. On the right side the first term denotes potential energy (in heat units), the second enthalpy and the third latent heat energy. We shall define

$$Q \equiv gz + c_p T + Lq.$$

For a total energy budget, kinetic energy should also be included. Its contribution to the heat budget, however, is very small compared to that of the other energy forms, and it will be considered separately later on. Since we are interested in fluxes with respect to the moving center, we shall let the cylinder travel with the storm and denote variables measured in the moving coordinate system with the subscript R. With this definition continuity demands that

$$\frac{\partial Q^*}{\partial t_R} = -\operatorname{div}_R(H) + Q_{eR} + Q_{sR} - R_{aR}. \quad (2)$$

Here the star denotes values integrated over the mass inside the cylinder, and the heat source $S = Q_{eR} + Q_{sR} - R_{aR}$, where Q_{eR} and Q_{sR} are latent and sensible heat transfer from earth to air, and R_{aR} is the net tropospheric radiational heat loss. The subscript R will hereafter be omitted from the source and sink terms.

Equation (2) may be divided as follows:

$$\frac{\partial}{\partial t_R}(gz + c_p T)^* = -\operatorname{div}_R(h) + Q_s + LP - R_a, \quad (3)$$

$$L\frac{\partial q^*}{\partial t_R} = -\operatorname{div}_R(Lq) + Q_e - LP. \quad (4)$$

Here P is precipitation, and $\operatorname{div}_R(h) + \operatorname{div}_R(Lq) = \operatorname{div}_R(H)$. Equation 4 permits later calculation of a separate moisture budget, including precipitation.

Observations of heat and moisture: For the purpose of determining the fluxes, data on temperature and height of the isobaric surfaces (altimeter correction D) were available at all flight levels; in addition, dewpoint temperatures (T_d) were measured on several of the lower altitude flights. Temperatures and dewpoints at ship's deck level, also sea surface temperatures, were composited on 25 August and, as far as possible, on 27 August from the file of ship reports already mentioned and from 960-mb flight data on 25 August. Analysis of T, D and T_d was performed on each flight level and tabulated on the grid of Fig. 2. Then T_d was converted to specific humidity q, and $\bar{T}$, $\bar{D}$ and $\bar{q}$ were computed at 10-mile radial intervals on each flight level, the bar denoting the azimuthal average. Next $\bar{T}$ was plotted on tephigrams at radii of 10, 20, 40, 60 and 80 n. mi.; curves of best fit were drawn to represent mean vertical soundings. These curves were extended beyond the B-47 flight level until they intersected the radiosonde ascents of the northern Bahamas. The specific humidities were treated similarly as far as possible; when these data were not recorded, relative humidity was assumed at 90 per cent of saturation.

Several results were slightly awkward, especially in the middle troposphere, where temperatures frequently were 1—3° C cooler than expected and the specific humidity at times exceeded saturation values. Possible causes of the low temperatures—especially whether real or instrumental—have been debated since the inception of these measurements. No satisfactory explanation is at hand, and it remains for new observational programs to apply conclusive tests. For this paper the uncertainty is not of decisive importance. In order to avoid excessive vertical instability below, and stability above, the flight levels between 500 and 600 mb, $\overline{T}$ was raised 1—2° C on several occasions, and the supersaturated dewpoints were disregarded as most likely due to observational shortcomings. If this procedure was unwarranted, some revision of the heat flux calculations will become necessary. This would not affect the general nature of most results, particularly on August 25 when these difficulties arose only rarely.

Figure 8 illustrates a sounding where hardly any adjustment of temperature was needed. Ship data in the surroundings of Daisy gave 26—27° C at pressures of about 1,010 mb. At the 20-mile radius surface pressure was estimated as close to 1,005 mb. These data, plus the adiabatic assumption, established the lowest point of the hurricane sounding of Fig. 8. From there a dry-adiabatic lapse rate can be drawn to the measured point at 960 mb which agrees with the general observation of dry-adiabatic conditions in the subcloud layer. The 960 mb flight leg was chosen because the cloud base was situated near this pressure in the interior of the storm; the airplane flew just underneath the clouds. With the top of the subcloud layer near 960 mb, a change in lapse rate is expected very close to this level. This is borne out by the points at 915 mb and 830 mb. Omitting three excessive dewpoints, the whole temperature curve is readily established. Above 500 mb the sounding was 2—3° C warmer than the nearest ascent in the Bahamas.

The top of the warm layer was situated near 150 mb which agrees well with the measured height of cloud tops (MALKUS et al., 1961). Below 500 mb the lapse rate was slightly greater, higher up slightly more stable than moist-adiabatic. Such a structure is reasonable. In the low and middle troposphere ventilation — to be discussed later — prevents the lapse rate from becoming fully moist-adiabatic. In the upper troposphere release of latent heat of fusion plus outward spreading of air ascended in the inner core with equivalent potential temperatures up to 360° A produce the small

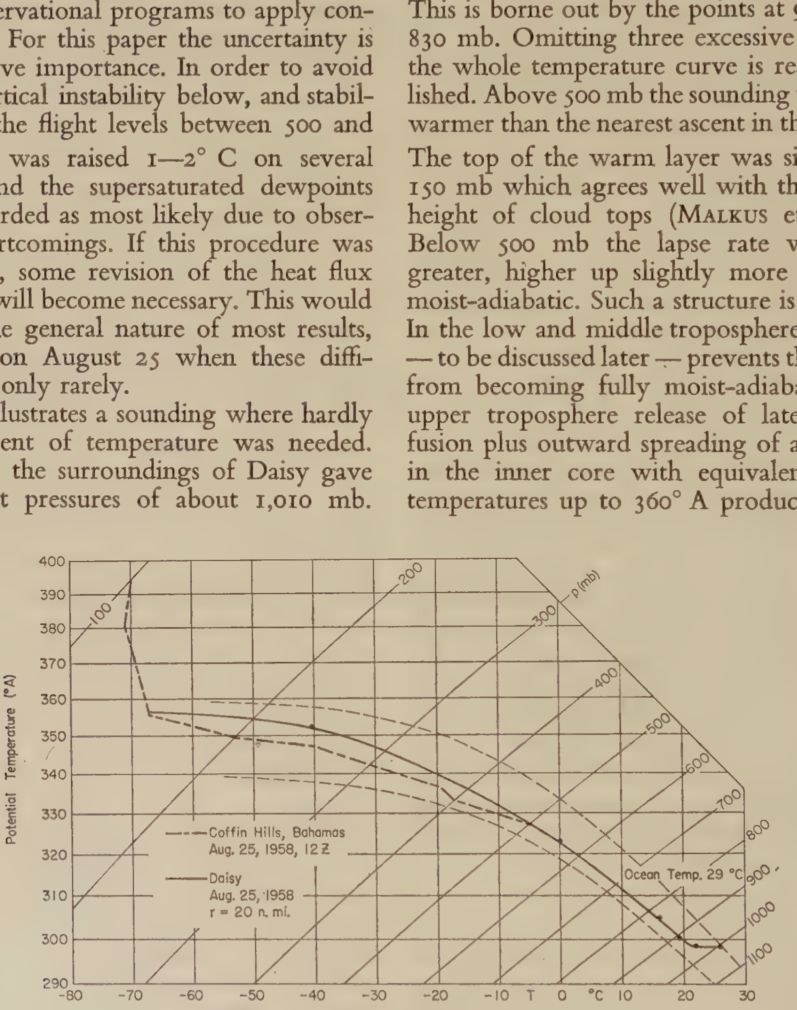

Fig. 8. Tephigram showing composited sounding for Daisy on August 25 at the 20-mile radius and the upper portion of the ascent at the nearest radiosonde station. Light dashed curves are moist adiabats. Ocean surface temperature, T_0, from ship reports was 28—29° C.

stability with respect to the moist-adiabatic ascent.

As a further test, the sounding of Fig. 8 may be checked for hydrostatic consistency against a vertical *D*-profile obtained independently from the aircraft absolute altimeter. For this calculation the height of the 250-mb surface was taken equal to the height of this surface as determined from radiosonde in the Bahamas. Agreement between *D*-values as calculated and as observed by the aircraft were well within range of measurement errors.

For the lateral flux calculations it is most convenient to utilize values integrated over the same pressure intervals chosen for Figs. 5—6. For vertical fluxes, means over areas between two radii are needed; these will be denoted with a wavy (~) bar. Appendices A and B (back) contain all necessary quantities for lateral flux calculations on 25 and 27 August. Since, on the latter day, only two missions were flown, the entire lower troposphere had to be interpolated. Hence the margin of uncertainty for all computations is greatest on this day.

Local changes of heat and moisture

The magnitude of $L\partial q^*/\partial t_R$ in equation (4) can be estimated from the moisture data in Tables A2 and B2 (Appendices). On August 25 the precipitable water content between the center and the 80-mile radius, area-weighted, was 5.6 gm/cm²; by the 27th it had risen to 6.5 gm/cm². This corresponds to a heat increment of 2.1×10^{12} cal/sec which proves to be about one-third the source term and an order of magnitude down relative to net advection. From Tables A4 and B4 (Appendices) the change in $c_pT + gz$ content between August 25 and 27 comes out 0.85×10^{12} cal/sec, or even smaller than the moisture change. On August 27 the cyclone attained maximum development, so that local change with respect to the center presumably was nil.

Lateral eddy transports of moisture and heat

The lateral component of flux divergence of a property N is determined from the radial transports

$$\iint \overline{Nv_R}\, rd\Theta \frac{dp}{g} = \iint \overline{N}\overline{v}_R\, rd\Theta \frac{dp}{g} + $$
$$+ \iint \overline{N'v_R}\, rd\Theta \frac{dp}{g} \qquad (5)$$

where the first term on the right gives the transport by the mass circulation and the second that due to asymmetries around each cylinder. Asymmetries with respect to Θ are denoted by primes and the subscript R has been omitted in the first term because $v \equiv v_R$. For evaluation of the eddy contribution only three flight levels were available: 830 and 560 mb on 25 August and 620 mb on 27 August. The uncertainty concerning data is such that a fully reliable determination cannot be made. Values of the eddy transport of moisture and heat, as obtained on the 80-mile radius are listed in Table I. It may be noted that a moisture transport of 1 kn × g/kg over a layer of 500 mb thickness gives 1.4×10^{12} cal/sec and that a heat transport of 1 kn × °C corresponds to 0.6×10^{12} cal/sec at the 80-mile radius. Eddy fluxes of this order have the same magnitude as the local changes and are much smaller than the flux due to the mean motion.

Table 1. Eddy moisture and heat fluxes

	Aug. 25		Aug. 27
	830 mb	570 mb	620 mb
$\overline{v'_R q'}$ (kn × g/kg)	—0.7	—1.5	0.7
$\overline{v'_R T'}$ (kn × °C)	—0.1	—1.2	—2.3

Total Heat Balance

In evaluating equation 3, then, $\partial Q^*/\partial t_R$ may be set equal to zero. Then the total heat source $S = Q_e + Q_s - R_a$ is given by the net transport of heat through a cylinder. Figs. 9—10 contain the lateral flux data and also the net heat source over areas with radial distance of 20 n.mi. as determined from $\mathrm{div}_R(H)$. The quantity $Q_a = Q_s + Q_e$ is obtained by setting

$$Q_a = \mathrm{div}_R(H) + R_a.$$

In a hurricane the main radiational surface presumably is transferred to the top of the outflow overcast which, as shown by cloud

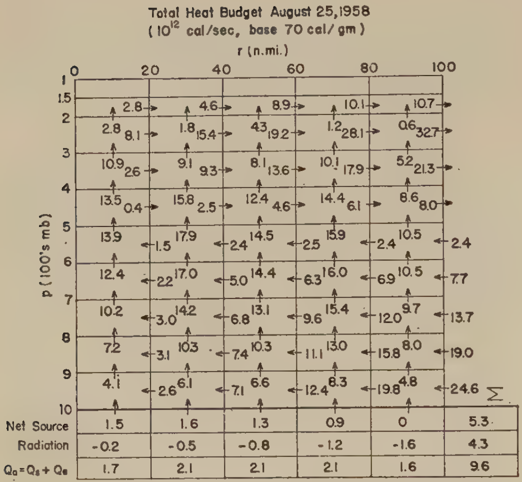

Fig. 9. Transport, sources, and sinks of total heat energy Q for Daisy on August 25. Lateral flows found by multiplication of lateral mass flow by $\overline{Q}$-70 (Table A8, Appendix). Vertical fluxes to meet continuity and net sources in radial intervals as residual. Total oceanic source Q_a, after allowance for radiation loss, in units 10^{12} cal/sec in each radial interval.

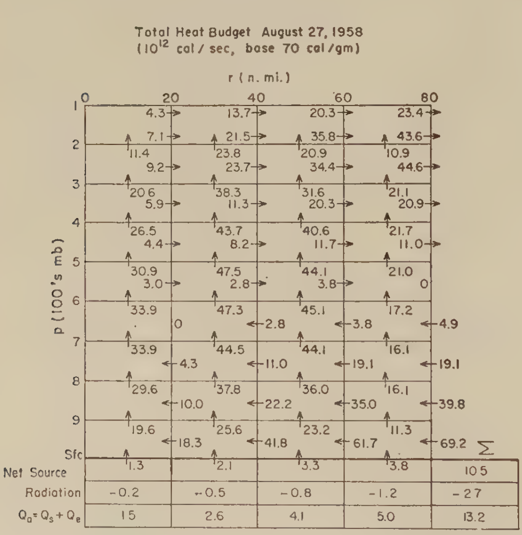

Fig. 10. Transports, sources and sinks of total heat energy Q for Daisy on August 27. Procedure and notation same as Fig. 9.

photographs, is very thick and may be assumed to act as a black body radiator in the first approximation. On 25 August the B-47 was quite close to the top of the thick cirrostratus at temperatures near −40° C, so that the cooling was about 0.24 ly/min or 2.7×10^{12} cal/sec inside the 80-mile radius if all incident sunlight was reflected. This corresponds to a mean tropospheric cooling of 1° C/day which appears reasonable and was adopted for estimating Q_a. It may be noted that there is a good chance that the net radiating surface was situated at a lower temperature on 27 August. If so, the radiation cooling would have been even smaller on that day. At an effective radiation temperature of −60° C, for instance, the cooling is 0.17 ly/min. Thus the hurricane outflow overcast, when thrust upward to high levels, protects the warm core.

From Figs. 9—10, Q_a was nearly twice as large as S on 25 August, whereas the difference was small on 27 August and and would have been even smaller with the assumption of a still higher and colder radiating shield. It should be noted that the value of S is uncertain to the extent that there are eddy transports of Q. As shown before, the eddy flux may be neglected in separate moisture and heat budgets. But the energy export by the mass circulation is a small difference between the import of latent heat and the export of $gz + c_pT$. It is possible to visualize an eddy flux of the same magnitude. Due to data uncertainties and insufficient number of flight levels, this subject cannot be pursued further. The reasonable results in our next section on sea-air exchange suggest that this unknown eddy heat flux is not large.

The oceanic source and air-sea exchange

We should now like to be able to divide the total oceanic source down into its latent and sensible heat contributions in order to complete an independent moisture budget. We should also like to examine the oceanic exchange requirements to compare with the model of MALKUS and RIEHL (1960) and to assess a drag coefficient for later use in constructing Daisy's momentum and energy budgets. All these objectives may be achieved if the exchange coefficients for the flux of heat, moisture, and momentum from ocean to air are identical. With this, Q_s/Q_e can be determined from the Bowen ratio

$$r_B = \frac{c_p}{L}\,\frac{T_0 - T_a}{q_0 - q_a},$$

where the subscripts 'o' and 'a' refer to the sea surface and ship's deck level respectively. On the 25th, the ship reports gave $T_0 = 28$—$29°$ C so we have taken $T_0 = 28.5°$ C and $T_0 - T_a = 2.5°$ C. On August 27, ship reports were lacking; we have taken $T_0 = 28°$ C and $T_0 - T_a = 2°$ C since the storm center was about 150 n.mi. farther north. The drag coefficients, c_D, are computable alternatively from either of the well-known exchange formulas

$$\frac{Q_s}{A} = \varrho c_p c_D u_a (T_0 - T_a),$$

$$\frac{Q_e}{A} = \varrho L c_D u_a (q_0 - q_a),$$

where A is the ocean surface area, and u_a is the wind speed at ships' deck level. The specific humidity at the ocean surface, q_0, was found (using tables) from the saturation q at the sea surface temperature, while the q_a's were taken from Tables A2 and B2, which gave values consistent with cloud base at about 970—960 mb throughout. Table 2 shows the components and results of the exchange computation.

Except for the inmost radial interval on both days, the c_D's of Table 2 are slightly smaller than careful experimental determinations (DEACON, SHEPPARD, and WEBB, 1956) would lead one to expect. According to these authors, drag coefficients of 2.2—2.5×10^{-3} were indicated for winds greater than 10 m/sec, with about 1.4×10^{-3} for normal trade-wind speeds of 6—7 m/sec. The smaller coefficients of Table 2 may be due to omission of a small eddy Q export, or underestimate of the radiative sink, or other shortcomings of our data or procedures. Nevertheless, in view of the limitations, the results of the exchange computation are very satisfactory. The Bowen ratio averaged 0.18 on both the formation and mature days of Daisy, or enhanced by an order of magnitude compared to the normal trade, and 50—100 % larger than found by GARSTANG (1958) in moderate tropical disturbances. The oceanic latent heat source, relative to the normal trade, is up by a factor of 3—4 on the 25th and 5—6 on the 27th, while the sensible heat source has risen by factors of about 15 and 25, respectively. Even so, the oceanic source is still somewhat smaller than that predicted by RIEHL and MALKUS (1960) for their model moderate storm. On the 25th, the net Q flux divergence is 55 % that of the model, while it reached 78 % on the 27th. Since (area-averaged 0—80 n.mi.) Daisy's low-level winds were on her maximum day only 66 % that of the model and the remaining parameters entering the exchange computations were closely similar, the results of the comparison are consistent and encouraging.

4. The moisture budget and precipitation

The lateral component of the moisture flux divergence may be obtained from an equation like (5), neglecting the eddy term as found in Table I. Fig. 11 shows the resulting net latent heat inflow, which is made up of a large import at low levels, and a very small export aloft.

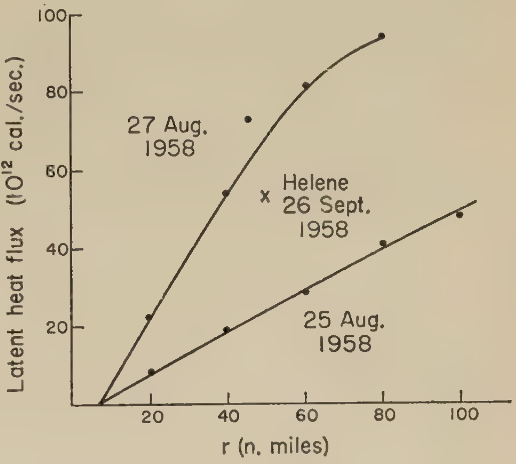

Fig. 11. Net latent heat import in troposphere as function of radius for Daisy August 25 and 27, also for Helene (September, 1958) at the 50-mile radius (denoted by the x).

To compute the precipitation within the storm core, in Table 3 we next convert the latent heat source to evaporation rate. It should be remembered here that evaporation is computed with respect to the storm center. Because of its propagation, the evaporation from any given ocean area was, of course, less. Table 3 nevertheless indicates the magnitude of water loss to be expected from a fixed ocean area in case of a stationary storm. This

Table 2. Air-sea exchange computation

A. August, 25

$\varrho = 1.2 \times 10^{-3}$ $T_0 = 28.5$ °C

	Radial interval (n.mi.)				
	0—20	20—40	40—60	60—80	80—100
Q_a ($\times 10^{-12}$ cal/sec)	1.7	2.1	2.1	2.1	1.6
$T_0 - T_a$ (°C)	2.5	2.5	2.5	2.5	2.5
$q_0 - q_a$ (g/kg)	5.3	5.5	5.5	5.6	5.8
r_B	0.19	0.18	0.18	0.18	0.17
A ($\times 10^{-14}$ cm^2)	0.43	1.29	2.15	3.01	3.87
Q_e/A (cal cm^{-2} sec^{-1})	3.32×10^{-2}	1.38×10^{-2}	0.83×10^{-2}	0.59×10^{-2}	0.36×10^{-2}
Q_s/A (cal cm^{-2} sec^{-1})	0.63×10^{-2}	0.25×10^{-2}	0.15×10^{-2}	0.11×10^{-2}	0.06×10^{-2}
u_a (m/sec)	23	17	13	11	9
c_D ($\times 10^3$)	3.8	2.0	1.6	1.3	1.0

Area averages (0—80 n.mi.):

$c_D = 1.7 \times 10^{-3}$

$Q_e/A = 1.0 \times 10^{-2}$ cal cm^{-2} sec^{-1} or 864 cal cm^{-2} per day

$Q_s/A = 0.18 \times 10^{-2}$ cal cm^{-2} sec^{-1} or 155 cal cm^{-2} per day

$r_B = 0.18$

B. August, 27

$\varrho = 1.15 \times 10^{-3}$ $T_0 = 28.0$ °C

	Radial Interval (n.mi.)			
	0—20	20—40	40—60	60—80
Q_a ($\times 10^{-12}$ cal/sec)	1.5	2.6	4.1	5.0
$T_0 - T_a$ (°C)	2	2	2	2
$q_0 - q_a$ (g/kg)	3.9	4.0	4.5	4.8
r_B	0.20	0.20	0.18	0.17
A ($\times 10^{-14}$ cm^2)	0.43	1.29	2.15	3.01
Q_e/A (cal cm^{-2} sec^{-1})	2.91×10^{-2}	1.70×10^{-2}	1.62×10^{-2}	1.42×10^{-2}
Q_s/A (cal cm^{-2} sec^{-1})	0.58×10^{-2}	0.33×10^{-2}	0.29×10^{-2}	0.24×10^{-2}
u_a (m/sec)	41	32	29	25
c_D ($\times 10^3$)	2.6	2.0	1.8	1.7

Area averages (0—80 n.mi.)

$c_D = 1.9 \times 10^{-3}$

$Q_e/A = 1.65 \times 10^{-2}$ cal cm^{-2} sec^{-1} or 1 425 cal cm^{-2} per day

$Q_s/A = 0.29 \times 10^{-2}$ cal cm^{-2} sec^{-1} or 250 cal cm^{-2} per day

$r_B = 0.18$

is of particular interest with respect to the calculation for 27 August which shows that evaporation rose to high values as Daisy's intensity increased. Had the storm become stationary for a day, measurable cooling of the ocean might have occurred in view of the evaporation rate, hence the intensity of the hurricane should have been adversely affected. Equation 4 may now be solved for the precipitation as residual (Fig. 12). Both on 25 and 27 August the lateral gradient of precipitation was very large, as expected, and could be represented as a straight line on semi-logarithmic paper. In view of the rate of stomr travel

Table 3. Moisture source

	Aug. 25	Aug. 27
Radius of area covered (n.mi.)	80	80
Total evaporative latent heat flux ($\times 10^{-12}$ cal sec^{-1})	6.8	11.2
Evaporation depths (cm/day)	1.4	2.3
Ratio of source to transport through boundary (per cent)	18	12

(average 6—7 knots), a stationary rain gauge passed by the center would have collected 4—5 inches on 25 August and 12 inches on 27 August. Neither amount is excessive, especially since the storm was rated by experienced meteorological observers of the research aircraft as a very "wet" one.

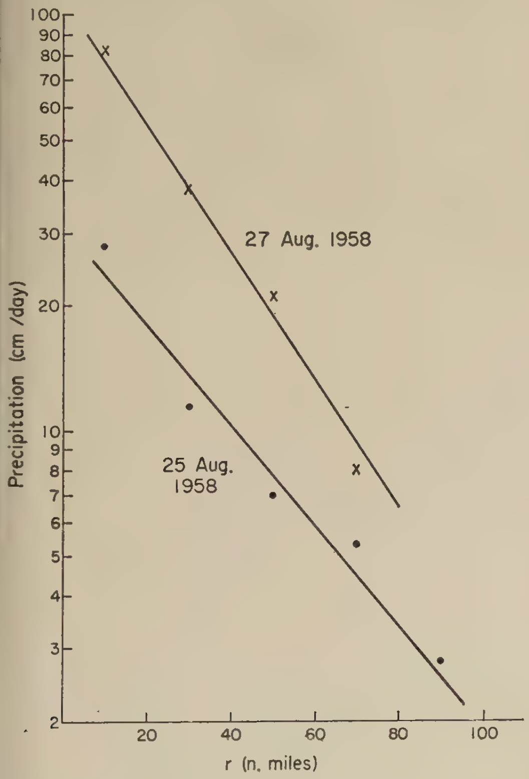

Fig. 12. Calculated radial distribution of precipitation for Daisy on August 25 and 27.

5. Vertical heat flux and the role of "hot towers"

Given the lateral heat transport of Figs. 9—10, vertical fluxes can be determined from continuity if there are no internal sources or sinks of Q. This is not quite true because of the radiation cooling. An estimate for the cooling of the whole mass has been obtained above, and it would be necessary to assign a vertical distribution of this cold source in order to include the heat sink for the vertical flux determination. This is difficult due to lack of knowledge about the radiation cooling as a function of height, and it is preferred to proceed without provision for radiation, especially as this would introduce only minor modifications.

In an analysis of the equatorial trough zone, RIEHL and MALKUS (1958) separated the vertical heat flux into contributions by transport in "hot" cumulonimbus cores, by recycling in thunderstorm downdrafts, and by "diffusion" through smaller cumuli in the manner of the vertical heat flux in the trade-wind areas (RIEHL ET AL., 1951). Since the air in the core of a hurricane is very moist throughout, a means for setting up strong downdrafts is lacking, and one would suppose that the second mechanism is negligible. If so, only the hot towers should be active above 500 mb, whereas lower down the smaller clouds may make a contribution in the layer where $\overline{Q}$ decreases upward, so that diffusion transports heat down the gradient.

The vertical mass transport M_z through a given isobaric surface may be divided

$$M_z = M_0 + (M_z - M_0), \qquad (6)$$

where M_0 denotes the mass flux which has risen from the subcloud layer, presumably in hot towers, and $M_z - M_0$ is the mass which has entered from the sides above the top of the subcloud layer. Let Q_0 denote the heat content of the air with characteristics of the subcloud layer and $\tilde{Q}$ the area-averaged heat content at any pressure surface. If all ascending mass not in hot towers has the heat content $\tilde{Q}$, and if internal sources and sinks are neglected, the vertical heat flux H_z through a given isobaric surface (cf. Fig. 13) is

$$H_z = \overline{Q}M_z = M_0 Q_0 + (M_z - M_0)\tilde{Q} \qquad (7)$$

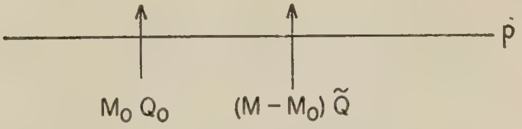

Fig. 13. Vertical heat flux mechanisms.

Here $\overline{Q}$ is the mean heat content which must be possessed by M_z in order to accomplish the heat transport prescribed by Figs. 9—10. It can be computed from these diagrams and Figs. 5—6. Values of Q for August 25 are contained in Table 4 A; none of these computations were carried out for 27 August because of lower reliability of the deduced fluxes on that day.

Table 4. Vertical heat flux calculations

August, 25

A. $\overline{Q}$ (cal/g)

Pressure (100's mb)	Radial interval (n.mi.)				
	0—20	20—40	40—60	60—80	80—100
2	83.4	82.9	83.4	82.0	82.0
3	83.0	82.5	82.6	82.0	82.0
4	82.5	81.6	81.5	81.3	80.5
5	82.4	81.4	81.2	81.0	80.2
6	82.6	81.6	81.2	81.1	80.2
7	83.3	82.0	81.4	81.2	80.5
8	84.7	82.7	82.0	81.5	80.6
9	89.5	85.6	83.7	82.4	80.7

B. Q_0 (cal/g)

	Radial interval (n.mi.)				
	0—20	20—40	40—60	60—80	80—100
Q_0	83.4	83.2	83.1	83.0	82.9

Area-averaged $Q_0 = 83.2$ cal/g

C. $\overline{Q} - \tilde{Q}$ (cal/g)

Pressure 100's mb	Radial interval (n.mi.)				
	0—20	20—40	40—60	60—80	80—100
2	0.85	0.6	1.3	0	0.1
3	1.6	1.4	1.7	1.3	1.3
4	1.5	0.9	1.3	1.4	0.8
5	1.5	0.8	1.0	1.2	0.6
6	2.0	1.0	1.0	1.1	0.4
7	2.4	1.4	1.1	1.0	0.4
8	3.8	2.0	1.5	1.1	0.3
9	8.1	4.4	3.0	1.7	0.2

D. $Q_0 - \tilde{Q}$ (cal/g)

Pressure 100's mb	Radial interval (n.mi.)				
	0—20	20—40	40—60	60—80	80—100
2	0.85	0.9	1.0	1.0	1.0
3	2.0	2.1	2.2	2.3	2.2
4	2.4	2.5	2.9	3.1	3.2
5	2.5	2.6	2.9	3.2	3.3
6	2.7	2.7	2.9	3.0	3.1
7	2.5	2.6	2.8	2.8	2.8
8	2.5	2.5	2.6	2.6	2.6
9	2.0	2.0	2.5	2.3	2.4

E. Fraction of vertical mass flux in hot towers

August, 25

$$\frac{\overline{Q} - \tilde{Q}}{Q_0 - \tilde{Q}}$$

Pressure (100's mb)	Radial interval (n.mi.)				
	0—20	20—40	40—60	60—80	80—100
2	1.00	0.67	~1.0	0	0.10
3	0.80	0.67	0.77	0.57	0.59
4	0.63	0.36	0.45	0.45	0.25
5	0.60	0.31	0.35	0.38	0.18

F. Mass flux rising in hot towers

August, 25

M_0 (10^{11} g/sec)

Pressure (100's mb)	Radial interval (n.mi.)				
	0—20	20—40	40—60	60—80	80—100
2	2.1	0.9	3.2	0	negligible
3	6.7	4.9	4.9*	4.8	2.5*
4	6.7	4.9	4.9*	5.6*	2.0*
5	6.7	4.9	4.6	5.5	1.9
9—5	6.7	4.9	4.6	5.5	1.9
M_0/A (9—5) gm cm^{-2}	15.6×10^{-3}	3.8×10^{-3}	2.1×10^{-3}	1.8×10^{-3}	0.5×10^{-3}

* Values slightly in excess of those for layer 900—500 mb indicate limit of computational reliability.

G. Per cent of vertical heat flux carried by hot towers

August, 25

$$\frac{M_0\,Q_0}{M_z\overline{Q}} = \frac{M_0 Q_0}{H_z}$$

Pressure (100's mb)	Radial interval (n.mi.)					
	0—20	20—40	40—60	60—80	80—100	Mean
2	100	67	98	0	~0	
3	82	71	79	62	62	71
4	66	41	52	50	30	48
5	65	36	42	45	23	42
Mean	78	54	68	*52	*38	

* Omitting 200 mb level

H. Vertical mass flux not in hot towers

$M_z - M_0$ (10^{11} g/sec)

Pressure (100's mb)	Radial interval (n.mi.)				
	0—20	20—40	40—60	60—80	80—100
2	0	0.5	~0	1.0	0.5
3	1.7	2.4	1.5	3.6	1.8
4	4.1	8.8	5.9	7.1	6.2
5	4.5	10.8	8.4	8.9	8.4
6	3.1	9.8	8.3	8.9	8.4
7	1.0	7.0	6.9	8.2	7.4
8	*	3.2	4.0	5.8	5.7
9	*	*	*	1.2	2.6

* Active turbulent diffusion.

Alternatively to equation 7, the vertical heat flux might also have been expressed by

$$H_z = \tilde{Q}M_z + \overline{Q^0 M_z^0}$$

where ^{0} denotes departure from the area average. As in the case of the equatorial trough study we prefer equation 6 to this formulation, because a transport $\tilde{Q}M_z$ does not occur at all and is merely a mathematical expression. We believe that equation 7 gives H_z in terms of components which have actual mechanistic existence.

Using mass continuity, we may solve equation 6 for M_0

$$M_0 = M_z \frac{\overline{Q} - \tilde{Q}}{Q_0 - \tilde{Q}}. \qquad (8)$$

At heights below the 500-mb level this relation may be modified to allow for diffusion $Q^0M_z^0$ by the widespread smaller towers. Thus

$$\overline{Q^0 M_z^0} = M_z\overline{Q} - M_0 Q_0 - (M_z - M_0)\tilde{Q} \quad (9)$$

for the lower layers. This relation can be evaluated if it is assumed that below the 500-mb level there is no "erosion" of the hot towers, i.e. M_0 and $M_0 Q_0$ are constant between 900 and 500 mb. Table 4B—H shows the remainder of the calculations for 25 August. We see that $\overline{Q} - \tilde{Q}$ is positive throughout, as expected (Table 4C). Furthermore, $Q_0 > \overline{Q}$ everywhere except at 800 and 900 mb at the inner wall and at 900 mb in the intervals 20—40 and 40—60 n.mi. (Table 4 A—B). This indicates that diffusion is very active up to about 700 mb near the eye and up to 850 mb a little farther out. Beyond this convective core and above 700 mb near the eye $\overline{Q^0 M_z^0}$ proved negligible.

The ratio $M_0/M_z = (\overline{Q} - \tilde{Q})/(Q_0 - \tilde{Q})$ in Table 4E is somewhat irregular but in general decreases outward, as expected. Although the irregularities may arise from our data, sampling and computational deficiencies there was a clear suggestion in the cloud mapping (MALKUS ET AL., loc. cit.) that within the core ($r < 100$ n.mi.) convective activity was highly concentrated in the eye wall and again at about 60 n.mi., with more tower-free spaces intervening. M_0 itself shows a rather uniform distribution with radial interval out to 80 n.mi.; however, the last line in Table 4F shows that per unit surface area, hot tower mass ascent is strongly concentrated in the inmost core. Along the vertical, M_0 remained closely constant in view of the buoyancy in the cumulonimbus cores which permits the mass to ascend rapidly without much lateral mixing. In contrast, the mass flow $M_z - M_0$ (Table 4H) with less buoyancy, cannot penetrate to the high troposphere; in fact, it diminishes immediately above the level of non-divergence near 500 mb. In consequence of this distribution, the percentage of H_z carried by the hot towers increases upward and decreases outward (Table 4G). The hot cores thus play an ever-increasing role as the center is approached, and they furnish the primary mechanism for heat flux to the high troposphere. Nevertheless, there was no requirement on August 25 that all rising mass go up in hot towers, nor was there any need to introduce recycling. It may be suggested that the potential intensity of a hurricane is related to the fraction of M_z channelled through the hot towers and its current intensity to the magnitude of M_0. These points are pursued in the following sections.

Number of hot towers

We may now compare the mass flux requirements in hot towers (Table 4 F) with the observed number penetrating the upper NHRP flight level (237 mb or about 37,000 ft) and with computations on the dynamics of individual cumulonimbus in Daisy[2]. From the latter, the ascent rate at this level of a buoyant element 4 km in diameter was about 12 m/sec. The photographs discussed by Malkus et al. and other evidence gave this as the typical horizontal dimension of the penetrative towers on the 25th.

The upward mass flux M_T through 237 mb effected by one hot tower with an area A_T, density ϱ_T, and rising at a rate W_T therefore is

$$M_T = \varrho_T A_T W_T \cong 6 \times 10^{10} \text{ g/sec}$$

where $\varrho_T \approx 0.4 \times 10^{-3}$ g cm^{-3}. From Table 4 F, the total mass flux M_0 within 100 n.mi. is about 15×10^{11} g/sec, which means that 25 active hot towers at a time are required within the storm core. The film measurements gave about 60 within 200 n.mi., so that the agreement could hardly be better, allowing for the fact that some of the towers photographed had ceased their actively rising phase when counted.

Is it also significant to note that, within 100 n.mi. on the 25th, the total mass in hot towers rising through the 500-mb level was 23.6×10^{11} g/sec or within computational error of the lateral mass inflow in the layer 1,000—900 mb at the 100 n.mi. boundary (22.0×10^{11} g/sec from Fig. 5). We suggest the correspondence between supply of subcloud air and hot tower ascent; this is supported by evidence on August 27. By the mature day, inflow (at 80 n.mi.) in the 1,000—900 mb layer had increased over the 25th by a factor of 56.7/17.5 = 3.25, while the number of penetrative hot towers within 200 n.mi. was assessed from the photographs as about 200, or an increase of a factor of 3.3 over the 25th! We shall explore some further aspects of the relationships of hot towers to hurricane development and maintenance in the next section on ventilation.

6. Ventilation

Early computations of the mean wind distribution in tropical storms at upper levels (E. JORDAN, 1952) indicated that $\overline{v}$ vanishes a few thousand feet above the surface, so that most inflow takes place in the subcloud layer. Later computations of the average wind field in Atlantic hurricanes (MILLER, 1957) and of several but not all individual cases from research flight information (SIMPSON and RIEHL, 1958; GANGOPADHYAYA and RIEHL, 1959) as well as Figs. 5—6 of this article, have shown that finite values of $\overline{v}$ can occur well above the subcloud layer and that the maximum inflow on occasion was situated as high or higher than the 700-mb level, at least at a radius of several hundred miles. Since Q decreased above the subcloud layer in every case investigated, such radial motion introduces lower values of Q (lower temperature and/or lower humidity, mainly the latter) into a hurricane or tropical depression, thus acting as a constraint on hurricane formation and maintenance.

This advection, called *ventilation*, may be defined for symmetrical circulations by

$$V_e = M_i(Q_i - Q_0) \qquad (10)$$

where M_i is the lateral inflow above the mixed layer and Q_i is its heat content. The principle of conservation of energy may be written for a volume as depicted in Fig. 14

$$M\frac{\partial Q^*}{\partial t_R} = M_0 Q_0 + \sum^{n} \Delta M_i Q_i - \sum^{m} \Delta M_u Q_u \qquad (11)$$

where M is mass and use has been made of mass continuity in the form

$$M_0 + \sum^{n} \Delta M_i = \sum^{m} \Delta M_u = M_u$$

where the subscripts 'i' and 'u' denote inflow and the summations are made (generally at

---

[2] Some of these calculations (for August 27) have been published by Malkus (1960). Similar calculations for the 25th, quoted here, are unpublished at the present time.

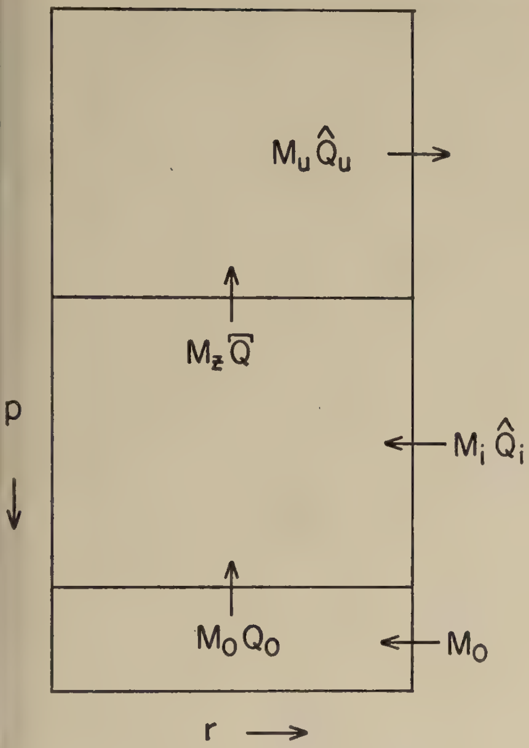

Fig. 14. Illustrating ventilation schematically.

100 mb-intervals) over the inflow and outflow layers, respectively. At the 900-mb level we shall assume undiluted upflow at the heat content of the air in the mixed surface layer, which may include contributions by the local oceanic heat source. Analogous to equation 7 we define

$$\sum^{n} \Delta M_i Q_i = M_i \hat{Q}_i$$

$$\sum^{m} \Delta M_u Q_u = M_u \hat{Q}$$

Then

$$M\frac{\partial Q^*}{\partial t_R} = M_0 Q_0 + M_i\hat{Q}_i - M_u\hat{Q}_u \qquad (12)$$

Ventilation may be introduced explicitly by adding and subtracting the identity (10). Then

$$M\frac{\partial Q^*}{\partial r_R} = M_u(Q_0 - \hat{Q}_u) + M_i(\hat{Q}_i - Q_0) \qquad (13)$$

The criterion for the growth of the disturbance is

$$\frac{M_i}{M_u} \underset{>}{\leq} \frac{Q_0 - \hat{Q}_u}{Q_0 - \hat{Q}_i} \qquad (14)$$

For example, given $Q_0 - \hat{Q}_u = 1$ cal/g and $Q_0 - \hat{Q}_i = 2$ cal/g, them the disturbance will grow if $M_i/M_u < 0.5$. From boundary observations all values are given except Q_0 which, when a large boundary such as the 5-degree radius is considered, may be taken as the heat content of the inflowing trade-wind air. In case of large mid-tropospheric inflow at the usual minimum of Q_i there, ventilation must act to weaken a storm.

For Daisy, the complete information is already contained in Figs. 9—10 and indeed the computation from equation 14 does not add to this information, but merely helps to establish a simple picture. We find that $M_i/M_u = 0.65$ at the 100 n.mi. radius on 25 August; further $\hat{Q}_i = 80.1$ and $\hat{Q}_u = 81.2$ cal/g. If the surface value of 83.2 cal/g is used for Q_0 at 900 mb, then $(Q_0 - \hat{Q}_u)/(Q_0 - \hat{Q}_i) = 0.65$. Within the limits of the computation, the equal sign of equation 14 applies. This shows there is at least no tendency for the environment to suppress the developing storm. Given an oceanic heat source, it can maintain the existing circulation against radiation and provide for some heat export and internal increase of heat content with time.

It is probable that the main utility of the ventilation calculation, as formulated here in equation 14, lies in applying it at an outer radius, say 300 n.mi., to potentially formative situations. This will indicate whether internal heating is strongly hindered. Given a mature hurricane, it will show whether weakening is likely to set in through increase of ventilation across the boundary of the calculation. In the case of Daisy where core data were available, we may explore the effects of ventilation in more mechanistic detail.

Table 5A shows the individual terms in equation 11 for the 25th (boundary 100 n.mi.) and for the 27th (80 n.mi.). On the former day we took Q_0 and M_0 from Table 4, and and on the latter day Q_0 was assumed as 84.0 cal/g (see Appendix B8) and M_0 was taken as equal to the lateral boundary inflow between 1,000—900 mb. On the 25th, the storm is gaining ground; the net warming (ignoring

Table 5. Ventilation.

A. Effect upon heat budget

Date	Unit: 10^{12} cal/sec			
	$M \partial Q^* / \partial t_R$	$M_0 Q_0$	$\Sigma M_i Q_i$	$\Sigma M_u Q_u$
Aug. 25—Actual	+11.8	196.3	340.	524.9
Aug. 25—No ventilation	+26.9	550.8	—	524.9
Aug. 27—Actual	—0.5	476.3	486.5	963.3
Aug. 27—No ventilation	+20.7	984.0	—	963.3

B. Parameters and comparisons

	Aug. 25	Aug. 27
Boundary radius (n. mi.)	100	80
$\tilde{Q}_0$ (cal/g)	83.2	84.0
M_0 (g/sec)	23.6×10^{11}	56.7×10^{11}
Increase in M_0 for no ventilation (%)	280 %	107 %
Increase in Q_a for no ventilation (%)	18 %	41 %

radiation) is comparable to the oceanic source. On the 27th, it is barely holding its own.

We may next inquire what degree of constraint upon Daisy's potential development was imposed by ventilation. It is interesting to note from Fig. 6 that on the mature day her total mass inflow at 80 n.mi. was almost exactly equal to that of the model moderate hurricane of Malkus and Riehl, and yet her winds, eye-wall surface pressure and oceanic source fell somewhat short of those they calculated. In the model, ventilation was not considered, the entering mass all arrived in the layer 1,000—900 mb, and the vertical soundings at each radius were governed by wet-adiabatic ascent of subcloud air. Therefore the hypothetical computation in Table 5 A was carried out; it places all Daisy's inflow in the layer 1,000—900 mb and raises it in hot towers M_0 with heat content Q_0, leaving the outflow unaltered. To raise the heat content of the additional inflow from its subcloud values at the boundary to Q_0 would require an enhanced oceanic source of only 18 % on the 25 th, but of 41 % on the 27th.

Since the rate of warming $M \partial Q^* / \partial t_R$ is more than doubled by this alteration on the 25th, and raised from a slight cooling to a significant warming on the 27th, one might infer that Daisy would have become an extreme storm, were only the constraint of ventilation removed. This, however, is not quite the case.

Malkus and Riehl showed that the intensity of a hurricane is proportional to the excessive heat content of the air rising in the inmost core. On August 25—27, Daisy's vertical sounding at 20 n.mi. radius was somewhat cooler than prescribed by adiabatic ascent of surface air, due to introduction of the ventilation inflow at mid-levels. Thus to assess how deep Daisy would have been without ventilation, we made hydrostatic computations at the 20 n.mi. radius assuming now an undilute wet-adiabatic sounding at the heat content Q_0 for each day. On the 25th, the surface pressure could have been lowered 10—12 mb by removal of the Q_i air and substitution of undilute ascent, while on the 27th the figure is about 8—10 mb.

Using the dynamic relationships of the model, we find that on the 25th, this lowering of eye-wall pressure and the accompanying increase of wind speed would readily enhance the oceanic source more than the 18 % required to maintain the new subcloud inflow at the 25th Q_0, thus allowing Q_0 to increase further and the storm to continue deepening, while this is not so on August 27th. On the 27th, lowering the eye-wall pressure by 8—10 mb, or to the values for the model moderate storm, increases the inner wind to about 57 m/sec, or again just comparable to the model. With the prevailing air-sea temperature difference, this wind increase permits the oceanic source to become just marginally large enough to maintain the new status quo. In fact, the work of Malkus and Riehl (equation 42, loc. cit.) suggests that now the upper limit of development has been reached for this air-sea property difference, when inmost pressures are to be maintained by ascent of subcloud air.

Thus while ventilation prevented Daisy from quite realizing her full potential, which was approximately that of the model moderate storm, it cannot be offered as the reason she did not achieve extreme intensity. To do that, she would have had either to move over warmer water or been able to lower her core pressure by some other means than hot tower ascent only, such as perhaps by an eye wall slanting outward over the inner rain area. We may suggest, however, that ventilation may be the critical inhibitor in the development in many or most cases from tropical disturbance to model moderate hurricane. Whether a storm like Daisy could have continued to intensify beyond August 25 had she not been able to concentrate an increasing percentage of her inflow in the subcloud layer, and what permitted her to do this where other storms fail are questions we raise for further hurricane research to explore. We turn next to the motion field and kinetic energy budgets of Daisy as she actually was observed.

7. The kinetic energy budget

The kinetic energy equation may be written

$$\varrho \frac{dK}{dt} = -g\varrho \mathbf{v} \cdot \nabla D + \mathbf{v} \cdot \frac{\partial \boldsymbol{\tau}}{\partial z} \qquad (15)$$

Here K is kinetic energy per unit mass, ϱ density, $\mathbf{v}$ the horizontal vector wind and $\boldsymbol{\tau}$ the horizontal shearing stress vector. Further it has been assumed that all dissipation of kinetic energy takes place by vertical turbulence, an assumption which will be examined further below. Equation 15 will be integrated over a volume α between two concentric cylinders with use of mass continuity. In the integration of the frictional term it will be assumed that $\boldsymbol{\tau} = \mu \frac{\partial \mathbf{v}}{\partial z}$, where μ is the coefficient of turbulent mass exchange, and that at ship's deck level $\boldsymbol{\tau}_0 = c_D \varrho_0 \mathbf{v}_0 V_0$ where c_D is the drag coefficient, $\mathbf{v}_0$ the vector wind and V_0 its magnitude at this level. Then

$$M \frac{\partial K^*}{\partial t_R} = -\int_\sigma K \varrho c_{nR}\, d\sigma - \int \mathbf{v} \cdot \nabla D\, dA\, dp$$
$$- c_D \varrho_0 \widetilde{V_0^3} A - \int_\alpha \mu \left(\frac{\partial V}{\partial z}\right)^2 d\alpha, \qquad (16)$$

if there is no transfer of kinetic energy through the top of the storm by shearing stresses.

Local change: The total kinetic energy was 0.6×10^{14} kj inside the 80-mile radius on 25 August and 1.3 such units on 27 August. Since the flight data for 28 August indicate that the storm was still growing in energy between the 27th and 28th, a uniform growth rate of 0.4×10^{14} kj/day will be used. This corresponds to 0.46×10^9 kj/sec or 0.1×10^{12} cal/sec in heat units; about an order of magnitude less than $M \frac{\partial Q^*}{\partial t_R}$ which itself could be neglected compared to the heat transports and sources. Such a situation is usually found in energy budget calculations. It must nevertheless be recognized that it is this very small increment which is of greatest interest in hurricanes.

Kinetic energy advection: The transport of kinetic energy by the mass circulation $\overline{K}M_r$ is readily determined from vertical profiles of $\overline{K}$ and the mass flow. But the contribution due to $\overline{v'_R K'}$ is difficult to assess because of the few flight levels and data uncertainties. Table 6 shows the available "eddy" transports.

Table 6. Eddy transport of kinetic energy

10^7 kj/sec/100 mb

	Radius (n.mi.)			
	20	40	60	80
25 Aug. 237 mb	—.2	—.4	—.2	1.9
560 mb	—.7	—3.5	—.3	—1.7
810 mb	—.9	1.7	2.9	—1.2
27 Aug. 237 mb	1.9	14.2	23.2	31.0
630 mb	9.9	11.0	10.1	14.4

They are irregular in sign on the 25th and much smaller than on 27 August, when this transport was directed outward at both flight levels, especially in the high troposphere. This suggests that the mass outflow took place in organized channels of relatively high speed. In order to obtain values integrated over the troposphere some assumptions must be made. On 25 August the arithmetic mean of the three flight levels was taken and applied to a layer of 800-mb thickness. On 27 August the values measured at 237 mb were applied to a layer of 200-mb thickness and those measured at 620 mb to a layer of 600-mb thickness.

Table 7 summarizes the kinetic energy transports. Flux due to mass circulation increased by an order of magnitude between the two days, largely because of the increase in mass circulation itself. On 25 August the "eddy" transport was only a small fraction of that due to the mean circulation and is best neglected, especially in view of the irregular distribution of signs in Table 6. On 27

Table 7. Kinetic energy transport

	Radius (n.mi.)			
	20	40	60	80
Aug. 25:				
$\overline{K}\,\overline{v}$ 10^7 kj/sec	—18.3	—23.1	—26.5	—25.0
$\overline{K'v'_R}$ 10^7 kj/sec	— 4.0	— 4.8	— 4.8	— 3.2
Total 10^{14} kj/day	— 0.2	— 0.2	— 0.2	— 0.2
Aug. 27:				
$\overline{K}\,\overline{v}$ 10^7 kj/sec	—280	—394	—490	—490
$\overline{K'v_R}$ 10^7 kj/sec	64	94	106	146
Total 10^{14} kj/day	—1.6	—2.6	—3.3	—3.9

August, however, the "eddy" flux was about 25 per cent of the mean flux at all radii, and it opposed the transport by the mean circulation. This contribution will be retained. But the limitations of the whole calculation in Tables 6—7 are evident.

Kinetic energy source: In determining the source term only the contribution by the mass circulation was evaluated. This term is readily computed within the limits of accuracy of the mass circulation. Since the contours of the isobaric surfaces formed nearly concentric circles, the contributions by $\overline{v'_R \frac{\partial D'}{\partial r}}$ and $\overline{u' \frac{\partial D'}{r\partial \Theta}}$ most likely were small. Thus, $-\int \mathbf{v}\cdot \nabla D\, dA\, dp = -\int \bar{v} \frac{\partial \bar{D}}{\partial r}\, dA\, dp$. The distribution of $\bar{D}$ is shown in Fig. 15 for 25 August. As will be expected in a warm-core vortex, the negative D's $\left(\text{as also } \frac{\partial \bar{D}}{\partial r}\right)$ decreased upward and outward. In the high troposphere the D-gradient was directed outward beyond the 50-mile radius. Thus the main seat of kinetic energy production was in the low levels where the mass flows in and the D-gradient is large. In the layer 500—300 mb, and in the upper troposphere inside the 50-mile radius, the outflow did work against the pressure field. But, since the D-gradient was small here compared to the low levels, the kinetic energy sink was much smaller than the source. Beyond the 50-mile radius, the circulation acted to generate kinetic energy at almost all heights.

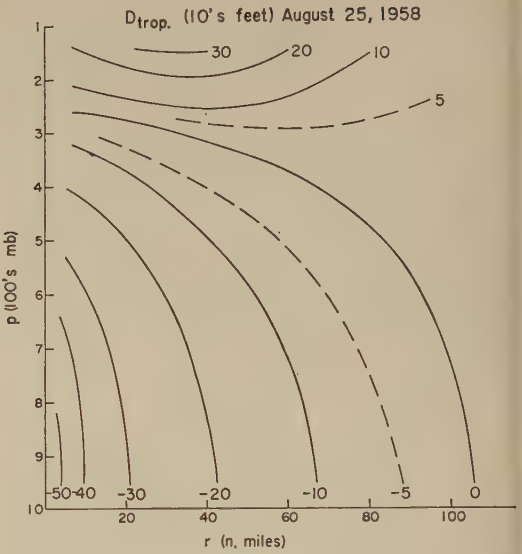

Fig. 15. Vertical cross section of altimeter correction with respect to the mean tropical atmosphere on August 25.

Tables 8—9 contain the kinetic energy budget. For 27 August four 20-mile intervals are shown. On 25 August values were somewhat more irregular, presumably because all energy transformations were much smaller; it is preferred to show only two radial intervals, for the inner and the outer region. The unit chosen is 10^{14} kj so that the transformations may be compared with total kinetic energy inside the 80-mile radius ($\sim 1 \times 10^{14}$ kj). Signs have been chosen so that the positive sign

Table 8. Kinetic energy budget (August 25)

(10^{14} kj/day)

	Radius (n.mi.)		
	0—40	40—80	0—80
Advection	.20	.02	.22
Production	1.06	1.34	2.40
Local Change	.13	.22	.35
Ground Dissipation	.57	.81	1.38
Advection plus Production	1.26	1.36	2.62
Local Change plus Ground Dissipation	.70	1.03	1.73
Left over for Internal Friction	.56	.33	.89
Ratio of Internal to Ground Friction	1.0	.4	

Table 9. Kinetic energy budget (August 27)
(10^{14} kj/day)

	Radius (n.mi.)				
	0—20	20—40	40—60	60—80	0—80
Advection	1.6	1.0	.7	—.3	3.0
Production	1.0	2.0	1.5	1.4	5.9
Local Change	.1	.1	.1	.1	.4
Ground Dissipation	.6	.8	.7	.7	2.8
Advection plus Production	2.6	3.0	2.2	1.1	8.9
Local Change plus Ground Dissipation	.7	.9	.8	.8	3.2
Left over for Internal Friction	1.9	2.1	1.4	.3	5.7
Ratio of Internal to Ground Friction	3.2	2.6	2.0	.4	

denotes a contribution toward increasing kinetic energy. The line marked "local change" refers to the change with respect to the moving system as defined above. Evidently, this term is very small, and essentially we deal with a balance between production and advection on one hand, and frictional dissipation on the other.

From Tables 7—9 all terms, except the time change, have the magnitude of total kinetic energy after integration over a day; on the 27th, in fact, the total energy is replaced completely every 2—3 hours. This helps to understand why the energy of hurricanes runs down very quickly in the inner core after they strike land.

On 25 August advection contributed little to storm growth and maintenance. Transport through the 80-mile radius was negligible, so that in this development stage the production mechanism in the interior was all-important. On the 27th, transport through the 80-mile radius contributed no less than three units, which is an order of magnitude larger than on 25 August. From Table 9 the maximum transport actually occurred near the 60-mile radius. Thus the energy imported was made available almost wholly to the inner zone.

In contrast to the large increase in advection, production inside the 80-mile radius merely doubled between the two days. Hence energy production shifted outward as the storm grew, since presumably the three units advected toward the core were generated mainly within the peripheral circulation. For comparison, PALMÉN and RIEHL (1957) computed 4.1 units for production inside the 120-mile radius for the mean hurricane, a value closer to Daisy on the 25th than the 27th. All interest now turns on the question of the disposal of the large amount of energy produced within the storm and imported toward its core.

Dissipation in the surface boundary layer: From equation 16 the dissipation of kinetic energy in the surface boundary layer is proportional to V_0^3 averaged over the area of calculation. This quantity was not available on either day, and in fact it cannot be obtained from aircraft missions. Various studies of upper winds, based on radio-wind and pilot balloon observations, have indicated that V varies little with height from the surface to the middle troposphere. PALMÉN and RIEHL (1957) actually assumed a slight decrease of windspeed from 950 mb toward the ocean. For determination of ground friction in Daisy, uniform speed from the lowest flight level down was postulated. On 25 August the legs at 960, 915, 830 and 560 mb support this assumption quite well. On 27 August, the 620-mb-level was the lowest one flown, and the windfield observed there must be assumed to be representative also of surface conditions.

An assumption must also be made about the drag coefficient, a subject discussed by Palmén and Riehl and in Section 3 herein. The dependence of c_D on wind speed, sea condition, and other parameters is a difficult topic and not yet solved satisfactorily especially at high wind speeds. In view of the somewhat low values found for Daisy in Table 2 and the uncertainties in its calculation, a uniform value of $c_D = 2.5 \times 10^{-3}$ was used in the energy and momentum budgets, as the most probable value from previous investigations. Should this procedure have been incorrect, it will be necessary to revise the ground dissipation in Tables 8—9 downward substantially. It appears certain, at least, that this term has not been underestimated.

Granted the general accuracy of the ground dissipation calculation, it is of interest that on 27 August, and to a lesser degree on 25 August, this dissipation was nearly independent of the radius. Thus

$$\overline{V_0^3} r^2 = \text{const} \tag{17}$$

for constant c_D. Malkus and Riehl (1960) found a similar distribution in a semi-theoretical model. For a symmetrical vortex, equation 17 becomes

$$V_0 r^x = V_0 r^{0.66} = \text{const} \tag{18}$$

Many calculations of the exponent x in equation 18 have been made in the literature. Values between 0.5 and 0.6 have given good fit in a large number of cases. In Daisy $x = 0.55$ verifies on 27 August. Since $\overline{V_0^3} > \overline{V}_0^3$, a coefficient somewhat lower than that computed for the symmetrical vortex should be expected; the range 0.5 to 0.6 appears excellent. Thus there is a suggestion of a frequent occurrence in hurricanes: that *dissipation of kinetic energy in the surface layer is independent of distance from the center.*

Internal Friction: The most spectacular result of Tables 8—9 is the large residual imbalance which developed between our two days and which must be attributed to a great increase in internal friction. For the general circulation it has been estimated that internal and ground dissipation may be equal. This value is not exceeded on 25 August when, also, the ratio of internal to ground friction decreased outward strongly as would be expected from the radial distribution of turbulence elements.

On 27 August the ratio decreased outward as on 25 August and was reduced to the same magnitude beyond the 60-mile radius. In the inner zone the calculated values are so strong (though well in keeping with the character of the type of circulation investigated) that the result must be considered as quite tentative. Extensive investigation of other cases plus further observations are requisite for confirmation. It is of interest, however, that the problem of disposal of kinetic energy generated also arose in the hurricane model of Malkus and Riehl (1960). In the kinetic energy budget (Fig. 9 of their report) the ground dissipation is comparable to that of 27 August. Balance is made in the lowest kilometer (the sole object of that study) by upward transport. If the computations had been extended higher up, import plus production by pressure forces would have had to be balanced by internal dissipation, and it is likely that the required magnitude would have been as large as on 27 August.

Thus the semi-theoretical work predicted the difficulty encountered in Daisy. The possibility exists that an important contribution may be made here toward understanding the limits of wind speeds attained in hurricanes by means of a constraint which grows in relative importance with the storm. In the following, possible mechanisms for achieving the internal dissipation will be taken up.

Dissipation may be accomplished by vertical and/or lateral eddies within the hurricane structure. An attractive possibility exists along the vertical. As discussed above and also by Malkus et al. (1961) in the cloud study of Daisy, most ascent is likely to have taken place in narrow towers covering only a few per cent of the area. The vertical velocity then is large (Fig. 7) and individual elements may be expected to reach the high troposphere with little loss of kinetic energy. In spite of the sampling difficulties, the high-level NHRP aircraft encountered speeds near 80 knots in Daisy and 95 knots in Helene of 1958 at 240 mb on just a few passes. These high-wind areas were very localized. The suggested picture is that the high-energy stream reaches the upper troposphere in narrow columns and then is brought rapidly in contact with environmental air which has already lost its energy by mixing and motion toward higher pressure. In the course of this contact the high energy of the fresh stream is given up to the low-energy surroundings, and this may be the mechanism of the internal dissipation process. If so, an Austausch coeffficient of 10^3 g cm^{-1}sec^{-1} would be required in view of the existing shears, if one wishes to apply this form of turbulence expression. The value is not excessive under the circumstances, especially when it is considered that Riehl et al. (1951) required a coefficient of 500 g cm^{-1}sec^{-1} for momentum balance of the average trades in the northeastern Pacific Ocean.

On account of the uniformity of wind with height below 500 mb, the dissipating mechanism just outlined may not be important there. Yet the small-scale wind fluctuations are such that judgment must be reserved. It should be added that Gray (1961) has computed strong frictional forces in the low and middle troposphere in dynamical calculations.

Considering next the possibility of lateral stresses, we shall investigate the radial stress of the tangential wind which is likely to make the largest contribution. This stress $\tau_{\Theta r} = \mu_r \left(\frac{\partial u}{\partial r} + \frac{u}{r}\right)$, and its radial derivative

$$\frac{\partial \tau_{\Theta r}}{\partial r} = \mu_r \left[\frac{\partial^2 u}{\partial r^2} + \frac{1}{r}\frac{\partial u}{\partial r} - \frac{u}{r^2}\right] = \mu_r \frac{\partial \zeta_\Theta}{\partial r}, \quad (19)$$

where μ_r is the lateral exchange coefficient for momentum and ζ_Θ is the relative vorticity of the tangential wind. Dissipation of kinetic energy by internal friction (IF) of this character

$$IF = \int\int \frac{\mu_r}{\varrho} \frac{\partial \zeta_\Theta}{\partial r} u dA \frac{dp}{g} \quad (20)$$

This formula was evaluated assuming μ_r independent of height and neglecting the horizontal correlations of $\frac{\partial \zeta_\Theta}{\partial r}$ and u which may be a substantial omission. However, only an order of magnitude estimate is wanted for comparison with previous calculations. DEFANT (1921) estimated $A = 5 \times 10^7$ g cm^{-1} sec^{-1} for the heat balance of the general circulation, and GRIMMINGER (1938) obtained 4×10^5 to 5×10^7 from the spread of moisture on isentropic charts. If the order of magnitude of A and μ in lateral turbulence is the same, then μ_r between 10^5 and 10^7 would be reasonable. Table 10 contains the calculated coefficients for August 25 and 27, where a uniform density of 10^{-3} g cm^{-3} has been used.

Values in Table 10 superficially lie within the acceptable order of magnitude range; they are also time and space dependent. On 25 August a uniform value of 1 unit is suggested within the limits of accuracy of the data. The same value applies on 27 August outside the 60-mile radius. In the interior, however, a strong rise in turbulence is indicated.

Table 10. Coefficient of horizontal turbulent exchange (μ_r)

Unit: 10^6 g cm^{-1} sec^{-1}

	Radial interval (n.mi.)			
	0—40	40—80		
25 August	0.7	1.5		
	0—20	20—40	40—60	60—80
27 August	7.4	6.6	1.7	0.9

As a check whether the order of magnitude in Table 10 is acceptable, the momentum budget will be computed in the next section. It will be shown there, what is not obvious from the energy calculations, namely that the large values of μ_r imply unreasonably large amounts of momentum transport outward, much more than can be ascribed to the range of error in our calculations. It follows that the high coefficients of Table 10 must be rejected and that in all likelihood internal dissipation of kinetic energy takes place by means of vertical turbulence.

One other aspect of the large internal dissipation should be brought out. If all energy dissipated by this mechanism were to go into sensible heat,

$$IF = cp \frac{dT}{dt} M, \quad (21)$$

where dT/dt is the mean temperature change of the mass M due to internal friction. Of course, IF may go over into other energy forms. But, assuming equation 21 to hold, we obtain temperature changes as shown in Table 11. In the core values are very large indeed. Of course, individual air particles will seldom, if ever, remain there for a whole day. But if they merely stay inside the 40-mile radius for 12 hours, net warming of 1—2° C can result. This is the order of magnitude of the radiational cold source; hence in terms of source and sink computations the effect is by no means negligible.

Table 11. Substantial temperature change due to IF

	Radial interval (n.mi.)			
	0—20	20—40	40—60	60—80
27 August °C/day	4.0	1.8	0.8	0.1

8. The budget of absolute angular momentum

The momentum balance will be taken up in stationary coordinates, and several terms will be omitted which arise when the origin of the coordinate system is referred to a moving frame. Since storm propagation was very slow, this is considered to be a permissible simplification of a computational system which otherwise would be quite complicated. The momentum equation, including vertical and lateral stress terms, then is given by

$$\varrho \frac{d\Omega}{dt} = \varrho \frac{d}{dt}\left(ur + \frac{fr^2}{2}\right) = -\frac{\partial p}{\partial \Theta} + \mu_z r \frac{\partial \tau_{\Theta z}}{\partial z} + \mu_r r \frac{\partial \tau_{\Theta r}}{\partial r}, \qquad (22)$$

where a constant Coriolis parameter f has been used. With the continuity equation $\varrho \frac{d\Omega}{dt} = \frac{\partial \varrho\Omega}{\partial t} + \nabla \cdot \varrho\Omega \mathbf{v}$. Neglecting $\frac{\partial \varrho\Omega}{\partial t}$ and integrating over the volume α

$$\int_\sigma \varrho\Omega c_n d\sigma = -\int r\tau_{\Theta o} dA + \mu_r \int r \frac{\partial \zeta_\Theta}{\partial r} d\alpha \qquad (23)$$

Here the advective term has been transformed to a surface integral over the bounding surface, and it has been assumed that the stress vanishes at the top of the storm. If the surface integral in equation 23 is evaluated between two radii and from the ground to the top of the system,

$$\int_\sigma \varrho\Omega c_n d\sigma =$$

$$= \iint \Omega v r d\Theta \frac{dp}{g}\Big]_{r_2} - \iint \Omega v r d\Theta \frac{dp}{g}\Big]_{r^1}. \qquad (24)$$

Contributions to advection arise (cf. PALMÉN and RIEHL, 1957) from the transport of relative and of earth's angular momentum by the mass circulation, and from the correlations of u with v and w. Figures 16 and 17 show the fluxes due to the mass circulation integrated over the layers of inflow and outflow. The transport of earth's angular momentum makes no contribution to the net balance. It is of importance, however, for determination of the vertical fluxes. Figures 18—19 contain the same fluxes, together with the residuals to be balanced and, in the lower portion, the net balance for the whole troposphere on each day. As in the kinetic energy budget, the correlation

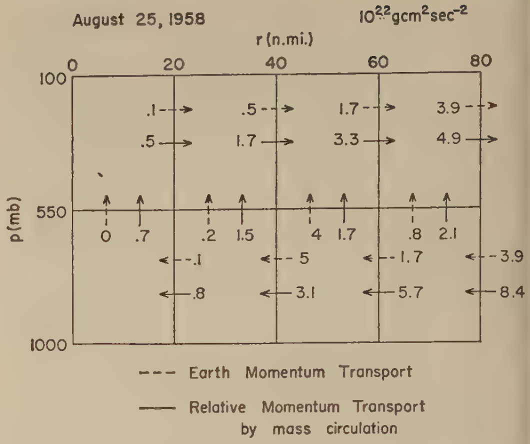
August 25, 1958
10^{22} gcm^{2}sec^{-2}
r (n.mi.)
0
20
40
60
80
p (mb)
100
550
1000
.1
.5
.5
1.7
1.7
3.3
3.9
4.9
0
.7
.2
1.5
4
1.7
.8
2.1
-.1
.8
-5
3.1
-1.7
5.7
-3.9
8.4
--- Earth Momentum Transport
—— Relative Momentum Transport by mass circulation

Fig. 16. Transport of absolute angular momentum by mass circulation on August 25.

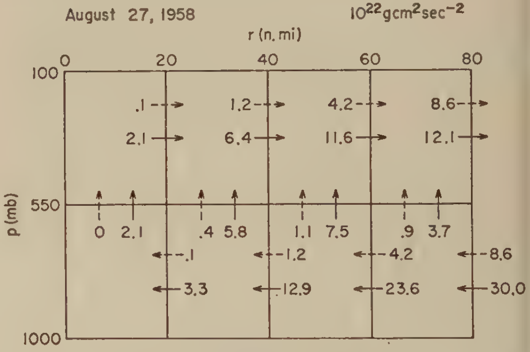
August 27, 1958
10^{22} gcm^{2}sec^{-2}
r (n. mi)
0
20
40
60
80
p (mb)
100
550
1000
.1
2.1
1.2
6.4
4.2
11.6
8.6
12.1
0
2.1
.4
5.8
1.1
7.5
.9
3.7
-.1
3.3
-1.2
12.9
-4.2
23.6
-8.6
30.0

Fig. 17. Transport of absolute angular momentum by mass circulation on August 27.

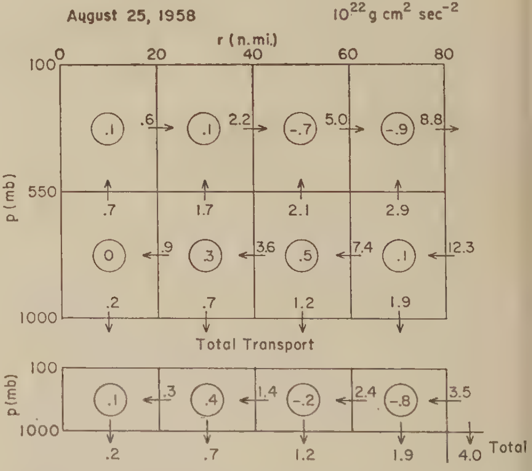
August 25, 1958
10^{22} g cm^2 sec^{-2}
r (n.mi.)
0
20
40
60
80
p (mb)
100
550
1000
.1
.6
.1
2.2
-.7
5.0
-.9
8.8
.7
1.7
2.1
2.9
0
.9
.3
3.6
.5
7.4
.1
12.3
.2
.7
1.2
1.9
Total Transport
100
1000
.1
.3
.4
1.4
-.2
2.4
-.8
3.5
.2
.7
1.2
1.9
4.0
Total

Fig. 18. Upper part: Transport of Fig. 16 repeated, also transfer to ocean and residuals in circles on August 25. Lower part: total lateral momentum transport, transfer to ocean and residuals.

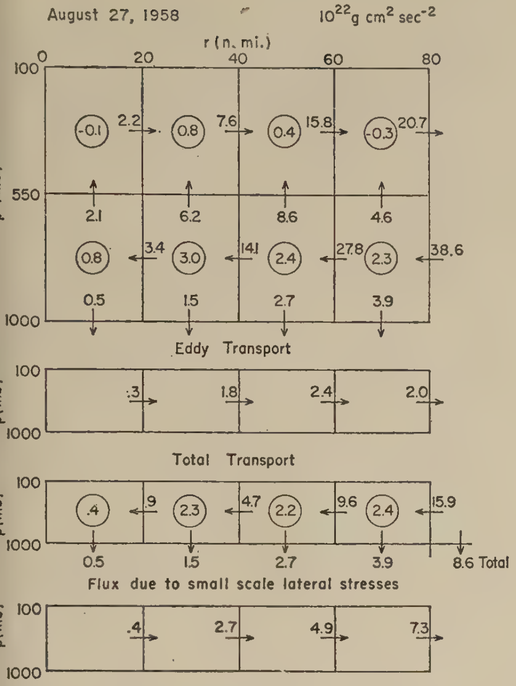

Fig. 19. Same as Fig. 18 for August 27, with intermediate line for eddy momentum flux. Residual to be exported by small-scale eddy stresses shown in line at bottom.

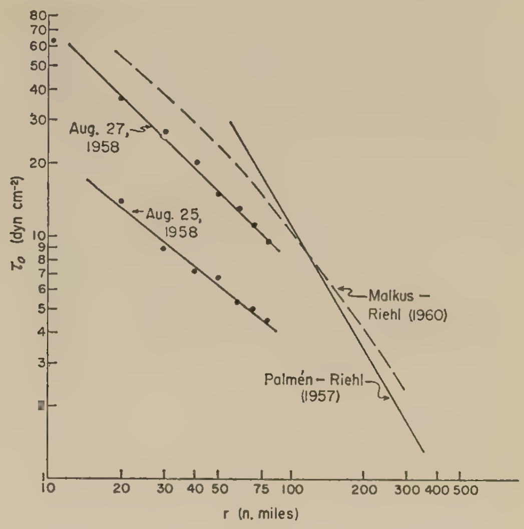

Fig. 20. Distribution of surface stress in Daisy and comparison with previous calculations.

of u' and v' contributed very little on 25 August and acted to transfer momentum outward on 27 August. The momentum flux to the surface was calculated from

$$\int r\tau_{\Theta 0} dA = \int c_D \varrho_0 V_{\Theta 0} V_0 dA, \qquad (25)$$

where on the 27th the 620-mb wind distribution was used to represent the surface wind field as in the energy budget. Figure 20 shows the distribution of τ_0 which is very similar to that of $\tau_{\Theta 0}$.

Transfer to the sea more than doubled between the two days; but on the 27th it still was well below that computed by PALMÉN and RIEHL (1957) for the mean hurricane. This is due to the fact that, as mentioned earlier, Daisy's winds were much weaker than those of the mean hurricane. On the 25th inward transport of momentum by the mass circulation equalled the transport to the ocean within the limits of accuracy of the calculations. The eddy fluxes, as already mentioned, proved to be small and of uncertain sign, as in case of the energy calculations. External forcing of the storm by eddy import of absolute angular momentum into the inner region was not the mechanism that gave birth to Daisy.

The slight inbalance on the 25th could result from some underestimate of the inflow or overestimate of the transport to the ground. It could well be that outside the 40-mile radius c_D was less than .0025 since winds decreased rapidly outward and were only 20—30 knots beyond the 60-mile radius. On the other hand, there is certainly nothing left over for lateral re-export by small-scale stresses. If $\mu_r = 1 \times 10^6$ g cm^{-1} sec^{-1} computed in Table 10 for August 25 is used in the lateral stress term of equation 23, an outward transport through the 80-mile radius is computed, which is about twice the total import by the mass circulation. It follows that the lateral exchange coefficient must have a magnitude of not more than 10^5 g cm^{-1} sec^{-1} on that day for momentum balance, that therewith dissipation of kinetic energy also must have taken place mainly by means of vertical eddies.

On the 27th a small amount of momentum was exported by the $\overline{u'v'}$ correlation so that this type of stress, far from importing momentum, actually removed it from the core as also on most other occasions where calculations have been performed. After taking account of this transport, about half of the imported momentum was given off to the ocean surface, and the balance on this day must be re-exported by small-scale lateral stresses. If the coefficients of Table 10 are used for this purpose, the outward flux exceeds the total import by a very large amount, almost an order of magnitude. If a uniform coefficient of 1×10^6 g cm^{-1} sec^{-1} is taken, the export across the 80-mile radius is 9.5 units. From the bottom of Fig. 19, the required export is 7.3 units. Hence this order of magnitude of the coefficient is satisfactory on the 27th. The lateral exchange still rose by an order of magnitude as the hurricane matured.

In conclusion of the energy and momentum sections the following may be summarized:

1) The inward momentum and energy transport took place by means of the mass circulation.

2) "Eddy" transports of angular momentum and energy were negligible or were directed outward.

3) Transport of momentum to the ocean very nearly satisfied balance requirements on the 25th. There is no need to invoke lateral momentum export by small-scale stresses. Hence the internal dissipation of kinetic energy —equal to the ground dissipation in the core— must have taken place by means of vertical eddies. The lateral exchange coefficient μ_r has a magnitude of not more than 1×10^5 g cm^{-1} sec^{-1}.

4) On 27 August interaction with the ground did not satisfy momentum balance. At this well-developed stage it is necessary to postulate lateral momentum export with coefficient of 1×10^6 g cm^{-1} sec^{-1}, hence one order of magnitude larger than on 25 August. Therefore this constraint upon the storm's growth becomes important. However, lateral coefficients computed from momentum and energy budget are not compatible if the assumption is made that all momentum transfer and all energy dissipation go by way of this process. One must postulate that the kinetic energy is dissipated by vertical turbulence. This requires a coefficient μ_z of 1,000 g cm^{-1} sec^{-1}; this is not considered excessive.

5) Internal dissipation on the 27th becomes so strong as to be able to affect the heat budget. If the energy dissipated is converted to sensible heat, a source with magnitude of $\dot{Q}_s$ is obtained inside the 40-mile radius.

6) There are strong indications that the surface dissipation of kinetic energy is independent of distance from the center, and that this may be a general feature of hurricanes which explains the observed surface wind profile along the radius.

7) The calculations have shown that both from momentum and energy viewpoints resistance against storm growth rose rapidly with intensification due to increasing importance of lateral and vertical turbulence. There is, however, no reason to suppose that this increase in the magnitude of the resistive effects relative to the generative terms is not present in each instance of storm development. Hence the calculations shed no light on the question why some hurricanes remain minimal while others rise to great intensity. It is probable that the peak intensity of each hurricane is controlled by external, not internal, factors.

9. Two-dimensional analysis and conclusions

The question may be asked what the results of this study portend with respect to understanding the hurricane engine, and with respect to future researches and observations. As case histories accumulate, one can of course proceed from the hundredth to the thousandth detail and demonstrate certain differences between individual storms. But is it worthwhile to do this? What can be said more generally about the mechanisms of hurricane maintenance from the present data? Is it necessary to treat a vortex, fully turbulent along all coordinates, and with turbulence also time dependent? How important is it that the air winds its way inward in rather tortuous selective channels which produce micro-patterns in the horizontal velocity field and that the bulk of the ascent appears concentrated in hot towers covering only a small fraction of the hurricane's area?

The Daisy data have in fact confirmed the importance of the hot tower mechanism and the concentration of the storm's heat release into 100—200 individual buoyant elements. If the details of the activity on these small scales are decisive for storm growth and maintenance, then the prospect for solving the large-scale hurricane problems and achieving predictive models recedes into the dim future. On the contrary, we shall conclude by offering the hope that the dynamic and thermal effects of these small scales of motion can be introduced or parameterized effectively in a relatively simple framework, without dwelling on their complex details which may differ from case to case and from time to time.

The most favorable situation would exist if it can be shown that the significant features of the hurricane can be grasped with two-dimensional models. In this respect, a hopeful start was made by MALKUS and RIEHL (1960). The preceding Daisy calculations are promising along the same line in that lateral eddy transports of heat and moisture proved small, and especially in that the much-vaunted $u'v'$ correlation was small with sign opposite to that postulated by its proponents; even the kinetic energy transport by the $K'v'$ correlation on 27 August was small enough so that it could have been neglected within limits of all other calculations. Outside the core, the $u'v'$ correlation appears to act in the same sense as in the core, at least to several hundred miles distance from a hurricane center (RIEHL, 1961).

Some of the interior mechanisms whose magnitudes are significant and which have been assessed here, such as internal and boundary friction along vertical and lateral axes may be expected to develop during any successful storm and hence should most probably be treated as necessary but dependent features, as should the local heat source, provided of course that the hurricane does not move to an area of much lower ocean temperatures or over land.

We now have a good quantitative, mechanistic, and thermal-dynamic picture of how the core of a moderate-strength hurricane operates, but the environmental and peripheral conditions which, only rarely, permit this engine to start and keep developing have not been found, although perhaps we know better how and where to seek them. It is highly probable that a storm's structure at maturity and the degree of its development are functions of large-scale interaction between the storm as a whole and the surrounding atmosphere, particularly as this does or does not permit a large inflow to develop in the lowest layer and ascend, with increasing heat content, in hot towers; our work suggests this is the key to the development of the core, which distinguishes a hurricane from other tropical storms. Two constraints upon hurricane development have been emphasized: ventilation and internal energy dissipation. Of these constraints, ventilation is a function of external parameters as far as one can see now. The question of what governs the vertical distribution of inflow stands out as one of the most important unresolved problems raised for future investigation.

Internal energy dissipation, according to our hypothesis, results from selective ascent of air in narrow channels. As indicated above, air moves from bottom to top of the troposphere in these channels in about 30 minutes; hence the tendency toward conservation of momentum and energy during such ascent will be high, and a large decrease of kinetic energy will occur when mixing finally does take place in the upper troposphere.

On the whole simple models such as developed by PALMÉN and RIEHL (1957) and by MALKUS and RIEHL (1960) have been supported by the present calculations. For guidance in development of complete two-dimensional models and quantitative prediction of hurricanes it appears appropriate, therefore, to present in closing a few illustrations of Daisy as this storm appears in two-dimensional form. At first, the mass flow of Figs. 5—6 may be represented in form of Stokes' stream functions (Figs. 21—22). As already emphasized, the main features in which the mass flow deviates from earlier models is the high level of non-divergence which results in importation of air with lower heat content than that of the surface layer. On August 25 the streamlines, which are also trajectories of the steady-state motion, and the lines of equal Q are fairly parallel, except in the inner core (Fig. 23). On the 27th (Fig. 24)

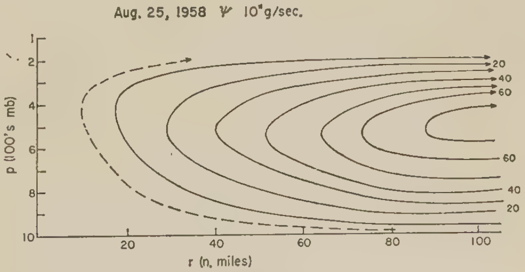

Fig. 21. Stokes stream function ψ (units 10^{11} g/sec) for August 25.

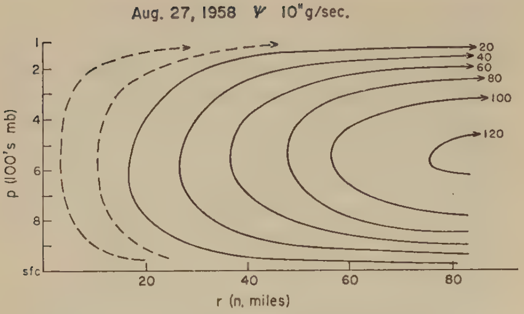

Fig. 22. Stokes stream function ψ (units 10^{11} g/sec) for August 27.

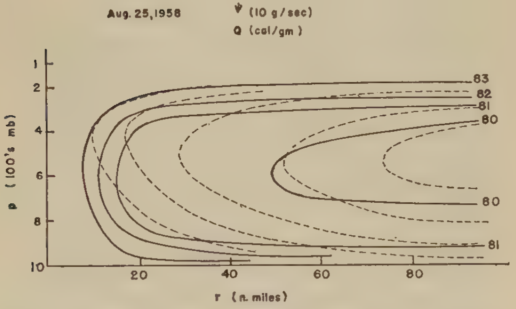

Fig. 23. Stokes stream function (dashed) and lines of constant heat content (solid) for August 25.

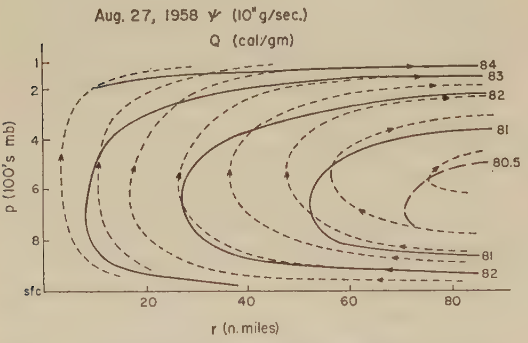

Fig. 24. Stokes stream function (dashed) and lines of constant heat content (solid) for August 27.

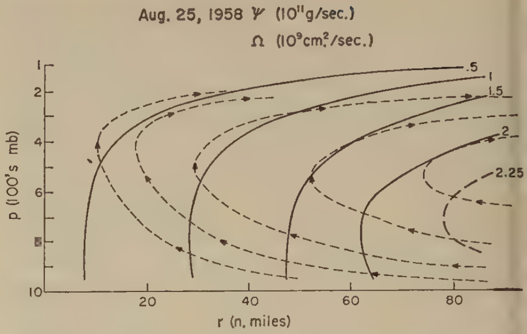

Fig. 25. Stokes stream function (dashed) and lines of constant absolute angular momentum (solid) for August 25.

the trajectories cross more strongly toward higher Q above the level of non-divergence, indicating increased effects of the oceanic heat source and transfer by rising undilute cumulonimbi and the mass they shed. Thus, in two-dimensional representation, the selective vertical motion in hot towers can be replaced by a mean vertical motion spread over the whole area, but only if $\tilde{Q}$ is replaced by $\overline{\tilde{Q}}$ for the vertical redistribution of heat.

The streamlines also cross toward lower absolute angular momentum up to the level of non-divergence on the 25th (Fig. 25), while higher up the momentum is roughly constant along these lines. This extension of the "friction layer" to the whole inflow layer must be accepted as realistic. It indicates the depth to which the flow is essentially controlled by transfer processes at the ocean surface and may be thought to correspond to the depth of the cloud layer in the trades (RIEHL and MALKUS, 1957). On 27 August (Fig. 26) the streamlines cross toward lower momentum at least up to 300 mb, and this might be taken to reflect the rising importance of lateral shearing stresses on that day. In the outflow layer the momentum again is as constant as drawing within observational limits permits.

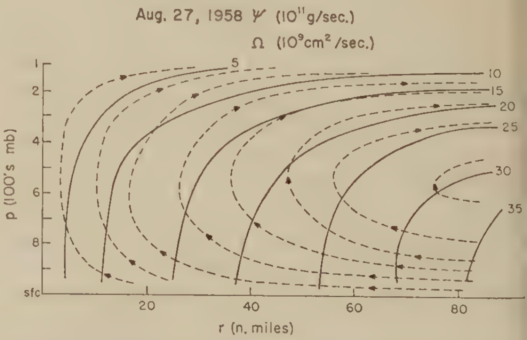

Fig. 26. Stokes stream function (dashed) and lines of constant absolute angular momentum (solid) for August 27.

We wish finally to investigate further whether the mean stream-function representation of Figs. 21—22 also is promising from the vorticity standpoint. While undoubtedly there are frictional influences on the vorticity field, it may still be presumed that the major configuration of the vorticity field is linked to the distribution of convergence and divergence so that, in the first approximation, the theorem of conservation of potential vorticity may hold. If so,

$$\frac{\zeta_{a_2}}{\zeta_{a_1}}=\frac{\Delta p_2}{\Delta p_1}, \tag{26}$$

where ζ_a is the absolute vorticity, Δp the pressure-depth of the column considered and the integration is carried out between the radii r_2 and r_1. Figures 27—28 contain the absolute vorticity cross sections, which are rather similar. Equation 25 was tested for five streamtubes of the inflow layer on the 25th and for four tubes on the 27th. No calculations were performed in the outflow region, but one can see qualitatively by comparison with Figs. 21—22 that decreasing ζ_a and Δp coincide. Table 12 gives the results for the inflow layer where it must be noted that only rough answers can be expected in view of the uncertainties in drawing the streamtubes, especially at the 80-mile radius which was taken as r_1.

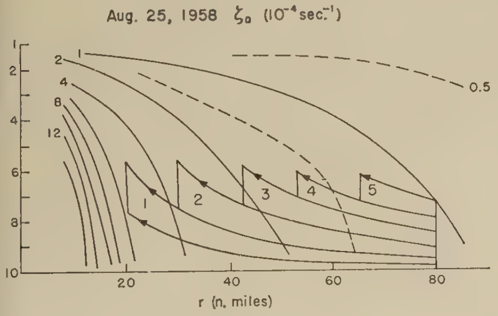

Fig. 27. Vertical cross section of absolute vorticity on August 25 and selected streamtubes from Fig. 21.

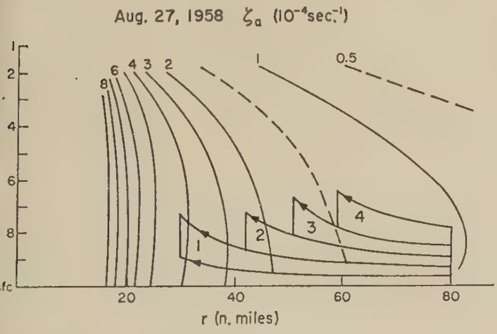

Fig. 28. Vertical cross section of absolute vortcity on August 27 and selected streamtubes from Fig. 22.

Table 12. Test of conservation of potential vorticity

	Streamtube				
	1	2	3	4	5
25 August					
ζ_{a_2}/ζ_{a_1}	4.5	3.2	1.8	1.5	1.3
$\Delta p_2/\Delta p_1$	4.5	3.6	2.5	1.6	1.5
27 August					
ζ_{a_2}/ζ_{a_1}	4.1	2.3	1.5	1.4	—
$\Delta p_2/\Delta p_1$	4.5	3.5	2.8	1.8	—

Agreement is satisfactory, especially along the mean trajectories which have the largest pressure changes; altogether percentages decrease together for ζ_{a_2}/ζ_{a_1} and $\Delta p_2/\Delta p_1$. Hence, from the dynamical viewpoint, it will be quite legitimate to treat the stream-function field as representing the synoptic-scale motion in Daisy. This outcome is particularly gratifying, as it is just the vorticity aspect of the hurricane which might have been affected strongly by the hot tower ascents which, after all, cross the mean streamtubes everywhere except perhaps in the eye wall.

Given conservation of potential vorticity in a steady two-dimensional field, the transport of absolute vorticity is constant after integration over, say the inflow layer. This property of constant vorticity transport was used by Riehl and Fultz (1958) to compute the velocity profile in a three-wave dishpan experiment and by Krishnamurti (1961) to determine the velocity field of the subtropical jetstream. The calculation appears promising also for the hurricane since the vorticity increases as the mass flow decreases inward. Then

$$\xi_a M_r=\text{const }(r). \tag{26}$$

Table 13 contains the result. Within reasonable limits the vorticity flux is constant.

In conclusion, it appears hopeful to attempt two-dimensional models of the hurricane core,

Table 13. Transport of absolute vorticity in inflow layer

Unit: 10^8 g sec^{-2}

	Radius (n.mi.)			
	20	40	60	80
25 August	6.7	7.0	6.0	6.0
27 August	14.2	14.6	14.0	13.0

provided the vital convective-scale processes are adequately parameterized and entered in the thermal budgets where their transports and releases are vital in the basic machinery. It appears likely that scales of motion intermediate between convection and the hurricane itself, such as lateral eddy transports, are not essential in the core; thus a "separation of scales of motion" may provide a framework of future useful attack upon this problem, as it has for other thermally-driven circulations in the tropics (MALKUS, 1956).

Acknowledgement

This work could not have been executed without the remarkable achievement of the National Hurricane Research Project in obtaining the days of flight records in Daisy, their care in reducing these, and their generosity and constant effort in providing them to us, supplemented by their experienced assistance at every phase. We are especially grateful to the directors of this program, R. H. Simpson, R. C. Gentry and H. Hawkins.

The research was supported by the Office of Naval Research and the United States Weather Bureau.

APPENDIX A

Quantities for lateral flux calculation

25 August, 1958

1. Temperature $\overline{T}$ (°C)

Pressure (100's mb)	Radius (n.mi.)				
	20	40	60	80	100
2—1.5	—58.1	—58.9	—59.0	—59.0	—59.0
3—2	—38.0	—39.0	—39.3	—39.5	—39.5
4—3	—21.7	—22.7	—23.0	—23.1	—23.1
5—4	—9.9	—11.1	—11.5	—11.9	—11.9
6—5	—1.1	—2.3	—2.5	—2.8	—2.8
7—6	5.9	5.1	4.9	4.9	4.9
8—7	11.7	11.1	11.0	11.0	11.0
9—8	16.8	16.3	16.2	16.1	16.1
10—9	21.7	21.2	21.1	21.0	21.0

2. Specific humidity $\overline{q}$ (g/kg)

Pressure (100's mb)	Radius (n.mi.)				
	20	40	60	80	100
2—1.5	—	—	—	—	—
3—2	0.3	0.2	0.1	—	—
4—3	1.5	1.2	0.8	0.6	0.3
5—4	3.0	2.8	2.3	2.0	1.7
6—5	5.8	5.2	5.0	4.5	4.2
7—6	8.2	7.7	7.3	7.1	6.8
8—7	11.0	10.2	10.1	10.0	9.9
9—8	13.6	12.9	12.6	12.4	12.3
10—9	17.7	17.0	16.5	16.2	16.0
Total precip. moisture (g)	6.1	5.7	5.5	5.3	5.1

3. gD^* (10^6 cm^2/sec^2)

Pressure (100's mb)	Radius (n.mi.)					Height of mean tropical atmosphere (10's m)
	20	40	60	80	100	
2—1.5	6	7	5	3	2	1329
3—2	4	3	2	2	2	1103
4—3	—3	1	0	1	1	862
5—4	—5	—1	—1	0	1	672
6—5	—6	—3	—2	—1	1	515
7—6	—8	—4	—3	—1	0	380
8—7	—9	—5	—3	—1	0	261
9—8	—9	—6	—4	—1	—1	155
10—9	—9	—6	—4	—2	—1	58

D^* deviation from mean tropical atmosphere.

4. $c_p\overline{T}$ (cal/g)

Pressure (100's mb)	Radius (n.mi.)				
	20	40	60	80	100
2—1.5	51.4	51.2	51.2	51.2	51.2
3—2	56.2	55.9	55.9	55.8	55.8
4—3	60.1	59.8	59.8	59.7	59.7
5—4	62.9	62.6	62.5	62.4	62.4
6—5	65.0	64.7	64.7	64.6	64.6
7—6	66.7	66.5	66.4	66.4	66.4
8—7	68.0	67.9	67.9	67.9	67.9
9—8	69.3	69.1	69.1	69.1	69.1
10—9	70.4	70.3	70.3	70.3	70.3

5. $g\bar{Z}$ (cal/g)

Pressure (100's mb)	Radius (n.mi.)				
	20	40	60	80	100
2—1.5	32.0	32.1	32.0	32.0	32.0
3—2	26.6	26.5	26.5	26.5	26.5
4—3	20.1	20.1	20.1	20.1	20.1
5—4	16.0	16.1	16.1	16.1	16.2
6—5	12.2	12.3	12.3	12.3	12.3
7—6	8.9	9.0	9.0	9.1	9.1
8—7	6.0	6.1	6.2	6.2	6.3
9—8	3.5	3.6	3.6	3.7	3.7
10—9	1.2	1.3	1.3	1.4	1.4

7. $L\bar{q}$ (cal/g)

Pressure (100's mb)	Radius (n.mi.)				
	20	40	60	80	100
2—1.5	—	—	—	—	—
3—2	0.2	0.1	0.1	—	—
4—3	0.9	0.7	0.5	0.4	0.1
5—4	1.8	1.7	1.4	1.2	1.0
6—5	3.5	3.1	3.0	2.7	2.5
7—6	4.9	4.6	4.4	4.3	4.1
8—7	6.6	6.1	6.0	6.0	5.9
9—8	8.2	7.7	7.6	7.5	7.4
10—9	10.6	10.2	9.9	9.7	9.6

6. $g\bar{Z} + c_p\bar{T}$ (cal/g)

Pressure (100's mb)	Radius (n.mi.)				
	20	40	60	80	100
2—1.5	83.4	83.2	83.2	83.1	83.1
3—2	82.7	82.5	82.4	82.3	82.3
4—3	80.1	79.9	79.8	79.8	79.8
5—4	78.9	78.7	78.6	78.5	78.5
6—5	77.2	77.0	76.9	76.9	77.0
7—6	75.6	75.5	75.5	75.5	75.5
8—7	74.1	74.0	74.1	74.1	74.1
9—8	72.8	72.7	72.7	72.8	72.8
10—9	71.6	71.6	71.6	71.6	71.6

8. $\bar{Q} = g\bar{Z} + c_p\bar{T} + L\bar{q}$ (cal/g, base 70)

Pressure (100's mb)	Radius (n.mi.)				
	20	40	60	80	100
2—1.5	13.4	13.2	13.2	13.1	13.1
3—2	12.9	12.6	12.5	12.3	12.3
4—3	11.0	10.6	10.3	10.2	9.9
5—4	10.7	10.4	10.0	9.7	9.5
6—5	10.7	10.1	9.9	9.6	9.5
7—6	10.5	10.1	9.9	9.8	9.6
8—7	10.7	10.1	10.1	10.1	10.0
9—8	11.0	10.4	10.3	10.3	10.2
10—9	12.2	11.8	11.5	11.3	11.2

APPENDIX B

Quantities for lateral flux calculation

27 August, 1958

1. Temperature $\bar{T}$ (°C)

Pressure (100's mb)	Radius (n.mi.)				
	15	20	40	60	80
1.5—1	—69.4	—69.8	—71.1	—72.2	—72.7
2—1.5	—52.6	—53.2	—55.7	—57.5	—59.0
3—2	—33.8	—34.6	—37.3	—38.4	—39.8
4—3	—16.5	—17.4	—19.9	—21.1	—22.5
5—4	—4.9	—5.7	—8.0	—9.3	—10.5
6—5	3.5	2.7	0.8	—0.6	—1.6
7—6	9.9	9.0	7.6	6.4	5.6
8—7	15.1	14.6	13.4	12.3	11.4
9—8	19.8	19.4	18.3	17.3	16.6
sfc—9	24.0	23.7	23.3	22.9	22.6

2. Specific humidity $\bar{q}$ (g/kg)

Pressure (100's mb)	Radius (n.mi.)				
	15	20	40	60	80
1.5—1	—	—	—	—	—
2—1.5	—	—	—	—	—
3—2	1.1	1.0	0.8	0.6	0.5
4—3	3.1	2.7	2.2	2.0	1.8
5—4	5.7	5.2	4.2	3.9	3.7
6—5	8.6	7.7	6.8	6.1	5.7
7—6	11.4	10.3	9.5	8.5	8.0
8—7	14.0	12.8	12.0	11.0	10.4
9—8	16.5	15.3	14.4	13.5	13.0
sfc—9	19.7	18.3	17.4	17.1	16.7
Total precip. moisture (g)	7.4	7.0	6.6	6.3	6.0

3. gD^* (10^6 cm²/sec²)

Pressure (100's mb)	Radius (n.mi.)					Height of mean tropical atmosphere (10's m)
	15	20	40	60	80	
1.5—1	3	4	5	6	8	1536
2—1.5	—19	—15	—14	—10	—6	1329
3—2	—23	—19	—16	—14	—10	1103
4—3	—28	—16	—13	—9	—7	862
5—4	—34	—18	—16	—12	—9	672
6—5	—42	—21	—17	—13	—11	515
7—6	—43	—22	—16	—12	—11	380
8—7	—44	—23	—16	—12	—11	261
9—8	—46	—27	—19	—15	—11	155
sfc—9	—46	—27	—19	—15	—11	76—58

D^* deviation from mean tropical atmosphere.

4. $c_p\overline{T}$ (cal/gm)

Pressure (100's mb)	Radius (n.mi.)				
	15	20	40	60	80
1.5—1	48.9	48.7	48.4	48.2	48.1
2—1.5	52.9	52.8	52.2	51.8	51.4
3—2	57.4	57.2	56.6	56.4	56.0
4—3	61.6	61.3	60.7	60.4	60.1
5—4	64.4	64.1	63.6	63.3	63.0
6—5	66.4	66.2	65.7	65.4	65.1
7—6	68.0	67.8	67.2	67.1	66.9
8—7	69.1	69.0	68.7	68.5	68.2
9—8	70.3	70.2	69.9	69.7	69.5
sfc—9	71.3	71.2	71.1	71.1	71.0

5. $g\overline{Z}$ (cal/g)

Pressure (100's mb)	Radius (n.mi.)				
	15	20	40	60	80
1.5—1	36.2	36.2	36.2	36.3	36.3
2—1.5	30.8	30.9	30.9	31.0	31.1
3—2	25.4	25.5	25.5	25.6	25.7
4—3	19.6	19.9	20.0	20.0	20.1
5—4	15.0	15.4	15.5	15.5	15.6
6—5	11.2	11.7	11.8	11.8	11.9
7—6	7.9	8.4	8.5	8.6	8.7
8—7	5.1	5.6	5.8	5.8	5.9
9—8	2.5	3.0	3.2	3.3	3.4
sfc—9	0.7	1.0	1.1	1.1	1.1

6. $g\overline{Z} + c_p\overline{T}$ (cal/g)

Pressure (100's mb)	Radius (n.mi.)				
	15	20	40	60	80
1.5—1	85.1	84.9	84.6	84.5	84.4
2—1.5	83.7	83.7	83.1	82.8	82.5
3—2	82.8	82.7	82.1	82.0	81.7
4—3	81.2	81.2	80.7	80.4	80.2
5—4	79.4	79.5	79.1	78.8	78.6
6—5	77.6	77.9	77.5	77.2	77.0
7—6	75.9	76.2	75.9	75.7	75.6
8—7	74.2	74.6	74.5	74.3	74.1
9—8	72.8	73.2	73.1	73.0	72.9
sfc—9	72.0	72.2	72.2	72.2	72.1

7. $L\overline{q}$ (cal/g)

Pressure (100's mb)	Radius (n.mi.)				
	15	20	40	60	80
1.5—1	—	—	—	—	—
2—1.5	—	—	—	—	—
3—2	0.7	0.6	0.5	0.3	0.3
4—3	1.9	1.7	1.4	1.2	1.1
5—4	3.5	3.1	2.5	2.4	2.2
6—5	5.2	4.7	4.1	3.7	3.5
7—6	6.9	6.2	7.2	6.6	6.2
8—7	8.4	7.7	5.7	5.1	4.8
9—8	10.0	9.2	8.7	8.1	7.8
sfc—9	11.8	11.0	10.5	10.3	10.1

8. $\overline{Q} = g\overline{Z} + c_v\overline{T} + L\overline{q}$ (cal/g, base 70)

Pressure (100's mb)	Radius (n.mi.)				
	15	20	40	60	80
1.5—1	15.1	14.9	14.6	14.5	14.4
2—1.5	13.7	13.7	13.1	12.8	12.5
3—2	13.5	13.3	12.6	12.3	12.0
4—3	13.1	12.9	12.1	11.6	11.3
5—4	12.9	12.6	11.6	11.2	10.8
6—5	12.8	12.6	11.6	10.8	10.4
7—6	12.8	12.4	11.6	10.8	10.4
8—7	12.6	12.3	11.7	10.9	10.3
9—8	12.8	12.4	11.8	11.1	10.7
sfc—9	13.8	13.2	12.7	12.5	12.2

REFERENCES

AUSMAN, M., 1959: *Some computations of the inflow angle in hurricanes near the ocean surface.* Dep't Meteor., Univ. Chicago. Report under Contract No. N6ori-02036 to Office of Naval Research. Unpublished.

COLÓN, J. ET AL., 1961: *Hurricane Daisy, 1958.* Manuscript to appear in Preprint Series of National Hurricane Research Project, U.S. Weather Bureau, Dep't of Commerce, Washington, D.C.

DEACON, E. L., SHEPPARD, P. A. and WEBB, E. K., 1956 Wind profiles over the sea and the drag at the se surface. *Australian Jour. Phys.*, **9**, pp. 511—541.

DEFANT, A., 1921: Die Zirkulation der Atmosphäre i den gemässigten Breiten der Erde. *Geografiska Anna ler*, **3**, p. 209.

GANGOPADHYAYA, M. and RIEHL, H., 1959: Exchange o heat, moisture, and momentum between hurrican

Ella (1958) and its environment. *Quart. J. Roy. Met. Soc.*, **85**, pp. 278—287.

Gray, W. S., 1961: *On the balance of forces in hurricanes.* Colorado State University, Atmospheric Research Report No. 1, Fort Collins, Colo.

Grimminger, G., 1938: The intensity of lateral mixing in the atmosphere as determined from isentropic charts. *Trans. Amer. Geophysical Union*, **19**, p. 163.

Groening, H. V., 1960: *Wind and pressure fields in the stratosphere over the West Indies in August 1958.* National Hurricane Research Project, Preprint Series No. 35. U.S. Dep't of Commerce, Weather Bureau, Washington, D.C.

Hughes, L. A., 1952: On the low-level wind structure of tropical storms. *J. Meteor.*, **9**, pp. 422—428.

Jordan, E. S., 1952: An observational study of the upper-wind circulation around tropical storms. *J. Meteor.*, **9**, pp. 340—346.

Jordan, C. L., Lt. Comdr. D. A. Hurt, Jr., USN, and Lt. C. A. Lowrey, USN, 1960: On the structure of hurricane Daisy on August 27, 1958. *J. Meteor.*, **17**, pp. 337—348.

Krishnamurti, T. N., 1961: The subtropical jet stream of winter. *J. Meteor.* (in press).

Krueger, D. W., 1959: A relation between the mass circulation through hurricanes and their intensity. *Bull. Amer. Meteor. Soc.*, **40**, pp. 182—190.

Malkus, J. S., 1956: On the maintenance of the trade winds. *Tellus*, **8**, pp. 335—350.

— 1958: On the thermal structure of the hurricane core. Proc. Tech. Conf. on Hurricanes, Miami, Florida, Nov. 1958. *Amer. Met. Soc.*

— 1960: *Recent developments in the study of penetrative convection and an application to hurricane cumulonimbus towers.* Proc. First Conf. on Cumulus Convection, Wentworth, New Hampshire, 1959, 65—84.

Malkus, J. S. and Riehl, H., 1960: On the dynamics and energy transformations in steady state hurricanes. *Tellus*, **12**, pp. 1—21.

Malkus, J. S., Ronne, C. and Chaffee, M., 1961: Cloud patterns in hurricane Daisy, 1958. *Tellus*, **13**, pp. 8—30.

Miller, B. I., 1957: *The three-dimensional wind structure around a tropical cyclone.* National Hurricane Research Project, Preprint Series No. 15. U.S. Dep't. of Commerce, Weather Bureau, Washington, D.C.

Palmén, E. and Riehl, H., 1957: Budget of angular momentum and energy in tropical cyclones. *J. Meteor.*, **14**, pp. 150—159.

Riehl, H. et al., 1951: The northeast trade of the Pacific Ocean. *Quart. J. Roy. Meteor. Soc.*, **77**, pp. 598—626.

Riehl, H. and Malkus, J. S., 1957: On the heat balance and maintenance of circulation in the trades. *Quart. J. Roy. Meteor. Soc.*, **83**, pp. 21—30.

Riehl, H. and Fultz, D., 1958: The general circulation in a steady rotating dishpan experiment. *Quart. J. Roy. Meteor. Soc.*, **84**, pp. 389—418.

Riehl, H. and Malkus, J. S., 1958: On the heat balance in the equatorial trough zone. *Geophysica* **6**, pp. 503—538.

Riehl, H., 1954: *Tropical Meteorology.* New York: McGraw-Hill Book Co. 394 pp.

Riehl, H., 1961: On the mechanisms of angular momentum transport in hurricanes. *J. Meteor.*, **18**, pp. 113—115.

Simpson, R. H. and Riehl, H., 1958: *Mid-tropospheric ventilation as a constraint on hurricane development and maintenance.* Proc. Tech. Conf. on Hurricanes, Miami, Florida, Nov. 1958.

United States Weather Bureau, 1956: *Objectives and design of the National Hurricane Research Project.* National Hurricane Research Project, Preprint Series No. 1. U.S. Dep't. of Commerce, Weather Bureau, Washington, D.C.

PRINTED IN SWEDEN
ESSELTE, STHLM 61

Contribution No. 1157

Särtryck ur Tellus nr 2, 1961

Theory of Very Long Waves in a Zonal Atmospheric Flow[1, 2]

By PIERRE WELANDER,

Swedish Research Council of the Natural Sciences and Woods Hole Oceanographic Institution

(Manuscript reiceved February 1, 1961)

Abstract

A derivation is given of the general wave equation for small quasi-static adiabatic perturbations in a zonal atmospheric flow. This equation is then specialized to the case of very long waves (wave-length 10,000 km or more). The proper modelling is obtained by assuming the (non-dimensional) wave number to be of order unity and by the assumptions of strong rotational constraint ($Ro \ll 1$), strong dynamic stability ($Ri \gg 1$) but weak stratification $\left(\frac{\Delta\Theta}{\Theta} \ll 1\right)$. The long waves obtained by the present model move at a speed that, to the first order, is independent of the wave number but dependent on the product $Ro \cdot Ri$. A solution is worked out in the β-plane approximation, assuming a basic wind and potential temperature that vary linearly with pressure. The existence of stationary waves in this case is demonstrated. The effect of different boundary conditions is discussed. Some consequences of the theory of interest in connection with numerical weather prediction are pointed out.

1. Introduction

On the hemispherical 500 mb maps of the atmosphere one observes clearly the existence of very long waves, with wave-lengths in the range 10,000—20,000 km. (Fig. 1.) These waves, that appear in the westerly flow of middle latitudes, remain stationary or show only a slow motion.

The first theory for long waves of this type was developed by Rossby (1939) for the case of a barotropic atmosphere (pressure depends only on density). Rossby assumed a uniform zonal flow and perturbations independent of the latitude coordinate. He further simplified the problem by introducing the so-called β-plane in which the only effect of the earth's curvature considered was the variation with latitude of the vertical component of earth's rotation. Rossby's theory gives waves moving with the speed

$$c=U-\frac{\beta}{k^2} \tag{1}$$

where U is the speed of the basic current, is the wave-number and $\beta=\frac{2\Omega}{R}\cos\varphi$ (Ω i

---

[1] Submitted to the National Science Foundation under Grant No. NSF-7368.

[2] Contribution No. 1157 from Woods Hole Oceanographic Institute.

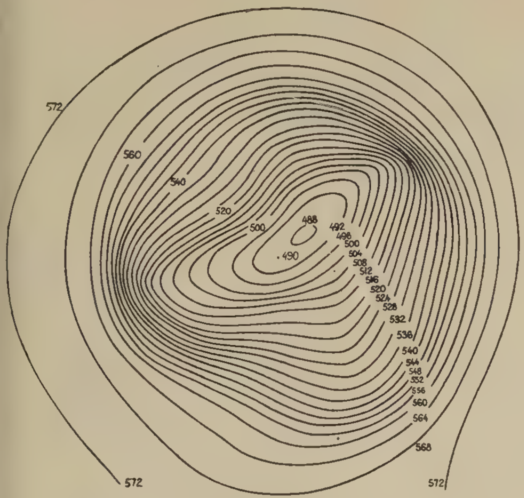

Fig. 1. Mean heigt field at 500 mb on the Northern Hemisphere. in February.

the angular velocity of earth, R the radius of earth and φ the latitude). For moderately long waves Rossby's formula is in reasonable agreement with the observations. For the very long waves that we discuss the second term in (1) will dominate, and the waves should have a strong retrograde motion. Also, the wave-speed should be very sensitive to small changes in the wave-number in this range. These results are not confirmed by the observations.

Later investigators have tried to improve Rossby's theory. HAURWITZ (1940) considered the same problem on a sphere. FJORTOFT (1950) and HOLMBOE (1953) have discussed the effects of a non-uniform basic flow. The behaviour of the waves in a physically more realistic atmosphere of baroclinic (non-barotropic) type has been studied by CHARNEY (1947), EADY (1949), FJORTOFT (1950), THOMPSON (1953) and KUO (1952). In the baroclinic theories the basic velocity is mostly assumed to vary linearly with height and the static stability is assumed constant. All changes are assumed to take place adibatically.

For very large wave-lengths these theories give generally a strong retrograde motion of the waves. In fact, many of baroclinic theories give precisely the Rossby solution in the limit of the very long waves.

A recent paper by BURGER (1959) has thrown some doubt on the simplified vorticity equation, from which most of the earlier theories start at, in the case of planetary-scale motion. For these reasons a new derivation of the wave equation that is appropriate for the very long waves seems to be needed, and an attempt in that direction is made in the present paper.

The start is made from the hydrodynamic and thermodynamic equations governing small quasi-static and adiabatic perturbations of a zonal current, retaining the spherical geometry of the problem. A single wave-equation with the associated boundary conditions is then derived for the geopotential of a pressure surface. The wave equation and the boundary conditions are now non-dimensionalized, so that all variables of the problem become of order 1. Certain non-dimensional coefficients, such as the Rossby number, the Richardson number and a stratification number will enter naturally in the equation. One has also a non-dimensional frequency and the non-dimensional wave-numbers (scaling by the period and the radius of the earth respectively). For the very long waves the non-dimensional zonal wave-number becomes of order 1. In this case it has been found possible to apply an expansion after small Rossby numbers and small inverse Richardson numbers. Finally, the study is limited to waves of small non-dimensional frequencies.

It has been attempted to justify the above expansion method in terms of the characteristic numbers that one can compute for the real atmosphere. It seems that the method will work satisfactorily for the problem we consider. It can certainly not be used for waves much shorter than 10,000 km.

The boundary conditions have been discussed in some detail. A comparison is made between the condition of vanishing vertical velocity and vanishing individual pressure change at the ground. In the upper atmosphere it is required that the geopotential remains finite when the pressure goes to zero, i.e. that the atmosphere has a limited thickness.

Numerical results have been worked out in a "β-plane" approximation for the special case where the basic zonal velocity and the potential temperature vary linearly with pressure. Diagrams will show the wave speed and the vertical structure of the waves.

A few words should be said about the coordinates used in the general derivation. The coordinates appearing are x, y, z or x, y, p. The coordinates x, y, z are not rectangular coordinates, but are quasi-coordinates that depict the spherical geometry. The rules of computation become accordingly different. For example, the operators $\frac{\partial}{\partial x}$ and $\frac{\partial}{\partial y}$ do not commute. The coordinates x, y, p are treated the same way. The only difference is that the pressure p replaces z as vertical coordinate and z, or in our case rather the geopotential $\phi = gz$, enters as dependent variable. These coordinates go together with the hydrostatic approximation. The transformation formulas are given by Eliassen (1949).

2. Basic Equations

Let φ be the latitude (counted positive northward), λ the longitude (counted positive eastward) and r the distance from the earth's centre. We introduce the quasi-coordinates x and y by the non-integrable relations

$$dx = r\cos\varphi\, d\lambda$$

$$dy = r d\varphi$$

We further introduce the height $z = r - R$, where R is the radius of earth. Let (u, v, w) be the velocity in the x-y-z system, p the pressure, ϱ the density, T the temperature, q the heat per unit mass, c_v the specific heat per unit mass, (F_x, F_y, F_z) the frictional force per unit mass, g the acceleration of gravity, Ω the magnitude of earth's angular velocity, $f = 2\,\Omega \sin\varphi$ the double vertical component and $e = 2\,\Omega\cos\varphi$ the double horizontal component of the same angular velocity. The basic hydrodynamic and the thermodynamic equations are then

$$\frac{du}{dt} - \left(f + \frac{u}{r}\operatorname{tg}\varphi\right)v + \left(e + \frac{u}{r}\right)w = -\frac{1}{\varrho}\left(\frac{\partial p}{\partial x} + F_x\right) \qquad (2)$$

$$\frac{dv}{dt} + \left(f + \frac{u}{r}\operatorname{tg}\varphi\right)u + \frac{vw}{r} = -\frac{1}{\varrho}\left(\frac{\partial p}{\partial y} + F_y\right) \qquad (3)$$

$$\frac{dw}{dt} - eu - \frac{u^2 + v^2}{r} = -\frac{1}{\varrho}\left(\frac{\partial p}{\partial z} + F_z\right) - g \qquad (4)$$

$$\frac{d\varrho}{dt} + \varrho\left(\frac{\partial u}{\partial x} + \frac{\partial v}{\partial y} - \frac{\operatorname{tg}\varphi}{r}v + \frac{\partial w}{\partial z} + \frac{2}{r}w\right) = 0 \qquad (5)$$

$$\frac{dq}{dt} = p\frac{d}{dt}\left(\frac{1}{\varrho}\right) + c_v\frac{dT}{dt} \qquad (6)$$

$$p = p(\varrho, T) \qquad (7)$$

where $\frac{d}{dt} = \frac{\partial}{\partial t} + u\frac{\partial}{\partial x} + v\frac{\partial}{\partial y} + w\frac{\partial}{\partial z} \cdot g$ will include the centrifugal forces due to earth's basic rotation. It is permissible to assume this apparent gravity constant and directed vertically. Consistently, the earth's surface should then be assumed spherical.

(2, 3, 4) are the equations of motion, (5) the continuity equation, (6) the first law of thermodynamics and (7) the equation of state. If q is known, or if it can be related to the other variables, we have six equations for the unknown quantities u, v, w, p, ϱ, and T. The boundary conditions are not considered at present.

3. General assumptions

The following general assumptions are made –

i) The depth (scale-depth) of the atmosphere is much smaller than the radius of earth.

ii) The vertical derivative of any of the physical variables is large compared to the horizontal derivatives.

iii) The pressure is hydrostatic.

iv) Friction and non-adiabatic heating are neglected.

v) The equation of state is the ideal gas law.

The assumptions (i) and (ii) allow us to replace r by R in the above equations. The approximation holds good also when further vertical derivatives are taken. In (1) y becomes a true coordinate, $y = R\varphi$. The assumptions further allow us to neglect the terms $\frac{uw}{R}$ and $\frac{vw}{R}$ in the equations of motion and the term $\frac{2}{R}w$ in the continuity equation.

The assumption (ii) combined with the continuity equation gives that $w \ll u$, v and the term ew in (2) may be dropped.

The assumption (iii) states that $\frac{\partial p}{\partial z} = -g\varrho$, the assumption (iv) that $F_x = F_y = F_z = 0$ and $\frac{dq}{dt} = 0$, and the assumption (vii) that $p = R_M \varrho T$, where R_M is the gas constant per gram.

Once the hydrostatic assumption is made there is some advantage in using a new coordinate system in which the geopotential $\phi = gz$ of a given pressure surface becomes a dependent variable, while the pressure becomes an independent vertical coordinate. The transformation of the hydrodynamic and the thermodynamic equations to the p-system has been carried out by ELIASSEN (1949). In this new system the density disappears from the equations of motion as well as from the continuity equation. The adiabatic equation in combination with the equation of state gives $\frac{d}{dt}\left(\frac{1}{\varrho}p^{\frac{1}{\varkappa}}\right) = 0$ with $\varkappa = \frac{c_p}{c_v}$, and here $\frac{1}{\varrho}$ can be replaced by $-\frac{\partial \phi}{\partial p}$ according to the hydrostatic equation. The two equations of motion, the continuity equation and the transformed adiabatic equation become finally

$$\frac{du}{dt} - \left(f + \frac{u}{R}\operatorname{tg}\varphi\right) v = -\frac{\partial \phi}{\partial x} \tag{8}$$

$$\frac{dv}{dt} + \left(f + \frac{u}{R}\operatorname{tg}\varphi\right) u = -\frac{\partial \phi}{\partial y} \tag{9}$$

$$\frac{\partial u}{\partial x} + \frac{\partial v}{\partial y} - \frac{\operatorname{tg}\varphi}{R} v + \frac{\partial \omega}{\partial p} = 0 \tag{10}$$

$$\frac{d}{dt}\left(p^{\frac{1}{\varkappa}} \frac{\partial \phi}{\partial p}\right) = 0 \tag{11}$$

where (u, v, ω) is the velocity in the p-system and $\frac{d}{dt} = \frac{\partial}{\partial t} + u\frac{\partial}{\partial x} + v\frac{\partial}{\partial y} + \omega\frac{\partial}{\partial p}$. In the above equations the x- and y-derivatives are evaluated along surfaces $p = \text{const}$. The velocity components u and v are identical with the same components in the z-system. The vertical velocity ω has, however, a different meaning in the p-system. ω stands for $\frac{dp}{dt}$ and represents thus the total rate of change of the pressure.

We next turn to the boundary conditions. Since the model is non-viscous and the changes are assumed to be adiabatic the only condition needed at the earth's surface is that the vertical velocity vanish: $w = 0$ at $z = 0$. Since $\phi = gz$ and $\frac{d\phi}{dt} = g\frac{dz}{dt} = gw$ the boundary condition in the p-system is

$$\frac{d\phi}{dt} = 0 \quad \text{at } \phi = 0 \tag{12}$$

This condition is of a different type from the one applying in the z-system, the surface $\phi = 0$ being unknown from the beginning.

What condition should be applied at the upper boundary of the atmosphere is more uncertain. In the real atmosphere frictional effects become very dominant at great heights, since the kinematic viscosity increases to the same extent as the density decreases. Thus it may be unrealistic to retain, in our ideal fluid model, waves that are very energetic at great heights and thus would be subjected to a very strong damping in reality. Formally such waves are eliminated by applying a sufficiently strong condition at the upper boundary. The condition normally used in problems of the present type is that ω should disappear at $p = 0$. This is a relatively weak condition. A more reasonable condition seems to be that the geopotential ϕ remains finite, requiring that the atmosphere has a limited extension out in space. This is a stronger condition than $\omega = 0$. We state the condition in the form

$$\phi < \infty \quad \text{when } p = 0 \tag{13}$$

In the y-direction there are no boundary conditions but one has to require regularity at certain critical points, such as the pole. However, the final wave equation that we will discuss contains y parametrically and the regularity becomes only a local problem. In this case, we can simply exclude the region close to the critical points from our analysis.

4. Wave Form Perturbation Equations

Consider a steady axially symmetric state of the atmosphere satisfying the equations (8—13). This state may be described by a geopotential $\Phi(y, p)$. The corresponding density distribution $Q(y, p)$ can be found from the hydrostatic equation, and the temperature $T(y, p)$ from the equation of state. The zonal velocity $U(y, p)$ is obtained from the second equation of motion, that in this case reduces to

$$\left(f+\frac{\mathrm{tg}\,\varphi}{R}U\right)U=-\frac{\partial\Phi}{\partial y} \tag{14}$$

We consider now small perturbations from this basic state. We shall assume from the beginning that these have a wave form. Thus we put

$$\begin{aligned} u &= U(y, p)+u'(y, p)\,e^{i(kx+\nu t)} \\ v &= v'(y, p)\,e^{i(kx+\nu t)} \\ \omega &= \omega'(y, p)\,e^{i(kx+\nu t)} \\ \phi &= \Phi(y, p)+\phi'(y, p)\,e^{i(kx+\nu t)} \end{aligned} \tag{15}$$

There is no restriction laid on the problem by assuming the wave form (15). In fact, this is the natural separation form of the perturbation equations. The restriction comes later by our assumption of real values of the frequency ν. This means that we only conside the neutral waves.

The appearance of x in the above forn may be puzzling, since x has been defined a a quasi-coordinate. In fact, the x in (15) has different meaning than in (1). In a spherica wave the longitudinal angle λ enters in factor $e^{in\lambda}$, where n is an integer givin the mode. We formally identify this facto with e^{ikx} to have a notation in accordanc with the β-plane analysis. x and k are then to b defined as follows —

$$\begin{aligned} x &= R\cos\varphi\cdot\lambda \\ k &= \frac{n}{R\cos\varphi} \end{aligned} \tag{16}$$

The important thing to remember here i that k, the zonal wave number, is a functio of the latitude.

The differential equations for u', v', ω' an ϕ' are given by the following scheme o coefficients:

$$\begin{array}{cccccc} u' & v' & w' & \phi' & & \\ \hline i(\nu+kU) & -\left(f+\frac{\mathrm{tg}\,\varphi}{R}U\right)+U_y & U_p & ik & & \\ f+\frac{2\,\mathrm{tg}\,\varphi}{R}U & i(\nu+kU) & 0 & \frac{\partial}{\partial y} & & (17 \\ ik & \frac{\partial}{\partial y}-\frac{\mathrm{tg}\,\varphi}{R} & \frac{\partial}{\partial p} & 0 & =0 & \\ 0 & \Phi_{yp} & \Lambda & i(\nu+kU)\frac{\partial}{\partial p} & & \end{array}$$

where

$$\Lambda = p^{-\frac{1}{\varkappa}}\left(p^{\frac{1}{\varkappa}}\Phi_p\right)_p = -\frac{1}{Q}\frac{1}{\Theta}\frac{\partial\Theta}{\partial p} \tag{18}$$

(Θ is the potential temperature $T\left(\frac{p_0}{p}\right)^{\frac{\varkappa-1}{\varkappa}}$).

5. Wave Equation for ϕ'

The next step is to derive a single wave equation and the associated boundary conditions for ϕ'. One has here the difficulty that the coefficients of the perturbations equation are functions of y and p, so that the differential operators do not normally commute. One straightforward way to derive a wav equation is, however, found: in the first second and fourth equations the coefficient of u', v' and ω' do not contain any y- or p derivatives. From these equations we ca thus by an algebraic elimination express u v' and ω' in terms of ϕ'. Inserting these ex pressions in the third equation, that is, the continuity equation, we have a single equation for ϕ'.

The first step of elimination gives us expressions of the form

$$u' = \left(A\frac{\partial}{\partial y} + B\frac{\partial}{\partial p} + C\right)\phi'$$
$$v' = \left(D\frac{\partial}{\partial y} + E\frac{\partial}{\partial p} + F\right)\phi' \qquad (19)$$
$$\omega' = \left(G\frac{\partial}{\partial y} + H\frac{\partial}{\partial p} + I\right)\phi'$$

and after insertion in the continuity equation one finds the following second order partial differential equation for ϕ:

$$\left\{D\frac{\partial^2}{\partial y^2} + (E+G)\frac{\partial^2}{\partial y \partial p} + H\frac{\partial^2}{\partial p^2} + \right.$$
$$+\left(ikA + D_y - \frac{\operatorname{tg}\varphi}{R}D + F + G_p\right)\frac{\partial}{\partial y} +$$
$$+\left(ikB + E_y - \frac{\operatorname{tg}\varphi}{R}E + H_p + I\right)\frac{\partial}{\partial p} +$$
$$\left. + ikC + F_y - \frac{\operatorname{tg}\varphi}{R}F + I_p\right\}\phi' = 0 \qquad (20)$$

The coefficients A, $B - I$ are given below:

$$A = -\left\{\Lambda\left(f + \frac{\operatorname{tg}\varphi}{R}U - U_y\right) + U_p\Phi_{yp}\right\}\cdot\frac{1}{N}$$
$$B = -U_p(\nu + kU)^2\cdot\frac{1}{N}$$
$$C = k\Lambda(\nu + kU)\cdot\frac{1}{N}$$
$$D = -i\Lambda(\nu + kU)\cdot\frac{1}{N}$$
$$E = -i\left(f + \frac{2\operatorname{tg}\varphi}{R}U\right)U_p(\nu + kU)\cdot\frac{1}{N}$$
$$F = ik\Lambda\left(f + \frac{2\operatorname{tg}\varphi}{R}U\right)\cdot\frac{1}{N} \qquad (21)$$
$$G = i\Phi_{yp}(\nu + kU)\cdot\frac{1}{N}$$
$$H = -i(\nu + kU)\left[\left(f + \frac{2\operatorname{tg}\varphi}{R}U\right)\left(f + \frac{\operatorname{tg}\varphi}{R}U - \right.\right.$$
$$\left.\left. - U_y\right) - (\nu + kU)^2\right]\cdot\frac{1}{N}$$
$$I = -ik\left(f + \frac{2\operatorname{tg}\varphi}{R}U\right)\Phi_{yp}\cdot\frac{1}{N}$$

where

$$N = \Lambda\left(f + \frac{2\operatorname{tg}\varphi}{R}U\right)\left(f + \frac{\operatorname{tg}\varphi}{R}U - U_y\right) +$$
$$+\left(f + \frac{2\operatorname{tg}\varphi}{R}U\right)U_p\Phi_{yp} - \Lambda(\nu + kU)^2$$

The boundary conditions (12, 13) become

$$\left\{(\Phi_y D + \Phi_p G)\frac{\partial}{\partial y} + (\Phi_y E + \Phi_p H)\frac{\partial}{\partial p} + \right.$$
$$\left. + i(\nu + kU) + \Phi_y F + \Phi_p I\right\}\phi' = 0 \text{ at } \Phi = 0 \quad (22)$$
$$\phi' < \infty \quad \text{at } p = 0$$

6. Non-dimensional Form

The previous equations can be brought to a non-dimensional form, in which all variables become of order 1. It is advantageous to work with such a form, since one can see directly the mathematical consequences of different physical assumptions.

At the moment we put no restriction on the horizontal and vertical scales of the basic and the perturbed states, except the one given by assumption (ii). We denote by l_0 and l the meridional wave numbers characterizing the basic state and the perturbation state, respectively. The zonal wave number k of the perturbation has already been introduced. To describe the scale in the vertical direction we introduce further the vertical wave numbers m_0 and m for the basic state and the perturbation state, respectively. We will also need the amplitude of the zonal velocity U_0, the relative variation of the potential temperature $\frac{\Delta\Theta}{\Theta_0}$ over the layer of the atmosphere considered and the standard values of pressure and density at the ground p_0 and ϱ_0.

We shall make the assumption for the basic state that the Coriolis force is at least comparable to the centrifugal force and that the vertical variation of the velocity is at least of order U_0. These assumptions, that are quite weak, allow us to normalize U by the so-called thermal wind relation.

We put

$$y^* = l_0 y,\ p^* = m_0 p \text{ and}$$

$$\frac{\partial}{\partial y} = l_0 \frac{\partial}{\partial y^*},\ \frac{\partial}{\partial p} = m_0 \frac{\partial}{\partial p^*} \text{ etc.}$$

(applying to the basic state)

$$y^{**} = ly,\ p^{**} = mp \quad \text{and } \frac{\partial}{\partial y} = l \frac{\partial}{\partial y^{**}},$$

$$\frac{\partial}{\partial p} = m \frac{\partial}{\partial p^{**}} \text{ etc.} \tag{23}$$

(applying to the perturbation state)

$$U^* = \frac{U}{U_0}$$

$$(\Phi_{yp})^* = \frac{\Phi_{yp}}{m_0 \Omega U_0}$$

The variables denoted by stars should be of order 1.

In their non-dimensional form, the wave equation and the associated boundary conditions will depend on nine independent non-dimensional coefficients. The coefficients can be chosen in different ways but those appearing most naturally are the following:

$\alpha = kR$ $\beta_0 = l_0 R,\ \beta = lR$ $\gamma_0 = m_0 p_0,\ \gamma = m p_0$	the non-dimensional wave numbers
$\delta = \frac{\nu}{\Omega}$	the non-dimensional frequency
$\varepsilon = \frac{U_0}{R\Omega}$	the Rossby number (Ro)
$\eta = \frac{U_0^2}{\frac{p_0}{\varrho_0}\frac{\Delta\Theta}{\Theta_0}}$	the inverse Richardson number (Ri^{-1}) [3]
$\sigma = \frac{\Delta\Theta}{\Theta_0}$	the stratification numbe

We do not write out the non-dimensiona equations explicitly but proceed directly t the expansion step.

7. Expansion of the Coefficients *A*, *B* – *I*

We now make the following importan assumptions:

i) The non-dimensional wave numbers ar of the order 1 $(\alpha, \beta_0, \beta, \gamma_0, \gamma \sim 1)$.

ii) The Rossby number and the invers Richardson number are small compare to 1 $(\varepsilon, \eta \ll 1)$.

iii) The theory is restricted to values of th non-dimensional frequency that are smal compared to 1 $(\delta \ll 1)$.

The assumption (i) does not mean that th non-dimensional wave numbers have to b close to 1 but only that they are of order from point of view of the expansion. Th actual limits on the wave numbers is commented on further.

The assumption (iii) concerns our eigenvalue parameter and we do not, of course dispose over this. The assumption is still legitimate but we must check our final result to be sure that we are in the range of validit of our assumptions.

Later on we will confine ourselves to case where the stratification parameter σ takes o relatively small values. In total, we can therefore say that we concern ourselves with th *largest-scale motion* in an atmosphere of *strong rotational constraints, strong dynamic stability* and *weak static stability.*

With these assumptions an expansion of th coefficients A, $B - I$ after δ, ε and η seem possible. In making the expansion one mus keep in mind that nothing has been assumed so far about the relative smallness of δ, ε and η. This is important since different ratios of these three parameters will occur. Care must be taken to keep all terms that can contribute, up to the order we want to consider, when these ratios are varied freely.

---

[3] Usually the Richardson number is defined as $Ri = \frac{\frac{g}{\Theta}\frac{\partial\Theta}{\partial z}}{\left(\frac{\partial U}{\partial z}\right)^2}$. With the hydrostatic assumption we can write this $\frac{\frac{1}{\varrho\Theta}\frac{\partial\Theta}{\partial p}}{\left(\frac{\partial U}{\partial p}\right)^2}$, and as a representative number for th whole atmosphere we may take $Ri \sim \frac{\frac{1}{\varrho_0\Theta_0}\frac{\Delta\Theta}{p_0}}{\frac{u_0^2}{p_0^2}} = \frac{\frac{p_0}{\varrho_0}\frac{\Delta\Theta}{\Theta_0}}{u_0^2}$

After these preliminary remarks we proceed directly to write down the expressions for the coefficients A, $B-I$, retaining only the leading terms:

$$A = -\frac{1}{2\Omega\sin\varphi}\left[1 - \frac{1}{\cos\varphi}U^*\varepsilon + \ldots\right]$$

$$B = -\frac{\varrho_0 U_0}{\frac{\Delta\Theta}{\Theta_0}}\frac{U^*_{p^*}}{4\sin^2\varphi\,\Lambda^*}\left[(\delta+\alpha U^*\varepsilon)^2 + \ldots\right]$$

$$C = \frac{k}{4\sin^2\varphi}\frac{1}{\Omega}\left[\delta + \alpha U^*\varepsilon + \ldots\right]$$

$$D = \frac{-i}{4\sin^2\varphi}\frac{1}{\Omega}\left[\delta + \alpha U^*\varepsilon \ldots\right]$$

$$E = \frac{-i}{2\sin\varphi}\frac{\varrho_0 U_0}{\frac{\Delta\Theta}{\Theta_0}}\left[\delta + \alpha U^*\varepsilon + \ldots\right]$$

$$\begin{aligned} F = {} & \frac{ik}{2\sin\varphi}\frac{1}{\Omega}\left[1 + \left(-\frac{1}{2\cos\varphi}U^* + \right.\right. \\ & \left. + \frac{1}{2\sin\varphi}\beta_0 U^*_{y_*}\right)\varepsilon - \\ & \left. - \frac{U^*_{p^*}}{2\sin\varphi}\frac{1}{\Lambda^*}(\Phi_{yp})^*\eta + \ldots\right] \end{aligned} \tag{25}$$

$$G = \frac{i\varrho_0 U_0}{\frac{\Delta\Theta}{\Theta_0}}\frac{(\Phi_{yp})^*}{\Lambda^*}\frac{1}{4\sin^2\varphi}\left[\delta + \alpha U^*\varepsilon + \ldots\right]$$

$$H = -\frac{i\varrho_0\Omega}{m_0\frac{\Delta\Theta}{\Theta_0}}\frac{1}{\Lambda^*}\left[\delta + \alpha U^*\varepsilon + \ldots\right]$$

$$\begin{aligned} I = {} & -\frac{ik\varrho_0 U_0}{\frac{\Delta\Theta}{\Theta_0}}\frac{(\Phi_{yp})^*}{2\sin\varphi\,\Lambda^*}\left[1 - \frac{1}{\cos\varphi}U^*\cdot\varepsilon - \right. \\ & \left. - \frac{1}{2\sin\varphi}\frac{U^*_{p^*}(\Phi_{yp})^*}{\Lambda^*}\cdot\eta + \ldots\right] \end{aligned}$$

8. Relation between Velocity and Geopotential

Inserting the above expressions for A, $B-I$ in the relations (19) one finds –

$$\begin{aligned} u' = {} & -\frac{1}{2\Omega\sin\varphi}\left\{(1 + \ldots)\frac{\partial}{\partial y^{**}} - \right. \\ & - \left[\frac{\gamma}{2\beta\sin\varphi}\frac{U^*_{p^*}}{\Lambda^*}\frac{\eta}{\varepsilon}(\delta+\alpha U^*\varepsilon)^2 + \ldots\right]\frac{\partial}{\partial p^*} \\ & \left. + \mathrm{o}(\delta,\varepsilon)\right\}\phi' \end{aligned}$$

$$\begin{aligned} v' = {} & \frac{ik}{2\Omega\sin\varphi}\left\{\mathrm{o}(\delta,\varepsilon)\frac{\partial}{\partial y^{**}} - \left(\frac{\gamma}{\alpha}\frac{U^*_{p^*}}{\Lambda}\frac{\delta\eta}{\varepsilon} + \ldots\right)\frac{\partial}{\partial p^{**}}\right. \\ & \left. + 1 + \ldots\right\}\phi' \end{aligned} \tag{26}$$

$$\begin{aligned} \omega' = {} & -\frac{i\varrho_0\Omega}{\frac{\Delta\Theta}{\Theta_0}}\left\{\mathrm{o}(\varepsilon\delta,\,\delta^2)\frac{\partial}{\partial y^{**}} + \right. \\ & + \left[\frac{\gamma}{\gamma_0}\frac{1}{\Lambda^*}(\delta+\alpha U^*\varepsilon) + \ldots\right]\frac{\partial}{\partial p^{**}} - \\ & \left. - \alpha\frac{U^*_{p^*}}{\Lambda^*}\varepsilon + \ldots\right\}\phi' \end{aligned}$$

In the expression for ω' use has been made of the relation

$$(\Phi_{yp})^* = -2\sin\varphi\, U^*_{p^*} + \mathrm{o}(\varepsilon) \tag{27}$$

(thermal wind)

One sees that the geostrophic approximation, in which the horizontal Coriolis force and pressure gradient balance, becomes good if $\delta\eta \ll \varepsilon$, i.e., the atmosphere should have a strong dynamic stability but not too strong rotational constraint! It becomes better for smaller frequencies and is certainly good for the stationary waves, to the present order of approximation. Since $\frac{\delta}{\varepsilon} \sim \frac{c}{U_0}$ for the longest waves, where c is the wave speed, we can also express it so that the geostrophic approximation is good when the ratio of the wave speed to the speed of the basic zonal current is small compared to the Richardson number. For the real atmosphere this condition is mostly satisfied. It may be of interest to note that in the case when the geostrophic approximation becomes invalid, the deviation becomes larger for v' than for u'.

Computing the divergence $D = \frac{\partial u'}{\partial x} + \frac{\partial v'}{\partial y} - \frac{\operatorname{tg}\varphi}{R} v'$ and the vertical component of vorticity $Z = \frac{\partial v'}{\partial x} - \frac{\partial u'}{\partial y} + \frac{\operatorname{tg}\varphi}{R} u'$ one verifies easily that these are of the same order, while in several earlier studies it has been assumed that $D \ll Z$. The fact that D and Z should be of the same order for the largest scales of motion in the atmosphere has already been pointed out by Burger (1959).

9. Wave Equation

Inserting the expanded expressions $A, B - I$ in the wave equation (20) one finds

$$\begin{aligned}
&\Big\{ o(\delta, \varepsilon) \frac{\partial^2}{\partial y^{**2}} + o(\eta) \frac{\partial^2}{\partial y^{**} \partial p^{**}} + \\
&+ \left[\frac{\gamma}{\gamma_0^2} \frac{1}{\Lambda^*} \left(\frac{\delta\eta}{\varepsilon^2} + \alpha U^* \frac{\eta}{\varepsilon} \right) + \ldots \right] \frac{\partial}{\partial p^{**2}} + \\
&+ \left[\frac{\beta\gamma_0}{2 \sin\varphi} \left(\frac{U^*_{p^*}}{\Lambda^*} \right)_{p^*} \cdot \frac{\delta\eta}{\varepsilon} + \ldots \right] \frac{\partial}{\partial y^{**}} + \\
&+ \Big[\gamma_0 \left(\frac{1}{\Lambda^*} \right)_{p^*} \left(\frac{\delta\eta}{\varepsilon^2} + \alpha U^* \frac{\eta}{\varepsilon} \right) + \\
&+ \left(\frac{\beta_0}{2 \sin\varphi} \left(\frac{U^*_{p^*}}{\Lambda^*} \right)_{y^*} - \frac{\cos\varphi}{2 \sin^2\varphi} \frac{U^*_{p^*}}{\Lambda^*} \right) \\
&\frac{\delta\eta}{\varepsilon} + \ldots \Big] \frac{\partial}{\partial p^{**}} + \alpha \frac{\cos\varphi}{2 \sin^2\varphi} - \\
&- \alpha\gamma_0 \left(\frac{U^*_{p^*}}{\Lambda^*} \right)_{p^*} \frac{\eta}{\varepsilon} + \frac{\alpha\gamma_0}{2 \sin\varphi} \left(\frac{U^*_{p^*}}{\Lambda^*} \right)_{p^*} \cdot \\
&\cdot \frac{\eta^2}{\varepsilon} + \ldots \Big\} \phi' = 0 \qquad (28)
\end{aligned}$$

All terms that can become of order 1 or more are retained. The first thing to note is that the $\frac{\partial^2}{\partial y^{**2}}$- and $\frac{\partial^2}{\partial y^{**} \partial p^{**}}$ - terms are small. The $\frac{\partial}{\partial y^{**}}$ - term is small if $\delta\eta \ll \varepsilon$. If $\delta\eta \geq \varepsilon$ it is of order one or more but it would certainly be small compared to the $\frac{\partial^2}{\partial p^{**2}}$ - and $\frac{\partial}{\partial p^{**}}$ – terms. To the first order the y-derivatives disappear thus from the problem and y can be treated parametrically. This means, in physical terms, that the behaviour of the long waves is determined essentially by the vertical and not the horizontal structure of the atmosphere.

The goodness of the first approximation depends, of course, on the actual values of δ, ε, η and the non-dimensional wave-numbers. Inspecting (28) it seems as if the first approximation may hold equally well for the higher zonal and vertical modes while the higher meridional modes obviously bring in the $\frac{\partial}{\partial y^{**}}$-term. However, we can only judge the tendency from (24), for when the wave-numbers get large enough to change the order of the terms the whole expansion breaks down and other terms in the coefficients A, – – I take over.

Once we have made the comparison between the different terms and decided which terms should enter in the first approximation we can, of course, change the vertical scaling as we like. Since our main interest is in the basic vertical mode it seems convenient to choose p_0 as vertical scale and put $p^{**} = p^* = \frac{p}{p_0}$, $\gamma = \gamma_0 = 1$. Further, we write

$$\frac{\delta}{\alpha\varepsilon} = \frac{\nu}{kU_0} = - \frac{c}{U_0} = - c' \qquad (29)$$

where c' is the ratio of the wave speed c and the speed of the current U_0. The negative sign is chosen to make the wave velocity positive for eastward moving waves (these correspond to negative frequencies).

Considering only the leading terms in (28), in accordance with our previous analysis, we have then

$$\begin{aligned}
&(U^* - c') \frac{\partial}{\partial p^*} \left(\frac{1}{\Lambda^*} \frac{\partial \phi'}{\partial p_*} \right) + \\
&+ \left[\frac{1}{2} \frac{\cos\varphi}{\sin^2\varphi} \frac{\varepsilon}{\eta} - \left(\frac{U^*_{p^*}}{\Lambda^*} \right)_{p^*} \right] \phi' = 0 \qquad (30)
\end{aligned}$$

The only physical parameter entering this equation is $\frac{\varepsilon}{\eta}$, i.e., the product of the Rossby and the Richardson numbers. It is seen the zonal wave number, after introducing the wave speed, has dropped out of the equation.

10. Boundary Conditions

The expanded form of the boundary conditions is –

$$\frac{1}{Q^* \Lambda^*} (\delta + \alpha U^* \varepsilon) \frac{\partial \phi'}{\partial p^*} =$$

$$= \left(\frac{\alpha U^*_{p^*}}{Q^* \Lambda^*} \varepsilon - \frac{\Delta \Theta}{\Theta_0} \cdot \delta \right) \phi' \quad \text{at } \Phi = 0$$

$$\phi' < \infty \quad \text{at } p^* = 0 \tag{31}$$

Here use has been made of the relations

$$\Phi_y = -2\Omega \sin\varphi \, U(1 + o(\varepsilon)),$$

$$\Phi_p = -\frac{1}{Q}, \; Q^* = \frac{Q}{\varrho_0}$$

Now, the meridional variation of the basic pressure at the ground is given by $\frac{\partial p}{dy} = -2\Omega$ $\sin\varphi \, \varrho_0 U_{z=0}(1 + o(\varepsilon))$. $U_{z=0}$ is normally small but in a general case we should assume it to be of order U_0. The total meridional variation of the pressure will then be of the order $R\Omega\varrho_0 U_0$ or $\frac{M^2}{\varepsilon}$ p_0, where M is the Mach number or the Froude number). The relative variation becomes small and we may then replace the surface $\Phi = 0$ by the surface $p = p_0$, if $M^2 \ll \varepsilon$, i.e., if the Mach number square is small compared to the Rossby number. This condition is normally satisfied.

The stratification number $\sigma = \frac{\Delta\Theta}{\Theta_0}$ is relatively small for the real atmosphere. One may therefore feel justified in dropping the terms proportional to this parameter in (31). In this case, the boundary conditions, after introducing the wave speed c', could be written –

$$(U^* - c') \frac{\partial \phi'}{\partial p^*} = U^*_{p^*} \phi' \quad \text{at } p^* = 1$$

$$\phi' < \infty \quad \text{at } p^* = 0 \tag{32}$$

The first condition in (33) is equivalent to $\omega = 0$ at $p^* = 1$, which condition has been used in many earlier investigations. A more precise analysis of the error contained in this approximation will be given later.

11. Justification of the Expansion

The validity of the previous expansion of the coefficients A, $B - I$ will depend on the actual smallness of the parameters δ, ε, and η. To get an estimate of these we start out from the following basic figures:

$R \simeq 6.4 \cdot 10^6$ m, $\Omega \simeq 7.3 \cdot 10^{-5}$ s^{-1}, $p_0 \simeq 10^5$ kg m^{-1} s^{-2}, $\varrho_0 \simeq 1.3$ kg m^{-3}. The vertical variation of the potential temperature over the main part of the atmosphere seems to lie in the range 30—60° A, and thus we put $\sigma \simeq 0.1$—0.2. We assume the period of the waves to be at least, say, 10 days and range up to infinity for the purely stationary waves. With these values the non-dimensional parameters of interest are estimated for three different amplitudes of the zonal current, $U_0 = 5$, 15 and 25 ms^{-1}:

Table 1. Numerical values of the characteristic parameters

	δ	ε	η	σ	M	$\frac{\delta}{\varepsilon}$	$\frac{\eta}{\varepsilon}$	$\frac{\delta\eta}{\varepsilon}$	$\frac{M^2}{\varepsilon}$
$U_0 = 5$ ms^{-1} . . .	0—0.1	0.01	0.002—0.004	0.1—0.2	0.02	0—10	0.2—0.4	0—0.04	0.04
$U_0 = 15$ ms^{-1} . . .	0—0.1	0.04	0.02—0.04	0.1—0.2	0.06	0—3	0.5—1	0—0.01	0.1
$U_0 = 25$ ms^{-1} . . .	0—0.1	0.06	0.05—0.1	0.1—0.2	0.1	0—2	1—2	0—0.2	0.2

With δ, ε and η in the above ranges the expansion is convergent and the first approximation is reasonably good, provided we limit ourselves to the basic mode in the vertical and to wave numbers less than 5—6 in the horizontal (corresponding to a wave length of 6,000—8,000 km). For the higher modes in the vertical the wave lengths must be more than 10,000 km to make the expansion valid.

The fact that $\frac{\eta}{\varepsilon}$ comes out so close to 1 indicates a balance between all the terms retained in the wave equation (30). The numbers $\frac{M^2}{\varepsilon}$

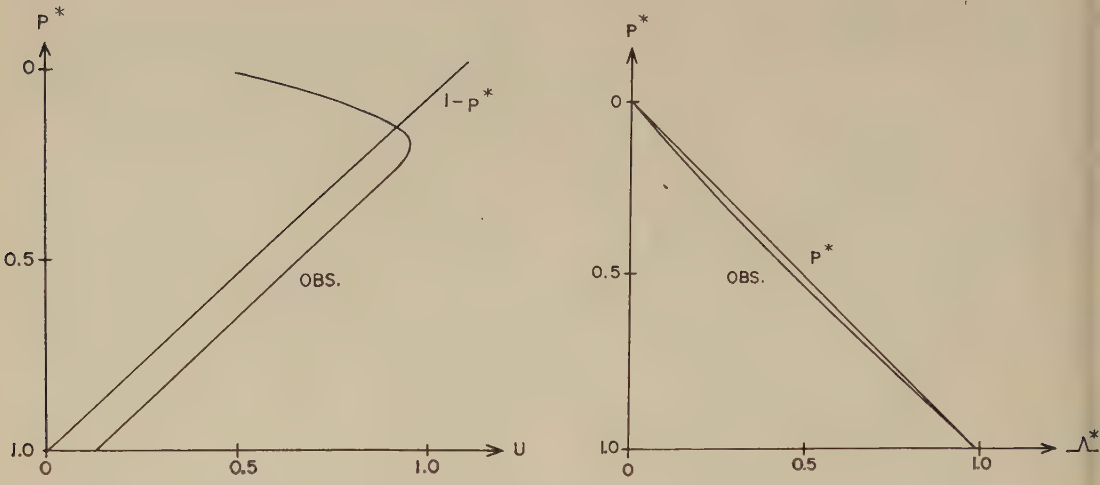

Fig. 2. Assumed and observed profiles for U^* and Λ^{*-1}. Observations in winter at 50° N.

and σ seem to be small enough to give us some confidence in the simplified boundary condition (33). The smallness of $\frac{\delta\eta}{\varepsilon}$, finally, confirms the idea of a close geostrophic balance of the long waves.

12. An approximate solution for the case $U^* = 1 - p_0^*, \Lambda^* = p^{*-1}$

It has so far not been found possible to derive solutions valid over the whole sphere. One can, however, derive solutions that corresponds to the so-called β-plane solutions constructed in many earlier theories. As pointed out later the β-plane derivation yields, to the first order, the same wave equation as derived here. Equation (30) has simply to be replaced by

$$(U^* - c')\frac{\partial}{\partial p^*}\left(\frac{1}{\Lambda^*}\frac{\partial\phi'}{\partial p^*}\right) + \left[R\Omega\frac{\beta}{f^2}\frac{\varepsilon}{\eta} - \left(\frac{U^*_{p^*}}{\Lambda^*}\right)_{p^*}\right]\phi' = 0 \qquad (30\,a)$$

where f is the Coriolis parameter and β is the meridional variation of this parameter, respectively. In the β-plane approximation these are treated as constants.

As one simple case we make now the basic wind and potential temperature be linear functions of p. The wind is assumed to be zero at the ground, but one can of course always superimpose uniform currents (this will only correspond to a slight change in ε and η, and in the bottom boundary condition). The normalized profiles are

$$U^* = 1 - p^*$$
$$\Lambda^* = p^{*-1}$$

The variation of Λ inversely to the pressure is due to the appearance of the density in the denominator. To our degree of approximation we can put the density proportional to the pressure.

As an example, we show profiles for U^* and Λ^{*-1} computed from atmospheric data (mean winter condition at 50° N) and according to the assumed laws – (Fig. 2).

In the present case equation (30) reduces to the form

$$(1 - c' - p^*)\frac{\partial}{\partial p^*}\left(p^*\frac{\partial\phi'}{\partial p^*}\right) + \left(1 + \frac{R\Omega\beta}{f^2}\frac{\varepsilon}{\eta}\right)\phi' = 0 \qquad (34)$$

The boundary conditions become

$$c'\frac{\partial\phi'}{\partial p^*} = \phi^* \quad \text{at } p^* = 1 \qquad (35)$$
$$\phi' < \infty \qquad \text{at } p^* = 0$$

(34, 35) formulates an eigen-value problem with c' as the eigen-value parameter. c' is assumed to be real (neutral waves). The assumption that the (non-dimensional) frequency is small should not be interpreted as a condition that c' is small, it merely requires that $c' \ll \varepsilon^{-1}$.

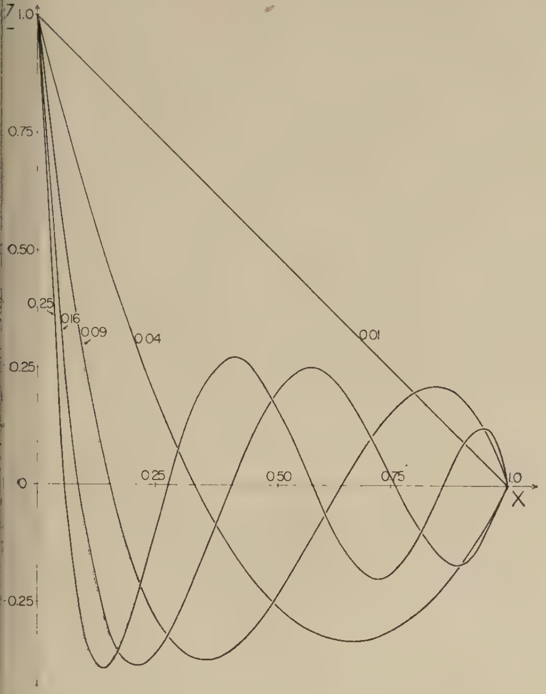

Fig. 3. Profiles of the stationary waves. The horizontal coordinate is ξ.

It has been found advantageous to transfer the eigen-value parameter to the boundary condition, by introducing the new independent variable

$$\xi = \frac{p^*}{1 - c'} \tag{36}$$

For the sake of simplicity we introduce further

$$Z = \phi', \quad \lambda = 1 + \frac{\beta}{f^2} \frac{\varepsilon}{\eta} \tag{37}$$

Finally, with γ entering only parametrically, we may replace all partial derivatives by total derivatives. (34, 35) then take on the form

$$(1 - \xi) \frac{d}{d\xi} \left(\xi \frac{dZ}{d\xi} \right) + \lambda Z = 0 \tag{38}$$

$$\begin{aligned} \frac{dZ}{d\xi} &= \frac{1 - c'}{c'} Z \quad &\text{at } \xi = \frac{1}{1 - c'} \\ Z &< \infty \quad &\text{at } \xi = 0 \end{aligned} \tag{39}$$

Equation (38) is of hypergeometric type. It has singularities at $\xi = 0$ and 1. Solutions that remain finite throughout the interval $0 \leq \xi \leq 1$ are found when $\lambda = n^2$, $(n = 0, 1, 2 \ldots)$. These will be eigen-solutions for the stationary waves. They are all polynomials. The first few are listed below:

$$\begin{aligned} Z_0 &= 1 \\ Z_1 &= 1 - \xi \\ Z_2 &= 1 - 4\xi + 3\xi^2 \\ Z_3 &= 1 - 9\xi + 18\xi^2 - 10\xi^3 \\ Z_4 &= 1 - 16\xi + 60\xi^2 - 80\xi^3 + 35\xi^4 \\ Z_5 &= 1 - 25\xi + 150\xi^2 - 350\xi^3 + 350\xi^4 - 126\xi^5 \end{aligned} \tag{40}$$

Graphs of these are seen in Fig. 3.

When λ is different from an integer square travelling waves do occur. These move very slowly compared to the Rossby waves. The wave speed and the vertical profile of the waves can be found as follows. For all values of λ the solution regular at $\xi = 0$ is given by

$$Z = 1 - \lambda\xi - \lambda \frac{1 - \lambda}{4} \xi^2 - \lambda \frac{1 - \lambda}{4} \frac{\lambda - 4}{9} \xi^3 + \ldots \tag{41}$$

The series can be used for $\xi < 1$. By (41) Z has been computed for different values of ξ and λ and the manifold of solutions has been constructed (Fig. 4). Points have then been sought at which the curves of solution are tangent to a straight line through $(+1, 0)$. If ξ_0 is the abscissa for such a point, the value of c' is found from the relation $\xi = \frac{1}{1 - c'}$, and the eigen-solution is represented by the part of the curve from $\xi = 0$ to ξ_0 (Fig. 5). The procedure is easily understood if we note that the condition $\frac{dZ}{d\xi} = \frac{1 - c'}{c'} Z$ integrates to $Z = \text{const.}\ (\xi - 1)$ if use is made of the above relation between ξ and c'. The wave speed can be directly read as a function of λ in Fig. 6.

13. Influence of σ in the Boundary Condition

Of the approximations made the most serious one may be the neglect of terms proportional to $\sigma \left(= \frac{\Delta \Theta}{\Theta_0} \right)$ in the boundary condition.

Retaining these terms the condition replacing (35) is –

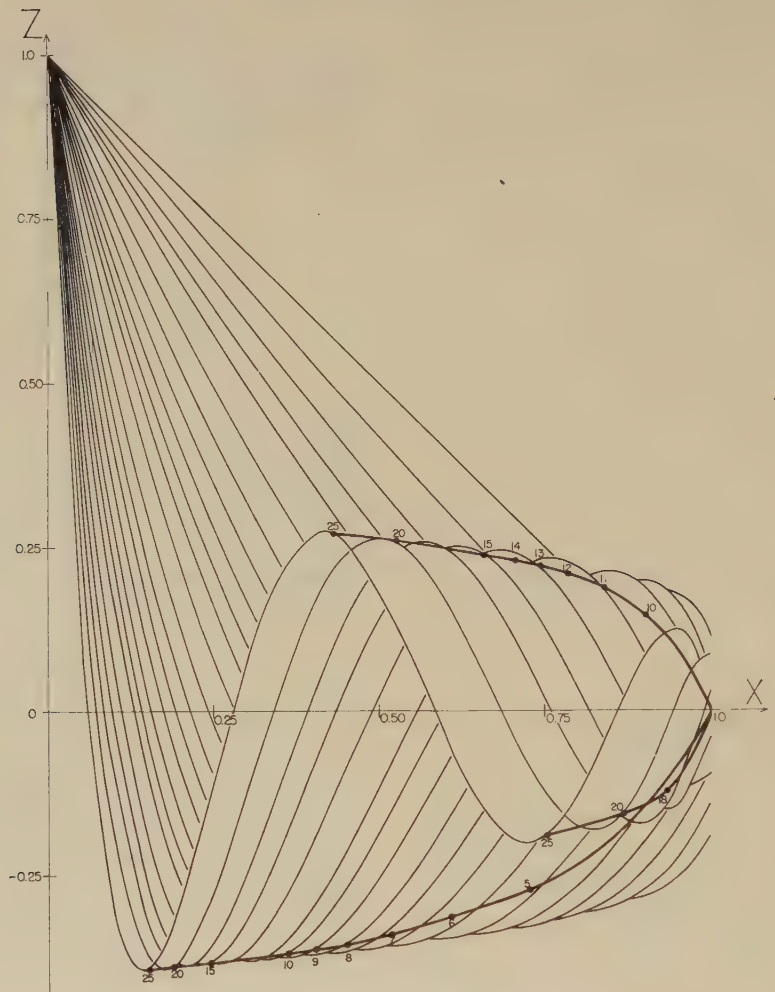

Fig. 4. The manifold $Z(\xi, \lambda)$. The horizontal coordinate is ξ.

$$\begin{aligned} c' \frac{\partial \phi'}{\partial p^*} &= (1 - c'\sigma)\phi' \quad &\text{at } p^* = 1 \\ \phi' &< \infty \quad &\text{at } p^* = 0 \end{aligned} \qquad (42)$$

or transformed to the new variables

$$\begin{aligned} \frac{dZ}{d\xi} &= \frac{(1 - c')(1 - \sigma c')}{c'} Z \quad \text{at } \xi = \frac{1}{1 - c'} \\ Z &< \infty \quad \text{at } \xi = 0 \end{aligned} \qquad (43)$$

In the stationary case ($c' = 0$) the condition is the same as (39). In the case of travelling waves the condition differs but there is little difficulty to extend the previous analysis to this case. The graphical method functions again but the straight lines have now to be replaced by the family of curves $Z = \text{const.} \dfrac{\xi - 1}{\xi^{\sigma}}$. The resulting wave speeds have been computed for $\sigma = 0.2$ and the result is shown in Fig. 7. One verifies that little is changed for stationary or slowly moving waves.

14. Difference between the Spherical and β-Plane Coordinates

Using the β-plane coordinates and repeating the derivations of Section II—V a different

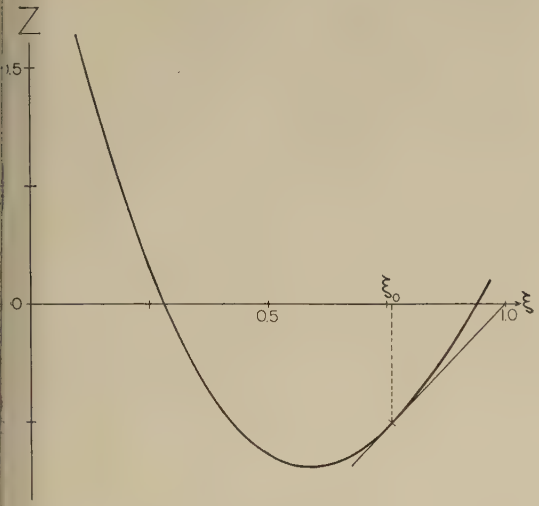

Fig. 5. Construction for the travelling waves $\left(\xi_0 = \frac{1}{1-c'}\right)$.

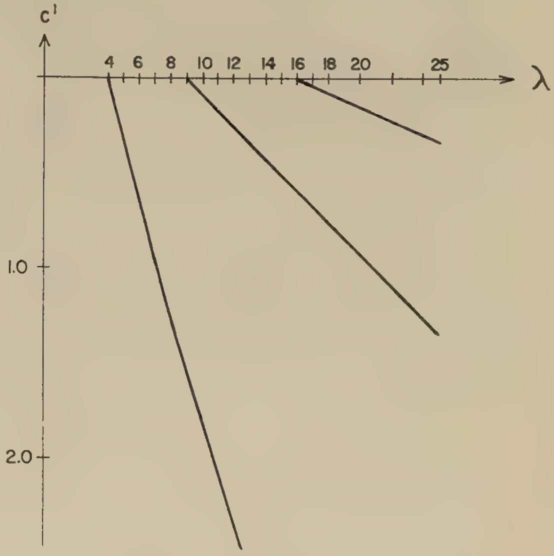

Fig. 6. c' as function of λ.

set of equations arise. However, making the same non-dimensionalization and expansion as before, the first order wave equation agrees with equation (30). Thus, the main spherical effect seems to be contained in the β-term. This result is, however, a special one, and one should not be led to the conclusion that the β-plane coordinates generally work correctly for the largest scales of motions in the atmosphere. A closer analysis shows that the β-plane can be used only when the meridional coupling of the waves is slight, and the perturbation motion is closely geostrophic. Both these conditions are met with in our first order theory.

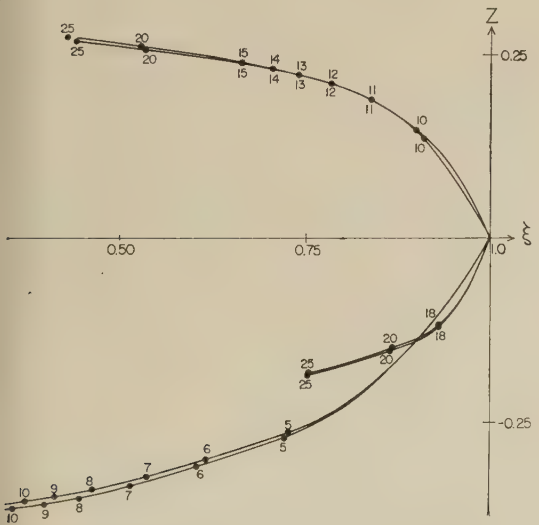

Fig. 7. Influence of σ on ξ_0. The curves represent the two cases $\sigma = 0$ and $\sigma = 0.2$.

It may be of value to give the specific rules of computation that should be added in a β-plane analysis to make this a true spherical analysis. Subject only to our general assumptions in Section 3, the rules turn out to be the following –

i) In the equations of motion the Coriolis parameter f should be replaced by $f + \frac{\operatorname{tg}\varphi}{R}u$.

ii) In the continuity equation the term $\frac{\partial v}{\partial y}$ should be replaced by $\frac{\partial v}{\partial y} - \frac{\operatorname{tg}\varphi}{R}v$

The operators $\frac{\partial}{\partial x}$ and $\frac{\partial}{\partial y}$ do not commute but follow the rule

$$\frac{\partial^2}{\partial y \partial x} = \frac{\partial^2}{\partial x \partial y} + \frac{\operatorname{tg}\varphi}{R}\frac{\partial}{\partial x}$$

(When wave numbers are introduced, the meridional wave number becomes accordingly a function of y).

iii) Not only f but also β (and what higher y-derivatives of f that occur) should be considered functions of y. At the end one introduces $f = 2\Omega \sin\varphi$ $\beta = \frac{2\Omega}{R}\cos\varphi$, etc.

As one simple example, we compute the divergence of the geostrophic wind by the two methods. In the β-plane as well as in the spherical case the geostrophic equations are, by definition,

$$\begin{aligned} -fv &= -\frac{\partial\phi}{\partial x} \\ fu &= -\frac{\partial\phi}{\partial y} \end{aligned} \tag{44}$$

The expressions for the divergence (D) are however, formally different. In the β-plane we have $D = \frac{\partial u}{\partial x} + \frac{\partial v}{\partial y}$ and insertion of (44) gives

$$D = -\frac{\beta}{f^2}\frac{\partial\phi}{\partial x} \tag{45}$$

In the spherical case we have

$D = \frac{\partial u}{\partial x} + \frac{\partial v}{\partial y} - \frac{\operatorname{tg}\varphi v}{R}$. Inserting (44) gives –

$$\begin{aligned} D = \frac{1}{f}\left(\frac{\partial^2}{\partial y \partial x} - \frac{\partial^2}{\partial x \partial y}\right)\phi - \frac{\beta}{f^2}\frac{\partial\phi}{\partial x} - \\ -\frac{\operatorname{tg}\varphi}{R}\frac{1}{f}\frac{\partial\phi}{\partial x} = -\frac{\beta}{f^2}\frac{\partial\phi}{\partial x} \end{aligned} \tag{46}$$

where the rule (ii) has been applied. Thus the results are identical. From point of view of the spherical analysis the success of the β-plane computation can be considered as the cancellation of two errors: the term $\frac{-\operatorname{tg}\varphi}{R}v$ is neglected in the divergence but at the same time we force a commutation of $\frac{\partial}{\partial x}$ and $\frac{\partial}{\partial y}$. Obviously the outcome of the two methods will not be the same when we have a general non-geostrophic motion and the one obtained from the spherical analysis has, of course, to be considered as the more correct one.

15. Some Comments on the Problem of Numerical Weather Prediction

In the attempts to make numerical weather predictions the difficulty of getting a correct movement of the very long waves have been noticed. In these computations the starting point is usually the vorticity equation. This equation reads –

$$\begin{array}{ccccc} \dfrac{\partial Z}{\partial t} & +u\dfrac{\partial Z}{\partial x} & +v\dfrac{\partial Z}{\partial y} & +w\dfrac{\partial Z}{\partial p} & +ZD \\ \mathrm{o}(\delta) & \mathrm{o}(\varepsilon) & \mathrm{o}(\varepsilon) & \mathrm{o}\left(\eta, \dfrac{\delta\eta}{\varepsilon}\right) & \mathrm{o}\left(\eta, \dfrac{\delta\eta}{\varepsilon}\right) \end{array}$$

$$\underbrace{\underset{\mathrm{o}(1)}{+fD} + \underset{\mathrm{o}(1)}{\beta v}}_{\left(\mathrm{o}\left(\delta, \varepsilon, \frac{\delta\eta}{\varepsilon}\right)\right)} + \underset{-}{\frac{\partial\omega}{\partial x}\frac{\partial v}{\partial p}} - \underset{\mathrm{o}\left(\eta, \frac{\delta\eta}{\varepsilon}\right)}{\frac{\partial\omega}{\partial y}\frac{\partial u}{\partial p}} = 0 \tag{47}$$

Inserting the expressions for u', v', ω' from (26) in the linearized form of (47) we can estimate the order of the different terms. These orders, apart from a common factor $R^{-2}\phi'$, are written under the equation (47). From the point of view of our theory, the only term that can be safely neglected is $\frac{\partial w}{\partial x}\frac{\partial v}{\partial p}$ (it does not occur at all in the linearized theory). fD and βv are both of order 1 but $fD + \beta v$ is of order $\mathrm{o}\left(\delta, \varepsilon, \frac{\delta\eta}{\varepsilon}\right)$. Since δ, ε and η may be of the same order all the other terms have then to be retained. This is in accordance with the analysis of Burger (1958).

The fact that the divergence term and the β-term balance out, to the first order, will of course not in itself display the quasi-stationary character of the longest waves. The motion of the waves is now determined by higher order terms, but whether or not they become quasi-stationary cannot be decided merely by inspecting the vorticity equation. For one thing, the boundary conditions have to be considered.

The barotropic model states the conservation of absolute vorticity: $\frac{d}{dt}(Z+f) = 0$. This case is obtained from (47) by putting $\frac{\partial}{\partial p} = 0$, $D = 0$. This is not a consistent approximation for the very long waves. In this case the β-term alone is of order 1 and our first order theory gives only the result $v' = 0$. In fact, a more consistent approximation would be to conserve the relative vorticity: $\frac{dZ}{dt} = 0$, i.e., neglect completely the effect of earth's rotation in the vorticity equation. In this case, of course, both the divergence and the β-term disappear.

In the derivation of the wave equation directly from the equations of motion, the continuity equation and the adiabatic equation the difficulty of cancelling first order does not occur. Thus, one may try to construct a scheme for numerical prediction for the largest scales of motion along a similar line. The equation used for the actual time-integration should then be the adiabatic equation. This equation would give a prediction of the potential temperature and thus through the hydrostatic equation also of the geopotential, if initial geopotential and velocity fields are known. To make a new time-step one has then to determine the new velocity field. For this, one has at one's disposal, the continuity equation and the two horizontal equations of motion.

In the first approximation, these equations of motion would be the geostrophic wind equations, but one would probably like to go one step further. One should still be able to treat the motion as balanced, i.e., merely solve for a steady state flow under the given pressure forces. The computation of the vertical velocity by help of the continuity equation is not critical in the case of the largest scales of motion, for the divergence will then be comparable to the individual terms in the continuity equation.

Acknowledgements

The author wants to acknowledge the valuable help given by Dr. B. Bolin and Dr. N. Phillips in discussions of the present problem.

Thanks are further due to Mrs. M. Thayer, Mrs. B. Curl and Mrs. M. Brown for the technical help. The work was performed under the auspices of the National Science Foundation.

REFERENCES

Burger, A. P., 1958: Scale consideration of planetary motions of the atmosphere, *Tellus* **10**, No. 2, pp. 195—205.

Charney, J., 1947: The dynamics of long waves in a baroclinic westerly current, *J. Meteor.* **1**, No. 1, pp. 135—162.

Eady, E., 1949: Long waves and cyclone waves, *Tellus* **1**, No. 3, pp. 33—52.

Eliassen, A., 1949: The quasistatic equations of motion with pressure as independent variable. *Geofysiska Publ.* **17**, No. 3, pp. 1—44.

Fjørtoft, R., 1950: Application of integral theorems in deriving criteria of stability for laminar flows and for the baroclinic circular vortex. *Geofysiska Publ.* **17**, No. 6, pp. 1—52.

Haurwitz, B., 1940: The motion of atmospheric disturbances, *J. Marine Res.* Vol. **3**, pp. 35—50.

Holmboe, J., 1953: *The Upper Level Winds Project*, Final Report GRD, Air Force Cam bridge Res. Centre, Cambridge, Mass.

Kuo, H. L., 1952: Three-dimensional disturbances in a baroclinic zonal current. *J. Meteor.* **9**, pp. 260—278.

Rossby, C. G., 1939: Relation between variations in intensity of the zonal circulation of the atmosphere and the displacement of the semipermanent centers of action, *J. Marine Res.* Vol. **2**, pp. 38—55.

Thompson, P. D., 1953: On the theory of large-scale disturbances in a two-dimensional baroclinic equivalent of the atmosphere, *Quart. J. Roy. Meteor. Soc.*, **79**, No. 339, pp. 51—69.

PRINTED IN SWEDEN
ESSELTE, STHLM 61

Contribution No. 1158

Reprinted for private circulation from
THE JOURNAL OF GEOLOGY
Vol. 69, No. 5, September 1961
Copyright 1961 by the University of Chicago
PRINTED IN U.S.A.

BEACH CHANGES BASED ON DAILY MEASUREMENTS OF FOUR CAPE COD BEACHES[1]

JOHN M. ZEIGLER[2] AND SHERWOOD D. TUTTLE[3]

ABSTRACT

This is a descriptive report. It presents hundreds of beach profile measurements—many taken daily. Measurements are given in graphic form. The data are processed to show daily changes in the volumes of the beaches studied and daily changes of cut or fill at points across the beaches.

During the span of a year or two the beach surface will oscillate within an eight to ten foot vertical envelope as cut and fill occurs along the beach profile. The foreshore may approach 150 feet in width or be less than 50 feet wide.

Daily net fluctuations of cut and fill are different for different parts of the beach. Daily net fluctuations are greatest near low water and the mid-foreshore, being 0.2 and 0.3 feet there. Although numerical data in the nearshore zone are scant, the writers believe that cut and fill is similar to the foreshore and mean low water zones. Maximum variation is perhaps less because at times the entire covering of sand is removed and erosion of the underlying fluvioglacial deposits does not take place as fast as that of the loose sand on the beach.

INTRODUCTION

For those whose work may bring them to a beach, as well as those who come to beaches for pleasure, the single most important fact about a beach is that it is undergoing continual change. Gilbert (1890) defined a beach as "the zone occupied by shore-drift in transit." Johnson emphasized that beach deposits are in more or less active transit (1919, p. 162), and Cuchlaine A. M. King writes in a recent textbook, "A beach is one of the most variable of landforms; it can be there one day and gone the next." She continues: "Beach changes can be measured over an interval of relatively short duration, unlike many other geomorphic processes. The difficulty arises because the observations, under the conditions in which the changes are most rapid, are by no means easy to make. The complexity of the forces causing the beach changes is another major difficulty; it is this that makes the mechanism of the detailed processes causing beach movement so little understood" (King, 1959, p. 1). We can only agree most wholeheartedly. The graphs and numbers derived from daily measurements of four beaches on Outer Cape Cod presented in this report substantiate all the above statements and, in addition, provide a basis for quantitative description.

A program of beach investigations was carried out by personnel of the Woods Hole Oceanographic Institution under the sponsorship of the Geography Branch of the Office of Naval Research. During this time reports of several aspects of the geomorphology, sedimentation, and hydrodynamics have been published (Zeigler and Ronne, 1957; Miller and Zeigler, 1958*a;* Miller and Zeigler, 1958*b;* Zeigler and Ronne, 1958; Miller and Zeigler, 1959; and Zeigler, Hayes, and Tuttle, 1959). In addition, thirteen unpublished status reports were prepared for ONR Geography Branch.

Measurements of topographic changes on Cape Cod beaches began in August, 1953, at Nauset (Orleans), Highland, Race Point, Sandy Neck (Barnstable), and Duxbury. In the beginning the beaches were surveyed about once a month using a dory on the seaward ends of the lines. Subsequently, measurements were made at more frequent intervals on land only, with Duxbury and Sandy Neck being dropped. During the spring and summer of 1957 daily measurements at every other low tide were made at Highland and High Head (fig. 1). During winter and spring of 1958 measurements were made daily at four beach areas: New Beach, Race Point, High Head, and Highland. These four areas were selected because they could all be more or less easily reached by roads, and they were close enough together so that they could be visited consecutively within a few hours. Also, they represented a variety of settings and orientations (see table 1).

---

[1] Contribution No. 1158 from the Woods Hole Oceanographic Institution. Manuscript received December 27, 1960.

[2] Woods Hole Oceanographic Institution, Woods Hole, Massachusetts.

[3] State University of Iowa, Iowa City, Iowa.

New Beach and Race Point study areas can be located on the U.S. Geological Survey Provincetown quadrangle (7½ minute sheet, surveyed 1941). New Beach was measured at the north end of the improved public beach which is located at the west end of a new major divided highway (U.S. Highway 6) some two miles west of Provincetown. The water immediately offshore at New Beach is called Herring Cove. The Race Point area is located about 1,000 yards west along the beach from the Race Point Coast Guard Station.

High Head and Highland areas are shown on the U.S. Geological Survey, North Truro quadrangle (7½ minute sheet, surveyed 1941–42). High Head is located 500 yards

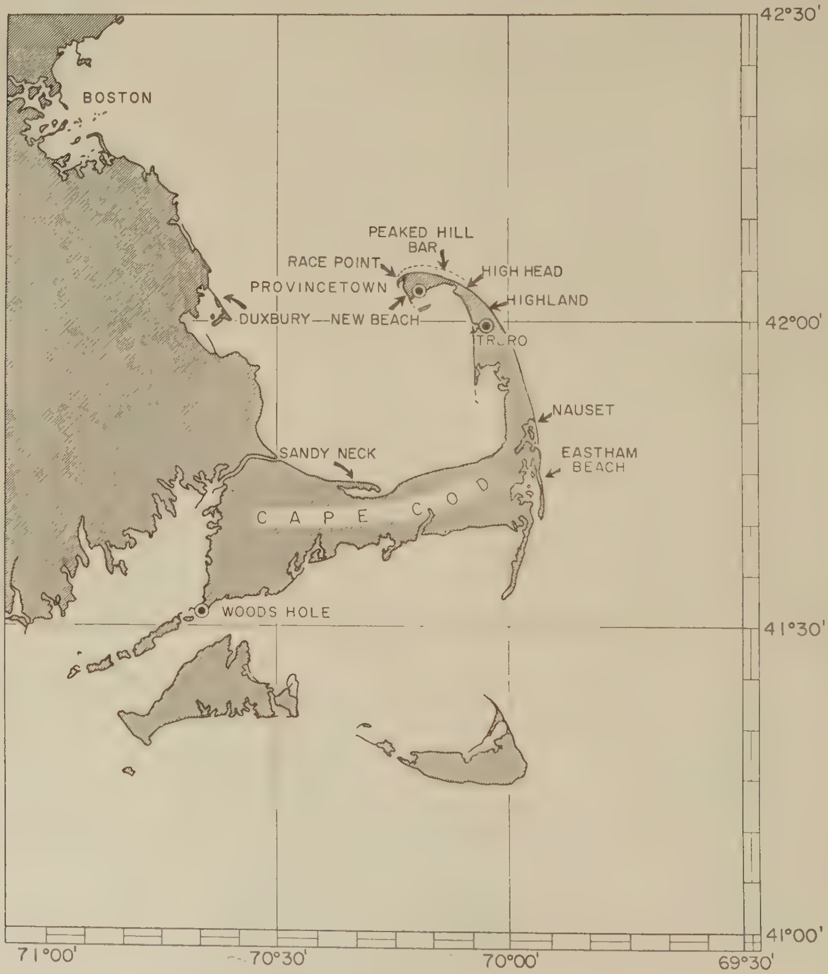
BOSTON
PEAKED HILL BAR
RACE POINT
HIGH HEAD
PROVINCETOWN
HIGHLAND
DUXBURY
NEW BEACH
TRURO
NAUSET
EASTHAM BEACH
SANDY NECK
CAPE COD
WOODS HOLE
42°30'
42°00'
41°30'
41°00'
71°00'
70°30'
70°00'
69°30'

Fig. 1.—Index map, Cape Cod and beaches studied

north of the High Head Coast Guard Station, now abandoned. It can be reached by an unimproved road from Highway 6 along the south side of Pilgrim Lake. The Highland site is located about 150 yards southeast of the Highland Coast Guard Station, also abandoned. It is about 1,200 yards northwest along the cliffs from the Cape Cod Lighthouse. The Highland area can be reached by paved road which ends at a parking lot at Highland. Precise locations at all profile lines can be obtained from Woods Hole.

Table 1 (in part after Zeigler, Hayes, and Tuttle, 1959) shows some of the geographic factors that are involved in analyzing changes on the beaches studied.

At this point we should note some basic differences between the profile areas (see table 1 and fig. 1). They face different directions and therefore would not be expected to react in the same way to the same sea conditions. Waves are highest at Highland and lowest at New Beach. High Head is directly in the lee of Peaked Hill Bar, and Race Point, in the lee of the same bar, is also at the terminus of this bar where things are changing rapidly. We believe this accounts in part for the abrupt day-to-day changes at Race Point.

The ranges of the tide on Outer Cape Cod are given in the Tide Tables as follows: Provincetown, mean 9.1′, spring 10.6′; Race Point, mean 9.0′, spring 10.4′; Cape Cod Lighthouse, mean 7.6′, spring 8.8′ (Coast and Geodetic Survey, 1960, p. 202) (see fig. 1). The data used in this paper involves a total of 834 measured profiles distributed as follows:

Location	Profiles	Date
Highland.........	335	Dec., 1956; Jan.–Oct., 1957; Jan.–May, 1958
High Head........	304	Jan.–Oct., 1957; Jan.–May, 1958
Race Point........	90	Jan.–May, 1958
New Beach.......	105	Jan.–May, 1958

Descriptions of New England weather are numerous, ranging from Mark Twain to the Weather Bureau's tabulations. In terms of Cape Cod beaches, several factors are sig-

TABLE 1

FACTORS WHICH AFFECT TOPOGRAPHIC CHANGES ON STUDIED BEACHES*

	Trend of Coast	Fetch 90° to Coast (Nautical Miles)	Fetch 45° to Coast (Nautical Miles)	Type Coast behind Beach	Source of Sand (Nautical Miles)	Net Direction Long Shore Drift	Open Fetch to Northeasterly Storms (Nautical Miles)	Proximity of Offshore Bars	Nearshore Bars
New Beach...	320°–140° T. NW.–SE.	16	17 W. 18 S.	Dune area (Provincelands)	10 Cliffs at Highland	Southeasterly	None	None, or poorly developed	None or poorly developed
Race Point...	043°–221° T. NE.–SW.	37	90 N.×E. 21 W.×N.	Dune area (Provincelands)	Cliffs at Highland 8 southeasterly	Northwesterly	Tangent to coast line	Terminus of Peaked Hill Bar	Complex and changing
High Head...	290°–110° T. W.NW.–E.SE.	80	65 N.NW. 110 E.NE.	Dune area (Provincelands)	1.5 Cliffs at Highland	Northwesterly	250 (Bay of Fundy)	1,000 feet origin of Peaked Hill Bar	Complex, migratory
Highland.....	308°–128° T. NW.–SE.	95	100 N., unlimited E.	High cliffs of glacial drift	Cliffs behind beach 0	Northerly	260 (Bay of Fundy)	2,000 feet	Numerous and complex

* After Zeigler, Hayes, and Tuttle, 1959, table 1.

nificant. The area is one of storminess; maps of North America showing storm tracks portray a general convergence across Cape Cod. Wind roses for this edge of the North Atlantic are generally symmetrical. Wind velocities are not extremely high, but winds of 45–55 mph are common in winter. The wave types produced by this changeable weather are complex off Cape Cod, and surf is almost always a mixture of several wave types at a time; regular swells are rarely present. Summer weather combines gentle breezes or flat calms with thunderstorms and an occasional tropical hurricane.

Surf statistics based on summaries of visual observations kept at Coast Guard Stations are published by Helle (1958), and sea state hindcasts are available for the deep water areas off Cape Cod (Neumann and James, 1955). Although we made repeated efforts to measure sea state by techniques that ranged from automatic offshore pressure recorders (placed and tended by boats) to time-lapse photography, we failed to obtain quantitative data about the sea state in any long-term consistent manner. Visual field estimates of surf height and wave periods were made each time a beach profile was measured. Because good sea state data were not obtained, we were unable to relate changes in the sea to observed changes along the beach profiles.

BEACH PROFILE MEASUREMENTS

Elevations along profiles across four beaches were measured at low tide approximately five days a week, but during some storms elevations were measured every low tide. Eight to ten pipes were driven into the beach in a line across each study area, and, when pipes were washed out, they were replaced if possible. The shoremost stake, or point of origin, for each line of stakes was placed at the landward edge of the beach (fig. 2). The elevations of the tops of the pipes were determined and rechecked by a transit survey. When measuring the beach profile, the observer had only to measure the exposed height of the pipes and later subtract it from the elevation of the top of the pipe, thereby obtaining the elevation of the beach surface. In this way, daily elevation data were secured. All measurements were converted to elevations above or below mean low water. These elevations are given in figures 3, 4, and 5. Tables presenting the data were so lengthy that unfortunately they could not be included in this paper.

One may use these data in a variety of ways, a few of which will be discussed. Changes can be pictured in terms of volumes and volume changes (figs. 3, 4, and 5). The area under each profile to mean low water datum was calculated as the sum of the areas of several trapezoids. This was converted to volume by multiplying area by one foot along the beach (right angles to the profile line). The volumes, therefore, represent a slice of beach one foot wide (parallel to the shore) with a length from the base of the dunes to mean low water and a thickness from the beach surface to a horizontal plane through mean low water rather than the bottom, since the actual thickness of beach sand is not known.

In another attempt to show the rate and nature of the changes, the elevation data of the stakes were plotted in terms of time (figs. 3, 4, and 5). Here, the time of the measurements is shown on the x-axis and the elevations of the beach at each stake on the y-axis. The observations for each of the eight pipes appear as lines crossing the diagram. Lines are dashed when observations were taken more than one day apart. Volumes for that beach are plotted. Also included are wind data, obtained from the Race Point Coast Guard Station in 1957 and from our own anemometer and vane mounted in Provincetown in 1958. Wind direction is given in terms of its angle to the particular beach being studied.

The writers intended to compare various beach changes, such as volume or slope or width with the seasons of the year as Shepard (1950), Shepard and Inman (1951), and Inman (1953) did on the West Coast. However, after examining our own data, we decided there was not enough of it. Closely spaced observations were made over a period of only 15 months, covering roughly 5 consecutive seasons: 2 winters, 2 springs, 1 summer, plus a fragment of fall. If one wishes to use an objective test for trend, at least twenty observations ordered in time are required. Clearly, we are short of observations on a monthly basis and are hardly started on a four-monthly basis; however, we have ample data to support discussion of daily beach changes. The observations are still being taken, and it is our hope they can be extended through at least twenty consecutive seasons.

Figures 3, 4, and 5 can be used in a variety of ways with a little practice. For example, one can observe the change in elevation with time of a distinct point in the beach. In figure 4, for example, the point

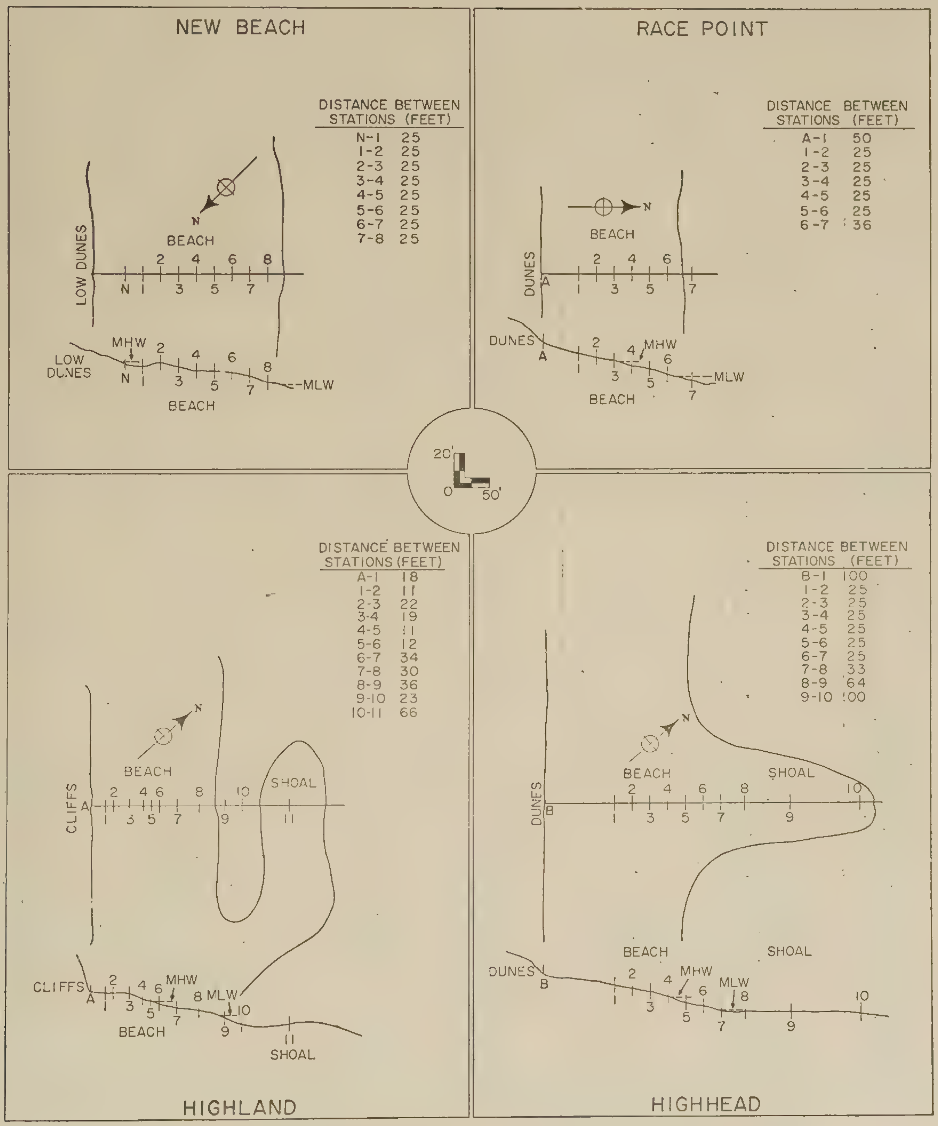
NEW BEACH
DISTANCE BETWEEN STATIONS (FEET)
N-1 25
1-2 25
2-3 25
3-4 25
4-5 25
5-6 25
6-7 25
7-8 25
N
LOW DUNES
BEACH
2 4 6 8
N 1 3 5 7
MHW
LOW DUNES
MLW
BEACH
RACE POINT
DISTANCE BETWEEN STATIONS (FEET)
A-1 50
1-2 25
2-3 25
3-4 25
4-5 25
5-6 25
6-7 36
N
DUNES
BEACH
A 1 2 3 4 5 6 7
DUNES
MHW
MLW
BEACH
20'
0
50'
DISTANCE BETWEEN STATIONS (FEET)
A-1 18
1-2 11
2-3 22
3-4 19
4-5 11
5-6 12
6-7 34
7-8 30
8-9 36
9-10 23
10-11 66
N
CLIFFS
BEACH
SHOAL
A 1 2 3 4 5 6 7 8 9 10 11
CLIFFS
MHW
MLW
BEACH
SHOAL
HIGHLAND
DISTANCE BETWEEN STATIONS (FEET)
B-1 100
1-2 25
2-3 25
3-4 25
4-5 25
5-6 25
6-7 25
7-8 33
8-9 64
9-10 100
N
DUNES
BEACH
SHOAL
B 1 2 3 4 5 6 7 8 9 10
BEACH
SHOAL
DUNES
MHW
MLW
HIGHHEAD

FIG. 2.—Location of points measured in plan and profile at the beaches studied

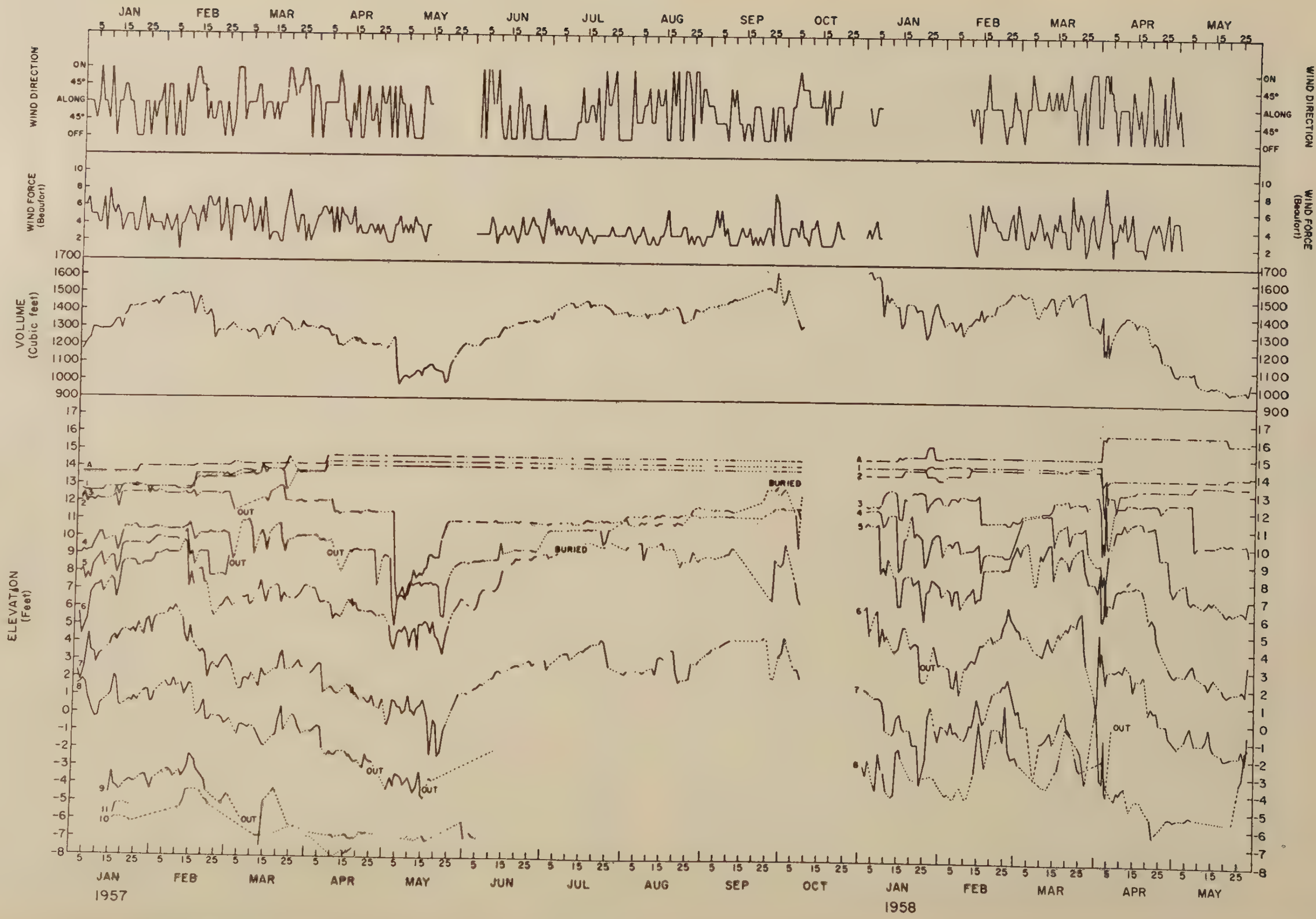

FIG. 3.—Elevations at measured points (*A* through *10*) on Highland Beach, January, 1957, to May, 1958. Volumes, wind force, and wind direction with respect to the beach are also presented for the

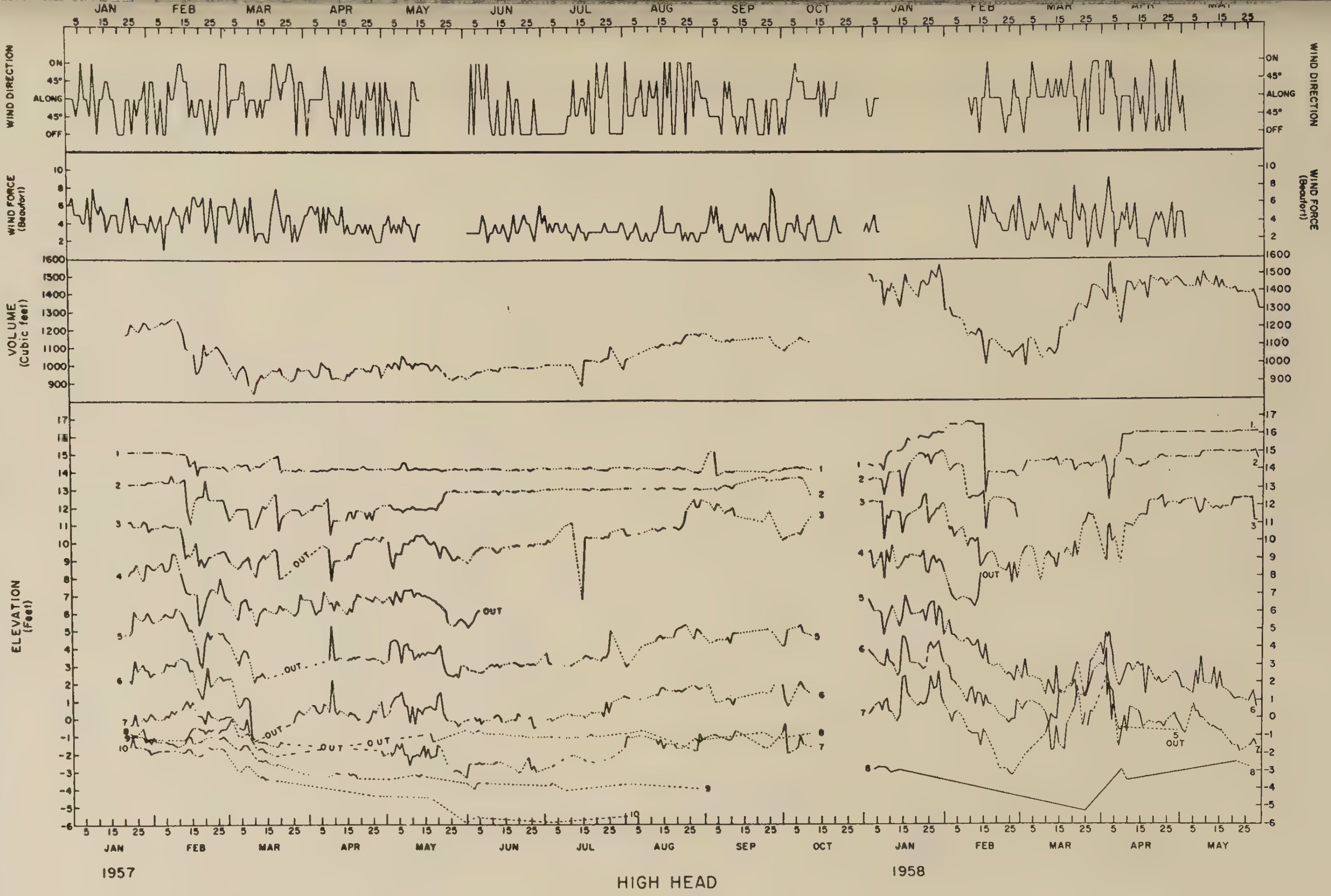

FIG. 4.—Elevations at measured points (*1* through *10*) on High Head Beach, January, 1957, to May, 1958. Volume, wind force, and wind direction with respect to the beach are also presented for the same time interval.

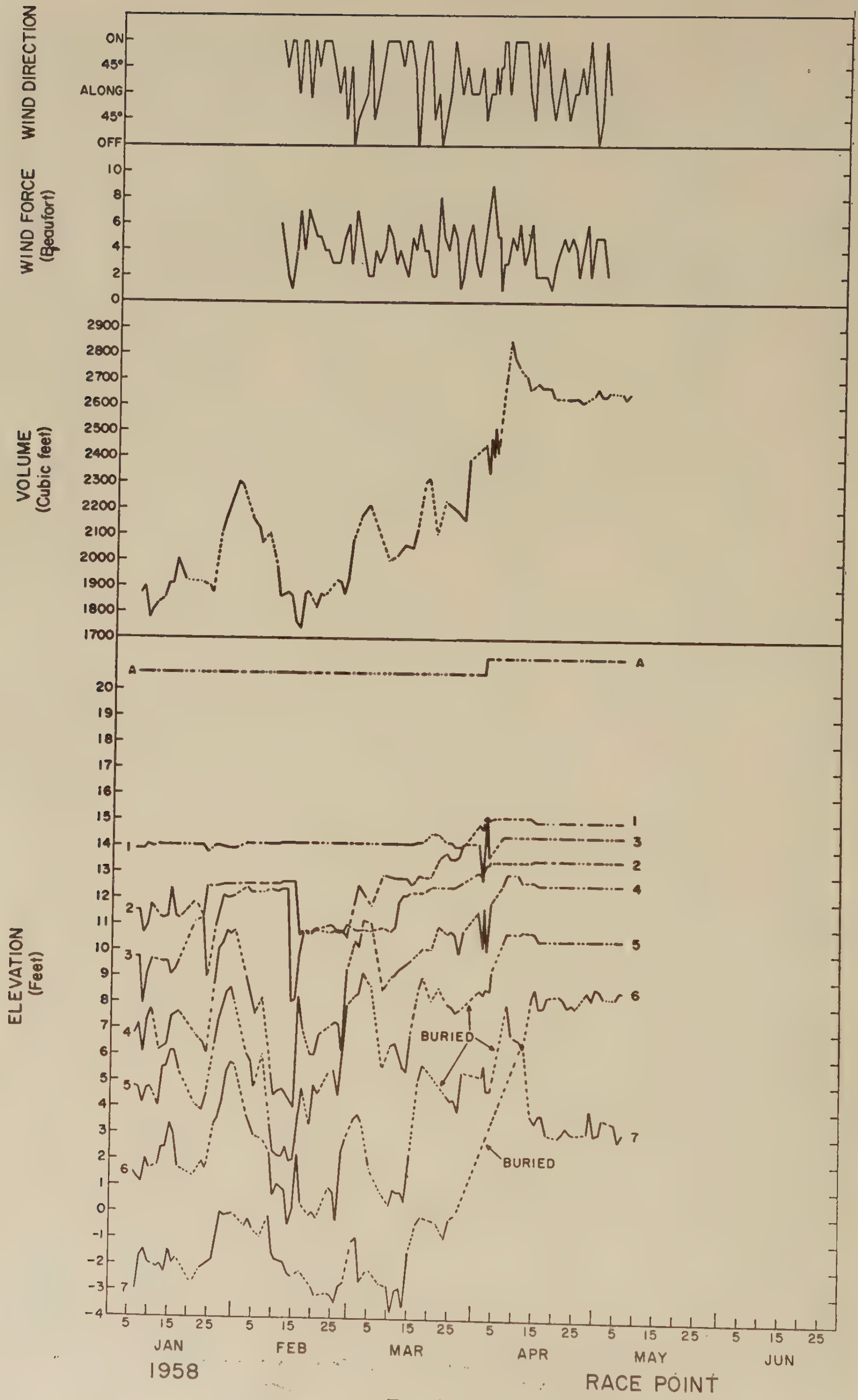

FIG. 5*a*

FIG. 5.—Elevations at measured points: 5*a* (*1* through *7*), at Race Point Beach; and 5*b*, New Beach (*N* through *8*), January, 1958, to May, 1958. Volume, wind force, and wind direction with respect to the beach are also presented for the same time interval.

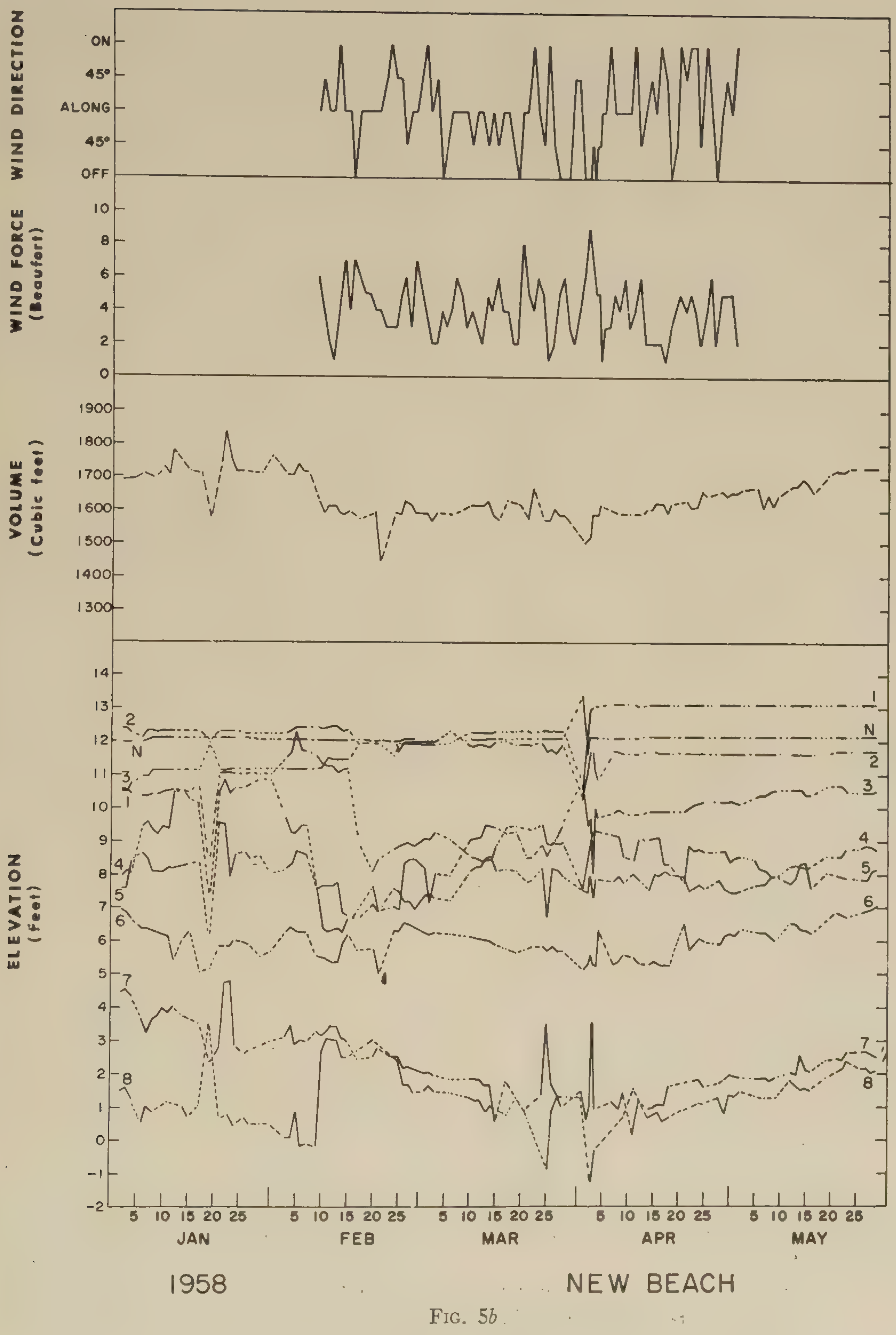
WIND DIRECTION
ON
45°
ALONG
45°
OFF
WIND FORCE (Beaufort)
10
8
6
4
2
0
VOLUME (Cubic feet)
1900
1800
1700
1600
1500
1400
1300
ELEVATION (feet)
14
13
12
11
10
9
8
7
6
5
4
3
2
1
0
-1
-2
1
N
2
3
4
5
6
7
8
5 10 15 20 25
JAN
FEB
MAR
APR
MAY
1958
NEW BEACH

FIG. 5b

farthest back at the backshore (Stake 1) changed very little from January, 1957, until January, 1958; then the elevation slowly increased almost two feet by February, 1958, at which time a scarp formed and the elevation was lowered two feet, etc.

The same sort of reasoning applies to all other points measured on the beach. Location of the measuring stations was given in plan and profile on figure 2. Specific wind conditions for any of the changes can be had from the figures with a little effort.

CUT AND FILL

Data have been organized to show the monthly average of the daily changes in net cut or fill which takes place on beaches studied by us (figs. 6, 7, and 8). Each point along the profile is identified by a stake number. The greatest net change per day observed during the month is also given as well as the number of observations used to determine the average. For example, using figure 6, one can see that the backshore at Highland represented by stakes 1, 2, and 3 showed net daily changes (cut or fill) of about 0.2 feet per day in January, 1957. The greatest net daily change at the backshore observed during that month (January) was about 1.0 foot per day near high water (Stake 3). The foreshore (Stakes 4, 5, 6, 7, and 8) had average net changes slightly different for each stake, but at the middle part of the foreshore (Stake 6) the average daily net change was about 0.4 foot, and the maximum daily change observed for January was about 1.4 feet (Stake 6). The same observation can be made for the other months and other beaches. Since there is an average daily topographic change of 0.2–0.3 feet across the foreshore, sediment samples taken within about 3 inches of the surface will be material that was affected by waves during the last tidal cycle.

It should be pointed out that these net daily averages do not represent merely a movement of a few tenths of a foot per day of sand measured at any one point; that is, they do not represent the gross movement. One of the writers observed the top of a buried pipe on the foreshore of Highland emerge from the sand until about three inches of pipe were exposed, and within five minutes the pipe became buried again. The net change was close to zero, but an enormous amount of material had been moved in a matter of minutes.

It is of interest to note the rapidity and eccentricity of changes at Race Point. This beach changes so much that its appearance is visibly different from day to day. Many beach scarps form here; pipes along the profile lines are frequently buried from one day to the next; digging for pipes at measurement time is routine.

Profiles showing the various beaches at their fullest and leanest during the period when surveys were being conducted were plotted as the highest and lowest recorded elevations for each stake. These elevations were plotted together, making an envelope which encloses the maximum measured variations for each beach area (fig. 9). As expected, these diagrams show that the middle and lower foreshore undergo greater cut and fill than the higher parts of the beach. The diagrams show clearly that one should expect the beach surface to move up and down vertically 9 or 10 feet. We measured a cut of 8 feet between October 10, 1955, and October 20, 1955, at Highland. The numbers presented here probably do not represent the maximum change.

One may say that sediment samples taken within 5–10 feet of the surface may have been exposed to waves at least once within the last year. Inferences drawn from sediment parameters of beach samples should be made in terms of realistic depths of cut and fill.

Cut and fill in the zone of breaking waves and offshore is not well documented. The points are difficult to reach even at low water. Another deterrent, but one which gives information, is that the measuring stakes are sometimes buried or sometimes carried away. One may deduce a range of cut and fill of approximately 5–6 feet in the immediate offshore region of our profiles. Figure 9 seems to support this guess.

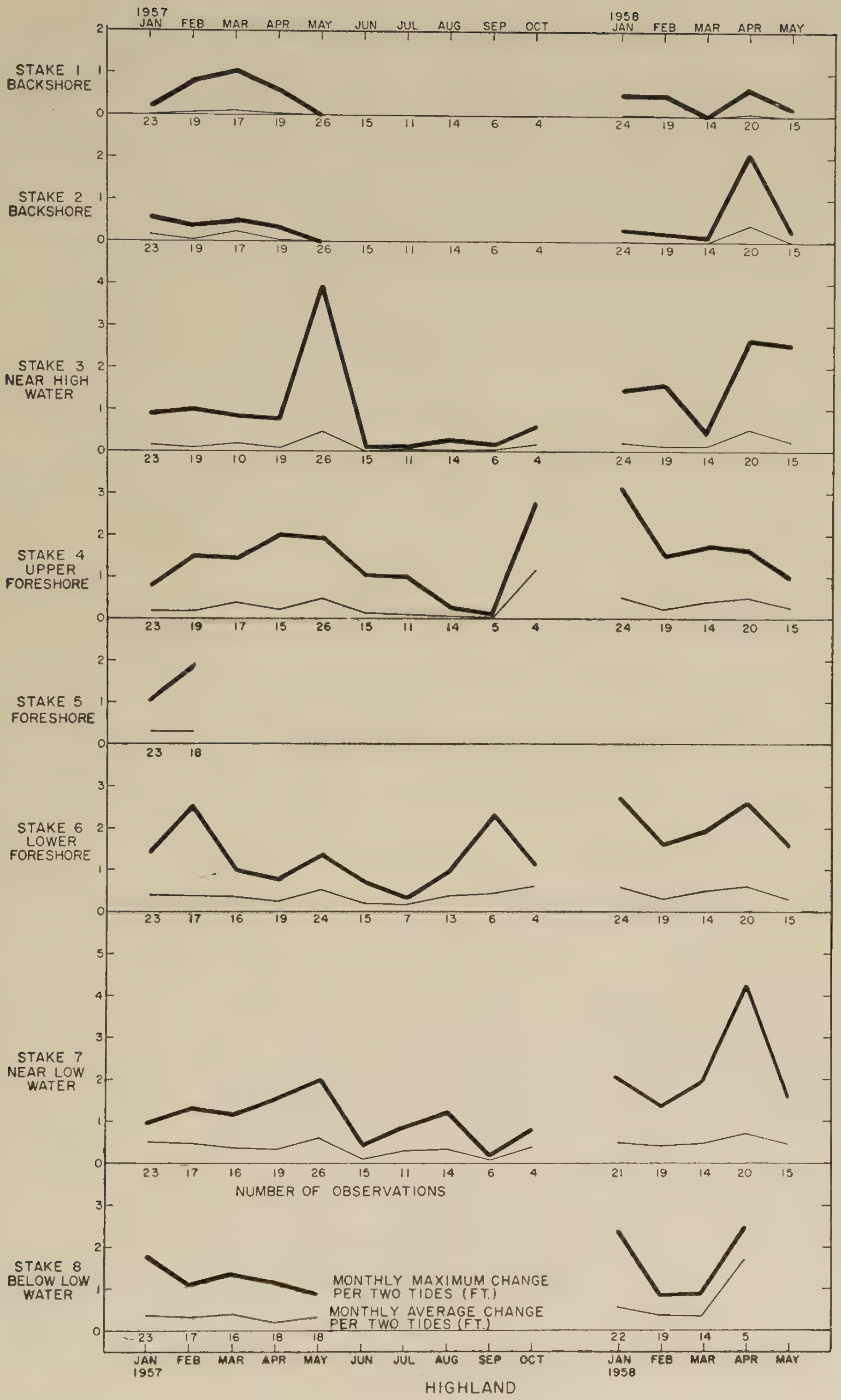

FIG. 6.—Monthly average of daily changes in net cut or fill which took place at Highland Beach, January, 1957, to May, 1958.

Our comparisons of daily changes nearshore are too scattered to be considered reliable; but our opinion, based on visual familiarity in the field, is that the daily changes are similar and of the same order of magnitude as those of the lower foreshore. The mechanism of movement is different, however.

The nearshore areas of Highland and High Head are greatly influenced by lateral passage of nearshore bars. The bars tend to move across the profile; however, they can

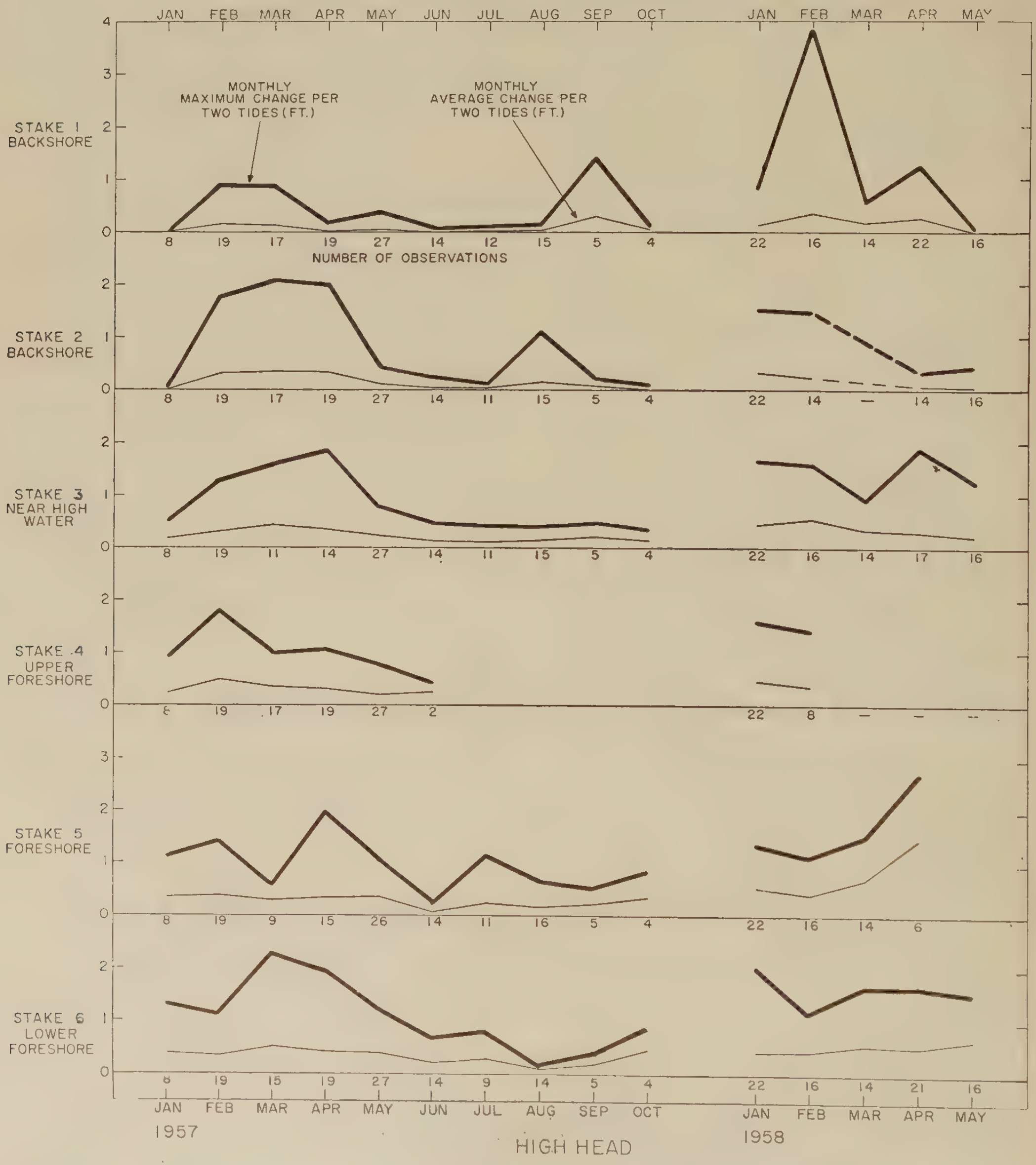

Fig. 7.—Monthly average of daily changes in net cut or fill which took place at High Head Beach, January, 1957, to May, 1958.

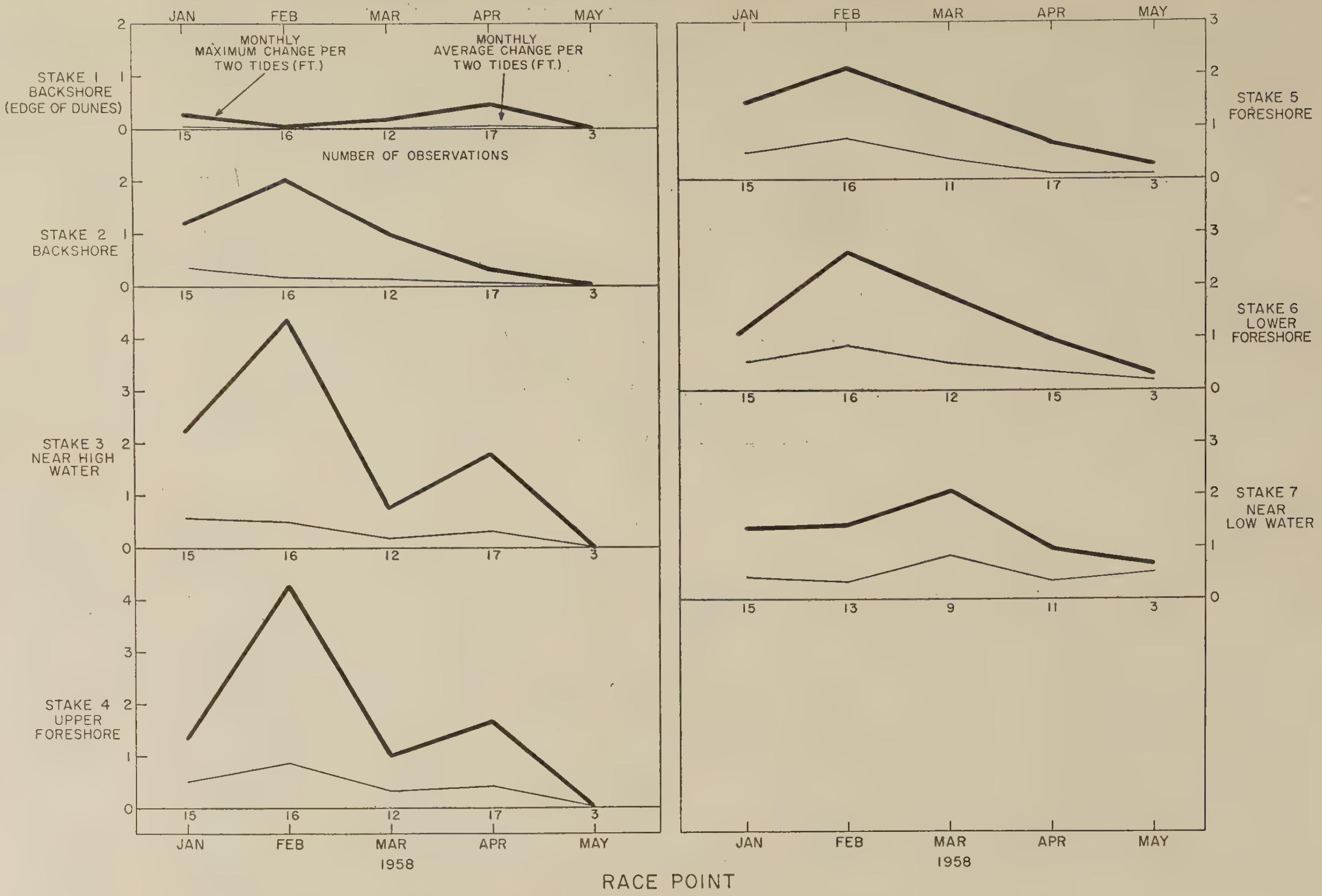

Fig. 8.—Monthly average of daily changes in net cut or fill which took place at Race Point

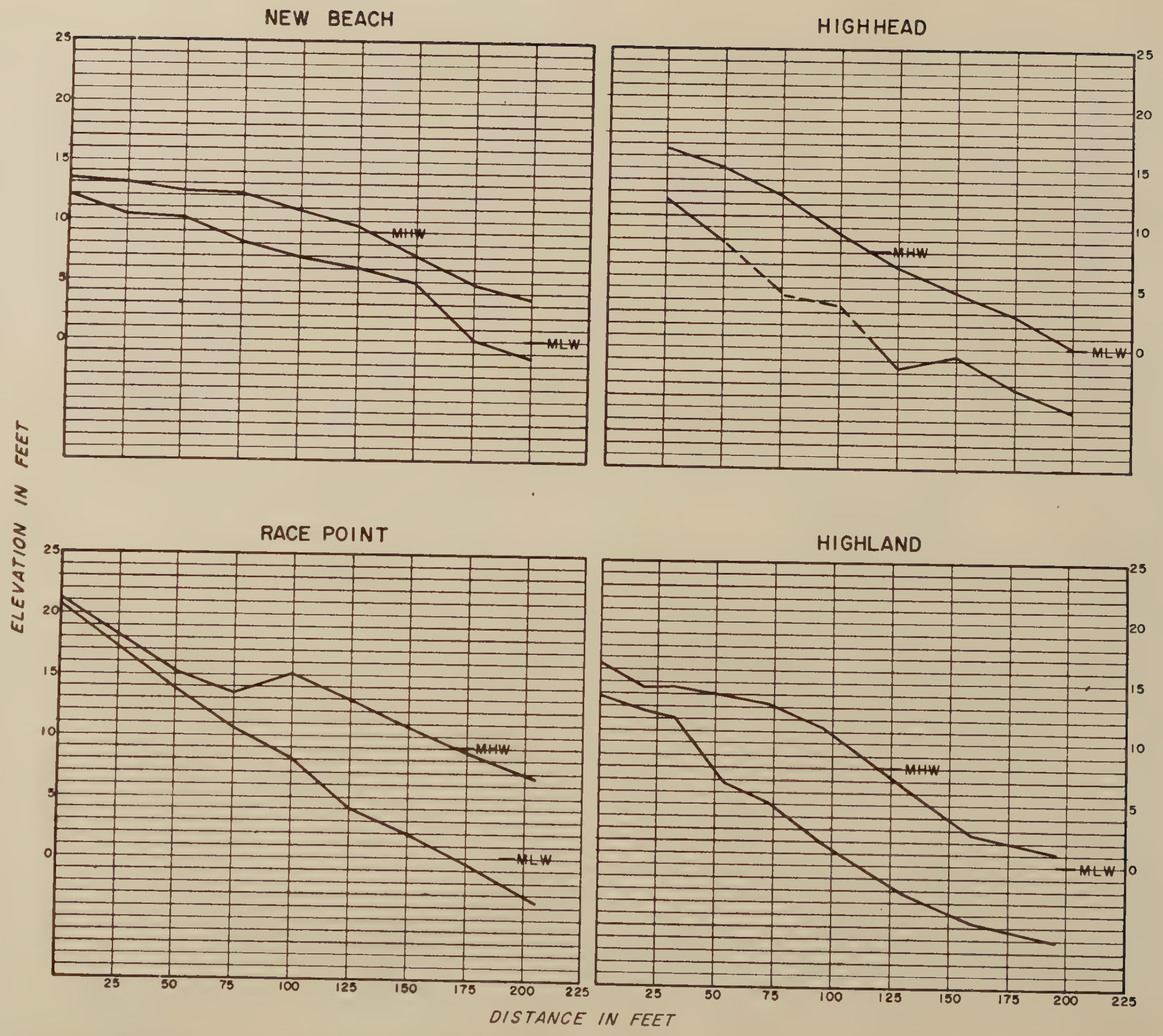

FIG. 9.—Envelope of maximum and minimum elevations observed at Highland, High Head, Race Point, and New Beach from January, 1957, to May, 1958.

be cut or filled on an onshore-offshore direction as well, if the sea state demands it. Stakes 9 and 10 at Highland often were buried when the nearshore bar shifted landward.

Some of our pipes penetrated the sand cover and entered fluvioglacial deposits (Stakes 9 and 10) at Highland only a few inches below the sand. Thus we conclude that the sand cover just beyond the foreshore is considerably thinner than on the foreshore itself, and at times the underlying glacial deposits are eroded. This would somewhat limit the daily changes observed because the glacial deposits are more resistant to erosion.

The rapidity with which change takes place on a beach is both a blessing and an irritation. Because conditions change, it is a splendid place to investigate causes of change. At the same time the complex changing places a severe burden on the investigator to collect his sediment samples in such a way that the samples represent the model he desires and not a dozen other things. We have pointed out that vast quantities of sediment are moved about near the surface of beaches each day and suggest that the numbers given here will help future sampling programs. Yet no sample program at the edge of the sea can free itself from limitations arising from the fact that four distinctly different hydrodynamic zones which overlap each other are compressed into a relatively narrow strip between the backshore and the nearshore. Sediment is transported by different mechanism in the zone of shoaling waves, zone of breaking waves, and zone of swash and backwash (Miller and Zeigler, 1958). The backshore, where wind moves material most of the time, is different from all the others.

REACH VARIATION

At the time of each profile measurement the observer noted the position of the reach of the previous high tide. Profiles were measured at the time of low tide. The location or distance from the point of origin and elevation of the reach could subsequently be determined from the profiles.

The variation in the position of the reach from day to day illustrates quantitatively the lateral shifting effect of the tidal oscillation on these beach slopes. Four interacting factors determine the extent and elevation of the reach in addition to the usual tidal forces: the neap and spring tidal fluctuations, the direction and velocity of the wind, the occurrence of storms and storm waves, and the slope of the beach. Comparison of reach data, with the wind force and wind direction curves on the isopleth diagrams (figs. 3, 4, and 5), show that, as one would expect, the reach was high and far inland at times of strong onshore winds and low and seaward on the beach during times of offshore winds. Other high reaches occur during times of spring high tides. The storm of April 1–3, 1958, which blew onshore, caused high reaches on all of the ocean beaches. Despite the fact that the wind was logged as offshore at New Beach during this storm, large waves were refracted around the end of Race Point against this beach, and the reach was also very high there.

Variation in the reach shows that the turbulent area of breaking waves and running oscillates considerably up and down the beach (table 2). The importance of this is that the sediment pattern is related to hydrodynamic zones across the beach, and, if these zones shift, the sediment characteristic of a particular hydrodynamic environment also shifts.

Classically, the inner margin of the foreshore is defined as the upper limit of wave swash on the beach. The variations of the reach, described above, illustrate a major difficulty in trying to define quantitatively, the foreshore on these particular beaches.

NEARSHORE BARS

A peculiar arrangement of bars begins at Highland and ends at Race Point. Peaked Hill Bar has its origin tangent to the beach at Highland (fig. 1). This bar extends gradually offshore for a distance of approximately

2,000 feet at a very flat angle to the coast; then, as the coast bends almost 90° at Race Point, the Peaked Hill Bar also hooks sharply at its end and disappears, not making the turn which the coast does.

Sand moves in a series of giant ripples or bars between Peaked Hill Bar and the beach. These smaller bars are commonly strongly transverse both to Peaked Hill Bar and the beach as well. When the end of one of the bars intersects the coast, a spit or tongue of land appears at nearly right angles to the beach. We were puzzled for a long time by these peculiar spits until we related them to the giant sand waves moving past the coast.

The High Head profile was purposely located at one of these transverse bars or spits (fig. 2). While we were never certain what was going on offshore, because Stakes 9, 10, and 11 were lost, we could measure the rate with which the beach end of the bar moved. The bar did not move with uniform speed; rather it remained more or less stationary for a few weeks then shifted laterally 25–75 feet per day for a few days before stopping for a while. The bar moved about 100 yards in three months and then just disintegrated and disappeared. In all probability its landward end simply swung offshore as part of an underwater giant ripple system. New bars formed from time to time in the same area. The following are the notes of Herman Tasha and Graham Giese, of Provincetown, who formed the permanent field party:

> A spit about 100 feet wide and 150 feet long appeared across the High Head line in May 1957 [normal to the shore]. Its position remained unchanged from about May 8th through May 27th. As estimated during times of low tide, the volume of the spit occasionally shrank or grew.
>
> At the High Head profile, a spit lying across the profile line moved an estimated 75 feet laterally to the northwest between March 11th and 12th, 1957. Another spit, at the same location, shifted 25 feet to the northwest between March 27 and 28.

TABLE 2

VARIATION IN THE POSITION OF THE BEACH

	Min. Distance Seaward of Origin	Max. Distance Seaward of Origin	Max. Elev. above Mean Low Water	Min. Elev. above Mean Low Water
Highland.......	−15′	109′	16.0′	6.4′
High Head......	−56′	200′	22.3′	2.1′
Race Point......	25′	220′	18.8′	3.5′
New Beach	0	119′	13.4′	8.0′

SUMMARY

Engineers and contractors engaged in the design and construction of man-made structures on a beach should be aware of the magnitude and rapidity of beach changes. Foundations and footings must be put deep enough so that they are not eroded out. Figure 9 indicates that about ten feet of vertical change may be expected across these beaches and many tens of feet of widening or narrowing. The military engineer must keep in mind that certain beach characteristics, such as slopes, widths, scarps, etc., may change within a few days, and constant beach reconnaissance is needed. The individual landowner with a cottage and beach should be aware of what to expect from the usual fluctuations and erosion on his beach without demanding or paying for beach protection structures which may not make a difference anyhow.

Without good sea state measurements and numerical descriptions, the usefulness of our profile measurements is limited. We would like to explain the daily fluctuations of the beaches in terms of specific sea state characteristics. We are unable to do this. Causes must be related to a theoretical laboratory and field analyses of the hydrodynamics of the associated waves. Including the condition of the beach and sea state, there are a considerable number of other variables that can be used to explain beach changes. At the moment this very dynamic region cannot be clearly defined quantitatively. Some parts of the data from the zone of breaking waves may never be satisfactorily collected since observing and recording surf characteristics in mid-winter during a northeast storm on an open New England beach can be a pretty discouraging business. We found several theoretically valid procedures for measuring sea state beyond our physical and financial limits.

ACKNOWLEDGMENTS.—The authors wish again to express appreciation to the numerous people who have contributed to the beach studies project at the Woods Hole Oceanographic Institution. The early surveys were made by Carlyle R. Hayes and the later daily measurements by Herman Tasha and Graham Giese, of Provincetown, Massachusetts. Mrs. Barbara Gill compiled most of the data. The work was carried out under ONR Geography Branch Contract No. Nonr-1254(00) (NR-388-018). Particular thanks are due to R. L. Miller, whose interest in the sea and all aspects of the nearshore has been valuable to us beyond measure.

REFERENCES CITED

COAST AND GEODETIC SURVEY, 1960, Tides tables East Coast, North and South America, p. 275: U.S. Dept. of Commerce.

GILBERT, GROVE K., 1890, Lake Bonneville: U.S. Geol. Survey Mono. 1.

HELLE, JAMES R., 1958, Surf statistics for the coast of the United States: Beach Erosion Board, Tech. Memo. 108.

INMAN, D. L., 1953, Areal and seasonal variations in beach and nearshore sediments at La Jolla, California: Beach Erosion Board, Tech. Memo. 39.

JOHNSON, DOUGLAS W., 1919, Shore processes and shoreline development, p. 584: New York, John Wiley & Sons.

KING, C. A. M., 1959, Beaches and coasts, p. 403: London, Edward Arnold & Co.

MILLER, ROBERT L., and ZEIGLER, JOHN M, 1958*a*, A model relating dynamics and sediment pattern in equilibrium in the region of shoaling waves, breaker zone, the foreshore: Jour. Geology, v. 66, no. 4, p. 417–441.

——— — ——— 1958*b*, A study of the relation between dynamics and sediment pattern in the region of shoaling waves, breaker zone, and foreshore. 5th International Sedimentological Congress, Geneva, Switzerland: Eclogae Geol. Helvet., v. 51, no. 3, p. 542–551.

——— — ——— 1959, Comparison of theoretical near-bottom mass transport velocities with observed sediment size and sorting patterns, p. 635: 1st International Oceanographic Congress, Preprints.

NEUMANN, G., and JAMES, P. W., 1955, North Atlantic coast wave statistics hindcast by the wave spectrum method: Beach Erosion Board, Tech. Memo 57.

SHEPARD, F. P., 1950, Beach cycles in southern California: Beach Erosion Board, Tech. Memo. 20.

——— and INMAN, D. L., 1951, Sand movement on the shallow intercanyon shelf at La Jolla, California: Beach Erosion Board, Tech. Memo. 26.

ZEIGLER, JOHN M., 1960, Beach studies in the Cape Cod area conducted during the period August 1953–April 1960: Unpublished reference no. 60-20, Woods Hole Oceanographic Institution.

———, HAYES, CARLYLE R., and TUTTLE, SHERWOOD, D., 1959, Beach changes during storms on outer Cape Cod, Massachusetts: Jour. Geology, v. 67, p. 318–336.

——— and RONNE, F. C., 1957, Time lapse photography—an aid to the studies of shorlines, p. 1–6: Research Review, Office of Naval Research, April, 1957.

——— — ——— 1958, Coastline photographs, p. 40–41: Industrial photography, October, 1958.

Contribution No. 1159

Deep-Sea Research, 1961, Vol. 7, pp. 298 to 300. Pergamon Press Ltd., London. Printed in Great Britain

LETTER TO THE EDITORS

Nitrogen fixation in the Sargasso Sea

(*Received* 31 *December* 1960)

THE stratification of surface ocean waters is normally accompanied by the depletion of plant nutrients, which are assimilated by the phytoplankton more rapidly than they are regenerated *in situ* or mixed upward from the deeper waters through the thermal gradient. In temperate and semi-tropical waters in the summer and in most tropical waters at all times, the levels of inorganic nitrogen, phosphorus, silicon and other essential nutrients are reduced to extremely low and often undetectable levels in the upper, euphotic layer.

This situation obtains in the Sargasso Sea near Bermuda from May until the seasonal thermocline breaks down in the late fall or early winter. Concentrations of combined nitrogen (nitrate plus nitrite) typically range from 0·1 to 0·5 $\mu g\ A/L$, phosphate-phosphorus 0·05 to 0·10 $\mu g\ A/L$ in the upper 100 m during this period. The abundance and rate of production of phytoplankton are at minimal levels under these conditions, the latter ranging from about 0·05 to 0·10 g carbon assimilated/m^2/day, as low as has been reported anywhere in the oceans (MENZEL and RYTHER, 1960).

During this period of nutrient impoverishment, there characteristically appears in the surface layer a noticeably dense population of the bluegreen alga, *Trichodesmium thiebautii*, whose fusiform colonies are clearly visible to the naked eye from shipboard. Although their vertical distribution has not been investigated, the visual impression is that the organisms are largely confined to the upper one or two metres. Because of this and because the organisms are discontinuously distributed in relatively large colonies or clumps, they are seldom sampled or counted in the routine 250 ml phytoplankton samples which are taken from various depths at biweekly intervals in this area (HULBURT *et al.*, 1960).

A semi-quantitative record of the seasonal distribution of *Trichodesmium* at Station S, 15 miles SE of Bermuda, for 1960 is shown below. The data were obtained by towing a metered No. 8 plankton net at the surface for approximately 15 minutes every two weeks. The values do not give an accurate picture of quantitative distribution, but serve to illustrate the fact that the organism occurs in this region only during the summer and fall when surface temperatures are above 25° and the waters are thermally stratified.

Date	*No. colonies*/m^3
Before July 11	rare or absent
July 11	0·8
July 27	2·4
August 12	4·4
August 29	2·5
September 15	6·7
October 7	23·5
October 25	1·7
After October 25	rare or absent

During the winter, when *Trichodesmium* is absent at station S, conspicuous quantities of the alga were observed by the junior authors South of Bermuda where the surface waters are permanently stratified (RYTHER and MENZEL, 1960) and in the Caribbean Sea. Quantitative estimates were not made, but the organisms appeared to be as abundant in these southern waters in winter as in the Bermuda region in summer. In September 1960, large quantities of the alga were observed at the surface off the edge of the continental shelf as far north as 38° (R. F. VACCARO, personal communication).

These observations are in substantial agreement with numerous reports in the literature (e.g., CLEVE, 1897 ; WILLE, 1904 ; and FARREN, 1932) to the effect that *Trichodesmium thiebautii* is a tropical species extending its distribution into temperate waters in summer or carried northward by current systems such as the Gulf Stream. Since it occurs in quantity only when the water is thermally stratified and is nutrient-impoverished and when other phytoplankton are at their seasonal minima of abundance, the ability of *Trichodesmium* to fix atmospheric nitrogen was considered a strong possibility. Although classified as a member of the Oscillatoriaceae, in which nitrogen fixation has not previously been demonstrated, neither the taxonomy of this organism nor the ability of bluegreens as a group to fix nitrogen have been adequately studied to exclude the possibility of what would appear, from ecological considerations, to be a logical adaptation of this organism to its natural environment.

The ^{15}N method for detecting nitrogen fixation has been adapted by DUGDALE, *et al.* (1959) to the measurement of nitrogen fixation rates in aquatic communities. The following procedure is carried out after placing a sample of water in a 1 litre boiling flask having a standard taper joint at the neck, and into which a specially designed gas flushing unit is fitted -

(1) atmospheric N_2 (as well as other gases) is flushed from the water with a mixture of 80/20 $He/0_2$ at a pressure of 0·8 atm ;
(2) 0·2 atm. N_2 enriched to 99·8 atom per cent ^{15}N is added to the flask and equilibrated with the aqueous phase by shaking ;
(3) the sample is incubated within the flask under the conditions selected for the experiment ;
(4) the organic fraction is converted to ammonia by micro-Kjeldahl digestion, distilled, titrated for total N and converted to N_2 with alkaline hypobromite ;
(5) the $^{15}N/^{15}N$ ratio determined with a mass spectrometer, the ratio converted to atom per cent ^{15}N, and the enrichment over the normal atom per cent ^{15}N of the organic material calculated.

Material for the experiment was collected on September 30, 1960 by towing a No. 8 plankton net at the surface. Upon return to the laboratory *Trichodesmium* colonies were selected from the net tow and inoculated into flasks containing surface seawater. One flask was enriched with phosphate, trace metals and vitamins. The flasks were incubated for 5 hours in a water-cooled box fitted with neutral density filters and placed in open sunlight (simulated *in situ* incubation). Following incubation, the particulate fraction, containing the *Trichodesmium*, was separated from the salt-water by filtration through fine-mesh parachute material, resuspended in distilled water, brought to the boil, transferred to a polyethylene bottle with 2 drops of H_2SO_2, and frozen. Subsequent analysis was carried out at the University of Pittsburgh with the following results :

% Incident (Light)	*Atom % (N15)*	*Atom % (Excess)*	*μg N (Fixed)*	*mg. N (in Sample)*
100	·372	·011	0·13	1·2
50	·367	·006	0·06	1·0
25	·364	·003	0·03	1·0
10	·363	·002	0·01	0·7
Dark	·361	·000	0·00	1·2
100 (enriched)	·361	·000	0·00	0·9
Standards	·361	—	—	—

The entire procedure has been carefully calibrated using converted ammonium sulphate as a reference standard. The least significant difference for pairs of samples at the 95 per cent confidence level is ·003 atom per cent excess ^{15}N. Two lots of untreated sample set aside to provide an initial nitrogen isotope ratio were accidentally contaminated making it necessary to discard them. However, isotope ratio determinations made at the University of Pittsburgh upon organic matter from natural waters have so far never varied significantly from that of the standards and in fact usually agree within less than ·001 atom per cent of these standards. In the absence of direct standards we are assuming that the ammonium sulphate standard represents an adequate estimate of the normal isotope ratio of the samples. The atom per cent excess ^{15}N associated with each flask has been calculated by subtracting the above value, 0·361, from the atom per cent ^{15}N found in each at the end of the experiment.

Fixation of nitrogen appears to have occured in our experiment since 3 of the 4 flasks exposed to light show a statistically significant enrichment according to the criteria described above. Furthermore, there appears to be a clear, direct relationship between the level of light during incubation and nitrogen fixation rate, with no apparent fixation in the dark. It is also interesting to note that enrichment with a mixture of phosphate, vitamins and trace minerals inhibited fixation completely. Since *Trichodesmium* was the predominant organism in the flasks, the hypothesis for nitrogen fixing ability in this alga is strengthened. Confirmation will, of course, have to await its isolation in pure culture. The results of this experiment suggest that organic production in oligotrophic tropical seas is not limited by nitrogen, a conclusion reached by REDFIELD (1958) on hypothetical grounds and in essential agreement with the experiments of MENZEL and RYTHER (in press), who found that iron is the element critically limiting plant production in the Bermuda region.

**Dept. of Biological Sciences, University of Pittsburgh.* R. C. DUGDALE*
***Bermuda Biological Station.* DAVID W. MENZEL**
†Woods Hole Oceanographic Institution. JOHN H. RYTHER†

Contribution No. 281 *of the Bermuda Biological Station and No.* 1159 *of the Woods Hole Oceanographic Institution under Contract AT*(30–1)–2646 *with the U.S. Atomic Energy Commission and with partial support of N.S.F. Grant G* 10693.

REFERENCES

CLEVE, P. T. (1897) A treatise on the phytoplankton of the Atlantic and its tributaries and on the periodic changes of the plankton of Skagerak. Upsala.

DUGDALE, RICHARD C., DUGDALE, VERA ; NEESS, JOHN and SOERING, JOHN (1959) Nitrogen fixation in lakes. *Science* **130** (3379), 859–860.

FARRAN, G. P. (1932) The occurrence of *Trichodesmium thiebautii* off the south coast of Ireland. *Rapp. Proc. Verb. Cons. Int. Explor. Mer.* **77**, 60–64.

HULBURT, E. M., RYTHER, J. H. and GUILLARD, R. R. L. (1960) The phytoplankton of the Sargasso Sea off Bermuda. *J. du Cons. Int. Explor. Mer.* **25**, 115–128.

MENZEL, D. W. and RYTHER, J. H. (1960) The annual cycle of primary production in the Sargasso Sea off Bermuda. *Deep-Sea Res.* **6**, 351–367.

MENZEL, D. W. and RYTHER, J. H. (1961) Nutrients limiting the production of phytoplankton in the Sargasso Sea with special reference to iron. *Deep-Sea Res.* **7**, 276–281.

REDFIELD, A. C. (1958) Biological control of chemical factors in the environment. *Amer. Sci.* **46** (3), 205–221.

RYTHER, J. H. and MENZEL, D. W. (1960) The seasonal and geographical range of primary production in the western Sargasso Sea. *Deep-Sea Res.* **6**, 235–238.

WILLE, N. (1904) Die Schizophyeen der Plankton Expedition. *Ergebnisse der Plankton Exhibition der Humboldt-Stiftung*, **4**, 1–89.

Printed in Great Britain by The Salisbury Press Ltd., Publicity House, Wilton Road, Salisbury Wilts. (27343)

Contribution No. 1160

[EXTRACT FROM U.S. COAST GUARD BULLETIN NO. 46, PAGE 31–114]

PHYSICAL OCEANOGRAPHY OF THE GRAND BANKS REGION AND THE LABRADOR SEA IN 1960[1]

by Floyd M. Soule, Peter A. Morrill, and Alfred P. Franceschetti (U.S. Coast Guard)

The U.S.C.G.C. *Evergreen* again served as the oceanographic vessel of the International Ice Patrol for 1960. No marked alterations affecting the oceanographic work were made in the vessel since the 1959 season.

The *Evergreen* departed Argentia, Newfoundland, on 1 April to conduct the first survey of the 1960 season. In addition to covering the southern and eastern slopes of the Grand Banks, this survey extended south to latitude 37°30′ N., in order to take stations in conjunction with the Woods Hole Oceanographic Institution's research vessels, *Chain*, *Atlantis*, and *Crawford* on the Gulf Stream Survey, 1960, under the direction of Mr. F. C. Fuglister. A total of 68 stations were taken during the first survey of which the first 31 were a part of Gulf Stream, 1960. Although original plans called for a two cast station to the bottom, it was found that the winch would overheat if more than 4,000 meters of wire were let out and consequently 4,000 meters was set as the maximum station depth. The survey proceeded without major interruption and was completed at station 7351 on 17 April and the *Evergreen* returned to Argentia.

The second survey was made in two phases. The first phase consisted of 70 stations taken in a counterclockwise direction on the eastern and northeastern slopes of the Grand Banks. Although heavy weather caused minor delays, the first phase was completed on 9 May at station 7421. Due to an erratic functioning loran receiver, the *Evergreen* returned to Argentia for repairs. After a 1-day stay, *Evergreen* departed on the second phase of the survey which was to make a quantitative evaluation of the wind effect on iceberg movement. Three days were lost in trying to locate an iceberg that was both free from field ice and not aground. On the late evening of 16 May, a drydock type iceberg, 85 feet high and 405 feet long was located in the Labrador Current. Although heavy fog persisted for 95 percent of the observation period and the winds were light, the preliminary evaluation is believed to be a success. In all, eight parachute drogues were launched during the 4 days of observations.

The third oceanographic survey consisted solely of an occupation of the Bonavista triangle. The survey commenced at the northern corner of the triangle on 3 June and proceeded in a counterclockwise direction without interruption. At station 7451 on 6 June, the survey was completed and *Evergreen* proceeded into Bonavista Bay to conduct iceberg demolition tests which have been described in the preceding section of this bulletin.

---

[1] To be reprinted as Contribution No. 1160 in the Collected Reprints of the Woods Hole Oceanographic Institution.

After completing the demolition tests, the *Evergreen* returned to Argentia on 13 June and departed from there on 17 June to conduct the fourth oceanographic survey which covered the waters over and immediately seaward of the southern and eastern slopes of the Grand Banks from just westward of the Tail of the Banks to the latitude of Flemish Cap. This survey included 86 stations taken between 18 June and 1 July with the work of collection of data beginning at the southwestern end of the area and progressing northward. Between stations 7467 and 7468, 36 hours were lost when the loran receiver transformer burned out and a spare one had to be flown down from Argentia. The survey resumed after a successful airdrop was made. At station 7537, the fourth survey was completed and *Evergreen* proceeded to St. Johns, Newfoundland, for a brief period of rest and relaxation.

On 5 July, *Evergreen* departed St. Johns to conduct the 1960 postseason cruise which was to include an occupation of the Bonavista triangle and a section across the Labrador Sea from South Wolf Island, Labrador to Cape Farewell, Greenland. The 30 stations of the Bonavista triangle were occupied between 6 and 8 July after which the *Evergreen* proceeded to within 5 miles of South Wolf Island to commence the Labrador Sea section, where on 10 July, the work of collection of data was resumed. The survey proceeded without interruption until shortly after the taking of station 7588, located on the Greenland continental slope, heavy concentrations of storis were encountered. At station 7588, *Evergreen* was approximately 36 miles off Cape Farewell. *Evergreen* then proceeded slowly through various leads in the ice until at 17 miles from Cape Farewell and still 5 miles short of proposed station 7589, the ice became impassable. An attempt was made to take station, but the rapidly moving ice floes threatened to close in on the ship. As there was no indication of more favorable ice conditions in the near future, the survey ended and *Evergreen* returned to Boston via Argentia and Woods Hole. Thus ended the 1960 oceanographic data collection.

The oceanographic work was under the supervision of Lt. P. A. Morrill who was assisted by Lt. (jg.) T. F. Budinger for the first, second, and third surveys, and by Oceanographer Alfred P. Franceschetti for the fourth and postseason surveys. Other assistants in the observational work included R. C. Norris, aerographer's mate first class; F. N. Brown, yeoman first class; D. P. Wagner, aerographer's mate second class; W. C. Carpenter, yeoman second class, and L. E. Dawson, aerographer's mate third class. Temperature and salinity observations were made at each of the 325 stations. At the 21 stations forming the section across the Labrador Sea, the observations extended from the surface to as near the bottom as was practicable. The 31 stations that comprised a part of the Gulf Stream, 1960, survey were similarly taken except that a maximum depth of 4,000 meters was imposed. At the remaining stations, observations were limited to the upper 1,500 meters. The intended depths of observations were 0, 25, 50, 75, 100, 150, 200, 300, 400, 600, 800, 1,000 and thence by 500-meter intervals except for the Gulf Stream, 1960, stations which, below the 1,000-meter level, were 1,250, 1,500, 1,750, 2,000, 2,250, 2,500, 3,000, 3,500 and 4,000 meters. Temperatures were measured with protected deep sea reversing thermometers. Most of the thermometers used were of Richter and Wiese manufacture, with a scattering of Negretti and Zambra, Kahl Scientific Instrument Corp. and G. M. Manufacturing Co., instruments. Depths of observation were based on unprotected reversing thermometers made by Richter and Wiese and by Kahl. As in the past, a program of intercomparison of the protected thermometers was carried out in the field to permit a close control to be kept on the functioning of individual thermometers. The thermometers were used in pairs and one of each pair was shifted periodically so that any one thermometer was eventually paired with several other thermometers. Mean differences between the corrected readings of pairs of thermometers were adjusted to zero by the application of consistent corrections. In all, 2,150 comparisons were made. Of these, 683 involved thermometers having a range of −2° to +20° or more and had a standard deviation (difference between the corrected readings of a pair of thermometers) of ±0.013°. For the ranges of +3 to +13 (311 comparisons) and −2° to +8° (1,156 comparisons), where the scale is more open, the standard deviations were ±0.007° and ±0.008° respectively. Inasmuch as most of the observed temperatures listed in the Table of Oceanographic Data are based on the corrected readings of a pair of thermometers and since many of the thermometers used had recent laboratory comparisons with thermometers tested by the National Bureau of Standards, it is considered that the tabulated observed temperatures have an accuracy of 0.01° C.

As in past years, the routine salinity measurements were made with a Wenner salinity bridge with a precision of ±0.005°/₀₀. This year the observed salinities listed in the Table of Oceanographic Data are considered to have an accuracy equal to this precision. As mentioned in Bulletins Nos. 44 and 45 of this series, efforts to arrive at a better standardization of salinities have been in progress for some time. During the 1959 ice season, 11 large samples (ca. 12 gallons each) of actual surface sea water, distributed over the salinity range from 31 to 36.4°/₀₀, were collected from the Ice Patrol operating area and stored in polyethylene drums. In February 1960, these samples were divided, some portions of each being transferred to polyethylene and glass containers for further storage, and other portions being measured after a few days storage in glass bottles. The measurements consisted of precise determinations of chlorinity by the Volhardt method, with checks against silver of high purity; and of electrical impedance by means of the Coast Guard's Wenner salinity bridge. The procedures followed and the results obtained in the precise chlorinity determinations are given in appendix 1. Other details regarding location of origin and date of collection of the large samples are given in appendix 2.

Three measurements of each sample were made on the Coast Guard bridge during each of two runs on 25 and 26 February 1960. The samples were also measured on the Woods Hole Oceanographic Institution's bridges No. 1 and No. 2 on 16 March 1960. Schleicher and Bradshaw of WHOI considered, from an examination of Thomas, Thompson, and Utterback's work on the electrical conductivity of sea water,[2] that the relationship between conductivity and salinity of sea water could be expressed by a second degree relationship over the salinity range from 30 to 40°/₀₀. They took actual high salinity Atlantic water (ca. 36°/₀₀) and concentrated it to about 40°/₀₀ by slow evaporation. From this they prepared five samples, distributed in salinity from 30 to 40°/₀₀, by dilution with conductivity water. From the second degree relationship and measurements of the ratios of the salinities of the prepared samples they determined the shape of their calibration curve and fixed it laterally by the measurement of Copenhagen water.

The Coast Guard has always used an assumed linear relationship between conductivity and salinity over a lesser range of about 31 to 36½°/₀₀ but has avoided the assumption that Copenhagen water has the same chlorinity-conductivity relationship as actual newly collected sea water. The February 1960 measurements present an opportunity of examining the magnitude of the errors involved in assuming a linear relationship between conductivity and salinity of sea water over this range, of determining the corrections to salinities published in the Ice Patrol bulletins for the postwar years, and the variations between the chlorinity-conductivity relationship of sea water and of several batches of Copenhagen water.

In assuming a linear relationship between conductivity and salinity, the calibration curve of the Coast Guard's bridge has the form $S=\frac{A}{B+m}-C$ where m is the reading of the variable impedance in the X-dial arm of the bridge at balance corresponding to a salinity S; and A, B, and C are constants which depend in part on the arbitrary selection of one point on the curve. In the 1957 calibration curve this point was an X-dial reading of 49.911 corresponding to $S=35$°/₀₀ and the numerical expression was

---

[2] Thomas, Bertram D., Thomas G. Thompson, and Clinton L. Utterback, The electrical conductivity of sea water. Jour. Conseil, v. 9, pp. 28–35, 1934.

$$S=\frac{9817.725}{200.2+m}-4.2534 \qquad (1)$$

The best fit of the February 1960 measurements to this curve was obtained by using a standardization correction of 0.054 in X-dial reading so that a reading of 49.857 corresponded to a salinity of 35‰.

After the addition of 0.143 to the values of m (bringing the selected point to $S=35$‰ corresponding to $m=50.000$) a preliminary evaluation was made of the constants for a calibration curve assuming a second degree relationship between conductivity and salinity. In the relationship assumed, $C=C_{35}(K+LS+MS^2)$ where C is the conductivity at any salinity S and C_{35} is the conductivity at a salinity of 35‰ and K, L, and M are constants. This calibration curve has the form:

$$S=\frac{-L\pm\sqrt{L^2-4M\left[K-\frac{(m'+B)}{(m+B)}\right]}}{2M}$$

where K, L, M, and m are as above and m' is the value of the X-dial reading corresponding to a salinity of 35‰ and B is a constant depending on the impedances of the bridge not associated with the electrolyte under measurement.[3] Where m_1, m_2, m_3 and m_4 are the X-dial readings at balance corresponding to salinities S_1, S_2, S_3 and S_4 respectively, B may be evaluated by solution of the following quadratic:

$$B^2\begin{bmatrix} S_1S_2(S_2-S_1)(m_3-m_4) \\ +S_1S_3(S_3-S_1)(m_4-m_2) \\ +S_1S_4(S_4-S_1)(m_2-m_3) \\ +S_2S_3(S_3-S_2)(m_1-m_4) \\ +S_2S_4(S_4-S_2)(m_3-m_1) \\ +S_3S_4(S_4-S_3)(m_1-m_2) \end{bmatrix} + B\begin{bmatrix} S_1S_2(S_2-S_1)(m_3-m_4)(m_1+m_2) \\ +S_1S_3(S_3-S_1)(m_4-m_2)(m_1+m_3) \\ +S_1S_4(S_4-S_1)(m_2-m_3)(m_1+m_4) \\ +S_2S_3(S_3-S_2)(m_1-m_4)(m_2+m_3) \\ +S_2S_4(S_4-S_2)(m_3-m_1)(m_2+m_4) \\ +S_3S_4(S_4-S_3)(m_1-m_2)(m_3+m_4) \end{bmatrix}$$

$$+\begin{bmatrix} S_1S_2(S_2-S_1)(m_3-m_4)m_1m_2 \\ +S_1S_3(S_3-S_1)(m_4-m_2)m_1m_3 \\ +S_1S_4(S_4-S_1)(m_2-m_3)m_1m_4 \\ +S_2S_3(S_3-S_2)(m_1-m_4)m_2m_3 \\ +S_2S_4(S_4-S_2)(m_3-m_1)m_2m_4 \\ +S_3S_4(S_4-S_3)(m_1-m_2)m_3m_4 \end{bmatrix}=0$$

---

[3] Considering that the adjacent arms of the bridge containing the X- and Y-cells have some small amount of impedance not associated with the electrolytes contained in the cells and that the other two arms of the bridge are each made up of a fixed impedance and a variable impedance, let r be the impedance not associated with the electrolyte in the X-cell arm, let R be the fixed impedance in the X-dial arm, let R_2 be the total impedance of the Y-dial arm and let R_4 be the total impedance of the Y-cell arm. Then $B=R-r\frac{R_2}{R_4}$

the published salinities. Of the various partial and complete calibration measurements made in the postwar period prior to February 1960, those made in February–March 1948, are considered the most reliable and have been accepted. The cumulative discrepancy of these measurements from the February 1960, measurements, as obtained from the successive intercomparison of different batches of Copenhagen standard water, amounts to 0.085 in X-dial reading. The reconciliation of this difference between the two ends of the 12-year period may be treated in different ways. It has been assumed here that this difference occurred gradually, at the rate of 0.007 per year (ca. $0.001\,{}^{\circ}/_{\circ\circ}$S) from 1948 to 1960, and that this drift may represent a slow increase in conductivity of the Copenhagen water from solution of the glass containing-ampules during storage. Three different calibration curves were used during the period; the 1948 curve for 1948–49, the 1950 curve for 1950–56 and the 1957 curve for 1957 and subsequent measurements. The arbitrarily selected point was different for each of the curves so that a salinity of $35\,{}^{\circ}/_{\circ\circ}$ corresponded to the following X-dial readings: 1948 curve, 50.255; 1950 curve 50.100; 1957 curve, 49.911. The significant chronology of the intercomparison of the different batches of Copenhagen water, in X-dial reading, was as follows:

February–March 1948	P15=50.040
Season of 1951	P18 greater than P15 by 0.140
March 1953	P17 greater than P15 by 0.135
Season of 1956	P22 greater than P17 by 0.120
March–May 1957	P22 greater than P23 by 0.009
February 1960	P23=49.857
February 1960	P29=49.902

From the foregoing, then, the corrected values of X-dial reading which should have been used in standardization for the appropriate calibration curve used, are as follows:

1948 curve 1948	P15=50.040
1948 curve 1949	P15=50.033
1950 curve 1950	P15=49.871
1950 curve 1951	P15=49.864
1950 curve 1951	P18=50.004
1950 curve 1952	P15=49.857
1950 curve 1952	P18=49.997
1950 curve 1953	P15=49.850
1950 curve 1953	P17=49.985
1950 curve 1954	P17=49.978
1950 curve 1955	P17=49.971
1950 curve 1956	P17=49.964
1950 curve 1956	P22=50.084
1957 curve 1957	P22=49.888
1957 curve 1957	P23=49.879
1957 curve 1958	P23=49.872
1957 curve 1959	P23=49.865
1957 curve 1960	P23=49.857
1957 curve 1960	P29=49.902

The application of standardization corrections necessary to conform to these values requires the following corrections to the published salinities. It will be noted that while the corrections are tabulated below to the nearest 0.001‰, the salinities published were given to the nearest 0.01‰ and the precision of the measurements was 0.005‰.

Survey	Station	‰
1948:		
1st	3576–3599	−0.002
2d	3600–3616	0.000
3d	3617–3658	+0.001
Postseason	3659–3715	+0.001
Postseason	3716–3746	0.000
1949:		
1st and 2d	3747–3810	+0.003
3d	3811–3872	+0.001
4th	3873–3902	+0.003
5th	3903–3932	+0.006
Postseason	3933–3999	+0.001
1950:		
1st	4000–4068	+0.029
2d	4069–4144	+0.027
3d	4145–4174	+0.030
4th	4175–4238	+0.028
Postseason	4239–4306	+0.028
1951:		
1st	4307–4385	+0.023
2d	4386–4452	+0.031
2d	4453–4464	+0.028
3d	4465–4559	+0.025
Postseason	4560–4613	+0.031
1952:		
1st	4614–4740	+0.026
2d	4741–4840	+0.028
3d	4841–4940	+0.024
Postseason	4941–4970	+0.029
Postseason	4971–4980	+0.027
Postseason	4981–4984	+0.029
Postseason	4985–4988	+0.031
Postseason	4989–4994	+0.028
1953:		
1st	4995–5060	+0.030
2d	5061–5141	+0.035
3d, 4th	5142–5248	+0.029
Postseason	5249–5300	+0.030
1954:		
1st	5301–5393	+0.023
2d	5394–5476	+0.019
3d	5477–5566	+0.028
4th	5567–5661	+0.018
Postseason	5662–5740	+0.022
1955:		
1st and 2d	5741–5877	+0.027
3d	5878–5983	+0.022
Postseason	5984–6036	+0.025
1956:		
1st	6037–6122	+0.009
2d	6123–6217	+0.002
3d	6218–6284	+0.008
Postseason	6285–6335	+0.003
1957:		
1st	6336–6431	+0.032
2d	6432–6503	+0.041
2d	6504–6519	+0.040
Postseason	6520–6572	+0.042
1958:		
1st	6573–6660	+0.037
2d	6661–6740	+0.038
3d	6741–6835	+0.042
Postseason	6836–6889	+0.039
1959:		
1st	6890–6976	+0.012
2d and 3d	6977–7149	+0.009
4th and postseason	7150–7283	+0.011

It is now of interest to examine the departures of Copenhagen water from the conductivity-chlorinity relationship existing in actual sea water which has not been stored in glass containers, as represented by the discrepancies between the salinities corresponding to the stated chlorinities of the Copenhagen water and the salinities corresponding to the X-dial readings of the Copenhagen water as given above. The comparison follows.

Year	Batch	Prepared	Stated Cl‰	Equivalent S‰	S‰ by conductivity	S(conductivity) minus S(Cl) in ‰
1948	P15	1937	19.393	35.034	35.033	−0.001
1949	P15	1937	19.393	35.034	35.035	+.001
1950	P15	1937	19.393	35.034	35.036	+.002
1951	P15	1937	19.393	35.034	35.037	+.003
1952	P18	1949	19,376	35.004	35.016	+.012
1953	P17	1948	19.386	35.022	35.018	−.004
1954	P17	1948	19.386	35.022	35.019	−.003
1955	P17	1948	19.386	35.022	35.020	−.002
1956	P17	1948	19.386	35.022	35.022	.000
1957	P22	1954	19.375	35.002	35.004	+.002
1957	P23	1955	19.376	35.004	35.005	+.001
1958	P23	1955	19.376	35.004	35.006	+.002
1959	P23	1955	19.376	35.004	35.007	+.003
1960	P29	1959	19.370	34.993	35.001	+.008

It will be seen that the major discrepancies in the above table occur with 3 year old P18 where the difference was .012°/₀₀ and 1 year old P29 with a difference of .008°/₀₀ in apparent salinity. Otherwise, batches P15 (even at age 14 years), P17, P22 and P23 would have given a negligible error if they had been used as conductivity standards.

The corrections to the salinities for the period 1948 through 1959 imply corrections to the dynamic heights used in the preparation of dynamic topographic charts for the same period. While, for the most part, the relative topography remains unchanged, corrections are required to reduce all charts to a common basis before charts of the same area can be compared. The following corrections, in dynamic millimeters, should be applied to the published dynamic topographic charts to make their dynamic heights comparable. These corrections do not necessarily apply to the dynamic heights of individual stations published in the tables of oceanographic data, as consultation of the texts of the various bulletins will indicate that in some cases partial corrections have been made in the tabulated data.

Year	Bulletin No.	Figure No.	Page No.	Millimeters
1948	34	17	Facing page 73	+1. 5
		19	Facing page 74	+0. 2
		26	Facing page 74	−8. 3
		27	Page 79	−0. 8
		31	Page 84	[1] −1. 1
1949	35	14	Page 57	−9. 9
		15	Page 58	−9. 9
		16	Page 59	−0. 7
		18	Page 66	−9. 9
		20	Page 68	−4. 6
		23	Page 72	−1. 1
1950	36	16	Facing page 66	−22. 0
		17	Facing page 66	−20. 5
		18	Facing page 66	−21. 2
		23	Facing page 80	−22. 8
		29	Facing page 88	−31. 8
1951	37	7	Page 21	−17. 4
		8	Page 22	[2] −23. 5
		8	Page 22	[3] −21. 2
		9	Page 23	−19. 0
		18	Page 48	−23. 5
		21	Page 51	−35. 3
1952	38	7	Page 35	−29. 6
		8	Page 36	−19. 7
		9	Page 37	−21. 2
		10	Page 38	−18. 2
		11	Page 43	−22. 0
		13	Page 47	[4] −30. 7
		13	Page 47	[5] −33. 0
		13	Page 47	[6] −35. 3
		13	Page 47	[7] −31. 9

See footnote at end of table.

Year	Bulletin No.	Figure No.	Page No.	Milli-meters
1953	39	14	Page 51	−22.8
		15	Page 52	−26.5
		16	Page 53	−22.0
		17	Page 54	−22.0
		19	Page 62	−22.8
		37	Page 81	−34.1
1954	40	15	Page 85	−17.4
		16	Page 86	−14.4
		18	Page 88	−21.2
		19	Page 89	−13.7
		20	Page 92	−16.7
		24	Page 99	−25.0
1955	41	13	Page 64	−20.5
		14	Page 65	−12.9
		15	Page 66	−24.3
		16	Page 67	−19.0
		19	Page 75	−28.4
1956	42	12	Page 38	−6.81
		13	Page 39	−1.5
		14	Page 40	−6.1
		15	Page 41	−9.9
		20	Page 54	−3.4
1957	43	19	Page 84	−24.3
		20	Page 85	[8] −31.1
		20	Page 85	[9] −30.3
		21	Page 86	−31.9
		25	Page 99	−63.7
1958	44	19	Page 34	−28.1
		20	Page 35	−28.8
		21	Page 36	−31.9
		22	Page 37	−29.6
		33	Page 56	−39.2
1959	45	44	Page 101	−9.1
		45	Page 102	−6.8
		46	Page 103	−6.8
		47	Page 104	−8.3
		48	Page 105	−8.3
		51	Page 109	−12.5

[1] Southern section only, from Labrador to Cape Farewell.
[2] All but southernmost section.
[3] Southernmost section only.
[4] Labrador current.
[5] Center west of 50° W.
[6] Center east of 50° W.
[7] West Greenland current.
[8] Except sections extending south and west from Flemish Cap.
[9] Flemish Cap sections only.

It will be noted that the salinities characterizing the intermediate and deep water of the Labrador Sea as given in tabular form on page 103 of bulletin No. 43 of this series (season of 1957) and on page 60 of bulletin No. 44 (1958 season) should be corrected to the following values:[4]

	1957	*1958*
Intermediate water	34.86_5	34.86_1
2000 meters	34.92_9	34.92_2
2500 meters	34.93_6	34.93_0
3000 meters	34.93_3	34.91_5
3500 meters	34.90_7	34.89_6

While the tabulation of the salinity corrections being listed according to stations permits the correction of specific sections of salinity, the corrections to certain illustrations are not apparent as for instance the curves representing the T–S relationship of the water masses found in the Grand Banks region. For those, the following corrections to the salinities are necessary.

Year	*Bulletin No.*	*Figure*	*Page*	*Correction to salinity in ⁰/₀₀*
1949	35	17	63	$+0.00_2$
1950	36	22	78	$+0.02_8$
1951	37	11	31	$+0.02_4$
1952	38	12	44	$+0.02_6$
1953	39	36	77	$+0.03_0$
1954	40	22	95	$+0.02_3$
1955	41	17	70	$+0.02_7$
1956	42	16	44	$+0.00_6$ Interchange titles of figures 16 and 17.
1957	43	22	89	$+0.03_6$
1958	44	24	41	$+0.04_0$
1959	45	49	107	$+0.01_0$

It should be noted that beginning with the 1956 season, the T–S curves for the year have been compared with postwar averages. The average curves shown are in error and should be disregarded. The corrected postwar averages are compared with the prewar averages in figure 30.

Other published figures show potential densities and need the following corrections:

Year	*Bulletin No.*	*Figure*	*Page*	*Correction to σ_θ*
1953	39	40	87	$+0.02_2$
		41	87	$+0.02$
		42	87	$+0.02_4$ for broken lines $+0.02_2$ for solid lines
		44	89	$+0.024$
		43	90	Station 4971–4980, $+0.02_2$ 4981–4984, $+0.02_3$ 4985–4988, $+0.02_5$ 4989–4994, $+0.02_2$
1954	40	33, 34, 35, 36, 37	109–113	$+0.01_8$ except $+0.02_2$ for the broken lines in figure 37.
1955	41	22	79	$+0.02_0$

---

[4] In all the bulletins of this series an inferior final digit in a number indicates that that digit is in doubt and the number has not been rounded off. Thus a salinity of 34.89_6 would be rounded off to 34.90.

In bulletin 42, figures 23, 24, 25 and 26, year to year fluctuations in the temperature, salinity, and density of the intermediate and deep water of the Labrador Sea were presented for the prewar and postwar periods. With the necessary corrections applied to the postwar data much of the difference between the two periods disappears. Figure 26 of bulletin 42 has been redrawn with corrected values and extended through 1960 and is presented in this bulletin as figure 44.

Figures 24 through 28 show chronologically the dynamic topography found during the four surveys made during the season and the postseason occupation of the Bonavista triangle. Notable in the first survey, figure 24, is the weakness of the Labrador Current at the Tail of the Banks, the relatively small area of cold mixed water southeastward of the Tail, and the correspondingly great northwestward and westward incursion of Atlantic Current water toward the Grand Banks at the 42d and 44th parallels.

Comparison of figure 24 with figure 25 indicates a weakening of the Labrador Current between about latitudes 45° N., and 45°30′ N. (the northern margin of the first survey and the southwestern margin of the second survey). The pronounced meander of Atlantic Current water toward the Grand Banks seen at the 44th parallel in figure 24 is probably responsible for the clockwise eddy present in the southern edge of the second survey between longitudes 46° W., and 47° W. It is also noted that figure 25 shows some possibility of bergs moving southeastward between Flemish Cap and the Grand Banks.

Figure 26 shows the dynamic topography of the Bonavista triangle found during the third survey. The current pattern along the southwestern side of the triangle is somewhat simpler than usual, although the westward flow near the southern corner may recurve eastward south of the surveyed area instead of continuing westward across the banks as suggested by the figure.

The fourth survey (fig. 27) again shows a warm water clockwise eddy, centered at about 44°30′ N., 48° W., which is considered to be a remnant of an earlier meander of the Atlantic Current. Between this eddy and another Atlantic Current meander northeastward of it, there is a weak eastward meander of Labrador Current water. As in the second survey, some of the Labrador Current meanders onto the Grand Banks at about the 46th parallel. The southern edge of the surveyed area shows a remarkably wide quiet area south of the northernmost band of the Atlantic Current.

Comparison of figure 28 with figure 26 shows that there was a slight weakening of the Labrador Current between the third survey and the postseason cruise. Normally the change would be in the other direction. The geographical division between the eastern and western branches of the Labrador Current changed offshore during the interval. Figure 26 indicates that southward moving bergs crossing the 49th parallel eastward of about 51°40′ W., would follow the eastern branch

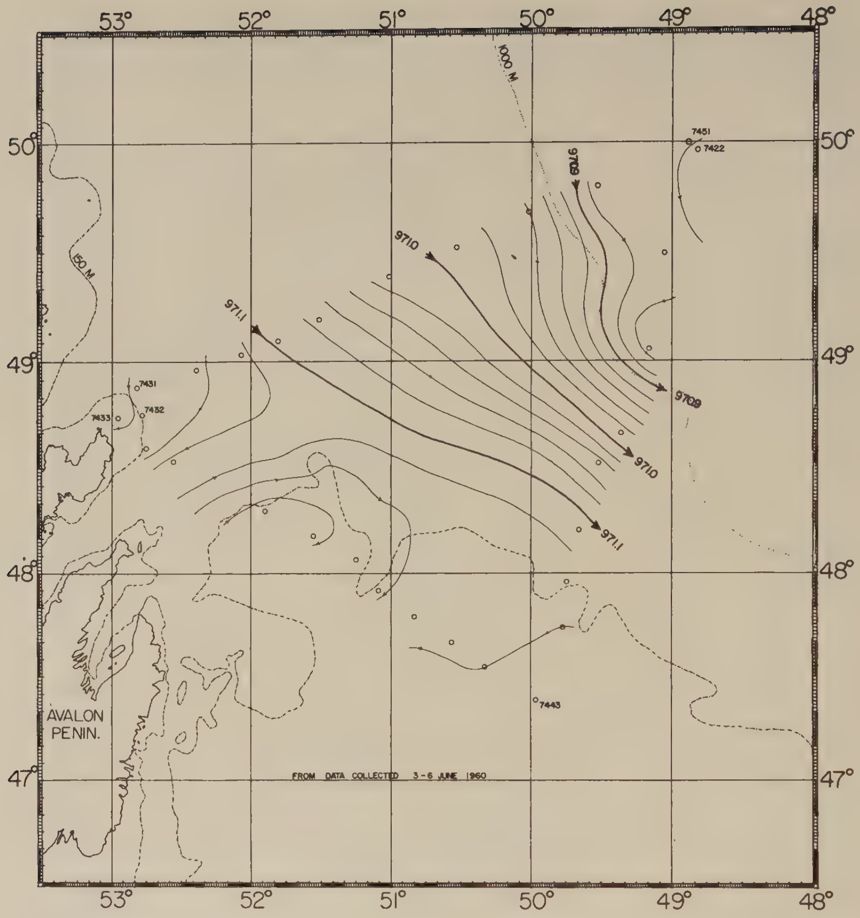
53°
52°
51°
50°
49°
48°
50°
49°
48°
47°
1000 M.
150 M.
7451
7422
7431
7432
7433
7443
971.0
971.1
970.9
971.0
971.1
AVALON PENIN.
FROM DATA COLLECTED 3-6 JUNE 1960

Figure 26.—Dynamic topography of the sea surface relative to the 1,000-decibar surface, from data collected 3–6 June 1960. Oceanographic station positions are indicated and the station numbers given at turning points.

whereas during the postseason occupation of the Bonavista triangle, figure 28 indicates that only such bergs as might cross the 49th parallel eastward of about 50°30′ W., would follow the eastern branch.

The first survey, the southern part of the second survey and the fourth survey covered areas in the Grand Banks region from which sufficient earlier data are available to permit the designation of normal temperature-salinity relationships of the Labrador Current and Atlantic Current water masses and the virtual water mass of mixed water derived from these two water masses. Figure 29 compares the T–S relationships of the Labrador Current water, Atlantic Current water and mixed water found during the above mentioned surveys in 1960 with the mean relationships for the 13-year period 1948–60.

Whereas the temperature minimum in the Labrador Current characteristically occurs at a depth of about 75 meters, in 1960 it occurred

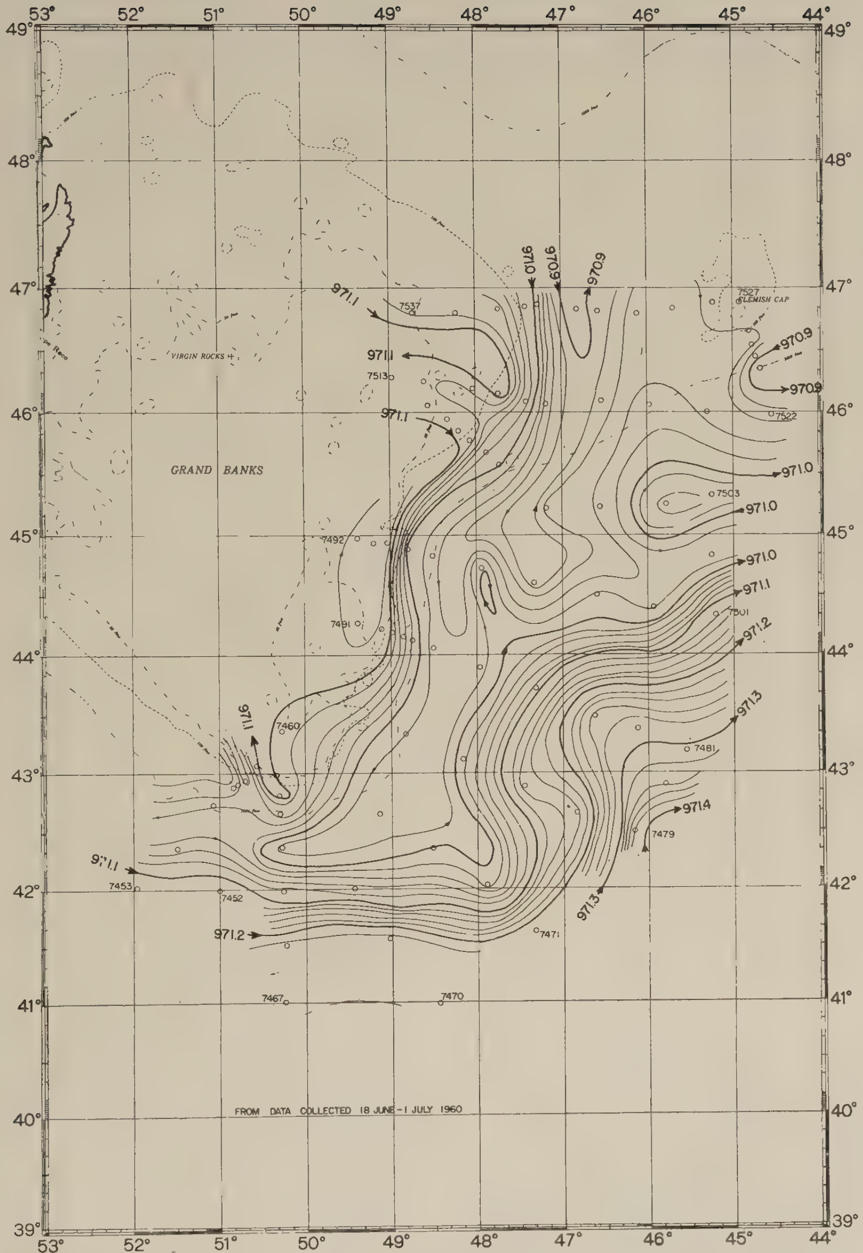
53°
52°
51°
50°
49°
48°
47°
46°
45°
44°
49°
48°
47°
46°
45°
44°
43°
42°
41°
40°
39°
VIRGIN ROCKS
GRAND BANKS
FLEMISH CAP
971.0
970.9
970.9
971.1
971.1
971.1
970.9
970.9
971.0
971.0
971.0
971.1
971.2
971.3
971.4
971.1
971.1
971.2
971.3
7537
7513
7527
7522
7503
7501
7492
7491
7460
7481
7479
7453
7452
7471
7467
7470
FROM DATA COLLECTED 18 JUNE–1 JULY 1960

FIGURE 27.—Dynamic topography of the sea surface relative to the 1,000-decibar surface, from data collected 18 June–1 July 1960. Oceanographic station positions are indicated and the station numbers given at turning points.

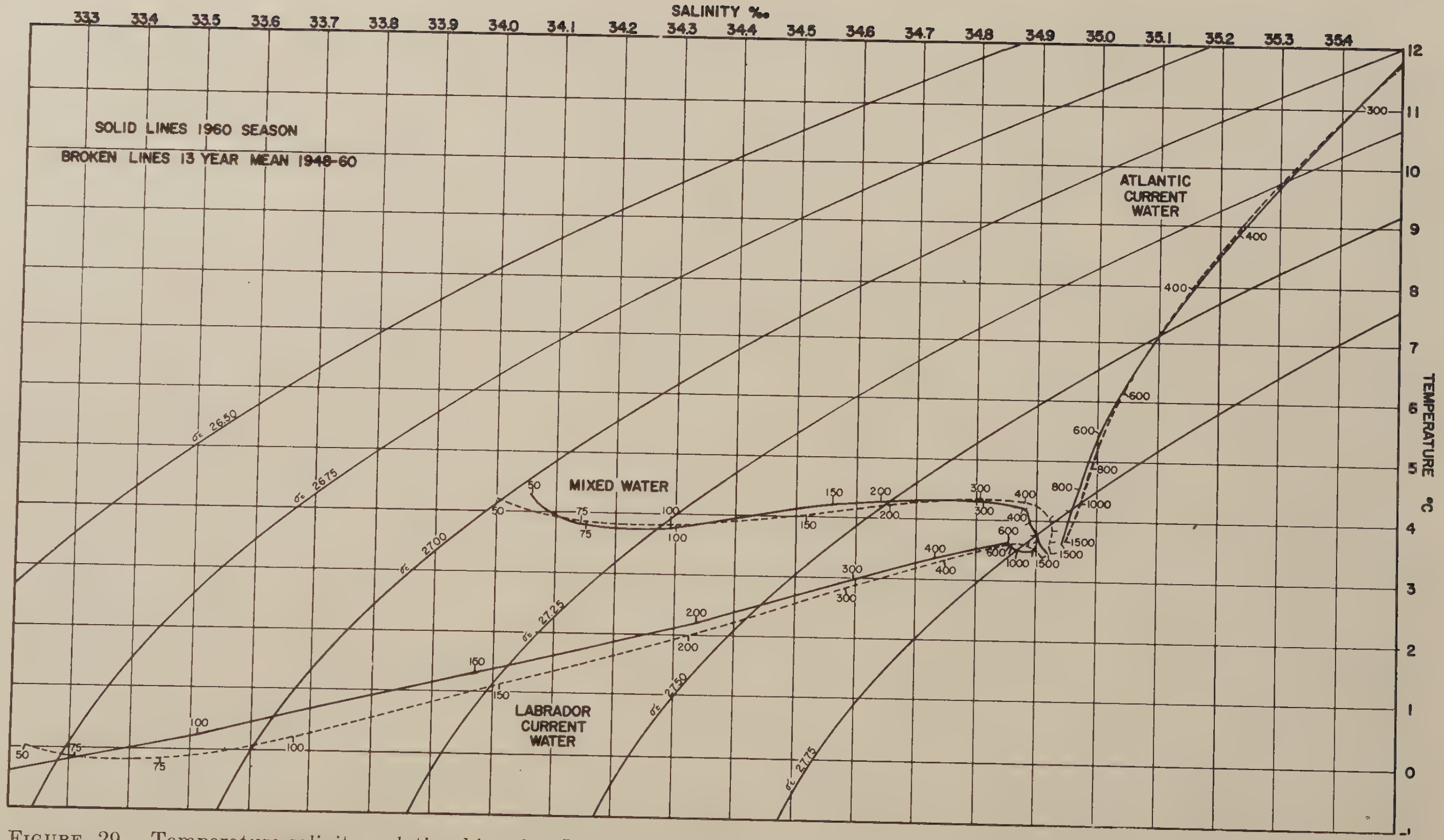

FIGURE 29.—Temperature-salinity relationships for Labrador Current water, Atlantic Current water and mixed water found in the Grand Banks region. Solid lines show conditions found during 1960 and broken lines represent the 13-year means for the period 1948–60. An approximate depth scale is given in meters.

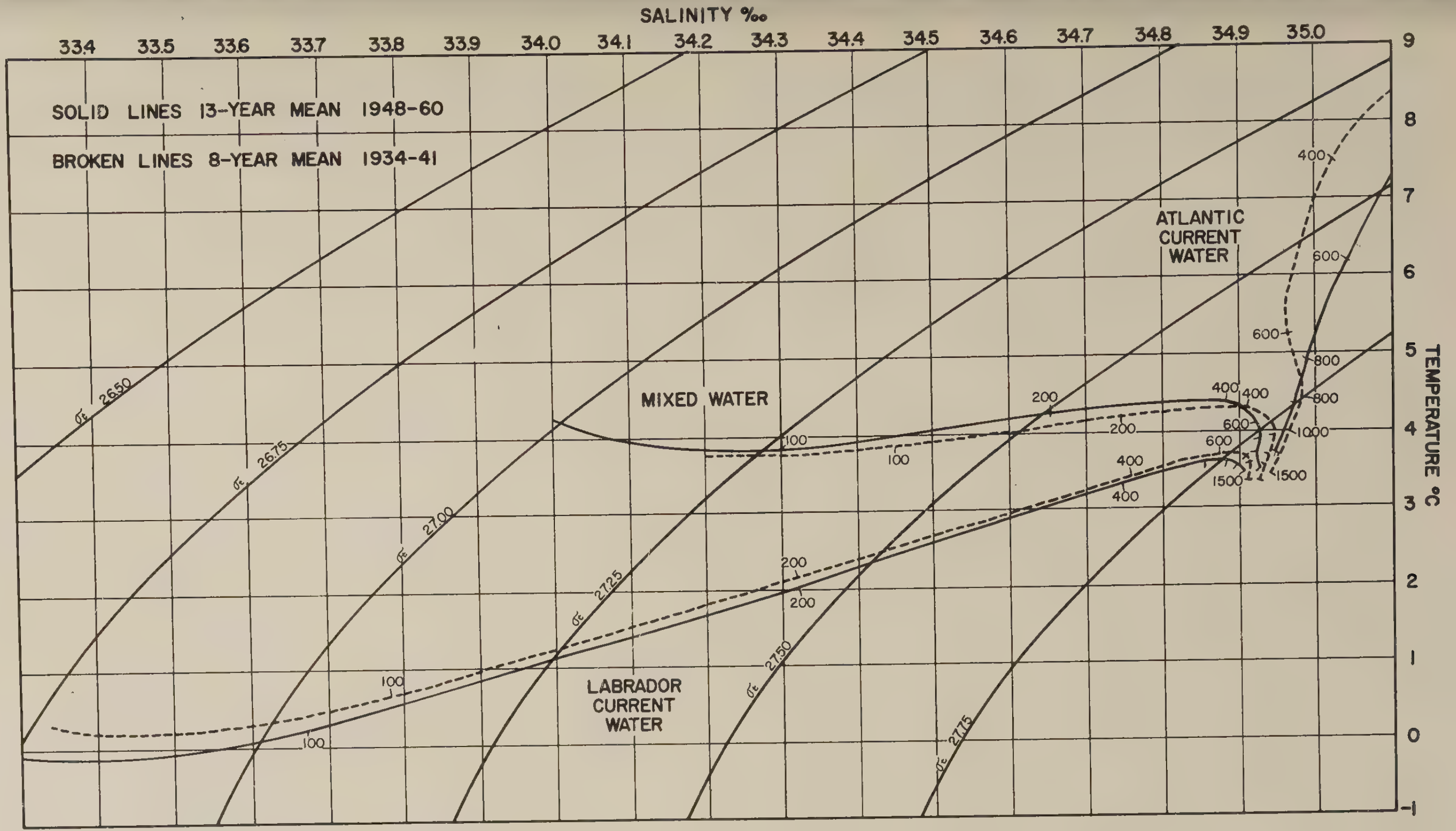

FIGURE 30.—Mean temperature-salinity relationships for Labrador Current water, Atlantic Current water and mixed water found in the Grand Banks region during the period 1948–60 (shown as solid lines) compared with means for the period 1934–41 (shown as broken lines).

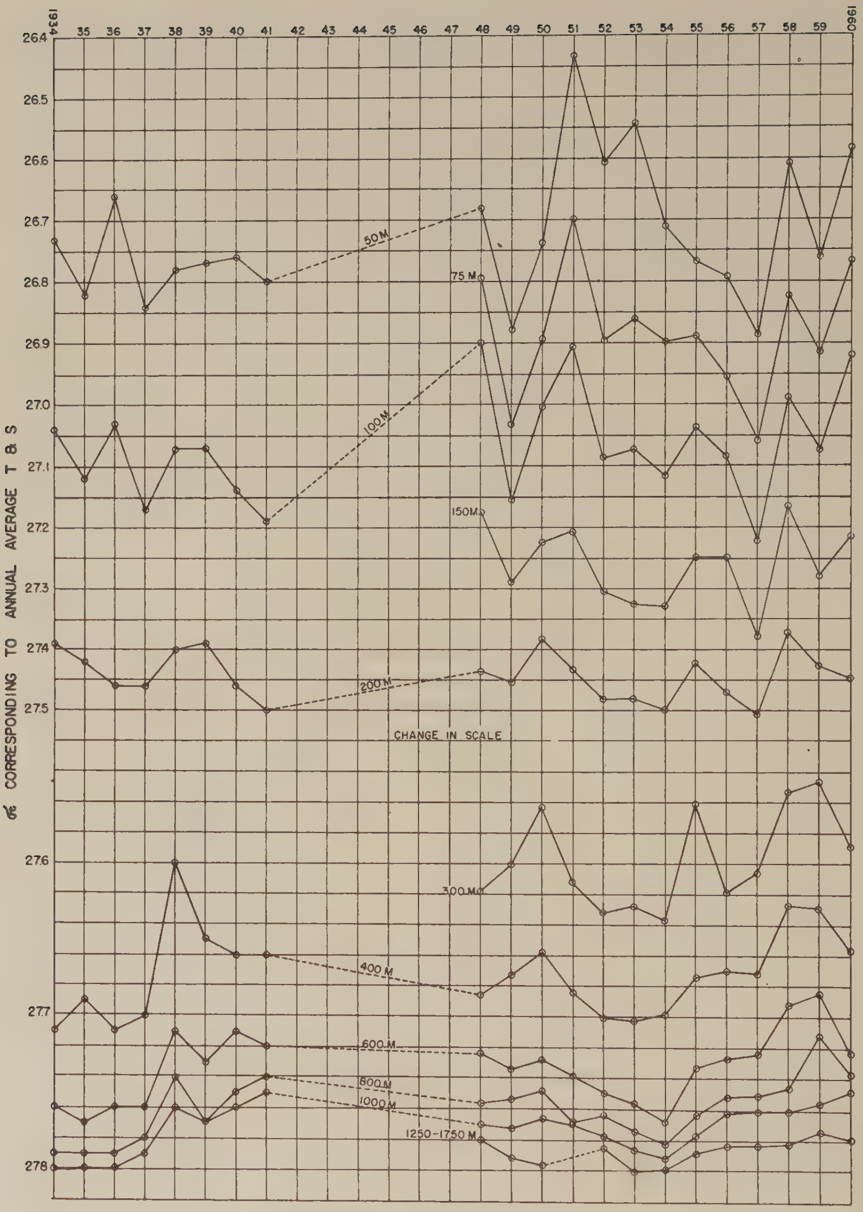

FIGURE 31.—Year-to-year fluctuations in density of the Labrador Current water found in the Grand Banks region at selected levels 1934–41 and 1948–60. The plotted points represent values of σ_t corresponding to the average temperature and average salinity for the particular year and level.

The temperature and salinity distribution found along the extra-southerly sections of the first survey are shown in figures 32–35. Departures of the individual stations from the specified meridian may be seen by referring to figure 24. The various bands of current shown in the dynamic topographic chart can also be identified in the temperature and salinity sections. Comparing the two sections it will be seen that the highest temperature in the western section is slightly warmer than in the eastern section. Otherwise the temperatures and salinities within particular current bands show little difference between the two sections.

The section along the meridian of 50°15′ W., has been occupied by ships of the International Ice Patrol before. In 1938, the *General Greene* occupied the section during the period when the *Armour Hansen* and *Altair* were engaged in their investigation of the Gulf Stream system in the Azores sector. The *Evergreen* occupied the section in 1950 at the time of Operation Cabot and again in 1958 as a part of the activity of the International Geophysical Year.

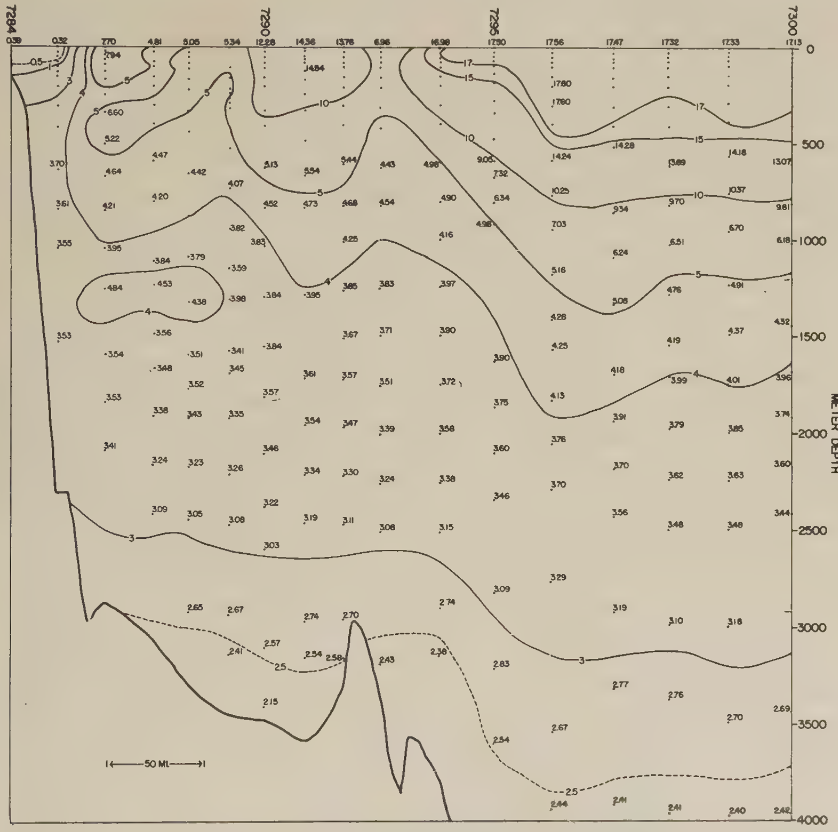

FIGURE 32.—Temperature distribution along meridional section at 48°30′ W., from data collected 2–7 April 1960.

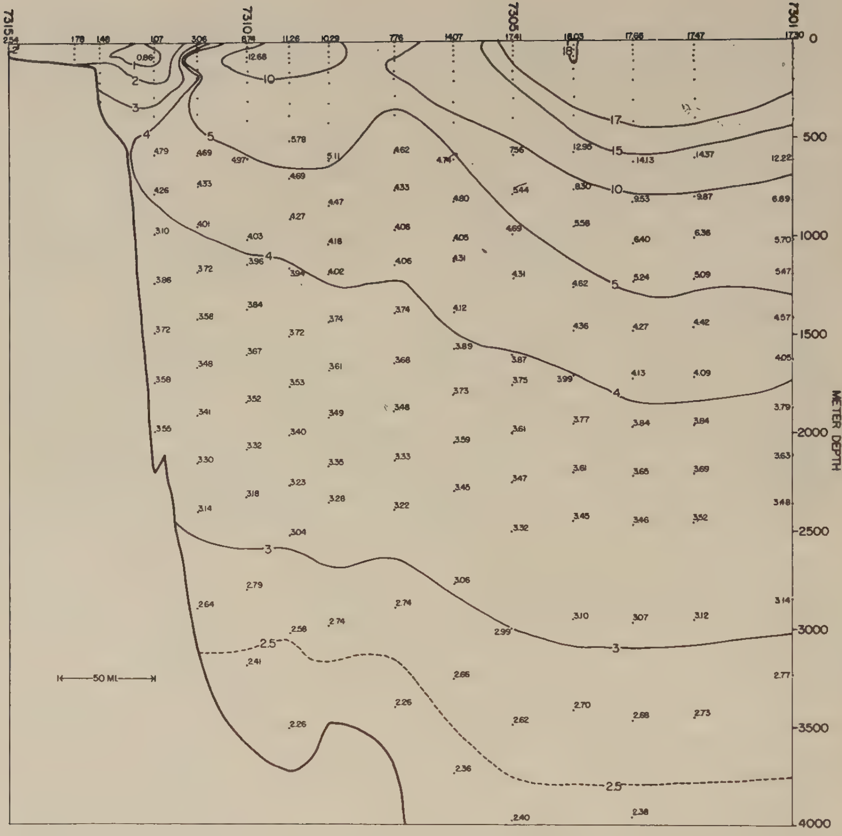

FIGURE 33.—Salinity distribution along meridional section at 48°30′ W., from data collected 2–7 April 1960.

The dynamic topography of the sea surface shown in figure 24 is referred to the 1,000-decibar surface. While this reference surface is satisfactory for studies of the Labrador Current in the Grand Banks region, the motionless surface beneath the Atlantic Current is more nearly the 2,000-decibar surface and this deeper surface was used for reference in studying the velocity distribution and volume and heat transports of the Atlantic Current at the section located along 50°15′ W. Figure 24 is still useful in showing the current pattern even though the absolute velocities are in error.

Figure 36 is a schematic representation of the bands of the Labrador and Atlantic Currents as they usually are found crossing a section along this meridian and is presented here to facilitate a discussion of the 1960 occupation of the section in comparison with the earlier occupations. An important part of the Atlantic Current crosses the section as A in figure 36. Some of A recurves toward Bermuda as B, some recurves northwestward as D and some continues to the eastward as C. D again recurves to the eastward after being joined by a part of the Atlantic Current, G, which recurved northwestward west of the section. G may be considered to include a small amount of water from the U.S. and Canadian shelves, and G and D together make up E. The Labrador Current, F, crossing the section to the westward, recurves and recrosses the section, with some admixture of water from G and D, as mixed water paralleling and on the northern side of E. The net contribution of the Atlantic Current to the eastward of the Grand Banks, then, is E plus C.

The following table summarizes the volume transports of these various components found during the four occupations. Units are millions of cubic meters per second. Values of components are computed except where otherwise indicated. Values derived by sum or difference of other components are indicated by (d). Values determined graphically by planimeter are indicated by (p). Some of the values are less reliable and are considered estimates labeled (e). It appears that in 1960, a closed counterclockwise eddy was present near the southern end of the section and consequently the southeastward

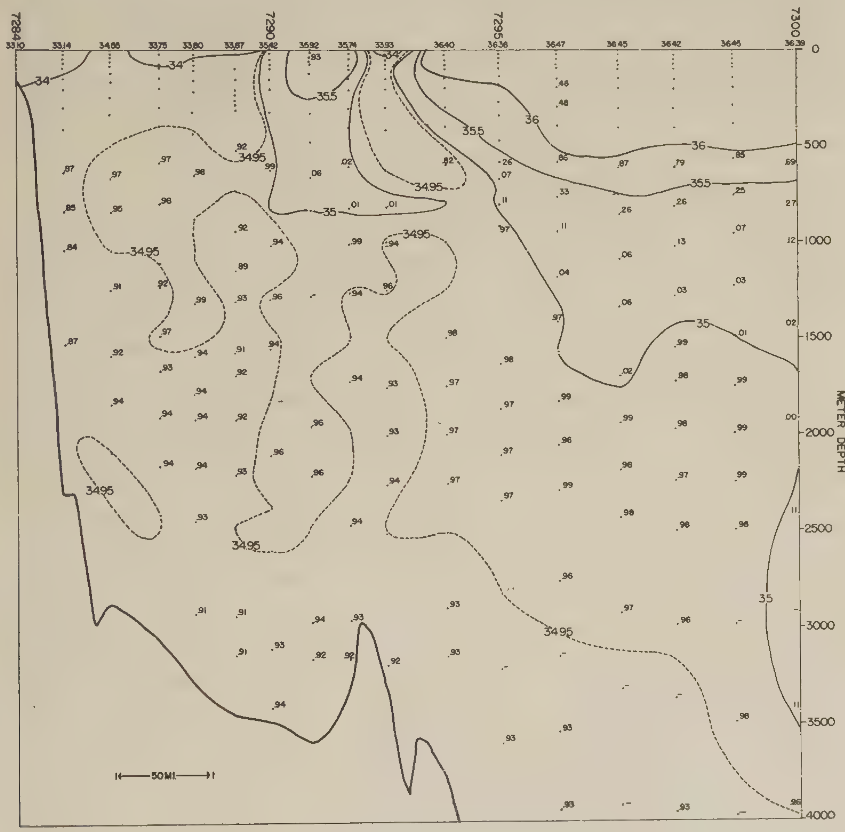

FIGURE 34.—Temperature distribution along meridional section at 50°15′ W., from data collected 7–10 April 1960.

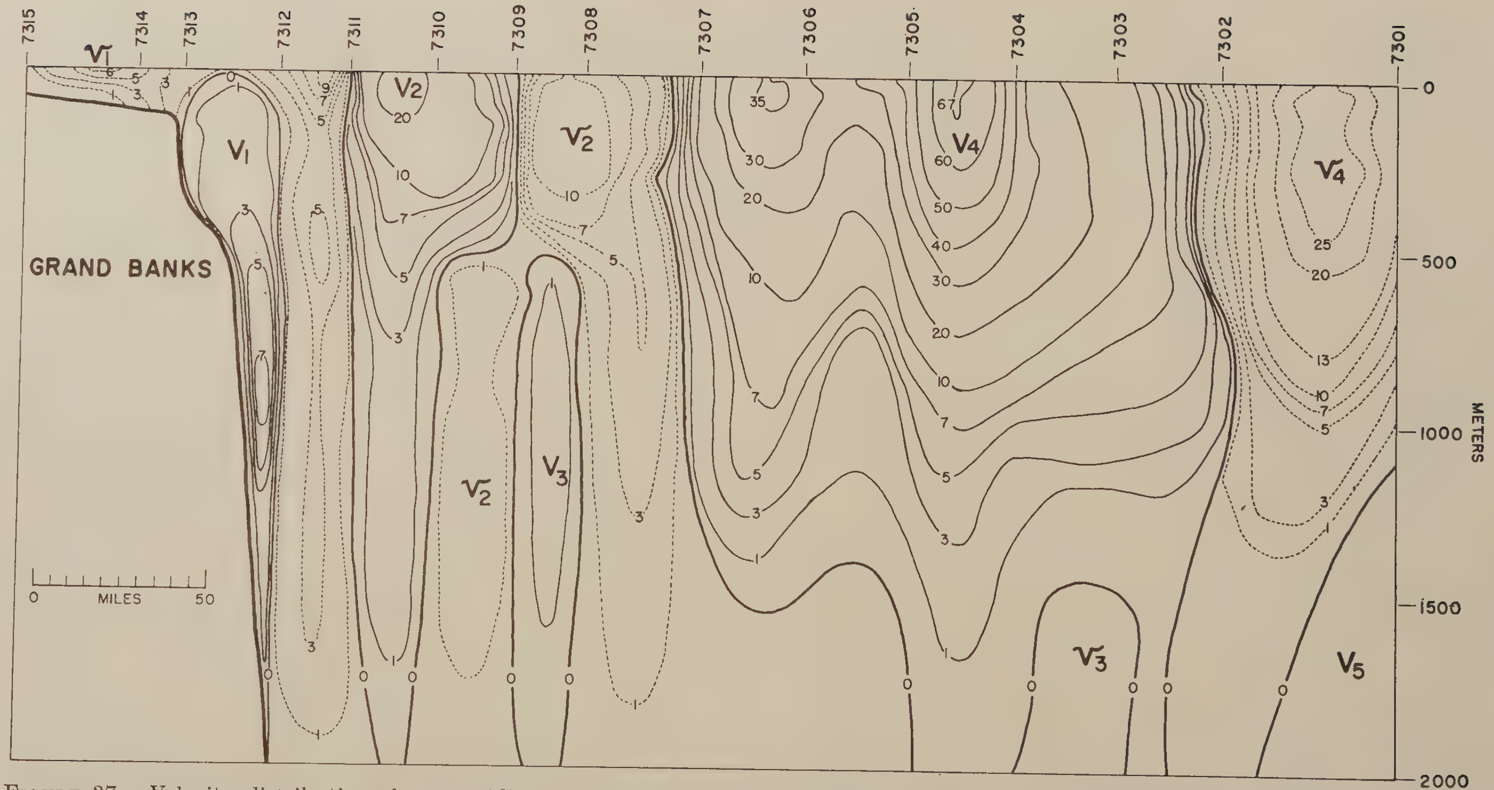

FIGURE 37.—Velocity distribution along meridional section at 50°15′ W., from data collected 7–10 April 1960. Velocities are referred to the 2,000-decibar surface. Easterly-flowing currents are shown as solid lines and westerly-flowing currents are shown as broken lines.

Grand Banks for this occupation of the section are given below in comparison with similar quantities for earlier occupations:

	E		*C*		*E+C*	
	Heat transport	*Mean temperature*	*Heat transport*	*Mean temperature*	*Heat transport*	*Mean temperature*
1938	--------	--------	--------	--------	312.	13. 0
1950	--------	--------	--------	--------	779.	13. 4
1958	159.	12. 1	447.	13. 5	606.	13. 1
1960	37.	8. 8	521.	13. 0	558.	12. 6

The lower mean temperature found during this occupation is noted as well as the fact that the 1960 measurements were made earlier in the spring. Although the Atlantic Current extends to considerable depth, since the highest velocity occurs in the upper layers and the heat transport and mean temperature are weighted according to velocity distribution seasonal changes in temperature in the upper layers cannot be disregarded and at this writing the significance of seasonal changes in heat transport and mean temperature cannot be accurately assessed in consideration of the above tabulated values.

From the 14 stations (7294–7307) which were located south of 41° N., during the first survey 53 observations from the water beneath the Atlantic Current were examined for potential temperature-salinity relationship and a curve representing them has been shown as a solid line in figure 38. Because of the small number of observations the curve has uncertainties, but at potential temperatures above about 2.6° it departs toward lower salinities from the curve shown by Bradshaw and Schleicher[6] for the deep water west of Bermuda. At lower potential temperatures there is no significant difference. The broken line in figure 38 is taken from Bradshaw and Schleicher. Fourteen observations from the deeper water beneath the Atlantic Current, made during the 1958 occupation of this section are shown as circles in figure 38.

A number of sections across the Labrador Current have been repeatedly occupied in connection with the routine current surveys of the Grand Banks region and on the postseason cruises. The locations of these sections are as follows: Sections NW., SW., and SE. are the northwestern, southwestern and southeastern sides of the Bonavista triangle which is defined by its corners located at 50° N., 49° W.; 47°20′ N., 50° W., and just off Cape Bonavista, Newfoundland; Section H is roughly parallel to SE. and extends northeasterly from about 47°10′ N., 49°15′ W.; section G extends northeasterly from about 47°10′ N., 48°40′ W.; section F_2 is an east-west section between the Grand Banks and Flemish Cap at the parallel of 47°15′ N.; section F is similar to F_2 but about 30 miles farther south; section T extends southeasterly from about 46°20′ N., 49° W.; section U ex-

---

[6] Bradshaw, Alvin L., and Karl E. Schleicher "A Conductivity Bridge for the Measurement of Salinity of Sea Water" Woods Hole Oceanographic Institution Reference No. 56–20. Unpublished Manuscript.

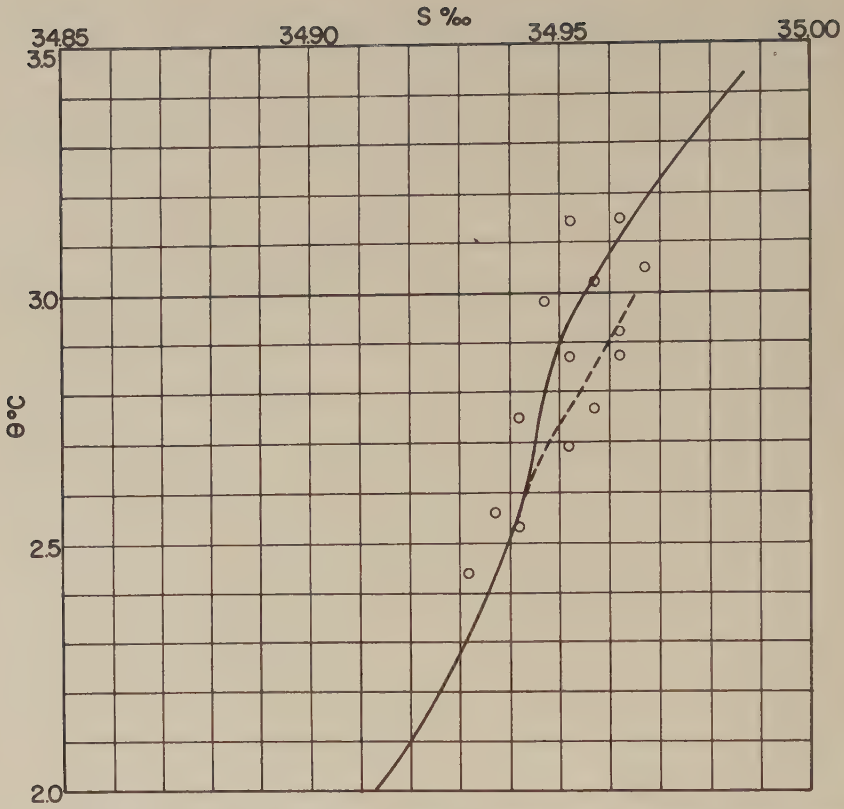

FIGURE 38.—Potential temperature-salinity relationship found beneath the Atlantic Current south of the Grand Banks 2–10 April 1960 (solid line) and 23–26 May 1958 (circles) compared with the relationship reported by Bradshaw and Schleicher for the deep water west of Bermuda (broken line).

tends easterly from the Grand Banks at about 45° N.; section W extends southerly from the Grand Banks along the meridian of 50°15′ W.; the South Wolf Island section extends northeasterly from South Wolf Island, Labrador, and is a part of the section across the Labrador Sea from South Wolf Island to Cape Farewell, Greenland.

A sufficient number of occupations of many of these sections has permitted the development of tentative normal seasonal variation relationships. Those previously developed for the Labrador Current were published as follows:

Sections NW., SW., and SE	bulletin No. 39 (season of 1953)
Sections F and G	bulletin No. 42 (season of 1956)
South Wolf Island section	bulletin No. 44 (season of 1958)

Tentative normals for sections T, U, and W have been redetermined and are shown herewith in figure 39. All occupations of these sections through 1960 were grouped according to months. The monthly groups from mid-April to mid-May were then averaged and plotted against their mean dates as the circles shown in the figure. Average mean monthly rates of change were then used to extend the lines in each direction from these circled points. While the tentative normals shown in figure 39 are better than those previously published in Bulletin 36 of this series, the remaining irregularities indicate that there are still imperfections in the curves.

Data are insufficient to determine even tentative normals for sections H and F_2.

Volume transport, mean temperature, minimum observed temperature and heat transport were evaluated for 23 occupations of such sections in 1959 and 18 occupations in 1960, and are tabulated below in comparison with seasonal normal values where they are available. Temperatures are given in °C, volume transport in millions of cu.m/sec. and heat transport in millions of cu.m°C/sec. Figure 40 is a schematic diagram representing the circulation deduced from the volume transports found during the 1960 surveys and listed in the table. In the first survey the Labrador Current was warmer than normal both as to mean temperature and minimum observed temperature. Recurvature after passing latitude 45° N., reduced the volume transport from greater than normal at section U to decidedly below normal at section W. In the second survey very nearly normal volume at section G did not suffer the usual losses and so was above normal at sections F and T. Mean temperatures were near normal at G and F and above normal at T. The coldest water graded from colder than normal in the north to warmer than normal in the south.

In both the third survey and postseason occupations of the Bonavista triangle the volume transports appearing in figure 40 have been adjusted so that the volume entering past section NW equals the sum of the volumes leaving across the other two sections. Considering this "mean triangle" the volume transport was about a million cu.m/sec. above normal during the third survey and about a quarter of a million above normal during the postseason cruise. Minimum temperatures were about normal in both occupations. Mean temperatures, however, went from near normal during the third survey to about 0.9° above normal during the postseason cruise. During the fourth survey, the mean temperature anomalies warmed from -0.2 at section F to $+0.3$ at U and dropped to slightly below normal at W. Volumes were below normal at F and T and above normal at U and W. These changes are considered to result from losses of Labrador Current water seaward and additions of warmer water from the Grand Banks.

Off South Wolf Island both the volume transport and mean temperature were above normal with a resulting large heat transport.

Section U has been occupied 56 times during 21 different years and the occupation during the first survey of 1960 is the first time that a positive temperature has been recorded as the minimum observed

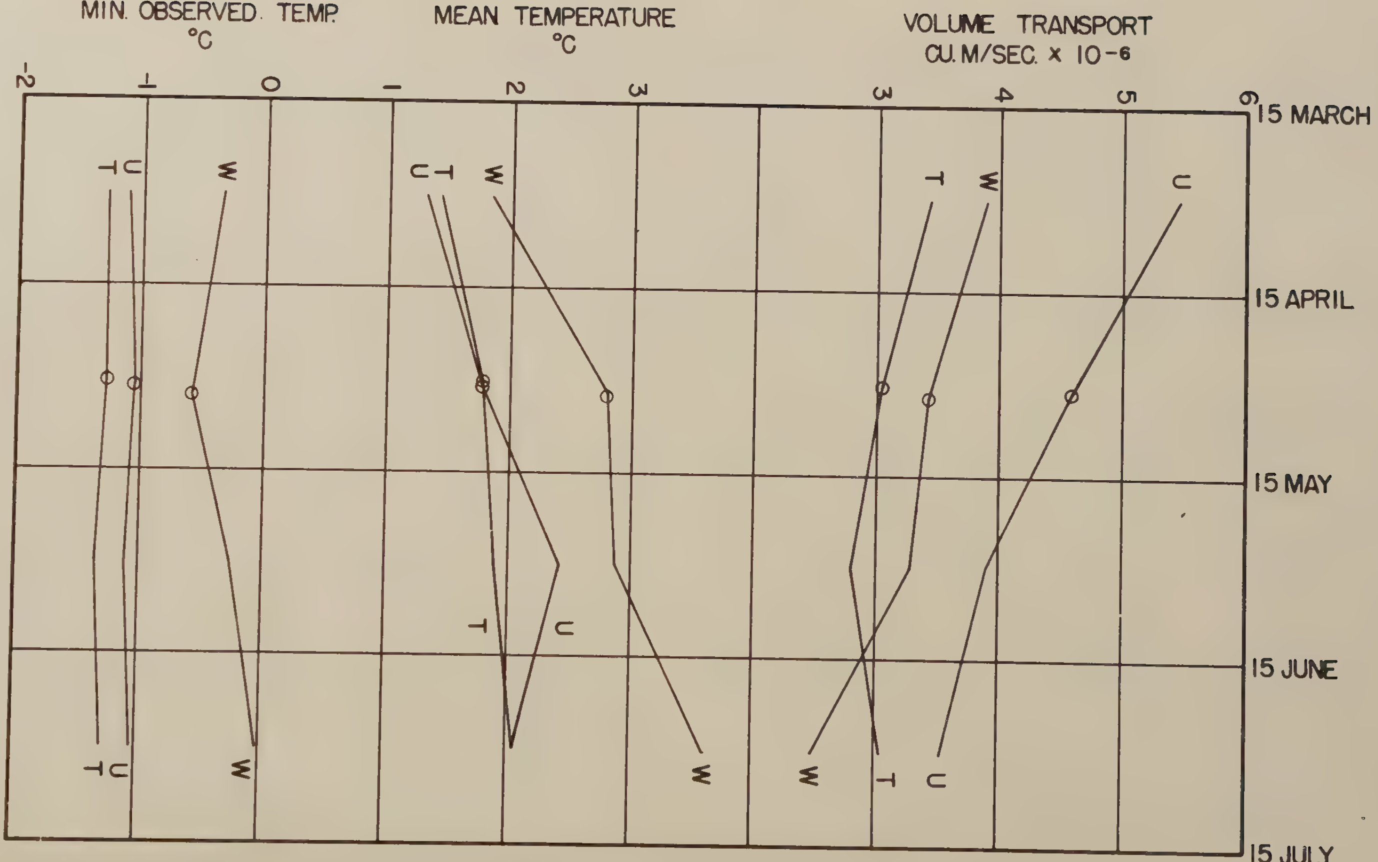

FIGURE 39.—Tentative normal seasonal change in volume transport, mean temperature and minimum observed temperature of the Labrador Current at sections T, U and W.

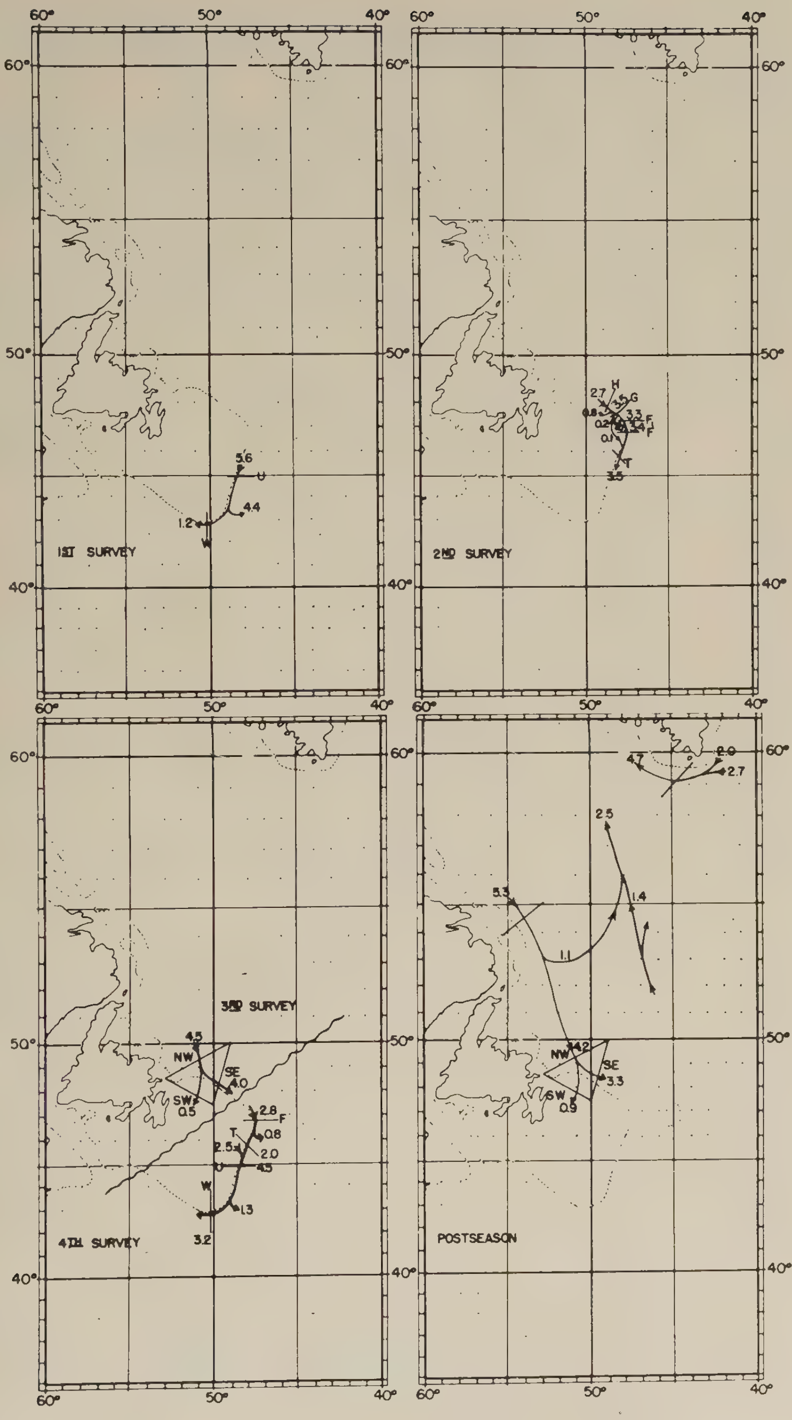
60°
50°
40°
1ST SURVEY
5.6
U
4.4
1.2
W
2ND SURVEY
2.7
H
G
3.3
F
0.2
0.1
T
3.5
3RD SURVEY
4TH SURVEY
NW
4.5
SE
4.0
SW
0.5
2.8
F
T
0.8
2.5
2.0
4.5
U
W
1.3
3.2
POSTSEASON
4.7
2.9
2.7
2.5
5.3
1.4
1.1
4.2
NW
SE
3.3
SW
0.5

FIGURE 40.—Schematic representation of circulation deduced from sections occupied in 1960. Numerals indicate volume transport in units of $m^3 \times 10^6$/sec.

SUMMARY OF VELOCITY SECTIONS ACROSS THE LABRADOR CURRENT

SECTIONS OCCUPIED IN 1959

	Volume transport			Mean Temperature			Minimum observed temperatures			Heat transport		
	1959	Normal	Anomaly	1959	Normal	Anomaly	1959	Normal	Anomaly	1959	Normal	Anomaly
First survey:												
F	4.17	2.75	+1.42	1.24	1.58	−0.34	−1.33	−1.26	−0.07	5.15	4.34	+0.81
T	3.72	3.24	+0.48	1.39	1.61	−0.22	−1.33	−1.27	−0.06	5.18	5.22	−0.04
U	5.38	5.13	+0.25	1.12	1.49	−0.37	−1.31	−1.09	−0.22	6.05	7.64	1.59
W	6.48	3.79	+2.69	1.67	2.03	−0.36	−0.55	−0.38	−0.17	10.85	7.69	+3.16
Second survey:												
F	2.40	2.93	−0.53	1.08	1.79	−0.71	−1.47	−1.29	−0.18	2.59	5.24	−2.65
T	1.93	2.97	−1.04	1.97	1.81	+0.16	−1.41	−1.30	−0.11	3.80	5.38	−1.58
U	3.72	4.48	−0.76	1.52	1.89	−0.37	−0.85	−1.07	+0.22	5.65	8.47	−2.82
W	3.99	3.45	+0.54	0.90	2.74	−1.84	−0.94	−0.58	−0.36	3.58	9.45	−5.87
Third survey:												
F	4.30	3.13	+1.17	0.34	2.02	−1.68	−1.41	−1.33	−0.08	1.45	6.32	−4.87
T	4.14	2.82	+1.32	1.49	1.90	−0.41	−1.41	−1.34	−0.07	6.17	5.36	+0.81
U	4.14	3.87	+0.27	1.29	2.39	−1.10	−1.07	−1.10	+0.03	5.34	9.25	−3.91
W	3.30	3.30	0.00	1.93	2.86	−0.93	−0.14	−0.30	+0.16	6.38	9.44	−3.06
Fourth survey:												
NW	2.49	3.73	−1.24	−0.17	1.21	−1.38	−1.70	−1.67	−0.03	−0.43	4.51	−4.94
SW	0.24	0.51	−0.27	0.49	−0.30	+0.79	−1.65	−1.64	−0.01	0.12	−0.15	+0.27
SE	3.68	3.14	+0.54	1.97	1.73	+0.24	−1.42	−1.54	+0.12	7.26	5.43	+1.83
H	4.24			1.92			−1.57			8.16		
G	3.40	2.68	+0.72	2.17	2.12	+0.05	−1.55	−1.32	−0.23	7.38	5.68	+1.70
F_2	4.26			2.48			−1.40			10.55		
F	2.67	3.27	−0.60	1.51	2.17	−0.66	−1.11	−1.35	+0.24	4.03	7.10	−3.07
Post season:												
NW	4.59	4.30	+0.29	1.56	1.57	−0.01	−1.66	−1.57	−0.09	7.15	6.75	+0.40
SW	0.52	0.71	−0.19	2.41	0.33	+2.08	−1.64	−1.65	+0.01	1.26	0.23	+1.03
SE	4.74	3.44	+1.30	2.01	2.15	−0.14	−1.44	−1.61	+0.17	9.52	7.40	+2.12
South Wolf Island	5.14	6.42	−1.28	2.25	3.03	−0.78	−1.47	−1.45	−0.02	11.55	19.45	−7.90

SECTIONS OCCUPIED IN 1960

	Volume transport			Mean Temperature			Minimum observed temperatures			Heat transport		
	1960	Normal	Anomaly	1960	Normal	Anomaly	1960	Normal	Anomaly	1960	Normal	Anomaly
First survey:												
U	5.59	5.03	+0.56	1.77	1.55	+0.22	0.02	−1.09	+1.11	9.89	7.80	+2.09
W	1.23	3.73	−2.50	2.58	2.13	+0.45	0.86	−0.42	+1.28	3.19	7.94	−4.75
Second survey:												
H	2.65			0.92			−1.58			2.44		
G	3.53	3.48	+0.05	1.56	1.66	−0.10	−1.56	−1.24	−0.32	5.52	5.78	−0.26
F_2	3.28			1.38			−0.95			4.54		
F	3.40	2.88	+0.52	1.79	1.74	+0.05	−1.01	−1.29	+0.28	6.09	5.01	+1.08
T	3.41	3.03	+0.38	2.72	1.81	+0.91	−0.80	−1.27	+0.47	9.27	5.48	+3.79
Third survey:												
NW	4.79	3.55	+1.24	1.46	1.10	+0.36	−1.67	−1.70	+0.03	7.02	3.90	+3.12
SW	0.47	0.46	+0.01	0.47	−0.48	+0.95	−1.64	−1.63	−0.01	0.22	−0.22	+0.44
SE	3.84	3.06	+0.78	1.16	1.62	−0.46	−1.65	−1.52	−0.13	4.44	4.96	−0.52
Fourth survey:												
F	2.85	3.33	−0.48	2.04	2.24	−0.20	−1.54	−1.36	−0.18	5.83	7.46	−1.63
T	1.99	3.02	−1.03	2.26	2.04	+0.22	−1.26	−1.29	+0.03	4.50	6.16	−1.66
U	4.54	3.59	+0.95	2.44	2.10	+0.34	−1.36	−1.05	−0.31	11.08	7.54	+3.54
W	3.24	2.76	+0.48	3.18	3.32	−0.14	−0.48	−0.11	−0.37	10.29	9.16	+1.13
Post season:												
NW	4.49	3.97	+0.52	2.71	1.36	+1.35	−1.62	−1.63	+0.01	12.19	5.40	+6.79
SW	0.79	0.60	+0.19	0.34	−0.02	+0.36	−1.63	−1.64	+0.01	0.27	−0.01	+0.28
SE	3.05	3.28	−0.23	2.48	1.93	+0.55	−1.57	−1.57	0.00	7.56	6.33	+1.23
South Wolf Island	5.27	4.37	+0.90	2.56	2.21	+0.35	−1.67	−1.54	−0.13	13.47	9.66	+3.81

temperature. The mean temperature during the postseason occupation of the Bonavista triangle was the warmest on record with 25 occupations during 13 years.

Figures 41 through 43 show the dynamic topography in the vicinity of the Labrador Sea section and the temperature and salinity distribution found along that section during the postseason cruise. As the stations were disposed in the form of a single section, rather than a network, the dynamic topography along the section is somewhat conjectural especially in the quieter water of the central Labrador Sea. The Labrador Current, divided by the shoal off Hamilton Inlet, and the outer part of the West Greenland Current off Cape Farewell are recognizable. In the temperature section, the characteristic frigid water over the shelf and temperature maximum tongue extending downward toward the continental slope identify the Labrador Current. In 1960, this temperature maximum tongue was warmer than usual. On the Greenland side the temperature maximum of greater than 6° identifies the Irminger Current component of the West Greenland Current. As previously noted, sea ice prevented the extension of the section beyond station 7588 so no information is available regarding the shape of the isotherms and isohalines in the colder fresher water inshore of the core of the Irminger Current water.

The temperature minimum remnant in the intermediate water of the Labrador Sea was warmer than usual with a coldest observation of 3.23°. The depth of the temperature maximum beneath it was shoaler than usual, located near 1,500 meters. The deep salinity maximum layer appears to have been centered at about 2,500 meters.

In considering the volume transport, mean temperature and heat transport of the West Greenland Current at the time of the 1960 occupation of the Labrador Sea section reasonable assumptions were made in extrapolating a section of anomaly of specific volume from station 7588 to the beach as well as in the extrapolation of isotherms. The resulting figures for volume transport, mean temperature and heat transport of the West Greenland Current were 6.09, 4.95, and 30.17 respectively. Comparable normal values, from the curves published in bulletin 35 of this series, are 4.70, 4.50, and 21.14. The corresponding figures for 1959 were 7.56, 4.29, and 32.40 when the normal values were 4.37, 5.14, and 22.49.

Considering the West Greenland Current to be made up of an Irminger Current component of constant mean temperature of 5.5° and an East Greenland Current component of constant mean temperature of 3.2° these components had volume transports of 4.64 and 1.45 respectively in 1960 compared with seasonal normals of 2.65 and 2.05 and in 1959 they were 3.57 and 3.99 compared with seasonal normals of 3.70 and 0.67. Thus in 1959, the Irminger Current component was near normal and the East Greenland Current component had a large positive anomaly. In 1960, the East Greenland Current component

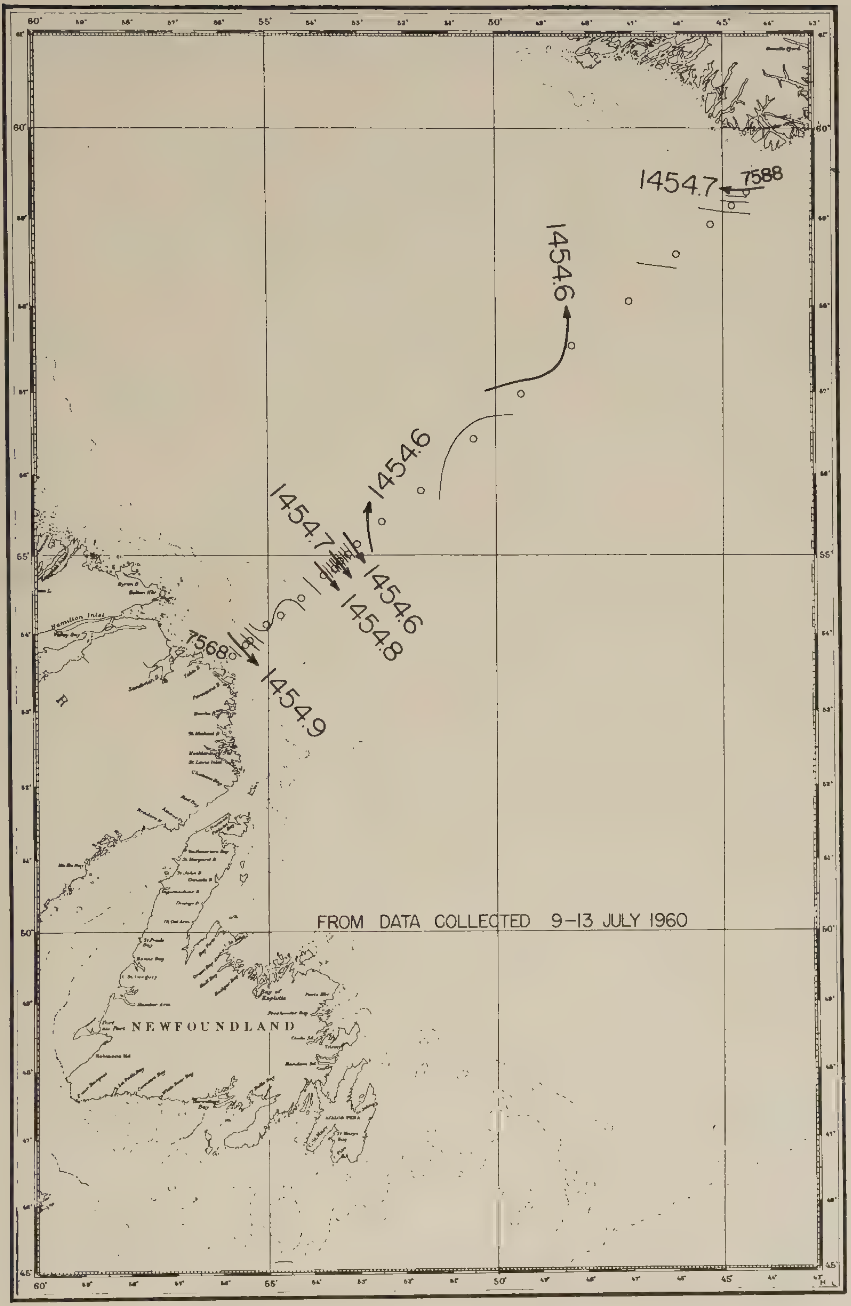

1454.7
7588
1454.6
1454.6
1454.7
1454.6
1454.8
7568
1454.9
NEWFOUNDLAND
Hamilton Inlet
FROM DATA COLLECTED 9-13 JULY 1960
60°
55°
50°
45°

FIGURE 41.—Dynamic topography of the sea surface relative to the 1,500-decibar surface from data collected 10–13 July 1960. Oceanographic station positions are indicated by circles.

was below normal and the Irminger Current component had a large positive anomaly.

In 1959, the net volume transport above the reference surface between Cape Farewell and South Wolf Island was computed to be 2.37 northwesterly. In 1960, this net transport was computed to be 1.91 also northwesterly.

Analysis of the intermediate water and deep water of the Labrador Sea section, after the manner described in Bulletin 42 of this series, gave the following characteristic values for 1959 and 1960:

	1959		*1960*	
	Temperature	*Salinity*	*Temperature*	*Salinity*
Intermediate water	3.36	34.83_5	3.37	34.87_0
2,000 meters	3.19	34.90_3	3.17	34.92_5
2,500 meters	2.84	34.91_6	2.94	34.93_0
3,000 meters	2.37	34.89_8	2.43	34.92_5
3,500 meters	1.70	34.87_8	1.72	34.91_0

The values of σ_t corresponding to the average temperature and average salinity have been shown in figure 44 for the deep water levels for each year that the Labrador Sea section has been occupied since 1934. Differences between prewar and postwar means are not significant. Examination of temperatures and salinities show a small increase in both temperature and salinity from prewar means to postwar means with changes becoming less at greater depths. At 2,000 meters, the change in salinity was 0.006‰ and in temperature 0.06°. At deeper levels the changes were not significant.

In figure 45 the mean potential temperature of the deep water of the Labrador Sea is plotted against mean salinity for particular levels. Ellipses show the standard deviation of individual postwar years from the 13-year mean 1948–60.

Assumptions occasionally must be made as to the ratio of the draft of a berg to its height above water. If the berg is homogeneous and floating with one-eighth of its mass above the water line this ratio would be 7/1 for a berg of rectangular shape or tabular with a flat top and vertical sides. If it is spherical in shape, the ratio is 3.5/1. Even smaller values exist for odd shapes like a mount or pinnacle on a raft or with extensive ledges. This ratio has frequently been assumed to be 5 or 6 to 1 for average bergs. Additional experience indicates that an average figure is nearer that for a sphere than that for a rectangular shape. This emphasizes the need for considering the total vector of forces moving bergs, that is, the effect of wind and water forces.

During the second survey, a study of the wind effect on icebergs was made with Lieut. (jg.) T. F. Budinger, USCG, as project officer. The primary objective of the study was to determine the direct effect of the wind and the indirect effect of the wind driven current on the movement of icebergs and thereby improve iceberg movement for-

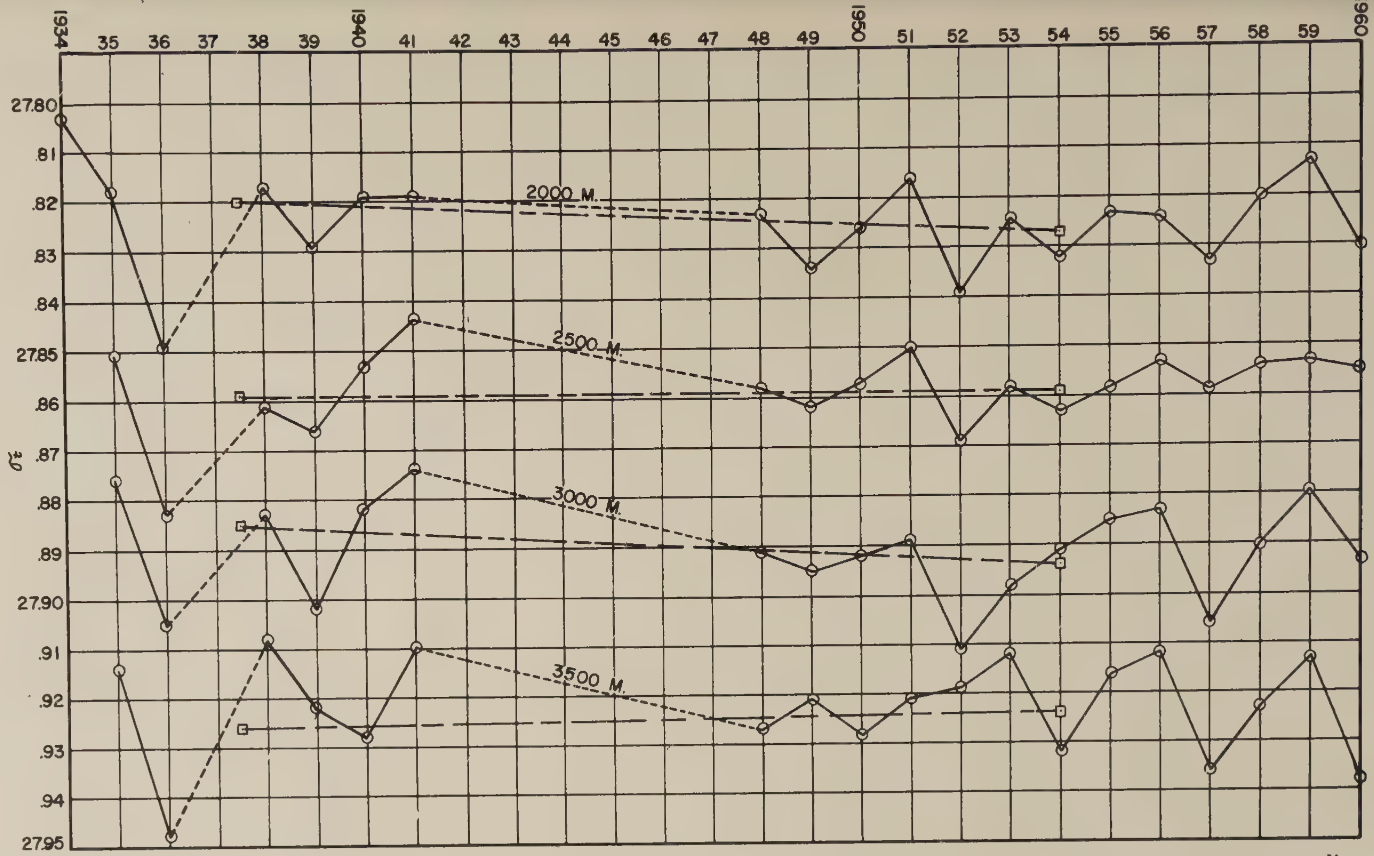

FIGURE 44.—Year-to-year variations in the deep water of the Labrador Sea as represented by the value of σ_t corresponding to the average temperature and salinity for the year.

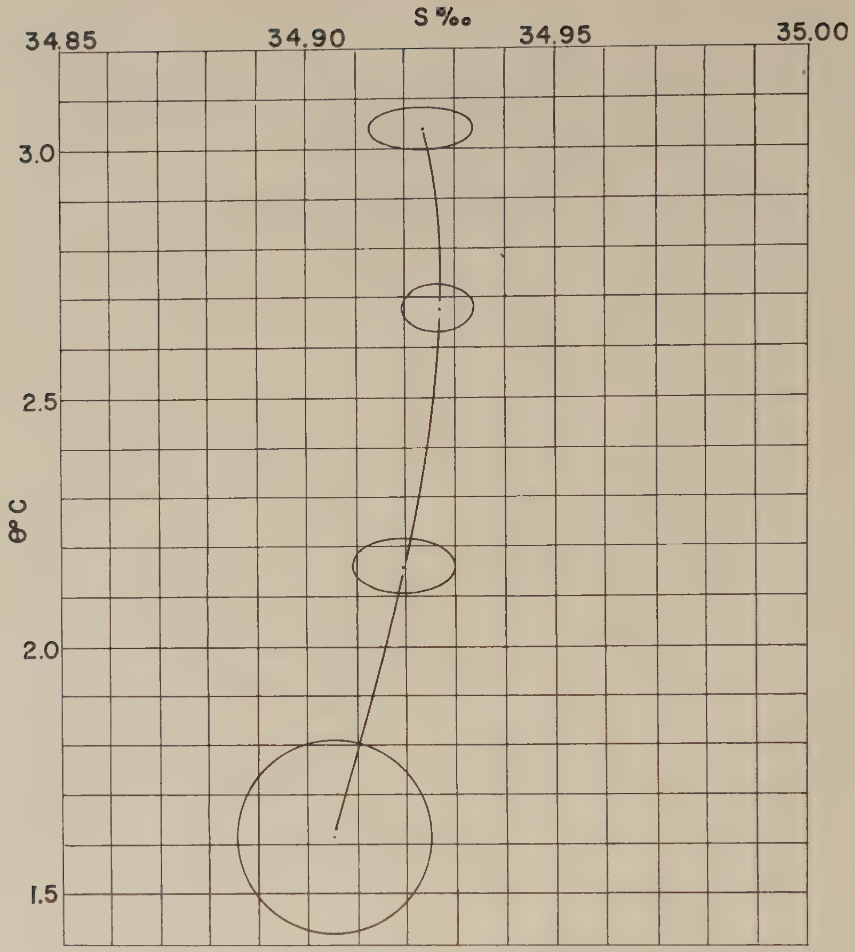

FIGURE 45.—Potential temperature-salinity relationship for the deep water of the Labrador Sea. Ellipses show standard deviation of postwar years from the 13-year mean 1948–60.

casting techniques. A secondary objective was to investigate Ekman's empirical equation for the velocity of a wind driven current.

To accomplish these objectives, the following measurements were made: Wind velocity by means of automatic and hand held wind measuring devices; ship's position by means of loran; surface current by means of a geomagnetic electrokinetograph and surface and subsurface currents by means of plotting the drift of three parachute drogues. The observation period lasted 83 hours during which time 66 loran fixes were obtained, 16 geomagnetic electrokinetograph surface current determinations were made, hourly wind velocity measurements taken, and half hourly radar ranges of iceberg and drogue reflectors recorded.

The parachute drogue measurements consisted of simultaneous radar tracking of three drogues relative to the iceberg. The drogues were placed approximately at the surface, at 250 feet, and at 500 feet. Each was suspended from a float consisting of a styrofoam float pierced by a 20-foot aluminum spar equipped with a battery powered flashing light and radar reflector. Unfortunately, the radar reflectors did not work as well as was expected and maximum radar range was 5 miles with occasional maximum ranges of less than 1 mile in choppy seas. Nevertheless, successful observations were taken and data recorded. At the present time it is felt that although some interesting results were obtained, the amount of data is insufficient to present a conclusive result. It is hoped that further studies can be made and more definite conclusions reached.

With reasonable assumptions regarding above water and below water areas and drag coefficients applied to theoretical hydrodynamical arguments an expression for windage was derived as:

$$\text{Iceberg velocity} = 0.023 \text{ wind.}$$

This was in good agreement with the preliminary data which indicate that the relation between wind speed and the movement imparted to an iceberg for wind speeds between 10 and 50 knots is linear and given by: Iceberg Vel.$=0.03K \cdot W$ with the movement directed 50° to the right of the surface wind.[7] The "shape" constant, K, varies from 0.7 for blocky or massive bergs to 1.4 for drydock or winged icebergs, W is the wind speed. As part of this investigation, a re-evaluation of the constant in Ekman's equation for the velocity of wind driven currents was accomplished by a rapid reduction of 77,828 observations made by lightships along the North American east coast. The value derived, 0.013, is in excellent agreement with Ekman's.

SUMMARY

1. Precise chlorinity determinations together with Wenner salinity bridge measurements of a collection of large samples of actual surface sea water samples over the range of salinities encountered in the Ice Patrol operating area has permitted a good calibration of the salinity bridge, an assessment of the errors involved in the use of several batches of Copenhagen standard water as standards of conductivity, and the determination of corrections to the previously published salinities of samples collected by the Ice Patrol during the period 1948 to 1959. These corrections and other corrections to salinity-dependent functions are tabulated.

2. Five dynamic topographic charts resulting from the four surveys made in the Grand Banks region during the season and the postseason occupation of the Bonavista triangle have been presented.

---

[7] Budinger, T. F. Wind Effect on Icebergs 1960, unpublished.

3. The temperature-salinity characteristics of the three water masses found in the Grand Banks region during the period from 1948–60 have been compared with conditions found during the 1960 season and with the means for the prewar period 1934–41.

4. During the first survey, two sections were extended southward from the Grand Banks to completely cross the Atlantic Current. For one of these sections, the volume and heat transports and mean temperature of the several branches of the Atlantic Current crossing the section have been presented in comparison with similar values found during the occupations of this section in 1938, 1950, and 1958.

5. The volume and heat transports and mean and minimum observed temperatures found during 23 occupations of sections across the Labrador Current in 1959 and 18 occupations of such sections in 1960 have been presented in comparison with tentative seasonal normals.

6. New tentative seasonal normal relationships for the Labrador Current at sections T, U, and W have been presented.

7. The characteristic temperature and salinity of the intermediate and deep waters of the Labrador Sea from the 1960 postseason cruise have been presented in comparison with earlier values, and the year to year fluctuations in density of the deep water at specific levels has been shown for all occupations of the Labrador Sea section from 1934 to 1960.

8. Some experiments using parachute drogues in measuring the effect of wind on the movement of icebergs have been described.

Appendix I

EXACT CHLORINITY DETERMINATIONS

By Lieut. (jg.) T. F. Budinger

General: On 8 February 1960 an investigation was initiated to determine the exact halogen content in 12 sea-water samples taken from the surface waters of the Grand Banks and contiguous areas of the North Atlantic Ocean. These samples were obtained by the International Ice Patrol Oceanographic Unit in 1959 and stored in polyethylene containers of ca. 12-gallon capacity until February 1960 when they were transferred to chemically clean containers of suitable size and quantities to allow distribution for calibration and analytical work by other investigators. This is a final technical report on the project completed 28 February 1960.

Techniques: Twelve Ice Patrol samples ranging in salinity from about 31°/₀₀ to 36.4°/₀₀ (intervals of approximately 0.5°/₀₀) were analyzed together with two Normal Water samples (batches P–28 and P–29) prepared by the Hydrographical·Laboratories in Copenhagen, Denmark. The analyses were conducted by two very precise techniques which can be made complimentary one to the other thus allowing intercomparison and confidence, or doubt, as the case might be, in the final results. The Ice Patrol surface samples were analyzed by a comparison technique with the Normal Water, P–28. The procedure is essentially the Volhardt technique as modified by Dittmar (1884),[1] S. P. L. Sørensen (1902),[2] and Bjørn-Andersen (1911).[3] The resulting weight titration technique gives high precision commensurate with the size of sample, strength of titration liquids, and analytical care. An extremely precise technique following the same general procedure as developed by the investigators listed above was used by Miss I. Knudsen (1937)[4] in comparing Urnormal 1937 water with P, P–11, and P–15 batches. The technique employed in the Ice Patrol analyses is a slight modification of the above procedures to accommodate the available apparati at the Marine Biological Laboratories in Woods Hole, Mass. The criteria for choice of solution strengths and quantities of samples were to maintain the highest theoretical precision in accomplishing replicate analyses of 12 samples and to allow intercomparison of the comparison analyses with "atomic weight silver" analyses. The second procedure used for control was pure silver analyses of the chlorinity of P–28 and Ice Patrol sample No. 1 as defined subsequent to the change in atomic weights of silver and chlorine in 1940.

Other techniques have been used for the precise analysis of sea-water chlorinity. Deacon [5] and Thompson and Wirth [6] used pure individually under magnification and dried at 225° C. before weighing. All silver masses were determined by double weighings on a Micro balance (sensitivity 1/200 mg.) and corrected for buoyancy, 0.01°/oo impurity, and probable moisture pick-up during weighing period. To each silver sample ca. 20 ml. conc. HNO_3 (nitrogen oxide free) were added and after slight heating on a water bath the $AgNO_3$ solution was brought up to ca. 200 ml. with conductivity water. To these solutions, P–28 and sample No. 1 were added and mixed. All work was accomplished in darkness and conductivity water was used throughout. The procedure thereafter followed that of the comparison technique with the exception that the mixtures were repeatedly shaken over a period of 12 hours before filtering and very little (ca. 1 ml. of NH_4SCN) was required by the excess silver nitrate.

Results: The results of these analyses are shown in the following table. The examination of P–28 by pure silver yielded values in remarkable agreement with the stated value:

P–28 by Silver	
19.3738	Mean=19.374$_3$
19.3747	
	Stated value=19.374

Silver analyses of Ice Patrol sample No. 1 compare very favorably with the results of the comparison technique:

By comparison	By silver
19.390$_8$	19.389$_6$

As a further check on the entire comparison technique and solution ratios, P–29 Normal Water was run as an unknown and confidence in all of the results may be inferred from the agreement between the stated value and the determined chlorinity:

By comparison	Stated value
19.369$_8$	19.370

As a final check, the determinations were examined to see if the amount of excess $AgNO_3$ caused random or directional deviation from the mean. The random deviation noted indicates that neither a determinate solution ratio error nor an indeterminate washing technique error exists. It is believed the precision could be improved slightly had weight burettes and larger samples been used. The precision of the chlorinity values given for Ice Patrol samples is ±0.002°/oo Cl and the accuracy is believed to be very nearly ±0.002°/oo Cl.

Chlorinity and Salinity

International Ice Patrol Sea-water Samples

Sample	Chlorinity ‰ determinations	Chlorinity ‰ mean*	Precision	Salinity ‰
7	17.2026 17.2035 17.2008	17.2023	±0.001	31.080
15	17.5079 17.5123	17.5101	±0.002	31.636
11	17.6976 17.7027	17.7001	±0.002	31.979
14	17.9711 17.9709	17.9710	±0.001	32.468
3	18.2860 18.2861	18.2860	±0.000	33.036
10	18.5620 18.5606	18.5613	±0.001	33.533
5	18.8269 18.8249	18.8259	±0.001	34.011
6	19.0862 19.0860	19.0861	±0.000	34.480
1	19.3890 19.3926	19.3908	±0.002	35.030
No. 1 Silver	19.3913 19.3879	19.3896	±0.002	35.028
9	19.6721 19.6737	19.6729	±0.001	35.540
8	20.1623 20.1658	20.1640	±0.002	36.426
P-29	19.3658 19.3695 19.3741	19.3698	±0.003	34.992
P-28 Silver	19.3738 19.3747	19.3743	±0.0005	35.001

*Fourth decimal not significant.

REFERENCES

1. Dittmar, W. 1884. Report on researches into the composition of ocean water collected by H.M.S. *Challenger*. Challenger Repts., Physics and Chem., vol. 1, p. 4, 1884.
2. Forch, Carl, Martin Knudsen, and S. P. L. Sørensen. 1902. Bericht über die Konstantenbestimmungen zur Aufstellung der hydrographischen Tabellen. Mèmoires de l'Academie Royale des Sciences et des Letters de Danemark, Copenhague, Serie 6, Section des Sciences, vol. 12, No. 1, 1902.
3. Bjørn-Andersen, H. 1912. Exact determination of the chlorine in some samples of sea water from the Mediterranean. Rpt. on the Danish Oceanographical Expeditions 1908–1810. vol. 1, sec. 3. p. 195, 1902.
4. Jacobsen, J. P. and M. Knudsen, 1940. Urnormal 1937 or Primary Standard Sea-Water 1937. Association D'Océanographie Physique, Publ. Scientifique No. 7, 1940.
5. Deacon, G. E. R. 1933. An examination of 'eau de mer normale P–13, 28–VI–1929. Journal du Conseil, vol. 8, p. 59, 1933.
6. Thompson, T. G. and H. E. Wirth, 1931. The specific gravity of sea water at zero degrees in relation to the chlorinity. Journal du Conseil, vol. 6. No. 2, p. 232, 1931.
7. Hermann, F. 1951. High accuracy potentiometric determination of the chlorinity of sea water. Journal du Conseil, vol. 17, No. 3, p. 223, 1951.
8. Bather, J. M. and J. P. Riley, 1953. The precise and routine potentiometric determination of the chlorinity of sea water. Journal du Conseil, vol. 18, No. 3, p. 277, 1953.

Appendix 2

Data on origin of 12-gallon polyethylene drum samples

Drum	Origin				Surface salinity at time of collection	S by Cl	Date drum sample divided
	Station	N. lat.	W. long.	Date of collection			
7	7244	48–25	52–14	2 Aug. 1959	31.07	31.080	15 Feb. 1960
15	7160	48–45.5	52–47	16 June 1959	31.60	31.636	16 Feb. 1960
11	7254	48–10	49–43	3 Aug. 1959	31.69	31.979	16 Feb. 1960
14	6899	43–00	50–14	6 Apr. 1959	32.47	32.468	16 Feb. 1960
3	6929	44–13	49–23	12 Apr. 1959	33.03	33.036	15 Feb. 1960
10	6910	42–02.5	47–49	9 Apr. 1959	33.54	33.533	16 Feb. 1960
5	6924	44–00	48–30	11 Apr. 1959	34.00	34.011	17 Feb. 1960
6	6922	43–41	47–19	11 Apr. 1959	34.46	34.480	16 Feb. 1960
1	6991 7028	41–31.5 44–52	50–14 45–18	2 May 1959 8 May 1959	34.80 35.25	35.030	16 Feb. 1960
9	6995 7004	41–06 42–39.5	48–14 46–51	3 May 1959 5 May 1959	35.28 35.75	35.540	17 Feb. 1960
8	6905	41–05.5	50–12	7 Apr. 1959	36.30	36.426	17 Feb. 1960

For the most part the column headings are self explanatory. The surface salinity at the time of collection of the large sample was that of a sample collected by Nansen bottle as measured by the Coast Guard Oceanographic Unit's Wenner bridge whereas the large sample was taken from the ship's fire main after thorough flushing of the system. While most of the differences between the surface salinity at the time of collection and the subsequent salinity by Cl are small, drums 11 and 8 showed large differences. In the case of drum 11, there was a considerable salinity gradient near the surface so that the fact that the fire main intake was below the surface may explain the higher drum salinity. No such explanation can be offered for the large difference in the case of drum 8 which leaves the possibility of inadequate flushing of the fire main system (this was one of the first drums collected in 1959 and personnel had little previous experience in this method of collection), contamination from other than sea water sources, and excessive evaporation. Since each of the last two possibilities depend on a leaky seal, they seem improbable because in the case of a leaky seal the contamination from rain water would probably greatly reduce the salinity. One other drum which did have a leaky seal changed from approximately 36.0°/oo upon collection on 10 April 1959 to 33.22°/oo in February 1960. Confidence in the seal is justified by the fact that at the end of the first survey, before the drum was put ashore for storage, a small sample was withdrawn and measured approximately 36.39°/oo by conductivity. Drums 1 and 9 were composites, each being mixtures of about equal parts of drums which were about ¼°/oo on either side of the desired salinities.

TABLE OF OCEANOGRAPHIC DATA

The data collected in 1960 are tabulated below. The individual station headings give the station number, date, geographical position, depth of water and dynamic height of the sea surface used in the construction of the dynamic topographic charts shown in figures 24, 25, 26, 27, 28, and 41. The depths of water are rough approximations, being the uncorrected sonic soundings based on a sounding velocity of 800 fathoms per second and containing an additional mechanical speed error of about 1/60. Where the depths of scaled values are enclosed in parentheses, the data are based on extrapolated vertical distribution curves of temperature or salinity or both. Asterisks appearing before observed temperatures indicate that these temperatures were determined from the depth of reversal and the corrected reading of an unprotected thermometer. The symbol σ_t signifies 1000 (density−1) at atmospheric pressure and temperature t.

TABLE OF OCEANOGRAPHIC DATA

Observed values			Scaled values			
Depth, meters	Temperature, °C.	Salinity, °/₀₀	Depth, meters	Temperature, °C.	Salinity, °/₀₀	σ_t
Station 7284; 2 April; 43°55′ N., 49°15′ W.; depth 159 m.; dynamic height						
0	0. 39	33. 10	0	0. 39	33. 10	26. 56
25	0. 43	33. 15	25	0. 43	33. 15	26. 61
50	0. 47	33. 18	50	0. 47	33. 18	26. 63
75	0. 50	33. 18	75	0. 50	33. 18	26. 62
100	0. 58	33. 25	100	0. 58	33. 25	26. 68
Station 7285; 2 April; 43°36′ N., 48°52.5′ W.; depth 2,286 m.; dynamic height 970.983						
0	0. 32	33. 14	0	0. 32	33. 14	26. 60
25	0. 34	33. 13	25	0. 34	33. 13	26. 59
51	0. 34	33. 16	50	0. 35	33. 15	26. 62
75	0. 70	33. 49	75	0. 70	33. 49	26. 86
101	1. 15	33. 80	100	1. 15	33. 79	27. 08
151	2. 28	34. 30	150	2. 27	34. 29	27. 40
202	2. 77	34. 54	200	2. 75	34. 52	27. 55
303	3. 41	34. 72	300	3. 40	34. 70	27. 60
414	3. 82	34. 83	400	3. 80	34. 82	27. 69
637	3. 70	34. 87	600	3. 72	34. 86	27. 72
840	3. 61	34. 85	800	3. 61	34. 84	27. 72
1,038	3. 55	34. 84	1,000	3. 56	34. 83	27. 71
1,526	3. 55	34. 87	1,500	3. 55	34. 86	27. 74
Station 7286; 3 April; 43°19′N., 48°32′ W.; depth 2,834 m.; dynamic height 971.047						
0	7. 70	34. 55	0	7. 70	34. 55	26. 97
21	7. 87	34. 54	25	7. 88	34. 54	26. 95
42	7. 94	34. 56	50	7. 93	34. 56	26. 96
62	7. 90	34. 57	75	7. 85	34. 55	26. 96
83	7. 79	34. 55	100	7. 69	34. 55	26. 98
125	7. 47	34. 57	150	7. 00	34. 57	27. 10
166	7. 91	34. 58	200	5. 75	34. 55	27. 25
249	4. 86	34. 51	300	6. 33	34. 87	27. 42
333	6. 60	34. 94	400	5. 90	34. 94	27. 54
498	5. 22	34. 95	600	4. 62	34. 95	27. 70
665	4. 64	34. 97	800	4. 30	34. 95	27. 73
841	4. 21	34. 96	1,000	3. 98	34. 95	27. 77
1,040	3. 95	34. 96	1,250	3. 85	34. 90	27. 74
1,246	4. 84	34. 91	1,500	3. 61	34. 90	27. 77
1,588	3. 54	34. 92	1,750	3. 52	34. 92	27. 79
1,834	3. 53	34. 94	2,000	3. 46	34. 94	27. 81
2,086	3. 41	34. 95				
Station 7287; 3 April; 42°54.5′ N., 48°29.5′ W.; depth 3,054 m.; dynamic height 971.011						
0	4. 81	33. 75	0	4. 81	33. 75	26. 72
24	4. 83	33. 74	25	4. 81	33. 74	26. 72
72	4. 44	33. 91	50	4. 70	33. 79	26. 77
99	5. 19	34. 17	75	4. 43	33. 84	26. 84
150	4. 39	34. 31	100	5. 19	34. 16	27. 01
200	4. 74	34. 58	150	4. 39	34. 31	27. 21
299	5. 17	34. 82	200	4. 74	34. 58	27. 39
396	5. 17	34. 96	300	5. 17	34. 81	27. 52
588	4. 47	34. 97	400	5. 16	34. 95	27. 64
798	4. 20	34. 98	600	4. 45	34. 96	27. 73
1,107	3. 84	34. 95	800	4. 19	34. 97	27. 77
1,229	4. 53	34. 92	1,000	3. 96	34. 95	27. 77
1,485	3. 54	34. 97	1,250	3. 73	34. 91	27. 76
1,663	3. 48	34. 93	1,500	3. 55	34. 96	27. 82
1,908	3. 38	34. 94	1,750	3. 42	34. 93	27. 81
2,156	3. 24	34. 94	2,000	3. 27	34. 93	27. 82
2,404	3. 09	34. 95	2,250	3. 18	34. 94	27. 84
			(2,500)	3. 03	34. 94	27. 86
Station 7288; 3 April; 42°38.5′ N., 48°35′ W.; depth 3,283 m.; dynamic height 970.983						
0	5. 05	33. 81	0	5. 05	33. 81	26. 74
27	5. 05	33. 80	25	5. 05	33. 80	26. 74
53	6. 65	34. 27	50	6. 51	34. 17	26. 85
80	5. 67	34. 32	75	5. 82	34. 30	27. 05
110	5. 54	34. 32	100	5. 58	34. 31	27. 08
166	6. 39	34. 77	150	6. 16	34. 66	27. 29
220	6. 21	34. 86	200	6. 28	34. 84	27. 41
330	5. 03	34. 87	300	5. 19	34. 86	27. 56
438	4. 85	34. 97	400	4. 90	34. 95	27. 67
655	4. 42	34. 98	600	4. 52	34. 97	27. 73
872	4. 00	34. 96	800	4. 14	34. 96	27. 76
1,089	3. 79	34. 95	1,000	3. 80	34. 95	27. 79
1,318	4. 38	34. 99	1,250	4. 23	34. 97	27. 76
1,592	3. 51	34. 94	1,500	3. 81	34. 95	27. 79
1,670	3. 52	34. 94	1,750	3. 49	34. 93	27. 80
1,918	3. 43	34. 94	2,000	3. 36	34. 93	27. 81
2,169	3. 23	34. 94	2,250	3. 17	34. 93	27. 83
2,420	3. 05	34. 93	2,500	2. 98	34. 92	27. 85
2,921	2. 65	34. 91	(3,000)	2. 60	34. 90	27. 86
Station 7289; 3 April; 42°17.5′ N., 48°36′ W.; depth 3,438 m.; dynamic height 970.984						
0	5. 34	33. 87	0	5. 34	33. 87	26. 76
105	5. 20	34. 17	25	5. 31	33. 92	26. 81
158	4. 47	34. 49	50	5. 28	34. 00	26. 87
212	4. 56	34. 66	75	5. 25	34. 07	26. 93
238	4. 88	34. 77	100	5. 22	34. 15	27. 00
264	4. 91	34. 82	150	4. 56	34. 42	27. 28
290	5. 02	34. 87	200	4. 53	34. 60	27. 43
317	5. 11	34. 91	300	5. 04	34. 88	27. 60
526	4. 42	34. 92	400	4. 84	34. 90	27. 63
732	4. 07	34. 95	600	4. 30	34. 92	27. 71
941	3. 82	34. 92	800	3. 98	34. 93	27. 75
1,148	3. 59	34. 89	1,000	3. 75	34. 91	27. 76
1,307	3. 98	34. 93	1,250	3. 86	34. 91	27. 75
1,572	3. 41	34. 91	1,500	3. 67	34. 91	27. 77
1,690	3. 46	34. 92	1,750	3. 44	34. 91	27. 79
1,920	3. 38	34. 92	2,000	3. 34	34. 92	27. 81
2,202	3. 26	34. 93	2,250	3. 22	34. 92	27. 82
2,470	3. 08	34. 95	2,500	3. 05	34. 93	27. 84
2,937	2. 67	34. 91	3,000	2. 58	34. 90	27. 86
3,133	2. 41	34. 91				
Station 7290; 4 April; 42°00′ N., 48°34′ W.; depth 3,475 m.; dynamic height 971.132						
0	12. 28	35. 42	0	12. 28	35. 42	26. 87
26	12. 30	35. 41	25	12. 30	35. 41	26. 87
52	12. 33	35. 42	50	12. 32	35. 41	26. 86
78	12. 40	35. 45	75	12. 40	35. 44	26. 87
105	12. 28	35. 42	100	12. 31	35. 41	26. 87
156	11. 84	35. 36	150	11. 90	35. 36	26. 91
208	10. 78	35. 33	200	11. 05	35. 33	27. 03
313	10. 97	35. 33	300	9. 95	35. 32	27. 23
416	6. 36	34. 99	400	6. 90	35. 03	27. 47
625	5. 13	34. 99	600	5. 26	34. 98	27. 65
830	4. 52	35. 01	800	4. 61	35. 00	27. 74
1,034	3. 83	34. 94	1,000	3. 94	34. 94	27. 76
1,294	3. 84	34. 96	1,250	3. 83	34. 95	27. 78
1,551	3. 84	34. 94	1,500	3. 86	34. 94	27. 77
1,811	3. 57	34. 95	1,750	3. 65	34. 94	27. 79
2,103	3. 46	34. 96	2,000	3. 49	34. 95	27. 82
2,374	3. 22	34. 95	2,250	3. 33	34. 95	27. 83
2,598	3. 03	34. 95	2,500	3. 10	34. 94	27. 85
3,108	2. 57	34. 93	3,000	2. 69	34. 93	27. 88
3,407	2. 15	34. 94				

TABLE OF OCEANOGRAPHIC DATA—Continued

Station 7291; 4 April; 41°39′ N., 48°31′ W.; depth 3,585 m.; dynamic height 971.095

Observed values			Scaled values			
Depth, meters	Temperature, °C.	Salinity, ‰	Depth, meters	Temperature, °C.	Salinity, ‰	σ_t
0	14.36	35.92	0	14.36	35.92	26.83
20	14.41	35.92	25	14.38	35.91	26.82
41	14.45	35.93	50	14.39	35.92	26.83
61	14.44	35.92	75	14.40	35.91	26.82
82	14.45	35.92	100	14.47	35.91	26.80
122	14.54	35.93	150	14.45	35.93	26.83
162	------	35.92	200	13.55	35.78	26.90
245	12.12	35.54	300	10.48	35.31	27.13
327	9.84	35.26	400	8.94	35.23	27.33
481	7.38	35.23	600	6.36	35.11	27.61
663	5.54	35.06	800	4.85	35.02	27.73
835	4.73	35.02	1,000	4.33	34.99	27.77
1,282	3.93	------	1,250	4.00	34.97	28.78
1,712	3.61	34.95	1,500	3.76	34.96	27.80
1,960	3.54	34.96	1,750	3.59	34.94	27.80
2,210	3.34	34.96	2,000	3.50	34.95	27.82
2,459	3.19	34.95	2,250	3.31	34.95	27.84
2,965	2.74	34.94	2,500	3.15	34.94	27.84
3,155	2.54	34.93	3,000	2.70	34.93	27.87

Station 7292; 4 April; 41°19′ N., 48°32′ W.; depth 3,310 m.; dynamic height 971.178

Observed values			Scaled values			
Depth, meters	Temperature, °C.	Salinity, ‰	Depth, meters	Temperature, °C.	Salinity, ‰	σ_t
0	13.76	35.74	0	13.76	35.74	26.82
26	13.77	35.75	25	13.77	35.74	26.82
51	13.73	35.74	50	13.74	35.73	26.82
77	13.69	35.74	75	13.70	35.73	26.83
102	13.69	35.73	100	13.70	35.73	26.83
152	11.74	35.28	150	11.83	35.31	26.88
203	11.05	35.18	200	11.10	35.18	26.91
305	9.47	35.15	300	9.54	35.14	27.15
406	7.58	35.01	400	7.67	35.02	27.36
610	5.44	35.02	600	5.63	35.01	27.63
811	4.68	35.01	800	4.73	35.01	27.73
1,010	4.25	34.99	1,000	4.26	34.99	27.77
1,261	3.85	34.94	1,250	3.86	34.94	27.77
1,509	3.67	34.95	1,500	3.68	34.94	27.79
1,720	3.57	34.94	1,750	3.55	34.93	27.79
1,968	3.47	34.95	2,000	3.42	34.94	27.82
2,216	3.30	34.95	2,250	3.26	34.94	27.83
2,466	3.11	34.94	2,500	3.19	34.93	27.83
2,958	2.70	34.93	3,000	2.68	34.92	27.87
3,156	2.58	34.92				

Station 7293; 4 April; 41°00′ N., 48°32′ W.; depth 3,292 m.; dynamic height 971.052

Observed values			Scaled values			
Depth, meters	Temperature, °C.	Salinity, ‰	Depth, meters	Temperature, °C.	Salinity, ‰	σ_t
0	6.96	33.93	0	6.96	33.93	26.59
26	6.94	33.96	25	6.95	33.95	26.62
52	7.85	34.37	50	7.72	34.33	26.81
78	9.04	34.78	75	8.80	34.72	26.95
104	9.53	34.99	100	9.41	34.94	27.02
155	8.05	34.84	150	8.24	34.86	27.15
208	7.07	34.81	200	7.25	34.81	27.26
312	5.50	34.80	300	5.69	34.79	27.44
413	4.60	34.80	400	4.72	34.79	27.56
622	4.43	34.95	600	4.45	34.92	27.70
827	4.54	35.01	800	4.54	34.99	27.74
998	4.00	34.94	1,000	4.01	34.93	27.75
1,248	3.83	34.96	1,250	3.84	34.95	27.78
1,497	3.71	34.95	1,500	3.73	34.94	27.79
1,752	3.51	34.93	1,750	3.50	34.92	27.80
2,002	3.39	34.93	2,000	3.37	34.92	27.81
2,254	3.24	34.94	2,250	3.22	34.93	27.83
2,506	3.08	34.95	2,500	3.10	34.94	27.85
3,199	2.43	34.92	3,000	2.64	34.92	27.88

Station 7294; 5 April; 40°29.5′ N., 48°30.5′ W.; depth 3,768 m.; dynamic height 971.171

Observed values			Scaled values			
Depth, meters	Temperature, °C.	Salinity, ‰	Depth, meters	Temperature, °C.	Salinity, ‰	σ_t
0	16.98	36.40	0	16.98	36.40	26.61
25	17.00	36.39	25	17.00	36.40	26.60
50	17.02	36.40	50	17.02	36.40	26.60
75	16.37	36.23	75	16.37	36.23	26.62
100	15.74	36.10	100	15.74	36.10	26.66
149	14.50	35.92	150	14.48	35.92	26.81
199	13.72	35.77	200	13.70	35.76	26.85
299	11.97	35.51	300	11.95	35.50	27.01
398	9.79	35.29	400	9.75	35.28	27.23
597	4.98	34.82	600	5.00	34.81	27.55
793	4.90	35.02	800	4.88	35.01	27.72
988	4.16	34.95	1,000	4.15	34.94	27.74
1,241	3.97	34.95	1,250	4.00	34.95	27.77
1,495	3.90	34.98	1,500	3.92	34.97	27.79
1,747	3.72	34.97	1,750	3.71	34.96	27.81
1,998	3.58	34.97	2,000	3.57	34.96	27.82
2,252	3.38	34.97	2,250	3.39	34.96	27.84
2,505	3.15	34.95	2,500	3.15	34.94	27.84
2,898	2.74	34.93	3,000	2.59	34.92	27.88
3,144	2.38	34.93				

Station 7295; 5 April; 40°00′ N., 48°26′ W.; depth 4,846 m.; dynamic height 971.420

Observed values			Scaled values			
Depth, meters	Temperature, °C.	Salinity, ‰	Depth, meters	Temperature, °C.	Salinity, ‰	σ_t
0	17.50	36.38	0	17.50	36.38	26.46
22	17.50	36.38	25	17.50	36.37	26.46
46	17.51	36.37	50	17.49	36.36	26.45
68	17.46	36.37	75	17.20	36.25	26.44
92	16.54	36.18	100	16.45	36.17	26.56
137	15.85	36.15	150	15.60	36.11	26.71
182	14.92	36.02	200	14.64	35.97	26.82
271	13.50	35.76	300	13.35	35.70	26.88
339	13.14	35.64	400	12.50	35.65	27.01
470	11.65	35.68	600	8.75	35.22	27.35
583	9.05	35.26	800	6.35	35.10	27.60
674	7.32	35.07	1,000	4.85	34.96	27.68
801	6.34	35.11	1,250	4.47	34.97	27.73
911	4.98	34.97	1,500	4.08	34.97	27.78
1,630	3.90	34.98	1,750	3.76	34.97	27.81
1,868	3.75	34.97	2,000	3.60	34.96	27.82
2,106	3.60	34.97	2,250	3.50	34.96	27.83
2,342	3.46	34.97	2,500	3.34	34.95	27.83
2,820	3.09	34.95	3,000	2.95	34.94	27.86
3,210	2.83	------				
3,598	2.54	34.93				

Station 7296; 5 April; 39°27.5′ N., 48°26′ W.; depth 5,413 m.; dynamic height 971.737

Observed values			Scaled values			
Depth, meters	Temperature, °C.	Salinity, ‰	Depth, meters	Temperature, °C.	Salinity, ‰	σ_t
0	17.56	36.47	0	17.56	36.47	26.52
25	17.56	36.47	25	17.56	36.47	26.52
50	17.59	36.47	50	17.59	36.47	26.51
75	17.58	36.47	75	17.58	36.47	26.51
100	17.59	36.47	100	17.59	36.47	26.51
149	17.59	36.47	150	17.59	36.46	26.51
199	17.60	36.48	200	17.60	36.47	26.52
299	17.60	36.48	300	17.60	36.47	26.52
395	------	36.47	400	17.16	36.47	26.62
584	14.24	35.86	600	13.90	35.81	26.85
767	10.25	35.33	800	9.67	35.28	27.24
945	7.03	35.11	1,000	6.27	35.09	27.61
1,180	5.16	35.04	1,250	5.41	35.01	27.66
1,412	4.28	34.97	1,500	4.27	34.98	27.76
1,567	4.25	35.00	1,750	4.16	34.98	27.77
1,828	4.13	34.99	2,000	3.85	34.96	27.79
2,056	3.76	34.96	2,250	3.72	34.97	27.81
2,286	3.70	34.99	2,500	3.51	34.97	27.83
2,760	3.29	34.96	3,000	3.12	34.94	27.85
3,145	3.00	------				
3,538	2.67	34.93				
3,933	2.44	34.93				

TABLE OF OCEANOGRAPHIC DATA—Continued

Station 7297; 6 April; 38°55.5′ N., 48°26′ W.; depth 5,321 m.; dynamic height 971.780

Observed values			Scaled values			
Depth, meters	Temperature, °C.	Salinity, °/oo	Depth, meters	Temperature, °C.	Salinity, °/oo	σ_t
0	17.47	36.45	0	17.47	36.45	26.52
26	17.48	36.45	25	17.48	36.44	26.52
52	17.49	36.44	50	17.48	36.43	26.51
77	17.49	36.44	75	17.48	36.43	26.51
102	17.49	36.44	100	17.49	36.43	26.51
153	17.49	36.44	150	17.49	36.43	26.51
204	17.50	36.44	200	17.50	36.43	26.50
306	17.51	36.44	300	17.50	36.43	26.50
408	16.96	36.31	400	16.98	36.31	26.54
614	14.28	35.87	600	14.45	35.89	26.79
858	9.34	35.26	800	10.52	35.40	27.19
1,090	6.24	35.06	1,000	7.45	35.13	27.47
1,338	5.08	35.06	1,250	5.51	35.06	27.68
1,692	4.18	35.02	1,500	4.68	35.04	27.77
1,938	3.91	34.99	1,750	4.12	35.01	27.80
2,183	3.70	34.98	2,000	3.84	34.98	27.81
2,430	3.56	34.98	2,250	3.66	34.97	27.82
2,922	3.19	34.97	2,500	3.52	34.97	27.83
3,318	2.77	------	3,000	3.10	34.96	27.87
3,914	2.41	34.95				

Station 7298; 6 April; 38°26.5′ N. 48°28′ W.; depth 5,303 m.; dynamic height 971.738

Observed values			Scaled values			
Depth, meters	Temperature, °C.	Salinity, °/oo	Depth, meters	Temperature, °C.	Salinity, °/oo	σ_t
0	17.32	36.42	0	17.32	36.42	26.53
26	17.34	36.42	25	17.33	36.41	26.53
51	17.34	36.42	50	17.33	36.41	26.53
77	17.31	36.42	75	17.31	36.41	26.54
102	17.32	36.42	100	17.32	36.41	26.53
152	17.32	36.42	150	17.32	36.41	26.53
203	17.27	36.40	200	17.31	36.40	26.53
305	16.71	36.28	300	16.75	36.28	26.57
407	16.11	36.16	400	16.15	36.16	26.62
611	13.69	35.79	600	13.82	35.80	26.86
816	9.70	35.26	800	9.98	35.30	27.20
1,021	6.51	35.13	1,000	6.85	35.13	27.56
1,282	4.76	35.03	1,250	4.99	35.03	27.72
1,545	4.19	34.99	1,500	4.31	34.99	27.76
1,721	3.99	34.98	1,750	3.92	34.97	27.79
1,976	3.79	34.98	2,000	3.77	34.97	27.81
2,234	3.62	34.97	2,250	3.61	34.97	27.82
2,493	3.48	34.98	2,500	3.48	34.97	27.84
2.982	3.10	34.96	3,000	3.08	34.95	27.86
3,363	2.76	------				
3,954	2.41	34.93				

Station 7299; 6 April; 37°55′ N., 48°27′ W.; depth 5,303 m.; dynamic height 971.726

Observed values			Scaled values			
Depth, meters	Temperature, °C.	Salinity, °/oo	Depth, meters	Temperature, °C.	Salinity, °/oo	σ_t
0	17.33	36.45	0	17.33	36.45	26.56
24	17.35	36.43	25	17.35	36.42	26.54
48	17.31	36.43	50	17.30	36.42	26.55
72	17.31	36.44	75	17.30	36.42	26.55
96	17.28	36.42	100	17.29	36.42	26.55
144	17.30	36.42	150	17.29	36.41	26.54
192	17.29	36.44	200	17.30	36.43	26.55
288	17.32	36.43	300	17.31	36.42	26.54
382	17.33	36.42	400	17.00	36.35	26.57
568	14.18	35.85	600	13.52	35.76	26.89
759	10.37	35.35	800	9.58	35.28	27.26
952	6.70	35.07	1,000	6.41	35.05	27.56
1,238	4.91	35.03	1,250	4.90	35.02	27.73
1,490	4.37	35.01	1,500	4.36	35.00	27.77
1,743	4.01	34.99	1,750	3.99	34.98	27.79
1,992	3.85	34.99	2,000	3.83	34.98	27.81
2,241	3.63	34.99	2,250	3.62	34.98	27.83
2,491	3.48	34.98	2,500	3.48	34.97	27.84
2,988	3.18	------	3,000	3.17	34.97	27.87
3,490	2.70	34.98				
3,979	2.40	------				

Station 7300; 7 April; 37°22.5′ N., 48°25′ W.; depth 5,305 m.; dynamic height 971.745

Observed values			Scaled values			
Depth, meters	Temperature, °C.	Salinity, °/oo	Depth, meters	Temperature, °C.	Salinity, °/oo	σ_t
0	17.13	36.39	0	17.13	36.39	26.56
25	17.16	36.39	25	17.16	36.39	26.56
50	17.19	36.40	50	17.19	36.39	26.56
75	17.17	36.39	75	17.17	36.39	26.56
100	17.18	36.39	100	17.18	36.39	26.56
150	17.17	36.39	150	17.17	36.38	26.55
200	17.18	36.39	200	17.18	36.38	26.55
300	17.18	36.40	300	17.18	36.39	26.56
401	16.67	36.27	400	16.66	36.26	26.58
604	13.07	35.69	600	13.15	35.59	26.83
809	9.81	35.27	800	9.97	35.28	27.19
1,016	6.18	35.12	1,000	6.48	35.12	27.60
1,443	4.32	35.02	1,250	5.17	35.05	27.72
1,683	3.96	35.00	1,500	4.25	35.00	27.78
1,926	3.74	35.00	1,750	3.90	34.99	27.81
2,171	3.60	35.00	2,000	3.69	34.99	27.83
2,416	3.44	35.11	2,250	3.55	35.02	27.87
3,434	2.69	35.11	2,500	3.39	35.10	27.95
3,956	2.42	34.96	3,000	3.01	35.10	27.99

Station 7301; 7 April; 37°28.5′ N.; 49°30.5′ W.; depth 5,321 m.; dynamic height 971.637

Observed values			Scaled values			
Depth, meters	Temperature, °C.	Salinity, °/oo	Depth, meters	Temperature, °C.	Salinity, °/oo	σ_t
0	17.30	36.40	0	17.30	36.40	26.52
26	17.31	36.39	25	17.31	36.39	26.52
52	17.31	36.39	50	17.30	36.39	26.52
77	17.28	36.39	75	17.28	36.38	26.54
103	17.27	36.39	100	17.27	36.38	26.54
153	17.27	36.39	150	17.27	36.38	26.54
205	17.16	36.36	200	17.17	36.35	26.53
308	16.91	36.31	300	16.93	36.30	26.54
409	15.62	36.08	400	15.76	36.09	26.66
613	12.22	35.57	600	12.44	35.61	26.99
817	6.89	35.09	800	7.33	35.12	27.48
1,020	5.70	35.09	1,000	5.85	35.08	27.65
1,191	5.47	35.10	1,250	5.25	35.08	27.73
1,413	4.57	35.02	1,500	4.36	34.99	27.76
1,628	4.05	34.97	1,750	3.92	34.97	27.79
1,868	3.79	34.99	2,000	3.71	34.97	27.81
2,110	3.63	34.97	2,250	3.55	34.96	27.82
2,356	3.48	34.97	2,500	3.38	34.95	27.83
2,838	3.14	34.95	3,000	3.02	34.94	27.86
3,329	2.77	34.94				

Station 7302; 8 April; 37°58.5′ N., 50°16′ W.; depth 5,413 m.; dynamic height 971.768

Observed values			Scaled values			
Depth, meters	Temperature, °C.	Salinity, °/oo	Depth, meters	Temperature, °C.	Salinity, °/oo	σ_t
0	17.47	36.45	0	17.47	36.45	26.52
25	17.52	36.44	25	17.52	36.45	26.51
50	17.52	36.45	50	17.52	36.45	26.51
75	17.51	36.45	75	17.51	36.45	26.51
100	17.50	36.44	100	17.50	36.44	26.50
150	17.41	36.43	150	17.41	36.43	26.52
201	17.38	36.42	200	17.38	36.41	26.52
302	17.30	36.41	300	17.30	36.40	26.53
401	17.16	36.37	400	17.16	36.36	26.54
600	14.37	35.87	600	14.35	35.87	26.79
803	9.87	35.26	800	9.86	35.26	27.20
1,008	6.36	35.02	1,000	6.53	35.02	27.52
1,214	5.09	35.04	1,250	4.99	35.02	27.72
1,461	4.42	35.00	1,500	4.20	34.99	27.78
1,712	4.09	34.97	1,750	4.06	34.96	27.77
1,960	3.84	34.97	2,000	3.81	34.96	27.80
2,205	3.69	34.97	2,250	3.65	34.96	27.81
2,454	3.52	34.97	2,500	3.49	34.96	27.83
2,949	3.12	34.95	3,000	3.08	34.94	27.85
3,448	2.73	34.93				

TABLE OF OCEANOGRAPHIC DATA—Continued

Observed values			Scaled values			
Depth, meters	Temperature, °C.	Salinity, °/oo	Depth, meters	Temperature, °C.	Salinity, °/oo	σ_t
Station 7303; 8 April; 38°28.5′ N.; 50°22.5′ W.; depth 5,394 m.; dynamic height 971.766						
0-------	17.66	36.48	0-------	17.66	36.48	26.49
26------	17.66	36.48	25------	17.66	36.47	26.49
52------	17.67	36.48	50------	17.66	36.47	26.49
78------	17.67	36.49	75------	17.66	36.48	26.50
104-----	17.65	36.49	100-----	17.66	36.48	26.50
155-----	17.66	36.49	150-----	17.66	36.48	26.50
206-----	17.56	36.47	200-----	17.57	36.46	26.51
310-----	17.45	36.45	300-----	17.46	36.44	26.52
414-----	17.41	36.43	400-----	17.42	36.42	26.52
622-----	14.13	35.81	600-----	14.45	35.86	26.77
828-----	9.53	35.21	800-----	9.70	35.28	27.24
1,033---	6.40	35.10	1,000---	6.42	35.11	27.60
1,230---	5.24	35.10	1,250---	5.15	35.08	27.74
1,476---	4.27	35.00	1,500---	4.25	34.99	27.77
1,721---	4.13	35.01	1,750---	4.10	34.99	27.79
1,968---	3.84	34.98	2,000---	3.81	34.97	27.80
2,218---	3.65	34.97	2,250---	3.65	34.96	27.81
2,468---	3.46	34.99	2,500---	3.43	34.96	27.83
2,964---	3.07	34.96	3,000---	3.05	34.95	27.86
3,462---	2.68	34.94				
3,961---	2.38	34.92				
Station 7304; 8 April; 38°58′ N., 50°18.5′ W.; depth 5,394 m.; dynamic height 971.683						
0-------	18.03	36.49	0-------	18.03	36.49	26.42
24------	18.03	36.49	25------	18.03	36.48	26.42
49------	18.03	36.49	50------	18.02	36.48	26.42
73------	18.02	36.50	75------	18.01	36.49	26.43
97------	18.01	36.50	100-----	18.00	36.49	26.43
145-----	17.80	36.49	150-----	18.00	36.48	26.42
194-----	17.78	36.50	200-----	17.95	36.49	26.44
291----	17.57	36.47	300-----	17.45	36.44	26.53
385-----	16.46	36.21	400-----	16.20	36.16	26.61
570-----	12.95	35.67	600-----	12.20	35.56	27.00
758-----	8.30	35.11	800-----	7.69	35.08	27.41
946-----	5.58	35.02	1,000---	5.43	35.00	27.64
1,258---	4.62	34.95	1,250---	4.67	34.95	27.70
1,470---	4.36	35.01	1,500--	4.32	35.00	27.77
1,702---	4.00	34.99	1,750---	3.95	34.98	27.79
1,950---	3.77	34.97	2,000---	3.74	34.97	27.81
2,198---	3.61	34.98	2,250 --	3.58	34.97	27.83
2,445---	3.45	34.97	2,500---	3.42	34.96	27.83
2,931---	3.10	34.95	3,000---	3.05	34.94	27.85
3,411---	2.70	------				
Station 7305; 9 April; 39°28.5′ N., 50°15′ W.; depth 5,449 m.; dynamic height 971.400						
0-------	17.41	36.36	0-------	17.41	36.36	26.47
25------	17.42	36.36	25------	17.42	36.36	26.47
50------	17.36	36.35	50------	17.36	36.35	26.47
74------	17.27	36.33	75------	17.26	36.32	26.48
99------	17.08	36.32	100-----	17.07	36.31	26.52
148-----	15.79	36.04	150-----	15.80	36.02	26.60
197-----	14.84	35.88	200-----	14.78	35.86	26.70
296-----	12.59	35.48	300-----	12.55	35.47	26.87
392-----	11.72	35.48	400-----	11.55	35.45	27.04
584-----	7.56	35.04	600-----	7.39	35.03	27.41
781-----	5.44	34.99	800-----	5.36	34.98	27.63
980-----	4.69	34.99	1,000---	4.65	34.98	27.72
1,212---	4.31	34.99	1,250---	4.30	34.98	27.75
1,600---	3.87	34.97	1,500---	4.02	34.96	27.77
1,750---	3.75	34.96	1,750---	3.74	34.95	27.79
2,000---	3.61	34.97	2,000---	3.61	34.96	27.82
2,247---	3.47	34.96	2,250---	3.45	34.95	27.82
2,496---	3.32	34.96	2,500---	3.31	34.95	27.84
2,991---	2.99	34.95	3,000---	3.00	34.94	27.86
3,482---	2.62	34.94				
3,974---	2.40	34.94				
Station 7306; 9 April; 39°59.5′ N., 50°17′ W.; depth 5,394 m.; dynamic height 971.242						
0-------	14.07	35.83	0-------	14.07	35.83	26.82
26------	14.05	35.82	25------	14.05	35.81	26.82
51------	14.07	35.82	50------	14.06	35.81	26.82
77------	14.04	35.82	75------	14.03	35.81	26.82
103-----	13.95	35.81	100-----	13.95	35.80	26.83
153-----	13.83	35.81	150-----	13.85	35.80	26.85
205-----	13.32	35.67	200-----	13.37	35.68	26.86
308-----	12.16	35.52	300-----	12.25	35.53	26.97
410-----	8.70	35.09	400-----	9.10	35.12	27.22
605-----	4.74	34.84	600-----	4.83	34.83	27.58
816-----	4.80	34.99	800-----	4.80	34.97	27.70
1,015---	4.05	34.94	1,000---	4.12	34.94	27.75
1,114---	4.31	35.00	1,250---	4.23	34.99	27.78
1,386---	4.12	34.99	1,500---	3.95	34.96	27.78
1,562---	3.89	34.96	1,750---	3.75	34.95	27.79
1,800---	3.73	34.96	2,000---	3.64	34.95	27.80
2,043---	3.59	34.96	2,250---	3.50	34.96	27.83
2,291---	3.45	34.97	2,500---	3.28	34.95	27.84
2,766---	3.06	34.96	3,000---	2.87	34.93	27.86
3,248---	2.66	34.90				
3,732---	2.36	34.91				
Station 7307; 9 April; 40°29′ N., 50°15′ W.; depth 3,695 m.; dynamic height 971.107						
0-------	7.76	33.95	0-------	7.76	33.95	26.49
23------	7.83	34.06	25------	7.85	34.08	26.59
45------	8.70	34.42	50------	8.85	34.48	26.75
70------	9.57	34.76	75------	9.77	34.80	26.86
93------	10.20	34.98	100-----	10.23	35.01	26.94
139-----	10.04	35.08	150-----	9.88	35.07	27.04
185-----	9.01	35.01	200-----	8.60	34.96	27.17
278-----	6.11	34.69	300-----	5.80	34.64	27.31
372-----	4.75	34.66	400-----	4.72	34.68	27.47
562-----	4.62	34.90	600-----	4.55	34.90	27.67
758-----	4.33	34.94	800-----	4.27	34.94	27.73
960-----	4.06	34.97	1,000---	4.08	34.96	27.77
1,140---	4.06	34.98	1,250---	3.94	34.96	27.78
1,388---	3.74	34.96	1,500---	3.72	34.95	27.80
1,642---	3.68	34.96	1,750---	3.60	34.95	27.81
1,888---	3.48	34.96	2,000---	3.41	34.95	27.83
2,138---	3.33	34.95	2,250---	3.25	34.94	27.83
2,389---	3.22	34.95	2,500---	3.11	34.94	27.85
2,889---	2.74	34.94	3,000---	2.65	34.93	27.88
3,394---	2.26	34.91				
Station 7308; 9 April; 41°02.5′ N., 50°11′ W.; depth 3,475 m.; dynamic height 971.113						
0-------	10.29	34.73	0-------	10.29	34.73	26.70
26------	10.25	34.72	25------	10.25	34.71	26.70
53------	10.48	34.88	50------	10.45	34.86	26.78
79------	11.19	35.19	75------	11.07	35.13	26.88
106-----	11.64	35.07	100-----	11.55	35.09	26.76
158-----	8.31	34.81	150-----	8.87	34.85	27.04
211-----	6.89	34.67	200-----	7.23	34.69	27.16
317-----	6.68	34.81	300-----	6.72	34.78	27.30
418-----	5.95	34.95	400-----	6.08	34.92	27.50
614-----	5.11	35.00	600-----	5.15	34.99	27.67
821-----	4.47	34.99	800-----	4.52	34.98	27.73
1,031---	4.18	34.97	1,000---	4.23	34.96	27.75
1,188---	4.02	34.96	1,250---	4.15	34.95	27.75
1,428---	3.74	34.95	1,500---	3.70	34.94	27.79
1,672---	3.61	34.95	1,750---	3.56	34.94	27.80
1,916---	3.49	34.94	2,000---	3.44	34.93	27.81
2,162---	3.35	34.94	2,250---	3.31	34.94	27.83
2,354---	3.28	34.96	2,500---	3.15	34.94	27.84
2,981---	2.74	34.93	3,000---	2.70	34.92	27.87

TABLE OF OCEANOGRAPHIC DATA—Continued

Station 7309; 10 April; 41°22.5′ N., 50°10′ W.; depth 3,731 m.; dynamic height 971.141

Observed values			Scaled values			
Depth, meters	Temperature, °C.	Salinity, ‰	Depth, meters	Temperature, °C.	Salinity, ‰	σ_t
0	11. 26	35. 15	0	11. 26	35. 15	26. 86
26	11. 30	35. 15	25	11. 30	35. 14	26. 85
52	11. 53	35. 21	50	11. 51	35. 19	26. 85
78	11. 59	35. 27	75	11. 56	35. 25	26. 89
104	11. 02	35. 16	100	11. 14	35. 17	26. 90
155	11. 05	35. 23	150	10. 40	35. 21	27. 07
207	8. 47	34. 89	200	8. 75	34. 92	27. 12
311	6. 81	34. 80	300	7. 00	34. 80	27. 28
374	8. 43	34. 94	400	7. 81	34. 95	27. 28
501	5. 78	35. 00	600	5. 22	34. 98	27. 65
694	4. 69	34. 98	800	4. 48	34. 97	27. 73
901	4. 27	34. 97	1,000	4. 20	34. 96	27. 76
1,252	3. 94	34. 96	1,250	3. 96	34. 95	27. 70
1,503	3. 72	34. 96	1,500	3. 75	34. 95	27. 79
1,754	3. 53	34. 94	1,750	3. 55	34. 93	27. 79
2,006	3. 40	34. 94	2,000	3. 40	34. 93	27. 81
2,261	3. 23	34. 92	2,250	3. 23	34. 92	27. 82
2,514	3. 04	34. 94	2,500	3. 05	34. 93	27. 84
3,012	2. 58	34. 93	3,000	2. 60	34. 92	27. 88
3,507	2. 26	34. 90				

Station 7310; 10 April; 41°44.5′ N., 50°07.5′ W.; depth 3,585 m.; dynamic height 971.104

Observed values			Scaled values			
Depth, meters	Temperature, °C.	Salinity, ‰	Depth, meters	Temperature, °C.	Salinity, ‰	σ_t
0	8. 74	34. 36	0	8. 74	34. 36	26. 67
25	8. 99	34. 42	25	8. 99	34. 43	26. 69
50	11. 65	35. 25	50	11. 65	35. 25	26. 86
75	12. 68	35. 51	75	12. 68	35. 51	26. 87
100	11. 77	35. 32	100	11. 77	35. 32	26. 89
150	10. 18	35. 13	150	10. 18	35. 13	27. 03
201	8. 53	34. 95	200	8. 55	34. 95	27. 17
302	6. 41	34. 80	300	6. 45	34. 80	27. 36
400	5. 78	34. 91	400	5. 77	34. 90	27. 53
597	4. 97	34. 90	600	4. 93	34. 89	27. 62
799	3. 98	34. 91	800	3. 98	34. 90	27. 73
1,004	4. 03	34. 96	1,000	4. 05	34. 95	27. 76
1,136	3. 96	34. 95	1,250	3. 91	34. 94	27. 77
1,362	3. 84	34. 94	1,500	3. 75	34. 94	27. 78
1,597	3. 67	34. 95	1,750	3. 60	34. 93	27. 79
1,836	3. 52	34. 93	2,000	3. 40	34. 92	27. 81
2,079	3. 32	34. 92	2,250	3. 25	34. 92	27. 82
2,324	3. 18	34. 92	2,500	3. 05	34. 92	27. 84
2,799	2. 79	34. 92	3,000	2. 35	34. 91	27. 89
3,181	2. 41	34. 92				

Station 7311; 10 April; 42°09′ N.; 50°06′ W.; depth 3,091 m.; dynamic height 971.020

Observed values			Scaled values			
Depth, meters	Temperature, °C.	Salinity, ‰	Depth, meters	Temperature, °C.	Salinity, ‰	σ_t
0	3. 06	33. 41	0	3. 06	33. 41	26. 63
23	3. 09	33. 45	25	3. 25	33. 52	26. 71
46	6. 43	34. 25	50	6. 70	34. 29	26. 92
69	7. 66	34. 57	75	7. 60	34. 55	27. 00
92	6. 83	34. 52	100	6. 60	34. 50	27. 10
137	5. 28	34. 47	150	4. 87	34. 43	27. 26
183	3. 50	34. 34	200	3. 90	34. 44	27. 37
275	5. 64	34. 84	300	5. 54	34. 85	27. 51
364	5. 26	34. 90	400	5. 14	34. 90	27. 60
538	4. 69	34. 95	600	4. 57	34. 94	27. 70
732	4. 33	34. 95	800	4. 23	34. 94	27. 74
936	4. 00	34. 95	1,000	3. 95	34. 94	27. 76
1,166	3. 72	34. 93	1,250	3. 70	34. 92	27. 78
1,410	3. 58	34. 92	1,500	3. 55	34. 91	27. 78
1,658	3. 48	34. 92	1,750	3. 45	34. 91	27. 79
1,902	3. 41	34. 93	2,000	3. 35	34. 92	27. 81
2,150	3. 30	------	2,250	3. 25	34. 92	27. 82
2,400	3. 14	34. 93	2,500	3. 00	34. 92	27. 85
2,892	2. 64	34. 92	3,000	2. 57	34. 91	27. 87

Station 7312; 10 April; 42°31′ N., 50°03.5′ W.; depth 2,195 m., dynamic height 971.041

Observed values			Scaled values			
Depth, meters	Temperature, °C.	Salinity, ‰	Depth, meters	Temperature, °C.	Salinity, ‰	σ_t
0	1. 07	33. 25	0	1. 07	33. 25	26. 66
23	1. 00	33. 32	25	1. 00	33. 31	26. 71
47	1. 00	33. 30	50	1. 00	33. 30	26. 70
70	0. 86	33. 32	75	0. 85	33. 36	26. 76
94	0. 86	33. 55	100	0. 92	33. 57	26. 92
140	1. 29	33. 90	150	1. 40	33. 94	27. 18
186	1. 81	34. 13	200	1. 96	34. 17	27. 33
280	2. 66	34. 49	300	2. 92	34. 53	27. 54
375	3. 80	34. 72	400	3. 93	34. 75	27. 61
570	4. 79	34. 95	600	4. 70	34. 94	27. 68
772	4. 26	34. 94	800	4. 23	34. 92	27. 72
1,226	3. 86	34. 93	1,000	4. 08	34. 92	27. 74
1,479	3. 72	34. 93	1,250	3. 86	34. 92	27. 76
1,735	3. 58	34. 92	1,500	3. 70	34. 92	27. 78
1,984	3. 55	34. 93	1,750	3. 55	34. 91	27. 78
			2,000	3. 55	34. 92	27. 79

Station 7313; 10 April; 42°58.5′ N.; 50°01.5′ W.; depth 344 m.; dynamic height 971.056

Observed values			Scaled values			
Depth, meters	Temperature, °C.	Salinity, ‰	Depth, meters	Temperature, °C.	Salinity, ‰	σ_t
0	1. 48	33. 10	0	1. 48	33. 10	26. 50
25	1. 45	33. 09	25	1. 45	33. 09	26. 50
50	1. 35	33. 14	50	1. 35	33. 14	26. 55
75	1. 02	33. 26	75	1. 02	33. 26	26. 66
100	2. 06	33. 57	100	2. 06	33. 57	26. 85
150	2. 87	34. 17	150	2. 87	34. 17	27. 25
200	2. 59	34. 24	200	2. 59	34. 24	27. 33
300	3. 38	34. 56	300	3. 38	34. 56	27. 51

Station 7314; 10 April; 43°11.5′ N., 50°00′ W.; depth 110 m.; dynamic height 971.065

Observed values			Scaled values			
Depth, meters	Temperature, °C.	Salinity, ‰	Depth, meters	Temperature, °C.	Salinity, ‰	σ_t
0	1. 78	33. 01	0	1. 78	33. 01	26. 41
27	1. 64	33. 05	25	1. 64	33. 04	26. 45
53	1. 27	33. 18	50	1. 30	33. 16	26. 57
80	1. 29	33. 33	75	1. 25	33. 29	26. 67

Station 7315; 10 April; 43°45′ N., 50°03.5′ W.; depth 68 m.; dynamic height 971.054

Observed values			Scaled values			
Depth, meters	Temperature, °C.	Salinity, ‰	Depth, meters	Temperature, °C.	Salinity, ‰	σ_t
0	2. 54	32. 63	0	2. 54	32. 63	26. 05
27	2. 44	32. 64	25	2. 45	32. 63	26. 06
54	1. 91	32. 86	50	2. 00	32. 82	26. 25

Station 7316; 11 April; 43°17.5′ N., 50°40′ W.; depth 90 m.; dynamic height 971.066

Observed values			Scaled values			
Depth, meters	Temperature, °C.	Salinity, ‰	Depth, meters	Temperature, °C.	Salinity, ‰	σ_t
0	2. 65	33. 01	0	2. 65	33. 01	26. 35
24	2. 29	33. 11	25	2. 30	33. 10	26. 45
49	2. 39	33. 17	50	2. 40	33. 16	26. 49
73	2. 01	33. 51	75	2. 00	33. 51	26. 81

Station 7317; 11 April; 43°11′ N., 50°48.5′ W.; depth 166 m.; dynamic height 971.047

Observed values			Scaled values			
Depth, meters	Temperature, °C.	Salinity, ‰	Depth, meters	Temperature, °C.	Salinity, ‰	σ_t
0	3. 76	33. 49	0	3. 76	33. 49	26. 62
20	4. 35	33. 70	25	4. 30	33. 70	26. 75
39	4. 14	33. 72	50	4. 50	33. 85	26. 84
58	4. 81	33. 99	75	5. 30	34. 03	26. 89
78	5. 40	34. 18	100	5. 85	34. 11	26. 89
117	6. 25	34. 47				

TABLE OF OCEANOGRAPHIC DATA—Continued

Observed values			Scaled values			
Depth, meters	Temperature, °C.	Salinity, ‰	Depth, meters	Temperature, °C.	Salinity, ‰	σ_t
Station 7318; 11 April; 43°08′ N., 50°52.5′ W.; depth 631 m.; dynamic height 971.050						
0	4.40	33.59	0	4.40	33.59	26.64
25	5.01	33.86	25	5.01	33.86	26.79
50	5.69	34.05	50	5.69	34.05	26.85
76	8.03	34.62	75	8.05	34.62	26.99
101	9.12	34.86	100	9.10	34.85	27.00
152	7.60	34.69	150	7.70	34.69	27.09
202	7.25	34.80	200	7.25	34.78	27.23
303	5.26	34.76	300	5.35	34.75	27.46
404	3.72	34.71	400	3.80	34.70	27.59
606	3.72	34.81	600	3.70	34.79	27.67
Station 7319; 11 April; 42°58′ N., 51°05.5′ W.; depth 1,481 m.; dynamic height 971.080						
0	6.59	34.16	0	6.59	34.16	26.82
23	6.89	34.36	25	6.90	34.36	26.95
48	7.40	34.52	50	7.50	34.53	26.99
71	8.46	34.78	75	8.40	34.77	27.05
96	8.10	34.75	100	7.75	34.71	27.10
142	5.08	34.34	150	4.85	34.31	27.17
190	3.73	34.21	200	3.65	34.20	27.21
286	3.17	34.23	300	3.15	34.25	27.29
382	3.13	34.40	400	3.25	34.44	27.43
575	4.51	34.79	600	4.50	34.89	27.66
770	4.45	34.95	800	4.35	34.92	27.71
960	3.71	34.88	1,000	3.75	34.88	27.73
1,431	3.62	------				
Station 7320; 11 April; 42°46.5′ N., 51°21′ W.; depth 2,012 m.; dynamic height 971.058						
0	3.00	33.37	0	3.00	33.37	26.60
23	6.09	34.11	25	6.10	34.11	26.86
46	6.16	34.20	50	6.20	34.22	26.93
69	6.61	34.35	75	6.50	34.34	26.98
92	6.15	34.35	100	5.90	34.31	27.04
138	4.47	34.22	150	4.55	34.25	27.15
185	4.85	34.35	200	4.75	34.36	27.22
277	4.32	34.49	300	4.45	34.54	27.39
367	4.99	34.75	400	4.95	34.77	27.52
546	4.91	34.94	600	4.80	34.93	27.66
722	4.51	34.96	800	4.50	34.95	27.71
902	4.43	34.96	1,000	4.40	34.95	27.72
1,352	3.72	34.94				
Station 7,321; 11 April; 42°21′ N.; 51°35′ W.; depth 3,237 m.; dynamic height 971.013						
0	5.45	33.49	0	5.45	33.49	26.44
21	5.24	33.53	25	5.20	33.52	26.51
42	5.16	33.54	50	5.10	33.67	26.64
63	4.98	33.94	75	4.90	34.10	26.99
84	4.93	34.23	100	4.90	34.24	27.10
126	4.91	34.25	150	4.60	34.38	27.25
169	4.32	34.51	200	4.50	34.59	27.42
253	4.83	34.76	300	4.90	34.82	27.57
338	4.94	34.90	400	4.80	34.91	27.65
509	4.53	34.95	600	4.35	34.93	27.71
682	4.11	34.94	800	4.10	34.93	27.74
862	4.05	34.94	1,000	3.95	34.93	27.75
1,308	3.70	34.94				

Observed values			Scaled values			
Depth, meters	Temperature, °C.	Salinity, ‰	Depth, meters	Temperature, °C.	Salinity, ‰	σ_t
Station 7322; 11 April; 42°10′ N., 50°52′ W.; depth 3,292 m.; dynamic height 971.047						
0	5.68	33.46	0	5.68	33.46	26.39
25	5.90	33.52	25	5.90	33.52	26.41
50	5.77	33.69	50	5.77	33.69	26.56
75	7.17	34.23	75	7.17	34.23	26.80
100	9.17	34.84	100	9.17	34.84	26.98
148	7.30	34.67	150	7.25	34.74	27.20
198	6.26	34.67	200	6.25	34.66	27.27
298	5.18	34.75	300	5.15	34.74	27.47
397	5.66	35.01	400	5.65	35.00	27.62
597	4.47	34.98	600	4.45	34.97	27.74
798	4.25	34.97	800	4.25	34.96	27.75
1,003	3.88	34.94	1,000	3.90	34.94	27.77
1,513	3.66	34.95				
Station 7323; 12 April; 41°59.5′ N., 49°32′ W.; depth 3,127 m.; dynamic height 971.112						
0	11.16	35.09	0	11.16	35.09	26.83
24	11.21	35.09	25	11.20	35.08	26.82
47	11.59	35.26	50	11.60	35.25	26.88
71	11.73	35.33	75	11.80	35.35	26.92
95	12.29	35.49	100	12.30	35.48	26.92
142	12.37	35.50	150	12.25	35.47	26.93
190	11.62	35.38	200	11.25	35.32	27.00
285	7.49	34.88	300	7.30	34.87	27.30
381	5.99	34.85	400	5.90	34.85	27.47
577	4.76	34.94	600	4.70	34.94	27.68
777	4.08	34.94	800	4.05	34.93	27.74
982	3.68	34.91	1,000	3.70	34.90	27.76
1,491	3.66	34.93				
Station 7324; 12 April; 41°36′ N., 47°17.5′ W.; depth 4,280 m.; dynamic height 971.309						
0	15.08	35.96	0	15.08	35.96	26.71
22	15.12	35.98	25	15.10	35.97	26.72
45	15.14	35.98	50	15.10	35.98	26.72
67	15.11	35.98	75	15.05	35.98	26.73
90	15.05	35.99	100	15.00	35.98	26.74
134	14.77	35.99	150	14.60	35.97	26.83
179	14.31	------	200	14.20	35.96	26.90
269	13.80	35.90	300	13.15	35.78	26.98
414	10.66	35.34	400	10.95	35.39	27.11
620	6.98	35.05	600	7.35	35.07	27.45
826	5.56	35.07	800	5.50	35.05	27.67
1,035	5.04	35.10	1,000	5.15	35.08	27.74
1,555	3.89	34.99				
Station 7325; 12 April; 41°58.5′ N., 47°54′ W.; depth 3,932 m.; dynamic height 971.176						
0	11.98	35.28	0	11.98	35.28	26.82
20	11.96	35.27	25	11.95	35.26	26.82
40	11.95	35.26	50	12.05	35.31	26.84
61	12.18	35.38	75	11.80	35.30	26.88
81	11.69	35.29	100	11.95	35.36	26.90
121	12.28	35.46	150	12.30	35.47	26.92
161	12.33	35.49	200	11.55	35.40	27.00
242	10.76	35.32	300	9.20	35.12	27.20
319	8.70	35.08	400	7.75	35.07	27.39
471	6.96	35.08	600	5.70	35.00	27.61
618	5.50	35.00	800	4.25	34.92	27.72
790	4.27	34.93	1,000	4.00	34.91	27.74
1,252	3.69	34.90				

TABLE OF OCEANOGRAPHIC DATA—Continued

Station 7326; 13 April; 42°22.5′ N., 48°30′ W.; depth 2,475 m.; dynamic height 971.011

Observed values			Scaled values			
Depth, meters	Temperature, °C.	Salinity, °/oo	Depth, meters	Temperature, °C.	Salinity, °/oo	σ_t
0	5.54	33.77	0	5.54	33.77	26.65
26	5.54	33.77	25	5.55	33.76	26.65
52	5.73	33.98	50	5.70	33.95	26.79
79	5.72	34.19	75	5.70	34.15	26.94
105	4.76	34.28	100	5.00	34.26	27.11
157	6.13	34.72	150	5.90	34.65	27.31
209	5.79	34.78	200	5.85	34.76	27.40
314	5.37	34.91	300	5.40	34.88	27.55
417	4.98	34.94	400	5.00	34.93	27.64
623	4.51	34.97	600	4.60	34.96	27.71
828	4.05	34.94	800	4.15	34.93	27.73
1,037	3.62	34.87	1,000	3.70	34.88	27.74
1,563	3.51	34.88				

Station 7327; 13 April; 42°43.5′ N., 49°07.5′ W.; depth 2,378 m.; dynamic height 971.047

Observed values			Scaled values			
Depth, meters	Temperature, °C.	Salinity, °/oo	Depth, meters	Temperature, °C.	Salinity, °/oo	σ_t
0	0.73	33.11	0	0.73	33.11	26.55
25	0.85	33.21	25	0.85	33.21	26.64
50	1.16	33.46	50	1.16	33.46	26.81
74	4.69	34.13	75	4.70	34.13	27.04
99	2.01	33.94	100	2.00	33.92	27.13
148	1.24	33.89	150	1.25	33.89	27.15
197	1.66	34.06	200	1.65	34.05	27.26
296	2.04	34.23	300	1.05	34.24	27.38
393	2.98	34.54	400	3.00	34.55	27.55
586	3.78	34.84	600	3.80	34.83	27.69
777	3.68	34.86	800	3.70	34.85	27.72
970	3.62	34.89	1,000	3.65	34.89	27.75
1,450	3.75	34.95				

Station 7328; 13 April; 43°20′ N., 48°47.5′ W.; depth 1,957 m.; dynamic height 970.919

Observed values			Scaled values			
Depth, meters	Temperature, °C.	Salinity, °/oo	Depth, meters	Temperature, °C.	Salinity, °/oo	σ_t
0	1.75	33.53	0	1.75	33.53	26.83
23	1.66	33.77	25	1.65	33.78	27.04
46	1.90	33.98	50	1.95	34.01	27.21
69	2.22	34.26	75	2.25	34.26	27.38
92	2.33	34.30	100	2.40	34.32	27.42
139	2.75	34.46	150	2.90	34.50	27.52
185	3.24	34.64	200	3.30	34.66	27.61
277	3.70	34.79	300	3.75	34.79	27.66
368	3.87	34.85	400	3.85	34.84	27.69
549	3.78	34.87	600	3.75	34.86	27.72
727	3.67	34.85	800	3.65	34.85	27.72
897	3.60	34.86	1,000	3.60	34.86	27.74
1,302	3.52	34.90				

Station 7329; 13 April; 43°06′ N., 48°09′ W.; depth 3,081 m.; dynamic height 970.987

Observed values			Scaled values			
Depth, meters	Temperature, °C.	Salinity, °/oo	Depth, meters	Temperature, °C.	Salinity, °/oo	σ_t
0	9.54	34.79	0	9.54	34.79	26.88
27	9.33	34.77	25	9.35	34.76	26.89
54	8.43	34.62	50	8.60	34.62	26.91
81	9.28	34.86	75	9.05	34.80	26.97
108	7.45	34.65	100	8.10	34.66	27.01
162	1.99	34.19	150	3.25	34.28	27.30
216	2.60	34.44	200	2.40	34.36	27.45
324	3.31	34.69	300	3.15	34.63	27.59
410	3.65	34.76	400	3.60	34.74	27.64
610	3.79	34.86	600	3.75	34.85	27.71
806	3.58	34.86	800	3.60	34.85	27.73
1,010	3.59	34.86	1,000	3.60	34.85	27.73
1,525	3.50	34.93				

Station 7330; 13 April; 42°51.5′ N., 47°30.5′ W.; depth 3,840 m.; dynamic height 970.994

Observed values			Scaled values			
Depth, meters	Temperature, °C.	Salinity, °/oo	Depth, meters	Temperature, °C.	Salinity, °/oo	σ_t
0	5.79	33.72	0	5.79	33.72	26.58
26	5.72	33.74	25	5.50	33.73	26.63
51	5.30	33.77	50	5.30	33.76	26.88
77	4.76	33.84	75	4.80	33.82	26.79
102	4.22	34.38	100	4.30	34.32	27.24
155	4.78	34.60	150	4.70	34.57	27.39
206	4.57	34.68	200	4.60	34.66	27.47
308	5.51	34.97	300	5.45	34.93	27.58
507	4.66	34.95	400	5.10	34.95	27.64
609	4.36	34.96	600	4.40	34.95	27.72
810	3.97	34.93	800	4.00	34.93	27.75
1,014	3.86	34.94	1,000	3.90	34.93	27.76
1,522	3.51	34.93				

Station 7331; 14 April; 42°37′ N., 46°51′ W.; depth 4,114 m.; dynamic height 971.180

Observed values			Scaled values			
Depth, meters	Temperature, °C.	Salinity, °/oo	Depth, meters	Temperature, °C.	Salinity, °/oo	σ_t
0	13.88	35.77	0	13.88	35.77	26.81
26	13.95	35.78	25	13.95	35.77	26.81
51	13.95	35.77	50	13.95	35.77	26.81
77	13.95	35.78	75	13.95	35.77	26.81
102	13.86	35.77	100	13.85	35.76	26.82
155	12.67	35.56	150	12.75	35.57	26.91
206	11.12	35.32	200	11.35	35.34	26.99
308	8.64	35.04	300	8.80	35.05	27.21
361	6.38	34.71	400	6.10	34.74	27.35
535	5.24	34.88	600	5.15	34.91	27.61
703	4.94	34.97	800	4.70	34.96	27.70
890	4.44	34.96	1,000	4.30	34.95	27.73
1,379	3.76	34.95				

Station 7332; 14 April; 42°23′ N., 46°11′ W.; depth 4,663 m.; dynamic height 971.500

Observed values			Scaled values			
Depth, meters	Temperature, °C.	Salinity, °/oo	Depth, meters	Temperature, °C.	Salinity, °/oo	σ_t
0	15.42	36.10	0	15.42	36.10	26.74
26	15.42	36.10	25	15.40	36.09	26.74
52	15.42	36.10	50	15.40	36.09	26.74
78	15.43	36.10	75	15.40	36.09	26.74
104	15.21	36.06	100	15.25	36.06	26.75
157	14.32	35.90	150	14.45	35.91	26.81
209	14.80	36.06	200	14.75	36.03	26.84
313	14.84	36.07	300	14.85	36.06	26.85
348	13.95	35.81	400	13.35	35.72	26.90
585	11.32	35.43	600	11.00	35.39	27.10
700	8.19	35.15	800	7.65	35.13	27.44
987	6.54	35.12	1,000	6.50	35.11	27.59
1,366	4.53	35.05				

Station 7333; 14 April; 42°44′ N., 45°43.5′ W.; depth 4,572 m.

Observed values			Scaled values			
Depth, meters	Temperature, °C.	Salinity, °/oo	Depth, meters	Temperature, °C.	Salinity, °/oo	σ_t
0	15.09	36.05	0	15.09	36.05	26.77
26	15.01	36.02	25	15.00	36.02	26.78
52	14.97	36.02	50	14.95	36.01	26.79
78	14.91	36.01	75	14.90	36.00	26.79
104	14.85	35.99	100	14.85	35.99	26.79
156	14.35	35.89	150	14.40	35.90	26.81
208	14.75	36.03	200	14.65	35.99	26.83
312	13.92	35.86	300	14.05	35.87	26.87

TABLE OF OCEANOGRAPHIC DATA—Continued

Observed values			Scaled values			
Depth, meters	Temperature, °C.	Salinity, °/oo	Depth, meters	Temperature, °C.	Salinity, °/oo	σ_t
Station 7334; 14 April; 43°11′ N., 45°18′ W.; depth 4,637 m.; dynamic height 971.368						
0	14.96	36.05	0	14.96	36.05	26.80
26	14.92	36.06	25	14.90	36.05	26.82
51	14.89	36.05	50	14.90	36.05	26.82
77	14.88	36.06	75	14.90	36.05	26.82
102	14.89	36.04	100	14.90	36.04	26.81
154	14.74	36.04	150	14.75	36.03	26.84
206	14.85	36.07	200	14.85	36.05	26.84
308	14.20	35.93	300	14.25	35.93	26.87
397	12.69	35.65	400	12.60	35.64	26.98
592	8.78	35.17	600	8.65	35.16	27.32
786	6.08	35.05	800	5.55	35.03	27.65
986	4.74	34.99	1,000	4.75	34.98	27.70
1,493	3.70	34.93				
Station 7335; 14 April; 43°19.5′ N., 46°00′ W.; depth 4,846 m.; dynamic height 971.314						
0	14.36	35.89	0	14.36	35.89	26.80
26	14.36	35.89	25	14.35	35.88	26.81
52	14.38	35.90	50	14.35	35.89	26.81
79	14.40	35.91	75	14.40	35.90	26.81
104	14.43	35.91	100	14.40	35.90	26.81
157	14.44	35.91	150	14.45	35.90	26.80
210	14.37	35.91	200	14.40	35.90	26.81
314	12.57	35.58	300	12.80	35.62	26.93
420	10.35	35.31	400	10.80	35.35	27.10
630	6.48	34.99	600	7.05	35.04	27.46
841	4.78	34.95	800	5.10	34.96	27.65
1,053	4.24	34.95	1,000	4.40	34.94	27.71
1,588	3.62	34.92				
Station 7336; 15 April; 43°30′ N., 46°40′ W.; depth 4,618 m.; dynamic height 971.144						
0	10.54	34.90	0	10.54	34.90	26.79
26	10.69	34.94	25	10.65	34.93	26.80
51	11.59	35.16	50	11.55	35.15	26.81
77	12.28	35.34	75	12.20	35.32	26.82
102	11.40	35.11	100	11.55	35.14	26.80
154	11.05	35.16	150	11.05	35.15	26.90
205	9.95	35.07	200	10.05	35.07	27.02
307	8.51	35.09	300	8.60	35.08	27.26
416	6.34	34.93	400	6.65	34.95	27.45
623	4.78	34.94	600	4.95	34.93	27.64
831	4.15	34.93	800	4.25	34.92	27.72
1,040	4.05	34.95	1,000	4.10	34.93	27.74
1,564	3.52	34.94				
Station 7337; 15 April; 43°42′ N., 47°18′ W.; depth 4,206 m.; dynamic height 971.172						
0	11.55	35.50	0	11.55	35.50	27.07
27	11.55	35.50	25	11.55	35.49	27.07
53	11.57	35.49	50	11.55	35.48	27.06
80	11.62	35.50	75	11.60	35.49	27.06
105	11.60	35.50	100	11.60	35.49	27.06
159	11.60	35.51	150	11.60	35.50	27.07
212	11.62	35.50	200	11.60	35.50	27.07
317	11.63	35.50	300	11.60	35.49	27.06
315	11.60	35.50	400	9.10	35.18	27.26
472	6.92	34.92	600	5.55	34.92	27.57
631	5.22	34.93	800	4.60	34.96	27.71
794	4.61	34.97	1,000	4.25	34.95	27.74
1,213	3.88	34.95				

Observed values			Scaled values			
Depth, meters	Temperature, °C.	Salinity, °/oo	Depth, meters	Temperature, °C.	Salinity, °/oo	σ_t
Station 7338; 15 April; 43°57′ N., 47°55′ W.; depth 4,060 m.; dynamic height 971.181						
0	11.33	35.43	0	11.33	35.43	27.06
26	11.33	35.43	25	11.30	35.42	27.07
51	11.35	35.43	50	11.35	35.42	27.06
77	11.34	35.43	75	11.35	35.42	27.06
102	11.35	35.44	100	11.35	35.43	27.06
153	11.36	35.44	150	11.35	35.43	27.06
204	11.38	35.43	200	11.30	35.42	27.07
306	11.46	35.47	300	11.45	35.46	27.07
409	8.34	34.98	400	8.60	35.02	27.22
612	5.60	34.95	600	5.75	34.94	27.56
818	4.41	34.95	800	4.55	34.94	27.70
975	3.98	34.92	1,000	4.00	34.92	27.75
1,541	3.67	34.93				
Station 7339; 15 April; 44°02.5′ N., 48°28.5′ W.; depth 3,658 m.; dynamic height 971.047						
0	10.99	35.16	0	10.99	35.16	26.91
23	10.98	35.16	25	10.95	35.15	26.92
46	10.98	35.16	50	10.95	35.15	26.92
69	10.98	35.16	75	10.90	35.15	26.93
92	10.75	35.16	100	10.60	35.14	26.97
139	10.03	35.12	150	9.60	35.05	27.08
185	8.13	34.88	200	7.75	34.85	27.21
277	5.71	34.73	300	5.55	34.74	27.42
413	4.91	34.82	400	4.95	34.80	27.54
619	4.61	34.94	600	4.20	34.92	27.73
826	4.02	34.95	800	4.00	34.94	27.76
985	4.07	34.94	1,000	4.05	34.93	27.74
1,542	3.52	34.89				
Station 7340; 15 April; 44°07.5′ N., 48°48′ W.; depth 1,637 m.; dynamic height 970.932						
0	1.50	33.58	0	1.50	33.58	26.89
24	1.84	33.64	25	1.85	33.63	26.91
46	1.92	33.67	50	2.00	33.70	26.95
69	2.18	33.91	75	2.25	33.96	27.14
91	2.40	34.14	100	2.60	34.22	27.32
138	3.48	34.56	150	3.45	34.57	27.52
184	3.35	34.65	200	3.45	34.67	27.60
275	3.98	34.83	300	3.95	34.83	27.67
416	3.84	34.87	400	3.85	34.86	27.71
620	3.62	34.86	600	3.65	34.85	27.72
822	3.56	34.84	800	3.55	34.84	27.72
1,028	3.53	34.89	1,000	3.55	34.87	27.75
1,542	3.48	34.91				
Station 7341; 16 April; 44°10′ N., 48°57′ W.; depth 607 m.; dynamic height 971.039						
0	0.15	33.16	0	0.15	33.16	26.62
22	0.19	33.17	25	0.15	33.18	26.65
45	0.12	33.32	50	0.20	33.35	26.78
68	0.44	33.50	75	0.50	33.51	26.90
91	0.63	33.57	100	0.70	33.61	26.97
135	0.97	33.79	150	1.10	33.87	27.15
181	1.49	34.06	200	1.60	34.11	27.31
272	2.11	34.36	300	2.30	34.40	27.49
358	2.81	34.52	400	3.00	34.57	27.57
528	3.63	34.78	(600)	3.80	34.84	27.70

TABLE OF OCEANOGRAPHIC DATA—Continued

Station 7342; 16 April; 44°12.5′ N., 49°08.5′ W.; depth 168 m.; dynamic height 971.118

Observed values			Scaled values			
Depth, meters	Temperature, °C.	Salinity, ‰	Depth, meters	Temperature, °C.	Salinity, ‰	σ_t
0	0.01	33.06	0	0.01	33.06	26.56
25	0.04	33.11	25	0.04	33.11	26.59
51	0.31	33.41	50	0.25	33.40	26.83
76	0.36	33.41	75	0.35	33.40	26.82
101	0.37	33.42	100	0.35	33.41	26.83
152	0.43	33.45	150	0.40	33.43	26.84

Station 7343; 16 April; 44°13.5′ N., 49°14′ W.; depth 84 m.; dynamic height 971.124

Observed values			Scaled values			
Depth, meters	Temperature, °C.	Salinity, ‰	Depth, meters	Temperature, °C.	Salinity, ‰	σ_t
0	0.04	33.10	0	0.04	33.10	26.58
25	0.13	33.17	25	0.13	33.17	26.64
49	0.17	33.20	50	0.15	33.19	26.66
74	0.22	33.30	75	0.20	33.29	26.73

Station 7344; 16 April; 44°18′ N., 49°31′ W.; depth 55 m.; dynamic height 971.131

Observed values			Scaled values			
Depth, meters	Temperature, °C.	Salinity, ‰	Depth, meters	Temperature, °C.	Salinity, ‰	σ_t
0	0.58	33.04	0	0.58	33.04	26.51
25	0.61	33.07	25	0.61	33.07	26.53
50	0.59	33.07	50	0.59	33.07	26.53

Station 7345; 16 April; 45°01′ N., 49°32′ W.; depth 71 m.; dynamic height 971.131

Observed values			Scaled values			
Depth, meters	Temperature, °C.	Salinity, ‰	Depth, meters	Temperature, °C.	Salinity, ‰	σ_t
0	0.22	32.98	0	0.22	32.98	26.48
25	0.25	32.99	25	0.25	32.99	26.49
51	0.17	33.15	50	0.20	33.13	26.61

Station 7346; 16 April; 44°56.5′ N., 49°03′ W.; depth 91 m.; dynamic height 971.123

Observed values			Scaled values			
Depth, meters	Temperature, °C.	Salinity, ‰	Depth, meters	Temperature, °C.	Salinity, ‰	σ_t
0	0.03	33.05	0	0.03	33.05	26.55
25	0.03	33.22	25	0.03	33.22	26.69
50	0.06	33.23	50	0.06	33.23	26.69
75	0.07	33.25	75	0.07	33.25	26.71

Station 7347; 16 April; 44°55′ N., 48°54′ W.; depth 612 m.; dynamic height 971.068

Observed values			Scaled values			
Depth, meters	Temperature, °C.	Salinity, ‰	Depth, meters	Temperature, °C.	Salinity, ‰	σ_t
0	0.14	33.13	0	0.14	33.13	26.60
24	0.08	33.12	25	0.05	33.11	26.60
48	0.02	33.19	50	0.05	33.20	26.68
72	0.25	33.43	75	0.35	33.46	26.87
96	0.68	33.67	100	0.75	33.68	27.02
144	1.16	33.84	150	1.20	33.84	27.12
192	1.32	33.93	200	1.30	33.92	27.18
287	1.40	33.97	300	1.50	34.02	27.25
383	...	34.44	400	2.30	34.47	27.55
575	3.74	34.85	(600)	3.95	34.89	27.72

Station 7348; 16 April; 44°52.5′ N., 48°39′ W.; depth 1,628 m.; dynamic height 970.943

Observed values			Scaled values			
Depth, meters	Temperature, °C.	Salinity, ‰	Depth, meters	Temperature, °C.	Salinity, ‰	σ_t
0	2.11	33.56	0	2.11	33.56	26.83
25	2.09	33.61	25	2.09	33.61	26.87
50	2.15	33.87	50	2.15	33.87	27.07
75	2.35	33.98	75	2.35	33.98	27.14
100	2.36	34.19	100	2.36	34.19	27.30
149	2.66	34.45	150	2.65	34.44	27.49
199	3.00	34.58	200	3.00	34.57	27.57
299	4.23	34.83	300	4.20	34.82	27.65
392	3.79	34.80	400	3.75	34.79	27.66
587	3.64	34.84	600	3.65	34.83	27.70
780	3.59	34.81	800	3.60	34.86	27.74
985	3.55	34.88	1,000	3.55	34.87	27.75
1,517	3.50	34.87				

Station 7349; 16 April; 44°48′ N., 48°23′ W.; depth 2,560 m.; dynamic height 970.942

Observed values			Scaled values			
Depth, meters	Temperature, °C.	Salinity, ‰	Depth, meters	Temperature, °C.	Salinity, ‰	σ_t
0	2.10	33.40	0	2.10	33.40	26.70
23	2.07	33.39	25	2.10	33.40	26.71
45	1.92	33.73	50	1.95	33.77	27.01
68	2.15	33.98	75	2.25	34.02	27.19
91	2.39	34.18	100	2.75	34.25	27.33
135	3.93	34.59	150	3.95	34.61	27.50
180	4.01	34.68	200	4.15	34.69	27.54
271	4.49	------	300	4.45	34.79	27.59
406	4.23	34.90	400	4.20	34.89	27.70
609	3.77	34.89	600	3.80	34.88	27.73
812	3.68	34.90	800	3.70	34.89	27.75
1,014	3.55	34.90	1,000	3.60	34.89	27.76
1,521	3.44	34.91				

Station 7350; 16 April; 44°40.5′ N., 47°54′ W.; depth 3,383 m.; dynamic height 970.916

Observed values			Scaled values			
Depth, meters	Temperature, °C.	Salinity, ‰	Depth, meters	Temperature, °C.	Salinity, ‰	σ_t
0	2.23	33.38	0	2.23	33.38	26.67
15	2.24	33.36	25	2.25	33.40	26.70
29	2.26	33.41	50	2.00	33.81	27.04
44	2.01	33.78	75	2.05	34.10	27.27
58	1.92	33.91	100	2.75	34.40	27.45
88	2.12	------	150	4.45	34.72	27.54
117	3.72	34.66	200	4.90	34.81	27.56
175	5.03	34.81	300	4.30	34.86	27.66
365	4.14	34.90	400	3.70	34.89	27.75
552	3.77	34.89	600	3.85	34.90	27.74
743	3.99	34.94	800	3.90	34.93	27.76
943	3.76	34.93	1,000	3.80	34.92	27.77
1,464	3.53	34.93				

Station 7351; 17 April; 44°39.5′ N., 47°17′ W.; depth 3,804 m.; dynamic height 970.938

Observed values			Scaled values			
Depth, meters	Temperature, °C.	Salinity, ‰	Depth, meters	Temperature, °C.	Salinity, ‰	σ_t
0	2.52	33.71	0	2.52	33.71	26.91
27	2.55	33.71	25	2.55	33.70	26.91
53	2.96	33.86	50	2.90	33.83	26.98
80	2.85	34.04	75	2.90	34.00	27.12
106	2.45	34.17	100	2.50	34.15	27.27
160	2.70	34.41	150	2.65	34.36	27.43
212	2.92	34.76	200	2.85	34.68	27.66
318	5.03	34.94	300	4.65	34.90	27.66
405	4.60	34.93	400	4.60	34.92	27.68
609	3.96	34.90	600	4.00	34.89	27.72
816	3.80	34.89	800	3.80	34.88	27.73
1,026	3.79	34.92	1,000	3.80	34.91	27.76
1,556	3.48	34.92				

TABLE OF OCEANOGRAPHIC DATA—Continued

Station 7352; 1 May; 45°16′ N., 47°03′ W.; depth 3,228 m.; dynamic height 970.976

Observed values			Scaled values			
Depth, meters	Temperature, °C.	Salinity, ‰	Depth, meters	Temperature, °C.	Salinity, ‰	σ_t
0	5.37	34.08	0	5.37	34.08	26.92
26	5.38	34.175	25	5.40	34.18	27.00
53	5.59	34.25	50	5.55	34.25	27.04
78	6.31	34.445	75	6.20	34.42	27.09
105	5.73	34.44	100	5.85	34.44	27.15
157	5.61	34.68	150	5.65	34.64	27.33
209	5.74	34.805	200	5.70	34.78	27.43
314	3.46	34.70	300	3.75	34.71	27.60
361	3.68	34.775	400	3.75	34.80	27.67
541	4.03	34.895	600	4.00	34.89	27.72
721	3.96	34.89	800	4.05	34.90	27.72
921	3.73	34.91	1,000	4.20	34.91	27.72
1,382	3.64	34.93				

Station 7353; 2 May; 45°15′ N., 47°45′ W.; depth 2,743 m.; dynamic height 970.970

Observed values			Scaled values			
Depth, meters	Temperature, °C.	Salinity, ‰	Depth, meters	Temperature, °C.	Salinity, ‰	σ_t
0	4.95	34.03	0	4.95	34.03	26.93
25	4.89	34.03	25	4.89	34.03	26.94
52	4.86	34.02	50	4.85	34.02	26.94
77	4.88	34.19	75	4.90	34.17	27.05
103	4.77	------	100	4.80	34.25	27.12
154	4.59	34.41	150	4.60	34.40	27.26
206	4.08	34.61	200	4.15	34.59	27.46
309	3.92	34.71	300	3.95	34.70	27.57
369	3.89	34.77	400	3.90	34.79	27.65
551	3.86	34.875	600	3.80	34.88	27.73
731	3.69	34.89	800	3.65	34.89	27.75
917	3.58	34.895	1,000	3.55	34.90	27.77
1,400	3.32	34.915				

Station 7354; 2 May; 45°31′ N., 48°06′ W.; depth 1,335 m.; dynamic height 971.045

Observed values			Scaled values			
Depth, meters	Temperature, °C.	Salinity, ‰	Depth, meters	Temperature, °C.	Salinity, ‰	σ_t
0	−0.51	32.88	0	−0.51	32.88	26.44
24	−0.60	32.90	25	−0.60	32.92	26.47
48	−0.62	33.18	50	−0.50	33.20	26.70
72	0.71	33.48	75	1.10	33.56	26.90
96	4.87	34.10	100	4.90	34.11	27.00
143	5.16	34.205	150	5.15	34.21	27.05
192	4.91	34.295	200	4.90	34.32	27.17
288	5.01	34.76	300	4.75	34.74	27.52
358	3.30	34.66	400	3.40	34.71	27.64
537	3.78	34.86	600	3.75	34.86	27.72
716	3.68	34.85	800	3.65	34.87	27.74
901	3.62	34.89	1,000	3.60	34.89	27.76
1,202	3.52	34.88				

Station 7355; 2 May; 45°37′ N., 48°13′ W.; depth 640 m.; dynamic height 971.131

Observed values			Scaled values			
Depth, meters	Temperature, °C.	Salinity, ‰	Depth, meters	Temperature, °C.	Salinity, ‰	σ_t
0	−0.42	32.72	0	−0.42	32.72	26.31
24	−0.43	32.72	25	−0.45	32.72	26.31
48	−0.52	32.74	50	−0.55	32.75	26.34
71	−0.85	32.98	75	−0.80	33.01	26.56
95	−0.48	33.21	100	−0.45	33.23	26.72
142	0.24	33.48	150	0.30	33.50	26.90
190	0.70	33.64	200	0.95	33.70	27.02
285	3.12	34.18	300	3.05	34.22	27.28
364	2.51	34.42	400	2.85	34.51	27.53
502	3.71	34.78	500	3.70	34.77	27.66

Station 7356; 2 May; 45°43′ N., 48°20′ W.; depth 174 m.; dynamic height 971.124

Observed values			Scaled values			
Depth, meters	Temperature, °C.	Salinity, ‰	Depth, meters	Temperature, °C.	Salinity, ‰	σ_t
0	0.18	32.69	0	0.18	32.69	26.25
26	−0.41	32.735	25	−0.40	32.73	26.32
51	−0.74	32.98	50	−0.75	32.98	26.53
77	−0.60	33.10	75	−0.60	33.09	26.60
102	−0.22	33.32	100	−0.25	33.30	26.76
152	0.06	33.40	150	0.05	33.40	26.84

Station 7357; 2 May; 45°46′ N., 48°26′ W.; depth 115 m.; dynamic height 971.121

Observed values			Scaled values			
Depth, meters	Temperature, °C.	Salinity, ‰	Depth, meters	Temperature, °C.	Salinity, ‰	σ_t
0	−0.31	32.73	0	−0.31	32.73	26.31
25	−0.34	32.73	25	−0.34	32.73	26.31
49	−0.80	32.97	50	−0.80	32.97	26.52
74	−0.55	33.12	75	−0.55	33.13	26.64
98	−0.09	33.28	100	−0.10	33.28	26.74

Station 7358; 2 May; 45°50′ N., 48°33′ W.; depth 95 m.; dynamic height 971.120

Observed values			Scaled values			
Depth, meters	Temperature, °C.	Salinity, ‰	Depth, meters	Temperature, °C.	Salinity, ‰	σ_t
0	0.54	32.85	0	0.54	32.85	26.36
26	0.57	32.85	25	0.55	32.85	26.36
53	0.51	32.85	50	0.55	32.85	26.36
79	−0.21	33.17	75	−0.05	33.13	26.62

Station 7359; 2 May; 46°03′ N., 48°54′ W., depth 84 m.; dynamic height 971.110

Observed values			Scaled values			
Depth, meters	Temperature, °C.	Salinity, ‰	Depth, meters	Temperature, °C.	Salinity, ‰	σ_t
0	0.63	32.89	0	0.63	32.89	26.39
28	0.61	32.89	25	0.60	32.89	26.39
55	0.04	33.16	50	0.15	33.11	26.59

Station 7360; 2 May; 46°09′ N., 49°08′ W.; depth 68 m. dynamic height 971.123

Observed values			Scaled values			
Depth, meters	Temperature, °C.	Salinity, ‰	Depth, meters	Temperature, °C.	Salinity, ‰	σ_t
0	0.95	32.83	0	0.95	32.83	26.33
26	0.91	32.84	25	0.90	32.84	26.34
51	0.83	32.865	50	0.85	32.86	26.36

Station 7361; 2 May; 45°59′ N., 48°30′ W.; depth 95 m.; dynamic height 971.107

Observed values			Scaled values			
Depth, meters	Temperature, °C.	Salinity, ‰	Depth, meters	Temperature, °C.	Salinity, ‰	σ_t
0	0.36	32.84	0	0.36	32.84	26.37
26	0.35	32.835	25	0.35	32.85	26.38
52	0.01	33.19	50	0.05	33.17	26.65
78	0.35	33.42	75	0.30	33.41	26.83

Station 7362; 2 May; 45°56′ N., 48°11′ W.; depth 124 m.; dynamic height 971.115

Observed values			Scaled values			
Depth, meters	Temperature, °C.	Salinity, ‰	Depth, meters	Temperature, °C.	Salinity, ‰	σ_t
0	0.22	32.86	0	0.22	32.86	26.39
26	0.21	32.86	25	0.20	32.86	26.39
51	0.03	32.92	50	0.05	32.92	26.45
77	−0.04	33.25	75	−0.05	33.22	26.69
103	0.24	33.43	100	0.20	33.40	26.83

TABLE OF OCEANOGRAPHIC DATA—Continued

Observed values			Scaled values			
Depth, meters	Temperature, °C.	Salinity, °/oo	Depth, meters	Temperature, °C.	Salinity, °/oo	σ_t
Station 7363; 2 May; 45°54′ N., 47°55′ W.; depth 265 m.; dynamic height 971.120						
0	0.13	32.84	0	0.13	32.84	26.38
25	0.14	32.84	25	0.14	32.84	26.38
50	−0.28	32.88	50	−0.28	32.88	26.43
75	−0.75	33.08	75	−0.75	33.08	26.61
101	−0.33	33.215	100	−0.35	33.21	26.70
150	0.76	33.65	150	0.76	33.65	27.00
201	0.92	33.745	200	0.90	33.74	27.06
Station 7364; 3 May; 45°53′ N., 47°45′ W.; depth 677 m.; dynamic height 971.063						
0	0.16	32.87	0	0.16	32.87	26.40
23	0.13	32.88	25	0.15	32.90	26.42
45	0.58	33.04	50	0.30	33.07	26.56
68	−0.49	33.19	75	−0.40	33.21	26.71
91	−0.18	33.325	100	0.00	33.34	26.79
135	0.83	33.68	150	0.90	33.74	27.06
181	1.12	33.86	200	1.40	33.97	27.21
272	2.51	34.44	300	2.60	34.48	27.52
367	2.83	34.57	400	3.00	34.61	27.60
567	3.78	34.84	(600)	3.95	34.88	27.71
Station 7365; 3 May; 45°49′ N., 47°20′ W.; depth 1,372 m.; dynamic height 970.936						
0	0.99	33.48	0	0.99	33.48	26.84
26	1.81	33.68	25	1.80	33.68	26.95
50	2.67	33.95	50	2.67	33.95	26.92
76	2.56	34.085	75	2.60	34.07	27.20
100	2.12	34.14	100	2.12	34.14	27.29
152	2.55	34.415	150	2.50	34.40	27.47
202	2.64	34.48	200	2.65	34.47	27.52
302	3.34	34.695	300	3.30	34.69	27.63
332	3.63	34.77	400	3.70	34.81	27.69
507	3.77	34.87	600	3.70	34.87	27.74
687	3.66	34.87	800	3.60	34.88	27.75
815	3.61	34.88	1,000	3.55	34.88	27.75
1,324	3.47	34.88				
Station 7366; 3 May; 45°46′ N., 46°44′ W.; depth 2,834 m.; dynamic height 970.999						
0	7.26	34.61	0	7.26	34.61	27.10
26	7.27	34.61	25	7.25	34.61	27.10
52	7.26	34.61	50	7.25	34.61	27.10
78	7.26	34.615	75	7.25	34.61	27.10
104	7.27	34.62	100	7.25	34.62	27.11
155	7.26	34.62	150	7.25	34.62	27.11
207	6.68	34.725	200	6.75	34.71	27.25
311	5.46	34.82	300	5.60	34.81	27.47
376	4.80	34.88	400	4.80	34.89	27.63
564	4.35	34.975	600	4.30	34.97	27.75
751	4.14	34.95	800	4.10	34.95	27.76
945	3.89	34.95	1,000	3.85	34.95	27.78
1,440	3.55	34.94				

Observed values			Scaled values			
Depth, meters	Temperature, °C.	Salinity, °/oo	Depth, meters	Temperature, °C.	Salinity, °/oo	σ_t
Station 7367; 3 May; 45°44′ N., 46°10′ W.; depth 3,383 m.; dynamic height 970.995						
0	6.51	34.43	0	6.51	34.43	27.06
26	6.49	------	25	6.50	34.43	27.06
52	6.49	34.43	50	6.50	34.43	27.06
79	6.50	34.43	75	6.50	34.43	27.06
105	6.50	34.44	100	6.50	34.44	27.06
156	6.67	34.685	150	6.65	34.66	27.22
209	6.38	34.79	200	6.45	34.77	27.34
314	5.33	34.89	300	5.50	34.88	27.54
363	5.07	34.89	400	4.85	34.89	27.62
546	3.96	34.89	600	3.85	34.89	27.73
730	3.66	34.88	800	3.60	34.87	27.75
928	3.54	34.87	1,000	3.55	34.88	27.75
1,452	3.56	34.92				
Station 7368; 3 May; 45°39.6′ N., 45°33.8′ W.; depth 3,621 m.; dynamic height 970.879						
0	3.73	34.25	0	3.73	34.25	27.24
26	3.74	34.26	25	3.75	34.26	27.25
51	4.03	34.30	50	4.00	34.30	27.25
77	3.75	34.475	75	3.75	34.45	27.39
102	3.58	34.60	100	3.60	34.60	27.53
152	4.67	34.87	150	4.60	34.85	27.62
204	4.52	34.87	200	4.55	34.87	27.65
306	3.67	34.82	300	3.70	34.82	27.70
375	3.66	34.81	400	3.65	34.82	27.70
568	3.65	34.87	600	3.60	34.87	27.75
763	3.54	34.865	800	3.55	34.87	27.75
958	3.47	34.88	1,000	3.45	34.88	27.76
1,460	3.41	34.91				
Station 7369; 3 May; 45°41.1′ N., 44°40.5′ W.; depth 4,352 m.; dynamic height 970.929						
0	3.64	33.58	0	3.64	33.58	26.71
26	4.30	33.905	25	4.30	33.90	26.90
52	4.35	34.005	50	4.35	34.00	26.97
78	3.86	34.155	75	3.95	34.15	27.14
105	3.50	34.26	100	3.55	34.24	27.25
156	3.65	34.44	150	3.60	34.42	27.39
208	4.26	34.745	200	4.10	34.67	27.54
313	5.17	35.01	300	5.05	34.97	27.67
416	4.40	34.945	400	4.50	34.96	27.72
622	3.86	34.92	600	3.90	34.92	27.76
828	3.50	34.90	800	3.55	34.90	27.77
1,034	3.61	34.93	1,000	3.60	34.93	27.79
1,550	3.41	34.935				
Station 7370; 4 May; 46°06.4′ N., 44°46.9′ W.; depth 3,731 m.; dynamic height 970.921						
0	4.41	33.97	0	4.41	33.97	26.94
26	4.41	33.975	25	4.40	33.97	26.95
52	4.39	34.00	50	4.40	34.00	26.97
78	4.05	34.20	75	4.10	34.17	27.14
104	3.59	34.29	100	3.65	34.27	27.26
155	4.25	34.65	150	4.15	34.61	27.48
207	3.59	34.635	200	3.70	34.64	27.55
311	4.14	34.88	300	4.05	34.85	27.68
414	3.89	34.87	400	3.90	34.87	27.72
621	3.77	34.90	600	3.75	34.90	27.75
828	3.57	34.88	800	3.60	34.89	27.76
1,034	3.69	34.925	1,000	3.65	34.92	27.78
1,549	3.45	34.93				

TABLE OF OCEANOGRAPHIC DATA—Continued

Observed values			Scaled values			
Depth, meters	Temperature, °C.	Salinity, °/₀₀	Depth, meters	Temperature, °C.	Salinity, °/₀₀	σ_t
Station 7371; 4 May; 46°32.4′ N., 44°53.5′ W.; depth 704 m.; dynamic height 970.875						
0	3.61	34.12	0	3.61	34.12	27.15
24	3.58	34.12	25	3.60	34.12	27.15
50	3.56	34.12	50	3.56	34.12	27.15
74	3.44	34.42	75	3.45	34.42	27.40
100	3.37	34.50	100	3.37	34.50	27.47
149	3.66	34.69	150	3.65	34.69	27.59
199	3.82	34.79	200	3.80	34.79	27.66
299	3.73	34.85	300	3.70	34.85	27.72
399	3.64	34.86	400	3.65	34.86	27.73
600	3.56	34.88	600	3.56	34.88	27.75
Station 7372; 4 May; 46°39.5′ N., 44°56.1′ W.; depth 223 m.; dynamic height 970.898						
0	3.61	34.08	0	3.61	34.08	27.11
23	3.60	34.09	25	3.60	34.09	27.12
47	3.59	34.09	50	3.60	34.09	27.12
70	3.59	34.10	75	3.55	34.14	27.17
94	3.40	34.31	100	3.40	34.33	27.33
141	3.53	34.51	150	3.55	34.55	27.49
188	3.71	34.72	(200)	3.75	34.77	27.65
Station 7373; 4 May; 46°50.9′ N., 45°01.1′ W.; depth 183 m.; dynamic height 970.894						
0	3.67	34.06	0	3.67	34.06	27.09
21	3.63	34.08	25	3.60	34.08	27.12
41	3.59	34.09	50	3.50	34.15	27.18
62	3.31	34.205	75	3.45	34.31	27.31
83	3.55	34.38	100	3.60	34.48	27.43
125	3.69	34.65	(150)	3.75	34.81	27.68
Station 7374; 4 May; 46°50.9′ N., 44°46.3′ W.; depth 152 m.; dynamic height 970.885						
0	3.63	34.09	0	3.63	34.09	27.12
27	3.61	34.09	25	3.60	34.09	27.12
53	3.56	34.09	50	3.55	34.09	27.13
80	3.18	34.32	75	3.25	34.28	27.30
106	3.20	34.39	100	3.20	34.37	27.39
Station 7375; 4 May; 46°50.2′ N., 44°55.1′ W.; depth 179 m.; dynamic height 970.894						
0	3.65	34.06	0	3.65	34.06	27.10
25	3.63	34.06	25	3.63	34.06	27.10
51	3.59	34.07	50	3.60	34.07	27.11
75	3.57	34.08	75	3.57	34.08	27.12
101	3.35	34.31	100	3.35	34.31	27.32
151	3.66	34.70	150	3.65	34.70	27.60
Station 7376; 4 May; 46°48.8′ N., 45°15.1′ W.; depth 220 m.; dynamic height 970.906						
0	3.78	34.06	0	3.78	34.06	27.08
25	3.77	34.07	25	3.77	34.07	27.09
50	3.75	34.07	50	3.75	34.07	27.10
75	3.74	34.08	75	3.74	34.08	27.11
101	3.40	34.23	100	3.40	34.23	27.25
150	4.03	34.55	150	4.03	34.55	27.44
201	3.88	34.71	200	3.90	34.70	27.58

Observed values			Scaled values			
Depth, meters	Temperature, °C.	Salinity, °/₀₀	Depth, meters	Temperature, °C.	Salinity, °/₀₀	σ_t
Station 7377; 4 May; 46°47′ N., 45°40′ W.; depth 256 m.; dynamic height 970.901						
0	3.95	34.11	0	3.95	34.11	27.11
24	3.95	34.12	25	3.95	34.12	27.12
49	3.95	34.12	50	3.95	34.12	27.12
72	3.99	34.175	75	4.00	34.19	27.16
97	3.67	34.405	100	3.70	34.41	27.37
145	4.23	34.58	150	4.25	34.60	27.46
193	4.32	34.74	200	4.25	34.75	27.58
242	3.92	34.80	250	3.90	34.81	27.67
Station 7378; 4 May; 46°46.5′ N., 45°54′ W.; depth 348 m.; dynamic height 970.881						
0	3.98	34.16	0	3.98	34.16	27.14
24	3.99	34.15	25	4.00	34.16	27.14
48	3.93	34.16	50	3.95	34.18	27.16
72	3.55	34.415	75	3.60	34.43	27.39
96	4.03	34.56	100	4.05	34.57	27.46
145	4.12	34.67	150	4.10	34.68	27.54
193	4.08	34.765	200	4.05	34.77	27.62
289	3.81	34.85	(300)	3.80	34.86	27.72
Station 7379; 4 May; 46°43′ N., 46°33′ W.; depth 732 m.; dynamic height 970.878						
0	3.92	34.13	0	3.92	34.13	27.12
25	3.93	34.13	25	3.93	34.13	27.12
50	3.96	34.13	50	3.96	34.13	27.12
75	3.56	34.26	75	3.56	34.26	27.27
100	4.10	34.62	100	4.10	34.62	27.50
149	4.16	34.745	150	4.15	34.75	27.59
199	3.92	34.81	200	3.90	34.81	27.67
299	3.84	34.87	300	3.85	34.87	27.72
388	3.68	34.88	400	3.65	34.88	27.74
551	3.53	34.87	(600)	3.50	34.87	27.76
Station 7380; 5 May; 46°42′ N., 46°52′ W.; depth 1,234 m.; dynamic height 970.887						
0	2.22	34.08	0	2.22	34.08	27.24
26	2.24	34.08	25	2.25	34.08	27.23
51	2.26	34.26	50	2.25	34.26	27.38
77	2.22	34.335	75	2.20	34.33	27.44
103	2.48	34.44	100	2.45	34.43	27.49
153	2.70	34.53	150	2.70	34.52	27.55
204	3.16	34.68	200	3.10	34.67	27.64
307	3.69	34.81	300	3.65	34.80	27.68
406	3.77	34.87	400	3.80	34.86	27.72
607	3.73	34.875	600	3.75	34.87	27.73
807	3.66	34.87	800	3.65	34.87	27.74
1,007	3.54	34.86	1,000	3.55	34.86	27.74
Station 7381; 5 May; 46°41′ N., 47°12′ W.; depth 649 m.; dynamic height 970.929						
0	0.92	33.66	0	0.92	33.66	27.00
25	0.85	33.67	25	0.85	33.67	27.01
50	1.15	33.78	50	1.15	33.78	27.07
76	1.19	33.94	75	1.20	33.94	27.20
101	1.48	34.09	100	1.45	34.09	27.30
150	1.94	34.27	150	1.94	34.27	27.42
201	2.41	34.45	200	2.40	34.45	27.52
302	3.25	34.70	300	3.20	34.70	27.65
403	3.73	34.84	400	3.70	34.83	27.70
607	3.66	34.86	600	3.65	34.87	27.74

TABLE OF OCEANOGRAPHIC DATA—Continued

Observed values			Scaled values			
Depth, meters	Temperature, °C.	Salinity, °/oo	Depth, meters	Temperature, °C.	Salinity, °/oo	σ_t
Station 7382; 5 May; 46°40′ N., 47°25′ W.; depth 329 m.; dynamic height 971.011						
0	−0.04	32.98	0	−0.04	32.98	26.50
23	−0.56	33.13	25	−0.45	33.17	26.67
46	0.52	33.40	50	0.45	33.41	26.82
69	0.09	33.445	75	0.10	33.46	26.88
92	0.13	33.51	100	0.15	33.54	26.94
137	0.45	33.68	150	0.65	33.75	27.08
182	1.21	33.99	200	1.45	34.07	27.29
274	2.47	34.41	(300)	2.80	34.54	27.55
Station 7383; 5 May; 46°38′ N., 47°38′ W.; depth 172 m.; dynamic height 971.059						
0	−0.21	32.70	0	−0.21	32.70	26.28
26	−0.25	32.70	25	−0.25	32.70	26.28
52	−0.37	32.72	50	−0.35	32.72	26.30
78	−1.01	33.05	75	−0.95	33.01	26.56
104	−0.06	33.36	100	−0.20	33.31	26.77
155	1.13	33.91	150	1.00	33.84	27.13
Station 7384; 5 May; 46°38′ N., 48°13′ W.; depth 117 m.; dynamic height 971.060						
0	0.28	32.77	0	0.28	32.77	26.32
26	0.16	32.78	25	0.15	32.78	26.33
51	0.24	32.82	50	0.25	32.82	26.36
76	−0.26	33.09	75	−0.25	33.07	26.58
102	0.33	33.425	100	0.25	33.30	26.74
Station 7385; 5 May; 46°43′ N., 48°38′ W.; depth 97 m.; dynamic height 971.055						
0	0.88	32.85	0	0.88	32.85	26.35
26	0.67	32.86	25	0.70	32.86	26.36
52	0.58	32.86	50	0.60	32.86	26.37
84	0.32	33.46	75	0.40	33.30	26.73
Station 7386; 5 May; 47°13′ N., 49°13′ W.; depth 102 m.; dynamic height 971.063						
0	0.53	32.80	0	0.53	32.80	26.33
28	0.34	32.82	25	0.35	32.82	26.35
55	0.36	32.825	50	0.35	32.82	26.35
83	−0.16	33.01	75	0.00	32.93	26.46
Station 7387; 5 May; 47°13′ N., 48°36′ W.; depth 119 m.; dynamic height 971.062						
0	0.21	32.70	0	0.21	32.70	26.26
26	0.25	32.76	25	0.25	32.76	26.31
53	0.40	32.81	50	0.40	32.81	26.35
80	−0.32	33.07	75	−0.20	33.02	26.51
106	0.02	33.30	100	−0.10	33.25	26.72
Station 7388; 6 May; 47°12′ N., 48°03′ W.; depth 166 m.; dynamic height 971.059						
0	−0.20	32.73	0	−0.20	32.73	26.31
25	−0.21	32.72	25	−0.21	32.72	26.30
51	−0.43	32.80	50	−0.40	32.80	26.38
76	−0.56	33.08	75	−0.55	33.02	26.55
102	−0.14	33.265	100	−0.15	33.24	26.72
152	0.76	33.63	150	0.70	33.62	26.98

Observed values			Scaled values			
Depth, meters	Temperature, °C.	Salinity, °/oo	Depth, meters	Temperature, °C.	Salinity, °/oo	σ_t
Station 7389; 6 May; 47°11.5′ N., 47°40′ W.; depth 216 m.; dynamic height 971.066						
0	−0.23	32.68	0	−0.23	32.68	26.27
26	−0.37	32.66	25	−0.35	32.66	26.25
52	−0.81	32.80	50	−0.75	32.79	26.38
78	−0.95	32.99	75	−0.90	32.96	26.52
104	−0.71	33.18	100	−0.75	33.15	26.66
155	0.60	33.58	150	0.45	33.54	26.92
207	0.95	33.79	200	0.90	33.76	27.08
Station 7390; 6 May; 47°11′ N., 47°22′ W.; depth 402 m.; dynamic height 971.086						
0	−0.51	32.71	0	−0.51	32.71	26.30
26	−0.50	32.74	25	−0.50	32.74	26.33
51	−0.58	32.75	50	−0.60	32.75	26.34
77	−0.80	32.92	75	−0.80	32.90	26.46
102	−0.93	33.045	100	−0.90	33.02	26.57
153	−0.20	33.36	150	−0.30	33.33	26.79
204	0.89	33.78	200	0.75	33.73	27.06
306	2.74	34.54	300	2.60	34.49	27.53
Station 7391; 6 May; 47°10′ N., 46°53′ W.; depth 1,189 m.; dynamic height 970.907						
0	1.23	33.77	0	1.23	33.77	27.06
26	1.44	33.89	25	1.40	33.89	27.14
51	1.35	33.935	50	1.35	33.93	27.18
77	1.53	34.12	75	1.50	34.11	27.32
101	1.84	34.23	100	1.85	34.22	27.38
153	2.27	34.38	150	2.25	34.38	27.47
205	2.67	34.52	200	2.65	34.51	27.55
308	3.51	34.76	300	3.40	34.74	27.66
405	3.74	34.83	400	3.75	34.83	27.69
607	3.69	34.88	600	3.70	34.88	27.74
811	3.54	34.89	800	3.55	34.89	27.76
1,013	3.49	34.86	1,000	3.50	34.87	27.76
Station 7392; 6 May; 47°10′ N., 46°42′ W.; depth 658 m.; dynamic height 970.891						
0	3.62	34.09	0	3.62	34.09	27.12
24	3.59	34.10	25	3.55	34.10	27.14
48	3.28	34.09	50	3.30	34.09	27.15
73	3.09	34.24	75	3.30	34.25	27.28
97	2.62	34.325	100	2.70	34.34	27.40
144	3.88	34.64	150	3.90	34.65	27.54
193	3.89	34.73	200	3.90	34.74	27.61
290	3.92	34.84	300	3.90	34.84	27.69
388	3.72	34.84	400	3.70	34.84	27.71
585	3.47	34.875	(600)	3.45	34.88	27.76
Station 7393; 6 May; 47°11.5′ N., 46°22′ W.; depth 318 m.; dynamic height 970.879						
0	3.65	34.10	0	3.65	34.10	27.13
25	3.63	34.09	25	3.63	34.09	27.12
50	3.62	34.09	50	3.62	34.09	27.12
74	3.50	34.22	75	3.50	34.22	27.24
99	3.60	34.50	100	3.60	34.51	27.46
148	4.09	34.73	150	4.10	34.73	27.58
197	3.92	34.785	200	3.90	34.79	27.65
296	3.72	34.85	300	3.70	34.85	27.72

TABLE OF OCEANOGRAPHIC DATA—Continued

Observed values			Scaled values			
Depth, meters	Temperature, °C.	Salinity, °/oo	Depth, meters	Temperature, °C.	Salinity, °/oo	σ_t
Station 7394; 6 May; 47°16′ N., 45°50′ W.; depth 289 m.; dynamic height 970.893						
0	3.70	34.06	0	3.70	34.06	27.09
26	3.64	34.07	25	3.65	34.07	27.11
51	3.57	34.08	50	3.55	34.08	27.12
77	3.57	34.07	75	3.55	34.07	27.12
102	3.31	34.335	100	3.30	34.30	27.32
153	3.85	34.64	150	3.80	34.61	27.52
206	3.71	34.72	200	3.70	34.71	27.61
256	3.71	34.775	250	3.70	34.77	27.66
Station 7395; 6 May; 47°19′ N., 45°27′ W.; depth 218 m.; dynamic height 970.912						
0	3.68	34.05	0	3.68	34.05	27.08
25	3.63	34.06	25	3.63	34.06	27.10
50	3.58	34.08	50	3.58	34.08	27.12
75	3.54	34.09	75	3.54	34.09	27.13
100	3.53	34.10	100	3.53	34.10	27.14
150	3.61	34.42	150	3.61	34.42	27.39
200	3.79	34.63	200	3.79	34.63	27.54
Station 7396; 6 May; 47°23′ N., 44°58′ W.; depth 170 m.; dynamic height 970.897						
0	3.60	34.05	0	3.60	34.05	27.09
27	3.59	34.09	25	3.60	34.09	27.12
52	3.49	34.10	50	3.50	34.10	27.14
78	3.37	34.11	75	3.40	34.12	27.17
103	3.15	34.34	100	3.15	34.32	27.35
158	3.82	34.63	150	3.70	34.59	27.51
Station 7397; 6 May; 47°30′ N., 45°13′ W.; depth 223 m.; dynamic height 970.905						
0	3.65	34.06	0	3.65	34.06	27.10
26	3.66	34.07	25	3.66	34.07	27.11
52	3.61	34.06	50	3.60	34.06	27.10
78	3.49	34.06	75	3.50	34.06	27.11
103	3.29	34.18	100	3.30	34.16	27.21
154	3.50	34.53	150	3.50	34.51	27.47
206	3.70	34.71	200	3.65	34.69	27.59
Station 7398; 6 May; 47°40′ N., 45°38′ W.; depth 329 m.; dynamic height 970.877						
0	3.63	34.08	0	3.63	34.08	27.11
24	3.63	34.08	25	3.60	34.08	27.11
49	3.59	34.095	50	3.60	34.10	27.13
73	3.54	34.34	75	3.55	34.35	27.33
97	2.96	34.435	100	3.00	34.44	27.46
146	3.34	34.63	150	3.40	34.64	27.58
195	3.79	34.775	200	3.80	34.78	27 65
292	3.70	34.86	(300)	3.70	34.87	27.74
Station 7399; 7 May; 47°42′ N., 45°45′ W.; depth 433 m.; dynamic height 970.869						
0	3.43	34.25	0	3.43	34.25	27.27
24	3.43	34.23	25	3.40	34.23	27.25
50	3.30	34.23	50	3.30	34.23	27.26
74	2.53	34.365	75	2.55	34.37	27.45
99	2.63	34.47	100	2.60	34.47	27.52
148	3.04	34.605	150	3.10	34.61	27.59
198	3.94	34.80	200	3.95	34.80	27.65
297	3.78	34.83	300	3.85	34.83	27.68
396	3.56	34.88	(400)	3.80	34.88	27.73
Station 7400; 7 May; 47°46′ N., 45°58′ W.; depth 1,042 m.; dynamic height 970.862						
0	3.06	34.28	0	3.06	34.28	27.32
25	3.12	34.28	25	3.12	34.28	27.32
50	3.12	34.25	50	3.12	34.26	27.30
75	2.98	34.48	75	2.98	34.48	27.49
100	2.92	34.53	100	2.92	34.53	27.54
149	3.23	34.63	150	3.25	34.63	27.58
199	3.70	34.77	200	3.70	34.77	27.66
299	3.80	34.83	300	3.80	34.83	27.69
399	3.76	34.88	400	3.75	34.88	27.73
600	3.54	34.87	600	3.54	34.87	27.74
804	3.48	34.89	800	3.50	34.89	27.77
1,008	3.43	34.905	1,000	3.45	34.90	27.78
Station 7401; 7 May; 47°58′ N., 46°25′ W., depth 1,189 m.; dynamic height 970.881						
0	2.27	34.10	0	2.27	34.10	27.25
25	2.27	34.09	25	2.27	34.09	27.24
50	2.36	34.14	50	2.36	34.14	27.27
75	2.36	34.38	75	2.36	34.38	27.46
100	2.50	34.43	100	2.50	34.43	27.49
150	2.81	34.55	150	2.81	34.55	27.56
200	3.14	34.65	200	3.14	34.65	27.61
300	3.56	34.80	300	3.56	34.80	27.69
400	3.65	34.85	400	3.65	34.85	27.72
602	3.69	34.88	600	3.70	34.88	27.74
807	3.61	34.87	800	3.60	34.87	27.75
1,014	3.51	34.895	1,000	3.55	34.89	27.76
Station 7402; 7 May; 48°17′ N., 45°58′ W.; depth 1,006 m.; dynamic height 970.862						
0	3.50	34.28	0	3.50	34.28	27.28
23	3.36	34.32	25	3.55	34.33	27.31
46	3.23	34.38	50	3.25	34.38	27.38
70	3.27	34.40	75	3.25	34.43	27.42
93	2.97	34.52	100	3.00	34.54	27.54
138	3.27	34.62	150	3.35	34.65	27.59
185	3.56	34.73	200	3.60	34.74	27.64
278	3.81	34.82	300	3.80	34.83	27 69
357	3.72	34.86	400	3.70	34.86	27.73
547	3.60	34.87	600	3.60	34.87	27.75
737	3.56	34.885	800	3.50	34.89	27.77
951	3.43	34.90	1,000	3.40	34.90	27.79
Station 7403; 7 May; 48°37′ N., 45°30′ W., depth 878 m.; dynamic height 970.865						
0	3.65	34.30	0	3.65	34.30	27.29
26	3.55	34.315	25	3.55	34.31	27.30
52	3.26	34.38	50	3.30	34.38	27.38
78	3.17	34.495	75	3.20	34.48	27.47
103	2.98	34.52	100	3.00	34.52	27.53
156	3.22	34.61	150	3.20	34.60	27.57
207	3.59	34.755	200	3.55	34.73	27.64
303	3.82	34.86	300	3.80	34.86	27.72
399	3.75	34.86	400	3.80	34.86	27.72
597	3.59	34.85	600	3.60	34.85	27.73
797	3.43	34.88	(800)	3.40	34.88	27.77

TABLE OF OCEANOGRAPHIC DATA—Continued

Observed values			Scaled values			
Depth, meters	Temperature, °C.	Salinity, °/oo	Depth, meters	Temperature, °C.	Salinity, °/oo	σ_t
Station 7404; 7 May; 49°02′ N., 45°02′ W., depth 1,408 m.; dynamic height 970.862						
0	3.16	34.31	0	3.16	34.31	27.34
26	3.10	34.32	25	3.10	34.32	27.36
52	2.54	34.33	50	2.60	34.33	27.40
77	2.87	34.44	75	2.85	34.42	27.46
103	3.05	34.52	100	3.00	34.51	27.52
152	3.34	34.70	150	3.30	34.69	27.63
205	3.62	34.80	200	3.45	34.79	27.69
308	3.65	34.84	300	3.65	34.83	27.70
400	3.66	34.85	400	3.68	34.85	27.72
602	3.61	34.86	600	3.60	34.86	27.74
806	3.53	34.88	800	3.55	34.88	27.75
1,010	3.48	34.88	1,000	3.50	34.88	27.76
1,274	3.46	34.89				
Station 7405; 7 May; 49°10′ N., 45°40′ W., depth 2,432 m.; dynamic height 970.861						
0	4.54	34.54	0	4.54	34.54	27.38
24	4.55	34.55	25	4.55	34.55	27.39
48	4.45	34.55	50	4.40	34.55	27.41
72	3.13	34.50	75	3.10	34.50	27.50
96	3.08	34.53	100	3.10	34.54	27.53
144	3.42	34.65	150	3.50	34.66	27.59
192	3.55	34.78	200	3.55	34.79	27.68
288	3.69	34.85	300	3.70	34.85	27.72
355	3.62	34.85	400	3.65	34.85	27.72
542	3.62	34.875	600	3.60	34.88	27.75
737	3.56	34.88	800	3.65	34.89	27.75
938	3.90	34.91	1,000	3.85	34.91	27.75
1,447	3.38	34.925				
Station 7406; 8 May; 49°19′ N., 46°20′ W., depth 3,054 m.; dynamic height 970.878						
0	5.30	34.63	0	5.30	34.63	27.36
26	5.30	34.63	25	5.30	34.63	27.36
52	5.27	34.63	50	5.25	34.63	27.37
78	5.09	34.63	75	5.10	34.63	27.39
104	4.88	34.635	100	4.90	34.63	27.41
155	4.12	34.62	150	4.20	34.62	27.49
207	3.95	34.74	200	3.95	34:72	27.59
311	3.97	34.85	300	3.95	34.84	27.68
400	3.83	34.87	400	3.85	34.87	27.72
600	3.65	34.88	600	3.65	34.88	27.74
801	3.58	34.90	800	3.60	34.90	27.77
1,006	3.49	34.91	1,000	3.50	34.91	27.79
1,522	3.41	34.94				
Station 7407; 8 May; 48°59′ N., 46°38′ W., depth 2,816 m.; dynamic height 970.852						
0	3.49	34.49	0	3.49	34.49	27.45
26	3.50	34.49	25	3.50	34.49	27.45
51	3.06	34.55	50	3.05	34.55	27.54
77	3.08	34.58	75	3.05	34.58	27.56
103	3.00	34.56	100	3.00	34.57	27.57
153	3.01	34.615	150	3.00	34.61	27.60
205	3.30	34.735	200	3.25	34.72	27.66
308	3.63	34.84	300	3.60	34.83	27.71
414	3.62	34.84	400	3.65	34.84	27.71
621	3.57	34.865	600	3.60	34.86	27.74
829	3.47	34.885	800	3.50	34.88	27.76
1,037	3.50	34.90	1,000	3.50	34.90	27.78
1,557	3.39	34.92				
Station 7408; 8 May; 48°36′ N., 46°57′ W., depth 2,542 m.; dynamic height 970.844						
0	3.27	34.42	0	3.27	34.42	27.42
26	3.23	34.435	25	3.25	34.43	27.42
53	3.23	34.465	50	3.25	34.46	27.45
79	3.34	34.54	75	3.30	34.53	27.50
105	2.98	34.58	100	3.05	34.57	27.56
157	3.20	34.71	150	3.15	34.69	27.64
210	3.39	34.78	200	3.35	34.77	27.69
315	3.65	34.85	300	3.60	34.84	27.72
413	3.63	34.88	400	3.65	34.87	27.74
619	3.58	34.88	600	3.60	34.88	27.75
822	3.48	34.88	800	3.50	34.88	27.76
1,029	3.47	34.90	1,000	3.50	34.90	27.78
1,545	3,33	34.91				
Station 7409; 8 May; 48°13′ N., 47°18′ W; depth 1,792 m.; dynamic height 970.881						
0	1.84	33.71	0	1.84	33.71	26.97
25	0.95	33.98	25	0.95	33.98	27.25
51	1.53	34.17	50	1.45	34.16	27.36
76	2.14	34.34	75	2.15	34.33	27.44
102	2.59	34.445	100	2.30	34.44	27.52
152	2.94	34.56	150	2.90	34.55	27.56
204	3.08	34.62	200	3.05	34.61	27.59
306	3.59	34.82	300	3.55	34.80	27.69
392	3.65	34.85	400	3.65	34.85	27.72
588	3.59	34.87	600	3.60	34.87	27.75
784	3.56	34.87	800	3.55	34.87	27.75
984	3.47	34.89	1,000	3.45	34.89	27.77
1,489	3.35	34.915				
Station 7410; 8 May; 47°54′ N., 47°37′ W; depth 375 m.; dynamic height 971 018						
0	0.48	32.61	0	0.48	32.61	26.19
23	−0.66	32.77	25	−0.65	32.80	26.39
46	−0.65	33.06	50	−0.65	33.10	26.62
68	−0.33	33.215	75	−0.15	33.30	26.76
92	0.29	33.49	100	0.40	33.54	26.93
137	0.99	33.77	150	1.25	33.89	27.15
183	1.99	34.20	200	2.15	34.33	27.44
275	2.81	34.53	300	2.95	34.61	27.60
366	3.22	34.68	(400)	3.35	34.72	27.65
Station 7411; 8 May; 47°46.5′ N., 47°48′ W; depth 309 m.; dynamic height 971.096						
0	0.66	32.54	0	0.66	32.54	26.11
24	−0.59	32.59	25	−0.60	32.59	26.21
49	−1.23	32.72	50	−1.20	32.73	26.34
73	−1.46	32.83	75	−1.45	32.83	26.43
97	−1.23	32.895	100	−1.15	32.92	26.49
146	−0.11	33.335	150	−0.05	33.38	26.82
195	0.80	33.73	200	0.85	33.77	27.09
292	2.88	34.505	300	3.00	34.56	27.56
Station 7412, 8 May; 47°42′ N., 48°11′ W; depth 240 m.; dynamic height 971.086						
0	0.63	32.57	0	0.63	32.57	26.17
25	−0.52	32.64	25	−0.52	32.64	26.25
50	−1.21	32.78	50	−1.21	32.78	26.38
75	−1.22	32.81	75	−1.22	32.81	26.41
100	−1.34	32.90	100	−1.34	32.90	26.48
151	0.05	33.30	150	0.00	33.30	26.75
201	1.54	34.05	200	1.50	34.04	27.26

TABLE OF OCEANOGRAPHIC DATA—Continued

Observed values			Scaled values			
Depth, meters	Temperature, °C.	Salinity, °/oo	Depth, meters	Temperature, °C.	Salinity, °/oo	σ_t
Station 7413; 8 May; 47°41′ N., 48°32′ W; depth 214 m.; dynamic height 971.022						
0	0. 55	32. 96	0	0. 55	32. 96	26. 45
26	0. 12	33. 10	25	0. 10	33. 10	26. 59
51	0. 18	33. 17	50	0. 15	33. 17	26. 64
76	−0. 41	33. 24	75	−0. 40	33. 23	26. 72
102	0. 00	33. 41	100	−0. 05	33. 40	26. 84
153	0. 29	33. 54	150	0. 25	33. 53	26. 93
204	2. 47	34. 475	200	0. 30	34. 41	27. 63
Station 7414; 8 May; 47°39′ N., 48°56′ W; depth 179 m.; dynamic height 971.083						
0	0. 44	32. 40	0	0. 44	32. 40	26. 02
24	0. 79	32. 445	25	0. 75	32. 45	26. 04
49	−1. 56	32. 68	50	−1. 55	32. 68	26. 31
72	−1. 54	32. 80	75	−1. 50	32. 81	26. 42
97	−1. 26	32. 94	100	−1. 20	32. 96	26. 53
145	0. 06	33. 41	(150)	0. 20	33. 45	26. 87
Station 7415; 9 May; 47°50′ N., 48°48′ W; depth 220 m.; dynamic height 971.059						
0	−0. 51	32. 44	0	−0. 51	32. 44	26. 09
25	−1. 57	32. 62	25	−1. 57	32. 62	26. 26
51	−1. 58	32. 81	50	−1. 60	32. 80	26. 41
76	−1. 39	32. 96	75	−1. 40	32. 95	26. 52
102	−0. 16	33. 29	100	−0. 15	33. 26	26. 73
152	0. 09	33. 485	150	0. 05	33. 47	26. 90
203	1. 02	33. 92	200	1. 00	33. 91	27. 19
Station 7416; 9 May; 48°05′ N., 48°41′ W. depth 322 m.; dynamic height 970.996						
0	0. 81	33. 06	0	0. 81	33. 06	26. 52
25	0. 50	33. 12	25	0. 50	33. 12	26. 58
50	−0. 26	33. 25	50	−0. 26	33. 25	26. 72
74	−0. 57	33. 315	75	−0. 55	33. 32	26. 79
99	−0. 28	33. 515	100	−0. 35	33. 53	26. 95
148	1. 11	33. 93	150	1. 15	33. 95	27. 21
198	1. 66	34. 245	200	1. 70	34. 25	27. 41
297	2. 78	34. 58	300	2. 80	34. 59	27. 59
Station 7417; 9 May; 48°12′ N., 48°36′ W. depth 677 m.; dynamic height 970.956						
0	1. 26	33. 15	0	1. 26	33. 15	26. 56
24	0. 20	33. 13	25	0. 20	33. 13	26. 61
49	−0. 34	33. 35	50	−0. 30	33. 37	26 82
73	0. 03	33. 65	75	0. 10	33. 66	27. 04
99	0. 94	33. 80	100	0. 95	33. 81	27. 11
147	1. 66	34. 17	150	1. 70	34. 19	27. 36
196	2. 68	34. 52	200	2. 70	34. 53	27. 55
295	3. 42	34. 74	300	3. 45	34. 74	27. 65
396	3. 64	34. 83	400	3. 65	34. 83	27. 70
598	3. 68	34. 88	600	3. 65	34. 88	27. 74
Station 7418; 9 May; 48°28′ N., 48°18′ W. depth 1,939 m.; dynamic height 970.878						
0	1. 82	33. 74	0	1. 82	33. 74	26. 99
25	1. 53	34. 05	25	1. 53	34. 05	27. 27
50	1. 90	34. 25	50	1. 90	34. 25	27. 40
76	2. 23	34. 38	75	2. 20	34. 38	27. 48
101	2. 21	34. 445	100	2. 20	34. 44	27. 53
150	2. 63	34. 56	150	2. 63	34. 56	27. 59
200	3. 17	34. 69	200	3. 17	34. 69	27. 64
301	3. 61	34. 825	300	3. 60	34. 82	27. 71
386	3. 61	34. 84	400	3. 65	34. 84	27. 71
573	3. 53	34. 845	600	3. 55	34. 85	27. 73
757	3. 47	34. 85	800	3. 45	34. 85	27. 74
950	3. 45	34. 87	1,000	3. 45	34. 87	27. 76
1,440	3. 43	34. 905				
Station 7419; 9 May; 48°48′ N., 48°02′ W. depth 2,286 m.; dynamic height 970.860						
0	4. 20	34. 52	0	4. 20	34. 52	27. 41
25	3. 87	34. 52	25	3. 87	34. 52	27. 44
51	3. 45	34. 51	50	3. 50	34. 51	27. 47
76	2. 80	34. 52	75	2. 80	34. 51	27. 53
102	2. 82	34. 55	100	2. 80	34. 55	27. 56
152	2. 73	34. 61	150	2. 75	34. 61	27. 62
202	3. 21	34. 70	200	3. 15	34. 70	27. 65
304	3. 66	34. 845	300	3. 65	34. 84	27. 71
396	3. 64	34. 85	400	3. 65	34. 85	27. 72
594	3. 53	34. 86	600	3. 55	34. 86	27. 74
794	3. 42	34. 85	800	3. 45	34. 85	27. 74
994	3. 46	------	1,000	3. 50	34. 87	27. 76
1,496	3. 37	34. 90				
Station 7420; 9 May; 49°02′ N., 47°51′ W. depth 2,395 m.; dynamic height 970.863						
0	4. 41	34. 52	0	4. 41	34. 52	27. 38
25	4. 31	34. 52	25	4. 31	34. 52	27. 40
51	3. 28	34. 525	50	3. 40	34. 53	27. 49
76	3. 06	34. 53	75	3. 05	34. 53	27. 52
102	2. 54	34. 55	100	2. 60	34. 55	27. 58
152	2. 42	34. 56	150	2. 45	34. 57	27. 61
204	2. 82	34. 68	200	2. 80	34. 67	27. 66
306	3. 42	34. 775	300	3. 40	34. 77	27. 69
384	3. 58	34. 82	400	3. 60	34. 82	27. 71
578	3. 52	34. 85	600	3. 55	34. 85	27. 73
775	3. 42	34. 84	800	3. 40	34. 84	27. 74
972	3. 42	34. 85	1,000	3. 15	34. 85	27. 77
1,474	3. 38	34. 90				
Station 7421; 9 May; 49°20′ N., 47°40′ W.; depth 2,560 m.; dynamic height 970.844						
0	3. 51	34. 54	0	3. 51	34. 54	27. 49
26	3. 39	34. 53	25	3. 40	34. 53	27. 49
52	3. 11	34. 52	50	3. 15	34. 52	27. 51
78	2. 51	34. 54	75	2. 60	34. 54	27. 57
104	2. 54	34. 605	100	2. 55	34. 59	27. 62
154	3. 18	34. 735	150	3. 10	34. 72	27. 68
206	3. 61	34. 845	200	3. 55	34. 83	27. 71
310	3. 60	34. 84	300	3. 60	34. 84	27. 72
416	3. 56	34. 84	400	3. 55	34. 84	27. 72
623	3. 45	34. 84	600	3. 45	34. 84	27. 73
829	3. 42	34. 84	800	3. 40	34. 84	27. 74
1, 036	3. 45	34. 895	1, 000	3. 45	34. 89	27. 77
1, 554	3. 34	34. 895				

TABLE OF OCEANOGRAPHIC DATA—Continued

Station 7422; 3 June; 50°02′ N., 48°49′ W.; depth 2,030 m.; dynamic height 970.846

Observed values			Scaled values			
Depth, meters	Temperature, °C.	Salinity, °/₀₀	Depth, meters	Temperature, °C.	Salinity, °/₀₀	σ_t
0	6.58	34.60	0	6.58	34.60	27.18
25	6.17	34.59	25	6.17	34.59	27.23
50	4.67	34.63	50	4.67	34.63	27.44
75	3.81	34 62	75	3.81	34.62	27.52
100	3.39	34.62	100	3.39	34.62	27.57
149	3.62	34.74	150	3.60	34.74	27.64
199	3.42	34.76	200	3.40	34.76	27.68
299	3.63	34.85	300	3.60	34.85	27.73
385	3.46	34.85	400	3.45	34.86	27.75
585	3.49	34.88	600	3.50	34.88	27.76
792	3.45	34.89	800	3.45	34.89	27.77
990	3.44	34.885	1,000	3.40	34.89	27.78
1,486	3.38	34.93				

Station 7423; 3 June; 49°49′ N., 49°32′ W.; depth 1,298 m.; dynamic height 970.867

Observed values			Scaled values			
Depth, meters	Temperature, °C.	Salinity, °/₀₀	Depth, meters	Temperature, °C.	Salinity, °/₀₀	σ_t
0	4.73	33.80	0	4.73	33.90	26.85
26	6.18	34.59	25	6.10	34.58	27.23
52	5.42	34.59	50	5.50	34.59	27.31
78	3.27	34.61	75	3.55	34.60	27.53
104	3.25	34.67	100	3.25	34.65	27.60
155	2.87	34.69	150	2.90	34.69	27.67
206	3.07	34.75	200	3.05	34.74	27.69
310	3.40	34.80	300	3.35	34.79	27.70
376	3.31	34.81	400	3.35	34.82	27.73
566	3.55	34.86	600	3.55	34.86	27.74
758	3.54	34.87	800	3.55	34.87	27.75
957	3.48	34.87	1,000	3.50	34.87	27.76
1,256	3.49	34.89				

Station 7424; 3 June; 49°47′ N., 50°01′ W.; depth 622 m.; dynamic height 970.960

Observed values			Scaled values			
Depth, meters	Temperature, °C.	Salinity, °/₀₀	Depth, meters	Temperature, °C.	Salinity, °/₀₀	σ_t
0	3.85	32.91	0	3.85	32.91	26.16
25	−0.48	33.07	25	−0.48	33.07	26.59
50	−0.25	33.50	50	−0.25	33.50	26.93
75	0.55	33.82	75	0.55	33.82	27.14
101	0.79	33.99	100	0.75	33.99	27.27
151	1.38	34.23	150	1.35	34.23	27.42
201	1.80	34.38	200	1.80	34.38	27.51
301	3.72	34.65	300	3.75	34.65	27.55
399	3.68	34.84	400	3.70	34.84	27.71
595	3.59	34.86	(600)	3.60	34.86	27.74

Station 7425; 3 June; 49°31′ N., 50°32′ W.; depth 313 m.; dynamic height 970.994

Observed values			Scaled values			
Depth, meters	Temperature, °C.	Salinity, °/₀₀	Depth, meters	Temperature, °C.	Salinity, °/₀₀	σ_t
0	3.51	32.71	0	3.51	32.71	26.03
26	2.12	32.95	25	2.15	32.95	26.34
51	−0.11	33.12	50	0.00	33.12	26.61
77	−0.62	33.39	75	−0.55	33.37	26.83
103	−0.08	33.645	100	−0.15	33.62	27.03
153	0.85	34.06	150	0.80	34.04	27.30
205	1.98	34.33	200	1.90	34.31	27.45
308	3.15	34.69	300	3.05	34.66	27.63

Station 7426; 3 June; 49°23′ N., 51 01′ W.; depth 348 m.; dynamic height 971.010

Observed values			Scaled values			
Depth, meters	Temperature, °C.	Salinity, °/₀₀	Depth, meters	Temperature, °C.	Salinity, °/₀₀	σ_t
0	3.44	32.59	0	3.44	32.59	25.95
26	−1.14	32.84	25	−0.90	32.83	26.41
52	−1.49	33.10	50	−1.45	33.09	26.63
78	−0.88	33.29	75	−0.90	33.26	26.76
104	−0.30	33.50	100	−0.45	33.47	26.92
155	1.10	33.93	150	1.00	33.88	27.16
206	1.45	34.21	200	1.40	34.18	27.38
310	2.98	34.66	300	2.85	34.62	27.62

Station 7427; 3 June; 49°12′ N., 51°32′ W.; depth 318 m.; dynamic height 971.079

Observed values			Scaled values			
Depth, meters	Temperature, °C.	Salinity, °/₀₀	Depth, meters	Temperature, °C.	Salinity, °/₀₀	σ_t
0	3.73	32.31	0	3.73	32.31	25.69
25	0.34	32.63	25	0.34	32.63	26.20
51	−1.22	32.84	50	−1.20	32.84	26.43
76	−1.55	32.94	75	−1.50	32.94	26.52
102	−1.32	33.07	100	−1.35	33.06	26.61
151	−0.51	33.39	150	−0.55	33.37	26.83
202	1.06	33.91	200	1.00	33.90	27.18
304	2.34	34.41	300	2.30	34.40	27.49

Station 7428; 3 June; 49°06′ N., 51°49′ W.; depth 300 m.; dynamic height 971.098

Observed values			Scaled values			
Depth, meters	Temperature, °C.	Salinity, °/₀₀	Depth, meters	Temperature, °C.	Salinity, °/₀₀	σ_t
0	3.56	32.10	0	3.56	32.10	25.56
24	2.52	32.38	25	2.45	32.39	25.87
49	−0.86	32.76	50	−0.85	32.76	26.35
74	−1.47	32.85	75	−1.45	32.85	26.44
98	−1.45	32.975	100	−1.40	32.99	26.56
147	−0.54	33.345	150	−0.50	33.36	26.82
196	0.06	33.71	200	0.15	33.74	27.10
294	2.42	34.41	(300)	2.55	34.44	27.50

Station 7429; 4 June; 49°02′ N., 52°05′ W.; depth 293 m.; dynamic height 971.125

Observed values			Scaled values			
Depth, meters	Temperature, °C.	Salinity, °/₀₀	Depth, meters	Temperature, °C.	Salinity, °/₀₀	σ_t
0	3.20	32.26	0	3.20	32.26	25.70
25	−0.91	32.59	25	−0.91	32.59	26.23
50	−1.59	32.72	50	−1.59	32.72	26.35
74	−1.62	32.77	75	−1.65	32.77	26.39
99	−1.59	32.85	100	−1.60	32.85	26.46
149	−1.41	33.01	150	−1.40	33.01	26.58
199	−0.60	33.33	200	−0.85	33.33	26.81
283	2.16	34.33				

Station 7430; 4 June; 48°58′ N., 52°24′ W.; depth 342 m.; dynamic height 971.149

Observed values			Scaled values			
Depth, meters	Temperature, °C.	Salinity, °/₀₀	Depth, meters	Temperature, °C.	Salinity, °/₀₀	σ_t
0	2.50	32.33	0	2.50	32.33	25.82
25	−1.22	32.66	25	−1.22	32.66	26.29
51	−1.67	32.78	50	−1.70	32.78	26.39
76	−1.54	32.86	75	−1.55	32.86	26.46
102	−1.49	32.88	100	−1.50	32.88	26.47
152	−1.29	32.97	150	−1.30	32.97	26.54
202	−0.76	33.19	200	−0.80	33.17	26.68
304	1.15	33.93	300	1.05	33.90	27.18

Station 7431; 4 June; 48°53′ N., 52°50′ W.; depth 223 m.; dynamic height 971.154

Observed values			Scaled values			
Depth, meters	Temperature, °C.	Salinity, °/₀₀	Depth, meters	Temperature, °C.	Salinity, °/₀₀	σ_t
0	4.61	31.69	0	4.61	31.69	25.12
26	0.97	32.34	25	1.00	32.34	25.94
52	−1.43	32.775	50	−1.35	32.75	26.36
78	−1.51	32.83	75	−1.50	32.82	26.42
104	−1.54	32.90	100	−1.55	32.89	26.48
155	−1.14	33.08	150	−1.20	33.06	26.61
207	−0.59	33.31	200	−0.65	33.29	26.77

Station 7432; 4 June; 48°45′ N., 52°47′ W.; depth 132 m.; dynamic height 971.158

Observed values			Scaled values			
Depth, meters	Temperature, °C.	Salinity, °/₀₀	Depth, meters	Temperature, °C.	Salinity, °/₀₀	σ_t
0	4.63	31.69	0	4.63	31.69	25.12
25	−0.52	32.50	25	−0.52	32.50	26.13
49	−1.57	32.72	50	−1.60	32.72	26.35
74	−1.60	32.79	75	−1.60	32.79	26.40
98	−1.61	32.80	100	−1.60	32.80	26.41
128	−1.58	32.85				

TABLE OF OCEANOGRAPHIC DATA—Continued

Station 7433; 4 June; 48°44′ N., 52°58′ W.; depth 121 m.; dynamic height 971.169

Observed values			Scaled values			
Depth, meters	Temperature, °C.	Salinity, ‰	Depth, meters	Temperature, °C.	Salinity, ‰	σ_t
0	6.30	30.80	0	6.30	30.80	24.23
28	−0.22	32.44	25	0.05	32.29	25.94
55	−1.30	32.595	50	−1.20	32.58	26.22
83	−1.53	32.67	75	−1.50	32.65	26.28
			(100)	−1.60	32.71	26.34

Station 7434; 4 June; 48°45′ N., 52°45′ W.; depth 220 m.; dynamic height 971.149

Observed values			Scaled values			
Depth, meters	Temperature, °C.	Salinity, ‰	Depth, meters	Temperature, °C.	Salinity, ‰	σ_t
0	4.51	31.71	0	4.51	31.71	25.15
25	1.96	32.44	25	1.96	32.44	25.95
52	−1.60	32.71	50	−1.60	32.70	26.33
77	−1.61	32.795	75	−1.60	32.79	26.40
103	−1.60	32.80	100	−1.60	32.80	26.41
154	−0.60	33.305	150	−0.70	33.27	26.76

Station 7435; 4 June; 48°32′ N., 52°33.5′ W.; depth 269 m.; dynamic height 971.115

Observed values			Scaled values			
Depth, meters	Temperature, °C.	Salinity, ‰	Depth, meters	Temperature, °C.	Salinity, ‰	σ_t
0	4.97	31.79	0	4.97	31.79	25.16
23	1.96	32.48	25	1.85	32.51	26.01
46	−1.09	32.81	50	−1.10	32.82	26.41
69	−1.36	32.885	75	−1.40	32.90	26.48
92	−1.51	32.97	100	−1.45	33.01	26.58
138	−1.21	33.20	150	−1.30	33.31	26.81
184	0.27	33.605	200	0.70	33.74	27.07
221	1.25	33.935				

Station 7436; 4 June; 48°18′ N., 51°54′ W.; depth 192 m.; dynamic height 971.162

Observed values			Scaled values			
Depth, meters	Temperature, °C.	Salinity, ‰	Depth, meters	Temperature, °C.	Salinity, ‰	σ_t
0	5.22	31.59	0	5.22	31.59	24.98
26	−0.30	32.375	25	−0.25	32.35	26.00
52	−1.43	32.65	50	−1.35	32.64	26.27
78	−1.64	32.69	75	−1.60	32.68	26.31
104	−1.41	32.85	100	−1.45	32.82	26.42
155	−1.33	32.97	150	−1.30	32.96	26.53

Station 7437; 4 June; 48°11′ N., 51°34′ W.; depth 220 m.; dynamic height 971.162

Observed values			Scaled values			
Depth, meters	Temperature, °C.	Salinity, ‰	Depth, meters	Temperature, °C.	Salinity, ‰	σ_t
0	4.25	31.91	0	4.25	31.91	25.33
25	0.63	32.12	25	0.63	32.12	25.78
50	−1.44	32.57	50	−1.44	32.57	26.22
75	−1.56	32.72	75	−1.56	32.72	26.34
100	−1.47	32.74	100	−1.47	32.74	26.36
150	−0.84	33.03	150	−0.84	33.03	26.57
200	0.33	33.43	200	0.33	33.43	26.84

Station 7438; 4 June; 48°04′ N., 51°15′ W.; depth 179 m.; dynamic height 971.146

Observed values			Scaled values			
Depth, meters	Temperature, °C.	Salinity, ‰	Depth, meters	Temperature, °C.	Salinity, ‰	σ_t
0	3.95	32.14	0	3.95	32.14	25.54
25	2.30	32.20	25	2.30	32.20	25.73
51	−1.47	32.635	50	−1.40	32.63	26.26
76	−1.38	32.74	75	−1.40	32.74	26.36
101	−1.54	32.84	100	−1.50	32.83	26.43
152	0.04	33.33	150	0.00	33.31	26.76

Station 7439; 4 June; 47°55′ N., 51°06′ W.; depth 181 m.; dynamic height 971.142

Observed values			Scaled values			
Depth, meters	Temperature, °C.	Salinity, ‰	Depth, meters	Temperature, °C.	Salinity, ‰	σ_t
0	4.11	32.18	0	4.11	32.18	25.55
25	2.02	32.28	25	2.02	32.28	25.81
50	−0.84	32.69	50	−0.84	32.69	26.29
75	−1.14	32.82	75	−1.14	32.82	26.41
100	−1.06	32.91	100	−1.06	32.91	26.48
140	−0.03	33.25				

Station 7440; 4 June; 47°48′ N., 50°50′ W.; depth 117 m.; dynamic height 971.130

Observed values			Scaled values			
Depth, meters	Temperature, °C.	Salinity, ‰	Depth, meters	Temperature, °C.	Salinity, ‰	σ_t
0	3.95	32.24	0	3.95	32.24	25.62
25	1.79	32.50	25	1.79	32.50	26.01
50	−1.15	32.64	50	−1.15	32.64	26.27
76	−1.49	32.785	75	−1.45	32.78	26.39
106	−0.52	33.115	100	−0.75	33.06	26.59

Station 7441; 5 June; 47°40′ N., 50°49′ W.; depth 110 m.; dynamic height 971.125

Observed values			Scaled values			
Depth, meters	Temperature, °C.	Salinity, ‰	Depth, meters	Temperature, °C.	Salinity, ‰	σ_t
0	4.42	32.51	0	4.42	32.51	25.78
25	2.74	32.56	25	2.74	32.56	25.98
50	1.05	32.75	50	1.05	32.75	26.26
74	0.30	32.92	75	0.30	32.93	26.45
104	0.24	33.33	100	0.25	33.27	26.72

Station 7442; 5 June; 47°33′ N., 50°20′ W.; depth 104 m.; dynamic height 971.120

Observed values			Scaled values			
Depth, meters	Temperature, °C.	Salinity, ‰	Depth, meters	Temperature, °C.	Salinity, ‰	σ_t
0	4.79	32.69	0	4.79	32.69	25.88
24	2.57	32.68	25	2.55	32.68	26.09
49	0.69	32.79	50	0.70	32.80	26.32
74	0.32	32.945	75	0.30	32.95	26.46
99	0.16	33.20	100	0.15	33.20	26.67

Station 7443; 5 June; 47°23′ N., 49°58′ W.; depth 91 m.; dynamic height 971.118

Observed values			Scaled values			
Depth, meters	Temperature, °C.	Salinity, ‰	Depth, meters	Temperature, °C.	Salinity, ‰	σ_t
0	4.42	32.60	0	4.42	32.60	25.87
24	2.73	32.695	25	2.25	32.70	26.13
49	−0.21	32.78	50	−0.20	32.79	26.36
78	−0.29	33.005	75	−0.25	32.99	26.52

Station 7444; 5 June; 47°44′ N., 49°47′ W.; depth 115 m.; dynamic height 971.120

Observed values			Scaled values			
Depth, meters	Temperature, °C.	Salinity, ‰	Depth, meters	Temperature, °C.	Salinity, ‰	σ_t
0	4.17	32.47	0	4.17	32.47	25.78
25	2.81	32.70	25	2.81	32.70	26.09
50	0.29	32.80	50	0.29	32.80	26.34
75	−0.34	32.96	75	−0.34	32.96	26.49
100	−0.19	33.19	100	−0.19	33.19	26.68

Station 7445; 5 June; 47°58′ N., 49°45′ W.; depth 168 m.; dynamic height 971.132

Observed values			Scaled values			
Depth, meters	Temperature, °C.	Salinity, ‰	Depth, meters	Temperature, °C.	Salinity, ‰	σ_t
0	3.76	32.28	0	3.76	32.28	25.66
24	1.79	32.455	25	1.75	32.45	25.98
49	−1.14	32.65	50	−1.15	32.65	26.28
74	−1.58	32.75	75	−1.55	32.75	26.36
99	−1.35	32.875	100	−1.35	32.89	26.47
148	0.19	33.455	(150)	0.20	33.48	26.91

TABLE OF OCEANOGRAPHIC DATA—Continued

Station 7446; 5 June; 48°12′ N., 49°40′ W.; depth 223 m.; dynamic height 971.109

Observed values			Scaled values			
Depth, meters	Temperature, °C.	Salinity, °/oo	Depth, meters	Temperature, °C.	Salinity, °/oo	σ_t
0	3.85	32.14	0	3.85	32.14	25.55
25	−0.67	32.66	25	−0.67	32.66	26.27
51	−1.62	32.84	50	−1.55	32.83	26.43
76	−1.65	32.955	75	−1.65	32.95	26.53
102	−0.99	33.175	100	−1.05	33.16	26.68
152	−0.02	33.50	150	−0.10	33.48	26.90
203	1.33	33.97	200	1.25	33.95	27.20

Station 7447; 5 June; 48°31′ N., 49°31′ W.; depth 594 m.; dynamic height 971.043

Observed values			Scaled values			
Depth, meters	Temperature, °C.	Salinity, °/oo	Depth, meters	Temperature, °C.	Salinity, °/oo	σ_t
0	3.95	32.31	0	3.95	32.31	25.67
18	0.79	32.685	25	0.75	32.78	26.30
38	−1.45	32.96	50	−1.00	33.03	26.57
56	−1.42	33.065	75	−0.70	33.30	26.78
72	−0.74	33.27	100	−0.40	33.47	26.92
112	−0.25	33.55	150	1.00	33.89	27.17
150	1.00	33.89	200	1.55	34.17	27.36
225	1.86	34.30	300	2.80	34.57	27.58
307	2.90	34.60	400	3.30	34.70	27.64
482	3.65	34.78				

Station 7448; 5 June; 48°40′ N., 49°22′ W.; depth 1,042 m.; dynamic height 970.983

Observed values			Scaled values			
Depth, meters	Temperature, °C.	Salinity, °/oo	Depth, meters	Temperature, °C.	Salinity, °/oo	σ_t
0	4.00	32.36	0	4.00	32.36	25.71
20	−1.27	32.87	25	−1.20	32.94	26.51
39	−0.84	33.20	50	−0.70	33.33	26.81
59	−0.42	33.46	75	0.05	33.59	26.99
79	0.24	33.625	100	0.65	33.80	27.12
118	1.12	33.97	150	1.35	34.13	27.34
157	1.40	34.165	200	2.10	34.37	27.48
236	2.74	34.545	300	2.85	34.64	27.63
322	2.84	34.67	400	3.25	34.75	27.68
482	3.63	34.84	600	3.65	34.85	27.72
668	3.64	34.85	800	3.60	34.88	27.75
867	3.57	34.89	(1,000)	3.55	34.90	27.77

Station 7449; 5 June; 49°04′ N., 49°10′ W.; depth 1,765 m.; dynamic height 970.853

Observed values			Scaled values			
Depth, meters	Temperature, °C.	Salinity, °/oo	Depth, meters	Temperature, °C.	Salinity, °/oo	σ_t
0	5.99	34.37	0	5.99	34.37	27.08
26	5.86	34.535	25	5.85	34.53	27.22
51	3.06	34.465	50	3.10	34.47	27.48
77	2.66	34.56	75	2.70	34.55	27.57
102	2.96	34.655	100	2.90	34.65	27.64
154	3.06	34.69	150	3.05	34.69	27.65
205	3.18	34.755	200	3.15	34.75	27.69
307	3.33	34.79	300	3.30	34.79	27.71
414	3.40	34.83	400	3.40	34.82	27.73
622	3.52	34.87	600	3.50	34.87	27.76
833	3.46	34.875	800	3.50	34.87	27.76
1,043	3.44	34.87	1,000	3.45	34.87	27.76
1,277	3.46	34.905				

Station 7450; 6 June; 49°30′ N., 49°04′ W.; depth 1,810 m.; dynamic height 970.870

Observed values			Scaled values			
Depth, meters	Temperature, °C.	Salinity, °/oo	Depth, meters	Temperature, °C.	Salinity, °/oo	σ_t
0	5.87	34.19	0	5.87	34.19	26.95
26	5.09	34.355	25	5.10	34.35	27.17
52	5.05	34.52	50	5.05	34.50	27.29
78	3.47	34.64	75	3.75	34.62	27.53
104	3.17	34.69	100	3.25	34.68	27.62
156	3.08	34.72	150	3.10	34.72	27.68
208	3.23	34.755	200	3.20	34.75	27.69
312	3.41	34.80	300	3.40	34.80	27.71
421	3.37	34.815	400	3.40	34.81	27.72
630	3.47	34.83	600	3.45	34.83	27.72
841	3.45	34.85	800	3.45	34.85	27.74
1,052	3.46	34.885	1,000	3.45	34.88	27.76
1,581	3.37	34.915				

Station 7451; 6 June; 50°00′ N., 48°53′ W.; depth 2,030 m.; dynamic height 970.868

Observed values			Scaled values			
Depth, meters	Temperature, °C.	Salinity, °/oo	Depth, meters	Temperature, °C.	Salinity, °/oo	σ_t
0	5.69	34.35	0	5.69	34.35	27.10
23	5.12	34.565	25	5.05	34.57	27.35
47	4.33	34.60	50	4.25	34.60	27.46
70	3.52	34.59	75	3.45	34.60	27.54
95	2.97	34.62	100	2.95	34.62	27.61
141	2.83	34.63	150	2.85	34.64	27.63
188	3.05	34.68	200	3.10	34.69	27.65
283	3.27	34.755	300	3.30	34.76	27.69
380	3.38	34.81	400	3.35	34.81	27.72
568	3.33	34.82	600	3.35	34.82	27.73
755	3.45	34.84	800	3.50	34.85	27.74
952	3.46	34.855	1,000	3.50	34.86	27.75
1,447	3.44	34.89				

Station 7452; 18 June; 41°59′ N., 51°00′ W.; depth 3,292 m.; dynamic height 971.144

Observed values			Scaled values			
Depth, meters	Temperature, °C.	Salinity, °/oo	Depth, meters	Temperature, °C.	Salinity, °/oo	σ_t
0	12.47	33.47	0	12.47	33.47	25.33
24	11.63	33.83	25	11.65	33.85	25.78
50	11.96	35.28	50	11.96	35.28	26.84
74	12.44	35.49	75	12.40	35.49	26.91
99	12.29	-----	100	12.25	35.50	26.95
148	12.27	35.52	150	12.25	35.50	26.95
198	10.78	35.24	200	10.70	35.23	27.02
297	7.71	34.96	300	7.65	34.96	27.31
339	6.80	34.905	400	5.90	34.88	27.49
502	4.32	34.83	600	4.25	34.89	27.69
662	4.16	34.90	800	4.00	34.92	27.75
843	3.95	34.93	1,000	3.90	34.93	27.76
1,327	3.70	34.93				

Station 7453; 19 June; 41°59′ N., 51°58′ W.; depth 4,023 m.; dynamic height 971.121

Observed values			Scaled values			
Depth, meters	Temperature, °C.	Salinity, °/oo	Depth, meters	Temperature, °C.	Salinity, °/oo	σ_t
0	11.10	33.12	0	11.10	33.12	25.32
25	9.35	33.18	25	9.35	33.18	25.65
51	1.52	33.15	50	1.75	33.15	26.54
77	3.55	33.61	75	3.30	33.57	26.74
103	4.33	33.96	100	4.20	33.91	26.92
153	7.52	------	150	7.25	34.43	26.95
205	8.32	34.96	200	8.25	34.92	27.20
308	6.83	34.97	300	6.95	34.97	27.43
406	5.31	34.88	400	5.40	34.89	27.56
610	4.93	35.00	600	4.95	34.99	27.69
815	4.06	34.95	800	4.10	34.95	27.76
1,017	3.99	34.96	1,000	4.00	34.96	27.78
1,519	3.68	34.95				

Station 7454; 19 June; 42°21′ W.; 51°30′ W.; depth 2,926 m.; dynamic height 971.042

Observed values			Scaled values			
Depth, meters	Temperature, °C.	Salinity, °/oo	Depth, meters	Temperature, °C.	Salinity, °/oo	σ_t
0	8.50	32.78	0	8.50	32.78	25.48
25	8.03	33.12	25	8.03	33.12	25.81
52	3.75	33.53	50	4.15	33.50	26.60
77	3.65	33.84	75	3.65	33.81	26.89
103	3.26	33.94	100	3.30	33.92	27.02
154	4.06	34.32	150	4.00	34.30	27.25
206	3.03	34.35	200	3.15	34.35	27.37
309	3.57	34.63	300	3.55	34.60	27.53
378	4.87	34.91	400	4.25	34.91	27.71
568	4.43	34.94	600	4.30	34.93	27.71
759	3.85	34.90	800	3.85	34.90	27.74
949	3.83	34.92	1,000	3.80	34.92	27.77
1,426	3.56	34.92				

TABLE OF OCEANOGRAPHIC DATA—Continued

Observed values			Scaled values			
Depth, meters	Temperature, °C.	Salinity, °/₀₀	Depth, meters	Temperature, °C.	Salinity, °/₀₀	σ$_t$
Station 7455; 19 June; 42°44′ N., 51°05′ W.; depth 1,774 m.; dynamic height 971.052						
0	10.02	33.07	0	10.02	33.07	25.46
26	9.82	33.22	25	9.85	33.22	25.60
52	6.23	33.54	50	8.85	33.51	26.00
78	3.95	33.86	75	4.50	33.82	26.82
105	3.94	34.09	100	3.95	34.05	27.06
156	4.62	34.61	150	4.50	34.54	27.39
208	4.03	34.64	200	4.10	34.63	27.50
313	4.67	34.87	300	4.85	34.84	27.58
405	4.47	34.88	400	4.50	34.88	27.65
610	3.70	34.85	600	3.75	34.85	27.71
816	3.72	34.88	800	3.70	34.88	27.74
1,022	3.63	34.89	1,000	3.65	34.88	27.74
1,539	3.58	34.93				
Station 7456; 19 June; 42°52′ N., 50°50′ W.; depth 1,070 m.; dynamic height 971.067						
0	11.14	33.33	0	11.14	33.33	25.47
23	7.39	33.39	25	7.05	33.41	26.18
47	3.21	33.66	50	3.45	33.78	26.89
70	7.49	34.59	75	7.55	34.62	27.06
93	7.98	34.76	100	7.65	34.74	27.14
139	5.91	34.66	150	5.90	34.65	27.31
186	5.85	34.62	200	5.80	34.65	27.32
279	5.58	34.78	300	5.55	34.78	27.45
369	3.52	------	400	5.20	34.78	27.49
547	3.65	34.79	600	3.65	34.81	27.69
735	3.73	34.86	800	3.70	34.86	27.73
927	3.69	34.86	1,000	3.60	34.86	27.74
Station 7457; 19 June; 42°54′ N., 50°47′ W.; depth 637 m.; dynamic height 971.079						
0	11.56	33.39	0	11.56	33.39	25.44
25	9.88	33.40	25	9.88	33.40	25.75
51	6.33	34.125	50	6.45	34.08	26.78
76	8.87	34.78	75	8.75	34.72	26.96
103	7.34	34.60	100	7.50	34.61	27.06
153	5.74	34.50	150	5.85	34.51	27.21
204	6.93	34.67	200	6.80	34.66	27.20
307	4.28	34.65	300	4.50	34.65	27.47
408	3.63	34.71	400	3.65	34.70	27.60
611	3.71	34.83	600	3.70	34.82	27.70
Station 7458; 19 June: 42°57′ N., 50°42′ W.; depth 170 m.; dynamic height 971.054						
0	11.18	33.39	0	11.18	33.39	25.51
25	6.41	33.57	25	6.41	33.57	26.39
51	2.34	33.61	50	2.65	33.61	26.83
76	8.41	------	75	8.30	34.69	27.01
103	5.55	34.32	100	5.85	34.34	27.07
153	3.83	34.11	150	3.95	34.13	27.12
Station 7459: 19 June: 43°03′ N., 50°34′ W.; depth 93 m.; dynamic height 971.091						
0	8.83	33.11	0	8.83	33.11	25.68
26	7.26	32.88	25	7.25	32.89	25.74
51	0.17	32.97	50	0.45	32.97	26.47
78	0.56	33.33	75	0.50	33.30	26.72
Station 7460: 19 June: 43°21′ N., 50°16′ W.; depth 60 m.; dynamic height 971.095						
0	8.12	32.76	0	8.12	32.76	25.52
25	5.65	32.81	25	5.65	32.81	25.89
51	1.74	33.01	50	1.85	33.01	26.42
Station 7461; 19 June; 42°59′ N., 50°20′ W.; depth 91 m.; dynamic height 971.082						
0	6.05	32.57	0	6.05	32.57	25.65
25	1.82	32.77	25	1.82	32.77	26.22
50	0.07	32.98	50	0.07	32.98	26.50
75	−0.09	33.21	75	−0.09	33.21	26.69
Station 7462; 19 June; 42°48′ N., 50°18′ W.; depth 293 m.; dynamic height 971.102						
0	5.68	32.61	0	5.68	32.61	25.73
23	2.65	32.72	25	2.45	32.73	26.14
48	−0.48	32.86	50	−0.45	32.90	26.45
70	−0.34	33.11	75	−0.30	33.13	26.63
95	−0.17	33.25	100	−0.15	33.27	26.74
141	0.16	33.44	150	0.50	33.51	26.90
188	2.36	33.81	200	2.55	33.91	27.07
281	3.81	34.54				
Station 7463; 19 June; 42°38′ N., 50°18′ W.; depth 2,012 m.; dynamic height 971.070						
0	7.05	32.68	0	7.05	32.68	25.61
25	1.58	32.77	25	1.58	32.77	26.24
52	0.10	33.12	50	0.25	33.10	26.58
76	−0.23	33.26	75	−0.20	33.25	26.72
102	0.12	33.40	100	0.10	33.38	26.82
153	3.00	33.95	150	2.80	33.90	27.05
203	1.39	34.00	200	1.50	34.00	27.23
303	3.02	34.52	300	2.95	34.49	27.50
394	3.32	34.67	400	3.35	34.71	27.64
589	3.69	34.84	600	3.70	34.84	27.71
780	3.69	34.87	800	3.70	34.87	27.74
982	3.67	34.89	1,000	3.65	34.89	27.75
1,483	3.55	34.92				
Station 7464; 20 June; 42°21′ N., 50°17′ W.; depth 2,743 m.; dynamic height 970.972						
0	9.86	33.15	0	9.86	33.15	25.55
26	6.40	33.56	25	6.70	33.56	26.35
52	3.49	33.84	50	3.75	33.82	26.89
76	3.01	34.01	75	3.05	34.00	27.10
102	4.23	34.34	100	4.05	34.31	27.26
153	3.85	34.49	150	3.90	34.48	27.40
203	3.30	34.52	200	3.35	34.52	27.49
304	4.84	34.90	300	4.80	34.88	27.62
400	4.81	34.97	400	4.82	34.97	27.69
597	4.08	34.94	600	4.05	34.94	27.75
793	3.91	34.93	800	3.90	34.93	27.76
995	3.90	34.96	1,000	3.90	34.95	37.78
1,505	3.70	34.95				
Station 7465; 20 June; 41°58′ N., 50°16′ W.; depth 3,566 m.; dynamic height 971.083						
0	12.13	33.11	0	12.13	33.11	25.12
25	8.39	33.82	25	8.39	33.82	26.31
50	6.26	33.86	50	6.26	33.86	26.65
75	11.27	35.13	75	11.27	35.13	26.85
100	10.89	35.17	100	10.89	35.17	26.95
151	9.06	34.99	150	9.10	34.99	27.11
201	7.49	34.83	200	7.55	34.83	27.22
301	3.48	34.45	300	3.55	34.45	27.41
377	5.41	34.94	400	5.30	34.93	27.60
571	4.26	34.91	600	4.25	34.92	27.72
771	4.26	34.97	800	4.20	34.96	27.76
965	3.97	34.99	1,000	3.95	34.95	27.77
1,450	3.74	34.95				

TABLE OF OCEANOGRAPHIC DATA—Continued

Observed values			Scaled values			
Depth, meters	Temperature, °C.	Salinity, ‰	Depth, meters	Temperature, °C.	Salinity, ‰	σ_t
Station 7466; 20 June; 41°30′ N., 50°14′ W.; depth 3,931 m.; dynamic height 971.252						
0	16.70	35.64	0	16.70	35.64	26.09
25	16.42	35.70	25	16.42	35.70	26.21
51	15.62	36.02	50	15.65	36.00	26.61
76	15.12	35.94	75	15.15	35.94	26.68
102	13.71	35.70	100	13.95	35.71	26.76
152	13.14	35.64	150	13.15	35.64	26.87
203	12.38	35.52	200	12.45	35.52	26.92
305	10.71	35.32	300	10.80	35.33	27.08
394	8.24	35.03	400	8.20	35.03	27.28
585	5.96	35.01	600	5.85	35.00	27.59
773	4.93	34.97	800	4.85	34.97	27.69
971	4.41	34.97	1,000	4.40	34.97	27.74
1,474	3.94	34.97				
Station 7467; 20 June; 41°00′ N., 50°15′ W.; depth 4,023 m.; dynamic height 971.257						
0	15.66	34.63	0	15.66	34.63	25.56
26	15.94	35.33	25	15.95	35.32	26.02
52	14.89	35.87	50	15.00	35.85	26.64
78	14.15	35.76	75	14.20	35.77	26.76
104	13.81	35.73	100	13.85	35.74	26.81
155	13.27	35.66	150	13.30	35.67	26.87
208	12.93	35.62	200	13.00	35.63	26.89
312	10.51	35.28	300	10.80	35.32	27.08
410	8.74	35.16	400	8.95	35.24	27.33
615	6.25	35.05	600	6.45	35.05	27.55
820	4.68	34.97	800	4.85	35.01	27.72
1,025	4.29	34.97	1,000	4.35	34.97	27.75
1,538	3.84	34.98				
Station 7468; 20 June; 42°00′ N., 49°27′ W.; depth 3,252 m.; dynamic height 971.063						
0	12.24	33.09	0	12.24	33.09	25.08
24	8.08	33.13	25	8.05	33.14	25.83
49	4.40	33.58	50	4.40	33.58	26.64
73	2.88	33.67	75	3.15	33.68	26.84
99	2.52	33.82	100	2.55	33.83	27.01
147	2.88	34.09	150	3.25	34.11	27.17
196	3.89	34.41	200	3.90	34.41	27.35
295	3.70	34.60	300	3.75	34.61	27.52
353	4.12	34.74	400	4.30	34.81	27.63
539	4.82	35.00	600	4.60	34.97	27.72
731	3.80	34.90	800	3.90	34.92	27.76
929	4.03	34.95	1,000	3.95	34.94	27.76
1,451	3.48	34.88				
Station 7469; 22 June; 41°33′ N., 49°02′ W.; depth 3,109 m.; dynamic height 971.229						
0	15.84	34.60	0	15.84	34.60	25.50
25	15.19	35.51	25	15.19	35.51	26.34
51	14.45	35.79	50	14.50	35.79	26.70
76	13.62	35.65	75	13.65	35.66	26.79
102	13.16	35.62	100	13.20	35 60	26.83
152	12.40	35.49	150	12.45	35.50	26.91
203	12.06	35.44	200	12.10	35.45	26.94
305	10.24	35.19	300	10.35	35.21	27.08
416	7.31	34.92	400	7.75	34.97	27.31
622	4.64	34.87	600	4.95	34.88	27.60
827	4.61	35.00	800	4.60	34.98	27.72
1,033	4.10	34.95	1,000	4.20	34.96	27.76
1,549	3.71	34.96				

Observed values			Scaled values			
Depth, meters	Temperature, °C.	Salinity, ‰	Depth, meters	Temperature, °C.	Salinity, ‰	σ_t
Station 7470; 23 June; 40°59′ N., 48°28′ W.; depth 3,383 m.; dynamic height 971.270						
0	16.43	34.99	0	16.43	34.99	25.66
24	16.89	35.43	25	16.85	35.43	25.90
49	14.14	35.57	50	14.15	35.56	26.53
73	13.36	35.54	75	13.30	35.53	26.76
98	12.68	35.42	100	12.65	35.42	26.81
147	12.34	35.46	150	12.35	35.46	26.90
196	12.32	35.52	200	12.30	35.51	26.95
294	10.68	35.34	300	10.60	35.33	27.12
402	8.34	35.09	400	8.40	35.09	27.30
602	6.01	35.06	600	6.05	35.01	27.50
899	4.47	34.98	800	5.00	34.99	27.69
1,095	4.16	34.97	1,000	4.30	34.97	27.75
1,581	3.57	34.92				
Station 7471; 23 June; 41°37′ N., 47°20′ W.; depth 4,335 m.; dynamic height 971.241						
0	15.10	34.42	0	15.10	34.42	25.52
24	12.92	34.22	25	13.00	34.25	25.84
49	14.25	35.56	50	14.20	35.56	26.60
73	13.21	35.53	75	13.20	35.53	26.78
98	13.04	35.58	100	13.00	35.57	26.85
145	12.08	35.40	150	12.05	35.40	26.91
194	11.73	35.36	200	11.65	35.36	26.95
292	10.61	35.31	300	10.45	35.29	27.11
403	7.62	34.945	400	7.70	34.95	27.30
594	5.42	34.94	600	5.40	34.96	27.62
792	5.14	35.05	800	5.10	35.04	27.71
980	4.15	34.95	1,000	4.15	34.94	27.74
1,347	3.70	34.92				
Station 7472; 23 June; 42°01′ N., 47°54′ W.; depth 3,400 m.; dynamic height 971.006						
0	11.52	33.31	0	11.52	33.31	25.39
25	8.93	33.28	25	8.93	33.28	25.80
50	4.63	33.69	50	4.63	33.69	26.70
75	3.27	33.89	75	3.27	33.89	26.99
100	2.78	34.11	100	2.78	34.11	27.14
150	3.95	34.51	150	3.95	34.51	27.42
200	3.48	34.56	200	3.48	34.56	27.51
300	4.13	34.78	300	4.13	34.78	27.62
389	4.49	34.89	400	4.50	34.89	27.66
587	4.46	34.98	600	4.45	34.98	27.74
783	4.30	34.99	800	4.25	34.99	27.77
983	3.95	34.97	1,000	3.95	34.96	27.78
1,494	3.57	34.93				
Station 7473; 23 June; 42°21′ N., 48°31′ W.; depth 3,383 m.; dynamic height 971.000						
0	11.90	33.13	0	11.90	33.13	25.18
25	4.98	33.48	25	4.98	33.48	26.50
50	4.54	33.99	50	4.54	33.99	26.94
75	5.21	34.28	75	5.20	34.28	27.10
100	6.31	34.57	100	6.31	34.57	27.19
149	5.37	34.57	150	5.30	34.57	27.32
198	4.79	34.62	200	4.80	34.62	27.42
298	4.98	34.82	300	5.00	34.82	27.56
394	4.64	34.89	400	4.10	34.89	27.71
590	4.46	34.97	600	4.45	34.97	27.74
786	4.45	34.98	800	4.40	34.98	27.74
984	3.89	34.94	1,000	3.90	34.94	27.77
1,497	3.50	34.92				

TABLE OF OCEANOGRAPHIC DATA—Continued

Observed values			Scaled values			
Depth, meters	Temperature, °C.	Salinity, °/oo	Depth, meters	Temperature, °C.	Salinity, °/oo	σ_t
Station 7474; 23 June; 42°40′ N., 49°08′ W.; depth 2,652 m.; dynamic height 970.970						
0	8.46	32.55	0	8.46	32.55	25.30
25	4.27	33.32	25	4.27	33.32	26.44
51	2.77	------	50	2.80	33.62	26.83
76	2.47	33.95	75	2.50	33.94	27.10
102	2.74	34.18	100	2.70	34.15	27.25
152	2.96	34.44	150	2.95	34.42	27.45
203	3.55	34.62	200	3.50	34.54	27.49
305	4.23	34.86	300	4.20	34.84	27.66
405	4.08	34.89	400	4.10	34.89	27.71
605	3.98	34.91	600	4.00	34.91	27.74
807	3.78	34.92	800	3.80	34.91	27.76
1,006	3.61	34.92	1,000	3.65	34.92	27.78
1,510	3.47	34.93				
Station 7475; 24 June; 43°20′ N., 48°50′ W.; depth 2,012 m.; dynamic height 970.981						
0	7.53	32.64	0	7.53	32.64	25.51
25	5.58	32.96	25	5.58	32.96	26.01
50	1.99	33.65	50	1.99	33.65	26.88
75	1.04	33.86	75	1.04	33.86	27.15
100	2.64	34.20	100	2.64	34.20	27.30
150	3.40	34.44	150	3.40	34.44	27.42
201	3.96	34.65	200	3.95	34.65	27.53
301	3.78	34.73	300	3.80	34.73	27.61
400	4.23	34.86	400	4.23	34.86	27.67
599	4.05	34.92	600	4.05	34.92	27.73
798	3.71	34.90	800	3.70	34.90	27.76
999	3.50	34.90	1,000	3.50	34.90	27.78
1,501	3.36	34.93				
Station 7476; 24 June; 43°07′ N., 48°09′ W.; depth 3,219 m.; dynamic height 971.002						
0	8.20	32.36	0	8.20	32.36	25.20
24	2.74	32.66	25	2.70	32.69	26.08
49	0.14	33.28	50	0.15	33.30	26.74
74	0.27	33.55	75	0.30	33.54	26.93
99	0.63	33.76	100	0.65	33.77	27.10
147	1.63	34.17	150	1.70	34.19	27.36
197	2.73	34.44	200	2.75	34.46	27.50
296	4.88	34.89	300	4.85	34.89	27.62
396	4.65	34.93	400	4.65	34.93	27.68
593	4.00	34.91	600	4.00	34.91	27.74
789	3.87	34.93	800	3.85	34.93	27.76
989	3.75	34.93	1,000	3.75	34.93	27.77
1,490	3.50	34.93				
Station 7477; 24 June; 42°53′ N., 47°27′ W.; depth 3,658 m.; dynamic height 971.157						
0	16.31	35.08	0	16.31	35.08	25.75
24	15.19	35.19	25	15.15	35.20	26.11
48	13.23	35.46	50	13.20	35.46	26.73
72	12.72	35.46	75	12.65	35.45	26.83
97	12.18	35.40	100	12.15	35.40	26.89
144	11.85	35.41	150	11.75	35.39	26.96
192	10.78	35.25	200	10.60	35.22	27.04
289	8.18	35.00	300	8.05	35.00	27.29
389	7.06	35.01	400	6.90	35.00	27.45
582	4.40	34.85	600	4.40	34.88	27.66
773	4.54	34.99	800	4.50	34.98	27.73
968	4.04	34.94	1,000	4.00	34.94	27.76
1,462	3.66	34.93				

Observed values			Scaled values			
Depth, meters	Temperature, °C.	Salinity, °/oo	Depth, meters	Temperature, °C.	Salinity, °/oo	σ_t
Station 7478; 24 June; 42°39′ N., 46°51′ W.; depth 3,841 m.; dynamic height 971.145						
0	15.28	34.13	0	15.28	34.13	25.26
24	14.62	34.10	25	14.50	34.10	25.41
48	10.67	34.48	50	10.65	34.50	26.47
72	10.21	34.61	75	10.20	34.63	26.64
96	9.98	34.76	100	9.85	34.75	26.80
143	7.69	34.69	150	7.70	34.72	27.12
192	7.94	34.93	200	7.85	34.92	27.26
288	6.42	34.83	300	6.35	34.84	27.40
372	5.78	34.87	400	5.75	34.89	27.52
561	5.39	35.02	600	5.30	35.02	27.68
754	4.90	35.03	800	4.80	35.03	27.74
949	4.40	35.01	1,000	4.35	35.00	27.77
1,448	3.72	34.94				
Station 7479; 24 June; 42°30′ N., 46°09′ W.; depth 4,572 m.; dynamic height 971.388						
0	19.48	35.91	0	19.48	35.91	25.61
25	19.52	35.94	25	19.52	35.94	25.62
49	17.22	36.01	50	17.20	36.01	26.26
74	15.32	35.80	75	15.30	35.81	26.55
98	15.27	35.95	100	15.20	35.92	26.66
146	13.39	35.60	150	13.35	35.60	26.80
196	13.14	35.63	200	13.10	35.62	26.87
294	12.03	35.47	300	11.85	35.45	26.98
331	10.46	35.28	400	9.30	35.16	27.21
491	7.65	35.00	600	7.50	34.92	27.31
645	5.46	34.89	800	5.45	35.01	27.65
834	5.43	35.04	1,000	5.15	35.03	27.70
1,357	4.59	35.00				
Station 7480; 25 June; 42°53′ N., 45°49′ W.; depth 4,663 m.; dynamic height 971.334						
0	17.95	34.82	0	17.95	34.82	25.17
23	18.04	35.37	25	18.00	35.37	25.58
45	17.97	35.37	50	17.05	35.39	25.82
67	14.05	35.48	75	13.75	35.47	26.62
89	13.05	35.44	100	12.90	35.40	26.74
135	12.53	35.26	150	12.40	35.32	26.78
180	12.24	35.45	200	12.00	35.43	26.94
269	11.31	35.38	300	9.50	34.96	27.02
291	9.61	34.96	400	8.05	34.93	27.23
469	7.03	34.91	600	6.15	34.94	27.50
669	5.65	34.99	800	5.00	34.97	27.68
862	4.65	34.96	1,000	4.45	34.96	27.73
1,390	3.90	34.96				
Station 7481; 25 June; 43°11′ N., 45°34′ W.; depth 4,801 m.; dynamic height 971.301						
0	17.35	35.71	0	17.35	35.71	25.99
26	17.34	35.72	25	17.35	35.72	26.00
52	15.91	36.01	50	16.05	35.99	26.51
78	14.69	35.81	75	14.80	35.83	26.67
103	13.40	35.58	100	13.65	35.77	26.88
156	13.15	35.68	150	13.20	35.69	26.90
207	12.67	35.55	200	12.75	35.57	26.91
310	11.60	35.47	300	11.70	35.47	27.03
387	10.26	35.31	400	10.10	35.29	27.18
579	6.99	35.08	600	6.80	35.06	27.51
773	5.03	34.96	800	4.95	34.96	27.67
975	4.62	35.00	1,000	4.60	34.99	27.73
1,494	3.81	34.95				

TABLE OF OCEANOGRAPHIC DATA—Continued

Station 7482; 25 June; 43°23′ N., 46°08′ W.; depth 4,663 m.; dynamic height 971.298

Observed values			Scaled values			
Depth, meters	Temperature, °C.	Salinity, °/oo	Depth, meters	Temperature, °C.	Salinity, °/oo	σ_t
0	17.25	35.57	0	17.25	35.57	25.91
27	17.24	35.65	25	17.25	35.65	25.97
53	16.37	36.16	50	15.40	36.11	26.53
80	15.65	36.04	75	15.80	36.07	26.64
106	14.32	35.79	100	14.65	35.85	26.72
160	13.74	35.74	150	13.85	35.75	26.82
214	13.13	35.66	200	13.30	35.68	26.87
320	11.42	35.43	300	11.75	35.47	27.02
404	9.19	35.13	400	9.30	35.15	27.20
606	5.68	34.92	600	5.80	34.92	27.54
811	4.57	34.94	800	4.65	34.94	27.69
1,016	4.31	34.97	1,000	4.35	34.96	27.74
1,531	3.72	34.94				

Station 7483; 25 June; 43°30′ N., 46°38′ W.; depth 4,390 m.; dynamic height 971.267

Observed values			Scaled values			
Depth, meters	Temperature, °C.	Salinity, °/oo	Depth, meters	Temperature, °C.	Salinity, °/oo	σ_t
0	17.36	35.72	0	17.36	35.72	25.91
24	17.22	35.735	25	17.20	35.74	26.05
48	16.00	36.08	50	15.95	36.07	26.60
72	15.51	36.02	75	15.45	36.00	26.66
97	14.85	35.90	100	14.80	35.89	26.71
144	13.95	35.78	150	13.90	35.78	26.82
193	13.58	35.76	200	13.45	35.75	26.90
290	11.81	35.51	300	11.50	35.47	27.07
375	9.44	35.20	400	9.00	35.17	27.27
566	6.20	35.02	600	6.00	35.02	27.59
760	5.13	35.02	800	5.05	35.02	27.71
957	4.64	35.02	1,000	4.55	35.01	27.76
1,464	3.69	34.92				

Station 7484; 25 June; 43°43′ N., 47°19′ W.; depth 4,115 m.; dynamic height 971.096

Observed values			Scaled values			
Depth, meters	Temperature, °C.	Salinity, °/oo	Depth, meters	Temperature, °C.	Salinity, °/oo	σ_t
0	16.38	35.12	0	16.38	35.12	25.77
25	15.74	34.95	25	15.74	34.95	25.79
50	8.42	34.38	50	8.42	34.38	26.74
75	10.04	34.91	75	10.04	34.91	26.89
100	8.85	34.95	100	8.85	34.90	27.08
150	8.95	34.90	150	8.95	34.95	27.11
200	8.60	34.99	200	8.60	34.99	27.19
300	4.93	34.64	300	4.93	34.64	27.42
349	4.96	34.78	400	4.85	34.82	27.57
521	4.67	34.92	600	4.55	34.94	27.70
692	4.45	34.96	800	4.15	34.93	27.73
878	3.98	34.91	1,000	3.90	34.91	27.75
1,367	3.62	34.91				

Station 7485; 25 June; 43°55′ N., 47°58′ W.; depth 3,658 m.; dynamic height 970.972

Observed values			Scaled values			
Depth, meters	Temperature, °C.	Salinity, °/oo	Depth, meters	Temperature, °C.	Salinity, °/oo	σ_t
0	8.64	32.67	0	8.64	32.67	25.37
25	3.78	33.21	25	3.78	33.21	26.41
51	2.63	33.80	50	2.65	33.79	26.81
76	2.67	34.02	75	2.65	34.01	27.15
102	3.15	34.23	100	3.10	34.21	27.27
152	3.39	34.47	150	3.35	34.45	27.43
202	3.58	34.62	200	3.55	34.61	27.54
304	4.18	34.82	300	4.15	34.81	27.64
397	4.38	34.91	400	4.40	34.91	27.69
596	4.11	34.92	600	4.10	34.92	27.74
790	3.92	34.93	800	3.90	34.93	27.76
991	3.59	34.91	1,000	3.60	34.91	27.78
1,490	3.50	34.92				

Station 7486; 26 June; 44°04′ N., 48°30′ W.; depth 2,743 m.; dynamic height 970.963

Observed values			Scaled values			
Depth, meters	Temperature, °C.	Salinity, °/oo	Depth, meters	Temperature, °C.	Salinity, °/oo	σ_t
0	9.50	33.08	0	9.50	33.08	25.56
25	4.97	33.44	25	4.97	33.44	26.47
52	2.53	33.94	50	2.70	33.91	27.06
77	2.74	34.12	75	2.70	34.10	27.21
103	3.48	34.27	100	3.40	34.25	27.27
154	3.85	34.58	150	3.80	34.55	27.47
206	3.69	34.58	200	3.70	34.58	27.50
309	4.39	34.83	300	4.35	34.81	27.62
398	4.45	34.91	400	4.45	34.91	27.69
600	4.08	34.92	600	4.08	34.92	27.74
802	3.81	34.92	800	3.80	34.92	27.77
1,006	3.65	34.91	1,000	3.65	34.91	27.77
1,518	3.49	34.90				

Station 7487; 26 June; 44°08′ N., 48°45′ W.; depth 1,591 m.; dynamic height 971.017

Observed values			Scaled values			
Depth, meters	Temperature, °C.	Salinity, °/oo	Depth, meters	Temperature, °C.	Salinity, °/oo	σ_t
0	6.94	32.54	0	6.94	32.54	25.52
24	3.58	32.78	25	3.55	32.79	26.10
49	2.51	33.15	50	2.50	33.16	26.48
74	−0.19	33.34	75	−0.20	33.35	26.80
98	0.96	33.81	100	1.00	33.82	27.12
147	1.50	34.11	150	1.50	34.13	27.33
197	2.27	34.38	200	2.30	34.39	27.48
296	3.23	34.685	300	3.25	34.68	27.62
402	3.58	34.80	400	3.60	34.79	27.68
602	3.70	34.82	600	3.70	34.82	27.70
803	3.59	34.87	800	3.60	34.87	27.75
1,009	3.55	34.87	1,000	3.55	34.87	27.75
1,523	3.56	34.92				

Station 7488; 26 June; 44°10′ N., 48°53′ W.; depth 626 m.; dynamic height 971.041

Observed values			Scaled values			
Depth, meters	Temperature, °C.	Salinity, °/oo	Depth, meters	Temperature, °C.	Salinity, °/oo	σ_t
0	6.42	32.38	0	6.42	32.38	25.46
25	2.27	32.73	25	2.27	32.73	26.16
52	−0.75	33.04	50	−0.55	33.02	26.55
77	−0.63	33.29	75	−0.65	33.26	26.75
103	0.02	33.54	100	−0.05	33.51	26.93
154	1.05	33.92	150	0.95	33.89	27.17
205	1.95	34.26	200	1.85	34.23	27.38
308	2.95	34.60	300	2.85	34.57	27.58
410	3.46	34.77	400	3.40	34.76	27.68
609	3.69	34.85	600	3.70	34.85	27.72

Station 7489; 26 June; 44°11′ N., 48°59′ W.; depth 167 m.; dynamic height 971.099

Observed values			Scaled values			
Depth, meters	Temperature, °C.	Salinity, °/oo	Depth, meters	Temperature, °C.	Salinity, °/oo	σ_t
0	6.28	32.36	0	6.28	32.36	25.46
25	−1.24	32.79	25	−1.24	32.79	26.39
50	−1.15	33.03	50	−1.15	33.03	26.58
75	−0.55	33.24	75	−0.55	33.24	26.73
99	−0.31	33.415	100	−0.30	33.42	26.87
149	0.90	33.85	150	0.90	33.85	27.15

Station 7490; 26 June; 44°13′ N., 49°07′ W.; depth 60 m.; dynamic height 971.118

Observed values			Scaled values			
Depth, meters	Temperature, °C.	Salinity, °/oo	Depth, meters	Temperature, °C.	Salinity, °/oo	σ_t
0	6.32	32.49	0	6.32	32.49	25.55
18	0.55	32.73	25	0.25	32.79	26.34
43	−0.91	32.96	(50)	−1.00	33.01	26.56

TABLE OF OCEANOGRAPHIC DATA—Continued

Station 7491; 26 June; 44°16′ N., 49°24′ W.; depth 53 m.; dynamic height 971.122

Observed values			Scaled values			
Depth, meters	Temperature, °C.	Salinity, °/oo	Depth, meters	Temperature, °C.	Salinity, °/oo	σ_t
0	9.02	32.62	0	9.02	32.62	25.28
15	------	32.62	25	5.75	32.80	25.87
40	1.00	33.07	(50)	−0.25	33.15	26.64

Station 7492; 26 June; 44°59′ N., 49°24′ W.; depth 64 m.; dynamic height 971.127

Observed values			Scaled values			
Depth, meters	Temperature, °C.	Salinity, °/oo	Depth, meters	Temperature, °C.	Salinity, °/oo	σ_t
0	7.52	32.47	0	7.51	32.47	25.38
26	3.95	32.47	25	4.00	32.47	25.80
51	−0.85	32.91	50	−0.80	32.90	26.46

Station 7493; 26 June; 44°57′ N., 49°12′ W.; depth 98 m.; dynamic height 971.136

Observed values			Scaled values			
Depth, meters	Temperature, °C.	Salinity, °/oo	Depth, meters	Temperature, °C.	Salinity, °/oo	σ_t
0	6.84	32.43	0	6.84	32.43	25.44
23	6.20	32.43	25	5.40	32.47	25.65
48	0.01	32.72	50	−0.10	32.73	26.30
71	−0.86	32.86	(75)	−1.00	32.88	26.45

Station 7494; 26 June; 44°56′ N., 49°02′ W.; depth 549 m.; dynamic height 971.134

Observed values			Scaled values			
Depth, meters	Temperature, °C.	Salinity, °/oo	Depth, meters	Temperature, °C.	Salinity, °/oo	σ_t
0	5.05	32.35	0	5.05	32.35	25.60
20	4.59	32.36	25	3.60	32.45	25.82
40	−1.31	32.74	50	−1.35	32.79	26.39
60	−1.36	32.85	75	−1.05	33.00	26.56
80	−0.96	33.06	100	−0.70	33.16	26.67
120	−0.41	33.26	150	0.05	33.51	26.93
160	0.23	33.59	200	0.90	33.85	27.15
240	1.53	34.12	300	1.95	34.30	27.39
320	------	34.36	400	2.55	34.48	27.53
485	3.06	34.61				

Station 7495; 26 June; 44°53′ N., 48°47′ W.; depth 2,195 m.; dynamic height 970.996

Observed values			Scaled values			
Depth, meters	Temperature, °C.	Salinity, °/oo	Depth, meters	Temperature, °C.	Salinity, °/oo	σ_t
0	5.95	32.71	0	5.95	32.71	25.78
26	5.56	32.83	25	5.55	32.83	25.91
52	3.62	33.64	50	3.80	33.59	26.71
78	1.62	33.74	75	1.95	33.73	26.97
103	1.22	33.96	100	1.25	33.93	27.19
156	1.49	34.18	150	1.40	34.15	27.36
208	2.17	34.41	200	2.05	34.37	27.49
311	3.57	34.74	300	3.40	34.70	27.63
413	4.24	34.88	400	4.15	34.86	27.68
619	3.74	34.88	600	3.80	34.88	27.73
826	3.57	34.89	800	3.60	34.88	27.75
1,040	3.51	34.89	1,000	3.55	34.89	27.76
1,583	3.52	34.89				

Station 7496; 26 June; 44°50′ N., 48°31′ W.; depth 2,561 m.; dynamic height 970.962

Observed values			Scaled values			
Depth, meters	Temperature, °C.	Salinity, °/oo	Depth, meters	Temperature, °C.	Salinity, °/oo	σ_t
0	7.13	32.89	0	7.13	32.89	25.76
25	6.98	33.56	25	6.98	33.56	26.31
49	2.25	33.69	50	2.25	33.69	26.92
73	2.29	33.97	75	2.45	33.99	27.14
97	3.41	34.12	100	3.45	34.14	27.17
147	3.83	34.44	150	3.85	34.45	27.38
196	4.02	34.64	200	4.05	34.65	27.52
293	4.46	34.84	300	4.20	34.85	27.67
351	4.44	34.91	400	4.20	34.92	27.73
537	4.18	34.95	600	4.00	34.93	27.75
730	3.73	34.90	800	3.75	34.91	27.76
924	3.73	34.92	1,000	3.70	34.92	27.78
1,426	3.53	34.93				

Station 7497; 26 June; 44°44′ N., 47°57′ W.; depth 3,484 m.; dynamic height 970.999

Observed values			Scaled values			
Depth, meters	Temperature, °C.	Salinity, °/oo	Depth, meters	Temperature, °C.	Salinity, °/oo	σ_t
0	9.31	33.30	0	9.31	33.30	25.75
27	4.60	33.80	25	5.05	33.76	26.71
52	6.19	34.41	50	6.00	34.35	27.02
79	6.76	34.52	75	6.70	34.51	27.10
104	6.77	34.52	100	6.75	34.52	27.10
157	6.68	34.67	150	6.70	34.65	27.20
210	5.84	34.72	200	6.00	34.71	27.35
314	4.96	34.86	300	5.10	34.83	27.55
394	4.35	34.87	400	4.35	34.87	27.67
591	3.76	34.88	600	3.75	34.88	27.73
791	3.61	34.90	800	3.60	34.89	27.76
993	3.57	34.90	1,000	3.55	34.90	27.77
1,505	3.46	34.92				

Station 7498; 27 June; 44°37′ N., 47°20′ W.; depth 3,885 m.; dynamic height 970.914

Observed values			Scaled values			
Depth, meters	Temperature, °C.	Salinity, °/oo	Depth, meters	Temperature, °C.	Salinity, °/oo	σ_t
0	9.85	33.21	0	9.85	33.21	25.60
26	4.75	33.76	25	4.50	33.76	26.77
53	3.08	34.06	50	3.25	34.02	27.10
79	3.57	34.27	75	3.50	34.23	27.24
105	3.62	34.41	100	3.60	34.38	27.35
157	3.77	34.60	150	3.75	34.57	27.49
209	3.62	34.83	200	3.65	34.78	27.66
314	4.51	34.91	300	4.40	34.90	27.68
412	4.28	34.93	400	4.35	34.93	27.71
619	------	34.89	600	3.74	34.90	27.76
826	3.73	34.91	800	3.75	34.91	27.76
1,034	3.80	34.93	1,000	3.80	34.93	27.77
1,555	3.43	34.92				

Station 7499; 27 June; 44°30′ N., 46°36′ W.; depth 3,858 m.; dynamic height 970.996

Observed values			Scaled values			
Depth, meters	Temperature, °C.	Salinity, °/oo	Depth, meters	Temperature, °C.	Salinity, °/oo	σ_t
0	10.38	33.38	0	10.38	33.38	25.65
25	10.63	33.58	25	10.63	33.58	25.76
51	10.79	34.01	50	10.80	34.01	26.06
76	3.13	34.13	75	3.65	34.12	27.15
102	4.14	34.40	100	4.00	34.38	27.31
152	4.72	34.68	150	4.70	34.67	27.47
203	4.68	34.75	200	4.70	34.74	27.52
305	4.76	34.92	300	4.75	34.90	27.64
346	4.18	34.86	400	4.10	34.87	27.70
594	3.89	34.91	600	3.90	34.91	27.75
789	3.82	34.92	800	3.80	34.92	27.77
991	3.57	34.90	1,000	3.55	34.90	27.77
1,502	3.42	34.91				

Station 7500; 27 June; 44°24′ N., 45°57′ W.; depth 3,913 m.; dynamic height 970.974

Observed values			Scaled values			
Depth, meters	Temperature, °C.	Salinity, °/oo	Depth, meters	Temperature, °C.	Salinity, °/oo	σ_t
0	9.60	32.65	0	9.60	32.65	25.20
25	3.40	33.24	25	3.40	33.24	26.47
51	1.58	33.71	50	1.65	33.69	26.97
76	2.46	34.02	75	2.45	34.01	27.16
102	4.53	34.45	100	4.40	34.42	27.31
152	5.16	34.67	150	5.10	34.66	27.42
202	4.78	34.74	200	4.80	34.73	27.50
304	4.49	34.85	300	4.50	34.84	27.62
404	4.40	34.91	400	4.40	34.91	27.69
605	3.97	34.91	600	4.00	34.91	27.74
805	3.75	34.90	800	3.75	34.90	27.75
1,007	3.69	34.91	1,000	3.70	34.91	27.77
1,515	3.49	34.91				

TABLE OF OCEANOGRAPHIC DATA—Continued

Station 7501; 27 June; 44°20′ N., 45°13′ W.; depth 4,206 m.; dynamic height 971.118

Observed values			Scaled values			
Depth, meters	Temperature, °C.	Salinity, °/₀₀	Depth, meters	Temperature, °C.	Salinity, °/₀₀	σ_t
0	12.68	33.22	0	12.68	33.22	25.10
24	10.02	33.33	25	10.00	33.38	25.71
49	8.08	34.23	50	8.10	34.25	26.69
73	9.24	34.69	75	9.25	34.70	26.86
98	9.52	34.90	100	9.40	34.89	26.98
146	6.20	34.44	150	6.10	34.44	27.12
195	5.15	34.42	200	5.20	34.44	27.23
293	6.15	34.81	300	6.10	34.81	27.41
398	5.16	34.80	400	5.15	34.80	27.52
591	4.12	34.87	600	4.10	34.87	27.70
780	4.04	34.89	800	4.05	34.89	27.71
979	3.91	34.91	1,000	3.90	34.91	27.75
1,489	3.62	34.94				

Station 7502; 27 June; 44°50′ N., 45°15′ W.; depth 4,298 m.; dynamic height 970.979

Observed values			Scaled values			
Depth, meters	Temperature, °C.	Salinity, °/₀₀	Depth, meters	Temperature, °C.	Salinity, °/₀₀	σ_t
0	11.97	33.37	0	11.97	33.37	25.35
25	7.43	33.53	25	7.43	33.53	26.22
52	3.91	33.91	50	4.25	33.90	26.90
77	4.61	34.33	75	4.55	34.30	27.19
103	3.85	34.32	100	3.95	34.32	27.28
154	4.57	34.62	150	4.50	34.60	27.43
205	4.11	34.64	200	4.15	34.64	27.50
308	4.41	34.83	300	4.40	34.82	27.62
406	4.87	34.98	400	4.85	34.97	27.68
610	4.10	34.94	600	4.15	34.94	27.74
814	3.92	34.93	800	3.95	34.93	27.75
1,016	3.75	34.94	1,000	3.80	34.94	27.78
1,522	3.44	34.92				

Station 7503; 27 June; 45°20′ N., 45°15′ W.; depth 4,298 m.; dynamic height 971.039

Observed values			Scaled values			
Depth, meters	Temperature, °C.	Salinity, °/₀₀	Depth, meters	Temperature, °C.	Salinity, °/₀₀	σ_t
0	12.21	33.17	0	12.21	33.17	25.15
25	7.86	33.46	25	7.86	33.46	26.11
50	1.00	33.47	50	1.00	33.47	26.84
75	6.28	34.38	75	6.28	34.38	27.05
100	6.30	34.47	100	6.30	34.47	27.12
151	5.49	34.50	150	5.50	34.49	27.23
201	5.67	34.65	200	5.65	34.65	27.34
301	5.79	34.91	300	5.80	34.90	27.52
401	4.79	34.90	400	4.80	34.90	27.64
598	4.27	34.93	600	4.30	34.93	27.71
798	4.01	34.94	800	4.00	34.94	27.76
1,000	3.85	34.93	1,000	3.85	34.93	27.76
1,507	3.48	34.92				

Station 7504; 28 June; 45°16′ N., 45°48′ W.; depth 3,585 m.; dynamic height 971.053

Observed values			Scaled values			
Depth, meters	Temperature, °C.	Salinity, °/₀₀	Depth, meters	Temperature, °C.	Salinity, °/₀₀	σ_t
0	11.63	33.66	0	11.63	33.66	25.64
26	8.70	33.77	25	8.85	33.76	26.18
51	10.17	34.98	50	10.10	34.91	26.89
76	10.44	35.13	75	10.40	35.13	27.00
101	9.17	34.92	100	9.25	34.93	27.04
153	8.41	34.96	150	8.45	34.96	27.19
204	6.95	34.81	200	7.10	34.82	27.29
305	5.75	34.87	300	5.80	34.86	27.49
401	5.41	34.95	400	5.40	34.95	27.61
597	4.74	34.98	600	4.75	34.98	27.70
791	4.24	34.97	800	4.20	34.97	27.77
989	3.94	34.95	1,000	3.95	34.95	27.77
1,484	3.56	34.93				

Station 7505; 28 June; 45°14′ N., 46°33′ W.; depth 3,383 m.; dynamic height 970.966

Observed values			Scaled values			
Depth, meters	Temperature, °C.	Salinity, °/₀₀	Depth, meters	Temperature, °C.	Salinity, °/₀₀	σ_t
0	10.71	33.58	0	10.71	33.58	25.74
26	8.49	33.58	25	8.50	33.58	26.10
51	4.06	34.03	50	4.25	34.00	26.99
77	3.38	34.16	75	3.45	34.15	27.18
102	3.73	34.34	100	3.70	34.32	27.30
153	3.95	34.53	150	3.90	34.52	27.44
204	4.38	34.71	200	4.35	34.70	27.53
306	4.05	34.82	300	4.10	34.81	27.65
403	4.03	34.88	400	4.05	34.88	27.70
606	3.71	34.88	600	3.75	34.88	27.73
811	3.64	34.89	800	3.65	34.89	27.75
1,015	3.57	34.89	1,000	3.60	34.89	27.76
1,532	3.41	34.93				

Station 7506; 28 June; 45°14′ N., 47°11′ W.; depth 3,329 m.; dynamic height 970.942

Observed values			Scaled values			
Depth, meters	Temperature, °C.	Salinity, °/₀₀	Depth, meters	Temperature, °C.	Salinity, °/₀₀	σ_t
0	7.79	33.11	0	7.76	33.11	25.84
24	5.86	33.31	25	5.80	33.32	26.27
48	2.14	33.99	50	2.15	34.00	27.18
72	2.32	34.24	75	2.35	34.25	27.36
97	2.57	34.32	100	2.60	34.33	27.40
144	3.05	34.49	150	3.10	34.51	27.51
192	3.49	34.66	200	3.55	34.68	27.59
289	4.18	34.82	300	4.15	34.83	27.65
398	3.98	34.89	400	4.00	34.89	27.72
588	3.61	34.84	600	3.60	34.84	27.72
792	3.57	34.86	800	3.55	34.86	27.74
994	3.52	34.89	1,000	3.55	34.89	27.76
1,505	3.40	34.91				

Station 7507; 28 June; 45°35′ N., 47°44.5′ W.; depth 1,317 m.; dynamic height 971.003

Observed values			Scaled values			
Depth, meters	Temperature, °C.	Salinity, °/₀₀	Depth, meters	Temperature, °C.	Salinity, °/₀₀	σ_t
0	6.68	32.63	0	6.68	32.63	25.62
25	1.95	32.99	25	1.95	32.99	26.36
51	−0.46	33.32	50	−0.35	33.31	26.77
76	0.52	33.72	75	0.50	33.71	27.06
103	1.86	34.11	100	1.70	34.07	27.27
153	1.72	34.20	150	1.70	34.19	27.36
204	2.28	34.45	200	2.20	34.43	27.52
307	3.23	34.63	300	3.15	34.62	27.59
407	3.63	34.74	400	3.60	34.73	27.63
610	3.67	34.83	600	3.65	34.83	27.70
814	3.60	34.84	800	3.60	34.84	27.72
1,117	3.54	34.84	1,000	3.55	34.84	27.72

Station 7508; 28 June; 45°40′ N., 47°54′ W.; depth 647 m.; dynamic height 971.005

Observed values			Scaled values			
Depth, meters	Temperature, °C.	Salinity, °/₀₀	Depth, meters	Temperature, °C.	Salinity, °/₀₀	σ_t
0	6.80	32.43	0	6.80	32.43	25.44
24	3.73	32.72	25	3.70	32.72	26.03
49	−0.63	32.86	50	−0.65	32.89	26.45
73	−0.99	33.23	75	−0.95	33.24	26.75
99	−0.36	33.42	100	−0.35	33.42	26.87
147	0.85	33.86	150	0.90	33.90	27.19
196	1.68	34.49	200	1.70	34.49	27.60
295	2.64	34.71	300	2.65	34.71	27.71
394	3.31	34.80	400	3.35	34.81	27.72
597	3.70	34.88	600	3.70	34.88	27.75

TABLE OF OCEANOGRAPHIC DATA—Continued

Observed values			Scaled values			
Depth, meters	Temperature, °C.	Salinity, °/oo	Depth, meters	Temperature, °C.	Salinity, °/oo	σ_t
Station 7509; 28 June; 45°46′ N., 48°04′ W.; depth 172 m.; dynamic height 971.098						
0	6.32	32.30	0	6.32	32.30	25.40
25	5.99	32.32	25	5.99	32.32	25.46
50	−0.76	32.82	50	−0.76	32.82	26.40
76	−1.14	33.05	75	−1.10	33.05	26.60
101	−0.66	33.25	100	−0.70	33.23	26.73
152	0.06	33.56	150	0.05	33.55	26.96
Station 7510; 28 June; 45°51′ N., 48°12′ W.; depth 104 m.; dynamic height 971.091						
0	7.69	32.57	0	7.69	32.57	25.44
26	1.99	32.51	25	2.20	32.51	25.98
52	−1.26	32.80	50	−1.00	32.77	26.37
78	−1.02	32.98	75	−1.05	32.95	26.52
104	−0.28	33.30	100	−0.40	33.25	26.74
Station 7511; 28 June; 45°56′ N., 48°20′ W.; depth 91 m.; dynamic height 971.095						
0	8.02	32.60	0	8.01	32.60	25.42
24	7.15	32.60	25	6.80	32.60	25.58
49	−0.93	32.81	50	−0.90	32.83	26.41
73	−0.23	33.22	75	−0.20	33.24	26.72
Station 7512; 28 June; 46°04′ N., 48°34′ W.; depth 75 m.; dynamic height 971.094						
0	7.83	32.62	0	7.83	32.62	25.46
25	5.93	32.60	25	5.93	32.60	25.70
49	−0.55	32.92	50	−0.55	32.93	26.48
64	−0.17	33.24				
Station 7513; 28 June; 46°18′ N., 48°58′ W.; depth 70 m.; dynamic height 971.095						
0	8.18	32.66	0	8.18	32.66	25.44
26	5.54	32.68	25	5.60	32.67	25.78
51	1.00	32.91	50	1.20	32.89	26.35
Station 7514; 29 June; 46°15′ N., 48°35′ W.; depth 89 m.; dynamic height 971.086						
0	7.59	32.60	0	7.59	32.60	25.47
25	4.97	32.63	25	4.97	32.63	25.83
49	0.12	32.93	50	0.10	32.94	26.47
74	0.06	33.34	(75)	0.05	33.35	26.80
Station 7515; 29 June; 46°12′ N., 48°02′ W.; depth 117 m.; dynamic height 971.092						
0	7.19	32.49	0	7.19	32.49	25.52
25	3.11	32.47	25	3.11	32.47	25.88
50	−1.20	32.78	50	−1.20	32.78	26.38
75	−1.37	32.94	75	−1.37	32.94	26.52
100	0.13	33.40	100	0.13	33.40	26.84

Observed values			Scaled values			
Depth, meters	Temperature, °C.	Salinity, °/oo	Depth, meters	Temperature, °C.	Salinity, °/oo	σ_t
Station 7516; 29 June; 46°10′ N., 47°45.5′ W.; depth 174 m.; dynamic height 971.102						
0	5.87	32.28	0	5.87	32.28	25.56
25	4.41	32.34	25	4.41	32.34	25.66
50	−1.20	32.78	50	−1.20	32.78	26.38
75	−1.24	32.95	75	−1.24	32.95	26.52
100	−0.94	33.18	100	−0.94	33.18	26.70
150	−0.06	33.50	150	−0.06	33.50	26.92
Station 7517; 29 June; 46°05′ N., 47°25′ W.; depth 649 m.; dynamic height 971.032						
0	6.49	32.41	0	6.49	32.41	25.47
25	3.99	32.74	25	3.99	32.74	26.02
52	−1.14	33.025	50	−0.65	33.05	26.58
77	−1.14	33.23	75	−1.15	33.25	26.76
103	−0.13	33.53	100	−0.20	33.49	26.92
154	1.17	33.925	150	1.05	33.89	27.17
206	1.90	34.33	200	1.80	34.28	27.43
309	2.95	34.625	300	2.85	34.60	27.60
404	3.54	34.82	400	3.55	34.81	27.70
593	3.65	34.85	600	3.65	34.85	27.72
Station 7518; 29 June; 46°04.5′ N., 47°10.5′ W.; depth 593 m.; dynamic height 970.948						
0	6.20	32.62	0	6.20	32.62	25.68
25	3.08	33.27	25	3.08	33.27	26.52
51	0.32	33.63	50	0.35	33.61	26.99
76	0.74	33.93	75	0.70	33.92	27.22
102	1.62	34.18	100	1.55	34.16	27.35
152	2.54	34.46	150	2.50	34.45	27.51
203	2.61	34.58	200	2.60	34.57	27.60
305	3.03	34.70	300	3.00	34.69	27.66
371	3.43	34.81	400	3.45	34.81	27.71
568	3.62	34.84	600	3.60	34.84	27.72
771	3.58	34.86	800	3.60	34.86	27.74
1,088	3.51	34.88	1,000	3.55	34.87	27.75
Station 7519; 29 June; 46°05.5′ N., 47°32′ W.; depth 686 m.; dynamic height 970.931						
0	7.89	33.32	0	7.89	33.32	25.98
25	6.50	33.92	25	6.50	33.92	26.66
51	3.96	34.22	50	4.00	34.21	27.18
76	4.02	34.40	75	4.00	34.39	27.32
102	4.04	34.46	100	4.05	34.45	27.36
152	4.10	34.66	150	4.10	34.65	27.52
203	4.30	34.78	200	4.30	34.77	27.60
305	4.25	34.86	300	4.25	34.86	27.67
407	3.74	34.86	400	3.80	34.86	27.72
601	3.70	34.87	600	3.70	34.87	27.74
Station 7520; 29 June; 46°04′ N., 45°59′ W.; depth 1,829 m.; dynamic height 970.962						
0	7.84	33.25	0	7.84	33.25	25.94
25	7.94	33.62	25	7.94	33.62	26.23
50	5.40	34.02	50	5.40	34.02	26.88
75	1.55	33.99	75	1.55	33.99	27.21
100	2.72	34.28	100	2.72	34.28	27.35
149	2.90	34.39	150	2.90	34.39	27.43
198	3.09	34.51	200	3.10	34.51	27.51
298	4.41	34.88	300	4.40	34.88	27.66
371	4.03	34.86	400	4.00	34.87	27.71
560	3.90	34.90	600	3.85	34.90	27.74
752	3.67	34.90	800	3.65	34.89	27.75
943	3.59	34.86	1,000	3.55	34.86	27.74
1,424	3.45	34.87				

TABLE OF OCEANOGRAPHIC DATA—Continued

Observed values			Scaled values			
Depth, meters	Temperature, °C.	Salinity, ‰	Depth, meters	Temperature, °C.	Salinity, ‰	σ_t
Station 7521; 29 June; 46°00′ N., 45°18′ W.; depth 3,072 m.; dynamic height 970.946						
0	9.14	33.43	0	9.14	33.43	25.89
22	9.06	33.68	25	8.60	33.72	26.20
45	3.99	34.11	50	3.90	34.13	27.12
67	3.65	34.19	75	3.70	34.24	27.23
90	3.86	34.35	100	3.90	34.39	27.33
135	3.93	34.57	150	4.50	34.67	27.49
180	5.69	34.89	200	5.65	34.92	27.56
270	5.41	35.00	300	5.10	34.97	27.66
376	4.24	34.90	400	4.15	34.90	27.71
569	3.69	34.88	600	3.60	34.88	27.75
767	3.53	34.87	800	3.55	34.88	27.75
955	3.49	34.88	1,000	3.50	34.88	27.76
1,424	3.42	34.91				
Station 7522; 29 June; 45°59′ N., 44°33′ W.; depth 3,695 m.; dynamic height 970.924						
0	9.82	34.06	0	9.82	34.06	26.27
25	9.19	34.06	25	9.19	34.06	26.37
51	6.60	34.34	50	6.75	34.33	26.94
76	5.19	34.47	75	5.25	34.47	27.25
102	4.59	34.59	100	4.65	34.58	27.40
152	4.08	34.67	150	4.10	34.67	27.54
204	3.91	34.76	200	3.95	34.75	27.61
306	3.88	34.85	300	3.90	34.85	27.70
408	3.95	34.91	400	3.95	34.90	27.73
607	3.81	34.92	600	3.80	34.91	27.76
803	3.62	34.90	800	3.65	34.90	27.76
1,006	3.65	34.92	1,000	3.65	34.92	27.78
1,515	3.42	34.93				
Station 7523; 30 June; 46°22′ N., 44°40′ W.; depth 1,737 m.; dynamic height 970.885						
0	9.17	33.99	0	9.17	33.99	26.32
25	7.15	34.28	25	7.15	34.28	26.85
52	4.01	34.46	50	4.25	34.45	27.34
77	3.77	34.51	75	3.80	34.50	27.43
103	3.51	34.57	100	3.55	34.63	27.55
154	3.63	34.71	150	3.65	34.69	27.59
205	3.63	34.79	200	3.65	34.78	27.66
308	3.60	34.84	300	3.60	34.84	27.72
407	3.62	34.86	400	3.60	34.86	27.74
606	3.54	34.87	600	3.55	34.87	27.75
802	3.47	34.87	800	3.50	34.87	27.76
1,006	3.47	34.87	1,000	3.45	34.87	27.76
1,519	3.46	34.91				
Station 7524; 30 June; 46°28′ N., 44°44′ W.; depth 633 m.; dynamic height 970.906						
0	9.28	33.96	0	9.28	33.96	26.28
25	8.63	34.02	25	8.63	34.02	26.43
51	3.88	34.35	50	4.05	34.34	27.28
76	3.27	34.47	75	3.30	34.46	27.45
102	3.25	34.53	100	3.25	34.52	27.50
152	3.42	34.66	150	3.40	34.65	27.59
204	3.76	34.83	200	3.75	34.81	27.68
306	3.70	34.84	300	3.70	34.84	27.71
406	3.69	34.86	400	3.70	34.86	27.73
605	3.64	34.88	600	3.65	34.87	27.74
Station 7525; 30 June; 46°33′ N., 44°46′ W.; depth 217 m.; dynamic height 970.942						
0	9.10	33.99	0	9.10	33.99	26.33
25	8.37	33.98	25	8.37	33.98	26.44
50	6.46	34.16	50	6.46	34.16	26.85
75	3.41	34.15	75	3.41	34.15	27.19
100	3.25	34.33	100	3.25	34.33	27.33
150	3.26	34.52	150	3.26	34.52	27.50
200	3.47	34.65	200	3.47	34.65	27.58
Station 7526; 30 June; 46°39′ N., 44°48′ W.; depth 169 m.; dynamic height 970.928						
0	9.18	34.01	0	9.18	34.01	26.34
25	6.65	34.02	25	6.65	34.02	26.72
50	4.22	34.06	50	4.22	34.06	27.04
75	3.23	34.25	75	3.23	34.25	27.13
100	3.41	34.38	100	3.41	34.38	27.37
150	3.64	34.60	150	3.64	34.60	27.52
Station 7527; 30 June; 46°53′ N., 44°55′ W.; depth 153 m.; dynamic height 970.938						
0	9.34	33.98	0	9.34	33.98	26.29
25	8.72	33.99	25	8.72	33.99	26.39
50	5.67	34.05	50	5.67	34.05	26.87
75	3.42	34.22	75	3.42	34.22	27.24
100	3.48	34.42	100	3.48	34.42	27.40
135	3.44	34.50	(150)	3.45	34.53	27.48
Station 7528; 30 June; 46°53′ N., 45°13′ W.; depth 224 m.; dynamic height 970.935						
0	9.47	33.98	0	9.47	33.98	26.26
25	8.73	33.94	25	8.73	33.94	26.35
50	5.71	34.05	50	5.71	34.05	26.86
74	3.49	34.30	75	3.50	34.30	27.30
99	3.47	34.42	100	3.45	34.42	27.40
148	3.36	34.56	150	3.35	34.57	27.53
198	3.66	34.71	(200)	3.65	34.71	27.61
Station 7529; 30 June; 46°50′ N., 45°42′ W.; depth 281 m.; dynamic height 970.954						
0	9.30	33.82	0	9.30	33.82	26.17
25	8.75	33.87	25	8.75	33.87	26.30
49	5.59	33.99	50	5.60	33.99	26.82
74	5.69	34.09	75	5.65	34.09	26.90
98	3.26	34.19	100	3.25	34.20	27.24
147	3.71	34.54	150	3.70	34.55	27.48
196	3.81	34.73	200	3.80	34.73	27.61
255	3.77	34.74				
Station 7530; 30 June; 46°48′ N., 46°07′ W.; depth 329 m.; dynamic height 970.955						
0	9.36	33.74	0	9.36	33.74	26.09
24	8.39	33.91	25	8.40	33.91	26.38
49	8.79	34.02	50	8.75	34.02	26.40
74	3.66	34.08	75	3.65	34.09	27.12
99	3.35	34.26	100	3.35	34.27	27.29
147	3.67	34.53	150	3.70	34.54	27.47
197	3.77	34.73	200	3.75	34.73	27.61
296	3.71	34.86	(300)	3.70	34.87	27.74

TABLE OF OCEANOGRAPHIC DATA—Continued

Observed values			Scaled values			
Depth, meters	Temperature, °C.	Salinity, ‰	Depth, meters	Temperature, °C.	Salinity, ‰	σ_t
Station 7531: 30 June; 46°49′ N., 46°34′ W.; depth 622 m.; dynamic height 970.908						
0	8.16	33.52	0	8.16	33.52	26.12
19	8.08	33.66	25	6.95	33.82	26.52
39	4.08	34.28	50	3.25	34.30	27.32
58	2.57	34.32	75	2.70	34.36	27.42
78	2.77	34.37	100	3.15	34.45	27.45
117	3.49	34.515	150	3.90	34.71	27.59
156	4.01	34.75	200	3.85	34.78	27.64
235	3.75	34.81	300	3.75	34.85	27.71
304	3.76	34.85	400	3.65	34.86	27.73
444	3.62	34.87				
Station 7532; 30 June; 46°50′ N., 46°49′ W.; depth 1,234 m.; dynamic height 970.895						
0	8.05	33.51	0	8.05	33.51	26.12
25	4.37	33.59	25	4.37	33.59	26.65
50	2.81	34.12	50	2.81	34.12	27.23
75	2.32	34.32	75	2.32	34.32	27.42
100	2.98	34.47	100	2.98	34.47	27.49
148	2.52	34.53	150	2.55	34.53	27.57
198	2.82	34.64	200	2.85	34.65	27.64
298	3.75	34.85	300	3.75	34.85	27.71
396	3.70	34.87	400	3.70	34.87	27.74
593	3.61	34.88	600	3.60	34.88	27.75
782	3.50	34.89	800	3.50	34.89	27.77
1,090	3.46	34.90	1,000	3.50	34.90	27.78
Station 7533; 30 June; 46°52′ N., 47°17′ W.; depth 622 m.; dynamic height 970.995						
0	6.74	32.64	0	6.74	32.64	25.54
23	5.10	32.69	25	4.95	32.72	25.90
47	1.37	33.17	50	1.25	33.20	26.61
70	−0.44	33.49	75	−0.30	33.52	26.95
94	0.45	33.65	100	0.50	33.71	27.06
140	1.11	34.07	150	1.35	34.13	27.35
186	2.13	34.38	200	2.20	34.42	27.52
280	2.84	34.79	300	3.00	34.66	27.64
369	3.62	34.62	400	3.60	34.81	27.70
547	3.63	34.865	(600)	3.65	34.88	27.74
Station 7534; 30 June; 46°51′ N., 47°25′ W., depth 320 m.; dynamic height 971.018						
0	6.76	32.47	0	6.76	32.47	25.48
23	1.85	32.77	25	1.65	32.78	26.24
47	−1.47	33.01	50	−1.45	33.03	26.59
70	−1.28	33.28	75	−1.05	33.32	26.81
94	−0.16	33.52	100	−0.05	33.58	26.98
141	1.24	34.00	150	1.35	34.05	27.27
188	1.92	34.28	200	2.00	34.30	27.43
282	2.66	34.52	(300)	2.80	34.56	27.57
Station 7535; 30 June; 46°50′ N., 47°44′ W.; depth 170 m.; dynamic height 971.037						
0	6.03	32.30	0	6.03	32.30	25.44
25	1.14	32.48	25	1.14	32.48	26.04
51	−1.54	32.85	50	−1.45	32.82	26.42
76	−1.46	32.99	75	−1.45	32.98	26.55
102	−0.70	33.25	100	−0.75	33.23	26.73
152	0.29	33.53	150	0.25	33.52	26.93

Observed values			Scaled values			
Depth, meters	Temperature, °C.	Salinity, ‰	Depth, meters	Temperature, °C.	Salinity, ‰	σ_t
Station 7536; 1 July; 46°49′ N., 48°14′ W.; depth 119 m.; dynamic height 971.074						
0	7.26	32.33	0	7.26	32.33	25.31
25	3.77	32.56	25	3.77	32.56	25.89
51	−0.86	32.85	50	−0.75	32.84	26.42
76	−0.93	33.03	75	−0.90	33.02	26.57
102	0.06	33.33	100	0.00	33.30	26.75
Station 7537; 1 July; 46°48′ N., 48°44′ W.; depth 93 m.; dynamic height 971.079						
0	7.01	32.44	0	7.01	32.44	25.43
26	5.27	32.44	25	5.30	32.44	25.64
53	0.32	32.87	50	0.90	32.82	26.32
79	−0.08	33.26	75	0.00	33.21	26.69
Station 7538; 6 July; 50°03′ N., 49°05′ W.; depth 1,728 m.; dynamic height 970.853						
0	8.52	33.81	0	8.52	33.81	26.28
24	6.25	34.33	25	6.20	34.34	27.02
49	4.05	34.56	50	4.00	34.56	27.46
73	3.38	34.66	75	3.40	34.67	27.61
97	3.47	34.72	100	3.45	34.73	27.64
147	3.41	34.78	150	3.40	34.78	27.69
196	3.44	34.81	200	3.50	34.81	27.71
293	3.51	34.84	300	3.50	34.84	27.73
388	3.52	34.88	400	3.50	34.87	27.76
582	3.45	34.87	600	3.45	34.87	27.76
778	3.34	34.87	800	3.35	34.87	27.77
978	3.36	34.88	1,000	3.35	34.88	27.77
1,483	3.40	34.92				
Station 7539; 6 July; 49°52′ N., 49°36′ W.; depth 1,170 m.; dynamic height 970.892						
0	7.81	32.68	0	7.81	32.68	25.50
24	0.59	33.85	25	0.60	33.86	27.17
48	0.51	34.03	50	0.55	34.05	27.33
72	1.81	34.30	75	1.80	34.31	27.46
97	1.92	34.42	100	2.00	34.42	27.53
144	2.45	34.51	150	2.50	34.53	27.57
192	2.76	34.62	200	2.80	34.63	27.62
289	3.26	34.78	300	3.30	34.78	27.70
386	3.40	34.82	400	3.40	34.82	27.73
580	3.38	34.85	600	3.40	34.85	27.75
776	3.45	34.87	800	3.45	34.87	27.76
976	3.44	34.87	1,000	3.45	34.88	27.76
1,130	3.45	34.89				
Station 7540; 6 July; 49°45′ N., 50°00′ W.; depth 627 m.; dynamic height 970.946						
0	7.95	32.18	0	7.95	32.18	25.88
24	4.66	33.01	25	4.55	33.05	26.20
48	−0.81	33.69	50	−0.75	33.70	27.11
72	0.06	33.88	75	0.20	33.91	27.24
97	1.45	34.15	100	1.45	34.16	27.36
144	1.49	34.32$_5$	150	1.60	34.35	27.42
192	2.50	34.55	200	2.55	34.57	27.61
289	3.21	34.74	300	3.25	34.75	27.68
386	3.39	34.80	400	3.40	34.80	27.71
581	3.42	34.83	(600)	3.45	34.83	27.72

TABLE OF OCEANOGRAPHIC DATA—Continued

Observed values			Scaled values			
Depth, meters	Temperature, °C.	Salinity, °/₀₀	Depth, meters	Temperature, °C.	Salinity, °/₀₀	σ_t
Station 7541; 6 July; 49°34′ N., 50°28′ W.; depth 336 m.; dynamic height 970.994						
0	8.74	31.87	0	8.74	31.87	24.74
25	2.18	32.82	25	2.18	32.82	26.24
51	−1.44	33.09	50	−1.25	33.09	26.71
76	−0.87	33.34	75	−0.90	33.33	26.82
102	−0.10	33.72	100	−0.20	33.70	27.09
152	0.88	34.09	150	0.80	34.07	27.33
203	2.15	34.43	200	2.05	34.41	27.52
305	3.21	34.76	300	3.35	34.75	27.67
Station 7542; 6 July; 49°24′ N., 51°01′ W.; depth 340 m.; dynamic height 971.066						
0	9.15	30.40	0	9.15	30.40	23.52
25	1.54	32.53	25	1.54	32.53	26.05
50	−1.24	32.92	50	−1.24	32.92	26.50
75	−1.30	33.12	75	−1.30	33.12	26.66
101	−1.30	33.30	100	−1.30	33.30	26.80
151	0.39	33.77	150	0.35	33.76	27.07
201	1.45	34.16	200	1.45	34.15	27.35
302	2.74	34.60	300	2.70	34.58	27.59
Station 7543; 6 July; 49°13′ N., 51°32′ W.; depth 320 m.; dynamic height 971.066						
0	9.74	30.21	0	9.74	30.21	23.28
24	−0.52	32.19	25	−0.55	32.21	25.90
49	−0.67	32.81	50	−0.70	32.81	26.40
74	−1.26	33.13	75	−1.25	33.14	26.67
99	−1.23	33.32	100	−1.20	33.33	26.83
147	−0.24	33.76	150	−0.15	33.78	27.15
197	1.63	34.16	200	1.70	34.18	27.35
296	3.05	34.67	(300)	3.15	34.69	27.64
Station 7544; 6 July; 49°06′ N., 51°51′ W.; depth 294 m.; dynamic height 971.091						
0	8.91	30.18	0	8.91	30.18	23.39
25	4.99	32.22	25	4.99	32.22	25.50
50	−0.75	32.90	50	−0.75	32.90	26.46
75	−1.45	33.04	75	−1.45	33.04	26.60
100	−1.18	33.18	100	−1.18	33.18	26.70
149	−0.63	33.58	150	−0.60	33.59	26.95
199	0.88	34.00	200	0.85	34.01	27.28
274	2.55	34.46	(300)	3.10	34.62	27.60
Station 7545; 6 July; 49°00′ N., 52°08′ W.; depth 294 m.; dynamic height 971.152						
0	10.58	30.66	0	10.58	30.66	23.50
25	−1.11	32.45	25	−1.11	32.45	26.12
51	−1.42	32.67	50	−1.40	32.66	26.29
76	−1.58	32.74	75	−1.55	32.74	26.34
102	−1.57	32.80	100	−1.50	32.79	26.40
152	−1.50	32.91	150	−1.50	32.90	26.48
202	−0.95	33.44	200	−0.95	33.42	26.90
278	2.04	34.315	(300)	2.80	34.53	27.55
Station 7546; 7 July; 48°52′ N., 52°27′ W.; depth 355 m.; dynamic height 971.168						
0	8.41	31.74	0	8.41	31.74	24.68
19	4.38	32.22	25	2.70	32.37	25.83
39	−1.37	32.70	50	−1.50	32.75	26.36
59	−1.62	32.79	75	−1.60	32.83	26.43
79	−1.57	32.84	100	−1.50	32.87	26.46
118	−1.47	32.90	150	−1.35	32.93	26.51
157	−1.33	32.94	200	−0.45	33.28	26.76
236	0.20	33.56	(300)	1.65	34.07	27.28

Observed values			Scaled values			
Depth, meters	Temperature, °C.	Salinity, °/₀₀	Depth, meters	Temperature, °C.	Salinity, °/₀₀	σ_t
Station 7547; 7 July; 48°46′ N., 52°40′ W.; depth 236 m. dynamic height 971.164						
0	10.03	31.04	0	10.03	31.04	23.88
25	5.39	32.20	25	5.39	32.20	25.43
52	−1.43	32.75	50	−1.43	32.75	26.36
75	−0.94	32.85	75	−0.94	32.85	26.43
99	−1.33	32.93	100	−1.35	32.94	26.52
149	−1.13	33.19	150	−1.10	33.20	26.72
199	−0.40	33.52	200	−0.90	33.53	26.98
Station 7548; 7 July; 48°44′ N., 52°45′ W.; depth 163 m; dynamic height 971.155						
0	9.35	31.03	0	9.35	31.03	23.99
25	2.56	32.35	25	2.56	32.35	25.83
50	−1.49	32.75	50	−1.49	32.75	26.36
75	−1.59	32.82	75	−1.59	32.82	26.43
100	−1.49	32.94	100	−1.49	32.94	26.52
150	−1.09	33.16	150	−1.09	33.16	26.68
Station 7549; 7 July; 48°44′ N., 52°57′ W.; depth 99 m.; dynamic height 971.167						
0	12.25	30.78	0	12.25	30.78	23.29
25	−0.88	32.41	25	−0.88	32.41	26.08
52	−1.40	32.59	50	−1.35	32.57	26.22
77	−1.47	32.69	75	−1.45	32.68	26.31
Station 7550; 7 July; 48°38′ N., 52°44′ W.; depth 158 m.; dynamic height 971.138						
0	9.59	31.18	0	9.59	31.18	24.06
25	−0.41	32.45	25	−0.41	32.45	26.09
51	−1.44	32.68	50	−1.40	32.67	26.30
77	−1.52	32.80	75	−1.50	32.79	26.40
103	−1.47	32.91	100	−1.50	32.89	26.47
153	−1.40	32.96	150	−1.40	32.96	26.53
Station 7551; 7 July; 48°34′ N., 52°34′ W.; depth 236 m.; dynamic height 971.129						
0	9.58	31.40	0	9.58	31.40	24.24
26	3.21	32.31	25	3.30	32.30	25.72
51	−1.47	32.72	50	−1.40	32.71	26.33
77	−1.63	32.79	75	−1.60	32.78	26.39
102	−1.43	32.89	100	−1.45	32.88	26.47
152	−1.22	33.195	150	−1.25	33.18	26.70
203	−0.47	33.47	200	−0.50	33.45	26.90
Station 7552; 7 July; 48°18′ N., 52°01′ W.; depth 179 m.; dynamic height 971.134						
0	10.35	31.29	0	10.35	31.29	24.03
25	6.81	32.14	25	6.81	32.14	25.22
51	−1.48	32.73	50	−1.40	32.72	26.34
77	−1.52	32.83	75	−1.50	32.82	26.42
103	−1.38	32.94	100	−1.35	32.93	26.51
153	−0.76	33.36	150	−0.80	33.34	26.82
Station 7553; 7 July; 48°12′ N., 51°48′ W.; depth 177 m.; dynamic height 971.142						
0	10.43	31.35	0	10.42	31.35	24.06
26	4.45	32.05	25	4.50	32.04	25.41
52	−1.39	32.61	50	−1.20	32.58	26.22
78	−1.53	32.76	75	−1.50	32.74	26.36
104	−1.42	32.88	100	−1.45	32.86	26.45
145	−1.25	33.10	(150)	−1.20	33.12	26.66

TABLE OF OCEANOGRAPHIC DATA—Continued

Observed values			Scaled values			
Depth, meters	Temperature, °C.	Salinity, ‰	Depth, meters	Temperature, °C.	Salinity, ‰	σ_t
Station 7554; 7 July; 48°04′ N., 51°30′ W.; depth 164 m.; dynamic height 971.116						
0	11.00	31.58	0	11.00	31.58	24.14
25	0.53	32.43	25	0.53	32.43	26.03
50	−1.39	32.66	50	−1.39	32.66	26.29
74	−1.52	32.78	75	−1.50	32.78	26.39
99	−1.41	32.89	100	−1.45	32.90	26.54
149	0.06	33.34	150	0.10	33.35	26.80
Station 7555; 7 July; 47°55′ N., 51°12′ W.; depth 142 m.; dynamic height 971.097						
0	9.34	32.05	0	9.34	32.05	24.78
25	1.83	32.58	25	1.83	32.58	26.07
50	−1.32	32.78	50	−1.32	32.78	26.36
75	−1.19	32.86	75	−1.19	32.86	26.45
100	−0.36	33.14	100	−0.36	33.14	26.64
130	0.01	33.30				
Station 7556; 7 July; 47°48′ N., 50°53′ W.; depth 140 m.; dynamic height 971.098						
0	9.06	32.12	0	9.06	32.12	24.88
25	3.44	32.47	25	3.44	32.47	25.85
50	−0.53	32.77	50	−0.53	32.77	26.35
75	−0.51	33.02	75	−0.51	33.02	26.55
100	−0.04	33.27	100	−0.04	33.27	26.73
Station 7557; 7 July; 47°40′ N., 50°34′ W.; depth 135 m.; dynamic height 971.105						
0	8.77	32.18	0	8.77	32.18	24.97
25	4.76	32.34	25	4.76	32.34	25.62
50	0.63	32.79	50	0.63	32.79	26.32
75	0.01	32.94	75	0.01	32.94	26.47
100	0.11	33.27	100	0.11	33.27	26.73
Station 7558; 7 July; 47°32′ N., 50°17′ W.; depth 98 m.; dynamic height 971.109						
0	8.97	32.13	0	8.97	32.13	24.90
25	6.05	32.47	25	6.05	32.47	25.53
50	1.65	32.72	50	1.65	32.72	26.19
75	−0.21	33.08	75	−0.21	33.08	26.59
90	−0.03	33.16	(100)	0.05	33.21	26.69
Station 7559; 7 July; 47°28′ N., 50°00′ W.; depth 86 m.; dynamic height 971.102						
0	9.12	32.30	0	9.12	32.30	25.01
25	6.36	32.58	25	6.36	32.58	25.62
50	0.89	32.78	50	0.89	32.78	26.29
70	−0.73	32.98	(75)	−1.00	33.03	26.57
Station 7560; 8 July; 47°45′ N., 49°47′ W.; depth 110 m.; dynamic height 971.098						
0	8.41	32.23	0	8.41	32.23	25.06
25	4.24	32.47	25	4.24	32.47	25.77
50	−0.24	32.80	50	−0.24	32.80	26.37
75	−0.15	33.03	75	−0.15	33.03	26.55
100	−0.16	33.17	100	−0.16	33.17	26.66

Observed values			Scaled values			
Depth, meters	Temperature, °C.	Salinity, ‰	Depth, meters	Temperature, °C.	Salinity, ‰	σ_t
Station 7561; 8 July; 47°58′ N., 49°44′ W.; depth 170 m.; dynamic height 971.066						
0	8.74	31.64	0	8.74	31.64	24.55
25	1.72	32.56	25	1.72	32.56	26.06
50	−1.36	32.81	50	−1.36	32.81	26.41
75	−1.44	32.98	75	−1.44	32.98	26.55
100	−1.40	33.03	100	−1.40	33.03	26.59
150	0.57	33.75	150	0.57	33.75	27.09
Station 7562; 8 July; 48°09′ N., 49°37′ W.; depth 212 m.; dynamic height 971.097						
0	8.42	31.50	0	8.42	31.50	24.49
25	−0.57	32.62	25	−0.57	32.62	26.23
50	−1.57	32.81	50	−1.57	32.81	26.42
75	−1.39	32.94	75	−1.39	32.94	26.52
100	−1.44	33.09	100	−1.44	33.09	26.63
150	−0.22	33.55	150	−0.22	33.55	26.97
200	1.56	34.14	200	1.56	34.14	27.33
Station 7563; 8 July; 48°29′ N., 49°22′ W.; depth 603 m.; dynamic height 971.034						
0	9.43	31.25	0	9.43	31.25	24.15
22	7.42	32.67	25	7.15	32.70	25.61
46	5.34	32.83	50	4.00	32.95	26.18
68	−0.89	33.43	75	−0.70	33.47	26.93
92	0.15	33.57	100	0.10	33.66	27.04
136	1.35	34.115	150	1.50	34.18	27.37
182	1.83	34.31	200	2.00	34.37	27.49
273	2.79	34.64	300	2.90	34.67	27.66
365	3.14	34.745	400	3.25	34.76	27.69
551	3.56	34.84	(600)	3.65	34.86	27.73
Station 7564; 8 July; 48°36′ N., 49°19′ W.; depth 1,097 m.; dynamic height 970.988						
0	9.83	31.86	0	9.83	31.86	24.55
25	3.59	32.84	25	3.59	32.84	26.14
51	−1.01	33.29	50	−0.95	33.30	26.57
76	0.09	33.74	75	0.05	33.74	27.11
102	0.72	33.99	100	0.65	33.97	27.26
151	0.53	34.16	150	0.55	34.15	27.33
202	2.08	34.45	200	2.00	34.44	27.54
304	3.00	34.71	300	2.95	34.70	27.67
404	3.20	34.78	400	3.20	34.77	27.71
604	3.45	34.84	600	3.45	34.84	27.73
803	3.60	34.88	800	3.60	34.88	27.75
1,002	3.48	34.89	1,000	3.50	34.89	27.77
Station 7565; 8 July; 49°03′ N., 49°13′ W.; depth 1,728 m.; dynamic height 970.875						
0	9.48	32.88	0	9.48	32.88	25.40
25	6.10	34.14	25	6.10	34.14	26.88
51	3.37	34.50	50	3.40	34.49	27.46
76	3.12	34.64	75	3.15	34.64	27.60
102	3.16	34.71	100	3.15	34.70	27.65
152	3.35	34.76	150	3.35	34.76	27.68
202	3.41	34.81	200	3.40	34.81	27.72
304	3.45	34.84	300	3.45	34.83	27.72
406	3.44	34.84	400	3.45	34.84	27.73
608	3.49	34.85	600	3.50	34.85	27.74
809	3.42	34.88	800	3.45	34.88	27.76
1,012	3.45	34.89	1,000	3.45	34.89	27.77
1,522	3.38	34.93				

TABLE OF OCEANOGRAPHIC DATA—Continued

Observed values			Scaled values			
Depth, meters	Temperature, °C.	Salinity, °/oo	Depth, meters	Temperature, °C.	Salinity, °/oo	σ_t
Station 7566; 8 July; 49°36′ N., 49°09′ W.; depth 1,673 m.; dynamic height 970.859						
0	9.49	33.52	0	9.49	33.52	25.90
25	5.49	34.51	25	5.49	34.51	27.25
51	3.44	34.53	50	3.45	34.53	27.48
76	3.16	34.64	75	3.15	34.63	27.59
103	3.31	34.69	100	3.30	34.68	27.62
153	3.58	34.77	150	3.55	34.76	27.67
204	3.35	34.79	200	3.35	34.79	27.70
307	3.40	34.82	300	3.40	34.82	27.73
409	3.57	34.87	400	3.55	34.86	27.74
607	3.63	34.89	600	3.60	34.89	27.76
802	3.45	34.88	800	3.50	34.88	27.76
1,007	3.48	34.89	1,000	3.45	34.89	27.77
1,522	3.36	34.90				
Station 7567; 8 July; 50°00′ N., 49°00′ W.; depth 1,875 m.; dynamic height 970.866						
0	8.50	33.96	0	8.50	33.96	26.48
24	4.48	34.04	25	4.50	34.05	27.00
49	3.58	34.62	50	3.55	34.62	27.55
73	3.26	34.68	75	3.25	34.69	27.63
98	3.42	34.75	100	3.45	34.75	27.66
146	3.55	34.80	150	3.55	34.80	27.69
195	3.62	34.82	200	3.60	34.82	27.71
293	3.57	34.83	300	3.55	34.82	27.71
404	3.58	34.83	400	3.55	34.83	27.71
606	3.37	34.85	600	3.40	34.84	27.74
810	3.36	34.85	800	3.35	34.84	27.74
1,014	3.27	34.85	1,000	3.30	34.85	27.76
1,526	3.43	34.91				
Station 7568; 10 July; 53°43′ N., 55°48′ W.; depth 113 m.; dynamic height 1454.933						
0	7.64	25.86	0	7.64	25.86	20.15
25	−1.62	32.51	25	−1.62	32.51	26.17
50	−1.65	32.64	50	−1.65	32.64	26.28
75	−1.67	32.69	75	−1.67	32.69	26.32
100	−1.59	32.76	100	−1.59	32.76	26.37
Station 7569: 10 July: 53°51′ N., 55°30.5′ W.; depth 223 m.; dynamic height 1454.888						
0	4.11	27.17	0	4.10	27.17	21.59
24	−1.39	32.48	25	−1.40	32.49	26.15
48	−1.67	32.68	50	−1.65	32.70	26.33
72	−1.50	32.85	75	−1.45	32.87	26.46
96	−1.08	33.08	100	−1.10	33.11	26.64
144	−1.27	33.39	150	−1.20	33.43	26.91
192	−0.62	33.76	(200)	−0.50	33.82	27.20
Station 7570; 10 July; 53°54′ N., 55°25′ W.; depth 179 m.; dynamic height 1454.879						
0	5.51	26.04	0	5.51	26.04	20.57
25	0.00	32.23	25	0.00	32.23	25.89
50	−0.97	32.98	50	−0.97	32.98	26.53
75	−1.22	33.20	75	−1.22	33.20	26.72
101	−1.26	33.36	100	−1.25	33.35	26.84
151	−0.87	33.65	150	−0.90	33.64	27.07
Station 7571; 10 July; 54°06′ N., 55°02′ W.; depth 163 m.; dynamic height 1454.834						
0	5.21	29.61	0	5.21	29.61	23.42
25	−1.20	32.63	25	−1.20	32.63	26.26
50	−1.55	32.90	50	−1.55	32.90	26.49
75	−1.22	33.19	75	−1.22	33.19	26.79
100	−1.20	33.36	100	−1.20	33.36	26.85
150	−0.89	33.70	150	−0.89	33.70	27.12
Station 7572; 10 July; 54°14′ N., 54°45′ W.; depth 183 m.; dynamic height 1454.865						
0	5.00	26.99	0	5.00	26.99	21.37
25	−0.81	32.43	25	−0.81	32.43	26.09
50	−1.42	32.98	50	−1.42	32.98	26.55
75	−1.09	33.18	75	−1.09	33.18	26.71
100	−1.19	33.34	100	−1.19	33.34	26.84
150	−0.99	33.64	150	−0.99	33.64	27.07
Station 7573; 10 July; 54°26′ N., 54°16′ W.; depth 214 m.; dynamic height 1454.835						
0	4.49	28.90	0	4.49	28.90	22.92
24	−1.41	32.66	25	−1.40	32.67	26.30
48	−1.36	33.04	50	−1.35	33.06	26.10
71	−1.21	33.22	75	−1.20	33.26	26.77
95	−1.23	33.45	100	−1.15	33.49	26.96
142	−0.59	33.83	150	−0.30	33.91	27.26
190	1.32	34.31	(200)	1.25	34.39	27.56
Station 7574; 10 July; 54°44′ N., 53°48′ W.; depth 320 m.; dynamic height 1454.807						
0	3.33	30.67	0	3.33	30.67	24.32
23	−1.49	32.83	25	−1.50	32.85	26.46
46	−1.21	33.21	50	−1.40	33.22	26.74
69	−1.16	33.28	75	−1.15	33.35	26.84
92	−1.09	33.58	100	−0.95	33.62	27.06
137	−0.47	33.83	150	−0.20	33.94	27.28
184	0.50	34.14	200	0.85	34.21	27.44
276	2.72	34.58	(300)	3.35	34.70	27.63
Station 7575; 10 July; 54°50′ N., 53°34′ W.; depth 654 m.; dynamic height 1454.758						
0	3.49	30.77	0	3.49	30.77	24.50
24	−0.35	33.27	25	−0.40	33.28	26.76
47	−0.98	33.51	50	−0.95	33.54	26.99
71	−0.59	33.72	75	−0.55	33.75	27.14
94	−0.32	33.87	100	−0.05	33.91	27.25
140	1.71	34.32	150	2.05	34.39	27.50
187	3.41	34.64	200	3.45	34.65	27.58
281	3.82	34.74	300	3.90	34.76	27.63
372	4.23	34.85	400	4.25	34.86	27.67
551	4.22	34.88	(600)	4.25	34.89	27.69
Station 7576; 10 July; 54°56′ N., 53°24′ W.; depth 1,600 m.; dynamic height 1454.687						
0	2.41	31.66	0	2.41	31.66	25.29
26	0.27	33.55	25	0.30	33.53	26.95
51	1.27	34.20	50	1.20	34.18	27.39
77	1.96	34.35	75	1.90	34.33	27.46
103	3.50	34.61	100	3.35	34.59	27.54
153	4.45	34.79	150	4.40	34.78	27.58
205	4.25	34.80	200	4.25	34.80	27.62
308	4.49	34.87	300	4.45	34.86	27.65
410	4.34	34.91	400	4.35	34.90	27.69
615	3.64	34.84	600	3.70	34.85	27.72
820	3.46	34.87	800	3.50	34.86	27.75
1,024	3.33	34.86	1,000	3.35	34.86	27.76
1,536	3.46	34.89	1,500	3.20	34.89	27.80

TABLE OF OCEANOGRAPHIC DATA—Continued

Station 7577; 10 July; 55°00′ N., 53°16′ W.; depth 2,103 m.; dynamic height 1454.636

Observed values			Scaled values			
Depth, meters	Temperature, °C.	Salinity, ‰	Depth, meters	Temperature, °C.	Salinity, ‰	σ_t
0	3.39	32.24	0	3.39	33.24	26.47
25	1.26	33.66	25	1.26	33.66	26.97
50	1.19	34.19	50	1.19	34.19	27.40
75	3.11	34.54	75	3.11	34.54	27.53
100	4.34	34.80	100	4.34	34.80	27.60
150	4.59	34.90	150	4.59	34.90	27.66
200	4.40	34.90	200	4.40	34.90	27.68
300	4.17	34.90	300	4.17	34.90	27.71
410	3.81	34.89	400	3.90	34.89	27.73
615	3.42	34.87	600	3.45	34.87	27.76
819	3.34	34.87	800	3.35	34.87	27.77
1,024	3.26	34.87	1,000	3.30	34.87	27.78
1,541	3.46	34.92	1,500	3.45	34.91	27.79
2,059	3.20	34.94				

Station 7578; 11 July; 55°08′ N., 53°02′ W.; depth 2,761 m.; dynamic height 1454.599

Observed values			Scaled values			
Depth, meters	Temperature, °C.	Salinity, ‰	Depth, meters	Temperature, °C.	Salinity, ‰	σ_t
0	5.76	33.73	0	5.76	33.73	26.60
25	5.34	34.58	25	5.34	34.58	27.32
50	4.71	34.66	50	4.71	34.66	27.46
75	4.14	34.73	75	4.14	34.73	27.58
100	4.10	34.86	100	4.10	34.86	27.69
149	4.08	34.90	150	4.10	34.90	27.72
199	3.86	34.88	200	3.90	34.88	27.72
299	3.69	34.89	300	3.70	34.89	27.75
391	3.59	34.89	400	3.55	34.89	27.76
587	3.47	34.88	600	3.45	34.88	27.76
783	3.31	34.87	800	3.30	34.87	27.78
979	3.26	34.865	1,000	3.25	34.87	27.78
1,470	3.42	34.91	1,500	3.40	34.91	27.80
1,961	3.18	34.94				
2,454	------	34.92				

Station 7579; 11 July; 55°26′ N., 52°29′ W.; depth 3,292 m.; dynamic height 1454.612

Observed values			Scaled values			
Depth, meters	Temperature, °C.	Salinity, ‰	Depth, meters	Temperature, °C.	Salinity, ‰	σ_t
0	7.55	34.48	0	7.55	34.48	26.95
26	5.98	34.68	25	6.00	34.68	27.32
51	4.27	34.71	50	4.35	34.71	27.54
76	3.75	34.73	75	3.75	34.73	27.61
102	3.46	34.73	100	3.50	34.73	27.64
152	3.34	34.77	150	3.35	34.78	27.69
203	3.36	34.795	200	3.35	34.79	27.70
305	3.47	34.83	300	3.45	34.83	27.72
404	3.45	34.84	400	3.45	34.84	27.73
604	3.39	34.85	600	3.40	34.85	27.75
807	3.29	34.855	800	3.30	34.85	27.76
1,011	3.29	34.86	1,000	3.30	34.86	27.77
1,509	3.43	34.90	1,500	3.40	34.90	27.79
2,016	3.35	34.94				
2,522	2.94	34.95				
3,234	1.61	34.90				

Station 7580; 11 July; 55°50′ N., 51°40′ W.; depth 3,493 m.; dynamic height 1454.617

Observed values			Scaled values			
Depth, meters	Temperature, °C.	Salinity, ‰	Depth, meters	Temperature, °C.	Salinity, ‰	σ_t
0	7.87	34.63	0	7.87	34.63	27.02
24	6.26	34.665	25	6.20	34.67	27.30
48	3.95	34.67	50	3.90	34.68	27.56
72	3.81	34.71	75	3.75	34.71	27.60
96	3.68	34.74	100	3.65	34.74	27.63
143	3.54	34.77	150	3.55	34.77	27.67
190	3.43	34.79	200	3.40	34.79	27.70
286	3.34	34.81	300	3.35	34.81	27.72
382	3.35	34.83	400	3.35	34.83	27.73
575	3.34	34.845	600	3.35	34.85	27.75
772	3.23	34.85	800	3.25	34.85	27.76
972	3.24	34.855	1,000	3.25	34.86	27.77
1,466	3.47	34.90	1,500	3.45	34.90	27.78
1,967	3,38	34.92				
2,475	3.19	34.93				
2,981	2.63	34.945				
3,399	1.66	34.90				

Station 7581; 11 July; 56°26′ N., 50°30′ W.; depth 3,658 m.; dynamic height 1454.636

Observed values			Scaled values			
Depth, meters	Temperature, °C.	Salinity, ‰	Depth, meters	Temperature, °C.	Salinity, ‰	σ_t
0	7.94	34.58	0	7.94	34.58	26.97
25	6.79	34.58	25	6.79	34.58	27.14
51	5.16	34.64	50	5.20	34.64	27.39
76	4.11	34.735	75	4.20	34.73	27.57
102	3.83	34.795	100	3.85	34.79	27.65
151	3.82	34.855	150	3.85	34.85	27.70
202	3.64	34.825	200	3.65	34.83	27.70
304	3.65	34.85	300	3.65	34.85	27.72
403	3.58	34.87	400	3.55	34.87	27.75
602	3.41	34.86	600	3.45	34.86	27.75
800	3.32	34.84	800	3.35	34.84	27.74
996	3.29	34.84	1,000	3.30	34.84	27.75
1,486	3.47	34.88	1,500	3.45	34.87	27.76
1,992	3.40	34.895				
2,492	3.12	34.91				
3,002	2.68	34.91				
3,500	1.65	34.90				
3,600	1.59	34.89				

Station 7582; 11 July; 57°00′ N., 49°27′ W.; depth 3,694 m.; dynamic height 1454.603

Observed values			Scaled values			
Depth, meters	Temperature, °C.	Salinity, ‰	Depth, meters	Temperature, °C.	Salinity, ‰	σ_t
0	7.87	34.64	0	7.87	34.64	27.03
25	5.75	34.69	25	5.75	34.69	27.36
50	3.96	34.70	50	3.96	34.70	27.57
76	3.40	34.71	75	3.40	34.71	27.63
101	3.40	34.75	100	3.40	34.75	27.67
151	3.40	34.78	150	3.45	34.78	27.68
201	3.68	34.84	200	3.65	34.84	27.71
302	3.57	34.855	300	3.60	34.85	27.73
402	3.45	34.85	400	3.45	34.85	27.74
604	3.44	34.87	600	3.45	34.87	27.76
810	3.44	31.88	800	3.45	34.89	27.77
1,018	3,48	34.90	1,000	3.50	34.90	27.78
1,511	3.44	34.91	1,500	3.45	34.91	27.79
2,015	3.37	34.93				
2,515	3.12	34.945				
3,018	2.74	34.94				
3,517	1.79	34.915				
3,616	1.70	34.90				

TABLE OF OCEANOGRAPHIC DATA—Continued

Observed values			Scaled values			
Depth, meters	Temperature, °C.	Salinity, °/oo	Depth, meters	Temperature, °C.	Salinity, °/oo	σ_t
Station 7583; 12 July; 57°33′ N., 48°20′ W.; depth 3,475 m.; dynamic height 1454.602						
0	6.94	34.69	0	6.94	34.69	27.20
25	6.41	34.70	25	6.41	34.70	27.28
50	4.27	34.79	50	4.27	34.79	27.61
75	4.06	34.87	75	4.06	34.87	27.70
100	4.39	34.93	100	4.39	34.93	27.71
150	4.20	34.92	150	4.20	34.92	27.72
200	4.01	34.90	200	4.01	34.90	27.73
300	3.74	34.88	300	3.74	34.88	27.74
401	3.60	34.88	400	3.60	34.88	27.75
599	3.35	34.86	600	3.35	34.86	27.76
799	3.37	34.855	800	3.40	34.86	27.76
996	3.30	34.86	1,000	3.30	34.86	27.77
1,505	3.47	34.895	1,500	3.45	34.89	27.77
2.007	3.38	34.93				
2,509	3.05	34.95				
3,003	2.59	34.93				
3,340	1.78	34.90				
Station 7584; 12 July; 58°05′ N., 47°07′ W.; depth 3,200 m.; dynamic height 1454.608						
0	7.18	34.72	0	7.18	34.72	27.19
25	6.27	34.72	25	6.27	34.72	27.32
50	5.29	34.80	50	5.29	34.80	27.50
75	4.86	34.90	75	4.86	34.90	27.63
101	4.73	34.93	100	4.75	34.93	27.66
152	4.71	34.96	150	4.75	34.96	27.69
202	4.34	34.93	200	4.35	34.93	27.71
303	4.10	34.92	300	4.10	34.92	27.74
404	3.98	34.925	400	4.00	34.92	27.75
604	3.70	34.90	600	3.70	34.90	27.76
805	3.56	34.89	800	3.60	34.89	27.76
1,004	3.52	34.89	1,000	3.50	34.89	27.77
1,498	3.50	34.92	1,500	3.50	34.92	27.80
2,000	3.31	34.94				
2,503	2.84	34.93				
3,000	1.90	34.91				
Station 7585; 12 July; 58°36′ N., 46°02′ W.; depth 2,578 m.; dynamic height 1454.630						
0	7.32	34.72	0	7.32	34.72	27.17
25	6.08	34.72	25	6.08	34.72	27.34
51	5.27	34.92	50	5.30	34.92	27.60
76	5.19	34.95	75	5.20	34.95	27.63
101	5.02	34.95	100	5.05	34.95	27.65
153	4.78	34.955	150	4.85	34.95	27.67
204	4.35	34.915	200	4.40	34.92	27.70
305	4.01	34.875	300	4.05	34.88	27.70
406	3.95	34.89	400	3.95	34.89	27.72
607	3.79	34.88	600	3.80	34.88	27.73
807	3.55	34.86	800	3.60	34.86	27.74
1,006	3.63	34.88	1,000	3.65	34.88	27.74
1,502	3.34	34.92	1,500	3.35	34.92	27.81
2,004	2.94	34.93				
2,507	2.38	34.90				

Observed values			Scaled values			
Depth, meters	Temperature, °C.	Salinity, °/oo	Depth, meters	Temperature, °C.	Salinity, °/oo	σ_t
Station 7586; 13 July; 58°57′ N., 45°17′ W.; depth 2,468 m.; dynamic height 1454.631						
0	6.82	34.65	0	6.82	34.65	27.19
24	6.18	34.66	25	6.15	34.66	27.29
48	6.03	34.71	50	6.00	34.71	27.35
72	5.32	34.77	75	5.30	34.80	27.50
96	5.10	34.94	100	5.10	34.94	27.63
145	5.00	34.97	150	5.00	34.97	27.68
193	5.00	34.99	200	5.00	34.99	27.69
289	4.67	34.98	300	4.60	34.98	27.72
387	4.29	34.96	400	4.25	34.96	27.75
580	3.90	34.92	600	3.85	34.92	27.76
776	3.58	34.89	800	3.60	34.89	27.76
972	3.56	34.895	1,000	3.55	34.89	27.76
1,460	3.39	34.87	1,500	3.35	34.87	27.77
1,948	2.90	34.90				
2,438	2.19	------				
Station 7587; 13 July; 59°10′ N., 44°50′ W.; depth 2,103 m.; dynamic height 1454.643						
0	5.48	33.75	0	5.48	33.75	26.65
25	5.52	33.83	25	5.52	33.83	26.71
51	6.14	35.02	50	6.10	35.02	27.58
76	5.86	35.04	75	5.90	35.04	27.62
102	5.58	35.05	100	5.60	35.05	27.66
152	5.30	35.025	150	5.35	35.03	27.67
204	5.21	35.02	200	5.20	35.02	27.69
306	5.03	35.00	300	5.05	35.00	27.69
408	4.69	34.98	400	4.80	34.98	27.70
613	4.15	34.93	600	4.20	34.93	27.72
794	3.88	34.92	800	3.85	34.92	27.76
996	3.60	34.915	1,000	3.60	34.92	27.79
1,498	3.14	34.90	1,500	3.15	34.90	27.81
2.004	2.48	34.905				
Station 7588; 13 July; 59°19′ N., 44°29′ W.; depth 1,116 m.; dynamic height 1454.698						
0	4.75	34.44	0	4.75	34.44	27.28
25	6.20	34.86	25	6.20	34.86	27.44
51	6.41	34.95	50	6.40	34.95	27.48
76	6.51	34.97	75	6.50	34.97	27.49
101	6.46	34.98	100	6.45	34.98	27.49
161	6.19	34.95	150	6.25	34.96	27.51
212	5.96	35.02	200	6.00	35.00	27.57
313	5.72	35.04	300	5.75	35.04	27.63
413	5.33	35.03	400	5.40	35.03	27.67
612	4.76	34.97	600	4.80	34.98	27.70
810	4.54	34.955	800	4.60	34.96	27.71
1,007	4.05	34.92	1,000	4.05	34.92	27.74

U.S. GOVERNMENT PRINTING OFFICE : 1961 O—617199

Contribution No. 1165

CONTRIBUTIONS FROM THE CUSHMAN FOUNDATION
FOR FORAMINIFERAL RESEARCH
VOLUME XII, PART 3, JULY, 1961

227. *GLOBIGERINA INCOMPTA*, A NEW SPECIES OF PELAGIC FORAMINIFERA FROM THE NORTH ATLANTIC[1,2]

by
RICHARD CIFELLI
U. S. National Museum, Washington, D. C.

ABSTRACT

A new Recent species of pelagic Foraminifera, **Globigerina incompta**, is recognized from the surface waters of the North Atlantic. This is a common pelagic form, but has been interpreted in various ways by previous workers. Reasons for considering it a separate species are discussed.

INTRODUCTION

The new Recent foraminifer described here, *Globigerina incompta,* was encountered in plankton tows collected from the North Atlantic. This appears to be a common and widely distributed pelagic form in the North Atlantic, but because of its small size and relatively simple structure there has probably been a reluctance in the past to recognize it as a separate species. *G. incompta* is comparable to *G. dutertrei* as originally described and figured by d'Orbigny (1839). However, that name is no longer available for the form indicated in d'Orbigny's figure because the lectotype, as figured (Banner and Blow, 1960, p. 11, pl. 2, fig. 1) is not the same and is comparable to *G. eggeri.* The selection of this lectotype is the latest in a series of complications that has plagued d'Orbigny's species since it was originally described. Most persons appear to have considered *G. dutertrei* as a life stage or variety of *G. eggeri* or *G. pachyderma.* However, *G. dutertrei* as illustrated by d'Orbigny, here redescribed as *G. incompta,* is morphologically separable from *G. eggeri,* and, moreover, is a much more common form in the North Atlantic Slope waters than *G. eggeri.* The relationship to *G. pachyderma* is still not clear, but the evidence for *G. incompta* and *G. pachyderma* being life stages of a single species is inconclusive and even somewhat contradictory. Therefore, it is believed that the species originally described by d'Orbigny and now recognizable and distinguishable from other species should be retained; it is for this reason that *G. incompta* is proposed here.

MATERIAL

This species was collected from oblique plankton tows, through the upper 200 meters of water, in a series of stations extending across the North Atlantic Slope waters into the Sargasso Sea. The hauls were taken in August, 1960, from the R/V *Crawford* during a Woods Hole Oceanographic Institution cruise. The collections were made as a part of a cooperative program with the Woods Hole Oceanographic Institution to study the ecology of pelagic Foraminifera in the North Atlantic. Travel and ship facilities for this work have been supplied by Woods Hole Oceanographic Institution under contract with The Office of Naval Research (NONR - 2196 (00)). Shipboard assistance and certain collateral data have been available from scientists supported by The United States Atomic Energy Commission (under grant AT (30-1)-1918).

A number 10 net with apertures of 0.158 mm. and a mouth diameter of three quarter meters was used for the towing. The locations of the stations and the percentages of *G. incompta* compared to the total foraminiferal populations are shown in table 1. The percentages of *G. eggeri* to *G. incompta* are also shown for comparison.

---

[1] Published by permission of the Secretary, Smithsonian Institution

[2] Contribution No. 1165 from the Woods Hole Oceanographic Institution

EXPLANATION OF PLATE 4

FIGS.		PAGE
1-7.	*Globigerina incompta* Cifelli, n. sp.; all magnifications × 95. 1, Holotype, U.S.N.M. no. 628588; a, dorsal view; b, ventral view; c, edge view. 2, Paratype, U.S.N.M. no. 628589; a, dorsal view; b, ventral view; c, edge view. 3, Paratype, U.S.N.M. no. 628590; a, dorsal view; b, ventral view; c, edge view. 4, Paratype, U.S.N.M. no. 628591; a, dorsal view; b, ventral view; c, edge view. 5, Paratype, U.S.N.M. no. 628592; a, dorsal view; b, ventral view; c, edge view. 6, Paratype, U.S.N.M. no. 628593; a, dorsal view; b, ventral view; c, edge view. 7, Paratype, U.S.N.M. no. 628594; a, dorsal view; b, ventral view; c, edge view.	84

Reprinted from CONTRIBUTIONS FROM THE CUSHMAN FOUNDATION FOR FORAMINIFERAL RESEARCH
Volume XII, Part 3, July, 1961

Table 1. Collecting stations and relative abundance of *Globigerina incompta* and *Globigerina eggeri*

Station	N. Latitude	W. Longitude	Percent *G. incompta*	Percent *G. eggeri*/*G. incompta*
Slope				
1	39° 48′	71° 12′	32	0
2	39° 36′	71° 06′	40	0
3	38° 39′	69° 33′	32	6
4	38° 46′	70° 20′	8	32
5				
6	38° 12.5′	69° 18′	13	57
Gulf Stream				
7	37° 21′	69° 07′	1	0
Sargasso				
8	37° 12′	68° 48′	1	0
9	36° 23′	68° 04′	2	25 (1 spec.)
10	35° 35′	67° 20′	2	0
11	35° 47′	66° 29′	3	0

The holotype and paratypes were all collected from station 3, latitude 38° 39′ N, longitude 69° 33′ W. These specimens are deposited in the national collections of Foraminifera, U. S. National Museum. The illustrations of the specimens were prepared by Mr. Lawrence Isham, scientific illustrator, U. S. National Museum.

Globigerina incompta n. sp.

Plate 4, figures 1-7

Diagnosis.—Test small, coiled low trochospirally, slightly convex on the dorsal side; periphery lobulate, subquadrilateral in side view, rounded in edge view; chambers inflated to slightly appressed, numbering about 9 to 14 and arranged in 2 to slightly less than 3 whorls, with marked increase in size of chambers between whorls; usually 4, but sometimes 4 and a portion of a fifth, chambers visible from the ventral side; final chamber overlapping on ventral side and thus oblique to axis of coiling; sutures radial, deeply depressed; umbilicus deep, but not particularly broad; aperture an elongate rounded opening at the base of the final chamber extending into and beyond the umbilicus, close to the periphery; only the aperture of the final chamber visible from the surface; a thin porous lip projecting at the top of the aperture; wall thin, porous; surface spinose.

Chambers.—The initial whorl consists of a minute proloculus and 4 or 5 additional small chambers. An abrupt increase in size generally occurs at about the sixth and again at about the eighth chamber. There are 4 or 4½ chambers in the second whorl and from 1 to 3 in the final, incomplete whorl. The cameral and spiral sutures are deeply depressed and sharply defined throughout so that the details of the chambers are clearly visible on the test. The last 4 chambers are relatively large and the increase in size of these is uniform. The final chamber is usually highly inflated and is mostly, but not always, the largest. Because of the uniformly large size of the last four chambers the periphery, in ventral view, is subquadrilateral. In most specimens there are 4 chambers visible from the ventral side but in some there are 4 and a portion of a fifth; the peripheries of these are less quadrilateral. The final chamber overlaps considerably more on the ventral side than do the previous ones, but the amount of overlap is highly variable.

Aperture.—The aperture is at the base of the final chamber and opens into a deep but fairly narrow umbilicus. It extends beyond the umbilicus in most specimens, occasionally almost reaching the periphery. The aperture varies from an elongate narrow opening to one that is rather broad and semi-circular. The aperture of the penultimate chamber can sometimes be seen through this opening, but it connects with the final chamber and does not appear to open directly into the umbilicus. The lip of the aperture of the final chamber is thin, delicate and porous; it was not observed on all of the specimens.

Surface.—Live and wet preserved specimens are covered with fine, elongate spines. These are easily destroyed, however, and are practically never seen on dry specimens. The wall is thin and highly porous and translucent; through it the protoplasm can be seen. It is a dark olive color. The surface of dry specimens is spinose.

Coiling.—No actual count of coiling ratios was made, but in the material examined the majority of specimens are dextral. The coiling direction of this species, however, may be temperature controlled, as has been reported to be the case in other pelagic Foraminifera.

Dimensions.—(in mm.)

	Total no. chambers	Diam. 1st whorl	Diam. 2nd whorl	Diam. Max.	Thick.
Holotype USNM no. 628588	14	.06	.18	.36	.21
Paratype USNM no. 628589	14	.11	.37	.51	.26
Paratype USNM no. 628590	11	.08	.18	.33	.22
Paratype USNM no. 628591	13	.08	.19	.32	.34
Paratype USNM no. 628592	11	.07	.18	.28	.16
Paratype USNM no. 628593	12	.06	.20	.32	.19
Paratype USNM no. 628594	13	.07	.19	.34	.22

Comparisons and remarks.—This species is common in parts of the North Atlantic and will probably be familiar to persons acquainted with Recent pelagic Foraminifera. However, because of its small size and rather generalized characters it probably has, in the past, been regarded as a juvenile or variant form of some other species with which it is associated. My first impression was that this species represented an immature stage of *Globigerina eggeri* Rhumbler, which it closely resembles, in mode of coiling and in inflation of chambers. It was not possible to establish a transition, however, and after study of many specimens I concluded that this small form was a separate species. It is distinguishable from *G. eggeri* in the following ways:

1 — The test of *Globigerina incompta* is coiled low trochospirally while that of *G. eggeri* is high, even in small specimens.

2 — The umbilicus is a larger, more open area in *G. eggeri.* The apertures of the chambers on the ventral side can often be seen in the umbilicus in *G. eggeri,* while only the aperture of the final chamber is visible in the umbilical area of *G. incompta.*

3 — The aperture of *G. eggeri* opens to, and does not extend beyond, the umbilicus. In *G. incompta* the aperture also opens to the umbilicus, but is variable in length, extending outward beyond the umbilicus and almost to the periphery. Of particular importance also is the fact that *G. incompta* was found to be very common in the plankton tows studied from the North Atlantic while *G. eggeri* was rare. In fact, *G. incompta* appears to be one of the most characteristic species of the North Atlantic Slope waters, along with *G. inflata* and *G. bulloides.* In one 200 meter plankton sample collected in August, 1960, at latitude 39° 36′ N and longitude 71° 06′ W, *G. incompta* was the dominant species and made up 40 percent of the foraminiferal population. In eleven 200 meter plankton samples collected August, 1960, from the North Atlantic Slope waters, the Gulf Stream and the Sargasso Sea, the ratio of *G. eggeri* to *G. incompta* varied from 0 - 57 percent (Table 1). If *G. incompta* were an early stage of *G. eggeri* it would be difficult to understand why so small a percentage of individuals succeed in achieving an adult stage.

Comparing favorably and apparently identical with *Globigerina incompta* is *G. dutertrei* d'Orbigny as originally described and figured by d'Orbigny (1839, p. 84, pl. 4, figs. 19-21). However, the lectotype of *G. dutertrei* selected by Banner and Blow (1960, p. 11, pl. 2, fig. 1) is not identical. The lectotype as figured is, in my opinion, inseparable from *G. eggeri.* I have observed both forms in a bottom sample from off the coast of Cuba, one of the areas from which d'Orbigny recorded *G. dutertrei.* The form comparable to d'Orbigny's figure also compares favorably and is identical with *G. incompta,* although the Cuban specimens have somewhat fewer chambers and slightly less lobulate peripheries. The other form, referable to the lectotype, is clearly of the *G. eggeri* type; besides being larger and having more chambers, it has a higher, less flat coil and has a larger umbilicus and a very broad umbilical aperture. D'Orbigny did not distinguish the two forms and apparently included both in his concept of *G. dutertrei.* It is unfortunate that the lectotype which was selected is not the form figured by d'Orbigny, since that specimen now becomes the name bearer of the species; d'Orbigny's figure no longer has nomenclatural status, even though it appears to be an accurate illustration. This further complicates a species that has already caused much difficulty in interpretation. *G. dutertrei* now becomes a senior subjective synonym of *G. eggeri.*

A species very similar to *Globigerina incompta* is *G. megastoma* Earland from the Antarctic region. The latter species, however, has a higher spire and a broader aperture. It is also a larger form and has a more elongate final chamber.

The relationships of this species to the form occurring in the Antarctic region and identified as *Globigerina dutertrei* by authors is problematic. Brady (1884, p. 601) regarded *G. dutertrei* as a typical Antarctic species and believed that it was the southern counterpart of *G. pachyderma* which, according to him, does not occur in the Antarctic region. Heron-Allen and Earland (1922, pp. 189-192) recognized *G. dutertrei* as a dominant form in the Antarctic but maintained that it is replaced by and intergrades with *G. pachyderma* in the lowermost latitudes. They felt that *G. pachyderma* is actually a variety of *G. dutertrei,* "due to the suppression of the comparatively large single aperture of the typical *G. dutertrei* combined with a reduction of the general dimensions and particularly with a massive thickening of the shell wall" (Heron-Allen and Earland, 1922, p. 192). Phleger, Parker and Pierson (1953, p. 13) and Uchio (1960, p. 5), on the other hand, consider it unlikely that the thick-walled Antarctic form is conspecific with the species described by d'Orbigny from the coast of Cuba. Uchio (1960, p. 5) found that *G. dutertrei* (of authors, not d'Orbigny) is dominant in the Antarctic sediments, while *G. pachyderma,* a small form, is of secondary importance. *G.* cf. *G. bulloides,* the only foraminifer occurring in the Antarctic plankton tows, is rare in the bottom sediments. *G. pachyderma* intergrades with *G. dutertrei* and Uchio believes that the Antarctic *G. dutertrei* is the adult stage of *G. pachyderma* (Uchio, 1960, p. 5). The original *G. dutertrei* of d'Orbigny, he feels, is the early stage of *G. eggeri.*

In the Arctic region *G. pachyderma* is dominant in the bottom sediments while a form resembling a juvenile *G. eggeri* or *G. bulloides* is the only foraminifer occurring in the plankton tows of the upper 200 meters of water. The line figure of the plankton form given by Bé (1960, fig. 1c) is suggestive of a type comparable to *G. incompta* although the Arctic form appears to be smaller. In addition, the coil of the Arctic form is sinistral while that of the present species is dextral. Like Uchio, Bé considers this form to be a life stage of *G. pachyderma.* Unlike Uchio, however, Bé regards *G. pachyderma* to be the *adult* stage. According to Bé (1960, p. 65) the juvenile achieves the adult characters by descending to deep waters, below 200 meters. The morphologic changes involved are "in the addition of a reduced final chamber and in the crystalline thickening of the test."

Part of the difficulty in comparing the Arctic and Antarctic forms is that despite the fair abundance of records and discussions of these forms there have been very few descriptions and, more important, illustrations. Without adequate illustrations and descriptions it is impossible to make meaningful comparisons. The figure of *G. dutertrei* given by Brady (1884, pl. 81, fig. 1) shows a form that appears to be comparable to *G. pachyderma* Earland. The Antarctic form figured by Ovey (*in* Wiseman and Ovey, 1950, p. 65, pl. 2, fig. 1a-c) compares well with *G. incompta,* but only a single specimen is figured, and nothing can be determined about the population structure. Conceivably the species described by d'Orbigny and revived here might be a life stage of *G. pachyderma;* the interpretations of Uchio and Bé seem reasonable if only the areas that they have studied are considered. However, it hardly seems justifiable to regard *G. incompta* a life from of *G. pachyderma* in the lower latitudes where *G. incompta* is common and *G. pachyderma* is rare or absent. Moreover, it is difficult to see how *G. pachyderma* could be an adult stage in the Arctic and a young stage in the Antarctic. Another possibility is that *G. incompta* is a geographic subspecies of *G. pachyderma.* However, this cannot be determined at the present since the descriptions and illustrations are inadequate and the records of occurrences of the high latitude forms cannot be evaluated. For now it seems best to retain for the lower latitudes, at least, a species comparable to the one that d'Orbigny originally described as *G. dutertrei,* even though a name change is involved.

BIBLIOGRAPHY

Banner, F. T., and Blow, W. H., 1960, Some primary types of species belonging to the superfamily Globigerinacea: Contr. Cushman Found. Foram. Research, vol. 11, pt. 1, pp. 1-41, pls. 1-8.

Bé, A. W. H., 1960, Some observations on arctic planktonic Foraminifera: Contr. Cushman Found. Foram. Research, vol. 11, pt. 2, pp. 64-68, 1 table, 1 text fig.

Brady, H. B., 1884, Report of the Foraminifera dredged by the H. M. S. *Challenger* during the years 1873-1876: Challenger Exped. 1873-1876, Rept., London, Zool., vol. 9, pt. 22, pp. 1-84, pls. 1-115.

Heron-Allen, E., and Earland, A., 1922, Protozoa, part II - Foraminifera: British Antarctic ("Terra Nova") Exped., 1910, Nat. Hist. Rept., Zool., vol. 6, pp. 25-268, pls. 1-8, 1 text fig.

Orbigny, A. d', 1839, Foraminifères: *In* R. de la Sagra, Histoire physique, politique et naturelle de l'Île de Cuba: Paris, Bertrand, pp. 1-224 (Plates published separately).

Phleger, F. B, Parker, F. L., and Peirson, J. F., 1953, North Atlantic Foraminifera: Repts. Swedish Deep-Sea Exped., vol. 7, fasc. 1, pp. 3-122, pls. 1-12, 38 tables, 26 text figs.

Uchio, T., 1960, Planktonic Foraminifera of the Antarctic Ocean: Spec. Publ. Seto Marine Biol. Lab., Biol. Results of Japanese Antarctic Res. Exped., no. 11, pp. 3-10, pl. 1, 1 text fig.

Wiseman, J. D. H., and Ovey, C. D., 1950, Recent investigations on the deep-sea floor: Proc. Geol. Ass., vol. 61, pt. 1, pp. 28-84, pls. 1-3, 3 tables, 2 text figs.

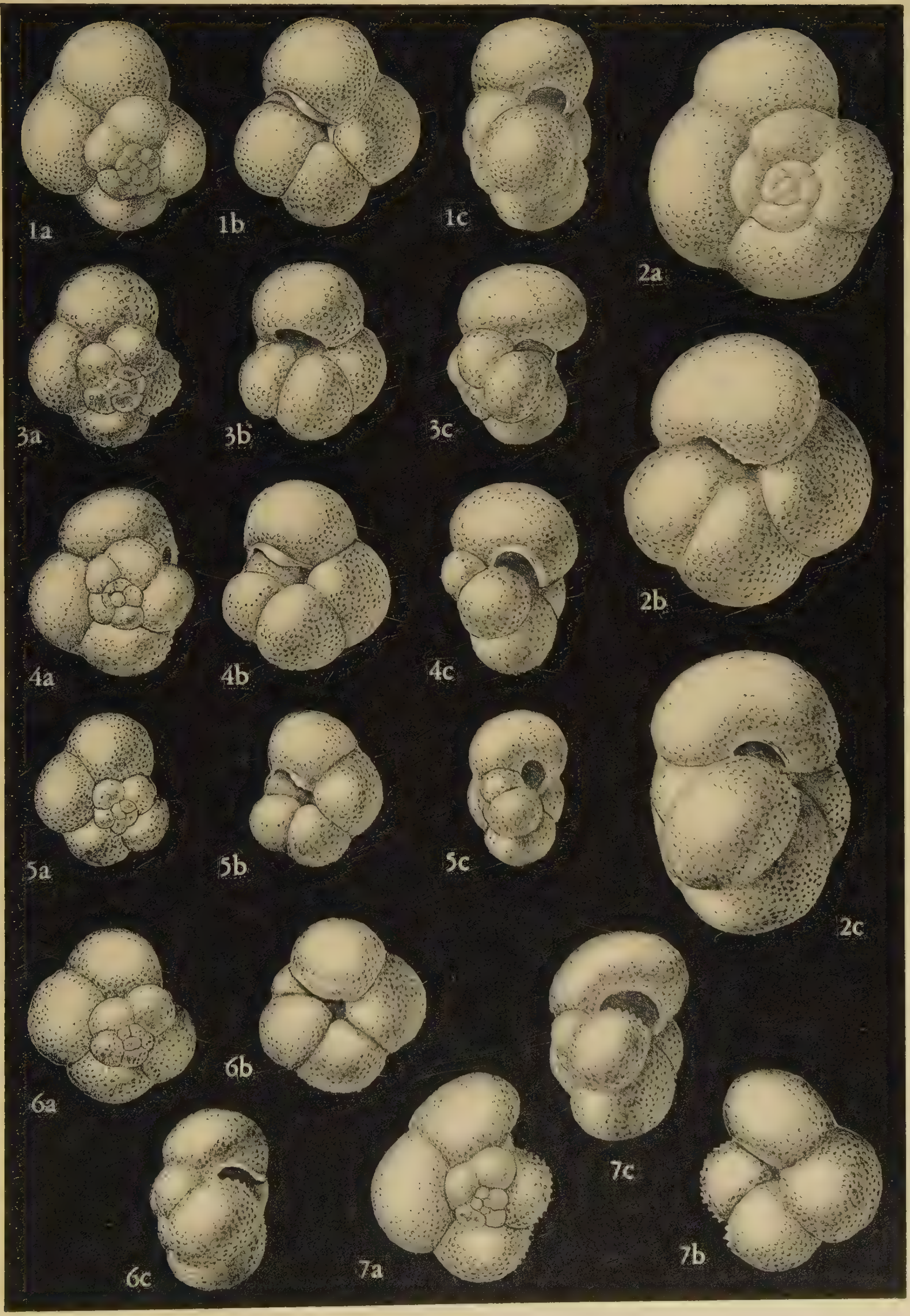
1a
1b
1c
2a
3a
3b
3c
2b
4a
4b
4c
5a
5b
5c
2c
6a
6b
7c
6c
7a
7b

Cifelli: *Globigerina incompta*, n. sp., from N. Atlantic

Särtryck ur Tellus nr 4, 1961

The Stability of Thermoclinic Jets

By MELVIN E. STERN, Woods Hole Oceanographic Institution

(Manuscript received February 6, revised version August 28, 1961)

Abstract

A laminar jet, in a "shallow layer" of water of density $\varrho - \Delta\varrho$ is in geostrophic equilibrium above a much deeper and resting layer of water of density ϱ. We compare the quasi-hydrostatic energy releasing process in this thermoclinic model with other baroclinic and barotropic models. It is first shown that a small amplitude disturbance can grow only if there is a transfer of *kinetic energy* from the horizontal variations in the mean jet and that conversions of mean potential energy can only occur concomitantly with, or as a finite amplitude result of this process. We also examine the perturbation equation for values of the stream Rossby number which are much less than unity and show that the finite depth of the thermocline inhibits inflectional instability of the jet. The generalization of Lord Rayleigh's theorem shows that the jet is stable if the gradient of *potential* vorticity does not vanish. In general, there is a critical value of the ratio of the radius of deformation $\left(f^{-1}\sqrt{gH_0\Delta\varrho/\varrho}\right)$ to the half width of the jet above which quasi-geostrophic disturbances will start to grow. It is proposed that meanders of the synoptic Gulf Stream will develop when the jet becomes "excessively" deep and that the effect of such instabilities is to limit the depth of the main thermocline in the interior of the ocean.

1. Statement of the Problem

We shall call the geostrophic laminar current, which is shown schematically in Fig. 1, a thermoclinic jet since it is a useful abstraction (Rossby, 1936); Stommel, 1953) of the thermal structure of the Gulf Stream. It consists of a homogeneous layer of light water of mean depth H_0 lying above a much deeper layer of water which is denser by an amount $\Delta\varrho \ll \varrho$. The latter is resting in a coordinate system which is rotating at $\omega = f/2$ rads./sec. The velocity in the upper layer is $V^*(x)$ directed along the y axis (or into the page) and this is balanced by the hydrostatic pressure gradient due to the elevation of the free surface. The characteristic width of the jet is denoted by $2L$ and V is the maximum speed.

The mutual adjustment of the free surface and the interface, which is necessary to bring about this inviscid equilibrium, allows us to express the hydrostatic pressure gradient in the upper layer in terms of its thickness $[h^*(x)]$ as: $g' dh^*/dx$ where $g' = g\Delta\varrho/\varrho$ is a "reduced" value of gravity. Under the conditions stated below[1] a similar simplification may be made for a perturbation $[h'(x, y, t)]$ which is introduced upon this mean field, so that if $h_T = h^* + h'$ denotes the total thickness of the upper layer then $g'\nabla h_T$ is the horizontal pressure gradient

---

[1] The hydrostatic (or shallow water) approximation may be defended when the mean depth of the top layer (H_0) and the bottom layer (H_b) are both small compared to the horizontal scale of the perturbation (L). On the other hand it may be shown that the ratio of the pressure gradients in the two layers is small to order H_0/H_b provided the stream Rossby number (R) and the rotational Froude number (F) are of magnitude unity or less (see eq. 10 for definitions of R, F). Thus the validity of this approximation and the analogy of the two layer model in Fig. 1 with the one layer model in Fig. 2, depend on the inequalities $H_0/L \ll H_b/L \ll 1$ when $R \leq 1$ and $F \leq 1$.

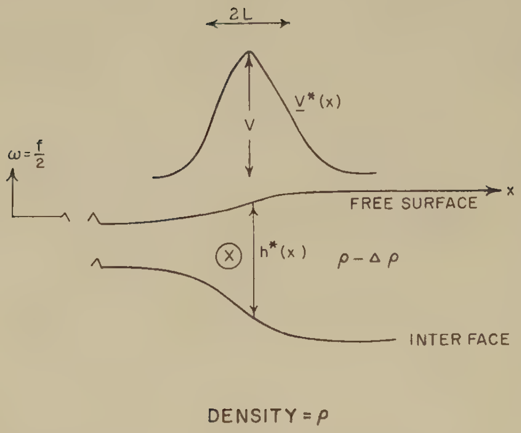

Fig. 1. A schematic diagram of a two layer thermoclinic jet. The lower layer of density ϱ is infinitely deep and resting. The geostrophically balanced velocity field $V^*(x)$ is directed along the y axis (into the page) and its maximum value is V. The section shown is supposed to occur at very large distances from the axis of the rotating system (f-plane).

therein. When these conditions are fulfilled then the dynamical model in Fig. 1 is analogous to the single fluid model shown in Fig. 2, in which gravity is reduced to g'. Although short-wave Helmholtz instabilities, associated with the interfacial shear in Fig. 1, have been filtered by the hydrostatic approximation it will be seen that either model has available potential energy as well as kinetic energy of horizontal shear. Both of these energy sources can be tapped by a superimposed perturbation. In Section 2 we shall examine certain integrals of the motion and show that the kinetic energy releasing process is the more fundamental one in the thermoclinic model. If an initially small disturbance releases potential energy from the mean flow it can only do so with a concomitant release of kinetic energy by the action of the Reynolds stress. This model then is fundamentally different from, and a logical extreme to, models having a uniformly distributed baroclinic zone (Charney, 1947; Eady, 1949) and which release only potential energy in the limit of small Rossby number. Kotchin's (1932) model of a Margules front separating two layers of the *same* thickness exhibits a similar potential energy conversion for long wave-length disturbances. Solberg (1930) has also considered the polar front instability in which both fluids are of infinite vertical extent. My understanding is that the instability mechanism here is due to vertical shear across the interface.

The classical Rayleigh-Tollmien theory (Lin, 1955) of two-dimensional inviscid shearing flow has established that a symmetric jet is unstable. Haurwitz and Panofsky (1950) have suggested this as a mechanism for meanders in the Gulf Stream (see Fuglister and Worthington, 1951, for the observational data which supports this picture). For zonal barotropic currents on a rotating sphere Kuo (1948) has generalized Lord Rayleigh's criterion to show that an extreme value of absolute vorticity is necessary for instability of the profile. The thermoclinic model allows a modification of this energy releasing process by virtue of the vertical velocities which work against the gravitational field. Nevertheless, a simple generalization of the foregoing criteria is possible which shows that "large-scale" instabilities will occur only when the profile has a maximum (or minimum) of *potential* vorticity. We point out the stabilizing influence of the finite depth of the thermocline and suggest the relevance of this quantity to the problem of the stability of the Gulf Stream.

2. The Energetics of Thermoclinic Jets

If $\mathbf{V}(x, y, t)$ denotes the total horizontal component of velocity in Figure 2 (or in the upper layer of Fig. 1) and $h_T(x, y, t)$ the thickness of the layer then the momentum and continuity equations are—

$$\frac{\partial \mathbf{V}}{\partial t} + \mathbf{V}\cdot\nabla\mathbf{V} + 2\boldsymbol{\omega}\times\mathbf{V} = -g'\nabla h_T \qquad (1)$$

$$\frac{\partial h_T}{\partial t} + \nabla\cdot\mathbf{V}h_T = 0 \qquad (2)$$

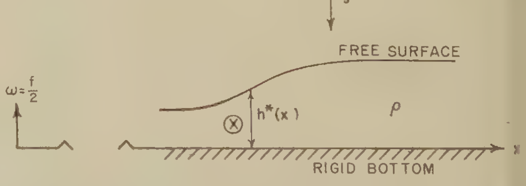

Fig. 2. A single layer system which is equivalent to Fig. 1 with respect to the dynamics of quasi-hydrostatic disturbances. $g' = g\Delta\varrho/\varrho$ is the "reduced" value of gravity.

Let us resolve the velocity into a mean component $\mathbf{V}^*(x)$ directed along the y axis and a perturbation $\mathbf{V}'(x, y, t)$ which has magnitudes (u', v') along (x, y). With a similar decomposition of $h_T = h^* + h'$ the linearized perturbation equations are—

$$\frac{\partial \mathbf{V}'}{\partial t} + 2\boldsymbol{\omega} \times \mathbf{V}' + \mathbf{V}^* \cdot \nabla \mathbf{V}' + \mathbf{V}' \cdot \nabla \mathbf{V}^* = -g' \nabla h' \tag{3}$$

$$\frac{\partial h'}{\partial t} + \nabla \cdot (\mathbf{V}^* h' + \mathbf{V}' h^*) = 0 \tag{4}$$

An interesting energy equation may now be formed by multiplying (3) by $h^*\mathbf{V}'$ and (4) $g'h'$. Denoting an average value over the entire horizontal plane by a bar we then get

$$\frac{\partial}{\partial t}\frac{1}{2}\,\overline{h^*\mathbf{V}'^2} + \frac{1}{2}\,\overline{h^*\mathbf{V}^* \cdot \nabla \mathbf{V}'^2} + {} + \overline{h^*\mathbf{V}' \cdot \mathbf{V}' \cdot \nabla \mathbf{V}^*} = -g'\,\overline{h^*\mathbf{V}' \cdot \nabla h'} \tag{5}$$

$$\frac{\partial}{\partial t}\frac{1}{2}\,g'\overline{h'^2} + g'\overline{h' \nabla \cdot \mathbf{V}^* h'} + g'\overline{h' \nabla \cdot \mathbf{V}' h^*} = 0 \tag{6}$$

In proceeding further we make use of the boundary condition that the normal component of $\mathbf{V}'$ vanishes at the x-boundaries and the downstream variation is well behaved (e.g. periodic in y). Note that the second term in (5) vanishes because the undisturbed velocity field has no horizontal divergence and also $\nabla \cdot h^*\mathbf{V}^* = 0$. Likewise, the second term in (6) vanishes and these equations become—

$$\frac{\partial}{\partial t}\frac{1}{2}\,\overline{h^*\mathbf{V}'^2} = -\overline{h^*\mathbf{V}' \cdot \mathbf{V}' \cdot \nabla \mathbf{V}^*} + g'\overline{h' \nabla \cdot \mathbf{V}' h^*} \tag{7}$$

$$\frac{\partial}{\partial t}\frac{1}{2}\,g'\overline{h'^2} = -g'\,\overline{h' \nabla \cdot \mathbf{V}' h^*} \tag{8}$$

Equation (7) may be interpreted as a statement of the rate of increase of the perturbation kinetic energy in the undisturbed depth h^*. The first term on the right represents a conversion of kinetic energy as the result of the Reynolds stress acting on the horizontal shear of the mean field. The second term represents work done against the gravitational field and will have a counterpart in the increase or decrease of the potential energy of the mean field. Note that in (8) there is an equal and opposite transfer to perturbation potential energy so that the sum of (7) and (8) is—

$$\frac{\partial}{\partial t}\left\{\frac{1}{2}\,\overline{h^*\mathbf{V}'^2} + \frac{1}{2}\,g'\overline{h'^2}\right\} = -\overline{h^*\mathbf{V}' \cdot \mathbf{V}' \cdot \nabla \mathbf{V}^*}$$

$$= -\overline{h^* u' v' \frac{\partial V^*_{(x)}}{\partial x}} \tag{9}$$

Since both integrands on the left side of (9) are positive definite it follows that spontaneous instabilities can only occur if $-\overline{h^*\mathbf{V}' \cdot \mathbf{V}' \cdot \nabla \mathbf{V}^*}$ is positive, i.e., the mean field must do work on the perturbation through the Reynolds stress. If this term were zero or negative neither $\mathbf{V}'$ nor h' could increase with time. This energy equation implies that the simple meander theory of STOMMEL (1953) is untenable, for in his model $h^*(x)$ is linear and $\partial V^*/\partial x = 0$. In that case $^1/_2\,\overline{h^* V'^2} + {}^1/_2\,g'\overline{h'^2}$ is conserved and a small disturbance could not grow unless the boundaries were squeezed. We also conclude that in the thermoclinic model, which we are about to consider in more detail, the shearing mechanism is fundamental to instability despite the availability of potential energy as represented by the departures of the surfaces from equi-potentials. This statement does not imply that there is no conversion of mean potential energy to the perturbation, but rather that if such occurs it can only be as a concomitant to the shearing mechanism. It should be borne in mind that this conclusion is based on the initial hypothesis that the bottom layer is very deep. Accordingly, this approximation may have the effect of eliminating certain modes of instability which are of interest.

3. The Stability of Quasi-Geostrophic Disturbances

The stability of the dynamical system (eq. (3) and (4)) depends on two "external" non-dimensional parameters:

$$R \equiv V/fL \qquad F \equiv f^2L^2/g'H_0 \tag{10}$$

The stream Rossby number (R) measures the ratio of inertial to coriolis force, for perturbations which have characteristic horizontal dimensions of order L (the half width of the jet) or greater. The rotational Froude number (F) is a measure of the vertical velocity of the perturbation, since the ratio of total horizontal convergence to either component ($\partial u'/\partial x$) is of order RF. One would like to discuss the stability characteristics for all values of R and F, using suitable profiles which describe the form of the mean flow. However, the analytical difficulties are such that we must satisfy ourselves with partial solutions, each of which is valid over certain ranges of the parameters. For example, when $F \ll 1$ the barotropic non-divergent theory is applicable and the necessary condition for instability requires that the jet have an inflection point. The case which is considered below is equivalent to an asymptotic[2] expansion of (3) and (4) in the Rossby number and is valid for $R \ll 1$ and F of order unity or less (as compared with the conclusion in Sec. 2 where the Rossby number may be as large as unity).

Equations (1) and (2) imply the conservation of the vertical component of potential vorticity. If $\zeta^*(x)$ denotes the undisturbed value of relative vorticity and $\zeta'(x, y, t)$ the perturbation vorticity then we have:

$$\left(\frac{\partial}{\partial t} + V^*(x)\frac{\partial}{\partial y} + v'\frac{\partial}{\partial y} + u'\frac{\partial}{\partial x}\right)\frac{f+\zeta^*+\zeta'}{h^*+h'} = 0 \tag{11}$$

When linearized eq. (11) becomes

$$\frac{1}{h^*(x)}\left(\frac{\partial}{\partial t} + V^*(x)\frac{\partial}{\partial y}\right)\zeta' - \frac{f+\zeta^*}{h^*}\cdot \cdot\left(\frac{\partial}{\partial t} + V^*\frac{\partial}{\partial y}\right)h' + u'\frac{\partial}{\partial x}\frac{f+\zeta^*}{h^*} = 0 \tag{12}$$

At this stage we introduce the geostrophic approximations:

$$v = g'/f\,\frac{\partial h'}{\partial x} \qquad u' = -g'/f\,\frac{\partial h'}{\partial y}$$

$$\zeta' = \frac{\partial v'}{\partial x} - \frac{\partial u'}{\partial y} = g'/f\,\nabla^2 h'$$

and therefore "correct to order R" eq. (12) becomes

$$\left(\frac{\partial}{\partial t} + V^*\frac{\partial}{\partial y}\right)\nabla^2 h' - \frac{f}{g'}\left(\frac{f+\zeta^*}{h^*}\right)\cdot \left(\frac{\partial}{\partial t} + V^*\frac{\partial}{\partial y}\right)h' - h^*\left(\frac{\partial}{\partial x}\frac{f+\zeta^*}{h^*}\right)\frac{\partial h'}{\partial y} = 0 \tag{13}$$

Let

$$h' = \phi(x)e^{i\alpha(y-ct)}, \quad c \equiv a + ib \tag{14}$$

and denote $P(x) = (f+\zeta^*)/h^*$ as the undisturbed potential vorticity. We then obtain the eigen-value equation

$$\phi''(x) - [\alpha^2 + fP(x)/g']\phi - \frac{h^*P'(x)\phi}{V^*(x) - c} = 0$$

$$\phi(\pm\infty) = 0 \tag{15}$$

where a prime denotes differentiation with respect to x. We now parallel Lord Rayleigh's technique (LIN, 1955) by multiplying (15) by the conjugate eigen-function $(\hat{\phi})$ and average the result over all values of x. When the imaginary part is set equal to zero one obtains

$$b\int_{-\infty}^{+\infty}\frac{h^*P'(x)\phi\hat{\phi}}{(V^*-a)^2+b^2}\,dx = 0 \tag{16}$$

It then follows that if there are unstable eigen functions (i.e. $b > 0$) then $P'(x)$ must vanish at some point which is at a finite distance from the centre of the jet. If $P'(x)$ were always of the same sign then (16) could not be satisfied. It is therefore necessary that the potential vorticity

$$P(x) = \frac{f+\zeta^*(x)}{h^*(x)} \tag{17}$$

have a maximum (or minimum) interior to the endpoints of the jet, in order that the latter be unstable. The derivation of this criterion is such that it can only be relied upon in the limit of small Rossby number ($\zeta^* \ll f$). Utilizing this approximation we may alternatively conclude that the flow is stable if

$$h^*\frac{d}{dx}\frac{f+\zeta^*}{h^*} = V^{*\prime\prime}(x) - \frac{f+\zeta^*}{g'h^*}fV^*$$

$$\cong V^*(V^{*\prime\prime}/V^* - f^2/g'h^*)$$

is never zero. Let us consider the class of velocity profiles for which $V^{*\prime\prime}/V^*$ is always finite and let max. $V^{*\prime\prime}/V^*$ denote its greatest value

---

[2] The y-wavelength is restricted to be of order L or greater and the time scale (period) of order L/V or greater. These assertions lead to a self consistent expansion of (3) and (4) whose zero order term is identical to that (15a) which is obtained by the simple derivation given below.

(for example: $V^*(x) \neq 0$ except at $x = \pm\infty$ where V^* goes to zero as some positive power of $1/x$). From the above equation it then follows that the mean field is stable if

$$\frac{f^2}{g' H_{+\infty}} > \max. \frac{V^{*''}(x)}{V^*(x)}$$

$$H_{+\infty} \equiv h^*(\infty) \tag{18}$$

Therefore a given $V^*(x)$ profile (corresponding to sufficiently small Rossby number) can be stabilized with respect to quasi-geostrophic modes by a uniform reduction of the thickness of the upper layer (other things being equal) to the point where (18) is satisfied.

On the other hand, it is easy to establish *instability* at sufficiently large h^* by noting that in this limit ($F \ll 1$) $P(x) \to 0$ while $h^* P'(x) \to d\zeta^*/dx$. In this case (15) reduces to

$$\phi''(x) - \alpha^2\phi - \frac{V^{*''}(x)}{V^* - c}\phi = 0$$

$$\phi(\pm\infty) = 0 \tag{19}$$

which is mathematically identical to the classical equation for two-dimensional inviscid instability. Tollmien's theorem (Lin, 1955) tells us that (for symmetrical V^*) there are marginally unstable solutions in the vicinity of certain discrete wave-numbers (α). Therefore, with a given profile, there must exist a maximum critical depth $[(H_{+\infty})]_{\mathrm{cr.}}$ above which the mean field is unstable and this number is bounded by:

$$0 < \frac{f^2}{g'(H_{+\infty})_{\mathrm{cr.}}} < \max. \frac{V^{*''}}{V^*(x)} \tag{20}$$

The phase speed of the neutral disturbance is equal to the mean speed of the jet at the potential vorticity extremum.

More precise specifications of these quantities require the solution of the eigenvalue equation (15), which is equivalent (correct to order R) to the following non-dimensional equation:

$$\phi''(\xi) - [\alpha_0^2 + F]\phi - \frac{\overline{W}''(\xi) - F\overline{W}(\xi)}{\overline{W} - c_0}\phi = 0$$

$$\phi(\pm\infty) = 0 \tag{15a}$$

where

$$\xi = x/L, \qquad V^*(x) = V\overline{W}(\xi)$$

$$c_0 = c/V \qquad \alpha_0 = \alpha L.$$

Although (15a) is difficult to solve in general, it is possible to obtain particular solutions for the case of the "Bickley Jet": $\overline{W} = \operatorname{sech}^2 x\ \xi$ (Savic, 1941). By direct substitution one finds that $\phi = \operatorname{sech}^2 \xi$ satisfies (15a) provided $\frac{1}{6}\alpha_0^2 = c_0 = \frac{1}{6}(4 - F)$. Therefore long quasi-stationary waves ($\alpha_0 \sim 0$, $c_0 \sim 0$) are neutral at $F \sim 4$. Using Tollmien's perturbation technique (Lin, loc. cit.) one can readily show that unstable solutions exist in the neighborhood of the neutral ones and that $F < 4$ is a sufficient condition for the instability of a Bickley Jet.

4. Discussion

Let us use the Bickley Jet profile to make some order of magnitude estimates of the depth of the upper layer which is necessary for instability. Consider water with a vertical temperature difference of 10° C (or air with a 1° C increase in potential temperature), $f = 10^{-4}$ sec^{-1}, and a jet half width of $L = 50$ km. Then $F = 4$ when $H_{+\infty} = 250$ meters. When this critical depth is exceeded the jet will be unstable to long waves provided the Rossby number is sufficiently small. To fulfill this, and validate the asymptotic theory, the amplitude of the jet must be less than $V \ll fL = 5$ meters/sec.

As regards the Gulf Stream, it should be pointed out that observations of the mean shear indicate that the characteristic Rossby number is not small but of order unity. Furthermore the restriction on the depth of the bottom layer in this model is such as to preclude other types of modes which are associated with the baroclinic structure of the jet. Nevertheless it is believed that the criterion for instability which is expressed by an extremum in the potential vorticity has a range of applicability which is greater than that which is indicated by the formal limits of validity of this theory. The relevance of this criterion to the stability of the Gulf Stream is supported by the observation of Stommel (1958 Fig. 65, based on a section at Lat. 38° N) that the layer between 17° C and 19° C is approximately one of constant potential vorticity. The disruption of the Gulf Stream north of Cape Hatteras may act as a control on the maximum depth of the thermocline in the interior of the ocean as well as along the western boundary.

Acknowledgement

The simple derivation of the instability criterion in Sec. 3 and the connection of the model with the criteria of Rayleigh and Kuo is the result of a suggestion made by Prof. Jule Charney of M.I.T. who read an earlier manuscript. This work was supported by funds from the U.S. Office of Naval Research and is W.H.O.I. contribution No. (1166).

REFERENCES

Charney, J. G., 1947: The Dynamics of Long Waves in a Baroclinic Westerly Current. *J. Meteor.*, **4**, pp. 135—162.

Eady, E. T., 1949: Long Waves and Cyclone Waves. *Tellus*, Vol. **1**, pp. 33—52.

Fuglister, F. C. and Worthington, L. V., 1951: Some results of a multiple ship survey of the Gulf Stream. *Tellus*, Vol. **3**, pp. 1—14.

Haurwitz, B. and Panofsky, H. A., 1950: Stability and Meandering of the Gulf Stream, *Transaction American Geophysical Union*, Vol. **31**, pp.

Kuo, H. L., 1949: Dynamic Instability of Two-Dimensional Nondivergent Flow in a Barotropic Atmosphere. *J. Meteor.*, **6**, pp. 105—122.

Kotschin, N., 1932: On the Stability of Margules Surfaces of Discontinuity, *Beiträge zur Physik der freien Atmosphäre* XVIII, pp. 129—164.

Lin, C. C., 1955: *The theory of Hydrodynamic Stability*, Cambridge Univ. Press.

Phillips, N., 1954: Energy Transformations and Meridional Circulations Associated with Simple Baroclinic Waves in a Two-level, Quasi-geostrophic Model, *Tellus*, Vol. **6**, pp. 273—286.

Pocinki, L. S., 1955: *The Stability of a Simple Baroclinic Flow with Horizontal Shear.* Geophysical Research Paper No. 38. AFCRC-TR-55-212.

Rossby, C. G., 1936: *Dynamics of Steady Ocean Currents in the Light of Experimental Fluid Mechanics.* P.P.O.M. Vol. 5, No. 1, 43 pp.

Savic, 1941: *Phil. Mag.* **32**, 245.

Solberg, H., 1930: *Das Zyklonenproblem.* Verh. III. Intern. Kongress für techn. Mechanik.

Stommel, H., 1953: Examples of the Possible Role of Inertia and Stratification in the Dynamics of the Gulf Stream System. *Jour. Mar. Res.* **12**, pp. 184—195.

— H., 1958: *The Gulf Stream.* U. of California Press, Berkeley.

PRINTED IN SWEDEN
ESSELTE, STHLM 62

Contribution No. 1167

Made in United States of America
Reprinted from LIMNOLOGY AND OCEANOGRAPHY
Vol. 6, No. 3, July, 1961
pp. 262–270

ECOLOGICAL AND PHYSIOLOGICAL STUDIES ON MARINE NEMATODES FROM A SMALL SALT MARSH NEAR WOODS HOLE, MASSACHUSETTS

BY WOLFGANG WIESER AND JOHN KANWISHER

ECOLOGICAL AND PHYSIOLOGICAL STUDIES ON MARINE NEMATODES FROM A SMALL SALT MARSH NEAR WOODS HOLE, MASSACHUSETTS[1]

Wolfgang Wieser and John Kanwisher
Department of Zoology, University of Vienna and
Woods Hole Oceanographic Institution, Woods Hole, Massachusetts[2]

ABSTRACT

Some physiological experiments have been performed on some marine nematodes from a soft-bottom community where they are numerically the most abundant group of the meiofauna. They appear to account for a quarter to a third of the biological activity in such a bottom. Different types of the same size show a three times variation in rate of O_2 uptake. A correlation seems to exist between respiration rate and feeding type.

INTRODUCTION

The physiology and the physiological-ecological relationships of the small invertebrate (meiofauna) communities of marine substrates have never been investigated; a first attempt is presented in this paper. A soft-bottom habitat was chosen for analysis in view of the increased occupation in recent years with this type of environment as an ecosystem (Smidt 1951, Sanders 1956, 1960, Teal 1959a, Pomeroy 1959, Wieser 1960). The investigation was confined to the nematodes which in soft-bottom substrates represent by far the most abundant group of small invertebrates (Wieser 1960).

MATERIALS AND METHODS

Quantitative samples were taken by means of plastic tubes of 10 and 1 cm^2 cross section pushed into the mud by hand. In the latter case the whole sample was sorted out under the microscope, in the former only a fraction of it. For the counting of the nematodes a "Bogorov tray," which is commonly employed for the counting of plankton, was found useful.

For experimental purposes samples were taken to the laboratory and kept as close as possible to the temperature which prevailed in the habitat at collecting time by using a cold room or refrigerator when necessary. The samples were collected between October, 1958, and June, 1959, when the water temperature varied from –1.5°C to 18°C.

Volume and weight determinations of nematodes were carried out as described by Wieser (1960).

Oxidation-reduction potential profiles were made by pushing a platinum electrode down into the core. The calomel reference made contact with the sediment at the surface.

Latent oxygen combining capacity of the sediment at different depths was measured by extruding 1 ml of the sediment into a bottle containing aerated sea water. This was immediately sealed with an oxygen electrode (Kanwisher 1959) and the time course of disappearance of the dissolved oxygen was followed on a recorder.

The anaerobic survival of nematodes was studied in Thunberg tubes that were flushed more than 20 times with tank nitrogen, then closed and left in a refrigerator for varying periods of time.

Determinations of oxygen consumption were made by the cartesian diver method as described by Holter and Linderstrøm-Lang (1943) and by Zeuthen (1947). The divers had a volume ranging from 6.5 to 37.4 μl and volume changes could be read to 0.001 μl/hr in the smallest and 0.006 μl/hr in the largest diver. The divers were filled with sea water and the nematode(s) transferred by means of a fine steel needle (Kerr pulp files no. 1). After the nematode(s) had sunk to the bottom of the diver, the superfluous water was sucked out with a fine pipette. Consequently, the volume of the water drop was

---

[1] This work was supported by National Science Foundation Grant G-4813.

[2] Contr. No. 1167 from the Woods Hole Oceanographic Institution.

not exactly controlled. The neck of the diver was closed with a KOH (conc.) and an oil seal, but no special flotation medium seal was put in. The volume of the gas space was determined by weighing the diver on a torsion balance with the water drop and the seals in their place. The experiments were performed either on single individuals or on batches of up to 5 equal-sized specimens. The experimental temperature was usually 20°C, in some cases 21 and 22°C, all ± 0.01°C. All values were corrected for 20°C, assuming the temperature/metabolism relationship of Krogh's standard curve (Krogh 1941; *cf.* Overgaard Nielsen 1949). The animals used had been kept in the laboratory for varying amounts of time, mostly 1 to 5 days, but sometimes as much as 16 days. Food was available in the form of mud and detritus from the original sample. Thermal adjustment to the experimental temperature was short, not more than a few hours, which, in view of the small size of the animals and the absence of temperature compensation in their metabolism (see below), should be sufficient. This is in agreement with the findings of Overgaard Nielsen (1949) in terrestric nematodes.

HABITAT

The habitat investigated was the sandy mud at the edge of a small *Spartina* marsh on Penzance Point, near Woods Hole, Massachusetts. The sediment actually covers old portions of the Spartina flat. From about 2 cm downwards dead roots of *Spartina alterniflora* are mixed into the sediment until they form a dense mat through which the plastic tube can be pushed only with difficulty. The sediment is sandy with a high proportion of silt and mud. Its appearance in a core is dark grey to black, overlain by a lighter and fluffier layer of detritus of varying thickness. All the samples were taken from a very small area which is covered by water of normal oceanic salinity at high tide and uncovered at low tide.

The general picture of the bottom sediment as a habitat is as follows. The interstitial water is trapped between the sediment particles and so supplies very little oxygen by its movement. Some oxygen is supplied by diffusion from the surface through this water phase. But the *in situ* biological demand is greater than this supply below about 1 cm and the environment becomes anaerobic. The redox potential drops very quickly at this level to values as low as –400 mv. No oxygen could be detected by probing with an oxygen electrode below 1 cm. Any doubt about the completeness of the anaerobicity inferred by the redox potential is removed by the rapid rate at which the sediment combines with oxygen when placed in aerated sea water. This is some thousand times faster than the oxygen consumption at the surface of an undisturbed core.

DISTRIBUTION OF NEMATODES

The population density of the nematode fauna at the collecting site varies from 1.4 to 2.1 × $10^6/m^2$. A list of the species found (Table 1) suggests that the distribution of several forms is patchy. Some species may be present in fall, but absent (or not detectable) in spring. While this cannot be verified for the less common species, it is certain for *Metoncholaimus pristiurus*, one of the most abundant species in the two November samples but entirely absent in the June sample. Moreover, repeated attempts to find this species for the measurement of oxygen consumption failed after about the middle of December. From that time on, *M. pristiurus* seems to be replaced by its close relative, *Oncholaimus campylocercoides*.

The data on the vertical distribution show that the dominant species are also those that penetrate most deeply into the mud. The decrease in number of specimens with increasing depth need not necessarily reflect an actual impoverization of the fauna but may be due to the reduction of available space since with increasing depth there is an enormous increase in the amount of dead *Spartina* roots per volume of mud. For example in the June sample, which did not contain any nematodes below 4 cm, the 0–2 cm layer contained no roots while in the 2–4 cm and the 4–6 cm layers the filter dried weight of *Spartina* roots amounted to 263 mg/cm^2 and 500 mg/cm^2 respectively.

TABLE 1. *Species and weight composition of nematode fauna in Penzance Marsh, Woods Hole*

	Species composition (% of population)						Biomass (% wt)	
Sample no.	Pen-1	Pen-2			Pen-12		Pen-1	Pen-12
Vertical sections (cm)		0–2	2–4	4–6	0–2	2–4		
Metoncholaimus pristiurus	38.3	3.9	1.8	12.5			57.3	
Sabatiera vulgaris	29.9	13.3	30.9	37.5	12.8	4.8	22.3	14.4
Spirina parasitifera	16.5	27.6	32.7		25.6	71.5	9.1	37.0
Halichoanolaimus longicaudatus	1.5	1.3	14.5				0.2	
Tripyloides gracilis	3.1	15.8					4.9	
Metalinhomoeus typicus	0.8	1.3	7.3				0.3	
Pareurystomina flagellicaudata	0.4	1.3					0.2	
Terschellingia n. sp.	1.1	1.8	1.8	37.5	7.7		0.3	1.6
Theristus setosus	0.8	5.3			5.1		0.6	4.7
Oncholaimus campylocercoides	0.4		1.8		9.0	14.3	0.2	16.4
Anticoma litoris	3.8				21.8		3.1	14.4
Terschellingia longicauda	1.1						0.2	
Theristus frictor	1.1						0.3	
Nudora lineata	0.8						0.3	
Spilophorella paradoxa		2.0	1.8					
Halalaimus pachydermatus		2.0	1.8					
Chromadora axi		3.3						
Monoposthia costata		1.3						
Desmolaimus fennicus		1.3						
Prochromadorella neapolitana		1.3						
Pareurystomina typicum		0.6						
Dermatolaimus elegans			1.8					
Hypodontolaimus carinatus		9.2			1.3			1.0
Paracanthonchus caecus		3.9			6.4			2.9
Hypodontolaimus balticus		2.6			1.3			1.0
Axonolaimus spinosus		0.6			1.3			0.2
Neochromadora poecilosoma					6.4			5.1
Odontophora papusi					1.3			0.4
Chromadorina germanica						4.8		0.4
Specimens examined	261	152	55	8	78	21		
Specimens/cm^2	213	71	68	5	170	24		
Specimens/cm^2 total	213	144			194			
Other meiofauna groups	4	5						
Biomass (wet wt g/m^2)							18.4	8.7
Collecting date	11/4/58	11/11/58			6/26/59			
Water temperature °C	8.5	9.0			18.0			

Moore (1931), Rees (1940), Mare (1942), Bougis (1946), and Smidt (1951) all agree that most nematodes can be found in the upper 4 cm of the mud, that they reach further down than the other groups of metazoans, and that the lower limit of the vertical penetration of marine nematodes into the mud lies around 8 cm. Within the limits of the present investigation these conclusions are supported by the data summarized in Table 1.

ANAEROBIC SURVIVAL

In view of the low E_h and the latent oxygen combining capacity below 1 cm in the mud it seems clear that all species we found must be able to tolerate highly reduced conditions. Moore (1931) found living nematodes in mud samples kept for a month in a reduced state in a rubber stoppered bottle. We have checked our material by putting 5 samples of mud together with a small amount of water into 5 Thunberg tubes, flushing the

TABLE 2. *Anaerobic survival of Penzance nematodes*

Sample no.	1, 2	3	4, 5
Number of days at reduced conditions	10–11	21	50–60
E_h volts at surface of mud	–.01 to –.04	?	–.06 to –.16
Anticoma litoris	→	→	→
Stenolaimus marioni	→	→	→
Longicyatholaimus quadriseta	→	→	→
Prochromadorella neapolitana	→	→	→
Sabatiera vulgaris	→	→	→
Sabatiera cupida	→	→	→
Odontophora papusi	→	→	→
Steineria n. sp.	→	→	→
Nudora lineata	→	→	
Hyalacanthion n. sp.	→	→	
Chromaspirina ciliata	→	→	
Chromaspirina n. sp.	→	→	
Spilophorella paradoxa	→	→	
Monoposthia duodecimalata	→	→	
Desmodora cephalata	→	→	
Paracanthonchus caecus	→	→	
Tripyloides gracilis	→		
Spirina parasitifera	→		
Ascolaimus elongatus	→		
Chromadora axi	→		
Oncholaimus campylocercoides	→		
Theristus setosus	→		
Oncholaimus paralangrunensis	→		
Monoposthia costata	→		
Hypodontolaimus carinatus	→		
Neochromadora poecilosoma	→		
Axonolaimus spinosus	→		

latter with nitrogen and storing them in a refrigerator at about 7°C. Before closing, some methylene blue was added to each Thunberg tube. The tubes were opened after a period from 10 to 60 days, the redox potentials at the surface of the mud were read and representative samples of the living nematodes were picked out under the microscope. The list of the species found (Table 2) again reflects the patchy distribution of some of the species. For this reason the absence of certain species in the most highly reduced samples, 4 and 5, cannot be taken as proof that these species would not survive extreme conditions. Since our negative E_h values indicate the absence of dissolved oxygen, it is safe to assume that all nematode species listed in Table 2 are able to live anaerobically for some time. It might be added that in samples 4 and 5 the mud was completely black and smelled of H_2S. In all samples the methylene blue was decolorized and turned blue again after exposure to air.

RESPIRATION

Despite the fact that all mud-inhabiting nematodes must be able to live anaerobically for some time, they can be kept for long periods in a well-aerated medium. Since the water overlying the Penzance Point mud at high tide is saturated with oxygen and stirs to a varying extent the top layer of the substrate, there must exist at times a mud-water interface in which the oxygen content falls from saturation to near zero and in which, consequently, nematodes have the opportunity of using oxygen for their metabolism. The thickness of this layer is probably never greater than 1 cm, but this upper centimeter is by far the most densely populated of all layers in the mud (Smidt 1951). This means that in large portions of the meiofauna of marine muds, periods of aerobic and anaerobic metabolism might alternate with each other. We can thus justify oxygen consumption determinations of metabolism in these mud-inhabiting animals. Such data for a number of the Penzance species is summarized in Table 3 and Figure 1. It was possible to measure representatives of most of the abundant and moderately abundant species listed in Table 1.

Although a great number of species belong to the size group from 2 to 8 μg, there is a considerable spread in the oxygen consumption, ranging from an average of 370 mm³/g/hr in *Spirina parasitifera* to 1,800 mm³/g/hr in *Axonolaimus spinosus*. This will be discussed below.

Comparison of the oxygen consumption of animals collected in winter and in summer or fall gives no indication that the species examined are able to compensate their metabolism for temperature changes. This means that in winter the metabolism of the whole nematode fauna will be very much reduced, which is in agreement with the findings by Wieser and Kanwisher (1960) for *Enoplus communis* and by Overgaard Nielsen (1949) for terrestric nematodes.

The range of variability in respiration rate

TABLE 3. *Oxygen consumption of Penzance nematodes, range and mean in parentheses*

	mm³ O₂/g/hr at 20°C	No. of determinations	Wet wt (μg)
Axonolaimus spinosus	1070–2580 (1800)	3	1.5– 2.9 (2.0)
Oncholaimus paralangrunensis	1210–1640 (1410)	5	3.4– 7.2 (5.7)
Bathylaimus kanwisheri	1300	1	5.0
Tripyloides gracilis	940–1860 (1285)	10	4.5– 8.6 (6.0)
Oncholaimus campylocercoides	860–1260 (1100)	6	11.0–22.0 (16.5)
Metoncholaimus pristiurus	610–1350 (918)	13	17.0–26.0 (21.2)
Theristus setosus	410–1100 (741)	16	5.0– 8.4 (6.5)
Odontophora papusi	660– 920 (726)	5	2.2– 5.0 (4.2)
Bolbella tenuidens	485– 815 (650)	2	16.0–26.0 (21.0)
Sabatiera vulgaris + *S. cupida*	455– 765 (605)	6	3.4–11.0 (7.3)
Monoposthia costata *Nudora lineata* }	445– 760 (590)	7	2.6– 3.9 (3.3)
Paracanthonchus caecus	356– 790 (563)	7	3.2– 5.5 (4.4)
Anticoma litoris	400– 625 (488)	6	7.0– 9.6 (8.3)
Terschellingia sp.	450	1	3.0
Spirina parasitifera	290– 540 (367)	6	4.1– 7.0 (5.9)
Halichoanolaimus longicauda	224– 510 (346)	4	21.0–57.0 (36.8)

lies around 100% in most species. While we believe that even under completely homogeneous experimental conditions the oxygen consumption of any species of invertebrates might vary by about 100%, the following possible sources of experimental variability should be mentioned. The weight determinations are based on the measurement of length and width of the animals and are therefore bound to introduce errors of as much as 10%. The animals were not starved before the experiments and thus might have been in different states of nutrition. However, Overgaard Nielsen (1949) has found that starving up to 7 days has no effect on the oxygen consumption of terrestric nematodes. The absence of an extra flotation medium seal might have allowed the flotation medium to penetrate at varying lengths into the neck of the diver, but the uncontrolled variability in the volume of the gas space so caused should not have exceeded 10%.

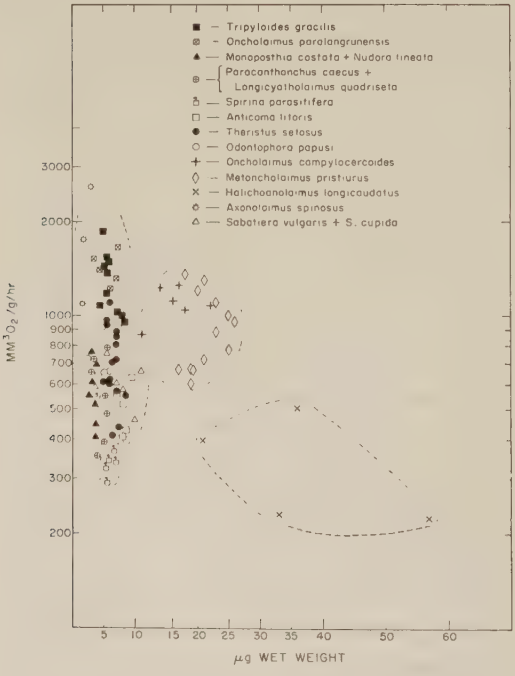

FIG. 1. Oxygen consumption of the more abundant species of nematodes from Penzance Point marsh near Woods Hole, Mass. Each convention denotes one experiment.

DISCUSSION

The density of the nematode fauna in the littoral mud of Penzance Point varies from 1.4 to 2.1 × $10^6/m^2$. This may be compared with a density from 2.8 × $10^5/m^2$ to 1.8 × $10^6/m^2$ in the offshore muds of Buzzards Bay in the same area (Wieser 1960). Smidt (1951) found about 1.0 × $10^6/m^2$ in the intertidal mud of the Danish Wadden Sea, but Rees (1940) about 10 times as many in the intertidal of the Bristol Channel. Thus it appears that the differences in population density between various intertidal areas are greater than those that might be encountered between the intertidal and the shallow sublittoral of the same area.

The nematode biomass can be estimated from volume determinations as used by Overgaard Nielsen (1949) and by Wieser (1960). This has been done for samples Pen-1 and Pen-12, using an average value for all adults of one species and assuming that the average weight of the juveniles was half that of the adults. This produces wet weights of 18.4 g/m^2 for the November sample (Pen-1), and 8.7 g/m^2 for the June sample (Pen-12). The smaller value for the June sample may be significant since at this time of year the large species *Metoncholaimus pristiurus* which dominated the November sample could not be found. Values of 8.7 g/m^2 and 18.4 g/m^2 indicate that the nematode biomass in the Penzance Point mud is about 10 times richer than the soft-bottom habitats of the shallow sublittoral. The corresponding figures are 0.4–2.5 g/m^2 for Buzzards Bay (12–30 m deep; Wieser 1960) and 1.15 g/m^2 for Plymouth Sound, England (45 m deep; Mare 1942). On the other hand, there is close agreement with the values given for certain types of terrestric habitats. Overgaard Nielsen (1949) found in Danish grass fields the biomass of the nematodes to vary between 6 and 17.8 g/m^2.

Our measurements of Q_{O_2} on most of the abundant nematode species permit the calculation of the total respiration of the nematode fauna per unit of surface area. As has been pointed out, the mud below 1 cm is always highly reduced and yet contains a considerable number of nematodes. Since our measurements were made with air in the cartesian diver, such a use of the figures assumes that nematodes have the same energy requirements whether living aerobically or anaerobically. The only indication that this is so comes from our repeated observations that the nematodes in question show identical speed and type of movement in an aerated dish and in a Thunberg tube with a highly reduced substrate.

The oxygen consumption of the nematode populations in samples Pen-1 and Pen-12 can be calculated, using the average Q_{O_2} values listed in Table 3 and the weight distribution given in Table 1. There are only few and relatively rare species of which the oxygen consumption is not known and these are assigned Q_{O_2} values of closely related species. In such a manner a total oxygen consumption of 13.9 cc/m^2/hr for Pen-1 and of 5.1 cc/m^2/hr for Pen-12 is found for a temperature of 20°C. In calculating these values the juveniles of each species were assumed to possess the same respiration rate as the adults. This assumption is certainly incorrect (see Overgaard Nielsen 1949, Wieser and Kanwisher 1960) but the error introduced by it is small. The total oxygen consumption of the nematode fauna of Danish grass fields measured at 16°C by Overgaard Nielsen varied between 5.8 and 17.3 cc/m^2/hr and thus agrees well with the data from the Penzance salt marsh.

Oxygen consumption per unit area of the bottom was determined as a measure of the energy utilization of the entire bottom community. Cores taken in plastic tubes were layered with sea water. Mineral oil was added on top to prevent gas exchange with the air. The sea water was kept mixed by stirring with a wire loop. The decrease in dissolved oxygen with time was followed by determinations made on 1-ml samples withdrawn by syringe. In November (Pen-1) the bottom consumption averaged 36 cc/m^2/hr while the spring determinations (Pen-12) gave a value of 26 cc/m^2/hr. Thus the nematode fauna appears to account for 25 to 33% of the biological activity in the bottom. We have estimated that the macrofauna respiration accounts for 10 to 15% additional of the bottom total. The remainder, more than half, can reasonably be allocated to the smaller forms, bacteria and protozoa. It may be that the highly reduced conditions of the bottom sediments tend to eliminate the larger forms and so produce an opportunity for the biochemically more ingenious bacteria to take over.

Anaerobic processes yield only about 10% of the energy that could be derived by complete oxidation of a food (Brand 1946). Thus the nematodes would have partially to digest a larger quantity of food if an energy requirement equal to that in air has to be satisfied. Using the dominant species of the November samples, *Metoncholaimus pristiurus*, the following calculation can be made. The average weight of an animal is 20 μg and it consumes about 1,000 m^3 O_2/g/hr at 20°C, or .02 m^3 O_2/hr/animal. Since the consumption of one liter of oxygen corresponds to the combustion of 1.34 g of carbohydrate, one animal in the presence of oxygen used about .029 μg of carbohydrate per hour which, according to the assumption made above, corresponds to about .29 μg of carbohydrate per hour under anaerobic conditions. The intestine of *M. pristiurus* measures on the average, 450 × 50 μ which corresponds to a volume of .00088 mm^3. If the specific gravity of the Penzance Point mud were only slightly higher than 1 (which is certainly too low), one intestine full of mud weighs about 1 μg. Supposing the total content of the intestine were to consist of digestible material with the caloric value of carbohydrate, the nematode could live on it for three hours under anaerobic conditions if it spent as much energy as it does under experimental conditions in the presence of oxygen at 20°C. If only 10% of the mud consisted of digestible material, one filling of the intestine would last for not more than 18 min.

Such a rapid rate makes our measured values of oxygen consumption less convincing. It is likely that in an undisturbed natural substrate, the animal would spend less energy than it would in a drop of water at the bottom of a cartesian diver. However, it is not likely that the experimental figures differ from the values to be expected in nature by, say, 500%. Also the possibility should be considered that nematodes may not, after all, spend as much energy under anaerobic conditions as they do in the presence of oxygen. Either case would make the nematodes energetically less important in the community than we have estimated.

The large range of variation in the respiration rate of nematode species (Fig. 1) is difficult to reconcile with the assumption made by several authors (Müller 1943, Krüger 1952, Bertalanffy 1957, and others) that within a taxonomic group interspecific differences in respiration rate can be sufficiently explained by differences in size (weight or surface) of the species concerned. The range of variation from 370 to 1,800 mm^3 O_2/g/hr in species that differ only little in weight and not at all in surface/volume ratio (see Wieser and Kanwisher 1960) seems to point definitely toward basic metabolic differences in these species. Similar large differences between related species of the same size group were found by Schwartzkopff and Wesemeier (1959) and by Wesemeier (1960) in mollusks.

We may rule out the possibility that different species are differentially harmed by the presence of oxygen since, as already mentioned, all species can be kept alive for long periods in an oxygenated medium. On the other hand, there is a clear correlation between oxygen consumption and degree of activity of the species. The species with respiration rates between 300 and 500 mm^3/g/hr are definitely more sluggish than those with respiration rates of 700 mm^3/g/hr and more. The species with respiration rates of greater than 1,200 mm^3/g/hr are almost constantly active in a dish, either swimming with whip-like motions of the whole body (*Axonolaimus spinosus*, *Oncholaimus paralangrunensis*) or continuously coiling and uncoiling (*Tripyloides gracilis*, *Bathylaimus kanwisheri*). On the other hand, *Spirina parasitifera* and *Anticoma litoris* can often be observed lying motionless in a rigid position at the bottom of the dish or coiled around shreds of algae or sand grains.

Different levels of oxygen consumption may also be explained by the existence of a correlation between respiration rate and feeding type. If the shape of the buccal cavity is pictured alongside a list of species arranged according to levels of oxygen consumption (Fig. 2) it is found that large buccal cavities are typical of species with high oxygen consumption, small buccal cavities of species with low oxygen consumption. The only exception to this rule is the largest species found, *Halichoanolaimus longicaudatus*. The three species with an average oxygen consumption between 350 and 500 mm^3 O_2/g/hr belong to what Wieser (1953) has called group 1-A, in which the

Axonolaimus spinosus	1800
Oncholaimus paralangrunensis	1410
Bathylaimus kanwisheri	1300
Tripyloides gracilis	1285
Oncholaimus campylocercoides	1100
Metoncholaimus pristiurus	918
Theristus setosus	741
Odontophora papusi	726
Bolbella tenuidens	650
Sabatiera vulgaris + S. cupida	605
Monoposthia costata Nudora lineata	590
Paracanthonchus caecus	563
Anticoma litoris	488
Terschellingia sp.	450
Spirina parasitifera	367
Halichoanolaimus longicauda	346

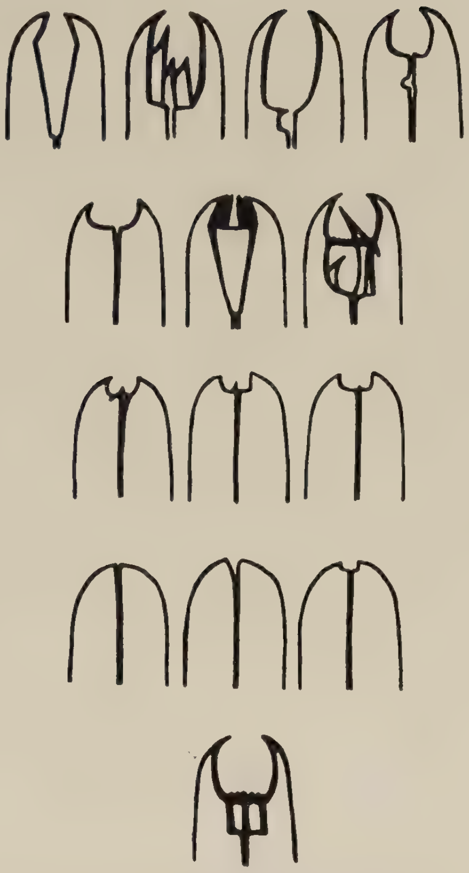

FIG. 2. Average respiration rate, in mm^3 O_2/g/hr, of nematode species from Penzance Point marsh near Woods Hole, Mass., together with outline drawings of anterior end of species studied in order to show relationship between respiration rate and shape of buccal cavity.

buccal cavity is either absent or very small (in the above-mentioned paper the genus *Spirina* was erroneously referred to group 2-A). The species with an average oxygen consumption of approximately 600 mm^3 O_2/g/hr belong to group 2-A which is characterized by a medium-sized buccal cavity and the possession of small teeth. The remaining species all of which have respiration rates above 650 mm^3 O_2/g/hr are in groups 1-B and 2-B which possess large buccal cavities, either armed with teeth or unarmed.

The most plausible interpretation of this relationship is that the different types of buccal cavities represent different feeding types and that the amount of oxygen required to sustain the metabolic and behavioral functions of these feeding types is also different; for example, the species with large buccal cavities may be non-selective deposit feeders and ingest a large amount of material of which they use only a fraction; while the species with small buccal cavities may be selective deposit or epigrowth feeders in which the ratio of digested to ingested material is higher. Obviously, the non-selective feeders would have to roam about more widely, and so be more active than the selective feeders. This is in agreement with observations on the general activity in the species concerned. The exceptional position of *Halichoanolaimus longicaudatus* may be due to a mode of feeding different from that of the other species with large buccal cavities. It may be pointed out that the genus *Halichoanolaimus* (together with the genus *Sphaerolaimus* which is not represented in the material) contains species in which predatory feeding habits are better established than in any other species of marine nematodes (Ditlevsen 1919, 1921, Allgén 1939, Wieser 1960).

REFERENCES

Allgén, C. 1939. Räuberische Ernährungsweise mariner Nematoden, insbesondere Halichoanolaimini. Fol. Zool. Hydrobiol., **9:** 321–325.

Bertalanffy, L. v. 1957. Quantitative laws in metabolism and growth. Quart. Rev. Biol., **32:** 217–231.

Bougis, P. 1946. Analyse quantitative de la microfaune d'une vase marine a Banyuls. C. R. Acad. Sci., **222:** 1122–1124.

Brand, T. v. 1946. Anaerobiosis in Invertebrates. Biodynamica Monogr. no. 4. Biodynamica, Normandy, Missouri, 328 pp.

Ditlevsen, H. 1919. Marine free-living nematodes from Danish waters. Vid. Medd. Dansk naturh. Foren., **70:** 147–214.

———. 1921. Marine free-living nematodes from the Auckland and Campbell islands. Vid. Medd. Dansk naturh. Foren., **73:** 1–32.

Holter, H., and K. Linderstrøm-Lang. 1943. On the Cartesian Diver. C. R. Lab. Carlsberg, Sér. chim., **24:** 333–478.

Kanwisher, J. W. 1959. Polarographic oxygen electrode. Limnol. Oceanogr., **4:** 210–217.

Krogh, A. 1941. The comparative physiology of respiratory mechanisms. Philadelphia, Univ. Pennsylvania Press, 172 pp.

Krüger, F. 1952. Über die Beziehung des Sauerstoffverbrauches zum Gewicht bei *Eisenia foetida* (Sav.) (Annelida Oligochaeta). Z. vgl. Physiol., **34:** 1–5.

Mare, M. 1942. A study of a marine benthic community with special reference to the micro organisms. J. Mar. Biol. Ass. U.K., **25:** 517–554.

Moore, H. B. 1931. The muds of the Clyde Sea area. J. Mar. Biol. Ass. U.K., **17:** 325–358.

Müller, I. 1943. Untersuchungen zur Gesetzlichkeit des Wachstums. IX. Z. vgl. Physiol., **30:** 139–144.

Nielsen, C. O. 1949. Studies on the soil microfauna. II. The soil inhabiting nematodes. Natura Jutlandica, **2:** 1–131.

Pomeroy, L. R. 1959. Algal productivity in salt marshes of Georgia. Limnol. Oceanogr., **4:** 386–397.

Rees, C. B. 1940. A preliminary study of the ecology of a mud-flat. J. Mar. Biol. Ass. U.K., **24:** 185–199.

Sanders, H. L. 1956. Oceanography of Long Island Sound, 1952–1954. X. Biology of marine bottom communities. Bull. Bingham Oceanogr. Coll., **15:** 345–414.

———. 1960. Benthic studies in Buzzards Bay. III. The structure of the soft-bottom community. Limnol. Oceanogr., **5:** 138–153.

Schwartzkopff, J., and H. Wesemeier. 1959. Zur Frage der Abhängigkeit des Sauerstoffverbrauchs vom Körpergewicht bei Gastropoden und Bivalviern. Naturwiss., **46:** 273.

Smidt, E. 1951. Animal production in the Danish Waddensea. Medd. Komm. Danmark. Fisk. Havunders. Ser. Fisk., **11:** 1–151.

Teal, J. M. 1959. Energy flow in the salt marsh ecosystem. Salt Marsh Conference March 1958. Mar. Inst. Univ. Georgia, Athens, Georgia, pp. 101–104.

Wesemeier, H. 1960. Untersuchungen über die Stoffwechselreduktion. Z. vgl. Physiol., **43:** 1–28.

Wieser, W. 1953. Die Beziehung zwischen Mundhöhlengestalt, Ernährungsweise und Vorkommen bei freilebenden marinen Nematoden. Ark. Zool. Ser. 2, **4:** 439–484.

———. 1960. Benthic studies in Buzzards Bay, II. The meiofauna. Limnol. Oceanogr., **5:** 121–137.

———, and J. W. Kanwisher. 1960. Growth and metabolism of a marine nematode, *Enoplus communis* Bast. Z. vgl. Physiol., **43:** 29–36.

Zeuthen, E. 1947. Body size and metabolic rate in the animal kingdom, with special regard to the marine micro-fauna. C. R. Lab. Carlsberg, Sér. chim., **26:** 17–161.

Contribution No. 1168

Interstitial Waters of Recent Marine Muds Off Cape Cod

Abstract. Interstitial waters of Recent muds off Cape Cod have salinities higher than the present ocean water in the same location and *p*H values lower than normal sea water in equilibrium with the atmosphere. The salinities may be either "paleosalinities" or an effect produced by behavior of the clay-water system as a semipermeable membrane. The low *p*H values are due to higher pressures of CO_2 in the sediment, probably coming from bacterial decomposition of organic matter.

On a recent cruise of the research vessel *Atlantis* of the Woods Hole Oceanographic Institution, several piston cores of bottom muds were taken and "squeezed" to remove the interstitial water. The stations occupied were all in the vicinity of 41°55′N, 69°30′W, in a small area of Recent grey muds several miles off Nauset light on the outer part of Cape Cod. Two layers were penetrated, a section of grey, slightly silty homogeneous clay, 1 to 6 m thick, at the top, and a section of brown and grey sandy and pebbly clay, at least 2.5 m thick, below. The upper grey clay contains a few marine mollusk shells, and is estimated to contain 2 to 5 percent $CaCO_3$. The lower brown sandy clay contains many carbonaceous fragments. Tentatively, the lower zone is correlated with the late Pleistocene, and the upper with the Recent. An oxidized transition zone of about 30 cm separates the two zones.

Samples of the cores were squeezed in a modified filter press of special design (*1*) to extract the interstitial water. The Na^+ activity of these waters and the bottom sea water, hereafter called "sodium-ion," were measured by a Na^+ sensitive glass electrode. This electrode should have no interference by other ions in sea water or interstitial water (*2*). Differences of electromotive force between standard Copenhagen water and the unknowns were read to ± 0.05 mv; it is estimated that the ratios reported are accurate to ± 1 percent of the number given. Chlorinity of the same samples was determined by $AgNO_3$ titration (Knudsen method). In addition, some *in situ* measurements of sodium-ion were made by pushing the glass electrode into the soft sediment. The values of sodium-ion determined by direct *in situ* measurement and by determinations on the squeezed waters are much the same.

Sodium-ion and chlorinity of bottom sea water and interstitial water plotted against depth in one core is shown in Fig. 1; the values are given as ratios to standard Copenhagen water (chlorinity = 19.374). The bottom water in this area is considerably less saline than that of the normal open sea throughout the year, mainly because fresh water funnels out of the Gulf of Maine past Cape Cod. The interstitial waters are all higher in sodium-ion and chlorinity than the overlying sea water, but less than Copenhagen water. The $\text{sodium-ion}_{\text{sample}}/\text{sodium-ion}_{\text{standard}}$ and $\text{chlorinity}_{\text{sample}}/\text{chlorinity}_{\text{standard}}$ ratios are in good agreement except for the bottom sea water, in which the $\text{sodium-ion}_{\text{sample}}/\text{sodium-ion}_{\text{standard}}$ is appreciably lower than the $\text{chlorinity}_{\text{sample}}/\text{chlorinity}_{\text{standard}}$.

The salinity change between bottom water and interstitial water may be explained by one of two alternatives. One is that some process is operating that is concentrating the salts in the sediment as the water of compaction is expressed upwards. It may be considered that the compacting clay-water system acts as a semi-permeable membrane, and only water is expressed, the hydrated ions being held behind.

An alternative is that this water is trapped unmodified sea water, and the salinities are "paleosalinities" (*3*). If this were so, it would suggest that the sediments accumulated in the past, when the hydrographic situation affecting sea water composition was somewhat different than that of today. For example, the sediments might have been accumulating during a time of decreased precipitation that resulted in less fresh water dilution from the Gulf of Maine than at present.

The choice between these alternatives can be made more easily after the completion of studies in progress on the behavior of clay-water systems under pressure as semi-permeable membranes and after more oceanic sediments are sampled to see if the effect is general or restricted to this area.

Determinations of *p*H by ordinary glass electrode were made *in situ* and on the expressed interstitial waters. The results showed that the *in situ p*H ranges from 7.4 to 7.8, whereas in the interstitial waters which were aerated in the squeezing process, it ranges from 8.1 to 8.2, a figure one would normally expect from sea water in equilibrium with the atmosphere. The simplest explana-

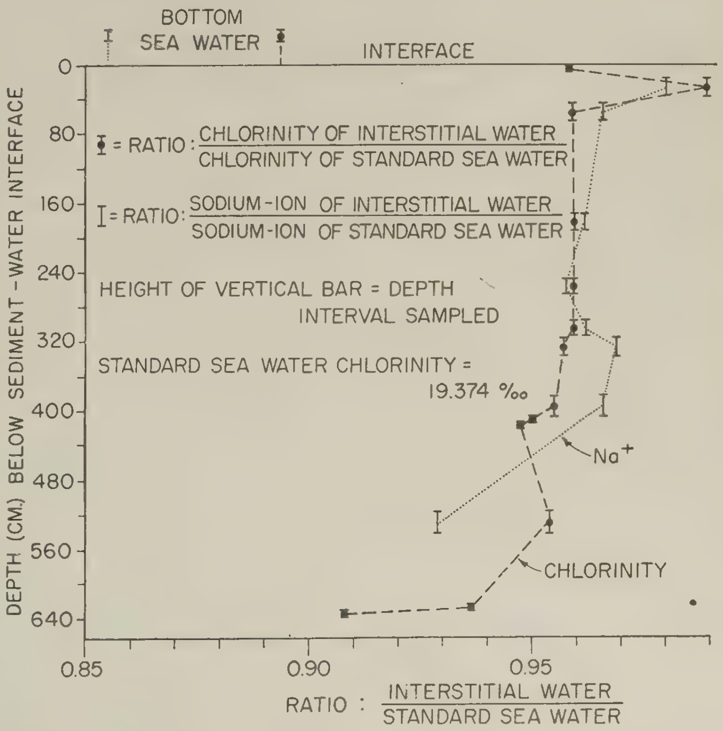

Fig. 1. Sodium-ion and chlorinity of bottom sea water and interstitial water plotted against depth.

tion for this discrepancy is that the CO_2 pressure in the sediment is higher than that in equilibrium with the atmosphere, and it is this that keeps the *p*H down. A calculation of the CO_2 pressure based on the *p*H change indicates that CO_2 pressure in the sediment is almost ten times that of the atmosphere. Measurements with a glass electrode, with a saturometer technique (*4*), indicated that the *in situ* sediment water is saturated with respect to $CaCO_3$ (calcite). The increased CO_2 is most likely the result of bacterial oxidation of organic matter. If this is so, CO_2 apparently diffuses upward through the sediment too slowly to allow the sediment to equilibrate with the overlying sea water, which, at this location, is almost certainly close to equilibrium with the atmosphere. Saturation with respect to calcite indicates that the solid carbonate shells are quick to equilibrate with the increased CO_2 by dissolving slightly (*5*).

RAYMOND SIEVER, ROBERT M. GARRELS
JOHN KANWISHER, ROBERT A. BERNER
Woods Hole Oceanographic Institution,
Woods Hole, Massachusetts, and
Harvard University, Cambridge,
Massachusetts

References and Notes

1. R. Siever, *J. Sediment. Petrol.*, in press.
2. G. Eisenman, D. O. Rudin, J. U. Casby, *Science* **126**, 831 (1957).
3. B. Kullenberg, *Medd. Oceanog. Inst. Göteborg* **6**, (1952).
4. P. K. Weyl, *J. Geol.* **69**, 32 (1961).
5. This research was supported by various grants from the Petroleum Research Fund, American Chemical Society; the Committee on Experimental Geology, Harvard University; The Office of Naval Research, under Contract NONR 2196 (00), NR 083 (004); and the Woods Hole Oceanographic Institution. This paper is Contribution No. 1168 from the Woods Hole Oceanographic Institution. Chlorinity analyses were made by D. R. Waldbaum.

3 May 1961

Reprinted from: **Science** 134 (3485): 1071-1072.

Contribution No. 1168
Woods Hole
Oceanographic Institution

Contribution No. 1170

Deep-Sea Research, 1961, Vol. 8, pp. 95 to 110. Pergamon Press Ltd., London. Printed in Great Britain

On the Abyssal Circulation of the World Ocean—IV

Origin and rate of circulation of deep ocean water as determined with the aid of tracers

BERT BOLIN* and HENRY STOMMEL**

(*Received* 10 *January* 1961)

Abstract—Using box models, and the observed distribution of temperature, salinity and radiocarbon estimates are made of the origins and rate of flow of waters that make up the Common Water in the Pacific and Indian Oceans, and Antarctic Intermediate Water. Difficulties in extending the computation to Antarctic Bottom Water are described. Emphasis is placed upon questions of computational reliability and the occurrence of ' ill-conditioned ' equations.

INTRODUCTION

RADIOACTIVE tracers such as radio-carbon have recently been applied to ocean circulation studies. So far, relatively few measurements are available and it has been possible to deduce only certain overall characteristics of the circulation of the sea. Thus CRAIG (1957) obtained a preliminary idea of the turnover time for the deep sea with the aid of C^{14} measurements. Recently BROECKER *et al.* (1960) and BIEN *et al.* (1960) have published more extensive measurements of C^{14} in the Atlantic and Pacific oceans and also tried to draw some conclusions regarding the circulation of these oceans. It is interesting to note, however, that in none of these studies has our quite extensive knowledge of the distribution of temperature and salinity been systematically utilized. Obviously the heat and salt can also be looked upon as tracers and used for circulation studies, as has, of course, also been done extensively in the past. By combining the comparatively few measurements of C^{14} with the large amount of information concerning the distribution of temperature and salt, more far-reaching conclusions can be drawn concerning the ocean circulation, and indeed the potentialities of such a technique have not been exhausted.

In making use of the few observations so far available, it is necessary to construct a very simplified picture of the ocean in order to obtain any results at all. We shall here use the so called ' box models.' It is assumed that the ocean water in each one of these boxes is well mixed and that the exchange between them can be expressed by first order processes. Certain difficulties are encountered if dividing the ocean into a large number of boxes (which actually correspond to a finite difference approximation of the appropriate equations for the transfer of matter) but we shall here restrict ourselves to a few very simple cases in which no ambiguity arises.

The following discussion will be essentially restricted to a discussion of the origin of the Common Water in the Pacific, the formation of Antarctic Bottom Water and the rate of flow of Intermediate Water towards the north in the Atlantic Ocean.

---

*Institute of Meteorology, Royal University of Stockholm.
**Pierce Hall, Harvard University.

2. THE ORIGIN OF COMMON WATER

(*a*) *Formulation of a model*

The most voluminous water mass in the world ocean is the deep water of the Indian and Pacific Oceans which MONTGOMERY (1958) has named Common Water. Reasons for supposing the Common Water to be a mixture of Atlantic Deep Water and Antarctic Bottom Water are put forth in Part II of this series. There must also be some mixture with the Pacific and Indian waters which immediately overlie the Common Water, and some heating from geothermal heat entering from the bottom also seems likely (WOOSTER and VOLKMANN 1960). We address ourselves to the problem of determining the relative contributions of these various components to the Common Water, and the rates at which they are added. First numerical values of the temperature, salinity, and radio-carbon to be associated with each of these water masses are chosen, as given in Table 1.

Table 1.

	N.A.D.W.	A.A.B.W.	P.+ I.I.W.	C.W.	
	$i = 1$	$i = 2$	$i = 3$	$i = 4$	*Allowed range*
T_i °C	2·5	0·0	4·0	1·5	± 0·1°
S_i ‰	34·90	34·70	34·40	34·70	± 0·03°
C_i	0·90	0·88	0·87	0·77	± 0·03°

The numerical values chosen to represent entire water mass are to a large extent arbitrary : the temperature and salinity being taken from MONTGOMERY (1958) and the values of radiocarbon from BROECKER *et al.* (1960) and BIEN *et al.* (1960).

It has been puzzling to some investigators as to how one can justify breaking up a continuous distribution of properties into several discrete boxes. Approximate methods using finite differences do much the same, but the number of boxes is taken to be as large as possible. Here we use very few boxes – but there is an important justification, based on the distribution of water in various temperature and salinity classes as tabulated by MONTGOMERY, COCHRANE and POLLAK (1958). FIG. 1 is a summary diagram directly taken from the graphs of the above authors (whose work must be consulted for accurate numerical values). The greatest volume of water occurs in the Common Water mode in the Pacific and Indian Oceans (shaded, white and stippled bars). The North Atlantic Deep Water and Antarctic Bottom Water occur as two distinct separate modes (black bars) in the Atlantic. There is even a weak mode at the temperature–salinity classes representative of the Intermediate Water. That the volumes occur in distinct modes indicates that there really are ‘ natural mixed boxes ’ in the ocean – even if their boundaries are diffuse – and the location of the modes guides our choice of representative values. The situation is not so clear when we must consider surface water.

In setting up the conservation laws expressing the various mass fluxes (in cm^3/yr.) from the i^{th} water mass to the j^{th} are denoted by K_{ij}. Thus, for example the amount of salt flux from the North Atlantic Deep Water ($i = 1$) into the Common Water ($i = 4$) is $K_{14}S_1$. In the following applications we write the flux of mass out of the Common Water as K_4, neglecting the second subscript because we are only writing, at this point,

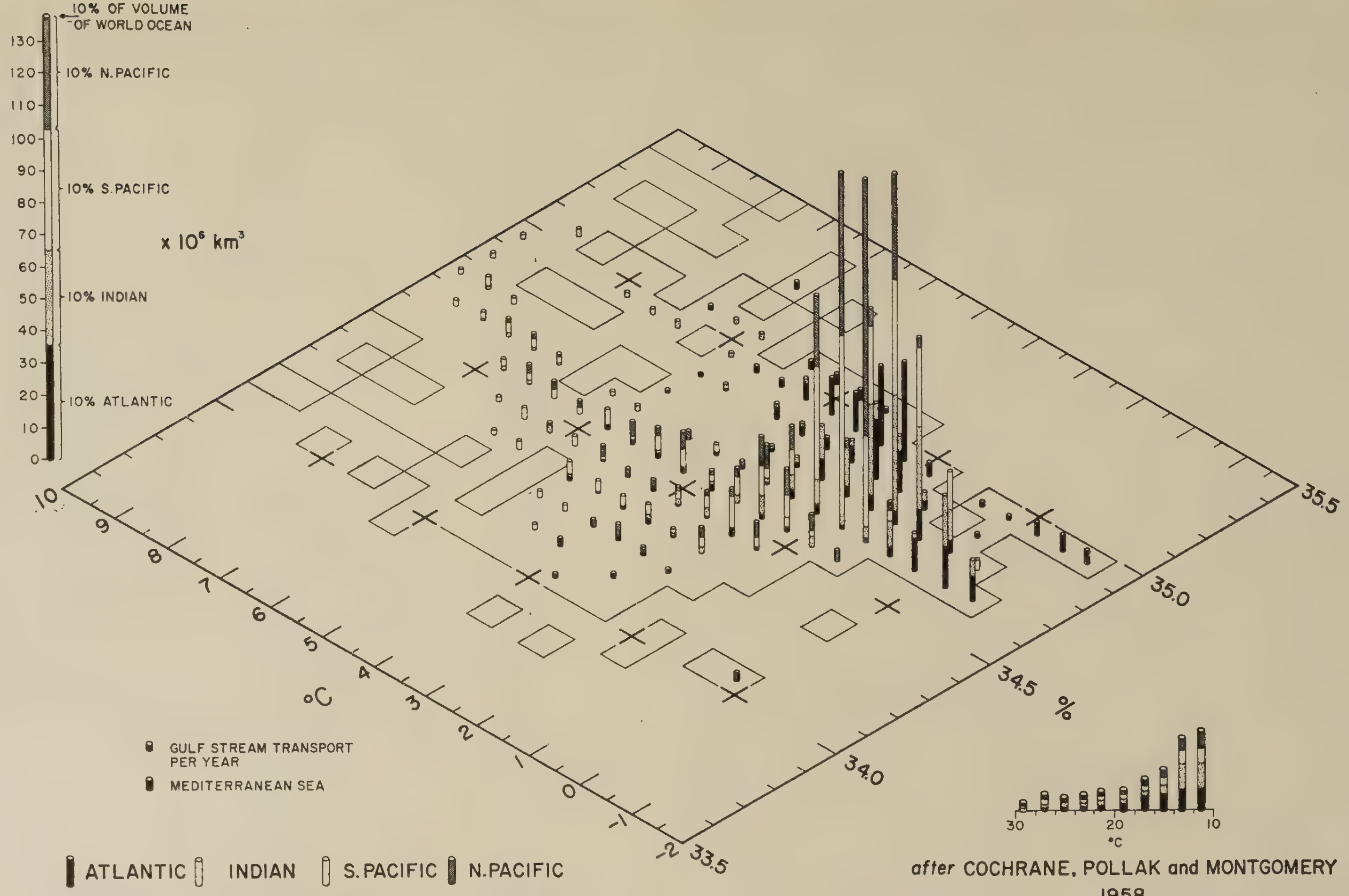

FIG. 1. Frequency distribution of the water masses of the world oceans. (after COCHRANE, POLLAK, MONTGOMERY, 1958).

conservation laws for the Common Water, and it is not relevant to note where the Common Water flows (although considerations in Part II suggest that it is mainly upward through the thermocline). We may also neglect the subscript j in the other K's because it is here, always understood to be 4.

Model I : With these conventions, the conservation laws of mass, heat, salt, and radiocarbon in the Common Water may be written as :

$$(1)\quad K_1 + K_2 + K_3 - K_4 = 0$$

$$(2)\quad K_1S_1 + K_2S_2 + K_3S_3 - K_4S_4 = 0$$

$$(3)\quad K_1T_1 + K_2T_2 + K_3T_3 - K_4T_4 = -HM_4$$

$$(4)\quad K_1C_1 + K_2C_2 + K_3C_3 - K_4C_4 = \lambda M_4C_4$$

On the right hand side the term HM_4 represents the rate of gain of heat due to geothermal flux through the bottom. It is constructed by noting that for a flux of 50 gm cal $\mathrm{cm}^{-2}\,\mathrm{yr}^{-1}$, a column of water 2500 m deep would increase in temperature at a rate $H = 2 \times 10^{-4}\,°\mathrm{C\,yr}^{-1}$. This must be multiplied by the mass of the Common Water $M = 6 \times 10^{23}$ gm, to represent the rate of heat added to the whole Common Water, and when entered on the right hand side requires the minus sign. The right hand side of the radio carbon conservation equation represents radio active decay, the decay rate being $\lambda = 1{\cdot}2 \times 10^{-4}\,\mathrm{yr}^{-1}$. The rate of loss of radio carbon in the entire Common Water mass is λM_4C_4, and is entered on the right hand side with a positive sign.

The numerical work is somewhat simplified if we introduce

$$X_i = K_i\,10^4/M_4$$

and substitute

$$S_i' = S_i - 34{\cdot}00$$

for the salinity so as to remove the large constant part of the salinity. The equation may then be written in terms of numbers with order of magnitude near unity

$$X_1 + X_2 + X_3 - X_4 = 0$$

$$S_1'\,X_1 + S_2'\,X_2 + S_3'\,X_3 - S_4'\,X_4 = 0$$

$$T_1\,X_1 + T_2\,X_2 + T_3\,X_3 - T_4\,X_4 = -2{\cdot}0$$

$$C_1\,X_1 + C_2\,X_2 + C_3\,X_3 - C_4\,X_4 = 1{\cdot}2\,C_4$$

The solutions are (values of coefficient 5 from Table 1) after conversion to conventional oceanographic units ($10^6\,\mathrm{m^3/sec}$) and dropping superfluous significant figures

$$K_1 = 3{\cdot}9 \times 10^6\,\mathrm{m^3/sec}$$

$$K_2 = 9{\cdot}6 \times 10^6\,\mathrm{m^3/sec}$$

$$K_3 = 2{\cdot}6 \times 10^6\,\mathrm{m^3/sec}$$

$$K_4 = 16{\cdot}2 \times 10^6\,\mathrm{m^3/sec}$$

the decimal figure being insignificant. The residence time in the Common Water is $M_4/K_4 = 3{\cdot}7 \times 10^{10}$ secs $= 1200$ years.

As a result of the calculations it appears that the main source of the Common Water is the Antarctic Bottom Water, which flows in at a rate of 10 million tons/sec; the North Atlantic Deep Water inflow is 4 million tons/sec, and the accession from the Intermediate Water only 3 million tons/sec. In the salt flux equation the main balance of terms occurs between the highly saline North Atlantic Deep Water and the much fresher Intermediate Water. There is little net exchange of salt between the Bottom Water and Common Water because they are so nearly the same in salinity. The heat balance is interesting because the only cooling tendency operation is the inflow of Antarctic Bottom Water. This is balanced by roughly equal influxes of heat from three heat sources : North Atlantic Deep Water, Intermediate Water, and flow through the ocean bottom. The balance of radiocarbon is largely between influx from Antarctic Bottom Water and *in situ* decay, contributions from other sources being considerably smaller.

The proportional parts of different waters going up to make Common Water are

Model I

Atlantic Deep Water	X_1/X_4	0·24
Antarctic Bottom Water	X_2/X_4	0·60
Pacific and Indian Intermediate Water	X_3/X_4	0·16

(*b*) *Other models*

Quite different models could have been constructed if we had not included all the information which has been put into model I. For example, several years ago, before radiocarbon data was available, a calculation from temperature and salinity data alone might have been attempted. It is clear from FIG. 2 that according to conventional water mass analysis, the Common Water cannot be a mixture of

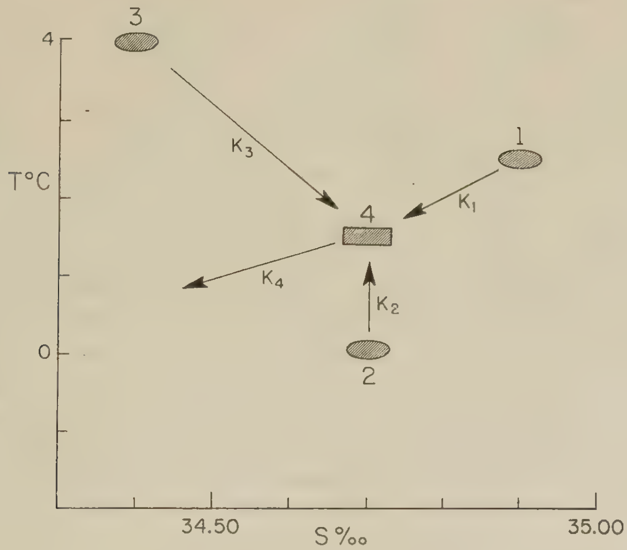

FIG. 2. Temperature–salinity diagram showing the characteristics of the water masses being mixed to form Common Water.

Atlantic Deep Water and Antarctic Bottom Water alone, because it lies above the line joining them. Therefore let us compute the proportional parts of the three components from equations (1), (2) and (3), neglecting equation (4) and setting the right hand side of (3) equal to zero. The result of this model, which we call Model II, is

$$X_1/X_4 = 0{\cdot}29$$

$$X_2/X_4 = 0{\cdot}52$$

$$X_3/X_4 = 0{\cdot}19$$

It is interesting to note that these figures compare favourably with those computed from Model I. The absolute fluxes X_i cannot be computed because the system is homogeneous. Were we to include the heat flux through the bottom the model would not be computable but under-determined. The proportion of water from the Intermediate Water (X_3/X_4) is small, however, and this suggests construction of Model III, in which we set $X_3 = 0$ in equations (1), (2) and (3), and still neglecting radio carbon (equation (4)), try to compute the fluxes by retaining the heating term on the right hand side.

MODEL III

$$X_1 = 0{\cdot}00$$

$$X_2 = 1{\cdot}33$$

$$X_4 = 1{\cdot}33$$

$$K_1 = 0{\cdot}0$$

$$K_2 = 2{\cdot}6 \times 10^6 \text{ m}^3/\text{sec}$$

$$K_4 = 2{\cdot}6 \times 10^6 \text{ m}^3/\text{sec}$$

$$X_1/X_4 = 0{\cdot}0 \qquad X_2/X_4 = 1{\cdot}0$$

Residence Time : 23×10^{10} sec; 7300 years

The results of Model III are substantially different from either I or II. The model implies that Common Water is pure Antarctic Bottom Water, very slowly heated from below. Assuming that there is no addition of Intermediate Water assures that there can be no addition of North Atlantic Deep Water, and vice versa, as can be seen from Fig. 2. The residence time is much greater than that from Model I, and is at variance with the radiocarbon data. Of course the actual heat flux through the bottom is poorly known. Were we to use equations (1), (2) and (4) so as to base the calculation on radiocarbon, and to avoid the problematical temperature equation (3), we could construct yet another model, Model IV, which is underdetermined unless we specify one of the fluxes. Again we set $X_3 = 0$ – that is, assume no addition of Intermediate Water – and obtain

MODEL IV

$$X_1 = 0{\cdot}00 \qquad X_1/X_4 = 0$$

$$X_2 = 8{\cdot}40 \qquad X_2/X_4 = 1$$

$$X_4 = 8{\cdot}40$$
$$K_2 = 16{\cdot}8 \times 10^6 \text{ m}^3 \text{ sec}^{-1}$$
$$K_4 = 16{\cdot}8 \times 10^6 \text{ m}^3 \text{ sec}^{-1}$$

Residence Time : 1050 years

Model IV has much the same residence time as Model I, but the proportional parts are very different. Model IV is equivalent to the Common Water part of the model proposed by Broecker *et al.* (1960) and appears to be inconsistent with the constraints imposed by the T–S diagram.

(*c*) *Computational reliability*

There is a pitfall hidden in the numerical solution of systems of equations such as the above, which in application to oceanographical problems was first pointed out by Defant (1941) in a review of two papers by Hidaka (1940). Some of the equations

Table 2. *Model* I.

	X_1	X_2	X_3	X_4
A. Original Values	1·982	4·857	1·321	8·160
B. Changed values on left hand side				
$T_1 + 0{\cdot}1\ °C$	1·945	4·922	1·297	8·164
$T_1 - 0{\cdot}1\ °C$	2·020	4·789	1·346	8·155
$T_2 + 0{\cdot}1\ °C$	1·888	5·025	1·259	8·171
$T_2 - 0{\cdot}1\ °C$	2·070	4·700	1·380	8·149
$T_3 + 0{\cdot}1\ °C$	1·957	4·900	1·305	8·163
$T_3 - 0{\cdot}1\ °C$	2·007	4·812	1·338	8·157
$T_4 + 0{\cdot}1\ °C$	1·829	5·130	1·219	8·178
$T_4 - 0{\cdot}1\ °C$	2·134	4·585	1·423	8·141
$S_1 + 0{\cdot}03‰$	1·835	4·935	1·427	8·196
$S_1 - 0{\cdot}03‰$	2·155	4·765	1·197	8·117
$S_2 + 0{\cdot}03‰$	1·575	5·072	1·613	8·260
$S_2 - 0{\cdot}03‰$	2·356	4·659	1·053	8·067
$S_3 + 0{\cdot}03‰$	1·869	4·916	1·402	8·188
$S_3 - 0{\cdot}03‰$	2·082	4·804	1·249	8·135
$S_4 + 0{\cdot}03‰$	1·314	5·210	1·801	8·325
$S_4 - 0{\cdot}03‰$	2·624	4·517	0·8604	8·001
$C_1 + 0{\cdot}03$	1·827	4·581	1·218	7·625
$C_1 - 0{\cdot}03$	2·166	5·184	1·444	8·794
$C_2 + 0{\cdot}03$	1·623	4·219	1·082	6·925
$C_2 - 0{\cdot}03$	2·468	5·721	1·645	9·834
$C_3 + 0{\cdot}03$	1·876	4·668	1·250	7·794
$C_3 - 0{\cdot}03$	2·010	5·068	1·401	8·570
$C_4 + 0{\cdot}03$	1·445	3·903	0·9636	6·312
$C_4 - 0{\cdot}03$	2·962	6·600	1·975	11·54
C. Changed values on the right hand side				
Bottom heating				
$- HM_4 \times 0$	2·356	4·188	1·571	8·114
$- HM_4 \times \frac{1}{2}$	2·169	4·522	1·446	8·137
$- HM_4 \times 2$	1·608	5·525	1·072	8·205
$- HM_4 \times 5$	0·4861	7·531	0·3241	8·341
$C_4 + {\cdot}03$	2·067	5·008	1·378	8·453
$C_4 - {\cdot}03$	1·897	4·706	1·256	7·867

may be so nearly the same that changes within the limits of confidence of the coefficients may make enormous differences in the computed values of the X_i. Another way of saying this is that the determinant of the left hand side of the set of equations nearly vanishes. Such equations are called ‘ ill-conditions equations ’ and the numerical results are not reliable.

The most rudimentary way to check the solutions of a model to see if they are ill-conditioned is to vary each coefficient in turn, and compute the X_i separately for each case. The following table shows the values of the X_i in Model I computed for changes of temperature, salinity, and radio carbon. For example, the values of the X_i computed by increasing the salinity S_1 assigned to the North Atlantic Deep Water by 0·03‰, and leaving all other terms unchanged are $X_1 = 1{\cdot}812$, $X_2 = 4{\cdot}891$, X_3 — 1·410, $X_4 = 8{\cdot}113$. As Table 2 shows, there is no indication that the equations are ill-conditioned, most of the X_i varying only slightly for varying the coefficients. The X_i are most sensitive to changes in C_4, and to a lesser extent upon C_2, S_4 and S_2 The need for good sampling to obtain a representative value of radiocarbon in the Common Water (C_4) is emphasized. Fortunately, the X_i are not strongly sensitive to T_3, S_3 and C_3 because representative values for the Pacific and Indian Intermediate Waters are hard to decide upon. The actual amount of bottom heating due to flux of geothermal heat from the ocean bed is difficult to assess. Therefore in Table 2 we exhibit the effect upon the computed X_i of several values of heat flux other than the original value. These calculations show that rather wide ranges of choice in the assigned bottom heating does not seriously change X_4, the total flux in the model, but does effect somewhat the relative proportion of the different water masses that go to make up the Common Water when it is taken to be as much as five times the assigned value – this seems to be an extreme assumption, however.

Calculations also show that the Models II, III and IV are computationally reliable, but as they do not seem to be oceanographically meaningful, in light of their conflict with Model I, we shall not pursue them further here.

3. ORIGIN OF ANTARCTIC BOTTOM WATER

In setting up Model I, we wrote conservation equations only for the Common Water, and did not enquire into the formation of other water masses. We now proceed to construct a model, Model V, in which conservation laws are also written for the Antarctic Bottom Water. We choose this water mass as the natural next step in complication because it is most strongly linked to the Common Water. We also introduce another water mass, Weddell Shelf Water, Type 5, as a contributing source. Plausible reasons for this choice are given by DEACON (1937) and FOFONOFF (1956). There is considerable difficulty in deciding just what values of temperature salinity and radiocarbon to assign to this new water type – it is in fact a hypothetical water mass. We choose the following values : $T_5 = -1{\cdot}9$ °C, $S'_5 = 0{\cdot}63$, $C_5 = 0{\cdot}88$. The temperature and salinity are taken to correspond to FOFONOFF's estimate, the radiocarbon to BROECKER's.

The configuration of water types and connecting mass fluxes K_{ij} is more complex, as shown in FIG. 3. It is necessary to retain both indices. Eight equations may now be written to determine these fluxes : four for conservation in Common Water (Type Y) and four for Antarctic Bottom Water (Type Z).

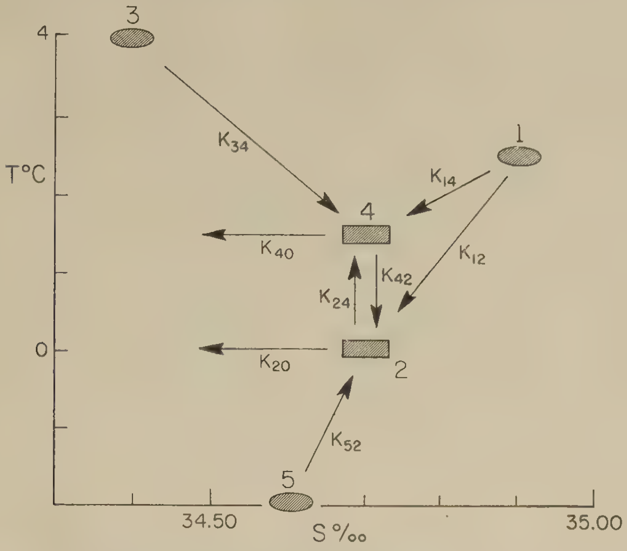

FIG. 3. Model for exchange of water between Common Water (C.W.), Antarctic Surface Water (A.S.W.), Antarctic Bottom Water (A.A.B.W.), Pacific and Indian Intermediate Water (P.+ I.I.W.), and North Atlantic Deep Water (N.A.D.W.).

The equations are

$$(Y)\begin{cases} K_{14}+K_{34}+K_{24}-K_{42}-K_{40}=0 \\ T_1K_{14}+T_3K_{34}+T_2K_{24}-T_4K_{42}-T_4K_{40}=-HM_4 \\ S_1K_{14}+S_3K_{34}+S_2K_{24}-S_4K_{42}-S_4K_{40}=0 \\ C_1K_{14}+C_3K_{34}+C_2K_{24}-C_4K_{42}-C_4K_{40}=\lambda\, M_4C_4 \end{cases}$$

$$(Z)\begin{cases} K_{12}+K_{52}-K_{24}+K_{42}-K_{20}=0 \\ T_1K_{12}+T_5K_{52}-T_2K_{24}+T_4K_{42}-T_2K_{20}=-HM_2 \\ S_1K_{12}+S_5K_{52}-S_2K_{24}+S_4K_{42}-S_2K_{20}=0 \\ C_1K_{12}+C_5K_{52}-C_2K_{24}+C_4K_{42}-C_2K_{20}=\lambda\, M_2C_2 \end{cases}$$

Making the substitution $X_{ij}=K_{ij}/M_4$ and assuming $M_2=M_4/10$.

$$X_{14}+X_{34}+X_{24}-X_{42}-X_{40}=0$$

$$2{\cdot}50X_{14}+4{\cdot}0X_{34}+0{\cdot}00X_{24}-1{\cdot}5X_{42}-1{\cdot}50X_{40}=-2{\cdot}0$$

$${\cdot}90X_{14}+{\cdot}40X_{34}+{\cdot}70X_{24}-{\cdot}70X_{42}-{\cdot}70X_{40}=0$$

$${\cdot}90X_{14}+{\cdot}87X_{34}+{\cdot}88X_{24}-{\cdot}77X_{42}-{\cdot}77X_{40}={\cdot}924$$

$$X_{12}+X_{52}-X_{24}+X_{42}-X_{20}=0$$

$$2{\cdot}50X_{12}-1{\cdot}90X_{52}-0X_{24}+1{\cdot}50X_{42}-0X_{20}=-0{\cdot}2$$

$${\cdot}90X_{12}+{\cdot}63X_{52}-{\cdot}70X_{24}+{\cdot}70X_{42}-{\cdot}70X_{20}=0$$

$${\cdot}90X_{12}+{\cdot}88X_{52}-{\cdot}88X_{24}+{\cdot}77X_{42}--{\cdot}88X_{20}=0{\cdot}106$$

Numerical solutions of the various X_{ij} are given in Table 3.

Table 3.

	Fluxes from source types				*exchange between 2 and 4*		*loss to outside*		
	X_{12}	X_{14}	X_{34}	X_{52}	X_{24}	X_{42}	X_{20}	X_{40}	$(X_{42} + X_{40})$
Model I	—	1·982	1·321	—	4·857	—	—	—	8·160
Model V original values	− 0·4689	1·982	1 321	− 1·340	4·857	− 1·049	− 7·714	9·209	8·160
$S_5 - 0{\cdot}20$‰	0·9122	1·982	1·321	0·6757	4·857	− 0·7978	− 4·067	8·958	8·160
$S_5 + 0{\cdot}20$‰	0·2187	1·982	1·321	0·3364	4·857	− 0·9239	− 5·898	9·084	8·160
$C_5 - 0{\cdot}10$	− 0·1901	1·982	1·321	− 0·5431	4·857	− 0·5045	− 6·094	8·664	8·160
$C_5 + 0{\cdot}10$	1·004	1·982	1·321	2·869	4·857	+ 1·827	0·8439	6·333	8·160

In Table 3 the values of the fluxes X_{14}, X_{24}, X_{34}, and $(X_{42} + X_{40})$ which correspond to the numbers calculated before in Model I are very stable computationally for very large variations in the salinity and radiocarbon values assigned to the Weddell Shelf Water. The other quantities (which are essentially the new features of Model V which I does not contain) X_{12}, X_{52}, X_{42} representing flow into the Antarctic Bottom Water and X_{20} that portion of the flow out of the Antarctic Bottom Water that does *not* enter the Common Water, exhibit two disconcerting features :

(1) they vary widely with the assigned values of S_5, and C_5, and hence are computationally unstable.

(2) they are often negative which is inconsistent with their definition – and a check of the stability of the only case (last row) in which all the X_{ij} are positive indicates that even for the smaller variations in all the coefficients applied to Model I, the equations are ill-conditioned with respect to the X_{i2} and X_{20}. Model V is therefore an unreliable model in all those respects where it attempts to improve upon model I.

4. FLOW OF ANTARCTIC INTERMEDIATE WATER IN THE ATLANTIC

Through studies by DEFANT (1936), SVERDRUP (1939), WÜST (1936, 1957), and others we have a fair knowledge of the meridional flow of water masses in the South Atlantic Ocean. Thus, Atlantic Surface Water slowly flows polewards while the Antarctic Surface Water is found in a northward current underneath, extending down to about 1200 metres (Antarctic Intermediate Water). Also in the bottom layers the Antarctic water flows northward and in the layer between, the Atlantic Deep Water gradually drifts southward mixing with the water masses above and below. FIG. 4 shows a north–south cross section through the Atlantic Ocean. The salinity and temperature data are taken from the *Meteor* Expedition (WÜST, 1936) while in FIG. 4 (c) all available data of C^{14} essentially due to the work by BROECKER *et al.* (1960) is displayed. The tongue of cold and comparatively fresh water flowing northward in a layer between approximately 300 and 1200 metres is clearly shown in all three graphs, the C^{14} values being significantly lower than in the waters above and below. Of course the number of C^{14} analyses is still small and the position of the isopleths quite uncertain. Due to the inadequacy of the data any refined analysis of the kind presented by DEFANT and SVERDRUP using C^{14}-measurements is not justified but we shall here simply try to estimate the average northward flow of this Intermediate Water and also the residence time for water in this part of the Atlantic Ocean.

Let us consider this intermediate water mass extending from 50° south to 10° north and from 300 to 1200 metres depth. The total amount of water then would be $0{\cdot}45 \times 10^{23}$ g. This water originates from the surface water in the Antarctic and mixes with the surface waters in the middle and equatorial latitudes as well as with the deep water during its northward motion. Let us denote these four water masses with the indices 6 to 9 respectively, and Table 4, (Model VI) gives the appropriate mean values for these water masses to be used in a box model similar to the one advanced in paragraph 2 (Model I).

Forming again the system of equations that expresses the conservation of the characteristic values given in Table 4 for the Atlantic Intermediate Water with due regard taken to radioactive decay of C^{14} yields the same four equations as given in paragraph 2, except that we should here completely disregard the loss or gain of heat due to thermal flux from below which had to be considered in the case of the Common Water in the Pacific. Inserting the values in Table 4 (Model VI) then gives the following solution

Table 4.

		A.A.S.W.	A.S.W.	A.D.W.	A.I.W.
		$i = 6$	$i = 7$	$i = 8$	$i = 9$
Model VI	T_i °C S_i ‰ C_i	2·2 34·25 0·88	14·5 35·40 0·94	3·0 34·85 0·90	5·5 34·60 0·87
Model VII	T_i °C S_i ‰ C_i	3·2 34·20 0·88	15·5 35·60 0·95	3·1 34·90 0·90	6·0 34·80 0·87

$$K_6 = 3.6 \times 10^6 \text{ m}^3/\text{sec}$$

$$K_7 = 1.4 \times 10^6 \text{ m}^3/\text{sec}$$

$$K_8 = 0.4 \times 10^6 \text{ m}^3/\text{sec}$$

$$K_9 = 5.4 \times 10^6 \text{ m}^3/\text{sec}$$

The residence time for Intermediate Water becomes about 250 years. Assuming that the water during this time gradually moves northward yields a velocity of about 0·05 cm/sec. The accuracy of the values given above is of course dependent upon the certainty with which representative values can be assigned to the different boxes. The computation has therefore been repeated changing the temperature by $\pm 1.0°$ for the Atlantic Surface Water and by 0·2° for the other water masses, similarly the salinity was varied by $\pm$ 0·3‰ and 0·1‰ respectively and the C^{14}-values by $\pm$ 0·02 for all water masses. Naturally the values were most sensitive to changes in the C^{14}-activity, particularly to the value assigned for the Intermediate Water itself. $C_9^{14} = 0.89$ increased the rate of overturning by a factor of four while $C_9^{14} = 0.85$ gave values a little larger than half of those given above. (Table 5).

When varying the salinity negative K_1-values were obtained in three cases and the computation is thus on the margin of being stable. On the other hand the variation of 0·3‰ and 0·1‰ for Surface and Deep Waters respectively is rather large and since the other K-values change moderately, we shall accept the computations as a reasonable first approximation.

Of course the boundaries of the Intermediate Water are somewhat arbitrary which will certainly also influence the results. To check the accuracy of the present computation in this respect it was carried through assuming the Intermediate Water extending for lat 40 °S to lat 10 °N. Assigning appropriate values for temperature, salinity and C^{14}-activity as given in Table 5 (Model VII) gives the following values for the exchange coefficients.

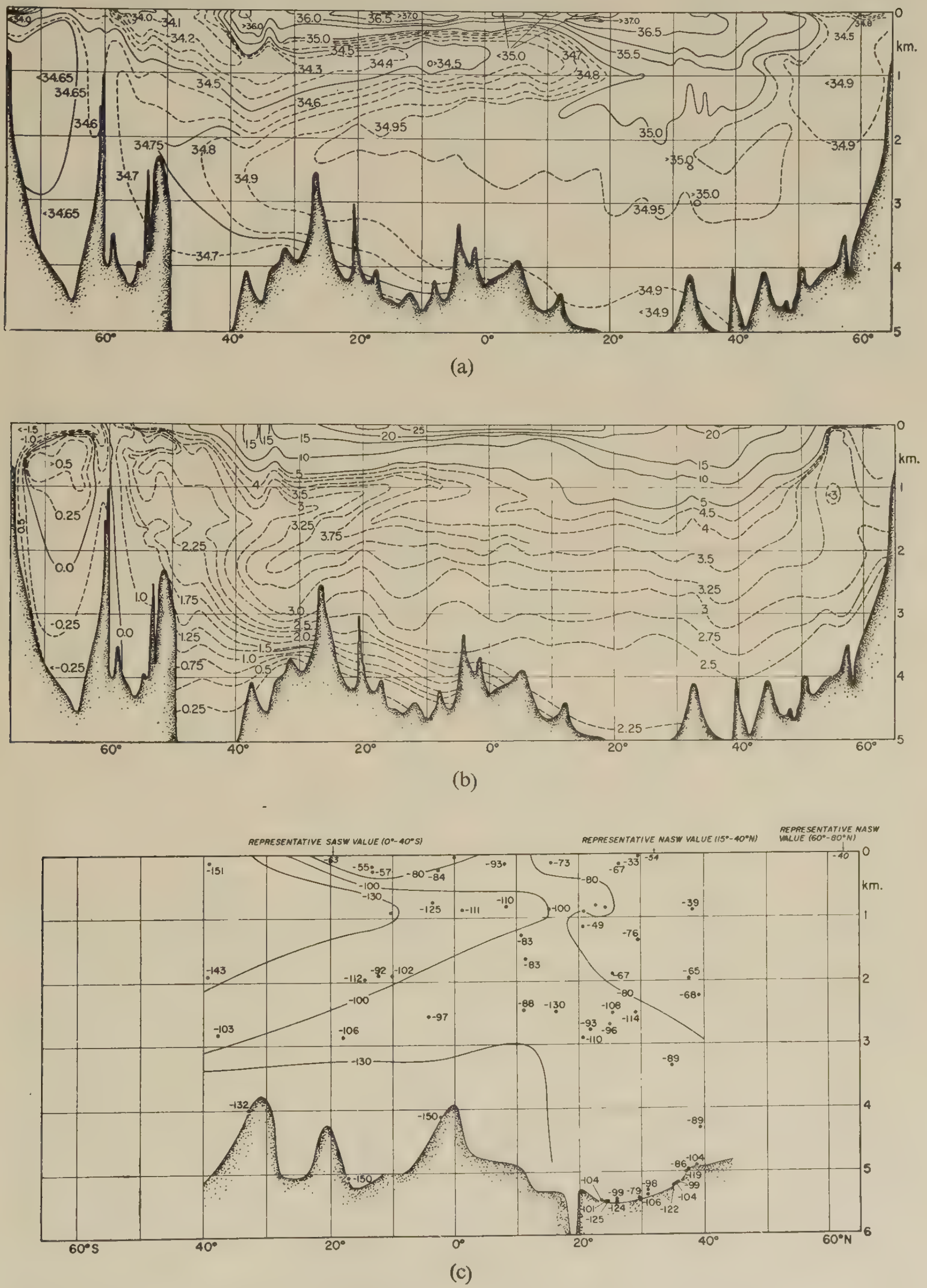

FIG. 4. Meridional distribution of salinity (‰) (a), temperature (°C) (b) and C^{14}-activity (c) putting the activity of modern (pre-bomb) wood equal to unity. Temperature and salinity data from WÜST (1936), C^{14}-data from BROECKER *et al.* (1960).

$$K_6 = 1{\cdot}4 \times 10^6 \text{ m}^3/\text{sec}$$

$$K_7 = 0{\cdot}8 \times 10^6 \text{ m}^3/\text{sec}$$

$$K_8 = 1{\cdot}4 \times 10^6 \text{ m}^3/\text{sec}$$

$$K_9 = 3{\cdot}6 \times 10^6 \text{ m}^3/\text{sec}$$

Table 5.

	K_6		K_7		K_8		K_9	
	VI	VII	VI	VII	VI	VII	VI	VII
Original values	3·6	1·4	1·4	0·8	0·4	1·4	5·4	3·6
$T_6 + 0{\cdot}2$ °C	3·5	1·3	1·4	0·8	0·6	1·5	5·5	3·6
$T_6 - 0{\cdot}2$ °C	3·6	1·4	1·5	0·8	0·3	1·4	5·4	3·6
$T_7 + 1{\cdot}0$ °C	3·5	1·3	1·3	0·8	0·7	1·6	5·5	3·7
$T_7 - 1{\cdot}0$ °C	3·6	1·4	1·5	0·9	0·2	1·3	5·3	3·6
$T_8 + 0{\cdot}2$ °C	3·6	1·3	1·4	0·8	0·4	1·5	5·4	3·6
$T_8 - 0{\cdot}2$ °C	3·6	1·4	1·4	0·8	0·4	1·4	5·4	3·6
$T_9 + 0{\cdot}2$ °C	3·6	1·4	1·5	0·9	0·2	1·3	5·3	3·6
$T_9 - 0{\cdot}2$ °C	3·5	1·3	1·4	0·8	0·6	1·6	5·5	3·7
$S_6 + 0{\cdot}1$‰	4·8	1·6	1·6	0·9	− 0·4	1·3	6·0	3·8
$S_6 - 0{\cdot}1$‰	2·9	1·1	1·3	0·8	0·9	1·6	5·1	3·5
$S_7 + 0{\cdot}3$‰	4·8	1·8	1·6	0·9	− 0·5	1·2	5·9	3·8
$S_7 - 0{\cdot}3$‰	2·6	0·9	1·3	0·8	1·1	1·7	5·0	3·4
$S_8 + 0{\cdot}1$‰	3·7	1·6	1·4	0·9	0·4	1·3	5·5	3·8
$S_8 - 0{\cdot}1$‰	3·4	1·1	1·4	0·8	0·5	1·6	5·3	3·5
$S_9 + 0{\cdot}1$‰	2·3	0·8	1·2	0·8	1·3	1·8	4·8	3·4
$S_9 - 0{\cdot}1$‰	5·1	2·0	1·7	0·9	− 0·7	1·0	6·1	3·9
$C_6 + 0{\cdot}02$	2·4	1·1	1·0	0·7	0·3	1·2	3·7	3·0
$C_6 - 0{\cdot}02$	6·9	1·7	2·8	1·1	0·8	1·9	10·5	4·7
$C_7 + 0{\cdot}02$	3·0	1·2	1·2	0·7	0·4	1·3	4·6	3·2
$C_7 - 0{\cdot}02$	4·4	1·6	1·8	1·0	0·5	1·6	6·7	4·2
$C_8 + 0{\cdot}02$	3·4	1·1	1·3	0·7	0·4	1·2	5·1	3·0
$C_8 - 0{\cdot}02$	3·8	1·8	1·5	1·1	0·5	1·9	5·8	4·8
$C_9 + 0{\cdot}02$	13·3	3·3	5·3	2·0	1·8	3·6	20·4	8·9
$C_9 - 0{\cdot}02$	2·1	0·8	0·8	0·5	0·2	0·9	3·1	2·2

In this case the total amount of Intermediate Water is 0·37 × 10^{23} g, and thus the residence time becomes 300 years. The stability of the computations has also been checked in the same way as given above for Model VI. Again the result was most sensitive to changes in the C^{14} activity for the Intermediate Water. For $C_9^{14} = 0{\cdot}89$ the rates of exchange were increased by a factor of about 2·5, if decreasing C_9^{14} to 0·85 the values were about 0·6 of those quoted above.

We may summarize our results in the following way : Antarctic Water flows northward underneath the Atlantic Surface Water at a rate of 1·5 – 5 × 10^6 m³/sec at latitudes 40 °–50 °S, corresponding to an average velocity of 0·03 – 0·1cm/sec. Present observations of C^{14}-activity in the Southern Atlantic make it quite unlikely that the velocity could be more than 0·2 cm/sec. This water, Atlantic Intermediate Water, mixes with the surface water above and the Deep Atlantic Water below by incorporating water from above and below of about equal amounts. Since presumably very little water returns directly from this layer to the Antarctic region we estimate the average upward motion into the Atlantic Surface Water and the downward motion into the Atlantic Deep Water to 1·5 – 5 × 10^6 m³/sec, half of which may be considered as a net upward or downward flow and the other half as large scale eddy exchange. With due regard to the total size of the area considered the net upward or downward motion may be estimated to 1 – 3 m/year. It is interesting to compare this value with the corresponding net upward motion in the Pacific Ocean (approximately represented by K_4 in section 2) of about 2 m/year. Finally the residence time for water in the Intermediate Layer of the Atlantic Ocean before being mixed or transferred upward or downward is about 300 years, but possibly as long as 400 years or as short as about 100 years. More extensive measurements of C^{14} activity, or preferably of a more short-lived radioisotope, can be expected to improve on these quite approximate results.

It is important to compare the net flow of Antarctic Intermediate Water as obtained by this water-mass model with the numerical values obtained by WÜST (1957) on the basis of geostrophic calculations. There are, of course, arbitrary elements in WÜST'S calculations – particularly the choice of reference level – but these arbitrary elements are probably less significant in WÜST'S study than in our own, and so we are inclined to accept WÜST'S transport figures as a test of our model. Some further comments on WÜST'S calculations have been made in another place (STOMMEL 1958).

As WÜST points out (1957, p. 372–3) the geostrophic flow in the Antarctic Intermediate Water does not show up as maximum velocity at depth, in the core, as might be expected, so in the summary figures for whole profiles WÜST sums transports of Surface, Central and Intermediate Waters. For our purposes we want to isolate the transport of the Intermediate Water, and this introduces an arbitrary element. One way to obtain figures is to sum the geostrophic transports between 300 m and 1200 m for every profile and full width of the ocean. These figures are shown in Table 6.

Table 6. WÜST'S (1957) *Transports summed between* 300 m *and* 1200 m (*in* 10^6 m³/sec, *plus means northward*)

Profile	*Latitude*	*Transport*
(III)	(49 °S)	(+ 14·3)
(I)	(41 °S)	(− 16·0)
IV	33 °S	+ 9·4
II	28 °S	+ 12·2
VII	22 °S	+ 12·1
VI	15·5 °S	+ 6·3
VIII	9·5 °S	+ 6·1
XIII	6–19 °N	+ 1·8

Both profiles III and I are rather far south, and are not closed off to solid land on the eastern end, so one is inclined to omit them* from comparison with our model. The average northward transport in the remaining six profiles is 8 × 10^6 m³/sec which somewhat exceeds the upper limit of transport values obtained by our model – a discrepancy for which we do not find any easy answer except to hope that with increasing amounts of radio-carbon data, more geostrophic calculations, and more refined models it will eventually be resolved.

---

*In such high latitudes the Intermediate Water extends to the surface – as a glance at FIG. 4 (a) confirms – and one should properly change the depth interval and include Ekman transport due to wind-stress.

Acknowledgement—The present investigation was begun while one of us (B.B.) spent three months at Woods Hole Oceanographic Institution as a fellow of the Carnegie Institution of Washington, D.C. Many of the computations were made by Mrs. JACQUELINE WEBSTER, for whose care and interest the authors are sincerely grateful.

Contribution No. 1170 *from the Woods Hole Oceanographic Institution.*

REFRERNCES

BIEN, G. S. ,RAKESTRAW, N. W. and SUESS, H. S. (1960) Radiocarbon concentration in Pacific Ocean water. *Tellus*, **12**, 436–443.

BROECKER, W. S., GERARD, R., EWING, M. and HEEZEN, B. C. (1960) Natural radiocarbon in the Atlantic Ocean, *J. Geophys. Res.*, **65**, 2903–2931.

COCHRANE, J. D. (1958) The frequency distribution of water characteristics in the Pacific Ocean. *Deep-Sea Res.*, **5**, 111–127.

CRAIG, H. (1957) The natural distribution of radiocarbon and the exchange time of carbon dioxide between atmosphere and sea. *Tellus*, **9**, 1–17.

DEACON, G. E. R. (1937) The Hydrology of the Southern Ocean. *Discovery Rep.*, **15**, 1–124.

DEFANT, A. (1936) Quantitative Untersuchungen zur Statik und Dynamik des Atlantischen Ozeans : Ausbreitungs- und Vermischungsvorgänge im antarktischen Bodenstrom und im subantarktischen Zwischenwasser. *Meteor* Exped. *Wissescchafftliche Ergebnisse*, Bd **VI**, Teil II, 2 Lief.

DEFANT, A. (1941) Die absolute Berechnung ozeanischer Ströme nach dem dynamischen Verfahren. *Ann. d. Hydr. usw.*, **69**, Heft. 6, 169–173.

FOFONOFF, N. P. (1956) Some properties of sea-water influencing the formation of Antarctic Bottom Water. *Deep-Sea Res.*, **4**, 32–35.

HIDAKA, K. (1940) Absolute Evaluation of Ocean Currents in Dynamical Calculation. *Proc. Imp. Acad.* Tokyo **16**, No. 8, 391–397.

MONTGOMERY, R. B. (1958) Water characteristics of Atlantic Ocean and world ocean. *Deep-Sea Res.*, **5**, 134–148.

POLLAK, M. J. (1958) Frequency distribution of potential temperatures and salinities in the Indian Ocean. *Deep-Sea Res.*, **5**, 128–133.

STOMMEL, H. (1958) Review of G. Wüst's *Meteor* Report (1957). *Trans. Amer. Geophys. Un.*

STOMMEL, H. and ARONS, A. B. (1960) On the abyssal circulation of the world ocean—II. An idealized model of the circulation pattern and amplitude in oceanic basins. *Deep-Sea Res.*, **6**, 217–233.

SVERDRUP, H. U. (1939) Lateral mixing in the deep water of the south Atlantic Ocean. *J. of Mar. Res.*, Vol. **II**, 195–207.

WOOSTER, W. and VOLKMANN, G. (1960) Indications of Deep Pacific Circulation from the Distribution of Properties at five kilometres. *J. Geophys. Res.*, **65**, 1239–1249.

WÜST, G. (1936) Die Stratosphäre des Atlantischem Ozeans. *Wissenschaftliche Ergbenisse des Deutscher Atlantischer Expedition auf dem Meteor.* Bd. **VI**, Erster Teil, p. 109 ff.

WÜST, G. (1957) Stromgeschwindigkeiten und Strommengen in der Tiefen des Atlantischen Ozeans. *Wissenschaftliche Ergebnisse des Deutscher Atlantischer Expedition auf dem Meteor.* Bd. **VI**, Zweiter Teil, 261–420.

Printed in Great Britain by The Salisbury Press Ltd., Publicity House, Wilton Road, Salisbury, Wilts. (30312)

Contribution No. 1171

Journal of Geophysical Research Volume 66, No. 9 September 1961

Lava-Sea-Air Contact Areas as Sources of Sea-Salt Particles in the Atmosphere[1]

A. H. Woodcock and A. T. Spencer

Woods Hole Oceanographic Institution, Woods Hole, Massachusetts

Abstract. One theory of individual raindrop formation requires a giant hygroscopic particle ($\geq 10^{-12}$ gram) as an initiating nucleus. For this and other reasons, natural sources of these nuclei are of interest to meteorologists. The sea surface is normally a source of relatively low numbers of these nuclei. Enormous numbers are present, however, in the steam clouds arising when molten lava encounters sea water. Observations of the number and the size of the steam-cloud particles or nuclei are given. Samples of these particles were taken from aircraft within the cloud during the 1960 Kilauea eruption in Hawaii. Other samples were taken from experimental clouds formed in the laboratory. Microscope and flame-photometric methods of analysis showed the particles to be, in major part, sea salt. Size distribution studies reveal that the flash boiling, resulting from lava-sea-air contact, produces salt nuclei of a size range in large part like that normally arising from the sea. The rate of production of these nuclei, expressed as grams per unit of surface, is from 1 to 6 million times greater from steaming lava than from the average sea surface.

1. Introduction

Recent eruptions of the Kilauea volcano on the island of Hawaii have produced large steam clouds in areas where the lava, at a temperature of about 1000°C [*Eaton and Murata*, 1960], flowed into the sea (Fig. 1). This flow continued for several weeks, and marked changes in visibility occurred 320 km away at Honolulu on the island of Oahu. Also, aircraft and surface ships observed dense haze at much greater distances over the North Pacific.

Simpson [1950] reported the formation of the haze associated with the 1950 eruption. During the 1960 eruption, S. Price (personal communication, 1960) noted that haze formation followed the entry of the lava streams into the sea, and he supposed that the haze-producing particles were largely sea salts which were thrown into the air by the violent vaporization or flash boiling of the sea in contact with the lava. The present study confirms Price's idea that the steam-cloud particles are largely sea salts.

Recent work has emphasized the meteorological and geochemical importance of large airborne salt nuclei produced by the sea [*Blanchard*, 1961; *Eriksson*, 1959; *Woodcock and Blanchard*, 1955; *Woodcock*, 1952, 1960]. The role of this marine aerosol in the formation of the large cloud droplets essential to accretional growth of raindrops is becoming recognized [*Mason*, 1957]. It is pertinent to expand our knowledge of the sea as a source of atmospheric salts to include those unusual areas and times at which the heat of volcanic activity forces salts into the air at an extraordinary rate.

The role of explosive volcanoes in occasionally adding vast quantities of finely divided material to the atmosphere is well known [*Symons*, 1888]. Eruptions of the nonexplosive shield-type volcanoes of Hawaii can also add great quantities of finely divided (hygroscopic) material to the air by the relatively slow but long-sustained flow of lava into the sea. It is supposed that other volcanic activity at or near sea level, such as that of Myojin-Sho near Japan [*Dietz and Sheehy*, 1954] will be especially productive of atomized sea salt.

The purpose of this paper is to present data on the size distributions of the salt particles added to the air in the steam clouds and to make estimates of the rates of production. These data were obtained over Hawaiian lava flows and in experimentally produced clouds in the laboratory. In the concluding section, estimates are made of the total quantities of particles added to the atmosphere by a major lava flow, and some discussion is given of physical factors which may alter these quantities.

2. Natural Steam-Cloud Particles

In this section a brief discussion is presented of the techniques used to sample the steam-cloud

---

[1] Contribution 1171 of the Woods Hole Oceanographic Institution.

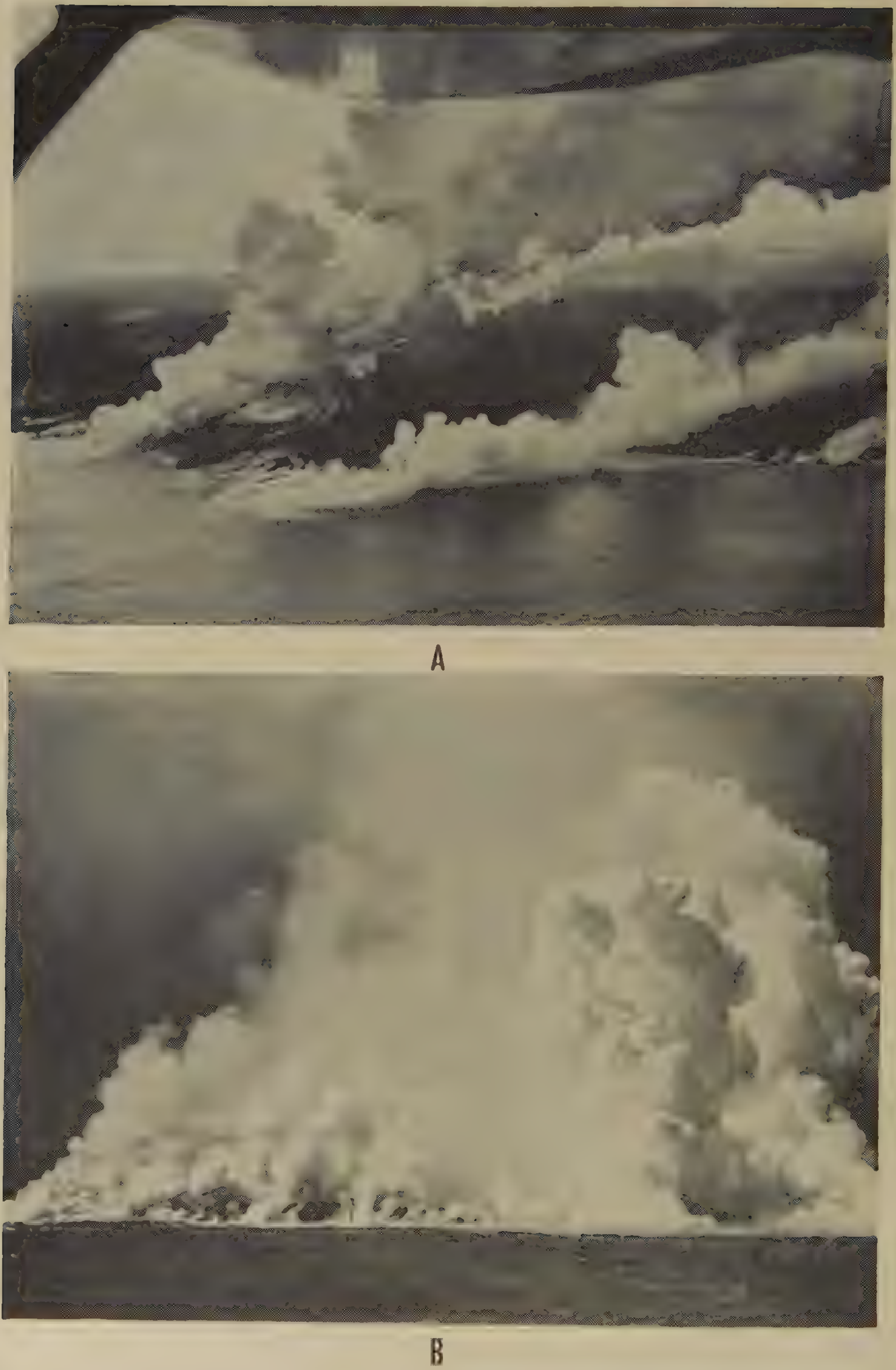

Fig. 1. Steam clouds formed as lava from the 1960 eruption of Kilauea enters the sea in the Puna district, island of Hawaii. Scale in picture *B*, may be judged from height of lava near sea, which is about four meters. Photograph *A* by Jack Pales, U.S.W.B., and photograph *B* by Robert Haugen of the National Park Service, Hawaii.

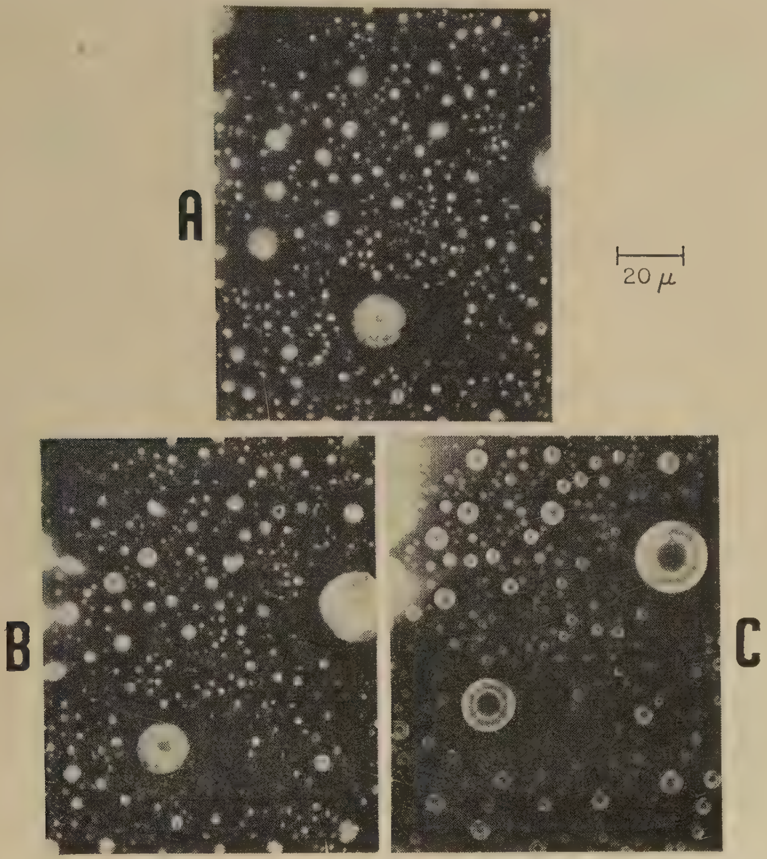

Fig. 2. Photomicrographs of steam-cloud particles on surface of sampling slide which was exposed to different relative humidities. See text for discussion.

particles and of the physical-chemical methods which show that they are largely sea salt.

Fifteen samples of the steam-cloud particles were collected on two sampling days by causing the particles to impinge upon prepared 1 × 20 mm glass slides. These slides were exposed from aircraft by means of a device previously described by *Woodcock* [1952, p. 208]. Flight speeds of 40 m $\sec^{-1}$ were used, and the samples were taken in the smaller steam clouds, such as those at the left in Figure 1*B*. Droplets and moist particles of certain size ranges impinge upon and adhere to these slides. A hydrophobic Dri-film coating causes droplets on them to form hemispheres [*Woodcock and Gifford*, 1949], thus simplifying volume estimates from diameter measurements.

Figure 2 shows photomicrographs of these steam-cloud particles. They contain cubic crystals at relative humidities of 71 per cent and less,[2] as shown in pictures *B* and *A*. They change phase at 74 per cent and are completely liquified at 77 per cent. These are properties of sea-salt particles [*Twomey*, 1953, 1954].

Examination with a microscope of many hundreds of droplets, such as those in Figure 2*C*, revealed that there were practically no insoluble particles present on the slides. Since soil, sand, and other small insoluble particles are readily deposited on the slides, the absence of these materials suggests that small particles of lava

---

[2] Immersion of the slides in water-vapor-saturated air over a 35 per cent solution of sulfuric acid and water (RH 71%) causes the amorphous mass of sodium chloride crystals usually formed to slowly recrystallize into larger cubic crystals of a lower-energy state.

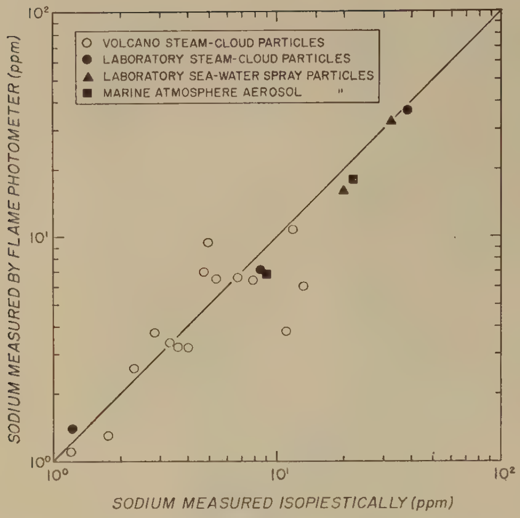

Fig. 3. Comparison of isopiestic and flame-spectrophotometer measurements of sodium in steam-cloud and other particles. Most of the scatter of the observations about the 45° line is attributed to the normal error of the two methods. See text.

or other materials are not carried upward very far in these clouds.

From diameter measurements of the hemispheric droplets, at a relative humidity of 91 per cent, and from the vapor pressure of concentrated sea water, one can compute the weight of sea salt W (grams) in each droplet.

$$W = V\,dC \qquad (1)$$

where

V = volume of hemispheric droplets (μ^3).
d = density of droplets [*Higashi, Nakamura, and Hara*, 1931] (g ml^{-1}).
C = concentration of salts in droplets by weight fraction [*Arons and Kientzler*, 1954].

The weights of salt in a great many droplets on each of the slides were thus determined. Estimates were then made of the total sea salt in all the droplets on the slides, the number of which usually greatly exceed those actually measured under the microscope. Subsequently all the salts on each slide were dissolved in from 50 to 200 mg of distilled water, and a sodium analysis was made with a flame spectrophotometer. Thus it was possible to compare the concentrations of sodium in these solutions, which were computed from the isopiestically determined weights of sea salt, to the sodium concentrations photometrically measured. These small-volume samples were readily measured with a modified Beckman 4040 atomizer burner.

Figure 3 shows a comparison of the sodium amounts derived by the two methods, the isopiestically determined sodium concentrations being derived from the product of the sea-salt weights and the ratio of the sodium in the sea to the total salts. Three of the 22 observations fall outside the range of error expected from the combined errors of the two methods. These unusual observations may be due to a lowering of the surface tension by contaminating films, resulting in a flattening of the larger droplets and an overestimate of their size and sodium content by the isopiestic technique. They can also result from the occasional failure of the larger particles, on that fraction of the slide area used for measurement under the microscope, to be representative of those on the slide as a whole.

Among 20 test measurements of the error of the flame photometer in the range of concentration concerned, 90 per cent showed an error of < ±10 per cent. All fell within ±15 per cent of the test solutions. The error of the isopiestic method, as used here, is about ±20 per cent.

From the agreement revealed in Figure 3, and from the other properties of the crystalline particles previously mentioned, it is concluded that the steam-cloud particles are in major part sea salt.

3. Steam-Cloud Salt Particles Compared with Salt Nuclei in Marine Air

As an aid in thinking about the meteorological role of volcano steam-cloud salt particles, it is useful to derive their spatial distributions and to compare them with those of salt particles normally found in the air over the sea.

Figure 4, curve *A*, shows an average steam-cloud particle distribution curve, compared with the normal range of average concentration in maritime air under wind forces 3, 5, 7, and 12. Curve *A* is based upon micrometer measurements of the numbers and sizes of many hundreds of individual particles. These measurements are then readily converted to spatial distribution in the air, using the observed aircraft speeds and slide exposure durations and areas.

The potency of the lava-sea-air contact zone

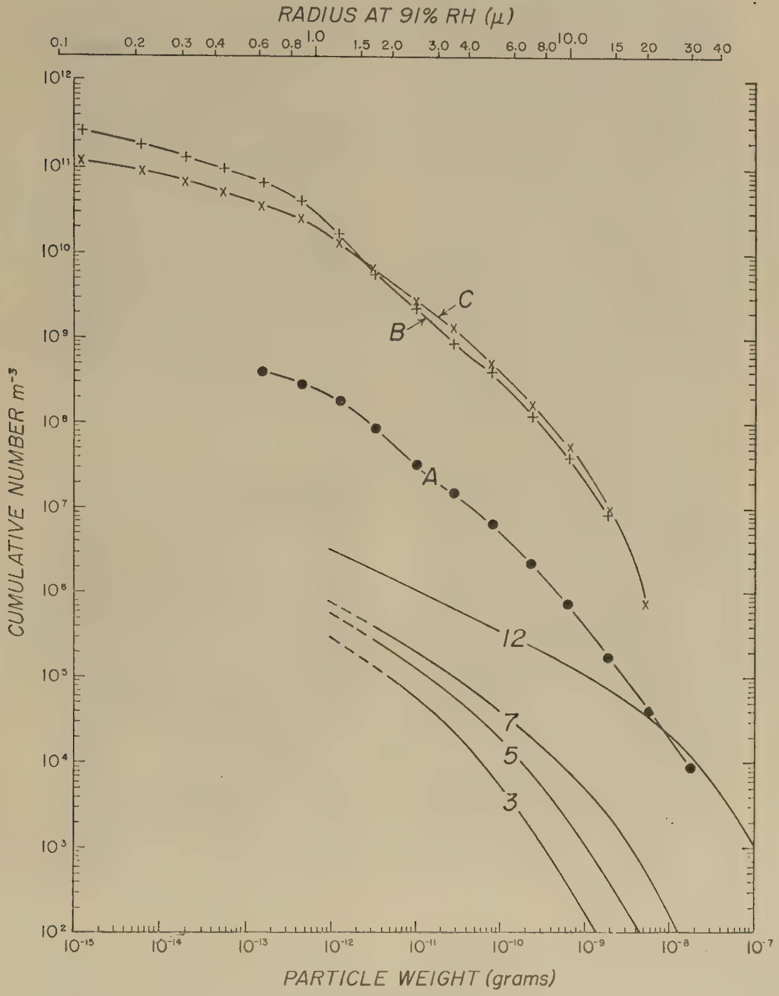

Fig. 4. Cumulative steam-cloud particle distribution curves (*A*, *B*, and *C*) compared with average salt-particle distributions found at the 300- to 600-meter altitudes over the sea during winds of forces 3, 5, 7 and 12. Symbols representing particle counts are plotted at the lower limiting particle weight of each weight range category. Curve *A* represents average particle concentrations in natural steam clouds, and *B* and *C* give concentrations in artificially formed clouds in the laboratory. Upper scale gives particle size as measured under the microscope and converted to equivalent spherical radius.

as a source of salt particles is obvious. It is notable that this zone produces especially great numbers of smaller particles and that the range of size is comparable to that of particles normally arising from the sea throughout most of the size range.

It is probable, however, that the concentration of particles in the small steam clouds (i.e. 4×10^8 particles $m^{-3} \geq 3 \times 10^{-13}$ g) was lower than that which might have been found in the large clouds present during a main advance of lava into the sea, such as that shown at the top left side of Figure 1. Note the comparatively dense character of this cloud. This impression is also supported by the reported observation, during the great 1950 flow of lava into the sea, of about 10^{-9} gram of salt per cubic centimeter of air in Honolulu [*Simpson*, 1950], which was 320 km downwind from the source area. It seems that the salt particle concentration near the steam-cloud source in 1950 may have been much greater than the quantity reported here (i.e.

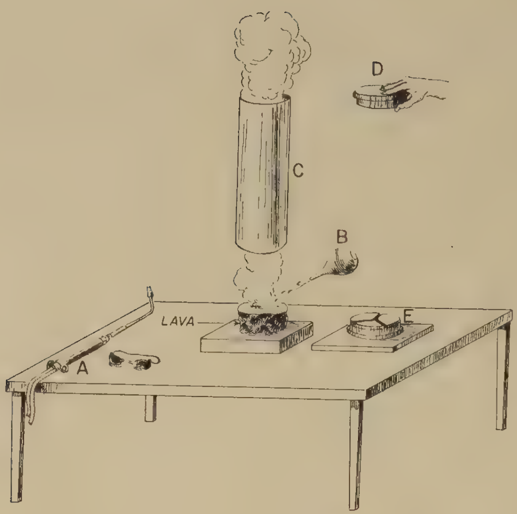

Fig. 5. Sketch illustrating method used to trap steam-cloud particles produced in the laboratory. Cylinder C is 44 cm long and 14 cm in diameter.

4×10^{-9} g cm^{-3}), which was measured only a fraction of a kilometer from the lava-sea-air contact zone.

It will be demonstrated later than there were probably many more small particles present in the Hawaiian steam cloud than those represented in curve A, Figure 4. These small particles add little, however, to the total mass per unit volume of air, which is discussed in the preceding paragraph. Langmuir has shown that the collection efficiency E, defined as the ratio of the actual deposition per unit surface on the slide or 'ribbon' to the total possible deposition under the sampling conditions, is negligible for the 1-mm-wide glass slides, at an air speed of 40 m sec^{-1} and for particles of density 1 and smaller than about 0.5-μ radius [*Langmuir and Blodgett*, 1945; *Woodcock and Gifford*, 1949]. Correction for E cannot be applied to these steam-cloud particle samples because particle size at sampling time is not known. It can be stated, however, from Langmuir's theoretical study of impact deposition on 'ribbons' [*Langmuir and Blodgett*, 1945], that E is at least 0.8 for particles $> 10^{-11}$ g and at least 0.5 for those $> 10^{-12}$ g. Failure to apply this E correction to the steam-cloud samples is not a serious handicap, however, in the present study.

A further, more serious, question about the natural steam-cloud samples concerns the degree to which droplet or particle coalescence, at the time of impact on the slides, may have altered the particle size distribution. A reasonable 'covering fraction' on the slides [see *Woodcock and Gifford*, 1949, p. 189, and *Langmuir*, 1944, pp. 59–70] could not be established since there was no way to know the particle sizes in the clouds and to adjust the sampling duration accordingly. Thus the size distribution curves should be regarded as a best approximation. The comparable nature of the size distributions on curves A, B, and C of Figure 4 cause the authors to think that coalescence has not greatly altered the distribution of the natural steam-cloud particles.

4. ESTIMATE OF RATE AT WHICH THE SALT AEROSOL WAS PRODUCED WHERE LAVA ENTERED SEA

Cine photographs of a small steam cloud, similar to that in which samples were taken, showed that the diameter of the plume at sampling level was much greater than the diameter close to the source. A rough value for the dilution factor of particles was derived from measurements on photographs of the relative diameters of the smoke plumes near the sampling altitude and close to the source area. From the airplane speed and the time required to pass through the steam clouds normal to their long axes, an estimate of the diameter at sampling altitude was made. With this diameter and the relative sizes derived from the steam-cloud photographs, the plume size near the source was derived.

Using this estimate of the enlargement of the steam-cloud plume from source to sampling level and a rate of rise derived from the angle of tilt of the plume in a known wind, a particle production rate P of about 1.4×10^{6} cm^{2} sec^{-1} was determined for those $\geq 3 \times 10^{-12}$ g.

$$P = CRV \tag{2}$$

where

C = number concentration of particles $\geq 3 \times 10^{-12}$ g at sampling level (95 cm^{-3}).
V = rate of rise of cloud normal to cross section (about 600 cm sec^{-1}).
R = ratio of cloud cross section at sampling level (3220 m^{2}) to that near source (129 m^{2}).

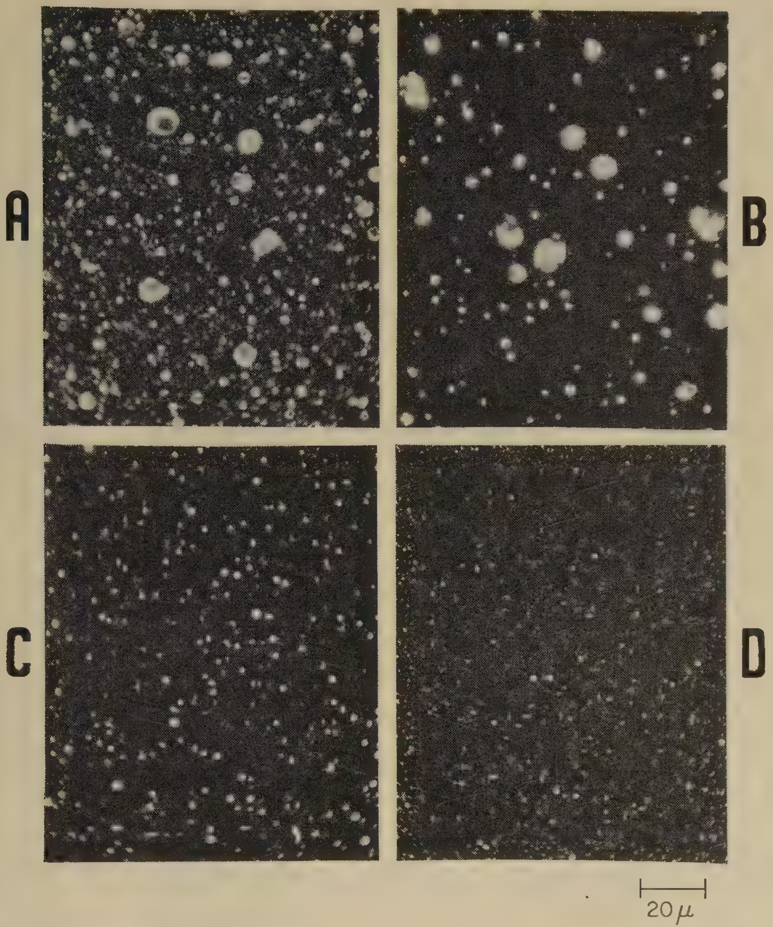

Fig. 6 Photomicrographs of salt crystals on glass slides exposed to fallout from laboratory steam cloud in sedimentation chamber. *A* shows excess 'covering fraction' or over-sampling [*Woodcock and Gifford*, 1949] from exposure to entire fallout. On slides *B*, *C*, and *D*, samples were taken from time 0 to 200, 200 to 1170, and 1170 to 7×10^4 seconds, respectively, thus avoiding over-sampling on any one slide. See text.

The sum of the weights of these particles gave a salt production rate of 4.5×10^{-5} g cm^{-2} sec^{-1}.

To test the above estimates and to learn whether smaller particles may also have been produced, it was decided to make miniature steam clouds in the laboratory. These tests are described in the following section.

5. Particles from Artificial Steam Clouds

A piece of lava from the Kilauea eruption of 1960 which D. H. Richter of the Hawaiian Volcano Observatory kindly sent to us was heated to a molten red-yellow state with an oxygen-acetylene torch, as suggested in Figure 5. When the incandescence had penetrated to a depth of about 1 cm, the flame was removed and the molten surface splashed with sea water B.[3] The steam cloud which arose from the lava was caused to flow through the cylindrical sedimentation chamber *C*. When steam was visibly entering the base of the open-ended cylinder and passing out at the top, a cover *D* was placed over the top, the lava removed, and the cylinder lowered over a prepared base *E*

---

[3] The lava in this case presented a relatively smooth surface to the water, a type of surface characteristic of pahoehoe lavas. It is thought that the porous surface of aa lavas would produce a different result when coated with sea water. (see end of section 8.)

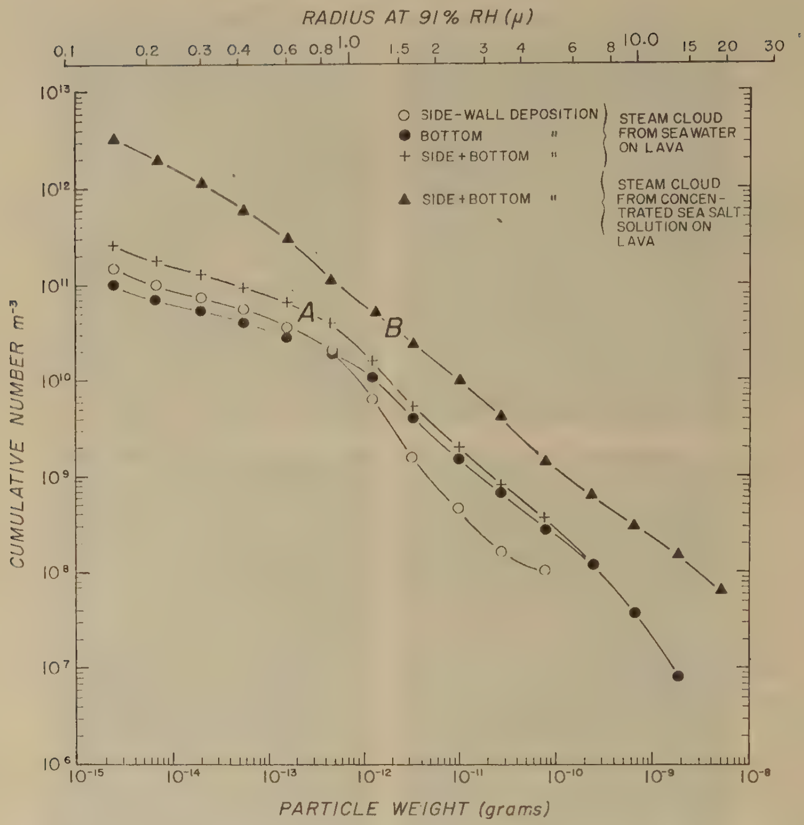

Fig. 7. Size distribution and relative deposition curves, representing steam-cloud particles deposited on the side walls and bottom of the sedimentation or fallout chamber. Symbols representing particle counts are plotted at the lower limiting particle weight of each weight range category.

containing a glass-slide sampling surface. All joints were effectively sealed with masking tape and the chamber set aside to await fallout of the particles.

The chamber was found to contain so many particles that the sampling slide was excessively covered, as illustrated in Figure 6*A*. This excess can result in particle coalescence on the slides as the crystals become relatively large droplets at the high relative humidities required to measure them isopiestically. Later samples were taken on several slides (see Fig. 6*B*, *C*, and *D*), thus avoiding this problem of an excess covering.

In Figure 4, curves *B* and *C*, it can be seen that the number of particles in the air close to the steaming lava surface in the laboratory is about two orders of magnitude greater throughout the range of sizes than the average of those sampled at about 100 m over the Hawaiian lava flow (curve *A*, Fig. 4). It will be shown below, however, that the actual particle production rate at the lava surface in the laboratory is near that estimated above from the natural steam clouds.

Metal foil was used as a lining for the inner surface of the sedimentation chamber in order to eliminate possible local charge effects which might cause side-wall deposition [*Schadt and Cadle*, 1957]. Later examination with a microscope of sections of this foil cut from the lining revealed, however, that deposition of particles seemed to occur. The steam-cloud sampling experiment was repeated with several thin glass slides attached to the walls of the chamber as well as to the bottom. As suspected, it was found that many of the smaller particles were depositing on the walls. Figure 7 shows the relative magnitude of this side-wall deposition, and Figure 8 shows photomicrographs of the particles on the side-wall slide surfaces. It can be seen in Figure 7

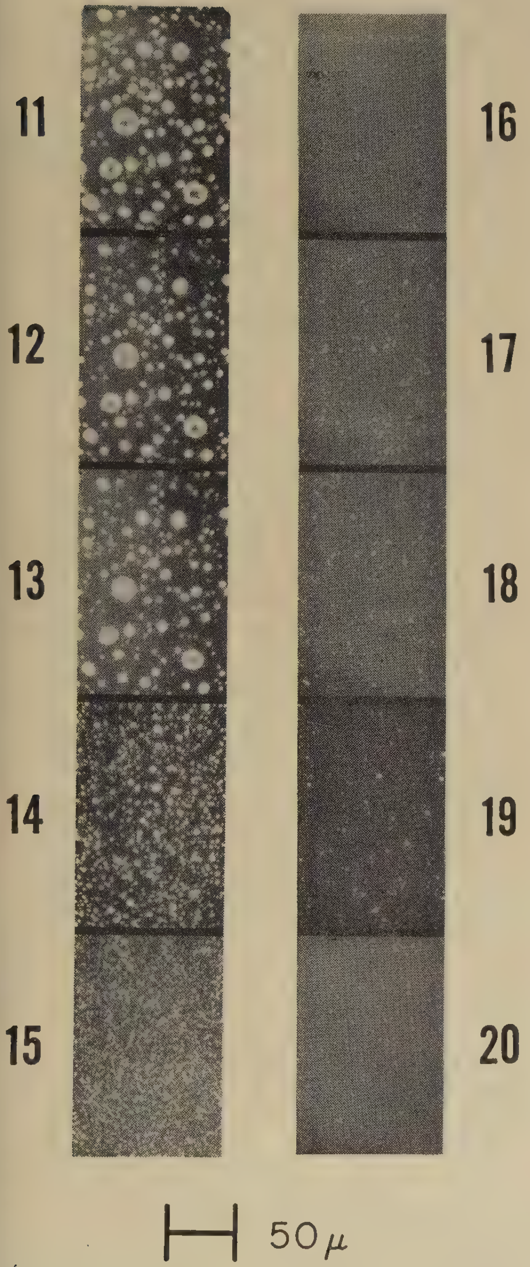

Fig. 8. Photomicrographs of laboratory steam-cloud particles, from saturated sea-salt solution on hot lava, deposited on glass sampling slides in sedimentation chambers. See text.

that wall deposition is greater for particles $< \text{about } 5 \times 10^{-13}$ g. It is supposed that this wall deposition is due to thermal effects.

Figure 8 further illustrates the sedimentation method for sampling salt crystals. The photographs show the steam-cloud particles, from a saturated sea-salt solution on hot lava, deposited on slides taken from the chamber. In frames 11, 12, and 13, the microscope was focused on the tops of the largest, medium-sized, and smallest cubic crystals, respectively, which were deposited by fallout on the bottom during the first 120 seconds. The purpose was to show something of the range of size of the cubic crystals of sodium chloride, which were clearly resolved under the microscope. Frames 14, 15 and 16 show deposition on other slides during successive periods of 900 seconds (i.e. 120 to 1020 seconds from time 0), 75,000 seconds, and 88,000 seconds, respectively. Side-wall deposition is shown on slides represented by frames 17, 18, and 19, which were attached near the top, middle, and bottom of the inner surface. Frame 20 shows the surface of the 'control' slide, which was exposed for 75,000 seconds to fallout from room air sealed in a separate sedimentation chamber.

A small Scholz condensation nucleus counter [*Landsberg*, 1938, p. 192] was used to demonstrate that the direct counts with the microscope of the individual particles falling in the sedimentation chamber actually represented most of the condensation nuclei present. Table 1 shows the results. For present purposes, the differences between the counts obtained by the two methods are not significant.

Many of the smaller particles, which are mere points of light on Figure 6*D*, were examined with an electron microscope. All particles were found to contain crystalline material, and cubic sodium-chloride crystals were visible in most of them. The smallest crystal seen was about 0.1 μ in diameter.

TABLE 1. Counts of Condensation Nuclei Made in Room Air and in the Laboratory Steam Cloud

	Scholz Counter*		Direct Count Steam-Cloud Particles with Microscope,†
Test No.	Room Air, N cm^{-3}	Steam Cloud, N cm^{-3}	N cm^{-3}
2	0.02×10^5	3.2×10^5	2.7×10^5
3	0.27×10^5	11×10^5	33×10^5

* An average, in each case, of many individual counts.

† Number computed from counts of more than 1800 crystals.

TABLE 2. Comparison of the Rates of Production of Salt Particles at the Surface of Molten Lava on the Puna Coast and in the Laboratory

	Puna Coast Steam-Cloud Particles, $\geq 3 \times 10^{-12}$ g (1)	Laboratory Steam Clouds: Sea Water Spray, Particles $\geq 3 \times 10^{-12}$ g (2)	Laboratory Steam Clouds: Sea Water Spray, All Particles (3)	Laboratory Steam Clouds: Saturated Solution Sea Salts, All Particles (4)
Salt production, grams cm^{-2} sec^{-1}	4.5×10^{-5}	7×10^{-5}	10×10^{-5}	45×10^{-5}
Particle production, number cm^{-2} sec^{-1}	1.4×10^{6}	2×10^{6}	100×10^{6}	745×10^{6}

Some difficulty was encountered with the nucleus counts due apparently to particle deposition on the walls of the short rubber tube leading from the cloud-filled chamber to the intake valve of the Scholz counter. This was solved by inserting a syringe needle through the tube wall at the counter intake orifice and, immediately before each sampling, drawing through the tube a volume of cloud air equal to several times the total inside volume of the tube. This step assured a minimum time for deposition on the inner walls of the tube.

On each occasion when steam clouds were sampled, background counts of condensation nuclei in the laboratory room air were also made. These are given in Table 1, with the condensation nucleus and salt crystal counts.

From the rate of rise, horizontal dimensions, and salt concentration of the miniature steam clouds, and from the surface area of the molten lava, estimates were made of the rate of production of salt particles P.

$$P = CAV/a \tag{3}$$

where

C = particle number cm^{-3}.
A = cross-section area of sedimentation chamber (154 cm^2).
V = rate of ascent of cloud (22 cm sec^{-1}).
a = area of hot lava surface (15 cm^2).

The average rate of production of particles was about 2×10^6 cm^{-2} sec^{-1}. This same expression can be similarly used to derive a total weight of sea salt of 7×10^{-5} g cm^{-2} sec^{-1}, when limited to particles having a weight $\geq 3 \times 10^{-12}$ g.

Table 2 shows a comparison of particle production by the laboratory steam cloud and by the Hawaiian clouds which were sampled. The quantities in columns 1 and 2 are regarded as an indication that the flash boiling process observed in the formation of the laboratory clouds also occurred in the formation of the natural clouds from the Hawaiian lava flows. From this result it is also concluded as probable that the numerous smaller particles found in the laboratory clouds were also present in the natural steam clouds, though unsampled owing to the limitations of the method used over the lava fields.

From the rate at which salt was driven off the lava surface by this flash boiling of the sea water, a rough estimate of the evaporation E and the heat utilization H were also made. These are expressed as follows:

$$E = W/S \tag{4}$$

where

E = sea water evaporated (g cm^{-2} sec^{-1}).
W = rate at which sea salt forced into air (g cm^{-2} sec^{-1}).
S = salinity of sea water, expressed as weight fraction.

$$H = Eh \tag{5}$$

where

H = calories used cm^{-2} sec^{-1}.
E = sea water evaporated (g cm^{-2} sec^{-1}).
h = heat of vaporization of sea water (cal g^{-1}).

By utilizing equations (3), (4), and (5), a quantity of about 2 cal cm^{-2} sec^{-1} was computed for the rate of consumption of heat during the few seconds of flash boiling of the water-coated hot lava. The physics handbook indicates a thermal conductivity of basalt of about 0.005 cgs units. Thus a brief heat flow of 2 cal/sec/cm² would be expected with a temperature gradient of about 1000°C in somewhat less than 1-cm thickness of lava. Some additional heat is also available from the latent heat of crystallization of the lava.

In making the above estimates of the rates at which water is vaporized, it is assumed that all of the salts are driven off into the air with the water vapor. It is observed, however, that some of the salts remain on the surface of our laboratory lava after it is dried and relatively cool. The extent to which a salt residue such as this may remain under natural conditions is uncertain. The above heat-flow estimate is therefore somewhat less than the actual amount.

As most of the water disappears and a salt brine is left, the particle production rate is apparently greatly increased, if the lava remains hot. This was tested in the laboratory by spraying a nearly saturated solution of sea salts on molten lava and trapping a portion of the white cloud of particles which arose. Figure 8, curve *B*, shows the comparative numbers and weights of the salt particles found; Table 2, column 4, shows the particle production rate; and Figure 8 shows photomicrographs of the particles formed. It is thought that this increase in the number of crystals may result from the availability of more heat for the fractionation process, which at present is unknown.

After the apparent vaporization of all water, the vapors rising from the salt-coated hot lava, when inhaled, are occasionally irritating to the nose and throat. D. E. Carritt, chemist of this laboratory, states that this irritant is probably HCl (and/or) H_2SO_4, resulting from the breakdown of the chlorides and sulfates.

J. P. Eaton has reported (personal correspondence) that rains falling from or through the steam clouds were occasionally acidic, causing a burning sensation to the skin and eyes. The above observations of the irritating character of the vapors suggests that in some cases a part of the lava remains hot enough, after contact with the sea, to break down salts remaining after the water is driven off.

It is an interesting fact that sea water droplets, when splashed or sprayed on molten lava, tend to flatten on the surface during vaporization and do not form the almost spherical, dancing droplets so characteristic of water on very hot metals. This difference in performance is thought to be due to the low thermal conductivity of lava, which is only about one-twentieth of that of steel and about a hundredth of that of copper.

It is of interest to meteorologists and others to compare the rates of production of salt particles by the hot lava in contact with the sea to that of the sea surface as a whole. *Blanchard* [1961] recently computed the average annual world fallout of sea salt to be 9×10^9 metric tons. This estimate is based upon measurements of salt found as particles at cloud levels in the atmosphere and salt in solution in falling rain. From Blanchard's estimate it is found that 1 m² of sea surface produces about 0.8 μg of salt per second, which reaches cloud-level altitudes. The total surface area of the oceans and seas assumed here is 3.6×10^8 km².

From the field and laboratory results given here it is computed that a square meter of lava produces from 0.7 to 4.5 grams of finely divided salt particles per second, or an amount equal to that produced on the average by about one to six million square meters of sea surface. In other words, the hot lava produces airborne salt from one to six million times faster per unit area than the average of the seas. Expressed in terms of particle number ($\geq 3 \times 10^{-12}$ gm), the range of rates of production, extended over the duration of the 1960 flow, is such that 2 to 7 km² of hot lava surface could double the salt-aerosol population within the first kilometer of the earth's atmosphere. These estimates emphasize again the relatively great particle productivity of hot lava at sea level.

6. Major Factors Affecting Density of Steam Clouds

Our experience with natural and artificial steam clouds has caused the authors to think that large differences should be found in the concentration of particles in these clouds. The physical factors producing these differences may be grouped under two headings: the rate and mechanics of availability of heat for the flash boiling of sea water and the manner in which the sea water is brought into contact with the lava.

Factors altering heat availability. Extreme examples of differences in the mechanics whereby

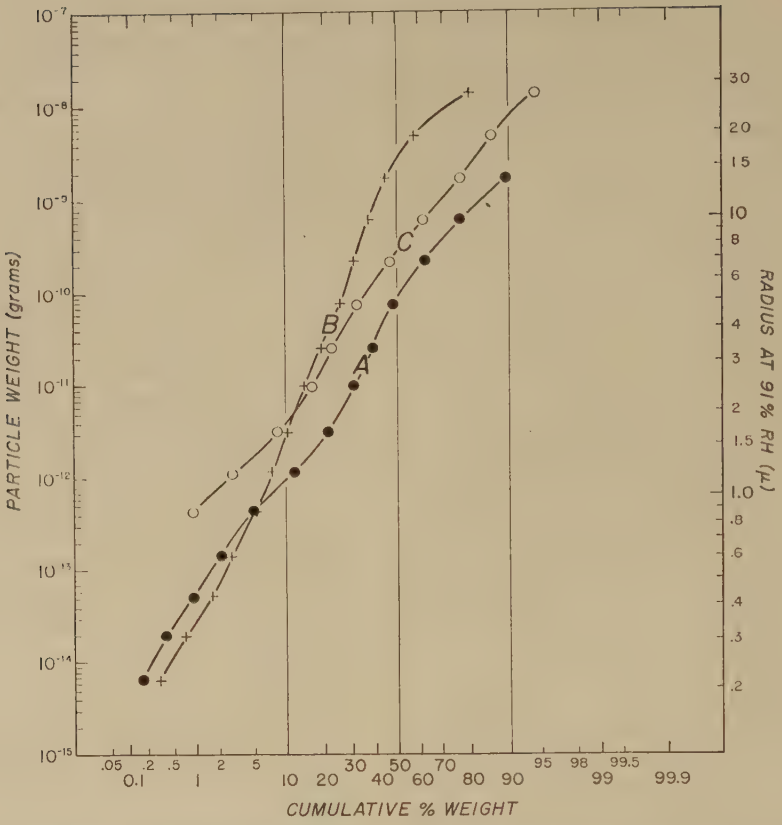

Fig. 9. Cumulative weight per cent distribution among steam-cloud particles formed in the laboratory. Curve *A* represents particles formed when sea water was sprayed on hot lava, and curve *B* represents those formed when a saturated sea-salt solution was used. *C* represents the distribution among the average volcano steam-cloud particles of Hawaii.

the hot lava enters the sea are shown in plates 1 and 3 of *MacDonald and Hubbard* [1951]. Plate 1 shows a large dense cloud rising when lava, advancing slowly along a broad front, encounters the sea. Plate 3 shows a negligible amount of steam around 'a stream of liquid rock gliding smoothly into the sea ···' In this latter example, the steady flow of fluid is thought to have formed a solidified lava 'tube' under water, which insulates the molten interior and greatly reduces the rate of transfer of heat to the sea as the lava continues its flow down the submarine slope. In contrast, plate 1 (and Fig. 1) is thought to represent a condition in which relatively small pieces or volumes of lava enter the sea intermittently.[4] In this case it is thought that lava tubes are not formed and that many small incandescent surfaces are exposed to water, dissipating much heat in the immediate vaporization of sea water. No doubt the slope of the shore and of the sea bottom influence the details of the mechanics of the encounter of lava and the sea, in addition to the effects of the fluidity of the lava, its gas content, and the rate at which it is arriving at the shore.

Effects of sea state on steam-cloud formation. If the sea is calm, it is thought that the width of the area of the zone of contact between sea and lava will be narrow. Heavy surf along the shore should act to broaden this zone and briefly but repeatedly to wet hot lava surfaces with relatively small amounts of water before its flow finally brings about complete submergence. Thus it is supposed that surf and heavy seas will increase the vaporization and atomization of water and salt above that occuring during calms.

---

[4] The presence of the steam makes it difficult if not impossible to see the details of the entry or contact process.

Effects of winds on cloud. In addition to the indirect effects of winds in causing waves on the sea, they can alter the steam-cloud particle concentration in at least two other ways.

First, winds can act to produce turbulent mixing of the clouds with the ambient air and thus to alter the rates of cooling of the sodium chloride vapor rising in some of them. This altered cooling rate will affect the salt crystal growth time and, as pointed out by *Schaefer* [1953, p. 82], cause differences in the sizes of the crystals produced.

Winds can alter the production of particles in another way—through the transport of spray and large salt particles from the lava-sea contact regions back over the approaching hot lava streams and fields. This requires a certain wind direction, of course. Thus the larger spray and salt particles, produced in the zones of explosive boiling and vaporization, would fall out of the steam clouds onto an even hotter surface, where they would be vaporized and would probably form smaller airborne particles.

Conditions resulting in contact between concentrated solutions of sea salts and hot lava can, as shown in Figure 8, produce many more particles than are formed when the presence of much water rapidly cools the lava surface. It is supposed that some of this increase in number may result from the vaporization and subsequent condensation of sodium chloride, which has a considerable vapor pressure at temperatures of 800° to 1000°C.

7. WEIGHT DISTRIBUTION AMONG THE SALT PARTICLES

Cumulative weight per cent distributions were derived from the data given in Figure 8, curves *A* and *B*, and Figure 4, curve *A*. The results of these computations are shown in Figure 9. Note that the median mass particle of curve *A*, which represents a sea-water steam cloud, is over an order of magnitude smaller than the median mass particle representing a cloud from a saturated sea salt solution (curve *B*). This result indicates that the particle size distribution produced probably differs from beginning to end of the flash boiling process as the salt concentration increases. Curve *C* of Figure 9, which represents an average of the natural steam-cloud particles, (i.e., curve *A*, Fig. 4), falls in major part between the two curves of the artificially formed particles. This result is tentatively interpreted to mean that the natural clouds were, at this time, largely a mixture of particles arising from the flash boiling of waters ranging in salt concentration from that of sea water to saturated solutions. The deficiencies of curve *C* for the smaller particles reflects the failure of the sampling technique used, as discussed.

8. CONCLUDING REMARKS

Meteorologists, geochemists, and others are increasingly concerned with information about salt particles from the sea which become airborne. These particles are thought to be essential in some cloud physics and other atmospheric processes, and in geochemistry, and are known to arise from bubbles present at the surface of the oceans [*Blanchard and Woodcock*, 1957]. It is important to explore more thoroughly the contribution of relatively short-term sources of these particles, such as volcanic activity at or near sea level.

Wexler [1953, p. 95] and *Menzel* [1953, p. 119] have noted the possible role of the freezing nuclei in volcanic dusts in causing large departures from average snowfall in the atmosphere, and in initiating long-term weather changes. The enormous production of giant salt nuclei by the lava-sea contact, and the potential role of these nuclei in the initial formation of raindrops, cause the authors to think that steam-cloud particles should be added to the growing list of factors influencing long-term weather changes.

Concerning the variability of cloud density, it is pertinent to state here that comparison of the range of rate of salt particle production on hot lava and the average of the oceans, such as that made at the end of section 5 above, are of limited meaning at this time. It seems likely that far greater rates will be found when it becomes possible to obtain samples from steam clouds that rise from the porous spongelike aa lava and especially from areas where explosive shattering of the lava surface occurs. A maximum rate of exchange of heat from the lava to the sea water and the air should attend the resulting rapid exposure of multiple hot surfaces. It is possible that a few square kilometers of hot lava, under certain conditions of contact with the sea, can produce a weight of sea-salt nuclei per unit of time equal to a large fraction of the total average production of all of the oceans of the earth. An occurrence such as this, in a relatively limited area, would be expected to produce changes in the radiation, precipitation, and thermodynamic characteristics of the atmosphere.

The results given in this paper are regarded as a beginning in the study of the salt-aerosol-producing capacity of the earth's lava-sea-atmosphere contact zones. In the future expansion of knowledge of this 'capacity' and its consequences, the following tentative steps seem pertinent at this time:

(*a*) The chemistry and the sizes of the aerosols produced by vapors arising from dry sea salts at various high temperatures should be investigated. This can be done in the laboratory.

(*b*) When eruptions and steam clouds occur, particle samples and counts of condensation nuclei should be made in the clouds by aircraft at various short distances from the source areas. The trapping of small volumes of these clouds seems to be the best method of obtaining these samples, since the number and size range of the particles make representative sampling by impingement alone very difficult. A study of the aerosol content, size, and rate of ascent of the steam clouds may be used to determine the variability of particle production rate under the changing conditions of steam-cloud formation by the lava and to test the estimates made in section 5 above.

(*c*) The great aerosol clouds from the lava-sea-atmosphere contact zones should be followed by specially instrumented aircraft to learn in what way events and properties within the air masses concerned mark them as unusual. It seems reasonable to regard these clouds as natural large-scale salt-seeding experiments, offering extraordinary observational opportunities. Study of the history of weather and other changes associated with these clouds, but far away from the source, may also give us some further ideas about the meteorological roles of the salt particles that are normally produced by the sea.

Acknowledgments. The authors thank Mr. Saul Price, USWB, Honolulu, and Dr. Harry Wexler, USWB, Washington, for their recognition of the rare opportunities for geophysical studies existing during the 1960 Kilauea eruption and for their efforts in aiding the first author during the field work in Hawaii. The first author also wishes to express his appreciation of the help given by Jerry P. Eaton, W. U. Ault, and D. H. Richter of the Kilauea Volcano Observatory, U.S.G.S., and Jack Pales and Colby Foss of the Mauna Loa Observatory, USWB, Hilo. The flying abilities and helpfulness of Mr. William Stearns of Murray Air, Ltd., of Hilo, Hawaii, made the sampling flights pleasurable as well as effective. Criticism of the manuscript by Adrian F. Richards was very useful.

The work was supported by the Office of Naval Research, contract NONR-798(00) (NR-082-124), and the National Science Foundation, grant 7366.

REFERENCES

Arons, A. B., and C. F. Kientzler, Vapor pressure of sea-salt solutions, *Trans. Am. Geophys. Union, 35,* 722–728, 1954.

Blanchard, D. C., The electrification of the atmosphere by particles from bubbles in the sea, Ph.D., thesis, Massachusetts Institute of Technology, 1961.

Blanchard, D. C., and A. H. Woodcock, Bubble formation and modification in the sea and its meteorological significance, *Tellus, 9,* 145–158, 1957.

Dietz, R. S., and M. J. Sheehy, Transpacific detection of Myojin volcanic explosions by underwater sound, *Bull. Geol. Soc. Am., 65,* 941–956, 1954.

Eaton, J. P., and K. J. Murata, How volcanoes grow, *Science, 132,* 925–938, 1960.

Eriksson, Erik, The yearly circulation of choride and sulfur; meteorological, geochemical and pedological implications, 1, *Tellus, 11,* 375–403, 1959.

Higashi, K., K. Nakamura, and R. Hara, The specific gravities and the vapor pressures of concentrated sea water at 0-175 °C, *J. Soc. Chem. Ind. Japan, 34* (Abstr. 72B), 166–172, 1931.

Landsberg, H., Atmospheric condensation nuclei, *Gerlands Beitr. Geophys., Suppl. 3:* 155–252, 1938.

Langmuir, I., and K. B. Blodgett, A mathematical investigation of water droplet trajectories, *Gen. Elec. Research Lab. Rept.,* Air Technical Service Command, contract W-33-038-AC-9151, pp.1-47, 1945.

Langmuir, Irving, Super-cooled water droplets in rising currents of cold saturated air, in *Precipitation Static Studies, Gen. Elec. Research Lab. Rept.,* Air Technical Service Command. contract N-33-106-SC-65. pp. 1–91, 1944.

MacDonald, G. A., and D. H. Hubbard, Volcanoes of Hawaii National Park, *Hawaii Nature Notes,* vol. 4, no. 2, 43 pp. Naturalist Division, Hawaii National Park, 1951.

Mason, B. J., *The Physics of Clouds,* Clarendon Press, Oxford, England, 1957.

Menzel, D. H., On the causes of the ice ages, in *Climatic Change. Evidence, Causes and Effects,* edited by Harlow Shapley, Harvard University Press, Cambridge, Mass., pp.117–121, 1953.

Schadt, C., and R. D. Cadle, Critical comparison of collection efficiencies of commonly used aerosol sampling devices, *Anal. Chem., 29,* 864–868, 1957.

Schaefer, V. J., Laboratory, field and flight experiments, *Final Report Project Cirrus, 1, R L 785,* General Electric Co., Schenectady, N. Y., 1953.

Simpson, R. H., A phenomenal haze in the Pacific, *Weatherwise,* 83–84, 1950.

Symons, G. J. (editor), The eruption of Krakatoa and subsequent phenomena, *Report of the Krakatoa Committee of the Royal Society,* London, 1888.

Twomey, S., The identification of individual hygroscopic particles in the atmosphere by the phase-transition method, *J. Appl. Phys., 24,* 1099–1102, 1953.

Twomey, S., The composition of hygroscopic particles in the atmosphere, *J. Meteorol., 11,* 334–338, 1954.

Wexler, H., On the causes of the ice ages, in *Climatic Change—Evidence, Causes and Effects,* edited by Harlow Shapley, Harvard University Press, Cambridge, Mass., pp. 73–105, 1953.

Woodcock, A. H., and Mary M. Gifford, Sampling atmospheric sea-salt nuclei over the ocean, *J. Marine Research, Sears Foundation, 8,* 177–197, 1952.

Woodcock, A. H., Atmospheric salt particles and raindrops, *J. Meteorol., 9,* 200–212, 1952.

Woodcock, A. H., and D. C. Blanchard, Tests of the salt-nuclei hypothesis of rain formation, *Tellus, 7,* 437–448, 1955.

Woodcock, A. H., The origin of trade-wind orographic shower rains, *Tellus, 12,* 315–326, 1960.

(Manuscript received May 8, 1961.)

Contribution No. 1173

Deep-Sea Research, 1961, Vol. 8, pp. 130 to 143. Pergamon Press Ltd., London. Printed in Great Britain

A description of Gulf Stream Meanders off Onslow Bay*

FERRIS WEBSTER

(*Received* 6 *February*, 1961)

Abstract—Data from a month of continuous surface observations across the Gulf Stream show a periodic time variation in the position of the current. The region studied is off Onslow Bay, North Carolina, where the current is close to the edge of the continental shelf. The dominant periods of the position variations correspond to the periods of the offshore winds, but no physical connection is apparent. The amplitude of these dominant variations, or meanders, is 10 km. Lunar components, either monthly or diurnal, have amplitudes which are, at most, small in comparison with those of the principal meanders.

Although the meanders off Onslow Bay may be analogous to the multiple currents found downstream, their periods eliminate them as incipient forms of the large-scale meanders. An average section of velocity and temperature during the month of observation is presented.

1. INTRODUCTION

MEANDERS are among the most intriguing and baffling aspects of the Gulf Stream System. Although meanders upstream from Cape Hatteras have been the subject of a certain amount of study, little is known of their existence or behaviour between the Florida Straits and Cape Hatteras, where the Gulf Stream flows close to shore over the Blake Plateau. This region would probably be a fruitful one for study, since the amplitude of lateral migrations of the current is constrained by the nearness of the continental shelf.

In order to seek information on the fine structure and time variation of the current in this region, a month-long cruise was made in the research vessel *Crawford* by W. S. von ARX, D. F. BUMPUS and C. G. DAY during May and June, 1958. The ship made 120 consecutive crossings of the axis of the Gulf Stream during a 28-day period (FIG. 1). Measurements were made of the surface salinity and velocity, and of the temperature to a depth of 200 m. The general procedure of this cruise was similar to one undertaken by von ARX, BUMPUS and RICHARDSON (1955) in the research vessel *Caryn*, but the duration and concentration of measurements were much greater.

Because the observations were restricted to a single lunar month, only a relatively small portion of the spectrum of Gulf Stream time variations could be sampled. Moreover, the time necessary to complete a single crossing of the current was about six hours, and hence the frequency of sections was too low to permit semidiurnal tidal effects to be measured. By extending the duration of measurements to 28 days, it was hoped that the lunar monthly effects, if any, could be observed. Hence, the data are most useful for determining the characteristics of time variations having periods greater than a day and less than a month.

2. BASIC DATA

Throughout the cruise, a bathythermograph (BT) measurement, giving temperature as a function of pressure to a depth of 200 m, was taken every half-hour. At the time of each BT lowering, a bucket sample of surface water was taken to be analysed later for salinity. The surface water velocity vector was determined hourly, by means of the geomagnetic electrokinetograph (GEK) (von ARX, 1950). The position of the ship at each BT and GEK observation was determined by a LORAN fix, to confirm the choice of ship's course to keep as close as possible to the planned cruise line. Each crossing was continued across the current as far as was necessary to define the onshore edge of the band of maximum velocity.

---

*Contribution No. 1173 from Woods Hole Oceanographic Institution.

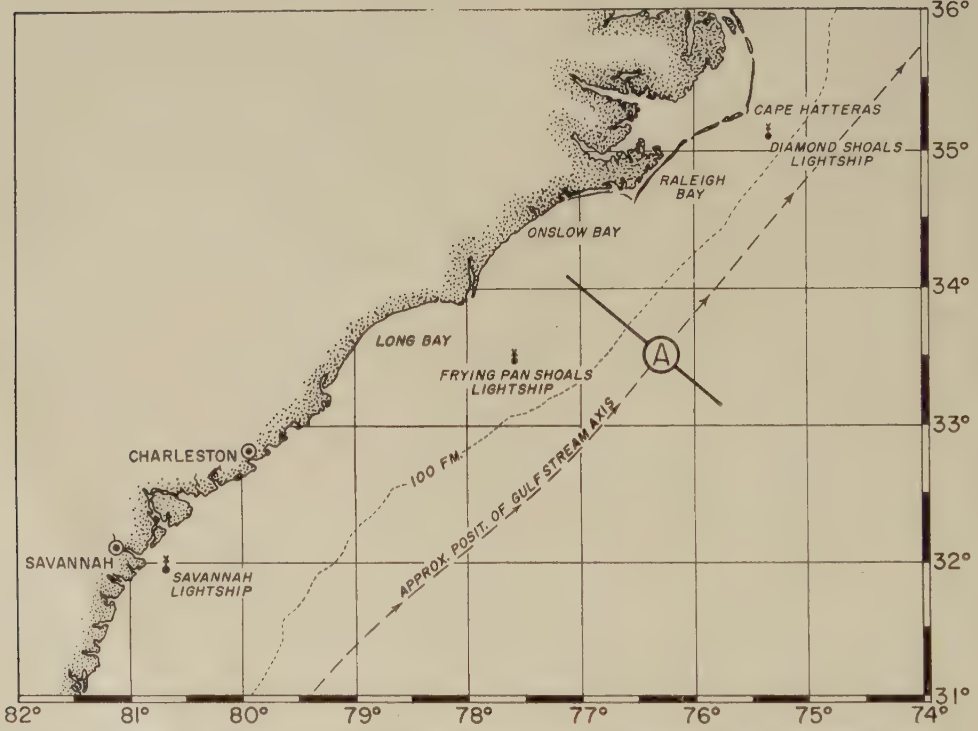
36°
35°
34°
33°
32°
31°
82°
81°
80°
79°
78°
77°
76°
75°
74°
CAPE HATTERAS
DIAMOND SHOALS LIGHTSHIP
RALEIGH BAY
ONSLOW BAY
LONG BAY
FRYING PAN SHOALS LIGHTSHIP
A
CHARLESTON
SAVANNAH
SAVANNAH LIGHTSHIP
100 FM.
APPROX. POSIT. OF GULF STREAM AXIS

FIG. 1. Onslow Bay area. Point ' A ' is the intersection of cruise path with the mean axis of the climatological mean Gulf Stream, as estimated by the U.S. Coast and Geodetic Survey.

The observations were plotted to form a set of space-time diagrams : namely those in which the values along the line of traverse were plotted against time of observation. Isopleths were drawn to connect the sections. These space-time diagrams bear some resemblance to the pattern of the stream as it might be if viewed from above. From above, the movement of the current is from right to left, whereas in the space-time diagrams, the passage of time is from left to right. Consequently, when the position of the current is moving towards the shore in time, the local direction of current flow is away from shore.

Surface Temperature

The surface temperatures were measured by means of a thermistor bead mounted in the bow of the *Crawford* about two feet below the water line. The resistance of the bead was recorded continuously on a strip chart recorder calibrated for temperature. This permitted the sharp temperature gradients to be well located in space and time (FIG. 2).

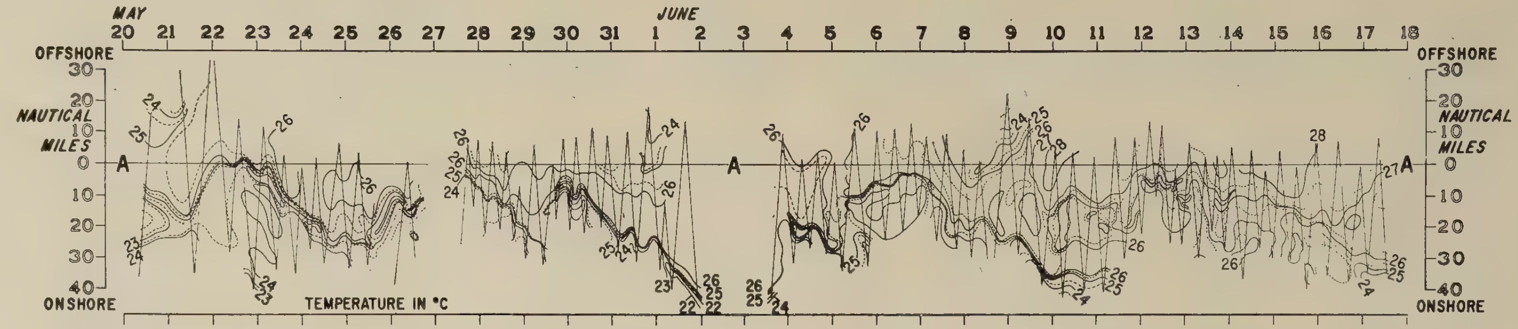

FIG. 2. Surface temperature, *Crawford* Cruise 18. From the 120 profiles of surface temperature the space-time diagram has been constructed. The straight slanting lines across the face of the diagram represent the path of the ship in space and time. Along this path, the temperature was measured continuously; between path lines, the isotherms were contoured smoothly.

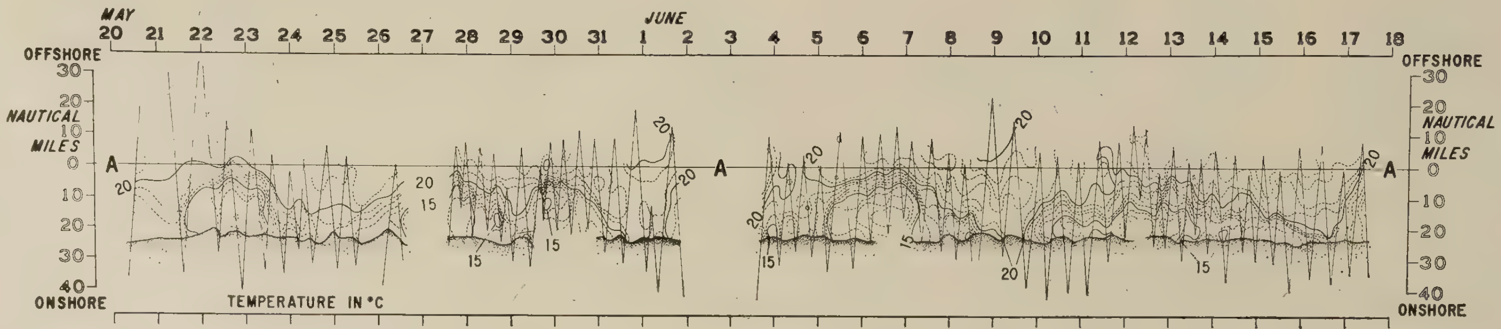

FIG. 3. 100 m temperature, *Crawford* Cruise 18, based on bathythermograph (BT) data. The stippled boundary of this diagram represents the position of the continental shelf at a depth of 100 m.

The surface temperatures were particularly susceptible to seasonal warming during the period of *Crawford* Cruise 18. The maximum temperature at the beginning of the cruise was about 25 °C, and at the end of the cruise, the maximum temperature was about 28 °C. This seasonal, or vernal warming tends to diminish the surface-temperature contrast across the Gulf Stream and makes the definition of the stream edges more difficult. In spite of the major handicap of vernal warning, the surface temperatures are nevertheless useful because they can be compared with the other physical quantities such as current velocity and salinity which were in general measured only at the surface.

100-*metre temperature*

Since BT lowerings were made at half-hourly intervals, the actual temperature gradients at a depth of 100 m may have been much sharper than the necessarily smoothed contours indicate (FIG. 3). However, the temperature at 100 m is relatively unaffected by vernal warming, so that it is more useful than surface temperature for comparison of the structure of the current between different portions of the cruise.

The fluctuations in the position of the edge of the continental shelf (FIG. 3) are due to uncertainties in position measurements and deviations of the ship's course from the cruise line. Loran signals were timed to an accuracy of about ± 3 micro-seconds, which, in this area, amounts to a probable positional error of ± 1 nautical mile. In addition, because of strong and variable cross-currents, the ship deviated from the planned cruise path. These deviations were as great as ten nautical miles on the first few crossings, but as the ability to keep the ship on course improved with practice, deviations from the cruise line were kept to less than two nautical miles after the first three or four days. Because of the irregularities in the edge of the continental shelf, the position of the edge at 100 m depth with respect to the point ' A ' can vary by as much as ± 4 nautical miles due to deviations from the path line. So, errors from Loran and bottom irregularities can combine to produce variations in the position of the 100 m contour as large as 10 nautical miles – enough to account for the fluctuations of the shelf edge shown in FIG. 3.

Depth of 20-*degree isotherm*

The topography of the 20-degree (Centigrade) isotherm (FIG. 4) was plotted in an attempt to determine the internal motions associated with meanders of the current. The isotherm for 20°C was chosen because shallower isotherms were subject to the distortions of vernal warming and deeper ones often dropped below the depth accessible to the BT.

Surface salinity

The surface water samples, which were routinely taken at the time of each BT lowering, were analyzed on a Schleicher-Bradshaw conductivity bridge. (SCHLEICHER and BRADSHAW, 1956). The surface salinity (FIG. 5) is determined on the assumption of a direct relation between conductivity and salinity, for which the conductivity bridge is calibrated.

General features of the space-time diagrams

Each of the space-time diagrams shows a series of lateral migrations, or meanders, of the current. The surface temperature diagram (FIG. 2) shows periodic occurrences of a sharp temperature gradient across the section. These sharp temperature gradients seem to form at an offshore position and to move onshore as time increases, generally becoming more intense. Since the local direction of current flow is exactly opposite to the direction of increasing time, the current is actually flowing offshore, decreasing in intensity as it does so. A region of sharp temperature gradient is followed by a broad diffuse temperature gradient which once again reforms into another offshore sharp gradient.

Surface readings, though suggestive, are not sufficient for delineating the meanders because the surface layer is influenced both by vernal warming and by shifting winds. Consequently, the temperature at a depth of 100 m (FIG. 3) and the depth of the 20°C isotherm (FIG. 4), are more useful in defining the centre of the Gulf Stream and its edges. It is found, upon comparing the surface velocity with the 100 m temperature, that the position of the 20°C isotherm at 100 m depth corresponds closely with the path of maximum downstream velocity as defined by the GEK on each crossing (FIG. 6). Hence, it is possible to define a centre of the stream using either the BT or the GEK; either the 20°C isotherm at 100 m depth or the maximum velocity across the section may be chosen as the centre of the stream in Onslow Bay.

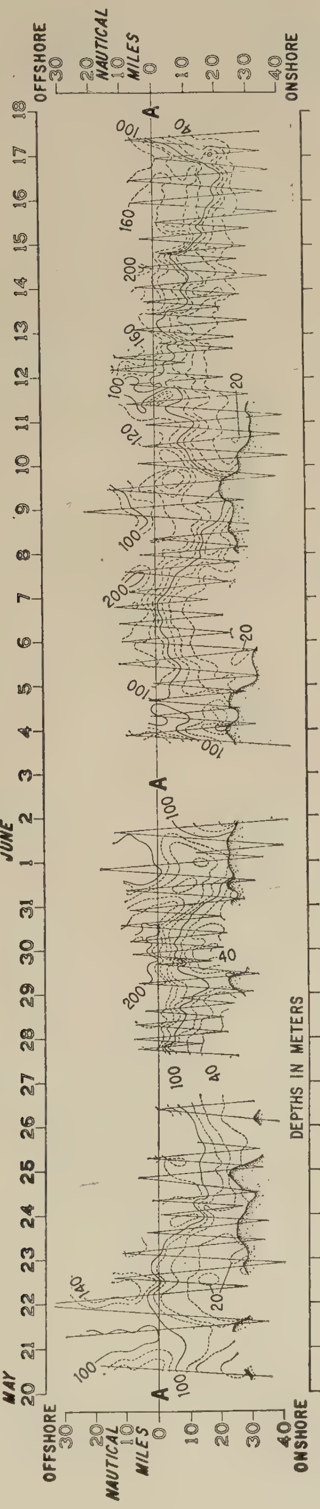

FIG. 4. Depth of 20°C isotherm, *Crawford* Cruise 18, based on BT observations.

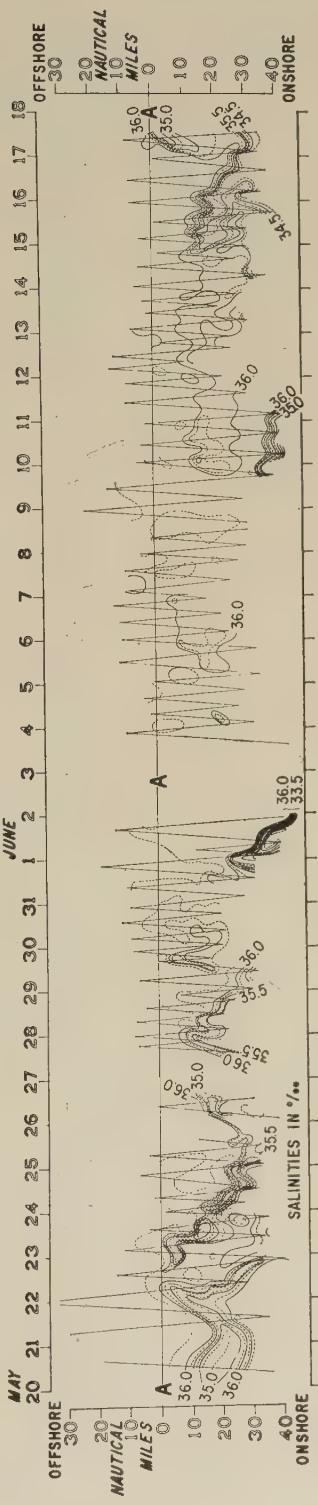

FIG. 5. Surface salinity, *Crawford* Cruise 18, from bucket samples of surface water.

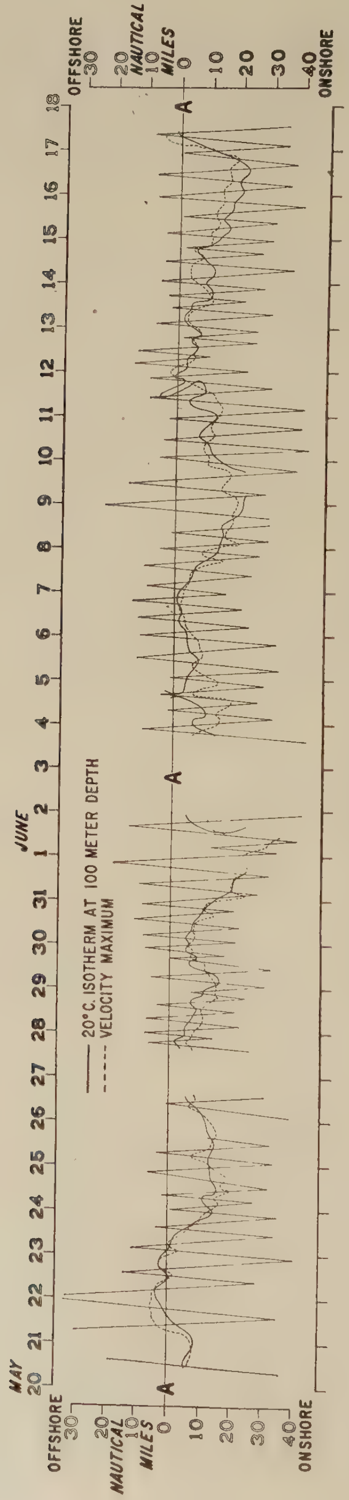

FIG. 6. Position of stream centre, *Crawford* Cruise 18.

3. ANALYSIS OF THE DATA

Cold tongues

Together, the surface temperature and salinity define bands, or tongues, of water both colder and less saline than that on either side.

These tongues are found shoreward of the stream centre. It will be noted that towards the end of the cruise, the salinity record shows another of these offshore-running tongues, but that the surface temperature record defines it only poorly. This is probably an effect of vernal warming, which gives a clue to the origin of the water in the tongues. A similar warming during this period was noted at Frying Pan Shoals Lightship, between Long Bay and Onslow Bay, where, between May 15 and June 15, the surface temperature increased from 19°C to 25°C.

In addition to the temperature, the salinity also gives a clue to the origin of the water in the tongues. Both the water temperature and salinity correspond generally to that of the onshore Carolina bays : Raleigh, Onslow and Long Bays. The temperature and salinity of the water in these regions were recorded during the cruise at lightships and have been tabulated by DAY (1959).

Table 1. *Comparison between lightship surface salinities and temperatures and those found in cold tongues during Crawford* 18 *Cruise.*

Date	*Crawford* 18 (*tongue*)		*Frying Pan Shoals* (*2 days earlier*)		*Frying Pan Shoals*		*Savannah*		*Diamond Shoals*	
	Temp. °C	Sal. ‰	Temp. °C	Sal. ‰	Temp. °C	Sal. ‰	Temp. °C	Sal. ‰	Temp. °C	Sal. ‰
May 24–25	22·5	34·5	21·5	33·0	22·0	34·0	24·0	31·0	21·5	32·0
May 28–29	23·0	34·0	22·5	34·0	22·0	35·0	24·0	31·0	—	—
May 31–June 2	22·0	32·5	22·0	33·0	24·0	35·0	24·0	31·5	22·0	31·5
June 10–11	23·5	34·0	23·0	34·0	24·0	35·0	27·0	30·0	21·5	31·5
June 15–17	26·0	33·5	26·0	33·5	25·0	33·0	26·0	32·0	25·5	33·5

Table 1 shows the temperatures and salinities as measured in the fresh cold tongues in the Gulf Stream and at the same time of the waters at Frying Pan Shoals and Savannah Lightships, both south of Onslow Bay, and at Diamond Shoals, north of Onslow Bay (FIG. 1). The water at Savannah Lightship is warmer and fresher than the water in the tongues, which eliminates it as a source of tongue water. The salinity of the water at Savannah a few days before the appearance of a cold tongue is always less than that in the tongue by about 3‰. The temperature and salinity are generally less at Diamond Shoals than in the tongues. Temperatures and salinities more compatible with those found in the tongues are found in the waters at Frying Pan Shoals. If this is indeed the source, best agreement is found when the values of temperature and salinity at Frying Pan Shoals are compared with those in the tongue at Onslow Bay two days later.

To illustrate the contrast between the shelf water and the water characteristic of the Gulf Stream in this region, note that the salinity of the water on the seaward side of the stream is consistently about 36·25‰ and the temperature ranges from 25° to 28°C. This is also typical of water in the main current on the shoreward side of the maximum flow. Hence, it appears that the water in the tongues is shelf water which has been entrained into the shoreward edge of the Gulf Stream current. The source of the tongue water is just south of the section under observation – probably Long Bay. This agrees with the conclusions of BUMPUS (1955), and BUMPUS and PIERCE (1955), that when the Florida Current moves onshore it will entrain shelf water. Other investigators have found similar occurrences of fresh and/or cool water. FORD, LONGARD and BANKS (1952) reported a slender filament of cold water along the shoreward edge of the Gulf Stream, downstream from Cape Hatteras. From the salinity of the filament, they concluded that its source was river runoff from the shelf near Cape Hatteras. Similarly, HELA and WAGNER (1954) report the occurrence of relatively fresh water on the western side of the Florida Current, off Miami, which seems to originate in the north-east area of the Gulf of Mexico.

The structure of the meanders as shown in the space-time diagrams suggests that each intense current forms onshore and moves offshore as it flows downstream. As the current flows offshore shelf water remains entrained along its shoreward side. If the meanders in the Onslow Bay region are characteristic of those throughout the Gulf Stream System, then we should expect to find water from a nearshore region generally present along the inshore edge of the current.

Periodic components of meanders

The Fourier components of the fluctuation positions of both the velocity maximum and the 20°C isotherm at 100 m depth were calculated. The lunar month of 27·55 days was chosen as a basic period, and the positions of these features were determined at 48 equidistant points during the month to establish a 48-ordinate scheme for harmonic analysis, as outlined by CONRAD and POLLAK (1950). The amplitudes of the components, up to the 12th harmonic, are shown in FIG. 7. The dominant harmonics are the fourth and the seventh, corresponding to periods of 6·9 and 3·9 days. There is no apparent reason to expect that the dominant harmonic components

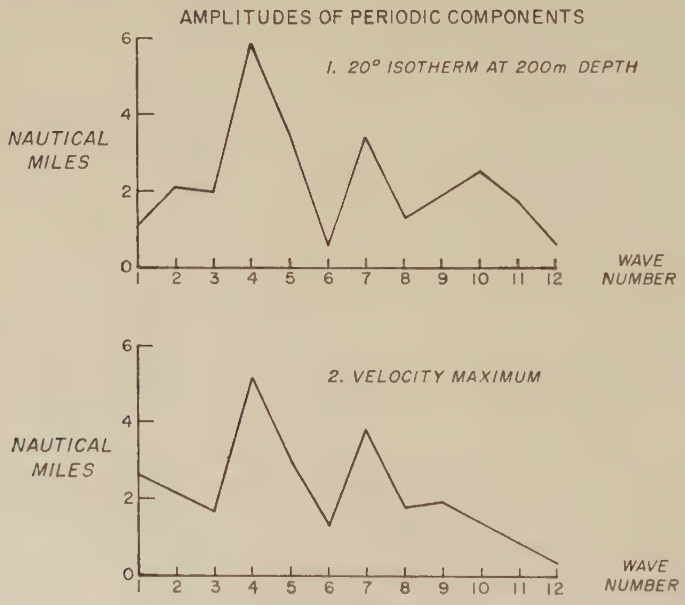

FIG. 7. Harmonic components of meanders.

should be exact sub-multiplies of a lunar month; hence the periods showing this characteristic should be regarded only as approximate. However, the prominent components have periods of the order of a week and amplitudes of about 10 km. It should be stressed that these harmonic components refer only to the *Crawford* Cruise 18 data; there is no evidence to indicate that these same periods and amplitudes would be found on another cruise.

Significantly, the amplitudes of the monthly (first harmonic) and fortnightly (second harmonic) components are comparatively small, being less than 2 nautical miles (3·7 km). Their unimportance indicates that the meanders are not induced primarily by long-period lunar effects.

Although the data are not suitable for analysis of diurnal components, it is evident from the space-time diagrams that the passage of each of the principal meanders (or shingles) is not a diurnal phenomenon, but requires a period of several days. It seems likely that, because of their relatively long time of passage, the meanders off Onslow Bay are not related to the daily outflow from the Gulf of Mexico, as suggested in the hypothesis advanced by von Arx, Bumpus and Richardson (1955).

A possible cause of the seven-day and four-day recurrence of meanders is revealed in a comparison of the meander positions, as indicated by the 20°C isotherm, with the atmospheric pressure field during the period of observations. The sea-level barometric pressure difference between Charleston, South Carolina, and Cape Hatteras was used as an index of the offshore wind. A higher pressure at Hatteras corresponds to an onshore wind. Fig. 8 shows the position of the 20°C isotherm at 100 m and the Hatteras-Charleston atmospheric pressure difference. There is an obvious similarity in periods, but no clear indication of synchronism. If it is

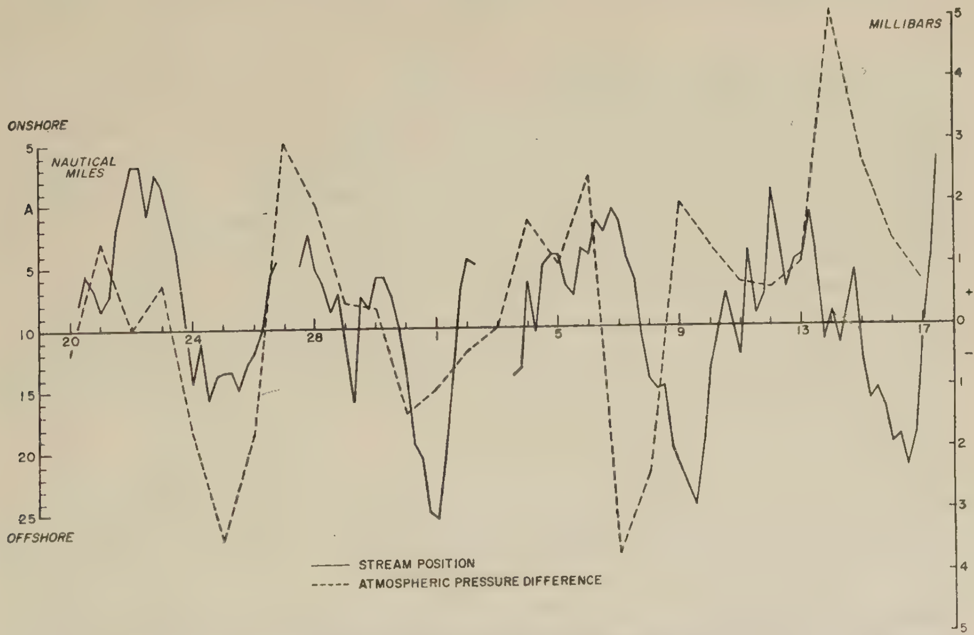

Fig. 8. Atmospheric pressure difference between Cape Hatteras and Charleston, and position of stream centre during *Crawford* Cruise 18.

assumed that there is a delay in the response of the stream position to persistent winds, then the atmospheric pressure difference can be lagged. FIG. 9 shows the result of introducing a lag of four and a half days, which gives the best correlation between atmospheric pressure and stream position. The stream positions (FIG. 9) were smoothed by combining the dominant harmonic components (4th, 5th and 7th) found in the Fourier analysis.

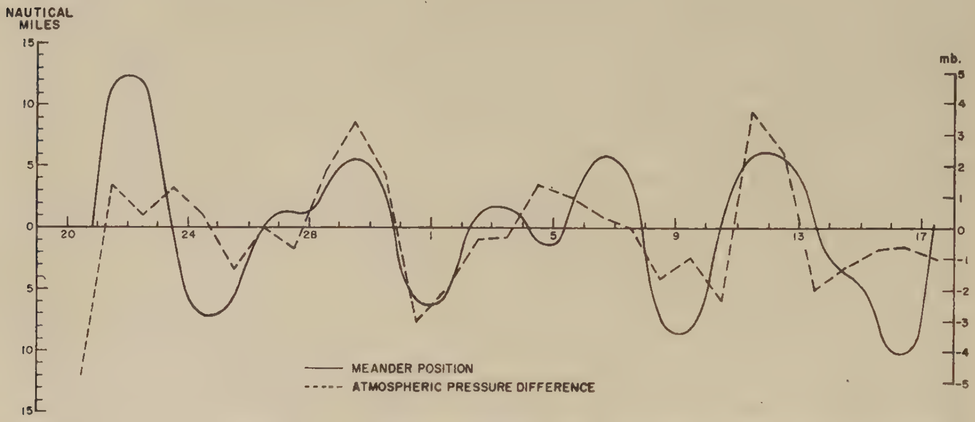

FIG. 9. Meander position, as a synthesis of the 4th, 5th and 7th harmonics of the Fourier analysis, and the Charleston-Hatteras atmospheric pressure difference, lagged four and one-half days.

The correlation between the two curves in FIG. 9 should not be interpreted as implying that the axis of the Gulf Stream is moved by the direct action of the wind. The kinetic energy contributed by the wind is several orders of magnitude less than is needed to sustain the meanders. An order of magnitude calculation shows that the energy added by the wind is two orders of magnitude less than the energy transferred from the meanders to the mean flow (WEBSTER, 1961). This energy transfer is probably an order of magnitude less than that needed to sustain the meanders.

Sea-level pressure differences between points across the axis of the current which would give an index of the intensity of the prevailing downstream winds showed no correlation with the stream meanders. The fact that the only correlation was found for the Hatteras-Charleston pressure suggests that the correlation might have been coincidental.

Characteristics of an average Gulf Stream

The Onslow Bay observations were further combined to portray an average cross-section of the surface layer temperature structure and the surface velocity profile for the period of the survey. The average downstream velocity profile ($\bar{v}$) and the average temperature structure are shown in FIG. 10. FIG. 11 shows, for comparison, a temperature cross-section and velocity profile for a single crossing of the current and might be considered to have some characteristic features common to all 120 crossings. Note that the characteristic instantaneous profile has much steeper temperature and velocity gradients. When time averages are taken of a shifting steep gradient, the gradient is blurred and tends to flatten out. This has been illustrated by FUGLISTER (1954) with respect to climatological temperature averages.

Any velocity, when measured with the GEK, is less than the actual surface water velocity by a factor which depends upon the depth of moving water in relation to the total depth of water. Because these depths cannot readily be measured, the factor is commonly determined empirically by calculating surface velocities from the discrepancies between LORAN and dead-reckoned positions. For the region of the Gulf Stream off Onslow Bay, it was found (von ARX, BUMPUS and RICHARDSON, 1955) that the GEK velocities should be multiplied by 1·46 ± 0·09 to correspond with the velocities as determined by dead-reckoning. All the GEK velocities obtained during *Crawford* Cruise 18 have been multiplied by this factor.

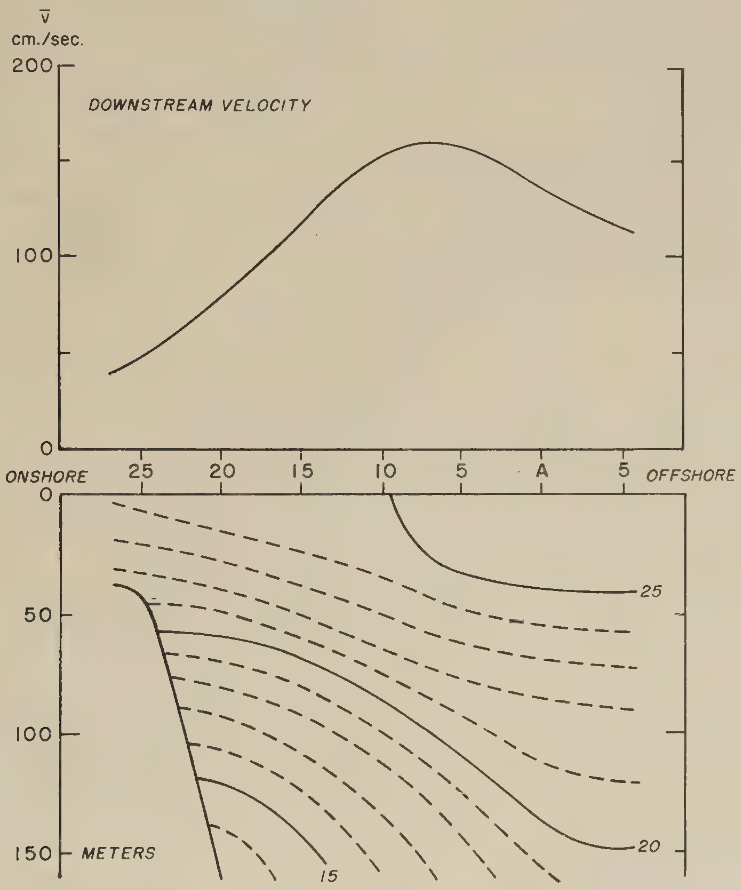

FIG. 10. Cross-section of average current during *Crawford* Cruise 18. Upper portion shows average downstream velocity, ($\bar{v}$). Lower portion shows average temperature section.

The cyclonic shear of the average velocity inshore of the velocity maximum is about 4·4 × 10^{-5} sec^{-1}, and the anti-cyclonic shear of the average velocity offshore is about 3·0 × 10^{-5} sec^{-1}. (For comparison, the Coriolis parameter at this latitude is 8 × 10^{-5} sec^{-1}). However, the cyclonic shear of the average velocity is much lower than the cyclonic shear of individual crossings. Von ARX (1951) gives individual values as high as 50 × 10^{-5} sec^{-1} for instantaneous cyclonic shears, and some instantaneous shears encountered on *Crawford* Cruise 18 were as large. The lower value results from the long-term averaging, so that the cyclonic shear of the average current for the month observed is less than the Coriolis parameter. To be realistic, a theory of the Gulf Stream should probably not imply a climatological average cylonic shear in excess of about 5 × 10^{-5} sec^{-1} in this region.

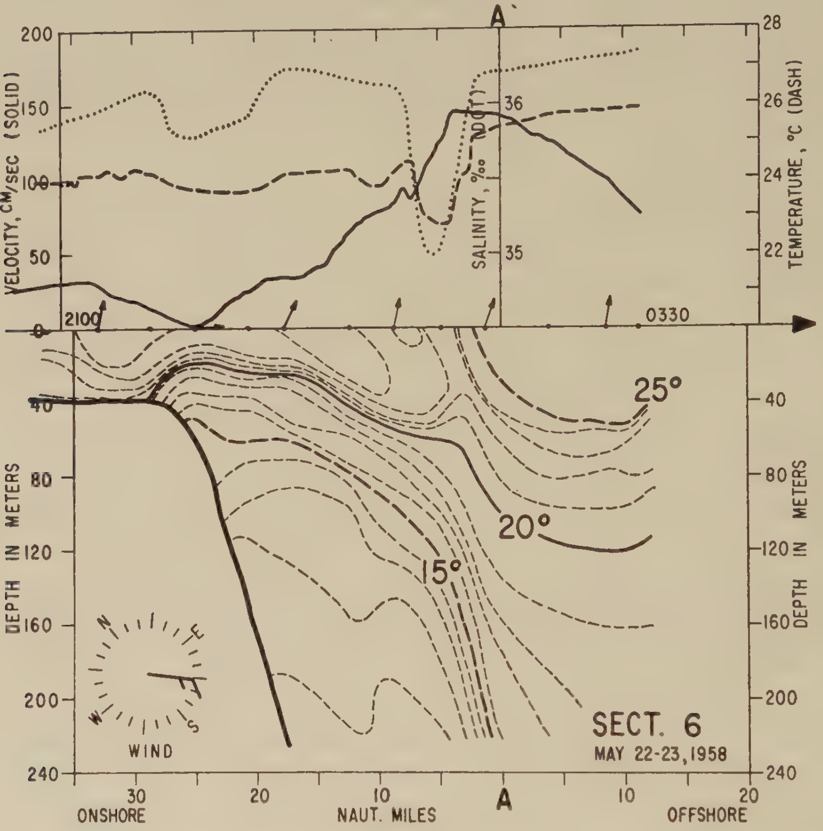

FIG. 11. Structure of a single crossing of the current. Lower part shows temperature structure and wind arrow. Above are : velocity (uncorrected GEK) cm/sec, solid line; Salinity, parts per thousand, dotted line; Temperature, degrees Centigrade, dashed line.

An idealized meander

The thermal structure of the upper 200 m layer may be determined from the BT data. In order to show this structure more clearly, an idealized diagram has been drawn, in space and time, which combines some features common to all the meanders. FIG. 12 is a diagram of the thermal structure of an idealized meander, in which the period of the meander was chosen to be seven days. Each of the meanders resembles a sort of skewed wave motion and consists of an intense offshore-running current (time 1 to 4 days), followed by a broad, confused flow onshore (time 4 to 7 days), then followed by another intense offshore current. The observations taken were not suitable to determine whether the cold subsurface water coinciding with the farthest offshore positions of the current maximum represents upwelling or not.

Comparisons with meanders farther downstream

The surface meander pattern in Onslow Bay as shown in the space-time diagrams has some similarity with the large-scale current pattern farther downstream. FUGLISTER (1951) presented an interpretation of the Gulf Stream beyond Cape Hatteras as a set of multiple currents. The meanders shown here are similar to the multiple currents because they appear to be more nearly a set of disconnected currents than a single current; each offshore-running current maximum seems to evolve anew rather than to be a continuation of a pre-existing current maximum. However, the space and time scales of the meanders off Onslow Bay are far different from those of the multiple currents beyond Cape Hatteras. There are only three or four currents comprising the multiple current system between Cape Hatteras and the Grand Banks. The length of each current is a thousand km or more, whereas the meanders off Onslow Bay probably have a length of the order of a hundred km. The multiple current pattern is either a permanent structural feature of the flow, or persists for a period of several months; the Onslow Bay meanders, on the other hand, pass by at a rate of one each week.

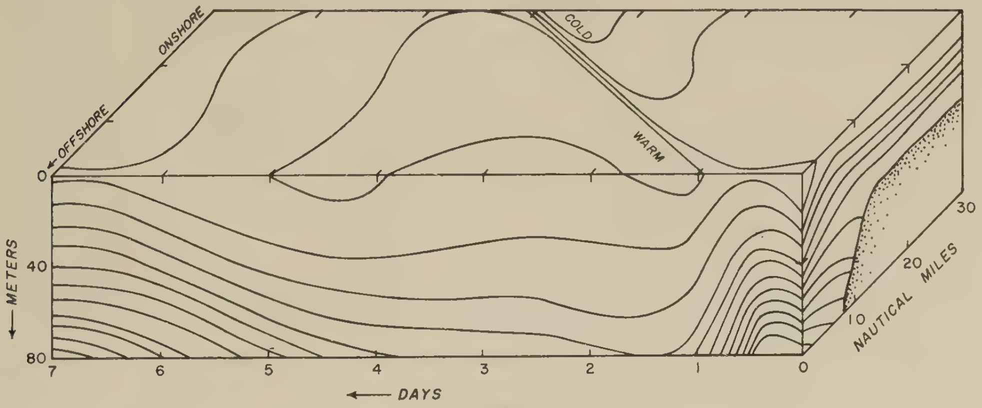

FIG. 12. Idealized meander structure.

Although there is uncertainty about the interpretation of the Gulf Stream currents between Cape Hatteras and the Grand Banks (FUGLISTER, 1955), it seems likely that currents in the region contain large-scale meanders (ISELIN and FUGLISTER, 1948; FORD and MILLER, 1952; FUGLISTER and WORTHINGTON, 1951). Such large-scale meanders are not an evolved form of the meanders observed off Onslow Bay. The meanders downstream from Cape Hatteras give the appearance of an amplifying disturbance (FUGLISTER and WORTHINGTON, 1951, FIG. 4). Were this assumption to be valid, the meanders excited upstream from Cape Hatteras and those which become amplified downstream would have similar periods. Since the time scale of the large-scale meanders appears to be at least an order of magnitude larger than the week-long periods observed off Onslow Bay, the meanders observed at Onslow Bay during the course of one month are probably not an incipient form of the larger meanders found farther downstream. If the large-scale meanders do have their origin upstream from Cape Hatteras, and have a period longer than a month, observations should be extended over several months to distinguish them.

Acknowledgments—The writer wishes to acknowledge the advice and encouragement of W. S. von Arx, who first suggested that this study be undertaken. Thanks are also due to B. A. Warren for helpful criticisms. The data used were collected under the direction of W. S. von Arx, with the assistance of D. F. Bumpus and C. G. Day. Much of the data reduction was performed by Mrs. N. Andersen. The work was made possible by funds supplied by the Office of Naval Research, under contract Nonr 2196 (00).

Woods Hole Oceanographic Institution,
Woods Hole, Mass.

REFERENCES

Bumpus, D. F. (1955) The circulation over the continental shelf south of Cape Hatteras. *Trans. Amer. Geophys. Un.* **36** (4), 601–611.

Bumpus, D. F. and Pierce, E. L. (1955) The hydrography and the distribution of chaetognaths over the continental shelf of North Carolina. *Pap. Mar. Biol. and Oceanogr., Suppl. Deep-Sea Res.*, **3**, 92–109.

Conrad, V. and Pollak, L. W. (1950) *Methods in Climatology*. 459 pp. Harvard University Press.

Day, C. G. (1959) Oceanographic observations, 1958 East Coast of the United States. *United States Fish and Wildlife Service, Special Sci. Rept.*, Fisheries No. 318, 119 pp.

Ford, W. L., Longard, J. R. and Banks, R. E. (1952) On the nature, occurrence and origin of cold low salinity water along the edge of the Gulf Stream. *J. Mar. Res.*, **11** (3), 281–293.

Ford, W. L. and Miller, A. R. (1952) The surface layer of the Gulf Stream and adjacent waters. *J. Mar. Res.*, **11**, (3), 267–280.

Fuglister, F. C. (1951) Multiple currents in the Gulf Stream System. *Tellus*, **3** (4), 230–233.

Fuglister, F. C. (1954) Average temperature and salinity at a depth of 200 meters in the North Atlantic. *Tellus*, **6** (1), 46–58.

Fuglister, F. C. (1955) Alternative analyses of current surveys. *Deep-Sea Res.*, **2** (3), 213–229.

Fuglister, F. C. and Worthington, L. V. (1951) Some results of a multiple ship survey of the Gulf Stream. *Tellus*, **3** (1), 1–14.

Hela, I. and Wagner, L. P. (1954) Note on tidal fluctuations in the Florida Current, in : *Marine Lab., Univ. of Miami, Tech. Rept.*, No. 54–7, 14–24.

Iselin, C. O'D. and Fuglister, F. C. (1948) Some recent developments in the study of the Gulf Stream. *J. Mar. Res.*, **7** (3), 317–329.

Schleicher, K. E. and Bradshaw, A. L. (1956) A conductivity bridge for measurement of the salinity of sea water. *J. du Cons.*, **22** (1), 9–20.

von Arx, W. S. (1950) An electromagnetic method for measuring the velocities of ocean currents from a ship under way. *Pap. Phys. Oceanogr. Meteor.*, **11** (3), 1–62.

von Arx, W. S. (1951) Some measurements of the surface velocities of the Gulf Stream. *Woods Hole Oceanogr. Inst., Tech. Rept.* Ref. No. 51–96 (unpublished manuscript).

von Arx, W. S., Bumpus, D. F. and Richardson, W. S. (1955) On the fine structure of the Gulf Stream front. *Deep-Sea Res.*, **3** (1), 46–65.

Webster, T. F. (1961) The effect of meanders on the kinetic energy balance of the Gulf Stream (to be published).

Printed in Great Britain by The Salisbury Press Ltd., Publicity House, Wilton Road, Salisbury, Wilts. (30315)

Contribution No. 1174

Särtryck ur Tellus nr 3, 1961

The Effect of Meanders on the Kinetic Energy Balance of the Gulf Stream

By FERRIS WEBSTER, Woods Hole Oceanographic Institution[1], Woods Hole, Massachusetts

(Manuscript received March 1, revised version June 28, 1961)

Abstract

Calculations have been made, using surface velocity observations, of the horizontal transfer of kinetic energy from meanders to mean flow at two separate localities in the Gulf Stream System. In both cases, it was found that there was a surface flow of kinetic energy from the meanders to the mean flow, exactly opposite to what would be expected if the meanders were frictionally driven. The observations suggest that the meanders derive energy from sources other than the kinetic energy of the mean flow. The role of the meanders in relation to the mean Gulf Stream appears analogous to that of large-scale eddies in relation to the general circulation of the atmosphere.

1. Introduction

Calculations have been made, for two separate regions, of the horizontal surface transfer of momentum by meanders in the Florida Current section of the Gulf Stream System. In both regions, it was found that the meanders transferred momentum against the velocity gradient, exactly opposite to what would be expected if they were frictionally driven. Or, in other words, there was at the surface, a net transfer of kinetic energy from the meanders to the mean flow.

Since no other such observations have been made of the transfer of kinetic energy in ocean currents, it has not been possible to determine the source of kinetic energy of meanders. It has been supposed by some (e.g.: ROSSBY, 1936, p. 6; STOMMEL, 1958, p. 107; VON ARX, 1954) that the meanders draw their energy from the kinetic energy of the mean flow and represent a mechanism for frictional dissipation of the mean flow. The observations here suggest that the opposite is true: that the mean flow is enhanced by the kinetic energy of meanders, and that the meanders should, therefore, derive their kinetic energy from sources other than the kinetic energy of the mean flow.

2. Observations

The data used to calculate eddy momentum fluxes were obtained from two separate sections across the axis of the Gulf Stream. One section is located off Onslow Bay, North Carolina, near Cape Hatteras, and the other is located in the Straits of Florida, running across the channel between Miami and Gun Cay, Bahamas. Figure 1 shows the location of these sections and their relation to the mean surface

---

[1] Contribution No. 1174 from the Woods Hole Oceanographic Institution.

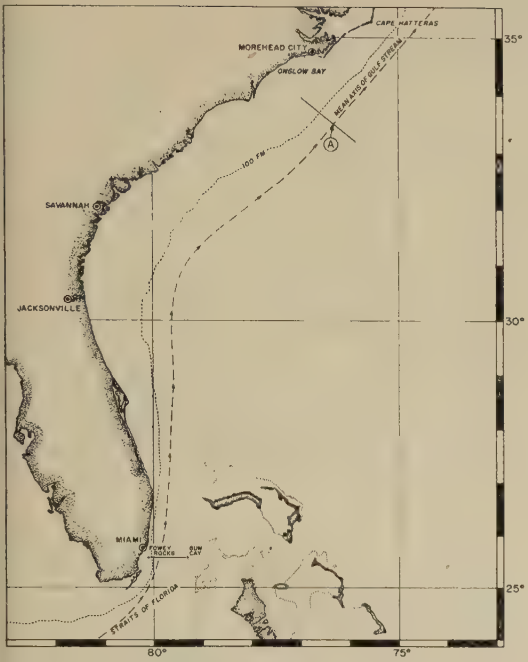

Fig. 1. Florida Current region.

axis of the Gulf Stream, as estimated by the United States Coast and Geodetic Survey.

GEK data. The necessary velocity measurements were made with the geomagnetic electrokinetograph (GEK), first described by VON ARX (1950). These measurements are usually less than the true surface velocity, depending mainly on the depth of moving water in relation to the total depth of water (LONGUET-HIGGINS, STERN, and STOMMEL, 1954). It is general practice to determine the reduction of GEK velocities for any region by calculating the average ratio between surface velocities measured by dead-reckoning methods and surface velocities measured with the GEK. This ratio (called "*k*") has been determined for the Onslow Bay area from several hundred measurements by VON ARX, BUMPUS, and RICHARDSON (1955), who found for *k*, 1.46 ± 0.09. In the Straits of Florida it has been calculated by HELA and WAGNER (1954) to be 1.68 ±0.30. That the Straits of Florida have a somewhat higher *k*-value than does Onslow Bay is a result of the shallower depth of water in the Straits. All GEK observations presented here have been corrected by the appropriate value of *k*.

Onslow Bay. The data off Onslow Bay were collected by W. S. von ARX, D. F. BUMPUS, and C. G. DAY on Cruise 18 of the research vessel CRAWFORD during May and June, 1958. The structure of the meanders observed during this period has been described by WEBSTER (1961). The CRAWFORD sailed back and forth along a single line at right angles to the mean axis of the Stream. An observation of the surface water velocity was made each hour by means of the GEK. During the twenty-eight days of the cruise, 620 separate measurements, or fixes, of the surface water velocity were made. Between fixes, the component of surface velocity at right angles to the course of the ship was recorded continuously. Since the ship's track was across the mean axis, this component was equivalent to the downstream surface velocity. For this portion of the Stream, "downstream" means in the direction 040°T.

The time-average downstream surface velocity ($\bar{v}$) profile determined from CRAWFORD Cruise 18 data has a cyclonic shear of approximately 4.4×10^{-5} sec^{-1}, and an anticylonic shear of approximately 3.0×10^{-5} sec^{-1}. The Coriolis parameter at this latitude has a value of 8.0×10^{-5} sec^{-1}. Because the averages of the cross-stream surface velocity ($\bar{u}$) are generally less than their standard deviations, the averages are not significantly non-zero. If there are mean cross-stream motions, they are less than 4 cm/sec.

Florida Straits. Between 1952 and 1958, the Marine Laboratory of the University of Miami was engaged in part of a long-term program to determine the characteristics of the Florida. Current as it flows through the channel between Fowey Rocks, Florida (near Miami), and Gun Cay, Bahamas. The channel at this point is about 43 nautical miles (80 kilometers) wide. A total of 632 GEK observations of velocity in the surface layer from 42 of the cruises made by the Marine Laboratory were available for analysis (University of Miami, 1954, 1955, 1957, 1958).

The region surveyed by the University of Miami was divided into longitudinal zones. Only the observations made between latitudes 25°30′N and 25°59′N were used in calculating the averages for each zone. The zones and the region are shown in Figure 2. The limits of the zones are as follows:

Zone	From	To	Width
1	80°05′.5 W	80°01′.5 W	4′.0
2	01′.4	79°58′.5	3′.0
3	79°58′.4	55′.5	3′.0
4	55′.4	52′.5	3′.0
5	52′.4	49′.5	3′.0
6	49′.4	44′.5	5′.0
7	44′.4	39′.5	5′.0
8	39′.4	34′.5	5′.0
9	34′.4	29′.5	5′.0
10	29′.4	24′.5	5′.0
11	24′.4	19′.5	5′.0

The western boundary of the channel, Fowey Rocks, is at 80°06′.5 W, and the eastern boundary, Gun Cay, is at 79°18′.5 W, so that the zones chosen cover nearly the entire channel, and include all the observations available. In the Straits of Florida region, one minute of longitude is equal to 0.911 nautical miles (1.69 km). Therefore the width of the widest zones is 4.55 nautical miles (8.45 km).

The averages of the northward component of surface velocity (v) and the eastward component (u) were calculated for each zone using all the GEK observations lying in that zone. These averages are tabulated in Table II, and plotted in Figure 3.

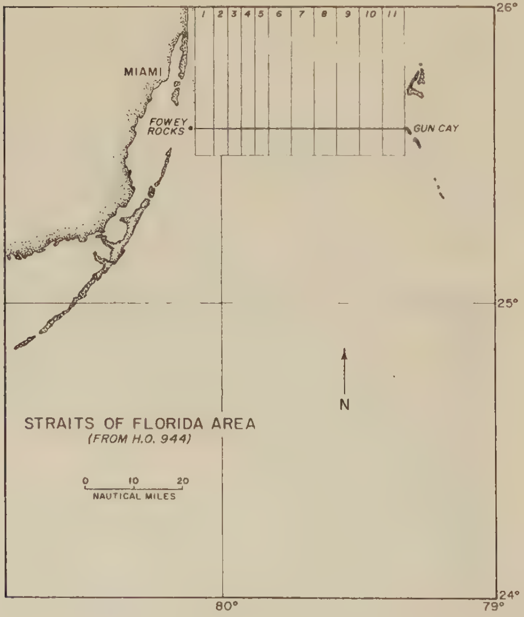

Fig. 2. Straits of Florida area, showing zones used to separate observations.

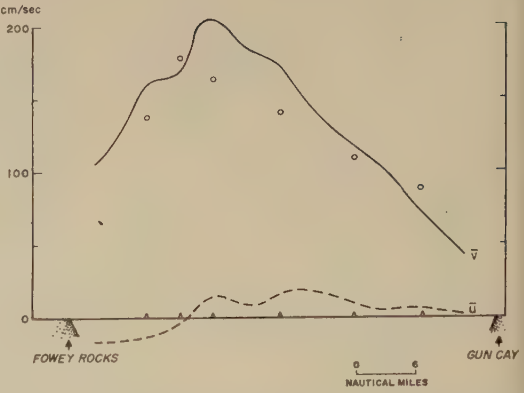

Fig. 3. Average velocity profile, Straits of Florida. Solid line is average downstream (north) velocity, dotted line is average cross-stream (east) velocity, and circles are velocity averages determined by Pillsbury.

The mean downstream velocity profile is asymmetrical, with a cyclonic shear region about 15 nautical miles (28 km) wide having a shear of approximately 3×10^{-5} sec^{-1}. The anticyclonic shear region is about 32 nautical miles (59 km) wide and has a shear of approximately 2×10^{-5} sec^{-1}. For comparison, the value of the Coriolis parameter at this latitude is 6.9×10^{-5} sec^{-1}. The cyclonic shear of the average stream is significantly less than that of the instantaneous stream, because variations in position of the latter produce a wide distribution of average velocity, and hence a profile more gentle than that which would be found on any particular crossing.

3. Energy Calculations

The transfer of kinetic energy from the eddies to the mean flow can be expressed as

$$\varrho\overline{u'v'}\frac{\partial \bar{v}}{\partial x} \qquad (1)$$

where a bar represents a time average of a quantity, a prime represents a deviation from the time average, u and v are the velocity components in the cross-stream (x) and downstream (y) direction, and ϱ is the density of the water. This method for treating perturbations of a mean flow was first developed by O. REYNOLDS (1895), and is outlined by LAMB (1932).

Table 1

Onslow Bay $k = 1.46$

Zone	$\bar{u}$ cm/sec		$\bar{v}$ cm/sec		$\overline{u'v'}$ cm²/sec²		$\frac{\partial \bar{v}}{\partial x}$ × 10⁻⁵sec⁻¹	$\varrho \overline{u'v'} \frac{\partial \bar{v}}{\partial x}$ 10⁻² ergs/cm³/sec	
6	+ 5.4	± 6.3	39.6	± 7.9	+ 210.2	± 279	2.13	+ 0.45	± 0.6
7	+ 2.6	± 7.2	53.6	± 13.0	— 72.1	± 503	2.68	— 0.19	± 1.3
8	+ 10.4	± 5.5	70.2	± 12.7	+ 236.3	± 341	4.35	+ 1.03	± 1.5
9	+ 6.9	± 6.6	95.9	± 9.1	+ 482.0	± 481	4.35	+ 2.10	± 2.1
10	— 4.8	± 8.0	118.1	± 8.8	+ 640.6	± 558	4.35	+ 2.79	± 2.4
11	+ 8.0	± 9.8	143.5	± 7.4	+ 648.8	± 364	3.84	+ 2.49	± 1.4
12	— 11.2	± 10.1	156.8	± 6.1	+ 335.6	± 409	0.71	+ 0.24	± 0.3
13	+ 2.2	± 6.0	157.2	± 6.4	+ 268.5	± 271	— 0.36	— 0.10	± 0.1
14	— 12.8	± 7.2	153.4	± 7.9	— 74.3	± 349	— 1.10	+ 0.08	± 0.4
15	+ 6.9	± 5.8	139.3	± 8.9	— 169.4	± 279	— 3.00	+ 0.51	± 0.8
16	— 3.8	± 5.4	126.0	± 8.3	— 61.9	± 253	— 2.21	+ 0.14	± 0.6
17	— 11.7	± 6.9	114.9	± 11.1	+ 72.4	± 349	— 2.85	— 0.21	± 1.0

Average Energy Flux: 79×10^{-4} ergs/cm³/sec.

Onslow Bay. For the Onslow Bay region, the data were divided into twelve zones across the current, each zone being 3 nautical miles wide. The eddy momentum transfer, $\overline{u'v'}$ was calculated by applying Simpson's rule to the value of $u'v'$, over the total time of observation, for each of the twelve zones. The value of $\frac{\partial \bar{v}}{\partial x}$ was calculated for each zone from the profile of average velocity ($\bar{v}$). Table 1 shows for each zone: $\overline{u'v'}$ the average transport of eddy momentum; $\frac{\partial \bar{v}}{\partial x}$ the shear of the average velocity; and the term (1) representing the production of mean kinetic energy by meanders. (ϱ was assumed constant, and equal to one gram per cubic centimeter.)

Figure 4 shows the distribution of (1) across the width of the current off Onslow Bay. The cross-stream integral of (1) is positive, indicating a net transfer of kinetic energy from the meanders to the mean current.

Florida Straits. The averages for the Florida Straits section were calculated by taking ensemble averages in each of the zones. That is, a barred quantity was evaluated as:

$$\overline{(\quad)} = \frac{1}{N} \sum_{i=1}^{N} (\quad)_i$$

where N is the total number of observations in the zone. The results of the calculations are tabulated in Table 2, and the profile of the term (1) across the current is shown in Figure 5. In this region, although there are points in the current where (1) is positive, the net production of mean kinetic energy across the whole stream is not significantly non-zero.

Statistical significance of results. The standard error of the means, $\bar{u}$, $\bar{v}$, and $\overline{u'v'}$ are given for each value in Tables 1 and 2. The standard error of a mean is defined, for large N, as $\sigma/\sqrt{N}$, where σ is the standard deviation of the sample from which the mean is calculated, and N is the number of individual observations.

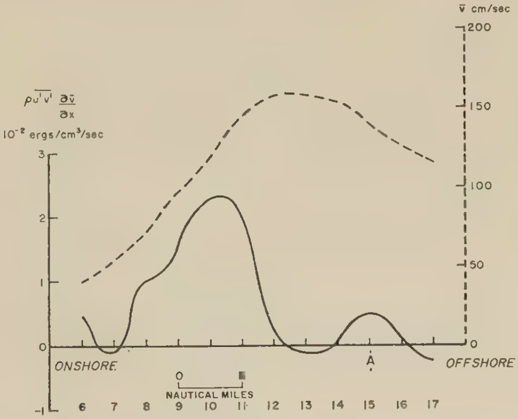

Fig. 4. Onslow Bay. Solid line: production of mean kinetic energy. Dotted line: mean downstream velocity.

Table 2

Florida Straits							$k = 1.68$			
Zone	$\bar{u}$ cm/sec		$\bar{v}$ cm/sec		$\overline{u'v'}$ cm²/sec²		$\frac{\partial \bar{v}}{\partial x}$ $\times 10^{-5}$ sec^{-1}	$\varrho \overline{u'v'} \frac{\partial \bar{v}}{\partial x}$ 10^{-2}ergs/cm³/sec	
1	—18.1	±3.5	103.1	±8.9	—411.7	±184	+4.27	—1.76	±0.78
2	—17.6	±6.4	129.9	±10.4	+259.0	±371	+5.68	+1.47	±2.11
3	—11.2	±5.7	160.7	±12.3	+270.0	±392	+3.60	+0.97	±1.41
4	—6.4	±4.5	164.8	±5.8	+975.4	±277	+4.27	+4.16	±1.18
5	+11.0	±6.7	202.8	±9.2	+357.0	±498	+1.97	+0.70	±0.98
6	+9.9	±4.2	188.0	±4.5	+333.2	±322	—2.35	—0.78	±0.76
7	+16.5	±5.7	167.0	±7.4	+15.2	±361	—3.34	—0.05	±1.21
8	+14.4	±4.2	131.4	±5.5	—13.2	±217	—3.55	+0.05	±0.77
9	+5.1	±4.4	107.2	±6.6	+140.6	±171	—3.43	—0.48	±0.59
10	+5.8	±4.5	73.5	±6.9	+122.7	±123	—3.75	—0.46	±0.46
11	+2.1	±4.4	43.9	±7.4	+281.2	±102	—3.49	—0.98	±0.36

Average Energy Flux: 3.0×10^{-4} ergs/cm³/sec.

4. Discussion of results

Scale of perturbations. The conclusions which can be derived directly from the evaluation of (1) across the Florida Current apply only to the surface layer of moving fluid, and only to the time scale of perturbations which the u' and v' characterize. That is, the results obtained say nothing directly about the energy balance below the surface nor about the eddy motions of other time scales.

PILLSBURY (1891) made a detailed study of the Florida Current at six anchor stations between Fowey Rocks and Gun Cay. His average surface velocities are plotted as circles in Figure 3 where they can be compared with the averages from the University of Miami GEK measurements. His observations show that the subsurface velocities are not greatly less than those at the surface, and suggest a qualitative similarity between surface and subsurface velocity fields. If so, then the energy transfer between eddies and mean flow calculated for the surface layers from GEK data may be representative of most of the current depth in the Florida Straits.

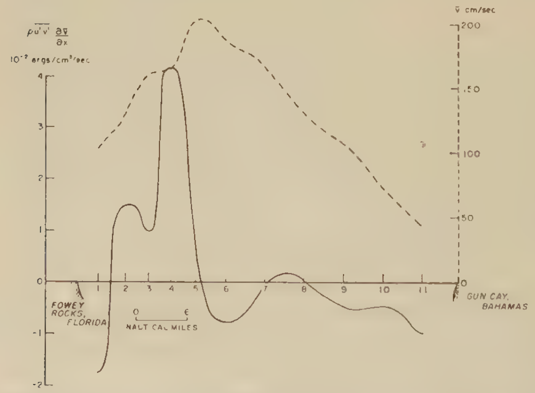

Fig. 5. Florida Straits. Solid line: production of mean kinetic energy. Dotted line: mean downstream velocity.

PILLSBURY also made a study of the time variations of current position, velocity, and width in the Florida Straits, and found monthly variations related to the declination of the moon, as well as daily, tidally-influenced oscillations. He concluded that the tidal components of the variations were significantly larger than those which could be attributed to non-tidal causes.

PARR (1937) analyzed a set of five anchor stations which were successively occupied for 24-hour periods in the Straits of Florida between Fowey Rocks and Gun Cay. He found that lunar periodicities were strongly indicated in the data, and he even combined data from station to station, by referring them to corresponding lunar hours.

More recently, MURRAY (1952) analyzed velocity fluctuations in the same region. These fluctuations, as determined with the GEK, had periods between a few hours and a day. Murray was unable to confirm Pillsbury's conclusion that there was a relationship between the transport and the declination of the moon, and found only inconclusive evidence of lunar effects. A further analysis of additional GEK data by Hela and Wagner (1954) indicated that some tidal variations in velocity did exist, but that they were strongly masked by non-tidal effects. Wertheim (1954) from electromagnetic measurements of total transport, found conclusive evidence of diurnal tidal influence in the transport through the Florida Straits.

In conclusion, although it is probably rash to ascribe the velocity fluctuations of the current through the Straits of Florida predominantly to tidal causes, the periods of the fluctuations are of the order of a day, and the deviations from the mean which are used here to calculate the eddy transport of momentum most likely are representative of meandering motion.

In Onslow Bay, the data were taken continously for a month, in contrast to the Florida Straits, where the data were obtained at intervals over the course of several years. The eddy momentum transfer calculated from the perturbations has periods ranging between a few hours and a week; that is the range of meander periods which were observed (Webster, 1961). Unfortunately, no systematic velocity measurements at depth, similar to those of Pillsbury in the Florida Straits, have ever been made in the Onslow Bay region.

We may conclude that both in the Florida Straits and in Onslow Bay, the calculated lateral surface transfer of momentum is produced by perturbations having periods of a day or longer. No observations have been made of perturbations of other time scales, in particular of small-scale perturbations, having periods which are small compared with the length of a day. Consequently, there is no evidence to suggest that small-scale perturbations would transport momentum in a manner similar to the meanders.

Regeneration Time. The magnitude and the lateral scale of the eddy kinetic energy release off Onslow Bay are similar to those in the Florida Straits. This apparent similarity between the two profiles suggests that there might be a characteristic scale of energy release throughout the whole region between the Straits of Florida and Cape Hatteras. However, a calculation of the time scales of the energy transfer reveals that the kinetic energy plays a different role in the mean kinetic energy balance in each region.

If the curves are integrated over their lengths, the average rate of surface transfer of energy from the meanders to mean flow is 79×10^{-4} ergs/cm^3/sec for Onslow Bay and 3.0×10^{-4} ergs/cm^3/sec for the Florida Straits. If the kinetic energy of the mean surface flow is averaged by integrating across the stream, the result is 7.3×10^3 ergs/cm^3 for Onslow Bay and 8.55×10^3 for the Florida Starits. If no other actions were present, the calculated rate of energy transfer would double the mean surface kinetic energy in 11 days in Onslow Bay and in 329 days in the Florida Straits.

The difference between the regeneration time of the surface kinetic energy in Onslow Bay and that in the Florida Straits may perhaps be explained partly by the confining channel of the latter. Near each shore there is a region where the meanders draw energy from the mean flow. This boundary layer effect is not so noticeable in the Onslow Bay region where the current is not closely confined by physical barriers.

In addition, the current through the Florida Straits may be more directly driven by a downstream pressure gradient. If so, then the meanders would contribute less to the mean flow than they do farther downstream where, possibly, the current is maintained by the cross-stream density field through the mechanism of meanders. At present, the measurements necessary to evaluate the role of downstream pressure gradients are not available.

Atmospheric Similarities. There is a similarity between the role of meanders in the Gulf Stream and the role of large-scale eddies in the atmosphere. Figure 6, adapted from Starr (1953) shows the production of zonal kinetic energy in arbitrary units, and the relative angular velocity as a function of latitude. When Figure 6 is compared with Figures 4 and 5, it can be seen that, for both systems, the maximum countergradient flow of momentum occurs in the region of maximum shear.

Several years' study of atmospheric transfer processes have established that the mean zonal flow is sustained by large-scale disturbances (Starr, 1953), and that the necessary meridional transports of momentum are effected by

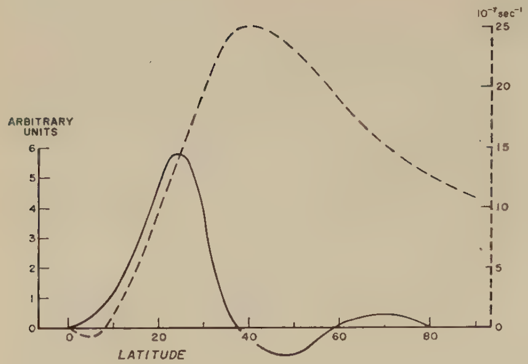

Fig. 6. Solid line: production of zonal kinetic energy, atmosphere. Dotted line: relative angular velocity. (from Starr, 1953, Figure 1.)

horizontal eddy exchange processes (Starr, 1954). The question of whether mean current systems in the ocean are maintained in an analogous manner cannot be answered until further observations are made.

Frictional models of the Gulf Stream (Stommel, 1948; Munk, 1950) require some sort of eddy dissipation which could conceivably be supplied by perturbations of meander scale. A coefficient of lateral eddy viscosity, or Austausch coefficient, may be defined on the assumption that the perturbations of the mean flow are analogous to an eddy frictional mechanism. However, the perturbations of the Gulf Stream flow, observed here, act exactly opposite to frictional effects, so that a viscosity coefficient calculated using them would be negative, and have questionable physical significance. It is possible that the necessary frictional dissipation is carried out by perturbations of a scale smaller than the meanders. If so, then the energy balance is analogous to that in the atmosphere, where the mean zonal flow is sustained by large-scale eddies, but dissipated by small-scale eddies and molecular viscosity.

5. Kinetic Energy Equation for the Mean Flow

The equation expressing the flux of energy in a turbulent flow was originally developed by O. Reynolds for a parallel non-rotating dissipative flow (Lamb, 1932). The corresponding general equation for the atmosphere has been given by Kuo (1951). The equations for ocean current systems are similar to those for the atmosphere because the coordinate frame for both systems is rotating, but dissimilar because the atmosphere is cyclic and centered about the axis of rotation, whereas ocean currents are a more local phenomenon. The action of winds upon the surface of the ocean is a mechanism whose atmospheric analogue is negligible.

The following model is a simple version of the Reynolds model, intended to provide an orientation. Better models may follow later.

Let us consider an ocean current, with a mean flow in the y-direction, having velocity components u, v, and w in the x, y, and z directions, x being directed to the right of y, and z being directed downward.

The momentum equations are

$$\varrho \frac{\partial u}{\partial t} + \varrho \mathbf{v} \cdot \nabla u = \varrho f v - \frac{\partial p}{\partial x} - X \qquad (1)$$

$$\varrho \frac{\partial v}{\partial t} + \varrho \mathbf{v} \cdot \nabla v = -\varrho f u - \frac{\partial p}{\partial y} - Y \qquad (2)$$

where ϱ is the density of the water, f is the Coriolis parameter, p is the pressure, and X and Y are components of a dissipative force. $\mathbf{v}$ is the three-dimensional velocity vector, $\mathbf{u}\mathbf{i} + \mathbf{v}\mathbf{j} + w\,\mathbf{k}$, and ∇ is the three-dimensional vector operator, $\mathbf{i}\frac{\partial}{\partial x} + \mathbf{j}\frac{\partial}{\partial y} + \mathbf{k}\frac{\partial}{\partial z}$. We shall omit explicit reference to the wind stress on the surface. With the aid of the continuity equation, $\frac{\partial \varrho}{\partial t} + \nabla \cdot \varrho \mathbf{v} = 0$, we may write (1) and (2) as:

$$\frac{\partial \varrho u}{\partial t} + \nabla \cdot \varrho u \mathbf{v} = \varrho f v - \frac{\partial p}{\partial x} - X \qquad (3)$$

$$\frac{\partial \varrho v}{\partial t} + \nabla \cdot \varrho v \mathbf{v} = -\varrho f u - \frac{\partial p}{\partial y} - Y \qquad (4)$$

The quantities u, v, and w can be separated into mean motion and deviations as:

$$u = \bar{u} + u'$$
$$v = \bar{v} + v'$$
$$w = \bar{w} = w'$$

where

$$\overline{(\ )} = \frac{1}{T}\int_{-\frac{T}{2}}^{\frac{T}{2}} (\ )\,dt.$$

The primes denote deviations from the time average. Terms of the form $\overline{u\,v}$ become $\bar u\,\bar v + \overline{u'\,v'}$.

Let us now multiply (3) by $\bar u$ and (4) by $\bar v$, and take time averages:

$$\bar u\frac{\partial}{\partial t}\varrho\bar u + \bar u\nabla\cdot\varrho\bar u\,\bar{\mathbf{v}} + \bar u\nabla\cdot\varrho\overline{u'\mathbf{v}'} =$$

$$= \varrho f\bar u\,\bar v - \bar u\frac{\partial\bar p}{\partial x} - \bar u\,\bar X \qquad (5)$$

$$\bar v\frac{\partial}{\partial t}\varrho\bar v + \bar v\nabla\cdot\varrho\bar v\,\bar{\mathbf{v}} + \bar v\nabla\cdot\varrho\overline{v'\mathbf{v}'} =$$

$$= -\varrho f\bar u\,\bar v - \bar v\frac{\partial\bar p}{\partial y} - \bar v\,\bar Y \qquad (6)$$

Equations (5) and (6) may be added, and with the aid of the continuity equation, written:

$$\varrho\frac{\partial}{\partial t}\bar k = -\mathbf{v}\cdot\nabla\bar k - \bar u\nabla\cdot\varrho\overline{u'\mathbf{v}'} - \bar v\nabla\cdot\varrho\overline{v'\mathbf{v}'}$$

$$-\bar u\frac{\partial p}{\partial x} - \bar v\frac{\partial p}{\partial y} - d \qquad (7)$$

where d is the dissipative force, $\bar u\,\bar X + \bar v\,\bar Y$, and $\bar k = \frac{\bar u^2 + \bar v^2}{2}$ is the total kinetic energy of the horizontal mean current. By definition, $\frac{\partial}{\partial t}\bar k = 0$.

If (7) is integrated over a cross-section of the current in the x-z plane, the result gives the balance of horizontal kinetic energy of the mean flow in a unit cross-section of the current:

①

$$0 = -\iint \mathbf{v}\cdot\nabla\bar k\,dx\,dz$$

②

$$-\iint \bar u\nabla\cdot\varrho\overline{u'\mathbf{v}'}\,dx\,dz$$

③

$$-\iint \bar v\nabla\cdot\varrho\overline{v'\mathbf{v}'}\,dx\,dz$$

④

$$-\iint\left(\bar u\frac{\partial\bar p}{\partial x} + \bar v\frac{\partial\bar p}{\partial y}\right)dx\,dz$$

⑤

$$-\iint d\,dx\,dz \qquad (8)$$

With the limited amount of information available now, it is not possible to evaluate each term in equation (8) for the Gulf Stream. However, an estimate of the role of some of the terms can be made.

First, consider terms ② and ③:

$$\bar u\nabla\cdot\varrho\overline{u'\mathbf{v}'} + \bar v\nabla\cdot\varrho\overline{v'\mathbf{v}'} = \bar u\frac{\partial}{\partial x}\varrho\overline{u'u'} + \bar u\frac{\partial}{\partial y}\varrho\overline{u'v'}$$

$$+\bar v\frac{\partial}{\partial x}\varrho\overline{u'v'} + \bar v\frac{\partial}{\partial y}\varrho\overline{v'v'}$$

$$+\bar u\frac{\partial}{\partial z}\varrho\overline{u'w'} + \bar v\frac{\partial}{\partial z}\varrho\overline{v'w'}$$

The axes were chosen so that the mean current is in the y-direction, so that $\bar v \gg \bar u$. In addition, the perturbations travel in the y-direction, so that for the time averaged velocity perturbation terms, $\frac{\partial}{\partial y} \approx 0$. Hence, terms ② and ③ become:

$$u\nabla\cdot\varrho\overline{u'\mathbf{v}'} + \bar v\nabla\cdot\varrho\overline{v'\mathbf{v}'} \simeq \bar u\frac{\partial}{\partial x}\varrho\overline{u'u'} + \bar v\frac{\partial}{\partial z}\varrho\overline{u'v'}$$

$$+\bar u\frac{\partial}{\partial z}\varrho\overline{u'w'} + \bar v\frac{\partial}{\partial z}\varrho\overline{v'w'}$$

The terms in $\overline{u'w'}$ and $\overline{v'w'}$ represent contributions of kinetic energy to the mean flow by vertical perturbations. Since observations of vertical motions are not available, this term has not been calculated. It might represent an important contribution to the mean down stream kinetic energy.

The term $v\frac{\partial}{\partial x}\varrho\overline{u'v'}$ includes the expression used in the surface calculation of this study. It may be re-written as

$$\overset{(a)}{\frac{\partial}{\partial x}(\varrho\bar v\cdot\overline{u'v'})} \quad \overset{(b)}{-\varrho\overline{u'v'}\frac{\partial\bar v}{\partial x}}$$

The term $\frac{\partial}{\partial x}\ (\varrho\bar{v}\cdot\overline{v'u'})$ represents an eddy advection across the boundaries of mean kinetic energy and can be integrated easily across a stream to become:

$$[\varrho\bar{v}\ \overline{v'u'}]_A - [\varrho\bar{v}\ \overline{v'u'}]_B$$

If the stream is bounded by walls, u' will be zero at the walls, or if the mean stream velocity drops to zero at each side of the current, $\bar{v}$ will be zero, and the term (a) is zero. Off Onslow Bay, where the current is not bounded by walls, and the observations did not cover the whole width of the current, calculation of the term (a) has revealed that its integral across the width of observations is zero. Hence the cross-stream integral of the term:

$$\varrho\overline{u'v'}\ \frac{\partial v}{\partial x} \qquad (1)$$

is a measure of the increase of mean kinetic energy at the expense of kinetic energy of horizontal eddy motion.

Maximum values of $\frac{\partial}{\partial x}\ \varrho\overline{u'u'}$ at the surface were observed to be almost as large as average values of $\frac{\partial}{\partial x}\ \varrho\overline{u'v'}$. However, since $v \gg u$, the term $u\ \frac{\partial}{\partial x}\ \varrho\overline{u'u'}$ is negligible in comparison with $\bar{v}\ \frac{\partial}{\partial x}\ \varrho\overline{u'v'}$.

Term ① represents the advection across the boundaries of the region under consideration of mean horizontal kinetic energy. Equation (8) states that this boundary advection ① must be balanced by the generation of mean kinetic energy by meanders, ② and ③, pressure forces, ④, and by the frictional dissipation, ⑤.

Proper measurements do not exist which will permit a calculation of the contribution of the pressure forces, ④, to the mean kinetic energy balance. Indications are that the downstream pressure gradient is important in the Florida Straits, but little is known about it in Onslow Bay. More reliable measurements are needed in both areas.

The frictional dissipation term, ⑤, was included in the equation to represent the general action of frictional stresses. Included in the term is the effect of wind stress at the surface. An order of magnitude calculation shows that the energy provided by the wind stress is one or two orders of magnitude less than the transfer of kinetic energy from the meanders to the mean flow. That is, if we assume a maximum wind stress of half a dyne/cm^2, a maximum velocity of 50 cm/sec, and a current depth of 500 meters, the energy transfer will be 5×10^{-4} ergs/cm^3/sec, for total correlation between winds and currents. Assuming only partial correlation, or more characteristic values of wind stress and meander velocity, the energy contributed to the meanders by the wind is about 1×10^{-4} ergs/cm^3/sec. In comparison with the transfer of energy between meanders and mean flow of 80×10^{-4} ergs/cm^3 sec, the wind would appear to be eliminated as a significant source of kinetic energy for the meanders.

6. Concluding Remarks

The similarity between these results and those in the atmosphere provides hope that a general study of the energy, momentum, and heat transfers in ocean currents would be as fruitful as such studies in the atmosphere have been. Perhaps, to some extent, meanders are to an ocean current what cyclones are to atmospheric circulation: a mechanism which sustains the mean flow and which provides transfers necessary for climatological balances.

A further program of systematic measurements in the Gulf Stream System is necessary to illuminate the large scale balances. Downstream from Cape Hatteras, especially, the tortuous course of the Gulf Stream has only recently been discovered, and the processes determining its nature are unknown. An extensive observation program might be undertaken initially with GEK surface velocity measurements. Hydrographic station data probably would not be suitable for velocity measurements because non-geostrophic and/or non-baroclinic velocity components might be an important constituent of the transfer process. A system which at present seems promising, and which ultimately might provide the vast amount of data necessary for an oceanic study comparable to that in the atmosphere, is that of anchored buoys, which record data at predetermined time intervals. Such a system could be scattered throughout the ocean, and could record data at any depth.

Acknowledgements

The writer is indebted to Dr. Kirk Bryan, Jr. for suggesting this study. Thanks are also due to Prof. V. P. Starr for encouragement and helpful suggestions, and to Bruce Warren and Prof. William von Arx for helpful criticisms.

REFERENCES

HELA, I., and WAGNER, L. P., 1954: *Note on tidal fluctuations in the Florida Current*, in Marine Lab., Univ. of Miami, Tech. Rept., No. 54—7, pp. 14—24.

KUO, H. L., 1951: A note on the kinetic energy balance of the zonal wind systems. *Tellus*, **3**, pp. 205—207.

LAMB, Sir H., 1932: *Hydrodynamics*, 6th ed., Cambridge, England, Cambridge University Press, 738 pp.

LONGUET-HIGGINS, M. S., STERN, M. E., and STOMMEL, H. M., 1954: The electrical field induced by ocean currents and waves, with applications to the method of towed electrodes. *Papers in Physical Oceanography and Meteorology*, **13**: 1, pp. 1—37.

MUNK, W. H., 1950: On the wind-driven ocean circulation. *Jour. Meteor.*, **7**, pp. 79—93.

MURRAY, K. M., 1952: Short period fluctuation of the Florida Current from geomagnetic electrokinetograph observations. *Bull. Mar. Sci., Gulf and Caribbean*, **2**, pp. 360—375.

PARR, A. E., 1937: Report of hydrographic observations at a series of anchor stations across the Straits of Florida *Bull. Bingham Oceanogr. Coll.*, **6**, pp. 1—62.

PILLSBURY, J. E., 1891: The Gulf Stream, a description of the methods employed in the investigation and the results of the research. *Rept. Supt., U. S. Coast and Geodetic Survey*, **1890**, App. 10.

REYNOLDS, O., 1895: On the dynamical theory of incompressible viscous fluids and the determination of the criterion. *Phil. Trans. Roy. Soc. London, A*, **186**, pp. 123—164.

ROSSBY, C.—G., 1936: Dynamics of steady ocean currents in the light of experimental fluids mechanics. *Papers in Physical Oceanography and Meteorology*, **5**:1, pp. 1—43.

STARR, V. P., 1953: Note concerning the nature of the large-scale eddies in the atmosphere. *Tellus*, **5**, pp. 494—498.

STARR, V. P., 1954: Commentaries concerning research on the general circulation. *Tellus*, **6**, pp. 268—272.

STARR, V. P., WHITE, R. M., 1951: A hemispherical study of the atmospheric angular momentum balance *Quart. J. Roy. Meteor. Soc.*, **77**, pp. 215—225.

STOMMEL, H. M., 1948: The westward intensification of wind-driven ocean currents. *Trans. Amer. Geophys. Union*, **29**, pp. 202—206.

STOMMEL, H. M., 1958: *The Gulf Stream*. Berkeley, U.S.A., Univ. of California Press, 202 pp.

UNIVERSITY OF MIAMI, MARINE LAB., 1954: *Some results of the Florida Current Study*, 1953. Technical Report No. 54—7, 100 pp.

UNIVERSITY OF MIAMI, MARINE LAB., 1955: *Some results of the oceanographic studies in the Straits of Florida and adjacent waters*. Technical Report, No. 55—1, 74+ pp.

UNIVERSITY OF MIAMI, MARINE LAB., 1957: *Tropical oceanography*, semi-annual report, March, 1957. Technical Report No. 57—9, 128 pp.

UNIVERSITY OF MIAMI, MARINE LAB., 1958: *A technical report of investigations for the period of June 25, 1956 to May 7, 1957*. Technical Report, No. 58—3, 55 pp.

VON ARX, W. S., 1950: An electromagnetic method for measuring the velocities of ocean currents from a ship under way. *Papers in Physical Oceanography and Meteorology*, **11**:3, pp. 1—62.

VON ARX, W. S., 1954: Measurements of the oceanic circulation in temperate and tropical latitudes. *Oceanographic Instrumentation, Nat. Res. Counc.* (U.S.) Publ., No. **309**, pp. 13—35.

VON ARX, W. S., BUMPUS, D. F., and RICHARDSON, W. S., 1955: On the fine structure of the Gulf Stream front. *Deep Sea Res.*, **3**, pp. 46—65.

WERTHEIM, G. K., 1954: Studies of the electric potential between Key West, Florida and Havana, Cuba. *Trans. Amer. Geophys. Union*, **35**, pp. 872—882.

WEBSTER, T. F., 1961: A description of Gulf Stream meanders off Onslow Bay. *Deep-Sea Res.* (in press).

PRINTED IN SWEDEN
ESSELTE. STHLM 61

Contribution No. 1176

Reprinted for private circulation from
PHYSIOLOGICAL ZOÖLOGY
Vol. XXXIV, No. 4, October 1961
Copyright 1961 by the University of Chicago
PRINTED IN U.S.A.

THE DEVELOPMENT OF SCHOOLING IN FISHES. II

EVELYN SHAW[1]
The American Museum of Natural History

INTRODUCTION

IN A previous study of the development of schooling in the atherinid fish, *Menidia* (Shaw, 1960), it was found that schooling developed gradually, appeared when the fish attained a certain size, and followed a characteristic pattern of approach and orientation. In a few preliminary experiments on the role of environmental conditions and of early experience with species mates, four fry (isolates) were successfully reared away from species mates to schooling age. The social responses of these fry were observed in one situation—presentation to schooling groups. They were presented individually and each responded by joining the schooling group. These isolates did not have any experience in the processes of parallel orientation nor had they ever contacted any other fish like themselves prior to the test situation. Yet, when presented to the schooling group, each was attracted to the school and followed it. Although there was some initial difficulty in orientation, the new fry were shortly indistinguishable from the other schooling fish. It was thought that the schooling group presented a strong stimulus situation to the isolates which resulted in approach and, as the stimulus moved off, in following. Unpublished observations (Shaw) show that isolates of another species, the cichlid, *Aequidens latifrons*, will also follow when placed with schooling fish but, in contrast, will not form a school when placed together with other isolates. In the latter situation the isolates probably presented equivalent stimuli to each other which resulted in aggregation, without parallel orientation. Because of the limited number of test animals in the first experiments with *Menidia* it was not possible to present *Menidia* isolates to one another to observe their responses. However, this was possible in the experiments described below—with somewhat different results.

Other points raised in the first experiment on the initiation of schooling concerned early experiences, and whether or not there is a certain critical period of time in development during which exposure to species mates is essential to later schooling initiation. The results of the experiments cited below, in which fish are raised under two different environmental situations, show that exposure to, and early experiential contact with, species mates may well be an essential element influencing the later establishment of schooling behavior, but that there may not be a critical time period.

---

[1] Contribution No. 1176 from the Woods Hole Oceanographic Institution, where part of this study was conducted as a visiting investigator during the summer of 1960. Research supported in part by Grant No. M2322, National Institutes of Health, and Grant No. G10832, National Science Foundation.

Material and Methods

GENERAL

The same species of fish were studied as in the previous experiments: *Menidia menidia* (Linnaeus) and *M. beryllina* (Cope). Adult fish were collected at the following localities: Sippiwissett, Great Pond, Green Pond, Stony Beach, Seapit River, Siaconsett Island, and Orleans. These species live sympatrically in shoal water (Rubinoff and Shaw, 1960) and during May, June, and July the adults spawn, coming very close to shore (Perlmutter, personal communication). The eggs are demersal (see Kuntz, 1916, for a description of their embryology) and are laid in clusters held together by adhesive threads.

During the spawning season, adults can be stripped of their gametes by applying gentle abdominal pressure; really ripe females extrude their eggs at the merest touch. Although many females did not produce mature eggs, males always had milt.

REARING TECHNIQUES

Ten females, mainly *M. menidia*, provided eggs for the various groups. The eggs were fertilized in shallow dishes, raised until hatching in polyethylene refrigerator dishes 5 inches square, and transferred at hatching to larger community bowls. Some hatched fry were reared in 10-gallon aquaria; others in large glass finger bowls 10 inches in diameter; others in 12 × 16-inch polyethylene basins; and others, individually, in 5-inch refrigerator dishes. This latter group constituted the main experimental units. Each day sea water in the small polyethylene dishes was changed and fresh sea water was added to the large containers. The fry were fed live nauplii of the brine shrimp *Artemia*, two days after hatching (Rubinoff, 1958). A total of 1,149 fry were reared in the laboratory. The laboratory was illuminated by both daylight and fluorescent light; the temperature ranged between 22°–27° C.

TESTING CONDITIONS

All observations were made in a doughtnut-shaped circular tank (Fig. 1) with an overhead light, either incandescent or fluorescent. The tank measured 18 inches in outside diameter and 12 inches in inside diameter, resulting in a channel 3 inches wide. The bottom of the tank was lined with sand, and sea water filled it up to 5 inches in height (between 6 and 7 liters of water). The tank was surrounded by an opaque shield and the front, or viewing part, was fitted with a one-way mirror. The water in the tank was changed at the start of each series of observations.

In test situations, three to five fry were introduced, one by one, at 3-minute intervals, into the same region of the tank. Observations were spoken into a Gray Audograph recording machine.

After all the fry had been added, they remained in the circular tank for at least ½ hour and on some occasions up to 2–3 hours. They were observed continuously for the first ½ hour; afterward they were usually observed at 15-minute intervals.

The indicated size of the fry was determined, in many instances, by watching fry swim over a marked grid. This was necessitated because our standard technique for measurement required killing the fry, which would have resulted in great depletion of our experimental groups.

EXPERIMENTAL

REARING TECHNIQUES

Here, as before, the same problems were encountered when fish were reared in isolation (Shaw, 1960). In conditions of isolation individuals are removed from species mates and raised in such fashion that they do not have visual or physical contact with their own species and grow in a relatively restricted environment. Non-transparent bowls with non-reflective interiors are used to eliminate visual access to the surrounding environment and to remove the possibility of the fish seeing his own image. In the previous experiments there was a high mortality and only four out of four hundred fry were reared in isolation from an early embryonic stage. Similarly, here, the mortality was also high among fry reared in isolation from early embryonic stages. They died within 5 days after hatching probably, as before, of starvation since they did not initiate feeding. Rearing conditions are listed below:

1. *Quasi-isolates.*—Seventy-six fry were isolated from their community groups 5–7 days after they had hatched. This was done for two reasons: (1) to see if, after feeding was started, the survival in isolation would be higher; and (2) to determine the effects of these experiences on subsequent behavior. Twenty-eight fish survived.

2. *Isolates.*—Eighty-nine fry were isolated as embryos. Nine survived: the remaining fry died within 5 days after hatching.

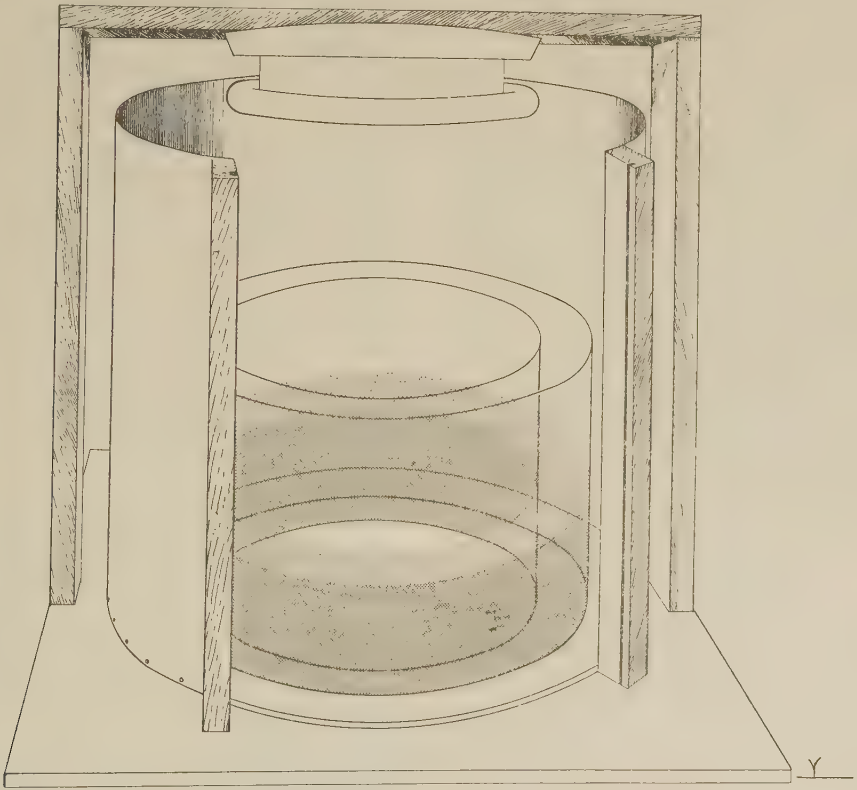

FIG. 1.—Circular tank, standardized testing apparatus for observations on schooling

3. *Crowded fry.*—In addition to these experimental groups, fifty to one hundred fry were raised in a 10-gallon tank. Since the development of schooling is described in terms of length of the fry, with age incidental, we wondered if these crowded conditions would produce a smaller fish which did not school even when its age compared favorably with the age at which fish usually school.

4. Forty fry were isolated at hatching. The water in their bowls was not changed; instead each day 10 cc. of water from community tanks, in which fry were feeding, was placed into the individual containers to try to encourage feeding by chemical stimulation. None survived.

5. Twelve were isolated as early embryos and placed together right after hatching. To our surprise they too, died.

EXPERIMENTAL PROCEDURES AND RESULTS

In the analysis of behavioral development, the methods whereby the animals are raised are an intrinsic part of understanding and interpreting the results, particularly in view of the fact that early experiences and environmental conditions influence greatly the appearance of certain behavioral characteristics (Shaw, 1961). Therefore, although it is not usual procedure, experimental methods are here incorporated with results, so that the methods of rearing will not be separated from the observed behavioral activities.

RESPONSES OF QUASI-ISOLATES TO ONE ANOTHER (TABLE 1)

Group a.—Five days after the start of isolation five fish approximately 7–8 mm. long were placed together in the circular tank. After three hours they had not aggregated[2] and they were returned to isolation.

Four days later the same group was retested, aggregating after one hour. They were measured (average, 9.2 mm. in length) and preserved.

Group b.—Four quasi-isolates approximately 8 mm. long were placed together for the first time 10 days after isolation started. They aggregated. Two days later, upon retesting, they again aggregated and showed some parallel orientation[3] which was disrupted when one or two fish darted away. After this test the fry were returned to isolation where they remained. Eighteen days later they had reached 13–15 mm. in length. Upon testing, after 15 minutes, two fish oriented parallel and two schooled. The schooling,[4] however, was erratic and was constantly disrupted when the two non-schooling fish darted about the tank.

Group c.—Another series of quasi-isolates was tested for the first time 12 days after the start of isolation. After five fish had been in the tank for 19 minutes, they lined up parallel, remained quite still, and showed variable distances from one another. Subsequently they aggregated and swam about randomly. They were replaced in isolation at the end of one hour. Two days later, upon retesting, they again lined up parallel within 5 minutes, but this time they swam together for about 2 seconds. During the following half-hour they showed parallel orientation, remaining stationary, or aggregating. They were measured (average, 10.4 mm. in length) and preserved.

Group d.—Eighteen days after the start of isolation, a group of four fry approximately 12 mm. in length (schooling usually begins at this length) was tested for the first time.

---

[2] *Aggregation:* the fry come together and remain near one another in random positional orientation.

[3] *Parallel orientation:* the fry, after coming together, line up parallel to one another, their heads facing in the same direction. They usually show staggered formation.

[4] *Schooling:* the fry after orienting parallel, begin to swim at the same speed and in the same direction.

The first quasi-isolate introduced into the tank darted around erratically and showed violent tail-wiggling. This did not cease when the second and third quasi-isolates were added; they all remained aloof. However, when the fourth quasi-isolate was introduced, Nos. 1 and 3 lined up parallel for several seconds, and when the fifth quasi-isolate was added, three of the fry oriented parallel, but remained quite still. At the end of 25 minutes they were still parallel but not moving. At the end of 150 minutes they were schooling. They were returned to isolation.

Two days later they were retested. By 15 minutes all five fry were schooling. They were returned to isolation. Nine days later (now 29 days after the start of isolation) they were again tested. Within 6 minutes the first two fry lined up parallel and began to school. As each fry was added, it joined the school.

Group e.—Thirty-three days after isolation, a group of five quasi-isolates approximately 15 mm. in length were placed together for the first time. Initially they showed darting movements. After 30 minutes they aggregated. At the end of 45 minutes they lined up parallel, but remained quite still. At the end of 90 minutes they started to school slowly and evenly with good orientation. They were returned to isolation and retested the next day when they schooled within 12 minutes.

ISOLATES (TABLE 1)

a) At the end of one month (3 weeks posthatching) in isolation, the fry were 11–12 mm. in length, the size at which schooling begins under typical laboratory conditions. At this time three isolates were placed, one by one, into the testing

TABLE 1

SUMMARY OF RESULTS OF SCHOOLING AMONG QUASI-ISOLATES AND ISOLATES

Group	No. of Fry	Tested Days after Isolation	Approximate Size (Mm.)	Previous No. of Tests	Time Together (Min.)	Responses at End of Time
Quasi-isolates:*						
a	5	5	7–8	0	180	No aggregation
		9	9.2†	1	60	Aggregation
b	4	10	8–9	0	30	Aggregation
		12	8–9	1	30	Aggregation, some parallel orientation
		30	13–14	2	12	Sporadic schooling
c	5	12	9–10	0	19	Parallel orientation, without moving forward
		14	10.4†	1	30	Parallel orientation, aggregation
d	4	18	12	0	25	Parallel orientation, but not moving
					150	Schooling
		20	12	1	15	Schooling
		29	13	2	12	Schooling
e	5	33	14–15	0	30	Aggregation
					45	Parallel, but not moving
					90	Schooling
		34	14–15	1	12	Schooling
Isolates:‡						
a	3	38	11–12	0	9	Schooling
b	3	42	13–14	0	10	Schooling

* Quasi-isolate Groups *a–e* were raised in community bowls during embryonic development and for five to seven days after hatching, at which time they were placed in isolation.

† Average.

‡ Isolate Groups *a* and *b* were raised in isolation from an early embryonic stage.

aquarium. Fry No. 2 was followed immediately by fry No. 1; within 6 minutes they oriented parallel, but remained stationary. When fry No. 3 was introduced initially it avoided Nos. 1 and 2 which approached it. However, after 2 minutes, No. 3 joined Nos. 1 and 2 and they formed an evenly spaced school.

b) A second group of three isolates, approximately 13–14 mm. long, was tested 42 days after isolation was started (4 weeks posthatching). The first fry introduced into the tank did not approach the second fry when it was introduced. Instead it circled the tank, swimming past fry No. 2, six times. However, when the third fry was added, Nos. 1 and 2 lined up parallel but did now show forward movement. Rather, they kept turning and following, circling (milling?) in a very small area and showing quick vibratory movements of the tail. When fry No. 3 joined them, all oriented parallel, approximately ½ cm. apart, and began to school. At this time ten minutes had elapsed from the start of the experiment.

RESPONSES OF QUASI-ISOLATES AND ISOLATES TO OTHER SPECIES

Certain quasi-isolates and isolates (neither group had previous experience) were placed for ½ hour (per test) with other species of fish which were matched as closely as possible in size. At the time of testing the fry had attained a schooling size of 12–15 mm. in length. Responses are presented in Table 2.

TABLE 2

RESPONSE OF QUASI-ISOLATES AND ISOLATES TO OTHER SPECIES

Fry No.[*]	Tested Days after Isolation	Species Presented	Previous Experience	Time Elapsed for Response (Min.)	Response of Isolate
1	19	*Spheroides*[†]	None	30	No approach; no withdrawal
2	19	*Spheroides*[†]	None	30	No approach; no withdrawal
3	20	*Apeltes*[‡]	None	30	Isolate approached once. Subsequently no approach; no withdrawal
4	20	*Apeltes*[†]	None	30	No approach; no withdrawal
	20	*Menidia*[§]	*Apeltes*	30	*Menidia* nipped at first. In 2 min. schooling started. Isolate followed
5	21	*Clupea*[†]	None	30	Darting motion; withdrawal
	21	*Menidia*[†]	*Clupea*	30	Darting motion
	21	*Menidia*[§]	*Clupea* and *Menidia*	30	Schooling—somewhat erratic, ½ hr.
6	28	*Fundulus*	None	20	No approach; no withdrawal by isolate. *Fundulus* did follow
	28	*Menidia*[§]	*Fundulus*	23	Schooling
7	28	*Fundulus*	None	20	*Fundulus* approaches slowly; isolate does not dart away. *Fundulus* follows isolate briefly
	28	*Menidia*[§]	*Fundulus*	2	Schooling
8[‖]	38	*Menidia*[§]	None	15	Aggregates, 2 min.; schooling, 15 min.
9[‖]	38	*Fundulus*	None	10	Isolate sporadically follows *Fundulus* and *Fundulus* follows sporadically

[*] Fry Nos. 1–7 were quasi-isolates.

[†] Recently caught in the field.

[‡] Lived in laboratory for 3 weeks.

[§] Laboratory-raised *Menidia*.

[‖] Fry Nos. 8 and 9 were isolates.

APPEARANCE OF SCHOOLING AMONG FISH RAISED UNDER CROWDED CONDITIONS

The fry in the group reared under crowded conditions in the aquarium tank did not grow as rapidly as the controls and, as a result, were smaller than the controls when the latter began to school. Schooling did not appear in the crowded fry (tested in the circular tank) until they had attained the appropriate length—two weeks after schooling began in the uncrowded controls.

General Observations

Observations on general development of schooling made in the previous experiment were confirmed. It was found that fish smaller than 7 mm. in length approached but did not show parallel orientation; that fry 8–10 mm. aggregated and showed temporary orientation; and that fry 11–12 mm. showed schooling orientation.

In previous experiments, fry developed in large troughs and observations were made of their behavior in their home troughs or bowls. In this experiment, fry were also observed in their home chambers, but, in addition, they were taken out of their rearing chambers and placed into the circular tank for observation. With this technique we learned that, generally, from three to five fry had to be in the tank before two fry would show parallel orientation; that, in several cases before the fry started to school in the tank they would line up together in staggered parallel formation but would not swim; and that they would remain almost stationary for a few seconds, then start swimming very slowly, gradually acquiring more speed in the next 20 seconds. In addition, we noted that in schooling, the fry were equidistant from both walls and generally about halfway up from the bottom.

Discussion

These findings emerged from the continuing studies on schooling development: schooling did appear among quasi-isolates and isolates placed together when they attained schooling size; initial latency of schooling in the testing situation was lower among isolates reared apart from an early embryonic age than among quasi-isolates reared apart 5–7 days posthatching; initial latency and length of isolation appear to be inversely related in the quasi-isolates; in preliminary experiments fry reared together during the posthatching period responded by approaching their own species and did not school with any other species.

Differences emerged in orientative processes and initial latency between the quasi-isolates and isolates and between two batches of quasi-isolates. Certainly these differences were not anticipated, particularly if we assumed that experienced fry would school more quickly than inexperienced fry. Is it possible that the experience of fry together for 5–7 days tends to inhibit schooling initially? During that time, fry show the behavioral patterns observed by Shaw (1960): "A fry frequently approached the tail, the head, or the lateral midbody region of another fry to within 5 mm.; both usually darted away rapidly." If these isolates retain experiences in which the typical behavior was at first approach and then withdrawal these early experiences may modify their responses to such an extent that they do not approach and school until the visual image becomes attractive.

Breder and Halpern (1946) reared *Brachydanio rerio* in total and in quasi-isolation (in the latter case they isolated the fish at 6 months for 6 months.) The quasi-isolates did not rejoin a school immediately but did rejoin after 1 day. Breder interpreted this, saying that the innate reaction to aggregation may evidently be modified by experience after it has once been exercised and then abandoned because of enforced isolation.

Kagan and Beach (1957) found that male rats reared in isolation but given 10 minutes of play experience each day tended to play, rather than to copulate, with females when they reached sexual maturity. They suggest that males were confronted with females under the same conditions and in the same setting that previously had been associated with playful interaction and that competing tendencies toward play and copulation were aroused. Although we are dealing here with a completely different phyletic level and behavioral situation, Kagan and Beach's suggestion may be relevant to the condition among our quasi-isolates.

Fry reared without contact with species mates showed almost immediate approach and subsequent following. Breder and Halpern (1946) also found this in their two isolates and suggested that aggregation in this species is not in the nature of a learned reaction but has its genesis in some innate mechanism. However, this does not explain it from the developmental viewpoint. According to Maier and Schneirla (1935) when an animal is first mildly stimulated visually a series of neural impulses from optic centers may stimulate motor centers where motor patterns may be already partially integrated, resulting in general approach. Schneirla (1959) states that the general disposition of lower vertebrates to approach the source of low-energy stimulation is clear and that fishes may respond rather consistently to moving stimuli of small area.

These findings suggest that there is no critical period when exposure to other fry is important in the schooling response.

VISUAL ORIENTATION

Quasi-isolates placed together prior to the time of schooling initiation showed behavior characteristic of their particular size; fry 5–7 mm. long showed an initial response of approach with subsequent darting-off; fry 8 mm. long approached but did not aggregate, whereas fry 9–10 mm. long approached, aggregated, and displayed some parallel orientation. It may be that, in fry at the early ages, the visuo-motor co-ordination is such that they cannot orient parallel, but when they attain 12 mm. in length their visuo-motor patterns are more highly developed and integrated, resulting in the capacity to orient after the more generalized response of approach. They certainly do not pass through stages characteristic of the earlier phases, which again suggests that the more complete development of visuo-motor co-ordination may be an important consideration in the start of schooling. Moreover, that the visual image and stimuli are important is suggested by the finding that, just prior to the initiation of schooling, fry frequently remained variable distances from one another, moved forward slightly and occasionally turned and reoriented—always in a small circumscribed area. This lining-up without the component of forward movement may result in a fry's being exposed to many and various kinds of visual stimuli, finally selecting and remaining a certain distance from the image which attracts but does not repel it (Parr, 1927). Schooling which includes, in addition to parallel orientation, the components of forward movement may occur incidentally when one fry begins to move away.

SPECIES RECOGNITION

The results of the studies on the responses of isolates and quasi-isolates to other species were too preliminary for conclusions. Nevertheless, they raised questions. For example, to what cues were the quasi-isolates (separated 19–25 days) responding when they responded to laboratory reared *Menidia*, but not to other species or to field-caught *Menidia*. This also seemed to be the case among the total isolates. Is it possible that there is some form of self-recognition, and consequently recognition of like forms among fish? Parr (1937) feels that it is not possible for a fish to see itself—especially a sleek one. He states that the possibility of self-recognition in the visual category rests upon the ability of the organism to bring its body within its own field of vision. Obviously, a fish cannot do this (except a sinuous one!). Moreover, a fish cannot touch itself (except with its fins). But what of other sensory cues, after ruling out vision? What of hearing, taste, smell, or patterns of water movement—limited, perhaps, but there is no reason to think a fish does not receive other sensations from its own body—if it has the ability to perceive that they are coming from itself. Parr also states "that the reaction of a schooling fish (mackerel) to the perception of others of its own kind cannot be in terms of a response to individuals recognized to be similar to itself, but must be based upon an automatic association mechanism of a different order in which the perception of another fish similar to itself fits as a key fits into a lock." The author agrees with Parr that the likelihood of self-recognition is indeed remote; but is it not possible that a fry responds to cues that are familiar through its own experiences with the environment and with processes of self-stimulation. According to Schneirla (1957) early self-stimulative relationships may provide a significant basis for later adjustments to new conditions involving members of the same species. Obviously, much work needs to be done in this area before we can really determine just how species recognition comes about.

SCHOOLING FRY IN THE SEA

What significance do these findings have in the coming together of fry in the sea? It may be that, prior to the onset of schooling and to the time the fry become part of plankton (Williams, personal communication), they gain recognition of one another sufficient to permit reidentification later on. If you recall (Shaw, *loc. cit.*) we found fry 7 mm. in length living along shallow banks which means that they hatched about one week earlier and therefore had one week's post-hatching experience together. If early experiences are critical, particularly to species-species responses, it may provide a fine adaptive mechanism which assures the coming together of these conspecific schooling groups even after extended periods of separation. A suggestion is made that, under certain conditions, mixed schools of fry may be a result of different species developing together in the same general area.

SUMMARY

1. Fry were reared under three conditions: isolation, quasi-isolation, and crowding. Each group schooled.

2. Initial latency of schooling was lower among total isolates than among quasi-isolates. In fact, initial latency and length of isolation appeared to be inversely related.

3. In preliminary experiments, fry (quasi-isolates) responded by approaching their own species and did not school with any other species.

4. Crowded fry schooled only when they attained the size at which schooling usually occurs in fry reared under uncrowded conditions.

LITERATURE CITED

BREDER, C. M., and HALPERN, F. 1946. Innate and acquired behavior affecting the aggregation of fishes. Physiol. Zoöl., **19**:154–90.

KAGAN, J., and BEACH, F. A. 1953. Effects of early experience on mating behavior in male rats. Jour. Comp. Phys. Psych., **46**:204–8.

KEENLEYSIDE, M. H. A. 1955. Some aspects of the schooling behavior of fish. Behaviour, **8**:183–248.

KUNTZ, A. 1916. Notes on the embryology and larval development of twelve teleostean fishes. Bull. U.S. Bur. Fish., **35**:87–134.

MAIER, N. R. F., and SCHNEIRLA, T. C. 1935. Principles of animal psychology. New York: McGraw-Hill Book Co.

PARR, A. E. 1927. A contribution to the theoretical analysis of the schooling behavior of fishes. Occasional Papers Bingham Oceanog. Coll., No. 1.

———. 1937. On self-recognition and social reaction in relation to biomechanics, with a note on terminology. Ecology, **18**:321–23.

RUBINOFF, I. 1958. Raising the atherinid fish *Menidia menidia* in the laboratory. Copeia, No. 2, pp. 146–47.

RUBINOFF, I., and SHAW, E. 1960. Hybridization in two sympatric species of atherinid fishes, *Menidia menidia* (Linnaeus) and *Menidia beryllina* (Cope). Amer. Mus. Novitates, No. 1999:1–13.

SCHNEIRLA, T. C. 1957. The concept of development in comparative psychology. Pp. 78–108 *in:* The concept of development, ed. Dale B. Harris. Minneapolis: University of Minnesota Press.

———. 1959. An evolutionary and developmental theory of biphasic processes underlying approach and withdrawal. *In:* Nebraska symposium on motivation. Lincoln: University of Nebraska Press.

SHAW, E. 1960. The development of schooling behavior in fishes. Physiol. Zoöl., **33**: 79–86.

———. 1961. Effects of altered environmental conditions on the appearance of sexual behavior in the platyfish. *In:* Roots of behavior, ed Eugene Bliss. New York: Paul B. Hoeber, Inc

Contribution No. 1177

RELATIVE IRON REQUIREMENT OF SOME COASTAL AND OFFSHORE PLANKTON ALGAE

By

JOHN H. RYTHER AND DANA D. KRAMER

Reprinted from *Ecology*, Vol. 42, No. 2, April, 1961

RELATIVE IRON REQUIREMENT OF SOME COASTAL AND OFFSHORE PLANKTON ALGAE

John H. Ryther
Woods Hole Oceanographic Institution

AND

Dana D. Kramer
Cornell University

Iron in the sea may exist in many physical and chemical forms of which the respective concentrations and availability to microorganisms are not well understood. There appears to be very little present in true solution in seawater (Cooper 1937) and that amount is believed to be insufficient to support phytoplankton at their normal concentrations (Harvey 1937). However, Harvey, and Goldberg (1952) and others have presented evidence that the algae can and do utilize particulate iron as their major source of this element, presumably by hydrolyzing particles adsorbed to their surfaces.

Regardless of the forms in which it exists and may be used, there is frequently very little iron of any kind in the open sea. Total concentrations normally range between 0 and 10 μg/L, about one-half of which will pass through a molecular filter (Lewis and Goldberg 1954, Shaeffer and Bishop 1958, Menzel, unpublished). For convenience, the fractions separated by such filtration techniques have been referred to as "particulate" and "dissolved" iron.

Gran (1933) was among the first to demonstrate that the addition of iron to seawater may stimulate the growth of phytoplankton. Since then many workers have proposed that iron may, at times, limit plant growth in the sea. Recent experiments by Menzel and Ryther (1961) have shown rather conclusively that iron is the most critical nutrient limiting primary production in the tropical and semi-tropical Western Atlantic.

Since iron is associated with land drainage, it is normally present at higher concentrations in coastal waters than in the open sea (cf. Schaeffer and Bishop, loc. cit.). The two regions therefore represent rather different chemical environments (in this and other respects) which could not only affect the general level of productivity but might conceivably provide a selective influence upon the kinds of organisms which could exist and compete with one another under the different conditions. The following experiments were designed to investigate the latter possibility.

Pure cultures of these organisms, listed with the location from which they were isolated, were used in the experiments:

1. *Cyclotella nana* (clone 13-1)	Atlantic Ocean: 33°11′N, 65°15′W
2. *Coccolithus huxleyi*	Atlantic Ocean: 32°10′N, 64°30′W
3. *Chaetoceros lorenzianus*	Atlantic Ocean: 32°10′N, 64°30′W
4. *Chaetoceros* sp. (clone BBSm)	Atlantic Ocean: 32°10′N, 64°30′W
5. *Pyramimonas* sp. (clone 2)	Great South Bay, Long Island, N. Y.
6. *Skeletonema costatum*	Long Island Sound

7. Unidentified cryptomonad (clone 3C)	Long Island Sound
8. *Amphidinium carteri*	Great Pond, Falmouth, Mass.
9. *Isochyris galbana*	Fish pond, Marine Biological Station, Port Erin

These organisms are maintained in pure culture at the Woods Hole Oceanographic Institution. They were all isolated by Dr. R. R. L. Guillard except for *Isochrysis galbana*, isolated and described by Dr. Mary Parke (Parke 1949). Species 1-4 may be considered and will be hereafter referred to as oceanic species, species 5-9 as coastal species.

The organisms are routinely grown at Woods Hole in an enriched seawater designated as medium "f" and consisting of the following addition to millipore-filtered seawater:

$NaNO_3$	150.0 mg/L
$NaHPO_4·H_2O$	10.0 mg/L
$Na_2SiO_3·9H_2O$	30.0 mg/L
Fe-EDTA	10.0 mg/L
Thiamin·HCl	0.2 mg/L
Biotin	1.0 µg/L
B_{12}	1.0 µg/L
$CuSO_4·5H_2O$	19.6 µg/L
$ZnSO_4·7H_2O$	44.0 µg/L
$CoCl_2·6H_2O$	22.0 µg/L
$MnCl_2·4H_2O$	360.0 µg/L
$Na_2moO_4·2H_2O$	30.0 µg/L

Fe-EDTA is the tetra-valent iron complex of ethylenediamine tetra-acetic acid.

For the experiments to determine iron requirement the organisms were inoculated into medium "f" minus its iron constituent and made from millipore-filtered offshore seawater. After one or 2 transfers through this medium, all the algae with one exception were obviously iron-limited and had ceased growing. The deficient cultures were then inoculated into a series of 50-ml cultures consisting of the same basic medium but enriched with varying concentrations of Fe-EDTA ranging in most cases from 0 to 130 µg Fe/L, but for the crytomonad, 0 to 260 ug/L, and for *Pyramimonas*, 0-1300 µg/L. The one organism which did not obviously develop an iron deficiency, *Coccolithus huxleyi*, was sub-cultured 6 times in the "f minus Fe" medium and then inoculated into the same series of media.

The cultures were grown at 20°C at approximately 1000 ft-c of light until their maximum population density was attained, a period which varied somewhat but ranged from 5-10 days. The population density was then estimated by cell counts with a hemocytometer, by optical density measurements at 750 mµ in a Beckman DU spectrophotometer and by chlorophyll *a* concentrations as determined by spectrophotometric measurements of acetone extracts following the method of Richards with Thompson (1952). Of the 3 methods, cell counts gave by far the most reproducible and interpretable results, despite some variability of cell size at different iron concentrations. These are the only data which will be reported here. In comparing cell counts with chlorophyll concentrations, an obvious increase was observed in the chlorophyll/cell value at successively higher levels of iron as has been reported elsewhere (cf. Fleischer 1935). There were indications that this value varied by more than an order of magnitude in some species, but the chlorophyll data were not sufficiently reliable to show this clearly.

The results of these experiments are reported as a series of curves typical of the "dose-response" curves employed in bioassay work. No attempt was made to define the concentrations of iron available to the organisms at any time. The data thus reflect the response of the algae to the amount of iron available, not to its instantaneous concentration. Even here, the quantity of iron available in the filtered seawater used as a base for the medium is not known, though it was below the level detectable by the ∝, ∝-bipyridyl method of Lewis and Goldberg (1954) and hence may be presumed to have been less than 5 µg/L. For these reasons, the exact iron requirement per cell of the respective organisms cannot be determined from our data with sufficient precision to warrant the attempt. However, the relative requirements of the oceanic and coastal species, as revealed by characteristic features of the dose-response curves, are of considerable ecological significance (Fig. 1).

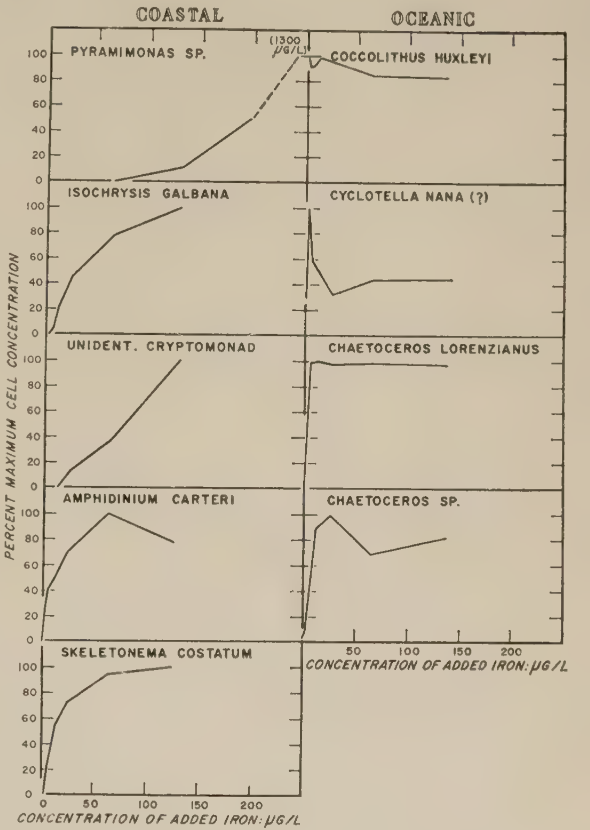

FIG. 1. Terminal population of algae attained in media enriched with various amounts of iron as Fe-EDTA, shown as percentage of maximum population developed for each organism.

Of the oceanic species, *Coccolithus huxleyi* could not be made to show an iron deficiency. After 6 transfers through Fe-deficient media and subsequent inoculation into the graded iron series, the greatest population (3×10^6 cells/ml) still developed in the control culture with no added iron. Apparently the iron originally present in the seawater was adequate for this growth.

All other species tested, once iron-deficient, showed no measurable growth in the control cultures containing no added iron. However, the 3 other oceanic species attained their maximum growth with 2.6 (*Cyclotella nana*), 6.5 (*Chaetoceros lorenzianus*) and 13-26 (*Chaetoceros* sp.) µg/Liter of iron respectively.

Of the coastal species 4 out of 5 failed to grow below 6.5 µg/L, the crytomonad did not increase significantly below 26 µg/L, and *Pyraminonas* sp. required at least 130 µg/L to initiate cell division. The maximum population densities were attained in iron levels of 65 µg/L for *Amphidinium carteri*, 130 µg/L for *Isochrysis galbana, Skeletonema costatum* and the crytomonad, and 1300 µg/L for *Pyramimonas* sp. Maximum populations of *Isochrysis, Skeletonema* and *Pyramimonas* were attained at the highest level of iron used, at which point growth may still have been iron limited.

We have defined the algae used in these experiments as "coastal" and "oceanic" on the basis of the regions from which they were isolated. We believe that the distinction may go beyond this, and that there are many species, perhaps including some of those tested here, which are restricted in their distribution to one or the other environment. For example, we have found *C. huxleyi* widespread in the open waters of the western Atlantic and the dominant organism during most of the year in the Sargasso Sea near Bermuda (Hulburt *et al.* 1960). Yet it is seldom encountered within the continental shelf waters off eastern United States and never in the shallow coastal waters. Other clones of *C. huxleyi* have been isolated from inshore northern waters (Mjaaland 1956), but that author points out that the species originally described by Lohmann (as *Pontosphaera huxleyi*) represents several taxonomic units. It is doubtful that the Woods Hole clone bears a close relationship, systematically or physiologically, to the forms with which Mjaaland worked, though this should be investigated.

Skeletonema costatum, on the other hand, is a ubiquitous diatom in estuaries and coastal waters throughout the world. It has seldom been reported in the open sea far from land and is probably always of neritic origin. It is significant in relation to these distributional patterns, that *Skeletonema* does not begin to grow at levels of iron which are sufficient to produce populations of *C. huxleyi* orders of magnitude greater than ever encountered in the sea.

Although the number of species used in our experiments was not large, the consistency of the results strongly indictates a general pattern of response. It is not unlikely that coastal and offshore species may respond differentially to the levels of other nutrients, but on the basis of our experiments and the little known of its distribution, iron appears to be one of the more likely factors controlling the distribution of plants in the sea.

SUMMARY

The relative iron requirement of 5 coastal and 4 oceanic species of plankton algae was determined by assaying the growth of iron-deficient cultures in media containing various amounts of Fe-EDTA. The oceanic species attained their maximum populations at levels of iron capable of supporting either no growth or a small fraction of the potential growth of the coastal species under the conditions of the experiment. It is suggested that the availability of iron may be a factor controlling the distribution of these and other species of marine phytoplankton in view of the association of this element with land drainage and its greater abundance in neritic waters.

REFERENCES

Cooper, L. H. N. 1937. Some conditions governing the solubility of iron. Proc. Roy. Soc. **124**: 299-307.

Fleischer, W. E. 1935. The relation between chlorophyll content and the rate of photosynthesis. J. Gen. Physiol. **18**: 573-597.

Goldberg, E. D. 1952. Iron assimilation by marine diatoms. Biol. Bull. **102**: 243-248.

Gran, H. H. 1933. Studies on the biology and chemistry of the Gulf of Maine. II. Distribution of the phytoplankton in August, 1932. Biol. Bull. **64**: 159-181.

Harvey, H. W. 1937. The supply of iron to diatoms. J. Mar. Biol. Ass. U. K. **22**: 205-219.

Hulburt, E. M., J. H. Ryther and R. R. L. Guillard. 1960. The phytoplankton of the Sargasso Sea off Bermuda. J. Cons. int. Explor. Mer. **25**: 115-128.

Lewis, G. L. Jr. and E. D. Goldberg. 1954. Iron in marine waters. J. Marine Res. **13**: 183-197.

Mjaaland, G. 1956. Some laboratory experiments on the coccolithophorid *Coccolithus huxleyi.* Oikos **7**: 251-255.

Menzel, D. W. and J. H. Ryther. 1961. Nutrients limiting the production of phytoplankton in the Sargasso Sea, with special reference to iron. Deep-Sea Res. 7.

Parke, Mary. 1949. Studies on marine flagellates. J. Mar. Biol. Ass. U.K. **28**: 255-286.

Richards, F. A. with T. G. Thompson. 1952. The estimation and characterization of plankton populations by pigment analysis. II. A spectro photometric method for the estimation of plankton pigments. J. Mar. Res. **11**: 156-172.

Schaeffer, M. B. and Y. M. M. Bishop. 1958. Particulate iron in the off-shore waters of the Panama Bight and in the Gulf of Panama. Limnology and Oceanog. **3**: 137-149.

Contribution No. 1177 from the Woods Hole Oceanographic Institution, with the partial support of Research Grant 10693 from the National Science Foundation.

Contribution No. 1183

Reprinted from BIOLOGICAL BULLETIN, Vol. 121, No. 1, pp. 92–107, August, 1961
Printed in U. S. A.

PRELIMINARY INVESTIGATION ON THE PHYSIOLOGY AND ECOLOGY OF LUMINESCENCE IN THE COPEPOD, METRIDIA LUCENS

CHARLES N. DAVID AND ROBERT J. CONOVER

Harvard College, Cambridge, Mass., and Woods Hole Oceanographic Institution, Woods Hole, Mass.

PRELIMINARY INVESTIGATION ON THE PHYSIOLOGY AND ECOLOGY OF LUMINESCENCE IN THE COPEPOD, METRIDIA LUCENS[1]

CHARLES N. DAVID AND ROBERT J. CONOVER

Harvard College, Cambridge, Mass., and Woods Hole Oceanographic Institution, Woods Hole, Mass.

Since the advent of the photomultiplier tube with greatly increased sensitivity to low light intensity, it has been possible to measure marine luminescence quantitatively. Luminescent flashes have been found to be far more prevalent at all depths in the sea than had generally been suspected (Clarke and Backus, 1956; Clarke and Breslau, 1959, 1960; Clarke and Hubbard, 1959; Clarke and Wertheim, 1956; Boden and Kampa, 1957, 1958; Kampa and Boden, 1957). Attempts to identify the source of this flashing, using the luminescence camera built by Breslau and Edgerton (1958), suggest that most of the luminescence is produced by planktonic organisms less than a centimeter long (Clarke and Breslau, 1959; Clarke, personal communication). Certain planktonic species whose luminescence has been investigated do not show spontaneous luminescence in the laboratory. Probably some of the luminescence which has been measured at sea may be artificially stimulated by the unavoidable motion of the photometer suspended from a research vessel. However, Kampa and Boden (1957) have concluded that some luminescence appears to be "natural" or "spontaneous."

Bioluminescence in a small planktonic animal has been examined particularly with a view toward evaluating its potential as a source of luminescence in the natural environment and determining the significance of the luminescence for the organism. The calanoid copepod, *Metridia lucens,* was the animal chosen.

This copepod was recognized as luminescent by Boeck (1865) who described the species. Several additional workers have made microscopic or field observations on the luminescent Copepoda (Dahl, 1893, 1894; Kiernik, 1908; Vanhöffen, 1895; Giesbrecht, 1895), but very little experimental work has been done.

In the present work preliminary investigation of certain physical properties of the luminescent emission and of the physiology of the luminescent mechanism has been attempted, in addition to the experiments designed to ascertain what ecological significance luminescence may have for this copepod.

The authors are indebted to Dr. George L. Clarke for his advice and criticism in planning the work and in the preparation of the manuscript. The authors also wish to express their thanks to Dr. W. D. McElroy, Dr. James F. Case, Dr. Edward R. Baylor and members of the staff of the Woods Hole Oceanographic Institution for their cooperation and assistance.

---

[1] Contribution No. 1183 from the Woods Hole Oceanographic Institution. Research supported by National Science Foundation Grants 3838 and 8913.

MATERIALS AND METHODS

The copepods used in the experiment were obtained in Cape Cod Bay about 3–5 miles northeast of the mouth of the Cape Cod Canal in 20–30 m. of water. Collections were made on two occasions, July 7 and August 16, 1960, with a ¾-meter #00 plankton net towed near the bottom. The *Metridia* were isolated from the catch and maintained in the laboratory approximately 40 animals to 1000 ml. of food culture. Laboratory cultures of the diatom *Thalassiosira fluviatilis* were used as food diluted 1:20 by volume with millipore-filtered sea water from Cape Cod Bay. This gave a concentration of 6000 to 10,000 cells/ml. in the final food culture. Either streptomycin or penicillin (50 mg./l.) was added to inhibit bacterial growth. For specific experiments, smaller groups of *Metridia* were kept in proportionately smaller volumes of food medium. All groups of animals were kept in a darkened refrigerator at 5–7° C.

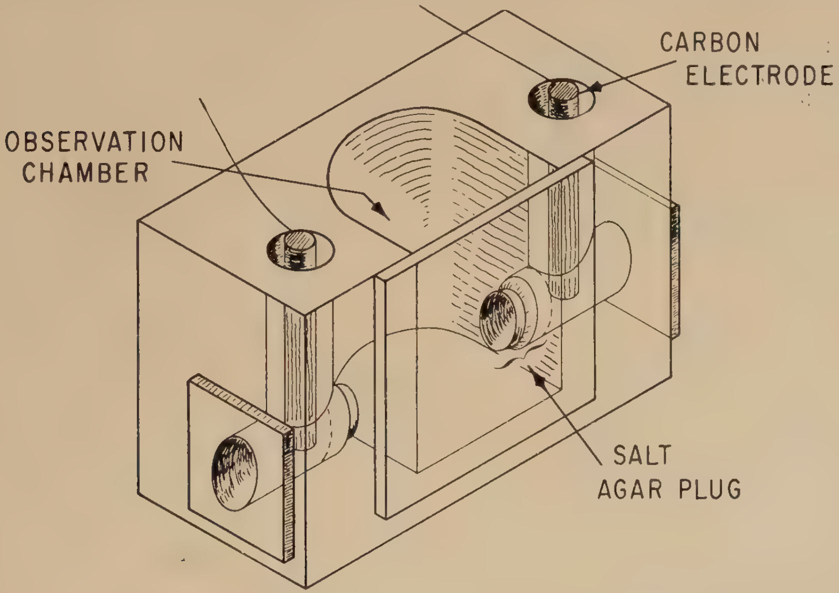

FIGURE 1. Electrode chamber used for stimulation of *Metridia*. For details see text.

Measurements of luminescence were made in a "black box" consisting of a tar-paper covered wooden frame built on top of a table. A large opening on one side of the box covered with a black cloth sleeve and drawstring permitted the investigator's head to remain inside the box for observations or to monitor recording and stimulating instruments outside the box.

The measurements of luminescence were made with the portable bathyphotometer designed and built by Breslau (1959), which employs a RCA 5819 photomultiplier tube with 1200 v. battery power and a transistor amplifier circuit. Experimental material was placed directly in front of the photomultiplier about 18 cm. from the sensitive surface. A Texas Instruments, Inc. single-channel, strip-chart recorder ("Recti/Riter") was used to record intensity (in μw./cm.^{2}) against time during each flash.

Since the *Metridia* do not generally luminesce spontaneously in the laboratory, mechanical or electrical stimulation must be applied to study the characteristics of the flashing. In order to standardize the stimulus delivered to the animals, a simple electrode chamber was constructed as shown in Figure 1. The device was cut out of a piece of lucite and the connecting holes between the two side chambers and the central chamber were filled with 3% agar made with millipore-filtered sea water. For experiments, carbon electrodes wired to a pulse regulator were placed in the side chambers and the whole device was filled with cooled sea water to complete the circuit. *Metridia,* either individually or in groups, were then placed in the central chamber for stimulation.

All stimulation was performed with alternating current controlled through an electronic switch and a continuously adjustable autotransformer, Variac Type W10MT. The switch regulated the duration of pulses to one-tenth of a second and the interval between pulses to two-tenths of a second. Although slightly sensitive to changes in salinity and temperature, the current was regulated accurately to one-tenth of an ampere. The chart speed of the recorder was varied for different experiments. The slower speed (6 in./hr.) was used to record the frequency and intensity of flashes. The faster speeds (6 or 12 in./min.) were used when a measure of total luminescent flux (area under intensity curve) or the duration of a flash was required.

Description and Distribution of Metridia lucens

Metridia lucens is a medium-sized copepod, virtually colorless in the living state. Its size varies between 2.4–3.0 mm. for females and 1.8–2.5 mm. for males.

Although *Metridia lucens* is a common copepod of temperate and boreal water, very little is known regarding its seasonal abundance or life-history. In the Gulf of Maine, Bigelow (1924) noted an increased abundance in the spring and again in September and October. Bigelow (1924) and Clarke (1933, 1934) observed extensive diurnal vertical migrations in this species. In the waters off the coast of Ireland it also seemed to have a period of maximum abundance in May and a smaller period of increase in the fall (Farran, 1920). During the spring it has been reported to be responsible for brilliant phosphorescence on the Irish coast (Farran, 1903, in Bigelow, 1924).

Little is known regarding the internal anatomy of the copepods. Among the calanoids only *Calanus finmarchicus* has been studied in detail (by Lowe, 1935). It is presumed that in the general features of its morphology *Metridia* does not differ greatly from *Calanus* although there doubtless are certain differences in structural detail.

The only light-sensitive organ in most copepods, including *Metridia,* is a single naupliar eye. It seems very doutbful that this organ can have any role in behavior requiring recognition of other organisms because it cannot form images. However, it can presumably detect intensity gradients (as in vertical migration) and possibly the plane of polarization of incident light.

Luminescent glands

The earliest workers recognized that the luminescence produced by *Metridia* was primarily external. Boeck (1865), who described *Metridia lucens,* noted that the light seemed to be produced in the head region and also from the abdomen. Vanhöffen (1895), working with the larger *M. longa,* observed luminescence distributed over most of the thorax as well as the head. In addition to the external secretion, he also felt that some light was produced internally which indicated the position of the secretory glands.

The authors observed that *Metridia lucens* seemed to produce luminescence, when stimulated electrically, chiefly from the anterior part of the head and from the region of the caudal rami. The separation of these two regions was sufficiently distinct that the light produced persisted sometimes as two discrete points for some seconds.

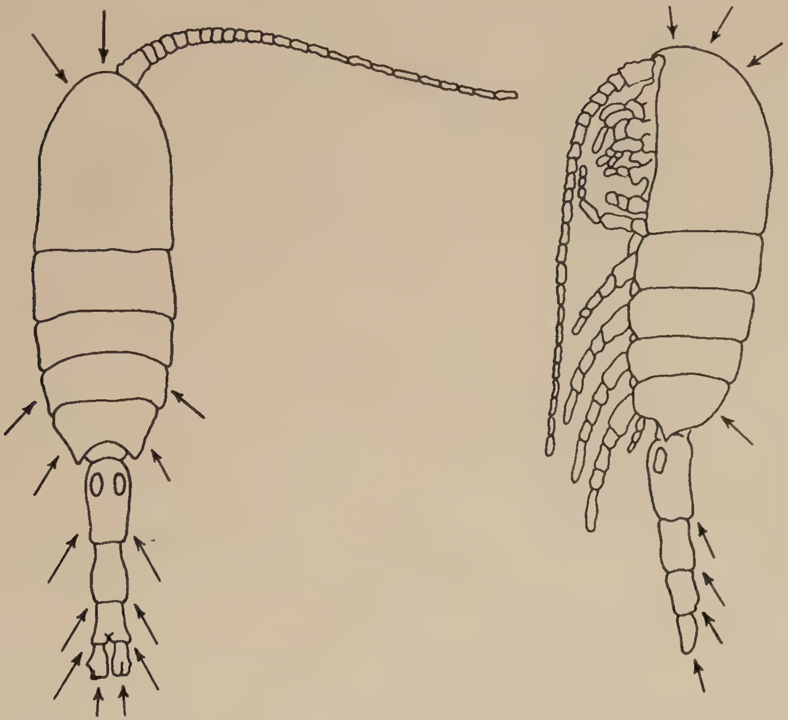

FIGURE 2. *Metridia lucens:* left, a dorsal view; right, a lateral view. Arrows indicate the general regions of the body where luminescent glands were found.

Due to the kindness of Dr. Robert Hessler, some histological preparations of *Metridia lucens,* fixed in Zenker's and stained with hematoxylin and eosin were available for study of the glands and their distribution. Figure 2 shows the regions of the body seen microscopically to produce luminescence in observations on living animals. Glands were located in the histological preparations in most of these places with definite concentrations on the anterior surface of the head and on the posterior portion of the abdomen.

The glands varied in shape somewhat depending on their location in the body. Those in the urosome had a long connecting duct between the glands and the external pore while those in the thorax opened directly to the outside through a short duct. In several cases masses of dark material which might be the luminescent substance were observed in these ducts.

Sewell (1932, 1947) describes the presence of external pores on the cuticle, presumably associated with glandular structures, in several groups of copepods including *Metridia*. It is not certain, however, that these are the openings to luminescent glands, particularly since such structures are found in several genera not presently known to be luminescent, notably *Eucalanus* and *Temora*. The distribution of these pores has not been worked out in detail for *Metridia lucens*.

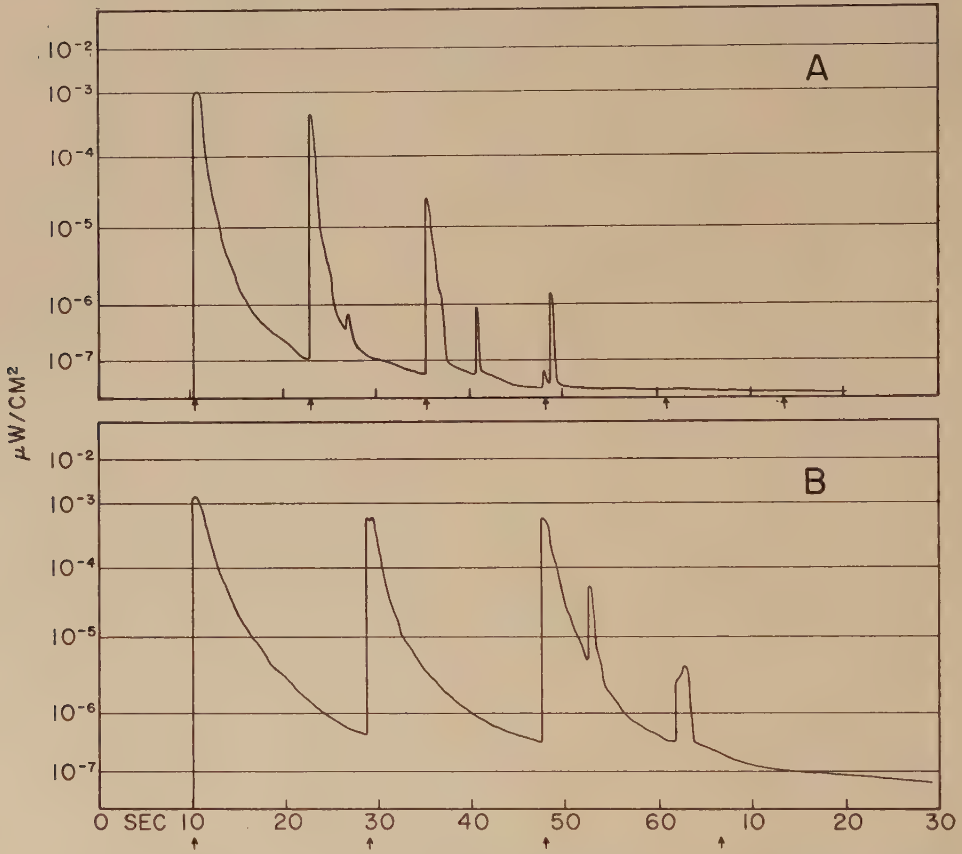

FIGURE 3. Luminescence of single *Metridia* when stimulated in the electrode chamber. Arrows along the time scale indicate instant of stimulation (0.7 amp.). Chart speed is 6 in./min. *A* shows curve for an animal tested six hours after capture; *B* shows curve for an animal tested after being kept in the laboratory for one month.

Physical characteristics of the luminescence

The luminescent emission of *Metridia lucens* is generally a bright flash of varying duration. According to Harvey (1952), luminescence in copepods results from the simultaneous discharge of substrate and enzyme into the surrounding medium; presumably the immediate peak emission occurs at the instant of initial contact between the reacting substances in the presence of oxygen. Generally a gradual decay follows as enzyme and substrate diffuse away into the medium, or perhaps as the substrate is used up.

The absolute intensity of the highest peak of the luminescent emission is in doubt because of the relatively slow response time of the equipment used. Furthermore, the maximum emission intensity varied to some extent for individual animals. However, the maximum intensity measured for *Metridia* was 1.2 × 10^{-3} μw./cm.^{2} at the working distance of 18 cm. (Fig. 3). With groups of 5 *Metridia,* there was an additive effect giving maximum intensities of up to 4.5 × 10^{-3}. The intensity of the response decreased after successive stimuli.

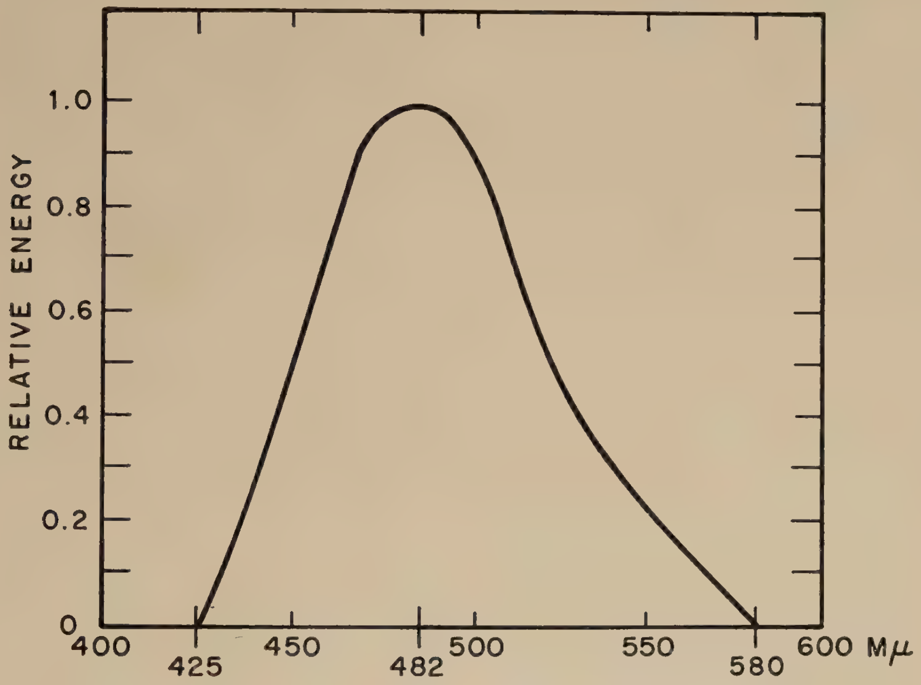

FIGURE 4. Spectrum of luminescent emission at 0° C. from crushed animals.

The duration of individual responses varied even more widely than the maximum intensities, and ranged from 3 seconds to 50 seconds for all luminescent responses with intensities between 10^{-3} and 10^{-4} μw./cm^2. There was no apparent relationship between the intensity of a luminescent emission and its duration. For example, two *Metridia,* exactly similar in laboratory history, both gave responses of 3 × 10^{-4} μw./cm.^{2}, one emission having a duration of 10 seconds, the other a duration of 50 seconds. If responses of a lower maximum intensity than 10^{-4} μw./cm.^{2} are considered, durations as short as 1 second have been measured, particularly at the end of fatigue experiments when the *Metridia* had already responded to 10 or 15 electrical stimuli.

Through the kindness of Dr. W. D. McElroy at the Marine Biological Laboratory, Woods Hole, Massachusetts, it was possible to measure the spectrum of *Metridia's* luminescent emission (Fig. 4). The apparatus used was an Aminco spectrophotofluorometer in circuit with a drum recorder ("x-y" recorder) and an oscilloscope. Because of the rapid decay in intensity of *Metridia's* luminescence, it was necessary to cool a number of the animals in crushed ice in order to slow down the enzyme reaction producing the luminescence. Then, by immediately crushing the animals in a small test tube directly in the spectrophotofluorometer, the luminescence remained at one intensity long enough to record the entire spectrum.

The peak of the spectrum for *Metridia* is around 482 mμ and is therefore similar to that of *Cypridina* and certain other luminescent Crustacea (Nicol, 1960). The curve is slightly skewed toward longer wave-lengths with about half the spectral energy falling in the range between 440 mμ and 525 mμ. The entire spectrum lies between 425 mμ and 580 mμ. This spectrum with its peak at 482 mμ coincides closely with the wave-lengths having maximum transmission through clear, oceanic sea water (Clarke, Chap. 6, 1954).

Experiments on physiology

In order to determine whether laboratory culture had any effect on the luminescence of *Metridia,* freshly captured specimens and some which had been maintained in the laboratory for a month were repeatedly stimulated until failure to respond to two successive stimuli indicated the onset of fatigue. A representative experiment shown in Figure 3 indicates that the maximum intensity and the rate of fatigue were not markedly different for the two specimens. The difference in flash duration is not significant considering the wide range of variation shown by this characteristic.

To study the effect of strength of the stimulating pulse on the luminescence, the current was increased from .3 amp. to .7 amp. which caused a significant increase in the intensity of the luminescence and in the number of responses to stimuli. However, pulses stronger than .7 amp. did not cause further increase in luminescence intensity but seemed to reduce the number of successive responses. Variations in the duration of the pulse over the range tested (.10–1.0 second) had little effect on the intensity or number of successive responses. However, short intervals, *i.e.,* 3 seconds, between pulses induced two or three times as many successive responses as were observed using longer intervals between pulses, *i.e.,* 10–45 seconds.

The effect of previous light- or dark-adaptation was tested with separate groups of animals kept at about 5° C. in the dark, in the light, and in a room exposed to diurnal light changes. The experiment was begun at 1700 on August 3 and the luminescence produced by each group was tested on August 5 and again on August 8 between 1000–1300. No statistically detectable difference was found between the three sets of animals. In another experiment twenty animals kept in a water bath at 5° C., where they were exposed to daily light variation, were tested at night (2330–0030) and during the day (1300–1400). In the case of a few animals the day-time response was somewhat lower than at night but there is no evidence in any of the data for a marked inhibition of luminescence by light or for a daily rhythm.

Having established the fact that the experimental techniques used had no appreciable effect on the luminescent response of *Metridia,* two more physiological experiments were performed. The first was designed to investigate an observation by the authors that animals which fed poorly still luminesced as vigorously as animals that fed well. Two groups of animals were set up, one fed on the regular culture medium and the other starved in millipore-filtered sea water. After one week, single stimulus tests were performed. On the basis of the total area under the intensity *vs.* time curve, the results showed no difference between the two

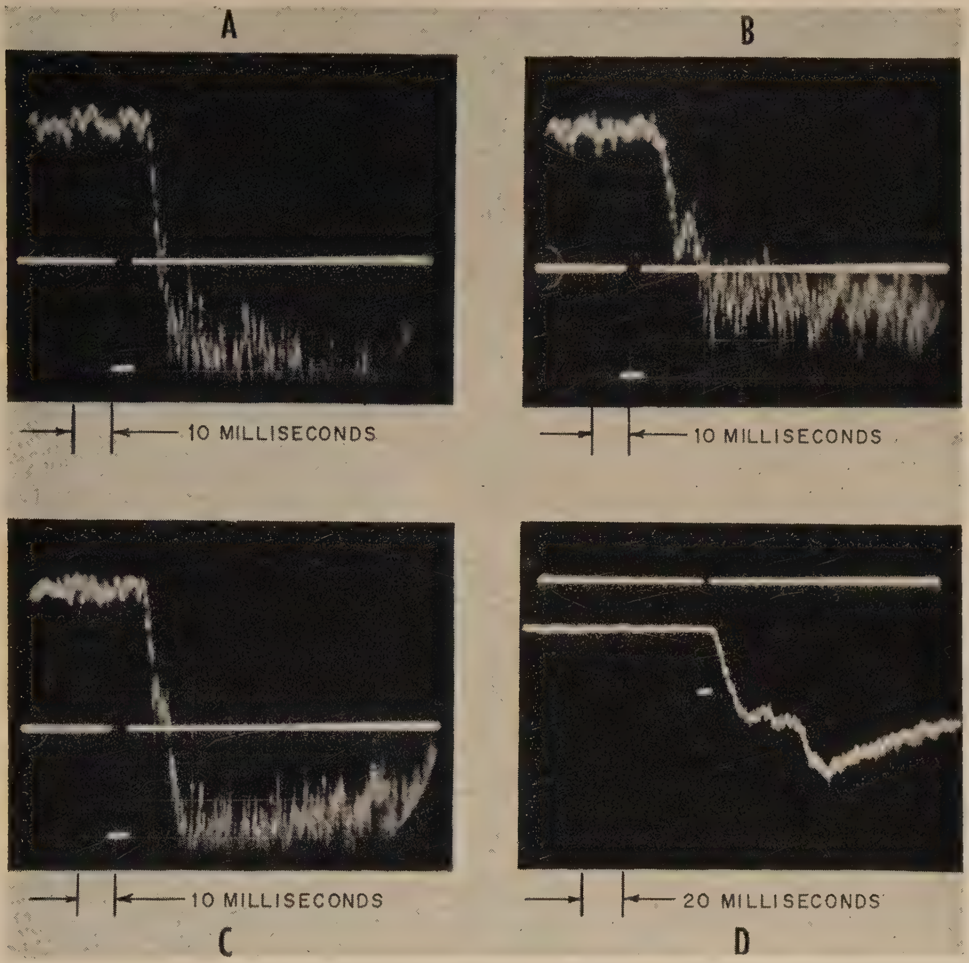

FIGURE 5. Lag time between stimulus and luminescent response. In all four cases the stimulus was 150 v./5 msc. represented by the break in the smooth horizontal trace. Downward deflection of the jagged upper trace (lower trace in *D*) represents luminescence measured by the photomultiplier. The lag times were: *A,* 8 msc.; *B,* 7 msc.; *C,* 8 msc. *D* shows the same type of measurement but includes more of the intensity curve and the stepwise rise to maximum intensity.

groups. However, when maximum intensity was considered, the results indicated statistically (Wilcoxen Ranked Sum) better luminescence for the starved group.

After the second week, repeated stimulus experiments were conducted on the two groups. Single stimulus data showed no statistical difference in the intensity of the response between the fed and starved groups, nor did the number of successive responses to repeated stimuli show a significant difference. At the end of the third week, however, experiments did demonstrate that the fed *Metridia* had a stronger luminescent response and the same group was able to respond to the electric stimulus a greater number of times than the starved animals.

In another series of experiments the length of time from the beginning of a stimulus to the beginning of a response (the lag time) was measured. For the necessary guidance and equipment to make these measurements, the authors are indebted to Dr. James F. Case at the Marine Biological Laboratory, Woods Hole, Mass. Single animals were tested in a small cell consisting of a 3-cm. piece of glass tubing with agar plugs and silver electrodes at either end. The electrodes were connected to a Grass S4 stimulator and the luminescence was measured with a RCA 931A photomultiplier in circuit with an oscilloscope. An automatic camera photographed the oscilloscope screen to record the results.

Using a stimulating pulse of 150 v. for 5 or 10 msc., the *Metridia* demonstrated a lag time (at room temperature) of 8–10 msc. to the beginning of the luminescent response and a lag time of 15–24 msc. to the maximum intensity of the response. The time to maximum intensity varied widely, depending on whether or not the rise to maximum intensity was direct or in a step-wise fashion, the latter giving lag times as long as 60 msc. (see Fig. 5). By observing the *Metridia* through a microscope during these experiments it was noticed that for a stimulus of 10 msc./150 v. usually both head and tail luminesced while for a stimulus of 5 msc./150 v. only the organs in the head region responded.

Experiments on behavior

Because it has often been suggested that luminescence functions as an escape mechanism for marine animals that luminesce by means of an extracellular discharge, the authors decided to investigate the behavior of *Metridia* in the presence of a predator. A series of experiments was conducted in the dark, in which possible planktonic predators on *Metridia* were placed individually with 10 *Metridia* in 600-ml. beakers. The species tested were: *Paraeuchaeta norvegica* (Copepoda), *Parathemisto* (*Euthemisto*) *gaudichaudii* (Amphipoda), and euphausiids, *Euphausia krohnii, Thysanoessa inermis, Nematoscelis megalops,* and *Meganyctiphanes norvegica.*

Each experiment was continued for at least two days and counts of the number of *Metridia* present were made at intervals of 12 to 16 hours. Only in the case of the two euphausiids, *Thysanoessa* and *Meganyctiphanes,* was there any predation on the *Metridia.* Although not every individual tested fed on *Metridia* with the same rapacity, *Meganyctiphanes* was by far the most successful predator. The best predators among the animals tested were then chosen for further examination.

The predator was placed in a 600-ml. beaker with 10 *Metridia* and this beaker was placed in the black box in front of the photometer. A cool water bath was used to keep the temperature in the experimental vessel between 10°–12° C. The photometer response was recorded at slow speed (6 in./hr.) so that each flash gave a spike indicating maximum intensity and time of occurrence. Analyzing the results of these experiments was complicated by the fact that both prey (*Metridia*) and predator (*Meganyctiphanes*) were luminescent. However, comparison of the characteristics of *Metridia* and *Meganyctiphanes* luminescence records when the animals were stimulated electrically showed that high intensity responses were almost surely due to *Metridia*. Even using a maximum stimulus (1.1 amp.), *Meganyctiphanes* never produced a response higher than 1×10^{-4} μw./cm.^{2} and it was generally much lower. Furthermore, the luminescent emission of *Meganyctiphanes* was usually a prolonged irregular glow (Fig. 6). The *Metridia*, by contrast, always gave a single flash that appeared as a perpendicular spike on the slow-speed record (see Fig. 7). Using these two criteria, a reasonable interpretation of the records could be made.

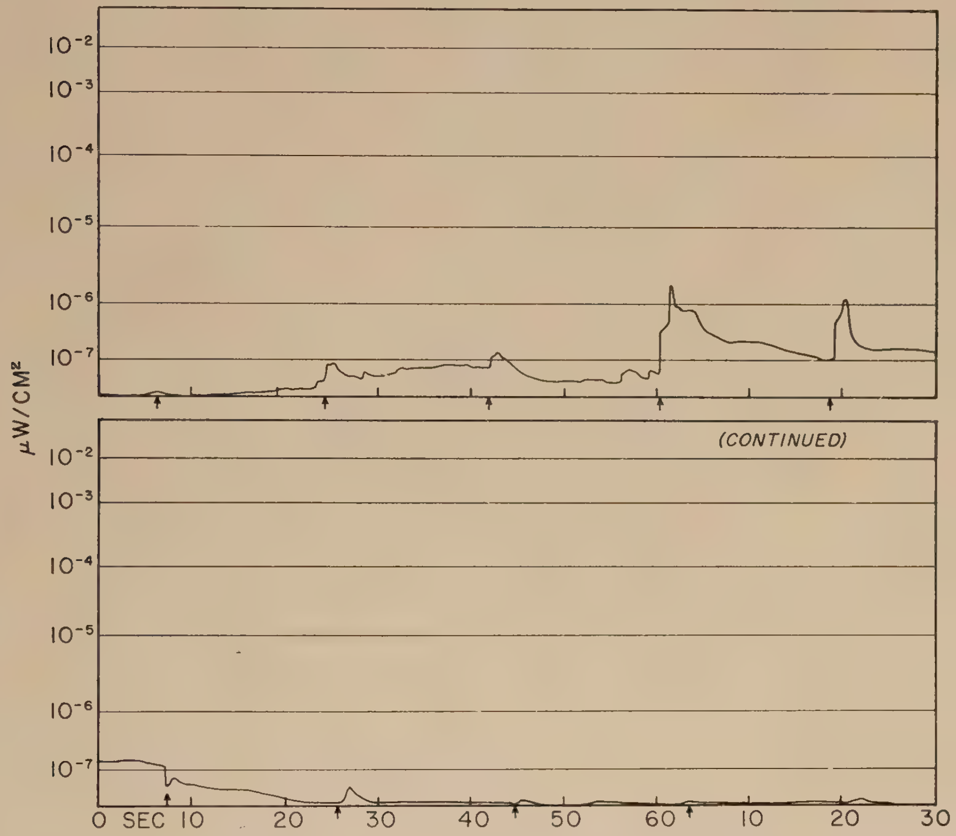

FIGURE 6. Luminescence of a single *Meganyctiphanes norvegica* when stimulated in the electrode chamber. Arrows along time scale indicate instant of stimulation. Chart speed is 6 in./min. The stimulus (0.7 amp.) was as strong as any ever used for *Metridia*. Low intensity of luminescence is notable in comparison to *Metridia's* bright flash.

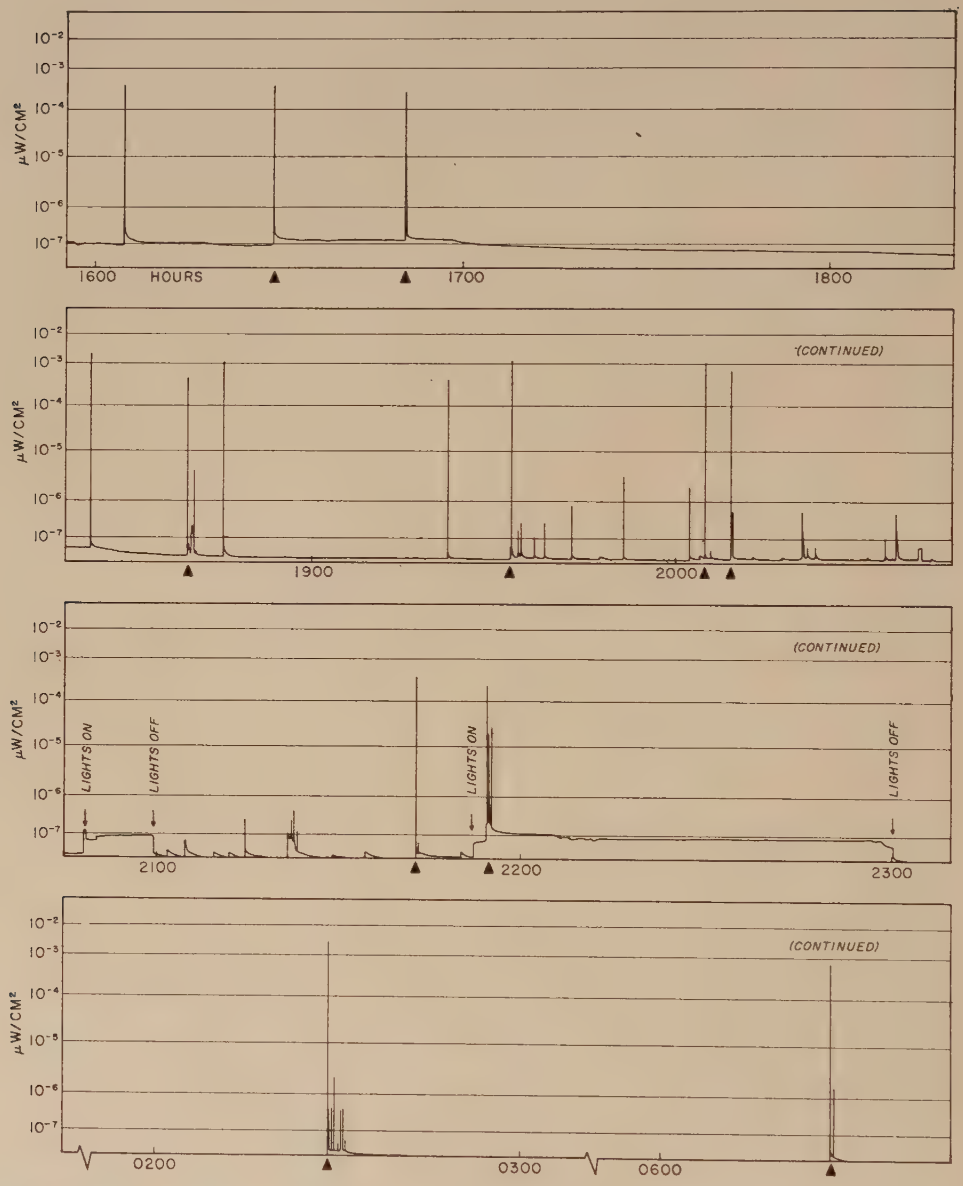

FIGURE 7. Record of behavior experiment 3 (see Table I). At the chart speed of 6 in./hr., luminescent flashes appear as spikes indicating maximum intensity and time of occurrence. Solid triangles indicate successful predation under interpretation outlined in text. The decreasing background intensity between 1600 and 1900 hours is due to the setting sun which reduced the ambient light in the laboratory. The increased background at 2045–2100 and 2150–2300 hours was caused by lights in the laboratory used to monitor the recorder.

A sample record from an experiment with both prey and predator present is show in Figure 7. All the experiments are summarized in Table I. Experiments 6 and 7 in the table show quite clearly that the two species when separated from each other ordinarily do not produce any spontaneous luminescence. Only a single weak flash (4×10^{-7} μw./cm.^{2}), which may have been caused by some accidental mechanical stimulus, was observed for the group of *Metridia* alone. The *Meganyctiphanes* alone produced no luminescence at all. This corroborates Mauchline's (1959) observation that *Meganyctiphanes* does not luminesce spontaneously in the laboratory except during the breeding season (Dec.–Feb.). On the other hand, when the two species were placed in the same container, considerable luminescence was observed and some *Metridia* were eaten (experiments 1–5). Since most of the flashes showed up on the record as single spikes, some with an intensity greater than 10^{-4} μw./cm.^{2} (see Fig. 7), it was concluded that the copepod was primarily responsible for the display.

TABLE I

Summary of behavior experiments.

The table shows the interrelationship between luminescence and predation in Metridia lucens. *For detailed explanation see text and Figure 8.*

Expt. No.	Date	Total time (hrs.)	Predator		No. of *Metridia*		Number of luminescent responses	
			No.	Species	In expt.	Eaten	Above 10^{-7} μw./cm.^{2}	Above 10^{-4} μw./cm.^{2}
1	8/12–13	15	1	*Meganyctiphanes norvegica*	9	8	30	15
2	8/17–18	8	1	*Meganyctiphanes norvegica*	10	3	17	3
3	9/14–15	16	1	*Meganyctiphanes norvegica*	10	10	33	14
4	9/16–17	13.5	1	*Meganyctiphanes norvegica*	11	5	41	21
5	9/18	10.5	1	*Meganyctiphanes norvegica*	10	4	23	1
6	8/13–14	15.75	—	—	10	0	1	0
7	8/14–15	9.5	1	*Meganyctiphanes norvegica*	0	—	0	0
8	8/11–12	7.25	2	*Parathemisto gaudichaudii*	10	0	1	0
9	8/19–20	15.5	1	*Parathemisto gaudichaudii*	9	0	0	0
10	8/18–19	15.5	2	*Thysanoessa inermis*	10	1	3	0
11	8/24–25	15	1	*Nematoscelis megalops*	10	0	1	0

On the original records (copied in Fig. 7), it was possible to distinguish two kinds of single spikes, ones representing only a single luminescent flash and ones where several tracings were actually superimposed. This latter kind represented several flashes of different intensities which occurred within an interval short enough (30–40 seconds) to prevent their resolution at the slow chart speed. Sometimes this multiple-flash sequence was spread out over a longer period of time and the smaller flashes were resolved on the record (*e.g.* 0230 hours in Fig. 7). The number of multiple-flash sequences was, in almost every case, exactly equal to the number of *Metridia* eaten. These sequences presumably represent a *Metridia's* capture (large flash) and subsequent struggle to escape (small flashes). The remaining spikes on the record (caused by single flashes) are presumed to represent successful escapes by *Metridia.*

In order to determine if the mere mechanical disturbance of another organism in the container could cause luminescence, groups of *Metridia* were tested with several other species in the container placed in front of the photometer. A large *Parathemisto* (*Euthemisto*) *gaudichaudii,* a vigorously swimming hyperiid amphipod, did not induce any luminescence when placed with *Metridia* nor did it eat any (Table I, experiments 8 and 9). Similar results were obtained with the euphausiid *Nematoscelis megalops* (experiment 11). When *Thysanoessa inermis* was used (experiment 10) a few flashes were produced and a single *Metridia* was eaten during the experiment. A further test of the effect of mechanical stimulation was made by vigorously stirring the water in a beaker containing *Metridia.* Considerable disturbance was necessary before any flashing occurred and even the most energetic agitation elicited a maximum response of only 6×10^{-5} μw./cm.^{2}, less than one tenth of the highest responses shown in Table I and Figure 7.

Direct observation of predation was also attempted in order to determine the nature of the luminescence stimulus. An infra-red-sensitive "sniper-scope" (Edmund Scientific Co.) was used with the infra-red source and a focusing lens placed behind the experimental beaker so that the animals appeared in opaque profile against a light background. The small *Metridia* were not always visible with this optical arrangement but some individuals were seen to be carried toward the euphausiid by the currents set up by the larger animal's pleopods. Sometimes the *Metridia* would dart away before reaching the *Meganyctiphanes,* but at other times the copepod would seem to come in contact with the euphausiid before darting away. On a few occasions the euphausiid started off as though in pursuit, but the actual act of capture was never observed.

These observations are in general agreement with those of Mauchline (1959) who found *Meganyctiphanes* capable of filter-feeding on organic detritus and even sucking into the "food basket" individual copepods (*Paraeuchaeta norvegica*) and *Sagitta* by lateral-ventral movements of the thoracic limbs. The animal can also seize larger objects by raptorial movements of the appendages but in the laboratory "no hunting or stalking of prey takes place" (Mauchline, 1959).

Discussion

Over the years there has been considerable speculation regarding the role of bioluminescence in the life of various marine organisms. In higher marine forms, luminescence has been found associated with either mating behavior, feeding mechanisms, or defense. Among planktonic species, however, there is less agreement as to its functional significance. Besides the three interpretations given above, it has been suggested that this phenomenon may often be coupled with other life processes in lower animals and therefore might have no function of its own (Russell and Yonge, 1928; Harvey, 1929). It has also been suggested that luminescence in planktonic and sessile creatures may serve as a "burglar alarm," thereby revealing a predator to its own enemies along the food chain (Burkenroad, 1943).

From the results of the behavior experiments with *Metridia,* it is apparent that there is some relationship between luminescence and the act of predation. Since the exact nature of the stimulus is still unknown, it is impossible to determine positively which, if any, of the above hypotheses is applicable. Nevertheless, some of the possibilities may be eliminated.

Any functional use of luminescence involving species recognition, such as mating display or warning systems to other individuals of danger, is doubtful because *Metridia* probably does not have an adequate image-forming eye. Of the remaining speculations presented above, the authors currently feel that the defense mechanism is the one most consistent with the experimental results. However, Burkenroad's hypothesis is not specifically ruled out.

The reasons for favoring the idea of an escape mechanism arise from: (1) certain of the physical and physiological characteristics of *Metridia's* luminescent emission, and (2) a unique pattern of behavior associated with luminescence in this copepod.

The maximum intensity of *Metridia's* luminescence is surprisingly brilliant. At the working distance (18 cm.) used in this study the flash was of the same order of magnitude as that of certain coelenterates and of the crustacean *Euphausia pacifica,* and greater than that of the teleost *Myctophum punctatum,* all measured at 1 cm. (Nicol, 1960). The duration of the flash is long and its spectral composition is similar to the spectrum of the transmission of light through sea water with the maximum of the two curves at nearly the same wave-length. It has also been shown that *Metridia* has an extremely short lag time between stimulus and response. The animal recovers quickly after stimulation and fatigues rather slowly on repeated stimulation, even after several weeks without food, suggesting that the ability to luminesce is important enough to the organism to be maintained under adverse conditions. All these characteristics of *Metridia's* luminescence, both physical and physiological, would certainly be selectively advantageous to the animal if its luminescence functioned as an escape mechanism.

The most significant evidence for the defense mechanism hypothesis, however, comes from observations of the behavior of single *Metridia* stimulated in the electrode chamber. On stimulation a point of luminescence was immediately produced and then in the majority of cases the animal appeared to dart off into the dark, leaving a bright luminescent spot at its original position and sometimes a trail of tiny luminescent specks that soon disappeared. Although the animal itself could not be seen during this reaction, the agitation of the water gave a clue to its behavior and its new position could be verified by passing a second electrical stimulus through the water and observing the new location of the resulting luminescent flash. The original luminescent emission remained a more or less discrete point of light for some seconds after stimulation.

Such a behavior pattern appears to the authors to indicate the manner in which *Metridia* escapes from *Meganyctiphanes.* Although the precise role that luminescence plays in this escape mechanism is still unknown, two speculations are possible. The luminescent emission may startle the attacker, interrupting its feeding procedure, or it may merely function as an attractive decoy. In either case, the *Metridia's* rapid departure from the spot where it had luminesced would complete the escape.

The possibility that luminescence only occurs when the *Metridia* is actually captured is not entirely eliminated. More definitive proof must await the elucidation of the specific stimulus that induces luminescence. Nevertheless the evidence presented here indicates that luminescence functions on the behavioral level as an escape mechanism for *Metridia*. It would then seem probable that luminescence, which is of such widespread occurrence in the oceans, may well have survival value in defense against predation in some similar manner for many other animals of the plankton.

SUMMARY

1. Skin glands believed to be the source of luminescence were found on the anterior portion of the head, on the last thoracic segment, and on the posterior margins of each segment of the abdomen.

2. The maximum intensity of the luminescent flash was 1.2×10^{-3} μw./cm.^{2} (at 18 cm.). The flash rose rapidly to peak intensity and then decayed slowly. The total duration of the flashes with peaks greater than 10^{-4} μw./cm.^{2} ranged from 3 to 50 seconds.

3. The peak of the luminescence spectrum occcurred at 482 mμ and the curve fell off to one-half the maximum value at 440 mμ and 525 mμ.

4. The ability of *Metridia* to luminesce on stimulation was found to be largely unaffected by prolonged laboratory culture. Starvation had little effect on the luminescence for the first three weeks and there was never any inhibition by previous light- or dark-adaptation.

5. With an increase in the strength of the electric stimulus from 0.3 amp. to 0.7 amp., the intensity of the luminescent flash was found to increase. With pulses stronger than 0.7 amp. no change in intensity was recorded but the number of successive responses to repeated stimuli was reduced. Duration of the pulse had little effect on the intensity or the number of successive responses.

6. *Metridia* showed a lag time of 8–10 msc. to the beginning of the luminescent response. The lag time to the peak of the luminescent response varied from 20 to 60 msc.

7. There was no spontaneous luminescence produced by groups of *Metridia* under conditions of constant darkness. However, the presence of certain planktonic predators, most notably *Meganyctiphanes norvegica,* caused a brilliant display of luminescence. The number of flashes attributable to *Metridia* was always greater than the number of *Metridia* eaten by the predator. There was little evidence that the luminescent euphausiid, *Meganyctiphanes,* flashed spontaneously either in the presence or absence of its prey.

8. Observations on the behavior of *Metridia* during and just after luminescence suggest that the flashing may be involved in an escape mechanism, but the precise effect of the light on the predator has not been determined.

LITERATURE CITED

BIGELOW, H. B., 1924. Plankton of the offshore waters of the Gulf of Maine. *Bull. U. S. Bur. Fish.,* **40**: pt. II, 509 pp.

BODEN, B. P., AND E. M. KAMPA, 1957. Records of bioluminescence in the ocean. *Pacific Sci.,* **2**: 229–235.

BODEN, B. P., AND E. M. KAMPA, 1958. Lumière, bioluminescens et migrations de la couche diffusante profande en Méditerranée occidentale. *Vie et Milieu,* **9**: 1–10.

BOECK, A., 1865. Oversigt over de ved Norges kyster iagttage Copepoder henhorende til Calanidernes Cyclopidermes og Harpactidernes familier. *Forh. Vidensk. Selsk. Krist.,* **7**: 226–282.

Breslau, L. R., 1959. The portable bathyphotometer. Unpublished manuscript. Reference No. 59–28, Woods Hole Oceanographic Institution.

Breslau, L. R., and H. E. Edgerton, 1958. The luminescence camera. *J. Biol. Photogr. Assoc.*, **26**: 49–58.

Burkenroad, M. D., 1943. A possible function of bioluminescence. *J. Mar. Res.*, **5**: 161–164.

Clarke, G. L., 1933. Diurnal migration of plankton in the Gulf of Maine and its correlation with changes in submarine irradiation. *Biol. Bull.*, **65**: 402–436.

Clarke, G. L., 1934. Further observations on the diurnal migration of copepods in the Gulf of Maine. *Biol. Bull.*, **67**: 432–455.

Clarke, G. L., 1954. Elements of Ecology. John Wiley and Sons, New York.

Clarke, G. L., and R. H. Backus, 1956. Measurements of light penetration in relation to vertical migration and records of luminescence of deep-sea animals. *Deep-Sea Res.*, **4**: 1–14.

Clarke, G. L., and L. R. Breslau, 1959. Measurements of bioluminescence off Monaco and Northern Corsica. *Bull. Inst. Oceanogr., Monaco,* **56**: (1147): 31 pp.

Clarke, G. L., and L. R. Breslau, 1960. Studies of luminescent flashing in Phosphorescent Bay, Puerto Rico, and in the Gulf of Naples using a portable bathyphotometer. *Bull. Inst. Oceanogr. Monaco,* **57** (1171): 32 pp.

Clarke, G. L., and C. J. Hubbard, 1959. Quantitative records of the luminescent flashing of oceanic animals at great depths. *Limnol. Oceanogr.*, **4**: 163–180.

Clarke, G. L., and G. K. Wertheim, 1956. Measurements of illumination at great depths and at night in the Atlantic Ocean by means of a new bathyphotometer. *Deep-Sea Res.*, **3**: 189–205.

Dahl, F., 1893. Pleuromma, ein Krebs mit Leuchtorgan. *Zool. Anz.*, **16**: 104–109.

Dahl, F., 1894. Leuchtende Copepoden. *Zool. Anz.*, **17**: 10–13.

Farran, G. P., 1920. On the local and seasonal distribution of the pelagic Copepoda of the southwest of Ireland. Publ. Circ., Cons. Perm. Int. Explor. Mer, No. 73, 30 pp.

Giesbrecht, W., 1895. Über das Leuchten der pelagischen Copepoden und das tierische Leuchten in allgemeinen. *Mitt. Zool. Sta. Neapel,* **11**: 631–694.

Harvey, E. N., 1929. Phosphorescence. Encyclopedia Brittanica, 14th ed., p. 117.

Harvey, E. N., 1952. Bioluminescence. Academic Press, New York.

Kampa, E. M., and B. P. Boden, 1957. Light generation in a sonic-scattering layer. *Deep-Sea Res.*, **4**: 73-92.

Kiernik, E., 1908. Über einige bisher unbekannte leuchtende Tiere. *Zool. Anz.*, **33**: 376–380.

Lowe, E., 1935. The anatomy of a marine copepod *Calanus finmarchicus* (Gunnerus). *Trans. Roy. Soc. Edinb.*, **58**: 561–603.

Mauchline, J., 1959. The biology of the euphausiid crustacean, *Meganyctiphanes norvegica* (M. Sars). *Proc. Roy. Soc. Edinb.*, **67**: 141–179.

Nicol, J. A. C., 1960. The Biology of Marine Animals. Sir Isaac Pitman, London.

Russell, F. S., and C. M. Yonge, 1928. The Seas. Frederick Warne, London.

Sewell, R. B. S., 1932. The Copepoda of Indian seas. Calanoida. *Mem. Indian Mus.*, **10**: 407 pp.

Sewell, R. B. S., 1947. The free-swimming planktonic Copepoda. Systematic account. *Sci. Repts., John Murray Expd.*, **8**: 303 pp.

Vanhöffen, E., 1895. Das Leuchten von *Metridia longa* Lubb. *Zool. Anz.*, **18**: 304–305.

Contribution No. 1186

Reprinted from Annals of The New York Academy of Sciences
Volume 95, Article 1, Pages 225-234
October 5, 1961

PHYSICAL ASPECTS OF DEDUCED AND ACTUAL CLIMATIC CHANGE

E. B. Kraus

*Woods Hole Oceanographic Institution, Woods Hole, Mass.**

Introduction

The general circulation is driven by differential heating, but the distribution of the heat sources and sinks depends on the circulation in turn. The system is complex, and allows a large number of different transient modes. In particular, the short-term fluctuations associated with colloidal or hydrodynamic instabilities appear to be mainly random. They may be able to create conditions that favor the reappearance of similar pattern for some time, but there is no evidence that they can perpetuate themselves. This assumption—plausible but unproved—is basic to all existing theories of the general circulation or of climatic change.

Feedback effects might cause oscillations of the earth's surface-atmosphere-ocean system. Examples are the oscillations of ice caps discussed by Brooks (1949), or the variations of CO_2 content studied by Plass (1956). The characteristic time scale of these changes is probably too long, however, for them to be initiated by any transient individual circulation pattern.

Our basic assumption is equivalent therefore to a belief that external changes or long-term feedback effects will cause changes in the frequency of various circulation modes and consequently in the mean regime. This, in turn, will effect such characteristic aspects of the climate as mean cloudiness or mean snow cover. On the other hand, the exceptional weather situations or the freak individual season are not believed to exert a significant, finite influence over a period of decades on the future mean circulation pattern.

I shall discuss the character of circulation changes that might be expected to result from some slight changes in the mean distribution of some external variables. The expected changes then will be matched against actually observed climatic changes.

Radiation Balance and Heat Transports

The earth's surface gains heat, and the atmosphere as a whole loses heat, by radiation. Balance is maintained by air currents that transport heat from the surface upward to regions where it can be lost by infrared radiation into space.

The atmosphere can reduce the direct radiational heat loss from the surface into space because of its absorbing components: chiefly water, carbon dioxide, and ozone. If the amount of these gases was larger, the greenhouse effect would be stronger; that means the surface would tend to be warmer, more heat would necessarily be transported upward by air current, and more radiant energy would be emitted from the atmosphere. The radiational change would be most important at frequencies not fully absorbed in a thin air layer.

---

* Contribution No. 1186 from Woods Hole Oceanographic Institution.

There is an important difference between the radiative effects of these 3 absorbing gases. Carbon dioxide and water vapor, with a constant or upward-decreasing mixing ratio, cool the atmosphere at all levels. On the other hand, the mixing ratio of ozone increases upward in the troposphere, and the presence of this gas tends to heat the air there. Radiational cooling by ozone becomes effective only above the 30-km. level. Carbon dioxide and water vapor have an over-all destabilizing effect. Ozone radiation tends to destabilize the air near the ground and above 30 km.; it increases vertical stability through most of the troposphere and lower stratosphere.

Sensible heat is transported upward in the atmosphere by a rising of warm air and the simultaneous sinking of cold air. This process increases the overall static stability of the atmosphere and lowers its center of gravity. Conditions will remain steady if the upward heat transport and the resultant decrease in potential energy are compensated by differential nonadiabatic heating and if the generation of kinetic energy is equal to the frictional dissipation. A horizontal—or more precisely, an isobaric—flux of sensible heat does not generate kinetic energy.

The presence of horizontal heating gradients allows potentially warm air from low latitutides to spread above cold air from high latitudes. This causes the over-all stable stratification of the atmosphere. It gives the isentropic surfaces—that is, the surfaces of equal potential temperature—an upward slope from warm to cold regions and permits the development of quasi-horizontal baroclinic eddies.

From the work of Charney (1947), Eady (1949), and others it is known that this baroclinic instability is favored by a small vertical stability and large horizontal temperature gradients: a state characterized by relatively closely-spaced and steeply-sloping surfaces. We should expect, in this case, frequent, fast-moving disturbances of relatively small horizontal extent. On the other hand, if the ratio of downward to meridional potential temperature gradients is large, the isentropic surfaces will be more parallel to the earth's surface. Small perturbations will be resisted because vertically displaced air masses will lack buoyancy. Air has to come then from a great horizontal distance, where the temperature is sufficiently different, before it can become involved in a developing perturbation. Zonal propagation would be more sluggish, and we might expect a stronger development of blocking highs, monsoon circulations, and similar standing circulations: a condition that may be denoted as increased continentality.

Let p_h denote the pressure at the local mean upper limit up to which latent and sensible heat is being transported by air currents from below. Though closely related, p_h is not identical with the pressure of the tropopause. Particularly in low latitudes, penetrating convection causes a downward transport of heat just below the tropopause, and this makes the level of zero enthalpy flux slightly lower than the actual tropopause.

The correlation coefficient $c\{p_h, T_0\}$ between p_h and the surface temperature T_0 was shown by Goody (1949) to be negative. Therefore:

$$c\{p_h, T_0\} < 0 \qquad c\{\pi_h^*, \tau_0^*\} > 0 \tag{1}$$

where the bar denotes a space average over the whole planet at a moment of time, π_h^* is the horizontal variance of p_h and τ_0^* that of T_0.

Goody has shown also that the level of zero enthalpy flux would be raised in middle and high latitudes by an over-all increase in the CO_2 mixing ratio. It would be somewhat lowered over the tropics by more O_3 in the lower stratosphere. This means that the mixing ratio of both gases is negatively correlated with π_h^*; but an increase in O_3 would tend to increase p_h, while an increase in CO_2 would tend to reduce it.

The CO_2 mixing ratio and the O_3 mixing ratio at the tropopause level are both positively correlated with the mean surface temperature T_0. Their correlation with the meridional surface temperature gradient and therefore with τ_0^* is negative. In the case of ozone, this is accentuated by the larger concentration of this gas in high latitudes; in the case of CO_2, the 14-μ absorption band tends to have a more effective shielding action at lower temperatures. The decrease of the over-all static stability, which must be associated with any increase in the CO_2 mixing ratio should therefore be concentrated mainly in extratropical latitudes, and this would favor the development of baroclinic disturbances there.

Compared to p_h the distribution of surface pressure p_0 may be assumed to be approximately uniform ($\pi_h^* \gg \pi_0^*$). The over-all generation of kinetic energy $\dot{K}$ in the troposphere is given approximately by:

$$\dot{K} \sim k\hat{\bar{H}}[l_n(\bar{p}_0/\bar{p}_h) + \pi_h^*/2\bar{p}_h^2] \tag{2}$$

The constant k depends only on the surface area and upon constant thermodynamic properties of the air; H is the vertical flux density of sensible heat, with the circumflex denoting a weighted vertical average.

The flux density of sensible heat has not been determined directly from observation. An estimate could be obtained indirectly from Equation (**2**), because $\bar{p}_h$ and π_h^* are observable and the value of $\dot{K}$ can be assessed with some confidence from estimates of the energy dissipation near the earth's surface. This yields a value of $\dot{K} \sim 0.5 \times 10^{22} - 1.0 \times 10^{22}$ erg sec.$^{-1}$ and of $\hat{\bar{H}} \sim 2000 - 3000$ erg cm.$^{-2}$ sec.$^{-1}$.

The vertical transport of sensible heat in the troposphere is likely to increase with increasing surface temperature and decreasing stability. The correlation between $\hat{\bar{H}}$ and the solar irradiation of the surface or between $\bar{H}$ and the CO_2 mixing ratio should therefore be positive. The value of $\hat{\bar{H}}$ would be reduced by an increased ozone concentration in the lower stratosphere and the upper troposphere.

An increased solar irradiation of the earth's surface would tend not only to reduce the mean downward gradient of potential temperature but would also increase the mean meridional gradient. This should lead to an over-all increase in kinetic energy generation and particularly to a more active development of baroclinic disturbances. An increase in ozone would tend to have the opposite effect: as discussed above, the greater stability and reduced meridional temperature variance would favor standing circulations and other indices of continentality at the expense of moving cyclonic circulation in this case.

Finally, an increase of CO_2 would tend to increase H and reduce p_h but it would tend also to reduce π_h^*. From Equation **2** it may be seen that the first two factors would make $\bar{K}$ larger; the third one would make it smaller. The over-all effect is probably one of increased $\dot{K}$. The decreased stability in middle and high latitudes would favor the incidence of baroclinic disturbances there, and this tendency would be amplified further by the effect of water in the atmosphere.

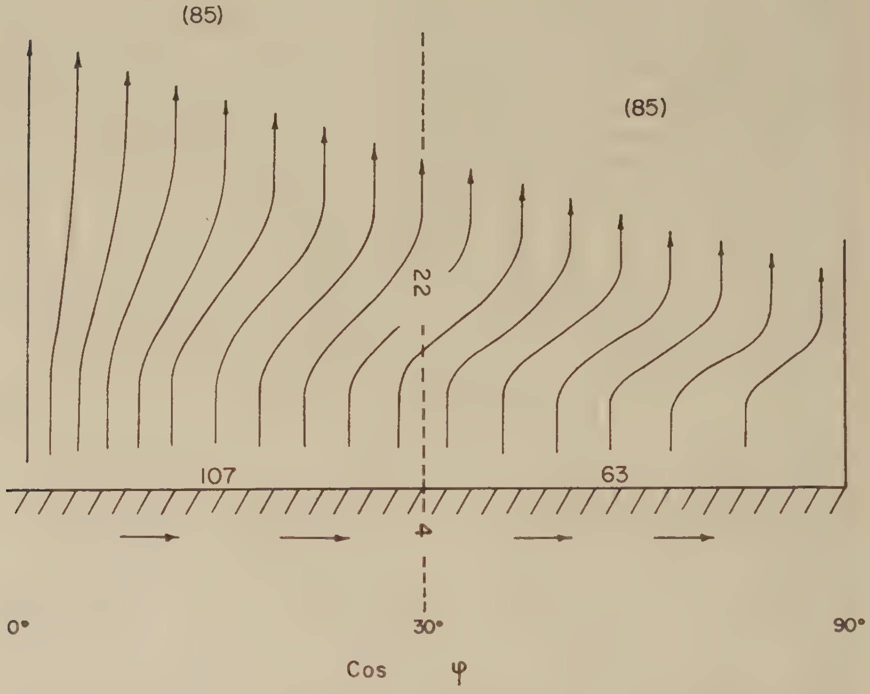

FIGURE 1. Schematic representation of heat transports in the northern hemisphere. Units are 10^{21} cal./yr.

The Circulation and the Hydrological Cycle

FIGURE 1 gives a schematic, order-of-magnitude representation of the latent and sensible heat transports in the troposphere and in the sea.

The net mean transport of heat across 30° N amounts to about 26×10^{21} cal./yr. Approximately 15 per cent of this transport, or 4×10^{21} cal./yr., is due to sea currents. The upward transport by air currents that originates at the surface amounts to about 340×10^{21} cal./yr. over the whole globe, or to about 10^5 erg cm.$^{-2}$ sec.$^{-1}$. Budyko (1956) states that about 82 per cent of this is latent heat, due to surface evaporation. The associated local heating of the atmosphere by condensation, as well as the radiative properties of the vapor itself and of the clouds, has a very large effect upon the distribution of heat sources and sinks, and therefore upon the circulation.

Both the CO_2 and the O_3 content of the atmosphere depend to some extent on factors that are independent of the circulation in the troposphere. The water vapor distribution on the other hand is so closely linked to atmospheric movements and temperature that it cannot be treated as an external influence. The amount of vapor that can be contained by the air decreases with decreasing temperature; it therefore decreases on the average upwards and polewards.

The radiational heat loss of the troposphere is closely related to the water vapor radiation from the layer immediately below p_h. The vapor pressure and temperature there cannot vary much with latitude. It is the mean temperature that would be registered by a celestial astronomer observing the earth in the 20 to 40 μ wave-length region. The total radiational heat loss through p_h appears to be more or less equally partitioned between the tropical and polar quarter of the troposphere, amounting to about 85×10^{21} cal./yr. for either, as indicated in FIGURE 1.

The radiational exchange between the atmosphere and the earth's surface also may be considered meridionally invariant as a first approximation. Although the surface radiates less energy at low temperatures near the poles, the back radiation from the atmosphere is reduced correspondingly because it originates from cold air layers that contain little water vapor. The net heat loss from the surface toward a cloudless sky may be estimated to be about 0.12 cal. $cm.^{-2}$ $min.^{-1}$ if the temperature is $-10°$ C. with a typical surface air vapor pressure of 3 mb.; it has the same estimated value of 0.12 cal. $cm.^{-2}$ $min.^{-1}$ if the temperature is 25° C. with a typical vapor pressure of 16 mb. The variations in the intermediate range are also small. The mean, area-weighted, zonal, heat loss by infrared radiation varies as a result by less than 20 per cent from its global average (Budyko, 1956). The variations that do exist are mainly due to the meridional variation in cloudiness.

As the infrared heat exchange between the atmosphere and the underlying surface is relatively invariant, the meridional variation of the surface radiation balance must be associated mainly with changes in the irradiation. The total radiation that reaches any latitude zone depends on the angle of the sun and on the cloudiness.

The relation between cloud amount and the radiation balance varies not only with the latitude but also with day and night or winter and summer. The amount of radiation that reaches the ground at any given point and time may be considered an approximately linear-decreasing function of the relative cloud amount n. On the other hand, the effective outgoing radiation appears to decrease with n^m, where $m \sim 1.5 - 2.0$.

In low latitudes the incoming radiation is so much larger than the outgoing radiation that any increase in cloudiness would cause a reduced surface radiation balance there. It can be estimated that at the time of the equinoxes this would apply anywhere between about 52° N and S. At 60°, however, a cloud amount $n > 0.7$ would increase the surface radiation balance; at 70° any value $n > 0.4$ would have the same effect. It follows that an increase in cloudiness would tend to reduce the surface temperature in low latitudes and would tend to increase surface temperatures at high and mid-latitudes, particularly in winter.

The over-all cloud amount can be expected to be positively correlated with $\dot{K}$. This is due to the relationship between cloudiness and vertical motion that in turn is related to $\dot{K}$. From the discussion in the preceding section it may be deduced therefore that the cloudiness is likely to increase if the intensity of solar radiation reaching the earth's surface became stronger. The cloudiness increase must be small enough for excess surface irradiation to remain positive. If that were not the case, the increased convection and clouds could not be maintained.

An increase in the CO_2 mixing ratio was expected to result in decreased stability and more frequent baroclinic disturbances in middle and high latitudes. The associated increase in cloudiness would reduce further the radiational surface heat loss there. It would contribute therefore to a decrease in the mean meridional surface temperature gradient.

An increase of tropospheric and lower stratospheric ozone would tend to reduce the incidence of clouds. A reduced mean cloud amount is likely to accentuate the temperature difference between the oceans and the continents favoring further an increased continentality.

If much water vapor is transported upward by air currents the precipitation and evaporation also must be relatively large. The heat of evaporation is withdrawn mainly from the ocean. Increased evaporation therefore would lead to lower ocean surface temperatures, particularly in low latitudes and vice versa. An increase in ozone would tend to suppress or reduce the air currents that remove heat and moisture from the sea surface in low latitudes. It is therefore likely to cause a reduced meridional evaporation gradient. The available potential energy would be used at the same time for the maintenance of large standing circulations with fewer, weaker traveling, extratropical cyclones. This would favor the occurrence of meridional sea currents, such as the Gulf Stream, which provide an effective mechanism for the poleward transport of the excess heat from the subtropics.

An increase in CO_2 would tend to increase the meridional evaporation gradient, and the relatively greater frequency of baroclinic disturbances is less favorable for the maintenance of strong meridional sea currents. A larger CO_2 mixing ratio would therefore probably cause a larger fraction of the meridional heat exchange to occur in the atmosphere, and a smaller fraction to occur in the sea. Any increase in the intensity of solar radiation is likely to have the same effect.

Comparison of Derived and Observed Climatic Changes

The argument of the two preceding sections is summarized in TABLE 1, which gives the expected sign of the correlation between characteristic circulation variables on the one hand and, on the other, the hypothetical variations of the solar constant, the CO_2 mixing ratio, or the O_3 mixing ratio at tropopause level.

Variations of total solar energy emission in excess of 1 per cent have not been observed, and are improbable on astrophysical grounds, but this does not affect the present argument, which deals only with derived terrestrial effects. It should be noted that a hypothetical increase in the solar constant or in the CO_2 mixing ratio would lead not only to increased mean surface temperatures but also to increased precipitation and decreased continentality. A reduction in the solar constant or in CO_2 content would of course have the opposite effect. Only changes initiated by ozone variations would cause increased surface temperature to be accompanied by reduced precipitation in low latitudes and vice versa.

The expected pattern of change, shown in TABLE 1, may now be compared with the actual pattern of change as derived from meteorological records over the past century. These actual changes have been summarized by, among others, Kraus (1958, 1960). They were characterized—up to about 1940—by an increase of approximately 0.01° C./yr. in the mean surface temperature. This increase appears to have been most pronounced in middle and high latitudes of the northern hemisphere, though it was not uniform in space or time even there. In low latitudes, precipitation decreased almost everywhere about the end of the last century. This decrease has received less attention than the temperature increase. It is therefore documented by FIGURE 2, which has been reproduced from one of the above-cited papers. The ordinate in this diagram represents the function

TABLE 1

EXPECTED SIGN VALUE OF CORRELATION BETWEEN CHARACTERISTIC CIRCULATION VARIABLES AND EXTERNAL VARIABLES

Mean value of characteristic circulation variables	Solar constant	CO_2*	O_3†
Surface temperature	+	+	+
Poleward surface temperature gradient	+	−	−
Tropopause height	+	+	−
Poleward tropopause slope	+	−	−
Precipitation	+	+	−
Poleward precipitation gradient	+	−	−
Baroclinic instability	+	+	−
Continentality	−	−	+
Ratio of atmospheric to oceanic meridional heat exchange	+	+	−

* Mean mixing ratio.

† Mean mixing ratio in lower stratosphere.

$$y(n) = 100 \sum_{l=1881}^{n} \left(\frac{r_l}{\bar{r}} - 1 \right) \tag{3}$$

where n is the running calendar year, l_1 the rainfall or stream discharge for the year l, and $\bar{r}$ the mean for the years 1881 to 1940. It is easily seen that y must be zero at the beginning of 1881 and at the end of 1940. The graph of y rises for $r_2 > \bar{r}$ and vice versa. It will be concave upward during the period when r is increasing with time, and convex when it is decreasing. The percentual deviation from $\bar{r}$ of the mean for any other period, for example, the years n to $(n + m)$, is given simply by $[y(n + m) - y(m)]/m$.

FIGURE 2 clearly indicates a higher precipitation level in the 19th century as compared with the first 40 years of the present century. The reduction of precipitation was associated with a reduced incidence of storms and a narrowing of the tropical rainfall belt. It is best observed on the tropical boundary of the arid zone, but was less pronounced or absent in the monsoon regions. Conditions there and in the center of the big continents at higher latitudes were characterized by an increase of the January-to-July pressure amplitude, which

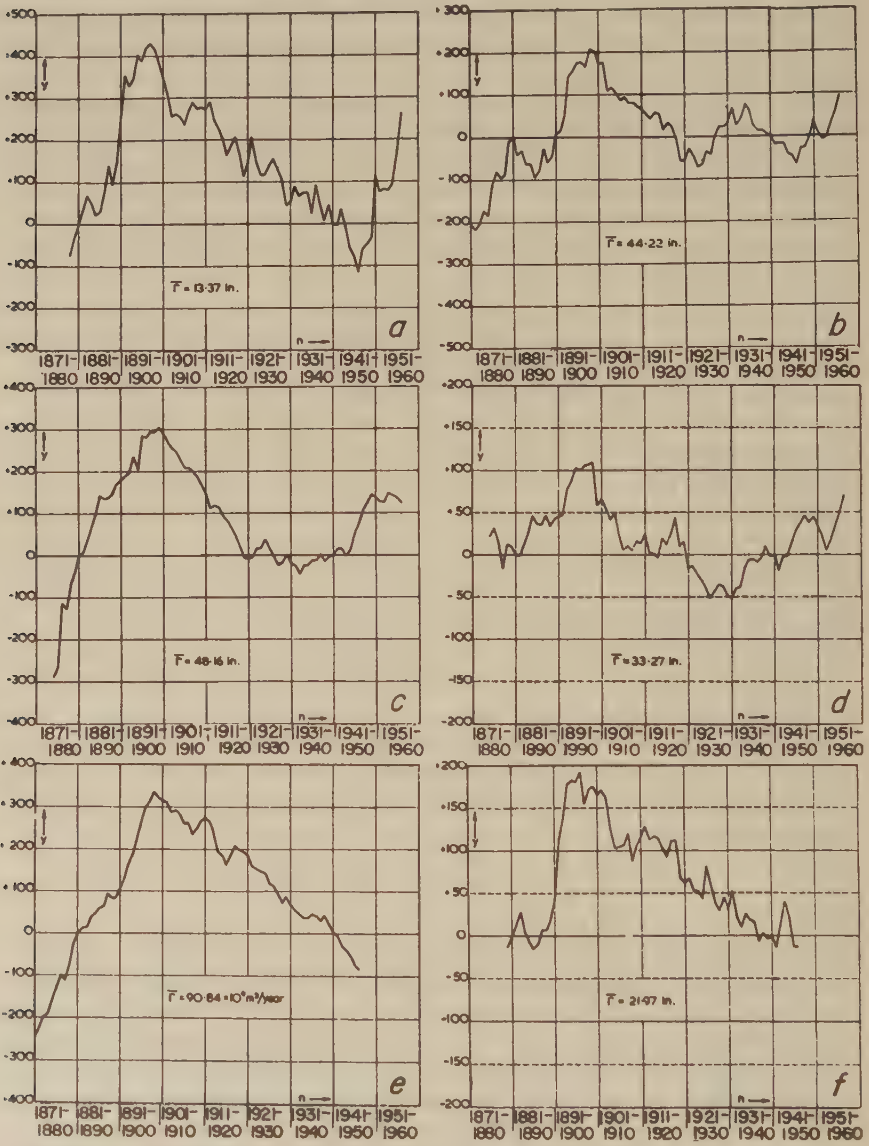

FIGURE 2. Cumulative percentual deviations from the 1881 to 1940 annual mean. Key: (*a*) N.W. New South Wales (Australian rainfall district No. 48); (*b*) Queensland Coast (Australian rainfall district No. 40); (*c*) Carolina Coast (mean of Charleston, S.C., and Cape Hatteras); (*d*) India (peninsula); (*e*) Nile river discharge at Aswan, Egypt; (*f*) Central Cape Province (South Africa rainfall district No. 16A).

suggests an increase in continentality. In the oceans, higher sea temperatures reported by Bjerknes (1959) and others were probably associated with decreased evaporative cooling in low latitudes.

During approximately the last 15 yr., the climatic trend appears to have been reversed. The warming in high latitudes seems to have ceased at least temporarily; at the same time most of the tropical regions and subtropical east coasts have become noticeably wetter again.

There is some evidence to suggest a Pleistocene glacial/pluvial sequence of basically the same character, although of larger amplitude than recent changes. Glacial ages were probably accompanied by wet conditions and therefore strong vertical heat flux in the tropics, and the end of the last ice age appears to have been associated with dryness at low latitudes and therefore with an increased meridional heat transport by sea currents.

If the arguments summarized in TABLE 1 are correct, it is not possible to explain either the pattern of recent climatic changes or the probable pluvial/glacial sequence of the Pleistocene by variations in the solar constant or in CO_2 content. Changes in the seasonal and meridional distribution of irradiation, caused by variations of the earth's orbital elements as calculated by Milankovitch, have not been considered here. They may have affected the Pleistocene sequence but they could not have produced the historic changes of recent times. The only type of variation that would be compatible with recent climatic changes—and that also could account qualitatively for the probable Pleistocene sequence—is the one initiated by ozone.

The quantity and the circulation of ozone in the upper stratosphere depends on solar ultraviolet radiation, which is known to vary to some extent, particularly at the shorter wave lengths. This suggests a possible link between climatic changes and the sun. However, any hypothesis would be on uncertain grounds until we know whether the existing ultraviolet variations can in fact influence significantly the formation of ozone and its transport to tropopause level.

Historical observations of the ozone distribution with height and latitude are insufficient for a test of the present argument. However, ozone is believed to have been possibly an agent of climatic change because of its effect upon tropospheric stability and tropical tropopause height. These last quantities have now been observed for a number of years, and this may permit a test of the present deductions with the aid of now available meteorological observations.

The changes that might be expected from CO_2 are different from those assumed to have occurred during the last million years. The possible result of a greatly increased CO_2 content is, however, of some speculative interest. It would be associated not only with a decreased meridional temperature gradient but also—because of high tropical evaporation and high polar rainfall—with an increased meridional salinity gradient near the ocean surface. This conceivably could lead to a reversal of the meridional circulation in the sea. Relatively warm, but highly saline and therefore dense, water would sink near the equator, to be replaced by fresher surface water from higher latitudes. This would be associated with a much higher temperature at depth, which would contribute additionally to a very high atmospheric CO_2 content. Conditions of this type may have prevailed conceivably during a major part of the earth's history, when the bulk of the deep seas were known to have been in fact very much warmer than today.

Summary

The effect of external variations on the general circulation is discussed. Hypothetical variations of the solar constant would be positively correlated with mean surface temperature, mean meridional surface temperature gradient, mean tropopause height, and mean meridional slope of the tropopause. Variations in the CO_2 mixing ratio would be positively correlated with surface temperature and tropopause height; the correlation with the temperature gradient and the tropopause slope would be negative. The ozone mixing ratio at tropopause level also should be positively correlated with the surface temperature; correlation with temperature gradient, tropopause height and slope should be all negative.

The stability of the troposphere would be decreased by an increase in the solar constant or the CO_2 mixing ratio; it would be increased by additional ozone. Water vapor always tends to destabilize the air. Its presence requires additional upward transport of heat by air currents. Clouds reduce surface temperature in low latitudes and increase it in high latitudes. The correlation between the mean cloud amount and the surface temperature gradient is therefore likely to be negative.

Comparison shows that neither CO_2 nor solar constant variations are compatible with the pattern of recent climatic change, or with the probable pattern of the glacial/pluvial Pleistocene sequence. Variation of the O_3 mixing ratio in the troposphere and lower stratosphere would be compatible with the observed pattern, at least qualitatively. A large increase in CO_2 may be accompanied by a reversal of the meridional circulation in the sea, and this could explain the high temperatures of the deep oceans before the Pleistocene.

Acknowledgment

I am indebted to C. Rooth for discussion and helpful criticism.

References

Bjerknes, J. 1959. The atmosphere and sun in motion. : 65–73. Rockefeller Inst. Oxford Univ. Press, New York, N.Y. London, England.

Brooks, C. E. P. 1949. Climate Through the Ages. McGraw-Hill. New York, N.Y.

Budyko, M. I. 1956. The heat balance of the earth's surface, Leningrad 255 pages (Translation prepared by Office of Technical Services, U.S. Dept. of Commerce). Washington, D.C.

Charney, J. G. 1947. The dynamics of long waves in a baroclinic westerly current. J. of Meteorol. **4:** 135.

Eady, E. T. 1949. Long waves and cyclone waves. Tellus. **1:** 33.

Goody, R. M. 1949. The thermal equilibrium at the tropopause and the temperature of the lower stratosphere. Proc. Roy. Soc. London. **A197:** 488.

Kraus, E. B. 1958. Recent climatic changes. Nature. **181:** 666.

Kraus, E. B. 1960. Synoptic and dynamic aspects of climatic change. Q. J. Research Meteorol. Soc. **86:** 1.

Plass, G. N. 1956. The carbon dioxide theory of climatic change. Tellus. **8:** 140.

Contribution No. 1189

(*Reprinted from Nature, Vol.* 191, *No.* 4784, *pp.* 157–158,
July 8, 1961)

Evidence of an Eastward Equatorial Undercurrent in the Atlantic from Measurements of Current Shear

RECENTLY there has been speculation as to the existence of an equatorial countercurrent in the Atlantic Ocean similar to the Cromwell Current[1,2] in the Pacific. G. Neumann[3] has cited evidence for such a current from early observations (1911) of anomalous drift currents and from a re-analysis of dynamic heights from oceanographical data along the equator. In the first two weeks of March, 1961, during an extensive bathymetry survey of the mid-Atlantic Ridge along the equator, I was able to make a number of measurements of horizontal current shear in the upper 100 m. surface water. The shears obtained at different points over an area extending from 19° W. to 10° W. longitude and from the equator to 3° S. latitude do indicate the presence of an eastward flowing equatorial undercurrent. The measurements were made from the R.V. *Chain* during the first part of a three-month cruise to study oceanographical problems associated with the Romanche Trench and the equatorial mid-Atlantic Ridge.

The current shear was measured by a method suggested to me by W. S. Richardson of this Institution. Two pitotmeters were mounted at the top and bottom, respectively, of the 600-ft. towed chain which carried thermistor elements for the continuous temperature profiling system[4]. When the ship was under way at a normal speed of 11 knots the shallow pitotmeter was at a depth of 15 m. and the deep pitotmeter at a depth of 105 m. The water speed past each pitotmeter was determined electrically from a differential pressure transducer driven by the pitot. By manoeuvring the ship at constant speed (11 knots) around a box course I could measure the vector difference between the current velocity at the pitotmeter and the drift velocity (wind drift and surface current) of the ship at the surface. By subtracting the result of one pitotmeter from that of the other I could determine the vector difference or shear between the current velocities at the two pitotmeters.

The preliminary results of shear measurements are shown on the chart in the accompanying Fig. 1. Each vector represents a measurement and gives the magnitude and direction of the difference: $\left[\overrightarrow{V}\,(15\text{ m.})-\overrightarrow{V}\,(105\text{ m.})\right]$, where $\overrightarrow{V}\,(15\text{ m.})$ is the current velocity at a depth of 15 m. and $\overrightarrow{V}\,(105\text{ m.})$ is the

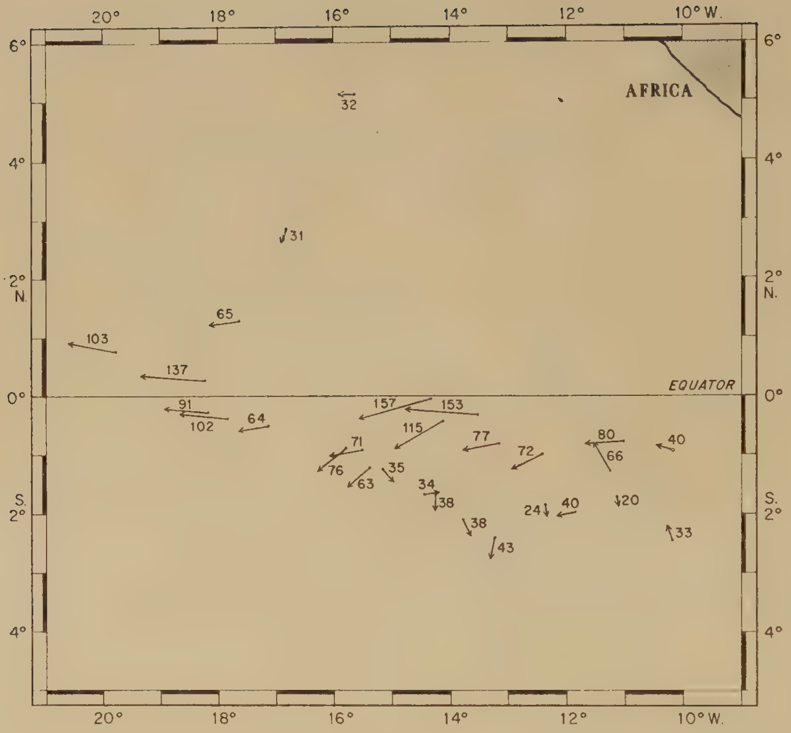

Fig. 1. Horizontal current shear $[V\ (15\text{ m.}) - \vec{V}\ (105\text{ m.})]$ measured near the equator during March 4–21, 1961 (shear magnitude in cm./sec. indicated beside each vector)

current velocity at 105 m. The magnitude of the shear in cm./sec. is indicated beside each vector. Clearly apparent in Fig. 1 is the unusually strong westerly shear of the 15-m. water over the 105-m. water along the equator. This shear was as high as 150 cm./sec. in two places. The shears shown give no information, of course, about absolute current velocities. However, determinations of the set of the ship while under way and while drifting indicate a current velocity at the surface of 40–60 cm./sec. to the westward at the equator. Because the current at 15 m. was about the same as that at the surface it is clear from the shears shown that the undercurrent at the 105-m.-level is toward the east along the equator and at some points as high as 100 cm./sec. The presence of this undercurrent was indicated very clearly during the lowering of a plankton net prior to a tow. When the net reached a depth of about 50 m. the wire angle changed drastically and stood out from the ship towards the east.

The shears shown in Fig. 1 indicate that the southern boundary of the undercurrent in these longitudes lies somewhere between 1° and 2° south latitude. The few measurements north of the equator show very little concerning the northern boundary of the undercurrent but suggest that the current is more or less symmetrical about the equator. The thermal structure of the water, which was recorded continuously throughout the survey to a depth of about 110 m., underwent an interesting transition whenever the ship crossed the boundary of the current. South of the current most of the total drop in temperature from 28° C. at the surface to 15° C. at 110 m. was concentrated within a very strong negative gradient at a depth of about 50 m. This gradient is the well-known equatorial discontinuity layer. Along the equator, however, the drop in temperature was distributed evenly from the surface to 110 m. with an approximately constant negative gradient.

This work was carried out under contract with the Office of Naval Research (*Nonr*-1367).

Measurements of the undercurrent are continuing aboard the R.V. *Chain* in this area at the time of writing. Detailed measurements of the undercurrents velocity profile are being made using current meters and current drogues by C. Parker.

ARTHUR D. VOORHIS
Woods Hole Oceanographic Institution, Mass.

[1] Cromwell, T., Montgomery, R. B., and Stroup, E. D., *Science*, **119**, 648 (1954).

[2] Knauss, J. A., *Deep-Sea Res.*, **6**, 265 (1960).

[3] Neumann, G., *Deep-Sea Res.*, **6**, 328 (1960).

[4] Hubbard, C. J., and Richardson, W. S., Woods Hole Oceanographic Institution Ref. No. 59-16 (1959).

Printed in Great Britain by Fisher, Knight & Co., Ltd., St. Albans

Contribution No. 1191

(*Reprinted from Nature, Vol.* 192, *No.* 4802, *pp.* 518–521,
November 11, 1961)

BIOLUMINESCENCE IN THE SURFACE WATERS OF THE SEA

By RICHARD H. BACKUS, CHARLES S. YENTSCH
and ASA WING

Woods Hole Oceanographic Institution, Woods Hole,
Massachusetts

RECENT work by Clarke *et al.*[1–4], who have lowered photomultiplier tubes to great depths at sea, have shown that flashing by bioluminescent organisms is present in varying degree at all depths in all localities of the ocean so far examined. Clarke's instrument detects bioluminescence resulting from the combined activities of a variety of organisms and only measures bioluminescence when the ambient light-level is low enough not to mask the flashes.

In order to make observations of bioluminescence independent of ambient light conditions we have devised an apparatus in which water from the sea surface is pumped at the rate of six gallons per minute through a darkened chamber fitted with a photomultiplier tube (*RCA* 6655–*A* with *S*11 spectral response). The tube is connected by appropriate circuiting to a recorder such that organisms luminescing while passing through the chamber are tallied and their numbers recorded at the end of either a 5-min. or a 1-hr. period. The effluent of the chamber may be strained with plankton nets for collecting its fauna and flora.

The plumbing system (Fig. 1) consists of the pump (Jabsco 2187), plastic intake and discharge hoses ½ in. in inside diameter, the viewing chamber (where the stream of water is about 2 in. wide and ¼ in. deep) and a flow-meter. The length of the intake hose was about 13 ft. in a harbour installation and about 50 ft. in a shipboard installation. In the harbour apparatus it took an organism somewhat more than 1 sec. to pass from the intake to chamber and in the shipborne apparatus about 5 sec. The intake of bioluminescent organisms into the plumbing system stimulates them to flash. Some flash at the point of intake and others all along the hose between intake and chamber, but, as our observations show, many flash in the chamber where the flow pattern is radically altered.

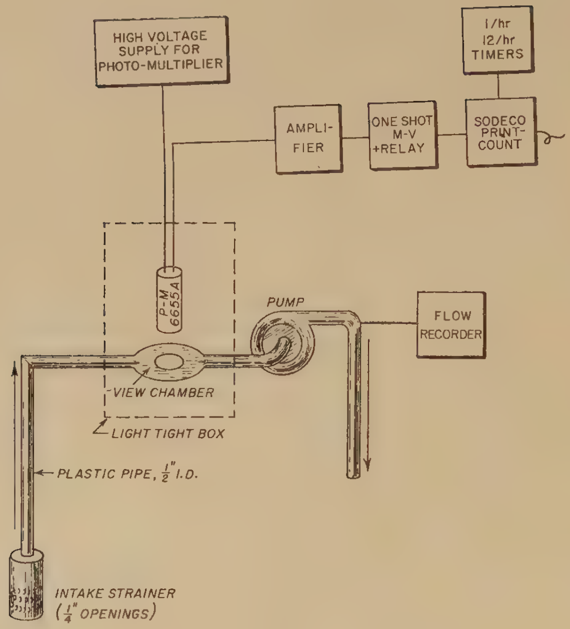
HIGH VOLTAGE SUPPLY FOR PHOTO-MULTIPLIER
1/hr
12/hr
TIMERS
AMPLI-FIER
ONE SHOT M-V +RELAY
SODECO PRINT-COUNT
P-M 6655A
PUMP
FLOW RECORDER
VIEW CHAMBER
LIGHT TIGHT BOX
PLASTIC PIPE, $\frac{1}{2}$" I.D.
INTAKE STRAINER ($\frac{1}{4}$" OPENINGS)

Fig. 1

At the shore installation counts were recorded by either a Hewlett–Packard print-out counter (Counter 523 *BN* and Printer 560–*A*) or a Sodeco 1*Tpb*53 print-out counter. At sea, counting was done with a simple solenoid-operated Sodeco counter which was read at appropriate times and re-zeroed.

Counts of flashes for 1-hr. periods for five days each in May and November 1960, in Great Harbor, Woods Hole, are shown in Fig. 2. A pronounced diurnal rhythm in activity is obvious. In May, maximum, or night-time, counts were about 700 times the minimum, or day-time counts, while in November these differed by a factor of about 100. Details of the rapid increase in count which occurs at sunset are shown in Fig. 3.

Table 1. Bioluminescence Counts (Period Totals) and Numbers of Organisms (per m.^{3} of Effluent) in Great Harbor, Woods Hole, December 2, 1960

Time (E.S.T.)	Bioluminescence	Diatoms*	Dinoflagellates†	Tintinnids*	Copepods‡
1330–1500	52	35,600	1,425	3,560	2,140
1730–1900	6,120	156,200	6,500	4,130	3,440

* Not luminescent.
† All (?) species luminescent.
‡ Some species luminescent.

Table 2. STATION DESCRIPTIONS

Station	Position	Date (1960)	Time (E.D.T.)	Depth* (fm.)	Surf. Temp. (°F.)
A	40° 39′ N., 72° 30′ W. to 40° 35′ N., 72° 41′ W.	Sept. 20	1230–2115	19–21	66·5
B	40° 29′ N., 72° 40′ W.	Sept. 21	0110–0130	24	62·8
C	40° 20′ N., 72° 39′ W.	Sept. 20–21	2310–0010	25	64·0
D	40° 06′ N., 72° 37′ W.	Sept. 21	0420–0445	29	—
E	39° 35′ N., 72° 32′ W. to 39° 23′ N., 72° 45′ W.	Sept. 21	1115–2100	44–50	65·4
F	38° 55′ N., 72° 34′ W.	Sept. 22	0055–0130	920–970	73·5
G	38° 28′ N., 72° 27′ W.	Sept. 22	0425–0450	1,470–1,475	74·8
H	37° 35′ N., 72° 15′ W. to 37° 26′ N., 72° 23′ W.	Sept. 22–23	1215–0730	1,680–1,760	71·9

* Bioluminescence observations and plankton samples were all taken from 1 m. under the surface.

Here counts every 5 min. are plotted relative to sunset for two days each in May and November 1960 and show that prior to sunset more bioluminescence occurred in May than November.

A No. 20 plankton net was used to strain the effluent for 1½ hr. at the time of minimum count and again for the same period at the time of maximum count on December 2, 1960. Counts of the principal groups found and the bioluminescence counts are given in Table 1. The numbers of organisms deemed potential sources of bioluminescence increased at night by factors of about 1·2–5. While a part of the increase in numbers of organisms in the night sample may be due to vertical migration, the species composition was quite different from that during day, which suggests that the water mass changed between sampling times.

Similar observations of bioluminescence were made at eight stations (Table 2) in the continental shelf and slope waters south of New England in September 1960. The plankton community was collected simultaneously by passing the effluent of the pump through a No. 20 plankton net. Three stations (*A*, *E* and *H*) were occupied for 6–10 hr., including the time of sunset, in order to study the diurnal variation of bioluminescence. The other five were used with these three for studying the geographical changes in night-time bioluminescence over the onshore–offshore section.

At stations *A*, *E* and *H* a diurnal rhythm in bioluminescence was observed similar to that described for Great Harbor. The observations for station *H*

Table 3. BIOLUMINESCENCE COUNTS (HOURLY TOTALS) AND NUMBERS OF ORGANISMS (PER M.^{3} OF EFFLUENT) AT STATION *H*

Time (E.D.T.)	Bio-lumin-escence	Diatoms	Dino-flagel-lates	Green flagel-lates	Tin-tinnids	Copepods
1400–1500	15	1,600,000	3,063	700,000	396	6,030
1600–1700	16	1,150,000	1,975	300,000	1,088	1,877
1800–1900	46	567,000	2,322	437,000	838	4,440
1900–2000	143	1,475,000	3,510	271,000	811	3,780

are shown in Fig. 4. Here, as at stations *A* and *E*, sharp increases in counting-rate were observed when the daylight intensity fell below about 500 foot-candles. This appeared to be true regardless of the magnitude of radiation during the day. Bioluminescence counts and counts of the principal organisms found in the effluent at station *H* during the afternoon and evening are shown in Table 3. Even considering the errors that may accrue due to plankton-counting techniques and to the loss of smaller organisms through the net it seems improbable that we would miss a vertical migration of plankton consistent with and of a magnitude sufficient to account for the diurnal changes in bioluminescence observed. Results at both stations *A* and *E* were similar.

Bioluminescence counts, counts of principal plankton organisms and amounts of net and total ('Millipore'-filtered) chlorophyll from the pump effluent during night hours at all stations are given in Table 4. Bioluminescence was at a maximum at *A*, the station nearest the coast, was low across the continental shelf (*B*–*D*) and rose to an intermediate value at the edge of the shelf (*E*) and remained moderately high at the stations in slope water (*F*–*H*). Numbers of dinoflagellates (mostly genus *Ceratium*) more or less

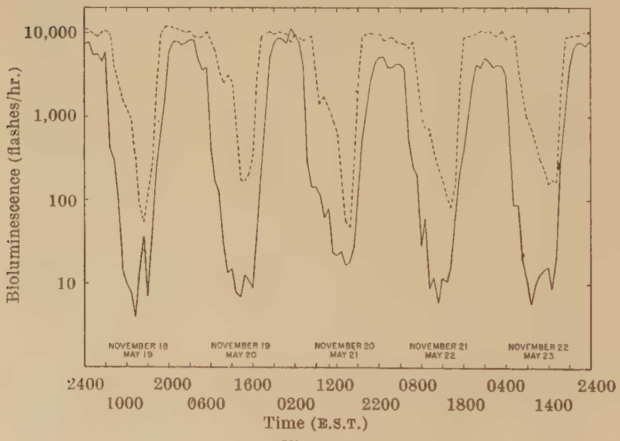

Fig. 2

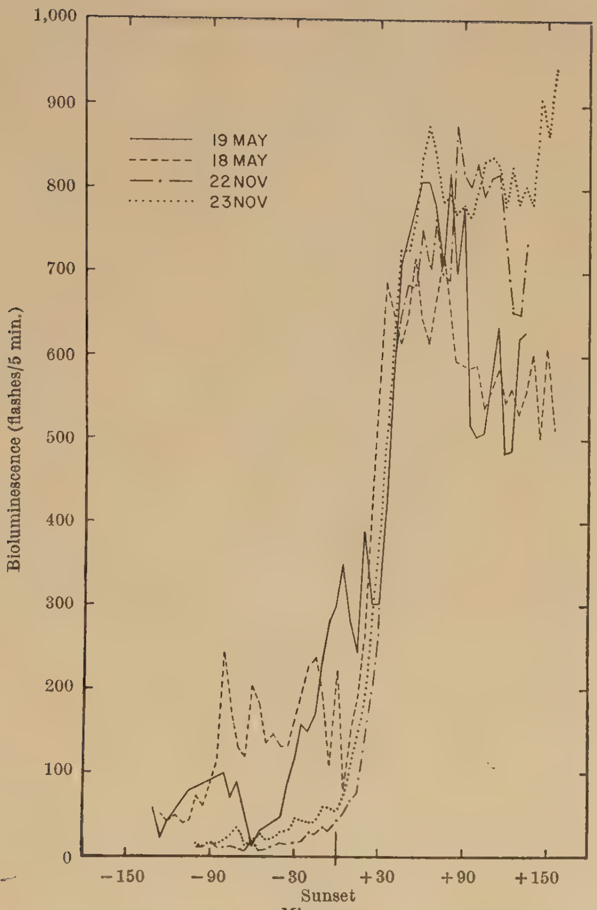

Fig. 3

followed this trend and it is probable that most of the bioluminescence we observed came from these organisms. The copepods were more numerous in slope water than at the stations on the shelf, but the cladocerans were present at the shelf stations and absent in the slope water. Tintinnids were absent at the shelf stations and present at the slope stations. The principal non-luminescent organisms encountered were diatoms. They were numerous on the shelf and, in general, diminished seaward except for the large population at station *H*. The distribution of total chlorophyll and net chlorophyll was also higher on the shelf than on the slope.

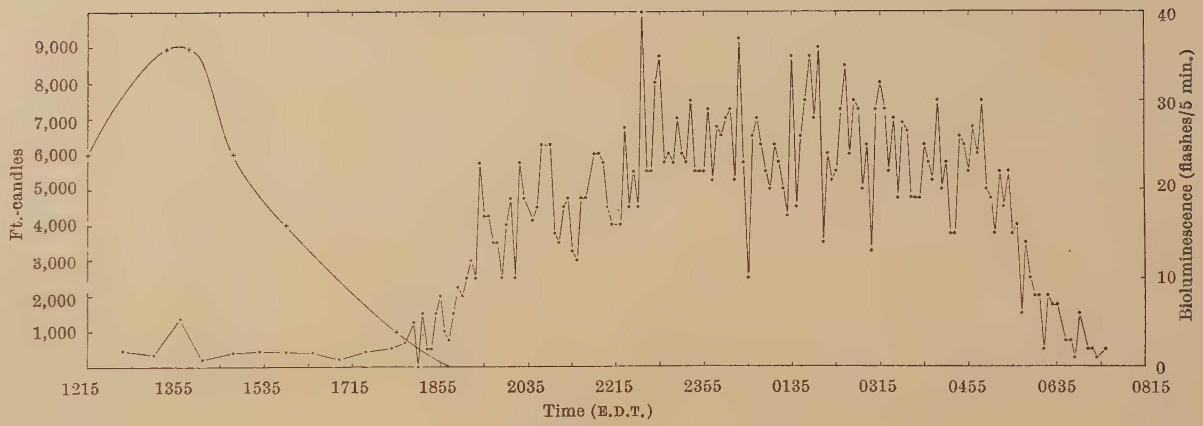
9,000
8,000
7,000
6,000
5,000
4,000
3,000
2,000
1,000
Ft.-candles
40
30
20
10
0
Bioluminescence (flashes/5 min.)
1215
1355
1535
1715
1855
2035
2215
2355
0135
0315
0455
0635
0815
Time (E.D.T.)

Fig. 4

Table 4. BIOLUMINESCENCE, PRINCIPAL PLANKTERS (NUMBER PER M.^{3}) AND CHLOROPHYLL (μGM./L.) AT STATIONS *A*–*H*

Station	Sampling period, E.D.T. (biolumin-escence)	Biolumin-escence* counts/5 min.	Sampling period, E.D.T. (plankton and chlorophyll)	Dino-flagellates	Copepods	Diatoms	Tintinnids	Cladocera	Chlorophyll†	
									Total	Net
A	1955–2115	33·2	2000–2100	514,000	1,710	32,600,000	—	2,020	0·36	0·0021
B	0110–0130	12·5	0108–0128	842,000	1,161	54,000,000	—	327	0·56	0·0063
C	2310–0010	1·9	2352–0012	2,000	1,183	53,000,000	—	312	0·37	0·0060
D	0420–0445	4·8	0420–0444	1,470	1,770	1,019,000	—	—	0·32	0·0020
E	1955–2100	16·0	2000–2100	4,370	5,400	8,010,000	344	98	0·21	0·0006
F	0055–0130	16·9	0113–0133	4,160	5,055	6,540	1,800	—	0·39	0·0018
G	0425–0450	12·7	0425–0445	1,839	4,500	3,150	1,300	—	0·21	0·0016
H	1955–2200	18·1	1900–2000	3,510	4,000	1,480,000	811	—	0·20	0·0013

* Flow-rate, 25 l./min.

† Chlorophyll determinations by the methods of Richards with Thompson (ref. 5) and Creitz and Richards (ref. 6).

It has been our experience that the larger dinoflagellates, which are important producers of bioluminescence, are missed when counts are made on raw sea-water samples of 100–200 ml., thus a fine plankton net had to be used to concentrate these organisms. We are aware that a great fraction of the phytoplankton passed through the No. 20 net[11]. Comparison of the net to total chlorophyll (Table 4) shows that the net entrained less than 1 per cent of all the photosynthetic autotrophs.

Our observations of the diurnal rhythm of bioluminescence are consistent with certain observations (summarized by Harvey[8]) of sea-water samples containing dinoflagellates held under various conditions of light and dark, and with recent observations of circadian rhythms of bioluminescence in laboratory cultures of dinoflagellates[9,10].

Seliger, Fastie and McElroy[7] have recently published observations of bioluminescence in Chesapeake Bay using an instrument which integrates light intensity over short periods rather than counting flashes. They observed no diurnal rhythm and concluded that changes in intensity throughout the water column were due to the vertical migration of organisms. In contrast, we feel that the diurnal pattern of bioluminescence observed by us largely results from the inactivation of the bioluminescent system of the organisms responsible by daylight. The discrepancy between the Chesapeake Bay and Woods Hole results may be due in part to the difference in instruments but more than likely comes mainly from the geographical difference.

This work was supported by the National Science Foundation (grant *NSF*–G9579 and grant *NSF*–G8339) and the Atomic Energy Commission (contract *AT*(30–1)–1918).

[1] Clarke, G. L., and Backus, R. H., *Deep-Sea Res.*, **4**, 1 (1956).

[2] Clarke, G. L., and Hubbard, C. J., *Limn. and Ocean.*, **4**, 163 (1959).

[3] Clarke, G. L., and Breslau, L. R., *Bull. Inst. Ocean., Monaco*, **1147**, 1 (1959).

[4] Clarke, G. L., and Breslau, L. R., *Bull. Inst. Ocean., Monaco*, **1171**, 1 (1960).

[5] Richards, F. A., with Thompson, T. G., *J. Mar. Res.*, **11**, 156 (1952).

[6] Creitz, G. I., and Richards, F. A., *J. Mar. Res.*, **14**, 211 (1955).

[7] Seliger, H. H., Fastie, W. G., and McElroy, W. D., *Science*, **133**, 699 (1961).

[8] Harvey, E. N., *Bioluminescence*, 128 (Academic Press, 1952).

[9] Haxo, F. T., and Sweeney, B. M., in Johnson, F. H. (edit.), *The Luminescence of Biological Systems*, 415 (Amer. Assoc. Adv. Sci., 1955).

[10] Sweeney, B. M., and Hastings, J. W., *J. Cell. Comp. Physiol.*, **49**, 115 (1957).

[11] Yentsch, C. S., and Ryther, J. H., *J. Cons. Int. l'Explor. Mer*, **24**, 231 (1959).

Printed in Great Britain by Fisher, Knight & Co., Ltd., St. Albans.

Contribution No. 1193

Benzpyrenes in Soil

Abstract. Benzpyrenes appear to be common and fairly abundant constituents of soils. Both the carcinogenic 3,4-benzpyrene and its inactive 1,2-isomer have been detected spectroscopically in extracts of soils from rural areas of the eastern United States.

Polynuclear aromatic hydrocarbons are commonly found in recent marine and nonmarine sediments (*1*, *2*). Evidence has now been obtained that both the strongly carcinogenic hydrocarbon 3,4-benzpyrene and its inactive isomer 1,2-benzpyrene are common and fairby abundant constituents of solids.

Table 1. 3,4-Benzpyrene in soils.

Origin and type of soil	Conc. (μg/kg)
Oak forest, West Falmouth, Cape Cod, Mass.	40
Pine Forest, West Falmouth, Cape Cod, Mass.	40
Mixed forest, West Falmouth, Cape Cod, Mass.	1300
Mixed forest, eastern Connecticut	240
Garden soil, West Falmouth, Cape Cod, Mass.	90
Plowed field, eastern Connecticut	900

A number of soils from rural areas of Massachusetts and Connecticut were analyzed. After the samples were dried to constant weight at 110°C, 50 g of each soil sample were weighed and extracted in a Soxhlet by benzene-methanol (1:1). The solvent was then removed in a rotating evaporator, and the remaining extract was treated with warm iso-octane-benzene (3:2). The soluble fraction was again dried, taken up in boiling iso-octane, and immediately adsorbed on an 8-ml column of alumina (Brockman II). The elution was carried out with a graded series of iso-octane-benzene mixtures. In some cases, yellow nonhydrocarbon materials broke through in the hydrocarbon-fractions; they were then removed by rechromatography under identical conditions. The hydrocarbons in the eluates were detected by ultraviolet spectrophotometry (Cary model 14 spectrophotometer); with a Sawicki chart (*3*) and a punched-card file of hydrocarbon spectra as aids in their identification. The spectra of 3,4-benzpyrene and 1,12-benzperylene, which both occur in soils, are very similar, but the presence of fine structure in the 383-mμ band together with a high 403-mμ band constitute conclusive evidence for the presence of 3,4-benzpyrene (*3*).

The hydrocarbon assemblage in all soil samples was found to be very similar even if the concentrations varied. The 1,2- and 3,4- isomers of benzpyrene were detected in all samples. Figure 1 is the spectrum of a typical benzpyrene fraction, contaminated with some chrysene (responsible for the background absorption) and some perylene (peaks at 434 and 428 mμ). The concentration of the biochemically active 3,4-benzpyrene was estimated from the intensity of the 403-mμ band (Table 1). In addition to the benzpyrenes, the following hydrocarbons were represented in all samples: phenanthrene, fluoranthene, pyrene, chrysene, perylene, and anthanthrene. Extensive rechromatography of the combined extracts provided evidence for the additional presence of anthracene, triphenylene, benzanthracene, benzfluorene, 1,12-benzperylene, and coronene.

Some soils may contain a much higher concentration of 3,4-benzpyrene than reported here. Kern (*1*), in his paper on the discovery of chrysene in some Swiss soils, describes the isolation of two additional hydrocarbons, not identified with certainty. The reported spectra and analytical data lead us to conclude that Kern already had isolated 3,4-benzpyrene [melting point: 171°C (benzpyrene: 177°C); molecular weight: 283 (benzpyrene: 252); log $\epsilon^{1\ \mathrm{percent}}_{1\ \mathrm{cm}}$ (at 296 mμ): 1.7 × 10^8 (benzpyrene: 2.2 × 10^8)]. According to Kern, this hydrocarbon was obtained in crystalline form with the remarkable yield of 21 mg/kg of soil.

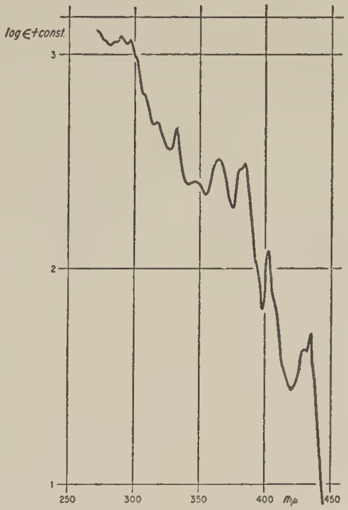

Fig. 1. Spectrum of a typical benzpyrene fraction, contaminated with some chrysene and some perylene (in iso-octane).

We believe that the occurrence of such hydrocarbon concentrations in rural soils distant from major highways and industries cannot be ascribed to fallout from polluted air. More likely, these hydrocarbons are indigenous to soil. They are among the pyrolytic products of wood and might be formed in soil by related low-temperature processes, as they also occur in the transformation of plant organic matter to peat and lignite. Alternatively, the hydrocarbons might be the products of the organisms which contribute their organic matter to the soils. These genetic mechanisms—if correct—imply that man has been in contact with carcinogenic hydrocarbons, not only during the industrial epoch, but during his entire history. It remains to be examined whether the concentration and availability of the benzpyrene in soil is sufficient to be of concern to those exposed to continued contact with soil (*4*).

MAX BLUMER
Woods Hole Oceanographic Institution,
Woods Hole, Massachusetts

References and Notes

1. W. Kern, *Helv. Chim. Acta* **30**, 1595 (1947).
2. W. G. Meinschein, *Bull. Am. Assoc. Petrol. Geologists* **43**, 925 (1959).
3. E. Sawicki, W. Elbert, T. W. Stanley, T. R. Hauser, F. T. Fox, *Anal. Chem.* **32**, 810 (1960).
4. This investigation has been supported by a research contract, NONR 2196(00), with the Office of Naval Research. This report is contribution No. 1193 of the Woods Hole Oceanographic Institution.

4 May 1961

Reprinted from: **Science**, 134 (3477); 474-475.

Contribution No. 1193
Woods Hole
Oceanographic Institution

Contribution No. 1194

Journal of Geophysical Research Volume 66, No. 7 July 1961

Some Heat-Flow Measurements in the North Atlantic[1]

John Reitzel

Woods Hole Oceanographic Institution
Woods Hole, Massachusetts

During the passage of R. V. *Chain* from Bermuda to Helsinki in July 1960, we made four determinations of the flow of heat through the sea bottom, in the fashion devised by *Bullard* [1954]. We measured the temperature gradient in the bottom sediments with thermometers in a cylindrical probe and found the thermal conductivity of the sediments near each station from a core sample. The results are given in Table 1.

TABLE 1

Station No.	1	2	3	4
N. Lat.	35°35′	35°35′	51°18′	53°53′
W. Long.	61°08′	61°15′	29°35′	24°05′
Water depth, m	4590	4680	3260	3350
dT/dz, °C/m	.062	.068	>.37	.073
K, 10^{-4} cal/cm sec °C	19.2		>17.	21.0
Q, 10^{-6} cal/cm² sec	1.20	1.31	>6.2	1.54

The gradients in this table are based on the temperature differences, extrapolated to long times, between two resistance thermometers in the bottom half of a steel probe of 3.2 cm outer diameter. These resistors were spaced 2.2 meters apart, with the lower resistor half a meter above the end of the probe. The higher one penetrated at least 1.8 meters into the sediments at every station, as was shown by the rise in its temperature over that of a resistor at the top of the probe. The ocean water about 100 meters above the bottom was taken to give a standard of zero temperature difference along the probe; this assumption is unlikely to lead to more than a per cent or two of error in the results.

Each value of K in the table is an average thermal conductivity along a core, reduced to sea-bottom pressure and temperature with the corrections given by *Ratcliffe* [1960]. The averages were taken from several direct measurements made in each core by the needle method described by *Von Herzen and Maxwell* [1959] supported by numerous determinations of water content.

The over-all experimental uncertainty in the heat-flow values is estimated to be about ±12 per cent, equally divided between uncertainties in the gradient and in the conductivity. Stations 1 and 2 are about 10 km apart, and both take their values of K from a single core taken between them. Part of the discrepancy between the two is probably due to local changes in thermal conductivity, and the mean of the two stations, 1.25×10^{-6} cal/cm² sec, is doubtless the best estimate of the heat flow in this vicinity. At station 3, the temperature gradient in the bottom exceeded the range of the instrument. No core was taken here, but we can safely suppose that the conductivity is higher than 17×10^{-4} cal/cm sec °C, to arrive at a lower limit for the heat flow.

The bottom near stations 1, 2, and 4 showed very little relief, though it had not the extreme flatness of a true abyssal plain. Station 3 was made on the mid-Atlantic ridge, in a small valley about 50 km northeastward of the main median valley, which could be plainly identified on our echo-sounding records. The high heat flow here is comparable to that observed by Bullard on the mid-Atlantic ridge at 47°N, as reported by *Hill* [1960]. A pipe dredge haul near station 3 brought up yellow mud with large and abundant shards of fresh volcanic glass, so it is evident that the excess heat flow here is accompanied by volcanism of Pleistocene or Recent date.

This work has been supported by a WHOI Associates' Fellowship and by contract Nonr 1367(00) with the Office of Naval Research.

---

[1] Contribution 1194 of the Woods Hole Oceanographic Institution.

REFERENCES

Bullard, E. C., The flow of heat through the floor of the Atlantic Ocean, *Proc. Roy. Soc. London A.*, *222*, 408–429, 1954.

Hill, M. N., A median valley of the mid-Atlantic ridge, *Deep-Sea Research*, *6*, 193-205, 1960.

Ratcliffe, E. H., The thermal conductivities of ocean sediments, *J. Geophys. Research*, *65*, 1535–1541, 1960.

Von Herzen, R., and Maxwell, A. E., The measurement of thermal conductivity of deep-sea sediments by a needle-probe method, *J. Geophys. Research*, *64*, 1557–1563, 1959.

(Received May 3, 1961.)

Contribution No. 1198

REPRINT FROM JOURNAL OF MARINE RESEARCH, VOLUME 19, 2, 1961

The Physiological Ecology of a Marine Diatom, Skeletonema costatum *(Grev.) Cleve*[1]

Herbert Curl, Jr., and Guy C. McLeod[2]
Woods Hole Oceanographic Institution
Woods Hole, Massachusetts

ABSTRACT

The marine plankton diatom, *Skeletonema costatum*, was isolated from local waters and cultured in enriched sea water. The effects of light, temperature, salinity, and concentrations of phosphorus and nitrogen on its growth and photosynthesis were determined separately and simultaneously. The effects of exocrine production by *Skeletonema* and grazing by copepods also were tested. The experimental results were used in developing an index of the photosynthetic potential of the diatom for seasonal hydrographic conditions found in the continental shelf waters south of Long Island.

Experimental results indicated that *Skeletonema* should have high photosynthetic rates and rapid cell division in late summer and early winter on the continental shelf by virtue of its responses to light and temperature alone. The usual concentrations of phosphorus and nitrogen on the shelf should not be limiting to this diatom.

The distribution and abundance of *Skeletonema* in 1956–1957 appeared to be in accord with predictions of potential photosynthesis except in offshore waters. Calculated photosynthetic rates and large standing crops occurred in late summer, decreasing toward late winter. The highest calculated photosynthetic rate in inshore waters was 29 °/₀ of the maximum rate, in July. The lowest calculated rates were for March through May.

Although the diatom ought to grow well offshore, it does not, apparently due to insufficient light during winter to support a stock for later growth. There is evidence that the lack of an undetermined nutrient also limits growth offshore.

Introduction. In natural phytoplankton populations, one algal species frequently predominates in numbers of individuals or in biomass. Such a situation may be taken as an indication of successful adaptation to prevailing environmental conditions, whether or not the species is an ecological dominant, in the sense of Shelford and Towler (1925). It should be possible to predict the physiological characteristics of an organism from its responses to the environ-

---

[1] Contribution No. 1198 from the Woods Hole Oceanographic Institution. This investigation was supported in part by a grant from the National Science Foundation (NSF 3892) and in part by a grant from the Atomic Energy Commission At(30-1)-1918.

[2] Present address: Carnegie Institute of Washington, Palo Alto California.

ment or, conversely, predict its responses in nature from physiological behavior in laboratory studies.

Frequently species that are important constituents of natural phytoplankton populations are singularly difficult to culture. However, *S. costatum* frequently is a major component of plankton blooms and grows extremely well in culture. It is present as far north as Thule, Greenland, and along the coast of the Gulf of Maine it is abundant and often "dominant" in summer and autumn (Bigelow 1926). It is the primary species in lower Narragansett Bay (Smayda 1957), Long Island Sound (Conover 1956) and Block Island Sound (Riley 1952), and has been very abundant in Chesapeake Bay (Cowles 1930) and at Beaufort, North Carolina (Manly 1953). In the Gulf of Mexico, it is abundant in spring and autumn though seldom if ever a primary species (Curl 1960). It seems to occur wherever plankton has been studied in coastal areas, except in the Arctic and Antarctic seas.

S. costatum was isolated in unialgal culture from Woods Hole Harbor in June 1957. Experiments were performed to study its responses to some of the chemical and physical variables important in local waters. Simultaneously, oceanographic cruises on the continental shelf south of Long Island yielded information on its distribution and abundance in natural populations, and associated hydrographic data. This paper correlates these laboratory and field observations.

Methods and Materials. Skeletonema was grown in enriched sea water (ESW), the composition of which is given in Table I. Sea water from Vineyard Sound, with an average salinity of 31 ‰, was filtered through a Millipore HA filter, enriched and autoclaved; its pH was 7.9–8.0 and its CO_2 concentration of 1.84 mmole; a five day supply of carbon at the maximum growth rates and cell concentrations used. The cultures were kept at 19–21°C under 10,000 lux illumination, and subcultures were made every fifth day. Rapidly growing cells, forming long chains, were used in the experiments.

TABLE I. CONCENTRATION OF ENRICHMENT ADDITIVES IN ESW MEDIUM (FORMULATED BY J. H. RYTHER).

Compound	Concentration	
	g/100 ml	mol. conc. μg–at/l
KNO_3	0.01	1000 NO_3–N
$Na_2HPO_4 \cdot 12\ H_2O$	0.002	50 PO_4–P
$Na_2SiO_3 \cdot 9\ H_2O$	0.0005	–
$Na_2S_2O_3$	0.00012	–
Ferric citrate	0.0003	–
Citric acid	0.0003	–
Vitamin B_{12}	0.12	–
Soil extract	0.5	–

Photosynthesis was measured by uptake of C^{14} according to the method of Steeman Nielsen (1952) as modified by Ryther (1954). The rates are expressed relative to the maximum value obtained in an entire series of experiments. The photosynthetic rate was determined after the cells had been exposed to the experimental conditions for periods which in different experiments lasted five or more days. The rates are therefore representative of the final experimental conditions in the culture.

RESULTS

Salinity. The effect of salinity on the rate of photosynthesis was studied in the range from 5–45°/oo. The Vineyard Sound sea water (31°/oo) was diluted with distilled water to give more dilute solutions; dried salt from local sea water was added to give higher concentrations.

Photosynthesis experiments, made one week after inoculation, showed the highest photosynthetic rates per cell at 15°/oo (Fig. 1). Considerable tolerance to higher salinities was evident. Throughout the salinity range of 11–40°/oo the rate of photosynthesis was at least half that of the maximum. When the salinity of the sea water was adjusted without adding nutrients, maximum photosynthesis occurred at 20°/oo. Both salinity and nutrients were diluted in the unenriched experiments, which may explain the lack of photosynthesis below 10°/oo. Carbon dioxide should not have been limiting at this concentration since 0.63 mmole/l was present initially.

Light and Temperature. Photosynthesis by cultures of *Skeletonema* in logarithmic growth phase was measured at temperatures from 5–30°C at light intensities varying from 0 to 36,000 lux. The incident light was attenuated

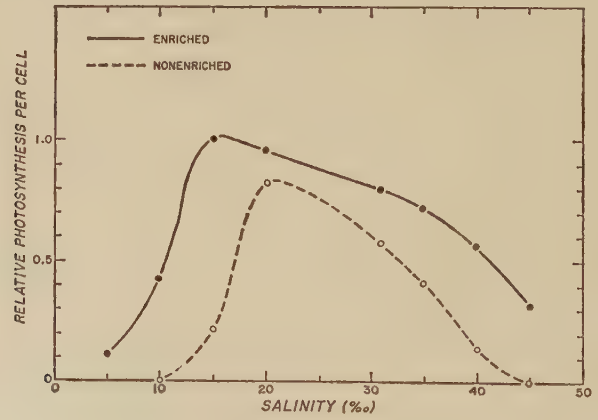

Figure 1. Relative photosynthesis in enriched and nonenriched sea water of varying salinities.

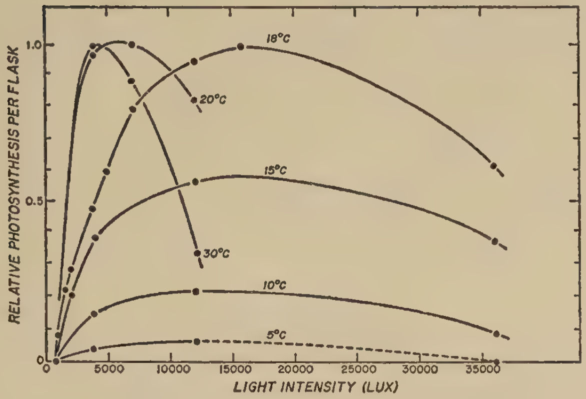

Figure 2. Relative photosynthesis as a function of light intensity at various temperatures.

with flat spectral distribution, neutral density filters. Replicates did not vary by more than 10°/₀; averages are plotted in Fig. 2. The point at which apparent zero photosynthesis occurs is the compensation intensity. In these experiments all of the curves can be extrapolated to a compensation intensity of about 1,000 lux.

At temperatures ranging 5–18°C, light saturation occurred at 12,000 to 16,000 lux. Below 18°C the rates decreased with temperature, but light saturation still occurred from 12,000 to 16,000 lux. Above 18°C the saturation intensity was reduced to 4,000–6,000 lux, and the range in which maximum relative photosynthesis took place became very narrow. The decrease in photosynthesis at high light and temperature may be a result of greatly enhanced cell respiration. Matsue (1954) found that the highest temperature tolerated by *Skeletonema* was between 37° and 40°C.

Nutrients. Experiments were conducted to determine the effect of varying concentrations of phosphorus and nitrogen upon photosynthetic ability. After a culture had passed the logarithmic phase of growth and the cells could be presumed to be deficient in nutrients, aliquots were inoculated into an ESW medium containing varying concentrations of phosphorus and nitrogen. After two days growth at 18°C and 8,000 lux, C^{14} was added and carbon uptake was measured at the end of two hours (Fig. 3). The rate of photosynthesis was higher with enrichment by either nitrogen or phosphorus concentration; for all phosphorus concentrations the increase in rate of photosynthesis as a function of nitrate increment was about equal. Since these experiments measured the "population" photosynthesis rates, the rates could increase with higher nutrient concentrations almost indefinitely as more biomass was produced. The scale of relative photosynthesis for the entire nutrient concentration

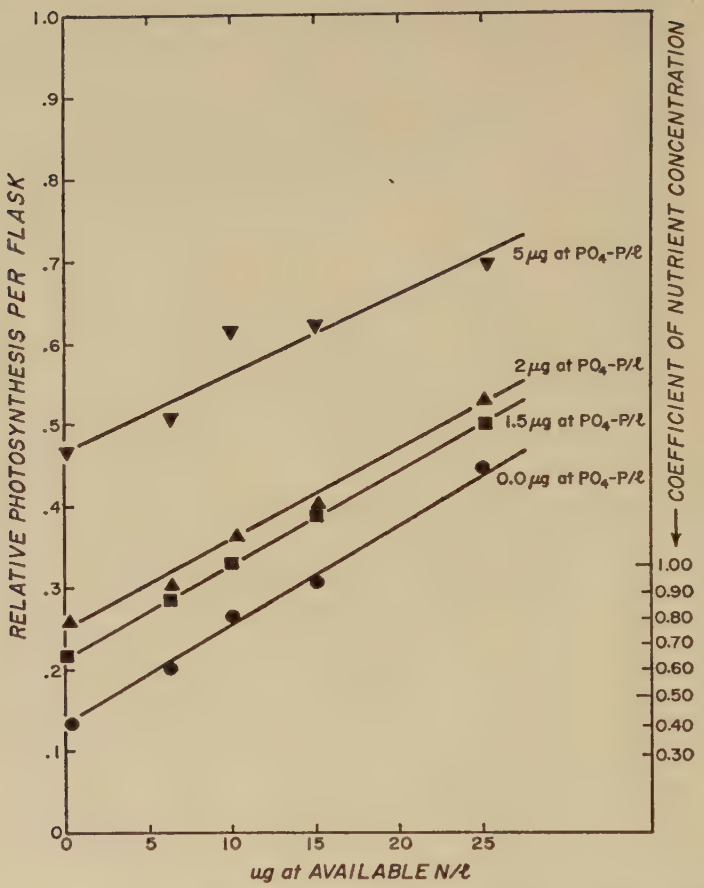

Figure 3. Relative photosynthesis as a function of low concentrations of phosphate phosphorus and available nitrogen. A scale of nutrient concentration coefficients replaces the scale of relative photosynthesis on the ordinate (see text).

range of the experiments has been discarded and a scale of nutrient concentration coefficients has been used in its place. The lower limit has been set at zero concentration. In order to have a coefficient of nutrient effect in the range 0–1.0, the upper limit has been set at the largest concentrations of phosphorus and nitrate that normally might be encountered in coastal Atlantic waters (0–1.0 μg-at available N/l, 0–1.5 μg-at PO_4–P/l) (Ketchum, *et al.* 1958).

Nutrients and Temperature. The effects of reduced amounts of nutrients on photosynthesis were studied at temperatures ranging from 5–30°C at a single light intensity (10,000 lux). Nitrate and phosphate were reduced to 0.1 the usual concentration, both separately and together. After inoculation from

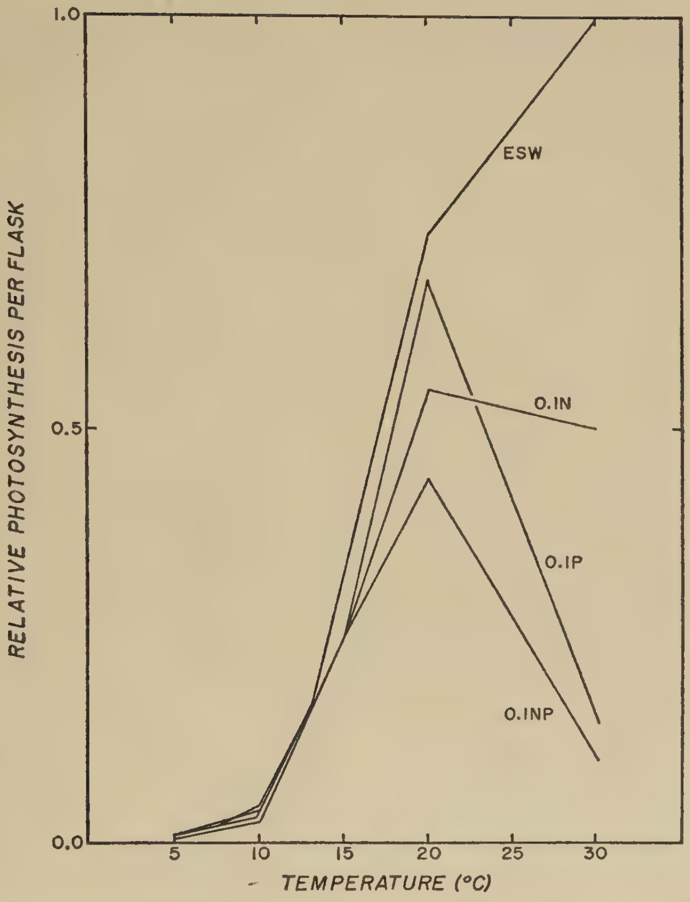

Figure 4. Relative photosynthesis as a function of temperature and nutrient concentration at 13,000 lux.

two-week old stock cultures, deficient in both phosphorus and nitrogen, the new cultures were equilibrated at the new temperature conditions for two days and then carbon fixation was measured for a two-hour period. Photosynthesis was at a maximum at 20°C at all nutrient dilutions (Fig. 4). The effect of reduced nitrogen alone was greater than reduced phosphorus at 20°C. The effect of reduced nutrients was greatest at the higher temperatures.

Studies of cell division rates at temperatures from 5–30°C were made at 13,000 lux in a complete medium and in a medium deficient in nutrients (Table II). Aliquots of a week-old culture growing in the ESW medium were inoculated into the ESW medium and into media deficient in nutrients, as used in the previous experiment. Cell counts were made daily until moribund

TABLE II. Maximum and Average Division Rates During the Logarithmic Growth-Phase of *Skeletonema costatum* Grown at 10,000 Lux and at Various Temperatures and Nutrient Concentrations for One Week*.

Medium	ESW		10% P		10% N		10% NP	
Temp. °C	max.	av.	max.	av.	max.	av.	max.	av.
30	4.28	0.94	3.17	1.02	4.25	1.19	1.35	1.05
20	4.28	1.21	3.45	1.35	4.35	1.22	3.17	1.24
15	3.17	1.24	3.27	1.28	3.17	1.24	1.66	0.89
10	–	0.47	–	0.50	–	0.51	–	0.51
5	–	0.21	–	0.0	–	0.08	–	0.01

* Division rate $k = \frac{1}{(t_2 - t_1)} \log_2 \frac{C_{t2}}{C_{t1}}$, where t = time in days and C_{t1} and C_{t2} are cell counts at beginning and end of the time $(t_2 - t_1)$.

cells were noted. The maximum and average division rates for the logarithmic portion of the curves are given in Table II. In the ESW medium the maximum division rate was 4.28 divisions per day at 20 and 30°C. This is the same value determined by Matsue (1954).

In a medium containing reduced phosphate, the fastest maximum division rate was observed at 20° (3.45) and the slowest at 30°C (3.17). The division rates in reduced nitrate were equivalent to those in full strength medium. Thus, decreased phosphate concentration was more effective than decreased nitrate concentration in lowering the division rate.

In reduced nitrate and phosphate, the division rates were lower than in any of the cultures maintained between 15° and 30°C. Under nutrient deficient conditions, the optimal temperature range for rapid cell division becomes narrower (stenothermal with respect to rate of cell division). The following division rates are recorded in the literature: 0.21–1.77 div./day during winter in nature (Riley 1952), 0.90–2.6 div./day at 10°C in culture (Braarud 1937, 1945).

Exocrines. In order to determine whether *Skeletonema* produces substances affecting its own growth or that of other algae, several liters of a week-old culture were centrifuged and the supernatant millipore-filtered. The filtrate was re-enriched and half was autoclaved for half an hour. Subcultures using both autoclaved and nonautoclaved aliquots were inoculated with *S. costatum*, *Chaetoceros ceratosporum*, *Corethron hystrix*, *Ditylum* sp. and *Phaeodactylum tricornutum.* Cell counts were made after inoculation and again after seven days incubation at 18°C under 7,000 lux (Table III).

In the autoclaved medium, *Skeletonema*, *Ditylum* and *Phaeodactylum* made good growth, *Chaetoceros* perished and *Corethron* grew slowly. In the nonautoclaved medium, *Chaetoceros* and *Ditylum* grew not at all and *Corethron* and *Skeletonema* required seven days to double their numbers. *Phaeodactylum*

TABLE III. Comparison of Seven-Day Growth Rates at 18°C, 7,000 Lux; Algae in Autoclaved and Nonautoclaved Filtrate from *Skeletonema* Cultures.

Diatom	Initial cell count (cells $\times 10^4$/ml)	ESW	Division per day autoclaved	Division per day nonautoclaved
Skeletonema costatum	4.0	1.2	1.1	0.04
Chaetoceros ceratosporum	0.75	1.0	0.0	0.00
Corethron hystrix	0.25	–	0.57	0.12
Ditylum sp.	0.03	–	0.81	0.00
Phaeodactylum tricornutum	2.2	1.0	1.0	0.60

showed the best growth, but this was equivalent to only 0.6 div./day. *Skeletonema* itself was also severely inhibited. *Chaetoceros* ordinarily grew well in an ESW medium but appeared to be extremely sensitive to substance(s) produced by *Skeletonema*.

Grazing. When plankton tows containing large quantities of *Skeletonema*, together with *Rhizosolenia*, *Nitzschia*, *Guinardia*, *Thalassionema*, and *Chaetoceros*, were set aside in the culture room, copepods (mainly *Acartia tonsa* and *Pseudocalanus* sp.) rapidly reduced the numbers of *Skeletonema*, leaving uneaten cells of *Rhizosolenia* which rapidly outgrew the other genera. *Skeletonema* seemed to be the favored food among the diatoms available, so far as these two species of copepods were concerned.

DISCUSSION

In comparing laboratory and natural populations, the environmental responses of an organism may be considered from different points of reference. In one, optimal growth conditions are determined in the laboratory and then similar conditions are sought in nature. Large populations would tend to occur where such conditions were found, and smaller populations elsewhere. However, the environmental and physiological conditions of the organism are changing with time. Riley, *et al.* (1949) attempted a prediction of productivity in nature based on laboratory results, taking these changing conditions into account by substituting into a differential equation.

Here an attempt is made to evaluate the potential productivity of *Skeletonema* on the continental shelf, on the basis of laboratory results, by determining the photosynthetic rates under the physical and chemical conditions obtaining at monthly intervals throughout the year. The potential or "predicted" productivity rates may be compared with the actual abundance and distribution of the populations in nature.

In our experiments, light and temperature were factors that interacted in such a way that they should be considered simultaneously. Salinity and the concentrations of available nutrients affect the photosynthetic rate, and the initial concentrations of phosphate and nitrate determine the size of the standing crop. *Skeletonema* inhibits its own growth when grown in dense cultures. Finally, the alga is consumed readily by some copepods.

To obtain data for natural conditions, the effects of salinity, light, temperature and nutrients on the potential photosynthesis of *Skeletonema* have been evaluated for the coastal waters south of Long Island, where observations were made during six cruises between September 1956 and September 1957. The data for adjoining stations have been combined and averaged over the depth of the wind-mixed layer, as determined by the pycnocline. This has been done separately for three depth ranges, *i. e.*, stations in water less than 100 m deep, between 100 and 500 m, and over 500 m. Values for months during which no observations were available were interpolated from smoothed seasonal curves.

For each group of stations the combined effect of light and temperature (Fig. 2) was determined as a per cent of the maximum photosynthesis obtained in the experiments (relative photosynthesis). Subsequently, the separate effects of salinity (Fig. 1) and of phosphate and nitrate (Fig. 3) were evaluated; the cumulative effects given by the product of each successive factor provided the potential productivity.

The average light intensity in the mixed layer was derived from the formula of Riley (1957), using Kimbal's (1928) tables. These data were reduced by 50°/₀ to eliminate the energy from wavelengths not available for photosynthesis. They have been converted from energy to intensity units by the relationship: 1 g cal/cm^2/min = 155×10^3 lux (Ryther 1956 b). The duration of daylight was taken from Baker (1938). Light attenuation coefficients were obtained either by secchi disc reading or by submarine photometer.

At the shallow stations (Table IV), on the basis of light and temperature alone, the highest potential photosynthetic rates occurred in July and September (72°/₀) and the lowest in midwinter (3–7°/₀). Introduction of the salinity effect decreases all monthly values without fundamental change in the pattern. The combined effect gives a maximum value of 57°/₀, and a minimum of 2.3°/₀. The nutrient effect further reduces these to 26°/₀ and 1.5°/₀. The same analysis has been applied to the results from the "intermediate" and deep stations (Tables V and VI). The cumulative effect of all factors shows that during most of the year the potential photosynthetic rates were higher at the intermediate stations than inshore. The potential ranged from 3–32°/₀ at the intermediate stations. At the deep stations the potential rates ranged from zero in winter, when the mixed layer was very deep, to values as high as 29–34°/₀ in summer and autumn.

The standing crops of *Skeletonema* observed in this case are shown in Fig. 5. The large populations observed from September through February correspond with the calculated high potential photosynthesis rates for the beginning of

TABLE IV. THE FRACTIONS (P) OF MAXIMUM PHOTOSYNTHESIS COMPUTED SUCCESSIVELY FOR TEMPERATURE AND LIGHT (t, i), SALINITY (s) AND NUTRIENTS (n). THE CUMULATIVE EFFECT (POTENTIAL PHOTOSYNTHESIS) IS GIVEN BY THE PRODUCT OF THESE (Ptisn).

DATA FOR STATIONS WITH WATER DEPTH OF 100 M OR LESS.

Date†	Light (lux)	Temp (°C)	P_{ti} (%)	Salinity (‰)	P_s (%)	P_{tis} (%)	PO_4–P (μg-at/liter)	Avail.N (μg-at/liter)	P_n (%)	P_{tisn} (%)	Calculated net C fixation (g/m²/day)	Per cent of total net photosynthesis	Net photosynthesis (g/m²/day)*
Sept.	7560	17	72	31.9	80	57	0.34	0.82	46	26	.131	84	.156
Oct.	6200	15	48	32.5	78	37	0.55	1.7	54	20	–	–	–
Nov.	2860	14	27	33.1	77	21	0.62	2.0	56	12	–	–	–
Dec.	2300	12	16	33.1	77	12	0.62	3.6	64	8	.596	101	.557
Jan.	2720	8	7	33.2	76	5.3	0.75	3.5	65	3	–	–	–
Feb.	2410	5	3	33.2	76	2.3	0.74	3.35	62	1.5	.072	13	.550
Mar.	6180	6	7	33.0	76	5.3	0.60	2.22	58	3	.000	0	.109
Apr.	8330	6	8	33.1	77	6.2	0.60	1.7	57	4	–	–	–
May	8520	8	16	33.1	77	12	0.48	1.25	50	6	.000	0	.106
June	7880	13	38	32.8	78	30	0.45	1.7	52	15	–	–	–
July	7200	17	72	32.5	78	56	0.33	1.8	51	29	.101	2	.500
Aug.	7400	16	60	32.6	78	47	0.33	1.5	50	24	–	–	–
Sept.	7610	16	63	32.7	78	49	0.32	1.01	50	25	–	–	–

* Calculated from Ryther and Yentsch (1958).

† Underlined months are those for which hydrographic data are available. Others are extrapolated.

TABLE V. THE FRACTIONS (P) OF MAXIMUM PHOTOSYNTHESIS COMPUTED SUCCESSIVELY FOR TEMPERATURE AND LIGHT (t, i), SALINITY (s), AND NUTRIENTS (n). THE CUMULTATIVE EFFECT (POTENTIAL PHOTOSYNTHESIS) IS GIVEN BY THE PRODUCT OF THESE (P_{tisn}).

DATA FOR STATIONS WITH WATER DEPTHS OF FROM 100 TO 500 M.

Date†	Light (lux)	Temp (°C)	P_{ti} (%)	Salinity (‰)	P_s (%)	P_{tis} (%)	PO_4–P	Avail.N	P_n (%)	P_{tisn} (%)	Calculated net C fixation (g/m²/day)	Per cent of total net photosynthesis	Net photosynthesis (g/m²/day)*
							(μg-at/liter)						
Sept.	8060	19	92	34.6	74	68	0.12	0.94	45	31	.001	0.5	0.19
Oct.	6590	18	77	34.4	74	57	0.20	1.50	48	26	–	–	–
Nov.	2090	15	25	33.4	77	19	0.40	2.50	54	10	–	–	–
Dec.	1670	15	15	34.0	74	11	0.50	4.15	64	7	.012	2	0.52
Jan.	1980	12	11	34.3	74	8	0.62	5.2	68	5	–	–	–
Feb.	1890	9	7	34.2	74	5	0.62	6.1	74	5	.025	15	0.16
Mar.	2600	8	9	33.8	76	7	0.52	3.42	60	4	.000	0	1.60
Apr.	2180	9	9	34.0	74	7	0.62	2.8	45	3	–	–	–
May	2240	10	10	34.1	75	8	0.41	1.05	50	4	.000	0	0.71
June	4810	13	32	33.8	76	24	0.30	1.00	50	4	–	–	–
July	7450	16	61	33.5	77	47	0.25	0.94	46	21	.000	0	0.37
Aug.	7330	17	72	33.9	76	55	0.35	2.00	52	28	–	–	–
Sept.	7900	17	73	34.3	74	54	0.52	3.1	60	32	–	–	–

* Calculated from Ryther and Yentsch (1958).

† Underlined months are those for which hydrographic data are available. Others are extrapolated.

TABLE VI. THE FRACTIONS (P) OF MAXIMUM PHOTOSYNTHESIS COMPUTED SUCCESSIVELY FOR TEMPERATURE AND LIGHT (t, i), SALINITY (s) AND NUTRIENTS (n). THE CUMULATIVE EFFECT (POTENTIAL PHOTOSYNTHESIS) IS GIVEN BY THE PRODUCT OF THESE (P_{tisn}).

DATA FOR STATIONS WITH WATER DEPTH OF FROM 500 TO 2000 M.

Date†	Light (lux)	Temp (°C)	P_{ti} (%)	Salinity (‰)	P_s (%)	P_{tis} (%)	PO_4–P (µg-at/liter)	Avail.N	P_n (%)	P_{tisn} (%)	Calculated net C fixation (g/m²/day)	Per cent of total net photosynthesis	Net photosynthesis (g/m²/day)*
Sept.	9230	23	88	35.6	73	64	0.13	0.55	45	29	0	0	0.21
Oct.	7550	21	97	35.5	72	70	0.20	1.00	47	33	–	–	–
Nov.	1090	18	17	35.0	75	13	0.30	2.00	52	7	–	–	–
Dec.	870	16	3	35.2	72	2	0.36	3.09	57	1.2	.000	0	0.18
Jan.	1040	14	15	35.4	72	11	0.53	5.6	72	8	–	–	–
Feb.	830	13	1	35.5	72	0.7	0.62	6.5	71	0.5	.000	0	0.10
Mar.	590	15	0	36.1	71	0	0.52	5.3	67	0	.000	0	0.56
Apr.	590	14	0	35.8	73	0	0.50	3.70	65	0	–	–	–
May	600	13	0	35.3	72	0	0.35	1.73	50	0	0	0	1.03
June	3950	17	45	35.2	72	32	0.25	1.00	47	15	–	–	–
July	7310	20	100	35.0	75	75	0.12	0.84	45	34	0	0	0.19
Aug.	5750	20	100	35.5	72	72	0.13	0.90	46	33	–	–	–
Sept.	4750	20	100	36.0	71	71	0.19	0.92	46	33	–	–	–

* Calculated from Ryther and Yentsch (1958).

† Underlined months are those for which hydrographic data are available. Others are extrapolated.

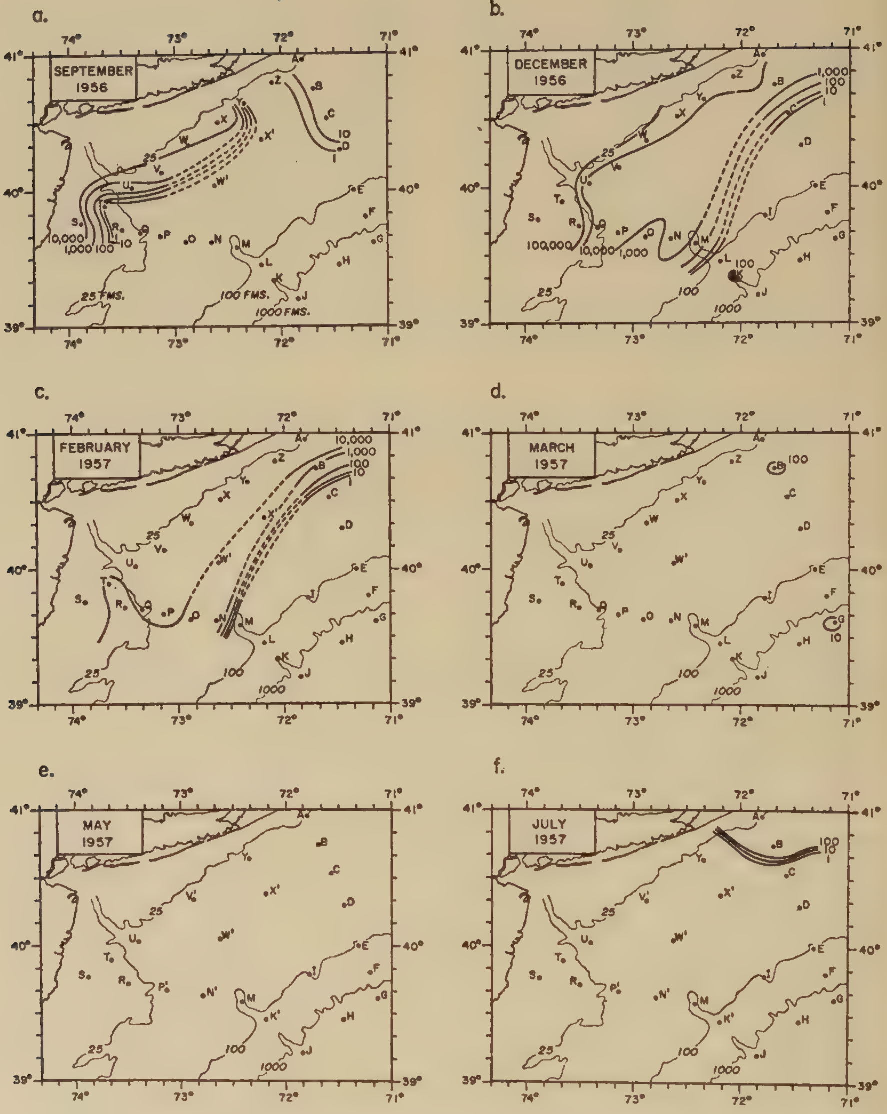
a.
SEPTEMBER 1956
10,000
1,000
100
10
1
25 FMS.
100 FMS.
1000 FMS.
b.
DECEMBER 1956
100,000
10,000
1,000
100
10
1
c.
FEBRUARY 1957
10,000
1,000
100
10
1
d.
MARCH 1957
100
10
e.
MAY 1957
f.
JULY 1957
100
10
1
25
100
1000
74°
73°
72°
71°
41°
40°
39°
A
B
C
D
E
F
G
H
I
J
K
L
M
N
O
P
Q
R
S
T
U
V
W
X
Y
Z
W'
X'
V'
N'
P'
K'

Figure 5 a–f. Distribution of *Skeletonema* (cells per liter) at 10 m depth on the continental shelf from September 1956 to July 1957.

this period. Likewise, the almost complete absence of cells from March onward corresponds with the calculated lack of photosynthesis by *Skeletonema* during this period. The appearance of a small bloom in July is in accordance with the prediction of an increase in *Skeletonema* photosynthesis in early summer (Table IV).

It would be ideal to be able to compare calculated potential photosynthesis with actually measured photosynthesis of the species, but only the total phytoplankton photosynthesis is available (last column, Tables IV, V, and VI).

For the shallow waters, at least, light and temperature appear to be the controlling influences on the seasonal appearance of *Skeletonema* whereas the size of the standing crop is controlled by an interaction of all the factors.

The fact that the population continues to increase from September through December may be explained by the supposition that the standing crop reflects a time lag between the environmental conditions and their expressions. Zooplankton grazing may be implicated also. Riley (1956) calculated that 65% of the phytoplankton produced in Long Island Sound was consumed by pelagic organisms. Our evidence indicates that *Skeletonema* is readily eaten by small copepods in "preference" to some other genera. Zooplankton volumes averaged 46% lower in the November-December cruise than in the September cruise. Volumes in February and March increased and were greatest in March (Curl, unpublished). Cladocera and copepods predominated in the samples. Grazing appears to be a plausible explanation of reduced cell numbers in September.

The intermediate and deep stations never supported large standing crops of *Skeletonema* despite good conditions for growth. Because zooplankton volumes were low at these stations, some factor not considered thus far must be limiting. Since the diatom is so obviously a neritic species, despite good growth conditions on the deep shelf, the factor (s) may be associated with proximity to either the benthos or land. *Skeletonema* requires both vitamin B_{12} (Droop 1955) and divalent sulfur (Lewin, personal communication), among other nutrients. The seaward advection, dilution by mixing, and biological destruction of such substances would make them unavailable to it on the deep shelf and would help to account for its observed spatial distribution.

Calculated zero potential photosynthesis at deep stations is indicative of deep mixing below the euphotic zone in winter (50% of the population may be below the compensation depth). However, when the thermocline is present, the potential photosynthetic rates are frequently more than double those close inshore. Nevertheless, *Skeletonema* is absent from offshore waters. One reason is that virtually no photosynthesis is possible during seven months of the year, and it has been shown that cells of *S. costatum* can survive only two months of darkness. Matsue (1954) found that *Skeletonema* could be kept in the dark up to 52 days without high mortality but that no cells survived beyond 60 days. Our experience agrees with this result. Moreover, if some substance derived from land drainage is essential for growth, it is even less likely to be found at the deep stations.

The circulation out of the lighted zone in winter is a condition to which almost all oceanic algae are subjected. A necessary consequence is that oceanic species must be able to tolerate periods of low illumination.

The photosynthesis of observed natural populations of *Skeletonema* can be estimated from our data. The maximum carbon fixation per cell is known from laboratory experiments, and the potential fraction of this value for each month has been calculated. These multiplied by the average cell concentration give the estimated carbon fixation by *Skeletonema* in nature. The highest photosynthetic rate observed in the laboratory was 1.76×10^{-3} mg C/10^4 cells/hour, calculated from C^{14} uptake. (*Chlorella*, which has one of the highest photosynthetic rates known, has a maximum reported rate of 16×10^{-3} mg C/hr/μl cell volume [Hill and Whittingham 1957] whereas *Skeletonema* fixed 2.8×10^{-3} mg C/hr/μl cell volume in our experiments.) The net carbon fixation at each station may be derived from the formula:

$$(\text{cells/m}^3) \times (1.76 \times 10^{-7}\ \text{mg C}) \times (\text{hrs daylight}) \times (\text{m depth}) \times (\%\ \text{max. photosynthesis}) = \text{gC/m}^2/\text{day}.$$

The depth used in this calculation is that of the mixed layer as previously used. In tables V–VII these computed values are compared with the observed total phytoplankton net photosynthesis computed from the data of Ryther and Yentsch (1958). A maximum of 0.596 gC fixed/m²/day by *S. costatum* is calculated for December at the shallow stations. These rates correspond to 100% of the observed fixation for this area and time. *Skeletonema* also could have accounted for 84% of the carbon fixation in September 1956. During the period of greatest carbon fixation, in March and May, it was not present. The comparative absence of *S. costatum* cells at the intermediate and deep stations throughout the year accounts for their lack of contribution to the total phytoplankton production.

Thus far, data for the seasonal occurrence of *Skeletonema* for one year have been examined. From similar data from inshore waters in other years it may be determined if the distribution of 1956–1957 was typical. Cell counts of *Skeletonema* from Vineyard Sound 1950–1951, Woods Hole 1956–1957 (Hulburt, unpublished), Narragansett Bay 1954–1955 (Smayda 1957), Block Island Sound 1949 (Riley 1952), Vineyard Sound 1935 (Lillick 1937), and Long Island Sound 1952–1954 (Conover 1956), were averaged for each month of the year irrespective of year or geography. Although the actual counts range from 0 to 20×10^6 cells per liter at any one particular place and time, the averages plotted against time yield a smooth bimodal curve (Fig. 6). The outstanding difference between the postulated shelf pattern and the inshore observations is the bimodal nature of the latter. The late autumn and winter peak occurs on the shelf but lags behind the high summer potential.

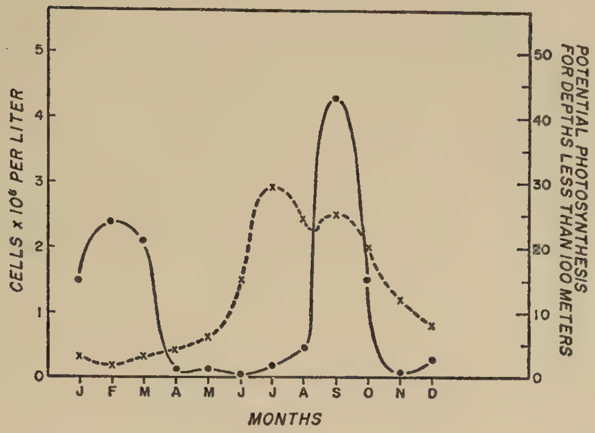

Figure 6. Averaged *Skeleotnema* concentrations in the inshore waters of the northeastern states, and calculated potential photosynthesis. Solid line, cell concentration; dashed line, potential photosynthesis.

A spring bloom of this species does not ordinarily occur in the self waters. For example, Bigelow (1926) says, this genus is "... closely confined to the immediate vicinity of the land in the Gulf of Maine and to the shallow water of the banks, where it flowers irregularly during summer and early autumn... In north European waters it has its maximum in spring but has been found flowering in autumn as well at many localities." The inshore spring flowering here and possibly the spring flowering in Europe must be a response to a factor not studied.

Conover (1956) and others have noted that *Thalassiosira nordenskioldii* Cl. occurs under nearly the same conditions as does *Skeletonema* and seems to be its closest competitor. The optima of light and temperature for the growth of *Skeletonema* are higher than those for *Thalassiosira*. Ryther (1956 a) derived an average relationship between light intensity and photosynthesis from studies of several species of diatoms, and a comparable curve has been derived for *Skeletonema* (Fig. 7). In the summertime *Skeletonema* tends to be favored by shade compared to the "average diatom" and would be inhibited at light intensities exceeding 25°/₀ of the surface value. If the mixed depth was as deep as the compensation depth or deeper, then *Skeletonema* would be able to equal the daily production of the "average diatom". In December, however, *Skeletonema* behaves like an "average diatom" at 12°C and can be significantly more productive than the average at 16°C. From a competitive viewpoint *Skeletonema* should fare best in early winter, and it certainly seems to do so.

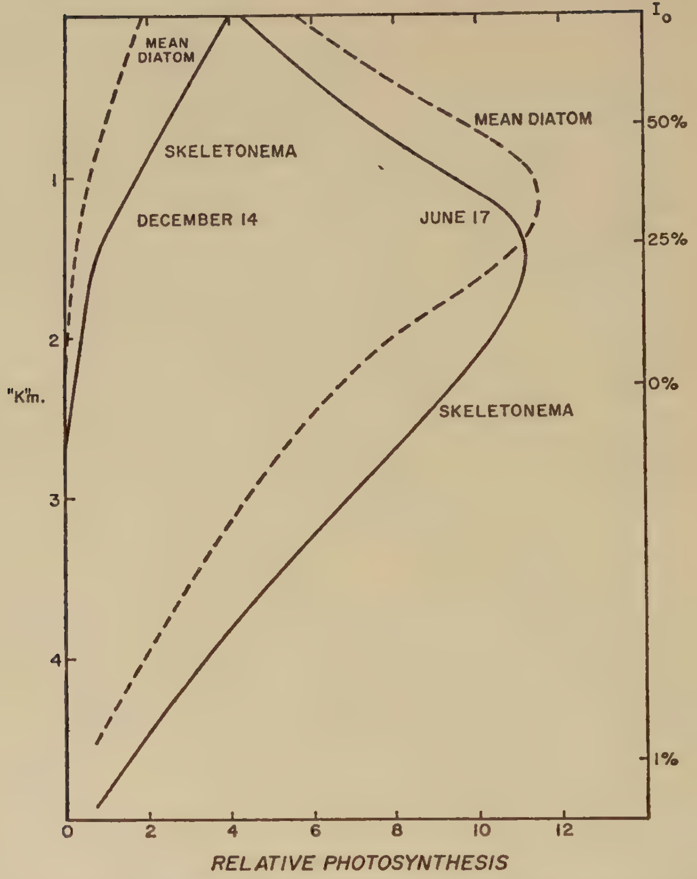

Figure 7. Integrated relative daily photosynthesis of *Skeletonema* as compared to that of the mean values for diatoms in general.

ACKNOWLEDGMENTS

Dr. E. M. Hulburt has been very helpful in supplying data on the occurrence of *Skeletonema* on the continental shelf. Drs. Joyce and Ralph Lewin kindly supplied helpful criticism. Dr. Takashi Ichiye, Florida State University, translated Matsue's (1954) paper. We are pleased to acknowledge the critical reading of the manuscript by B. H. Ketchum, J. H. Ryther, and V. T. Bowen.

REFERENCES

BAKER, J. R.

1938. Latitude and egg seasons in old world birds. Proc. zool. Soc. London, (A) *108*: 557–582.

BIGELOW, H. B.

1926. Plankton of the offshore waters of the Gulf of Maine. Bull. U. S. Bur. Fish., *40*: 1–509.

BRAARUD, T.

1937. A quantitative method for the experimental study of plankton diatoms. J. Cons. int. Explor. Mer., *12*: 321–332.

1945. Experimental studies on marine plankton diatoms. Abh. norske Vidensk. Acad., *10*: 3–16.

CONOVER, S.

1956. Oceanography of Long Island Sound, 1952–1954. IV. Phytoplankton. Bull. Bingham oceanogr. Coll., *15*: 62–112.

COWLES, R. P.

1930. A biological study of the offshore waters of Chesapeake Bay. Bull. U. S. Bur. Fish., *46*: 277–381.

CURL, HERBERT, JR.

1960. The phytoplankton of Apalachee Bay and the northeastern Gulf of Mexico. Publ. Inst. mar. Sci. Texas, *7*: 277–320.

DROOP, M. R.

1955. A pelagic diatom requiring cobalamin. J. Mar. biol. Ass. U. K., *34*: 229–231.

HILL, R. AND C. P. WHITTINGHAM

1957. Photosynthesis. Methuen and Co., Ltd., London. 175 pp.

KETCHUM, B. H., R. VACCARO, AND N. CORWIN

1958. The annual cycle of phosphorus and nitrogen in New England coastal waters. J. Mar. Res., *17*: 282–301.

KIMBALL, H. H.

1928. Amount of solar radiation that reaches the surface of the earth on the land and on the sea, and methods by which it is measured. Month. Weather Rev., *56*: 393–399.

LILLICK, L. C.

1937. Seasonal studies of the phytoplankton off Woods Hole, Massachusetts. Biol. Bull. Woods Hole, *73*: 488–503.

MANLY, J. O.

1953. Marine and brackish water diatoms of Beaufort, N. C. Duke University, Durham. Doctoral Dissertation.

MATSUE, YOSHIYUKE

1954. On the culture of the marine plankton diatom, *Skeletonema costatum* (Grev.) Cleve. in: Review of Fisheries Science in Japan. Jap. Soc. Adv. Sci., Tokyo. 41 pp. (Japanese).

RILEY, G. A.

1952. Phytoplankton of Block Island Sound, 1949. Bull. Bingham oceanogr. Coll., *13*: 40–64.

1956. Oceanography of Long Island Sound, 1952–1954. IX. Production and utilization of organic matter. Bull. Bingham oceanogr. Coll., *15*: 342–344.

1957. Phytoplankton of the north central Sargasso Sea, 1950–1952. Limnol. Oceanogr., *2*: 252–270.

RILEY, G. A., H. STOMMEL AND D. F. BUMPUS

1949. Quantitative ecology of the plankton of the western North Atlantic. Bull. Bingham oceanogr. Coll., *12*: 1–169.

Ryther, J. H.
1954. The ratio of photosynthesis to respiration in marine plankton algae and its effect upon the measurement of productivity. Deep-Sea Res., *2*: 134–139.
1956a. Interrelation between photosynthesis and respiration in the marine dinoflagellate *Dunaliella euchlora*. Nature, London, *178*: 861–862.
1956b. Photosynthesis in the ocean as a function of light intensity. Limnol. Oceanogr., *3*: 327–335.
Ryther, J. H. and C. S. Yentsch
1958. Primary production of continental shelf waters off New York. Limnol. Oceanogr., *3*: 327–335.
Shelford, V. E. and E. D. Towler
1925. Animal communities of the San Juan channel and adjacent areas. Publ. Puget Sound biol. Sta., *5*: 53–73.
Smayda, T. J.
1957. Phytoplankton studies in lower Narragansett Bay. Limnol. Oceanogr., *2*: 342–359.
Steeman Nielsen, E.
1952. The use of radio-active carbon (C^{14}) for measuring organic production in the sea. J. Cons. int. Explor. Mer., *18*: 117–140.

Printed in Denmark for the Sears Foundation for Marine Research,
Yale University, New Haven, Connecticut, U.S.A.
Bianco Lunos Bogtrykkeri A/S, Copenhagen, Denmark

Contribution No. 1199

Särtryck ur Tellus nr 2, 1961

Temperature and Steady State Vertical Heat Flux in the Ocean Surface Layers

By ERIC B. KRAUS and CLAES ROOTH, Woods Hole Oceanographic Institution[1]

(Manuscript received January 17, 1961)

Abstract

The occurrence of a quasi-isothermal surface layer is shown to be a necessary consequence of the vertical distribution of heat sources and sinks, which requires an upward transport of heat. The depth of the convective layer depends essentially on a balance between the absorption of visible radiation within the layer and the loss of heat at the surface. Variations in the profile below the isothermal layer are primarily caused by vertical motion. Numerical examples illustrate the effects of meteorological conditions on the heat loss and hence on the surface temperature and thermal structure below.

I. Introduction

Fig. 1 shows two sets of temperature soundings. The left hand side represents the vertical temperature distribution in the sea at 16° 25 N, 23° 09′ W and the potential temperature in the air over Sal (16° 44′ N, 22° 57′ W) in the Cape Verde Islands on the same day. The right hand side represents simultaneous soundings at 17° 33′ N, 81° 11′ W in the Caribbean and over Grand Cayman Island (19° 18′ N, 81° 22′ W). Why have these curves this particular shape, which is fairly typical for conditions in the eastern and western margins of the sub-tropical Atlantic? Why is the surface temperature about 26° C and not 22° or 30°.

A full answer to these questions requires a knowledge of the three dimensional distribution of temperature and velocity in the atmosphere and the oceans. It involves therefore a knowledge of the whole general circulation. The aim of the present discussion is more modest. It intends to show the dependency of the surface temperature and of the profile below upon the rate of upwelling and upon the climatic conditions above.

The sea is cooled by evaporation, conduction and infra-red radiation. These processes are concentrated on the surface. On the other hand, heating by the absorption of visible light from the sun and sky affects an appreciable depth, particularly in biologically unproductive offshore waters. There must be therefore a layer through which heat is transported upwards. As a result, the ocean surface should be somewhat cooler than the water below, an effect observed recently by Ewing and McAlister (1960).

In low latitudes where the sea gains more heat than it loses, the upward heat flux affects only a layer of limited depth. Absorption of solar energy in this layer must be sufficient to compensate for the heat loss from the surface. We may hence expect to find a level where the vertical heat flux changes direction. On the average, between 30° N and 30° S, the amount of energy lost from the surface is about 5—10 times as large as the amount which is being retained and becomes available for export by ocean currents to extra-tropical latitudes.

A turbulent upward flux of heat will be

---

[1] Contribution No. 1199 from the Woods Hole Oceanographic Institution.

07140 Sep.

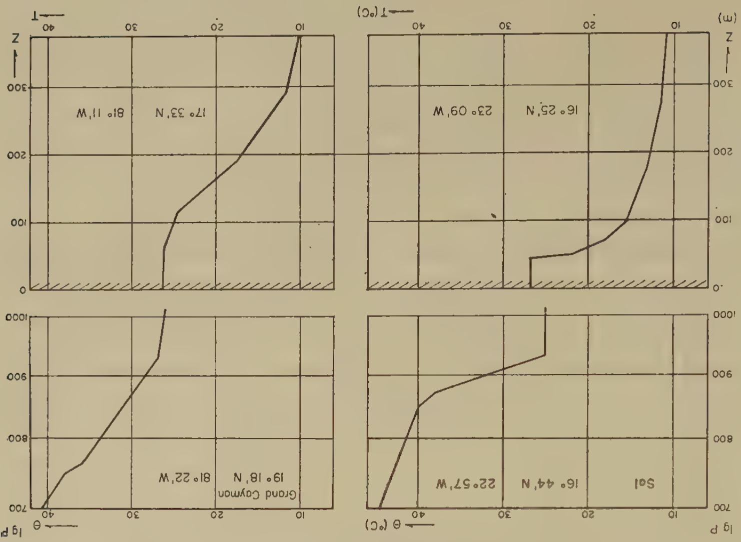

Fig. 1. Characteristic distribution of potential temperature in air and water.

associated with free convection. It generates kinetic energy and tends to produce a layer of nearly constant potential temperature. On the other hand, kinetic energy will be destroyed in the region of downward eddy flux. The stratification there would tend to be stable.

The argument does not indicate that the stirring of the sea surface layers is due to free convection alone. In fact, the kinetic energy created by the buoyancy forces is small compared to that transferred by wind stresses. Particularly in regions of fairly turbid water, and hence of only limited light penetration, wind mixing is likely to overshadow the effects of the upward heat flux. We do feel, however, that over a larger part of the sub-tropical oceans, the variation of the steady state vertical heat flux with depth and hence indirectly the meteorological conditions pertaining above, exerts a dominating influence on the thermal structure in the uppermost layers.

2. The Absorption of Radiant Energy in the Sea

Radiation from the sun and sky which penetrates the sea surface is mostly absorbed either directly or after multiple scattering. Only a small fraction of the incident energy is scattered back into the atmosphere. Both absorption and scattering vary with the wavelength. Pure ocean water is most transparent to blue light, it absorbs red light more rapidly and is practically opaque to infra-red radiation. The scattering is affected not only by water molecules but also by suspended particles, organisms and dissolved coloured substances. The transparency of sea water in nature is therefore affected by its biological productivity.

Although Beer's law is not strictly applicable in these circumstances, it is closely approximated below the top few metres, at least in the blue and green part of the spectrum. In the present study it will be assumed that the radiation flux in the sea can be represented by the function ($Se^{-\alpha z}$), where S is the flux per unit area across the sea surface and α is the extinction coefficient. (The vertical coordinate z is throughout considered to be 0 at the sea surface and counted positive downwards.)

A brief survey of radiation measurements up to the second world war can be found in Sverdrup, Johnson and Fleming (1942). Most of these measurements were carried out in comparatively turbid and biologically productive waters of the northern temperate zone. Measurements carried out later in sub-tropical regions showed smaller extinction coefficients.

With the sun at the zenith, and for very clear ocean water, Jerlov (1951) found that ten per cent of the incident vertical beam penetrated to a depth of about 35 metres and one per cent to 85 metres. These figures apply to the vertical component only and, according to Jerlov, have to be increased by about twenty per cent to obtain the total energy.

Jerlov's figures for clear ocean water may be compared with a series of twenty-seven measurements obtained in the Sargasso Sea 15 miles S. E. of Bermuda at 32° 10′ N, 64° 30′ W between 1957 and 1960, BERMUDA BIOLOGICAL STATION (1960). These measurements were carried out with a Weston 856 RR photo-electric cell. Incident solar and sky radiation was measured simultaneously with an Epley pyrheliometer. The extinction coefficients α varied in this series between 0.035 m^{-1} and 0.068 m^{-1}, with a mean of 0.048. This corresponds to an energy penetration of ten per cent to the 48 m level and of 1 per cent to about one hundred metres. Measurements described by CLARKE (1936) give even greater penetrations.

An accurate computation would have to include the spectral variation in α. For the present, fairly simple, model $\alpha = 0.05\ \mathrm{m}^{-1}$ will be assumed for the total extinction coefficient in the trade wind region. In biologically more productive and therefore more turbid tropical waters a value of 0.10 would be more appropriate. In temperate oceanic water Jerlov's figures suggest extinction coefficients approaching 0.2 m^{-1}.

Following BUDYKO (1956), the short wave radiation which penetrates the surface will be approximated by

$$S = 0.94\,(1-0.68\,n)\,S_0 \quad \text{cal cm}^2\ \text{day}^{-1} \qquad (1)$$

where S_0 is the solar and short wave sky radiation which reaches the ground, the factor 0.94 is due to an assumed reflection of 6 per cent (BUDYKO 1956, NEIBURGER 1954) and n is the cloud amount in tenths.

3. The Heat Loss from the Sea Surface

The sea surface loses heat by infra-red radiation, turbulent conduction and evaporation.

Following BRUNT (1944) and DORSEY (1940) the mean infra-red radiation balance at the sea surface can be approximated by:

$$Q_a = 0.985\,\sigma\,T_0^4\,(0.39 - 5.04\,.\,10^{-2}\sqrt{re_w}) \qquad (2)$$

where σ is Boltzman's constant, T_0 absolute temperature of the sea surface, e_w the corresponding saturation vapour pressure in mbs; the quantity r – the ratio of the vapour pressure in the air (at ship's level) to e_w – is closely related to the relative humidity.

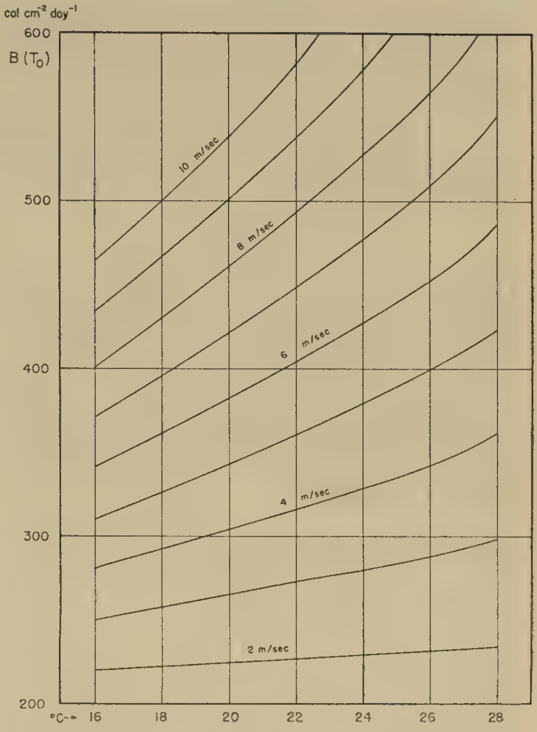

Fig. 2. The rate of heat loss, B, at the sea surface as a function of surface water temperature T_0 and wind speed ($n=0$, $r=0.8$, $R=0.1$).

When clouds reduce the effective outgoing radiation, the expression (2) is multiplied by a correction factor

$$1 - c\,n^2 \qquad (3)$$

where c, in the sub-tropics, is assumed equal to 0.6. A correction factor of this type is given by BUDYKO (1956), who also lists values of c, for other latitudes.

The conductive and evaporative heat losses can be expressed by

$$Q_h + Q_e = (1+R)\ LE = (1+R)\ LK^{\star}u\ (1-r)\,e_w \qquad (4)$$

with R denoting Bowen's ratio, L the latent heat of evaporation ($L = 585$ cal g^{-1}) and u the wind velocity. The mean value of the proportionality constant $K^{\star} = 1.5 \times 10^{-9}\ \mathrm{cm}^{-2}\ \mathrm{sec}^2$; in broad agreement with the finding of JACOBS (1951), MARCIANO and HARBEK (1954), BUDYKO (1956), KRAUS (1959) and other investigators.

From (2), (3) and (4) with u in m/sec:

$$B = Q_a + Q_h + Q_e = \qquad (5)$$

$$0.985\, T_0^4 \,(0.39 - 0.05\, re_w)\,(1 - 0.6\, n^2) + (1 + R)\,(1 - r)\; 5.26 \times 10^{-3}\, u\, e_w$$

$$(\text{cal cm}^{-2}\ \text{min}^{-1})$$

The value of e_w is fully determined by T_0. The heat loss B is therefore a function of T_0, the velocity u and the relative humidity r (relative to e_w). It has been plotted in Figure 2 for the special case $n = 0$, $R = 0.1$, $r = 0.8$. It should be noted that variations in u and r tend to affect B more strongly than the variation in T_0 likely to be encountered in the subtropical sea surface.

4. A steady state model; general discussion

To demonstrate the effects of the energy fluxes discussed above, the following simple model is considered.

A water volume is subject to warming in depth and cooling at the surface by radiation, convection and evaporation. At some depth D, not at the bottom but much deeper than the characteristic penetration depth α^{-1} of the visible light, the temperature T_0 and its vertical gradient are prescribed. Effects of horizontal advection are not considered, except for the inclusion of a divergence in the horizontal flow at the surface, compensated for, together with the evaporation, by a prescribed vertical velocity w at depth D. It is assumed that this divergence is confined to the well mixed surface layer, which we anticipate to find. Hence, the temperature of the outflowing water is equal to the surface temperature T_0 and w is constant below the surface layer at least to the depth D. Variations in salinity are not considered and the surface boundary layer described by Ewing is neglected.

Our problem is to determine the structure of the temperature field from the surface to the depth D, and its dependence upon the boundary conditions above and below.

The surface temperature T_0 is readily obtained from a consideration of the energy balance in the column between the surface and the depth D. In the notation of the previous sections we have:

$$S(1 - e^{-\alpha D}) = B\,(T_0) + cpw\,(T_0 - T_D) + K_D \gamma \qquad (6)$$

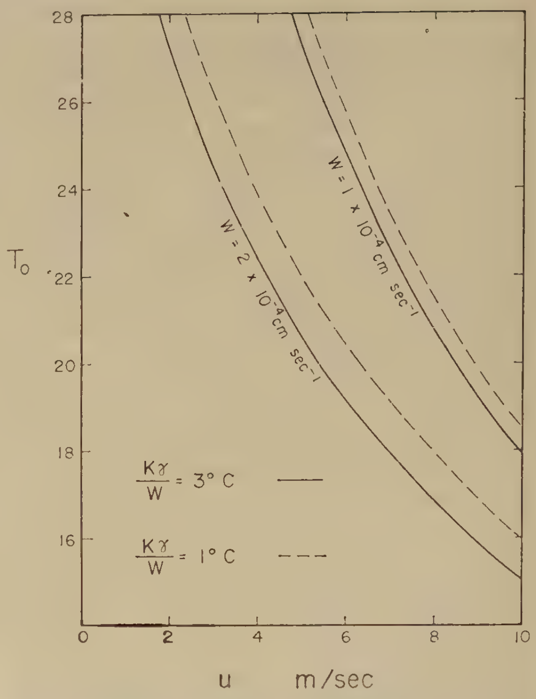

Fig. 3. Surface temperature according to equation (6), with $Kw^{-1} = 250$ m and other parameters as indicated on the diagram.

In this relation exp. $(-\alpha D)$ is negligibly small according to our basic assumptions. Some evidence, discussed below, suggests that the ratio K/w is a scale length which tends to be constant in large parts of the tropical oceans with a value of approximately 250 m. Figure 3 illustrates the relation between T_0 and the wind speed u for some values of w and $\left|\dfrac{K\gamma}{w}\right|$. D was taken as 500 m and values for T_0 and γ were chosen characteristic of data for low latitudes in the Atlantic ocean (FUGLISTER, 1960).

We shall now proceed to consider the temperature distribution for $0 < z < D$. Our equation (6) implies an upward transport of heat in some layer of depth of order α^{-1}. In these layers any motions induced by wind driven turbulence will tend to be amplified, and a convective regime with nearly isothermal conditions may be expected. Dependent upon the intensity of the convective and wind driven turbulence, this convective regime may penetrate more or less deeply beyond the level

$h^\star$, where balance is struck between the heat loss at the surface, and the total radiation energy absorbed in the layer above.

Since a treatment of the dynamics of this convective layer lies outside the scope of the present study, the following approximation is introduced:

An isothermal layer of temperature T_0 according to (6) corresponding to the entire convective layer described above, reaches down to some depth $h > h^\star$ where $\exp(-\alpha h^\star) = (S-B)/S$. For $z > h$ a constant coefficient K of vertical eddy transfer of heat is assumed to apply. At $z = D$, $T = T_D$ and $\frac{dT}{dz} = \gamma$, in accordance with the conditions applied to equation (6).

With these assumptions, together with the previously stated conditions of constant w below the isothermal layer the thermal energy equation can be integrated upwards from $z = D$, and h is determined by the requirement of temperature continuity: $T(h) = T_0$.

The appropriate equation is:

$$w\frac{dT}{dz} = K\frac{d^2T}{dz^2} + \frac{\alpha S}{\varrho c}e^{-\alpha z} \qquad (7)$$

and the solution:

$$T = T_D - \frac{S_0}{\varrho c(\alpha K + w)}\left(e^{-\alpha z} - e^{-\alpha D}\right) + \\ + \frac{K}{w}\left(\gamma - \frac{\alpha_0 S}{\varrho c(\alpha K + w)}e^{-\alpha D}\right)\left(e^{\frac{w}{K}(z-D)} - 1\right) \qquad (8)$$

The heat conduction term $K\frac{dT}{dz}$ at h is balanced by the excess radiation absorbed in the mixed layer, $S_0[\exp(-\alpha h^\star) - \exp(-\alpha h)]$. This balance is automatically secured by the determination of T_0 from the total energy budget for $0 \leq z < D$, equation (6).

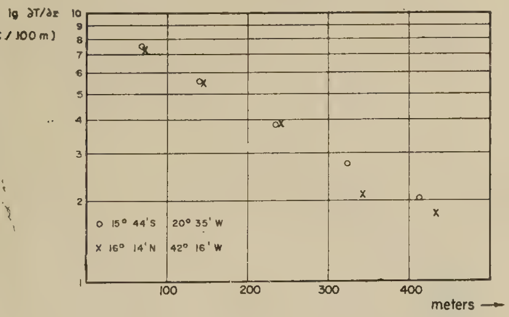

Fig. 4. Variation of $\frac{\partial T}{\partial z}$ with depth at two oceanographic stations.

It is evident from equation (7) that since the short wave radiation term is always positive and $\frac{\partial T}{\partial z}$ outside the convective layer is generally negative, $\frac{\partial^2 T}{\partial z^2}$ can be positive only in the presence of a sufficiently strong upwelling ($w < 0$). Dependent upon the value of the nondimensional numbers $N_1 = \alpha h^\star$ and $N_2 = \alpha K w^{-1}$, inflection points may or may not occur in the profile. The magnitude of N_1 indicates the proportion of the available radiation energy which is consumed for evaporation and N_2 shows the relative importance of the radiation and the heat conduction in the lower layers. A large value of $|N_2|$ indicates that the radiation term is of little importance in the interior part of the region, but for any $N_2 < 0$ a sufficiently small N_1 will introduce an inflection point in the profile, and a layer where the last term in (7) is not negligible.

It is also of interest to note, that if any single term in (7) is negligible, the solution for T according to the reduced equation is a simple exponential, with a characteristic scale length dependent upon which term is negligible. This fact affords us an opportunity to use observations for guidance as to the pertinent values of the scale lengths by simply making plots on a logarithmic scale of $\frac{\partial T}{\partial z}$ versus z on a linear scale.

Figure 4 shows such a plot for two oceanographic stations in the North and South Atlantic. The values fall approximately on a straight line indicating that a reduced form of (7) would indeed apply. Furthermore, since α^{-1} is at most about 30 m (cf. section 2 above), the scale length involved must be identified with Kw^{-1}. Similar plots for a number of oceanographic stations along 16° N and 15° S (FUGLISTER 1960) suggest that a value of about 250 m for this length is characteristic of about two thirds of the sub-tropical Atlantic. The adaptation of a constant Kw^{-1} is not justifiable for data along the margins of the ocean; in particular it is not applicable for the surroundings in figure (1).

5. Numerical Examples

Equations (6) and (8) were used to show how the surface temperature T_0 and the depth h of the isothermal layer are influenced by the meteorological conditions. The following parameters are common to all the examples:

$$D = 500\,\mathrm{m},\ T_D = 9^\circ\,\mathrm{C},\ \gamma = 0.8 \times 10^{-4\circ}\,\mathrm{C/cm}.$$

$$w = 1.5 \times 10^{-4}\ \ \mathrm{cm/sec}\quad Kw^{-1} = 2.5 \times 10^4\,\mathrm{cm}$$

The values of w and of $K\gamma w^{-1}$, (2° C), are seen to lie in between the parameters chosen for the curves in Fig. 3. The results are quite sensitive to the choice of parameters, a fact which will be further commented upon below. Tables 1—3 illustrated the effects of varying wind speed, relative humidity and cloudiness.

Table 1. The surface temperature T_0 and convective layer depth h as functions of the mean wind velocity *ce*. ($n = 0$, $r = 0.8$)

U (m/sec)	3	4	5	6	7	8	9	10
T_0 (°C)	28.8	25.9	23.4	21.5	19.9	18.5	17.3	16.2
h (m)		10	57	87	116	143	169	(200)

Table 2. T_0 and h as functions of the mean ratio r between the vapour pressures in the air, ea, and at the sea surface, ew. ($u = 5$, $n = 0$)

r	0.5	0.6	0.7	0.8	0.9
T_0		15.9	18.8	23.4	(32)
h		(200)	135	57	

Table 3. T_0 and h as functions of the mean cloudiness n (in tenths). ($u = 5$, $r = 0.8$)

n	0	2	4	6	8	10
T_0	23.4	20.2	16.9	(14)		
h	57	110	178			

It is evident that each of the parameters strongly influences the solution in this model. The same is true for the choice of w and T_0. The range of values of the various parameters, that produce reasonable results is quite limited, and the theory may therefore be said to have quite high information content within its range of validity.

6. Transients

We have limited our discussion to the steady state and our method of treatment cannot immediately be extended to the transient case.

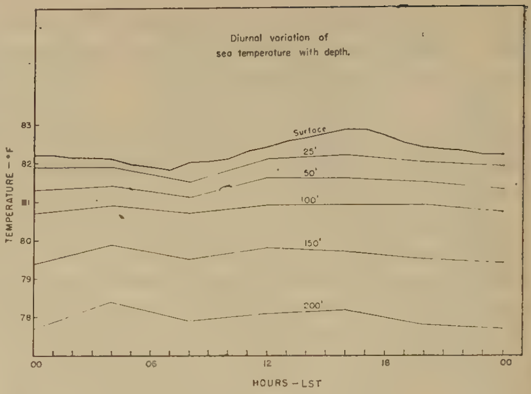

Fig. 5. Temperature variations in the surface layer of the sea, from Garstang (1958).

A brief discussion of some cases of transient development will however be given here, as it is felt that they shed more light on the role of the vertical heat flux.

We can distinguish between three major types of transients, according to the mechanisms and characteristic time scales involved.

The seasonal warming or cooling will cause changes in the total heat storages which are appreciable even compared with the total seasonal insolation (BRYAN and SCHROEDER, 1960).

Weather disturbances of various time scales and dimensions may provide intense wind mixing as well as changes in evaporation conditions, etc. Finally, the diurnal changes in insolation and wind and cloud patterns even on undisturbed days will introduce fluctuations from the idealized steady state with which we have been concerned in our specific model.

The diurnal change of the surface temperature profile in the tropical Atlantic 11° 11′ N, 52° 25′ W has been observed by GARSTANG (1958). Series of hourly or three hourly bathythermograph soundings are available also from Weathership station Echo (35° N, 48° W). Both series of data tend to show a slight increase in stability during day and a decrease during night.

In explanation it should be considered that during the day, absorption of radiation in a relatively shallow layer will suffice to balance the heat loss from the surface. The lower part of the quasi-isothermal layer gains heat and may become slightly more stable during this

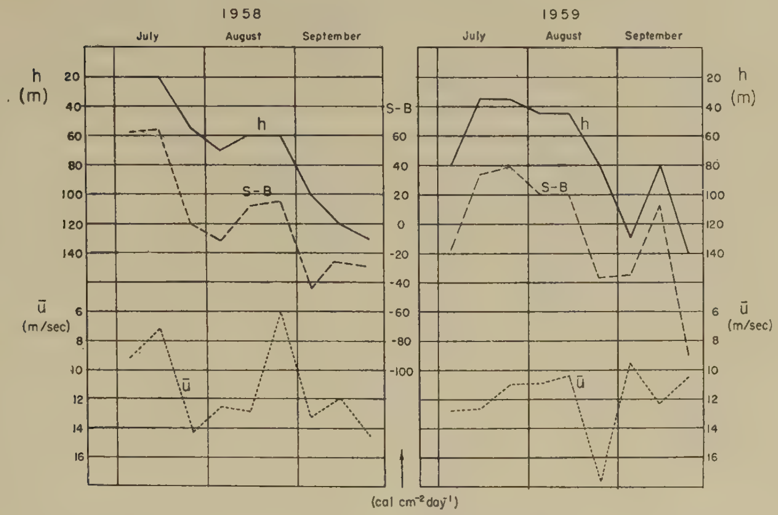

Fig. 6. Wind speed, *u*, rate of heat loss, *S - B*, and depth, *h*, of the "wind mixed layer" at weather ship station Echo.

period. The gain of heat is drawn upon during the night when the continuing surface heat loss causes convection to extend through the whole depth of the layer. The diurnal rhythm of convection below the cooled sea surface is therefore opposite to the diurnal rhythm of convection in the air over heated land.

In Garstang's records, as shown in Fig. 5, the mean temperature amplitude at 50 feet is about 0.12° C. The diurnal change in convection may conceivably affect the vertical movement of plankton in the tropics. In extra-tropical regions the diurnal change is likely to be masked by convection changes caused by synoptic disturbances.

Changes on a larger time scale outside the tropics in the northern Sargasso Sea, are illustrated by Fig. 6 which is based also on observations from Weather Ship station Echo (34° N, 48° W). The analysed periods covered late summer and early autumn in 1958 and 1959.

In view of NAMIAS' (1959) findings in the Pacific, it is of some general interest that the sea temperature at this station during summer 1958 was substantially higher than in 1959. This difference was characteristic for every calendar day between the first of July and the last of September. The mean value of T_0 was 76.8° F for August, 1959 against 80.5° F for August 1958. The corresponding July figures were 73.7° F and 77.3° F. The associated difference in the heat storage, that is the enthalpy integral between the surface and 200 metres amounted to about 30,000 cal./cm^2 equivalent to two months solar energy input.

Weather and bathythermograph observations were carried out during the observation periods usually at 3 hourly intervals. The heat loss *B* was computed from these observations by means of equation (5). The insolation *S* was estimated on the basis of table 135 in the Smithsonian Meteorological Tables (1951) with an assumed transmission coefficient of 0.9 and with the corrections for albedo and cloudiness given by equation (1).

All estimates were then averaged over ten day periods.

The exact individual results of the computations are doubtful because of unreliable and missing observations. However, the resulting uncertainties have less effect on the ten day means and figure (6) is believed to represent the character of the time change reasonably well.

It can be seen that changes in the mean depth *h* of the isothermal layer reflect changes in the heat balance *S - B*. There is no obvious correlation with the mean wind velocity as such—in keeping with the present argument.

7. Concluding Remarks

Within the framework of a very simple model we have endeavored to demonstrate that by way of affecting the heat losses from the ocean surface, in particular through changes in evaporation, the meteorological conditions over the ocean may excert a profound influence on the temperature T_0 and depth h of the so-called wind mixed surface layer. We realize that since a radiation excess or deficit of 100 cal./cm^2 day would change the temperature of a 50 m layer by only .02° C/day, advective effects as well as seasonal changes in the total heat content of a water column may be extremely important.

However, a greater challenge is offered by the lack of an adequate theory for the penetration of the convection beyond the depth $h^\star$ where the vertical heat flux changes direction. In a sense the classical treatment of the mixed boundary layer by Rossby and Montgomery (1935) represents a limiting case of negligible effects of the heating in depth. The same is true of a recent study by Kitaigorodsky (1960) who considers a case of finite heat supply $=S_0 - B$ in our notation, completely concentrated at the surface, which makes his mixed layer a true layer of forced convection, the depth of which is determined by a kind of Richardson number. The Rossby-Montgomery theory is included as a special case in Kitaigorodsky's work. Attempts at application of the formulae given by Kitaigorodsky did not seem to yield very satisfactory values of h for the cases tried. On the other hand, the procedure outlined in section 4, for finding h on the basis of T_D and γ at $D = 500$ m cannot possibly go far wrong if these values together with T_0 are reasonable. On these grounds it is felt that a true test of a model like this can be made only when it is complete in the sense of containing the dynamics of the combined forced and free convection associated with the mixed surface layer.

Finally, we wish to acknowledge the constructive criticism of our colleagues at the Woods Hole Oceanographic Institution, and the fact that one of us, C. Rooth, is supported under NSF grant No. G 7366.

REFERENCES

Bermuda Biological Station, 1960: Unpublished data. *Final Report Atomic Energy Commission Contract AT* (30—1)—2078.

Brunt, D., 1944: *Physical and Dynamical Meteorology*, Cambridge University Press.

Bryan, K. and Schroeder, E., 1960: Seasonal Heat Storage in the North Atlantic Ocean *J. Met. Am. Met. Soc.* **7**, pp. 670—674.

Budyko, M. I., 1956: *The Heat Balance of the Earth's Surface.* Translation prepared by Office of Technical Services, U.S. Department of Commerce of: Teplovoi balans zemmio poverblenosti Cjidrometeorologicheskoe izdatel'stvo, Leningrad 1960, 255 pages.

Clarke, G. L., 1936: Light Penetration in the Western North Atlantic, Conseil Permanent International par l'exploration de la mer, *Rapports et Procès-Verbaux* **101**.

Dorsey, E., 1940: *Properties of Ordinary Water Substance.* Am. Chem. Soc. Monographs, Reinholds Publishing Corporation, New York.

Ewing, G. and McAlister, 1960: On the Thermal Boundary Layer of the Ocean, *Science* **131**, pp. 1374—1376.

Fuglister, F., 1960: *Atlantic Ocean Atlas*, Woods Hole Oceanographic Institution.

Garstang, M., 1958: *Some Meteorological Aspects of the Low Latitude Tropical Western Atlantic*, Woods Hole Oceanographic Institution. Unpublished manuscript.

Jacobs, W., 1951: *Compendium of Meteorology*, Thomas F. Malone, Editor, Am. Met. Soc. — Boston — pp. 1057—1070.

Jerlov, N., 1951: *Swedish Deep Sea Expedition*, Reports 3, Physics and Chemistry, pp. 1—59.

Kitaigorodsky, S. A., 1960: On the Evaporation of the Thickness of the Windmixing layer in the Ocean. *Bull* (*Izveztija*) *Social Sci. USSR, Geoph. Series* pp. 284—287 in the translated issue, 425—431 in the original.

Kraus, E., 1959: The Evaporation-Precipitation Cycle of the Trades, *Tellus* **11**, pp. 147—158.

Marciano and Harbek, 1954: *Water Loss Investigations, Lake Hefner Studies*, Technical Report, U.S. Department of the Interior, Geological Survey Professional Paper 269.

Namias, J., 1959: Recent Seasonal Interactions between North Pacific Waters and the Overlying Atmospheric Circulation. *J. Geophysical Res.* **64**, pp. 631—646.

Neiburger, M., 1954: A note on the Reflection of Diffuse Radiation by the Sea Surface. *Trans. Am. Geoph. Soc.* **35**, pp. 729—732.

Rossby, C.-G. and Montgomery, 1935: The layer of frictional influence in Wind and Ocean Currents. Papers in *Physical Oceanography and Meteorology* **3**, No. 3.

Sverdrup, H. U., Johnsson and Fleming, 1942: *The Oceans.* Prentice Hall, Inc., New York.

PRINTED IN SWEDEN
ESSELTE, STHLM 61

Contribution No. 1208

A Multipurpose Large Volume Sea-Water Sampler[1]

R. H. Bodman, L. V. Slabaugh and V. T. Bowen
Woods Hole Oceanographic Institution

The need for large volumes of sea-water, from all depths, for radioisotope studies with carbon-14, tritium or fission-products, has resulted in the development of a variety of sampling devices. Most of these appear to us to suffer from two serious defects: one, they are clumsy to handle and often require large diameter wire for lowering; and two, they are special-purpose devices giving samples of little value except for a particular analysis. In fact, large volume samples from all depths are also needed for a variety of nonradiochemical purposes: trace element determinations, studies of organic matter, both dissolved and particulate, nutrilite studies of phytoplankton, and others. The device described below has been developed and used with a view to satisfying the disparate requirements of all these programs.

Principle of Operation. This sampler is a modified Kammerer bottle, built of aluminum and stainless steel, Neoprene or Polyethylene valves, and lined with Kel-F plastic. Models of 64 L and of 140 L capacity have been built. Their dimensions are identical except that the smaller has a 10″ diameter sample chamber. The drawings of the 140 L model in Fig. 1 will serve for description of both models.

The sample chamber is an aluminum cylinder, 15″ O.D., and 57¾″ long; at each end a 45° neck leads to a six″ opening. The whole inside chamber, and the outside of the valve opening for about ½″ are spray-coated with Kel-F plastic (Trifluoro, chloro ethylene polymer). Lugs with 13/16″ diameter holes are welded to the outside of the chamber in three vertical rows, each consisting of three lugs; by means of these the chamber is slipped into position on three rails of ¾″ diameter stainless steel rods. These rails are then bolted at each end to triangular aluminum plates, making a rigid frame. Between the top plate and the sample chamber is the upper valve plate, which also slides freely on the rails. The sample chamber is connected to each corner of the upper valve plate

---

[1] Contribution No. 1208 from the Woods Hole Oceanographic Institution.

REPRINT FROM JOURNAL OF MARINE RESEARCH, VOLUME 19, 3, 1961

by 14¹/₄″ lengths of chain. On the lower surface of the upper valve plate and on the upper surface of the bottom plate are neoprene and gum rubber valves, in the form of stoppers, which fit tightly in the 6″ openings of the sample chamber. On the upper surface of the upper valve plate is a catch held in the cocked position by the trigger of the release mechanism on the top plate. Thus, when cocked (Fig. 1 A), the sampler is open, the chamber hanging with its top opening about 7″ below the upper valve, and its bottom opening about 8″ above the bottom valve. When the messenger releases the trigger, both upper valve plate and sample chamber fall free; the inertia of each is sufficient to seat first the lower and then the upper valve, enclosing the sample to be collected.

Construction Details. Blueprints of engineering drawings of the sampler are available on request from the Woods Hole Oceanographic Institution; requests should be addressed to the third author.

Aluminum alloys of high corrosion resistance, like 6061-T6, should be used. It is also important that all moving parts be fitted very loosely, to allow accumulated salt particles to be flushed out easily.

Although handles, as shown in Fig. 1, are a real convenience, they have proved in practice to be quite vulnerable. One sampler, which has now been in use for two years with both handles gone, offers no serious problem in manipulation at sea, so these may be regarded as luxuries.

A small vent tube, ¹/₄″ I.D., as shown at the top of the sample chamber, is necessary to permit outflow of enough water to allow the valve to seat. This may be a standard one-way pressure relief valve or simply a short open tube; we have used both with no measurable difference in performance. The latter is somewhat more convenient as a point of attachment for an air pump to speed transfer of the water sample to shipping drums on deck.

The release mechanism, a stainless steel trigger (as shown in Fig. 1 A) slotted to permit the wire pennant to pass through it, is hinged on a pin at the bottom of the top plate. On the upper side of the top plate is a loosely attached trigger plate, through which the wire pennant is also passed. After passing through trigger plate, top plate and trigger, the wire is brought around a fixed semicylindrical bearing (3″ diameter), looped with a thimble over a ³/₈″ aluminum bar on the upper side of the top plate, and fastened with wire clamps. In the cocked position, the trigger engages the U-shaped catch on the upper surface of the upper valve plate. To prevent pre-tripping due to vibration during lowering, it is necessary that the springs (bronze leaf springs) shown holding the trigger forward in the cocked position be relatively strong. To overcome their action, and the frictional resistance of the release, a brass messenger of five pounds weight is needed. The trigger plate simply transfers the weight of the messenger to the trigger, in spite of moderate angular displacement of the wire pennant relative to the sampler.

The upper and lower valves consist of five pieces each: distally, a large spacer of $^1/_{16}''$ neoprene sheet; next a $^1/_2''$ thick circle of natural rubber gum cemented to a $^1/_2''$ thick circle of neoprene, shaped to fit the 6″ opening of the chamber; finally a Kel-F coated aluminum disk of $5^3/_4''$ diameter tapped to receive a $^3/_8''$ diameter stainless set screw, which holds the valve to the surface of the plate (see Fig. 1 B) and which can be tightened to compress and expand the valve to compensate for wear in use. When all adjustments are properly made, the water sample comes in contact with only the 6″ diameter ring of neoprene (about $^1/_4''$ wide), left uncovered by the Kel-F coated disk; the foam rubber contacts only the sides of the chamber opening.

The upper valve plate is weighted with three lead cylinders, each of five pounds. This has proved ample mass to seat the valve securely.

The Kel-F coating is applied by a standard commercial process licensed by the M. W. Kellogg Company. A directory of firms equipped to apply this material is obtainable from the Company.

Operation. In Fig. 2 is presented a block diagram of the rigging of the sampler on hydrographic wire. The six-foot pennant of the sampler is fastened through a heavy duty (at least 600 lbs. load) ball-bearing swivel to the end of the hydrographic wire. About six feet above the swivel is rigged a Nansen bottle with both protected and unprotected reversing thermometers. The sampler messenger, fitted with an arm long enough to by-pass the swivel, is hung by a light wire pennant from the Nansen bottle messenger-release mechanism. Tripping at depth is thus managed by first tripping the Nansen bottle, which then trips the sampler. The sample depth is determined from the thermometer readings, and proper operation of the sampler is determined by comparison of salinity between the sampler contents and that of the Nansen bottle.

Aside from the usual spectrum of ills to which a lowered hydrographic device is subject, two other problems are inherent in the design of this sampler:

A surge of the sea surface which meets the sampler when lowered will not fill the chamber fast enough to prevent its floating. In extreme cases this may trip the release—defining the sea-state beyond which work is no longer possible. In less than extreme conditions, the chamber may float up and seat the upper valve firmly enough to suspend the chamber from it; if not noticed, this results in lowering a bell closed at the top and in collecting a sample of surface water only slightly mixed with water from below. This can be completely prevented by clamping to one or two rails, just above the position of the lower lug when cocked, a stop which will not permit the barrel to rise enough to reach the upper valve in the cocked position.

Because of the relatively low mass of the sampler and its high cross-sectional and surface area, the sampler must not be lowered at too high winch speed, otherwise the wire will finally pass the sampler. Using $^3/_{16}''$ stainless wire, and the 140 L sampler illustrated herewith, a maximum speed of lowering of about

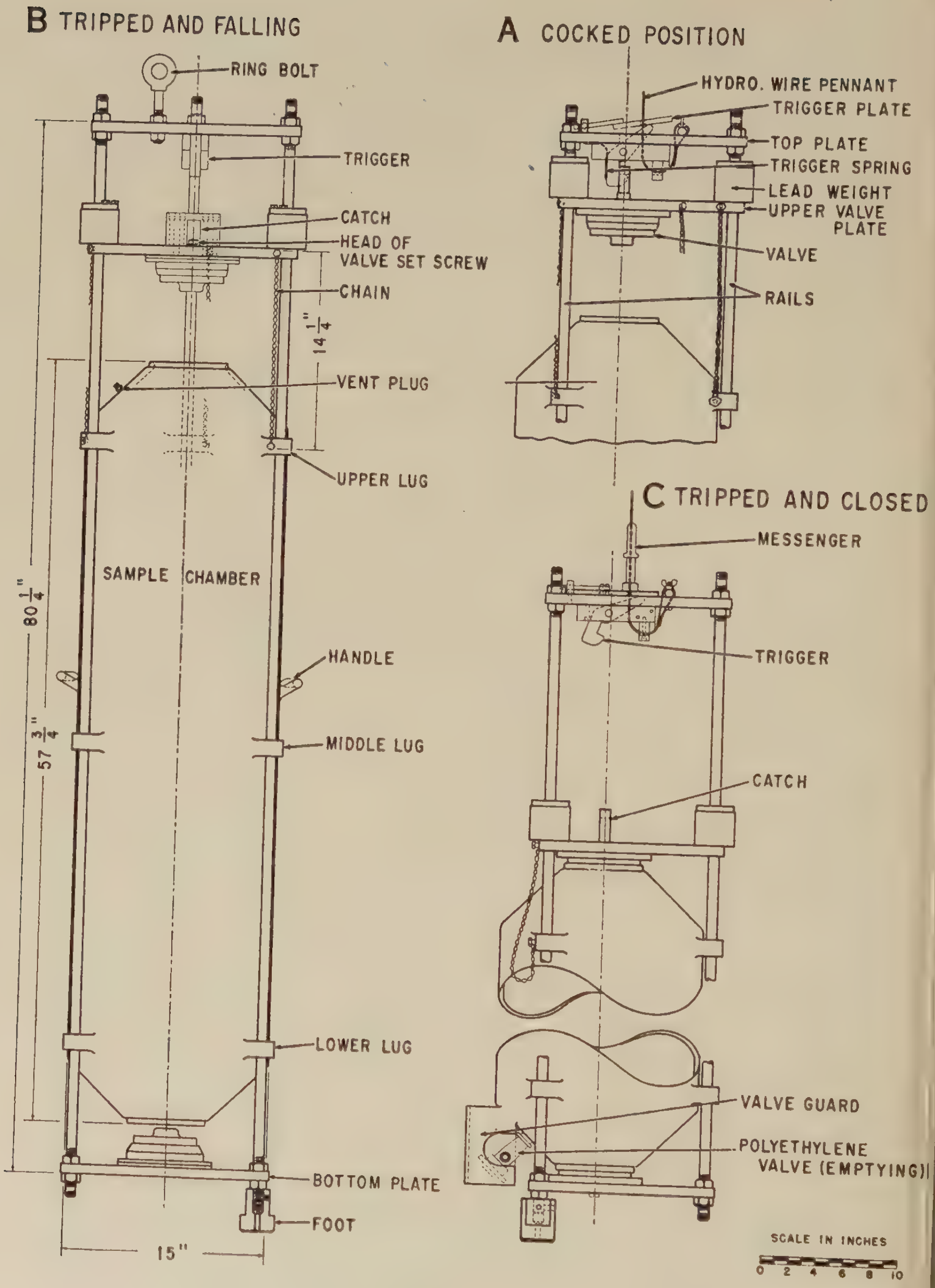
B TRIPPED AND FALLING
RING BOLT
TRIGGER
CATCH
HEAD OF VALVE SET SCREW
CHAIN
14 1/4"
VENT PLUG
UPPER LUG
SAMPLE CHAMBER
80 1/4"
57 3/4"
HANDLE
MIDDLE LUG
LOWER LUG
BOTTOM PLATE
FOOT
15"
A COCKED POSITION
HYDRO. WIRE PENNANT
TRIGGER PLATE
TOP PLATE
TRIGGER SPRING
LEAD WEIGHT
UPPER VALVE PLATE
VALVE
RAILS
C TRIPPED AND CLOSED
MESSENGER
TRIGGER
CATCH
VALVE GUARD
POLYETHYLENE VALVE (EMPTYING)
SCALE IN INCHES
0 2 4 6 8 10

Figure 1.

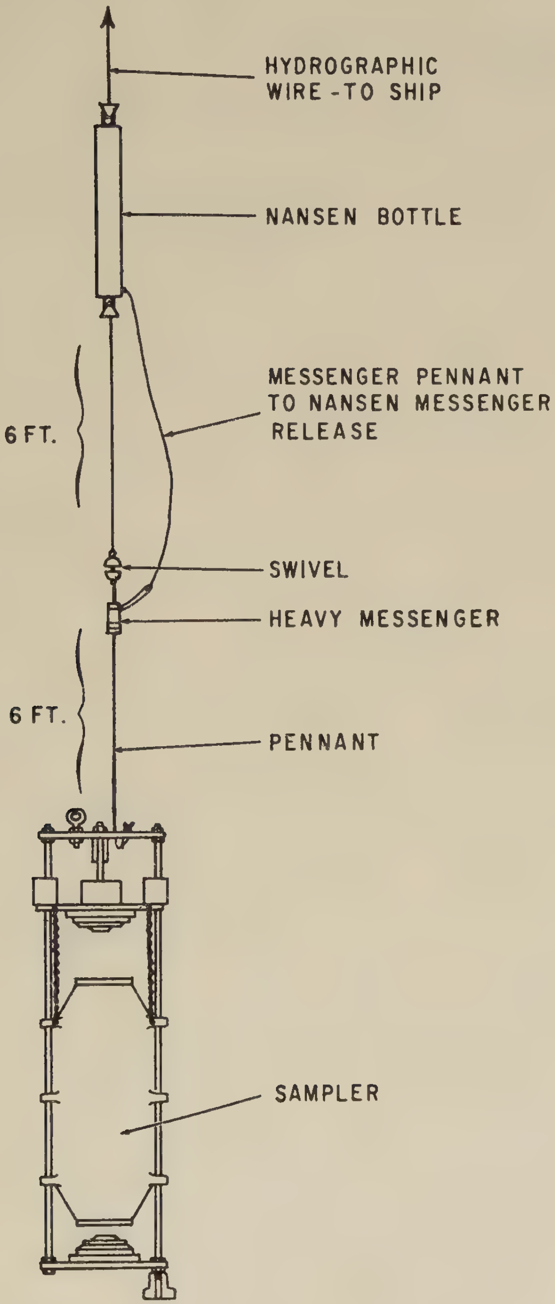
HYDROGRAPHIC WIRE - TO SHIP
NANSEN BOTTLE
MESSENGER PENNANT TO NANSEN MESSENGER RELEASE
6 FT.
SWIVEL
HEAVY MESSENGER
6 FT.
PENNANT
SAMPLER

Figure 2.

45 m/min. has been found to be safe. The full sampler can be raised at normal operating maximum speed.

During the operation of getting the cocked sampler over the side, considerable danger—in fact, substantial certainty—of a pre-trip exists. This is obviated by placing a large clamp on one rail to hold the upper valve plate in cocked position. After resetting the trigger if necessary, and after the Nansen bottle has been rigged, this clamp is removed just before lowering away.

No general prescription for ship handling can be made. The three devices now in use have seen service from RV PANULIRUS (50 feet) of the Bermuda Biological Station, and from RV BEAR (103 feet), RV CRAWFORD (125 feet) and RV CHAIN (215 feet) of the Woods Hole Oceanographic Institution fleet. In each case the details of rigging have presented new, but solvable, problems. Both $^5/_{32}$ and $^3/_{16}$ wire have been used; so far no sampler has been lost.

The stations for which these samplers are used normally require from 6–11 lowerings, and the time to empty the chamber through the $^1/_2''$ valve used is about 15 minutes. Thus the saving in ship time by having two samplers in use alternately rather soon pays for the second device. Operating in this way, a station with samples at surface, 100, 300, 500, 700, 1000, 1500, 2500, and 4000 m can be obtained in less than 10 hours.

Performance Data. Table I compares hydrographic data from a recent station made with the large volume sampler, with data from a regular hydrographic station made with Nansen bottles in series just before the large sampler station. In general the salinities of sampler and simultaneous Nansen bottle agree within the precision of the salinometer employed (Schleicher and Bradshaw, 1956). It is seen that the lowerings to 91 and to 297 m spanned regions of rapid change in salinity; in both cases the flushing of the large sampler has been thorough enough to show the difference in salinity over the approximately 5 m difference in depth (Fig. 2) between it and the Nansen bottle. This confirmation of the excellence of flushing, at least by comparison with the Nansen bottle, has been the usual observation whenever sharp gradients have been encountered.

So far these large samples have been used principally for radiochemical studies (Bowen and Sugihara, 1960), with complete satisfaction. Unpublished studies by Curl and Bowen have indicated they are also suitable for separation of organic particulate matter; others by Ryther have shown that the water is suitable for culture experiments with marine phytoplankton. We believe that, with slight modification, the samples would prove suitable for trace element analysis of both dissolved and particulate phases; as now used, the sample chamber is painted outside with a zinc chromate anti-corrosion paint. Although the filtered material from these samples showed less paint contamination than is usual from either Nansen or Van Dorn bottle samples, we believe trace element samples should be collected with an unpainted and probably freshly polished device.

TABLE I.

Cruise Chain 17
Position: 00° 13′S; 18° 34′W

Station Number 341
Date: 24-IV-61

Hydrographic Station			Large Sampler Station			
Corr. Depth (m)	Temp. (°C)	Salin. (°/oo)	Corr. Depth (m)	Nansen Temp. (°C)	Nansen Salin. (°/oo)	Sampler Salin. (°/oo)
1	29.27	35.350	1	–	–	35.008
30	27.13	36.051				
60	20.42	36.241				
99	16.05	35.704	91	15.16	35.596	35.526
149	14.22	35.443				
199	13.21	35.298				
248	12.13	35.170				
298	10.54	34.975	297	10.29	34.954	34.939
398	8.56	34.757				
			494	6.73	34.592	34.590
596	5.47	34.504				
			692	5.16	34.496	34.500
795	4.55	34.495				
994	4.39	34.612	987	4.39	34.616	34.616
1193	4.42	34.786				
1392	4.31	34.924				
			1494	4.07	34.966	34.961
1587	3.98	34.960				
1887	3.46	34.958				
2187	3.298	34.952				
2487	2.971	34.929	2485	2.961	34.933	34.930
2787	2.730	34.916				
3087	2.607	34.903				
3487	2.479	34.896				
3887	2.226	34.879				
4287	1.334	34.778				
4687	1.092	34.749				
5087	1.110	34.746	5003	1.120	34.758	34.754
5378	–	34.754				
5578	1.150	34.750				
5778	1.185	34.748				
6076	1.231	34.748				
6374	1.274	34.753				
6673	1.317	34.748				
			6774	1.33	34.748	34.899
6872	1.344	34.750				
7072	1.377	34.750	7072	1.41	34.750	34.753
7271	1.407	34.746				
7570	1.451	34.746				

Because of the large volume of sample obtained, very little change of temperature occurs during retrieval. Although no advantage has been taken of this fact so far, the samples would be very suitable for collection of living organisms, especially low-temperature stenotherms.

Acknowledgments. It is a pleasure to thank our many co-workers who have assisted in this development, both in making useful design suggestions and in working out safe procedures for ship handling. We are most grateful to personnel of the American Durafilm Company, Newton Lower Falls, Massachusetts, for assistance in technical aspects of the plastic coating. The original development work was supported very largely by the National Science Foundation — International Geophysical Year program. Additional support has been received from the Office of Naval Research and from the Atomic Energy Commission under grant AT(30–1)–2174.

REFERENCES

Schleicher, K. E. and Alvin Bradshaw
1956. A conductivity bridge for measurement of the salinity of sea water. J. Cons. int. Explor. Mer, *22*: 2–20.
Bowen, V. T. and T. T. Sugihara
1960. Strontium-90 in the "Mixed Layer" of the Atlantic Ocean. Nature, London, *186*: 71–72.

Contribution No. 1209

The Measurement of Dehydrogenase Activity in Marine Organisms[1]

Herbert Curl, Jr.[2]
Woods Hole Oceanographic Institution
Woods Hole, Massachusetts

Judith Sandberg[3]
Department of Biophysics
John Hopkins University
Baltimore, Maryland

Abstract. A method for the estimation of respiratory potential in marine biological material is discussed. The method, which depends upon photometric assay for a dehydrogenase enzyme by the reduction of tetrazolium salt, showed that activity measurements are positively, linearly, related to oxygen consumption measurements. Respiratory potential may be measured immediately upon securing the material, or at a later time.

INTRODUCTION

Studies of rates of energy transfer and metabolic turn-over in marine populations are dependent upon measurements of respiratory rates of samples of the populations or their components. The standard procedure for assessing such metabolic activity has been the measurement of oxygen consumption by the techniques of iodimetry (Winkler method), manometry, or by oxygen electrode. Among them, the techniques involve variables and inconsistencies that render intercomparison difficult. The most important variable is biological: the crowding of organisms at high density in a bottle, sometimes for extended periods, is a very unnatural condition. Since oxygen consumption itself is a function of the chain of respiratory enzymatic reactions interposed between oxidation of a substrate and the assimilation of oxygen, the unusual conditions present during the usual measurement of oxygen consumption may be avoided by determining the activity of one of the interposed enzyme systems either *in vitro* or *in vivo*.

---

[1] Contribution No. 1209 from the Woods Hole Oceanographic Institution. This study was aided by grants from the National Science Foundation (NSFG13272 and G8339).

[2] Present address: Department of Oceanography, Oregon State University, Corvallis, Oregon.

[3] Woods Hole Oceanographic Institution, Summer Student Fellow, 1960.

REPRINT FROM JOURNAL OF MARINE RESEARCH, VOLUME 19, 3, 1961

Some enzyme systems, *e. g.* the cytochromes, do not lend themselves to the "quick and dirty" methods that must by employed on shipboard, if not in the laboratory itself, because of their lability. However, a variety of biochemical techniques for the determination of dehydrogenase activity have appeared in recent years, and these are admirably suited for use with plankton organisms. Initially, the rate of reduction of redox dyes such as methylene blue was used, although there was no satisfactory evidence that a single component of a coupled enzyme system was being determined. Tetrazolium salts have found favor in recent years for determining dehydrogenase activity in histochemical preparations because the reaction could proceed aerobically and the resulting colored products could be determined with great sensitivity, although the reaction is not necessarily specific for a particular substrate (Novikoff 1955, Cooperstein *et al.* 1950).

Aleem (1955) attempted to determine the standing crop of phytoplankton by using a tetrazolium salt, assuming a constant respiration rate per unit weight of organic matter.

The tetrazolium salts are organic compounds which form stable colored compounds (formazans) upon reduction. This may be accomplished with various organic compounds such as ascorbic acid, or substrates or DPNH in the presence of flavine-containing enzyme. In aerobic metabolism, energy is obtained from a stepwise transfer of electrons from complex organic compounds to oxygen, the process of oxidative phosphorylation. Dehydrogenases oxidize or remove hydrogen atoms in a number of these steps. The tetrazoliums have the convenient attribute of intercepting hydrogen atoms, thereby becoming themselves reduced instead of the associated cytochromes. The reduction products, formazans, occur as water-insoluble precipitates in tissues, usually close to the sites of actual dehydrogenase activity. For quantitative purposes, the colored formazan may be extracted in an organic solvent and the concentration determined photometrically.

The objective of the study reported here was to develop a quantitative procedure for measuring the dehydrogenase enzyme activity in living tissues of phyto- and zoo-plankton at sea, as an indicator of the respiratory potential of the populations.

METHODS

Reagents. A variety of tetrazolium salts is commercially available and new ones appear at frequent intervals. Among those tested were TTC (Triphenyl tetrazolium chloride), Tetrazolium blue, Neo-tetrazolium chloride, Nitro blue tetrazolium and INT (2p Iodophenyl-5-phenyltetrazolium chloride).[4] Aqueous solutions of the salts were reduced with ascorbic acid, note being taken of the length of time required to produce a dense colored product. The

---

[4] All obtained from the Nutritional Biochemicals Corporation, Cleveland, Ohio.

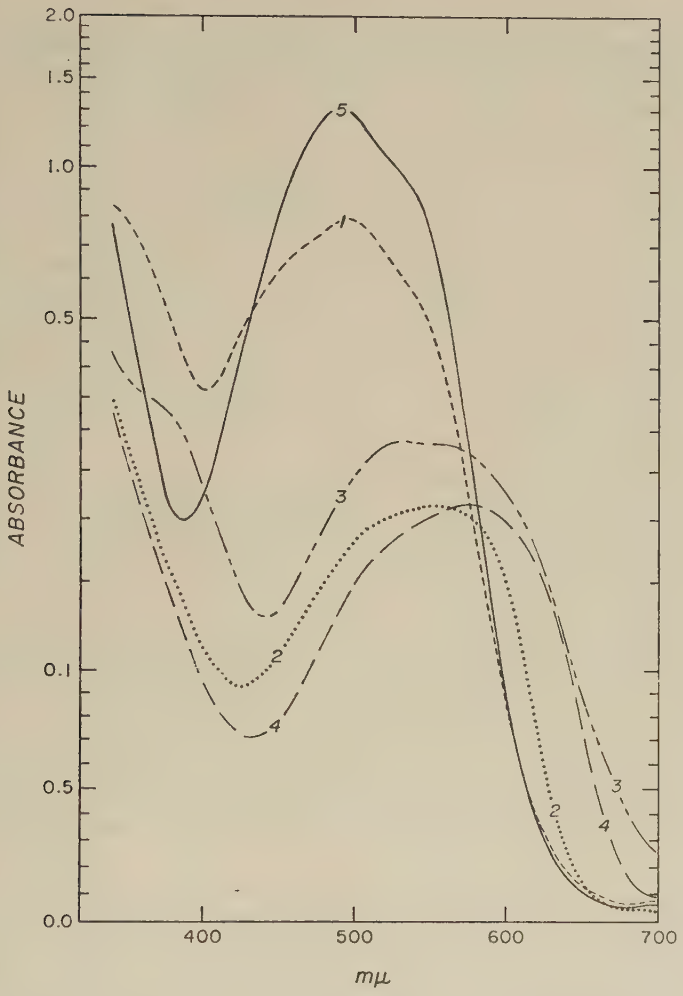

Figure 1. Absorption spectra of five formazans. Tetrazolium salts were reduced with ascorbic acid under aerobic conditions and the resulting formazan dissolved in TCE-acetone. INT (1), Neo-T (2), Nitro-BT (3), Tetrazolium Blue (4), TTC (5).

resulting formazans were extracted with a tetrachloroethylene-acetone mixture, and absorption curves were plotted with a Carey recording spectrophotometer (Fig. 1). INT and Neo-tetrazolium reduced immediately. Comparison of INT reduction under aerobic and anaerobic conditions showed no difference in amount of formazan formation. Nitro blue tetrazolium began reducing immediately but took about ten minutes to achieve maximum color. Blue tetrazolium and TTC showed no color after one hour; however, upon raising the pH, a formazan was produced very slowly by Blue tetrazolium, but not by TTC; in approximately 48 hours TTC also became reduced. Under anaerobic conditions it seems likely that these latter tetrazoliums would have reacted more quickly. INT was chosen for experimental purposes because it competed well with oxygen for liberated electrons, making anaerobiasis unnecessary, because it was reduced most rapidly of those tested, and because it gave the greatest sensitivity. INT formazan has a rather narrow peak of light absorption at 490 mμ and would be suitable for use with a spectrophotometer.

An INT solution was prepared by dissolving 100 mg of the substance in 50 ml of distilled water. A few drops of 3N sodium carbonate solution were added to bring the pH to approximately 7.5, thereby increasing the solubility of the salt. After filtering, the resulting clear, yellow-brown solution was kept under refrigeration. New solutions were prepared weekly, but if kept at 5°C they were stable for several months.

Sodium succinate was prepared weekly as a 0.4M stock solution in distilled water with a few drops of 3N sodium carbonate solution added, and refrigerated. Other substrates were prepared in a similar manner.

Phosphate buffer of pH 7.7 (0.2M) was prepared from KH_2PO_4 and NaOH solutions.

Biological Materials. Both intact and homogenized organisms were used. Intact organisms were wet-weighed and used immediately. Homogenates were prepared with a ground glass tissue grinder at concentrations of 25 mg of wet tissue per ml of homogenate, in distilled water. Grinding was performed with the apparatus immersed in ice. The homogenate was centrifuged for a few minutes to provide a supernatant fluid devoid of visible particles; usually one ml of this fluid was used in a reaction.

Procedure. One ml of homogenate or approximately 25 mg of intact organisms was added to a reaction mixture consisting of 2 ml phosphate buffer, 1 ml 0.4M sodium succinate, and 1 ml of 0.2% INT solution in screw-capped 15 ml test tubes; reaction mixture for one day was made up in these proportions in advance. No attempt was made to estimate the keeping properties of the reaction mixture beyond 24 hours. (Nachlas *et al.* [1960] found that their combination of reagents would keep for two weeks at 5°C. At −18°C the reaction mixture remained unchanged at the end of three months.) The tubes were placed at once in a covered constant-temperature bath for a carefully timed period.

The formazan produced is insoluble in water but is soluble in organic solvents such as isoamyl alcohol, chloroform, acetone and tetrachloroethylene. A suitable solvent would be immiscible with water, would not form unbreakable or strong emulsions with water, especially in the presence of much dissolved organic material, and should have a relatively low vapor pressure. A 1:1.5 mixture of tetrachloroethylene and acetone satisfied these requirements. Formazan formation may be stopped either by addition of HCl to lower the pH to 6 or simply by the addition of solvent. The usual procedure was to remove tubes from the incubator to an ice bath prior to addition of solvent.

Eight mls. of solvent were added to each tube and permitted to stand for various lengths of time with shaking. After brief centrifugation, solvent was pipetted from the tube into small screw-capped vials through filter paper. There appears to be no limit to how long the extracted formazan may be kept. Evaporation of solvent must be prevented, therefore discs of polyethylene sheeting were used as gaskets in both the reaction tubes and in the vials. Strong light will bleach formazan temporarily. Rather than work in subdued light, solutions of formazan were kept in a dark box or under black cloths.

Measurements of optical density of the extracted formazan were made at 490 mμ on a Beckman model B spectrophotometer against a reagent blank consisting of all reagents and homogenate except INT.

Measurements of oxygen uptake were made in aspirator bottles of from 130–500 ml capacity. The experimental animals were acclimated for 15–30 minutes in the dark, with water flowing through the bottle before the experiment began. The Winkler method was used in oxygen determinations.

RESULTS

The optimal conditions for various parameters in the reaction were investigated.

pH. The pH of the reaction mixture was varied from 6.8–8.0 (Fig. 2). Using homogenates of the marine minnow *Menidia menidia*, an optimum of 7.7 was found, but it should be possible to achieve good results throughout a range of 7.5–7.9.

Incubation Temperature. Homogenates of *M. menidia* were incubated with INT at temperatures of 25–50°C, with and without pre-incubation of the homogenate before addition of the reaction mixture (Figs. 3, 4).

Homogenates kept at 0–5°C showed no activity. When incubated at temperatures of 25, 30, 35 and 40°C, increased rate of reaction was observed with increasing temperature, except that the rate at 40°C was initially the same as that at 35°C and declined after 20 minutes incubation (Fig. 3). Homogenates were incubated at temperatures of 25–50°C for 20 minutes without addition of reaction mixture, after which they were incubated for 30 minutes at 34°C.

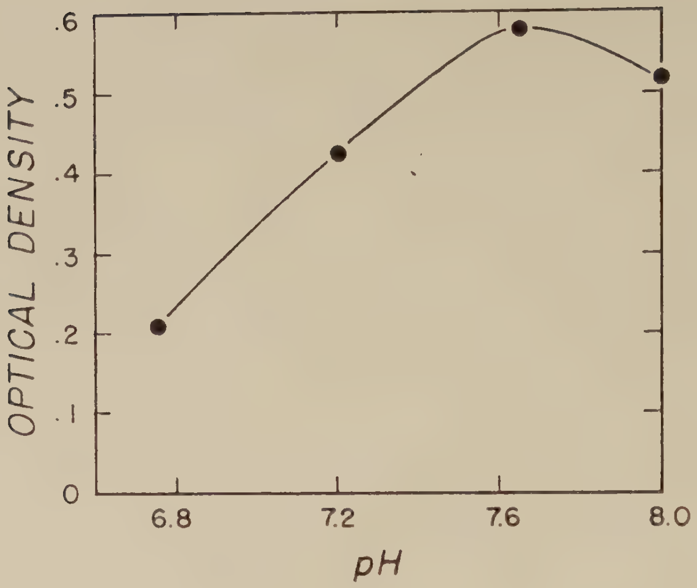

Figure 2. Reduction of INT as a function of pH; incubation 30 minutes at 35°C.

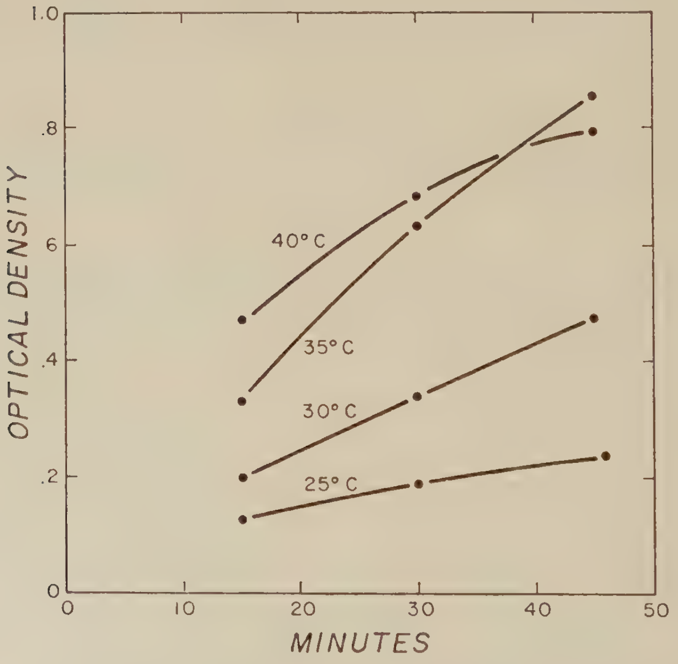

Figure 3. Reduction of INT as a function of time at various temperatures.

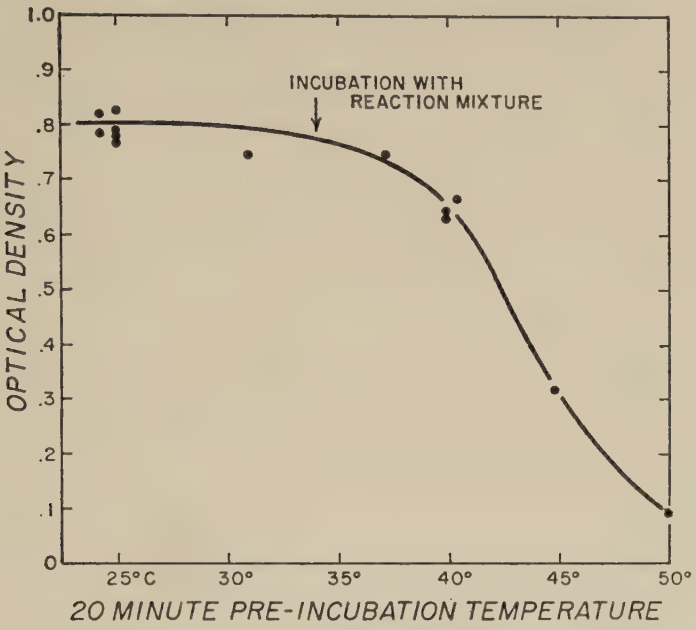

Figure 4. Effect of preincubation at various temperatures before addition of reaction mixture; reaction for 30 minutes at 35°C.

The amount of reduction decreased about 18% from 25–40°C. At higher temperatures, activity was greatly reduced (Fig. 4). An incubation temperature of 35°C was chosen for subsequent experiments and pre-incubation was avoided inasmuch as no increase in activity resulted. This regime gave the maximum rate of activity, linear with time, and gave no evidence of enzyme deactivation.

Reagent Concentration. It was desirable that the measured enzyme activity be independent of INT concentration. The concentration had to lie within the limits of decreasing the reaction rate by its scarcity or by inhibiting the reaction with an excess. The rate of reaction was measured with three stock concentrations of INT: 0.08, 0.04, 0.01% at a temperature of 35°C and at a homogenate concentration of 0.025 g/ml (Fig. 5). An INT concentration of 0.04% gave a reduction rate which was essentially linear for the first 30 minutes and gave the highest rate among the three concentrations. A concentration of 0.08% is still a very low one. Its obvious inhibiting action after 20 minutes may indicate that INT can so successfully compete for electrons that the intermediary metabolism dependent upon dehydrogenation is "starved".

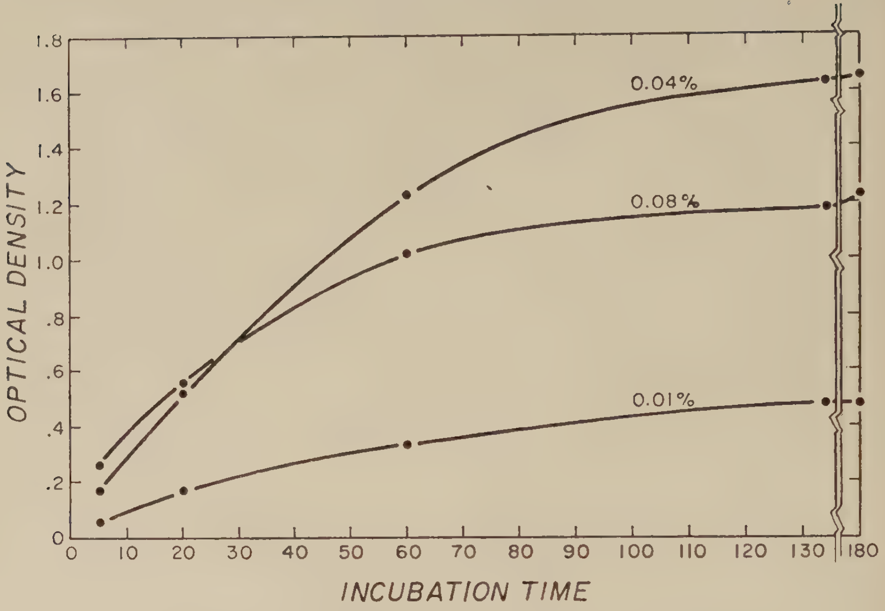

Figure 5. Effect of INT concentration and time on development of formazan, at 35°C.

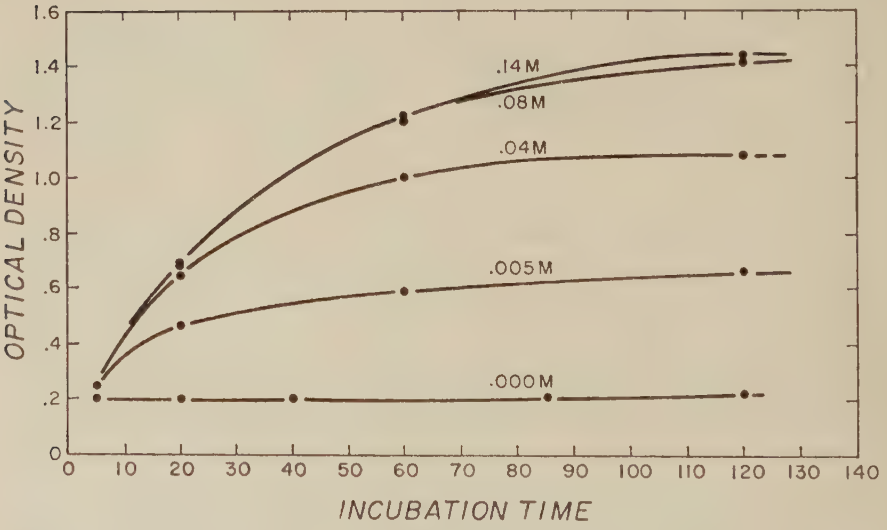

Figure 6. Effect of succinate concentration and time on development of formazan, using standard reaction mixture (see text).

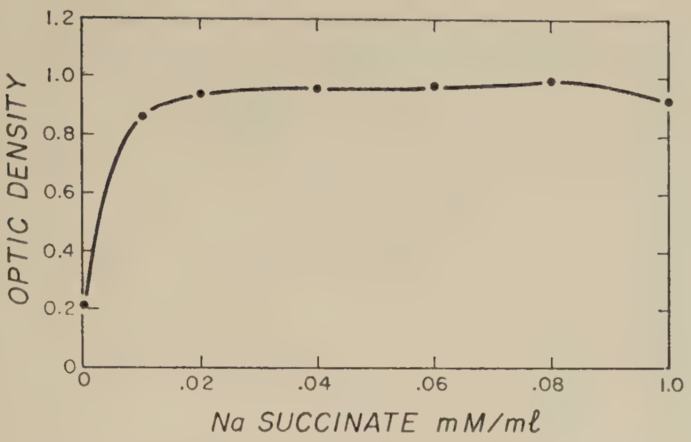

Figure 7. Effect of succinate concentration on formazan development, using standard reaction mixture.

Enzyme activity is proportional to substrate concentration up to some maximum and then becomes independent of further increase. It is particularly desirable to operate on a portion of the curve where the reduction rate is independent of substrate concentration. Four concentrations of sodium succinate were investigated (Fig. 6). The reaction rate increased with higher succinate concentrations up to 0.08M. Doubling this concentration had no significant effect upon the reaction rates.

A curve of initial velocity versus substrate concentration (Fig. 7) indicated that the maximum velocity was reached at a substrate concentration of 0.02M for a 20 minute incubation, other conditions being fixed. The standard succinate concentration was chosen to be 0.08M, for at this concentration the solution was substrate-saturated and no substrate inhibition was found below 1.0M succinate.

Incubation Time. The initial velocity of the reaction may be obtained from a curve of activity or optical density versus time (Figs. 3, 5, 6, 9). The initial velocity is obtained by extrapolating the curve to t = 0. For the standard reaction conditions, all the curves indicate linearity between activity and time up to at least 30 minutes. One interval on the linear portion may be taken to represent the initial velocity. The 20-minute interval was used as it was in the linear range and yielded a convenient optical density.

Enzyme Concentration. Presuming that substrate and indicator are present in unlimited quantities and that aerobic metabolism may be carried out, the reduction of indicator should proceed indefinitely and at a rate proportional to the concentration of enzyme. However, in *in vitro* experiments, substrate

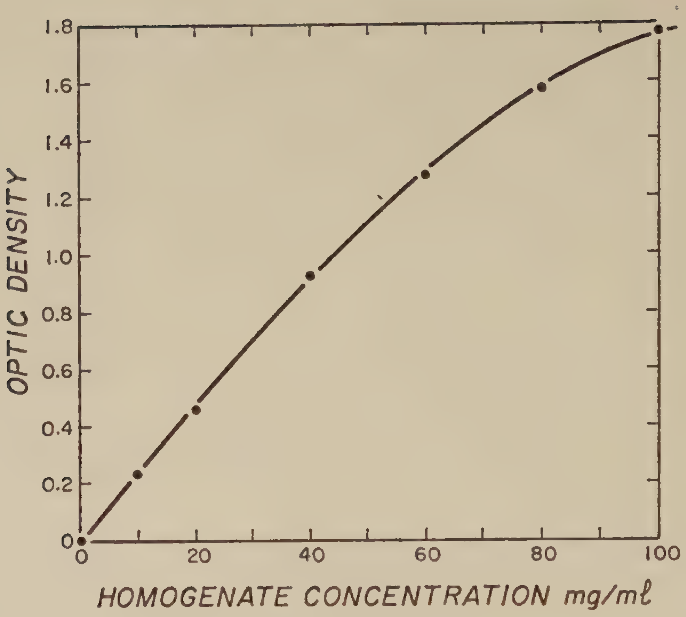

Figure 8. Effect of homogenate concentration on formazan development using standard reaction mixture.

and indicator are both ultimately limiting and the rate decreases. For a definite amount of formazan production to be proportional to the enzyme concentration, the formazan must be measured while the rate of production is constant and is limited only by enzyme concentration.

By varying the concentration of *M. menidia* homogenate, a linear relationship was obtained between formazan production and enzyme concentration up to 60 mg wet weight/ml homogenate (Fig. 8). Several concentrations of *Menidia* homogenate were incubated for various lengths of time. The effect of reagent depletion was most noticeable at the highest concentration of 10 mg/ml homogenate, occurring after about an hour. The concentration of 2.5 mg/ml homogenate gave a slowly decreasing rate of reduction but no evidence of sudden depletion for at least three hours (Fig. 9).

Substrate Dependence. It has been reported that cofactors are required for the *in vitro* use of substrates other than succinate (Kivy-Rosenberg *et al.*, 1959). We have demonstrated that homogenized organisms require exogenous substrate for reduction of significant amounts of indicator. Without substrate, only very slight activity was observed (Figs. 7 and 10). Sodium succinate was used in these experiments. In addition, the effects of alpha keto glutarate, malate, fumarate, glucose, and aspartic acid were determined. The use of substrates other than succinate gave an amount of reduction equivalent to that

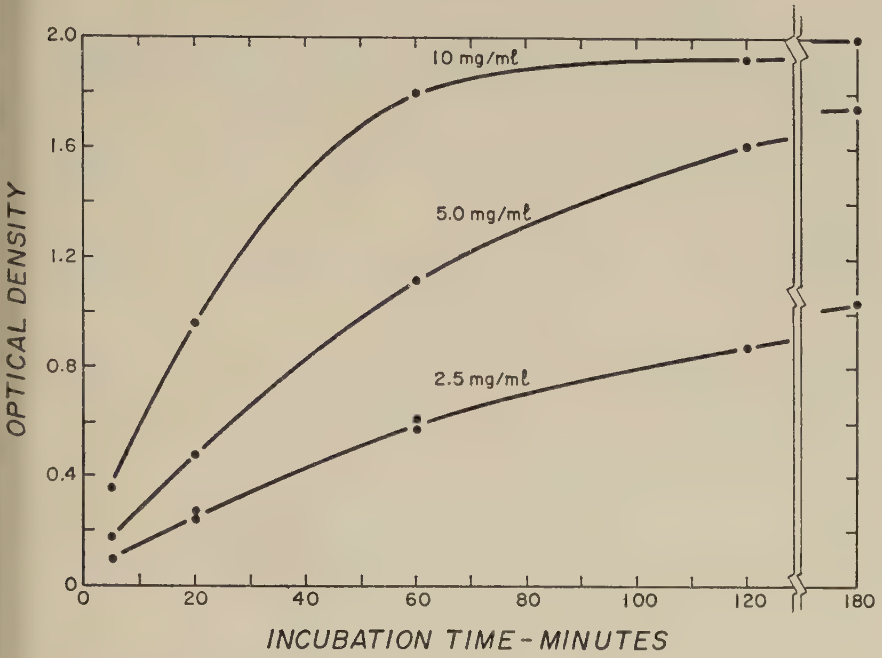

Figure 9. Effect of homogenate concentration and time on formazan development, using standard reaction mixture.

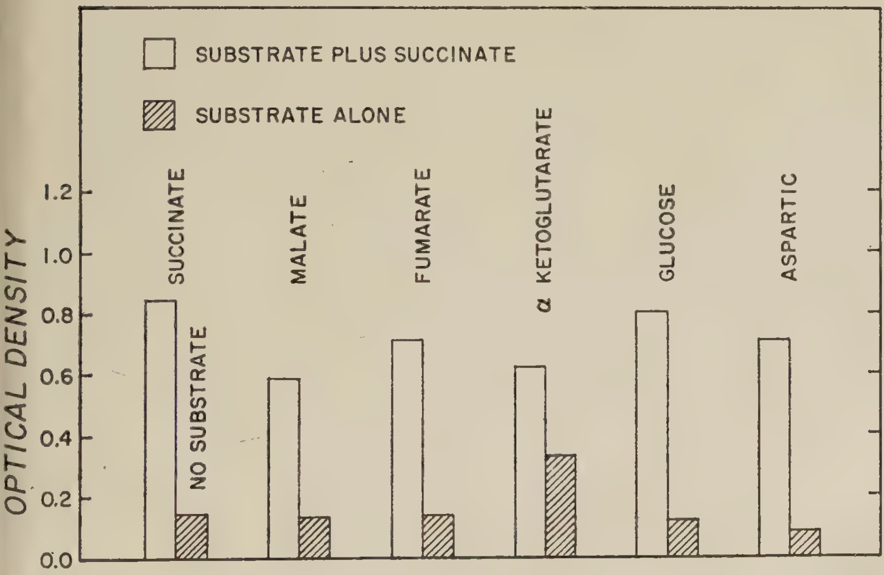

Figure 10. Effect of various substrates with and without added succinate on formazan development.

achieved with no substrate at all (Fig. 10). The combination of one of the other substrates with succinate gave values lower than the value obtained with succinate alone (with the exception of glucose-succinate). We may have some confidence that the method is specific for succinic dehydrogenase, since only this substrate with no cofactors has been used. Other endogenous substrates and their associated cofactors appear to be in too low supply to support significant reduction.

Reduction with intact organisms was less dependent upon an exogenous substrate source (succinate) than with homogenized organisms, but the addition of substrate accelerated the reaction by 10%.

Preparation of Biological Material. In order to adapt the technique to shipboard use, two additional problems were investigated: the feasibility of preservation of material for later analysis, and the desirability of homogenizing the sample either before or after reduction.

At 25°C, activity diminished by about 50% in 6 hours and was nil after 20 hours. A renewal of activity after 24 hours was observed as a result of bacterial growth. A high rate of activity may be preserved for 3 hours at 0°C, but this will diminish by 50% in 48 hours.

Freezing intact and homogenized organisms with dry ice at –60°C to maintain high activity was unsuccessful. Intact specimens appeared to give consistently lower values than homogenates.

Calibration. In the experiments described thus far, it has been shown that a good correlation exists between the quantity of biomass used and the resulting formazan production. However, we have demonstrated that the reaction is dependent upon a single substrate-specific enzyme, succinic dehydrogenase. The quantities of biomass used have been equated with corresponding quantities of enzyme, but no direct estimate of the actual enzyme content was made. Except as has been done indirectly in these experiments, no such estimate is feasible. It is possible either to measure the actual proton-accepting ability of a given amount of tetrazolium or to determine the amount of formazan produced proportional to the availability of a given number of protons. The latter course has been followed. Aliquots of an ascorbic acid solution providing 0.1 meq. H^+/ml were added to the standard reaction mixture and incubated until color formation had ceased (Fig. 11). Ascorbic acid in excess of 3 meq. H^+ did not exceed the proton-accepting capacity of the INT used in the mixture. Lower concentrations produced a linear relationship between the formazan produced and the proton supply. Thus, under the time, temperature, and pH regime used in these experiments, it is possible to express the enzyme activity observed as meq H^+transferred/g dry weight or organic weight/hour. When samples from natural populations are used, units of meq H^+transferred/m^3 sea water/hour would be appropriate.

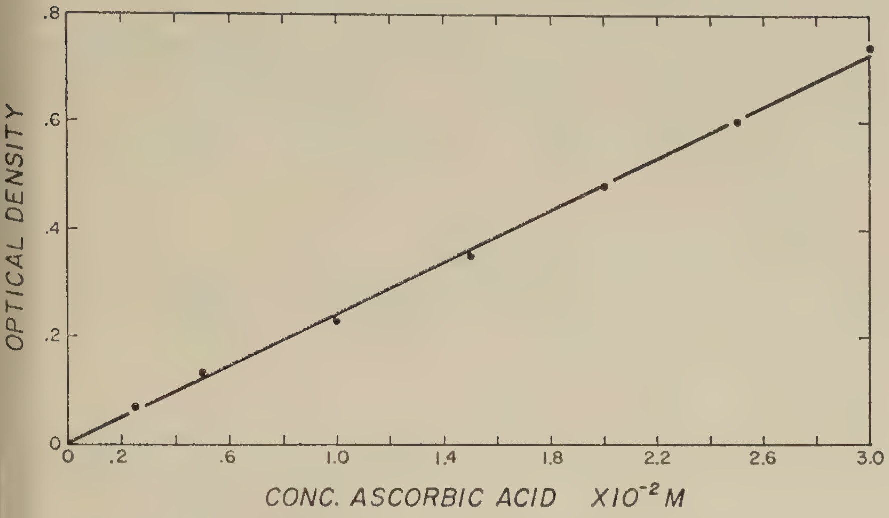

Figure 11. Calibration curve of formazan development optical density *vs.* concentration of ascorbic acid where 1 ml 0.01 M ascorbic acid is equivalent to 0.01 meq. H+.

Activity in Biological Material. We can report only preliminary results from two marine organisms used in laboratory experiments. These were the atherinid minnow, *M. menidia*, and a decapod crustacean, *Palaemonetes vulgaris* (Say).

Respiration rates of invertebrate animals vary with environmental conditions such as temperature and oxygen tension, and with species, size and activity. Though not a planktonic organism, *M. menidia* was used initially because it was easily obtained and weighed, and its tissues showed high activity. Oxygen uptake by a single fish was measured for 30 minutes, after which its tissues were homogenized and the dehydrogenase activity measured (Fig. 12). There is a positive, linear relationship between oxygen consumption and enzyme activity. Regression lines have been fitted to the experimental points by the method of least squares. The correlation coefficient (r) of 0.91 is significant at the 0.01 level. Neither regression line passes through the origin, although Y as a function of X approaches it closely. These data indicate that a small amount of enzyme activity should be observed in the complete absence of gaseous respiration. Rates of oxygen consumption above 0.4 ml/g/hr., as found in *M. menidia*, are normally associated with active and vigorous swimmers such as mackeral (*Scomber*) (Baldwin, 1924). The scatter of the points may be attributed to varying size and activity of the specimens, although specimens averaging 40 mm were used.

Enzyme activity per unit weight of material as a function of specimen size was also measured (Fig. 13). Activity decreased 50% with a ten-fold increase in body weight. A highly significant correlation coefficient of −0.99 has been

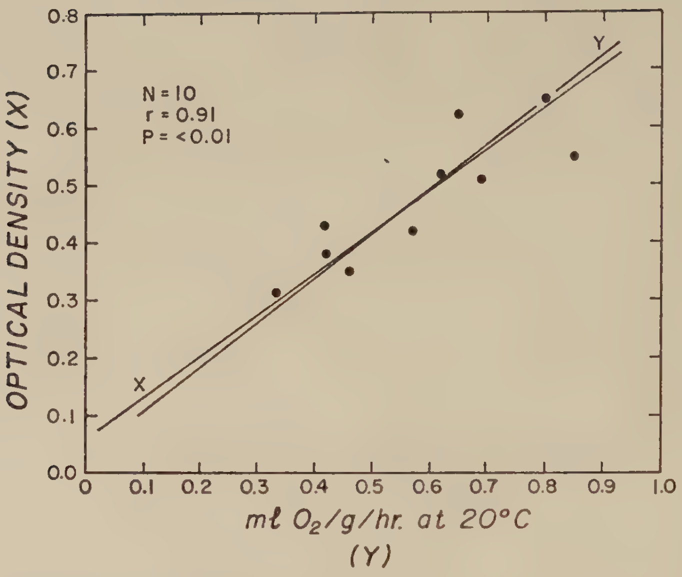

Figure 12. Oxygen consumption of *Menidia menidia* and equivalent formazan production of a homogenate containing 25 gm wet weight/ml of homogenate.

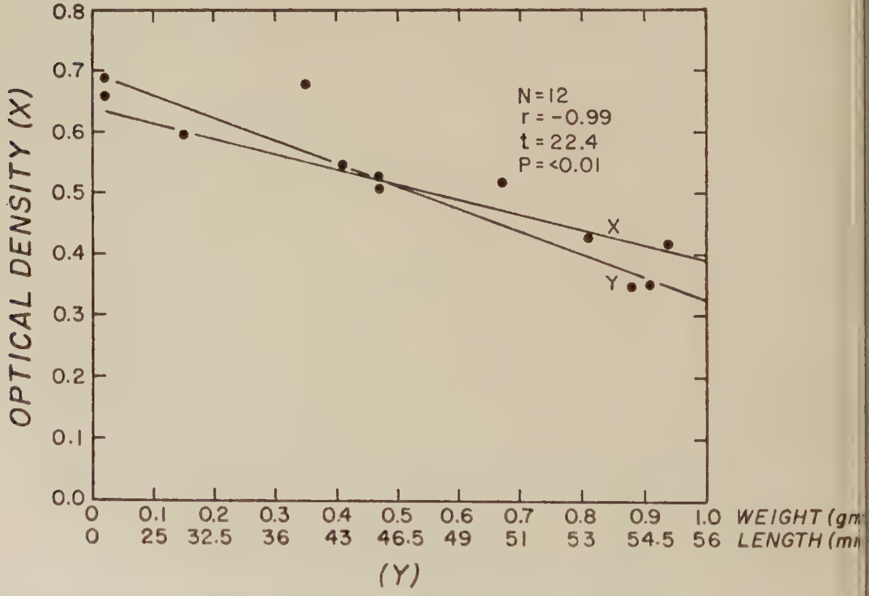

Figure 13. Formazan production per 25 mg wet weight of *Menidia* homogenate for various sizes of fish.

computed for this relationship. Since activity is plotted as a function of body size, the scatter in the data must be attributed to individual differences between specimens and to experimental errors. The data were replotted as enzyme activity for a whole organism against body weight. Oxygen consumption was replaced with formazan production in the formula:

$$cc\ O_2 = k\,W^x,$$

where k is a species constant, W is the wet weight of the organism, and x is ideally 0.66 if oxygen consumption is exactly related to surface area, since surface area changes as the $^2/_3$ power of the weight. The formula:

$$O.D. = 0.133\,W^{0.7}$$

fits the replotted data very closely. An exponent of $x = 0.7$ is a commonly reported value for *Menidia*-sized organisms (Zeuthen, 1953).

Several experiments were performed on freshly caught and starved fish. Starving for eight days decreased oxygen consumption by 40% and enzyme activity by 20% in 0.4–0.5 g specimens. Undoubtedly some of the observed depression of oxygen consumption is due to acclimatization to experimental conditions; depressed enzyme activity is probably a better indication of the physiological condition of the specimens

DISCUSSION AND CONCLUSIONS

The method of measuring respiratory potential described here should be a useful one for both laboratory and field work. It has the advantage of being technically uncomplicated and dispenses with the need of maintaining *in vivo* conditions during the measurement. Thus the technique, through the extraction of formazan, may be carried out on board a vessel, and the absorbance of the solution may be measured later, ashore. Care must be taken to prevent evaporation of the solvent and bleaching of the formazan.

The parameter being measured by our procedure has been called "respiratory potential" because the gross activity of an enzyme, which is unlimited by substrate concentration, should be constant per unit weight of enzyme. In effect, the amount of enzyme or, the capacity of the system, is being determined. This capacity or potential should be maximal with respect to the actual respiratory activity of the organism, which may depend upon food eaten, motor activity, temperature, etc. A linear relationship between gaseous respiration (oxygen consumption) and enzymatic activity (tetrazolium reduction) was found in *M. menidia*, indicating that measurements of dehydrogenase activity may be substituted for *in vivo* measurements of gaseous respiration. Preliminary work at sea indicates that all of the animals tested thus far (copepods, euphausids, pteropods, chaetognaths, amphipods) possess a succinic dehydrogenase. However, evidence is not yet at hand to determine whether the same linear relationship that was found for *M. menidia* holds for these invertebrates.

ACKNOWLEDGEMENT

We are grateful to Dr. V. T. Bowen for many helpful suggestions and comments and to Mr. Richard Stone for his valuable shipboard and laboratory assistance. Appreciation is extended to Dr. Max Blumer for his advice in choosing suitable solvents for the formazans and for the preparation of absorption spectra of the formazans on the Carey spectrophotometer. Thanks are due to Dr. Evelyn Kivy-Rosenberg for many helpful suggestions.

REFERENCES

Aleem, A. A.

1955. Measurement of plankton populations by triphenyltetrazolium chloride. Kieler Meeresforsch., *11*: 160–173.

Baldwin, F. M.

1924. Oxygen consumption in marine animals. Proc. Iowa Acad. Sci., *30*: 173–180.

Cooperstein, S. J., A. Lazarow, and N. J. Kurfess

1950. A microspectrophotometric method for the determination of succinic dehydrogenase. J. biol. Chem., *186*: 129–139.

Kivy-Rosenberg, E., J. Cascarano and G. Merson

1959. Examination of some DPN and TPN dependent dehydrogenase activity before and after relatively high doses of X irradiation of *Spisula* eggs. Biol. Bull. Woods Hole, *117*: 415.

Nachlas, M. M., S. I. Margulies and A. M. Seligman

1960. A colorimetric method for the estimation of succinic dehydrogenase activity. J. biol. Chem., *235*: 499–503.

Novikoff, A. B.

1955. Histochemical and cytochemical staining methods, *in* Analytical cytology. R. C. Mellers, ed. Blakeston Div. McGram Hill, New York. 500 pp.

Zeuthen, E.

1953. Oxygen uptake as related to body size in organisms. Quart. Rev. Biol., *28*: 1–11.

Contribution No. 121

Minimal light intensity and the dispersal of schooling fish (1, 2)

BY

EVELYN SHAW *

(Department of Animal Behavior,
The American Museum of Natural History,
New York 24, New York)

---

* The author wishes to acknowledge the fine assistance of Miss Joan BRICKER, a participant in the American Museum's Undergraduate Research Program.

1) This research was supported, in part, by the National Science Foundation grant no. G 10832 and the National Institutes of Health, grant no. M 2322.

2) Contribution no. 1211 from the Woods Hole Oceanographic Institution.

BULLETIN DE L'INSTITUT OCÉANOGRAPHIQUE, MONACO, N° 1213, 11 AOUT 1961.

Introduction

Vision is a critical factor in schooling (reviewed by ATZ, 1953; BREDER, 1959) and schooling fish generally disperse in the darkness of night (reviewed by LOUKASHKIN and GRANT, 1959). Periodically, however, there are reports from fishermen and investigators that orientated schools are seen at night; these observations were also made on *Menidia* by the author at Woods Hole, Massachusetts, during 1960. MOULTON (1960) found that *Anchoviella* and *Caranx* did not disperse after dark in laboratory tanks, and SPRINGER (1957) reports that *Jenkinsia* appeared in a very tight school near his boat, evidently attracted to its night light. BREDER, 1951, on the other hand, found *Jenkinsia* schools completely dispersed at night in the laboratory.

The problem appears not to be one of whether or not fish form schools at night, but rather, one of what is meant by night — in terms of the amount of light available to the fish and whether or not this amount is sufficient for schooling orientation to be present. A number of investigations have been carried out on minimal light values and schooling (ALI, 1959; HARDEN JONES, 1956; KUEHNE, 1958; LOUKASHKIN and GRANT, 1959; and STEVEN, 1959). Some results suggest that fish would be able to remain in schools on both moonlit and darker nights. Since *Menidia* (Atherinidae) were seen schooling on a bright moonlit night, experiments were carried out to find the approximately minimal amount of light necessary to the maintenance of schooling orientation.

A series of laboratory experiments were performed in which light intensity was reduced to the point where schooling orientation was disrupted and did not reappear until the light intensity was increased.

Procedures

Menidia are in-shore fishes, found near the surface in relatively shallow water, and around docks and jetties. Adults can be collected by seining and they are easily stripped of eggs and sperm. It is possible to rear the embryos and larvae in the laboratory from the egg-stage on (Rubinoff, 1958). They hatch about 10 days after fertilization, and are 4.5-5 mm in length; they start to school about three weeks after hatching when they are approximately 12 mm in length (Shaw, 1960, 1961). In these studies, laboratory-reared fry 12-18 mm long were observed — only those fry showing a strong schooling response, close fish to fish distances and continuous, rather than sporadic, schooling, were subjected to the various light intensities.

All testing was done in our standard testing apparatus, the circular tank (Shaw, 1961). The light source for the tank was a 12-inch circular, daylight fluorescent tube, 12 inches above the water level and directly over the circular channel. Three fry were placed into the channel, with the light on, and remained there for at least 1/2 hour before the light intensity was reduced. The maximum intensity, emitted by the circular tube, was 130 ft. candles. Light measurements were taken with a Photovolt Light photometer, model 200A. Its photoelectric cell was placed in the open center of the circular tank, at a level approximating mid-water in the channel. Light was reduced by neutral density filters, 14″ × 17″, prepared in our photography department; it was extremely difficult to obtain precisely the desired density in each filter. Enough were prepared to provide sufficient variety for many combinations of filters.

Light was reduced two ways, rapidly and gradually. When light was reduced gradually, the gradual reductions to different levels were made from 5 ft. candles down to the point where schooling stopped; the fish remained at each level for a certain length of time, 10 minutes or longer, before the light was reduced again. Rapid reduction of light was made to a number of different levels of intensity and the fish were observed at that level only; no further changes were made. For each series of tests of rapid or of gradual light reduction, a new batch of fry were used. Fry remained at each light level again for a minimum of ten minutes, which appeared to be an adequate length of time for any behavioral changes to appear. As a check, however, in five separate instances, fry remained at each intensity for one hour. No obvious differences in behavior were observed between those exposed to each level for 10 minutes and those exposed for one hour. At the end of each series of tests light was increased rapidly to 130 ft. candles to see if schooling started again.

Results

Twenty-eight separate experiments were performed; of these, 10 were subjected to gradual light reduction, 18 to rapid reduction. When light was reduced gradually, the school loosened between 0.35-0.12 ft. candles. This was noted in four experiments. The fry continued to show parallel orientation, after an initial disruption lasting between 2-5 minutes, but the fish-to-fish distances increased from approximately 1/4 - 1/2 inch to 3 to 5 inches. Schooling ceased at a number of different intensities (Table 1). Fry were found scattered over the bottom of the tank and tended to remain relatively motionless. No positional orientation was noted.

When light was reduced rapidly down to 1 or 2 ft. candles, the school was disrupted for 2-5 minutes, the fish-to-fish distances were increased and fry broke away from the group, swimming in another direction or darting about. The school then reformed and was maintained. When light was reduced rapidly down to intensities of 0.75-0.06 ft. candles, schooling was disrupted, the fry dispersed over the tank, and the school did not reform.

In the remaining experiments light was reduced gradually from 5 ft. candles, to a minimum of 1.75 ft. candles, and schooling was not disrupted at any point.

It was found that the tighter schools (fish-to-fish distances were small) did not break up until the intensity was lower than that at which the looser schools (greater fish-to-fish distances) were disrupted.

TABLE 1

RAPID REDUCTION	GRADUAL REDUCTION	
Ft. candles at which schooling was disrupted	Ft. candles at which fish-to-fish distances increased	Ft. candles at which schooling was disrupted
0.25	0.17	0.04
0.25	0.12	0.05
0.06	0.23	0.06
0.35	0.35	0.25
0.75	— 1)	0.08
0.25	—	0.15
0.25	—	0.12
0.10	—	0.05
0.65 *	—	0.03
	—	0.05

* Continued to school sporadically.

1) Not observed.

Discussion

Schooling disperses at a number of different light intensities in different species of fish. The table summarizes the results of other authors, in order of decreasing light values. Conversions were made to foot candles, wherever possible; the values, therefore, are approximate.

Species	Light reduced by	Light value (in ft. candles) at which schools dispersed.
Aqueidens (Shaw, unpublished)	rheostat	2.5
Rhinichthys (Kuehne, 1958)	neutral density filters	0.12
Semitolis (Kuehne, 1958)	” ” ”	0.17
Hepsitia (Steven, 1959)	natural daylight (?)	0.05
Bathystoma (Steven, 1959)	” ”	0.05
Menidia (present report)	neutral density filters	0.03 - 0.05
Moonlight (at Woods Hole) *		Ca. 0.012
Sardinops (Loukashkin & Grant, 1959)	bulbs & iris diaphragm	< 0.01
Phoxinus (Harden Jones, 1956)	rheostat	0.002
Oncorhynchus (Ali, 1959)	bulbs & filters	0.0001

The disparity in the minimal light values needed to disperse the school may be caused by several factors. The most obvious one is that of species differences. However, when the experimental methods are examined, it becomes apparent that many aspects of the experiments need to be clarified before these differences can be assigned to species variability. Some experimental aspects which introduce variability are technique : methods of light reduction and measurement; and the behavioral criterion, the meaning of schooling. Schooling according to Breder (1959) has a precise meaning — a school is an orientated group of fish moving in the same direction, at a uniform speed and the fish are regularly spaced from one another. Kuehne (1958), however, chose to accept Keenleyside's (1955) definition that an aggregation, a non-orientated group can also be called a school. Therefore, in what way group behavior changes, in Kuehne's experiments, is not certain. Kuehne increased the light intensity for dark-adapted fish until the fish gave *some* signs of parallel swimming or altered its swimming path in response to another fish — the light value at which these behavioral changes occurred was considered the visual threshold for schooling. Ali (1959) states that, among salmon, when the light intensity falls below the rod threshold (10^{-4} ft. candles) the school disbands. No other descriptions are given. Somewhat more detailed description of behavior in *Phoxinus* and *Hepsitia* are found in the papers of HARDEN JONES (1956), and STEVEN (1959); here, fish-to-fish distances increased gradually until the fish become independent of one another and either sink to the bottom *(Phoxinus)* or rise to the surface *(Hepsitia)*. LOUKASHKIN and GRANT (1959) by means of stroboscopic photography describe an activity in *Sardinops* which comes about in total darkness; the fish assume a head-up, tail down position, slowly rising to the surface. This same behavior was noted by this author in the acara, *Aequidens*, when it was suddenly placed in the dark.

---

* Personal comm., G. L. Clarke : “ ...the illumination from the full moon is 3×10^{-6} of that from the sun plus skylight at the same altitude. Referring to the chart “ Natural Illumination Charts,” published by the Bureau of Ships, Department of Navy, Report No. 374-1, September 1952 for Latitude 40°, the nearest one to Woods Hole, and assuming that on a night of full moon the altitude of the moon was the same as the maximum for the sun during the winter, you would obtain an illumination on horizontal surface of 1.2×10^{-2} foot candles. ”

In addition to insufficient material for comparison of the various behavioral changes, many technical aspects of each study are also non-equivalent. Methods of measuring the light are subject to error in all but the most sensitive of instruments. Types and shapes of containers serve to influence schooling patterns and the distribution of light. The place where readings are taken, in the water, above the water, in various parts of the tank, also produces variables. Methods of light reduction, neutral density filters, bulbs, diaphragms, and rheostats, produce variables; rheostats produce spectral shifts as the intensity changes. If equivalence could be established in these technical variables, we would be able to achieve some confidence in comparing results. However, the basic question remains unanswered. We do not know how much light enters the pupil of the fish's eye.

This is an important element and what is needed, now, are experiments in which the illumination reaching inside the eye and actually striking the retina is measured. Only then will we have a satisfactory way of determining the amount of light needed for the maintenance of schooling formation.

Summary

There are conflicting reports about the dispersal of schooling fish at night. One of the problems is what is meant by night in terms of light available to the schools. Experiments on young *Menidia* (12-18 mm in length) show that their schools will disperse at 0.05 ft. candles when the light is reduced with neutral density filters. A comparison of these results with the results of other investigators demonstrates a wide range of minimal light intensities at which schools disperse. This range may be due to species variation; it is difficult, however, to compare the results since a great variety of techniques were employed which intrinsically could give rise to a variety of results.

Résumé

Il y a des rapports contradictoires sur la dispersion des poissons en banc la nuit. L'un des problèmes est de savoir ce que l'on entend par « nuit » en fonction de la lumière reçue par les bancs. Des expériences sur de jeunes *Menidia* (12 à 18 mm de longueur) montrent que les bancs se dispersent à 0,5382 lux quand la lumière est réduite par des filtres neutres de densité. La comparaison de ces résultats avec les résultats d'autres chercheurs démontre que l'intensité lumineuse à laquelle les bancs se dispersent varie entre de larges limites. Cette marge peut être due à une variation suivant les espèces ; il est toutefois difficile de comparer les résultats, étant donné qu'ils ont été obtenus par des techniques très diverses qui pourraient intrinsèquement donner naissance à une certaine diversité des résultats.

References

ALI, M.A. 1959. — The ocular structure, retinomotor and photobehavioral responses of juvenile Pacific salmon. *Canad. J. Zool.*, **37**, pp. 965-996.

ATZ, J.W. 1953. — Orientation in schooling fishes. *Proc. Conf. Orientation in Animals.* — O.N.R., pp. 103-130.

BREDER, C.M., Jr. 1951. — Studies on the structure of the fish school. *Bull. Amer Mus. nat. Hist.*, **98**, pp. 1-28.

BREDER, C.M., Jr. 1959. — Studies on social grouping in fishes. *Bull. Amer. Mus. nat. Hist.*, **117**, pp. 395-481.

HARDEN JONES, F.R. 1956. — The behaviour of minnows in relation to light intensity. *J. exper. Biol.*, **33** (2), pp. 271-281.

KEENLEYSIDE, M.H.A. 1955. — Some aspects of the schooling behaviour of fish. *Behaviour*, **8** (2-3), pp. 183-247.

KUEHNE, R.A. 1958. — Studies on the schooling behavior of the minnows, *Semotilus* and *Rhinichthys.* Univ. of Mich. Ph. D. thesis.

LOUKASHKIN, A.S. and Norman GRANT. 1959. — Behavior and reactions of the Pacific sardine, *Sardinops caerulea* (Girard), under the influence of white and colored lights and darkness. *Proc. Calif. Acad. Sci.*, **29** (15), pp. 509-548.

MOULTON, J.H. 1960. — Swimming sounds and the schooling of fishes. *Biol. Bull.*, **119** (2), pp. 210-223.

RUBINOFF, I. 1958. — Raising the atherinid fish *Menidia menidia* in the laboratory. *Copeia*, N° 2, pp. 146-47.

SHAW, Evelyn. 1960. — The development of schooling behavior in fishes. *Physiol. Zool.*, **33** (2), pp. 79-86.

SHAW, Evelyn. 1961. — The development of schooling behavior in fishes. II. *Physiol. Zool.* (In press.)

SPRINGER, S. 1957. — Some observations on the behavior of schools of fishes in the Gulf of Mexico and adjacent waters. *Ecology*, **38** (1), pp. 166-171.

STEVEN, D.M. 1959. — Studies on the shoaling behavior of fish. I. Responses of two species to changes of illumination and to olfactory stimuli. *J. exper. Biol.*, **36** (2), pp. 261-280.

Contribution No. 121

(*Reprinted from Nature, Vol.* 192, *No.* 4798, *pp.* 156–157,
October 14, 1961)

Natural Glass from beneath Red Clay on the Floor of the Atlantic*

DURING April and May 1961 on a cruise of the R.V. *Chain*, a programme of coring deep-sea sediments from the Atlantic for geochemical investigations was conducted. At 19° 23′ N., 40° 53′ W. a modified Kullenberg corer was lowered through 4,430 m. of water to the summit of a rise on the ocean floor. The topography of the sea bed in this region is irregular, but between the hills and rises the average depth is approximately 4,900 m. At the point where the corer struck the sea bed the surface sediment is a red clay, but no sediment core was obtained since at a very short distance below the surface the red clay is underlain by solid material. The corer struck and broke the surface of this solid material, a fragment of which was recovered in the pilot corer, together with the overlying red clay. From the position of the solid fragment in the pilot corer the thickness of the clay can be estimated to be not more than 38 cm. The solid fragment is a very dark brown, almost black natural glass of irregular shape, but with approximate dimensions 3 cm. × 2·5 cm. × 1·3 cm. Two faces of the fragment were freshly broken surfaces. On two other faces a thin (1 mm.) zone of devitrification occurs with small areas of manganese deposition on the outer surface. The two other faces appear to be natural fractures. Internally the fragment contains small irregular cavities about which slight devitrification has also occurred. When collected the fragment showed a marked tendency to disintegrate into smaller fragments, a consequence, no doubt, of the impact of the corer on the brittle glass. Red clay containing broken shards of the same glass was found adhering to the piston of the main corer, and it is likely, therefore, that the glass formation is too extensive to be interpreted as a boulder contained within the red clay. It is believed to represent the solid surface on which the overlying sediments rest. So far as is known this is the first sample collected of solid rock indisputably from below the sediments of the deep Atlantic.

The glass fragment when collected weighed approximately 18 gm. Part of it was crushed and natural glass fragments hand-picked from devitrified material for chemical analysis. Examined optically these glass fragments appear homogeneous without crystallites, microlites or any other crystallization phenomena. The chemical composition of this glass is quite remarkable, namely (percentages). SiO_2 25·81, Al_2O_3 19·35, TiO_2 2·02, Fe_2O_3 15·05, FeO 0·63, MnO 0·15, MgO 1·29, CaO 1·25, Na_2O 1·68, K_2O 0·89, H_2O 31·02, P_2O_5 0·08, Cl_2 0·97; uncorrected total 100·19 per cent, less 0 for Cl 0·22 per cent; corrected total 99·97 per cent. It is quite different from compositions of natural igneous glasses from the continental regions of the world. The high chlorine content suggests contamination with sea salts. However, the fragments analysed were hand-picked from the interior of the larger fragment collected, and such a high chlorine content, equivalent to 1·6 per cent sodium chloride, cannot be attributed to surface contamination by sea water during collection. The high water content also suggests contamination with sea water. Attempts to determine the distribution of the water between loosely bound positions (H_2O-) and tightly bound positions (H_2O+) did not meet with success. The loss in weight on heating the powdered glass for 20 hr. at 108° C. corresponded to 22·18 per cent of the total powder, but this figure slowly rises with continued heating. Loss of water appears to be accompanied by crystallization of the glass so that any H_2O- figure determined does not correspond to the original material. Thus the total H_2O figure has not been broken down into H_2O+ and H_2O-. The very high Fe^{+++}/Fe^{++} ratio suggests that the material was hydrated while still in a molten condition, supporting the view that the water content of this glass is original, despite being so much greater than the water content of silicate glasses produced experimentally in the laboratory.

---

* Contribution No. 1215 from the Woods Hole Oceanographic Institution.

A more extensive account of the properties of this glass and its possible origin will be published elsewhere. Meanwhile we urge oceanographers to make further attempts to collect samples from the sub-sediment surface of the Atlantic floor in order to demonstrate whether this first sample is truly representative of that surface or merely an unusual type of limited distribution.

Grateful acknowledgment is made to all aboard the R.V. *Chain* for help in the coring operations and particularly to R. G. Leahy, P. L. Sachs and G. L. Erlanger. This work was supported by the U.S. Office of Naval Research under a contract with the Woods Hole Oceanographic Institution.

G. D. NICHOLLS
Department of Geology,
University of Manchester.

V. T. BOWEN
Woods Hole Oceanographic Institution,
Woods Hole, Mass.

Printed in Great Britain by Fisher, Knight & Co., Ltd., St. Albans

Contribution No. 1218

Made in United States of America
Reprinted from Limnology and Oceanography
Vol. 6, No. 4, October, 1961
pp. 388–399

GAS EXCHANGE IN A GEORGIA SALT MARSH

by John M. Teal and John Kanwisher

GAS EXCHANGE IN A GEORGIA SALT MARSH[1]

John M. Teal[2] and John Kanwisher

ABSTRACT

The oxygen consumption of the undisturbed marsh surface, of well-stirred mud samples, and of above- and below-ground portions of *Spartina* was measured as were oxygen and redox profiles and sediment particle size. All but the uppermost fraction of the sediment was oxygen free and the intensity of reduction was high in all but the best drained areas and was not correlated with amount of reduced material present. The latter was, however, roughly correlated with primary productivity. The rate of energy degradation of the bacteria living in the marsh mud was increased about 25 times when they were supplied with oxygen. *Spartina*, the major marsh producer, consumes more oxygen than any other group. Next in importance are the bacteria of the mud.

INTRODUCTION

There is a broad band of salt marshes running along the southeast coast of the United States which, because of their relative simplicity, make good subjects for ecological research. Most of the primary production can be attributed to *Spartina alterniflora*, the only important higher plant growing on the marshes. The remainder is due to the algae growing on the surface of the marsh mud. Considerable detritus is formed from products of primary production and much of this accumulates on the mud surface producing a black mud, rich in organic matter. In and on this mud live most of the marsh consumers from fiddler crabs to nematodes and bacteria. In this paper we are concerned with the role of the mud and its micro-fauna in the marsh energy budget and also with some of the properties of the mud which are important to organisms living in it.

METHODS

A series of random stations was chosen from a grid drawn on an aerial photograph of the marsh (Fig. 1). Cores were taken at these stations by pushing lucite tubing down into the mud and lifting the tube after stoppering the top. With the bottom then stoppered, the cores were easily brought into the laboratory for oxygen, redox, and gas exchange measurements.

The relative altitude of the stations was determined by measuring the maximum depth of water over the mud at one high tide. Particle size analyses of sediments from 8 stations were done by the pipette method described in the Field Manual of the Allan Hancock Foundation (1958). An estimate of organic content was made by igniting samples in a muffle furnace and correcting for the water of crystallization of the clays, on the assumption that the entire weight loss of the clay sample with the least loss on ignition was due to water loss.

Oxygen profiles down into the mud were made with a polarographic electrode (Kanwisher 1959), pushed into the mud and then moved laterally to determine the oxygen tension at a given depth. This technique is subject to errors of as much as 20% when tested with known tensions, but provides useful estimates where no other method is available.

Below the point where the oxygen electrode indicated anaerobicity the varying degrees of reduction were determined by the redox potential. Hayes, Reid, and Cameron (1958) have shown that the measurement of redox potential of sediments is complicated by the presence of H_2S which acts on the Pt electrode in an irreversible manner. Large electrodes gave better results than small ones. They also reported that different types of sediments produce curves of redox potential against depth that are not comparable. Our study dealt with

---

[1] Supported by National Science Foundation Grant G-6156 and G-4813. Contribution No. 30 from the Marine Institute, University of Georgia, Sapelo Island, Georgia, and No. 1218 of the Woods Hole Oceanographic Institution, Woods Hole, Massachusetts.

[2] Present address Institute of Oceanography, Dalhousie University, Halifax, Nova Scotia.

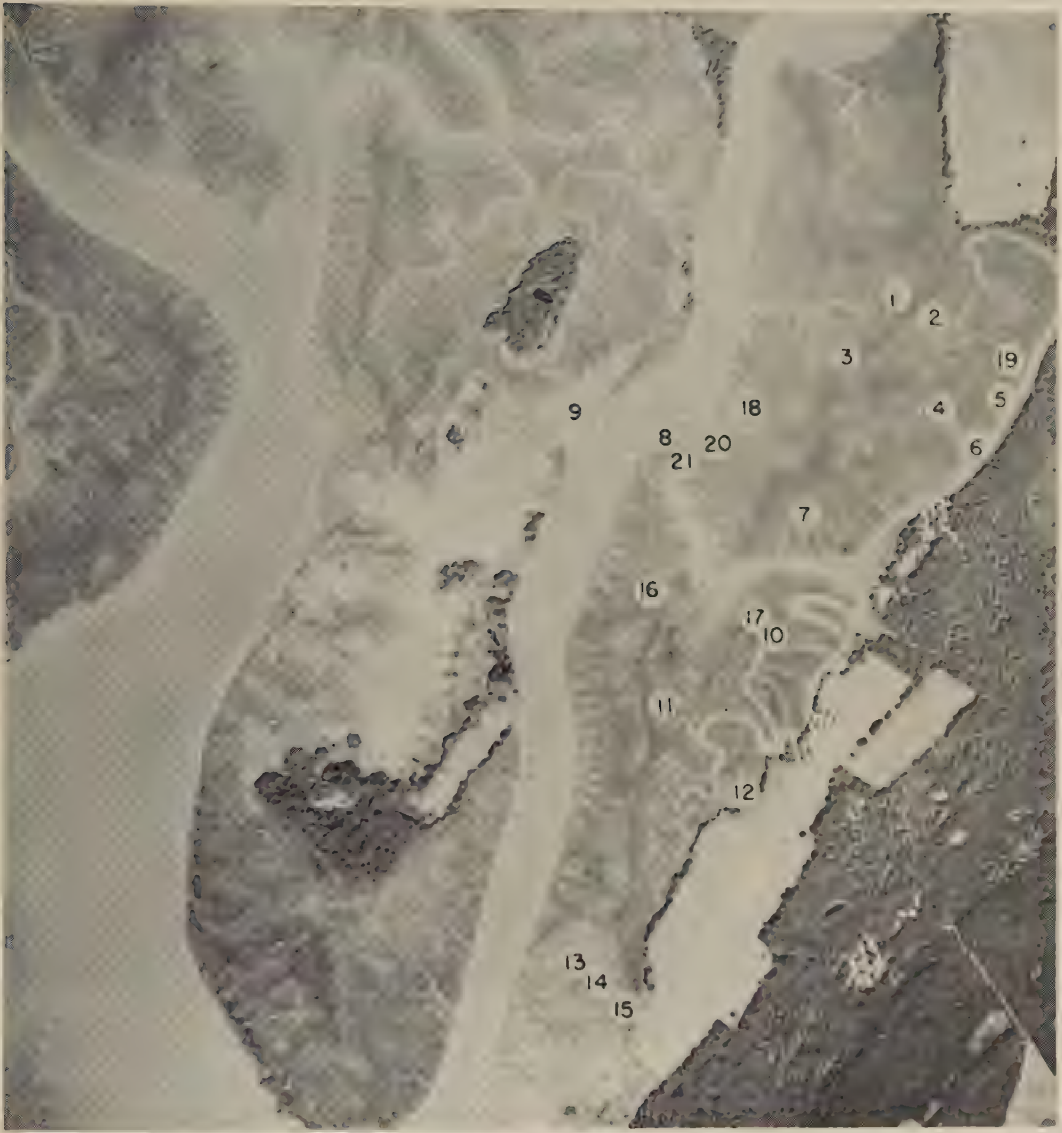

Fig. 1. Aerial photograph of Georgia salt marsh showing sites used in this study. Streamside marsh is narrow dark band along creeks, levees show as broad irregular grey just beyond. Distance from site 16 to site 17 is 0.4 km.

sediments that were all fairly similar or at most represented samples along a gradient and we used a relatively large 7-mm diameter electrode. Although the actual values we obtained may not accurately indicate the true state of reduction in the samples, they are a useful relative measure. We may note that in general the muds were brown in color at potentials above +0.100 v; grey from +0.100 v to –0.100 v; and black at potentials below –0.100 v. Also in the black regions the presence of H_2S was indicated by its odor. Duplication was poor in the less reduced cores that were visibly nonhomogeneous. Values from the black reduced muds could be repeated within 0.02 to 0.04 v.

The oxidation–reduction profiles were obtained by pushing the 7-mm Pt electrode slowly into the cores. Because of drift several minutes were allowed at each depth before each reading. A calomel electrode at the edge of the core completed the circuit. The pH of the muds varied from 6.5 in black areas to 7.4 in brown. This whole range would affect *r*H, when computed from *Eh*, by no more than 40–50 mv.

Such redox potentials are related to the intensity of reduction, but tell nothing about the amount of reduced material present, *i.e.* the amount of oxygen debt of the mud. Two methods were developed for such determinations. A 1-cm^3 sample of mud was taken with a small coring tube with a minimum of exposure to air. It was extruded into a 25-ml container of sea water. An oxygen electrode was immediately inserted for a stopper and the disappearance of the dissolved oxygen was recorded while the contents were vigorously stirred magnetically. In this way the mud particles were quickly dispersed throughout the water and given maximum access to oxygen. When the dissolved oxygen had nearly disappeared from the bottle, the stopper was removed, pure oxygen bubbled gently through the water for a few seconds to renew the supply, the stopper replaced and recording continued. Formalin was sometimes injected midway in a run to stop any oxygen consumption by living organisms and provide a way to compare chemical with biological consumption. Formalin is a reducing agent and so might increase oxygen consumption. Controls indicated no such effect.

In addition 1-cm^3 mud samples were placed in 20-ml syringes with 1 ml of sea water and a magnet. When the magnet was spun with a stirrer the mud slurry was thrown about in the syringe and aerated. Gas samples withdrawn at intervals were analyzed with an accuracy of 0.02% for O_2 and 0.015% for CO_2 (Scholander 1947).

Oxygen and CO_2 gas exchange at the mud surface was determined on 4-cm and 30-cm diameter cores brought into the laboratory. These were capped with several centimeters of air above the mud and serial gas samples were withdrawn with a syringe. Oxygen consumption and CO_2 production were determined with the ½-cc analyzer. As a check on this procedure several cores were fitted onto Scholander type volumetric respirometers and oxygen uptake was followed (Scholander, *et al.* 1952). RQ's were calculated from runs where both respiratory gases were measured.

Since the gas exchange of the marsh mud takes place under water for a considerable part of the time some measurements were made with cores in which the mud surface was covered with water. A layer of oil floated over the water reduced exchange with the air to a negligible amount. Water samples were taken at intervals and oxygen determined with the gasometric technique (Scholander, *et al.* 1955). If the water was not stirred an oxygen gradient developed. The layer just over the mud surface could become very depleted, or even anaerobic, in as little as one hour. This was prevented by stirring gently with a wire loop inserted through the oil layer. Oxygen uptake under these conditions was not significantly different from that measured in air and will not be referred to again. Very few places on the marsh had water stagnant enough to develop oxygen gradients at the mud surface.

The cores were taken so as to exclude crab burrows, mussels, snails, or *Spartina* plants. Data for gas exchange of the entire marsh community was obtained by following changes in composition of air under a gas-tight 5,000-cm^2 plywood box pushed into the mud to seal the edges. A rubber stopper in the top allowed samples to be withdrawn by a syringe. A cover of aluminum foil minimized heating by the sun. To obtain a measurable change in a few hours the air space under the box was kept to 15–20 cm. The plants were thus bent over.

The respiratory contribution of the above-ground parts of *Spartina* plants was determined by repeating runs after cutting the plants off at the mud surface. Independent checks were made using the ½-cc analyzer to follow the gas exchange of sections of *Spartina* leaf and stem enclosed in a 100-ml syringe.

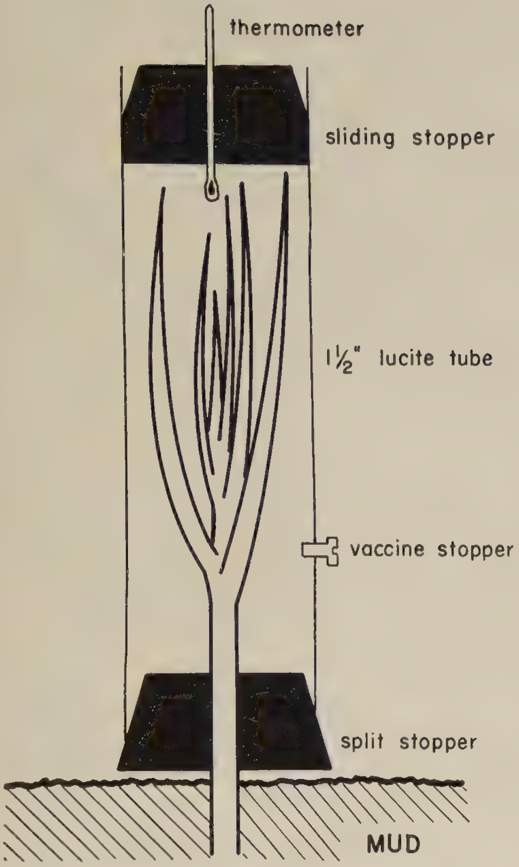

FIG. 2. Diagram of lucite tube used for comparing respiration of above- and below-ground parts of *Spartina* plant showing plant before it was cut off above lower stopper.

The *in situ* box measurements with the *Spartina* tops removed showed an oxygen consumption per unit area above that of the core samples even when allowance was made for the crabs, mussels, *etc.* Since the mud was anaerobic it seemed logical to suppose that the root system of the *Spartina* might obtain its oxygen through the aerial parts of the plant. Such root respiration was determined by measuring the gas passing into the cut-off stems. A plant was sealed in a section of lucite tube with a stopper at the top and another at the bottom bored to fit the stem snugly (Fig. 2). Respiration was measured with the plant intact and after the stem had been cut off just above the bottom stopper. The respiration of the underground parts of the plants could then be expressed as a percentage of the respiration of the intact plant.

RESULTS

The marsh profile with sampling sites is shown in Figure 3. The horizontal scale is distorted non-uniformly. The left side of the figure represents a tidal creek bank where the mud near low-water level contained a large proportion of sand and where *Spartina* did not grow. *Spartina* began to occur at about 1.2 m above mean low water where it grew to about 3 m in height, with the plants close together forming a dense luxuriant "streamside marsh." The break in elevation represents the little cliffs frequently found as a result of slumping of the marsh due to stream undercutting of the banks. The next series of stations were representative of the areas from the streamside marsh up to the top of the natural levee which forms along all of the larger tidal rivers and creeks. The *Spartina* grew to a height of about 1 m. In the levees, as on the rest of the marsh where the typical *Spartina* growth occurs, there was very little sand and the mud consisted of about equal parts silt and clay, most of the silt occurring in the 16–8, 8–4, and 4–2 μ fractions and 80% of the clay particles in the <1 μ fraction. After spring tides mud from all sites was about 65% water (expressed as a fraction of wet weight).

Behind the levees there is usually an extensive area where the *Spartina* is short, 0.5–0.7 m. Station 2 represented such a site at the beginning of a tidal creek well above low-water level. The two stations on the right represented places where the marsh abutted on the land. Here the soils became much more sandy, the *Spartina* was stunted, and shared the ground with other plants (*Distichlis*, *Salicornia*, *Sporobulus*).

Except for areas near low water, the fineness of the sediments prevented extensive movements of the interstitial water in spite of the changing hydraulic pressure due to the tides. A depression in the mud drains very slowly at low tide. In fact the entire surface of much of the short-*Spartina*

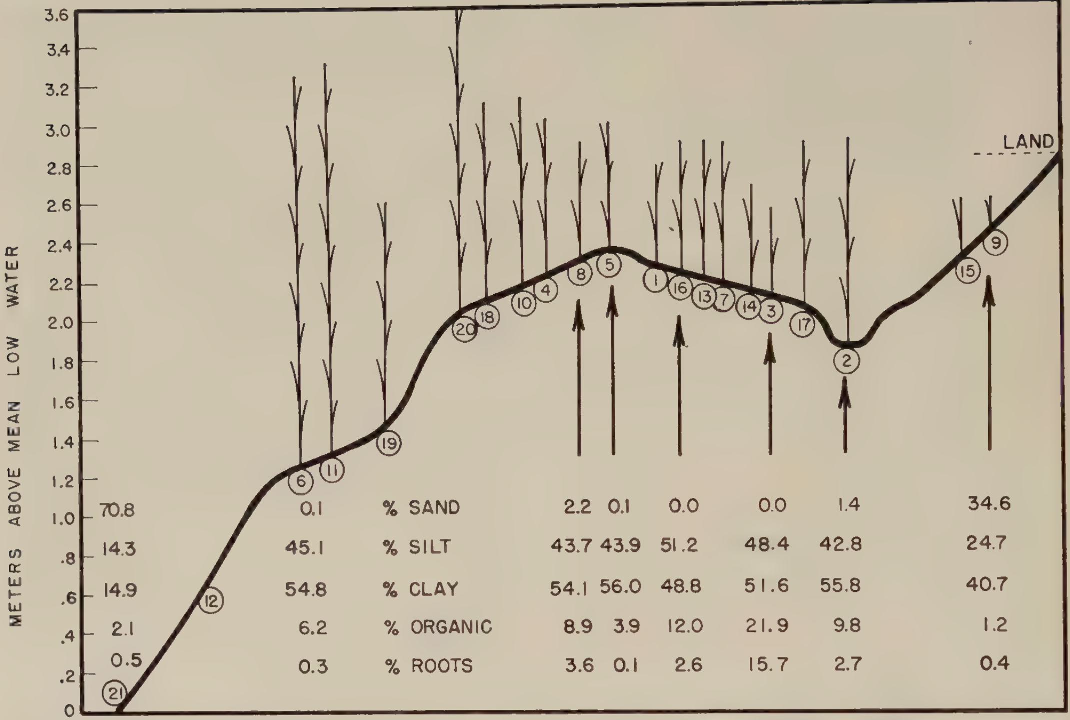
METERS ABOVE MEAN LOW WATER
3.6
3.4
3.2
3.0
2.8
2.6
2.4
2.2
2.0
1.8
1.6
1.4
1.2
1.0
.8
.6
.4
.2
0
LAND
21
12
6
11
19
20
18
10
4
8
5
1
16
13
7
14
3
17
2
15
9
% SAND 70.8 0.1 2.2 0.1 0.0 0.0 1.4 34.6
% SILT 14.3 45.1 43.7 43.9 51.2 48.4 42.8 24.7
% CLAY 14.9 54.8 54.1 56.0 48.8 51.6 55.8 40.7
% ORGANIC 2.1 6.2 8.9 3.9 12.0 21.9 9.8 1.2
% ROOTS 0.5 0.3 3.6 0.1 2.6 15.7 2.7 0.4

FIG. 3. Diagrammatic salt marsh section indicating elevation relative to low tide and height of mature *Spartina* plants at sampling sites. Sediment cores of 5 cm diameter from the upper 10 cm were used for particle size analysis. Horizontal scale is distorted non-uniformly.

marshes, behind the levees, had water on the surface continually during the spring tide period when drainage was so slow that it was not complete before a subsequent high tide arrived. Conversely some of the levee marsh dried out completely on the surface during neap tide intervals and the mud became very hard and caked.

The organic content of the muds was lowest near the low-water level and near the land, and was highest in the short *Spartina* marshes. The amount of roots, *etc.* in the mud was appreciable only in the higher parts of the marsh. In the short-*Spartina* areas this formed a peat-like layer from the surface to about 30 cm deep in which the mud particles were tightly held together by the roots. Aside from the roots, most of the organic matter was found in the silt fraction.

The Intensity of Reduction

We have divided the stations into three groups: Figure 4a includes sites on the outer sides of the levees; 4b, sites from the short-*Spartina* marshes; 4c, sites from the creeks and creek banks. The levee stations (Fig. 4a) except for No. 10 were relatively well drained with a firm mud. No. 10 was on the levee of a small creek where the mud was quite soft and resembled the creek banks more than the other levees. In spite of the relatively high redox values the oxygen electrode indicated a measurable oxygen tension down to 2 cm only in core 9. At other stations in the marsh there appeared to be no oxygen at a depth of more than a few millimeters. A similar situation was found in lakes by Hayes, *et al.* (1958). They thought mixing of the bottom was involved in the formation of the surface-"oxidized" but oxygen-free layer.

The creek stations, with the exception of No. 11, all had the very soft mud typical of these areas and showed a sharp decrease in potential just below the surface. These gave cores with the blackest mud and the strongest H_2S smell. No. 11 was unusual in

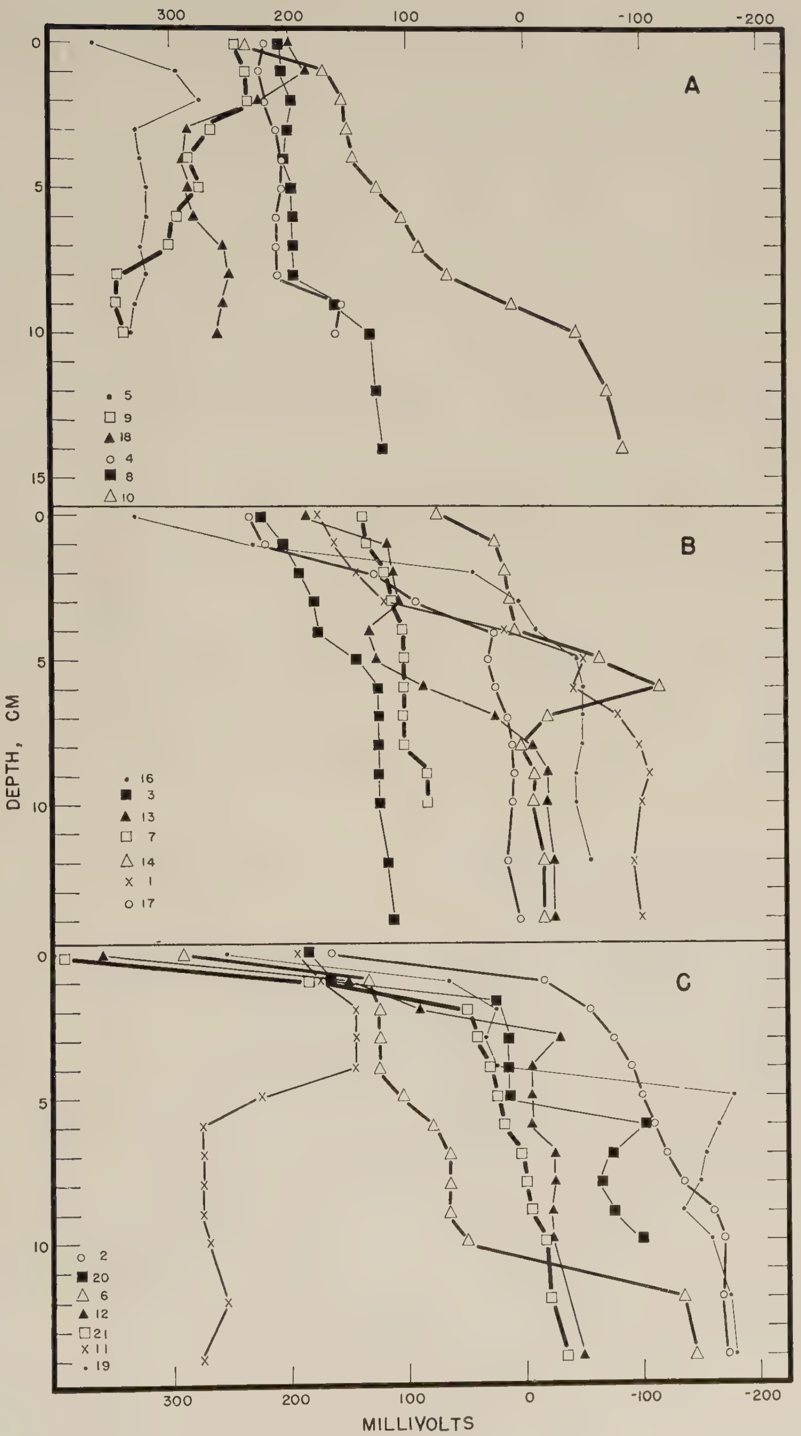

FIG. 4. Redox profiles from salt marsh sampling sites divided into three groups: a—sites on outer sides of levees; b—sites from short-*Spartina* marshes; c—sites from creeks and creek banks.

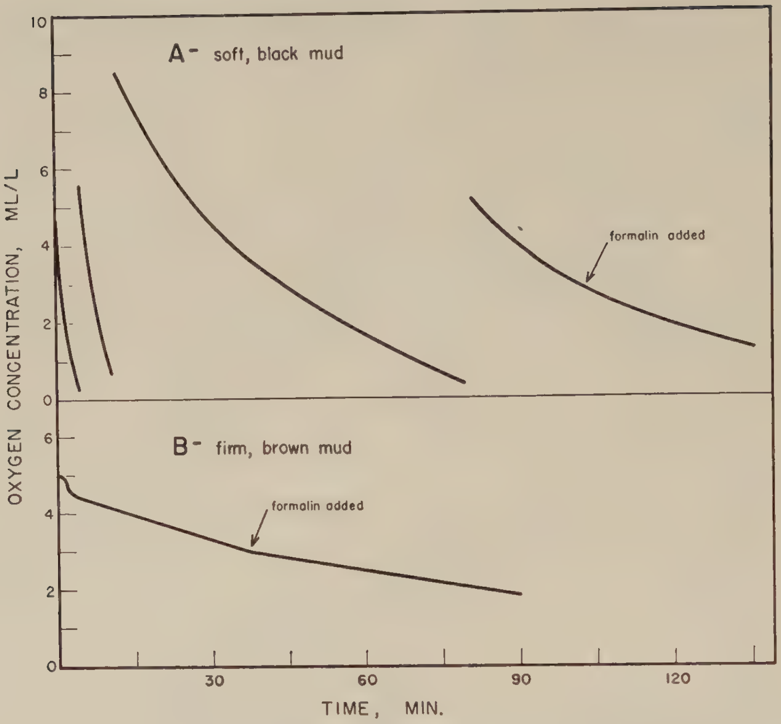

FIG. 5. Typical curves of oxygen consumption of well-stirred mud obtained with the oxygen electrode. Sample A is from a creek bank, B from a levee.

that it had a firm substratum and a steep bank next to the coring station where the stream was undercutting the bank.

The Pt electrode consistently indicated 2–3 cm lumps of black mud distributed in the brown mud layers by a potential of –0.100 v or below. This gave us confidence in the relative shapes of the curves indicated by such electrode potentials. Examination showed that these lumps had a piece of partly decayed plant material in their center. It seems reasonable that bacteria were living in the organic material, oxidizing it and consequently reducing the surrounding mud.

The redox profiles for the sites in the short-*Spartina* marshes (Fig. 4b) are intermediate between those for the levees and creek banks. Some show a definite break in the curve near the surface and others do not. This difference was correlated with the presence of a root mat and the hardness or softness of the mud. With a well-developed mat and firm soil, the burrows and holes in the soil could remain open, while in the soft areas openings in the mud collapsed and filled in as the tide rose.

It seems obvious from Figure 4 that small differences in redox potential in natural muds are not significant. But a series of determinations can be useful for the comparison of sediments especially as regards the change from oxidized to reduced conditions (Pearsall and Mortimer 1939), and when combined with other measurements, particularly in areas like salt marshes where the sediments are visible. Variations in such a situation may have meanings that would be puzzling to anyone forced to sample the mud at random from a position where he could not see it, as for example when sampling underwater sediments from a boat or ship.

The Quantity of Reduced Material

Figures 5a and b show two typical curves of mud oxygen consumption obtained with the oxygen electrode. The first

TABLE 1. *Oxygen uptake in well-stirred mud samples. "Final rate" is taken from the curve after sufficient time has elapsed for the rate to become relatively constant. Formalin decreases refer to final rates and not initial rates. Curves illustrated in Figure 3 are indicated*

Core	Depth (cm)	Initial rate—1st 15 min (mm^3/hr/ml)	Final rate (mm^3/hr/ml)	Decrease after adding formalin
6	0–1	260	–	–
	0–1	310	65	35%
	1½–2½	340	90	22%
	1½–2½	320	70	–
	3–4	230	80	0
	3–4	250	105	0
	4–5 (Fig. 3a)	680	70	0
	12–13	1,070	150	–
21	0–1	110	80	21%
	2½–3½	650	–	–
	4–5	350	90	31%
2	0–1	510		
	2½–3½	620		
	4½–5½	460		
4	0–1	220	85	27%
	3–4	730	75	51%
	6–7	470	105	21%
8	0–1	60	80	21%
	2–3	90		
	4–5 (Fig. 3b)	100	90	31%
7	0–1	131	122	50%
	1½–2½	336		
16	0–1	188	61	25%
	0–1	114	73	33%
	4–5	291	61	33%

is a sample from a creek bank station with very soft, black mud. Oxygen uptake was very rapid at first and gradually declined with time. There was no appreciable change in rate when formalin was injected. Figure 5b was derived from the 4–5 cm level of site 8 which represents the extreme case of a well-oxidized sample. It showed a low rate of oxygen uptake and in which living organisms or at least systems susceptible to formalin poisoning accounted for approximately ⅓ of the rate. A summary of the results is given in Table 1. The uptake varied in the first 15 min from 60 up to 1,000 mm^3 O_2/hr/ml mud; the highest values were obtained from deep levels of the soft, black cores; the lowest from the upper layers of the better oxidized sites.

The rapid initial oxygen uptake in these well-stirred mud samples is a convenient indicator of the comparative amount of reduced material present, at least in the salt marsh. Since all marsh sites should have the same sorts of reduced compounds, uptake by the easily oxidized portion will be proportional to total chemical uptake or oxygen debt.

Attempts to poison the initial rapid uptake with formalin were unsuccessful. Apparently the oxygen consumption during this phase was predominantly chemical. This conclusion is supported by the experiments done in the syringes. These showed that CO_2 production was initially very low in relation to the oxygen consumed. This would be the case with oxidation of metals, H_2S, *etc.*

The final or slow phase presents a contrast. There was usually about a 30% reduction in oxygen uptake following addition of formalin and the RQ measured in syringes was normal for respiratory processes, between 0.7 and 1. Occasionally in deeper levels of highly reduced cores there seemed to be no biological activity even in the slow phase.

Undoubtedly the biological part of the oxygen consumption was present from the beginning of the runs, but was overshadowed at the start by the high chemical demand. As the more highly reduced materials were oxidized and the chemical demand slowed, the biological respiration became relatively more important. Presumably if the experiments had been continued long enough only the biological part would have remained. This proved to be the case in similar experiments done with Nova Scotia lake sediments.

Gas Exchange of the Mud Surface

The results of 37 determinations of gas exchange across the mud surface of cores are summarized in Table 2. The cores are listed approximately in the order: creek bank, streamside marsh, levee, short-*Spartina* marsh, landward marsh edge. There

TABLE 2. *Oxygen consumption and RQ's of cores with undisturbed surfaces from Georgia salt marsh*

Site	O_2 consumption ($mm^3/cm^2/hr$)	RQ
21	3.6	–
2	5.0	.72
6	6.8	.54
11	5.6	–
19	5.5	–
18	5.1	–
20	4.3	–
10	5.3	.78
4	4.0	–
8	5.0	.70
5	7.4	.50
1	3.4	.96
13	4.4	–
16	4.4	–
7	5.5	–
14	2.9	–
3	8.4	.79
17	3.5	–
15	6.0	–
9	7.0	–

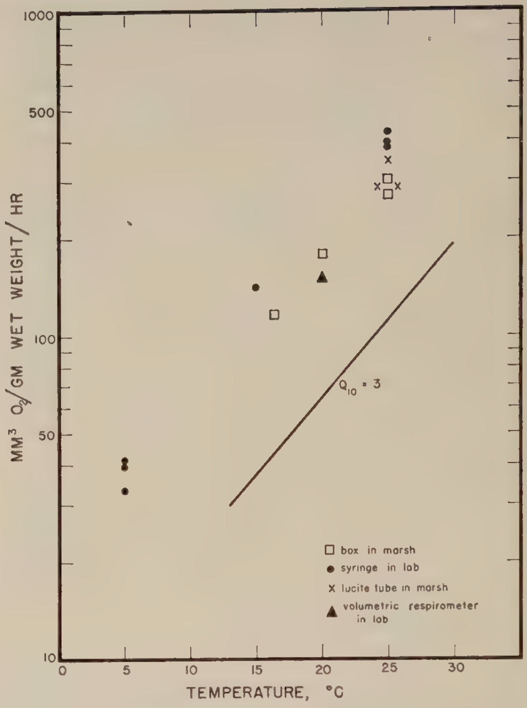

FIG. 6. Respiration of *Spartina alterniflora* from Georgia salt marsh plotted against temperature. Line indicates slope at which $Q_{10} = 3$.

was no discernible trend within the values and all lay fairly close to the mean 5.2 ± 1.8 mm³ $O_2/cm^2/hr$. This value represents respiration of bacteria, nematodes, *etc.* in the surface layers of the mud plus whatever chemical oxidation took place on the surface.

The 5,000-cm² box was used at three sites in the marsh (Table 3). Column 4 shows that cutting the grass off at the mud surface still resulted in an oxygen uptake per unit area much higher than that found with small cores. The underground parts of the plants showed oxygen uptake rates of 82, 73, 70, 67% of the above-ground portion. We have subtracted an amount equal to 73% of the grass respiration to give the results in the final column of Table 3. This represents the respiration of the mud and contained animals, macro-fauna such as crabs, mussels, and snails, and also the respiration of bacterial populations of such dead *Spartina* leaves as were lying on the surface of the mud.

Since the field data from the box in some cases were collected over several days while the temperature was fluctuating, it was possible to calculate a Q_{10} of 1.7 for the mud with the animals and grass roots. RQ's were calculated for the contents of the boxes giving a figure of 0.68 with the grass present and 0.82 with it removed.

Respiration of Spartina

Respiration determinations of undisturbed *Spartina* plants in the marsh were combined with laboratory measurements on parts of plants to give Figure 6. The data from the three types of measurements do not show significant differences and indicate a high Q_{10} of about 3.

DISCUSSION

The mud of the Georgia salt marshes is, over most of the marsh area, a very finely divided substrate holding from 50–70% of its weight in water when saturated. As has been noted, this water moves through the mud only slowly and the movement that does occur can be assumed to take place mostly through crab burrows, worm holes, and root holes. The bulk of the mud must receive oxygen, if at all, by diffusion from

TABLE 3. *Salt marsh respiration under ½-m² box. Values are given as mm³ O_2 used/cm²/hr*

1 Site	2 Temp.	3 Intact surface	4 Without *Spartina*	5 *Spartina* rate col. 3 – col. 4	6 Root rate	7 Mud rate col. 4 – col. 6
Creek head 1-m *Spartina*	17°	20	13	7	5.1	7.9
Short-*Spartina* marsh	25°	32.8	18.5	14.3	10.4	8.1
Levee marsh	20°	31.5	18.6	12.9	9.4	9.2

the surface. That this is a very slow process is evidenced by the absence of oxygen, presence of H_2S, and highly reduced conditions found below the top centimeter in all but the highest, best drained stations.

All of the primary production of organic matter occurs on or above the surface of the marsh and comes to lie on the surface as the plants die.

Surface animals can use the oxygen of the air and water to metabolize this potential food. But as soon as the organic material has been buried more than a few millimeters by either animal movement or further deposition on top, it is in an anaerobic environment. The bacteria and nematodes living there can only use it as food by parallel oxidizing and reducing reactions. The result is an accumulation of reduced end products such as CH_4, H_2S, and ferrous compounds.

The increasing degree of reduction (lower redox potential) suppresses biological activity by reducing the number of tolerant species and by limiting the number of reactions that can occur. The reduced materials will be transported slowly upwards by diffusion in a similar manner to the way in which oxygen moves down. They may form a food source at some higher level (lower redox potential) or they may combine with oxygen directly. We can assume the salt marsh soil to be relatively stable; that is to say, no great disturbances occur often enough to be important in terms of the life cycles of the organisms or the rates of the chemical reactions involved. This produces a horizontally stratified system which is highly reduced deep in the mud and has abundant free oxygen available on the surface. Between these two extremes diffusion and mixing will occur. If accumulation of organic matter is also relatively slow, oxygen will be consumed at a rate proportional to degradation of free energy by the organisms whether they are living at the surface or down in the mud. A kind of countercurrent exchange will prevent many of the reduced substances from escaping to the atmosphere. For example, H_2S is rarely smelled on the surface although it is present in large amounts 1 or 2 cm down; RQ's close to one also substantiate this. If reduction over the entire mud column and oxidation near the surface were not balanced, one would expect to find RQ's considerably greater than one reflecting the anaerobic production of CO_2. We can reasonably conclude then that the rate of oxygen consumption per unit area at the surface is an integrated measure of the energy degraded in the mud column. There remains a possibility that chemically resistant reduced compounds such as CH_4 diffuse all the way to the surface and are lost to the atmosphere.

If there is no appreciable accumulation of reduced material per unit time in the salt marsh soils, the actual amount of reduced substance present will have no relation to the biological activity, but will be related only to the ability of oxygen to penetrate into the mud. With an appreciable accumulation the figures for oxygen uptake per unit area of surface will have to be corrected to give a true measure of degradation in the mud column. The uptake of stirred mud from deep in the core divided by the time required for its accumulation would provide the necessary correction.

We might expect a positive relation between primary production or rate of deposition of the products of primary production and the amount of reduced material in areas with comparable oxygen supply. Figure 3 and Table 1 show some correlation between height of *Spartina* growth and the initial uptake of oxygen in stirred cores. Under non-tidal conditions, both in fresh and salt waters, where the supply of oxygen to the sediments is similar and where deposition and accumulation of reduced substances is appreciable, the measure of oxygen debt would serve as a useful index of biological activity in the mud.

Kato (1956) also measured the oxygen uptake by marine muds which were stirred and then allowed to settle. He similarly found that the chemical demand representing former biological activity exceeded the demand by living organisms.

Mortimer (1942) showed that a relation between the degree of reduction and amount of reduced material implies a correlation between redox potential and the square root of capacity to consume oxygen. We found no significant correlation using the values of initial consumption in stirred cores from Table 1 and the redox values in Figure 4.

There was no recognizable trend with depth or station in the data for respiration sensitive to formalin poisoning in the mixed mud samples. The average value was 28 $mm^3/hr/cm^3$ with a standard deviation of 16. The value for respiration of undisturbed mud cores was 5.2 $mm^3/hr/cm^2$, of which 0.2 $mm^3/hr/cm^2$ represents the respiration of the nematodes and annelids (authors' unpublished data) leaving some 5.0 $mm^3/hr/cm^2$ which might be attributed to the bacteria. If we assume that the average for the stirred cores holds to a depth of 5 cm (see Table 1), the oxygen uptake of the stirred mud would be 25 times that of the undisturbed core. Since some of the formalin-sensitive oxygen uptake may have been due to extracellular enzymes preserved by the normal reducing conditions, we can conclude that the bacteria exposed to oxygen consumed energy somewhat less than 25 times as fast as when in anaerobic conditions. It is probable that bacteria slow their metabolism considerably to compensate for the reduced free energy available under anaerobic conditions. They commonly reduce their metabolism under harsh conditions, *e.g.*, with spore formation. We know little about possible similar behavior of animals such as the nematodes which also exist anaerobically in the mud.

As we have pointed out above, the respiration of the undisturbed mud, excluding animals, was 5.0 mm^3 $O_2/hr/cm^2$. This value multiplied by the marsh area would not give the oxygen consumption for the marsh mud as a whole, because there are other surfaces through which oxygen is exchanged besides the visible mud surface, principally the burrows of crabs. The data from the boxes placed on the marsh included this exchange and gave an average of 8.4 mm^3 $O_2/hr/cm^2$ (Table 3). When we subtract the respiration due to the populations of animals such as crabs, nematodes, snails, *etc.* (Teal 1958 and authors' unpublished data) the remainder of 6.4 $mm^3/hr/cm^2$ represents the true areal value for the marsh. One can calculate that animal burrows made up 22% of the surface area of the mud if gas exchange was proportional to surface.

If we compare the value of 5 mm^3 $O_2/cm^2/hr$ for the bacteria with some of the values obtained for other marsh organisms, we find that aside from the *Spartina* which uses more free energy than bacteria, all the other organisms use less. The fiddler crabs which are the most conspicuous and abundant larger animals use on the average only 0.32 mm^3 $O_2/cm^2/hr$ and all of the herbivorous insects, crabs, mussels, snails, nematodes, and annelids together use 1.6 mm^3 $O_2/cm^2/hr$ on the average throughout the year (Teal 1958). In the marsh economy only the *Spartina* is more active (Table 3), using more than 3 times as much oxygen as the mud. In summer when the marsh grass crop is larger and the temperature higher the difference might well be greater. The producers are the most important consumers in the marsh. The bacteria are second and they account for more of the energy than all the remaining organisms together.

REFERENCES

HAYES, F. R., B. L. REID, AND M. L. CAMERON. 1958. Lake water and sediment. II. Oxidation–reduction relations at the mud–water interface. Limnol. Oceanogr., **3**: 308–317.

KANWISHER, J. 1959. Polarographic oxygen electrode. Limnol. Oceanogr., **4**: 210–217.

KATO, K. 1956. Chemical investigations on marine humus in bottom sediments. Mem. Fac. Fish. Hokkaido Univ., **4**: 91–209.

MORTIMER, C. H. 1942. The exchange of dissolved substances between mud and water in lakes. J. Ecol., **30**: 147–201.

PEARSALL, W. H., AND C. H. MORTIMER. 1939. Oxidation–reduction potentials in water-logged soils, natural waters and muds. J. Ecol., **27**: 483–501.

SCHOLANDER, P. F. 1947. Analyzer for accurate estimation of respiratory gases in one-half cubic centimeter samples. J. Biol. Chem., **167**: 235–250.

———, C. L. CLAFF, J. R. ANDREWS, AND D. F. WALLACH. 1952. Microvolumetric respirometry. J. Gen. Physiol., **35**: 375–395.

———, L. VAN DAM, C. L. CLAFF, AND J. W. KANWISHER. 1955. Microgasometric determination of dissolved oxygen and nitrogen. Biol. Bull., **109**: 328–334.

TEAL, J. M. 1959. Energy flow in the salt marsh ecosystem. Proc. Salt Marsh Conf. Univ. Georgia, pp. 101–107.

Report for the year 1961

Annual Report 1961

THE WOODS HOLE OCEANOGRAPHIC INSTITUTION

WOODS HOLE OCEANOGRAPHIC INSTITUTION

CONTENTS

TRUSTEES 4

MEMBERS OF THE CORPORATION 7

RESEARCH STAFF 10

ADMINISTRATIVE STAFF 14

DIRECTOR'S REPORT

REVIEW 15

RESEARCH

Physical Oceanography 17

Theoretical and Experimental Hydrodynamics 23

Marine Meteorology 24

Geophysics and Submarine Geology 28

Underwater Acoustics 31

Chemistry and Geochemistry 33

Marine Biology 36

Instrumentation 42

Fleet Operations 47

PERSONNEL

Honoraria 52

Visitors 53

Employees and Staff 55

Publications 58

TREASURER'S REPORT 62

BALANCE SHEETS 64

TRUSTEES

As of 31 December 1961

HONORARY TRUSTEES

Henry B. Bigelow, Founder Chairman, Museum of Comparative Zoology, Cambridge 38, Massachusetts

L. O. Colbert, 4408 29th Street, N.W., Washington, D. C.

Alexander Forbes, 610 Harland Street, Milton, Massachusetts

Horace S. Ford, 77 Massachusetts Avenue, Cambridge 39, Massachusetts

Frank A. Howard, 30 Rockefeller Plaza, New York, New York

A. G. Huntsman, 217 Indian Road, Toronto, Canada

Arnaud C. Marts, 521 Fifth Avenue, New York, New York

Lawrason Riggs, Riggs, Ferris and Geer, Room 1201, 74 Trinity Place, New York 6, New York

Harlow Shapley, Sharon Cross Road, Peterborough, New Hampshire

Henry L. Shattuck, 10 Milk Street, Boston, Massachusetts

Selman A. Waksman, Institute of Microbiology, Rutgers University, New Brunswick, New Jersey

TO SERVE UNTIL 1965

Harvey Brooks, Division of Engineering and Applied Physics, Pierce Hall, Harvard University, Cambridge 38, Massachusetts

Hudson Hoagland, Worcester Foundation for Experimental Biology, 222 Maple Avenue, Shrewsbury, Massachusetts

J. Seward Johnson, Cedar Lane Farm, Oldwick, New Jersey

Robert R. Shrock, Department of Geology and Geophysics, Massachusetts Institute of Technology, Cambridge 39, Massachusetts

Raymond Stevens, Arthur D. Little, Inc., 25 Acorn Park, Cambridge 40, Mass.

E. Bright Wilson, Jr., Department of Chemistry, Harvard University, Cambridge 38, Massachusetts

TO SERVE UNTIL 1964

Detlev W. Bronk, The Rockefeller Institute of Medical Research, 66th Street and York Avenue, New York 21, New York

Noel B. McLean, Edo Corporation, College Point 56, Long Island, New York

Daniel Merriman, Bingham Oceanographic Laboratory, Yale University, New Haven, Connecticut

Emanuel R. Piore, International Business Machines Corporation, 590 Madison Avenue, New York 22, New York

Alfred C. Redfield, Maury Lane, Woods Hole, Massachusetts

Gerard Swope, Jr., General Electric Co., 570 Lexington Avenue, New York, N. Y.

TRUSTEES

TO SERVE UNTIL 1963

James S. Coles, Bowdoin College, Brunswick, Maine

Carl H. Eckart, Scripps Institution of Oceanography, La Jolla, California

Homer H. Ewing, Greenville, Wilmington 7, Delaware

Cecil H. Green, 1000 Exchange Bank Bldg., Airlawn Station, Dallas 35, Texas

Milford R. Lawrence, Siders Pond Road, Falmouth, Massachusetts

Francis C. Welch, 73 Tremont Street, Boston, Massachusetts

TO SERVE UNTIL 1962

Charles Francis Adams, Raytheon Company, Spring Street, Lexington 73, Massachusetts

Columbus O'D. Iselin, Woods Hole Oceanographic Institution, Woods Hole, Massachusetts

Augustus P. Loring, Loring, Wolcott Office, Inc., 35 Congress Street, Boston, Massachusetts

Albert E. Parr, American Museum of Natural History, Central Park West at 79th Street, New York, New York

Athelstan F. Spilhaus, Institute of Technology, University of Minnesota, Minneapolis 14, Minnesota

Alfred M. Wilson, Minneapolis-Honeywell Regulator Co., 2747 4th Avenue, South, Minneapolis 8, Minnesota

EX. OFFICIO

Edwin D. Brooks, Jr., Treasurer, P. O. Box 1135, Boston 3, Massachusetts

Mary Sears, Woods Hole Oceanographic Institution, Woods Hole, Massachusetts

Paul M. Fye, Woods Hole Oceanographic Institution, Woods Hole, Massachusetts

OFFICERS

Noel B. McLean, Chairman of the Board of Trustees, Edo Corporation, College Point 56, Long Island, New York

Paul M. Fye, President of the Corporation, Woods Hole Oceanographic Institution, Woods Hole, Massachusetts

Edwin D. Brooks, Jr., Treasurer, P. O. Box 1135, Boston 3, Massachusetts

Mary Sears, Clerk of the Corporation, Woods Hole Oceanographic Institution, Woods Hole, Massachusetts

EDWARD HANSON SMITH

29 October 1889
29 October 1961

Rear Admiral Edward H. Smith, U.S.C.G. (ret.), the third director of the Institution (1950-1956), was born on Martha's Vineyard with the sea in his blood and with a craving for knowledge about the sea. He was graduated from what is now the Coast Guard Academy in 1914 and a few years later had an opportunity to serve with the International Ice Patrol. It was then that he came to know the Scientific Advisor to the Ice Patrol, Henry B. Bigelow. In the off season, while writing patrol reports, he studied at Harvard University with Dr. Bigelow. On completing his master's degree at Harvard (1924), he studied at the Geofysisk Institutt in Bergen, Norway, with Professor Bjorn Helland-Hansen, who with J. W. Sandström had advanced the method for computing dynamic currents. It was this work that laid the foundation for the present scientific approach of the Ice Patrol.

To learn more about icebergs, he went with the MARION as far as 70° North, then was assigned to Woods Hole in 1933 to command Base 18 on the site of the present aquarium of the U. S. Fish & Wildlife Service. When the base was decommissioned the next year, he remained in Falmouth to write the well-known MARION report which became his doctor's thesis (Harvard, 1934).

Although duty took him elsewhere, he never lost interest in oceanography and in the new Institution established in Woods Hole in 1930. It was therefore most fitting that in 1945 he was elected a Member of the Corporation and a Trustee, a post he held until becoming an Honorary Trustee in 1961. No one had a better background, through training and association with the traditions of Woods Hole, than Admiral Smith when he was elected director. During his term of office the Institution started its permanent growth. The Laboratory of Oceanography was built, the CRAWFORD was acquired and the Institution assumed responsibility for the educational aspects of oceanography. In short, the modernization of the Institution was begun and well established under his leadership.

MEMBERS OF THE CORPORATION

Charles Francis Adams, Raytheon Company, Spring Street, Lexington 73, Massachusetts

Oliver Ames, III, "Edgewater", Beverly Farms, Massachusetts

Philip B. Armstrong, Medical Center of Syracuse, State University of New York, Syracuse, New York

Eric G. Ball, Harvard Medical School, Shattuck Street, Boston, Massachusetts

Henry B. Bigelow, Museum of Comparative Zoology, Cambridge 38, Massachusetts

Detlev W. Bronk, The Rockefeller Institute of Medical Research, 66th Street and York Avenue, New York 21, New York

Edwin D. Brooks, Jr., P. O. Box 1135, Boston 3, Massachusetts

Harvey Brooks, Division of Engineering and Applied Physics, Pierce Hall, Harvard University, Cambridge 38, Massachusetts

George F. Carrier, Department of Mechanical Engineering, 211 Pierce Hall, Harvard University, Cambridge 38, Massachusetts

John P. Chase, 75 Federal Street, Boston, Massachusetts

C. Lloyd Claff, Single Cell Research Foundation, Inc., 5 Van Beal Road, Randolph, Massachusetts

L. O. Colbert, 4408 29th Street, N. W., Washington, D. C.

Kenneth S. Cole, National Institutes of Health, Bethesda 14, Maryland

James S. Coles, Bowdoin College, Brunswick, Maine

Edward M. Douglas, West Chop, Massachusetts

Henry B. DuPont, Wilmington, Delaware

Ferdinand Eberstadt, 39 Broadway, New York 6, New York

Carl H. Eckart, Scripps Institution of Oceanography, La Jolla, California

Harrison P. Eddy, c/o Metcalf & Eddy, 1300 Statler Building, Boston, Massachusetts

Gifford C. Ewing, P. O. Box 508, Rancho Santa Fé, California

Homer H. Ewing, Greenville, Wilmington 7, Delaware

Alexander Forbes, 610 Harland Street, Milton, Massachusetts

Horace S. Ford, 77 Massachusetts Avenue, Cambridge, Massachusetts

Paul M. Fye, Woods Hole Oceanographic Institution, Woods Hole, Massachusetts

John A. Gifford, 14 Wall Street, New York 5, New York

Cecil H. Green, 1000 Exchange Bank Building, Airlawn Station, Dallas 35, Texas

Paul Hammond, Hammond, Kennedy & Legg Co., 230 Park Avenue, New York, N. Y.

Caryl P. Haskins, Carnegie Institute of Washington, Washington, D. C.

MEMBERS OF THE CORPORATION

HUDSON HOAGLAND, Worcester Foundation for Experimental Biology, 222 Maple Avenue, Shrewsbury, Massachusetts

FRANK A. HOWARD, 30 Rockefeller Plaza, New York, New York

COLUMBUS O'D. ISELIN, Woods Hole Oceanographic Institution, Woods Hole, Massachusetts

FRANK B. JEWETT, JR., Vitro Corporation of America, 261 Madison Avenue, New York 16, New York

HOWARD C. JOHNSON, JR., United States Steel Co., 71 Broadway, New York 6, New York

J. SEWARD JOHNSON, Cedar Lane Farm, Oldwick, New Jersey

AUGUSTUS B. KINZEL, Union Carbide Corporation, 30 East 42nd Street, New York 17, New York

MILFORD R. LAWRENCE, Siders Pond Road, Falmouth, Massachusetts

ALFRED L. LOOMIS, Room 2420, 14 Wall Street, New York, New York

AUGUSTUS P. LORING, Loring, Wolcott Office, Inc., 35 Congress Street, Boston, Massachusetts

LEROY F. MAREK, Arthur D. Little Co., Inc., 30 Memorial Drive, Cambridge, Massachusetts

ARNAUD C. MARTS, 521 Fifth Avenue, New York, New York

ROBERT E. MCCONNELL, First National Bank, Hobe Sound, Florida

NOEL B. MCLEAN, Edo Corporation, College Point 56, Long Island, New York

DANIEL MERRIMAN, Bingham Oceanographic Laboratory, Yale University, New Haven, Connecticut

HENRY S. MORGAN, 2 Wall Street, New York, New York

HENRY A. MORSS, 61 Ballast Lane, Marblehead Neck, Massachusetts

FRANK PACE, General Dynamics Corporation, 445 Park Avenue, New York 22, New York

ALBERT E. PARR, American Museum of Natural History, Central Park West at 79th Street, New York, New York

JOHN C. PICKARD, Box 3684, Greenville, Delaware

SUMNER T. PIKE, Lubec, Maine

EMANUEL R. PIORE, International Business Machines Corp., 590 Madison Avenue, New York 22, New York

ALFRED C. REDFIELD, Maury Lane, Woods Hole, Massachusetts

GEORGE H. RICHARDS, 68 Williams Street, New York, New York

MEMBERS OF THE CORPORATION

Lawrence B. Richardson, General Dynamics Corporation, 1710 H. Street, N.W.
Washington 6, D. C.

Lawrason Riggs, Riggs, Ferris and Geer, Room 1201, 74 Trinity Place,
New York 6, New York

William W. Rubey, Institute of Geophysics, University of California,
Los Angeles 24, California

Francis C. Ryder, 37 Larchwood Drive, Cambridge 39, Massachusetts

Mary Sears, Woods Hole Oceanographic Institution, Woods Hole, Massachusetts

Frederick Seitz, Department of Physics, University of Illinois, Urbana, Illinois

Harlow Shapley, Sharon Cross Road, Peterborough, New Hampshire

Henry L. Shattuck, 10 Milk Street, Boston, Massachusetts

Robert R. Shrock, Department of Geoolgy and Geophysics, Massachusetts
Institute of Technology, Cambridge 39, Massachusetts

Athelstan F. Spilhaus, Institute of Technology, University of Minnesota,
Minneapolis 14, Minnesota

H. Burr Steinbach, Department of Zoology, University of Chicago,
Chicago 37, Illinois

Raymond Stevens, Arthur D. Little, Inc., 25 Acorn Park, Cambridge 40,
Massachusetts

Julius A. Stratton, President, Massachusetts Institute of Technology,
Cambridge 39, Massachusetts

Gerard Swope, Jr., General Electric Co., 570 Lexington Avenue, New York,
New York

Selman A. Waksman, Institute of Microbiology, New Bunswick, New Jersey

Thomas J. Watson, Jr., International Business Machines Corporation,
590 Madison Avenue, New York 22, New York

William Webster, 5 Upland Road, Wellesley, Massachusetts

Francis C. Welch, 73 Tremont Street, Boston, Massachusetts

Alfred M. Wilson, Minneapolis-Honeywell Regulator, 2747 4th Avenue South,
Minneapolis 8, Minnesota

E. Bright Wilson, Jr., Department of Chemistry, Harvard University,
Cambridge 38, Massachusetts

RESEARCH STAFF

Arnold B. Arons, Associate in Physical Oceanography
Professor of Physics, Amherst College

William D. Athearn, Research Associate in Geology

Richard H. Backus, Marine Biologist
Associate in Ichthyology, Harvard University

Lincoln Baxter II, Research Associate in Physics

Edward R. Baylor, Research Associate in Physiology

David L. Belding, Associate in Marine Biology (Emeritus)
Professor of Bacteriology and Experimental Pathology (Emeritus), Boston University

Bruce B. Benson, Associate in Physics
Professor of Physics, Amherst College

Henry B. Bigelow, Founder Chairman, Associate in Oceanography
Professor of Zoology (Emeritus), Harvard University; Research Oceanographer (Retired), Museum of Comparative Zoology

Duncan C. Blanchard, Research Associate in Meteorology

Max Blumer, Geochemist

Bert Bolin, Associate in Meteorology
Director, Institute of Meteorolgy, University of Stockholm;
Director, International Institute of Meteorology, Stockholm

Vaughan T. Bowen, Geochemist
Lecturer in Zoology, Yale University

Alvin L. Bradshaw, Research Associate in Oceanography

Robert R. Brockhurst, Research Associate in Physics

John G. Bruce, Jr., Research Associate in Oceanography

Kirk Bryan, Jr., Associate in Meteorology
U. S. Weather Bureau

Dean F. Bumpus, Oceanographer

Elizabeth T. Bunce, Research Associate in Physics

Andrew F. Bunker, Meteorologist
Adjunct Associate Professor in Oceanography, New York University

Cornelia L. Carey, Associate in Marine Bacteriology (Emeritus)
Associate Professor of Botany (Retired), Barnard College

Dayton E. Carritt, Chemist
Professor of Oceanography, Massachusetts Institute of Technology

Joseph Chase, Research Associate in Physical Oceanography

George L. Clarke, Marine Biologist
Associate Professor of Zoology, Harvard University

Nathaniel Corwin, Research Associate in Chemistry

C. Godfrey Day, Research Associate in Physical Oceanography

RESEARCH STAFF

Willard Dow, Electronics Engineer

Richard S. Edwards, Research Associate in Geophysics

Kenneth O. Emery, Geologist

Alan J. Faller, Meteorologist

Charles J. Fish, Associate in Marine Biology
Professor of Marine Biology, University of Rhode Island;
Director, Narragansett Marine Laboratory

Nicholas P. Fofonoff, Physical Oceanographer

David H. Frantz, Jr., Research Associate in Engineering

Frederick C. Fuglister, Physical Oceanographer

Paul M. Fye, Chemist; Director

Michael Garstang, Research Associate in Meteorology

John W. Graham, Research Associate in Geology

George D. Grice, Jr., Research Associate in Marine Zoology

Robert R. L. Guillard, Research Associate in Marine Biology

Earl E. Hays, Physicist

John B. Hersey, Geophysicist
Associate Professor of Oceanography, Massachusetts Institute of Technology

Louis N. Howard, Associate in Mathematics
Associate Professor of Mathematics, Massachusetts Institute of Technology

Edward M. Hulburt, Research Associate in Marine Biology

Columbus O'D. Iselin, Henry Bryant Bigelow Oceanographer
Associate Professor of Physical Oceanography, Harvard University;
Research Oceanographer, Museum of Comparative Zoology;
Professor of Oceanography, Massachusetts Institute of Technology

Holger W. Jannasch, Microbiologist

John W. Kanwisher, Biophysicist

Bostwick H. Ketchum, Senior Oceanographer
Lecturer in Biological Oceanography, Harvard University

David D. Ketchum, Research Associate in Electronics

Sydney T. Knott, Jr., Research Associate in Engineering

Robert H. Kraichnan, Associate in Theoretical Physics
Senior Research Scientist, Institute of Mathematical Sciences, New York University

Eric B. Kraus, Meteorologist
Visiting Professor of Meteorology and Research Associate, Bingham Oceanographic Laboratory, Yale University;
Visiting Scientist, National Center for Atmospheric Research, Boulder, Colorado

Edward J. Kuenzler, Research Associate in Marine Biology

RESEARCH STAFF

Richard G. Leahy, Associate in Geology
    Assistant Director of Laboratories, Division of Engineering and Applied Physics, Harvard University

Joseph Levine, Research Associate in Meteorology

Joanne S. Malkus, Meteorologist
    Professor of Meteorology, University of California at Los Angeles

Willem V. R. Malkus, Physical Oceanographer
    Professor of Geophysics, University of California at Los Angeles

Paul C. Mangelsdorf, Jr., Associate in Physical Chemistry
    Associate Professor of Physics, Swarthmore College

Frank J. Mather, III, Research Associate in Oceanography

James W. Mavor, Jr., Research Associate in Applied Physics

Giles W. Mead, Associate in Ichthyology
    Curator of Fishes, Harvard University

David W. Menzel, Associate in Marine Biology
    Assistant Director, Bermuda Biological Station for Research, Inc.

William G. Metcalf, Physical Oceanographer

Arthur R. Miller, Physical Oceanographer

Robert L. Miller, Associate in Submarine Geology
    Associate Professor in Marine Geophysics and Geology, Department of Geophyscial Sciences, University of Chicago

Hilary B. Moore, Associate in Marine Biology
    Professor in Marine Biology and Assistant Director, Marine Laboratory, University of Miami

James M. Moulton, Associate in Marine Biology
    Associate Professor of Biology, Bowdoin College

Jerome Namias, Associate in Meteorology
    Chief, Extended Forecast Branch, U. S. Weather Bureau

Geoffrey D. Nicholls, Associate in Geochemistry
    Senior Lecturer in Geochemistry, Department of Geology, University of Manchester, Manchester, England

Charles B. Officer, Jr., Associate in Geophysics
    Vice President, Alpine Geophysical Associates, Inc., Norwood, New Jersey

David M. Owen, Research Associate in Underwater Photography

Alfred C. Redfield, Senior Oceanographer (Emeritus)
    Professor of Physiology (Emeritus), Harvard University

Charles E. Renn, Associate in Engineering
    Professor of Sanitary Engineering and Water Resources, School of Engineering, The Johns Hopkins University

William S. Richardson, Physical Chemist

Helen M. Roberts, Associate in Mathematics
    Assistant Professor of Mathematics, University of Connecticut

RESEARCH STAFF

Allan R. Robinson, Associate in Physical Oceanography
Assistant Professor of Meteorology and Oceanography, Harvard University

F. Claude Ronne, Research Associate in Photography

Claës G. H. Rooth, Research Associate in Meteorology

John H. Ryther, Marine Biologist

Howard L. Sanders, Research Associate in Marine Biology
Instructor in Marine Ecology, Marine Biological Laboratory, Woods Hole

Harold E. Sawyer, Research Engineer

Arthur K. Saz, Marine Microbiologist
Chief, Medical and Physiological Bacteriology Section, Laboratory of Infectious Diseases, NIAID, National Institutes of Health

Rudolf S. Scheltema, Research Associate in Marine Biology
Faculty Member in Biology, Cape Cod Community College

William E. Schevill, Associate in Oceanography
Research Associate in Zoology, Museum of Comparative Zoology, Harvard University

Karl E. Schleicher, Research Associate in Physics

William C. Schroeder, Ichthyologist
Honorary Associate in Ichthyology, Museum of Comparative Zoology, Harvard University

Mary Sears, Planktonologist

Raymond Siever, Associate in Geology
Associate Professor of Geology, Harvard University

Floyd M. Soule, Associate in Physical Oceanography
Oceanographer, U. S. Coast Guard

Allard T. Spencer, Research Associate in Engineering

Edward A. Spiegel, Associate in Astrophysics
Research Scientist, Courant Institute of Mathematical Sciences, New York University

Athelstan F. Spilhaus, Associate in Physical Oceanography
Dean, Institute of Technology, University of Minnesota

Melvin E. Stern, Physicist

Henry M. Stommel, Associate in Physical Oceanography
Professor of Oceanography, Harvard University

Thomas T. Sugihara, Associate in Geochemistry
Professor of Chemistry, Clark University

William H. Sutcliffe, Jr., Research Associate in Marine Biology
Director, Bermuda Biological Station for Research, Inc.

Harry J. Turner, Jr., Marine Biologist
Lecturer in Zoology, University of New Hampshire; Faculty Member in Biology, Cape Cod Community College

Ralph F. Vaccaro, Research Associate in Microbiology

George Veronis, Mathematician

RESEARCH STAFF

Allyn C. Vine, Physical Oceanographer

Gordon H. Volkmann, Research Associate in Physical Oceanography

William S. von Arx, Physical Oceanographer
Professor of Oceanography, Massachusetts Institute of Technology

Arthur D. Voorhis, Research Associate in Physics

Robert G. Walden, Research Associate in Electronics

Stanley W. Watson, Research Associate in Marine Bacteriology

Pierre Welander, Physical Oceanographer
Docent, International Institute of Meteorology, Stockholm, Sweden

Geoffrey G. Whitney, Jr., Research Associate in Physical Oceanography

Alfred H. Woodcock, Oceanographer

George P. Woollard, Associate in Geophysics
Professor of Engineering Geology and Geophysics, University of Wisconsin

L. Valentine Worthington, Physical Oceanographer

Charles S. Yentsch, Research Associate in Marine Biology

John M. Zeigler, Research Associate in Marine Geology
Lecturer in Geology, University of Chicago

ADMINISTRATIVE STAFF

Paul M. Fye	Director
David D. Scott	Head, Administrative Branch
Jess H. Stanbrough	Technical Assistant to the Director
James R. Mitchell	Administrative Assistant to the Director
Ronald A. Veeder	Development Program Manager
W. Redwood Wright	Public Information Officer
Norman T. Allen	Archivist
Harvey MacKillop	Controller
Richard S. Edwards	Marine Superintendent
John F. Pike	Port Captain
L. Hoyt Watson	Personnel Manager

DIRECTOR'S REPORT

REVIEW

With the great surge of interest in oceanography in recent years it became apparent that the Institution should augment its long-standing program for the training of interested young people in the various branches of marine science. To this end, three years ago we re-examined our educational policies in some detail. It seems appropriate to devote this portion of our annual report to this important aspect of our work.

Education and research have gone hand in hand at the Institution since it was established. From 1930 through 1958 a total of 320 fellowships had been awarded. In the three-year period since 1958 we have accelerated this part of our educational program and have awarded 141 fellowships. Fortunately, the budget for this purpose has grown markedly — about fourfold — during this period and increased stipends have permitted us to select outstanding students in spite of the increasing competition for the best.

In addition to augmenting our fellowship program, we have improved our educational opportunities through the expansion of our university affiliations, both by continuing to have university faculty members on our staff and, more importantly, by obtaining part-time faculty appointments for Institution staff members. At present 15 of our senior staff hold faculty appointments at 8 universities.

We believe that an oceanographic career is best approached by way of thorough academic training in any one of the basic scientific disciplines, with concentration on the marine aspects of that discipline beginning at the time actual research is started. This opinion is based on the interdisciplinary nature of oceanography and on the research performance and leadership in the field by many scientists with various educational backgrounds. In keeping with this point of view the Institution has traditionally organized its educational activities toward three overlapping purposes: promoting interest in marine research at all academic levels; helping academic institutions to maintain teachers with marine interests on their faculties; and using our own staff and facilities to provide specific educational opportunities not available within the academic framework.

Although these purposes are pursued throughout the year, the greatest activity at Woods Hole naturally occurs during the summer when students and teachers from other institutions have the time to make use of our laboratories and shops, our research vessels and workboats, and the incomparable library we share with the Marine Biological Laboratory. In 1961, for example, there were 146 summer additions to our year-round roll, including 24 student fellows, eight postdoctoral fellows, 21 visiting investigators and 93 students with jobs in the laboratories or at sea. Of this last category, all but three were high school graduates and 39 held bachelor's or advanced degrees. An invasion of this sort, representing nearly a 40 per cent increase in our work force, inevitably puts a strain on our physical plant, but we have always managed to find or create the necessary laboratory space. In recent years the extra scientific berths aboard the CHAIN have made it possible for many budding oceanographers — as well as a number of senior university people — to get a taste of science at sea. Needless to say, summer at the Institution is a challenging and stimulating experience, for hosts and guests alike.

For the past several summers we have offered special courses as well as research opportunities. Since 1952 we have cooperated with the Marine Biological Laboratory in presenting a course in Marine Ecology. More recently, with the financial sponsorship of the National Science Foundation, we have given a summer course in Geophysical Fluid Dynamics. The course includes both lectures and original research. It has attracted considerable national and international interest. Last year there were 19 participants from outside the Institution, including six from European countries, two from Canada, one from India and one from South Africa.

A third course was initiated in 1961 on an experimental basis, largely as a response to a growing demand from universities which teach oceanography but have no sea-going ships. The new course, entitled Observational Physical Oceanography, offers a combination of classroom and field experience. Six students took part during the first year, five of them on fellowships. A series of introductory lectures was followed by a cruise on the CHAIN, after which the students worked up their own data under the supervision of staff oceanographers. The course was quite successful and is being continued. It is our hope eventually to develop similar courses in other areas of our interest, specifically biology, geology and chemistry, and to assign the ATLANTIS to this training program.

The Institution's contribution to education on a year-round basis takes a number of forms. In 1961, nine graduate students were engaged in full time research leading toward doctoral dissertations; three received their degrees during the year. In addition we awarded five year-round postdoctoral fellowships. The recipient of one of these has since joined our staff, indicating the mutual advantages of such a program. In addition, we participate in two continuing seminar programs: the Massachusetts Institute of Technology — Woods Hole Oceanographic Institution Seminar in Thermal Convection which meets once a month at each Institution, and our Monday night Journal Club sessions where papers are presented on the entire spectrum of the marine sciences.

We are also providing more formal opportunities for the continuing education of our own staff. An in-service course in mathematics has been conducted for several years and courses in other subjects, notably foreign languages, have been presented from time to time. Each year the Institution loses a sizable number of employees who return to college, from beginning freshmen to senior investigators whose research needs have spurred them to fill specific educational gaps. Many of these individuals receive support from the Institution's fellowship program. The Institution also encourages employees wishing to further their education by means of university extension courses.

Continued enhancement of the educational opportunities at Woods Hole is imperative as both the Institution and the field of oceanography continue to grow. The impact of our educational program is complex to assess. However, in following up on the summer fellows of one recent year, we have found that more than three out of four are continuing in marine studies. This represents the true rewards of the planning and effort that have gone into this aspect of our work.

RESEARCH

Physical Oceanography

The Romanche Trench. One of the most fruitful cruises of 1961 was a three-and-a-half-month trip by the CHAIN to the eastern equatorial Atlantic in the vicinity of the Romanche Trench. The cruise was divided into three legs, interrupted by stops at Freetown, Sierra Leone. There were some changes in the scientific party between legs; in all, 29 men and women took part. The following listing gives an indication of the amount and variety of work performed:

There were 53 hydrographic stations, four large-volume water sample stations, 675 bathythermograph observations, 78 plankton tows, 24 mid-water trawls, 60 parachute drogue observations, 20 scattering layer stations involving 350 pounds of explosives, 13 velocimeter lowerings, 40 current shear studies, 8 piston coring tube lowerings, 17 Van Veen bottom samplings, and one pipe dredge lowering. Bottom photographs were taken, temperature measurements were made with the towed thermistor chain and a new method of navigation with a gyro-mounted telescope was tested. Routine observations included continuous bottom profiling, continuous observation of atmospheric and oceanic carbon dioxide, dipnet collections of surface organisms and keeping records of sightings of whales, porpoises and birds.

The cruise had three major objectives: an intensive investigation of the Romanche Trench, a deep valley in the mid-Atlantic Ridge on the Equator at 19° West Longitude; locating a low area in the Ridge across which cold deep water from the Western Basin of the Atlantic is flowing into the Eastern Basin; and measurement of the Atlantic Equatorial Undercurrent, a strong current flowing to the eastward beneath the westbound surface current.

Hydrographic stations during the International Geophysical Year had shown that the coolest deep water in the Eastern Basin lay in the vicinity of the Romanche Trench, suggesting that this anomalously cold water was flowing across a sill somewhere in that region. The first leg of this cruise was devoted almost exclusively to an intensive bathymetric survey of both the trench itself and the area along the Ridge to the east, where there was some earlier evidence of a saddle across which the cold water might flow. The ship criss-crossed the area, steaming more than 4,600 miles to complete the survey; the bottom was reconstructed aboard ship with sheets of plastic as the survey progressed.

The Romanche Trench lies in the mid-Atlantic Ridge with its long axis oriented east and west. The area deeper than 3500 fathoms is roughly 10 miles wide and 50 miles long. Only two small areas, the larger being about five miles long, showed depths greater than 4000 fathoms. The deepest hole located on the cruise was 4180 fathoms, uncorrected for the speed of sound in water, or 7985 meters, corrected. The bathymetric survey did not disclose the sill depth of the trench, but thermal observations showed that the deep water in the trench has the same potential temperature as that found at 2250 fathoms in the Western Basin; suggesting that the southern boundary of the trench may be almost this deep. At the same time the deep water in the Eastern Basin adjacent to the trench was not so cold, indicating that the sill there is so shallow that it does not permit any significant overflow.

A region about 250 miles east of the trench at about 15° West seems most likely to be the overflow area, with a sill depth of about 3750 meters; hydrographic studies as well as the bathymetry there indicate that the cold Western

Basin water is filtering through a complex system of ridges and valleys into the Eastern Basin. That the overflow of cold water is relatively small is shown by the fact that it is identifiable in only a small area before its characteristic temperature is modified by mixing with the much greater volume of warmer Eastern Basin water as it moves away from the source region. No figures can yet be given for the magnitude of the overflow, but it is believed to be irregular, occurring in surges which may depend upon the rate of formation of bottom water or some phenomenon such as internal waves.

Interest in the eastward-flowing equatorial undercurrents has increased rapidly in the few years since Cromwell and others began investigating the equatorial undercurrent in the Pacific Ocean. The Cromwell Current, as this is often called, is a wide, flat stream running strongly to the eastward just a few meters below the westbound Pacific Equatorial Current. Preliminary observations made during the International Geophysical Year showed the presence of a similar undercurrent in the Atlantic Ocean which was examined in some detail on this cruise of the CHAIN.

Shallow hydrographic stations were made on two north-south sections across the Equator from 3°30′ South to 3°30′ North, at 18°30′ and 13°30′ West. The samples were analyzed for temperature, salinity and oxygen content. In addition, at each station a current meter was lowered to 500 meters to record relative currents. Parachute drogues were also used; two drogues were pulled under by the current but a third, with a more buoyant float, provided an impressive demonstration of the speed of the undercurrent. The

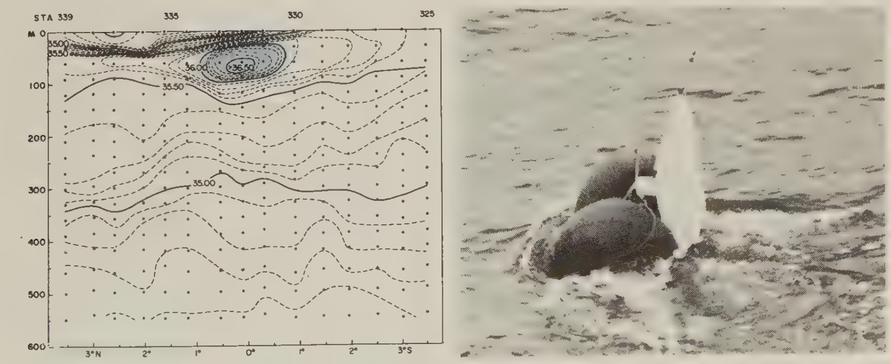

HAHN

Buoy towed by parachute drogue in equatorial undercurrent; Salinity profile across current at 13°30′ West.

float set off to the eastward leaving a wake like an outboard motorboat. The CHAIN followed it for 19 hours; the undercurrent was flowing eastward at about two knots and the surface current was moving westward at a little more than half a knot.

The undercurrent was also shown clearly by a number of measurements of horizontal shear made with pitotmeters attached to the thermistor chain. The measurements agreed well with those made by the drogues; they also indicated that the current is roughly symmetrical about the Equator with a southern boundary between 1° and 2° South. Evidence of the undercurrent was found at depths from 30 to 500 meters, with the highest speeds between 60 and 100 meters. It appears, however, that the undercurrent is not simply a broad, shallow ribbon but a very complicated stream.

The driving mechanism of the current is not yet known. Students of the Cromwell Current have suggested that vertical mixing at the surface along the Equator is involved. The temperature and oxygen profiles for the Atlantic undercurrent are similar to those of the Cromwell Current, but the salinity picture is quite different. A wide core of high salinity water right on the Equator in the Atlantic indicates that vertical mixing is not a major feature. Analysis of thermal data recorded with the thermistor chain shows that the isotherms diverge approaching the Equator from either side, indicating the presence of the undercurrent. In the same region there also appears to be intense production of internal waves with a period of 10 to 20 minutes and a wave length of 500 to 1000 meters.

Bottom water formation in the Mediterranean. The Mediterranean Sea has become of increasing interest, not only as a feature in its own right but because it can be regarded as a "model ocean" for studying processes which occur in the world oceans on a scale too large for detailed examination. In particular, the problem of bottom water formation in the Mediterranean is being studied as an aid to understanding the same phenomenon in the less accessible Antarctic area. The ATLANTIS spent three winter months in 1961 in the western Mediterranean; extensive hydrographic work was done on the CHAIN in the Eastern Mediterranean in the late summer; and another ATLANTIS cruise has been scheduled for the first few months of 1962. The ultimate purpose of these cruises is to determine the rate of bottom water formation in key Mediterranean areas: the Ligurian, Adriatic, and Cretan seas.

It is believed that new bottom water is formed when outside processes change the character of surface water so that it becomes sufficiently dense to sink to the bottom. In the Antarctic this process is the cooling and salting of the surface water accompanying the formation of sea ice. In the Mediterranean dense water is made by winter cooling and by extensive evaporation which removes fresh water from the sea surface. Accordingly, in conjunction with the hydrographic work measurements were made of humidity, solar radiation and back radiation, wind, precipitation and evaporation. New instrumentation has been and will continue to be developed for measurements of this sort; it is difficult to evaluate the data accumulated so far because of the interference introduced by the ship itself. However, there are indications that daily evaporative cooling in the Mediterranean is so great that the sinking process might be initiated by relatively small temperature changes, rather than large outbreaks of polar air as had been suspected.

The ATLANTIS made 138 hydrographic stations during her winter cruise, mostly in the Ligurian Sea; the CHAIN added 75 more in the Sea of Marmora, the Aegean Sea and the Cretan Sea. The data from these will be a valuable addition to the surprisingly scanty amount of information about a sea so well-traveled as the Mediterranean. Part of the CHAIN's work included a network of closely spaced stations in the Cretan Sea; the area north of the Island of Rhodes was well covered. Results seem to indicate a deep isolated water mass of high salinity. On the other hand, in a deep of 4500 meters southeast of Rhodes the deep water appears continuous with the surrounding waters but with little vertical mixing below what might be called sill depth at 2500 meters. The data agree with those of the French and earlier ATLANTIS stations except for surface water salinity differences which are probably seasonal effects. Unfortunately the amount of data available is still not sufficient to determine seasonal changes.

Gyres and Convergences in the North Atlantic. Evidence has been found that the circulation system of the Western North Atlantic may consist of two large gyres separated by a low pressure trough running southeast from the Flemish Cap. Sections made by F. R. S. ANTON DOHRN, V. F. S. GAUSS, R. R. S. DISCOVERY II, S. S. M. LOMONOSOV and the ATLANTIS, CRAWFORD and CHAIN have been examined. From the data were drawn plots of oxygen versus sigma-t, sigma-t profiles, temperature profiles and salinity anomalies; volume and oxygen anomaly transports were computed. The results of the investigation can be summarized as follows:

As it passes the southern extremity of the Grand Banks the Gulf Stream transports water with an oxygen-density relationship closely resembling the Sargasso Sea average established by Richards and Redfield (1955). The currents which flow to the north, off the Flemish Cap, transport water which has a temperature-salinity correlation similar to that of the Sargasso Sea but is richer in oxygen by about 1 ml/l at every sigma-t surface in the pycnocline. For this reason it is suggested that the Gulf Stream does not turn northward after passing the Grand Banks but continues to flow in a southeasterly direction, and that the currents which pass the Flemish Cap are part of a separate northerly gyre. There is evidence of a nearly permanent trough of low pressure between the gyres. It has also proved possible to estimate a new water budget consistent with the distribution of oxygen in the Western North Atlantic.

The area of salinity maximum in the region of the northeast trade winds in mid-Atlantic was examined in a CRAWFORD cruise in March. The salinity maximum is of interest because it is evidently an area where water mass formation is actively taking place as a result of convergence. However, it depends upon trade wind circulation, which was unfortunately well below normal during the CRAWFORD cruise as it has been on two earlier cruises to the area. Current measurements made from the ship with an anchored buoy as a reference point showed a northeasterly flow in the upper 240 meters. Normal currents in the area are westerly; this near-reversal of conditions is thought to be associated with an abatement of the trade winds. It is hoped that in the future productive experiments can be made with unattended instruments in the salinity maximum area.

Gulf Stream meanders. In October and November the CRAWFORD made seventy crossings of the Florida Current off Jacksonville in a study of the meanders of that portion of the Gulf Stream. Earlier analysis of data on the Florida current off Onslow Bay and Miami had indicated that the meanders are actually adding energy to the mean stream instead of dissipating it, as had been suspected. In the CRAWFORD cruise extensive use was made of the new *in situ* salinometer. Initial analysis of the data indicates that the

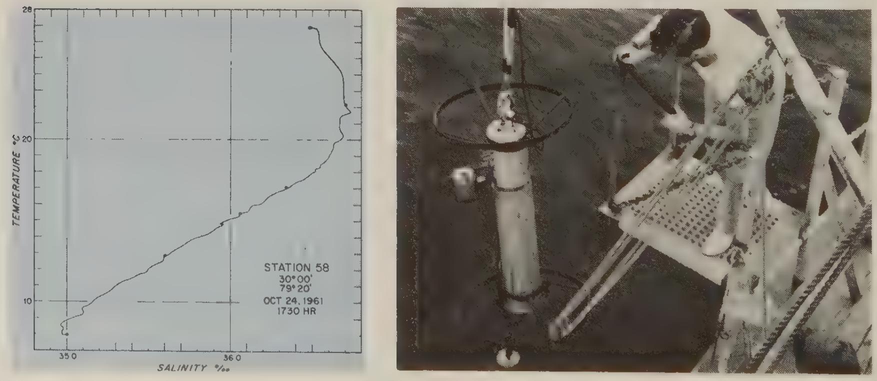

WRIGHT

Temperature-salinity curve from in situ salinometer lowering; Instrument comes aboard CRAWFORD.

instrument is particularly well suited to this sort of problem, as fine details and hitherto unsuspected time variations were discovered in the temperature and salinity structure of the region. In addition, an anchored buoy with two current meters was placed on the eastern side of the current. Results will be compared with dynamic velocity computations and with coincident surface measurements with the geomagnetic electrokinetograph (GEK). The data will be analyzed to determine the momentum transfer and the mechanism of the kinetic energy balance associated with the meandering of the current.

Non-tidal circulation on the continental shelf. The continuing drift bottle investigation of non-tidal circulation on the continental shelf has been augmented by the introduction of mushroom-shaped bottom drifters of brightly-colored plastic, developed at the Lowestoft Laboratory in England. Several thousand of these have been released with an encouraging percentage of returns. In one area off the Middle Atlantic States more than 26 per cent of the bottom drifters released in the fall were recovered, most of them along the shore. In the same area the only surface drift bottles recovered were those launched near the beach. Thus it appears that the autumnal offshore tendency at the surface is compensated for by a shoreward drift along the bottom, which fits the theory of an estuarine type of circulation on the continental shelf.

A series of cruises was made between Cape Cod and Cape Hatteras in an attempt to monitor any large scale changes in the circulation of the waters on the continental shelf. Some direct measurements of the drift were correlated with the density field and an encouraging result in the form of a regression equation was derived. The equation was used to compute velocity profiles for several sections across the shelf and the difference in these from summer to winter were related to expected seasonal changes in temperature and salinity in the area.

Theoretical and Experimental Hydrodynamics

The theoreticians continue their interest in exploring hydrodynamic phenomena that are related to oceanic circulation and in devising experimental and mathematical models which will permit an analysis of them.

The problem of penetrative convection has been considered by utilizing the peculiar properties of water near its freezing point. When a layer of water is maintained at 0°C at its bottom, while its top is somewhat greater than 4°C, then the system becomes unstable at a critical Rayleigh number, and one inquires as to how deeply the motions go inside the stable warm water. The finite amplitude theory of Malkus and Veronis (1958) was extended to this case. In addition, a different formulation of Malkus's turbulent convection theory is now being developed.

Experimental data on the instability of Ekman boundary layer flow is being analyzed and combined with theoretical investigations. The roll-like waves which are observed in the rotating tank offer a possible explanation of certain geophysical circulations that have banded structure. Construction has begun in the Laboratory of Oceanography of a new hydrodynamics laboratory to replace the one on the Institution dock which had fallen victim to a series of hurricanes over the years.

A series of numercial solutions has been completed for the non-linear thermocline problem as formulated by Robinson and Stommel (1959). The calculations were made, using an iterative method of Hartree's for solution of ordinary non-linear differential equations, on the Recomp II computer. It is believed that these new calculations will shed considerable light on which parameters determine the form and amplitude of the abyssal circulation and of the thermocline itself.

Some progress has been made in deriving stability criteria for the problem of the breaking up of jet-like streams into vortices. This bears on the problem of the formation of meanders in ocean currents like the Gulf Stream, and the development of cyclones in the atmosphere. In the Gulf Stream, for example, both the cross stream gradient of density and the mean velocity are known from previous literature to be potent mechanisms for producing unstable waves. The motions which may result when both these mechanisms are present are under discussion.

Marine Meteorology

Meteorology investigations in 1961 fell generally into two interrelated areas: the physics of convection, condensation and cloud formation, and the exchange of energy and matter across the sea surface.

Cloud physics. Laboratory studies of the convection of isolated masses of buoyant fluid, carried out in London and in Woods Hole, have helped in understanding the dynamics of convective clouds. The work was extended by field measurements of subtropical showers made in collaboration with the U. S. Weather Bureau in Miami, Florida. On two occasions giant cumulonimbus clouds with tops as high as 55,000 feet were observed to penetrate into the stratosphere. An analysis of time-lapse photographs and radar measurements showed that the extent to which a cloud penetrated the stratosphere was directly related to the intensity of vertical air motions within the cloud; a result which had been accurately predicted from the laboratory experiments.

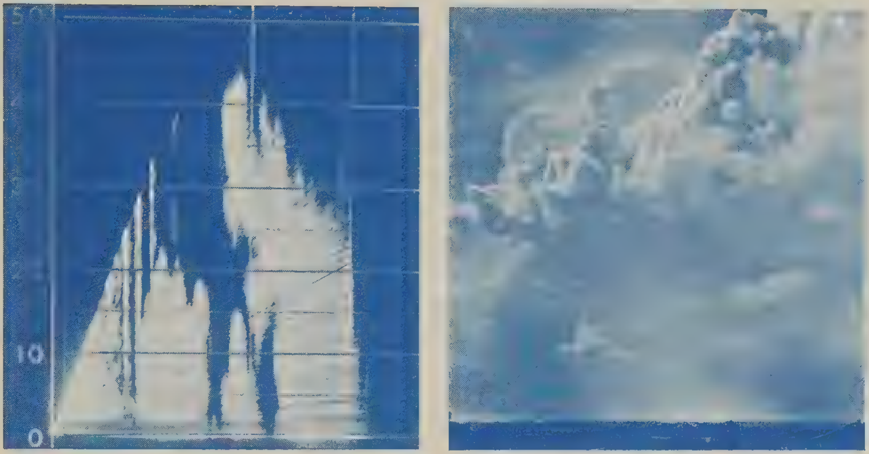

RONNE

Radar picture shows cross section of storm cloud at right.

The relationship between the dimensions of visible shower clouds and the echoes received from them on a high-power weather radar was also examined on the Miami trip and a close correspondence was found. The result is doubly valuable because it improves the use of radar for storm warning purposes as well as the interpretation of radar data in basic research.

Cloud photographs from the second of three flights made over the Pacific Ocean in 1957 have provided the data for cloud distribution there. Previous analyses of photographs made during the first flight have shown a pronounced alignment of cumulus clouds. From the maps made from the Flight II photographs, it appears that the upper air circulation exerts a control upon the trends of cloud activity and upon the organization of clouds into lines and groups. The trend toward deeper and more vigorous clouds occurs in discontinuous steps rather than in a continuous build-up from small cumulus to cumulonimbus.

The water vapor distribution data obtained off the Bahama Islands in 1960 from three airplanes flying one above another have been processed. The huge job of data reduction and spectral analysis was accomplished by the Recomp II computer, without which the project would have been impossible. The results give a clear two-dimensional picture of the water vapor distribution in the sub-cloud region of the trade winds. Cross-sectional graphs reveal many intrusions of dry air into the moist lower air. The spectral analysis shows a continuous increase in the variance of the mixing ratio from the 100-meter to the 100-kilometer scale.

The hot wire instruments used in field trips in 1960 to measure liquid water content in clouds and precipitation have now been calibrated. A high speed spark source aided in photographing droplets in the instrument wind tunnel; droplet counts from the photographs have made possible the precise calibration of the instrument's response to water drops. As a consequence final analysis of the cloud data can now be undertaken. This will, in turn, permit determinations to be made of the degree of mixing of buoyant cloud elements with the dry environmental air.

The meteorological instrumentation of the R4D aircraft has been improved by the addition of a microwave refractometer which gives faster measurements of the water vapor content of the air and makes possible more reliable computations of the water vapor flux through the atmosphere. It was used in flights over the Gulf of Maine, Buzzards Bay and Sebago Lake during a severe winter cold spell. An improved radiometer is also being developed for the airplane to measure the net flux of radiation through the atmosphere.

Sea salt nuclei and rain. The work of the salt nuclei project was concentrated largely upon preparation for and execution of a two-month field trip on the island of Hawaii, where previous investigations of orographic rains have been dubbed "Project Shower." Hawaii, largest of the Hawaiian Islands, is particularly suited for this sort of work because of its distance from other land areas to windward, its high annual rainfall and its accessible mountains which permit observations at various levels in the shower clouds. Evaluation of the data from the field trip is expected to help provide an integral picture of the life history of a shower-producing convective cell.

One of the purposes of the trip was to relate the various properties of raindrops in the showers to other variables such as the amounts of airborne salt, the water-vapor distribution in the trade winds, the total rainfall and saltfall on the watershed and the height of the trade inversion. To accomplish this, twenty battery-operated rain recorders were designed and built. The instruments make a photographic record of the number and size of raindrops falling on a glass plate each 30 seconds; about 1,400,000 observations were obtained, making possible a detailed study of the time and space variability of drop number and size in the showers.

Measurements of the sodium content of individual raindrops were made for the first time with a flame spectrophotometer developed at the Institution. The sodium concentration varied between one and twenty parts per million and was inversely related to drop size. Attempts will be made to relate these quantities to a model of shower rain formation.

Instruments were also built to measure potential gradient, space charge, bulk rain current and the charge and size of individual raindrops. The most important finding in this atmospheric-electric work, made with a six-foot cubical Faraday cage which was set up ashore and on the deck of a Coast Guard cutter, was that of the flux of positive charge from ocean to atmosphere in regions of breaking waves and foaming. This confirmed earlier evidence that the sea is a source of positive charge for the atmosphere. It has been estimated on the basis of laboratory experiments that about 160 amperes of positive current are continually flowing from the world ocean into the atmosphere.

The contact of molten lava with sea water forces great quantities of finely divided salt particles into the atmosphere. A study of these particles in steam clouds from the 1960 Kilauea eruption in Hawaii has been published. A major result was finding that the rate of production of the important "giant nuclei" (10^{-9} grams or larger) was very great; a new geochemical fact which may have widespread meterological significance. One way to make clear the magnitude of the production rate is to realize that a few square kilometers of hot lava surface in contact with sea water could, within the lifetime of an eruption, produce enough particles to double the number of giant nuclei in the lower kilometer of the entire earth's atmosphere.

The idea which motivated the first attempts (in 1947) to measure the distribution of sea-salt particles in marine air over the ocean has never been satisfactorily explored. This idea, briefly stated, was that the hygroscopic sea salt particles might cause significant amounts of latent heat of vaporization of water to be released in subsaturated air. Accumulated evidence and experience over the intervening years finally made it possible, in 1961, to construct a reasonable hypothesis which confirms the original idea. It now appears that the release of latent heat in some parts of the lower atmosphere over the sea can be an important factor in the initiation of cumulus clouds.

Convection Theoretical work on the relation between vortical motions in convective clouds and the formation of precipitation has opened up a whole field of problems involving the interaction of a fluid in motion with particle populations in suspension in the fluid. Studies of convection in populations of motile algae (bioconvection) show promise of shedding some light on the formation of intensive downdrafts in and under precipitating clouds.

Winter temperatures in New England. An attempt has been made to put the forecasting of winter temperatures in New England on a more objective basis by devising a geometrical grid as an index of the flow along the Atlantic side of the trans-Arctic Ridge in November. Lines of regression have been calculated relating the index with the winter temperature anomalies in southern New England in 21 cases. Rules are being developed for dealing with other cases in which the index alone does not adequately describe the flow of cold air.

Geophysics and Submarine Geology

The Mid-Atlantic Ridge. The Mid-Atlantic Ridge is an object of great scientific curiosity. During the past year some of its geological and geophysical characteristics were deciphered by scientists from the Institution. It was suspected that the depth of the Ridge near the equator limits the flow of deep, cold, Antarctic water from the western basin of the South Atlantic into the eastern. Accordingly a rather detailed bathymetric survey of the Ridge, the Romanche Trench, and adjacent waters between 10° and 20°W was made from the CHAIN in January. Geologically this trip was significant because it was one of the first times it was possible to examine the bottom of the Romanche Trench in considerable detail with the aid of anchored buoys for navigational reference. In addition many photographs were taken along the floor of the trench and some very important rock samples were recovered in cores.

On a subsequent cruise of the CHAIN, the Mid-Atlantic Ridge was visited twice more, each time near 29°N Lat., on the way to and from the Mediterranean. On the eastward crossing within a region two hundred miles long in an east-west direction by thirty miles wide, two possible breaks in the wall of the median rift were found. In one, there was a large boulder of volcanic rock with glassy outer surfaces; in the other calcareous sand or ooze. In a nearby depression quite similar to the rift in form, 500 overlapping photographs of the bottom revealed an extensive area of ripples in the sediment. These were presumably formed by bottom currents, but they are so criss-crossed by animal tracks that they are obviously not of recent origin.

Heat flow. In collaboration with a student from Cambridge University, several measurements of heat flow from the earth's interior were made on the same passage. The object was to determine whether the several high readings previously reported in mid-oceanic ridges signify a broad, regional heat maximum there or merely local patches. Although the data have not yet been completely worked up, the latter appears to be true.

Records of Sub-bottom echoes. Identification of sediments in deep-sea basins over extensive areas has been vastly improved by the development of a continuous seismic profiler (CSP), which can continuously record sub-bottom echoes from interfaces between contrasting rocks or sediments more than 1000 meters below the surface of the bottom just as routinely as echo soundings have been collected for many years. This instrument was used in topographically enclosed basins both in the Mediterranean, known to have a bottom of uniformly bedded sediments at least 30 or 40 meters thick, and in the North Atlantic basins where there are characteristic flat plains. In the Mediterranean the source of sediments in such basins is derived from the surrounding land areas and from volcanic ash. In the open ocean, however, it is believed that the sediments come mainly from adjacent submarine slopes. The CSP readily showed that the flat plains are actually formed by horizontally-bedded sediments which partially fill deep depressions in pre-existing surfaces to depths of 500 to 1000 meters. Outside these basin areas and the major abyssal plains, the sediments are by comparison thinner, which supports the generally accepted theory that abyssal plain sediments are transported from the continental slopes by turbidity currents. In the vicinity of Caryn seamount CSP records show at least 1000 meters of sediment horizontally bedded at its base, with the deeper layers dipping away from it. This indicates the likelihood that the seamount is older than the adjacent sediments and strengthens the argument that such sediments were deposited by turbidity currents.

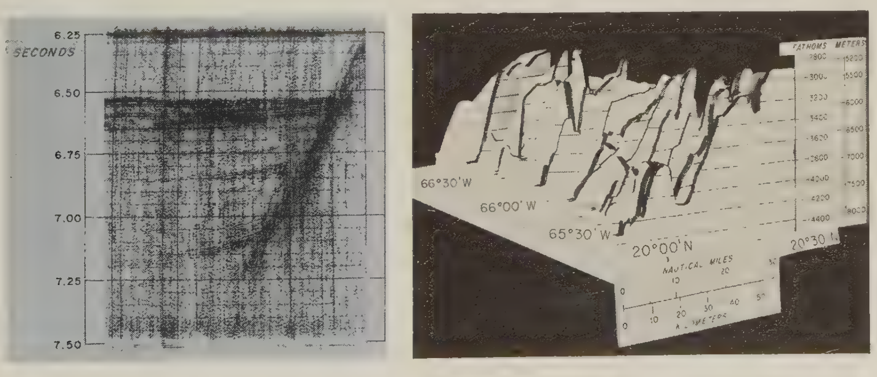

CSP record shows sediment beds dipping away from Caryn Seamount; Model based on Puerto Rico Trench bathymetry was made during CHAIN 19.

Deep-living coral and manganese modules. Topographic investigations on the Blake Plateau which started in 1954 led to the discovery this year of banks of coral at 450 fathoms. Earlier (1955) it had been found that the remarkably smooth-surfaced Blake Plateau is interrupted by sharp local hillocks rising several tens of fathoms above it. Subsequently some of these protuberances were detected as ridges or "welts" along corresponding depressions. During a cruise of the ATLANTIS (1961) these were ascertained to be banks of living coral on at least one major structure. These corals are being examined in collaboration with a scientist from the U. S. National Museum. It had been thought that the strikingly linear boundaries of the depressions in this area were indications of fault zones. However, CSP records reveal that the shallow beds terminate to form the walls of the depressions while deeper bedding continues beneath them without conspicuous evidence of faulting.

During the same cruise several hundred pounds of manganese nodules were collected on the plateau. These nodules and the live coral seem to be mutually exclusive, but their relationship is not yet thoroughly understood. Great interest has been shown in these manganese nodules and their chemical composition and probable mode of deposition, investigations of which are underway or being planned. Parenthetically, this very productive ATLANTIS trip was also part of the summer training program in oceanography. The cruise was under the direction of two experienced submarine geologists who were assisted by seven students ranging from a preparatory school boy to doctoral candidates in geology and geophysics.

Crustal structure. With the Carnegie Institution of Washington, the University of Wisconsin and others, the Institution took part in a cooperative seismic refraction study of the crustal structure beneath the Gulf of Maine. The BEAR acted as listening ship, first near the Maine coast and later near the continental slope between Brown's and George's banks. Shore parties from other institutions recorded signals in Maine while attempts were made at Woods Hole to monitor those received at several localities on Cape Cod, Block Island and Long Island by means of long-distance telephone lines. The reception aboard BEAR was excellent, as were the results from Maine.

The crustal studies in the Mediterranean, on the continental shelf south of Ireland and north of Puerto Rico (for Mohole site selection), all mentioned in previous reports, have been largely completed this year. Although the laboratory analyses of seismic refraction data is an exacting and protracted labor, sufficient information for planning further research has been obtained from a preliminary examination of the field data. The crustal structure, as determined during the Mohole survey, and photographs of the rock on the north wall of the Puerto Rico Trench led directly to successful dredging operations there in 1961. During the CHAIN cruise, four hauls dredged loose rock fragments of various sedimentary and crystalline rock, mostly serpentinite.

One fragment of serpentinite may have been broken off from an outcrop apparently from below the upper boundary of the lowest layer of the earth's crust. The significance of this exciting find is somewhat dimmed by uncertainty of the seismic shots and of the estimates of the depth where the rock was detached. Improving the latter will require the development of new techniques.

Transport of coastal sediments. Existing theory and wave equations did not provide an adequate mechanism for the transportation of fine silts and clays from cliffs along a beach to offshore sites of deposition. Known patterns of sediment distribution required some explanation besides rips and other narrow seaward currents. Furthermore, the wave equations for predicting the movement of particles of water beneath shoaling waves did not allow for any sort of return flow. Experiments from a wave tower located off the Tisbury beach on Martha's Vineyard have shown that there is a net seaward flow in the mid-depth waters beneath shoaling waves. The 1960 wave tower, a steel H-beam driven into the sand, was carried away by a hurricane. A sturdier structure was built in 1961 and equipped with instruments to measure the horizontal component of wave orbits at three points above the bottom simultaneously with observations of wave height, period and length. Despite delays caused by storms, several records were collected. Analysis of the data is still in progress, but it appears certain that the flow is strong enough to move large particles.

Underwater Acoustics

Since World War II the Institution has assisted the Navy in understanding the effects of the oceanic environment on the performance of underwater acoustical devices. An increased understanding of these automatically provides the oceanographer with a new technique for examining the oceans. Acoustical instruments serve observational purposes, such as the various sound pingers introduced by Edgerton and Cousteau to facilitate bottom photography and as adopted by Swallow to measure deep currents. These are now utilized at the Institution to monitor bottom coring operations and deep hydrographic casts. In 1961 they were used for positioning a rock dredge; later an underwater camera was added to photograph the bottom along the projected path of the dredge. This adaptation has greatly increased the efficiency of dredging, if only by assuring that the gear has made prolonged contact with the bottom.

A potential use of sound is to reveal the presence of and to track the movement of water masses by transmitting sound through them. Long distance transmission experiments in support of naval projects in the Bermuda area has produced striking evidence of large scale contrasts in the water masses in the Sargasso Sea. Although this is by no means a fully developed scientific tool, continued investigations may well lead to a powerful method in synoptic oceanography.

New long distance sound transmissions in the eastern Mediterranean in cooperation with NATO's SACLANT Research Center in La Spezia, Italy, have aided in understanding the bottom reflection process and the focusing of sound by variation of its velocity in sea water. Small explosive charges were used as sound sources for such work until a few years ago, when it became evident that the fine scale changes in both distance and time in the ocean would require more rapid observation than the use of explosives would permit. A great advantage was also apparent in correlating successive wave trains received from an impulse source that operated on a precise schedule. The "Sparker" and the "Boomer" (formerly called the "Thumper") were developed partly for this work and partly for seismic reflection work. Both devices were strengthened considerably in 1961: a "Sparker" designed for 25,000-joule electrical output was available for the CHAIN's work in the Mediterranean and a 13,000-joule "Boomer" was used repeatedly on the return trip across the Atlantic. Earlier in the year 5,000-joule "Sparkers" and "Boomers" permitted observations of deep bottom reflections and in horizontal sound transmissions over several tens of miles in the western North Atlantic. An extended use of underwater sound in geophysics and physical oceanography may now be possible with the advent of these new acoustic devices.

CHAIN's 25,000-joule "Sparker" proved capable of recording deep scattering layers from 2 to 20 kilocycles while the ship was underway at full speed. The first demonstration came in a four-day investigation of internal waves in the Strait of Gibraltar in collaboration with a scientist from La Spezia. Later observations were made in the Mediterranean whenever possible. Studies of this sort previously had been made only very laboriously with explosives; now continuous observations can be made of the frequency dependent phenomena of deep scattering layers.

Continuous deep profiles of sound velocity have been made from CHAIN with the National Bureau of Standards velocimeter. In addition, several profiles were made on two ATLANTIS cruises in the western basin of the North Atlantic. Results from these added to previous experience at the Institution and elsewhere suggest that this meter is a significantly better means of determining sound velocity as a function of depth than the earlier method of computing it from temperature, salinity and depth. Since this is the first program of continuous surface-to-bottom of any physical property of the deep sea, it should be watched with great interest by oceanographers for hints of telltale anomalies from which new understanding of deep water masses may come.

Chemistry and Geochemistry

Fallout fission products. Analyses for the fallout fission products strontium-90, cerium-144 and promethium-147 from both surface and deep water samples have continued to accumulate, confirming our belief that the first of these is a good tracer of water movement while the other two are moving principally with sinking particles. In many cases, by making reasonable assumptions about the time of massive delivery of fission products after a bomb-test series, it has been possible to estimate the rate of sinking of particle-populations of differing properties, both chemical and physical.

The strontium-90 data continue to show both an inexplicably high rate of delivery to the sea surface and a rate of down-mixing higher than expected. Two samples taken in 1959 from the Chukchi Sea, north of Bering Strait, were analyzed to see if high radioactivity in water of Pacific origin could be discerned as it moved northward into the Arctic Ocean; the samples showed strontium-90 no higher than is found at comparable latitudes in the North Atlantic.

The water sampling program developed well during the year. Six full stations were made on Institution cruises; three additional Chukchi Sea samples have been obtained with the help of the Fisheries Laboratory, University of Washington; surface samples are being taken twice a month on four weather ships in the Atlantic Ocean through cooperation with the U. S. Weather Bureau and the U. S. Coast Guard. The data should provide a good base line to support maximum interpretation of the movements of the new fallout expected in the spring of 1962 as a result of the Russian tests in the fall of 1961.

A series of cores was taken on the CHAIN from the Romanche Trench and from a line across the Sierra Leone and Cape Verde basins to the mid-Atlantic Ridge. The cores are expected to be of special interest as spanning the whole spectrum of variation in terrigenous contribution. They are being subjected to complicated cooperative analyses: major and minor elements at University of Manchester; interstitial water at Harvard University; heavy minerals at Woods Hole and Foraminifera at the United States National Museum. Clay minerals are also being looked at and several other sorts of analyses are still to be farmed out. An abortive coring attempt on the same cruise yielded a small piece of volcanic glass under conditions indicating it must have covered a considerable area on the east slope of the Ridge under about 14 inches of red clay. Analysis of the elements in this glass showed a most unusual composition which has led to much speculation on its origin. Other submarine glass samples will be analyzed for comparison.

A workable method for separating actinium from ocean sediments has been developed; measurable yields of a radioisotope showing a growth curve similar to that of actinium-227 have been obtained from high-uranium Caribbean samples. The next step is to use analysis of the dis-equilibrium between parent isotopes and the daughter actinium-227 to study both the rate of sediment accumulation and the extent of back diffusion of some natural radioelements.

Fossil pigments. The organic chemistry of a heavily pigmented fossil sea lily of Jurassic age has been studied in some detail. Four aromatic hydrocarbons have been identified, the structure of three major pigments has been tentatively established and partial evidence has been obtained for the constitution of a fourth; all the pigments and hydrocarbons are interrelated genetically and structurally. It is now possible to reconstruct the sequence from a simple biogenic pigment to the more complex fossil pigments and the hydrocarbons. Of special interest is the fact that several of the pigments but none of the hydrocarbons have a sterically strained structure. The conversion from the unstable, strained pigments to the stable hydrocarbons has proceeded only to a very small degree in spite of the long exposure in the sedimentary environment. This indicates a very low reactivity in the sediment and an excellent chance for the preservation of unstable biogenic products and reaction intermediates.

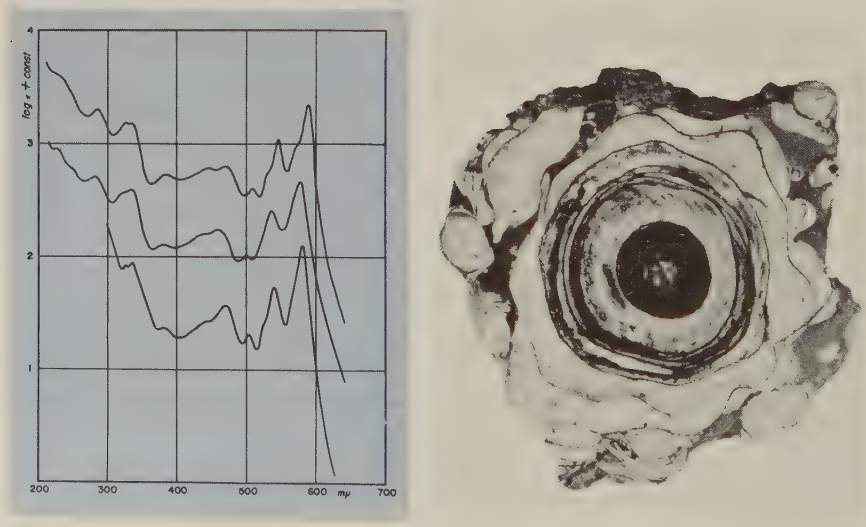

SPOONER

Section of fossil Crinoid (Millericrinus) and graph of absorption spectra of Fringelite D, E and F, the three major pigments.

The discovery of unusual aromatic hydrocarbons in the fossil has led to a more general search for such compounds in nature; a great many were found to occur in soil. Most surprising was the finding of 3.4-benzpyrene, a well-known and powerful carcinogen, at concentrations up to 1.3 mg/kg. This means carcinogens may be a much more common and unavoidable part of man's environment than had been suspected.

Work has also been continued on techniques for isolation and identification of very dilute organic compounds in sea water. For isolating non-polar, high-boiling materials the favored procedure now involves a solvent extraction with benzene followed by zone melting of the solution to concentrate the solutes. The concentrate is injected into the gas chromatograph at a temperature sufficiently low to elute the solvent while retaining the solutes; these are then analyzed by temperature programming of the column. This method avoids losses by evaporation and minimizes handling of the extracts.

Salt bridges for GEK cables. The use of salt bridges for cables in GEK technology has been applied successfully both for current measurements at sea and for measuring tidal flow in Woods Hole. With a polyethylene tube across Woods Hole channel from Juniper Point to Nonamesset Island, a continuous record of current flow was obtained. In addition to confirming the basic usefulness of the method, this experiment demonstrated that the Hole acts as a half-wave rectifier, with a total transport from west to east about twice that from east to west. Sea tests aboard the ATLANTIS showed that the salt bridge system permits easy compensation for GEK electrode sensitivity to salinity, temperature, pressure and oxygen tension.

Ion interactions in sea water. Estimation of ion interactions in sea water is needed for evaluation both of ionic activities and of the contributions of various constituents of sea water to its conductivity. To obtain basic data on simplified systems, various properties of mixed strong electrolyte solutions at constant molarity are being investigated. The solutions are: soldium chloride-magnesium chloride; magnesium chloride-magnesium sulfate; magnesium sulfate-sodium sulfate; sodium sulfate-sodium chloride. The molality of the first electrolyte is varied by alternate additions of small amounts of water and second electrolyte so that total molality is maintained at 0.7, in the range of sea water. The activities of the electrolytes, the aqueous vapor pressure of the solutions and their density will be measured; the experimental data will be compared with those predicted by various theories of inter-ionic effects.

Oxygen titration. An experimental study has been made of the Winkler titration method, the classical means of determining dissolved oxygen. Of four published methods for standardizing the titrant, only one was found to be capable of what can loosely be called "nearly adequate" precision and accuracy. Examination of other parts of the procedure showed a wider spread of results than had been estimated and indicated that the absolute value of error may be virtually independent of the concentration of dissolved oxygen in the sample. The results of these experiments are being used as the basis for modifying the procedure.

Zinc in sea water. A method for the determination of zinc in sea water has been developed as the first part of a general study of many of the minor and trace substances in the oceans. A guiding principle of this study has been that in order to describe the distribution of these substances in a manner adequate for present biochemical and geochemical considerations, analyses are necessary on a scale now achieved for major nutrients like phosphate and nitrate. The procedure that has been devised for zinc involves the use of anion exchange resins to collect the element from a large volume of sea water, followed by removal of the zinc from the resin column with a small volume of eluting agent. It is believed that this technique, which will be tested at sea in 1962, will prove suitable for collecting and concentrating several other trace elements.

In addition, the physical chemistry of zinc in sea water is being examined and tracer studies of the mechanisms of zinc accumulation by marine phytoplankton have been started. The sugars and sugar esters in local decapod Crustacea are being examined in relation to the life cycles and ecology of several species; this approach may soon be applied to planktonic Crustacea.

Marine Biology

The biological investigations at the Institution are a combination of laboratory and field studies aimed at understanding the environmental conditions which determine and control the size of populations, their growth and the distribution of individual species in the sea. The work includes organisms ranging in size from bacteria to whales and processes ranging from nutrition and food consumption to the visual physiology of Crustacea.

Arctic copepods. One of the most unusual opportunities of 1961 was provided by a collection of Arctic zooplankton gathered by an automatic sampler installed on the nuclear submarine SEADRAGON, which cruised from the North Atlantic to the Pacific Ocean via the North Pole in the late summer of 1960. The sampler, devised with the help of Institution scientists, took 12 samples every 24 hours while the submarine cruised under the ice: the first horizontal net collecting in this hard-to-reach area. Although limited in size and not too well preserved, the set of samples is valuable because it extends our understanding of the distribution of various copepods. It has been possible to recognize 18 species, of which six are cosmopolitan and 12 are cold water forms restricted to the northern hemisphere. Of these only one appears endemic to the Arctic.

Indicator species. Other work on the geographical distribution of zooplankton suggests that several species of copepods are useful as indicators of the movement of water. For example, the presence of offshore copepods at various times of the year on the Continental Shelf between Delaware Bay and Block Island Sound confirms earlier drift bottle evidence of an inshore flow of oceanic water in that area. Results of a continuing investigation of zooplankton distribution in Buzzards Bay, Cape Cod Bay and the Cape Cod Canal seem to confirm the idea that temperature and salinity are important limiting factors. Samples of some of these copepods have been subjected to laboratory experiments. It has been found that the grazing and predation are reduced when the organisms are transferred to unfavorable temperature conditions. The structure of the mouth parts is correlated with the usual type of feeding, whether filtering or grasping and chewing.

Zooplankton productivity. Other laboratory studies on the feeding of zooplankton have indicated that they have an unusually high efficiency of growth but a relatively poor efficiency of assimilation. For example, of the food ingested only 13% to 50% was assimilated and became useful for the animal's growth and metabolism. But, of this relatively small fraction, from 63% to 91% was transformed into growth of the organism. The well-fed animals appeared to use a mixture of carbohydrates and fats as their source of energy whereas starved animals burned fat almost entirely. When extended to a great many species with a wide variety of food sources, this type of experiment should aid in interpreting the overall energy cycle in the sea and supplement the information obtained from phytoplankton studies on the role of photosynthesis. Additional work on zooplankton feeding has shown that they are very fussy eaters. When fed mixtures of pure algal cultures most of the species tested preferred the larger species of phytoplankton. Although this would appear to place the populations of large phytoplankton under greater pressure than the small ones, such may not always be the case. For example, it was found that two-day-old larvae of a sedentary worm failed to develop if they were starved and could not develop when offered a moderately large species of phytoplankton as food, even though the same phytoplankton was adequate food for five-day-old larvae. On the other hand, a smaller species of phytoplankton was readily ingested by the two-day-old worm larvae and promoted rapid growth when it was available.

Preliminary experiments with two species of crustaceans, a fish and a mollusk indicate that ribonucleic acid, a necessary precursor to protein synthesis, may be used as an indicator of animal growth and as such has possibilities in estimates of zooplankton productivity.

Phosphorus metabolism of unicellular algae. Two interesting and important results have come from a continuing investigation of the phosphorus metabolism of unicellular algae, based upon the utilization of radioactive phosphorus. Even at very low concentrations of inorganic phosphate in the medium the cell is able to assimilate and incorporate phosphorus into protoplasm faster than it can make new protoplasm. Thus it appears that the rate of assimilation of inorganic phosphorus from the medium is unlikely to limit phytoplankton growth in the oceans although the total quantity of phosphorus in the water may limit the size of the population which can ultimately be developed. Bioassays for the availability of phosphorus in sea water continue to show lower concentrations than are determined by chemical analysis. This may reflect the inability of the organism to use some of the organic compounds that are detected chemically; indeed, continuing tests show that different species of unicellular marine algae differ in their ability to use dissolved organic phosphorus. The ability of these algae to assimilate phosphate from sea water depends upon the amount already present within the cell as well as the supply in the external medium. This result is not unexpected but the relationships are still obscure and studies of the internal physiology of the cell as it relates to phosphorus assimilation are being continued.

Other work has shown that dissolved phosphate in sea water can be concentrated at the surface by rising bubbles of air. As the bubbles break at the surface, absorbed surfactant organic binders of phosphate form monomolecular films which are subsequently compressed by a Langmuir type of circulation. The phosphate has been recovered from the rows of slick and foam where it is significantly more concentrated than between the rows. Thus adsorption to the bubbles driven into sea water by breaking waves may be an important mechanism for concentration and increasing the availability of phosphate and other materials in the ocean.

New photosynthesis technique for sparse phytoplankton population. New techniques for studying the photosynthesis of the marine populations of phytoplankton offer promise in areas where the total size of the population is very small. The population is concentrated many times by filtering on a membrane, then the membrane filter is placed in a special apparatus in which the rate of photosynthesis or respiration can be measured with an oxygen electrode. Since the response of such concentrated populations to changes in nutrient content of the water is very rapid this technique may accelerate studies of these interrelationships, which have been of interest for several years.

Nitrification process. The microorganisms responsible for the nitrification process in the sea, which were first successfully isolated from the open sea about two years ago, are now in continuous culture although they have not been freed of all bacterial contamination. It appears that the organisms may not be bacteria at all. They are unlike any known species of bacteria, including their own terrestrial nitrifying counterparts. They are larger than the nitrifying bacteria and have a complicated life cycle; examination with the electron microscope even casts doubt on any close relationship to bacteria. If further investigations substantiate these findings, this organism will be the first known chemosynthetic organism other than true bacteria, a fact which would help explain the failure of previous efforts to isolate nitrifying bacteria from the sea. New media have been devised in which the culture grows about 60 times as fast as in the medium originally used for its isolation; the importance of this more rapid growth to the physiological and biochemical studies now in progress cannot be overemphasized.

Bactericidal activity of sea water. It has been firmly established that a large organic molecule is responsible for the bactericidal activity of sea water. Now the molecule is being purified and separated by flash evaporation and electrophoresis so that specific studies of its chemical nature are rapidly becoming possible in spite of the relatively low concentrations in sea water. The active compound has turned out to be lethal for all Gram-positive bacteria but inactive against all Gram-negative bacteria that have been tested. For years it has been known that the marine bacteria are almost exclusively Gram-negative; this new discovery may point to the reason why. The active material has been found in all samples of sea water tested although it may be much more concentrated in some samples than in others. The fact that it is an inhibitor of penicillin-resistant staphylococci would be of prime importance in the medical field if adequate methods for its development and concentration could be worked out.

Light in the sea. Studies of light in the sea have followed three major lines: the direct measurement of light, the effects of suspended plant and inorganic material on the amount of light reaching various depths, and the bioluminescence of marine organisms. Light is not only absorbed in the sea by the particulate matter which is present but it is also changed in wavelength depending upon the amount of living phytoplankton in the water above. The shift in wavelength has been shown to be closely related to the amount of chlorophyll and the various carotenoids in the phytoplankton. In the deep sea, luminescent flashes have been recorded at every locality investigated, from near the surface to depths of more than 2,000 fathoms. The intensity of these bioluminescent flashes is about 100 times greater than that needed to attract crustaceans and more than 10 million times greater than the visual threshold for man and many marine animals. Laboratory studies have been made of various marine species, some of which had been maintained in culture and others which were freshly collected at sea. The luminescent glands of several species have been found to fluoresce in ultraviolet light, revealing the distribution and structure of the light organs to a degree of detail not otherwise possible. Histological examination of these glands and other evidence suggest that some marine species have a luminescence mechanism that differs both physiologically and biochemically from the mechanism which is becoming well understood through studies of terrestrial forms.

The deep benthos. Studies of the benthos in the deep sea were inaugurated between Woods Hole and Bermuda and have been very successful. New collecting methods have been developed which retain all the smaller organisms that were previously lost. As a result, much larger bottom populations have been found than on earlier surveys, indicating that the deep sea fauna may be much more significant than had been previously supposed. All of the collections from the great depths contain a large number of species but with no single one numerically dominant.

Borers. The buoy line between Woods Hole and Bermuda has provided an opportunity to learn about the attachment of organisms in deep water away from seasonal factors such as temperature and day-length. For this purpose wooden test panels have been attached to the mooring lines of the buoys at various depths. Several of the panels have shown no evidence of attached organisms or borers despite prolonged immersion, but a heavy infestation of a wood-borer, *Xylophaga,* was found on one panel which had been exposed for six months 10 meters above the bottom in 3000 meters of water. *Xylophaga* is not a common form in inshore waters and, because the specimens in the panel were juveniles, complete identification of the species has not been possible. Further tests are proposed in an effort to find out if such borers are common inhabitants of the deep sea.

Fish behavior and distribution. Students of fish behavior have long debated whether schooling is controlled by the eyes or the lateral line system. That vision plays a role has been established by using contact lenses which produce distortions of the visual field and corresponding distortions of schooling behavior. The same investigation has revealed that most fishes are far-sighted but that reef fishes are relatively near-sighted. A special adaptation has been found which permits flying fish to see equally well in air and water, two media of very different optical qualities.

The known distribution patterns of both tuna and swordfish have been extended during the past year. For the first time, catches south of the Grand Bahama Bank related the annual Cat Cay run of bluefin tuna to concentrations previously discovered in the Windward Passage in late April. An apparently separate group of giant bluefins was found ranging over a large area along the Atlantic side of the Bahamas where they were not known to occur previously. The trans-Atlantic migration of giant bluefin tuna was proved by tagging experiments; two specimens made the migration from Cat Cay to Bergen, Norway, in less than four months. Studies of the juveniles of tuna have been made both by X-ray techniques and by normal dissection methods. A nearly complete collection of juvenile tunas is now available for four species; important errors and omissions in the literature on these have been revealed.

BRAY

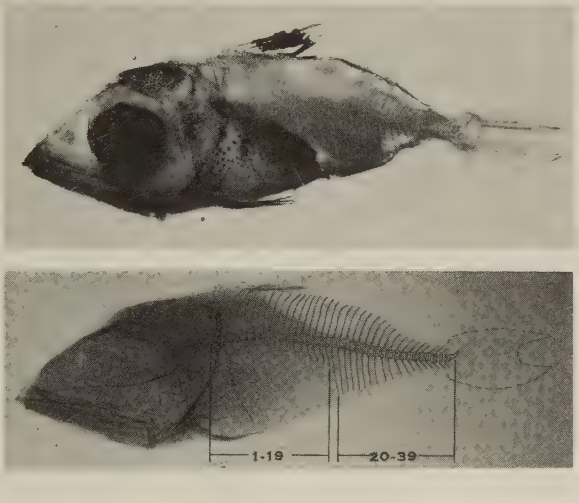

Larva of blackfin tuna 11.5 mm long. Soft X-ray (retouched) shows vertebral characteristics which distinguish species.

Work has been continued on the elasmobranchs, including sharks and skates, and an account is in preparation on the whiting, or silver hake, of the western Atlantic for inclusion in the memoir series, "Fishes of the Western North Atlantic."

Environmental cetology. Work in environmental cetology has been continued both offshore and nearshore, and even on the beach. A valuable opportunity to make observations on a living *Ziphius,* one of the little-known beaked whales, occured in March when a mature male was stranded on a beach in Newport, Rhode Island. Published information on this whale had been based on dead specimens only. Curiously enough, five months later another *Ziphius* was washed ashore dead on the outer beach at Orleans, Massachusetts.

Observations of migrating right whales in Cape Cod waters were made during April and May from the air and from shipboard. Attempts to take underwater motion pictures of the whales were terminated when one of them carried away the camera with a stroke of its tail.

The acoustic program has continued and the sounds of two previously unrecorded species have been added to the library. The known ranges of three species of porpoise have been extended with the aid of improved harpoons.

Instrumentation

Several of the instrumentation techniques which have been under development at the Institution for the past few years were made operational and applied as parts of working measurement systems in 1961.

Anchored buoy stations. The application of new instrumentation took place on the largest scale in the establishment of a line of anchored buoy stations between Woods Hole and Bermuda, as mentioned in last year's report. The buoy line represents an effort to obtain direct measurements of currents more frequently over a longer period and in a more extended area than has previously been possible. There has been a long-standing need for this sort of nearly-continuous sampling throughout an entire ocean basin.

The line, when complete, will consist of 20 moored buoys set at roughly equal intervals along the rhumb line from Gay Head, Martha's Vineyard, to St. George's, Bermuda. The buoys are foam-filled fiberglas doughnuts eight feet in diameter, painted bright orange for visibility. Each is mounted with a ten-foot tripod which houses wind recording instruments as well as a flashing light and a small radio transmitter as aids in locating the buoy. The anchor lines are half-inch polypropylene rope with current meters and other instruments shackled in at 500-meter intervals. In all, there are about 150 instruments, including wind gauges, current meters, tension meters, depth meters and inclinometers. Each one is self-contained, battery-powered and self-recording so that there are no electrical connections outside the instrument cases. The recordings are made in binary code on slowly-moving photographic film; each instrument can record up to 10,000 readings over a period of 100 days or more. At intervals of three to four months the line must be revisited, the records removed and the instruments recharged with fresh film and batteries. After the film is developed, the data are picked off by photoelectric scanning and fed into a computer for processing.

Fifteen buoy stations were set out in May and June. Long term series current measurements were obtained from all the deep water stations except those in the Gulf Stream, which were swept away; a stronger anchoring system is being devised for the Stream stations. The stations on the continental shelf failed in Hurricanes Esther and Frances, which crossed the line at several points, but the deep stations survived with slight damage to the surface floats. Examination of the data had not begun at year's end.

The buoy line is a good example of cross-fertilization among the disciplines at Woods Hole. The line has been used for corrosion studies in deep water and for collection of deep water biological fouling data. Also, the components of the current meter have been used in shipboard lowerings in studies of the Atlantic Equatorial Undercurrent and in conjunction with Project Mohole. Individual stations have been used by the International Ice Patrol and in measurements of fluctuations in the Florida Current; others are to be used in the Labrador Sea in early 1962 along with Swallow floats and classical hydrographic stations. Finally, the current meter is being modified so that its data can be telemetered to ship or shore by means of transponding radio buoys.

The transponding buoys, developed at Woods Hole several years ago, have been available commercially for about two years. A temperature sensor designed to provide a digital transmission from the buoys has been worked out and anchored stations utilizing this combination are in preparation. The same combination is being used with a recording temperature-and-depth package and parachute drogues to measure currents both in the open ocean and on the continental shelf. The transponding buoy has also been adapted to radio acoustic ranging.

Other systems of current measurement are also being applied. One involves a meter of the rotor type in combination with a camera for recording bottom currents; another recording current meter is being adapted for vertical soundings of horizontal velocity.

In situ salinometer. Several years of work on conducting cables and salinity sensors have led to an instrument which can be lowered to provide a continuous record of temperature and salinity versus depth. The salinity determinations of the instrument are less accurate than those obtained from Nansen bottle samples, but it has the important advantage that it picks up the fine structure that is not revealed by the discrete sampling of a bottle cast. The instrument was tested last summer and then was used later in the year to replace Nansen bottles in a study of the fluctuations of the Gulf Stream. Its major difficulty has been a long response time of the cell which compensates for pressure and temperature in the conductivity measurement; this is of little importance in the deep ocean where changes occur slowly, but in a region of sharp temperature gradients such as the Gulf Stream it has resulted in many spurious transient excursions of the salinity trace. The work of reducing the cell's response time is under way.

Gyro-Erected Optical Navigation (GEON). A new system for celestial navigation (whose acronym is GEON, for Gyro-Erected Optical Navigation) has been devised. This is a by-product of steps being taken toward the goals of some day determining the shape of the earth at sea and ultimately to determine the slope of the sea surface as an index of ocean current activity in the water column.

GEON consists of an equatorially mounted astronomical telescope equipped with very precise setting circles, all held in the plane of the local meridian by a Sperry Mark 19 Model 3a meridian gyrocompass. This miniature observatory has been mounted on the boat deck of the CHAIN; the system was tested extensively on both the Romanche Trench and the Mediterranean cruises. GEON proved capable of fixing the ship's position to an accuracy of one nautical mile with a single celestial sight. Moreover, because the meridian gyrocompass serves as a level reference the horizon need not be visible; a fix of position can be obtained by day or night provided the sky is not totally obscured.

In addition, the equatorial mounting of the telescope makes it possible to take photographs of star fields in the night sky with exposures as long as an hour. Stars as faint as the 14th magnitude have been photographed while the ship was underway at 13 knots. With a motion-picture camera mounted on the gyrocompass, time-lapse movies have been made, while underway, of

MERCHANT

VON ARX

GEON aboard CHAIN; 15-minute exposure with ship underway shows meteor crossing star clouds of Sagittarius and Ophiuchus.

the development of trade-wind cumulus clouds and of the optical properties of the atmosphere near the horizon.

Steps are being taken to improve the optical and mechanical parts of the equatorial mounting of the GEON system to reduce their contribution to the navigational errors. The ship's speed and the acceleration circuits and computer elements of the gyrocompass are also being modified in an effort to improve its performance. If these changes are successful enough to permit navigation accurate to one-tenth of a nautical mile — the predicted accuracy of the TRANSIT satellite navigational system — it may be possible to combine GEON and TRANSIT observations to obtain information on the slope of the earth's shape at sea to an accuracy in the order of 1 to 10 seconds of arc. Although this is far short of the accuracy required for the detection of sea slopes accompanying geostrophic motions in the water column, it is a firm step toward that goal in a closely related area. Present knowledge of the figure of the earth is based on astro-geodetic measurements from the land — only one-fourth of the earth's surface.

New gravity meter. Associated with the question of the slope of the sea surface is that of the change of geopotential along these slopes. Since gravity is the gradient of geopotential, it is desirable to be able to measure gravity on hydrographic stations as well as surface slope and the vertical distributions of water density so that geostrophic computations can be made without reference to a "level of no motion" or any equivalent assumption. Such an extension of present techniques would permit detection of geostrophic motions that are independent of the field of density within the sea; barotropic motions of this class may account for a large fraction of the total transport in some areas.

Accordingly, a new form of gravity meter has been developed for use aboard surface ships. It employs a stainless steel non-magnetic sphere falling slowly through a column of highly viscous silicone fluid. With careful control of the temperature of the fluid, the fall rate can be shown to be a linear function of the force of gravity. Each gravity measurement requires about an hour and can be made while the deep hydrographic cast is down to ensure that the ship's motion over the earth is so small that the Eötvös force can be neglected. It is expected that an overall accuracy of one part in a million can be achieved at sea with this instrument. A preliminary version was tested on the CHAIN between the latitudes of 1° South and 42° North; the change of gravity with latitude was observed to satisfy Clairaut's formula to an accuracy of 1 part in 10,000.

Instrumented wave tower. A third instrumented wave tower has been erected in Buzzards Bay on the site of the earlier ones which were swept away by autumn storms. It is considerably more sturdy than its predecessors, having been built on four eight-inch steel pipes driven 35 feet into the bay bottom and anchored with a series of flanges. It survived the worst weather of 1961 but has not yet been tested by a hurricane.

The tower is designed so that there is no cross bracing near the sea surface; except for the legs themselves there is nothing to interfere with the movement of the waves from eight feet below mean low water to 14 feet above it, where the instrument platform is located. A fine stainless steel wire is suspended from the platform into the water, measuring the resistance of the wire gives a continuous record of wave heights passing a point in space. At the same time observations of wind speed and direction are made. Converted to a frequency-modulated signal, the data are transmitted on demand to the laboratory, where they are recorded on multi-channel tape. The records can then be sampled in a variety of ways for analysis by computer.

The purpose of the initial experiments is to observe changes in the wave frequency spectra as wind conditions change. It is planned to add a movable boom with additional sensing wires so that directional components can be measured, as another step toward the ultimate goal of understanding the generation of wind waves. The tower may also serve as a base for observational studies of the surface interactions between the water and the atmosphere. Vertical transports of mass and energy and horizontal shear at near-surface layers will be investigated.

To help handle the massive quantities of data collected from the wave tower and by other continuous sampling techniques, a system for analogue-to-digital conversion has been installed as a direct link between tape-recorded analogue data and the Recomp II digital computer. This equipment has been used in experimental programs in many areas of research, including analyses of water circulation patterns in shoaling and breaking waves, microstructure of temperature measurements obtained by the thermistor chain in the upper layers of ocean water, and measurements of turbulence and heat exchange from sea surface through different levels of the atmosphere.

Computers. Computers are being used more and more in data reduction, but the laborious process of preparing them in a form that can be put into the computer has posed a problem. During the CHAIN cruise to the Mediterranean a first attempt was made to store data from many sources semi-automatically with an IBM system: navigation fixes, surface and subsurface temperatures, weather observations, water depths and attenuation settings from various instruments. The IBM equipment put data on cards and paper tape and then typed them out on typewriters in two of the ship's laboratories. The success of this experiment indicates a growing use of such methods.

Other techniques. Two other techniques tried during the same cruise were closed-circuit television and two modified versions of the airplane wing that had been tested on the CRAWFORD in 1960. The television cameras were designed for either air or water and, although most of the use was between locations on the ship, some examination was made of the screws and bottom of the ship and various pieces of submerged gear. As a visual link between the bridge and the activities on the fantail the TV greatly reduced the confusions of voice communications. One of the new extendable platforms was a styrofoam-filled aluminum catwalk supported on the outboard end by a streamlined float; the other was an inflatable rubber boom that skimmed along the surface. Used in dredging operations the booms extended the base line of the ship to provide a better means for determining acoustically the position of the dredge on the bottom.

Fleet Operations

Two changes in the research fleet marked the beginning of 1961. The ketch ARIES, which had been used primarily in deep water current measurements in the Bermuda area, was disposed of by sale to Mr. George Theodorocopoulos of New York. At about the same time, through the generosity of Mr. Louis E. Marron, the Institution took title to the 59-foot sportfisherman, the EUGENIE VIII. She was used throughout the year in migratory game fish studies and other biological work. The Japanese long-line technique which had been used on the CRAWFORD was adapted to the EUGENIE VIII with considerable success before she cruised south to work in Florida waters during the winter.

The major cruises of the year were made by the ATLANTIS and the CHAIN. The ATLANTIS spent three months on a winter trip to the Mediterranean. The CHAIN was away three and a half months in the spring in the Eastern Equatorial Atlantic, then spent four months on a trip into the eastern Mediterranean going as far as Istanbul, making scientific investigations on both ocean crossings and returning to Woods Hole the week before Christmas. In the Mediterranean cruises both ships worked extensively with foreign research vessels, including the ARAGONESE of La Spezia, Italy, and the fleet of the Oceanographic Museum in Monaco. Several foreign scientists spent time at sea on our vessels as observers or to carry out investigations and, in Monaco, Prince Rainier and Princess Grace honored the CHAIN by having Thanksgiving dinner aboard.

The longest CRAWFORD cruises were for a study of the salinity-maximum west of the Cape Verde Islands in the spring and, in the fall, a survey of Gulf Stream meanders which required 70 crossings of the Florida Current along the same 30-mile track off Jacksonville, Fla. The BEAR returned from the Bahamas early in the year and spent the winter in the Gulf of Maine on charter to a commercial firm calibrating a new Navy communications facility. During the rest of the year she was used primarily on short cruises in local waters.

The Institution fleet spent a total of 921 days at sea during the year and logged a total of 116,646 miles — a slight decrease from the record figure in 1960. It is interesting to note that in her 30th full year of service the ATLANTIS sailed 26,462 miles, which is more than once around the globe at the Equator and considerably more than the 14,100 miles she sailed in her first year and a half.

Other ships used in Institution work were the fishing vessel CAP'N BILL III, which was chartered frequently for a study of non-tidal drift on the continental shelf, and Mr. J. Seward Johnson's ketch the OCEAN PEARL which was made available in February for current measurements off the Atlantic side of Eleuthera Island in the Bahamas.

There was only one occasion on which hurricane evasion was necessary. In anticipation of Hurricane Donna in September, the ATLANTIS, the CRAWFORD and the BEAR sought shelter in Boston Harbor and the small craft were moved into the Eel Pond. The storm did no damage to the fleet, the docks or other Institution property.

There were no major foreign flights by the R4D aircraft in 1961. Most of the year's activities consisted of local trips except for some airborne coastal photography, including a flight along the Gulf Coast after the devastating Hurricane Carla. The Helio-Courier made one flight to Nova Scotia for whale spotting; otherwise it was used primarily in local work. On a number of occasions the plane worked in conjunction with the small research vessel ASTERIAS in whale observations in Cape Cod Bay.

A $3,876,000 contract for the construction of a research vessel was awarded in September to the Maryland Shipbuilding and Drydock Co. of Baltimore, Mr. Delivery is scheduled for December, 1962, and it is expected that the new ship's first major cruise will be to the Indian Ocean in early 1963. The new ship was named ATLANTIS II by popular acclaim and she is considered to be a replacement for the original ATLANTIS.

The ATLANTIS II will be built of steel and will have twin propellors powered by a uniflow reciprocating steam engine. Her principal specifications are: overall length, 210 feet; waterline length, 195 feet; beam, 44 feet; draft, 16 feet; displacement, 2,100 tons; cruising speed, 12 knots; range, 8,000 miles. She will have accommodations for a crew of 28 and a scientific party of 25. Among her special features will be anti-roll tanks and bilge keels for increased stability, a bow propulsion unit for maneuverability and an underwater observation chamber in the bow. There will be four fixed laboratories and deck space for portable laboratory units which can be used interchangeably. The ATLANTIS II was designed by the Bethlehem Steel Company's Shipbuilding Division in Quincy, Mass., with M. Rosenblatt & Son of New York as design associates. Hull models were tested in the towing tanks at Stevens Institute in Hoboken, N. J. Design and construction are being financed by The National Science Foundation.

The need for a ship to function as a replacement for the BEAR and the ASTERIAS has become apparent. Preliminary designs have been prepared and conversion possibilities are being considered with the goal of acquiring a multipurpose craft approximately 100 feet long.

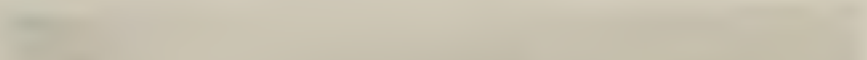

ATLANTIS II

PAINTING BY MINOT

ATLANTIS Days at Sea — 214 Total Miles Sailed — 26,462

CRUISE	DATES	AREA OF OPERATION	DAYS	CHIEF SCIENTIST
263	12 Jan.–16 April	Western Mediterranean	82	Miller
264	20 May–25 May	Woods Hole–Bermuda	7	H. L. Sanders
265	31 May–8 June	Woods Hole–Bermuda	9	Corwin
266	20 June–26 July	Blake Plateau	37	Stetson
267	4 Aug.	Local	7	Associates' Cruise
268	8 Aug.–12 Aug.	Woods Hole–Bermuda	5	Scheltema
269	15 Aug.–19 Aug.	Local	5	Mangelsdorf
270	22 Aug.	Local	1	Conover
271	5 Sept.–15 Sept.	Woods Hole–Bermuda	11	Stimson
272	19 Sept.–22 Sept.	Chelsea, Mass.	4	Hurricane Warning
273	26 Sept.–4 Oct.	Woods Hole–Bermuda	9	H. L. Sanders
274	17 Oct.–3 Dec.	Puerto Rico	47	Bruce

BEAR Days at Sea — 130 Total Miles Sailed — 10,000

CRUISE	DATES	AREA OF OPERATION	DAYS	CHIEF SCIENTIST
258	1 Jan.–6 Jan.	Bahamas	6	Athearn
259	7 Feb.–30 Mar.	Gulf of Maine	51	On Charter
260	10 May	Local	1	Compass Adjustment
261	22 May–26 May	Rhode Island Sound	5	Nalwalk
262	6 June–9 June	Cape Cod Bay	4	Hoskins
263	16 June	Local	1	Engine Adjustment
264	26 June–22 July	Gulf of Maine	27	Fahlquist
265	1 Aug.–11 Aug.	Continental Shelf	11	Backus
	14 Aug.	Local	1	Fejer
266	17 Aug.–28 Aug.	Shelf off Virginia	12	J. E. Sanders, Owen
267	30 Aug.	Local	1	Fejer
268	11 Sept.–15 Sept.	Cape Cod Bay	5	Watkins
	22 Sept.	Cape Cod Bay	1	
	28 Sept.–1 Oct.	Gulf of Maine	4	

CHAIN Days at Sea — 286 Total Miles Sailed — 42,984

CRUISE	DATES	AREA OF OPERATION	DAYS	CHIEF SCIENTIST
14	3 Jan.	Shipyard – Woods Hole	1	
15	9 Jan.–14 Jan.	Woods Hole – Bermuda	6	B. H. Ketchum
16	16 Jan.–21 Jan.	Bermuda – Woods Hole	6	Richardson
17	1 Feb.–17 May	Romanche Trench	104	Hays, Voorhis, Metcalf
18	29 May–4 June	Woods Hole – Bermuda	7	Richardson
19	13 June–7 July	Puerto Rico Trench	25	Hersey
20	20 July–2 Aug.	Woods Hole – Bermuda	13	Richardson
21	16 Aug.–18 Dec.	Mediterranean	124	Hersey, Hays

CRAWFORD Days at Sea — 191 Total Miles Sailed — 25,200

CRUISE	DATES	AREA OF OPERATION	DAYS	CHIEF SCIENTIST
57	3 Jan.	Shipyard – Woods Hole	1	
58	7 Jan.–10 Jan.	Gulf of Maine	4	Curl
59	17 Jan.–22 Jan.	Woods Hole – Bermuda	6	Yentsch
60	24 Jan.–3 Feb.	Chelsea, Mass.		At Shipyard
61	9 Feb.–4 April	Mid-Atlantic Northeast Trades	48	Worthington
62	19 Apr.–8 June	Gulf Stream, Bahamas	45	Mather, Bartlett
63	23 Jun.–4 July	Shelf – Gulf Stream	12	Kuenzler
64	24 July–30 July	Gulf of Maine	7	Clarke
65	4 Aug.	Local	1	Associates' Cruise
66	6 Aug.–9 Aug.	Woods Hole – Bermuda	4	Yentsch
67	13 Aug.–20 Aug.	Continental Shelf	7	B. H. Ketchum
68	28 Aug.–8 Sept.	East of Cape Hatteras	11	Parker
69	19 Sept.–22 Sept.	Chelsea, Mass.		Hurricane Warning
70	2 Oct.–18 Nov.	Florida Current	46	Webster
71	21 Nov.–9 Dec.	Chelsea, Mass.		At Shipyard

PERSONNEL

Honoraria

The following persons were awarded grants, honoraria or fellowships during 1961:

Roger W. Bachman	University of Michigan
Mario R. Capecchi	Antioch College
Frank Carey	Duke University
Robert J. Collier	Harvard University
Hugh Dingle	University of Michigan
Ivar Dugstad	University of Oslo
Walter Eckhart	Pembroke College, University of Cambridge
John Edinger	The Johns Hopkins University
George Field	Princeton University
Nicholas P. Fofonoff	Pacific Oceanographic Group, Nanaimo, British Columbia
Santanu K. Ghose	Florida State University
Philip Gossett	Amherst College
James R. Greaves	University of Minnesota
Kurt Hecht	Brown University
Bertil Hille	Yale University
Louis N. Howard	Massachusetts Institute of Technology
Robert H. Kraichnan	New York University
Frank Lipps	The Johns Hopkins University
Lionel W. MacMillan	University of British Columbia
Eric L. Mills	Yale University
Derek W. Moore	University of Bristol
Martin T. Mork	University of Oslo
S. Nagarajan	New York University
Norman S. Neidell	Imperial College, London, England
J. A. Colin Nicol	The Laboratory, Plymouth, England
Pearn P. Niiler	University of Cambridge
Dennis H. Peregrine	Churchill College, University of Cambridge

Honoraria

Donald C. Rhoads	University of Iowa
Robert S. Rhodes	Stanford University
Steven I. Rosencrans	Massachusetts Institute of Technology
Ira Rubinoff	Harvard University
Peter M. Saunders	Imperial College, London, England
Robert K. Sexton	Brooklyn College
Fred C. Shure	University of Michigan
Edward A. Spiegel	New York University
Bruce A. Warren	Massachusetts Institute of Technology
Charles G. Wing	Bowdoin College

Visitors

Scientists from this and many other countries honored the Institution with visits during 1961. Among these were:

Tokiharu Abe	Tokaiku Suisan Kenkyujo, Tokyo
Masateru Anraku	University of Hokkaido
Karl Banse	University of Washington
N. F. Barber	Dominion Physical Laboratory, D.S.I.R New Zealand
Willard Bascom	National Academy of Sciences
Neil L. Brown	Division of Fisheries and Oceanography, CSIRO, Cronulla
R. W. Burling	New Zealand Oceanographic Institute, D.S.I.R.
R. Morrison Cassie	New Zealand Oceanographic Institute, D.S.I.R.
Vivienne Cassie	New Zealand Oceanographic Institute, D.S.I.R.
Roland A. Cox	National Institute of Oceanography, Great Britain
Ronald I. Currie	National Institute of Oceanography, Great Britain
L. R. Day	Fisheries Research Board of Canada
Günter Dietrich	Institut für Meereskunde, Kiel, W. Germany
L. A. Earlston Doe	Bedford Oceanographic Institute, Canada
R. Dorrestein	K. Nederlands Meteorologisch Instituut, De Bilt

Visitors

T. ENGELSEN	N.D.R.E., Bergen, Norway
M. P. FOACHE	French Navy
G. E. FOGG	Westfield College, University of London
WILLIAM L. FORD	Defence Research Board, Canada
Y. FUJII	Transportation Research Institute, Japan
DAVID GARNER	New Zealand Oceanographic Institute, D.S.I.R.
T. F. W. HARRIS	C.S.I.R., South Africa
E. M. HASSAN	New York University
M. R. HOWE	Liverpool University
M. INOUE	Tokai University, Japan
HIDEO KAWAI	Tohoku Regional Fisheries Research Laboratory
FRITZ KOCZY	University of Miami, Coral Gables, Florida
WOLFGANG KRAUSS	Institut für Meereskunde, Kiel, W. Germany
G. LAMBERT	French Atomic Energy Commission
L. M. LAUZIER	Fisheries Research Board of Canada
ARTHUR J. LEE	Fisheries Laboratory, Lowestoft
JOHN R. LONGARD	Canadian Joint Staff, Washington
HUGH MCLELLAN	Agriculture and Mechanical College of Texas
YASUO MIYAKE	Meteorological Research Institute, Tokyo
HÅKON MOSBY	Universitet i Bergen
W. D. NESTEROFF	Sorbonne, University of Paris
J. A. C. NICOL	The Laboratory, Plymouth, England
G. D. NICHOLLS	Manchester University, Great Britain
MAKOTO OMORI	Hokkaido University
GOTE ÖSTLUND	Swedish Geological Survey
E. PASTEL	Office de la Recherche Scientifique et Technique Outre Mer
CHARLES E. RENN	Johns Hopkins University
V. ROMANOVSKY	Centre de Recherches et d'Etudes Océanographiques, Paris, France
P. SLIZEWICZ	French Atomic Energy Commission
M. J. TUCKER	National Institute of Oceanography, Great Britain
K. UMSHOHARA	Research Institute of Japan, Defense Agency
GEORG WÜST	Universität Kiel, W. Germany

Employees and Staff

The following were in the employ of the Institution for the twelve-month period ending December 31, 1961.

Allen, Ethel B.
Allen, Norman T.
Anders, Wilbur J.
Andersen, Neil R.
Andersen, Nellie T.
Anraku, Masateru
Athearn, William D.
Backus, Cyril
Backus, Harold
Backus, Jeanne
Backus, Richard H.
Barbour, Rose L.
Barrett, Joseph R., Jr.
Barstow, Elmer M.
Bartlett, Martin R.
Baxter, Lincoln II
Baylor, Edward R.
Bazner, Kenneth E.
Behrens, Henry G.
Bergstrom, Stanley W.
Betterly, Robert
Birch, Francis J.
Blanchard, Daniel J.
Blanchard, Duncan C.
Blumer, Max
Bodman, Ralph H.
Bowen, Vaughan T.
Bowman, Warren O.
Bradley, Mabel D.
Bradshaw, Alvin L.
Bray, W. Scott
Broadbent, Alice G.
Brockhurst, Robert R.
Broughton, Jane F.
Brown, Joseph C.
Bruce, John C. Jr.
Bryant, Edwin T.
Bumer, John Q.
Bumpus, Dean F.
Bunce, Elizabeth T.
Bunker, Andrew F.
Burnham, Charles A.
Byron, Paul C.
Cabral, John P.
Cabral, John V.
Cain, Henry A.
Cangiamila, Angelo
Carlson, Alfred G.
Carlson, Eric B.
Carlson, Ruth H. E.
Caron, Henri L.
Carritt, Dayton E.
Carter, Alwyn L.
Carter, Richard J.
Casiles, David F.
Caulfield, David D.
Cavanaugh, James J.
Chadwick, Constance W.
Chaffee, Margaret A.
Chalmers, Agnes C.
Chase, Joseph
Christian, John A.
Chute, Edward H.
Clarke, David B.
Clarke, George L.
Clarkin, William H.
Clarner, John P.
Colburn, Arthur D., Jr.
Condon, John W.
Conover, Robert J.
Cook, Alden H.
Cook, Hans
Copestick, Louis B.
Corwin, Nathaniel
Cory, Norman
Cotter, Jerome M.
Coughlin, Brooks W.
Crocker, Marion W.
Crouse, Porter A.
Davis, Charles A.
Day, C. Godfrey
Day, Joseph V.
Densmore, C. Dana
Devitt, Howard B.
Dimmock, Richard H.
Dimock, Alan D.
Dow, Willard
Dunkle, William M., Jr.
Edwards, Richard S.
Eldridge, Stanley N.
Erlanger, George L.
Ewing, William R., Jr.
Fahlquist, Davis A.
Faller, Alan J.
Farnum, Gregory N.
Ferguson, Sandra K.
Ferris, George A.
Fielden, Frederick E.
Fisher, Stanley O.
Flaherty, John J., Jr.
Foster, Donald B.
Frank, Winifred H.
Fraser, John G.
Fuglister, Cecelia B.
Fuglister, Frederick C.
Fye, Paul M.
Gallagher, Gloria S.
Gallagher, William F.
Gaskell, Fred
Giese, Graham S.
Gifford, James E.
Gill, Barbara L.
Gingrass, Norman
Graham, John W.

Employees and Staff

Graham, Russell G.
Grant, Carlton W., Sr.
Grant, Carlton W., Jr.
Grice, George D., Jr.
Guillard, Robert R. L.
Hahn, Jan
Halpin, William T.
Hannah, Mary Ann
Hatzikon, Kaleroy L.
Hayes, Carlyle R.
Hays, Earl E.
Hays, Helen C.
Hellwig, Jessica D.
Henderson, Arthur T.
Hersey, John B.
Hess, Frederick R.
Hessler, Robert R.
Hiller, Emerson H.
Hoadley, Lloyd D.
Hodgkins, Harry L.
Hodgson, Sloat F.
Houston, Leo C.
Howe, Malcolm R.
Howe, Paul M.
Howland, Myron P., Jr.
Howland, Paul C.
Hulburt, Edward M.
Hunt, Otis E.
Innis, Charles S., Jr.
Iselin, Columbus O'D
Jenkins, Delmar R.
John, Alfred C.
Johnston, Alexander T.
Kahler, Yolande A.
Kanwisher, John W.
Karram, Calvin D.
Ketchum, Bostwick H.
Ketchum, David D.
Knott, Sydney T., Jr.
Kostrzewa, John A.
Kraus, Eric B.
Kuenzler, Edward J.
Lambert, Joseph L.
Leiby, Jonathan
Levine, Joseph
Lyon, Thomas P.
Mackey, Malcolm R.
MacKillop, Harvey
Mather, Frank J., III
Matousek, William J.
Matthews, Francis S.
Mavor, James W., Jr.
McCormack, Eileen M.
McGill, David A.
McHardie, James
Mellor, Florence K.
Merchant, Floyd L.
Merrill, Emily B.
Metcalf, William G.
Miller, Arthur R.
Minot, Mary K.
Mitchell, James R.
Mizula, Joseph W.
Mogardo, Juanita A.
Moller, Donald A.
Morehouse, Clayton B.
Morrison, Kenneth
Motta, Joseph C.
Munns, Robert B.
Mysona, Eugene J.
Nalwalk, Andrew J.
Oliver, Isabel
Ortolani, Mary
Ostiguy, Betty P.
Owen, David M.
Palmieri, Michael, Jr.
Parker, Charles E.
Pasley, Gale G., Jr.
Patterson, John E.
Pennypacker, Thomas R.
Phillips, Helen F.
Pierce, George E.
Pierce, Samuel F.
Pike, John F.
Pimental, John M.
Poole, Stanley E.
Pratt, Richard M.
Price, Don L.
Prostredny, Evelyn
Randall, Vivian H.
Reitzel, John S.
Ribeiro, Joseph
Richardson, William S.
Riegel, Richard E., Jr.
Rogers, Henry A., Jr.
Rogers, M. Dorothy
Ronne, F. Claude
Rooth, Claës G. H.
Rose, Lawrence
Rossby, Harriet A.
Roy, Alfred J.
Ryther, John H.
Sachs, Peter L.
Salthouse, James E.
Sanders, Howard L.
Sawyer, Harold E.
Scheltema, Rudolf S.
Schevill, William E.
Schleicher, Karl E.
Schroeder, Elizabeth H.
Schroeder, William C.
Sears, Mary
Seibert, Harry
Shaleski, Eleanor M.
Sharp, Arnold G.
Shields, William J.
Shodin, Leonard F.
Shultz, William S.
Silverman, Maxwell
Slabaugh, Luther V.
Snyder, Robert M.
Soderland, Eloise M.
Solberg, Otto

Employees and Staff

Souza, Thomas A.
Spencer, Allard T.
Spooner, Charles E.
Stalcup, Marvel C.
Stanbrough, Jess H., Jr.
Stansfield, Richard
Stern, Melvin E.
Stetson, Thomas R.
Stevens, Raymond G.
Stillman, Stephen L.
Stimpson, John W.
Stimson, Paul B.
Stone, Richard A.
Sutcliffe, Thomas O.L.
Swinhart, Orrin L.
Tasha, Herman J.
Thurston, Theodore G.
Tometich, Louis J.
Turner, Harry J.
Turner, Mary A.
Vaccaro, Ralph F.
Veeder, Ronald A.
Veronis, George
Vine, Allyn C.
Volkmann, Gordon H.
von Arx, William S.
von Dannenberg, Carl R.
Voorhis, Arthur D.
Walden, Robert G.
Walker, Jean D.
Watkins, William A.
Watson, Margaret E.
Watson, Stanley W.
Webster, Jacqueline H.
Webster, T. Ferris
Weeks, Robert G.
Welch, Linda E.
Whitney, Geoffrey G., Jr.
Wilde, Phillips B.
Wilharm, Larry
Wilkins, Charles H.
Williams, George A.
Wilson, Esther N.
Wing, Asa S.
Wing, Carleton R.
Winslow, Elisha F.
Witzell, Warren E.
Woodcock, Alfred H.
Woodward, Fred C., Jr.
Woodward, Ruth F.
Worthington, L. Valentine
Wright, W. Redwood
Yentsch, Anne L.
Yentsch, Charles S.
Zeigler, John M.

Monaco, February 1961

MUNNS

Publications

During 1961, sixty-two papers bearing contribution numbers were published. See *Author, Subject-Locality, Taxonomic Index* published in 1957 for a complete list through 1956 and subsequent annual reports for the publications appearing since 1956. These are also listed in the back of the annual volume of *Collected Reprints.*

No. 1045. Alfred C. Redfield. The Tidal System of Lake Maracaibo, Venezuela. *Limnol. and Oceanogr.*, Vol. 6, No. 1, pp. 1-12. 1961.

No. 1050. S. M. Marshall and A. P. Orr. On the Biology of *Calanus finmarchicus.* XII. The Phosphorus Cycle: Excretion, Egg Production, Autolysis. *Jour. Mar, Biol. Assoc., U. K.*, Vol. 41, pp. 463-483. 1961.
R. J. Conover. Addendum. The Turnover of Phosphorus by *Calanus finmarchicus. Jour. Mar. Biol. Assoc., U. K.,* Vol. 41, pp. 484-488. 1961.

No. 1057. Francis A. Richards and Bruce B. Benson. Nitrogen/Argon and Nitrogen Isotope Ratios in Two Anaerobic Environments, the Cariaco Trench in the Caribbean Sea and Dramsfjord, Norway. *Deep-Sea Res.,* Vol. 7, No. 4, pp. 254-264. 1961.

No. 1063. Max Blumer and Gilbert Omenn. Fossil Chlorins in a Triassic Sediment. *Nature,* Vol. 191, No. 4784, pp. 161-162. 1961.

No. 1066. Earl E. Hays. Comparison of Directly Measured Sound Velocities with Values Calculated from Hydrographic Data. *Jour. Acoust. Soc., Amer.,* Vol. 33, No. 1, pp. 85-88. 1961.

No. 1072. George D. Grice. Calanoid Copepods from Equatorial Waters of the Pacific Ocean. *Fish. Bull., U. S. Fish and Wildlife Service (Fish. Bull.* No. 186) Vol. 61, pp. 171-246. 1961.

No. 1085. Richard H. Backus. Stranded Killer Whale in the Bahamas. *Jour. Mammal.,* Vol. 42, No. 3, pp. 418-419. 1961.

No. 1109. Robert L. Edwards. The Fishes of Richmond Gulf, Ungava, Canada. *Proc. Amer. Philosoph. Soc.,* Vol. 105, No. 2, pp. 196-205. 1961.

No. 1110. Joyce C. Lewin. The Dissolution of Silica from Diatom Walls. *Geochimica et Cosmochimica Acta,* Vol. 21, pp. 182-198. 1961.

No. 1114. J. E. G. Raymont and Robert J. Conover. Further Investigations on Carbohydrate Content of Marine Zooplankton. *Limnol. and Oceanogr.,* Vol. 6, No. 2, pp. 154-164. 1961.

No. 1118. J. H. Ryther, D. W. Menzel and R. F. Vaccaro. Diurnal Variations in Some Chemical and Biological Properties of the Sargasso Sea. *Limnol. and Oceanogr.,* Vol. 6, No. 2, pp. 149-153. 1961.

No. 1119. D. W. Menzel and J. H. Ryther. Annual Variations in Primary Production of the Sargasso Sea off Bermuda. *Deep-Sea Res.,* Vol. 7, No. 4, pp. 282-288. 1961.

No. 1120. John H. Ryther and David W. Menzel. Primary Production in the Southwest Sargassa Sea, January–February, 1960. *Bull. Mar. Sci., Gulf and Caribbean,* Vol. 11, No. 3, pp. 381-388. 1961.

No. 1121. David W. Menzel and John H. Ryther. Zooplankton in the Sargasso Sea off Bermuda and its Relation to Organic Production. *Jour. du Conseil,* Vol. 26, No. 3, pp. 250-258. 1961.

Publications

No. 1122. R. M. Pratt. Erratic Boulders from Great Meteor Seamount. *Deep-Sea Res.*, Vol. 8, No. 2, pp. 152-153. 1961.

No. 1123. D. W. Menzel and J. H. Ryther. Nutrients Limiting the Production of Phytoplankton in the Sargasso Sea, with Special Reference to Iron. *Deep-Sea Res.*, Vol. 7, No. 4, pp. 276-281. 1961.

No. 1127. George D. Grice. *Candacia ketchumi,* a New Calanoid Copepod from the North-Western Part of the Sargasso Sea. *Crustaceana,* Vol. 2, No. 2, pp. 126-131. 1961.

No. 1129. J. C. Swallow and L. V. Worthington. An Observation of a Deep Countercurrent in the Western North Atlantic. *Deep-Sea Res.*, Vol. 8, No. 1, pp. 1-19. 1961.

No. 1131. H. G. Farmer and D. D. Ketchum. Chap. 5. An Instrumentation System for Wave Measurements, Recording and Analysis. *Proc. Seventh Cong. Coastal Eng., The Hague, Netherlands, Aug. 1960, (Publ. Counc. Wave Res., Eng.)* Vol. 1, Ch. 5, pp. 77-99. 1961.

No. 1132. Rudolf S. Scheltema. Metamorphosis of the Veliger Larvae of *Nassarius obsoletus* (Gastropoda) in Response to Bottom Sediment. *Biol. Bull.,* Vol. 120, No. 1, pp. 92-109. 1961.

No. 1135. A. B. Arons, A. P. Ingersoll, and T. Green III. Experimentally Observed Instability of a Laminar Ekman Flow in a Rotating Basin. *Tellus,* Vol. 13, No. 1, pp. 31-39. 1961.

No. 1136. T. T. Sugihara and Vaughan T. Bowen. Radioactive Rare Earths from Fallout for a Study of Particle Movement in the Sea. In: Radioisotopes in the Physical Sciences and Industry, pp. 57-65. 1961.

No. 1137. Hartley Hoskins and S. T. Knott. Geophysical Investigation of Cape Cod Bay, Massachusetts, Using the Continuous Seismic Profiler. *Jour. Geol.,* Vol. 69, No. 3, pp. 330-340. 1961.

No. 1138. W. V. R. Malkus and G. Veronis. Surface Electroconvection. *The Physics of Fluids,* Vol. 4, No. 1, pp. 13-23. 1961.

No. 1139. Joseph Levine. A Spherical Vortex Model of the Buoyant Thermal in Cumulus and Dry Convection. *Schweizer Aero-Revue,* Zurich, Vol. 36, No. 2, pp. 100-101. 1961.

No. 1144. Parker D. Trask. Sedimentation in a Modern Geosyncline off the Arid Coast of Peru and Northern Chile. *Internat. Geol. Congr., XXI Session, Norden, 1960, Internat. Assoc. of Sedimentology,* Pt. 23, pp. 103-118. 1961.

No. 1145. Joanne S. Malkus, Claude Ronne and Margaret Chaffee. Cloud Patterns in Hurricane Daisy, 1958. *Tellus,* Vol. 13, No. 1, pp. 8-30. 1961.

No. 1146. Dean F. Bumpus. Drift bottle records for the Gulf of Maine, Georges Bank, and the Bay of Fundy, 1956-58. *U. S. Fish and Wildlife Service, Spec. Sci. Rept., Fish.,* No. 378, pp. 1-127. 1961.

No. 1147. R. R. Brockhurst, J. G. Bruce, Jr. and A. B. Arons. Refraction of Underwater Shock Waves by a Strong Velocity Gradient. *Jour. Acoust. Soc., Amer.,* Vol. 33, No. 4, pp. 452-456. 1961.

No. 1148. W. V. R. Malkus. Similarity arguments for fully developed turbulence, *Nuovo Cimento* Ser. 10, Vol. 22 (Suppl. 1): 376-384. 1961.

Publications

No. 1150. Jack McLachlan. The Effect of Salinity on Growth and Chlorophyll Content in Representative Classes of Unicellular Marine Algae. *Canadian Jour. Microbiol.*, Vol. 7, pp. 399-406. 1961.

No. 1152. Peter M. Saunders. An Observational Study of Cumulus. *Jour. Meteorol.*, Vol. 18, No. 4, pp. 451-467. 1961.

No. 1153. Bruce B. Benson and Peter D. M. Parker. Nitrogen/Argon and Nitrogen Isotope Ratios in Aerobic Sea Water. *Deep-Sea Res.*, Vol. 7, No. 4, pp. 237-253. 1961.

No. 1154. Bruce B. Benson and Peter D. M. Parker. Relations among the Solubilities of Nitrogen, Argon and Oxygen in Distilled Water and Sea Water. *Jour. Phys. Chem.*, Vol. 65, pp. 1489-1496. 1961.

No. 1155. M. Blumer and G. S. Omenn. Fossil Porphyrins: Uncomplexed Chlorins in a Triassic Sediment. *Geochimica et Cosmochimica Acta,* Vol. 25, pp. 81-90. 1961.

No. 1156. Herbert Riehl and Joanne Malkus. Some Aspects of Hurricane Daisy, 1958. *Tellus,* Vol. 13, No. 2, pp. 181-213. 1961. (Also, published as *National Hurricane Research Project, Rept.* No. 46 [multilithed]).

No. 1157. Pierre Welander. Theory of Very Long Waves in a Zonal Atmospheric Flow. *Tellus,* Vol. 13, No. 2, pp. 140-155. 1961.

No. 1158. John M. Zeigler and Sherwood D. Tuttle. Beach Changes Based on Daily Measurements of Four Cape Cod Beaches. *Jour. Geol.,* Vol. 69, No. 5, pp. 583-599. 1961.

No. 1159. R. C. Dugdale, David W. Menzel and John H. Ryther. Nitrogen Fixation in the Sargasso Sea. *Deep-Sea Res.* Vol. 7, No. 4, pp. 298-300. 1961.

No. 1160. Floyd M. Soule, Peter A. Morrill and Alfred P. Franceschetti. Physical Oceanography of the Grand Banks Region and the Labrador Sea in 1960. *U. S. Coast Guard Bull.,* No. 46, pp. 31-114. 1961.

No. 1165. Richard Cifelli. 227. *Globigerina incompta,* a New Species of Pelagic Foraminifera from the North Atlantic. *Contrib. Cushman Found. Foram. Res.,* Vol. 12, Pt. 3, pp. 83-86, Pl. 4. 1961.

No. 1166. Melvin E. Stern. The Stability of Thermoclinic Jets. *Tellus,* Vol. 13, No. 4, pp. 503-508. 1961.

No. 1167. Wolfgang Wieser and John Kanwisher. Ecological and Physiological Studies on Marine Nematodes from a Small Salt Marsh near Woods Hole, Massachusetts. *Limnol. and Oceanogr.,* Vol. 6, No. 3, pp. 262-270. 1961.

No. 1168. Raymond Siever, Robert M. Garrels, John Kanwisher and Robert A. Berner. Interstitial Waters of Recent Marine Muds off Cape Cod. *Science,* Vol. 134, No. 3485, pp. 1071-1072. 1961.

No. 1170. Bert Bolin and Henry Stommel. On the Abyssal Circulation of the World Ocean. IV. Origin and Rate of Circulation of Deep Ocean Water as Determined with the Aid of Tracers. *Deep-Sea Res.,* Vol. 8, No. 2, pp. 95-110. 1961.

No. 1171. A. H. Woodcock and A. T. Spencer. Lava-Sea-Air Contact Areas as Sources of Sea-Salt Particles in the Atmosphere. *Jour. Geophys. Res.,* Vol. 66, No. 9, pp. 2873-2887. 1961.

Publications

No. 1173. **Ferris Webster.** A Description of Gulf Stream Meanders off Onslow Bay. *Deep-Sea Res.*, Vol. 8, No. 2, pp. 130-143. 1961.

No. 1174. **Ferris Webster.** The Effect of Meanders on the Kinetic Energy Balance of the Gulf Stream. *Tellus,* Vol. 13, No. 3, pp. 392-401. 1961.

No. 1176. **Evelyn Shaw.** The Development of Schooling in Fishes. II. Physiol. Zoöl., Vol. 34, No. 4, pp. 263-272. 1961.

No. 1177. **John H. Ryther** and **Dana D. Kramer.** Relative Iron Requirement of Some Coastal and Offshore Plankton Algae. *Ecology,* Vol. 42, No. 2, pp. 444-446. 1961.

No. 1183. **Charles N. David** and **Robert J. Conover.** Preliminary Investigation on the Physiology and Ecology of Luminescence in the Copepod, *Metridia lucens. Biol. Bull.,* Vol. 121, No. 1, pp. 92-107. 1961.

No. 1186. **E. B. Kraus.** Physical Aspects of Deduced and Actual Climatic Change In: Solar Variations, Climatic Change, and Related Geophysical Problems. *Ann. N. Y. Acad. Sci.,* Vol. 95, Art. 1, pp. 225-234. 1961.

No. 1189. **Arthur D. Voorhis.** Evidence of an Eastward Equatorial Undercurrent in the Atlantic from Measurements of Current Shear. *Nature,* Vol. 191, No. 4784, pp. 157-158. 1961.

No. 1191. **Richard H. Backus, Charles S. Yentsch,** and **Asa Wing.** Bioluminescence in the Surface Waters of the Sea. *Nature,* Vol. 192, No. 4802, pp. 518-521. 1961.

No. 1193. **Max Blumer.** Benzpyrenes in Soil. *Science,* Vol. 134, No. 3477, pp. 474-475. 1961.

No. 1194. **John Reitzel.** Some Heat-Flow Measurements in the North Atlantic. *Jour. Geophys. Res.,* Vol. 66, No. 7, pp. 2267-2268. 1961.

No. 1198. **Herbert Curl, Jr.,** and **Guy C. McLeod.** The Physiological Ecology of a Marine Diatom, *Skeletonema costatum* (Grev.) Cleve. *Jour. Mar. Res.,* Vol. 19, No. 2, pp. 70-88. 1961.

No. 1199. **Eric B. Kraus** and **Claës Rooth.** Temperature and Steady State Vertical Heat Flux in the Ocean Surface Layers. *Tellus,* Vol. 13, No. 2, pp. 231-238. 1961.

No. 1208. **Ralph H. Bodman, Luther V. Slabaugh** and **Vaughan T. Bowen.** A Multipurpose Large Volume Sea-Water Sampler. *J. Mar. Res.,* Vol. 19, No. 3, pp. 141-148. 1961.

No. 1209. **Herbert Curl, Jr.** and **Judith Sandberg.** The Measurement of Dehydrogenase Activity in Marine Organisms. *J. Mar. Res.,* Vol. 19, No. 3, pp. 123-138. 1961.

No. 1211. **Evelyn Shaw.** Minimal Light Intensity and the Dispersal of Schooling Fish. *Bull. Inst. Océanogr., Monaco,* No. 1213, pp. 1-8, 1961.

No. 1215. **G. D. Nicholls** and **V. T. Bowen.** Natural Glass from Beneath Red Clay on the Floor of the Atlantic. *Nature,* Vol. 192, No. 4798, pp. 156-157. 1961.

No. 1218. **John M. Teal** and **John Kanwisher.** Gas Exchange in a Georgia Salt Marsh. *Limnol. and Oceanogr.,* Vol. 6, No. 4, pp. 388-399. 1961.

TREASURER'S REPORT

The accounts for the year 1961 have been audited by Lybrand, Ross Bros. & Montgomery.

The book value of endowment funds at December 31, 1961, was $3,549,925 of which $1,086,345 represented accumulated net gains from sales of investments. The market value of endowment assets on the same date, including real estate at book amount, was $5,980,290. Endowment fund investments and income received therefrom are summarized in Schedule C.

The plant fund accounts on the Balance Sheet reflect the changes during the year resulting from the sale of the Aries, the acquisition of two parcels of real estate, and the work on the new research vessel, as well as the usual addition to the plant reserve funds resulting from depreciation accruals and write-offs of deferred charges.

Income received on endowment assets was $190,208 for the year ended December 31, 1961, compared with $192,354 the previous year. Included in endowment income is $5,731 of parking lot income, which represented a 5 per cent return on this investment. The balance of the parking lot income, amounting to $11,786, was transferred to endowment assets, to amortize the costs of this property. A loss of $3,747.00 on 38 Water Street property incurred during renovation of the property for the new tenant was charged against endowment income. This makes a net real estate income included in endowment income of $1,984 for the year 1961. Endowment income represented a return on endowment fund assets of 3.2 per cent at year-end market quotation, 5.4 per cent on the book amount and 7.7 per cent on the contributed amount of the endowment fund.

Endowment income was allocated for 1961 operating expenses at the rate of 6 per cent of the book amount of original endowment funds, or $146,262. Of the balance of endowment income, $43,946, there was transferred to the income and salary stabilization reserve $42,984 and to unexpended balance of gifts from Oceanographic Associates as income from investment of life memberships $962.

The Institution's 1961 contribution to the Woods Hole Oceanographic Institution's Employees Retirement Trust amounted to $111,661. The trust is administered by three trustees. The balance of the old Retirement Fund, administered by the Treasurer, amounted to $75,931 as at December 31, 1961. The balance consisted of amounts on deposit in sixteen savings bank accounts held in trust for ten members of the plan. No contributions to the Old plan were made in 1961. Interest totalling $2,871 was credited to the savings accounts during the year.

In the financial statements that follow it is interesting to note that for each dollar spent 80 cents was spent for direct costs of research activity, 15 cents for general and administration expenses and 5 cents for plant operation and miscellaneous. Administrative salaries amounted to only 5 cents of each dollar of total expense. Included in the 15 cents of general and administration expenses was 4 cents for staff benefits (group insurance, social security taxes, and contributions to retirement plan).

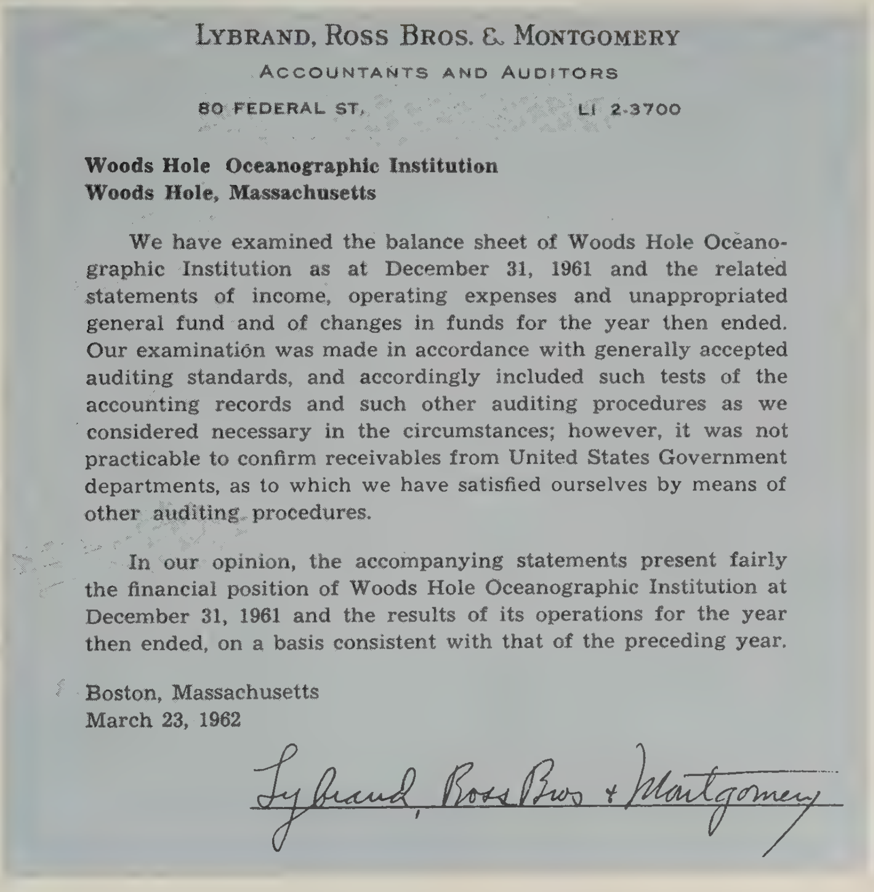

LYBRAND, ROSS BROS. & MONTGOMERY
ACCOUNTANTS AND AUDITORS
80 FEDERAL ST. LI 2-3700

Woods Hole Oceanographic Institution
Woods Hole, Massachusetts

We have examined the balance sheet of Woods Hole Oceanographic Institution as at December 31, 1961 and the related statements of income, operating expenses and unappropriated general fund and of changes in funds for the year then ended. Our examination was made in accordance with generally accepted auditing standards, and accordingly included such tests of the accounting records and such other auditing procedures as we considered necessary in the circumstances; however, it was not practicable to confirm receivables from United States Government departments, as to which we have satisfied ourselves by means of other auditing procedures.

In our opinion, the accompanying statements present fairly the financial position of Woods Hole Oceanographic Institution at December 31, 1961 and the results of its operations for the year then ended, on a basis consistent with that of the preceding year.

Boston, Massachusetts
March 23, 1962

Lybrand, Ross Bros + Montgomery

BALANCE SHEET

As at December 31, 1961

ASSETS

Endowment Fund Assets:		
Investments (Schedule C):		
Bonds (market quotations $1,858,641)		$1,918,334
Stocks (market quotations $3,897,958)		1,407,900
Real estate		162,390
		3,488,624
Cash		61,301
		3,549,925
Plant Fund Assets (note):		
Laboratory plant and equipment		920,425
Vessels and equipment		514,967
Other property		254,541
Vessels under construction		481,084
Total plant		2,171,017
Advance to current funds		821,282
		2,992,299
Current Fund Assets:		
Cash		919,883
Time deposit		50,000
Accounts receivable:		
U. S. Government	$230,241	
Other	10,873	241,114
Unbilled costs on research contracts:		
U. S. Government	758,194	
Other	11,337	769,531
Supplies inventories		43,128
Deferred charges		43,000
		2,066,656
Less advance from plant funds		821,282
		1,245,374
		$7,787,598

Note — Since 1945 the Institution has provided for depreciation of plant assets other than vessels at annual rates of 2% on building and 5% to 33⅓% on equipment, carrying the amounts to general plant and equipment reserve.

BALANCE SHEET

As at December 31, 1961

LIABILITIES

Endowment Funds:		
Unrestricted as to income	$2,000,000	
Unrestricted as to principal and income	42,160	$2,042,160
For upkeep of plant		419,420
Henry Bryant Bigelow Chair of Oceanography		2,000
Accumulated net gain on sales of investments		1,086,345
		3,549,925
Plant Funds:		
Invested in plant		2,171,017
Unexpended:		
Fund for design and construction of a research vessel		377,812
Fund for acquisition of capital assets		247,000
General plant and equipment reserve		144,366
Fund for construction of a small vessel		52,104
		2,992,299
Current Liabilities and Funds:		
Accounts payable and accrued expenses		226,737
Contribution payable to employees' retirement plan and trust		111,661
Unexpended balances of gifts and grants for research:		
Government	432,504	
Other	90,879	523,383
General fund:		
Income and salary stabilization reserve	354,441	
Unappropriated	29,152	383,593
		1,245,374
		$7,787,598

STATEMENT OF INCOME, OPERATING EXPENSES AND UNAPPROPRIATED GENERAL FUND

For the Year Ended December 31, 1961

INCOME:		
For sponsored research (including $1,027,309 gifts and grants expanded):		
For direct costs		$4,284,949
For indirect costs		952,316
Fees for use of facilities		144,236
		5,381,501
Endowment income (Schedule C)	$190,208	
Less amounts added to income and salary stabilization reserve ($42,984) and to unexpended balance of gifts from Oceanographic Associates ($962)	43,946	146,262
Miscellaneous		6,890
Total income availed of		5,534,653
OPERATING EXPENSES:		
Direct costs of research activity (Schedule A):		
Salaries and wages		1,404,702
Vessel operations		1,230,257
Materials and services		1,628,565
Travel		116,373
		4,379,897
Indirect costs:		
General and administration (Schedule B)	801,366	
Plant operation (Schedule B)	277,578	
Miscellaneous	6,526	1,085,470
Total operating expenses		5,465,367
Excess of income		69,286
Additions to plant from current funds — books and equipment purchased		43,799
		25,487
Unappropriated general fund, January 1, 1961		3,665
Unappropriated general fund, December 31, 1961		$ 29,152

STATEMENT OF CHANGES IN FUNDS

For the Year Ended December 31, 1961

	Endowment Funds	Plant Funds		Unexpended Balances of Gifts and Grants for Research	General Fund
		Invested in Plant	Unexpended	(note)	
BALANCE, December 31, 1960	$3,483,053	$2,005,387	$353,373	$ 473,549	$315,122
Gifts (including Associates life membership dues) and grants received	8,876		759,000*	1,077,143	
Additions from current year's revenues:					
Books and equipment purchased		43,799			
Provision for depreciation			95,877		
Provision for income and salary stabilization reserve					42,984
Excess of income over provisions and expenses					25,487
Net gain on sales of investments	57,996				
Proceeds from sale of assets			84,985		
Cost of assets disposed of		(300,437)			
Invested in plant		422,268	(422,268)		
Expended				(1,027,309)	
Funds received in 1961 applied to 1960 expenditures			(49,685)		
BALANCE, December 31, 1961	$3,549,925	$2,171,017	$821,282	$ 523,383	$383,593

*Includes $750,000 received on grant for design and construction of a research vessel.

NOTE — Unexpended balances consist of amounts received in advance of expenditure, and do not include receipts or expenditures under reimbursement type contracts.

Schedule A

DIRECT COSTS OF RESEARCH ACTIVITY

For the Year Ended December 31, 1961

	Salaries and Wages	Vessel Operations	Materials and Services	Travel	Total
U. S. GOVERNMENT CONTRACTS	$1,374,607	$1,148,586	$1,554,804	$105,388	$4,183,385
OTHER SPONSORED RESEARCH	7,250	59,967	31,930	2,417	101,564
Total direct costs of sponsored research	1,381,857	1,208,553	1,586,734	107,805	4,284,949
INSTITUTION RESEARCH	22,845	21,704	41,831	8,568	94,948
Total direct costs of research	$1,404,702	$1,230,257	$1,628,565*	$116,373	$4,379,897

*Includes grants and fellowships:

U. S. Government contracts	$21,200
Other sponsored research	23,146
Institution research	25,280
	$69,626

Schedule B

GENERAL AND ADMINISTRATION EXPENSES AND EXPENSES FOR PLANT OPERATION

For the Year Ended December 31, 1961

GENERAL AND ADMINISTRATION

GENERAL EXPENSES:		
Staff benefits:		
Contributions to retirement plan		$111,661
Social security taxes		54,217
Employee health benefits		20,769
Group insurance		6,779
		193,426
Shop services		136,532
Housing, net		1,421
ADMINISTRATION EXPENSES:		
Salaries and wages	$287,632	
Insurance, travel, supplies and other	182,355	469,987
		$801,366

PLANT OPERATION

Salaries and wages		$ 67,898
Provision for depreciation (credited to general plant and equipment reserve)		76,456
Other repair costs	$52,518	
Heat, light and power	32,164	
Other	48,542	133,224
		$277,578

Schedule C

SUMMARY OF INVESTMENTS

As at December 31, 1961

	Book Amount	% of Total	Market Quotation	% of Total	Endowment Income
BONDS:					
Government	$ 536,330	15.37	$ 533,946	9.02	$ 18,020
Railroad	410,325	11.76	379,080	6.40	19,923
Public utility	360,673	10.34	344,051	5.81	14,369
Industrial	435,299	12.48	422,445	7.14	17,893
Financial and investment	175,707	5.04	179,119	3.03	7,379
Total bonds	1,918,334	54.99	1,858,641	31.40	77,584
STOCKS:					
Preferred	259,746	7.45	250,988	4.24	12,500
Common:					
Public utility	330,728	9.48	1,148,152	19.40	29,069
Industrial	560,092	16.05	1,874,099	31.66	51,068
Miscellaneous	257,334	7.38	624,719	10.55	18,003
Total common stocks	1,148,154	32.91	3,646,970	61.61	98,140
Total stocks	1,407,900	40.36	3,897,958	65.85	110,640
REAL ESTATE	162,390	4.65	162,390*	2.75	1,984
Total investments	$3,488,624	100.00	$5,918,989	100.00	$190,208

*At book amount.

List of Contributions

LIST OF CONTRIBUTIONS
FROM THE WOODS HOLE OCEANOGRAPHIC INSTITUTION

See Author, Subject-Locality, Taxonomic Indexes, published in 1957, for a complete list through 1956.

No. 800. M. S. Gordon and Richard H. Backus. New Records of Labrador Fishes with Special Reference to Those of Hebron Fjord. *Copeia*, No. 1, pp. 17–20. 1957.

No. 801. Floyd M. Soule and J. E. Murray. Physical Oceanography of the Grand Banks and the Labrador Sea in 1955. *U. S. Coast Guard Bull.*, No. 41, pp. 59–114. 1956.

No. 802. James M. Moulton and Richard H. Backus. Annotated References Concerning the Effects of Man-Made Sounds on the Movements of Fishes. *Dept. Sea and Shore Fish., Fish. Circ.*, Augusta, Maine, No. 17, 8 pp. 1955.

No. 803. E. M. Hulburt, J. J. A. McLaughlin and P. A. Zahl. *Katodinium dorsalisulcum*, a New Species of Unarmored Dinophyceae. *Jour. Protozool.*, Vol. 7, No. 4, pp. 323–326. 1960.

No. 804. W. V. R. Malkus. Outline of a Theory of Turbulent Shear Flow. *Jour. Fluid Mech.*, Vol. 1, Pt. 5, pp. 521–539. 1956.

No. 805. John Mackiewicz and Richard H. Backus. Oceanic Records of *Lasionycteris noctivagans* and *Lasiurus borealis*. *Jour. Mammalogy*, Vol. 37, No. 3, pp. 442–443. 1956.

No. 806. Allyn C. Vine. Oceanographic Instrumentation. *Science*, Vol. 122, No. 3173, pp. 748–751. 1955.

No. 807. P. F. Scholander and William E. Schevill. Counter-Current Vascular Heat Exchange in the Fins of Whales. *Jour. Appl. Physiol.*, Vol. 8, No. 3, pp. 279–282. 1955.

No. 808. E. Steemann Nielsen. The Interaction of Photosynthesis and Respiration and Its Importance for the Determination of ^{14}C-Discrimination in Photosynthesis. *Physiologia Plantarum*, Vol. 8, pp. 945–953. 1955.

No. 809. Duncan C. Blanchard. The Supercooling, Freezing and Melting of Giant Waterdrops at Terminal Velocity in Air. Proceedings of the First Conference on the Physics of Cloud Precipitation Particles, Woods Hole, September 7–10, 1955. In: Artificial Stimulation of Rain, Pergamon Press Ltd., New York, London, Paris, pp. 233–249. 1957.

No. 810. Karl E. Schleicher and Alvin Bradshaw. A Conductivity Bridge for Measurement of the Salinity of Sea Water. *Jour. du Conseil*, Vol. 22, No. 1, pp. 9–20. 1956.

No. 811. G. W. Morgan. On the Wind-Driven Ocean Circulation. *Tellus*, Vol. 8, No. 3, pp. 301–320. 1956.

No. 812. Duncan C. Blanchard. Discussion of Raindrop Distributions Made during Project Shower, Hawaii, 1954. Proceedings of the First Conference on the Physics of Cloud Precipitation Particles, Woods Hole, September 7–10, 1955. In: Artificial Stimulation of Rain, Pergamon Press Ltd., New York, London, Paris, pp. 213–223. 1957.

No. 813. R. W. Holmes. The Annual Cycle of Phytoplankton in the Labrador Sea, 1950–51. *Bull. Bingham Oceanogr. Coll.*, Vol. 16, Art. 1, 74 pp. 1956. (Not included in *Collected Reprints*).

No. 814. Richard H. Backus, Stewart Springer and Edgar L. Arnold, Jr. A Contribution to the Natural History of the White-Tip Shark, *Pterolamiops longimanus* (Poey). *Deep-Sea Research*, Vol. 3, pp. 178–188. 1956.

No. 815. William E. Schevill. *Lagenorhynchus acutus* off Cape Cod. *Jour. Mammalogy*, Vol. 37, No. 1, pp. 128–129. 1956.

No. 816. P. F. Scholander, L. van Dam and Theodore Enns. Nitrogen Secretion in the Swimbladder of Whitefish. *Science*, Vol. 123, No. 3185, pp. 59–60. 1956.

No. 817. Harold E. Edgerton and Lloyd D. Hoadley. Cameras and Lights for Underwater Use. *Jour. Soc. Motion Pict. and Television Eng.*, Vol. 64, pp. 345–350. 1955.

No. 818. P. F. Scholander, John W. Kanwisher and D. C. Nutt. Gases in Icebergs. *Science*, Vol. 123, No. 3186, pp. 104–105. 1956.

No. 819. John H. Ryther. Photosynthesis in the Ocean as a Function of Light Intensity. *Limnol. and Oceanogr.*, Vol. 1, No. 1, pp. 61–70. 1956.

No. 820. William S. von Arx. An Experimental Approach to Problems in Physical Oceanography. In: Progress in Physics and Chemistry of the Earth, Pergamon Press Ltd., London, New York, Paris, Vol. 2, pp. 1–29. 1957.

No. 821. George L. Clarke and Gunther K. Wertheim. Measurements of Illumination at Great Depths and at Night in the Atlantic Ocean by Means of a New Bathyphotometer. *Deep-Sea Research*, Vol. 3, pp. 189–205. 1956.

No. 822. P. F. Scholander. Hydrostatic Pressure in Coconuts. *Plant Physiol.*, Vol. 30, No. 6, pp. 560–561. 1955.

No. 823. John C. Ayers. A Dynamic Height Method for the Determination of Currents in Deep Lakes. *Limnol. and Oceanogr.*, Vol. 1, No. 3, pp. 150–161. 1956.

No. 824. Parker D. Trask. The *Atlantis* Marine Geological Expedition to Peru and Chile. *Nature*, Vol. 177, pp. 454–455. 1956.

No. 825. John H. Ryther. The Measurement of Primary Production. *Limnol. and Oceanogr.*, Vol. 1, No. 2, pp. 72–84. 1956.

No. 826. Robert L. Miller. Trend Surfaces: Their Application to Analysis and Description of Environments of Sedimentation. 1. The Relation of Sediment-Size Parameters to Current-Wave Systems and Physiography. *Jour. Geology*, Vol. 64, No. 5, pp. 425–446. 1956.

No. 827. Joanne Starr Malkus. On the Maintenance of the Trade Winds. *Tellus*, Vol. 8, No. 3, pp. 335–350. 1956.

No. 828. Alfred C. Redfield and Arthur R. Miller. Water Levels Accompanying Atlantic Coast Hurricanes. In: Interaction of Sea and Atmosphere. *Meteorol. Monogr.*, Vol. 2, No. 10, pp. 1–23. 1957.

No. 829. Arthur R. Miller. The Effect of Steady Winds on Sea Level at Atlantic City. In: Interaction of Sea and Atmosphere. *Meteorol. Monogr.*, Vol. 2, No. 10, pp. 24–31. 1957.

No. 830. Francis A. Richards and Ralph F. Vaccaro. The Cariaco Trench, an Anaerobic Basin in the Caribbean Sea. *Deep-Sea Research*, Vol. 3, pp. 214–228. 1956.

No. 831. David C. Nutt and Lawrence K. Coachman. The Oceanography of Hebron Fjord, Labrador. *Jour. Fish. Res. Bd., Canada*, Vol. 13, No. 5, pp. 709–758. 1956.

No. 832. William E. Schevill and Barbara Lawrence. Food-Finding by a Captive Porpoise (*Tursiops truncatus*). *Breviora, Mus. Comp. Zool.*, No. 53, 15 pp. 1956.

No. 833. A. F. Bunker. Turbulence Measurements in a Young Cyclone over the Ocean. *Bull. Amer. Meteorol. Soc.*, Vol. 38, No. 1, pp. 13–16. 1957.

No. 834. Richard H. Backus and J. B. Hersey. Echo-Sounder Observations of Midwater Nets and Their Towing Cables. *Deep-Sea Research*, Vol. 3, pp. 237–241. 1956.

No. 835. Joseph Chase. The Bermuda-Azores High Pressure Cell. Its Surface Wind Circulation. *Miscelânea Geofísica*, Luanda, Angola, pp. 29–54. 1956. (In *Collected Reprints* for 1957).

No. 836. Frank J. Mather, III and Howard A. Schuck. Growth of Bluefin Tuna of the Western North Atlantic. *Fish. Bull.* 179, *Fish Bull., U. S. Fish and Wildlife Service*, Vol. 61, pp. 39–52. 1960.

No. 837. A. H. Woodcock. Dimorphism in the Portuguese Man-of-War. *Nature*, Vol. 178, No. 4527, pp. 253–255. 1956.

No. 838. E. M. Hulburt. The Taxonomy of Unarmored Dinophyceae of Shallow Embayments on Cape Cod, Massachusetts. *Biol. Bull.*, Vol. 112, No. 2, pp. 196–219. 1957.

No. 839. C. B. Officer, J. I. Ewing, R. S. Edwards and H. R. Johnson. Geophysical Investigations in the Eastern Caribbean: Venezuelan Basin, Antilles Island Arc, and Puerto Rico Trench. *Bull. Geol. Soc. Amer.*, Vol. 68, pp. 359–378. 1957.

No. 840. Francis A. Richards. On the State of our Knowledge of Trace Elements in the Ocean. *Geochimica et Cosmochimica Acta*, Vol. 10, No. 4, pp. 241–243. 1956.

No. 841. Henry R. Johnson, Richard H. Backus, J. B. Hersey and D. M. Owen. Suspended Echo-Sounder and Camera Studies of Midwater Sound Scatterers. *Deep-Sea Research*, Vol. 3, pp. 266–272. 1956.

No. 842. John H. Ryther. Interrelation between Photosynthesis and Respiration in the Marine Flagellate, *Dunaliella euchlora*. *Nature*, Vol. 178, pp. 861–862. 1956.

No. 843. Joanne Starr Malkus. Trade Cumulus Cloud Groups: Some Observations Suggesting a Mechanism of Their Origin. *Tellus*, Vol. 9, No. 1, pp. 33–44. 1957.

No. 844. Francis A. Richards. Some Current Aspects of Chemical Oceanography. In: Progress in Physics and Chemistry of the Earth, Pergamon Press Ltd., London, New York, Paris, Vol. 2, pp. 77–128. 1957.

No. 845. Henry Stommel. Florida Straits Transports, 1952–1956. *Bull. Mar. Sci., Gulf and Caribbean*, Vol. 7, No. 3, pp. 252–254. 1957.

No. 846. Henry Stommel. On the Determination of the Depth of No Meridional Motion. *Deep-Sea Research*, Vol. 3, pp. 273–278. 1956.

No. 847. Athelstan Spilhaus. Control of the World Environment. *Geogr. Rev.*, Vol. 46, No. 4, pp. 451–459. 1956.

No. 848. Henry B. Bigelow and William C. Schroeder. A Study of the Sharks of the Suborder Squaloidea. *Bull. Mus. Comp. Zool.*, Vol. 117, No. 1, pp. 1–150. 1957. (Not included in *Collected Reprints*).

No. 849. Duncan C. Blanchard. Electrically Charged Drops from Bubbles in Sea Water and Their Meteorological Significance. *Jour. Meteorol.*, Vol. 15, No. 4, pp. 383–396. 1958.

No. 850. H. Walden and H. G. Farmer. Auswertung von Seegangsregistrierungen des Forschungsschiffes "Atlantis" mit dem "Ship-Borne Wave Recorder" sowie Vergleich mit entsprechenden Seegangsberechnungen aus den Windverhaltnissen (Hindcasting). *Deutsche Hydrogr. Zeitschrift*, Bd. 10, Heft 4, pp. 121–134. 1957.

No. 851. Allyn C. Vine, Some Trends in Oceanographic Instrumentation. *Proc. UNESCO Symp. Phys. Oceanogr.*, Tokyo, 1955, pp. 49–52. 1957. (Not included in *Collected Reprints*).

No. 852. Francis A. Richards and Nathaniel Corwin. Some Oceanographic Applications of Recent Determinations of the Solubility of Oxygen in Sea Water. *Limnol. and Oceanogr.*, Vol. 1, No. 4, pp. 263–267. 1956.

No. 853. Irving I. Schell. On the Nature and Origin of the Southern Oscillation. *Jour. Meteorol.*, Vol. 13, No. 6, pp. 592–598. 1956.

No. 854. Richard H. Backus. Northern Record of the Snake Eel *Ophichthus gomesi* (Castelnau). *Copeia*, No. 1, p. 61. 1957.

No. 855. A. B. Arons and Henry Stommel. A β-Plane Analysis of Free Periods of the Second Class in Meridional and Zonal Oceans. *Deep-Sea Research*, Vol. 4, pp. 23–31. 1956.

No. 856. Gordon Volkmann, John Knauss and Allyn Vine. The Use of Parachute Drogues in the Measurement of Subsurface Ocean Currents. *Trans. Amer. Geophys. Union*, Vol. 37, No. 5, pp. 573–577. 1956.

No. 857. Richard H. Backus. Notes on Western North Atlantic Sharks. *Copeia*, No. 3, pp. 246–248. 1957.

No. 858. George L. Clarke and Richard H. Backus. Measurements of Light Penetration in Relation to Vertical Migration and Records of Luminescence of Deep-Sea Animals. *Deep-Sea Research*, Vol. 4, pp. 1–14. 1956.

No. 859. G. Veronis and Henry Stommel. The Action of Variable Wind Stresses on a Stratified Ocean. *Sears Found., Jour. Mar. Res.*, Vol. 15, No. 1, pp. 43–75. 1956.

No. 860. I. Friedman and A. H. Woodcock. Determination of Deuterium-Hydrogen Ratios in Hawaiian Waters. *Tellus*, Vol. 9, No. 4, pp. 553–556. 1957.

No. 861. J. I. Ewing, C. B. Officer, H. R. Johnson, and R. S. Edwards. Geophysical Investigations in the Eastern Caribbean: Trinidad Shelf, Tobago Trough, Barbados Ridge, Atlantic Ocean. *Bull. Geol. Soc. Amer.*, Vol. 68, pp. 897–912. 1957.

No. 862. James M. Moulton. Influencing the Calling of Sea Robins (*Prionotus* spp.) with Sound. *Biol. Bull.*, Vol. 111, No. 3, pp. 393–398. 1956.

No. 863. S. T. Knott and J. B. Hersey. Interpretation of High-Resolution Echo-Sounding Techniques and Their Use in Bathymetry, Marine Geophysics, and Biology. *Deep-Sea Research*, Vol. 4, pp. 36–44. 1956.

No. 864. H. B. Moore and E. G. Corwin. The Effects of Temperature, Illumination, and Pressure on the Vertical Distribution of Zooplankton. *Bull. Mar. Sci., Gulf and Caribbean*, Vol. 6, No. 4, pp. 273–287. 1956.

No. 865. Richard S. Edwards and Francis A. Richards. A Bottom-Water Sampler. *Deep-Sea Research*, Vol. 4, pp. 65–66. 1956.

No. 866. M. S. Rutstein. Flooded Quarries for Experimental Work. *Trans. Amer. Geophys. Union*, Vol. 35, No. 5, pp. 688–690. 1957.

No. 867. Irving Friedman, Daniel R. Norton, Douglas B. Carter and Alfred C. Redfield. The Deuterium Balance of Lake Maracaibo. *Limnol. and Oceanogr.*, Vol. 1, No. 4, pp. 239–246. 1956.

No. 868. M. S. Gordon. Observations on Osmoregulation in the Arctic Char (*Salvelinus alpinus* L.). *Biol. Bull.*, Vol. 112, No. 1, pp. 28–33. 1957.

No. 869. Helen S. Vishniac. On the Ecology of the Lower Marine Fungi. *Biol. Bull.*, Vol. 111, No. 3, pp. 410–414. 1956.

No. 870. W. S. Wooster and Bostwick H. Ketchum. Transport and Dispersal of Radioactive Elements in the Sea. In: The Effects of Atomic Radiation on Oceanography and Fisheries. *Nat. Acad. Sci.-Nat. Res. Council, Publ.* No. 551, Chap. 4, pp. 43–51. 1957.

No. 871. Bostwick H. Ketchum. The Effects of the Ecological System on the Transport of Elements in the Sea. In: The Effects of Atomic Radiation on Oceanography and Fisheries. *Nat. Acad. Sci.-Nat. Res. Council, Publ.* No. 551, Chap. 5, pp. 52–59. 1957.

No. 872. P. F. Scholander and John Krog. Countercurrent Heat Exchange and Vascular Bundles in Sloths. *Jour. Applied Physiol.*, Vol. 10, No. 3, pp. 405–411. 1957. (Not included in *Collected Reprints*).

No. 873. Lawrence K. Coachman, E. Hemmingsen and P. F. Scholander. Gas Enclosures in a Temperate Glacier. *Tellus*, Vol. 8, No. 4, pp. 415–423. 1956. (Not included in *Collected Reprints*).

No. 874. J. B. Hersey. Electronics in Oceanography. In: Advances in Electronics and Electron Physics, Academic Press, Inc., New York, Vol. 9, pp. 239–295. 1957. (Not included in *Collected Reprints*).

No. 875. Duncan C. Blanchard and A. H. Woodcock. Bubble Formation and Modification in the Sea and Its Meteorological Significance. *Tellus*, Vol. 9, No. 2, pp. 145–158. 1957.

No. 876. Harry J. Turner, Carl J. George and Joseph H. Connell. Eighth Report on Investigations of the Shellfisheries of Massachusetts. *Com. Mass., Dept. Nat. Res., Div. Mar. Fish.*, 25 pp. 1955.

No. 877. Floyd M. Soule and J. E. Murray. Physical Oceanography of the Grand Banks Region and the Labrador Sea in 1956. *U. S. Coast Guard Bull.*, No. 42, pp. 35–100. 1957. (In *Collected Reprints* for 1958).

No. 878. J. W. Kanwisher and H. Leivestad. Thermal Regulation in Whales. *Norwegian Whaling Gazette*, No. 1, pp. 1–5. 1957.

No. 879. P. F. Scholander and L. van Dam. Micro Gasometric Determination of Oxygen in Fish Blood. *Jour. Cell. and Comp. Physiol.*, Vol. 48, No. 3, pp. 529–532. 1956. No. 3, pp. 517–522. 1956.

No. 880. P. F. Scholander. Observations on the Gas Gland in Living Fish. *Jour. Cell. and Comp. Physiol.*, Vol. 48, No. 3, pp. 523–528. 1956.

No. 881. P. F. Scholander, L. van Dam and Theodore Enns. The Source of Oxygen Secreted into the Swimbladder of Cod. *Jour. Cell. and Comp. Physiol.*, Vol. 48, No. 3, pp. 517–522. 1956.

No. 882. H. L. Sanders. The Cephalocarida and Crustacean Phylogeny. *Syst. Zool.*, Vol. 6, No. 3, pp. 112–129. 1957.

No. 883. John C. Ayers and Roger Bachmann. Simplified Computations for the Dynamic Height Method of Current Determination in Lakes. *Limnol and Oceanogr.*, Vol. 2, No. 2, pp. 155–157. 1957.

No. 884. John M. Zeigler and F. C. Ronne. Time-Lapse Photography - - an Aid to Studies of the Shoreline. *Research Reviews*, Office of Naval Research, Washington, April, pp. 1–6. 1957.

No. 885. Shannon R. Torphy and John M. Zeigler. Submarine Topography of Eastern Channel, Gulf of Maine. *Jour. Geology*, Vol. 65, No. 4, pp. 433–441. 1957.

No. 886. Harry J. Turner and David L. Belding. The Tidal Migrations of *Donax variabilis* Say. *Limnol and Oceanogr.*, Vol. 2, No. 2, pp. 120–124. 1957.

No. 887. J. W. Kanwisher. Freezing and Drying in Intertidal Algae. *Biol. Bull.*, Vol. 113, No. 2, pp. 275–285. 1957.

No. 888. J. W. Kanwisher and Alfred Ebeling. Composition of the Swim-Bladder Gas in Bathypelagic Fishes. *Deep-Sea Research*, Vol. 4, pp. 211–217. 1957.

No. 889. A. H. Woodcock and A. T. Spencer, An Airborne Flame Photometer and its Use in the Scanning of Marine Atmospheres for Sea-Salt Particles. *Jour. Meteorol.*, Vol. 14, No. 5, pp. 437-447. 1957.

No. 890. Willem A. van Bergeijk and Emil Witschi. The Basila Papilla of the Anuran Ear. *Acta Anatomica*, Vol. 30, pp. 81–91. 1957. (Not included in *Collected Reprints*).

No. 891. P. F. Scholander, L. van Dam, J. W. Kanwisher, H. T. Hammel and M. S. Gordon. Supercooling and Osmoregulation in Arctic Fish. *Jour. Cell. and Comp. Physiol.*, Vol. 49, No. 1, pp. 5–24. 1957.

No. 892. P. F. Scholander and L. van Dam. The Concentration of Hemoglobin in Some Cold Water Arctic Fishes. *Jour. Cell. and Comp. Physiol.*, Vol. 49, No. 1, pp. 1–4. 1957.

No. 893. Charles S. Yentsch and John R. Ryther. Short-Term Variations in Phytoplankton Chlorophyll and Their Significance. *Limnol. and Oceanogr.*, Vol. 2, No. 2, pp. 140–142. 1957.

No. 894. Richard H. Backus and Harold Barnes. Television-Echo-Sounder Observations by Midwater Sound Scatterers. *Deep-Sea Research*, Vol. 4, pp. 116-119. 1957.

No. 895. Robert G. Walden, David D. Ketchum and David H. Frantz, Jr. Buoy Telemeters Ocean Temperature Data. *Electronics*, McGraw-Hill Co., New York, Vol. 30, No. 6, pp. 164–167. 1957.

No. 896. Richard H. Backus. The Fishes of Labrador. *Bull. Amer. Mus. Nat. Hist.*, Vol. 113, Art. 4, pp. 273-337. 1957. (Not included in *Collected Reprints*).

No. 897. Harold Barnes. The Northern Limit of *Balanus balanoides* (L). *Oikos*, Vol. 8, No. 1, pp. 1–15. 1957.

No. 898. Charles S. Yentsch. A Non-Extractive Method for the Quantitative Estimation of Chlorophyll in Algal Cultures. *Nature*, Vol. 179, pp. 1302-1304. 1957.

No. 899. Henry Stommel and George Veronis. Steady Convective Motion in a Horizontal Layer of Fluid Heated Uniformly from Above and Cooled Non-Uniformly from Below. *Tellus*, Vol. 9, No. 3, pp. 401–407. 1957.

No. 900. Arthur R. Miller. The Effects of Winds on Water Levels on the New England Coast. *Limnol. and Oceanogr.*, Vol. 3, No. 1, pp. 1–14. 1958.

No. 901. Frank J. Mather III and Robert H. Gibbs. Distributional Records of Fishes from Waters off New England and the Middle Atlantic States. *Copeia*, No. 3, pp. 242–244. 1957.

No. 902. John H. Ryther and Charles S. Yentsch. The Estimation of Phytoplankton Production in the Ocean from Chlorophyll and Light Data. *Limnol. and Oceanogr.*, Vol. 2, No. 3, pp. 281-286. 1957.

No. 903. W. H. Sutcliffe, Jr. An Improved Method for the Determination of Preserved Plankton Volumes. *Limnol. and Oceanogr.*, Vol. 2, No. 3, pp. 295–296. 1957.

No. 904. Dean F. Bumpus. Surface Water Temperature along Atlantic and Gulf Coasts of the United States. *U. S. Fish and Wildlife Service, Spec. Sci. Rept. — Fisheries*, No. 214, 153 pp. 1957. (Not included in *Collected Reprints*).

No. 905. William D. Athearn. Comparisons of Clay from the Continental Shelf off Long Island with the Gardiners Clay. *Jour. Geology*, Vol. 65, No. 4, pp. 448–449. 1957.

No. 906. John H. Ryther and Charles S. Yentsch. Primary Production of Continental Shelf Waters off New York. *Limnol. and Oceanogr.*, Vol. 3, No. 3, pp. 327–335. 1958.

No. 907. Vaughan T. Bowen and T. T. Sugihara. Strontium 90 in North Atlantic Surface Water. *Proc. Nat. Acad. Sci.*, Vol. 43, No. 7, pp. 576–580. 1957.

No. 908. L. V. Worthington and William E. Schevill. Underwater Sounds Heard from Sperm Whales. *Nature*, Vol. 180, p. 291. 1957

No. 909. Jan Hahn. Oceanus Goes to the Bottom of the Sea. *Oceanus*, Vol. 5, Nos. 1 and 2, pp. 20–31. 1957.

No. 910. J. C. Swallow and L. V. Worthington. Measurements of Deep Currents in the Western North Atlantic. *Nature*, Vol. 179, pp. 1183–1184. 1957.

No. 911. G. C. McLeod. The Effect of Circularly Polarized Light on the Photosynthesis and Chlorophyll *a* Synthesis of Certain Marine Algae. *Limnol. and Oceanogr.*, Vol. 2, No. 4, pp. 360–362. 1957.

No. 912. Robert H. Gibbs, Jr. A Taxonomic Analysis of *Myctophum affine* and *M. nitidulum*, Two Lantern-Fishes Previously Synonymized, in the Western North Atlantic. *Deep-Sea Research*, Vol. 4, pp. 230–237. 1957.

No. 913. E-an Zen. Preliminary Report on the Mineralogy and Petrology of Some Marine Bottom Samples off the Coast of Peru and Chile. *Amer. Mineralogist*, Vol. 42, pp. 889–903. 1957.

No. 914. James M. Moulton. Sound Production in the Spiny Lobster *Panulirus argus* (Latreille). *Biol. Bull.*, Vol. 113, No. 2, pp. 286–295. 1957.

No. 915. Joanne S. Malkus. On the Structure and Maintenance of the Mature Hurricane Eye. *Jour. Meteorol.*, Vol. 15, No. 4, pp. 337-349. 1958.

No. 916. G. G. Whitney, Jr. Factors Affecting the Accuracy of Thermometric Depth Determinations. *Jour. du Conseil*, Vol. 22, No. 2, pp. 167–173. 1957.

No. 917. Henry Stommel. A Survey of Ocean Current Theory. *Deep-Sea Research*, Vol. 4, pp. 149–184. 1957.

No. 918. Dean F. Bumpus. Oceanographic Observations 1956, East Coast of the United States. *U. S. Fish and Wildlife Service, Spec. Sci. Rept. — Fisheries*, No. 233, 132 pp. 1957. (Not included in *Collected Reprints*).

No. 919. John M. Zeigler, W. D. Athearn and H. Small. Profiles across the Peru-Chile Trench. *Deep-Sea Research*, Vol. 4, pp. 238–249. 1957.

No. 920. A. H. Woodcock. The Release of Latent Heat in Tropical Storms due to the Fall-Out of Sea-Salt Particles. *Tellus*, Vol. 10, No. 3, pp. 355-371. 1958.

No. 921. P. F. Scholander. Oxygen Dissociation Curves in Fish Blood. *Acta Physiol. Scand.*, Vol. 41, No. 4, pp. 340–344. 1957.

No. 922. Robert H. Gibbs, Jr. Preliminary Analysis of the Distribution of White Marlin, *Makaira albida* (Poey), in the Gulf of Mexico. *Bull. Mar. Sci., Gulf and Caribbean*, Vol 7, No. 4, pp. 360–369. 1957.

No. 923. Alfred C. Redfield. The Inadequacy of Experiment in Marine Biology. In: Perspectives in Marine Biology, Symposium held at Scripps Inst. of Oceanogr., Univ. Cal., March 24-April 2, 1956, Univ. California Press, pp. 17–23. 1958.

No. 924. Mary A. Plunkett. The Qualitative Determination of Some Organic Compounds in Marine Sediments. *Deep-Sea Research*, Vol. 4, pp. 259-262. 1957.

No. 926. Dean F. Bumpus, Joseph Chase, C. Godfrey Day, David H. Frantz, Jr., David D. Ketchum and Robert G. Walden. A New Technique for Studying Non-Tidal Drift with Results of Experiments off Gay Head, Mass., and in the Bay of Fundy. *Jour. Fish. Res. Bd., Canada*, Vol. 14, No. 6, pp. 931–944. 1957.

No. 927. Malcolm S. Gordon. Osmotic and Ionic Regulation in Scottish Brown Trout and Sea Trout (*Salmo trutta L.*). *Jour. Exper. Biol.*, Vol. 36, No. 2, pp. 253–260. 1959.

No. 928. H. Barnes and Margaret Barnes. The Rate of Development of *Balanus balanoides* (L.) Larvae. *Limnol. and Oceanogr.*, Vol. 3, No. 1, pp. 29–32. 1958.

No. 929. Theodore R. Folsom and Allyn C. Vine. On the Tagging of Water Masses for the Study of Physical Processes in the Oceans. In: The Effects of Atomic Radiation on Oceanography and Fisheries. *Nat. Acad. Sci.-Nat. Res. Council, Publ.* No. 551, Chap. 12, pp. 121–132. 1957.

No. 930. William S. von Arx. "Dister": A Displacement Sequence Stereoscope. *Jour. Meteorol*, Vol. 15, No. 2, pp. 230–231. 1958.

No. 931. William S. von Arx. Synoptic Photography. *Weather, Roy. Meteorol. Soc.*, London, pp. 179–197. 1958.

No. 932. Henry B. Bigelow and William C. Schroeder. Four New Rajids from the Gulf of Mexico. *Bull. Mus. Comp. Zool.*, Vol. 119, No. 2, pp. 201–233. 1958.

No. 933. G. Veronis. On the Transient Response of a β-plane Ocean. *Jour. Oceanogr. Soc., Japan*, Vol. 14, No. 1, pp. 1–5. 1958.

No. 934. William S. Richardson and Charles H. Wilkins. An Airborne Radiation Thermometer. *Deep-Sea Research*, Vol. 5, pp. 62–71. 1958.

No. 935. Joyce C. Lewin, R. A. Lewin and D. E. Philpott. Observations on *Phaeodactylum tricornutum*. *Jour. Gen. Microbiology*, Vol. 18, No. 2, pp. 420–426. 1958.

No. 936. Joyce C. Lewin. The Taxonomic Position of *Phaeodactylum tricornutum*. *Jour. Gen. Microbiology*, Vol. 18, No. 2, pp. 427–432. 1958.

No. 937. H. Barnes. Temperature and the Life Cycle of *Balanus balanoides* (L.). In: Marine Boring and Fouling Organisms, Univ. Washington Press, Seattle, pp. 234–245. 1959. (Not included in *Collected Reprints*).

No. 938. Harry J. Turner. The Effect of Nutrition on the Color of the Callus of *Polinices duplicatus*. *The Nautilus*, Vol. 72, No. 1, pp. 1–3. 1958.

No. 939. Henry Stommel, A. B. Arons and A. J. Faller. Some Examples of Stationary Planetary Flow Patterns in Bounded Basins. *Tellus*, Vol. 10, No. 2, pp. 179–187. 1958.

No. 940. Howard L. Sanders. Benthic Studies in Buzzards Bay. I. Animal-Sediment Relationships. *Limnol. and Oceanogr.* Vol. 3, No. 3, pp. 245–258. 1958.

No. 941. Dean F. Bumpus and C. Godfrey Day. Drift Bottle Records for the Gulf of Maine and Georges Bank, 1931–56. *U. S. Fish and Wildlife Service, Spec. Sci. Rept. — Fisheries*, No. 242, 61 pp. 1957.

No. 942. Frank J. Mather, III and Robert H. Gibbs, Jr. Distribution of the Atlantic Bigeye Tuna, *Thunnus obesus*, in the Western North Atlantic and the Caribbean Sea. *Copeia*, 1958, No. 3, pp. 237–239. 1958.

No. 943. W. V. R. Malkus and G. Veronis. Finite Amplitude Cellular Convection. *Jour. Fluid Mech.*, Vol. 4, Pt. 3, pp. 225–260. 1958.

No. 944. J. B. Hersey and M. S. Rutstein. Reconnaissance Survey of Oriente Deep (Caribbean Sea) with a Precision Echo Sounder. *Bull. Geol. Soc. Amer.*, Vol. 69, pp. 1297–1304. 1958.

No. 945. Alan J. Faller. An Optical Method for the Measurement of Surface Waves in the Laboratory. *Trans. Amer. Geophys. Union*, Vol. 39, No. 4, pp. 716–720. 1958.

No. 946. Bostwick H. Ketchum, John H. Ryther, Charles S. Yentsch and Nathaniel Corwin. Productivity in Relation to Nutrients. *Rapp. et Proc.-Verb., Cons. Perm. Internat. Explor. de la Mer*, Vol. 144, pp. 132–140. 1958.

No. 947. William C. Schroeder. The Lobster, *Homarus americanus*, and the Red Crab, *Geryon quinquedens*, in the Offshore Waters of the Western North Atlantic. *Deep-Sea Research*, Vol. 5, pp. 266–282. 1959.

No. 948. Susan I. Scholander and Joan T. Kanwisher. Latitudinal Effect on Respiration in Some Northern Plants. *Plant Physiol.*, Vol. 34, No. 5, pp. 574–576. 1958. (Not included in *Collected Reprints*).

No. 949. H. Barnes and Margaret Barnes. Further Observations on Self-Fertilization in *Chthamalus* sp. *Ecology*, Vol. 39, No. 3, p. 550. 1958.

No. 950. H. Barnes and Margaret Barnes. A Comparison of the Annual Growth Patterns of *Balanus balanoides* (L.) with Particular Reference to the Effect of Food and Temperature. *Oikos*, Vol. 10, No. 1, pp. 1–18. 1959.

No. 951. Takashi Ichiye. A Theory of Vertical Structure of Density in the Ocean. *Jour. Oceanogr. Soc., Japan*, Vol. 14, No. 2, pp. 35–40. 1958.

No. 952. Takashi Ichiye. Tsunami Waves—What are known about them—How we have studied them. *The Port Engineer*, Calcutta, India, Vol. 7, No. 1, pp. 5–19 [1–14]. 1958.

No. 953. Henry Stommel. Letter to the Editors: The Abyssal Circulation. *Deep-Sea Research*, Vol. 5, pp. 80–82. 1958.

No. 954. Bernhard Haurwitz, Henry Stommel and Walter H. Munk. On the Thermal Unrest in the Ocean. In: The Atmosphere and the Sea in Motion (The Rossby Memorial Volume), Rockefeller Institute Press, New York, pp. 74-94. 1959.

No. 955. G. C. McLeod. Delayed Light Action Spectra of Several Algae in Visible and Ultraviolet Light. *Jour. Gen. Physiol.*, Vol. 42, No. 2, pp. 243–250. 1958.

No. 956. John M. Zeigler, Carlyle R. Hayes and Sherwood D. Tuttle. Beach Changes during Storms on Outer Cape Cod, Massachusetts. *Jour. Geology*, Vol. 67, No. 3, pp. 318–336. 1959.

No. 957. James M. Moulton. The Acoustical Behavior of Some Fishes in the Bimini Area. *Biol. Bull.*, Vol. 114, No. 3, pp. 357–374. 1958.

No. 958. Robert L. Miller and John M. Zeigler. A Model Relating Dynamics and Sediment Pattern in Equilibrium in the Region of Shoaling Waves, Breaker Zone, and Foreshore. *Jour. Geology*, Vol. 66, No. 4, pp. 417-441. 1958.

No. 959. Floyd M. Soule and R. M. Morse. Physical Oceanography of the Grand Banks Region and the Labrador Sea in 1957. *U. S. Coast Guard Bull.*, No. 43, pp. 81–131. 1958.

No. 960. James M. Moulton. A Summer Silence of Sea Robins, *Prionotus* spp. *Copeia* 1958, No. 3, pp. 234–235. 1958.

No. 961. Robert H. Gibbs, Jr., and Bruce B. Collette. On the Identification, Distribution, and Biology of the Dolphins, *Coryphaena hippurus*, and *C. equiselis*. *Bull. Mar. Sci. Gulf and Carib.*, Vol. 9, No. 2, pp. 117–152. 1959.

No. 962. E-an Zen. Clay Mineral—Carbonate Relations in Sedimentary Rocks. *Amer. Jour. Sci.*, Vol. 257, pp. 29–43. 1959.

No. 963. Takashi Ichiye. The Response of a Stratified Bounded Ocean to Variable Wind Stresses. *Oceanogr. Mag.*, Tokyo, Japan, Vol. 10, No. 1, pp. 19–63. 1958.

No. 964. Theodore J. Smayda. The Seasonal Incoming Radiation in Norwegian and Arctic Waters, and Indirect Methods of Measurement. *Jour. du Conseil*, Vol. 24, No. 2, pp. 215–220. 1959.

No. 965. Theodore J. Smayda. Biogeographical Studies of Marine Phytoplankton. *Oikos*, Vol. 9, No. 2, pp. 158–191. 1958.

No. 967. Joanne S. Malkus and Georg Witt. The Evolution of a Convective Element: A Numerical Calculation. In: The Atmosphere and the Sea in Motion (The Rossby Memorial Volume), Rockefeller Institute Press, New York, pp. 425–439. 1958.

No. 968. Bostwick H. Ketchum and Vaughan T. Bowen. Biological Factors Determining the Distribution of Radio-Isotopes in the Sea. *Proc. 2nd Internat. Conference on the Peaceful Uses of Atomic Energy*, Geneva, Sept. 1–15, 1958, Vol. 18, pp. 429–433. 1958.

No. 969. Joanne Starr Malkus. On the Structure of the Trade Wind Moist Layer. *Papers in Physical Oceanography and Meteorology*, Vol. 13, No. 2, pp. 1–47. 1958. (Not included in *Collected Reprints*).

No. 970. Vaughan T. Bowen amd T. T. Sugihara. Marine Geochemical Studies with Fallout Radioisotopes. *Proc. 2nd Internat. Conference on the Peaceful Uses of Atomic Engery*, Geneva, Sept. 1–15, 1958, Vol. 18, pp. 434–438. 1958.

No. 971. Francis L. Parker and William D. Athearn. Ecology of Marsh Foraminifera in Poponesset Bay, Massachusetts. *Journ. Paleont.*, Vol. 33, No. 2, pp. 333–343. 1959.

No. 972. Charles S. Yentsch and Ralph F. Vaccaro. Phytoplankton Nitrogen in the Oceans. *Limnol. and Oceanogr.*, Vol. 3. No. 4, pp. 443–448. 1958.

No. 973. J. B. Hersey, Elizabeth T. Bunce, R. F. Wyrick, and F. T. Dietz. Geophysical Investigation of the Continental Margin between Cape Henry, Virginia, and Jacksonville, Florida. *Bull. Geol. Soc. Amer.*, Vol. 70, pp. 437–466. 1959.

No. 974. Melvin E. Stern. The Moving Flame Experiment. *Tellus*, Vol. 11, No. 2, pp. 175–179. 1959.

No. 975. Jack McLachlan and Guy C. McLeod. The Use of Conversion Factors for the Determination of the Concentration of Nutrients in Culture Media. *Limnol. and Oceanogr.*, Vol. 4, No. 2, pp. 218–219. 1959.

No. 976. Alfred C. Redfield. The Biological Control of Chemical Factors in the Environment. *Amer. Scientist*, Vol. 46, No. 3, pp. 205–222. 1958.

No. 977. C. Godfrey Day. Surface Circulation in the Gulf of Maine Deduced from Drift Bottles. *Fish. Bull.* 141, *U. S. Fish and Wildlife Service, Fish. Bull.*, Vol. 58, pp. 443–472. 1958.

No. 978. John H. Ryther, Charles S. Yentsch and Ralph F. Vaccaro. The Dynamics of a Diatom Bloom. *Biol. Bull.*, Vol. 115, No. 2, pp. 257–268. 1958.

No. 979. A. T. Spencer and D. C. Blanchard. A Portable Raindrop Recorder for Semi-Continuous Determination of Size Distributions. *Trans. Amer. Geophys. Union*, Vol. 39, No. 5, pp. 853–857. 1958.

No. 980. G. D. Nicholls, Herbert Curl, Jr., and V. T. Bowen. Spectrographic Analyses of Marine Plankton. *Limnol. and Oceanogr.*, Vol. 4, No. 4, pp. 472–478. 1959.

No. 981. Takashi Ichiye. On Convective Circulation and Density Distribution in a Zonally Uniform Ocean. *Oceanogr. Mag.*, Tokyo, Japan, Vol. 10, No. 1, pp. 97–135. 1958.

No. 982. T. T. Sugihara, H. I. James, E. J. Troianello and V. T. Bowen. Radiochemical Separation of Fission Products from Large Volumes of Sea Water. Strontium, Cesium, Cerium, and Promethium. *Analyt. Chem.*, Vol. 31, No. 1, pp. 44–49. 1959.

No. 983. P. F. Scholander. Counter Current Exchange: A Principle in Biology. *Hvaldrådets Skrifter*, No. 44, 24 pp. 1958.

No. 984. Charles S. Yentsch and John H. Ryther. Relative Significance of the Net Phytoplankton and Nanoplankton in the Waters of Vineyard Sound. *Jour. du Conseil*, Vol. 24, No. 2, pp. 231–238. 1959.

No. 985. G. Veronis. Cellular Convection with Finite Amplitude in a Rotating Fluid. *Jour. Fluid Mech.*, Vol. 5, Pt. 3, pp. 401-435. 1959.

No. 986. C. Godfrey Day. Oceanographic Observations, 1957, East Coast of the United States. *U. S. Fish and Wildlife Service, Spec. Sci. Rept. — Fisheries*, No. 282, 123 pp. 1959. (Not included in *Collected Reprints*).

No. 987. Alan J. Faller and William S. von Arx. The Modeling of Fluid Flow on a Planetary Scale. *Proceedings of the Seventh Hydraulics Conference*, Iowa Institute of Hydraulic Research, pp. 53–72. 1959.

No. 988. John M. Zeigler. Origin of the Sea Islands of the Southeastern United States. *Geogr. Rev.*, Vol. 49, No. 2., pp. 221–237. 1959.

No. 989. Malcolm S. Gordon. Ionic Regulation in the Brown Trout (*Salmo trutta L.*). *Jour. Exper. Biol.*, Vol. 36, No. 2, pp. 227–252. 1959.

No. 990. Francis A. Richards. Dissolved Silicate and Related Properties of Some Western North Atlantic and Caribbean Waters. *Sears Found., Jour. Mar. Res.*, Vol. 17, pp. 449–465. 1958. (In *Collected Reprints* for 1960).

No. 991. Sherwood D. Tuttle. Evolution of the New Hampshire Shore Line. *Bull. Geol. Soc., Amer.*, Vol. 71, pp. 1211–1222. 1960.

No. 992. Elizabeth Schroeder, Henry Stommel, David Menzel and William Sutcliffe, Jr. Climatic Stability of Eighteen Degree Water at Bermuda. *Jour. Geophys. Res.*, Vol. 64, No. 3, pp. 363-366. 1959.

No. 993. Jack McLachlan. The Growth of Unicellular Algae in Artificial and Enriched Sea Water Media. *Canad. Jour. Microbiol.*, Vol. 5, pp. 9–15. 1959.

No. 994. Gilbert L. Voss. The Cephalopods Collected by the R/V Atlantis during the West Indian Cruise of 1954. *Bull. Mar. Sci., Gulf and Caribbean*, Vol. 8, No. 4, pp. 369–389. 1958.

No. 995. John C. Ayers. The Hydrography of Barnstable Harbor, Massachusetts. *Limnol. and Oceanogr.*, Vol. 4, No. 4, pp. 448–462. 1959.

No. 996. Edward R. Baylor. The Responses of Snails to Polarized Light. *Jour. Exper. Biol.*, Vol. 36, No. 2, pp. 369–376. 1959.

No. 997. Guy C. McLeod and Jack McLachlan. The Sensitivity of Several Algae to Ultraviolet Radiation of 2537 Å. *Physiol. Plant.*, Vol. 12, pp. 306–309. 1959.

No. 998. H. Barnes. Regarding the Southern Limits of *Balanus balanoides* (L.). *Oikos*, Vol. 9, No. 2, pp. 139–157. 1958.

No. 999. C. B. Officer, J. I. Ewing, J. F. Hennion, D. G. Harkrider and D. E. Miller. Geophysical Investigations in the Eastern Caribbean: Summary of 1955 and 1956 Cruises. In: Physics and Chemistry of the Earth, Pergamon Press Ltd., New York, Vol. 3, pp. 17-109. 1959.

No. 1000. Alfred C. Redfield. The Influence of the Continental Shelf on the Tides of the Atlantic Coast of the United States. *Sears Found., Jour. Mar. Res.*, Vol. 17, pp. 432–448. 1958. (In *Collected Reprints* for 1960).

No. 1001. L. R. Breslau and H. E. Edgerton. The Luminescence Camera. *Jour. Biol. Photogr. Assoc.*, Vol. 26, No. 2, pp. 49–58, 1958.

No. 1002. Harry J. Turner, Jr. and James E. Hanks. Infestation of *Pecten irradians* by *Polydora*. *The Nautilus*, Vol. 72, No. 4, pp. 109–111. 1959.

No. 1003. Allan Robinson and Henry Stommel. The Oceanic Thermocline and the Associated Thermohaline Circulation. *Tellus*, Vol. 11, No. 3, pp. 295–308. 1959.

No. 1004. Allan Robinson and Henry Stommel. Amplification of Transient Response of the Ocean to Storms by the Effect of Bottom Topography. *Deep-Sea Research*, Vol. 5, pp. 312–314. 1959.

No. 1005. Sheina M. Marshall and A. P. Orr. Some Uses of Antibiotics in Physiological Experiments in Sea Water. *Sears Found., Jour. Mar. Res.*, Vol. 17, pp. 341–346. 1958. (In *Collected Reprints* for 1960).

No. 1006. Bert Bolin. On the Use of Tritium as a Tracer for Water in Nature. *Proc. 2nd Internat. Conference on the Peaceful Uses of Atomic Energy*, Geneva, Sept. 1–15, 1958, Vol. 18, pp. 336–338. 1958. (In *Collected Reprints* for 1959).

No. 1007. Bostwick H. Ketchum, Ralph F. Vaccaro and Nathaniel Corwin. The Annual Cycle of Phosphorus and Nitrogen in New England Coastal Waters. *Sears Found., Jour. Mar. Res.*, Vol. 17, pp. 282–301. 1958. (In *Collected Reprints* for 1960).

No. 1008. Henry Stommel. Florida Straits Transports: June 1956–July 1958. *Bull. Mar. Sci., Gulf and Caribbean*, Vol. 9, No. 2, pp. 222–223. 1959.

No. 1009. James B. Lackey. *Calkinsia aureus* gen. et sp. nov.; a New Marine Euglenid. *Trans. Amer. Micr. Soc.*, Vol. 79, No. 1, pp. 105–107. 1960.

No. 1010. Jack McLachlan and Charles S. Yentsch. Observations on the Growth of *Dunaliella euchlora* in Culture. *Biol. Bull.*, Vol. 116, No. 3, pp. 461–471. 1959.

No. 1011. John W. Graham. Metabolically Induced Precipitation of Trace Elements from Sea Water. *Science*, Vol. 129, No. 3360, pp. 1428–1429. 1959.

No. 1012. Joseph Levine. Spherical Vortex Theory of Bubble-Like Motion in Cumulus Clouds. *Jour. Meteorol.*, Vol. 16, No. 6, pp. 653–662. 1959.

No. 1013. John Kanwisher. Histology and Metabolism of Frozen Intertidal Animals. *Biol. Bull.*, Vol. 116, No. 2, pp. 258–264. 1959.

No. 1014. John Kanwisher. Polarographic Oxygen Electrode. *Limnol. and Oceanogr.*, Vol. 4, No. 2, pp. 210–217. 1959.

No. 1015. L. V. Worthington. The 18° Water in the Sargasso Sea. *Deep-Sea Research*, Vol. 5, pp. 297–305. 1959.

No. 1016. John H. Ryther. Potential Productivity of the Sea. *Science*, Vol. 130, No. 3376, pp. 602–608. 1959.

No. 1017. John W. Graham and Susan C. Cooper. Biological Origin of Manganese-Rich Deposits of the Sea Floor. *Nature*, Vol. 183, pp. 1050–1051. 1959.

No. 1018. Floyd M. Soule and R. M. Morse. Physical Oceanography of the Grand Banks Region and the Labrador Sea in 1958. *U. S. Coast Guard Bull.*, No. 44, pp. 29–99. 1960.

No. 1019. George L. Clarke and Charles J. Hubbard. Quantitative Records of the Luminescent Flashing of Oceanic Animals at Great Depths. *Limnol. and Oceanogr.*, Vol. 4, No. 2, pp. 163–180. 1959.

No. 1020. Richard Barakat. A Note on the Transient Stage of the Random Dispersal of Logistic Populations. *Bull. Math. Biophysics*, Vol. 21, pp. 142–151. 1959.

No. 1021. W. V. R. Malkus. Magnetoconvection in a Viscous Fluid of Infinite Electrical Conductivity. *Astrophys. Jour.*, Vol. 130, No. 1, pp. 259–275. 1959.

No. 1022. Carl E. Tschiegg and Earl E. Hays. Transistorized Velocimeter for Measuring the Speed of Sound in the Sea. *Jour. Acoust. Soc. Amer.*, Vol. 31, No. 7, pp. 1038–1039. 1959.

No. 1023. Henry Stommel and A. B. Arons. On the Abyssal Circulation of the World Ocean. I. Stationary Planetary Flow Patterns on a Sphere. *Deep-Sea Research*, Vol. 6, No. 2, pp. 140–154. 1960.

No. 1024. Patrick Butler. Palynological Studies of the Barnstable Marsh, Cape Cod, Massachusetts. *Ecology*, Vol. 40, No. 4, pp. 735-737. 1959. (Published posthumously).

No. 1025. Bert Bolin and Erik Eriksson. Changes in the Carbon Dioxide Content of the Atmosphere and Sea due to Fossil Fuel Combustion. In: The Atmosphere and the Sea in Motion (The Rossby Memorial Volume), Rockefeller Institute Press, New York, pp. 130–142. 1959.

No. 1026. John H. Ryther and R. R. L. Guillard. Enrichment Experiments as a Means of Studying Nutrients Limiting to Phytoplankton Production. *Deep-Sea Research*, Vol. 6, pp. 65–69. 1959.

No. 1027. Charles S. Yentsch and John H. Ryther. Absorption Curves of Acetone Extracts of Deep Water Particulate Matter. *Deep-Sea Research*, Vol. 6, pp. 72–74. 1959.

No. 1028. W. A. Mordy. Computations of the Growth by Condensation of a Population of Cloud Droplets. *Tellus*, Vol. 11, No. 1, pp. 16–44. 1959.

No. 1029. Irving I. Schell. On a Criterion of Representativeness of Sea Surface Temperature Date. *Bull. Amer. Meteorol. Soc.*, Vol. 40, No. 11, pp. 571–574. 1959.

No. 1030. J. S. Hart and Laurence Irving. The Energetics of Harbor Seals in Air and in Water with Special Consideration of Seasonal Changes. *Canad. Jour. Zool.*, Vol. 37, pp. 447–457. 1959.

No. 1031. Andrew F. Bunker. Heat and Water-Vapor Fluxes in Air Flowing Southward over the Western North Atlantic Ocean. *Jour. Meteorol.*, Vol. 17, No. 1, pp. 52–63. 1960.

No. 1032. JOSEPH CHASE. Wind-Induced Changes in the Water Column along the East Coast of the United States. *Jour. Geophys. Res.*, Vol. 64, No. 8, pp. 1013–1022. 1959.

No. 1033. HOWARD L. SANDERS. Benthic Studies in Buzzards Bay. III. The Structure of the Soft-Bottom Community. *Limnol. and Oceanogr.*, Vol. 5, No. 2, pp. 138–153. 1960.

No. 1034. J. S. MALKUS and H. RIEHL. On the Dynamics and Energy Transformations in Steady-State Hurricanes. *Tellus*, Vol. 12, No. 1, pp. 1–20. 1960.

No. 1035. BOSTWICK H. KETCHUM. Marine Pollution Problems in the North Atlantic Area. In: Biological Problems in Water Pollution, Trans. Second Seminar, April 20–24, 1959, Cincinnati, Ohio, Sponsorship, Water Supply and Water Pollution Research Program. *Robert A. Taft Sanitary Engineering Center, U.S. Dept. Health, Education and Welfare, Publ. Health Service, Technical Rept.*, No. W60–3, pp. 212–217. 1960 (Not included in *Collected Reprints*).

No. 1036. E-AN ZEN. Mineralogy and Petrography of Marine Bottom Sediment Samples Off the Coast of Peru and Chile. *Jour. Sed. Petrol.*, Vol. 29, No. 4, pp. 513–539. 1959.

No. 1037. H. BARNES and MARGARET BARNES. Note on Stimulation of Cirripede Nauplii. *Oikos*, Vol. 10, No. 1, pp. 19–23. 1959.

No. 1038. JOHN T. CONOVER. Seasonal Growth of Benthic Marine Plants as Related to Environmental Factors in an Estuary. *Publ., Inst. Mar. Sci., Univ. Texas*, Vol. 5, pp. 97–147. 1959.

No. 1039. JOHN H. RYTHER. Light Adaptation by Marine Phytoplankton. *Limnol. and Oceanogr.*, Vol. 4, No. 4, pp. 492–497. 1959.

No. 1040. WILLIAM E. SCHEVILL and RICHARD H. BACKUS. Daily Patrol of a *Megaptera*. *Jour. Mammalogy*, Vol. 41, No. 2, pp. 279–281. 1960.

No. 1041. A. C. REDFIELD. Biological Considerations — The Fourth Phase. Conference on Physical and Chemical Properties of Sea Water, Easton, Maryland, Sept. 4–5, 1958. *Nat. Acad. Sci. — Nat. Res. Council, Publ.* 600, pp. 101–112. 1959. (Not included in *Collected Reprints*).

No. 1042. D. W. MENZEL and J. H. RYTHER. The Annual Cycle of Primary Production in the Sargasso Sea off Bermuda. *Deep-Sea Research*, Vol. 6, No. 4, pp. 351–367. 1960.

No. 1043. GEORGE L. CLARKE and LLOYD R. BRESLAU. Measurements of Bioluminescence off Monaco and Northern Corsica. *Bull. Inst. Océanogr., Monaco*, No. 1147, pp. 1–31. 1959.

No. 1044. JOANNE S. MALKUS. Recent Developments in Studies of Penetrative Convection and an Application to Hurricane Cumulonimbus Towers. In: Cumulus Dynamics, Pergamon Press, London and New York, pp. 65–84. 1960.

No. 1045. ALFRED C. REDFIELD. The Tidal System of Lake Maracaibo, Venezuela. *Limnol. and Oceanogr.*, Vol. 6, No. 1, pp. 1–12. 1961.

No. 1046. WILLIAM S. RICHARDSON and CHARLES J. HUBBARD. The Contouring Temperature Recorder. *Deep-Sea Research*, Vol. 6, No. 3, pp. 239–244. 1960.

No. 1047. DAVID A. MCGILL, NATHANIEL CORWIN and BOSTWICK H. KETCHUM. The Temperature Correction of Oceanic Inorganic Phosphorus Analyses. *Deep-Sea Research*, Vol. 6, pp. 60–64. 1959.

No. 1048. C. GODFREY DAY. Oceanographic Observations, 1958, East Coast of the United States. *U. S. Fish and Wildlife Service, Spec. Sci. Rept. — Fisheries*, No. 318, 119 pp. 1959. (Not included in *Collected Reprints*).

No. 1049. John H. Ryther. Organic Production by Plankton Algae and its Environmental Control. In: Ecology of Algae, the Pymatuning Symposium in Ecology, 18–19 June 1959, *Spec. Publ.*, *Univ. Pittsburg Press*, No. 2, pp. 72–83. 1960.

No. 1050. S. M. Marshall and A. P. Orr. On the Biology of *Calanus finmarchicus*. XII. The Phosphorus Cycle: Excretion, Egg Production, Autolysis. *Jour. Mar. Biol. Assoc.*, *U. K.*, Vol. 41, pp. 463–483. 1961.

R. J. Conover. Addendum. The Turnover of Phosphorus by *Calanus finmarchicus*. *Jour. Mar. Biol. Assoc.*, *U. K.*, Vol. 41, pp. 484–488. 1961.

No. 1051. Joanne S. Malkus and Claude Ronne. Cloud Distributions over the Tropical Oceans in Relation to Large-Scale Flow Patterns. In: Physics of Precipitation, *Amer. Geophys. Union*, *Monogr.*, No. 5, pp. 45–60. 1960.

No. 1052. J. B. Hersey. Acoustically Monitored Bottom Coring. *Deep-Sea Research*, Vol. 6, No. 2, pp. 170–172. 1960.

No. 1053. Wolfgang Wieser and John Kanwisher. Vorschlag zum Anlegen einer "Stoffwechselkartei" für marine Tiergemeinschaften. *Zool. Anz.*, Vol. 165, Nos. 9/10, pp. 370–375. 1960.

No. 1054. Wolfgang Wieser. Benthic studies in Buzzards Bay. II. The Meiofauna. *Limnol. and Oceanogr.*, Vol. 5, No. 2, pp. 121–137. 1960.

No. 1055. Henry Stommel and A. B. Arons. On the Abyssal Circulation of the World Ocean. II. An Idealized Model of the Circulation Pattern and Amplitude in Oceanic Basins. *Deep-Sea Research*, Vol. 6, No. 3, pp. 217–233. 1960.

No. 1056. George C. Matthiessen. Observations on the Ecology of the Soft Clam, *Mya arenaria*, in a Salt Pond. *Limnol. and Oceanogr.*, Vol. 5, No. 3, pp. 291–300. 1960.

No. 1057. Francis A. Richards and Bruce B. Benson. Nitrogen/Argon and Nitrogen Isotope Ratios in Two Anaerobic Environments, the Cariaco Trench in the Caribbean Sea and Dramsfjord, Norway. *Deep-Sea Research*, Vol. 7, No 4, pp. 254–264. 1961.

No. 1058. Charles S. Yentsch. The Influence of Phytoplankton Pigments on the Colour of Sea Water. *Deep-Sea Research*, Vol. 7, No. 1, pp. 1–9. 1960.

No. 1059. Wolfgang Wieser and John Kanwisher. Growth and Metabolism in a Marine Nematode, *Enoplus communis* Bastian. *Zeits. Vergl. Physiol.*, Vol. 43, pp. 29–36. 1960.

No. 1060. Karl E. Schleicher. A Note on the Constancy of the T/S Relationship in a Water Mass. Die Expeditionen von F. F. S. "Anton Dohrn" und V. F. S. "Gauss" im Internationalen Geophysikalischen Jahr 1957/1958. *Deutsche Hydrogr. Zeitschr.*, *Ergänzungsheft*, Reihe B (4°), No. 3, pp. 46–48. 1959.

No. 1061. Wolfgang Wieser and John Kanwisher. Respiration and Anaerobic Survival in some Sea Weed-Inhabiting Invertebrates. *Biol. Bull.*, Vol. 117, No. 3, pp. 594–600. 1959.

No. 1062. Joyce C. Lewin and Ralph A. Lewin. Auxotrophy and Heterotrophy in Marine Littoral Diatoms. *Canadian Jour. Microbiol.*, Vol. 6, pp. 127–134. 1960.

No. 1063. Max Blumer and Gilbert Omenn. Fossil Chlorins in a Triassic Sediment. *Nature*, Vol. 191, No. 4784, pp. 161–162. 1961.

No. 1064. G. G. Whitney, Jr. Procedure for and Comments on Ice Point Tests of Deep Sea Reversing Thermometers. *Limnol. and Oceanogr.*, Vol. 5, No. 2, pp. 232–235. 1960.

No. 1065. Allan R. Robinson. The General Thermal Circulation in Equatorial Regions. *Deep-Sea Research*, Vol. 6, No. 4, pp. 311–317. 1960. (Reprints erroneously marked as Contribution No. 1081).

No. 1066. Earl E. Hays. Comparison of Directly Measured Sound Velocities with Values Calculated from Hydrographic Data. *Jour. Acoust. Soc., Amer.*, Vol. 33, No. 1, pp. 85–88. 1961.

No. 1067. John H. Ryther and David W. Menzel. The Seasonal and Geographical Range of Primary Production in the Western Sargasso Sea. *Deep-Sea Research*, Vol. 6, No. 3, pp. 235–238. 1960.

No. 1068. E. M. Hulburt, J. H. Ryther and R. R. L. Guillard. The Phytoplankton of the Sargasso Sea off Bermuda. *Jour. du Conseil*, Vol. 25, No. 2, pp. 115–128. 1960.

No. 1069. Alan J. Faller. Further Examples of Stationary Planetary Flow Patterns in Bounded Basins. *Tellus*, Vol. 12, No. 2, pp. 159–171. 1960.

No. 1070. Andrew A. Fejer and Richard H. Backus. Porpoises and the Bow-Riding of Ships Under Way. *Nature*, Vol. 188, No. 4752, pp. 700–703. 1960.

No. 1072. George D. Grice. Calanoid Copepods from Equatorial Waters of the Pacific Ocean. *Fish. Bull., U. S. Fish and Wildlife Service* (*Fish. Bull.* No. 186) Vol. 61, pp. 171–246. 1961.

No. 1073. John M. Zeigler, G. G. Whitney, Jr. and Carlyle R. Hayes. Woods Hole Rapid Sediment Analyzer. *J. Sed. Petr.*, Vol. 30, No. 3, pp. 490–495. 1960.

No. 1074. Richard Barakat and Robert Barakat. Optical Studies of the Diffraction of Water Waves by Circular and Thin Elliptic Cylinders. *Jour. Appl. Physics*, Vol. 31, No. 3, pp. 474–478. 1960.

No. 1075. H. Barnes and Margaret Barnes. The Effect of Temperature on the Oxygen Uptake and Rate of Development of the Egg-Masses of Two Common Cirripedes, *Balanus balanoides* (L.) and *Pollicipes polymerus* J. B. Sowerby. *Kieler Meeresforschungen*, Vol. 15, No. 2, pp. 242–251. 1959. (In *Collected Reprints* for 1960).

No. 1076. Richard H. Backus. Notes on Western North Atlantic Sharks, No. 2. *Copeia*, 1960, No. 3, pp. 243–245. 1960.

No. 1077. Kirk Bryan. The Instability of a Two-Layered System Enclosed between Horizontal, Coaxially Rotating Plates. *Jour. Meteorol.*, Vol. 17, No. 4, pp. 446–455. 1960.

No. 1078. J. H. Steele and C. S. Yentsch. The Vertical Distribution of Chlorophyll. *Jour. Mar. Biol. Assoc., U.K.*, Vol. 39, pp. 217–226. 1960.

No. 1079. W. A. Mordy. Differences in Coalescence Tendencies in Computed Condensation Cloud Droplet Spectra. In: Physics of Precipitation, *Amer. Geophys. Union, Monogr.*, No. 5, pp. 184–190. 1960.

No. 1080. James E. Hanks. A Method for Preparing the Marine Polychaete, *Pectinaria gouldi* (Verrill), for Histological Study. *Trans. Amer. Micr. Soc.*, Vol. 79, No. 4, pp. 470–471. 1960.

No. 1081. E. A. Spiegel and G. Veronis. On the Boussinesq Approximation for a Compressible Fluid. *The Astrophysical Jour.*, Vol. 131, No. 2, pp. 442–447. 1960.

No. 1082. G. Veronis. An Approximate Theoretical Analysis of the Equatorial Undercurrent. *Deep-Sea Research*, Vol. 6, No. 4, pp. 318–327. 1960.

No. 1083. Raymond Wexler and Ruth Wexler. Cold Clouds over Tropical Oceans. In: Cumulus Dynamics, Pergamon Press, London and New York, pp. 129–134. 1960.

No. 1084. Henry Stommel. Wind-Drift near the Equator. *Deep-Sea Research*, Vol. 6, No. 4, pp. 298–302. 1960.

No. 1085. Richard H. Backus. Stranded Killer Whale in the Bahamas. *Jour. Mammal.*, Vol. 42, No. 3, pp. 418–419. 1961.

No. 1086. Dean F. Bumpus. Sources of Water Contributed to the Bay of Fundy by Surface Circulation. *Jour. Fish. Res. Bd., Canada*, Vol. 17, No. 2, pp. 181–197. 1960.

No. 1087. G. Fraenkel. Lethal High Temperatures for Three Marine Invertebrates: *Limulus polyphemus*, *Littorina littorea* and *Pagurus longicarpus*. *Oikos*, Vol. 11, No. 2, pp. 171–182. 1960.

No. 1088. J. H. Ryther and E. M. Hulburt. On Winter Mixing and the Vertical Distribution of Phytoplankton. *Limnol. and Oceanogr.*, Vol. 5, No. 3, pp. 337–338. 1960.

No. 1089. C. Godfrey Day. Bottom Water Temperature on Browns Ledge off Southern Massachusetts. *Jour. du Conseil*, Vol. 25, No. 3, pp. 235–239. 1960.

No. 1090. George L. Clarke and Lloyd R. Breslau. Studies of Luminescent Flashing in Phosphorescent Bay, Puerto Rico, and in the Gulf of Naples Using a Portable Bathyphotometer. *Bull. Inst. Océanogr., Monaco*, No. 1171, 32 pp. 1960.

No. 1091. Floyd M. Soule and P. A. Morrill. Physical Oceanography of the Grand Banks Region and the Labrador Sea in 1959. *U. S. Coast Guard Bull.*, No. 45, pp. 98–154. 1960.

No. 1092. Frank J. Mather, III. Recaptures of Tuna, Marlin and Sailfish Tagged in the Western North Atlantic. *Copeia*, 1960, No. 2, pp. 149–151. 1960.

No. 1093. Thomas F. Budinger. Iceberg Detection by Radar. *U. S. Coast Guard Bull.*, No. 45, pp. 49–97. 1960.

No. 1094. A. H. Woodcock. The Origin of Trade-Wind Orographic Shower Rains. *Tellus*, Vol. 12, No. 3, pp. 315–326. 1960.

No. 1095. Vaughan T. Bowen and Thomas T. Sugihara. Strontium-90 in the 'Mixed Layer' of the Atlantic Ocean. *Nature*, Vol. 186, No. 4718, pp. 71–72. 1960.

No. 1096. Ralph F. Vaccaro and John H. Ryther. Marine Phytoplankton and the Distribution of Nitrite in the Sea. *Jour. du Conseil*, Vol. 25, No. 3, pp. 260–271. 1960.

No. 1097. Jack McLachlan. The Culture of *Dunaliella tertiolecta* Butcher — a Euryhaline Organism. *Canadian Jour. Microbiol.*, Vol. 6, pp. 367–379. 1960.

No. 1099. Harry J. Turner, Jr. and James E. Hanks. Experimental Stimulation of Gametogenesis in *Hydroides dianthus* and *Pecten irradians* during the Winter. *Biol. Bull.*, Vol. 119, No. 1, pp. 145–152. 1960.

No. 1100. Francis A. Richards. Some Chemical and Hydrographic Observations along the North Coast of South America — 1. Cabo Trés Puntas to Curaçao, Including the Cariaco Trench and the Gulf of Cariaco. *Deep-Sea Research*, Vol. 7, No. 3, pp. 163–182. 1960.

No. 1101. William G. Metcalf. A Note on Water Movement in the Greenland-Norwegian Sea. *Deep-Sea Research*, Vol. 7, No. 3, pp. 190–200. 1960.

No. 1102. Herbert Curl, Jr. Primary Production Measurements in the North Coastal Waters of South America. *Deep-Sea Research*, Vol. 7, No. 3, pp. 183–189. 1960.

No. 1103. John Kanwisher. pCO_2 in Sea Water and its Effect on the Movement of CO_2 in Nature. *Tellus*, Vol. 12, No. 2, pp. 209–215. 1960.

No. 1104. C. Godfrey Day. Oceanographic Observations, 1959, East Coast of the United States. *U. S. Fish and Wildlife Service, Spec. Sci. Rept.-Fisheries*, No. 359, 114 pp. 1960. (Not included in *Collected Reprints*).

No. 1106. Raymond G. Stross. Growth Response of *Chlamydomonas* and *Haematococcus* to the Volatile Fatty Acids. *Canadian Jour. Microbiol.*, Vol. 6, pp. 611–617. 1960.

No. 1107. Kirk Bryan and Elizabeth Schroeder. Seasonal Heat Storage in the North Atlantic Ocean. *Jour. Meteorol.*, Vol. 17, No. 6, pp. 670–674. 1960.

No. 1108. F. C. Fuglister. Atlantic Ocean Atlas of Temperature and Salinity Profiles and Data from the International Geophysical Year of 1957–1958. *Woods Hole Oceanogr. Inst. Atlas Series*, Vol. 1, 209 pp. 1960. (Not included in *Collected Reprints*).

No. 1109. Robert L. Edwards. The Fishes of Richmond Gulf, Ungava, Canada. *Proc. Amer. Philosoph. Soc.*, Vol. 105, No. 2, pp. 196–205. 1961.

No. 1110. Joyce C. Lewin. The Dissolution of Silica from Diatom Walls. *Geochimica et Cosmochimica Acta*, Vol. 21, pp. 182–198. 1961.

No. 1111. Bostwick H. Ketchum. Oceanographic Research Required in Support of Radioactive Waste Disposal. In: Disposal of Radioactive Wastes, International Atomic Energy Agency, Vienna, pp. 283–291. 1960.

No. 1112. Max Blumer. Pigments of a Fossil Echinoderm. *Nature*, Vol. 188, No. 4756, pp. 1100–1101. 1960.

No. 1114. J. E. G. Raymont and Robert J. Conover. Further Investigations on the Carbohydrate Content of Marine Zooplankton. *Limnol. and Oceanogr.*, Vol. 6, No 2, pp. 154–164. 1961.

No. 1115. Robert J. Conover. The Feeding Behavior and Respiration of Some Marine Planktonic Crustacea. *Biol. Bull.*, Vol. 119, No. 3, pp. 399–415. 1960.

No. 1116. George D. Grice. Copepods of the Genus *Oithona* from the Gulf of Mexico. *Bull. Mar. Sci., Gulf and Carib.*, Vol. 10, No. 4, pp. 485–490. 1960.

No. 1118. J. H. Ryther, D. W. Menzel and R. F. Vaccaro. Diurnal Variations in Some Chemical and Biological Properties of the Sargasso Sea. *Limnol. and Oceanogr.*, Vol. 6, No. 2, pp. 149–153. 1961.

No. 1119. D. W. Menzel and J. H. Ryther. Annual Variations in Primary Production of the Sargasso Sea off Bermuda. *Deep-Sea Research*, Vol. 7, No. 4, pp. 282–288. 1961.

No. 1120. John H. Ryther and David W. Menzel. Primary Production in the Southwest Sargasso Sea, January–February, 1960. *Bull. Mar. Sci., Gulf and Caribbean*, Vol. 11, No. 3, pp. 381–388. 1961.

No. 1121. David W. Menzel and John H. Ryther. Zooplankton in the Sargasso Sea off Bermuda and its Relation to Organic Production. *Jour. du Conseil*, Vol. 26, No. 3, pp. 250–258. 1961.

No. 1122. R. M. Pratt. Erratic Boulders from Great Meteor Seamount. *Deep-Sea Research*, Vol. 8, No. 2, pp. 152–153. 1961.

No. 1123. D. W. Menzel and J. H. Ryther. Nutrients Limiting the Production of Phytoplankton in the Sargasso Sea, with Special Reference to Iron. *Deep-Sea Research*, Vol. 7, No. 4, pp. 276–281. 1961.

No. 1124. Robert L. Miller and John M. Zeigler. A Study of the Relation between Dynamics and Sediment Pattern in the Zone of Shoaling Wave, Breaker, and Foreshore. *Eclogae Geol. Helv.*, Vol. 51, No. 3, pp. 542–551. 1958. (In *Collected Reprints* for 1960).

No. 1125. William S. Von Arx. The Line of Zero Set. *Deep-Sea Research*, Vol. 7, No. 3, pp. 219–220. 1960.

No. 1126. James M. Moulton. Swimming Sounds and the Schooling of Fishes. *Biol. Bull.*, Vol. 119, No. 2, pp. 210–223. 1960.

No. 1127. George D. Grice. *Candacia ketchumi*, a New Calanoid Copepod from the North-Western Part of the Sargasso Sea. *Crustaceana*, Vol. 2, No. 2, pp. 126–131. 1961.

No. 1128. J. M. Zeigler, W. S. Hoffmeister, Graham Giese and Herman Tasha. Discovery of Eocene Sediments in Subsurface of Cape Cod, Massachusetts. *Science*, Vol. 132, No. 3437, pp. 1397–1398. 1960.

No. 1129. J. C. Swallow and L. V. Worthington. An Observation of a Deep Countercurrent in the Western North Atlantic. *Deep-Sea Research*, Vol. 8, No. 1, pp. 1–19. 1961.

No. 1130. Willard Dow. A Telemetering Hydrophone. *Deep-Sea Research*, Vol. 7, No. 2, pp. 142–147. 1960.

No. 1131. H. G. Farmer and D. D. Ketchum. Chap. 5. An Instrumentation System for Wave Measurements, Recording and Analysis. *Proc. Seventh Cong. Coastal Eng., The Hague, Netherlands, Aug. 1960*, (*Publ. Counc. Wave Res., Eng. Found.*), Vol. 1, Ch. 5, pp. 77–99. 1961.

No. 1132. Rudolf S. Scheltema. Metamorphosis of the Veliger Larvae of *Nassarius obsoletus* (Gastropoda) in Response to Bottom Sediment. *Biol. Bull.*, Vol. 120, No. 1, pp. 92–109. 1961.

No. 1134. Alfred C. Redfield. The Distribution of Phosphorus in the Deep Oceans of the World. *Assoc. Océanogr. Phys., Union Géodés. et Géophys. Int., Proc. Verb.*, No. 7 (G 16), pp. 189–193. 1960.

No. 1135. A. B. Arons, A. P. Ingersoll and T. Green III. Experimentally Observed Instability of a Laminar Ekman Flow in a Rotating Basin. *Tellus*, Vol. 13, No. 1, pp. 31–39. 1961.

No. 1136. T. T. Sugihara and Vaughan T. Bowen. Radioactive Rare Earths from Fallout for a Study of Particle Movement in the Sea. In: Radioisotopes in the Physical Sciences and Industry, pp. 57–65. 1961.

No. 1137. Hartley Hoskins and S. T. Knott. Geophysical Investigation of Cape Cod Bay, Massachusetts, Using the Continuous Seismic Profiler. *Jour. Geol.*, Vol. 69, No. 3, pp. 330–340. 1961.

No. 1138. W. V. R. Malkus and G. Veronis. Surface Electroconvection. *The Physics of Fluids*, Vol. 4, No. 1, pp. 13–23. 1961.

No. 1139. Joseph Levine. A Spherical Vortex Model of the Buoyant Thermal in Cumulus and Dry Convection. *Schweizer Aero-Revue*, Zurich, Vol. 36, No. 2, pp. 100–101. 1961.

No. 1144. Parker D. Trask. Sedimentation in a Modern Geosyncline off the Arid Coast of Peru and Northern Chile. *Internat. Geol. Congr., XXI Session, Norden, 1960, Internat. Assoc. of Sedimentology*, Pt. 23, pp. 103–118. 1961.

No. 1145. Joanne S. Malkus, Claude Ronne and Margaret Chaffee. Cloud Patterns in Hurricane Daisy, 1958. *Tellus*, Vol. 13, No. 1, pp. 8–30. 1961.

No. 1146. Dean F. Bumpus. Drift bottle records for the Gulf of Maine, Georges Bank, and the Bay of Fundy, 1956–58. *U. S. Fish and Wildlife Service, Spec. Sci. Rept., Fish.*, No. 378, pp. 1–127. 1961. (Not included in *Collected Reprints*).

No. 1147. R. R. Brockhurst, J. G. Bruce, Jr. and A. B. Arons. Refraction of Underwater Shock Waves by a Strong Velocity Gradient. *Jour. Acoust. Soc., Amer.*, Vol. 33, No. 4, pp. 452–456. 1961.

No. 1150. Jack McLachlan. The Effect of Salinity on Growth and Chlorophyll Content in Representative Classes of Unicellular Marine Algae. *Canadian Jour. Microbiol.*, Vol. 7, pp. 399–406. 1961.

No. 1152. Peter M. Saunders. An Observational Study of Cumulus. *Jour. Meteorol.*, Vol. 18, No. 4, pp. 451–467. 1961.

No. 1153. Bruce B. Benson and Peter D. M. Parker. Nitrogen/Argon and Nitrogen Isotope Ratios in Aerobic Sea Water. *Deep-Sea Research*, Vol. 7, No. 4, pp. 237–253. 1961.

No. 1154. Bruce B. Benson and Peter D. M. Parker. Relations among the Solubilities of Nitrogen, Argon and Oxygen in Distilled Water and Sea Water. *Jour. Phys. Chem.*, Vol. 65, pp. 1489–1496. 1961.

No. 1155. M. Blumer and G. S. Omenn. Fossil Porphyrins: Uncomplexed Chlorins in a Triassic Sediment. *Geochimica et Cosmochimica Acta*, Vol. 25, pp. 81–90. 1961.

No. 1156. Herbert Riehl and Joanne Malkus. Some Aspects of Hurricane Daisy, 1958. *Tellus*, Vol. 13, No. 2, pp. 181–213. 1961. (Also, published as *National Hurricane Research Project, Rept.* No. 46 (multilithed)).

No. 1157. Pierre Welander. Theory of Very Long Waves in a Zonal Atmospheric Flow. *Tellus*, Vol. 13, No. 2, pp. 140–155. 1961.

No. 1158. John M. Zeigler and Sherwood D. Tuttle. Beach Changes Based on Daily Measurements of Four Cape Cod Beaches. *Jour. Geol.*, Vol. 69, No. 5, pp. 583–599. 1961.

No. 1159. R. C. Dugdale, David W. Menzel and John H. Ryther. Nitrogen Fixation in the Sargasso Sea. *Deep-Sea Research*, Vol. 7, No. 4, pp. 298–300. 1961.

No. 1160. Floyd M. Soule, Peter A. Morrill and Alfred P. Franceschetti. Physical Oceanography of the Grand Banks Region and the Labrador Sea in 1960. *U. S. Coast Guard Bull.*, No. 46, pp. 31–114. 1961.

No. 1165. Richard Cifelli. 227. *Globigerina incompta*, a New Species of Pelagic Foraminifera from the North Atlantic. *Contrib. Cushman Found. Foram. Res.*, Vol. 12, Pt. 3, pp. 83–86, Pl. 4. 1961.

No. 1166. Melvin E. Stern The Stability of Thermoclinic Jets. *Tellus*, Vol. 13, No. 4, pp. 503–508. 1961.

No. 1167. Wolfgang Wieser and John Kanwisher. Ecological and Physiological Studies on Marine Nematodes from a Small Salt Marsh near Woods Hole, Massachusetts. *Limnol. and Oceanogr.*, Vol. 6, No. 3, pp. 262–270. 1961.

No. 1168. Raymond Siever, Robert M. Garrels, John Kanwisher and Robert A. Berner. Interstitial Waters of Recent Marine Muds off Cape Cod. *Science*, Vol. 134, No. 3485, pp. 1071–1072. 1961.

No. 1170. Bert Bolin and Henry Stommel. On the Abyssal Circulation of the World Ocean. IV. Origin and Rate of Circulation of Deep Ocean Water as Determined with the Aid of Tracers. *Deep-Sea Research*, Vol. 8, No. 2, pp. 95–110. 1961.

No. 1171. A. H. Woodcock and A. T. Spencer. Lava-Sea-Air Contact Areas as Sources of Sea-Salt Particles in the Atmosphere. *Jour. Geophys. Res.*, Vol. 66, No. 9, pp. 2873–2887. 1961.

No. 1173. Ferris Webster. A Description of Gulf Stream Meanders off Onslow Bay. *Deep-Sea Research*, Vol. 8, No. 2, pp. 130–143. 1961.

No. 1174. Ferris Webster. The Effect of Meanders on the Kinetic Energy Balance of the Gulf Stream. *Tellus*, Vol. 13, No. 3, pp. 392–401. 1961.

No. 1176. Evelyn Shaw. The Development of Schooling in Fishes. II. *Physiol. Zoöl.*, Vol. 34, No. 4, pp. 263–272. 1961.

No. 1177. John H. Ryther and Dana D. Kramer. Relative Iron Requirement of Some Coastal and Offshore Plankton Algae. *Ecology*, Vol. 42, No. 2, pp. 444–446. 1961.

No. 1183. Charles N. David and Robert J. Conover. Preliminary Investigation on the Physiology and Ecology of Luminescence in the Copepod, *Metridia lucens*. *Biol. Bull.*, Vol. 121, No. 1, pp. 92–107. 1961.

No. 1186. E. B. Kraus. Physical Aspects of Deduced and Actual Climatic Change. In: Solar Variations, Climatic Change, and Related Geophysical Problems. *Ann. N. Y. Acad. Sci.*, Vol. 95, Art. 1, pp. 225–234. 1961.

No. 1189. Arthur D. Voorhis. Evidence of an Eastward Equatorial Undercurrent in the Atlantic from Measurements of Current Shear. *Nature*, Vol. 191, No. 4784, pp. 157–158. 1961.

No. 1191. Richard H. Backus, Charles S. Yentsch and Asa Wing. Bioluminescence in the Surface Waters of the Sea. *Nature*, Vol. 192, No. 4802, pp. 518–521. 1961.

No. 1193. Max Blumer. Benzpyrenes in Soil. *Science*, Vol. 134, No. 3477, pp. 474–475. 1961.

No. 1194. John Reitzel. Some Heat-Flow Measurements in the North Atlantic. *Jour. Geophys. Res.*, Vol. 66, No. 7, pp. 2267–2268. 1961.

No. 1198. Herbert Curl, Jr., and Guy C. McLeod. The Physiological Ecology of a Marine Diatom, *Skeletonema costatum* (Grev.) Cleve. *Sears Found., Jour. Mar. Res.*, Vol. 19, No. 2, pp. 70–88. 1961.

No. 1199. Eric B. Kraus and Claës Rooth. Temperature and Steady State Vertical Heat Flux in the Ocean Surface Layers. *Tellus*, Vol. 13, No. 2, pp. 231–238. 1961.

No. 1208. R. H. Bodman, L. V. Slabaugh and V. T. Bowen. A Multipurpose Large Volume Sea-Water Sampler. *Sears Found., Jour. Mar. Res.*, Vol. 19, No. 3, pp. 141–148. 1961.

No. 1209. Herbert Curl, Jr. and Judith Sandberg. The Measurement of Dehydrogenase Activity in Marine Organisms. *Sears Found., Jour. Mar. Res.*, Vol. 19, No. 3, pp. 123–138. 1961.

No. 1211. Evelyn Shaw. Minimal Light Intensity and the Dispersal of Schooling Fish. *Bull. Inst. Océanogr., Monaco,* No. 1213, pp. 1–8. 1961.

No. 1215. G. D. Nicholls and V. T. Bowen. Natural Glass from Beneath Red Clay on the Floor of the Atlantic. *Nature,* Vol. 192, No. 4798, pp. 156–157. 1961.

No. 1218. John M. Teal and John Kanwisher. Gas Exchange in a Georgia Salt Marsh. *Limnol. and Oceanogr.,* Vol. 6, No. 4, pp. 388–399. 1961.